MICROBIAL STRESS: FROM SENSING TO INTRACELLULAR AND POPULATION RESPONSES

EDITED BY: Daniela De Biase, John P. Morrissey and Conor P. O'Byrne
PUBLISHED IN: Frontiers in Microbiology

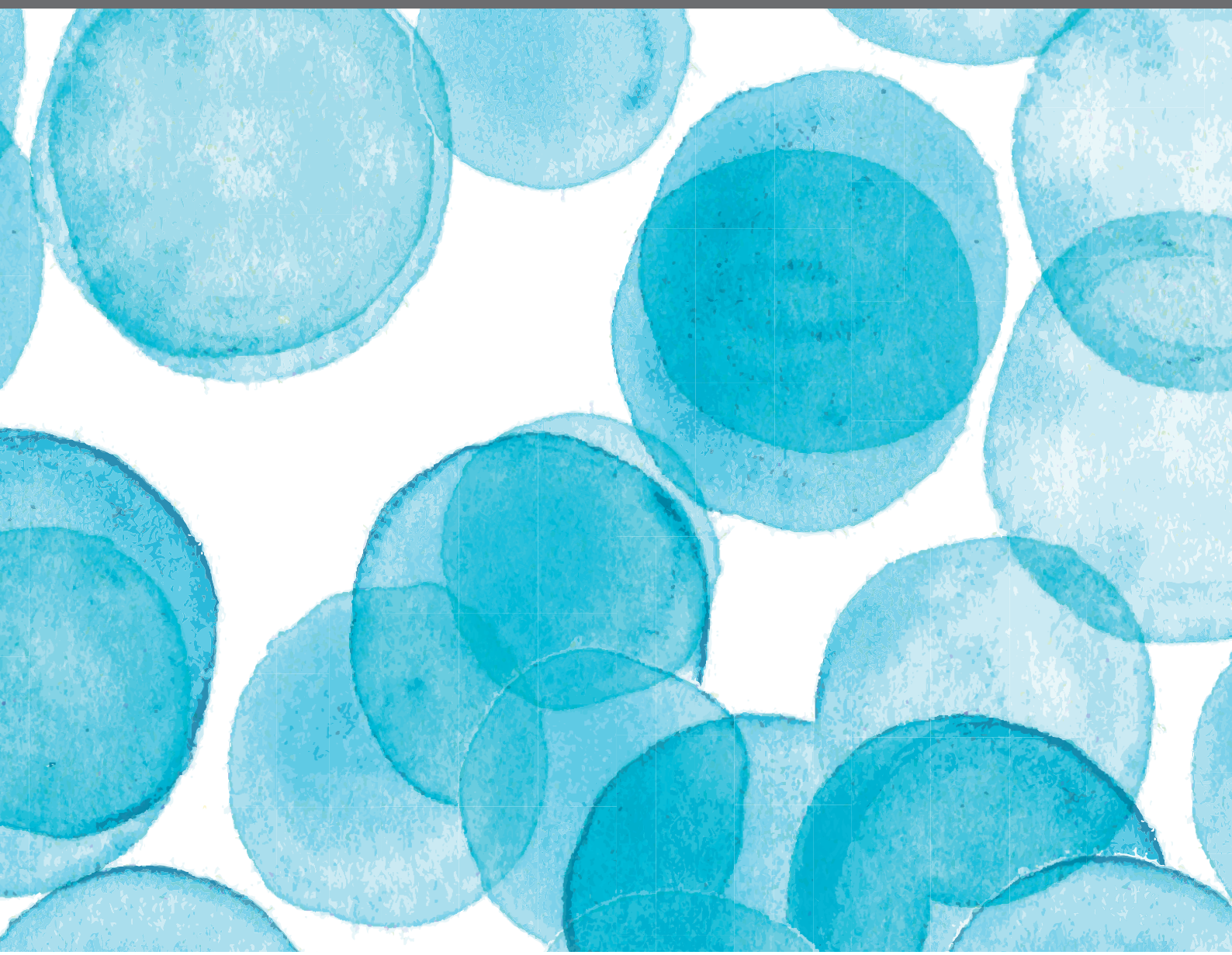

frontiers Research Topics

frontiers

ISSN 1664-8714
ISBN 978-2-88966-024-7
DOI 10.3389/978-2-88966-024-7

About Frontiers

Frontiers is more than just an open-access publisher of scholarly articles: it is a pioneering approach to the world of academia, radically improving the way scholarly research is managed. The grand vision of Frontiers is a world where all people have an equal opportunity to seek, share and generate knowledge. Frontiers provides immediate and permanent online open access to all its publications, but this alone is not enough to realize our grand goals.

Frontiers Journal Series

The Frontiers Journal Series is a multi-tier and interdisciplinary set of open-access, online journals, promising a paradigm shift from the current review, selection and dissemination processes in academic publishing. All Frontiers journals are driven by researchers for researchers; therefore, they constitute a service to the scholarly community. At the same time, the Frontiers Journal Series operates on a revolutionary invention, the tiered publishing system, initially addressing specific communities of scholars, and gradually climbing up to broader public understanding, thus serving the interests of the lay society, too.

Dedication to Quality

Each Frontiers article is a landmark of the highest quality, thanks to genuinely collaborative interactions between authors and review editors, who include some of the world's best academicians. Research must be certified by peers before entering a stream of knowledge that may eventually reach the public - and shape society; therefore, Frontiers only applies the most rigorous and unbiased reviews.
Frontiers revolutionizes research publishing by freely delivering the most outstanding research, evaluated with no bias from both the academic and social point of view. By applying the most advanced information technologies, Frontiers is catapulting scholarly publishing into a new generation.

What are Frontiers Research Topics?

Frontiers Research Topics are very popular trademarks of the Frontiers Journals Series: they are collections of at least ten articles, all centered on a particular subject. With their unique mix of varied contributions from Original Research to Review Articles, Frontiers Research Topics unify the most influential researchers, the latest key findings and historical advances in a hot research area! Find out more on how to host your own Frontiers Research Topic or contribute to one as an author by contacting the Frontiers Editorial Office: researchtopics@frontiersin.org

MICROBIAL STRESS: FROM SENSING TO INTRACELLULAR AND POPULATION RESPONSES

Topic Editors:
Daniela De Biase, Sapienza University of Rome, Italy
John P. Morrissey, University College Cork, Ireland
Conor P. O'Byrne, National University of Ireland Galway, Ireland

Citation: De Biase, D., Morrissey, J. P., O'Byrne, C. P., eds. (2020). Microbial Stress: From Sensing to Intracellular and Population Responses. Lausanne: Frontiers Media SA. doi: 10.3389/978-2-88966-024-7

Table of Contents

frontiers in Microbiology

EDITORIAL
published: 31 July 2020
doi: 10.3389/fmicb.2020.01667

Editorial: Microbial Stress: From Sensing to Intracellular and Population Responses

Daniela De Biase[1]*, *John P. Morrissey*[2] *and Conor P. O'Byrne*[3]

[1] Department of Medico-Surgical Sciences and Biotechnologies, Laboratory Affiliated to the Istituto Pasteur Italia – Fondazione Cenci Bolognetti, Sapienza University of Rome, Latina, Italy, [2] School of Microbiology, Centre for Synthetic Biology and Biotechnology, Environmental Research Institute, APC Microbiome Institute, University College Cork, Cork, Ireland, [3] Microbiology, School of Natural Sciences, College of Science, National University of Ireland, Galway, Ireland

Keywords: acid stress, second messengers, transcriptional regulation, cyanobacteria, pathogens, organic acids, oxidative stress, biotechnology

Editorial on the Research Topic

Microbial Stress: From Sensing to Intracellular and Population Responses

We initially devised this Research Topic (RT) as a valuable initiative to collect high-quality scientific articles from the participants of the 4th European Federation of Biotechnology (EFB) Microbial Stress meeting held in Kinsale, Ireland, April 2018. The scope of the RT is based on the scientific content of that "*Microbial Stress: from Systems to Molecules and back*" meeting. Indeed, over 40% of the articles eventually accepted for publication were contributed by meeting participants, but notably the remaining 60% was contributed by authors that work in this field. The collection of 22 original research and 2 review articles, contributed by 163 authors collectively, deal with the many different aspects of the microbial responses to biotic and abiotic stresses, relevant to many fields: from host-pathogen interactions to biotechnology, from bioremediation to food processing, from molecular and single-cell to population studies. The RT showcases the rapid developments of the microbial stress research on a range of microorganisms and stress conditions, and confirms that understanding microbial physiology under stress can be a trigger for the development of new methodologies as well as helping to integrate the knowledge from many different microbiological fields of research.

The retrospective analysis of the articles contributed to this RT allowed them to be assigned to one of four main sub-topics: (i) impact of weak organic acids and low pH on micro-organisms, from clinical to biotechnological contexts; (ii) adaptive responses in microbial pathogens to abiotic/environmental stress; (iii) oxidative and metal stress, from clinical to bioremediation contexts, and (iv) regulation of transcription and translation under stress, from epigenetic aspects to the role of second messengers and sRNAs.

WEAK ORGANIC ACIDS AND LOW pH STRESS

An area of intensive research deals with the microbial responses to acids (inorganic or organic) because these are common encounters that can affect or even be a threat to microbial growth, with implications in many area of clinical and applied microbiology research.

Using a bioinformatic analysis, Pennacchietti et al. showed that the glutamine-dependent acid resistance (AR2_Q) system in enteric bacteria is often associated with the glutamate-dependent AR system, the most potent AR system reported to date (De Biase and Pennacchietti, 2012). In addition, they developed a simple to perform, fast, and sensitive colorimetric assay which allowed

OPEN ACCESS

Edited by:
Jörg Stülke,
University of Göttingen, Germany

Reviewed by:
Thomas Schweder,
University of Greifswald, Germany
Matthew Cabeen,
Oklahoma State University, United States

***Correspondence:**
Daniela De Biase
daniela.debiase@uniroma1.it

Specialty section:
This article was submitted to Microbial Physiology and Metabolism, a section of the journal Frontiers in Microbiology

Received: *03 June 2020*
Accepted: *25 June 2020*
Published: *31 July 2020*

Citation:
De Biase D, Morrissey JP and O'Byrne CP (2020) Editorial: Microbial Stress: From Sensing to Intracellular and Population Responses. Front. Microbiol. 11:1667. doi: 10.3389/fmicb.2020.01667

the detection of the acid glutaminase, a key enzyme in AR2Q. The assay can find useful application in high-throughput phenotypic screens.

The use of weak organic acids was covered by three studies. Bushell et al. described a comprehensive characterization of the growth response of *Pseudomonas aeruginosa* to several organic acids over a range of pH values, with the long-term goal of using them in the treatment of topical infections caused by this pathogen. In their study, they found that the effects on the organic acids on growth could be best modeled with a non-parametric Gaussian process regression (rather than a parametric logistic approach), a finding that will undoubtedly help with modeling the growth behavior of other pathogens. Another study by Lourenço et al. provides insight into the effect of pH 4.0 and acetic acid or lactic acid on the efficacy of different azoles employed to treat vaginal candidiasis caused by two pathogenic fungi *Candida albicans* and *Candida glabrata*. In particular, acetic acid was shown to improve significantly the efficacy of all azoles tested, even on strains that were azole resistant. Thus, both studies point to an important role of these acids to treat infections or improve the efficacy of current therapeutic treatments.

A further article on yeast by Watcharawipas et al. reviewed the *Saccharomyces cerevisiae* response to sodium acetate. Sodium and acetic acid independently cause stress and activate appropriate responses in yeast but this article addressed the combined response to both. This illustrated the involvement of well-studied stress response mechanisms such as the Rim101 and Hog1 pathways, as well as a role for the ubiquitin ligase Rsp5. Rim101 is a transcriptional activator, mainly studied for its role in adaptation to alkaline stress, whereas Hog1 is a protein kinase that is a key mediator of the response to osmotic shock. It is still unknown how the different pathways interact to deliver an integrated response to combined stressors with different modes of action.

A link between acid stress and osmotic stress was studied by Chakraborty and Kenney who investigated the role of OmpR in *Salmonella enterica* serovar Typhimurium and *Escherichia coli* strain MG1655. The authors demonstrated that the acid stress regulon is rather different in the number of affected genes between the two microorganisms, whereas the number of genes affected under osmotic stress is similar. Notably, in both microorganisms, OmpR repressed *gltA*, coding for citrate synthase, which otherwise negatively affected cell growth during stress. Moreover, OmpR binding affinity for DNA increased at acidic pH. Control of intracellular enzyme activities in response to acid frequently occurs via conformational changes (Gut et al., 2006) and these mechanisms contribute significantly to the physiological response of the cell to acid stress, even when changes at the expression level are not detected.

MICROBIAL PATHOGENS ADAPTIVE RESPONSES TO STRESS

Using a label-free relative quantitative proteomics approach, Zai et al. performed a detailed study aimed at dissecting the responses of *Brucella abortus* to different stresses singly and when applied all together, the most likely situation encountered by this intracellular facultative microorganism when infecting the host. Overall the results using the multi-stress condition suggested that *B. abortus* by decreasing the oxidation of nutrients and amino acid use, reducing the secondary metabolite biosynthesis, enhancing iron acquisition and two-component systems better adapted to the intracellular environment. The importance of stress adaptation in the human food-borne pathogen *Listeria monocytogenes* is highlighted in a broad review by Bucur et al. The regulatory mechanisms that underpin thermal adaptation, acid resistance, osmoregulation, and other food processing/preservation stresses were all comprehensively reviewed. The adaptability of this pathogen makes it a significant challenge for food producers, and remains a significant public health risk.

Some pathogens, such as *Yersinia ruckeri*, have optimal growth at 28°C, but cause outbreaks in the fish host at 18°C. To gain insights into the genes preferentially expressed at lower temperature and which could play a role in virulence, Mendez et al. used Mini-*Tn5-lux-lac Km2* transposon to generate a library of 14,724 *Y. ruckeri* transconjugants, out of which 168 clones displayed β-galactosidase activity higher at 18°C than at 28°C. The *acrR* and *osmY* genes were analyzed in further detail by *in vivo* and *ex vivo* analysis of their promoters activation in different fish tissue during the colonization process via bioluminescence. The latter represents an interesting approach to significantly reduce the number of fish used in this kind of experiments. Another *in vivo* model, *Galleria mellonella* larvae, was used by Lee et al. to demonstrate that YfdX deficiency enhanced *S. enterica* serovar Typhi virulence while decreasing its susceptibility to penicillin G and carbenicillin. Through a combination of structural analyses (SEC-MALS, SAXS, crystallography) and mutagenesis studies the authors demonstrated that the tetrameric enzyme undergoes dissociation into dimers when the pH is increased from 5.5 to 8.0. Unlike the monomer, the oligomers were responsible for YfdX effectiveness *in vivo*, though the authors do not known if at different level/extent.

Metarizhium acridum alcohol dehydrogenase (*Ma*ADH1) expression and deletion effects on the growth and sporulation of this entomopathogenic fungi were investigated by Zhang et al. *M. acridum* belongs to a group of promising agents for biological control of pest insects such as locust and grasshopper in Africa, Asia and Australia. The authors showed that *Ma*ADH1 supports fungal growth and sporulation very likely because the enzyme detoxifies from acetaldehyde, in particular under hypoxic conditions.

A detailed analysis (hourly) of the transcriptome profile during the *E. coli* growth cycle in LB medium by Smith et al. revealed that the KEGG pathways "Ribosome" and "Microbial metabolism in diverse environments" were the most overrepresented in the different phases of growth (lag, exponential and stationary) when pH and nutrient availability change. Moreover, by using the persister phenotype as a proxy for changes in populations-wide heterogeneity, persisters were shown to increase during growth and the response of persisters formation to antibiotics was not only growth

phase-dependent, but also affected by the composition of the medium containing the antibiotic. Thus, medium composition is an important consideration when screening for antibiotics against persisters.

OXIDATIVE AND METAL STRESS

An interesting observation was made by Vijay et al. about the ultrastructure of *Mycobacterium tuberculosis* from sputum and from clinical isolates exposed to oxidative stress, antibiotic isoniazid or iron deprivation *in vitro*. Using Transmission Electron Microscopy, the authors demonstrated a significant reduction in thickness of the triple-layered cell envelope and the accumulation of intracytoplasmic lipid inclusions in all isolates exposed to the above stresses, but not in the *M. tuberculosis* H37Rv reference laboratory strain. The cellular adaptations in clinical isolates may well represent a signature of dormancy and antibiotic tolerance, making them possible targets for antibiotic treatment.

Oxidative stress is also encountered by pathogenic Group B *Streptococcus* in macrophages when they colonize the human female host. Korir et al. investigated the role of a putative NADH peroxidase Npx in protecting against phagosome-associated oxidative stress. They showed that a mutant lacking the corresponding gene (*npx*) was compromised for H_2O_2 survival and growth in human macrophages.

In yeast, oxidative stress is an issue both in pathogenic and biotechnological settings. For biotechnology, it is of interest to find ways to improve oxidative stress resistance and two papers addressed this. First, Vázquez et al. showed the protective effects of melatonin in different yeasts used in the beverage industry. This molecule is naturally produced by yeasts and knowledge of its protective effect open up possibilities to generate overproducing strains with enhanced stress tolerance. Liu et al. took a completely different approach that focused on creating a glutathione-dependent disulfide oxidoreductase gene (*GRX1*) with a noisy promoter. This also led to increased resistance to oxidative stress and highlights some interesting points around stochasticity and population structure: for example, whether natural variability is a positive or negative feature when engineering strains for biotechnology. This idea that yeast cultures display population heterogeneity is the focus of a separate study on the biotechnological yeast *Pichia pastoris* by Raschmanová et al. The authors used single cell approaches to identify four sub-populations that varied in the unfolded protein response and other cellular parameters. Understanding and controlling this has important implications for efficient production of recombinant proteins.

Mercury is a potent antimicrobial but resistance mechanisms have evolved in many microbial species. The mercury resistance gene cluster (*mer*) of the mercury resistant marine bacterium *Pseudomonas stutzeri* was characterized by Zheng et al. The cluster encodes transcriptional regulators (MerR and MerD), the structural genes required for the transport (MerP and MerT) and reductive detoxification of Hg^{2+} to Hg^0 (MerA) as well as MerF. The latter, which has homologs in several other pathogenic bacterial species, was shown by the authors to influence motility and biofilm formation and contribute to mercury resistance.

REGULATION OF TRANSCRIPTION UNDER STRESS

Dostálová et al. investigated the σ^D regulon of *Corynebacterium glutamicum*. The σ^D factor of RNAP, which belongs to a group of extracytoplasmic σ factors, was recently found to be involved in envelope stress response, synthesis of mycomembrane and formation of cell wall (Toyoda and Inui, 2018). The authors showed that σ^D increased the expression of 29 genes organized in 23 operons. Eleven promoter regions (encompassing 50 nucleotides) could be aligned and a consensus sequence derived. Using a combination of *in vitro* and *in silico* methods they provided evidence for overlapping functions of different sigma factors which should play a significant role in fine tuning of gene expression and coping with complex environmental stresses.

An interesting study on the global and specific changes in the m^5C methylome was presented in the cyanobacterium *Synechocystis* sp. PCC 6803 by Hu et al. The authors demonstrated that 72 h of nitrogen starvation had no effect on the proportion of global m^5C, rather on its distribution. In other words, nitrogen deficiency led to decrease of methylated sites, but the level of methylation of the m^5C sites increased to an extent that balanced the decrease in the total methylated sites. The epigenetic pattern was partly inherited and still detectable after 12 generations, thus pointing to the methylome as a way to detect the stress history of a specific microorganism. Notably, no correlation was identified between level of methylation and increase/decrease of gene expression. Nitrogen stress was also investigated in the cyanobacterium *Nostoc* sp. PCC7120 by Álvarez-Escribano et al., though at the transcriptional and post-transcriptional level. The authors performed a detailed molecular study and demonstrated that a feed-forward loop is taking place involving the sRNA NsrR1 and the transcriptional regulator NtcA, which activated the gene *nblA*, encoding a protein adaptor for phycobilisome degradation under nitrogen deficiency. The authors showed that NtcA directly represses NsrR1, which in turn, when expressed, was responsible for repressing *nblA* expression by direct binding to its mRNA 5′-UTR thereby interfering with the translation start, possibly causing *nlbA* mRNA destabilization.

The iron starvation response is important for virulence in pathogenic yeasts, so Benchouaia et al. used a transcriptomic and bioinformatic approach to study this in the human pathogen *C. glabrata*. By focusing on genes that responded differently to iron stress in *C. glabrata* and other yeasts, they identified novel genes required for surviving iron starvation in *C. glabrata*. The REGULOUT bioinformatic tool described in this paper is likely to be applicable also for other comparative transcriptomics studies.

The importance of cyclic dinucleotides in stress signaling and in modulating adaptive gene expression was reflected in three different papers and three distinct bacteria. While c-diAMP has been implicated as a second messenger in cell wall homeostasis

in response to osmotic stress in several bacterial species its role in the physiology of cyanobacteria had not been investigated. Agostoni et al. showed that c-di-AMP levels were modulated differently in two cyanobacterial species in response to osmotic stress (by salt or sorbitol), suggesting a role in osmotic stress adaptation in the genus *Synechocystis*. In *E. coli,* c-di-GMP is well-known to influence biofilm formation as a result of its role in regulating the production of surface structures called curli. Somorin et al. reported that some soil persistent strains of *E. coli* have lost curli production because of mutations that negatively affect c-di-GMP pools. These strains had a reduced capacity to produce biofilm, suggesting that there may be niches in the soil occupied by *E. coli* that do not require biofilm formation. The links between c-di-GMP and biofilm formation in the opportunistic human pathogen *P. aeruginosa* were investigated by Strempel et al. In this case, hypochlorite stimulated biofilm formation by inducing expression of a c-di-GMP synthase. Given that HClO is a common disinfectant, the potential to modulate the very complex intracellular c-di-GMP signaling network in a serious pathogenic bacterium highlighted the need to further explore and better understand such finely balanced systems.

AUTHOR CONTRIBUTIONS

All authors listed have made a substantial, direct and intellectual contribution to the work, and approved it for publication.

ACKNOWLEDGMENTS

This topic was organized to accompany the 4th EFB Meeting *Microbial Stress: from Systems to Molecules and Bac*k, held in Kinsale (Ireland), 23-25 April 2018. We would like to take this opportunity to thank all the conference participants, and especially those who contributed their work to this topic.

REFERENCES

De Biase, D., and Pennacchietti, E. (2012). Glutamate decarboxylase-dependent acid resistance in orally acquired bacteria: function, distribution and biomedical implications of the *gadBC* operon. *Mol. Microbiol.* 86, 770–786. doi: 10.1111/mmi.12020

Gut, H., Pennacchietti, E., John, R. A., Bossa, F., Capitani, G., De Biase, D., et al. (2006). *Escherichia coli* acid resistance: pH-sensing, activation by chloride and autoinhibition in GadB. *EMBO J.* 25, 2643–2651. doi: 10.1038/sj.emboj.7601107

Toyoda, K., and Inui, M. (2018). Extracytoplasmic function sigma factor sigma (D) confers resistance to environmental stress by enhancing mycolate synthesis and modifying peptidoglycan structures in *Corynebacterium glutamicum*. *Mol. Microbiol.* 107, 312–329. doi: 10.1111/mmi.13883

Conflict of Interest: The authors declare that the research was conducted in the absence of any commercial or financial relationships that could be construed as a potential conflict of interest.

frontiers in Microbiology

ORIGINAL RESEARCH
published: 22 November 2017
doi: 10.3389/fmicb.2017.02311

The Oxidative Stress Agent Hypochlorite Stimulates c-di-GMP Synthesis and Biofilm Formation in *Pseudomonas aeruginosa*

Nikola Strempel[1], Michael Nusser[1], Anke Neidig[1], Gerald Brenner-Weiss[1†] and Joerg Overhage[1,2†]*

[1] *Institute of Functional Interfaces, Karlsruhe Institute of Technology, Karlsruhe, Germany,* [2] *Department of Health Sciences, Carleton University, Ottawa, ON, Canada*

The opportunistic human pathogen *Pseudomonas aeruginosa* is able to survive under a variety of often harmful environmental conditions due to a multitude of intrinsic and adaptive resistance mechanisms, including biofilm formation as one important survival strategy. Here, we investigated the adaptation of *P. aeruginosa* PAO1 to hypochlorite (HClO), a phagocyte-derived host defense compound and frequently used disinfectant. In static biofilm assays, we observed a significant enhancement in initial cell attachment in the presence of sublethal HClO concentrations. Subsequent LC-MS analyses revealed a strong increase in cyclic-di-GMP (c-di-GMP) levels suggesting a key role of this second messenger in HClO-induced biofilm development. Using DNA microarrays, we identified a 26-fold upregulation of ORF PA3177 coding for a putative diguanylate cyclase (DGC), which catalyzes the synthesis of the second messenger c-di-GMP – an important regulator of bacterial motility, sessility and persistence. This DGC PA3177 was further characterized in more detail demonstrating its impact on *P. aeruginosa* motility and biofilm formation. In addition, cell culture assays attested a role for PA3177 in the response of *P. aeruginosa* to human phagocytes. Using a subset of different mutants, we were able to show that both Pel and Psl exopolysaccharides are effectors in the PA3177-dependent c-di-GMP network.

Keywords: *Pseudomonas aeruginosa*, bacterial stress response, biofilm formation, c-di-GMP, oxidative stress, pathogen

OPEN ACCESS

Edited by:
John P. Morrissey,
University College Cork, Ireland

Reviewed by:
Jerry Reen,
University College Cork, Ireland
Giordano Rampioni,
Università degli Studi Roma Tre, Italy

****Correspondence:***
Joerg Overhage
joerg.overhage@carleton.ca

† These authors are joint senior authors.

Specialty section:
This article was submitted to Microbial Physiology and Metabolism, a section of the journal Frontiers in Microbiology

Received: *18 September 2017*
Accepted: *08 November 2017*
Published: *22 November 2017*

Citation:
Strempel N, Nusser M, Neidig A, Brenner-Weiss G and Overhage J (2017) The Oxidative Stress Agent Hypochlorite Stimulates c-di-GMP Synthesis and Biofilm Formation in Pseudomonas aeruginosa. Front. Microbiol. 8:2311. doi: 10.3389/fmicb.2017.02311

INTRODUCTION

Pseudomonas aeruginosa is a widespread Gram-negative water and soil bacterium, which is in addition one of the most important opportunistic human pathogens causing severe infections in immunocompromised persons (Hancock and Speert, 2000; Stover et al., 2000). Moreover, *P. aeruginosa* is the leading cause of chronic pneumonia in patients suffering from cystic fibrosis (CF) (Rajan and Saiman, 2002). The high pathogenicity of *P. aeruginosa* is linked to its intrinsic resistance to several commonly used antibiotics, the ability to rapidly adapt to varying environmental conditions and the expression of a large arsenal of virulence factors, which facilitate bacterial invasion and the establishment of persistent infections in host organisms (Breidenstein et al., 2011).

Under environmental stress conditions, *P. aeruginosa* is able to form robust biofilms in which surface-associated bacteria are embedded in a self-produced matrix (extrapolymeric substances; EPS) (Costerton et al., 1994; Hall-Stoodley et al., 2004). This switch from a free-swimming motile to a sessile biofilm lifestyle starts with the attachment of bacterial cells to a surface (Hall-Stoodley et al., 2004) and is regulated by a complex regulatory network of different signaling pathways and is associated with overall changes in gene expression leading to an enhanced matrix production and to a loss of motility-related factors (Whiteley et al., 2001; Dötsch et al., 2012). Among others, nucleotide second messengers such as cyclic di-GMP (c-di-GMP), cell-density dependent quorum sensing, sigma factors and two-component regulatory systems play an important role in biofilm formation (Mikkelsen et al., 2011; Fazli et al., 2014). Living within such a biofilm provides bacteria protection against a variety of different stressors like toxic substances, antibiotics or the host immune system and is therefore considered as an adaptive resistance mechanism (Hall-Stoodley et al., 2004; Breidenstein et al., 2011).

During acute and chronic infections, bacteria are confronted with a variety of host defense mechanisms designed to kill and eliminate invading pathogens from the host organism. These mechanisms include the secretion of compounds with direct antimicrobial or immunomodulatory activities or the incorporation and subsequent clearance of bacteria by phagocytic cells (Williams et al., 2010; Gellatly and Hancock, 2013). With respect to *P. aeruginosa* lung infections, main actors in the fight against this pathogen are epithelial cells and immune cells belonging to the innate immune system, such as phagocytic neutrophils or activated alveolar macrophages (Gellatly and Hancock, 2013; Lovewell et al., 2014). One major killing agent of mammalian phagocytes and, at the same time a frequently used disinfectant, is the potent oxidant hypochlorite (HClO) (Hawkins and Davies, 1998). HClO is generated from hydrogen peroxide (H_2O_2) and chloride ions (Cl^-) in a chemical reaction which is catalyzed by the enzyme myeloperoxidase (MPO) and reacts with a large number of biomolecules, including proteins, lipids and DNA and thus rapidly induces bacterial cell death (Albrich et al., 1981; Rosen et al., 1990; Klebanoff, 2005; Gray et al., 2013a).

While several studies investigated the bacterial stress responses to the less reactive oxidant H_2O_2 (Palma et al., 2004; Chang et al., 2005; Salunkhe et al., 2005; Choi et al., 2007; Small et al., 2007a; Heo et al., 2010; Lan et al., 2010; Goldova et al., 2011; Hare et al., 2011; Romsang et al., 2013; Deng et al., 2014) information on the immediate response of *P. aeruginosa* to HClO as a component of the human first line of defense, its intracellular sensing and its implication on the adaptation of *P. aeruginosa* to a hostile environment still remains elusive. Earlier studies have shown that HClO influences energy, iron and polyphosphate metabolism in *P. aeruginosa* (Small et al., 2007a,b; Groitl et al., 2017), however, the impact of HClO on *P. aeruginosa* biofilm initiation and development has not been investigated so far.

In the present study, we show that sublethal HClO concentrations strongly induce early steps of biofilm formation in *P. aeruginosa* PAO1 by increasing intracellular levels of the second messenger c-di-GMP. Further analyses identified the diguanylate cyclase (DGC) PA3177 as part of the HClO-induced stress response and we demonstrate its involvement in motility, biofilm formation and interaction of *P. aeruginosa* with THP-1 macrophages.

MATERIALS AND METHODS

Organisms, Plasmids, Primers, and Growth Conditions

A list of bacterial strains and plasmids used in this study is provided in **Table 1**. *P. aeruginosa* PAO1 was either grown in complex Luria Bertani (LB) Miller broth (Carl Roth, Karlsruhe, Germany) or in BM2 minimal medium [62 mM potassium phosphate buffer, pH 7.0, 7 mM $(NH_4)_2SO_2$, 2 mM $MgSO_4$, 10 μM $FeSO_4$, 0.4% (w/v) Glucose] at 37°C and 170 rpm. In BM2-swarm medium, 7 mM $(NH_4)_2SO_4$ was substituted for 0.5% (w/v) casamino acids. *Escherichia coli* strains DH5α and BL21(DE3) were cultivated in LB medium at 37°C. For overexpression experiments, the arabinose-inducible expression vector pJN105 and the IPTG-inducible vector pET23a were used. Antibiotics ampicillin (100 μg/ml) and gentamicin (10 μg/ml for *E. coli*; 30 μg/ml for *P. aeruginosa*) were added for plasmid selection and/or maintenance.

Hypochlorite was added in the form of aqueous sodium hypochlorite (NaClO) or calcium hypochlorite [$Ca(ClO)_2$] solutions as mentioned within the text. For effects caused by both, NaClO and $Ca(ClO)_2$ treatment, the general term HClO was used within the manuscript.

Free chlorine concentrations of HClO solutions (VWR, Darmstadt, Germany) were determined prior to each assay using DPD Free Chlorine Powder Pillows (VWR, Darmstadt, Germany) according to the manufacturer's instructions.

The sequences of DNA primers (Eurofins MWG Operon, Germany) used in these studies are shown in Supplementary Tables S1 and S2.

Construction of Recombinant *P. aeruginosa* and *E. coli* Strains

Cloning procedures were performed with *E. coli* strain DH5α, proof-reading Platinum® *pfx* DNA polymerase and restriction enzymes from Thermo Fisher Scientific (St. Leon-Rot, Germany) according to standard protocols provided by the manufacturers. Primer sequences for subsequent cloning experiments are shown in Supplementary Table S1.

For overexpression in *P. aeruginosa*, ORF PA3177 was amplified from PAO1 genomic DNA using a XbaI restriction site flanked forward primer and a SacI site flanked reverse primer and the fragment was cloned into the arabinose-inducible broad host range vector pJN105 (Newman and Fuqua, 1999), resulting in pJN3177.

For overexpression in *E. coli* BL21 (DE3), ORF PA3177 was amplified from PAO1 genomic DNA using a BamHI restriction site flanked forward primer and a XhoI site flanked reverse primer followed by in-frame insertion into pET-23a(+) (Novagen, Merck, Darmstadt, Germany). The resulting plasmid pET3177 and the vector control pET23a were then transferred

TABLE 1 | Plasmids and bacterial strains used in this study.

	Description	Reference
Plasmids		
pJN105	Broad-host-range expression vector derived from pBBR1MCS-5, contains araC-p_{BAD}, L-arabinose-inducible, Gm^R	Newman and Fuqua, 1999
pJN3177	Overexpression of *P. aeruginosa* PA3177; arabinose-inducible, Gm^R	This study
pJN2133	Overexpression of *P. aeruginosa* PA2133; arabinose-inducible, Gm^R	Hickman et al., 2005
pET23a	*E. coli* expression vector, pBR322 origin, N-terminal T7-Tag, C-terminal His-Tag, T7 promoter, Amp^R	Novagen, Merck Millipore
pET3177	Vector for heterologous overexpression of PA3177 in *E. coli* BL21; Amp^R	This study
***P. aeruginosa* strains**		
PAO1	Wildtype strain	Stover et al., 2000
PAO1-PA3177Ω	PAO1 transposon insertion mutant, ID: PAO1_lux_66:D11, PA3177 knock-out, Tc^R	Lewenza et al., 2005
PAO1-Δ*pelF*	PAO1 deletion mutant, *pelF* (PA3059) knock-out	Ghafoor et al., 2011
PAO1-Δ*pslA*	PAO1 deletion mutant, *pslA* (PA2231) knock-out	Ghafoor et al., 2011
PAO1-Δ*pelF* Δ*pslA*	PAO1 deletion double mutant, *pelF* and *pslA* knock-out	Ghafoor et al., 2011
PAO1-*flgK*Ω	PAO1 transposon insertion mutant, ID:PAO1_lux_24:H1, *flgK*(PA1086) knock-out, Tc^R	Lewenza et al., 2005
PAO1-pJN105	Vector control strain	This study
PAO1-pJN3177	Overexpression of PA3177 in strain PAO1	This study
PAO1-pJN2133	Overexpression of PA2133 in strain PAO1	This study
PAO1-pJN3177-*gfp*	Overexpression of a PA3177-GFP fusion protein in strain PAO1	This study
PAO1-Δ*pelF*-pJN3177	Overexpression of PA3177 in strain PAO1-Δ*pelF*	This study
PAO1-Δ*pslA*-pJN3177	Overexpression of PA3177 in strain PAO1-Δ*pslA*	This study
PAO1-Δ*pelF* Δ*pslA*-pJN3177	Overexpression of PA3177 in strain PAO1-Δ*pelF* Δ*pslA*	This study
PAO1-*flgK*Ω-pJN3177	Overexpression of PA3177 in strain PAO1-*flgK*Ω	This study
***E. coli* strains**		
DH5α	Cloning strain	Invitrogen
BL21 (DE3)	Expression strain	Stratagene
BL21-pET23a	Vector control strain	This study
BL21-pET3177	Heterologous expression of PA3177 in strain BL21(DE3)	This study

Tc^R, tetracycline resistance; Gm^R, gentamicin resistance; Amp^R, ampicillin resistance.

into *E. coli* strain BL21 (DE3) by heat shock transformation (Hanahan, 1983). *E. coli* was chosen for the heterologous expression of PA3177 due to its fast growth to high cell densities and the availability of highly efficient and tightly regulated gene expression systems.

Susceptibility Tests in Microtiter Plates

Minimal inhibitory concentrations (MIC) of different antimicrobials for planktonic *P. aeruginosa* cells were assayed by a standard broth microdilution method in BM2 medium as described previously (Wiegand et al., 2008). Additionally, growth of *P. aeruginosa* PAO1 during 24 h in the presence of different NaClO concentrations was monitored using a microplate reader (TECAN, Männerdorf, Switzerland) under shaking conditions at 37°C.

Attachment Assay in Microtiter Plates

Attachment assays in 96-well polystyrene microtiter plates (Nunc, Thermo Fisher Scientific, St. Leon-Rot, Germany) were performed as previously described (Overhage et al., 2008) with the following minor modifications. *P. aeruginosa* PAO1 overnight cultures were washed and resuspended in BM2 medium, diluted to an optical density (OD_{600}) of 0.2 and transferred to microtiter plates. In case of antimicrobial treatment, respective agents were added at indicated sub-MIC concentrations. Attachment of *P. aeruginosa* overexpression strains PAO1-pJN105, PAO1-pJN3177 or PAO1-pJN2133, was evaluated in BM2 medium supplemented with 0.1% (w/v) L-arabinose (Sigma–Aldrich, Seelze, Germany) to induce recombinant gene expression. Microtiter plates were incubated for 2 h at 37°C without shaking followed by the quantification of biofilm biomass by crystal violet staining as previously described (Merritt et al., 2005). Experiments were performed at least in triplicate with multiple wells per condition. Statistical significance was verified by the non-parametric Mann–Whitney test.

Attachment on Microscope Slides and Fluorescence Microscopy

Attachment to a surface or interface is the initial step in the formation of biofilms. Attachment of *P. aeruginosa* PAO1 on glass microscope slides in the presence or the absence of NaClO (2 μg/ml) was analyzed as described previously (Bernard et al., 2009). The starting OD_{600} was 0.2 and

the slides were incubated for 2 h at 37°C without shaking. Following fixation with 3% (v/v) formaldehyde, the attached bacteria were stained with the DNA intercalating fluorescent dye SYTO9 (Life Technologies, Darmstadt, Germany) according to the manufacturer's instructions. Fluorescence microscopy was carried out using an Axioplan 2 imaging system (Carl Zeiss, Oberkochem, Germany) with appropriate filter sets at 100 x magnification. Experiments were performed in duplicate and repeated three times. For biomass quantification, the surface coverage of four different squares with a side length of 200 μm was calculated for each slide using *ImageJ* software. All data were statistically analyzed by the non-parametric Mann–Whitney test.

Nucleotide Extraction and c-di-GMP Quantification by LC-MS

Intracellular c-di-GMP levels in *P. aeruginosa* PAO1 and in *E. coli* BL21 were quantified using a liquid chromatography coupled tandem mass spectrometry (LC-MS) method described by Spangler et al. (2010). *P. aeruginosa* PAO1 overnight cultures were washed and resuspended in BM2 medium. The OD_{600} was adjusted to 1.0 in order to increase the cell mass required for the subsequent extraction procedure, and the cells were incubated in small petri dishes with sublethal concentrations of NaClO (8 μg/ml, due to increased starting cell numbers) or without NaClO for 1 h at 37°C. In case of experiments with PA3177-overexpressing *E. coli* strain BL21-pET3177 and vector control BL21-pET23a, bacterial overnight cultures were diluted 1:100 in LB containing ampicillin (100 μg/ml) and grown until mid-log phase at 37°C under shaking conditions. IPTG was added at a final concentration of 0.4 mM and bacteria were incubated for 5 h at 37°C and 170 rpm. Harvesting and nucleotide extractions were performed as described previously (Spangler et al., 2010; Strehmel et al., 2015) using 200 ng cXMP (Biolog, Bremen, Germany) as an internal standard. Extractions were performed in triplicate and assays were repeated at least with two independent bacterial cultures. Total protein contents of the samples were determined by the Pierce BCA Protein Assay Kit (Thermo Fisher Scientific, St. Leon-Rot, Germany) according to the manufacturer's instructions. LC-MS measurements were performed as described by Strehmel et al. (2015). Concentrations of c-di-GMP were normalized against total protein contents of respective cultures. Statistical significance was analyzed by the non-parametric Mann–Whitney test.

Gene Expression Analyses

For microarray analysis, overnight cultures of *P. aeruginosa* PAO1 were washed and resuspended in BM2 medium. After dilution to an OD_{600} of 0.2, 10 ml of the suspensions was transferred to a small petri dish (5 cm diameter; Sarstedt, Nuembrecht, Germany) and NaClO was added at a final concentration of 2 μg/ml. Untreated samples served as negative controls. Bacteria were incubated for 1 h at 37°C, mimicking growth during static attachment assays in 96-well microtiter plates in order to increase the cell mass required for subsequent RNA extractions and microarray analysis. RNA extraction, cDNA synthesis and processing was performed as described previously (Strempel et al., 2013). Samples from three independent experiments per condition each with a minimum of two technical replicates were pooled to detect significantly up- or down-regulated genes. Each sample was hybridized to two microarray *Affymetrix* Pae_G1a GeneChips ($n = 4$). Only genes which were more than 3-fold dysregulated in NaClO-treated bacteria were included in further analyses (Student t-test p-value ≤ 0.05). Complete microarray data is deposited in the ArrayExpress database under accession number E-MTAB-2876. These results were verified using qRT-PCR as described in the following on three additional, independent experiments.

For quantitative realtime-PCR (qRT-PCR), *P. aeruginosa* PAO1 overnight cultures were washed and diluted with BM2 medium to an OD_{600} of 0.2 followed by incubation with NaClO, $Ca(ClO)_2$, NH_2Cl, paraquat and H_2O_2 at indicated concentrations for 1 h at 37°C. For each condition, three independent experiments each with a minimum of two technical replicates were conducted. Untreated bacteria served as negative controls. RNA isolation, cDNA synthesis and subsequent qRT-PCR experiments were carried out as described previously (Strempel et al., 2013). Obtained Ct values were normalized to expression of housekeeping genes *rpoD* and *fabD* as described elsewhere (Schmidberger et al., 2013).

Motility Assays

Motility assays were performed as described elsewhere (Strehmel et al., 2015). Overnight cultures of strains PAO1-pJN3177 and PAO1-pJN105 were diluted 1:50 in LB medium containing 30 μg/ml gentamicin and 0.1% (w/v) arabinose and incubated for 5 h at 37°C and 170 rpm prior to inoculation of agar plates. LB or BM2 agar plates were also supplemented with 0.1% (w/v) arabinose and 30 μg/ml gentamicin. Assays were performed in triplicate and mean values of five plates per experiment were calculated. Statistical significance of the obtained results was examined by the non-parametric Mann–Whitney test.

Phagocytosis Assays with Human THP-1 Macrophages

Gene expression in phagocytized bacteria was analyzed using qRT-PCR following interaction with THP-1 human macrophage-like cells and *P. aeruginosa* PAO1. THP-1 cells (German Collection of Microorganisms and Cell Cultures – DSMZ, Braunschweig, Germany) were routinely cultured in complete RPMI-1640medium containing 10% (v/v) heat-inactivated FBS and 2 mM L-glutamine (Sigma–Aldrich, Hamburg, Germany) at 37°C and 5% CO_2. To start the experiment, cells were seeded out in 6-well microtiter plates at a density of 5×10^6cells per well. Differentiation into adherent macrophage-like cells was stimulated by the addition of 5 ng/ml PMA (Sigma–Aldrich, Hamburg, Germany) for 48 h as described previously (Park et al., 2007). *P. aeruginosa* PAO1 overnight cultures grown in BM2 were washed twice in complete RPMI medium and added to the THP-1 macrophages at a multiplicity of infection of 100. Interaction assays were carried out for 1h at 37°C. THP-1 cells without bacteria and *P. aeruginosa* incubated without THP-1 macrophages served as controls. After phagocytosis, supernatants

which contained residual planktonic bacteria were removed from the wells. After a washing step with PBS, complete RPMI medium supplemented with the antibiotic gentamicin at a final concentration of 400 μg/ml was added to the THP-1 monolayer and remaining extracellular bacteria were killed during a 30 min incubation step at 37°C as described previously (Neidig et al., 2013). Subsequently, the THP-1 cells were rinsed with complete RPMI medium and incubated with a 1:1 (v/v) mixture of *RNAprotect Bacteria Reagent* and complete RPMI medium for 5 min. During this incubation step, adherent THP-1 cells detached from the bottom of the 6-well plate and could be easily harvested by centrifugation (10 min, 5,000 × *g*, RT). All control samples were also treated with a 1:1 (v/v) mixture of *RNAprotect Bacteria Reagent* and complete RPMI medium prior to RNA isolation. Supernatants were discarded and cell pellets were stored at −80°C until needed. Total RNA was extracted using the *RNeasy Mini Kit* in combination with *QIAshredder* columns (Qiagen, Hilden, Germany) according to the manufacturer's protocol for total RNA isolation from animal cells. The obtained RNA was directly used for cDNA synthesis and subsequent qRT-PCR.

In vitro phagocytosis of PAO1 cultures by THP-1 was performed as described previously (Yeung et al., 2014) using mid-log bacterial cells and THP-1 at an MOI of 10. Three independent experiments with triplicates in each experiment were performed for each bacterial strain.

RESULTS

HClO Induces Biofilm Formation in *P. aeruginosa* PAO1

In order to determine appropriate NaClO concentrations for subsequent assays, the susceptibility of *P. aeruginosa* PAO1 toward NaClO was analyzed by MIC determination in BM2 minimal medium resulting in MIC values of 4 μg/ml free chlorine. This value was confirmed by monitoring bacterial growth during 24 h in the presence of different concentrations of NaClO (Supplementary Figure S1). Thus, for subsequent experiments sublethal concentrations of 2 μg/ml free chlorine were chosen.

Since adhesion of bacterial cells to a surface is among the first steps in the development of biofilms (Hall-Stoodley et al., 2004), we performed static attachment assays in 96-well microtiter plates to show a significant 2.8-fold increase in initial adhesion of *P. aeruginosa* PAO1 during 2 h exposure to 2 μg/ml NaClO (**Figure 1A**). Additional tests indicated a dose-dependent induction of attachment starting at concentrations as low as 0.5 μg/ml NaClO (**Figure 1B**). To verify these findings, *P. aeruginosa* attachment was also evaluated on glass microscope slides using fluorescence microscopy to show a similar 2.6-fold increase in the amount of attached bacteria in the presence of NaClO (**Figure 1C**).

In order to investigate whether this enhanced attachment was part of the general response to oxidative stress in *P. aeruginosa*, bacterial adhesion was monitored under different oxidative stress conditions. Evaluated substances included H_2O_2, calcium hypochlorite [$Ca(ClO)_2$], paraquat and monochloramine (NH_2Cl), a downstream reaction product of HClO. In each case, half of the determined MIC was used for the experiment [H_2O_2: 50 μg/ml, $Ca(ClO)_2$: 2 μg/ml, Paraquat: 1 μg/ml]. NH_2Cl and NaClO were applied at a molecular ratio of 1:1. Thus, final concentrations of NH_2Cl were equivalent to concentrations resulting from the reaction of 2 μg/ml NaClO with amines. In addition to NaClO, the strongest induction of attachment was found in response to $Ca(ClO)_2$ (+4.2-fold) and NH_2Cl (+1.9-fold). For H_2O_2, there was still a slight increase in attachment detectable (+1.5-fold), whereas cells incubated with paraquat did not show any difference in biomass compared to untreated controls (**Figure 1D**) indicating that attachment is not induced by oxidative stress in general.

The Second Messenger c-di-GMP Is Involved in the NaClO-Induced Biofilm Formation

Pseudomonas aeruginosa biofilm development is a complex adaptation which is regulated by a multitude of different signaling pathways including the second messenger c-di-GMP (Kalia et al., 2013; Fazli et al., 2014). In order to evaluate the involvement of c-di-GMP in the observed NaClO phenotype, intracellular c-di-GMP levels were quantified using LC-MS to show a significant increase in c-di-GMP levels by 8.7-fold in bacteria treated with NaClO (**Figure 2A**). With respect to absolute c-di-GMP levels, average concentrations of 201 pmol and 25 pmol c-di-GMP per mg protein in NaClO-treated and control cultures, respectively, were measured.

In order to test whether these increased c-di-GMP levels were an important factor for the NaClO-triggered initiation of biofilm formation, additional assays were performed with strain *P. aeruginosa* PAO1-pJN2133, which overexpresses the phosphodiesterase (PDE) PA2133 in the presence of 0.1% (w/v) arabinose leading to an enhanced and continuous c-di-GMP degradation and subsequently low intracellular c-di-GMP levels within the cell. Crystal violet staining after 2 h revealed a significant 1.4-fold increase in adhered biomass of PAO1-pJN105 in the presence of NaClO compared to the untreated control. In contrast, attachment was not affected in NaClO-treated cells of PAO1-pJN2133 in comparison to untreated bacteria (**Figure 2B**) suggesting an important role for c-di-GMP in NaClO-induced biofilm formation of *P. aeruginosa*.

Expression of the Putative DGC PA3177 Is Induced by HClO

Intracellular c-di-GMP levels are regulated by the activity of DGCs which catalyze c-di-GMP synthesis from two GTP molecules and c-di-GMP-degrading PDEs. DGCs are characterized by a conserved GGDEF domain, whereas PDEs harbor either an EAL or a HD-GYP motif (Hengge, 2009; Kalia et al., 2013). To investigate which DGCs or PDEs are responsible for the increase in c-di-GMP upon NaClO treatment, global gene expression analyses using DNA microarrays were performed and gene expression levels in response to NaClO (2 μg/ml, 1 h) were compared to those of untreated PAO1 cells. Out of the 33

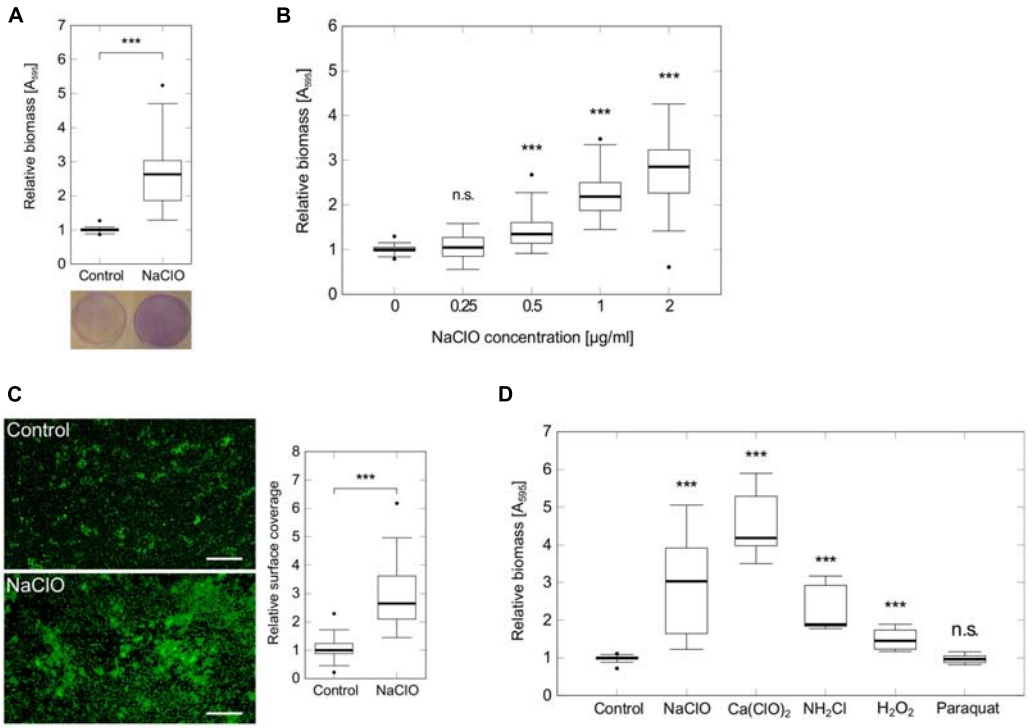

FIGURE 1 | Attachment of *P. aeruginosa* PAO1 in the presence of different oxidants. Attachment of *P. aeruginosa* PAO1 during 2 h incubation in the presence of sublethal NaClO concentrations **(A–C)** or half-MIC concentrations of oxidants NaClO (2 μg/ml), $Ca(ClO)_2$ (2 μg/ml), NH_2Cl (equivalent to 2 μg/ml NaClO), H_2O_2 (50 μg/ml) and paraquat (1 μg/ml) **(D)**. **(A,B,D)** Attachment was assayed in 96-well microtiter plates by crystal violet staining and subsequent measurement of A_{595}. Obtained values for treated samples were normalized against A_{595} of untreated controls (=relative biomass). Experiments were performed at least in triplicate, each with multiple wells per condition ($n \geq 18$). **(C)** *P. aeruginosa* PAO1 was incubated with sub-MIC concentrations of NaClO (2 μg/ml) in BM2 for 2 h in 50 ml reaction tubes containing glass microscope slides. Adhered bacteria were stained with the DNA-intercalating dye SYTO9 prior to visualization by fluorescence microscopy at 100× magnification (scale bar: 100 μm). Average surface coverages from 36 pictures per condition were calculated using *ImageJ*. Experiments were performed in triplicate. For all experiments, statistical significance was evaluated by the Mann-Whitney test (***$p \leq 0.001$, n.s., not significant). Boxes include median (thick horizontal line), 25th and 75th percentiles. Dots indicate extreme values considered as outliers.

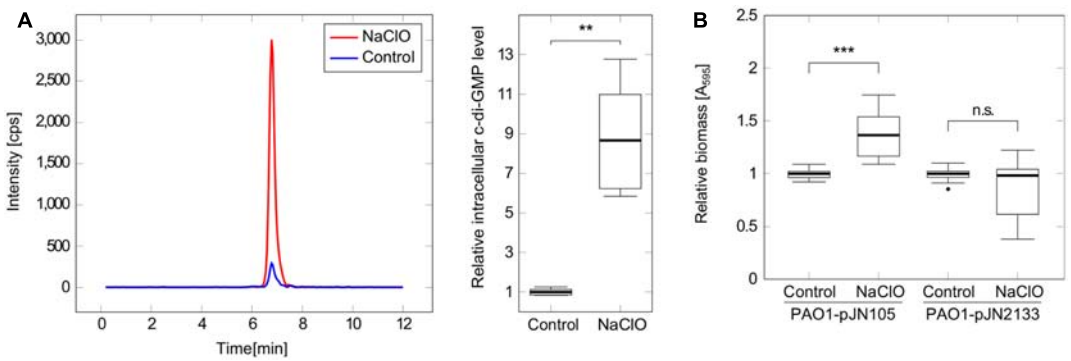

FIGURE 2 | Implication of c-di-GMP in the response of *P. aeruginosa* PAO1 to NaClO. **(A)** *P. aeruginosa* PAO1 was incubated with NaClO (8 μg/ml, OD_{600} = 1.0, BM2) for 1h followed by nucleotide extraction and quantification of intracellular c-di-GMP by LC-MS. Levels of c-di-GMP were normalized to the total protein content of the respective sample and compared to c-di-GMP levels in untreated controls (n = 6). The chromatogram shows c-di-GMP peaks of one representative measurement. **(B)** Attachment of *P. aeruginosa* in response to NaClO during overexpression of the c-di-GMP-degrading PDE PA2133 was evaluated by crystal violet staining. PAO1-pJN2133 and the vector control strain PAO1-pJN105 were incubated in 96-well microtiter plates either in the presence or in the absence of NaClO (2 μg/ml) for 2 h at 37°C followed by the quantification of biofilm biomass. BM2 was supplemented with 0.1% (w/v) arabinose to induce recombinant gene expression. Experiments were repeated four times, each with six wells per strain and condition (n = 24). Absorbance at 595nm (A_{595}) was determined and obtained values for NaClO-treated samples were normalized against the A_{595} of respective untreated controls (=relative biomass). Statistical significance was evaluated by the Mann–Whitney test (***$p \leq 0.001$, **$p \leq 0.01$, n.s., not significant). Boxes include median (thick horizontal line), 25th and 75th percentiles. Dots indicate extreme values considered as outliers.

genes which possess a DGC consensus sequence in *P. aeruginosa* (Kulasakara et al., 2006; Winsor et al., 2011), only ORF PA3177 showed statistically significant changes in gene expression levels and an upregulation by 26.2-fold in response to NaClO. Genes coding for PDEs were not affected by the oxidant (ArrayExpress E-MTAB-2876). The increase in PA3177 gene expression in response to NaClO was confirmed by qRT-PCR (**Table 2**). In addition, qRT-PCR experiments with the oxidants H_2O_2, paraquat, $Ca(ClO)_2$ and NH_2Cl indicated that the induction of PA3177 was not part of the general response of *P. aeruginosa* to oxidative stress. A strong increase in PA3177 expression was only found upon treatment with $Ca(ClO)_2$, NH_2Cl and NaClO. In contrast, in response to paraquat, PA3177 levels were only slightly enhanced and H_2O_2 did not affect PA3177 gene expression at all (**Table 2**).

Characterization of the DGC PA3177

According to the *Pseudomonas* Genome Database (Winsor et al., 2011), the gene product of ORF PA3177 is a hypothetical cytoplasmic protein with a predicted molecular weight of 34.4 kDa containing a GGDEF domain (here: GGEEF). However, previous studies failed to confirm a c-di-GMP-generating enzyme activity of the PA3177 homologue in *P. aeruginosa* PA14 and did not show a consistent impact of PA3177 on biofilm formation (Kulasakara et al., 2006; Merritt et al., 2010).

To investigate the DGC activity of *P. aeruginosa* PAO1 PA3177, the enzyme was heterologously expressed for 5 h in *E. coli* BL21-pET3177 to obtain a high protein concentration, which was confirmed by SDS-PAGE and MALDI-ToF mass spectrometry analysis. Nucleotides were extracted from BL21-pET3177 and subsequent quantification of intracellular c-di-GMP levels by LC-MS revealed a 26.1-fold increase in c-di-GMP synthesis upon overexpression of PA3177 compared to BL21-pET23a (**Figure 3A**), which confirmed its DGC activity.

To further characterize this DGC, the PA3177 overexpressing strain PAO1-pJN3177 was constructed in which PA3177 expression was under the control of an arabinose-inducible promoter. After 2 h of PA3177 expression, cultures of PAO1-pJN3177 showed a 2.4-fold enhancement in biofilm biomass in 96-well microtiter plates in comparison to vector control PAO1-pJN105 or uninduced PAO1-pJNPA3177 cultures (**Figure 3B**).

Since motility is also strongly regulated by c-di-GMP (Hengge, 2009), the main motility types of *P. aeruginosa* – swimming in aqueous environments, twitching on solid surfaces and swarming on semisolid surfaces – were evaluated during PA3177 overexpression. To this aim, overnight cultures of *P. aeruginosa* PAO1-pJN3177 and control strain PAO1-pJN105 were diluted 1:50 in LB broth supplemented with 0.1% (w/v) arabinose and grown for 5 h at 37°C. Of note, at this time point PAO1-pJN3177 formed already clearly visible cell aggregates in the flask indicating DGC activity (**Figure 3C**). In agreement with other studies which identified several DGCs as negative regulators of *P. aeruginosa* motility (Aldridge et al., 2003; Merritt et al., 2007), a 61% decrease in swimming ability was observed upon induction of PA3177 expression. Similar results were obtained for twitching motility after 72 h at 37°C (18% decrease) and swarming motility after 21 h at 37°C (99% decrease) in response to PA3177 overexpression (**Figure 3D**).

TABLE 2 | PA3177 gene expression in response to different oxidants[a].

Compound	Applied concentration	Relative gene expression[c]
NaClO	2 μg/ml free chlorine[b]	13.7 ± 0.9
$Ca(ClO)_2$	2 μg/ml free chlorine	86.0 ± 4.0
NH_2Cl	≙2 μg/ml free chlorine	28.6 ± 4.9
H_2O_2	50 μg/ml (1.47 mM)	1.2 ± 0.1
Paraquat	1 μg/ml (3.88 mM)	2.2 ± 0.2

[a]*P. aeruginosa PAO1 was incubated with different oxidants at indicated half-MIC concentrations in BM2 minimal medium for 1 h at 37°C followed by RNA isolation and qRT-PCR.* [b]*Free chlorine concentrations are shown in μg/ml as determined by the respective test kit. Since free chlorine is defined as a mixture of HClO, ClO^- and Cl_2 and therefore possesses a variable molecular mass, corresponding millimolar concentrations were not calculated.* [c]*Mean averages and standard deviations of three independent experiments, each analyzed at least in duplicate ($n \geq 6$). Ct values were normalized against expression of housekeeping genes rpoD and fabD and relative PA3177 expression in treated cells compared to untreated controls was calculated.*

Role of Pel and Psl exopolysaccharides

Several DGCs have been shown to induce attachment and biofilm formation by influencing flagella movement or stimulating extracellular matrix production (Klebensberger et al., 2009; Boehm et al., 2010; Malone et al., 2010; Petrova et al., 2014). To investigate in which way PA3177 modulates biofilm formation, plasmid pJN3177was transferred to a set of different *Pseudomonas aeruginosa* PAO1 mutants and attachment of respective strains was quantified after PA3177 induction. In addition to a *flgK* mutant with a defect in flagellum synthesis, mutants with defects in the Pel or Psl exopolysaccharide biosynthesis clusters were tested, since Pel and Psl have been identified to be important components for attachment and early biofilm formation in *P. aeruginosa* PAO1 (Evans and Linker, 1973; Friedman and Kolter, 2004; Jackson et al., 2004; Overhage et al., 2005). As shown in **Figure 4A**, a disrupted *pslA* gene or a simultaneous knock-out of Pel and Psl in the double mutant PAO1-Δ*pelF*Δ*pslA*-pJN3177 completely abolished the biofilm-inducing effect of PA3177. Furthermore, the single mutant PAO1-*pelF*-pJN3177 showed only a marginal 1.1-fold increase in attachment when PA3177 was overexpressed. In contrast, in the absence of *flgK,* overexpression of PA3177 in strain PAO1-*flgK*Ω-pJN3177 led to a 2.1-fold increase in attachment which was comparable to PAO1-pJN3177 cells (**Figure 4A**). In addition, we analyzed gene expression of *pelA* and *pslA* in PAO1-pJN3177and PAO1-pJN105 using qRT-PCR. Since the microarray data did not reveal any upregulation in gene expression after 1 h of incubation and to ensure appropriate expression levels of PA3177 in PAO1-pJN3177, we determined *pelA* and *pslA* gene expression after 4 h of PA3177 expression. In comparison to the vector control strain PAO1-pJN105, we obtained an enhanced expression of *pelA* and *pslA* by 2.6 ± 0.8- and 7.9 ± 1.0-fold, respectively, after 4 h of PA3177 over-expression.

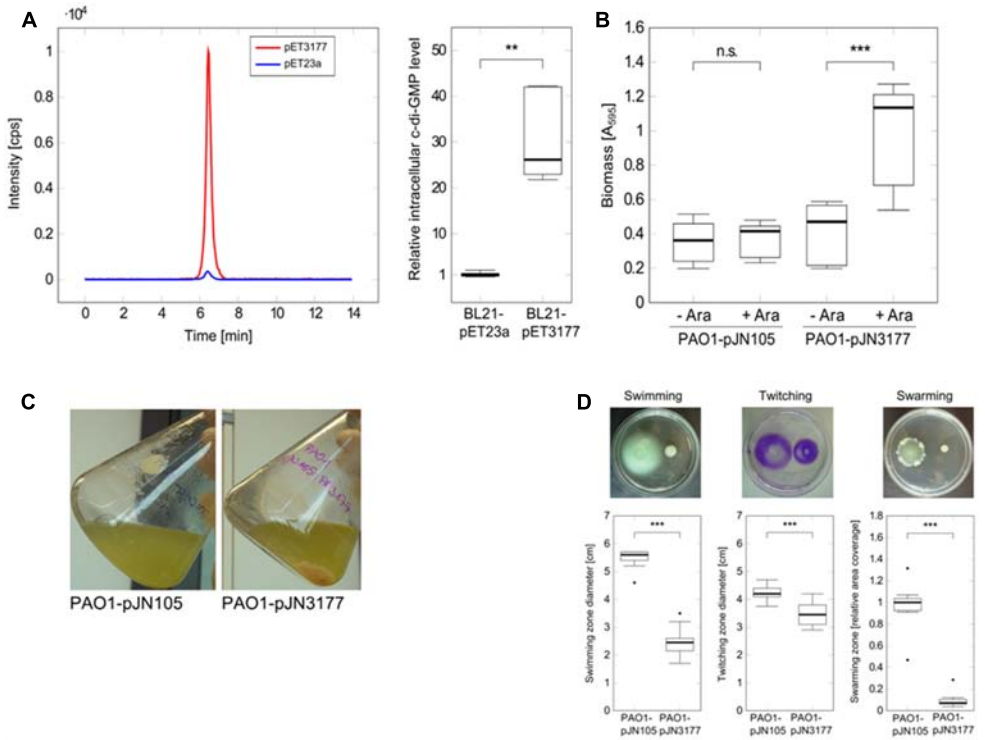

FIGURE 3 | Characterization of the DGC PA3177. **(A)** *E. coli* BL21-pET3177 and the vector control strain BL21-pET23a were grown in LB broth supplemented with 0.4 mM IPTG for 5 h at 37°C followed by nucleotide extraction and quantification of intracellular c-di-GMP by LC-MS. Levels of c-di-GMP were normalized to the total protein content of the respective sample and compared to c-di-GMP levels in empty vector control strain BL21-pET23a (n = 6). The chromatogram shows c-di-GMP peaks of one representative measurement. **(B)** Attachment of *P. aeruginosa* during PA3177 overexpression was evaluated by crystal violet staining. PAO1-pJN3177 and empty vector control strain PAO1-pJN105 were incubated in 96-well microtiter plates for 2 h at 37°C followed by biomass quantification. For recombinant gene expression, BM2 was supplemented with 0.1% (w/v) arabinose (+Ara). Cultures without arabinose (–Ara) served as negative controls. Experiments were carried out in triplicate, each with six wells per strain and condition (n = 18). **(C)** Planktonic growth during 5 h at 37°C. **(D)** Overnight cultures of PA3177-overexpressing strain *P. aeruginosa* PA01-pJN3177 and vector control PAO1-pJN105 were diluted in LB broth supplemented with 0.1% (w/v) arabinose and grown for 5 h at 37°C followed by evaluation of swimming, swarming and twitching motility. Assays were carried out with three independent bacterial cultures and at least four agar plates per experiment ($n \geq 12$). In all experiments statistical significance was evaluated by the Mann-Whitney test (***$p \leq 0.001$, **$p \leq 0.01$, n.s., not significant). Boxes include median (thick horizontal line), 25th and 75th percentiles. Dots indicate extreme values considered as outliers.

Next, we investigated whether Pel and Psl were implicated in the enhanced biofilm initiation in response to NaClO, i.e., under conditions in which the expression of PA3177 was naturally induced in PAO1 wildtype cells. To this aim, attachment of the deletion mutants PAO1-Δ*pelF,* PAO1-Δ*pslA* and of the double mutant PAO1-Δ*pelF*Δ*pslA* was analyzed in the presence of 2 μg/ml NaClO. Similar to PA3177 overexpression, NaClO treatment led to a significantly lower induction of attachment in the respective mutant strains in comparison to PAO1 wildtype (**Figure 4B**). Thus, the results demonstrate that both Pel and Psl polysaccharides are involved in the NaClO- and PA3177-dependent stimulation of biofilm formation in *P. aeruginosa* PAO1.

Identification of Alternative NaClO-Responsive DGCs

A *P. aeruginosa* PA3177 knock-out mutant (PAO1-PA3177Ω) of the *Pseudomonas aeruginosa* PAO1 mini-Tn*5 lux* transposon mutant library (Lewenza et al., 2005) was used in the following experiments. The correct insertion of the transposon cassette was confirmed by colony PCR. Susceptibility tests revealed equal MIC values of 4 μg/ml NaClO for PAO1-PA3177Ω and PAO1 wildtype. Phenotypical characterization of the PAO1-PA3177Ω mutant showed no changes in swimming, swarming or twitching motility as well as the ability to form biofilms compared to PAO1 wildtype (data not shown). Furthermore, subsequent attachment assays in the presence of NaClO demonstrated that a knock-out of PA3177 does not completely impede the biofilm-inducing effect of NaClO, since attachment of the mutant was still significantly enhanced compared to the untreated control (**Figure 5A**). However, this increase in attachment by 2.2-fold was significantly lower than the 2.6-fold increase of PAO1 wildtype.

The *P. aeruginosa* PAO1 genome encodes for at least 33 proteins with the GGDEF consensus sequence of DGCs (Kulasakara et al., 2006). Of note, not all of these proteins contain an intact GGDEF domain, and 16 proteins are hybrid proteins harboring an additional EAL domain being a typical functional domain of c-di-GMP-degrading phosphodiesterases (PDEs) (Kulasakara et al., 2006; Winsor et al., 2011). Most of these

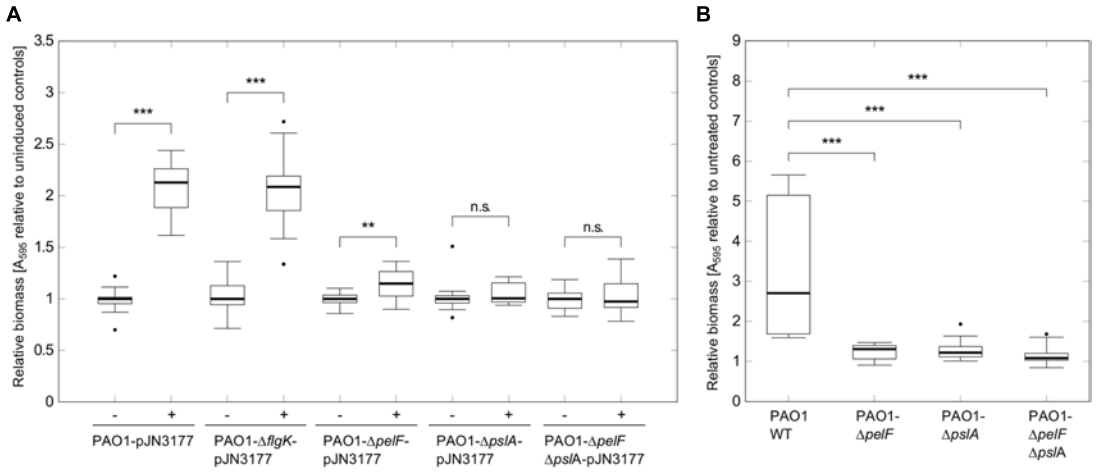

FIGURE 4 | Attachment assays with PAO1 mutants. **(A)** Attachment of *P. aeruginosa* PAO1 wildtype (WT) or PAO1 mutant strains during overexpression of PA3177 was evaluated by crystal violet staining. Bacteria were incubated in 96-well microtiter plates for 2 h at 37°C prior to biomass quantification. For recombinant gene expression, L was supplemented with 0.1% (w/v) arabinose (+). Cultures without arabinose (–) served as negative controls. **(B)** Attachment of *P. aeruginosa* PAO1 WT or PAO1 deletion mutants during NaClO treatment (2 μg/ml in BM2, 2 h) was evaluated by crystal violet staining. All experiments were carried out in triplicate, each with six wells per strain and condition (n = 18). Statistical significance was evaluated by the Mann–Whitney test (***$p \leq 0.001$, **$p \leq 0.01$, n.s., not significant). Boxes include median (thick horizontal line), 25th and 75th percentiles. Dots indicate extreme values considered as outliers.

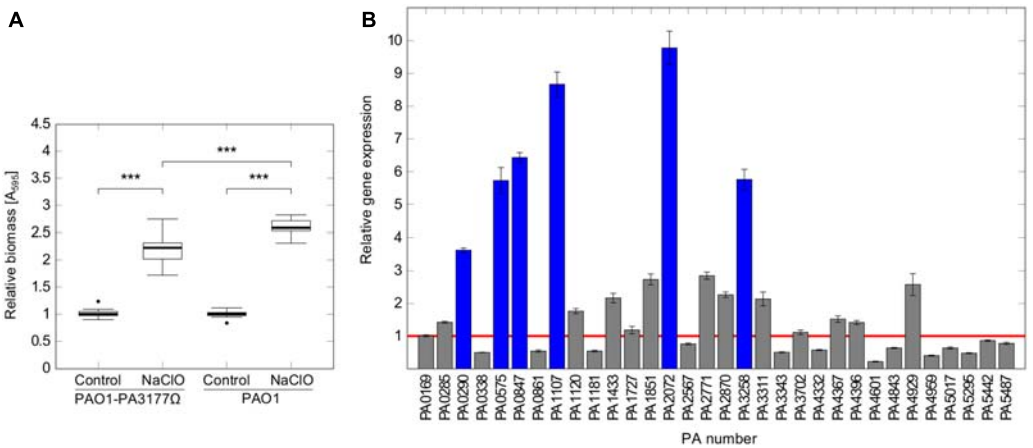

FIGURE 5 | Attachment and DGC expression in PAO1-PA3177Ω in response to NaClO. **(A)** Attachment of *P. aeruginosa* mutant strain PAO1-PA3177Ω and wildtype PAO1 after 2 h incubation with half-MIC concentrations of NaClO (2 μg/ml) compared to untreated controls was assayed in 96-well microtiter plates by crystal violet staining. To show alterations in attachment caused by NaClO, A_{595} of treated samples was normalized to A_{595} of untreated controls for each strain (=relative biomass). Statistical significance was evaluated by the Mann–Whitney test (***$p \leq 0.001$, $n \geq 12$). Boxes include median (thick horizontal line), 25th and 75th percentiles. Dots indicate extreme values considered as outliers. **(B)** *P. aeruginosa* mutant strain PAO1-PA3177Ω was treated with 2 μg/ml NaClO and relative gene expression levels of genes encoding DGCs in comparison to untreated control cultures were analyzed by qRT-PCR. The figure shows mean averages and standard deviations calculated from three experiments, each analyzed in duplicate (n = 6). Ct values were normalized against the expression of housekeeping genes *rpoD* and *fabD*. The red line corresponds to a relative gene expression level of 1, which means no change in gene expression. Blue bars indicate relative gene expression values ≥ 3.

hybrid proteins possess either a DGC or a PDE activity, whereas a dual DGC-PDE function has been confirmed for only few enzymes (e.g., PA4601) so far (Phippen et al., 2014). In contrast, the hybrid enzymes PA2567 and PA5017 have been identified as functional PDEs (Rao et al., 2009; Roy et al., 2012). So far, an actual DGC activity has been proposed for at least eleven putative DGCs of *P. aeruginosa* (Kulasakara et al., 2006; Merritt et al., 2007; Klebensberger et al., 2009; Petrova et al., 2014). Therefore, we hypothesized that in case of a PA3177 knock-out, alternative DGCs may adopt functions of PA3177 with respect to NaClO induced biofilm formation.

To test this idea, PAO1-PA3177Ω was incubated in the presence of sub-MIC concentrations of NaClO and expression of all putative DGCs was analyzed by qRT-PCR in order to detect changes in gene expression compared to untreated controls. Indeed, NaClO treatment induced the expression of

additional six alternative DGCs in the PAO1-PA3177Ω knock-out mutant by more than three-fold (**Figure 5B**). The strongest upregulation was found for PA2072 (9.8 ± 0.5-fold) and PA1107 (8.7 ± 0.4-fold), followed by PA0847 (6.4 ± 0.2-fold), PA3258 (5.8 ± 0.3-fold), PA0575 (5.7 ± 0.4-fold) and PA0290 (3.6 ± 0.1-fold). Of note, none of the mentioned DGCs were identified differentially regulated in above described microarray analysis of NaClO-treated PAO1 (ArrayExpressE-MTAB-2876). Additional qRT-PCR experiments on different cultures confirmed these results for PA0290, PA0575, PA0847, PA3258. Interestingly, an upregulation of PA1107 (5.5 ± 0.2-fold) and PA2072 (5.4 ± 0.2-fold) was observed in addition to PA3177 (13.7 ± 0.9-fold) in NaClO-treated PAO1 wildtype cells, however, the induction of these two DGCs in PAO1 WT was considerably lower than in the mutant strain PAO1-PA3177Ω. Overall, these results suggest that in addition to PA3177 additional DGCs exhibit an increase in gene expression in response to NaClO in the PAO1 wildtype and the PAO1-PA3177Ω mutant strain, indicating that a knock-out of PA3177 can be counterbalanced by one or more additional DGC activities within the c-di-GMP network of PAO1.

PA3177 Expression Is Induced in Contact with Phagocytes

HClO is generated in human immune cells during phagocytosis in a chemical reaction of H_2O_2 and Cl^- which is catalyzed by the MPO enzyme (Klebanoff, 2005; Groitl et al., 2017). Since HClO was able to activate PA3177 gene expression *in vitro*, in the next step, PA3177 expression was examined in *P. aeruginosa* PAO1 ingested by phagocytic cells in order to identify a role of PA3177 during host–pathogen interactions. Phagocytosis experiments were carried out with human THP-1 macrophage-like cells and *P. aeruginosa* PAO1 at a multiplicity of infection of 100. MPO expression in THP-1 macrophages had been previously confirmed by Hachiya et al. (2000). Phagocytic uptake of bacteria by THP-1 macrophages was confirmed by fluorescence microscopy using a *P. aeruginosa* strain which constitutively expressed the green fluorescent protein GFP. As a result, expression of PA3177 was upregulated by 9.5 ± 0.4-fold in phagocytized bacteria compared to PAO1 cells grown without any contact to THP-1 macrophages. However, when we investigated virulence of PAO1-PA3177Ω and PAO1 wildtype during phagocytosis using THP-1 cells and an MOI of 10, we did not observe any statistically significant changes in survival rates after 2 h of incubation (Supplementary Figure S2).

DISCUSSION

The second messenger c-di-GMP acts as a key regulator of motility and biofilm formation in many bacteria. Although much effort has been put into the elucidation of *P. aeruginosa* c-di-GMP signaling during the last decade, there is still a need for further investigation in order to obtain a complete view of cellular c-di-GMP actions and their implication in *P. aeruginosa* stress response and host-pathogen interactions (Hengge, 2009; Römling et al., 2013). For example, only a few environmental stimuli which influence the synthesis or degradation of c-di-GMP have been identified so far (Hoffman et al., 2005; Klebensberger et al., 2009; Malone et al., 2012; Li et al., 2013; Luo et al., 2015), and knowledge about detailed c-di-GMP effector pathways and connections to other stress-responsive networks is still incomplete (Hengge, 2009; Römling et al., 2013).

In this study, we demonstrate that the phagocytic killing agent and strong disinfectant HClO acts as an activator of c-di-GMP synthesis and subsequent attachment and biofilm formation in *P. aeruginosa*. The hyperattachment phenotype is prevented by overexpression of the c-di-GMP-degrading PDE PA2133 enabling a constant degradation of c-di-GMP in the respective strain *P. aeruginosa* PAO1-pJN2133 (Hickman et al., 2005) during NaClO incubation, which highlights the role of the second messenger in this adaptation process. Further results suggest an involvement of the DGC PA3177 whose expression was strongly stimulated by the HClO-releasing agents NaClO and $Ca(ClO)_2$ and NH_2Cl, which is an abundant secondary reaction product of HClO and nitrogen-containing organic compounds. In contrast, transcriptional levels were not altered or only marginally enhanced in response to the oxidants H_2O_2 and paraquat.

Several studies present evidence for the ability of bacteria to increase biofilm formation in response to sublethal concentrations of otherwise highly toxic agents such as antibiotics, detergents and biocides (Bagge et al., 2004; Hoffman et al., 2005; Linares et al., 2006; Klebensberger et al., 2009; Shemesh et al., 2010; Damron et al., 2011; Kaplan, 2011; Malone et al., 2012). However, a regulatory impact on c-di-GMP metabolism in *P. aeruginosa* has only been described for some agents including tobramycin and SDS and both toxic agents promote a sessile mode of growth of *P. aeruginosa* when applied at sublethal concentrations (Hoffman et al., 2005; Klebensberger et al., 2009). So far, the only studies in which sublethal doses of NaClO are linked to an enhanced bacterial biofilm formation deals with *E. coli* (Capita et al., 2014) and *Staphylococcus aureus* MRSA (Buzon-Duran et al., 2017). The authors propose that an increase in cell surface hydrophobicity caused by NaClO is responsible for the observed induction of biofilm formation in *E. coli*. However, a potential implication of c-di-GMP in the observed phenotype was not suggested in the respective study(Capita et al., 2014).

Our results indicate that the DGC PA3177 is specifically induced by HClO but not by oxidative stress in general. With respect to the tested agents, both HClO and NH_2Cl as well as H_2O_2 are able to directly generate oxidative damage of cellular macromolecules and additionally promote the synthesis of further highly reactive oxygen species, e.g., hydroxyl radicals (·OH) and singlet oxygen ($^1O_2$) which in turn intensifies the oxidative cell injury (Fang, 2004; Klebanoff, 2005). Similar mechanisms have been reported for the herbicide paraquat whose oxidative potential is predominantly caused by a massive production of superoxide anion radicals ($\cdot O_2$) upon cell contact (Cocheme and Murphy, 2008; Hare et al., 2011). $\cdot O_2$ stimulates the generation of reactive nitrogen species or is converted into the less reactive H_2O_2 by superoxide dismutase (Fang, 2004; Flannagan et al., 2009). A crucial difference between the tested oxidants is the rate at which they promote the reversible

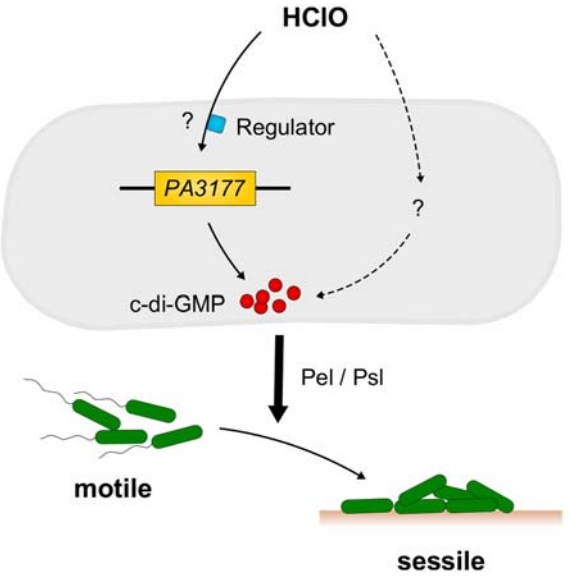

FIGURE 6 | Model of HClO-induced biofilm formation in *P. aeruginosa* PAO1. Sublethal concentrations of HClO-releasing agents NaClO and $Ca(ClO)_2$ are able to induce expression of *P. aeruginosa* PA3177 via a yet unknown regulatory pathway. PA3177acts as a DGC and catalyzes the formation of the second messenger c-di-GMP. These high intracellular c-di-GMP concentrations promote the switch from a free-living motile to a surface-associated sessile lifestyle and contribute to the development of persistent *P. aeruginosa* infections. Mutant analyses revealed an important role for the Pel and Psl exopolysaccharides as effectors in the PA3177-dependent pathway.

oxidation of methionine residues in proteins to methionine sulfoxides (Met-SO) (Drazic and Winter, 2014). In general, all tested oxidants are able to induce Met-SO formation; however, the reaction occurs considerably faster in case of HClO compared to the less reactive H_2O_2 (Pattison and Davies, 2001; Peskin and Winterbourn, 2001; Drazic and Winter, 2014). Met-SO generation by chloramines appears at medium rates depending on the chloramine type (Peskin and Winterbourn, 2001). Besides methionine oxidation, the oxidative modification of cysteine residues in proteins represents a second predominant reaction of HClO with cellular components (Pattison and Davies, 2001; Gray et al., 2013a). Pattison and Davies (2001) demonstrated that at molecular ratios $\leq$ 4:1 of HClO and proteins, 98% of applied HClO is consumed by methionine and cysteine oxidation. In addition to the lower reactivity of H_2O_2, *P. aeruginosa* possesses highly efficient H_2O_2 removal strategies such as glutathione peroxidases and catalases (Elkins et al., 1999; Lan et al., 2010) – a fact which might also contribute to the lack of Met-SO generation or cysteine oxidation by H_2O_2 in contrast to HClO *in vivo* (Romsang et al., 2013). An implication of both types of protein modification in HClO signaling in bacteria has been shown for *B. Subtilis* (Palm et al., 2012) and *E. coli* (Gebendorfer et al., 2012; Drazic et al., 2013; Gray et al., 2013b), but not for *P. aeruginosa* so far. To finally answer the question whether Met-SO generation represents a key factor in the described PA3177-mediated hyperattachment phenotype of *P. aeruginosa* in response to HClO and to identify potential modified residues in regulatory proteins, further analyses such as global mass spectrometry approaches as described by Rosen et al. (2009) would be required.

Using a PA3177 overexpression strain of *P. aeruginosa* PAO1, we were able to demonstrate a strong stimulating impact of PA3177 on self-aggregation, attachment and biofilm initiation whereas motility was strongly inhibited by the DGC. Similar cellular functions have been reported for the *P. aeruginosa* DGCs such as SiaD (PA0169), RoeA (PA1107) and YfiN (PA1120) (Klebensberger et al., 2009; Malone et al., 2010; Merritt et al., 2010). As a common feature, the expression of exopolysaccharide synthesis genes was affected by all mentioned DGCs (Klebensberger et al., 2009; Malone et al., 2010; Merritt et al., 2010). In general, changes in matrix production often play a role in the enhanced bacterial biofilm formation in response to most previously mentioned antimicrobials (Bagge et al., 2004; Hoffman et al., 2005; Linares et al., 2006; Klebensberger et al., 2009; Shemesh et al., 2010; Damron et al., 2011; Kaplan, 2011; Malone et al., 2012). In *B. subtilis*, for example, stimulation of biofilm formation by ClO_2 is associated with an enhanced matrix production mediated by the histidine kinase KinC (Shemesh et al., 2010). A similar induction of pellicle formation was also observed in *P. aeruginosa* PA14, but underlying mechanisms have not been further investigated in the respective study (Shemesh et al., 2010).

In *P. aeruginosa* biofilms, the main structural components are the polysaccharides alginate, Pel and Psl (Evans and Linker, 1973; Friedman and Kolter, 2004; Jackson et al., 2004). In contrast to alginate, which is primarily produced by mucoid strains at a later stage of biofilm development, Pel and Psl are already involved in early steps of biofilm formation like cell adhesion of *P. aeruginosa* non-mucoid variants, such as PAO1 (Wozniak et al., 2003; Overhage et al., 2005; Colvin et al., 2012; Cooley et al., 2013). In addition, flagella are important for initial cell surface attachment and biofilm formation (O'Toole and Kolter, 1998). Both flagella and exopolysaccharides are controlled by a complex regulatory network including c-di-GMP in *P. aeruginosa* (Ha and O'Toole, 2015). Using a subset of recombinant strains with mutations in genes related to flagella function (*flgK*) and exopolysaccharide synthesis (*pelF*, *pslA*), we were able to demonstrate a role of the Pel and Psl exopolysaccharides in the PA3177-mediated biofilm phenotype of *P. aeruginosa* PAO1, since in NaClO-treated *P. aeruginosa* deletion mutants the increase of attachment in the presence of NaClO was strongly inhibited when *pel* and/or *psl* genes were disrupted. Moreover, no increase in biofilm formation in response to a PA3177 overexpression was observed in the respective *pel* and *psl* deletion mutants.

Since PA3177 expression was also induced by contact with human macrophages, and given the fact that infected CF lungs bear an unusual high phagocytic burden and thus severely increased levels of HClO-generating MPO enzyme (Van Der Vliet et al., 2000; Downey et al., 2009), we can imagine an implication of this DGC in the development of persistent *P. aeruginosa* strains during chronic infections. Moreover, the applied HClO concentrations of 2 μg/ml are considered as physiologically

relevant, since it has been demonstrated previously that 5×10^6 stimulated neutrophils are able to generate 88 ± 24 nmol HClO (which corresponds to 4–5 μg HClO) within 2 h (Kalyanaraman and Sohnle, 1985) and the numbers of invading neutrophils have been estimated by approximately 1×10^4/ml during airway inflammations (Thomson et al., 2010). However, we were not able to identify a role of PA3177 in virulence and survival using THP-1 cells, since the knock-out PAO1-PA3177Ω mutant strain showed no differences compared to wildtype cells.

Previously, it has been shown that a PA3177 mutation in *P. aeruginosa* strain PA14 results in altered biofilm formation, however, the authors state that these results were not consistent (Merritt et al., 2010). Furthermore, Kulasakara et al. (2006) were able to show that a PA3177 knock-out in strain PA14 did not alter virulence or biofilm phenotypes.

The observation that in addition to PA3177 gene expression of other DGCs is induced in the presence of NaClO, in particular in the PA3177 knock-out mutant, emphasizes the importance of biofilm formation as an adaptation process for *P. aeruginosa* in response to HClO stress. Further studies have to be done to clarify if one or more DGC activities are involved in counterbalancing a PA3177 knock-out. These additional effects, the potential involvement of PA3177 in pathogenesis of *P. aeruginosa* as well as the regulatory cascade involved in the regulation of PA3177 gene expression will be investigated in more detail in the future.

Concluding, within this work we were able to identify the host defense compound and strong disinfectant HClO as a new environmental stimulus for c-di-GMP synthesis and biofilm formation in *P. aeruginosa* (**Figure 6**). The finding that expression of the HClO-responsive DGC PA3177 is also induced upon contact of *P. aeruginosa* cells with human macrophages highlights its potential role during host–pathogen interactions.

AUTHOR CONTRIBUTIONS

JO and GB-W conceived the experiments. NS and AN performed susceptibility tests, biofilm, motility and phagocytosis experiments and plasmid constructions. MN performed c-di-GMP quantification by LC-MS. NS, GB-W, and JO wrote the manuscript. All authors contributed to the final version of the manuscript, and all authors approved the final manuscript.

FUNDING

We gratefully acknowledge financial support by the BioInterfaces in Technology and Medicine (BIFTM) program of the Karlsruhe Institute of Technology (KIT) in the Helmholtz Association and start-up funds by Carleton University.

ACKNOWLEDGMENTS

We thank Bernd Rehm and Bob Hancock for kindly providing bacterial strains, Caroline Harwood for kindly providing plasmids used in this study, Robert Geffers for the microarray analysis, Boris Kühl for mass spectrometry measurements, Marie Eckstein and Linda Guedemann for technical assistance. We acknowledge support by Deutsche Forschungsgemeinschaft and Open Access Publishing Fund of Karlsruhe Institute of Technology.

SUPPLEMENTARY MATERIAL

The Supplementary Material for this article can be found online at: https://www.frontiersin.org/articles/10.3389/fmicb.2017.02311/full#supplementary-material

REFERENCES

Albrich, J. M., McCarthy, C. A., and Hurst, J. K. (1981). Biological reactivity of hypochlorous acid: implications for microbicidal mechanisms of leukocyte myeloperoxidase. *Proc. Natl. Acad. Sci. U.S.A.* 78, 210–214. doi: 10.1073/pnas.78.1.210

Aldridge, P., Paul, R., Goymer, P., Rainey, P., and Jenal, U. (2003). Role of the GGDEF regulator PleD in polar development of *Caulobacter crescentus*. *Mol. Microbiol.* 47, 1695–1708. doi: 10.1046/j.1365-2958.2003.03401.x

Bagge, N., Schuster, M., Hentzer, M., Ciofu, O., Givskov, M., Greenberg, E. P., et al. (2004). *Pseudomonas aeruginosa* biofilms exposed to imipenem exhibit changes in global gene expression and beta-lactamase and alginate production. *Antimicrob. Agents Chemother.* 48, 1175–1187. doi: 10.1128/AAC.48.4.1175-1187.2004

Bernard, C. S., Bordi, C., Termine, E., Filloux, A., and de Bentzmann, S. (2009). Organization and PprB-dependent control of the *Pseudomonas aeruginosa tad* Locus, involved in Flp pilus biology. *J. Bacteriol.* 191, 1961–1973. doi: 10.1128/JB.01330-08

Boehm, A., Kaiser, M., Li, H., Spangler, C., Kasper, C. A., Ackermann, M., et al. (2010). Second messenger-mediated adjustment of bacterial swimming velocity. *Cell* 141, 107–116. doi: 10.1016/j.cell.2010.01.018

Breidenstein, E. B., de la Fuente-Nunez, C., and Hancock, R. E. (2011). *Pseudomonas aeruginosa*: all roads lead to resistance. *Trends Microbiol.* 19, 419–426. doi: 10.1016/j.tim.2011.04.005

Buzon-Duran, L., Alonso-Calleja, C., Riesco-Pelaez, F., and Capita, R. (2017). Effect of subinhibitory concentrations of biocides on the architecture and viobility of MRSA biofilms. *Food Microbiol.* 65, 294–301. doi: 10.1016/j.fm.2017.01.003

Capita, R., Riesco-Pelaez, F., Alonso-Hernando, A., and Alonso-Calleja, C. (2014). Exposure of *Escherichia coli* ATCC 12806 to sublethal concentrations of food-grade biocides influences its ability to form biofilm, resistance to antimicrobials, and ultrastructure. *Appl. Environ. Microbiol.* 80, 1268–1280. doi: 10.1128/AEM.02283-13

Chang, W., Small, D. A., Toghrol, F., and Bentley, W. E. (2005). Microarray analysis of *Pseudomonas aeruginosa* reveals induction of pyocin genes in response to hydrogen peroxide. *BMC Genomics* 6:115. doi: 10.1186/1471-2164-6-115

Choi, Y. S., Shin, D. H., Chung, I. Y., Kim, S. H., Heo, Y. J., and Cho, Y. H. (2007). Identification of *Pseudomonas aeruginosa* genes crucial for hydrogen peroxide resistance. *J. Microbiol. Biotechnol.* 17, 1344–1352.

Cocheme, H. M., and Murphy, M. P. (2008). Complex I is the major site of mitochondrial superoxide production by paraquat. *J. Biol. Chem.* 283, 1786–1798. doi: 10.1074/jbc.M708597200

Colvin, K. M., Irie, Y., Tart, C. S., Urbano, R., Whitney, J. C., Ryder, C., et al. (2012). The Pel and Psl polysaccharides provide *Pseudomonas aeruginosa* structural redundancy within the biofilm matrix. *Environ. Microbiol.* 14, 1913–1928. doi: 10.1111/j.1462-2920.2011.02657.x

Cooley, B. J., Thatcher, T. W., Hashmi, S. M., L'her, G., Le, H. H., and Hurwitz, D. A. (2013). The extracellular polysaccharide Pel makes the attachment

of *P. aeruginosa* to surfaces symmetric and short-ranged. *Soft Matter* 9, 3871–3876. doi: 10.1039/c3sm27638d

Costerton, J. W., Lewandowski, Z., DeBeer, D., Caldwell, D., Korber, D., and James, G. (1994). Biofilms, the customized microniche. *J. Bacteriol.* 176, 2137–2142. doi: 10.1128/jb.176.8.2137-2142.1994

Damron, F. H., Davis, J., Michael, R., Withers, T. R., Ernst, R. K., Goldberg, J. B., et al. (2011). Vanadate and triclosan synergistically induce alginate production by *Pseudomonas aeruginosa* strain PAO1. *Mol. Microbiol.* 81, 554–570. doi: 10.1111/j.1365-2958.2011.07715.x

Deng, X., Liang, H., Ulanovskaya, O. A., Ji, Q., Zhou, T., Sun, F., et al. (2014). Steady-state hydrogen peroxide induces glycolysis in *Staphylococcus aureus* and *Pseudomonas aeruginosa*. *J. Bacteriol.* 196, 2499–2513. doi: 10.1128/JB.01538-14

Dötsch, A., Eckweiler, D., Schniederjans, M., Zimmermann, A., Jensen, V., Scharfe, M., et al. (2012). The *Pseudomonas aeruginosa* transcriptome in planktonic cultures and static biofilms using RNA sequencing. *PLOS ONE* 7:e31092. doi: 10.1371/journal.pone.0031092

Downey, D. G., Bell, S. C., and Elborn, J. S. (2009). Neutrophils in cystic fibrosis. *Thorax* 64, 81–88. doi: 10.1136/thx.2007.082388

Drazic, A., Miura, H., Peschek, J., Le, Y., Bach, N. C., Kriehuber, T., et al. (2013). Methionine oxidation activates a transcription factor in response to oxidative stress. *Proc. Natl. Acad. Sci. U.S.A.* 110, 9493–9498. doi: 10.1073/pnas.1300578110

Drazic, A., and Winter, J. (2014). The physiological role of reversible methionine oxidation. *Biochim. Biophys. Acta* 1844, 1367–1382. doi: 10.1016/j.bbapap.2014.01.001

Elkins, J. G., Hassett, D. J., Stewart, P. S., Schweizer, H. P., and McDermott, T. R. (1999). Protective role of catalase in *Pseudomonas aeruginosa* biofilm resistance to hydrogen peroxide. *Appl. Environ. Microbiol.* 65, 4594–4600.

Evans, L. R., and Linker, A. (1973). Production and characterization of the slime polysaccharide of *Pseudomonas aeruginosa*. *J. Bacteriol.* 116, 915–924.

Fang, F. C. (2004). Antimicrobial reactive oxygen and nitrogen species: concepts and controversies. *Nat. Rev. Microbiol.* 2, 820–832. doi: 10.1038/nrmicro1004

Fazli, M., Almblad, H., Rybtke, M. L., Givskov, M., Eberl, L., and Tolker-Nielsen, T. (2014). Regulation of biofilm formation in *Pseudomonas* and *Burkholderia* species. *Environ. Microbiol.* 16, 1961–1981. doi: 10.1111/1462-2920.12448

Flannagan, R. S., Cosío, G., and Grinstein, S. (2009). Antimicrobial mechanisms of phagocytes and bacterial evasion strategies. *Nat. Rev. Microbiol.* 7, 355–366. doi: 10.1038/nrmicro2128

Friedman, L., and Kolter, R. (2004). Two genetic loci produce distinct carbohydrate-rich structural components of the *Pseudomonas aeruginosa* biofilm matrix. *J. Bacteriol.* 186, 4457–4465. doi: 10.1128/JB.186.14.4457-4465.2004

Gebendorfer, K. M., Drazic, A., Le, Y., Gundlach, J., Bepperling, A., Kastenmuller, A., et al. (2012). Identification of a hypochlorite-specific transcription factor from *Escherichia coli*. *J. Biol. Chem.* 287, 6892–6903. doi: 10.1074/jbc.M111.287219

Gellatly, S. L., and Hancock, R. E. (2013). *Pseudomonas aeruginosa*: new insights into pathogenesis and host defenses. *Pathog. Dis.* 67, 159–173. doi: 10.1111/2049-632X.12033

Ghafoor, A., Hay, I. D., and Rehm, B. H. (2011). Role of exopolysaccharides in *Pseudomonas aeruginosa* biofilm formation and architecture. *Appl. Environ. Microbiol.* 77, 5238–5246. doi: 10.1128/AEM.00637-11

Goldova, J., Ulrych, A., Hercik, K., and Branny, P. (2011). A eukaryotic-type signalling system of *Pseudomonas aeruginosa* contributes to oxidative stress resistance, intracellular survival and virulence. *BMC Genomics* 12:437. doi: 10.1186/1471-2164-12-437

Gray, M. J., Wholey, W.-Y., and Jakob, U. (2013a). Bacterial responses to reactive chlorine species. *Annu. Rev. Microbiol.* 67, 141–160. doi: 10.1146/annurev-micro-102912-142520

Gray, M. J., Wholey, W.-Y., Parker, B. W., Kim, M., and Jakob, U. (2013b). NemR is a bleach-sensing transcription factor. *J. Biol. Chem.* 288, 13789–13798. doi: 10.1074/jbc.M113.454421

Groitl, B., Dahl, J. U., Schroeder, J. W., and Jakob, U. (2017). *Pseudomonas aeruginosa* defense systems against microbiocidal oxidants. *Mol. Microbiol.* 106, 335–350. doi: 10.1111/mmi.13768

Ha, D. G., and O'Toole, G. A. (2015). c-di-GMP and its effect on biofilm formation and dispersion: a *Pseudomonas aeruginosa* review. *Microbiol. Spectr.* 3:MB-0003-2014. doi: 10.1128/microbiolspec.MB-0003-2014

Hachiya, M., Osawa, Y., and Akashi, M. (2000). Role of TNFalpha in regulation of myeloperoxidase expression in irradiated HL60 promyelocytic cells. *Biochim. Biophys. Acta* 1495, 237–249. doi: 10.1016/S0167-4889(99)00168-8

Hall-Stoodley, L., Costerton, J. W., and Stoodley, P. (2004). Bacterial biofilms: from the natural environment to infectious diseases. *Nat. Rev. Microbiol.* 2, 95–108. doi: 10.1038/nrmicro821

Hanahan, D. (1983). Studies on transformation of *Escherichia coli* with plasmids. *J. Mol. Biol.* 166, 557–580. doi: 10.1016/S0022-2836(83)80284-8

Hancock, R. E., and Speert, D. P. (2000). Antibiotic resistance in *Pseudomonas aeruginosa*: mechanisms and impact on treatment. *Drug Resist. Updat.* 3, 247–255. doi: 10.1054/drup.2000.0152

Hare, N. J., Scott, N. E., Shin, E. H. H., Connolly, A. M., Larsen, M. R., Palmisano, G., et al. (2011). Proteomics of the oxidative stress response induced by hydrogen peroxide and paraquat reveals a novel AhpC-like protein in *Pseudomonas aeruginosa*. *Proteomics* 11, 3056–3069. doi: 10.1002/pmic.201000807

Hawkins, C. L., and Davies, M. J. (1998). Hypochlorite-induced damage to proteins: formation of nitrogen-centred radicals from lysine residues and their role in protein fragmentation. *Biochem. J.* 332, 617–625. doi: 10.1042/bj3320617

Hengge, R. (2009). Principles of c-di-GMP signalling in bacteria. *Nat. Rev. Microbiol.* 7, 263–273. doi: 10.1038/nrmicro2109

Heo, Y. J., Chung, I. Y., Cho, W. J., Lee, B. Y., Kim, J. H., Choi, K. H., et al. (2010). The major catalase gene (*katA*) of *Pseudomonas aeruginosa* PA14 is under both positive and negative control of the global transactivator OxyR in response to hydrogen peroxide. *J. Bacteriol.* 192, 381–390. doi: 10.1128/JB.00980-09

Hickman, J. W., Tifrea, D. F., and Harwood, C. S. (2005). A chemosensory system that regulates biofilm formation through modulation of cyclic diguanylate levels. *Proc. Natl. Acad. Sci. U.S.A.* 102, 14422–14427. doi: 10.1073/pnas.0507170102

Hoffman, L. R., D'Argenio, D. A., MacCoss, M. J., Zhang, Z., Jones, R. A., and Miller, S. I. (2005). Aminoglycoside antibiotics induce bacterial biofilm formation. *Nature* 436, 1171–1175. doi: 10.1038/nature03912

Jackson, K. D., Starkey, M., Kremer, S., Parsek, M. R., and Wozniak, D. J. (2004). Identification of *psl*, a locus encoding a potential exopolysaccharide that is essential for *Pseudomonas aeruginosa* PAO1 biofilm formation. *J. Bacteriol.* 186, 4466–4475. doi: 10.1128/JB.186.14.4466-4475.2004

Kalia, D., Merey, G., Nakayama, S., Zheng, Y., Zhou, J., Luo, Y., et al. (2013). Nucleotide, c-di-GMP, c-di-AMP, cGMP, cAMP, (p)ppGpp signaling in bacteria and implications in pathogenesis. *Chem. Soc. Rev.* 42, 305–341. doi: 10.1039/c2cs35206k

Kalyanaraman, B., and Sohnle, P. G. (1985). Generation of free radical intermediates from foreign compounds by neutrophil-derived oxidants. *J. Clin. Invest.* 75, 1618–1622. doi: 10.1172/JCI111868

Kaplan, J. B. (2011). Antibiotic-induced biofilm formation. *Int. J. Artif. Organs* 34, 737–751. doi: 10.5301/ijao.5000027

Klebanoff, S. J. (2005). Myeloperoxidase: friend and foe. *J. Leukoc. Biol.* 77, 598–625. doi: 10.1189/jlb.1204697

Klebensberger, J., Birkenmaier, A., Geffers, R., Kjelleberg, S., and Philipp, B. (2009). SiaA and SiaD are essential for inducing autoaggregation as a specific response to detergent stress in *Pseudomonas aeruginosa*. *Environ. Microbiol.* 11, 3073–3086. doi: 10.1111/j.1462-2920.2009.02012.x

Kulasakara, H., Lee, V., Brencic, A., Liberati, N., Urbach, J., Miyata, S., et al. (2006). Analysis of *Pseudomonas aeruginosa* diguanylate cyclases and phosphodiesterases reveals a role for bis-(3′-5′)-cyclic-GMP in virulence. *Proc. Natl. Acad. Sci. U.S.A.* 103, 2839–2844. doi: 10.1073/pnas.0511090103

Lan, L., Murray, T. S., Kazmierczak, B. I., and He, C. (2010). *Pseudomonas aeruginosa* OspR is an oxidative stress sensing regulator that affects pigment production, antibiotic resistance and dissemination during infection. *Mol. Microbiol.* 75, 76–91. doi: 10.1111/j.1365-2958.2009.06955.x

Lewenza, S., Falsafi, R. K., Winsor, G., Gooderham, W. J., McPhee, J. B., Brinkman, F. S., et al. (2005). Construction of a mini-Tn5-luxCDABE mutant library in *Pseudomonas aeruginosa* PAO1: a tool for identifying differentially regulated genes. *Genome Res.* 15, 583–589. doi: 10.1101/gr.3513905

Li, Y., Heine, S., Entian, M., Sauer, K., and Frankenberg-Dinkel, N. (2013). NO-induced biofilm dispersion in *Pseudomonas aeruginosa* is mediated by

an MHYT domain-coupled phosphodiesterase. *J. Bacteriol.* 195, 3531–3542. doi: 10.1128/JB.01156-12

Linares, J. F., Gustafsson, I., Baquero, F., and Martinez, J. L. (2006). Antibiotics as intermicrobial signaling agents instead of weapons. *Proc. Natl. Acad. Sci. U.S.A.* 103, 19484–19489. doi: 10.1073/pnas.0608949103

Lovewell, R. R., Patankar, Y. R., and Berwin, B. (2014). Mechanisms of phagocytosis and host clearance of *Pseudomonas aeruginosa*. *Am. J. Physiol. Lung Cell. Mol. Physiol.* 306, L591–L603. doi: 10.1152/ajplung.00335.2013

Luo, Y., Zhao, K., Baker, A. E., Kuchma, S. L., Coggan, K. A., Wolfgang, M. C., et al. (2015). A hierarchical cascade of second messengers regulates *Pseudomonas aeruginosa* surface behaviors. *mBio* 6:e02456-14. doi: 10.1128/mBio.02456-14

Malone, J. G., Jaeger, T., Manfredi, P., Dotsch, A., Blanka, A., Bos, R., et al. (2012). The YfiBNR signal transduction mechanism reveals novel targets for the evolution of persistent *Pseudomonas aeruginosa* in cystic fibrosis airways. *PLOS Pathog.* 8:e1002760. doi: 10.1371/journal.ppat.1002760

Malone, J. G., Jaeger, T., Spangler, C., Ritz, D., Spang, A., Arrieumerlou, C., et al. (2010). YfiBNR mediates cyclic di-GMP dependent small colony variant formation and persistence in *Pseudomonas aeruginosa*. *PLOS Pathog.* 6:e1000804. doi: 10.1371/journal.ppat.1000804

Merritt, J. H., Brothers, K. M., Kuchma, S. L., and O'Toole, G. A. (2007). SadC reciprocally influences biofilm formation and swarming motility via modulation of exopolysaccharide production and flagellar function. *J. Bacteriol.* 189, 8154–8164. doi: 10.1128/JB.00585-07

Merritt, J. H., Ha, D. G., Cowles, K. N., Lu, W., Morales, D. K., Rabinowitz, J., et al. (2010). Specific control of *Pseudomonas aeruginosa* surface-associated behaviors by two c-di-GMP diguanylate cyclases. *mBio* 1:e00183-10. doi: 10.1128/mBio.00183-10

Merritt, J. H., Kadouri, D. E., and O'Toole, G. A. (2005). Growing and analyzing static biofilms. *Curr. Protoc. Microbiol.* 00:1B.1.1–1B.1.17. doi: 10.1002/9780471729259.mc01b01s00

Mikkelsen, H., Sivaneson, M., and Filloux, A. (2011). Key two-component regulatory systems that control biofilm formation in *Pseudomonas aeruginosa*. *Environ. Microbiol.* 13, 1666–1681. doi: 10.1111/j.1462-2920.2011.02495.x

Neidig, A., Yeung, A., Rosay, T., Tettmann, B., Strempel, N., Rueger, M., et al. (2013). TypA is involved in virulence, antimicrobial resistance and biofilm formation in *Pseudomonas aeruginosa*. *BMC Microbiol.* 13:77. doi: 10.1186/1471-2180-13-77

Newman, J. R., and Fuqua, C. (1999). Broad-host-range expression vectors that carry the L-arabinose-inducible *Escherichia coli araBAD* promoter and the *araC* regulator. *Gene* 227, 197–203. doi: 10.1016/S0378-1119(98)00601-5

O'Toole G. A., and Kolter, R. (1998). Flagellar and twitching motility are necessary for *Pseudomonas* aeruginosa biofilm development. *Mol. Microbiol.* 30, 295–304. doi: 10.1046/j.1365-2958.1998.01062.x

Overhage, J., Campisano, A., Bains, M., Torfs, E. C., Rehm, B. H., and Hancock, R. E. (2008). Human host defense peptide LL-37 prevents bacterial biofilm formation. *Infect. Immun.* 76, 4176–4182. doi: 10.1128/IAI.00318-08

Overhage, J., Schemionek, M., Webb, J. S., and Rehm, B. H. A. (2005). Expression of the *psl* operon in *Pseudomonas aeruginosa* PAO1 biofilms: PslA performs an essential function in biofilm formation. *Appl. Environ. Microbiol.* 71, 4407–4413. doi: 10.1128/AEM.71.8.4407-4413.2005

Palm, G. J., Khanh Chi, B., Waack, P., Gronau, K., Becher, D., Albrecht, D., et al. (2012). Structural insights into the redox-switch mechanism of the MarR/DUF24-type regulator HypR. *Nucleic Acids Res.* 40, 4178–4192. doi: 10.1093/nar/gkr1316

Palma, M., DeLuca, D., Worgall, S., and Quadri, L. E. N. (2004). Transcriptome analysis of the response of *Pseudomonas aeruginosa* to hydrogen peroxide. *J. Bacteriol.* 186, 248–252. doi: 10.1128/JB.186.1.248-252.2004

Park, E. K., Jung, H. S., Yang, H. I., Yoo, M. C., Kim, C., and Kim, K. S. (2007). Optimized THP-1 differentiation is required for the detection of responses to weak stimuli. *Inflamm. Res.* 56, 45–50. doi: 10.1007/s00011-007-6115-5

Pattison, D. I., and Davies, M. J. (2001). Absolute rate constants for the reaction of hypochlorous acid with protein side chains and peptide bonds. *Chem. Res. Toxicol.* 14, 1453–1464. doi: 10.1021/tx0155451

Peskin, A. V., and Winterbourn, C. C. (2001). Kinetics of the reactions of hypochlorous acid and amino acid chloramines with thiols, methionine, and ascorbate. *Free Radic. Biol. Med.* 30, 572–579. doi: 10.1016/S0891-5849(00)00506-2

Petrova, O. E., Cherny, K. E., and Sauer, K. (2014). The *Pseudomonas aeruginosa* diguanylate cyclase GcbA, a homolog of *P. fluorescens* GcbA, promotes initial attachment to surfaces, but not biofilm formation, via regulation of motility. *J. Bacteriol.* 196, 2827–2841. doi: 10.1128/JB.01628-14

Phippen, C. W., Mikolajek, H., Schlaefli, H. G., Keevil, C. W., Webb, J. S., and Tews, I. (2014). Formation and dimerization of the phosphodiesterase active site of the *Pseudomonas aeruginosa* MorA, a bi-functional c-di-GMP regulator. *FEBS Lett.* 588, 4631–4636. doi: 10.1016/j.febslet.2014.11.002

Rajan, S., and Saiman, L. (2002). Pulmonary infections in patients with cystic fibrosis. *Semin. Respir. Infect.* 17, 47–56. doi: 10.1053/srin.2002.31690

Rao, F., Qi, Y., Chong, H. S., Kotaka, M., Li, B., Li, J., et al. (2009). The functional role of a conserved loop in EAL domain-based cyclic di-GMP-specific phosphodiesterase. *J. Bacteriol.* 191, 4722–4731. doi: 10.1128/JB.00327-09

Römling, U., Galperin, M. Y., and Gomelsky, M. (2013). Cyclic di-GMP: the first 25 years of a universal bacterial second messenger. *Microbiol. Mol. Biol. Rev.* 77, 1–52. doi: 10.1128/MMBR.00043-12

Romsang, A., Atichartpongkul, S., Trinachartvanit, W., Vattanaviboon, P., and Mongkolsuk, S. (2013). Gene expression and physiological role of *Pseudomonas aeruginosa* methionine sulfoxide reductases during oxidative stress. *J. Bacteriol.* 195, 3299–3308. doi: 10.1128/JB.00167-13

Rosen, H., Klebanoff, S. J., Wang, Y., Brot, N., Heinecke, J. W., and Fu, X. (2009). Methionine oxidation contributes to bacterial killing by the myeloperoxidase system of neutrophils. *Proc. Natl. Acad. Sci. U.S.A.* 106, 18686–18691. doi: 10.1073/pnas.0909464106

Rosen, H., Orman, J., Rakita, R. M., Michel, B. R., and VanDevanter, D. R. (1990). Loss of DNA-membrane interactions and cessation of DNA synthesis in myeloperoxidase-treated *Escherichia coli*. *Proc. Natl. Acad. Sci. U.S.A.* 87, 10048–10052. doi: 10.1073/pnas.87.24.10048

Roy, A. B., Petrova, O. E., and Sauer, K. (2012). The phosphodiesterase DipA (PA5017) is essential for *Pseudomonas aeruginosa* biofilm dispersion. *J. Bacteriol.* 194, 2904–2915. doi: 10.1128/JB.05346-11

Salunkhe, P., Töpfer, T., Buer, J., and Tümmler, B. (2005). Genome-wide transcriptional profiling of the steady-state response of *Pseudomonas aeruginosa* to hydrogen peroxide. *J. Bacteriol.* 187, 2565–2572. doi: 10.1128/JB.187.8.2565-2572.2005

Schmidberger, A., Henkel, M., Hausmann, R., and Schwartz, T. (2013). Expression of genes involved in rhamnolipid synthesis in *Pseudomonas aeruginosa* PAO1 in a bioreactor cultivation. *Appl. Microbiol. Biotechnol.* 97, 5779–5791. doi: 10.1007/s00253-013-4891-0

Shemesh, M., Kolter, R., and Losick, R. (2010). The biocide chlorine dioxide stimulates biofilm formation in *Bacillus subtilis* by activation of the histidine kinase KinC. *J. Bacteriol.* 192, 6352–6356. doi: 10.1128/JB.01025-10

Small, D. A., Chang, W., Toghrol, F., and Bentley, W. E. (2007a). Comparative global transcription analysis of sodium hypochlorite, peracetic acid, and hydrogen peroxide on *Pseudomonas aeruginosa*. *Appl. Microbiol. Biotechnol.* 76, 1093–1105.

Small, D. A., Chang, W., Toghrol, F., and Bentley, W. E. (2007b). Toxicogenomic analysis of sodium hypochlorite antimicrobial mechanisms in *Pseudomonas aeruginosa*. *Appl. Microbiol. Biotechnol.* 74, 176–185.

Spangler, C., Bohm, A., Jenal, U., Seifert, R., and Kaever, V. (2010). A liquid chromatography-coupled tandem mass spectrometry method for quantitation of cyclic di-guanosine monophosphate. *J. Microbiol. Methods* 81, 226–231. doi: 10.1016/j.mimet.2010.03.020

Stover, C. K., Pham, X. Q., Erwin, A. L., Mizoguchi, S. D., Warrener, P., Hickey, M. J., et al. (2000). Complete genome sequence of *Pseudomonas aeruginosa* PAO1, an opportunistic pathogen. *Nature* 406, 959–964. doi: 10.1038/35023079

Strehmel, J., Neidig, A., Nusser, M., Geffers, R., Brenner-Weiss, G., and Overhage, J. (2015). The sensor kinase PA4398 modulates swarming motility and biofilm formation in *Pseudomonas aeruginosa* PA14. *Appl. Environ. Microbiol.* 81, 1274–1285. doi: 10.1128/AEM.02832-14

Strempel, N., Neidig, A., Nusser, M., Geffers, R., Vieillard, J., Lesouhaitier, O., et al. (2013). Human host defense peptide LL-37 stimulates virulence factor production and adaptive resistance in *Pseudomonas aeruginosa*. *PLOS ONE* 8:e82240. doi: 10.1371/journal.pone.0082240

Thomson, E., Brennan, S., Senthilmohan, R., Gangell, C. L., Chapman, A. L., Sly, P. D., et al. (2010). Identifying peroxidases and their oxidants in the early

pathology of cystic fibrosis. *Free Radic. Biol. Med.* 49, 1354–1360. doi: 10.1016/j.freeradbiomed.2010.07.010

Van Der Vliet, A., Nguyen, M. N., Shigenaga, M. K., Eiserich, J. P., Marelich, G. P., and Cross, C. E. (2000). Myeloperoxidase and protein oxidation in cystic fibrosis. *Am. J. Physiol. Lung Cell. Mol. Physiol.* 279, L537–L546.

Whiteley, M., Bangera, M. G., Bumgarner, R. E., Parsek, M. R., Teitzel, G. M., Lory, S., et al. (2001). Gene expression in *Pseudomonas aeruginosa* biofilms. *Nature* 413, 860–864. doi: 10.1038/35101627

Wiegand, I., Hilpert, K., and Hancock, R. E. (2008). Agar and broth dilution methods to determine the minimal inhibitory concentration (MIC) of antimicrobial substances. *Nat. Protoc.* 3, 163–175. doi: 10.1038/nprot.2007.521

Williams, B. J., Dehnbostel, J., and Blackwell, T. S. (2010). *Pseudomonas aeruginosa*: host defence in lung diseases. *Respirology* 15, 1037–1056. doi: 10.1111/j.1440-1843.2010.01819.x

Winsor, G. L., Lam, D. K., Fleming, L., Lo, R., Whiteside, M. D., Yu, N. Y., et al. (2011). *Pseudomonas* genome database: improved comparative analysis and population genomics capability for *Pseudomonas* genomes. *Nucleic Acids Res.* 39, D596–D600. doi: 10.1093/nar/gkq869

Wozniak, D. J., Wyckoff, T. J. O., Starkey, M., Keyser, R., Azadi, P., O'Toole, G. A., et al. (2003). Alginate is not a significant component of the extracellular polysaccharide matrix of PA14 and PAO1 *Pseudomonas aeruginosa* biofilms. *Proc. Natl. Acad. Sci. U.S.A.* 100, 7907–7912. doi: 10.1073/pnas.1231792100

Yeung, A. T. Y., Janot, L., Pena, O. M., Neidig, A., Kukavica-Ibrulj, I., Hilchie, A., et al. (2014). Requirement of the *Pseudomonas aeruginosa* CbrA sensor kinase for full virulence in a murine acute lung infection model. *Infect. Immun.* 82, 1256–1267. doi: 10.1128/IAI.01527-13

Conflict of Interest Statement: The authors declare that the research was conducted in the absence of any commercial or financial relationships that could be construed as a potential conflict of interest.

The reviewer JR and handling Editor declared their shared affiliation.

frontiers in Microbiology

ORIGINAL RESEARCH
published: 29 November 2017
doi: 10.3389/fmicb.2017.02347

Relative Quantitative Proteomic Analysis of *Brucella abortus* Reveals Metabolic Adaptation to Multiple Environmental Stresses

Xiaodong Zai, Qiaoling Yang, Ying Yin, Ruihua Li, Mengying Qian, Taoran Zhao, Yaohui Li, Jun Zhang, Ling Fu, Junjie Xu and Wei Chen**

Laboratory of Vaccine and Antibody Engineering, Beijing Institute of Biotechnology, Beijing, China

Brucella spp. are facultative intracellular pathogens that cause chronic brucellosis in humans and animals. The virulence of *Brucella* primarily depends on its successful survival and replication in host cells. During invasion of the host tissue, *Brucella* is simultaneously subjected to a variety of harsh conditions, including nutrient limitation, low pH, antimicrobial defenses, and extreme levels of reactive oxygen species (ROS) via the host immune response. This suggests that *Brucella* may be able to regulate its metabolic adaptation in response to the distinct stresses encountered during its intracellular infection of the host. An investigation into the differential proteome expression patterns of *Brucella* grown under the relevant stress conditions may contribute toward a better understanding of its pathogenesis and adaptive response. Here, we utilized a mass spectrometry-based label-free relative quantitative proteomics approach to investigate and compare global proteomic changes in *B. abortus* in response to eight different stress treatments. The 3 h short-term *in vitro* single-stress and multi-stress conditions mimicked the *in vivo* conditions of *B. abortus* under intracellular infection, with survival rates ranging from 3.17 to 73.17%. The proteomic analysis identified and quantified a total of 2,272 proteins and 74% of the theoretical proteome, thereby providing wide coverage of the *B. abortus* proteome. By including eight distinct growth conditions and comparing these with a control condition, we identified a total of 1,221 differentially expressed proteins (DEPs) that were significantly changed under the stress treatments. Pathway analysis revealed that most of the proteins were involved in oxidative phosphorylation, ABC transporters, two-component systems, biosynthesis of secondary metabolites, the citrate cycle, thiamine metabolism, and nitrogen metabolism; constituting major response mechanisms toward the reconstruction of cellular homeostasis and metabolic balance under stress. In conclusion, our results provide a better understanding of the global metabolic adaptations of *B. abortus* associated with distinct environmental stresses. The identification of proteins necessary for stress resistance is crucial toward elucidating the infectious process in order to control brucellosis, and may facilitate the discovery of novel therapeutic targets and effective vaccines.

Keywords: *Brucella abortus*, proteomic, label-free, environmental stress, differentially expressed protein, metabolic pathway

OPEN ACCESS

Edited by:
Daniela De Biase,
Sapienza Università di Roma, Italy

Reviewed by:
Jayaseelan Murugaiyan,
Freie Universität Berlin, Germany
Eustache Paramithiotis,
Caprion, Canada
Carlos Rossetti,
Instituto Nacional de Tecnología Agropecuaria (INTA), Argentina

****Correspondence:***
Junjie Xu
xujunjie@sina.com
Wei Chen
cw0226@foxmail.com

Specialty section:
This article was submitted to Microbial Physiology and Metabolism, a section of the journal Frontiers in Microbiology

Received: *29 August 2017*
Accepted: *15 November 2017*
Published: *29 November 2017*

Citation:
Zai X, Yang Q, Yin Y, Li R, Qian M, Zhao T, Li Y, Zhang J, Fu L, Xu J and Chen W (2017) Relative Quantitative Proteomic Analysis of Brucella abortus Reveals Metabolic Adaptation to Multiple Environmental Stresses. Front. Microbiol. 8:2347. doi: 10.3389/fmicb.2017.02347

INTRODUCTION

Brucella (Brucellaceae) are gram-negative, facultative intracellular pathogens that cause brucellosis, which results in abortion and infertility in the natural host (Akpinar, 2016). Brucellosis is a major global zoonosis that infects approximately 500,000 people annually (Hasanjani Roushan and Ebrahimpour, 2015). *Brucella abortus*, *B. melitensis*, and *B. suis* are most pathogenic toward humans and have been listed as high priority biological agents (Doganay and Doganay, 2013). However, the pathogenic mechanisms of *Brucella* are currently not well understood. During invasion of the host tissue, the bacteria multiply inside phagocytic cells and eventually establish persistent infection and replication within the host (Ahmed et al., 2016). It appears that *Brucella* species do not depend on single discrete virulence factors such as cytolysins, capsules, exotoxins, secreted proteases, fimbriae, or phage-encoded toxins for their pathogenicity (He, 2012). Rather, their pathogenicity mainly depends on their capacity to survive and proliferate within host cells (Byndloss and Tsolis, 2016). During the invasion of host tissue, these bacteria are subjected to several severe stresses, including nutrient limitation, low pH, antimicrobial defenses, and extreme levels of reactive oxygen species (ROS) from the immune response of the host (Roop et al., 2009; Barbier et al., 2011; Olsen and Palmer, 2014). The pathogen may therefore be able to withstand the variety of stresses encountered during its intracellular infection (Lamontagne et al., 2009).

In recent years, proteomics has become an indispensable tool used to investigate the metabolic adaptation mechanisms of various organisms to multiple environmental stresses (Cash, 2011; Van Oudenhove and Devreese, 2013; Greco and Cristea, 2017). The assessment of differential proteome expression patterns of a pathogen under stress may contribute to a better understanding of pathogen adaptation and pathogenesis. Distinct environmental conditions can be simulated by *in vitro* models, in which bacterial cultures are exposed to different *in vivo*-mimicking conditions experienced in the cellular environment of the host. The metabolic adaptation of *Brucella* to specific stresses such as nutrient starvation, acidity, high temperature, or peroxide has been explored in previous studies (Teixeira-Gomes et al., 2000; Al-Dahouk et al., 2008, 2009, 2013). However, earlier proteomic approaches employed two-dimensional electrophoresis (2-D), and are therefore limited in their detection of alkaline and low-abundance proteins. Lamontagne et al. (2009) used an LC-MS approach to investigate and compare global proteomic changes in *B. abortus* at different times after infection *in vivo*, which provided insight into mechanisms utilized by *Brucella* to survive and proliferate within host cells. During the invasion of host tissue, *Brucella* is simultaneously subjected to a variety of harsh environments (Roop et al., 2009); however, previous proteomic studies failed to test a range of potential environmental stresses that the bacteria could be exposed to within the host.

In this study, we utilized a label-free relative quantitative proteomics approach to investigate and compare global proteomic changes in *B. abortus* in response to a variety of typical environmental stresses. A total of 2,272 proteins were identified and quantified, with significant changes observed in 1,221 under the multiple stress conditions tested. The differentially expressed proteins (DEPs) identified that were significantly changed under the stress treatments may provide novel insights into the global metabolic adaptations of *B. abortus* to multiple stresses. The identification of proteins necessary for stress resistance is crucial to elucidate the infection process and may facilitate the discovery of novel therapeutic targets and effective vaccines.

Abbreviations: 2-D, two-dimensional electrophoresis; CAMPs, cationic antimicrobial peptides; DEP, differentially expressed protein; LC-MS/MS, liquid chromatography coupled to tandem mass spectrometry; LTQ, Linear trap quadrupole; FDR, False discovery rate; COG, Clusters of orthologous groups; KEGG, Kyoto Encyclopedia of Genes and Genomes; STRING, Search Tool for the Retrieval of Interacting Genes/Proteins; LFQ, label-free quantitation; PCoA, principal coordinate analysis.

MATERIALS AND METHODS

Brucella Strains and Experimental Design

The *B. abortus* 104-M strain was obtained from the Lanzhou Institute of Biological Products in China (Yu et al., 2015). The cells were subjected to a control treatment [grown on tryptic soy broth (TSB), condition #1] and eight different stress treatments as previously described, with some modifications (Teixeira-Gomes et al., 2000; Al-Dahouk et al., 2008, 2009, 2013; Lamontagne et al., 2010). These included: (i) seven single-stress conditions: #2 serum stress [addition of 10% serum (obtained from healthy volunteers after informed consent; stored at −20°C)]; #3 nutrient starvation stress (grown in Sauton's glycerol medium); #4 physical/chemical stress [grown in an acidic, high-temperature, hyperhaline, and high osmotic pressure condition (pH 4.5, 45°C, NaCl 1 mol/L final concentration, sorbitol 1 mol/L final concentration)]; #5 peroxide/nitric oxide stress (addition of 50 mM H_2O_2 and 5 mM DETA-NO, final concentrations); #6 oxygen deficiency stress (incubation sealed); #7 iron-limited stress [addition of 50 μM final concentration of the Fe^{2+}-chelator 2,2′-dipyridyl (DIP; Sigma-Aldrich, Shanghai, China)]; #8 antibacterial stress (addition of polymyxin B to 100 μg/mL final concentration); and (ii) a multi-stress condition, consisting of a combination of conditions #2 to #8 (#9, see **Table 1** for details).

The cells were first cultured in TSB with continuous shaking (200 rpm) at 37°C for approximately 24 h until mid-log phase (OD_{600nm} = 1.0). The cells were harvested by concentrating the solution, and were then resuspended in the eight different growth conditions listed above and incubated for 3 h in a shaking incubator. Cultures were then serially diluted and plated on tryptic soy agar to determine their viability post-challenge. The survival percentage of the 3 h post-stress challenge was calculated by dividing the number of colony-forming units obtained from each stress treatment to that obtained from the control treatment, multiplied by 100. The survival experiments were performed at least three times for each treatment. All experiments involving live *B. abortus* 104-M were conducted in BSL-2 labs in line with health and safety guidelines.

TABLE 1 | Survival of *B. abortus* under environmental stress.

Group	Stress	Conditions	Cell survival rate (%)
1	TSB (Control condition)	37°C, TSB, pH 7.6	100
2	Serum stress	10% serum	65.85
3	Nutrient starvation stress	Sauton's glycerol medium	5.85
4	Physical/chemical stress	45°C, TSB, pH 4.5, NaCl 1 mol/L, Sorbitol 1 mol/L	36.59
5	Peroxide/nitric oxide stress	H_2O_2 50 mM, DETA-NO 5 mM	11.71
6	Oxygen deficiency stress	Incubation sealed	5.85
7	Iron-limited stress	Fe^{2+}-chelator 2,2′-dipyridyl 50 μM	73.17
8	Antibacterial stress	Polymyxin B 100 μg/mL	24.39
9	Multi-stress	42°C, Sauton's glycerol medium, pH 5.5, NaCl 0.5 mol/L, Sorbitol 0.5 mol/L, 5% serum, H_2O_2 25 mM, DETA-NO 2.5 mM, incubation sealed, Fe^{2+}-chelator 2,2′-dipyridyl 25 μM, polymyxin B 50 μg/mL	3.17

Protein Sample Preparation and Proteolytic Digestion

The protein samples were prepared as described previously (Zai et al., 2017). Briefly, cells cultured in each condition were harvested by centrifugation (7,000 × g for 15 min), and then washed three times with phosphate-buffered saline (PBS). The bacterial cells were resuspended in lysis buffer and disrupted by ultrasonication (25% amplitude, 15 min at 0°C). The resultant suspension was centrifuged (40,000 × g for 30 min) and the protein concentrations in the collected supernatants were measured using a BCA (bicinchoninic acid) protein assay kit (Thermo Fisher Scientific, Waltham, USA). The cell protein extracts were reduced in 1 mM dithiothreitol (25°C for 1 h) and then alkylated in 5.5 mM iodoacetamide (25°C for 1 h, in the dark). Sequencing-grade trypsin (Promega) was added to a final ratio of 1:50 (V:V) and the proteins were digested in solution overnight at 37°C.

Liquid Chromatography Coupled to Tandem Mass Spectrometry (LC-MS/MS)

All experiments were performed on an LTQ Q-Exactive HF mass spectrometer (Thermo Scientific, USA) coupled online with a nano-HPLC (Ultimate 3000, Thermo Scientific) (Scheltema et al., 2014). The peptides were loaded onto a trap column (C18, 3 μm particles, 100 μm × 2 cm) and separated on EASY-Spray columns (C18, 1.9 μm particles, 15 μm × 12 cm) with trapping at a flow rate of 600 nL/min (Kentache et al., 2017). The mobile phase A was 0.1% formic acid in water and the mobile phase B was 0.1% formic acid in acetonitrile. The peptides were eluted using a gradient (6–95% mobile phase B) during a 195-min LC run and then sprayed directly into the MS instrument.

The mass spectrometer was operated using the data-dependent top-15 method with automatic switching between MS and MS/MS scans (Kalayou et al., 2016). Full MS scans were acquired at a resolution of 120,000, with an automatic gain control target value of 3×10^6 ions or maximum injection time of 80 ms within the scan range 300–1,400 m/z. Peptide fragmentation was performed by higher energy collision dissociation (HCD) with the normalized collision energy set to 27 (Tutturen et al., 2014). The 15 highest-intensity ions were then selected for the collision-induced fragmentation at a resolution $R = 15{,}000$, an automatic gain control target value of 5×10^4 ions, or maximum fragment accumulation time of 45 ms. After the fragmentation event, dynamic exclusion of precursor ion masses for 12 s was used to avoid the repeated fragmentation of peaks. We excluded precursor ions with single, unassigned, or ≥ seven charge states from the fragmentation selection.

Protein Identification and Label-Free Quantification

Protein identification was performed by submitting raw data files to Proteome Discoverer software (Thermo Scientific, USA, v. 1.2). The MS/MS searches were performed using the SEQUEST (v. 28) algorithm against a database constructed from the UniProt entries for *B. abortus* 104-M (taxonomy: 1210454), which contained 3,072 protein sequences. The search parameters included specific digestion with trypsin with up to two missed cleavages allowed; carbamidomethylation (C) on cysteine was set as a fixed modification; and oxidation (M) on methylene and acetyl (protein-N term) on asparagine & glutamine were applied as variable modifications. The initial allowed mass deviation of the precursor ion was set to 15 ppm, and the allowed value for the fragment mass was set to 0.02 Da. Protein identifications that contained at least two identified peptides were accepted with a false discovery rate (FDR) less than 1.0% (Zai et al., 2017).

For protein quantification, a label-free experiment was performed as previously described (Pettersen et al., 2016; Schmidt et al., 2016). Briefly, raw data were imported into Proteome Discover 1.4 following the MS analysis. Protein abundance of was calculated on the basis of label-free quantitation intensity [LFQ]. For comparison, the protein abundance in the control group was set as a reference and the protein abundance in the other eight stress groups were aligned. Proteins identified in at least two out of nine groups were considered for label-free quantification. Those proteins exhibiting fold change >1.5 (P-value ≤0.05) between the treatment and the control were deemed up-regulated or down-regulated respectively. The MS proteomics data have been deposited in the ProteomeXchange Consortium via the jPOSTrepo (Japan ProteOme STandard Repository) with the data set identifier PXD007548 (Vizcaino et al., 2014; Okuda et al., 2017).

Bioinformatics Analyses

The calculation of protein molecular masses, pI, and peptide grand average of hydropathicity (GRAVY) values were carried out using the ProtParam tool from the ExPASy toolbox (Gasteiger et al., 2003). Protein transmembrane helices were predicted using TMHMM 2.0 (Krogh et al., 2001). The protein functions were assigned by the Clusters of Orthologous Groups (COG) database (Galperin et al., 2015). The pathways of proteins were analyzed using the Kyoto Encyclopedia of Genes and Genomes (KEGG) database (Kanehisa et al., 2017). Possible interactions between identified proteins were tested using the STRING tool (Search Tool for the Retrieval of Interacting Genes/Proteins) (Szklarczyk et al., 2017). Heatmaps of the proteins were generated using the versatile matrix visualization and analysis software Morpheus, available from the Broad Institute.

Experimental Design and Statistical Rationale

The proteomes of bacteria grown under the nine groups were investigated. For each condition, two biological replicates and two technical replicates were sampled, resulting in a total of four samples per condition for LC-MS/MS. Protein identifications should contain at least two identified peptides with a FDR less than 1.0%. Significant label-free changes in proteins were determined using the statistical analysis-based variance (ANOVA) test, which was performed on the protein LFQ values. Additionally, principal coordinate analysis (PCoA) was used to visualize the correlations among the nine groups. The Pearson's *r* correlation coefficient between the nine groups was also visualized by means of a correlation matrix. The expression patterns of the proteins grown under the nine conditions were presented in a heatmap with hierarchical clustering performed using a Euclidean distance metric and the average linkage method (Pettersen et al., 2016).

RESULTS

Experimental Design

Brucella spp. are facultative intracellular bacteria. During the invasion of host tissue, *Brucella* are subjected to various harsh environmental conditions including nutrient limitation, low pH, antimicrobial defenses, and extreme levels of ROS (Roop et al., 2009; Barbier et al., 2011; Olsen and Palmer, 2014). Correspondingly, *Brucella* is well-equipped from both a physiological and metabolic perspective to adopt to environmental stresses (Roop et al., 2009). Analysis of the differential proteome expression patterns of *Brucella* under stress should improve our understanding regarding its adaptation and pathogenesis. Thus, we chose a multiple-environmental-stress strategy to reveal the global metabolic adaptations of *B. abortus* to intravacuolar environmental conditions. These conditions included: (i) a control condition (growth on TSB, condition #1); (ii) seven single-stress conditions: (conditions #2–8) and (iii) a multi-stress condition (#9, see **Table 1** for details). The multi-stress condition constituted a combination of each single-stress condition, and may more realistically simulate the conditions experienced by *Brucella* during infection of the host. We investigated the survival rate and differential protein expression of *B. abortus* in the single-stress and multi-stress conditions compared with the control condition (**Figure 1**). The survival rates of *B. abortus* under the different stress conditions ranged from 3.17 to 73.17%. Nutrient starvation, physical/chemical starvation, peroxide/NO starvation, and anaerobic starvation resulted in low survival rates (**Table 1**). The multi-stress condition resulted in the lowest survival rates, and may constitute a more accurate reflection of the *in vivo* conditions of *B. abortus* under intracellular infection.

Coverage of the *B. abortus* Proteome

The goal of this study was to achieve substantial coverage of the *B. abortus* proteome under *in vitro* stress conditions. Accordingly, we applied a proteomics approach on whole cell lysates prepared from *B. abortus* grown in the nine groups described above. LC-MS/MS analysis of the resulting peptide mixtures generated 1.1 million spectra. The acquired raw MS data files were then analyzed and the spectral files matched to 27,076 unique peptides with an FDR of 1.0%. We mapped the unique peptides to the *B. abortus* 104-M UniProt database (3,072 protein sequences), and only proteins that were identified by at least two unique peptides were confirmed (Zai et al., 2017). A total of 2,289 proteins were identified by two repeats, which represents approximately 74.5% coverage of the predicted proteome (**Figure 2A**). Proteins identified in at least two out of nine groups (2,272) were considered for label-free quantification (**Figure 2B**). The distribution of the identified proteins with respect to pI, molecular weight, hydrophobicity, and transmembrane regions was consistent with the annotated proteins (Figure S1). Among the 2,289 identified proteins, 1,570 were annotated in the COG database. Almost all of the pivotal categories for *Brucella* were identified, suggesting good coverage and representation of the genomic content of *B. abortus* by the proteome. Table S1 lists all identified proteins with their accession numbers and calculated score.

Quantification Analysis of Proteins under Environmental Stress

We used high-resolution MS to quantitatively describe the protein profiles of *B. abortus* under stress conditions, and compared them with the expressed proteome in the control. Protein quantification allowed the characterization of proteins that were differentially expressed across the nine groups. Here, we obtained LFQ intensities for 2,272 quantified proteins. Their quantitative levels covered a 5-$\log_{10}$ dynamic range. The density plot of the log2 ratio between the stress group and control group closely matched a normal distribution, which indicated that the experimental procedure was performed without systematic bias toward the different samples. PCoA analysis indicated good homogeneity of the biological replicates and was able to discriminate nine distinct protein populations (**Figure 3A**). The Pearson's correlation coefficient *r* varied between 0.95 and 0.99, indicating that there were differences in the protein levels between the different stress conditions (**Figure 3B**).

We next explored differences between the protein profiles of *B. abortus* under the various stress conditions. Hierarchical

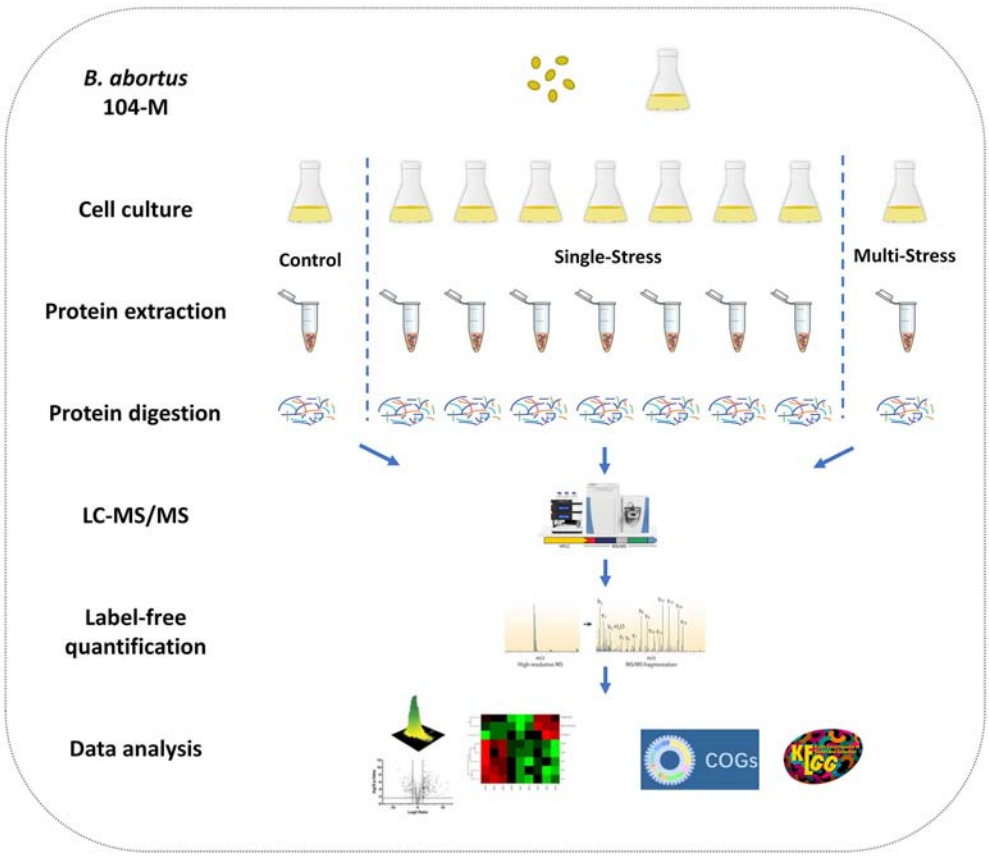

FIGURE 1 | Experimental design of the quantitative proteomics of *Brucella abortus* under environmental stress. A label-free relative quantitative proteomics approach was utilized to investigate and compare the global proteomic changes of *B. abortus* in response to a variety of distinct stresses including a control condition, seven single-stress conditions, and a multi-stress condition. Protein samples were prepared and proteolytic-digested using trypsin enzymes. Peptides were analyzed on a Q-Exactive HF MS coupled online with a nano-HPLC. The identified proteins were quantified using a label-free approach and further functionally analyzed using the COG and KEGG databases.

clustering was performed based on the LFQ intensities of the 2,272 proteins quantified in this study, and indicated distinguishable protein expression profiles between the nine different groups (**Figure 3C**). For each growth condition, a range of 1,967–2,109 proteins per group were identified (**Table 2**). About 87.6% of the detected proteins were common to all groups. Several of the identified proteins demonstrated a significant difference in abundance in stress compared to the control condition. The study identified DEPs in each stress condition whose quantitative levels varied by more than 1.5 fold from the respective LFQ intensity means in the control, i.e., 213, 413, 311, 451, 314, 357, 401, and 306 proteins in the eight stress conditions, respectively (Figure S2). Table S2 lists all the DEPs along with their accession numbers and LFQ intensities for each condition.

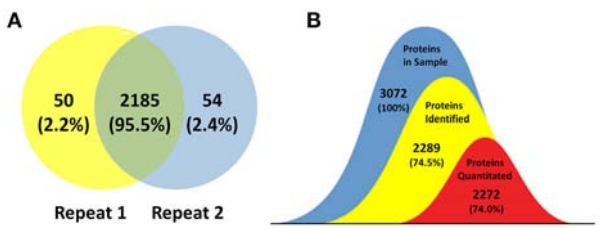

FIGURE 2 | Coverage of the *B. abortus* proteome by high-resolution mass spectrometry. **(A)** Venn plot of protein identification overlaps among two independent biological experiments. The number of proteins identified in the *B. abortus* proteome were 2,289, with 2,235 and 2,239 in the respective experiments. **(B)** The number of proteins identified in at least two out of nine groups and considered for label-free quantification was 2,272. The coverage of proteins identified and proteins quantitated in this study was 74.5 and 74%, respectively.

Metabolic Pathway Analysis of DEPs under Each Environmental Stress Condition

To understand the functional classification and metabolic pathways that were involved in the environmental stress response, the DEPs in each stress condition were functionally analyzed. All of the enriched KEGG pathways of *B. abortus* in response to each stress treatment are listed in **Table 3**. The results suggested that the metabolic adaptations of *B. abortus* to each environmental stress condition varied.

Brucella can persist for several weeks in the blood of an intraperitoneally-infected host (Vitry et al., 2014). Considering the role that serum stimulation has in intraperitoneally-infected

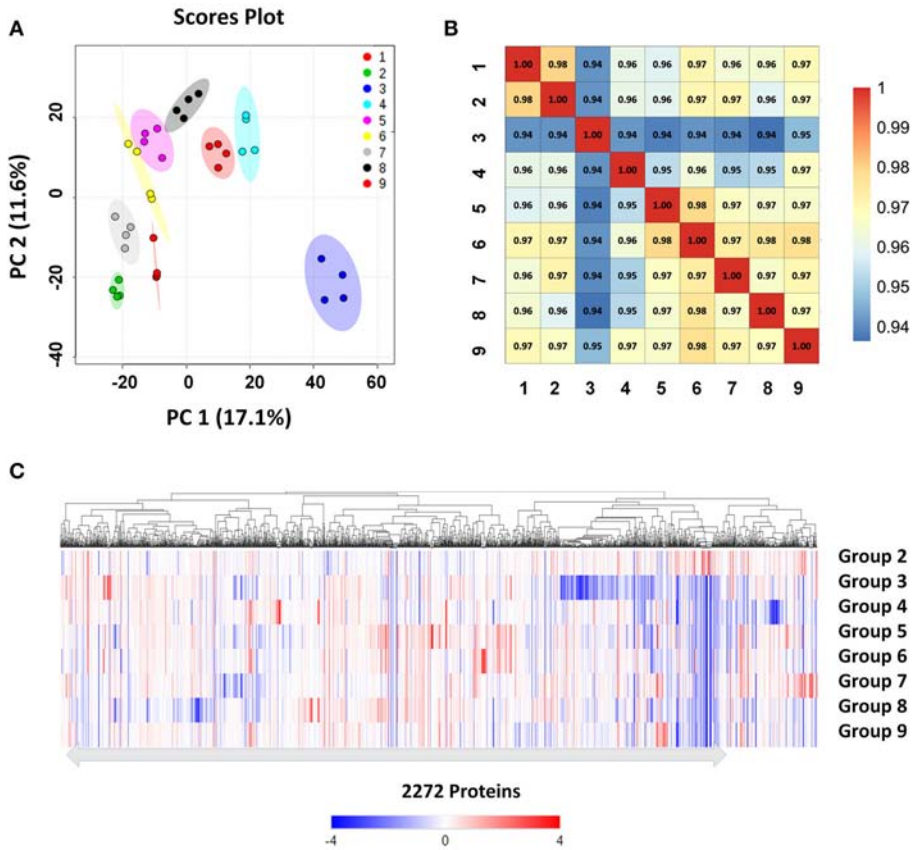

FIGURE 3 | Clustering and correlation of quantified proteins of *B. abortus* under environmental stress. **(A)** PCoA comparing the level of variance among the biological and technical replicates in the nine growth conditions for all the 2,272 proteins obtained after one-way ANOVA. Each dot represents an independent biological replicate. **(B)** Pearson's correlation coefficients of the protein intensities in all nine groups compared against each other. **(C)** Heatmap and hierarchical clustering of quantified proteins from cells under stress treatments. Hierarchical clustering was performed based on all quantified proteins. Relative protein expression under stress conditions was compared to the control condition.

hosts of *Brucella*, serum stress was chosen as single-stress condition #2. In this treatment, we discovered 125 and 88 up-regulated and down-regulated proteins, respectively, compared with the control. As shown in Figure S3A, the main enriched KEGG pathways for regulated proteins included biosynthesis of siderophore group non-ribosomal peptides, ABC transporters, synthesis and degradation of ketone bodies, thiamine metabolism, and two-component system. This suggests that *Brucella* may enhance its iron acquisition through the regulation of ABC transporters and biosynthesis of siderophores in order to adapt to the serum stress.

During the invasion of host tissue, a major hurdle in the infection of a host cell by *Brucella* is the lack of nutrients within the phagosome (Essenberg et al., 2002; Hanna et al., 2013; Barbier et al., 2017). Considering the role that nutrient starvation has in the intracellular replication of *Brucella*, nutrient stress was set as single-stress condition #3. Of the DEPs detected under this condition, 139 and 274 proteins were respectively up-regulated or down-regulated compared with the control. The primary enriched KEGG pathways for regulated proteins included two-component system, glycerophospholipid metabolism, ABC transporters, nitrogen metabolism, and porphyrin and chlorophyll metabolism (Figure S3B). This implies that *Brucella* may decrease its energy usage and secondary metabolite biosynthesis through the regulation of glycerophospholipid metabolism, nitrogen metabolism, and porphyrin and chlorophyll metabolism in response to nutrient starvation stress.

One major mechanism of *Brucella* pathogenesis is the capacity to survive in the acidic, high-temperature, hyperhaline, and high osmotic pressure environment inside macrophages (Detilleux et al., 1991; Liu et al., 2015). Given that physical/chemical stimulation influences the intracellular replication of *Brucella,* physical/chemical stress was set as single-stress condition #4. We discovered 120 and 191 up-regulated and down-regulated proteins present in the physical/chemical stress condition compared with the control. ABC transporters, thiamine metabolism, biosynthesis of siderophore group nonribosomal peptides, glycerophospholipid metabolism, and two-component system constituted the main enriched KEGG pathways (Figure S3C). *Brucella* may therefore decrease its energy usage and secondary metabolite biosynthesis through the regulation of

TABLE 2 | Overview of *B. abortus* proteins identified under environmental stress.

Group	Stress	Identified proteins	Unique A[a]	Unique B[b]	Common[c]	Up[d]	Down[e]
1	TSB (Control)	2,091	–	–	–	–	–
2	Serum stress	2,109	67	49	2,042	125	88
3	Nutrient starvation stress	1,967	49	173	1,918	139	274
4	Physical/chemical stress	2,001	46	136	1,955	120	191
5	Peroxide/NO stress	2,064	72	99	1,992	235	216
6	Oxygen deficiency stress	2,079	73	85	2,006	165	149
7	Iron-limited stress	2,085	68	74	2,017	169	188
8	Antibacterial stress	2,009	52	134	1,957	146	255
9	Multi-stress	2,046	58	103	1,988	116	190

[a] *Proteins unique to the stress condition.*
[b] *Proteins unique to the control.*
[c] *The common proteins identified in both the control and stress conditions.*
[d] *The up-regulated proteins under stress conditions.*
[e] *The down-regulated proteins under stress conditions.*

glycerophospholipid metabolism and thiamine metabolism in order to the physical/chemical stress.

The exogenous production of ROS such as O^{2-} and H_2O_2 by the host immune system has also been shown to be important for the survival of *Brucella* (Jimenez De Bagues et al., 2007). Nitric oxide produced by the macrophages were also crucial for phagocytes to control the intracellular replication of *Brucella* (Roop et al., 2009; Ronneau et al., 2016). Peroxide/nitric oxide stress was therefore set as single-stress condition #5. Of the DEPs detected in this treatment, 235 and 216 proteins were up-regulated or down-regulated respectively compared with the control. The main enriched KEGG pathways for regulated proteins included nitrogen metabolism, ABC transporters, biosynthesis of siderophore group nonribosomal peptides, thiamine metabolism, and two-component system (Figure S3D). The result suggests that *Brucella* may decrease its amino acid usage and secondary metabolite biosynthesis through the regulation of nitrogen metabolism and thiamine metabolism, meanwhile enhancing its iron acquisition through regulation of the two-component system and biosynthesis of siderophores in response to peroxide/NO stress.

The presence of oxygen has positive effects on the levels of proteins that are functional in aerobic respiration and purine metabolism, while low access to oxygen results in the induction of enzymes of mixed-acid fermentation and gluconate metabolism (James et al., 1995). Considering the role that oxygen deficiency plays in the intracellular replication of *Brucella,* oxygen deficiency stress was set as single-stress condition #6. In this treatment we discovered that 165 and 149 proteins were up-regulated or down-regulated respectively compared with the control. The main enriched KEGG pathways for the regulated proteins were two-component system, flagellar assembly, glycerophospholipid metabolism, quorum sensing, and ABC transporters (Figure S3E). Thus, *Brucella* may decrease its energy usage and virulence through the regulation of glycerophospholipid metabolism, two-component system, flagellar assembly and quorum sensing to manage oxygen deficiency stress.

Iron is an essential element for *Brucella* and is pivotal in host-pathogen interactions (Eskra et al., 2012; Roop, 2012). In the host, free iron levels are extremely low, resulting in iron limitation being a crucial stress (Braun, 2001). Iron-limitation stress was thus set as single-stress condition #7. We found that 169 and 188 proteins were respectively up-regulated or down-regulated in the iron-limited stress condition compared with the control. As indicated in Figure S3F, the main enriched KEGG pathways included oxidative phosphorylation, two-component system, biosynthesis of siderophore group nonribosomal peptides, nitrogen metabolism, and citrate cycle (TCA cycle). This result suggests that *Brucella* may decrease its energy usage through the regulation of oxidative phosphorylation, nitrogen metabolism and the TCA cycle, while enhancing its iron acquisition through the regulation of siderophore biosynthesis to adapt to the stress resulting from limited iron.

Antimicrobial peptides can limit the colonization of bacterial during infection in the innate defense, and therefore it is likely that *Brucella* encounters antimicrobial peptides within host microenvironments during infection (Martinez De Tejada et al., 1995). These peptides may be involved in environmental signaling that triggers changes in bacterial gene expression. Considering the role that antimicrobial peptide stimulation has in the intracellular replication of *Brucella*, antibacterial stress was set as single-stress condition #8. Of the DEPs in this treatment, 146 and 255 proteins were up-regulated or down-regulated respectively in comparison with the control. The main enriched KEGG pathways included two-component system, nitrogen metabolism, oxidative phosphorylation, biosynthesis of siderophore group nonribosomal peptides, and base excision repair (Figure S3G). This suggests that *Brucella* may decrease its energy usage through the regulation of oxidative phosphorylation and nitrogen metabolism, while enhancing its antimicrobial peptide resistance through regulation of the two-component system and base excision repair in response to antibacterial stress.

During the invasion of host tissue, *Brucella* experiences several stresses simultaneously, including nutrient limitation,

TABLE 3 | KEGG enrichment analysis of DEPs in response to each stress treatment.

Group	Stress	Pathway-ID	Description	Genes	*P*-value
2	Serum stress	ko01053	Biosynthesis of siderophore group nonribosomal peptides	5	0.0000683
		ko02010	ABC transporters	24	0.0056025
		ko00072	Synthesis and degradation of ketone bodies	3	0.0099555
		ko02040	Flagellar assembly	3	0.0099555
		ko00730	Thiamine metabolism	3	0.0608771
		ko02020	Two-component system	10	0.0702431
3	Nutrient starvation stress	ko02020	Two-component system	22	0.0061642
		ko00564	Glycerophospholipid metabolism	8	0.0065323
		ko02010	ABC transporters	44	0.0081475
		ko00910	Nitrogen metabolism	9	0.0120856
		ko00860	Porphyrin and chlorophyll metabolism	14	0.0258088
		ko01053	Biosynthesis of siderophore group nonribosomal peptides	4	0.0297269
		ko00790	Folate biosynthesis	7	0.0791646
		ko00072	Synthesis and degradation of ketone bodies	3	0.087634
4	Physical/chemical stress	ko02010	ABC transporters	35	0.000864
		ko00730	Thiamine metabolism	5	0.0065975
		ko01053	Biosynthesis of siderophore group nonribosomal peptides	4	0.0067706
		ko00564	Glycerophospholipid metabolism	6	0.0136601
		ko02020	Two-component system	15	0.0233687
		ko00072	Synthesis and degradation of ketone bodies	3	0.0297309
		ko00910	Nitrogen metabolism	6	0.0491114
5	Peroxide/nitric oxide stress	ko00910	Nitrogen metabolism	9	0.0041133
		ko02010	ABC transporters	38	0.0133396
		ko01053	Biosynthesis of siderophore group nonribosomal peptides	4	0.0170841
		ko00730	Thiamine metabolism	5	0.0196635
		ko02020	Two-component system	18	0.0242233
		ko00860	Porphyrin and chlorophyll metabolism	12	0.0415006
		ko00564	Glycerophospholipid metabolism	6	0.0440453
		ko01220	Degradation of aromatic compounds	5	0.0732277
6	Oxygen deficiency stress	ko02020	Two-component system	16	0.005989
		ko02040	Flagellar assembly	3	0.025681
		ko00564	Glycerophospholipid metabolism	5	0.0441204
		ko02024	Quorum sensing	15	0.0521694
		ko02010	ABC transporters	27	0.0600535
		ko00350	Tyrosine metabolism	4	0.0887595
		ko00920	Sulfur metabolism	5	0.0942084
7	Iron-limited stress	ko00190	Oxidative phosphorylation	29	1.32E-12
		ko02020	Two-component system	24	0.0000285
		ko01053	Biosynthesis of siderophore group nonribosomal peptides	6	0.0000445
		ko00910	Nitrogen metabolism	11	0.0000831
		ko00020	Citrate cycle (TCA cycle)	12	0.0005147
		ko01120	Microbial metabolism in diverse environments	43	0.0275001
		ko00072	Synthesis and degradation of ketone bodies	3	0.0502816
		ko00860	Porphyrin and chlorophyll metabolism	11	0.0627104
		ko00650	Butanoate metabolism	7	0.0673582
		ko02010	ABC transporters	33	0.0682408

(Continued)

TABLE 3 | Continued

Group	Stress	Pathway-ID	Description	Genes	*P*-value
8	Antibacterial stress	ko02020	Two-component system	24	0.0000861
		ko00910	Nitrogen metabolism	11	0.0001522
		ko00190	Oxidative phosphorylation	16	0.006429
		ko01053	Biosynthesis of siderophore group nonribosomal peptides	4	0.0173993
		ko03410	Base excision repair	5	0.0200875
		ko02010	ABC transporters	37	0.0246314
		ko01220	Degradation of aromatic compounds	5	0.0745956
		ko00130	Ubiquinone and other terpenoid-quinone biosynthesis	4	0.0879378
9	Multi-stress	ko02020	Two-component system	18	0.0019099
		ko00910	Nitrogen metabolism	8	0.0037586
		ko00730	Thiamine metabolism	5	0.007187
		ko01053	Biosynthesis of siderophore group nonribosomal peptides	4	0.0072753
		ko02010	ABC transporters	30	0.0313728
		ko03410	Base excision repair	4	0.0411957

low pH, antimicrobial defenses, and extreme ROS levels from the host immune response. Thus, the combination of stress conditions 2 to 8 was set as the multi-stress condition #9 that may better simulate the environments that *Brucella* may occur during host infection. We discovered that 116 and 190 proteins were respectively up-regulated or down-regulated in the multi-stress condition compared with the control. The primary enriched KEGG pathways included two-component system, nitrogen metabolism, thiamine metabolism, biosynthesis of siderophore group nonribosomal peptides, and ABC transporters (Figure S3H). *Brucella* may decrease its energy usage and secondary metabolite biosynthesis via the regulation of nitrogen metabolism and thiamine metabolism, while enhancing its iron acquisition and antimicrobial peptide resistance by regulating the two-component system and siderophore biosynthesis in order to cope with multiple stresses.

Compared with the single-stress condition, the enriched pathways of *B. abortus* in response to multi-stress conditions were more extensive and covered the primary enriched pathways of each single-stress condition. For example, the two-component system pathway enriched in the multi-stress condition was also enriched in all eight of the single-stress conditions, indicating its significance in the metabolic adaptation to multiple environmental stresses. The nitrogen metabolism pathway was enriched in the multi-stress condition and also in numerous single-stress conditions, including nutrient starvation stress, physical/chemical stress, peroxide/nitric oxide stress, iron-limited stress, and antibacterial stress. The DEPs included in this enriched pathway were similar in their regulatory patterns in both the single-stress and multi-stress treatments. The results suggested that the metabolic adaptations of *B. abortus* to multiple stresses constitute the synthesis of each environmental stress condition, and that the multiple stress treatment may better simulate the metabolic adaptations of *Brucella* during host infection.

Metabolic Pathway Analysis of DEPs under Various Stress Conditions

The functional analysis above indicated that *B. abortus* exhibited different metabolic adaptations to each environmental stress condition. To better understand the primary metabolic adaptations of *B. abortus* to various stress conditions, we summed all the DEPs in each stress condition, resulting in a total of 1,221 proteins that were differentially expressed in at least one stress condition compared with the control. The protein functions of all 1,221 DEPs in the eight stress conditions were assigned by the COG database. We identified 20 different COG phylogenetic protein groups (**Figure 4**), with the highest represented subsets in category E (amino acid transport and metabolism, 104 proteins), category K (transcription, 93 proteins), category C (energy production and conversion, 90 proteins), category P (inorganic ion transport and metabolism, 87 proteins), and category G (carbohydrate transport and metabolism, 63 proteins). Furthermore, 114 proteins were assigned only a putative function (category R), while 127 proteins remained without an allocated biological role (category S). The COG functional analysis suggested that energy usage-related categories (E, C, and G) and the iron acquisition-related category (P) were involved in the main metabolic adaptations of *B. abortus* to various stress conditions.

A putative protein-protein interaction network was then constructed from all high-confidence *B. abortus* protein interaction pairs that were matched with the 1,221 DEPs using the STRING tool (Szklarczyk et al., 2015). The KEGG pathway analysis showed a significant enrichment of DEPs (P-value $\leq$ 0.05). All 1,221 DEPs in the eight stress conditions were primarily enriched in oxidative phosphorylation, ABC transporters, two-component systems, biosynthesis of secondary metabolites, porphyrin and chlorophyll metabolism, glycerol phospholipid metabolism, the TCA cycle, thiamine metabolism, nitrogen metabolism, or were associated with carbon metabolism (**Figure 5**). The KEGG pathway analysis suggested that the

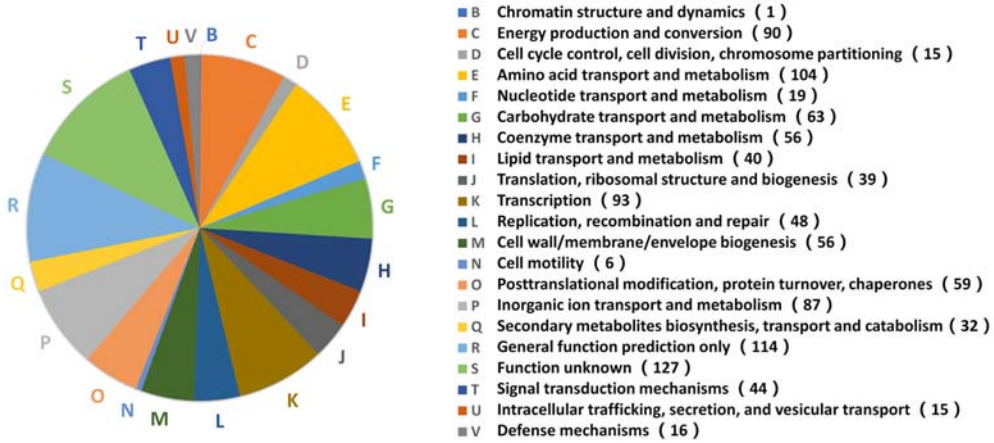

FIGURE 4 | Distribution of 1,221 DEPs in the stress treatments according to COG functions. A phylogenetic classification of DEPs in response to environmental stress was accomplished using the clusters of COGs. Letters displayed on the pie chart represent individual COGs with the numbers of proteins listed in brackets afterwards.

energy usage-related pathways and regulatory mechanism pathways constituted the primary pathways involved in the metabolic adaptation of *B. abortus* to various stress conditions. Table S3 lists the DEPs that were related to the main metabolic changes of *B. abortus* in response to stress treatments.

Main Metabolic Changes in Response to Environmental Stress

Oxidative phosphorylation is the process in which ATP is formed through using enzymes to oxidize nutrients (Dimroth et al., 2000). TCA cycle is a series of chemical reactions that produces ATP through the oxidation of acetyl-CoA. In this study, several proteins involved in oxidative phosphorylation and the TCA cycle, such as those associated with the NADH dehydrogenase (NDH) family, succinate dehydrogenase (SDH), and cytochrome *c* oxidase CcO, were abundantly down-regulated in response to both the single-stress and multiple-stress treatments (**Figures 6A,C**). A major hurdle in the infection of a host cell by *Brucella* is the lack of nutrients within the phagosome (Barbier et al., 2017). These results suggest that immediately after phagocytosis, *Brucella* reduces energy metabolism via the TCA cycle as the available extracellular nutrients decrease.

Two-component systems are adapted to respond to a wide variety of stress, including nutrients, quorum signals, antibiotics, temperature, pH, and so forth (Mascher et al., 2006). In this study, several proteins involved in two component system-controlled metabolic pathways, such as chromosomal replication initiator protein dnaA and nitrate reductase Nar, were decreased in abundance. Two-component system sensor histidine kinase PhoR/GlnL, hybrid sensor histidine kinase/response regulator ChvG, and transcriptional regulator RegB were up-regulated in response to several single-stress and multiple environmental stresses (**Figure 6B**). During the invasion of host tissue, *Brucella* must survive under several severe stresses through generating a suitable adaptive response to various signals (Viadas et al., 2010). Here, we found that the two-component system proteins were regulated in response to stress, which is essential for the persistence of *Brucella* within stressed environments in the host organism.

Cationic antimicrobial peptides (CAMPs) are crucial for the host defense against invasive bacterial infection (Alegado and Tan, 2008). The resistance of pathogenic bacteria toward antimicrobial peptides may also account for their virulence. In this study, several proteins involved in CAMPs resistance, such as the serine peptidase DegP and Hemolysin D (NL70_15120), were increased in abundance in our study. Transporter TolC and N-acetylmuramoyl-L-alanine amidase (NL70_04450) were down-regulated in response to several single environmental stresses, especially antibacterial stress (**Figure 6E**). These results indicated that the adopted mechanism of *Brucella* to resist host antimicrobials is important for persistent infection.

Siderophores are an important group of structurally diverse natural products that chelate iron and are important in the acquisition of the essential trace element iron by most microorganisms (Miethke and Marahiel, 2007). In the host, free iron levels are extremely low as the metal is largely bound to proteins. To overcome iron limitation, some bacteria and fungi produce siderophores. In this study, several proteins involved in the biosynthesis of siderophore group nonribosomal peptides, such as enterobactin biosynthetic enzymes EntA/B/E/F, were found to be up-regulated particularly in response to serum stress and iron-limitation stress (**Figure 6F**). These results indicated that *Brucella* has evolved strategies to overcome iron limitation and to compete with the iron sequestration immune mechanisms of the host.

We also observed specific variations in the amounts of multiple proteins involved in nitrogen metabolism, thiamine metabolism, and purine metabolism. In this study, nitrate reductase (Nar), nitrite reductase (NirK), and thiamine pyrophosphokinase (ThiN/E/G), which play essential roles in amino acid metabolism, and several enzymes participating in glycine, serine, and threonine metabolism, were relatively significantly differentially expressed in the different conditions (**Figure 6D**). Serine peptidase HtrA and heat shock protein

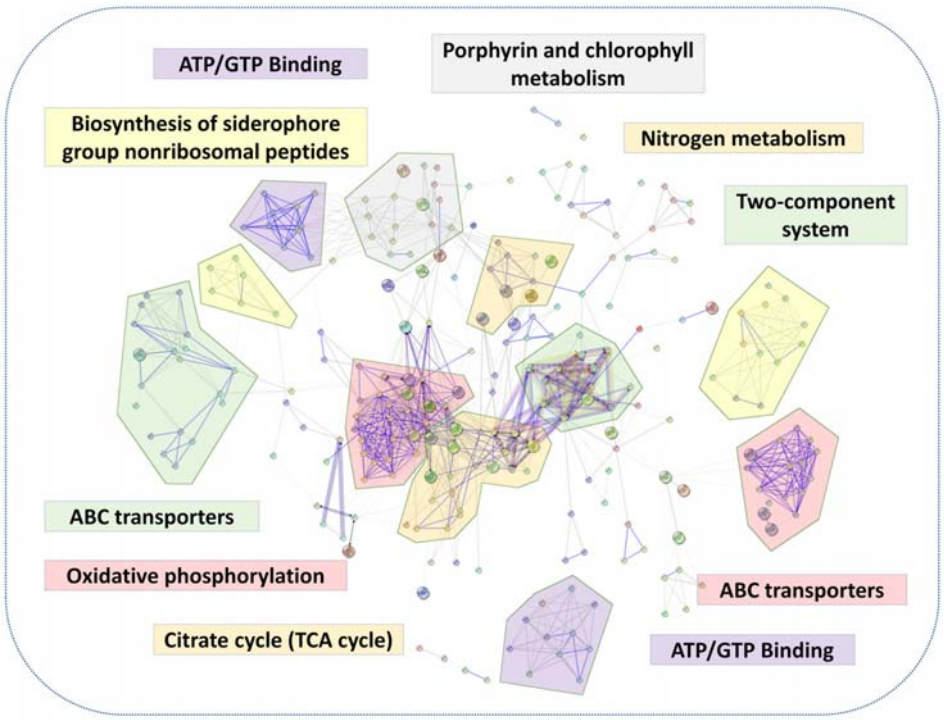

FIGURE 5 | The main metabolic changes of *B. abortus* in response to stress treatments. Possible interactions between DEPs under the stress treatments were tested using the STRING software tool. The network utilized *1st shell* that contained 442 nodes and 1,904 edges with confidence score (0.7). KEGG pathway analyses of DEPs indicated major metabolic adaptation mechanisms of *B. abortus* in response to multiple environmental stresses.

Hsp20 were observed to increase considerably under both the single-stress and multiple-stress treatments. The Cu-Zu superoxide dismutase SodC was found to increase during oxidative stress and multiple-stress treatments, but remained unchanged under the physical/chemical stress conditions of heat shock or acidic pH. Other proteins such as exopolyphosphatase (NL70_13665), ribonuclease H (RnhA), single-stranded DNA exonuclease (RecJ), and urea amidohydrolase (UreA/B/C) were also reduced in at least one of the stress conditions in our study.

DISCUSSION

The virulence of *Brucella* strains mainly depends on their capacity to survive and proliferate within host cells (Kohler et al., 2002). During the invasion of host tissue, *Brucella* is able to withstand the environmental stresses encountered and establish and maintain persistent intracellular residence (Roop et al., 2009). However, the mechanisms used by *Brucella* in intracellular infection are not fully understood. The aim of this work was to elucidate the regulatory processes of *Brucella* that enable survival under extreme stress by mirroring the possible living conditions of the bacteria in the host environment.

Multiple approaches have been used to investigate the proteomes of bacterial pathogens (Schmidt and Volker, 2011; Semanjski and Macek, 2016). Since bacteria are much smaller than mammalian host cells, the detection of bacterial proteins is difficult due to interference from the large excess of host proteins present. As a result of these challenges, the majority of bacterial proteomic datasets are still obtained from *in vitro* experiments (Cash, 2011). The main advantage of *in vitro* systems is the ability to implement a simple experimental design in a controlled manner using defined media and conditions. Although the *in vivo* approach in cultured cell lines reflects the conditions in infected hosts more closely than *in vitro* cultures, and reveals pathogenesis-related determinants present throughout the course of infection, it only partially describes the actual infection state due to the artificial conditions of the cell culture. Thus, *in vitro* approaches significantly contribute toward our understanding of the physiology of pathogenic bacteria and assist in identifying novel virulence factors that may represent potential biomarkers or drug targets. However, previous *in vitro* studies did not test the range of possible environment stresses that *Brucella* may be exposed to within the host. During the invasion of host tissue, *Brucella* is simultaneously subjected to a variety of harsh environments. Distinct environmental conditions can be simulated in *in vitro* models in which bacterial cultures are exposed to different *in vivo*-mimicking conditions similar to the cellular environment of the host. We therefore chose a multiple-environmental-stress strategy in order to reveal the global metabolic adaptations of *B. abortus* to intravacuolar environmental conditions.

We used a label-free proteomics approach to quantitatively elucidate the protein profiles of *B. abortus* under conditions of stress, and compared them with the expressed proteome in the control sample. The *in vitro* single-stress and multi-stress conditions simulated the *in vivo* conditions of *B. abortus*

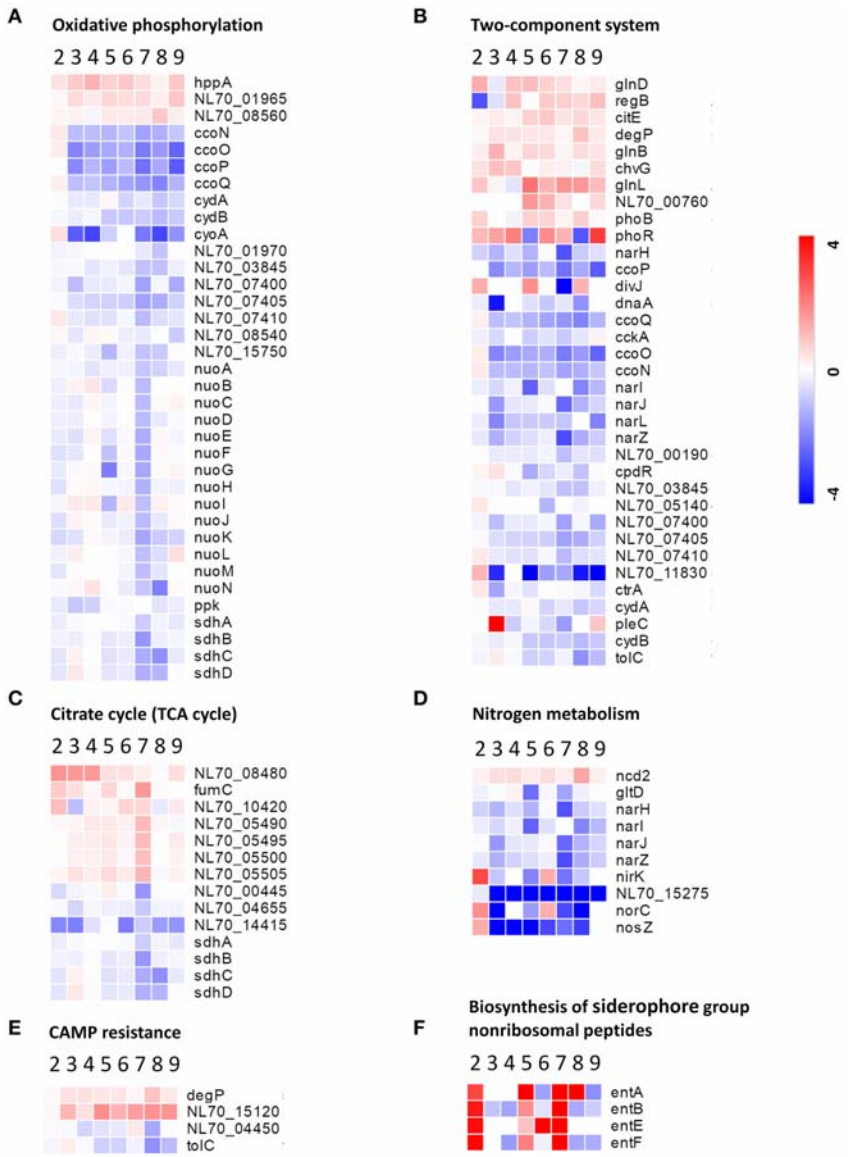

FIGURE 6 | Heatmap of DEPs related to the main metabolic changes of *B. abortus* in response to stress treatments. Fold change of proteins related to **(A)** oxidative phosphorylation, **(B)** two-component systems, **(C)** the citric acid cycle, **(D)** nitrogen metabolism, **(E)** cationic antimicrobial peptide resistance, and **(F)** biosynthesis of siderophore group nonribosomal peptides. The heatmap is shown in matrix format with rows representing the individual proteins and columns representing each stress condition. The red and blue colors reflect high and low fold changes, respectively.

under intracellular infection, with survival rates ranging from 3.17 to 73.17%. The results suggested that all of the single-stress conditions constituted harsh environments for *B. abortus*. The multi-stress condition resulted in the lowest survival rates, and may constitute a more accurate reflection of the *in vivo* conditions of *B. abortus* under intracellular infection. During the invasion of host tissue, *Brucella* is subjected to a harsh environment that results in the vast majority of the cells being killed within the macrophages (Di-Russo Case and Samuel, 2016). The *in vitro* stress treatments utilized in this study correspond well with the *in vivo* conditions of *Brucella* under intracellular infection.

The proteomic analysis identified and quantified a total of 2,272 proteins and 74% of the theoretical proteome, which has provided wide coverage of the *B. abortus* proteome. By replicating eight typical stress environments *in vitro,* we were able to investigate the influence of various stresses on the detected proteomes. The results indicated that there were different metabolic adaptations to different environmental stresses. The COG functional analysis of the 1,221 DEPs showed that energy usage-related categories (E, C, and G) and the iron acquisition-related category (P) were involved in the main metabolic adaptations of B. abortus to various stress conditions. While the KEGG pathway analyses revealed

that the majority of pathways were involved in oxidative phosphorylation, ABC transporters, two-component systems, biosynthesis of secondary metabolites, the citrate cycle, thiamine metabolism, and nitrogen metabolism; all representing major response mechanisms involved in the maintenance of cellular homeostasis and metabolic balance under stress. The multi-stress treatment was a combination of each single-stress, and may better reflect the metabolic response of *Brucella* under intracellular infection. Most of the regulated proteins in the multi-stress treatment were associated with oxidative phosphorylation, the citrate cycle, nitrogen metabolism, and biosynthesis of secondary metabolites, suggesting that *Brucella* may decrease the oxidation of nutrients, amino acid use and reduce secondary metabolite biosynthesis in order to adapt to the intracellular environment.

Teixeira-Gomes et al. (2000) studied the differences in protein synthesis patterns in *B. melitensis* 16M in response to heat, oxidative, and acidic pH stresses using a 2-D approach. The 19 resulting DEPs suggested that *B. melitensis* invoked an adaptive response to stress conditions. Al-Dahouk et al. characterized the proteome of *B. suis* at the late stage of *in vitro* infection, oxygen deficiency and long-term nutrient starvation using a 2-D approach, respectively (Al-Dahouk et al., 2008, 2009, 2013). The resulting 168, 37, and 30 DEPs indicated the regulatory mechanisms that reducing processes participating in energy, protein, and nucleic acid metabolism. Lamontagne et al. (2009) characterized the proteome of *B. abortus* strain 2308 and attenuated strain 19 that were infected into macrophages. The comparative analysis suggested that the *B. abortus* initially reduced the majority of biosynthesis and altered its respiration, but these adaptations were reversed later in the infection process.

Our observations are consistent with previous studies that suggest that *Brucella* may regulate its metabolism by decreasing its energy usage and secondary metabolite biosynthesis, while enhancing its iron acquisition and two-component system to cope with the intracellular environment (Kohler et al., 2002). In addition, we also discovered that some unique pathway categories and regulated genes play key roles in stress resistance, like thiamine metabolism and purine metabolism, thereby further elucidating the metabolic adaptation of *Brucella* to specific stressors. Furthermore, on comparison with the intracellular lifecycle of *Mycobacterium tuberculosis*, we discovered that the latter adapted to the intracellular environment by producing several key virulence factors which also appear on *Brucella* (Weiss and Schaible, 2015). For example, the virulence regulator PhoR in the two-component system plays a major role in *M. tuberculosis* pathogenicity and is also regulated in *Brucella* in response to stress (Ryndak et al., 2008; Broset et al., 2015). These findings may facilitate a better understanding of the metabolic adaptations of intracellular pathogens during their infection lifecycle.

The quantitative data obtained here are the most comprehensive to date that might capture the integral proteome profiling by *B. abortus* at a specific point in time. However, there may be some limitations regarding our experimental system. We used *in vitro* stress conditions to mimic the *in vivo* condition of *B. abortus* under intracellular infection by culturing the cells in a rich medium (TSB) until mid-log phase, and then transferring them to the stress treatments for 3 h. TSB is a standard culture medium that is routinely used as the control condition in proteomic analyses of *Brucella* under stress (Teixeira-Gomes et al., 2000). Compared with the extracellular lifecycle (represented here by culture on TSB), *Brucella* is subjected to severe nutrient limitation when invading the host tissue (represented by the treatments). Additionally, the selected 3 h treatment duration used constituted a short-term stress treatment that approximates the preliminary stage required for the survival of *Brucella* in the host cells (Lamontagne et al., 2009). We suspect that gradual metabolic changes may occur in *Brucella* after 3 h. However, we recommend that other conditions using different media and stress durations are tested in future research.

In conclusion, we have utilized a label-free relative quantitative proteomics approach to describe the protein profiles of *B. abortus* under different stress conditions. Under the multi-stress treatment, *B. abortus* experienced greater survival pressure in an environment that better imitates the intracellular environment of the host. Our results revealed differences in protein expression between the different stress treatments, providing new insight into the metabolic pathway of the response of *B. abortus* to multiple environmental stresses. Further studies into the proteins required for stress resistance under multiple environmental stresses are warranted to elucidate metabolic adaptation in *Brucella*. Continued efforts to elucidate the manner in which *Brucella* has adapted to its intracellular niche should provide valuable information for the discovery of novel therapeutic targets and effective vaccines in order to control brucellosis.

AUTHOR CONTRIBUTIONS

XZ, JX, and WC conceived and designed the experiments; XZ, QY, RL and LF performed the experiments; XZ, MQ and YY analyzed the data; YL, TZ and YY contributed to the reagents; XZ and JX wrote the paper. All authors read and approved the finalized manuscript.

FUNDING

This work was financially supported by the National Science and Technology Major Project of China (2013ZX09304101 and 2016ZX10004001). The funders had no role in the study design, data collection, interpretation, or decision-making in relation to submission for publication.

ACKNOWLEDGMENTS

We would like to thank Shanhu Li, Li Zhu, and Hengliang Wang at the Beijing Institute of Biotechnology for helpful discussions; and also thank Beijing BangFei Bioscience Co. Ltd. for technical assistance with the LC–MS/MS analysis.

SUPPLEMENTARY MATERIAL

The Supplementary Material for this article can be found online at: https://www.frontiersin.org/articles/10.3389/fmicb.2017.02347/full#supplementary-material

REFERENCES

Ahmed, W., Zheng, K., and Liu, Z. F. (2016). Establishment of chronic infection: brucella's stealth strategy. *Front. Cell. Infect. Microbiol.* 6:30. doi: 10.3389/fcimb.2016.00030

Akpinar, O. (2016). Historical perspective of brucellosis: a microbiological and epidemiological overview. *Infez. Med.* 24, 77–86.

Al-Dahouk, S., Jubier-Maurin, V., Neubauer, H., and Kohler, S. (2013). Quantitative analysis of the *Brucella suis* proteome reveals metabolic adaptation to long-term nutrient starvation. *BMC Microbiol.* 13:199. doi: 10.1186/1471-2180-13-199

Al-Dahouk, S., Jubier-Maurin, V., Scholz, H. C., Tomaso, H., Karges, W., Neubauer, H., et al. (2008). Quantitative analysis of the intramacrophagic *Brucella suis* proteome reveals metabolic adaptation to late stage of cellular infection. *Proteomics* 8, 3862–3870. doi: 10.1002/pmic.200800026

Al-Dahouk, S., Loisel-Meyer, S., Scholz, H. C., Tomaso, H., Kersten, M., Harder, A., et al. (2009). Proteomic analysis of *Brucella suis* under oxygen deficiency reveals flexibility in adaptive expression of various pathways. *Proteomics* 9, 3011–3021. doi: 10.1002/pmic.200800266

Alegado, R. A., and Tan, M. W. (2008). Resistance to antimicrobial peptides contributes to persistence of *Salmonella typhimurium* in the *C. elegans* intestine. *Cell Microbiol.* 10, 1259–1273. doi: 10.1111/j.1462-5822.2008.01124.x

Barbier, T., Nicolas, C., and Letesson, J. J. (2011). Brucella adaptation and survival at the crossroad of metabolism and virulence. *FEBS Lett.* 585, 2929–2934. doi: 10.1016/j.febslet.2011.08.011

Barbier, T., Zuniga-Ripa, A., Moussa, S., Plovier, H., Sternon, J. F., Lazaro-Anton, L., et al. (2017). Brucella central carbon metabolism: an update. *Crit. Rev. Microbiol*. doi: 10.1080/1040841X.2017.1332002. [Epub ahead of print].

Braun, V. (2001). Iron uptake mechanisms and their regulation in pathogenic bacteria. *Int. J. Med. Microbiol.* 291, 67–79. doi: 10.1078/1438-4221-00103

Broset, E., Martin, C., and Gonzalo-Asensio, J. (2015). Evolutionary landscape of the *Mycobacterium tuberculosis* complex from the viewpoint of PhoPR: implications for virulence regulation and application to vaccine development. *MBio* 6:e01289-15. doi: 10.1128/mBio.01289-15

Byndloss, M. X., and Tsolis, R. M. (2016). Brucella spp. virulence factors and immunity. *Annu. Rev. Anim. Biosci.* 4, 111–127. doi: 10.1146/annurev-animal-021815-111326

Cash, P. (2011). Investigating pathogen biology at the level of the proteome. *Proteomics* 11, 3190–3202. doi: 10.1002/pmic.201100029

Detilleux, P. G., Deyoe, B. L., and Cheville, N. F. (1991). Effect of endocytic and metabolic inhibitors on the internalization and intracellular growth of *Brucella abortus* in Vero cells. *Am. J. Vet. Res.* 52, 1658–1664.

Dimroth, P., Kaim, G., and Matthey, U. (2000). Crucial role of the membrane potential for ATP synthesis by F(1)F(o) ATP synthases. *J. Exp. Biol.* 203, 51–59.

Di-Russo Case, E., and Samuel, J. E. (2016). Contrasting lifestyles within the host cell. *Microbiol. Spectr.* 4:10.1128/microbiolspec.VMBF-0014-2015. doi: 10.1128/microbiolspec.VMBF-0014-2015

Doganay, G. D., and Doganay, M. (2013). Brucella as a potential agent of bioterrorism. *Recent Pat. Antiinfect. Drug Discov.* 8, 27–33. doi: 10.2174/1574891X11308010006

Eskra, L., Covert, J., Glasner, J., and Splitter, G. (2012). Differential expression of iron acquisition genes by *Brucella melitensis* and *Brucella canis* during macrophage infection. *PLoS ONE* 7:e31747. doi: 10.1371/journal.pone.0031747

Essenberg, R. C., Seshadri, R., Nelson, K., and Paulsen, I. (2002). Sugar metabolism by Brucellae. *Vet. Microbiol.* 90, 249–261. doi: 10.1016/S0378-1135(02)00212-2

Galperin, M. Y., Makarova, K. S., Wolf, Y. I., and Koonin, E. V. (2015). Expanded microbial genome coverage and improved protein family annotation in the COG database. *Nucleic Acids Res.* 43, D261–D269. doi: 10.1093/nar/gku1223

Gasteiger, E., Gattiker, A., Hoogland, C., Ivanyi, I., Appel, R. D., and Bairoch, A. (2003). ExPASy: the proteomics server for in-depth protein knowledge and analysis. *Nucleic Acids Res.* 31, 3784–3788. doi: 10.1093/nar/gkg563

Greco, T. M., and Cristea, I. M. (2017). Proteomics tracing the footsteps of infectious disease. *Mol. Cell. Proteomics* 16, S5–S14. doi: 10.1074/mcp.O116.066001

Hanna, N., Ouahrani-Bettache, S., Drake, K. L., Adams, L. G., Kohler, S., and Occhialini, A. (2013). Global Rsh-dependent transcription profile of Brucella suis during stringent response unravels adaptation to nutrient starvation and cross-talk with other stress responses. *BMC Genomics* 14:459. doi: 10.1186/1471-2164-14-459

Hasanjani Roushan, M. R., and Ebrahimpour, S. (2015). Human brucellosis: an overview. *Caspian J. Intern. Med.* 6, 46–47.

He, Y. (2012). Analyses of Brucella pathogenesis, host immunity, and vaccine targets using systems biology and bioinformatics. *Front. Cell. Infect. Microbiol.* 2:2. doi: 10.3389/fcimb.2012.00002

James, P. E., Grinberg, O. Y., Michaels, G., and Swartz, H. M. (1995). Intraphagosomal oxygen in stimulated macrophages. *J. Cell. Physiol.* 163, 241–247. doi: 10.1002/jcp.1041630204

Jimenez De Bagues, M. P., Loisel-Meyer, S., Liautard, J. P., and Jubier-Maurin, V. (2007). Different roles of the two high-oxygen-affinity terminal oxidases of *Brucella suis*: cytochrome c oxidase, but not ubiquinol oxidase, is required for persistence in mice. *Infect. Immun.* 75, 531–535. doi: 10.1128/IAI.01185-06

Kalayou, S., Granum, C., Berntsen, H. F., Groseth, P. K., Verhaegen, S., Connolly, L., et al. (2016). Label-free based quantitative proteomics analysis of primary neonatal porcine Leydig cells exposed to the persistent contaminant 3-methylsulfonyl-DDE. *J. Proteomics* 137, 68–82. doi: 10.1016/j.jprot.2015.12.007

Kanehisa, M., Furumichi, M., Tanabe, M., Sato, Y., and Morishima, K. (2017). KEGG: new perspectives on genomes, pathways, diseases and drugs. *Nucleic Acids Res.* 45, D353–D361. doi: 10.1093/nar/gkw1092

Kentache, T., Ben Abdelkrim, A., Jouenne, T., De, E., and Hardouin, J. (2017). Global dynamic proteome study of a pellicle-forming acinetobacter baumannii strain. *Mol. Cell. Proteomics* 16, 100–112. doi: 10.1074/mcp.M116.061044

Kohler, S., Foulongne, V., Ouahrani-Bettache, S., Bourg, G., Teyssier, J., Ramuz, M., et al. (2002). The analysis of the intramacrophagic virulome of Brucella suis deciphers the environment encountered by the pathogen inside the macrophage host cell. *Proc. Natl. Acad. Sci. U.S.A.* 99, 15711–15716. doi: 10.1073/pnas.232454299

Krogh, A., Larsson, B., Von Heijne, G., and Sonnhammer, E. L. (2001). Predicting transmembrane protein topology with a hidden Markov model: application to complete genomes. *J. Mol. Biol.* 305, 567–580. doi: 10.1006/jmbi.2000.4315

Lamontagne, J., Beland, M., Forest, A., Cote-Martin, A., Nassif, N., Tomaki, F., et al. (2010). Proteomics-based confirmation of protein expression and correction of annotation errors in the *Brucella abortus* genome. *BMC Genomics* 11:300. doi: 10.1186/1471-2164-11-300

Lamontagne, J., Forest, A., Marazzo, E., Denis, F., Butler, H., Michaud, J. F., et al. (2009). Intracellular adaptation of *Brucella abortus*. *J. Proteome Res.* 8, 1594–1609. doi: 10.1021/pr800978p

Liu, W., Dong, H., Li, J., Ou, Q., Lv, Y., Wang, X., et al. (2015). RNA-seq reveals the critical role of OtpR in regulating *Brucella melitensis* metabolism and virulence under acidic stress. *Sci. Rep.* 5:10864. doi: 10.1038/srep10864

Martinez De Tejada, G., Pizarro-Cerda, J., Moreno, E., and Moriyon, I. (1995). The outer membranes of Brucella spp. are resistant to bactericidal cationic peptides. *Infect. Immun.* 63, 3054–3061.

Mascher, T., Helmann, J. D., and Unden, G. (2006). Stimulus perception in bacterial signal-transducing histidine kinases. *Microbiol. Mol. Biol. Rev.* 70, 910–938. doi: 10.1128/MMBR.00020-06

Miethke, M., and Marahiel, M. A. (2007). Siderophore-based iron acquisition and pathogen control. *Microbiol. Mol. Biol. Rev.* 71, 413–451. doi: 10.1128/MMBR.00012-07

Okuda, S., Watanabe, Y., Moriya, Y., Kawano, S., Yamamoto, T., Matsumoto, M., et al. (2017). jPOSTrepo: an international standard data repository for proteomes. *Nucleic Acids Res.* 45, D1107–D1111. doi: 10.1093/nar/gkw1080

Olsen, S. C., and Palmer, M. V. (2014). Advancement of knowledge of Brucella over the past 50 years. *Vet. Pathol.* 51, 1076–1089. doi: 10.1177/0300985814540545

Pettersen, V. K., Mosevoll, K. A., Lindemann, P. C., and Wiker, H. G. (2016). Coordination of metabolism and virulence factors expression of extraintestinal pathogenic *Escherichia coli* purified from blood cultures of patients with sepsis. *Mol. Cell. Proteomics* 15, 2890–2907. doi: 10.1074/mcp.M116.060582

Ronneau, S., Moussa, S., Barbier, T., Conde-Alvarez, R., Zuniga-Ripa, A., Moriyon, I., et al. (2016). Brucella, nitrogen and virulence. *Crit. Rev. Microbiol.* 42, 507–525. doi: 10.3109/1040841X.2014.962480

Roop, R. M. II. (2012). Metal acquisition and virulence in Brucella. *Anim. Health Res. Rev.* 13, 10–20. doi: 10.1017/S1466252312000047

Roop, R. M. 2nd, Gaines, J. M., Anderson, E. S., Caswell, C. C., and Martin, D. W. (2009). Survival of the fittest: how Brucella strains adapt to their

intracellular niche in the host. *Med. Microbiol. Immunol.* 198, 221–238. doi: 10.1007/s00430-009-0123-8

Ryndak, M., Wang, S., and Smith, I. (2008). PhoP, a key player in *Mycobacterium tuberculosis* virulence. *Trends Microbiol.* 16, 528–534. doi: 10.1016/j.tim.2008.08.006

Scheltema, R. A., Hauschild, J. P., Lange, O., Hornburg, D., Denisov, E., Damoc, E., et al. (2014). The Q Exactive HF, a Benchtop mass spectrometer with a pre-filter, high-performance quadrupole and an ultra-high-field Orbitrap analyzer. *Mol. Cell. Proteomics* 13, 3698–3708. doi: 10.1074/mcp.M114.043489

Schmidt, A., Kochanowski, K., Vedelaar, S., Ahrne, E., Volkmer, B., Callipo, L., et al. (2016). The quantitative and condition-dependent *Escherichia coli* proteome. *Nat. Biotechnol.* 34, 104–110. doi: 10.1038/nbt.3418

Schmidt, F., and Volker, U. (2011). Proteome analysis of host-pathogen interactions: investigation of pathogen responses to the host cell environment. *Proteomics* 11, 3203–3211. doi: 10.1002/pmic.201100158

Semanjski, M., and Macek, B. (2016). Shotgun proteomics of bacterial pathogens: advances, challenges and clinical implications. *Expert Rev. Proteomics* 13, 139–156. doi: 10.1586/14789450.2016.1132168

Szklarczyk, D., Franceschini, A., Wyder, S., Forslund, K., Heller, D., Huerta-Cepas, J., et al. (2015). STRING v10: protein-protein interaction networks, integrated over the tree of life. *Nucleic Acids Res.* 43, D447–D452. doi: 10.1093/nar/gku1003

Szklarczyk, D., Morris, J. H., Cook, H., Kuhn, M., Wyder, S., Simonovic, M., et al. (2017). The STRING database in 2017: quality-controlled protein-protein association networks, made broadly accessible. *Nucleic Acids Res.* 45, D362–D368. doi: 10.1093/nar/gkw937

Teixeira-Gomes, A. P., Cloeckaert, A., and Zygmunt, M. S. (2000). Characterization of heat, oxidative, and acid stress responses in *Brucella melitensis*. *Infect. Immun.* 68, 2954–2961. doi: 10.1128/IAI.68.5.2954-2961.2000

Tutturen, A. E., Fleckenstein, B., and De Souza, G. A. (2014). Assessing the citrullinome in rheumatoid arthritis synovial fluid with and without enrichment of citrullinated peptides. *J. Proteome Res.* 13, 2867–2873. doi: 10.1021/pr500030x

Van Oudenhove, L., and Devreese, B. (2013). A review on recent developments in mass spectrometry instrumentation and quantitative tools advancing bacterial proteomics. *Appl. Microbiol. Biotechnol.* 97, 4749–4762. doi: 10.1007/s00253-013-4897-7

Viadas, C., Rodriguez, M. C., Sangari, F. J., Gorvel, J. P., Garcia-Lobo, J. M., and Lopez-Goni, I. (2010). Transcriptome analysis of the *Brucella abortus* BvrR/BvrS two-component regulatory system. *PLoS ONE* 5:e10216. doi: 10.1371/journal.pone.0010216

Vitry, M. A., Hanot Mambres, D., Deghelt, M., Hack, K., Machelart, A., Lhomme, F., et al. (2014). *Brucella melitensis* invades murine erythrocytes during infection. *Infect. Immun.* 82, 3927–3938. doi: 10.1128/IAI.01779-14

Vizcaino, J. A., Deutsch, E. W., Wang, R., Csordas, A., Reisinger, F., Rios, D., et al. (2014). ProteomeXchange provides globally coordinated proteomics data submission and dissemination. *Nat. Biotechnol.* 32, 223–226. doi: 10.1038/nbt.2839

Weiss, G., and Schaible, U. E. (2015). Macrophage defense mechanisms against intracellular bacteria. *Immunol. Rev.* 264, 182–203. doi: 10.1111/imr.12266

Yu, D., Hui, Y., Zai, X., Xu, J., Liang, L., Wang, B., et al. (2015). Comparative genomic analysis of *Brucella abortus* vaccine strain 104M reveals a set of candidate genes associated with its virulence attenuation. *Virulence* 6, 745–754. doi: 10.1080/21505594.2015.1038015

Zai, X., Yang, Q., Liu, K., Li, R., Qian, M., Zhao, T., et al. (2017). A comprehensive proteogenomic study of the human Brucella vaccine strain 104 M. *BMC Genomics* 18:402. doi: 10.1186/s12864-017-3800-9

Conflict of Interest Statement: The authors declare that the research was conducted in the absence of any commercial or financial relationships that could be construed as a potential conflict of interest.

frontiers in Microbiology

ORIGINAL RESEARCH
published: 11 January 2018
doi: 10.3389/fmicb.2017.02681

Ultrastructural Analysis of Cell Envelope and Accumulation of Lipid Inclusions in Clinical *Mycobacterium tuberculosis* Isolates from Sputum, Oxidative Stress, and Iron Deficiency

*Srinivasan Vijay[1,2], Hoang T. Hai[1], Do D. A. Thu[1], Errin Johnson[3], Anna Pielach[3], Nguyen H. Phu[4], Guy E. Thwaites[1,2] and Nguyen T. T. Thuong[1,2]**

[1] Oxford University Clinical Research Unit, Ho Chi Minh City, Vietnam, [2] Centre for Tropical Medicine and Global Health, Nuffield Department of Medicine, University of Oxford, Oxford, United Kingdom, [3] Sir William Dunn School of Pathology, University of Oxford, Oxford, United Kingdom, [4] Hospital for Tropical Diseases, Ho Chi Minh City, Vietnam

OPEN ACCESS

Edited by:
Daniela De Biase,
Sapienza Università di Roma, Italy

Reviewed by:
Etienne Dague,
Centre National de la Recherche Scientifique (CNRS), France
Gerald Larrouy-Maumus,
Imperial College London, United Kingdom
Marcos André Vannier-Santos,
Instituto Oswaldo Cruz, Fundação Oswaldo Cruz, Brazil

***Correspondence:**
Nguyen T. T. Thuong
thuongntt@oucru.org

Specialty section:
This article was submitted to Microbial Physiology and Metabolism, a section of the journal Frontiers in Microbiology

Received: 22 September 2017
Accepted: 22 December 2017
Published: 11 January 2018

Citation:
Vijay S, Hai HT, Thu DDA, Johnson E, Pielach A, Phu NH, Thwaites GE and Thuong NTT (2018) Ultrastructural Analysis of Cell Envelope and Accumulation of Lipid Inclusions in Clinical Mycobacterium tuberculosis Isolates from Sputum, Oxidative Stress, and Iron Deficiency. Front. Microbiol. 8:2681. doi: 10.3389/fmicb.2017.02681

Introduction: Mycobacteria have several unique cellular characteristics, such as multiple cell envelope layers, elongation at cell poles, asymmetric cell division, and accumulation of intracytoplasmic lipid inclusions, which contributes to their survival under stress conditions. However, the understanding of these characteristics in clinical *Mycobacterium tuberculosis* (*M. tuberculosis*) isolates and under host stress is limited. We previously reported the influence of host stress on the cell length distribution in a large set of clinical *M. tuberculosis* isolates (n = 158). Here, we investigate the influence of host stress on the cellular ultrastructure of few clinical *M. tuberculosis* isolates (n = 8) from that study. The purpose of this study is to further understand the influence of host stress on the cellular adaptations of clinical *M. tuberculosis* isolates.

Methods: We selected few *M. tuberculosis* isolates (n = 8) for analyzing the cellular ultrastructure *ex vivo* in sputum and under *in vitro* stress conditions by transmission electron microscopy. The cellular adaptations of *M. tuberculosis* in sputum were correlated with the ultrastructure of antibiotic sensitive and resistant isolates in liquid culture, under oxidative stress, iron deficiency, and exposure to isoniazid.

Results: In sputum, *M. tuberculosis* accumulated intracytoplasmic lipid inclusions. In liquid culture, clinical *M. tuberculosis* revealed isolate to isolate variation in the extent of intracytoplasmic lipid inclusions, which were absent in the laboratory strain H37Rv. Oxidative stress, iron deficiency, and exposure to isoniazid increased the accumulation of lipid inclusions and decreased the thickness of the cell envelope electron transparent layer in *M. tuberculosis* cells. Furthermore, intracytoplasmic compartments were observed in iron deficient cells.

Conclusion: Our ultrastructural analysis has revealed significant influence of host stress on the cellular adaptations in clinical *M. tuberculosis* isolates. These adaptations may contribute to the survival of *M. tuberculosis* under host and antibiotic stress conditions.

Variation in the cellular adaptations among clinical *M. tuberculosis* isolates may correlate with their ability to persist in tuberculosis patients during antibiotic treatment. These observations indicate the need for further analyzing these cellular adaptations in a large set of clinical *M. tuberculosis* isolates. This will help to determine the significance of these cellular adaptations in the tuberculosis treatment.

Keywords: *Mycobacterium tuberculosis*, ultrastructure, intracytoplasmic lipid inclusions, cell envelope, oxidative stress, iron deficiency and mesosome

INTRODUCTION

Mycobacterium tuberculosis (*M. tuberculosis*), causes tuberculosis (TB) and is a major public health problem (World Health Organization [WHO], 2015). The ability of *M. tuberculosis* cells to survive under host and antibiotic stress partly explains why *M. tuberculosis* is a successful human pathogen. Hence, cellular adaptations conferring stress tolerance in *M. tuberculosis* and in related species are an active area of research (Kieser and Rubin, 2014).

Investigations into cell biology of mycobacteria have revealed several unique characteristics in growth and division, which contributes to their survival under stress conditions (Thanky et al., 2007; Hett and Rubin, 2008; Kieser and Rubin, 2014). One such cellular structure is the complex cell envelope of mycobacteria (Brennan and Nikaido, 1995). Electron microscopy has revealed the ultrastructure of cell envelope layers in mycobacteria (Takade et al., 1983; Hoffmann et al., 2008; Zuber et al., 2008; Vijay et al., 2012). The cell envelope is essential for *M. tuberculosis* survival as it acts as a permeability barrier for the entry of antibiotics and also modulates host immune response (Jarlier and Nikaido, 1994; Briken et al., 2004; Torrelles and Schlesinger, 2010). Therefore, it is also an important drug and vaccine target (Chatterjee, 1997; Abrahams and Besra, 2016; Tima et al., 2017). The composition of cell envelope layers has been determined using cell envelope mutants (Etienne et al., 2002, 2005) and antibiotic treatments which inhibit the envelope synthesis in mycobacteria (Mdluli et al., 1998). These studies have advanced our understanding of the cell envelope role as a permeability barrier and in inhibiting phagocytosis of mycobacteria by macrophages (Mdluli et al., 1998; Etienne et al., 2002, 2005).

Another feature revealed by electron microscopy was the accumulation of intracytoplasmic lipid inclusions in mycobacteria under different host infection model systems (Peyron et al., 2008; Caire-Brandli et al., 2014; Barisch and Soldati, 2017a). In an *in vitro* human granuloma model of infection, *M. tuberculosis* cells accumulated lipid inclusions during infection of lipid loaded macrophages called foam cells (Peyron et al., 2008). Similarly, *M. avium* accumulated host-derived lipids as inclusions in foam cells and exhibited a thin cell envelope (Caire-Brandli et al., 2014). Recently, *M. marinum* was also found to have lipid inclusions derived from host lipids during the infection of *Dictyostelium* (Barisch and Soldati, 2017a). These studies have identified triacylglycerols as the major lipid in mycobacterial lipid inclusions derived from host cells (Peyron et al., 2008; Daniel et al., 2011; Caire-Brandli et al., 2014; Barisch and Soldati, 2017a). *M. tuberculosis* and *M. smegmatis* can also accumulate lipid inclusions containing triacylglycerols under *in vitro* stress conditions independent of host cells (Garton et al., 2002; Anuchin et al., 2009; Deb et al., 2009). Several studies have shown that *M. tuberculosis* uses diverse host carbon sources such as cholesterol, pyruvate, and glucose (Pandey and Sassetti, 2008; Marrero et al., 2013; Baker et al., 2014). Utilization of such diverse carbon sources by *M. tuberculosis* contributes to its pathogenesis and persistence in the host (Pandey and Sassetti, 2008; Marrero et al., 2013; Baker et al., 2014).

Importantly, the accumulation of lipid inclusions in *M. tuberculosis* was associated with persistence, antibiotic tolerance, cavitation, and poor treatment outcome (Deb et al., 2009; Russell et al., 2009; Daniel et al., 2011; Hammond et al., 2015; Kayigire et al., 2015; Sloan et al., 2015). It is possible that this is due to growth arrest of *M. tuberculosis* and loss of antimicrobial functions by foamy macrophages leading to persistent infection (Peyron et al., 2008; Daniel et al., 2011; Caire-Brandli et al., 2014). This phenomenon may lead to clinical complications, such as relapse of infection and the emergence of antibiotic-resistant *M. tuberculosis* (Cohen et al., 2013; Sebastian et al., 2017). Thus, intracytoplasmic lipid inclusions and the cell envelope are important for the survival of *M. tuberculosis*. The understanding of these cellular characteristics and their adaptations to stress in clinical *M. tuberculosis* isolates is limited. This understanding is vital for the development of novel therapeutic targets. In our previous study, we have observed that host stresses influenced cell length distribution in a large set (n = 158) of clinical *M. tuberculosis* isolates (Vijay et al., 2017). In this study we investigated the accumulation of lipid inclusions and cell envelope ultrastructure of *M. tuberculosis* in sputum by transmission electron microscopy (TEM). The ultrastructure of *M. tuberculosis* in sputum was compared with the ultrastructure of clinical *M. tuberculosis* isolates and H37Rv in liquid culture, and under conditions of oxidative stress, iron deficiency, and exposure to the antibiotic isoniazid.

MATERIALS AND METHODS

Bacterial Isolates

Six *M. tuberculosis* clinical isolates were selected from a collection of *M. tuberculosis* clinical isolates from pre-treated patients with pulmonary tuberculosis (n = 158) in Vietnam, along with the laboratory strain H37Rv. We selected three sensitive and three

TABLE 1 | *Mycobacterium tuberculosis* clinical strains selected for the study based on antibiotic sensitive and resistant phenotypes.

Strain name	Antibiotic resistance	*M. tuberculosis* lineages
C1	Sensitive	Indo-Oceanic
C2	STR, RIF	ND
C3	Sensitive	Indo-Oceanic
C4	STR	East Asian
C5	Sensitive	East Asian
C6	STR, RIF, INH, EMB	East Asian
H37Rv	Sensitive	Euro American

STR, streptomycin; RIF, rifampin; INH, isoniazid; EMB, ethambutol, ND, not determined.

antibiotic-resistant isolates as determined by drug susceptibility test for the electron microscopy analysis. **Table 1** presents drug sensitivity data.

Ethics Approval Statement

Between January 2015 and October 2016, patients were recruited from two district TB control units in Ho Chi Minh City (HCMC), Vietnam. The clinical *M. tuberculosis* isolates were collected from patients before treatment. The patients were ≥18 years of age, had clinical symptoms of active pulmonary TB, which was confirmed by chest X-ray and positive sputum culture, and none of the patients were HIV positive. Written informed consent was obtained from each patient in accordance with the declaration of Helsinki. Protocols were approved by the human subjects review committees, at the Hospital for Tropical Diseases HCMC, Vietnam (124/BVBNĐ.HĐĐĐ) and the Oxford Tropical Research Ethics Committee, United Kingdom (OxTREC Reference: 16-14).

Bacterial Culture

Mycobacterium tuberculosis isolates were cultured from sputum samples in bio safety level-3 laboratory and were stored as glycerol stocks in 7H9 media. These *M. tuberculosis* isolates were used for the experiments with a limited number of sub-culturing (approximately two to three passages) to avoid phenotypic/genotypic changes in clinical *M. tuberculosis* isolates. For mid-log culture, 50 ml culture tubes with 10 ml of 7H9T medium [7H9 broth supplemented with 10% oleic acid/albumin/dextrose/catalase (OADC) enrichment, and 0.05% Tween 80, BD Difco™] were inoculated with the clinical isolates and laboratory strain H37Rv, incubated at 37°C without shaking. The samples were processed for TEM at $O.D_{600}$ of 0.3–0.6.

Drug Susceptibility Test

Drug susceptibility was performed using BACTEC™ MGIT™ 960 SIRE Kit (BD), according to manufacturer guidelines. Drug susceptibility was tested for streptomycin (1.0 μg/ml), isoniazid (0.1 μg/ml), rifampicin (1.0 μg/ml), and ethambutol (5.0 μg/ml).

M. tuberculosis Lineage Identification

The lineages of the selected clinical *M. tuberculosis* isolates were determined in the previous study (Vijay et al., 2017).

Oxidative Stress, Iron Deficiency, and Isoniazid Treatment

For TEM analysis of *M. tuberculosis* cells under different stress conditions, *M. tuberculosis* culture in 7H9T medium at $O.D_{600}$ 0.3–0.5 was treated with H_2O_2 (Merk) at different concentrations, ranging from 21 to 210 mM for 48 h at 37°C and selected 21 mM H_2O_2-treated samples for electron microscopy (Voskuil et al., 2011). For iron deficiency, *M. tuberculosis* isolates were cultured in the presence of deferoxamine mesylate salt (DFO) (Sigma–Aldrich) at final concentrations of 100, 250, and 500 μM in 7H9T medium until the $O.D_{600}$ reached 0.3–0.5, with the 100 and 500 μM DFO-treated samples processed for electron microscopy (Pal et al., 2015). For isoniazid treatment, *M. tuberculosis* isolates were grown in the presence of isoniazid (Sigma–Aldrich) in 7H9T medium at a concentration of 0.015 μg/ml until the $O.D_{600}$ reached 0.3–0.5. All treated and untreated control isolates, along with about 500 μl of sputum with high density of acid fast bacilli (3+) as observed by microscopy from two pulmonary tuberculosis patients, were then processed for TEM.

Transmission Electron Microscopy

Mycobacterium tuberculosis cells were fixed as described previously (Vijay et al., 2012). *M. tuberculosis* cells were harvested by centrifugation and fixed in 1% (vol/vol) osmium tetroxide (Sigma–Aldrich) and 0.15 M sodium cacodylate buffer (pH 7.2) (Sigma–Aldrich) for 1 h at room temperature. After this samples were washed once with the same buffer, and post fixed for 2 h at room temperature in 0.15 M cacodylate buffer (pH 7.2) containing 2% (wt/vol) tannic acid and 2% (vol/vol) glutaraldehyde (both from Sigma–Aldrich). Samples were then washed once with 0.15 M cacodylate buffer and then refixed in 1% (vol/vol) osmium tetroxide overnight at 4°C and stored at 4°C for 2–4 weeks before further processing. Next the samples were washed with water and cells were re-suspended in 4% low melting point agarose, spun down, and stored at 4°C for few minutes. These samples were cut into small fragments of less than 1 mm^3 and stained with 0.5% uranyl acetate overnight and washed with water. Subsequent steps were performed using a Leica EM TP automated processing unit (Leica Microsystems). Samples were dehydrated in a graded series of ice cold ethanol (Merck) and then infiltrated with epoxy resin (Taab Low Viscosity Resin, Taab Laboratories) as follows: 25% resin in ethanol for 2 h, 50% resin for 3 h, 75% resin for 2 h, then 100% resin over 48 h with several changes of resin. Samples were polymerized in beem capsules at 60°C for 48 h. Ultrathin sections (90 nm) were obtained using a Leica UC7 Ultramicrotome and a Diatome Diamond Knife (Leica microsystems and Diatome). Sections were transferred to formvar coated 100 mesh Cu grids and post-stained with Reynolds' lead citrate (Reynolds, 1963). Sections were imaged on an FEI Tecnai 12 Transmission Electron Microscope operated at 120 kV using a Gatan OneView digital camera. In each condition approximately 100 *M. tuberculosis* cells per sample were observed, except sample S2 ($n = 10$ cells). Cell envelope layer measurements were carried out using ImageJ (Schneider et al., 2012).

RESULTS

M. tuberculosis in Sputum Displayed Triple Layered Cell Envelope and Accumulation of Intracytoplasmic Lipid Inclusions

Initially, we investigated *M. tuberculosis* cell envelope ultrastructure and lipid inclusions in pulmonary tuberculosis patient's sputum samples. The ultrastructure of these cells displayed a triple layered cell envelope which could be clearly distinguished as consisting of an electron dense outer layer (OL), electron transparent layer (ETL), and peptidoglycan layer (PGL) (**Figure 1**). *M. tuberculosis* cells in sputum were identified by the characteristic triple layered cell envelope of mycobacteria and distinguished from other bacteria present in the sputum (**Figures 1A–C**). *M. tuberculosis* cells revealed the accumulation of intracytoplasmic lipid inclusions in sputum sample S1 (**Figure 1A** and **Table 2**). The ETL of the cell envelope had an average thickness of 10.7 nm (±9 nm) in one of the patient sputum sample (S1) and 40 nm (±38 nm) in *M. tuberculosis* cells from another patient sputum sample (S2, **Figure 1B**). This revealed that *M. tuberculosis* cells in human hosts accumulate lipid inclusions and that envelope ultrastructure varies between hosts.

Strain-to-Strain Variation in Accumulation of Intracytoplasmic Lipid Inclusions among Clinical *M. tuberculosis* Isolates in Mid-Log Culture Condition

We analyzed the cellular ultrastructure of six clinical *M. tuberculosis* isolates (C1–C6) along with H37Rv under mid-log culture condition (**Figure 2A**). Major cellular ultrastructural features of *M. tuberculosis* isolates include the triple layered cell envelope, nucleoid, and cytoplasm. These features were similar in both sensitive (C1, C3, and C5) and resistant (C2, C4, and C6) *M. tuberculosis* isolates (**Figures 2A,B**). We also observed mild (**Figure 2A** and **Table 2**, C1, C2, C4, and C5) to extensive (**Figure 2A** and **Table 2**, C3) accumulation of cytoplasmic lipid inclusions in clinical *M. tuberculosis* isolates, but not in H37Rv and C6 (**Figure 2A** and **Table 2**). All *M. tuberculosis* isolates in mid-log condition had an ETL of average thickness 31.7 nm (±13.1 nm) (Supplementary Figure S1A). We also observed high variation in ETL thickness in the same cell and between different *M. tuberculosis* cells (Supplementary Figure S1A). Based on these *ex vivo* and *in vitro* ultrastructure of clinical *M. tuberculosis* isolates we further analyzed the cellular adaptations under different stress conditions.

Accumulation of Intracytoplasmic Lipid Inclusions Increased in Oxidative, Iron Deficiency, and Antibiotic Stresses

We observed *M. tuberculosis* cells with reduced acid fast staining and beaded appearance in sputum, oxidative stress, iron deficiency, and isoniazid treatment (**Figure 3**, $n \sim 100$–300 cells), and then we characterized the ultrastructure of *M. tuberculosis* under these conditions (**Figure 4**). H_2O_2 and isoniazid treatment resulted in a significant accumulation of intracytoplasmic lipid inclusions in clinical *M. tuberculosis* isolate C1 (**Figures 4A,B** and **Table 2**), but not in H37Rv and C4 (**Figures 4A,B** and **Table 2**). H37Rv and clinical *M. tuberculosis* isolates exposed to 100 μM DFO did not accumulate lipid inclusions (**Figure 4C** and **Table 2**) while all isolates treated with 500 μM DFO exhibited accumulation of lipid inclusions (**Figure 4C** and **Table 2**). Both H_2O_2 and DFO treatments also resulted in a thinner ETL, with thickness of 13 (±11 nm) and 10.5 nm (± 4 nm), respectively, in *M. tuberculosis* cell envelope as compared to untreated mid-log control (**Figure 4D** compared to **Figure 2B**, $P < 0.0001$ Mann–Whitney *U*-test; Supplementary Figures S1B,C). Similar to the observations in *M. tuberculosis* cells from sputum, different host and antibiotic stresses increased the accumulation of intracytoplasmic lipid inclusions and reduced the cell envelope ETL in *M. tuberculosis* isolates.

Unique Intracytoplasmic Compartment Observed in *M. tuberculosis* Cells under Iron Deficiency

In addition to the cellular adaptations observed above in different stress conditions, we also observed unique intracytoplasmic compartments in iron-deficient *M. tuberculosis* cells. This compartment was only observed in *M. tuberculosis* grown in the presence of 500 μM DFO and not in cells grown in 100 μM DFO and or the mid-log controls (**Figure 5**). Single intracytoplasmic compartments were observed in all three strains used in this experiment, H37Rv and clinical *M. tuberculosis* isolates (C1, C4), under iron deficiency (n = 50 cells observed in each strain) (**Figure 5A**). The average size of this compartment was 250 nm (±50 nm, n = 30 cells in total) (**Figure 5B**). At high magnification, we also observed membrane-like structure surrounding these intracytoplasmic compartments, some of which contained small circular units of diameter 17.4 nm (±3.6 nm) (**Figure 5C**).

DISCUSSION

We analyzed the lipid inclusions and cell envelope layers in clinical *M. tuberculosis* isolates *ex vivo* in sputum representing the host environment. We then compared this with the ultrastructure of clinical *M. tuberculosis* isolates and H37Rv in liquid culture and under different *in vitro* stress conditions. This revealed the accumulation of intracytoplasmic lipid inclusions in clinical *M. tuberculosis* isolates as a cellular adaptation in sputum, liquid culture, and under stress conditions. Analysis of six clinical *M. tuberculosis* isolates revealed isolate-to-isolate variation in the extent of lipid inclusions in mid-log culture and its increased accumulation under stress conditions. The thickness of *M. tuberculosis* cell envelope ETL was significantly reduced under different stress conditions. Formation of an intracytoplasmic compartment in *M. tuberculosis* cells was also observed under iron deficiency.

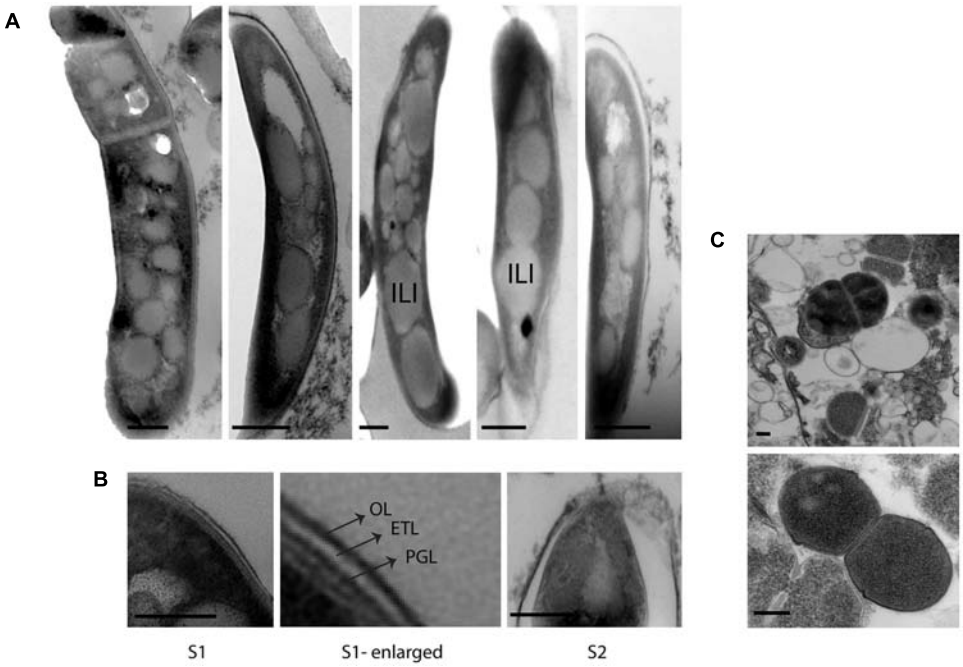

FIGURE 1 | Cellular ultrastructure of *M. tuberculosis* cells from patient sputum samples. **(A)** TEM images of *M. tuberculosis* cells with intracytoplasmic lipid inclusions in sputum sample S1. **(B)** TEM images of *M. tuberculosis* cells with detailed ultrastructure of cell envelope layers OL, ETL, and PGL from two different sputum samples S1 and S2. **(C)** TEM images of other bacterial cells in sputum sample S1. OL, outer layer; ETL, electron transparent layer; PGL, peptidoglycan layer; ILI, intracytoplasmic lipid inclusions; TEM, transmission electron microscopy. Scale bar = 200 nm.

Mycobacterium tuberculosis cells with lipid inclusions have been associated with foamy macrophages and unfavorable treatment outcome in tuberculosis patients (Garton et al., 2002; Peyron et al., 2008; Kayigire et al., 2015; Sloan et al., 2015). In the present study, clinical *M. tuberculosis* isolates displayed lipid inclusions even in liquid culture, which was not observed in the laboratory strain H37Rv. Similarly, *M. avium* and *M. marinum* also do not accumulate lipid inclusions in macrophages and the extracellular environment, respectively (Caire-Brandli et al., 2014; Barisch and Soldati, 2017a). This indicates that accumulation of lipid inclusions is a more prominent cellular adaptation in clinical *M. tuberculosis* isolates compared to laboratory strains of mycobacteria. Supporting this, we also observed increased accumulation of lipid inclusions under both oxidative stress and sub-inhibitory concentration of isoniazid only in clinical *M. tuberculosis* isolates. Isoniazid can also induce oxidative stress and may therefore link these findings (Timmins and Deretic, 2006). It will be interesting to study how other antibiotic treatments influences the accumulation of lipid inclusions in clinical *M. tuberculosis* isolates, as its accumulation may have a role in *M. tuberculosis* persistence to antibiotics (Hammond et al., 2015; Kayigire et al., 2015; Sloan et al., 2015).

TABLE 2 | Quantification of intracytoplasmic lipid inclusions (ILI) in *M. tuberculosis* isolates from the study ($n \sim 100$ cells in each isolate/condition, except S2, $n = 10$ cells).

Growth condition	**Sputum (*ex vivo*)**		**Mid-log (*in vitro*)**						
***Mtb* samples**	**S1**	**S2**	**Rv**	**C1**	**C2**	**C3**	**C4**	**C5**	**C6**
Average number of ILI per cell	4 (±2)	0	0	2 (±1)	2 (±1)	6 (±3)	4 (±1)	4 (±2)	0
Percentage of cells with ILI	90%	0%	0%	10%	5%	90%	80%	14%	0%
Average size of ILI (nm)	250 (±150)	NA	NA	65 (±25)	100 (±75)	250 (±150)	150 (±50)	120 (±40)	NA

Stress conditions	**H_2O_2**			**INH**		**DFO**				
***Mtb* samples**	**Rv-H**	**C1-H**	**C4-H**	**Rv-I**	**C1-I**	**Rv-D1**	**Rv-D2**	**C1-D1**	**C1-D2**	**C4-D2**
Average number of ILI per cell	2 (±1)	6 (±3)	4 (±2)	0	4 (±2)	0	5 (±3)	2 (±1)	14 (±7)	11 (±5)
Percentage of cells with ILI	1%	98%	50%	0%	55%	0	99%	15%	100%	100%
Average size of ILI (nm)	70 (±30)	250 (±130)	100 (±40)	NA	80 (±20)	NA	130 (±100)	70 (±50)	140 (±70)	170 (±120)

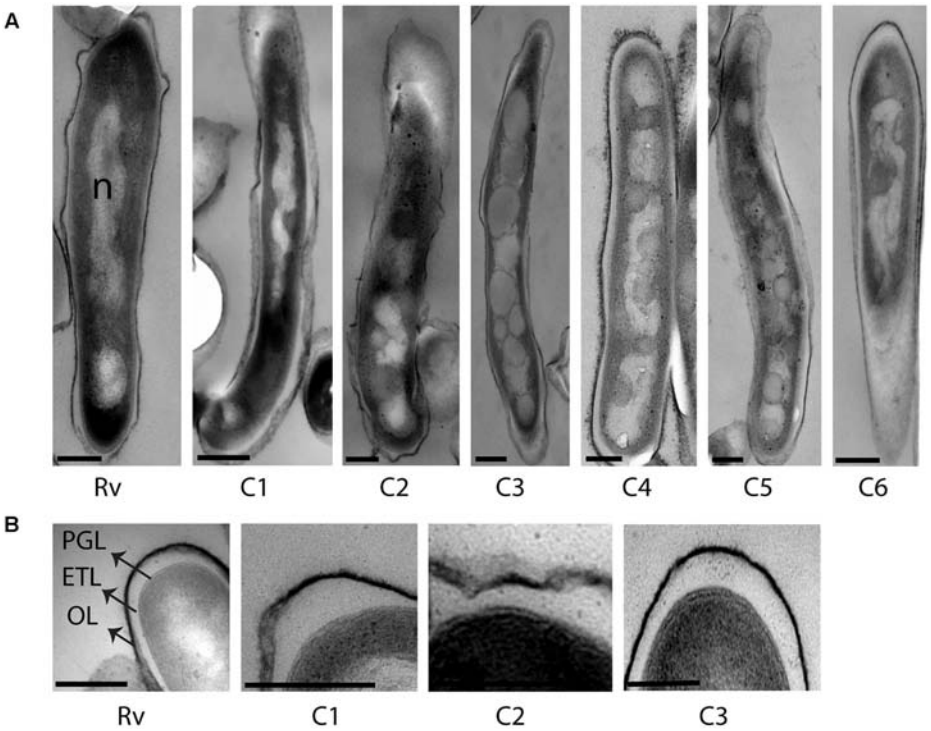

FIGURE 2 | Cellular ultrastructure of clinical *M. tuberculosis* strains under mid-log culture condition. **(A)** TEM images of H37Rv (Rv) and six clinical *M. tuberculosis* strains from mid-log culture (C1–C6). **(B)** TEM images of H37Rv and three clinical *M. tuberculosis* strains (C1–C3) with detailed ultrastructure of cell envelope layers in mid-log culture. OL, outer layer; ETL, electron transparent layer; PGL, peptidoglycan layer; ILI, intracytoplasmic lipid inclusions; n, nucleoid. Scale bar = 200 nm.

We observed increased accumulation of lipid inclusions in *M. tuberculosis* cells at 500 μM DFO compared to 100 μM DFO-treated cells under iron deficiency. DFO concentration-dependent accumulation of lipid inclusions were found in both clinical *M. tuberculosis* isolates and H37Rv. Supporting these observations it has also been reported that iron deficiency and oxidative stress can induce lipid accumulation in mycobacteria, which depends on host foamy macrophages (Bacon et al., 2007; Peyron et al., 2008). Host oxidative stress generates oxidized low-density lipoproteins, and oxygenated mycolic acids present in *M. tuberculosis*; both can trigger the differentiation of host macrophages into foamy cells (Peyron et al., 2008; Palanisamy et al., 2012). This in turn facilitates the accumulation of lipid inclusions in *M. tuberculosis* cells and provides a protective niche for its survival. Our host stress models were based on *in vitro* culture lacking foamy macrophages. Hence, accumulation of lipid inclusions in our host stress models in *M. tuberculosis* cells may have derived lipids from oleic acids present in the culture media, as seen in case of *M. smegmatis* (Garton et al., 2002; Anuchin et al., 2009).

Oxidative stress was also a co-factor in all of the stress conditions where we observed the increased accumulation of lipid inclusions in *M. tuberculosis* cells (Rodriguez and Smith, 2003; Timmins and Deretic, 2006). Transcriptional adaptation of *M. tuberculosis* in macrophages and under *in vitro* stress conditions strongly correlates with the ultrastructural adaptations observed here, indicating that under host stress *M. tuberculosis* shifts to a fatty acid-based metabolism (Schnappinger et al., 2003). Enzymes involved in fatty acid metabolism are also essential for *in vivo* growth and virulence (Munoz-Elias and McKinney, 2005; Reed et al., 2007). The accumulation of lipid inclusions is implicated in *M. tuberculosis* cell division arrest and induction of antibiotic tolerant dormant phenotype (Daniel et al., 2011; Caire-Brandli et al., 2014). This needs to be reinvestigated as our study shows that lipid inclusions *per se* may not inhibit cell division in *M. tuberculosis*. We observed *M. tuberculosis* cells with lipid inclusions growing in mid-log culture and under iron deficiency, similar to the growth observed in *M. marinum* with lipid inclusions (Barisch and Soldati, 2017a). It is possible that accumulation of lipids being a cellular adaptation that can facilitate *M. tuberculosis* entry into, and survival during dormancy (Barisch and Soldati, 2017b).

The unique triple layered cell envelope, reported in several laboratory mycobacterial strains and in clinical strains of *M. tuberculosis* (Takade et al., 1983; Brennan and Nikaido, 1995; Velayati et al., 2009; Vijay et al., 2012), was also observed in all of the clinical *M. tuberculosis* isolates in the present study. The ultrastructure of triple layered cell envelope from our study was also similar to the cell envelope ultrastructure of *M. tuberculosis* processed by cryofixation and rapid freeze substitution (Yamada et al., 2010, 2015). We also observed tearing of resin around *M. tuberculosis* cells in sputum, as observed in TEM images of *M. marinum* granulomas and *M. tuberculosis*

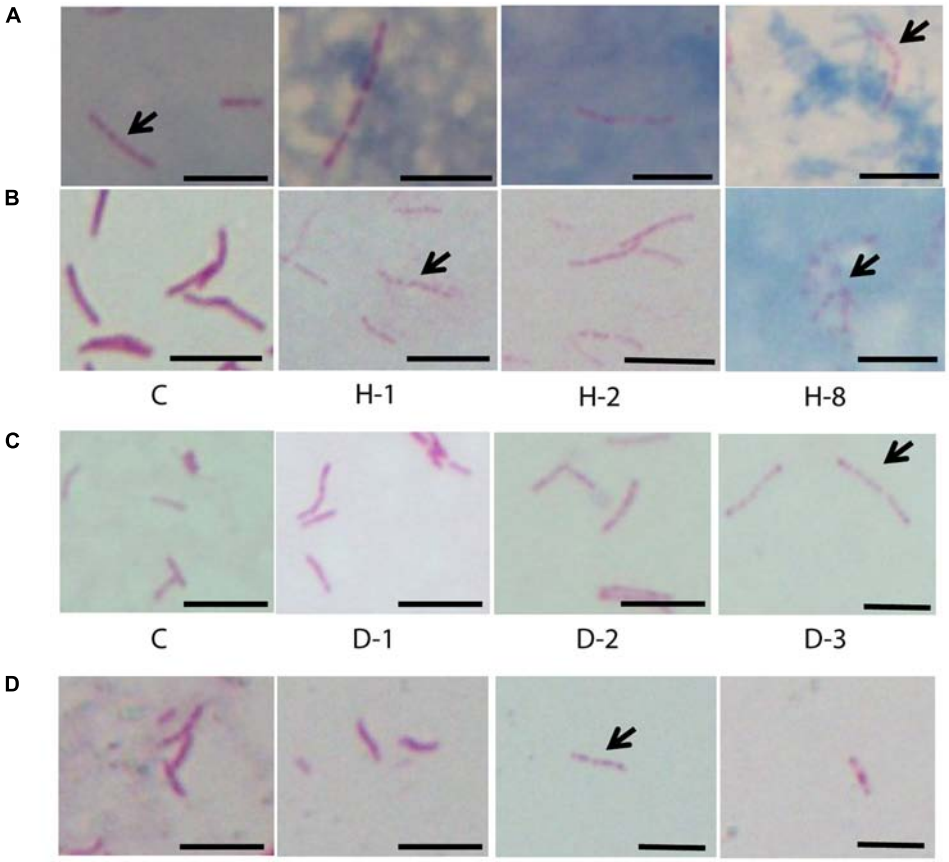

FIGURE 3 | Acid fast staining of *M. tuberculosis* cells in sputum, oxidative stress, iron deficiency, and isoniazid treatment. **(A)** Four sputum samples with *M. tuberculosis* cells ($n \sim 100$ cells). **(B)** Clinical *M. tuberculosis* strain treated with different concentrations of H_2O_2 for oxidative stress and **(C)** DFO for iron deficiency ($n = 300$ cells). **(D)** Clinical *M. tuberculosis* strains grown in the presence of isoniazid (0.015 μg/ml) ($n \sim 100$ cells). C, untreated control; H_2O_2 concentrations used are 21 (H-1), 42 (H-2), and 168 mM (H-8) and the concentrations of DFO are 100 (D-1), 250 (D-2), and 500 μM (D-3), arrow indicates beaded cells and scale bar = 5 μm.

cells (Bouley et al., 2001; Vijay et al., 2014). The thickness of the triple layers under mid-log growth conditions was consistent across the six clinical *M. tuberculosis* isolates and H37Rv used here. However, under stress conditions like sputum, oxidative stress, and iron deficiency, we observed a significant reduction in the thickness of cell envelope ETL, although the extent of this reduction varied between the two sputum samples despite a similar bacterial load. These findings suggest that the ETL can be reduced in thickness under host stress, which may vary from patient to patient. This needs to be investigated in a greater number of patients and correlated with aspects such as severity of tuberculosis symptoms and persistence to understand the clinical significance of such adaptations.

The ETL is mainly composed of lipids like mycolic acids (Mdluli et al., 1998; Wang et al., 2000) and transcriptional analysis of *M. tuberculosis* cells under host stress also indicate cell envelope remodeling and fatty acid degradation (Schnappinger et al., 2003). Cell envelope lipids are also involved in host immune modulation and virulence of *M. tuberculosis* strains (Karakousis et al., 2004; Makinoshima and Glickman, 2005). It has also been observed that under different stress conditions *M. tuberculosis* loses acid fastness due to loss of cell envelope lipids and it is associated with dormancy and antibiotic tolerance (Bhatt et al., 2007; Deb et al., 2009). We also observed reduced acid fast staining and *M. tuberculosis* cells with acid fast stained cytoplasmic beads in oxidative stress and iron deficiency. Such cells were also observed in some sputum samples and under isoniazid treatment, these observations strongly correlate with the ultrastructural adaptations such as reduced ETL and accumulation of lipid inclusions in our study. Further investigations are needed to understand the role of reduced cell envelope lipids on the accumulation of intracytoplasmic lipid inclusions in *M. tuberculosis*.

Reduction in the envelope lipids may enhance the permeability of cell envelope and influence the susceptibility of *M. tuberculosis* to antibiotics. Cell envelope modifications and enhanced antibiotic susceptibility in *M. smegmatis* have been observed under iron deficiency (Pal et al., 2015). Triacylglycerol is also a component of *M. tuberculosis* cell envelope and loss of acid fastness is observed under iron deficiency and in hypoxia (Rastogi et al., 2017). Such cell envelope modifications accompany non-replicative persistence and antibiotic tolerance of *M. tuberculosis*

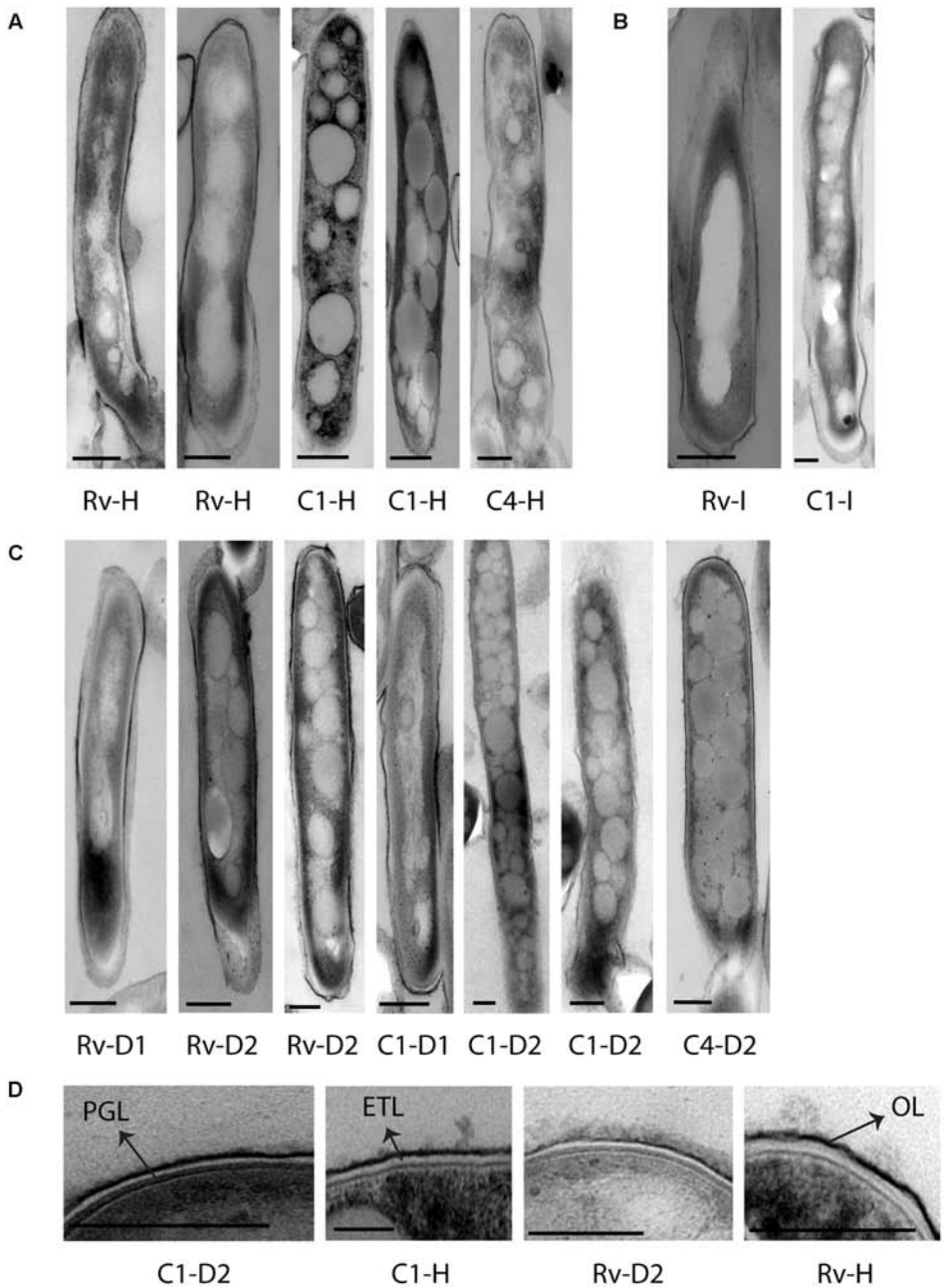

FIGURE 4 | Cellular ultrastructure of *M. tuberculosis* strains under H_2O_2, isoniazid treatment, and iron deficiency displaying accumulation of lipid inclusions and thin cell envelope ETL. **(A)** TEM images of H37Rv [Rv-H (two images)] and clinical *M. tuberculosis* strains [C1-H (two images) and C4-H] under H_2O_2 treatment. **(B)** TEM image of H37Rv and clinical *M. tuberculosis* strain grown under isoniazid treatment (Rv-I and C1-I). **(C,D)** TEM images of H37Rv and clinical *M. tuberculosis* strains grown under iron deficiency DFO-100 (Rv-D1, C1-D1) and 500 μM [Rv-D2 (two images), C1-D2 (two images) and C4-D2]. DFO, deferoxamine mesylate salt; OL, outer layer; ETL, electron transparent layer; PGL, peptidoglycan layer; scale bar = 200 nm.

in vitro (Rastogi et al., 2017). These observations indicate the influence of host factors on cellular adaptations in *M. tuberculosis* and antibiotic susceptibility. As there are multiple host factors and complex interactions influencing antibiotic susceptibility, this needs to be investigated further to identify the factors that can enhance susceptibility to antibiotics. There was significant variation in the accumulation of lipid inclusions in clinical *M. tuberculosis* isolates in mid-log culture. Such differences between *M. tuberculosis* isolates may have a clinical significance in persistence against host stress and antibiotics. Hence, variations in cellular adaptations need to be correlated with persistence and antibiotic tolerance among clinical *M. tuberculosis* isolates to understand its role in treatment failure.

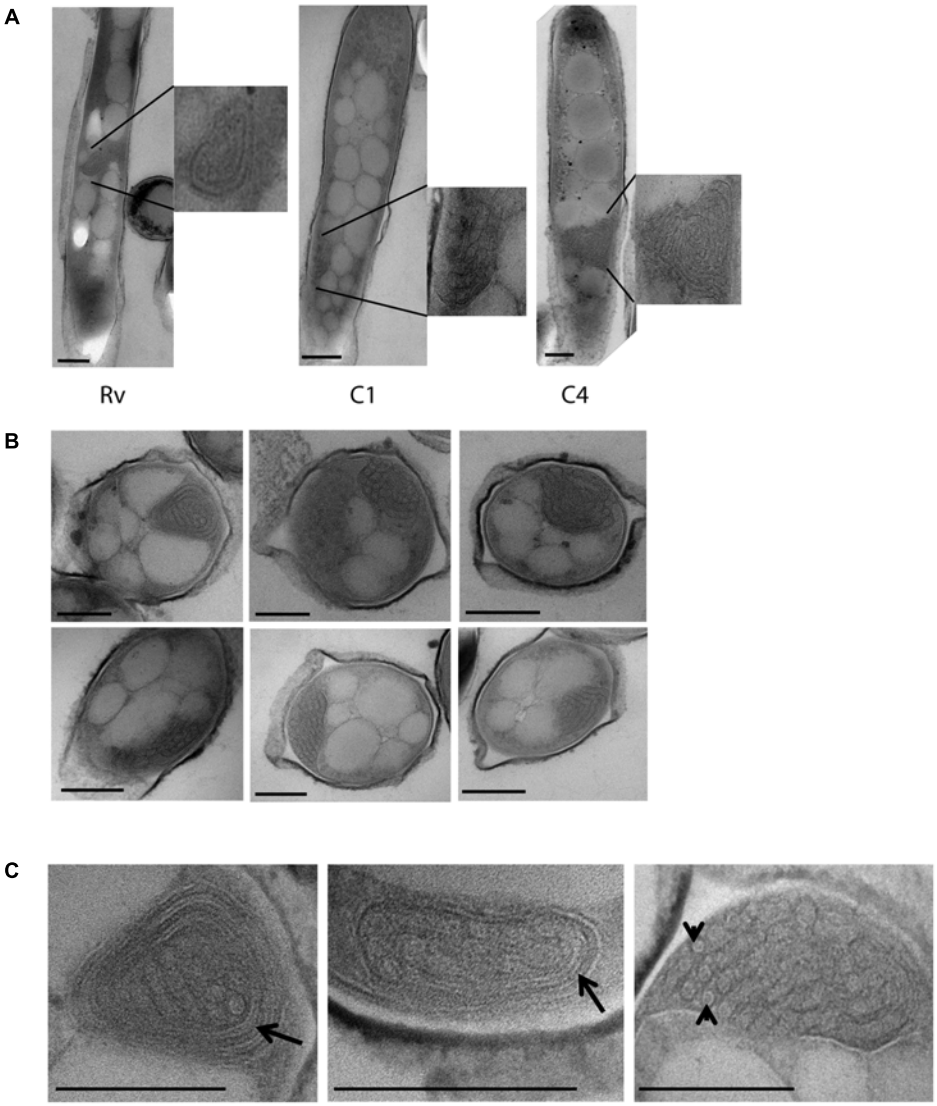

FIGURE 5 | Cytoplasmic compartments in *M. tuberculosis* strains under iron deficiency. **(A)** H37Rv (Rv) and clinical *M. tuberculosis* strains (C1, C4) grown under 500 μm DFO, displaying cytoplasmic compartments in cells along with enlarged images. **(B)** Multiple sections of *M. tuberculosis* cells grown under 500 μm DFO, with cytoplasmic compartment as indicated by asterisks. **(C)** Higher magnification images (40–50 K X) of cytoplasmic compartments from *M. tuberculosis* cells grown under 500 μm DFO, arrow indicates membrane-like structures surrounding the cytoplasmic compartment and arrowhead indicates subunits assembled inside the compartment. DFO, deferoxamine mesylate salt; scale bar = 200 nm.

Beijing lineage was shown to accumulate triacylglycerides and has triacylglyceride synthase gene (Rv 3130c) upregulated during *in vitro* growth (Reed et al., 2007). This gene is a member of DosR regulon, and some of the regulon genes are constitutively overexpressed in Beijing lineage (Domenech et al., 2017). DosR and WhiB3 have been shown to modulate lipid accumulation in *M. tuberculosis* (Singh et al., 2009), and also contribute to bacilli adaptation to hypoxia and redox stresses, respectively (Park et al., 2003; Saini et al., 2004; Singh et al., 2009). These proteins may play a role in the accumulation of lipid inclusions under oxidative stress and iron deficiency in clinical *M. tuberculosis* isolates. The mechanism of formation of lipid inclusions in mycobacteria also involves interactions with host lipid droplets and membrane phospholipids (Barisch and Soldati, 2017b). Thus, host stresses may induce significant cell biological adaptations in clinical *M. tuberculosis* isolates; its molecular mechanism needs to be further investigated.

In addition to reduction in the thickness of ETL and accumulation of lipid inclusions in *M. tuberculosis* cells, we also observed intracytoplasmic compartments under iron deficiency. These compartments were approximately 200 nm in size and were specifically observed in all *M. tuberculosis* isolates cultured under 500 μM DFO. It is possible that these compartments are mesosomes as observed in bacteria treated with antibiotics (Santhana Raj et al., 2007; Li et al., 2008). Studies have also shown the formation of intracellular compartments which accumulate

H_2O_2 under cellular damage (Ebersold et al., 1981; Li et al., 2008; Xin et al., 2014). Mesosomes and other such intracellular structures are considered as ultrastructural artifact induced under chemical fixation and dehydration process, and these are not observed under cryo-electron microscopy lacking such fixation (Pilhofer et al., 2010). In this study we have used primary fixation with osmium tetroxide for 1 h, and post-fixation with glutaraldehyde for 2 h. There is a possibility of such chemical fixation inducing the formation of intracellular structures, specifically under stress conditions. Cellular adaptations under iron deficiency may increase the probability of formation of such structures during chemical fixation, as we observed them only in *M. tuberculosis* cells under iron deficiency. In cryoelectron microscopy cells are imaged at frozen-hydrated state without chemical fixation or dehydration of cells and can avoid much of the fixation artifacts (Pilhofer et al., 2010). Cytoplasmic structure termed as stack has been reported in slow growing *Pseudomonas deceptionensis* M1 by TEM and also confirmed by cryo-electron microscopy (Delgado et al., 2013). If confirmed to be a true cellular structure by cryoelectron microscopy and specific for *M. tuberculosis* in iron deficiency. These compartments probably may have a role in iron storage.

Iron limitation has been a common host defense encountered by *M. tuberculosis*; hence, it has evolved mechanisms to sequester iron from the host by using siderophores like mycobactin (Rodriguez and Smith, 2003; Ratledge, 2004). Inside *M. tuberculosis* cells bacterioferritins BfrA and BfrB function as iron storage proteins. Recent observations have shown that BfrB can be encapsulated by the protein encapsulin to form nanocompartments *in vitro* (Reddy et al., 2012; Contreras et al., 2014). We observed arrangement of units with size ∼20 nm inside these intracytoplasmic compartments in *M. tuberculosis* cells, which is similar in size to the encapsulin observed *in vitro* (Contreras et al., 2014). These observations suggest that these intracytoplasmic compartments may be encapsulin-based nanocompartments in *M. tuberculosis*. They may be used to isolate excess of iron from generating oxidative cellular damage or a similar protective function under stress (Contreras et al., 2014). Iron storage has been essential for *M. tuberculosis* survival and virulence, hence has also been a potential novel drug target (Pandey and Rodriguez, 2012). It is important to investigate further the nature of these intracytoplasmic compartments in avirulent laboratory strains by cryo-electron microscopy and its role in *M. tuberculosis* survival under iron deficiency. Recent observations further implicate survival of *M. tuberculosis* in iron deficiency and accumulation of lipid inclusions to antibiotic tolerance and persistence (Baron et al., 2017; Kurthkoti et al., 2017).

In summary, we were able to demonstrate the major cellular adaptations of clinical *M. tuberculosis* isolates to host and antibiotic stress conditions. Further investigation of these cellular adaptations and their role in *M. tuberculosis* survival under stress is important. These will aide in our understanding of the ability of *M. tuberculosis* cells to persist during host and antibiotic stress. The variations in cellular response among clinical *M. tuberculosis* isolates may be associated with the persistence and treatment outcome among patients.

AUTHOR CONTRIBUTIONS

SV, NT, GT, NP, and EJ conceived and designed the experiments. SV, HH, and DT did the experiments. SV and AP did TEM analysis. SV, NT, GT, EJ, and AP analyzed and interpreted the data. SV, HH, DT, NP, NT, GT, AP, and EJ drafted and revised the manuscript and approved the final version.

FUNDING

This work was supported by the Wellcome Trust Training Fellowship in Public Health and Tropical Medicine (grant 097124/Z/11/Z to NT); the Wellcome Trust supporting the Major Overseas Program in Vietnam (grant 106680/Z/14/Z to GT).

ACKNOWLEDGMENTS

We acknowledge the work of staff from the District TB units in Districts 4 and 8, HCMC, particularly Drs. Pham Thi Thuy Lieu and Nguyen Van Thom, who initially diagnosed and studied the patients. We would like to thank all patients who participated in this study.

SUPPLEMENTARY MATERIAL

The Supplementary Material for this article can be found online at: https://www.frontiersin.org/articles/10.3389/fmicb.2017.02681/full#supplementary-material

REFERENCES

Abrahams, K. A., and Besra, G. S. (2016). Mycobacterial cell wall biosynthesis: a multifaceted antibiotic target. *Parasitology* doi: 10.1017/S0031182016002377 [Epub ahead of print].

Anuchin, A. M., Mulyukin, A. L., Suzina, N. E., Duda, V. I., El-Registan, G. I., and Kaprelyants, A. S. (2009). Dormant forms of *Mycobacterium smegmatis* with distinct morphology. *Microbiology* 155(Pt 4), 1071–1079. doi: 10.1099/mic.0.023028-0

Bacon, J., Dover, L. G., Hatch, K. A., Zhang, Y., Gomes, J. M., Kendall, S., et al. (2007). Lipid composition and transcriptional response of *Mycobacterium tuberculosis* grown under iron-limitation in continuous culture: identification of a novel wax ester. *Microbiology* 153(Pt 5), 1435–1444. doi: 10.1099/mic.0.2006/004317-0

Baker, J. J., Johnson, B. K., and Abramovitch, R. B. (2014). Slow growth of *Mycobacterium tuberculosis* at acidic pH is regulated by phoPR and host-associated carbon sources. *Mol. Microbiol.* 94, 56–69. doi: 10.1111/mmi.12688

Barisch, C., and Soldati, T. (2017a). *Mycobacterium marinum* degrades both triacylglycerols and phospholipids from its *Dictyostelium* host to synthesise its own triacylglycerols and generate lipid inclusions. *PLOS Pathog.* 13:e1006095. doi: 10.1371/journal.ppat.1006095

Barisch, C., and Soldati, T. (2017b). Breaking fat! How mycobacteria and other intracellular pathogens manipulate host lipid droplets. *Biochimie* 141, 54–61. doi: 10.1016/j.biochi.2017.06.001

Baron, V. O., Chen, M., Clark, S. O., Williams, A., Hammond, R. J. H., Dholakia, K., et al. (2017). Label-free optical vibrational spectroscopy to detect the metabolic state of *M. tuberculosis* cells at the site of disease. *Sci. Rep.* 7:9844. doi: 10.1038/s41598-017-10234-z

Bhatt, A., Fujiwara, N., Bhatt, K., Gurcha, S. S., Kremer, L., Chen, B., et al. (2007). Deletion of kasB in *Mycobacterium tuberculosis* causes loss of acid-fastness and subclinical latent tuberculosis in immunocompetent mice. *Proc. Natl. Acad. Sci. U.S.A.* 104, 5157–5162. doi: 10.1073/pnas.0608654104

Bouley, D. M., Ghori, N., Mercer, K. L., Falkow, S., and Ramakrishnan, L. (2001). Dynamic nature of host-pathogen interactions in *Mycobacterium marinum* granulomas. *Infect. Immun.* 69, 7820–7831. doi: 10.1128/IAI.69.12.7820-7831.2001

Brennan, P. J., and Nikaido, H. (1995). The envelope of mycobacteria. *Annu. Rev. Biochem.* 64, 29–63. doi: 10.1146/annurev.bi.64.070195.000333

Briken, V., Porcelli, S. A., Besra, G. S., and Kremer, L. (2004). Mycobacterial lipoarabinomannan and related lipoglycans: from biogenesis to modulation of the immune response. *Mol. Microbiol.* 53, 391–403. doi: 10.1111/j.1365-2958.2004.04183.x

Caire-Brandli, I., Papadopoulos, A., Malaga, W., Marais, D., Canaan, S., Thilo, L., et al. (2014). Reversible lipid accumulation and associated division arrest of *Mycobacterium avium* in lipoprotein-induced foamy macrophages may resemble key events during latency and reactivation of tuberculosis. *Infect. Immun.* 82, 476–490. doi: 10.1128/IAI.01196-13

Chatterjee, D. (1997). The mycobacterial cell wall: structure, biosynthesis and sites of drug action. *Curr. Opin. Chem. Biol* 1, 579–588. doi: 10.1016/S1367-5931(97)80055-5

Cohen, N. R., Lobritz, M. A., and Collins, J. J. (2013). Microbial persistence and the road to drug resistance. *Cell Host Microbe.* 13, 632–642. doi: 10.1016/j.chom.2013.05.009

Contreras, H., Joens, M. S., McMath, L. M., Le, V. P., Tullius, M. V., Kimmey, J. M., et al. (2014). Characterization of a *Mycobacterium tuberculosis* nanocompartment and its potential cargo proteins. *J. Biol. Chem.* 289, 18279–18289. doi: 10.1074/jbc.M114.570119

Daniel, J., Maamar, H., Deb, C., Sirakova, T. D., and Kolattukudy, P. E. (2011). Mycobacterium tuberculosis uses host triacylglycerol to accumulate lipid droplets and acquires a dormancy-like phenotype in lipid-loaded macrophages. *PLOS Pathog.* 7:e1002093. doi: 10.1371/journal.ppat.1002093

Deb, C., Lee, C. M., Dubey, V. S., Daniel, J., Abomoelak, B., Sirakova, T. D., et al. (2009). A novel *in vitro* multiple-stress dormancy model for *Mycobacterium tuberculosis* generates a lipid-loaded, drug-tolerant, dormant pathogen. *PLOS ONE* 4:e6077. doi: 10.1371/journal.pone.0006077

Delgado, L., Carrion, O., Martinez, G., Lopez-Iglesias, C., and Mercade, E. (2013). The stack: a new bacterial structure analyzed in the Antarctic bacterium *Pseudomonas deceptionensis* M1(T) by transmission electron microscopy and tomography. *PLOS ONE* 8:e73297. doi: 10.1371/journal.pone.0073297

Domenech, P., Zou, J., Averback, A., Syed, N., Curtis, D., Donato, S., et al. (2017). Unique regulation of the DosR regulon in the Beijing lineage of *Mycobacterium tuberculosis*. *J. Bacteriol* 199:e00696-16. doi: 10.1128/JB.00696-16

Ebersold, H. R., Cordier, J. L., and Luthy, P. (1981). Bacterial mesosomes: method dependent artifacts. *Arch. Microbiol.* 130, 19–22. doi: 10.1007/BF00527066

Etienne, G., Laval, F., Villeneuve, C., Dinadayala, P., Abouwarda, A., Zerbib, D., et al. (2005). The cell envelope structure and properties of *Mycobacterium smegmatis* mc2155: is there a clue for the unique transformability of the strain? *Microbiology* 151(Pt 6), 2075–2086.

Etienne, G., Villeneuve, C., Billman-Jacobe, H., Astarie-Dequeker, C., Dupont, M. A., and Daffe, M. (2002). The impact of the absence of glycopeptidolipids on the ultrastructure, cell surface and cell wall properties, and phagocytosis of *Mycobacterium smegmatis*. *Microbiology* 148(Pt 10), 3089–3100. doi: 10.1099/00221287-148-10-3089

Garton, N. J., Christensen, H., Minnikin, D. E., Adegbola, R. A., and Barer, M. R. (2002). Intracellular lipophilic inclusions of mycobacteria *in vitro* and in sputum. *Microbiology* 148(Pt 10), 2951–2958. doi: 10.1099/00221287-148-10-2951

Hammond, R. J., Baron, V. O., Oravcova, K., Lipworth, S., and Gillespie, S. H. (2015). Phenotypic resistance in mycobacteria: is it because I am old or fat that I resist you? *J. Antimicrob. Chemother.* 70, 2823–2827. doi: 10.1093/jac/dkv178

Hett, E. C., and Rubin, E. J. (2008). Bacterial growth and cell division: a mycobacterial perspective. *Microbiol. Mol. Biol. Rev.* 72, 126–156. doi: 10.1128/MMBR.00028-07

Hoffmann, C., Leis, A., Niederweis, M., Plitzko, J. M., and Engelhardt, H. (2008). Disclosure of the mycobacterial outer membrane: cryo-electron tomography and vitreous sections reveal the lipid bilayer structure. *Proc. Natl. Acad. Sci. U.S.A.* 105, 3963–3967. doi: 10.1073/pnas.0709530105

Jarlier, V., and Nikaido, H. (1994). Mycobacterial cell wall: structure and role in natural resistance to antibiotics. *FEMS Microbiol. Lett.* 123, 11–18. doi: 10.1111/j.1574-6968.1994.tb07194.x

Karakousis, P. C., Bishai, W. R., and Dorman, S. E. (2004). *Mycobacterium tuberculosis* cell envelope lipids and the host immune response. *Cell Microbiol.* 6, 105–116. doi: 10.1046/j.1462-5822.2003.00351.x

Kayigire, X. A., Friedrich, S. O., van der Merwe, L., Donald, P. R., and Diacon, A. H. (2015). Simultaneous staining of sputum smears for acid-fast and lipid-containing *Myobacterium tuberculosis* can enhance the clinical evaluation of antituberculosis treatments. *Tuberculosis* 95, 770–779. doi: 10.1016/j.tube.2015.08.001

Kieser, K. J., and Rubin, E. J. (2014). How sisters grow apart: mycobacterial growth and division. *Nat. Rev. Microbiol.* 12, 550–562. doi: 10.1038/nrmicro3299

Kurthkoti, K., Amin, H., Marakalala, M. J., Ghanny, S., Subbian, S., Sakatos, A., et al. (2017). The capacity of *Mycobacterium tuberculosis* to survive iron starvation might enable it to persist in iron-deprived microenvironments of human granulomas. *mBio* 8:e01092-17. doi: 10.1128/mBio.01092-17

Li, X., Feng, H. Q., Pang, X. Y., and Li, H. Y. (2008). Mesosome formation is accompanied by hydrogen peroxide accumulation in bacteria during the rifampicin effect. *Mol. Cell. Biochem.* 311, 241–247. doi: 10.1007/s11010-007-9690-4

Makinoshima, H., and Glickman, M. S. (2005). Regulation of *Mycobacterium tuberculosis* cell envelope composition and virulence by intramembrane proteolysis. *Nature* 436, 406–409. doi: 10.1038/nature03713

Marrero, J., Trujillo, C., Rhee, K. Y., and Ehrt, S. (2013). Glucose phosphorylation is required for *Mycobacterium tuberculosis* persistence in mice. *PLOS Pathog.* 9:e1003116. doi: 10.1371/journal.ppat.1003116

Mdluli, K., Swanson, J., Fischer, E., Lee, R. E., and Barry, C. E. III. (1998). Mechanisms involved in the intrinsic isoniazid resistance of *Mycobacterium avium*. *Mol. Microbiol.* 27, 1223–1233. doi: 10.1046/j.1365-2958.1998.00774.x

Munoz-Elias, E. J., and McKinney, J. D. (2005). *Mycobacterium tuberculosis* isocitrate lyases 1 and 2 are jointly required for *in vivo* growth and virulence. *Nat. Med.* 11, 638–644. doi: 10.1038/nm1252

Pal, R., Hameed, S., and Fatima, Z. (2015). Iron deprivation affects drug susceptibilities of mycobacteria targeting membrane integrity. *J. Pathog.* 2015:938523. doi: 10.1155/2015/938523

Palanisamy, G. S., Kirk, N. M., Ackart, D. F., Obregon-Henao, A., Shanley, C. A., Orme, I. M., et al. (2012). Uptake and accumulation of oxidized low-density lipoprotein during *Mycobacterium tuberculosis* infection in guinea pigs. *PLOS ONE* 7:e34148. doi: 10.1371/journal.pone.0034148

Pandey, A. K., and Sassetti, C. M. (2008). Mycobacterial persistence requires the utilization of host cholesterol. *Proc. Natl. Acad. Sci. U.S.A.* 105, 4376–4380. doi: 10.1073/pnas.0711159105

Pandey, R., and Rodriguez, G. M. (2012). A ferritin mutant of *Mycobacterium tuberculosis* is highly susceptible to killing by antibiotics and is unable to establish a chronic infection in mice. *Infect. Immun.* 80, 3650–3659. doi: 10.1128/IAI.00229-12

Park, H. D., Guinn, K. M., Harrell, M. I., Liao, R., Voskuil, M. I., Tompa, M., et al. (2003). Rv3133c/dosR is a transcription factor that mediates the hypoxic response of *Mycobacterium tuberculosis*. *Mol. Microbiol.* 48, 833–843. doi: 10.1046/j.1365-2958.2003.03474.x

Peyron, P., Vaubourgeix, J., Poquet, Y., Levillain, F., Botanch, C., Bardou, F., et al. (2008). Foamy macrophages from tuberculous patients' granulomas constitute a nutrient-rich reservoir for *M. tuberculosis* persistence. *PLOS Pathog.* 4:e1000204. doi: 10.1371/journal.ppat.1000204

Pilhofer, M., Ladinsky, M. S., McDowall, A. W., and Jensen, G. J. (2010). Bacterial TEM: new insights from cryo-microscopy. *Methods Cell Biol.* 96, 21–45. doi: 10.1016/S0091-679X(10)96002-0

Rastogi, S., Singh, A. K., Chandra, G., Kushwaha, P., Pant, G., Singh, K., et al. (2017). The diacylglycerol acyltransferase Rv3371 of *Mycobacterium tuberculosis* is required for growth arrest and involved in stress-induced cell wall alterations. *Tuberculosis* 104, 8–19. doi: 10.1016/j.tube.2017.02.001

Ratledge, C. (2004). Iron, mycobacteria and tuberculosis. *Tuberculosis* 84, 110–130. doi: 10.1016/j.tube.2003.08.012

Reddy, P. V., Puri, R. V., Khera, A., and Tyagi, A. K. (2012). Iron storage proteins are essential for the survival and pathogenesis of *Mycobacterium tuberculosis* in THP-1 macrophages and the guinea pig model of infection. *J. Bacteriol.* 194, 567–575. doi: 10.1128/JB.05553-11

Reed, M. B., Gagneux, S., Deriemer, K., Small, P. M., and Barry, C. E. III (2007). The W-Beijing lineage of *Mycobacterium tuberculosis* overproduces triglycerides and has the DosR dormancy regulon constitutively upregulated. *J. Bacteriol.* 189, 2583–2589. doi: 10.1128/JB.01670-06

Reynolds, E. S. (1963). The use of lead citrate at high pH as an electron-opaque stain in electron microscopy. *J. Cell Biol.* 17, 208–212. doi: 10.1083/jcb.17.1.208

Rodriguez, G. M., and Smith, I. (2003). Mechanisms of iron regulation in mycobacteria: role in physiology and virulence. *Mol. Microbiol.* 47, 1485–1494. doi: 10.1046/j.1365-2958.2003.03384.x

Russell, D. G., Cardona, P. J., Kim, M. J., Allain, S., and Altare, F. (2009). Foamy macrophages and the progression of the human tuberculosis granuloma. *Nat. Immunol.* 10, 943–948. doi: 10.1038/ni.1781

Saini, D. K., Malhotra, V., Dey, D., Pant, N., Das, T. K., and Tyagi, J. S. (2004). DevR-DevS is a bona fide two-component system of *Mycobacterium tuberculosis* that is hypoxia-responsive in the absence of the DNA-binding domain of DevR. *Microbiology* 150(Pt 4), 865–875. doi: 10.1099/mic.0.26218-0

Santhana Raj, L., Hing, H. L., Baharudin, O., Teh Hamidah, Z., Aida Suhana, R., Nor Asiha, C. P., et al. (2007). Mesosomes are a definite event in antibiotic-treated *Staphylococcus aureus* ATCC 25923. *Trop. Biomed.* 24, 105–109.

Schnappinger, D., Ehrt, S., Voskuil, M. I., Liu, Y., Mangan, J. A., Monahan, I. M., et al. (2003). Transcriptional adaptation of *Mycobacterium tuberculosis* within macrophages: insights into the phagosomal environment. *J. Exp. Med.* 198, 693–704. doi: 10.1084/jem.20030846

Schneider, C. A., Rasband, W. S., and Eliceiri, K. W. (2012). NIH Image to ImageJ: 25 years of image analysis. *Nat. Methods* 9, 671–675. doi: 10.1038/nmeth.2089

Sebastian, J., Swaminath, S., Nair, R. R., Jakkala, K., Pradhan, A., and Ajitkumar, P. (2017). *De novo* emergence of genetically resistant mutants of *Mycobacterium tuberculosis* from the persistence phase cells formed against antituberculosis drugs *in vitro*. *Antimicrob. Agents Chemother.* 61:e01343-16. doi: 10.1128/AAC.01343-16

Singh, A., Crossman, D. K., Mai, D., Guidry, L., Voskuil, M. I., Renfrow, M. B., et al. (2009). *Mycobacterium tuberculosis* WhiB3 maintains redox homeostasis by regulating virulence lipid anabolism to modulate macrophage response. *PLOS Pathog.* 5:e1000545. doi: 10.1371/journal.ppat.1000545

Sloan, D. J., Mwandumba, H. C., Garton, N. J., Khoo, S. H., Butterworth, A. E., Allain, T. J., et al. (2015). Pharmacodynamic modeling of bacillary elimination rates and detection of bacterial lipid bodies in sputum to predict and understand outcomes in treatment of pulmonary tuberculosis. *Clin. Infect. Dis.* 61, 1–8. doi: 10.1093/cid/civ195

Takade, A., Takeya, K., Taniguchi, H., and Mizuguchi, Y. (1983). Electron microscopic observations of cell division in *Mycobacterium vaccae* V1. *J. Gen. Microbiol.* 129, 2315–2320. doi: 10.1099/00221287-129-7-2315

Thanky, N. R., Young, D. B., and Robertson, B. D. (2007). Unusual features of the cell cycle in mycobacteria: polar-restricted growth and the snapping-model of cell division. *Tuberculosis* 87, 231–236. doi: 10.1016/j.tube.2006.10.004

Tima, H. G., Al Dulayymi, J. R., Denis, O., Lehebel, P., Baols, K. S., Mohammed, M. O., et al. (2017). Inflammatory properties and adjuvant potential of synthetic glycolipids homologous to mycolate esters of the cell wall of *Mycobacterium tuberculosis*. *J. Innate Immun.* 9, 162–180. doi: 10.1159/000450955

Timmins, G. S., and Deretic, V. (2006). Mechanisms of action of isoniazid. *Mol. Microbiol.* 62, 1220–1227. doi: 10.1111/j.1365-2958.2006.05467.x

Torrelles, J. B., and Schlesinger, L. S. (2010). Diversity in *Mycobacterium tuberculosis* mannosylated cell wall determinants impacts adaptation to the host. *Tuberculosis* 90, 84–93. doi: 10.1016/j.tube.2010.02.003

Velayati, A. A., Farnia, P., Ibrahim, T. A., Haroun, R. Z., Kuan, H. O., Ghanavi, J., et al. (2009). Differences in cell wall thickness between resistant and nonresistant strains of *Mycobacterium tuberculosis*: using transmission electron microscopy. *Chemotherapy* 55, 303–307. doi: 10.1159/000226425

Vijay, S., Anand, D., and Ajitkumar, P. (2012). Unveiling unusual features of formation of septal partition and constriction in mycobacteria–an ultrastructural study. *J. Bacteriol.* 194, 702–707. doi: 10.1128/JB.06184-11

Vijay, S., Nagaraja, M., Sebastian, J., and Ajitkumar, P. (2014). Asymmetric cell division in *Mycobacterium tuberculosis* and its unique features. *Arch. Microbiol.* 196, 157–168. doi: 10.1007/s00203-014-0953-7

Vijay, S., Vinh, D. N., Hai, H. T., Ha, V. T. N., Dung, V. T. M., Dinh, T. D., et al. (2017). Influence of stress and antibiotic resistance on cell-length distribution in *Mycobacterium tuberculosis* clinical isolates. *Front. Microbiol.* 8:2296. doi: 10.3389/fmicb.2017.02296

Voskuil, M. I., Bartek, I. L., Visconti, K., and Schoolnik, G. K. (2011). The response of mycobacterium tuberculosis to reactive oxygen and nitrogen species. *Front. Microbiol.* 2:105. doi: 10.3389/fmicb.2011.00105

Wang, L., Slayden, R. A., Barry, C. E. III, and Liu, J. (2000). Cell wall structure of a mutant of *Mycobacterium smegmatis* defective in the biosynthesis of mycolic acids. *J. Biol. Chem.* 275, 7224–7229. doi: 10.1074/jbc.275.10.7224

World Health Organization [WHO] (2015). *Global Tuberculosis Report 2015*. Geneva: World Health Organization.

Xin, L., Lipeng, Y., Jiaju, Q., Hanqing, F., Yunhong, L., Min, Z., et al. (2014). Revisiting the mesosome as a novel site of hydrogen peroxide accumulation in *Escherichia coli*. *Curr. Microbiol.* 69, 549–553. doi: 10.1007/s00284-014-0617-5

Yamada, H., Mitarai, S., Chikamatsu, K., Mizuno, K., and Yamaguchi, M. (2010). Novel freeze-substitution electron microscopy provides new aspects of virulent *Mycobacterium tuberculosis* with visualization of the outer membrane and satisfying biosafety requirements. *J. Microbiol. Methods* 80, 14–18. doi: 10.1016/j.mimet.2009.09.022

Yamada, H., Yamaguchi, M., Chikamatsu, K., Aono, A., and Mitarai, S. (2015). Structome analysis of virulent *Mycobacterium tuberculosis*, which survives with only 700 ribosomes per 0.1 fl of cytoplasm. *PLOS ONE* 10:e0117109. doi: 10.1371/journal.pone.0117109

Zuber, B., Chami, M., Houssin, C., Dubochet, J., Griffiths, G., and Daffe, M. (2008). Direct visualization of the outer membrane of mycobacteria and corynebacteria in their native state. *J. Bacteriol.* 190, 5672–5680. doi: 10.1128/JB.01919-07

Conflict of Interest Statement: The authors declare that the research was conducted in the absence of any commercial or financial relationships that could be construed as a potential conflict of interest.

frontiers in Microbiology

ORIGINAL RESEARCH
published: 05 April 2018
doi: 10.3389/fmicb.2018.00682

Genetic and Physiological Adaptations of Marine Bacterium *Pseudomonas stutzeri* 273 to Mercury Stress

Rikuan Zheng[1,2,3], *Shimei Wu*[4], *Ning Ma*[1,2,3] *and Chaomin Sun*[1,2]*

[1] Key Laboratory of Experimental Marine Biology, Institute of Oceanology, Chinese Academy of Sciences, Qingdao, China, [2] Laboratory for Marine Biology and Biotechnology, Qingdao National Laboratory for Marine Science and Technology, Qingdao, China, [3] College of Earth Sciences, University of Chinese Academy of Sciences, Beijing, China, [4] College of Life Sciences, Qingdao University, Qingdao, China

Mercury-mediated toxicity remains one of the greatest barriers against microbial survival, even though bacterial resistance to mercury compounds can occur. However, the genetic and physiological adaptations of bacteria to mercury stress still remains unclear. Here, we show that the marine bacterium *Pseudomonas stutzeri* 273 is resistant to 50 μM Hg^{2+} and removes up to 94% Hg^{2+} from culture. Using gene homologous recombination and complementation, we show that genes encoding Hg^{2+}-transport proteins MerT, MerP, the mercuric reductase MerA and the regulatory protein MerD are essential for bacterial mercuric resistance when challenged with Hg^{2+}. Further, mercury stress inhibits flagellar development, motility, chemotaxis and biofilm formation of *P. stutzeri* 273, which are verified by transcriptomic and physiological analyses. Surprisingly, we discover that MerF, a previously reported Hg^{2+}-transporter, determines flagellar development, motility and biofilm formation in *P. stutzeri* 273 by genetic and physiological analyses. Our results strongly indicate that MerF plays an integral role in *P. stutzeri* 273 to develop physiological responses to mercury stress. Notably, MerF homologs are also prevalent in different human pathogens. Using this unique target may provide novel strategies to control these pathogenic bacteria, given the role of MerF in flagella and biofilm formation. In summary, our data provide an original report on MerF in bacterial physiological development and suggest that the *mer* in marine bacteria has evolved through progressive, sequential recruitment of novel functions over time.

Keywords: marine, *Pseudomonas stutzeri*, mercury, stress, motility, flagella

OPEN ACCESS

Edited by:
Conor P. O'Byrne, National University of Ireland Galway, Ireland

Reviewed by:
Romé Voulhoux, UMR7255 Laboratoire d'Ingénierie des Systèmes Macromoléculaires (LISM), France
Calvin A. Henard, National Renewable Energy Laboratory (DOE), United States

***Correspondence:**
Chaomin Sun
sunchaomin@qdio.ac.cn

Specialty section:
This article was submitted to Microbial Physiology and Metabolism, a section of the journal Frontiers in Microbiology

Received: *01 February 2018*
Accepted: *22 March 2018*
Published: *05 April 2018*

Citation:
Zheng R, Wu S, Ma N and Sun C (2018) Genetic and Physiological Adaptations of Marine Bacterium Pseudomonas stutzeri 273 to Mercury Stress. Front. Microbiol. 9:682. doi: 10.3389/fmicb.2018.00682

INTRODUCTION

Mercury, as one of the most toxic heavy metals naturally present in the earth, endangers the environment and causes a variety of diseases in humans and animals (Dash and Das, 2012). Specifically, exposure to mercury stress can dramatically decrease reproduction like fertilization capability, hatchability, viability and sperm motility (Dietrich et al., 2010). In the aquatic environment including the ocean, increasing evidence indicates that sublethal mercury pollution may cause a long-term decline and eventual extinction of species by adversely affecting fertilization and limiting propagation of a species (Kime, 1995).

Since mercury is ubiquitous in the earth, microorganisms inevitably encounter this heavy metal in their natural environment (Singh et al., 2014). Responding to environmental changes is a fundamental property of unicellular organisms who directly interact with an ever-changing microenvironment (Singh et al., 2014). Mercuric effects on live microorganisms impact their physiology (Dietrich et al., 2010). Through evolution, motility and chemotaxis are remarkably evolved features of bacterial physiology and strengthen bacterial adaptive capabilities to mercuric stress (Gadd, 2010). Chemotaxis of a bacterium toward metal stress largely depends on its physiological capability to utilize or resist the metallic environment or bacterial swarming powered by rotating helical flagella, a universal movement patterns (Kearns, 2010). In addition, bacteria within a developing biofilm may require chemotaxis and/or motility to move along the surface, thereby facilitating the growth and spread of the biofilm (Stelmack et al., 1999). With extensive evolution, mercury-resistant bacteria obtain the *mer* (mercuric ion resistance) operon in their genome to respond to stress from toxic mercury compounds. The *mer* operon enables bacteria to survive in the presence of mercury and reduce it to volatile, less-toxic Hg^0, which diffuses out of the cell (Mathema et al., 2011).

Of the known bacterial heavy metal resistance systems, the *mer* operon is an intensively studied mercurial resistance system. Typically, the *mer* operon consists of a series of structural genes that transport and transform inorganic and organic mercury, such as mercuric reductase (MerA), organomercury lyase (MerB), periplasmic Hg^{2+} scavenging protein (MerP), one or more inner membrane spanning proteins (MerT, MerC, MerE, MerF, and MerG) that transport Hg^{2+} to the cytoplasm for reduction by MerA and regulatory proteins (MerR, MerD). Expression of the *mer* operon is tightly regulated by the dual function transcriptional regulator, MerR, which binds to the *mer* operator/promoter (O/P) region and acts as a transcriptional repressor or activator in the absence or presence of Hg^{2+} (Mathema et al., 2011). MerD, the other proposed regulatory protein of *mer* operon, may function as either an activator (Nucifora et al., 1989) or a repressor of the *mer* operon (Mukhopadhyay et al., 1991). MerD can form a ternary complex in association with O/P region and MerR to co-regulate the expression of *mer* operon (Champier et al., 2004). Following exposure to ionic Hg^{2+}, the toxic metal firstly binds to two cysteine residues at positions 14 and 17 of MerP (Steele and Opella, 1997), which directly transfers the Hg^{2+} to the mercury-specific transporter MerT (Schue et al., 2008). MerT transfers Hg^{2+} from its two cysteine residues located on the periplasmic side of the membrane to two cysteine residues located on the cytosolic side (Morby et al., 1995). Once bound on the cytosolic side of MerT, the Hg^{2+} is transferred directly to two cysteine residues within the amino-terminal domain of MerA (NMerA) (Schue et al., 2008) which then transfers the Hg^{2+} to two cysteine residues in the active site of MerA for NAD(P)H-dependent reduction to Hg^0 (Hong et al., 2014). The mercuric reductase MerA is the central enzyme in the microbial mercury detoxification system and *merA* is a suitable biomarker for examining the functional diversity of Hg detoxification (Boyd and Barkay, 2012). The *merE* gene is a predicted small ORF immediately following *merD* in many Gram-negative *mer* operon sequences, and it is proposed to encode a transporter of Hg^{2+} or methylmercury (Sone et al., 2017). MerF could transport ionic mercury from the periplasmic protein MerP across the bilayer to MerA and it plays a similar function as that of MerT (Barkay et al., 2003). However, the other functions of MerF toward mercury resistance are still unclear given that MerT is considered as the main transporter of mercury (Wahba et al., 2017).

Despite being the most studied bacterial toxic metal resistance loci, significant issues remain unknown to elucidate the genetic and physiological adaptations of bacteria to mercury stress, such as the relationship between each gene in the *mer* operon and bacterial physiology toward mercury resistance. While the role of the *mer* operon is well understood in terrestrial bacteria, however, it is not conclusive how *mer* works to cope with mercury stress in marine bacteria (Barkay et al., 2003). Notably, increasingly serious mercuric pollution in the ocean not only leads to food chain contamination, but also hastens ocean acidification (Wang et al., 2017). So, we must quickly develop cost-effective, sustainable and environmentally friendly remediation methods that facilitate the removal of mercury from contaminated ocean sites (Sone et al., 2013). But, we can only develop novel bioremediation strategies with a comprehensive understanding how *mer* systems function in response to the ever-increasing challenges of co-existing with mercury.

In this study, we show that the mercury resistant marine bacterium *P. stutzeri* 273 contains a *mer* gene cluster consisting of putative regulatory proteins (MerR, MerD), transporters (MerT, MerP, MerE, and MerF) and the mercuric reductase (MerA). Using genetic and transcriptomic assays, we demonstrate that *merT*, *merA*, *merP, merD,* and *merR* confer mercury resistance in *P. stutzeri* 273. Importantly, we identify novel functions of MerF to promote bacterial mercury resistance, such as the determination of flagellar development, motility, chemotaxis and biofilm formation. Finally, we propose a model for the mercury-adapted lifestyle of the bacterium *P. stutzeri* 273.

MATERIALS AND METHODS

Bacterial Strains and Media

Pseudomonas stutzeri 273 was isolated from the sediment samples collected by RV *KEXUE* during a cruise in the East China Sea in the year of 2014 (Wu et al., 2016). *P. stutzeri* 273 and its mutants were cultured in marine broth 2216E (5 g/L tryptone, 1 g/L yeast extract, one liter filtered seawater, pH adjusted to 7.4–7.6) or Luria Bertani (LB) medium (10 g/L peptone, 5 g/L yeast extract, 10 g/L NaCl, pH adjusted to 7.0) and incubated at 28°C under vigorous agitation at speed of 150 rpm. *Escherichia coli* DH5α was used as the host for plasmid construction, and *E. coli* S17-1 was used as a vector donor in conjugation. *E. coli* DH5α, *E. coli* SY327, and *E. coli* S17-1 were grown in LB medium at 37°C with shaking at speed of 150 rpm. When necessary, antibiotics were used at the following concentrations: chloramphenicol (Cm) and gentamicin (Gm) with a final concentration of 25 and 25 μg/mL, respectively (Wu et al., 2017).

Bioinformatic Analysis

The sequences of genes within the *mer* gene cluster of *P. stutzeri* 273, MerD and MerF protein sequences of other bacteria used in our study were obtained from GenBank. All of the bacterial MerF sequences were aligned using ClustalW2 (Larkin et al., 2007), and the phylogenetic tree was constructed with MEGA6.0 (Tamura et al., 2013). The complete genome sequence of *P. stutzeri* 273 has been deposited at GenBank under the accession number CP015641, and all the genome information of *P. stutzeri* 273 available in GenBank.

Determination of Mercury Minimal Inhibitory Concentrations (MIC), Growth Curves and Mercury Removal Rate in *P. stutzeri* 273 or *P. aeruginosa* PAO1

To determine the mercury MIC against *P. stutzeri* 273, fifty-microliter of mid-log-phase cultures was inoculated in 5 mL LB medium containing 0, 20, 40, 60, 80, 100, and 120 μM $HgCl_2$, respectively. Cultures were incubated at 28°C with the speed of 150 rpm for 24 h for each strain tested until confluent growth was observed in control (no $HgCl_2$) tubes, followed by examination of growth on the $HgCl_2$-supplemented groups. The MIC value was the lowest concentration of Hg^{2+} at which growth in LB medium was inhibited (Vetriani et al., 2005). Each treatment was performed in triplicate and the MIC was defined as the average number of three repeats. To determine the mercury MIC against *P. aeruginosa* PAO1, fifty-microliter of mid-log-phase cultures was inoculated in 5 mL LB medium containing 0, 0.1, 0.2, 0.3, 0.4, 0.5, 0.6, 0.7, 0.8, 0.9, and 1.0 μM $HgCl_2$, respectively. Other operations were performed as described above. To check the growth of *P. stutzeri* 273 under $HgCl_2$ stress, 1 mL overnight bacterial culture was inoculated in 100 mL flask at 28°C with the speed at 150 rpm in LB medium in the absence or presence of 20 μM or 50 μM $HgCl_2$. Bacterial growth status was monitored by measuring the OD_{600} value every 4 h until cell growth reached stationary phase. To determine the Hg^{2+} removal rate of *P. stutzeri* 273, *P. stutzeri* 273 was incubated at 28°C with speed of 150 rpm in LB medium supplemented with 20 μM or 50 μM $HgCl_2$ to OD_{600} value of 1.5. The supernatant of culture was collected by centrifugation (13,400 × *g*, 2 min). After which, the supernatant was thoroughly digested with nitric acid and perchloric acid, and diluted with Milli-Q water for Hg^{2+} concentration detection. The dissolved Hg^{2+} concentrations were measured with an inductively coupled plasma source mass spectrometer (Optima 7300 DV, PerkinElmer) (Han et al., 2014).

Construction of Deletion Mutants of Genes Within *mer* Gene Cluster and Complementation of Mutants for Mercury Sensitivity Assays

The *P. stutzeri* 273 derivatives (Δ*merA*, Δ*merP*, Δ*merR*, Δ*merT*, Δ*merD*, Δ*merE*, Δ*merF*, and Δ*fliC*) were constructed by allelic exchange as previously described (Wu et al., 2017). Briefly, fragments for mutant construction were amplified from the chromosome of *P. stutzeri* 273 by primers shown in Supplementary Table S1. Then, PCR fragments were purified, digested and ligated into the suicide vector pEX18Gm containing an *oriT* for conjugation. The resulting plasmid was transformed successively into *E. coli* SY327 and *E. coli* S17-1 by the $CaCl_2$ method. Mating between *P. stutzeri* 273 and *E. coli* S17-1 containing different plasmids was performed at 30°C for 24 h. Colonies growing on LB agar amended with Cm (25 μg/mL) and Gm (25 μg/mL) were single-event positive recombinant strains. The individual colony was picked and incubated overnight at 30°C with shaking in LB broth with Cm (25 μg/mL) and Gm (25 μg/mL), then diluted 1:1000 into fresh LB broth and plated onto LB agar plate amended with 10% sucrose and incubated for 48 h at 30°C. A single colony was re-streaked several times before being replicated onto a LB agar plate amended with Gm (25 μg/mL) to confirm sensitivity to gentamicin and loss of the pEX18GM vector. All double recombination mutants candidates were verified by PCR amplification and sequencing.

To construct complementary strains, pUCP18 was used as the mother plasmid, and *E. coli* DH5a was used as the host strain. Briefly, genes (*merT*, *merP*, *merF*, *merA*, and *merD*) derived from *P. stutzeri* 273 together with their native promoters were amplified from the wild-type strain by primers listed in Supplementary Table S2. Then, the corresponding PCR products were digested with *Hin*dIII and *Bam*HI and ligated into pUCP18 to produce pUCP18-*merT*, pUCP18-*merP*, pUCP18-*meF*, pUCP18-*merA,* and pUCP18-*merD*, respectively. The above resulting plasmids were separately transformed into the corresponding mutants Δ*merT*, Δ*merP*, Δ*merF*, Δ*merA,* and Δ*merD* with the $CaCl_2$ method (Lee et al., 2013; Weller-Stuart et al., 2017). The final complementary strains (Δ*merT*/c*merT*, Δ*merP*/c*merP*, Δ*merF*/c*merF*, Δ*merA*/c*merA*, and Δ*merD*/c*merD*) were verified by PCR amplification and sequencing.

Mercury sensitivity assays of *P. stutzeri* 273 wild type, different mutants and the corresponding complementations were performed on LB agar plates with different concentrations of $HgCl_2$. Cells were grown to the exponential phase in LB liquid medium and then diluted to an OD_{600} of 0.1. Five 10-fold dilutions were carried out and spotted on agar plates incubated at 28°C for 48 h. Each experiment was repeated three times.

Motility, Chemotaxis and Biofilm Formation Assays

For the motility assay, *P. stutzeri* 273 and correlative mutants were cultured in LB medium at 28°C with speed of 150 rpm to the OD_{600} of 1.2. Then 20 μL different culture was inoculated onto the center of 1% agar plate without or with 20 or 50 μM $HgCl_2$ and incubated for 5 days at 28°C (Radin et al., 2013). For the chemotaxis assay, wild type *P. stutzeri* 273 was cultured in LB medium at 28°C with speed of 150 rpm to the OD_{600} of 1.2. Then 20 μL culture was inoculated onto the center of 1% agar plate, and the filter paper containing 20 μL water or 20 or 50 μM $HgCl_2$ was loaded 2-cm away from the culture spot. Plates were incubated for 5 days at 28°C for further examination. For the biofilm formation assay, 50 μL of *P. stutzeri* 273 culture (OD_{600} about 0.8) was inoculated in a borosilicate tube containing 1 mL liquid

LB medium without or with 20 and 50 μM $HgCl_2$, respectively. The tubes were incubated at 28°C without shaking for 3 days for further biofilm assays. To quantify the amount of biofilm, the liquid LB medium and planktonic cells were removed from the borosilicate tubes, and the remaining biofilms were washed off with phosphate-buffered saline (PBS, pH 7.4) and stained with crystal violet. The stained biofilms were eluted in 100% ethanol and monitored for biofilm formation as determined by spectrophotometry at 595 nm (Lee et al., 2013). The biofilm formation assays for *P. stutzeri* 273 Δ*merF* and its complement were performed as described above.

Western Blotting

Bacterial lysates of wild type *P. stutzeri* 273 and *merF* deletion mutant were harvested and lysed in the sample buffer containing sodium dodecyl sulphate (SDS) and β-mercaptoethanol, then boiled for 10 min at 100°C. Same amount proteins from wild type and mutant were separated on 12% SDS-page gels, electro-transferred to nitrocellulose membranes and incubated with FliC primary antibody (BioLegend) and secondary antibody (Proteintech Group).

Quantitative Reverse Transcription-PCR (qRT-PCR)

For qRT-PCR, cells of *P. stutzeri* 273 or corresponding mutants incubated in LB medium amended without or with 20 or 50 μM Hg^{2+} to OD_{600} of 1.2. Cells were centrifuged at 6,000 × *g* for 10 min, total RNAs were extracted using the RNApure Bacteria Kit (DNase I) (CWBio, China). Total RNAs were reverse transcribed into cDNA, and the transcriptional levels of different genes were determined by qRT-PCR with Sybr Green Premix Low rox (MDbio, China) and the QuantStudioTM 6 Flex (Thermo Fisher Scientific, United States). RNA degradation was examined on 1% agarose gels. RNA purity was verified with NanoPhotometer R spectrophotometer (IMPLEN, Westlake Village, CA, United States). RNA concentration was determined by QubitR RNA Assay Kit in QubitR 2.0 Fluorometer (Life Technologies, Carlsbad, CA, United States). RNA integrity was assessed by RNA Nano6000 Assay Kit for the Bioanalyzer 2100 system (Agilent Technologies, Santa Clara, CA, United States). 16S rDNA was used as an internal reference. The relative gene expression was calculated using the $2^{-\Delta\Delta Ct}$ method with each transcript signal normalized to 16S rDNA (Petrus et al., 2015; Zhu et al., 2017). Transcript signals for each treatment were compared to the transcript signals from the control group. Specific primers for the genes within *mer* gene cluster and 16S rDNA were designed using Primer 5.0 as shown in Supplementary Table S3. All qRT-PCR runs were conducted with three biological and three technical replicates.

Transcriptional Profiling of *P. stutzeri* 273 Challenged With Different Concentrations of Hg^{2+}

Total RNAs of *P. stutzeri* 273 incubated in LB medium in the absence or presence of 20 or 50 μM of $HgCl_2$ with OD_{600} about 1.2 were extracted and checked as described above. Detailed protocols of RNA-seq are described in the Supplementary Information. qRT-PCR verification of transcriptional profiling data was performed as described above. Five genes (PS273GM-RS08590, *flgG*; PS273GM-RS08570, *flgC*; PS273GM-RS08525, *motA*; PS273GM-RS02905, *cheY*; PS273GM-RS08565, *flgB*) were chosen for verification of transcriptional profiling data by qRT-PCR. The specific primers were listed in Supplementary Table S3. The heat map was made by HemI 1.0 based on the KEGG enrichment results.

Transmission Electron Microscopy (TEM)

To examine the flagella formation, wild-type and relative mutants of *P. stutzeri* 273 were all examined using TEM with a JEOL JEM 12000 EX (equipped with a field emission gun) at 100 kV. The cell suspension was washed with sterile nutrient solution or Milli-Q water and centrifuged at 5,000 × *g* for 3 min. Finally, these samples were taken by immersing copper grids coated with a carbon film for 1 min in bacterial suspensions and washed for several minutes in distilled water and dried several minutes at room temperature (Bundeleva et al., 2014; Han et al., 2014).

Statistical Analysis

Tests for significance of the differences among groups were subjected to one-way analysis of variance (one-way ANOVA) and multiple comparisons by using the GraphPad Prism 5. Statistical significance was defined in our study by $P < 0.05$ (indicated by* in all figures), $P < 0.01$ (indicated by ** in all figures) or $P < 0.001$ (indicated by *** in all figures).

RESULTS

Characterization of Mercury Resistance Conferred by the *mer* Gene Cluster in *P. stutzeri* 273

Pseudomonas stutzeri 273 has its entire genome sequenced (NCBI accession number CP015641) (Wu et al., 2017). When analyzing the genome sequence of this bacterium, a candidate *mer* gene cluster between nucleotide 2193317 to nucleotide 2196970 was found in the chromosome of *P. stutzeri* 273. Notably, the *mer* gene cluster is located on a genomic island flanked by a transposase (WP_046622512.1) and a resolvase (WP_003089068.1) (**Figure 1A**). This *mer* gene cluster consists of two potential mercury-responsive regulatory proteins, MerR and MerD, the mercury transporters MerP, MerT, MerE, and MerF, and the mercuric ion reductase MerA, which reduces toxic Hg^{2+} to non-toxic Hg^0 (**Table 1**). To measure the potential mercury resistance conferred by the *mer* gene cluster, we examined the resistance of *P. stutzeri* 273 against Hg^{2+}. Our results showed that Hg^{2+} has a 60 μM minimum inhibition concentration against *P. stutzeri* 273 (**Figure 1B**). Notably, the Hg^{2+} MIC against *P. aeruginosa* PAO1 without *mer* gene cluster in the chromosome is 0.7 μM (Supplementary Figure S1), which is much lower than that of *P. stutzeri* 273. The bacteria could grow to a similar density in the presence of 20 μM Hg^{2+} or 50 μM Hg^{2+} compared to growth with no mercury, however, the time

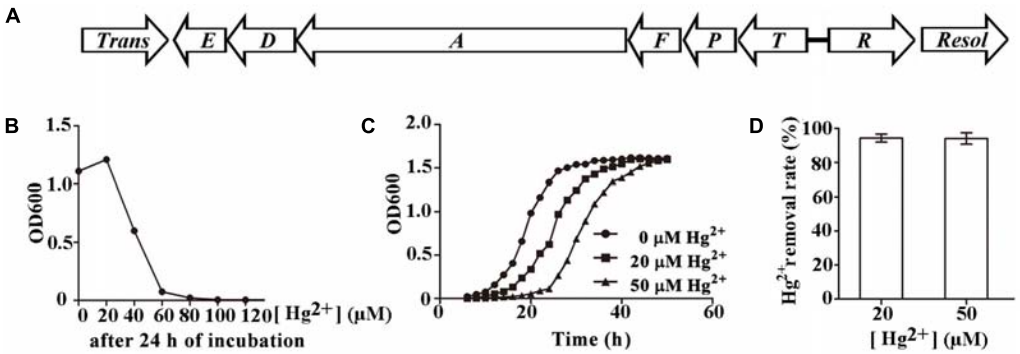

FIGURE 1 | Characterization of mercury resistance by *Pseudomonas stutzeri* 273. **(A)** Arrangement of potential *mer* gene cluster in *P. stutzeri* 273. *Trans*, transposase (PS273GM_RS09950); *E*, *merE* (PS273GM_RS09955); *D*, *merD* (PS273GM_RS09960); *A*, *merA* (PS273GM_RS09965); *F*, *merF* (PS273GM_RS09970); *P*, *merP* (PS273GM_RS09975); *T*, *merT* (PS273GM_RS09980); *R*, *merR* (PS273GM_RS09985); *Resol*, resolvase (PS273GM_RS09990). Locus tags indicated in the bracket. **(B)** Hg^{2+} MIC determination in *P. stutzeri* 273. **(C)** Growth style of *P. stutzeri* 273 in the absence or presence of Hg^{2+} (20 μM or 50 μM). **(D)** Hg^{2+} removal by *P. stutzeri* 273 with different concentrations of Hg^{2+}.

reaching stationary phase is 10 and 20 h later than that without mercury stress, respectively (**Figure 1C**). We then assessed the mercury removal property of *P. stutzeri* 273 by measuring metal depletion in culture supernatants by inductively coupled plasma-optical emission spectroscopy (ICP-OES). We found that up to 94% Hg^{2+} could be removed in both 20 and 50 μM Hg^{2+} conditions (**Figure 1D**). Taken together, these results indicate that *P. stutzeri* 273 is a good candidate to develop bioremediation products toward mercuric pollution in the marine environment.

Genetic and Biochemical Determination of Key Genes in the *mer* Gene Cluster of *P. stutzeri* 273 Conferring Mercury Resistance

Mer gene cluster is widely accepted to determine mercurial resistance of most bacteria (Barkay et al., 2003). We sought to elucidate which genes in the *mer* gene cluster are essential for mercury resistance in *P. stutzeri* 273. So, we constructed different deletion mutants (Δ*merA*, Δ*merP*, Δ*merR*, Δ*merT*, Δ*merD*, Δ*merE*, Δ*merF*) and tested their growth status in LB agar plates supplemented with different concentrations of Hg^{2+}. As expected, the wild type showed normal growth in the concentration of 50 μM Hg^{2+}. However, the mutants with deletion of *merA* (encoding the mercuric reductase) or *merT* (encoding the Hg^{2+}-transporter) exhibited the greatest sensitivity to the low concentration of Hg^{2+}, such that the cells could not even grow in the agar plate containing 20 μM Hg^{2+} (**Figure 2A**, middle panel). The deletion of *merD* (encoding the regulatory protein of *mer* gene cluster) affected bacterial growth to a certain extent in the presence of 20 μM Hg^{2+} (**Figure 2A**, middle panel), but cellular growth was completely inhibited by 50 μM Hg^{2+} (**Figure 2A**, right panel). The deletion of *merP* (encoding the Hg^{2+}-transporter) only affected bacterial growth under the 50 μM Hg^{2+} condition but not the low level Hg^{2+} condition (**Figure 2A**, middle and right panels). On the other hand, deletions of *merR* (encoding the regulatory protein of *mer* gene cluster), *merE* and *merF* (encoding Hg^{2+}-transporter) did not affect the mercury resistance of *P. stutzeri* 273, as the cells grew as well as the wild type in the presence of 50 μM Hg^{2+} (**Figure 2A**, right panel). To better understand how *merA*, *merP*, *merT,* and *merD* confer mercury resistance to *P. stutzeri* 273, we constructed complements (Δ*merA*/c*merA*, Δ*merP*/c*merP*, Δ*merT*/c*merT*, and Δ*merD*/c*merD*) of the above deletion strains and examined their growth in the presence of both low (20 μM) and high (50 μM) levels of Hg^{2+}. As expected, *merA*, *merP*, *merT,* or *merD* could complement the mercury sensitive phenotype of corresponding *P. stutzeri* 273 gene deletion strain (**Figure 2B**). These results clearly demonstrate that *merA*, *merP*, *merT,* and *merD* determine mercury resistance in *P. stutzeri* 273.

The metalloregulatory protein MerR acts as both a repressor and an activator of the transcription of the *mer* operon depending on the absence or presence of mercuric ions, respectively (Champier et al., 2004). MerR is the predominant regulator for mercury resistance, however, the function of the other potential regulator MerD remains speculative. To further clarify the function of MerD and MerR for mercury resistance in *P. stutzeri* 273, we detected the expression of other *mer* genes in the mutant Δ*merR* or Δ*merD* of *P. stutzeri* 273 by qRT-PCR in the presence of different concentrations of Hg^{2+}. Interestingly, in the absence of Hg^{2+}, the expression of all *mer* genes was up-regulated in the *merR* deletion mutant (**Figure 2C**, left panel), which indicates

TABLE 1 | Proteins involved in the mercury resistance of *Pseudomonas stutzeri* 273.

Protein designation	Size (amino acids)	Putative function
MerE	78	Methylmercury transport protein
MerD	121	Regulator protein
MerA	548	Mercuric ion reductase
MerF	81	Mercuric ion transport protein
MerP	91	Periplasmic mercuric ion binding protein
MerT	116	Mercuric ion transport protein
MerR	144	Regulator protein

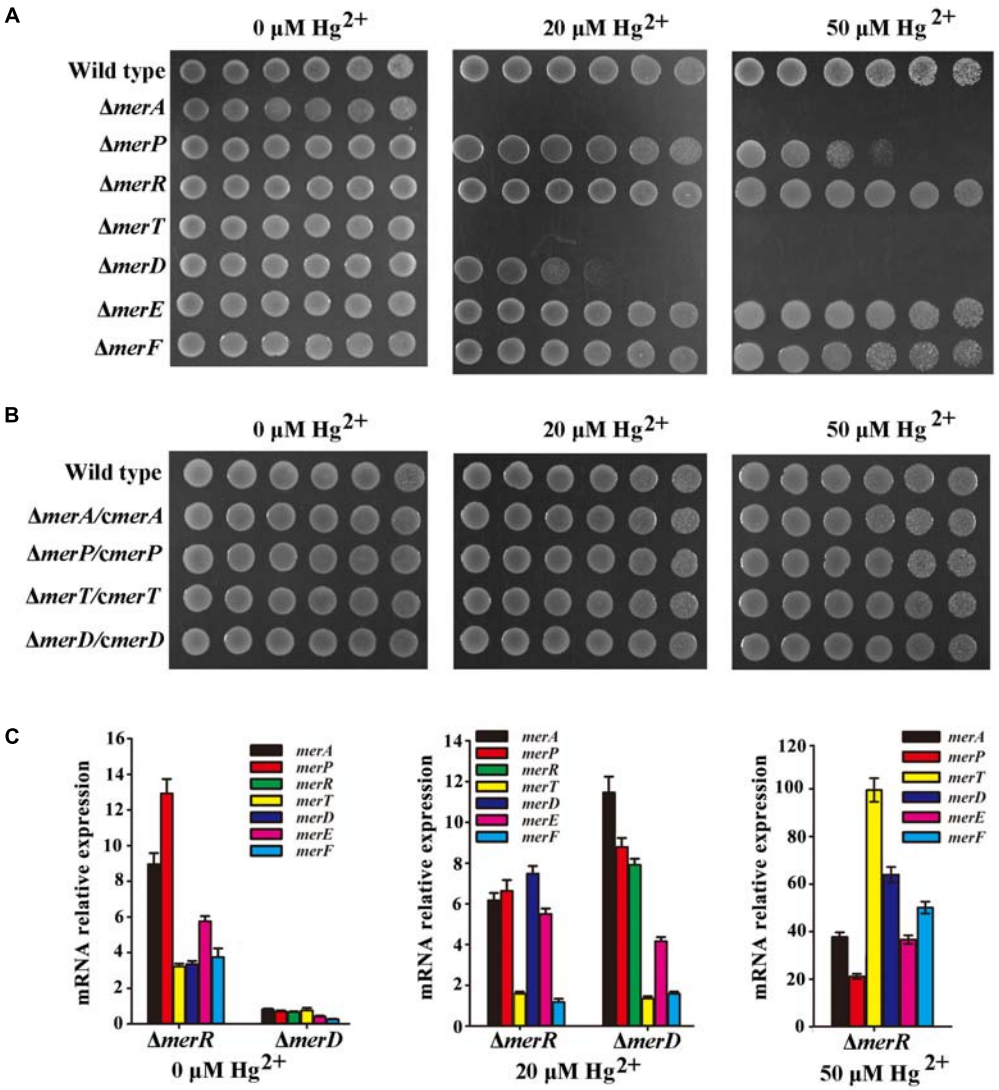

FIGURE 2 | Genetic and biochemical analyses of *mer* gene cluster function for mercury resistance in *P. stutzeri* 273. **(A)** Growth in LB solid media of wild type, mutant strains (Δ*merA*, Δ*merP*, Δ*merR*, Δ*merT*, Δ*merD*, Δ*merE*, and Δ*merF*) and **(B)** complemented strains (Δ*merA*/*c*Δ*merA*, Δ*merP*/*c*Δ*merP*, Δ*merT*/*c*Δ*merT*, and Δ*merD*/*c*Δ*merD*) of *P. stutzeri* 273. Five 10-fold dilutions spotted from left to right with the indicated concentration of Hg^{2+}. **(C)** Expression of each gene in the *mer* gene cluster of *P. stutzeri* 273 mutant with *merR* or *merD* deletion without Hg^{2+} (left panel), in the presence of 20 μM Hg^{2+} (middle panel). Expression of each gene in the *mer* gene cluster of *P. stutzeri* 273 mutant with *merR* deletion in the presence of 50 μM Hg^{2+} (right panel).

that merR is a repressor in *P. stutzeri* 273 in the absence of Hg^{2+}. However, the expression of all *mer* genes was down-regulated (**Figure 2C**, left panel) in the *merD* deletion mutant, which indicates that merD is an activator in *P. stutzeri* 273 in the absence of Hg^{2+}. When challenged with 20 μM Hg^{2+}, in the *merR* or *merD* deletion mutant, the expression of most *mer* genes was up-regulated from 4 to 12 times except for *merT* and *merF*, whose expression almost kept the same level when challenged with 20 μM Hg^{2+} (**Figure 2C**, middle panel). Notably, the expression of *merD* or *merR* was up-regulated about eight times in the *merR* or *merD* deletion mutant (**Figure 2C**, middle panel), which suggests that MerD or MerR might regulate the expression of the *mer* gene cluster when the other is absent. In the presence of 50 μM Hg^{2+}, the growth of the *merR* deletion mutant was completely inhibited, however, the *merR* deletion mutant grew very well with the expression of *merD* increased more than 60-fold (**Figure 2C**, right panel). Moreover, the expression of all other *mer* genes in *merR* deletion mutant was up-regulated from 20 to 100 times in the presence of 50 μM Hg^{2+} (**Figure 2C**, right panel). Together with the results of gene deletion and complement shown in **Figures 2A,B**, we propose that MerR is a repressor and MerD is an activator in the absence of Hg^{2+}, MerD acts as an activator in both low (20 μM) and high (50 μM) concentrations of Hg^{2+}, and MerR is only functional as an activator in the presence of low (20 μM) but not high (50 μM) concentration of Hg^{2+}.

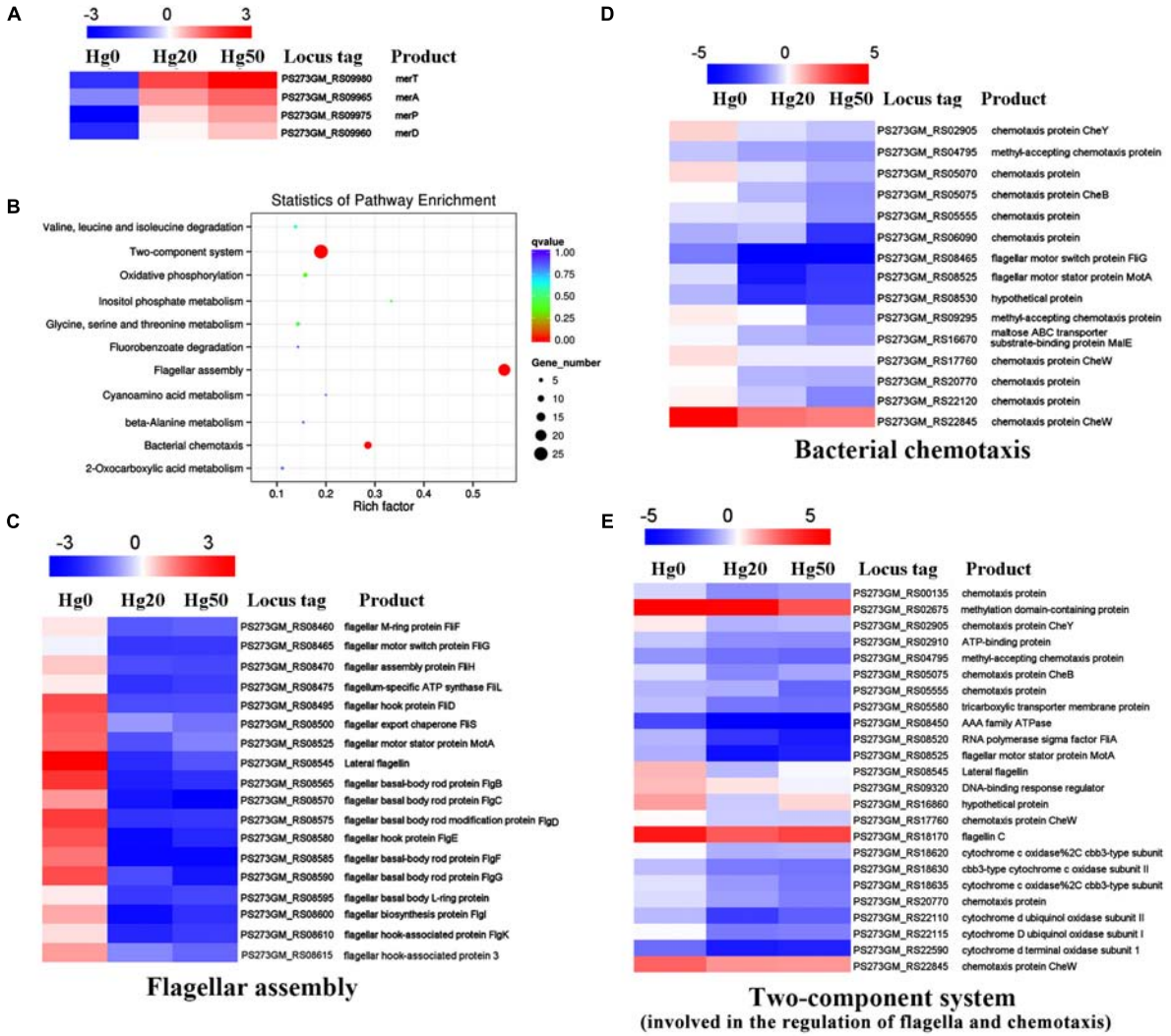

FIGURE 3 | Transcriptome profiles of *P. stutzeri* 273 challenged with different Hg^{2+} concentrations. **(A)** Heat map shows relatively up-regulated and differentially expressed Hg^{2+} stress-responsive genes (DEGs) within *mer* gene cluster in *P. stutzeri* 273 among Hg0, Hg20, and Hg50 enriched by KEGG analysis. **(B)** DEGs enriched KEGG pathway scatterplot of *P. stutzeri* 273 challenged with different Hg^{2+} concentrations. The Rich factor is the ratio of differentially expressed gene numbers annotated in this pathway term to all gene numbers annotated in this pathway term. The greater the Rich factor, the greater the degree of pathway enrichment. A *Q*-value is the corrected *p*-value ranging from 0 to 1, and a lower value indicates greater pathway enrichment. Heat map shows relatively down-regulated Hg^{2+} stress responsive DEGs that contribute to flagellar assembly **(C)**, bacterial chemotaxis **(D)** and two-component system involved in the regulation of flagella and chemotaxis **(E)** among Hg0, Hg20, and Hg50 enriched by KEGG analysis. The locus tag and its corresponding encoding product shown with the heat map. Heat map made using Heml 1.0.3.3.

Transcriptome Profiles of *P. stutzeri* 273 Challenged With Different Concentrations of Hg^{2+}

Mercury and its compounds exert inhibitory effects on the functioning of bacterial enzymes and proteins and render them useless. However, bacterial genetic and morphological flexibility along with immense physiological variability enable them to survive in extreme environmental conditions (Mathema et al., 2011). To reveal the overall responses when exposed to mercury stress, we performed transcriptome analyses of *P. stutzeri* 273 challenged with different concentrations of Hg^{2+}. As expected, expression of *merT*, *merA*, *merD,* and *merP* was significantly up-regulated with increasing Hg^{2+} concentrations (**Figure 3A**). These results are consistent with the genetic results (**Figure 2**) and confirm the importance of these genes to confer mercury resistance in *P. stutzeri* 273. KEGG enrichment analysis showed that flagellar assembly, bacterial chemotaxis and two-component system were enriched among the two-way comparison of Hg0 (absence of Hg^{2+}), Hg20 (presence of 20 μM Hg^{2+}), and Hg50 (presence of 50 μM Hg^{2+}) (**Figure 3B**). It is noteworthy that all of the genes expressed related to these three pathways were significantly down-regulated with increasing concentrations of

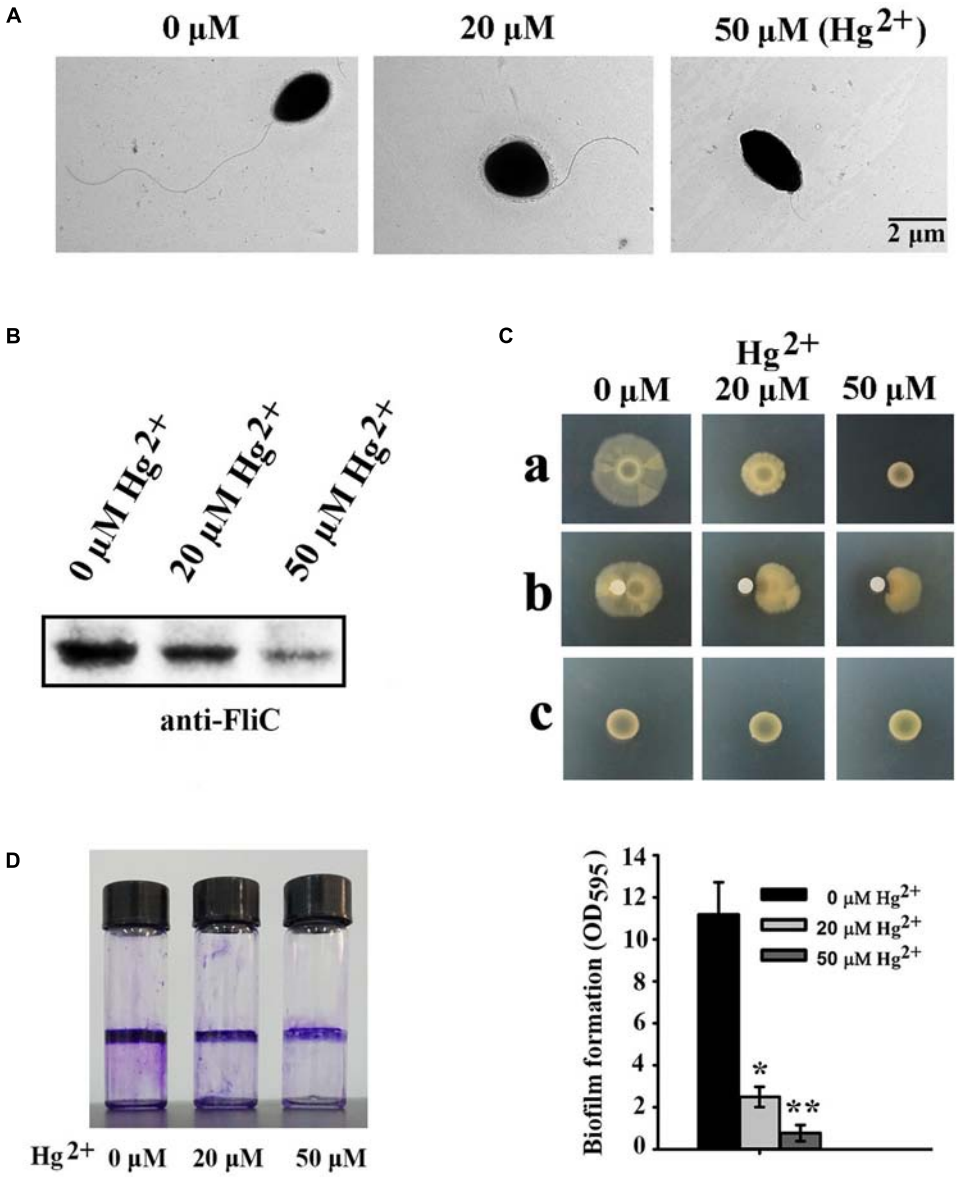

FIGURE 4 | Effects of different Hg^{2+} concentrations on *P. stutzeri* 273 physiology. **(A)** Effects of different Hg^{2+} concentrations on flagella formation in *P. stutzeri* 273 analyzed by TEM. Representative pictures are shown. **(B)** Western blot analysis of protein expression of the typical flagellar related gene *fliC*. **(C)** Effects of different concentrations of Hg^{2+} on motility (row a) and chemotaxis (row b) in *P. stutzeri* 273. Motility assays of *fliC* deletion mutant of *P. stutzeri* 273 in the absence or presence of Hg^{2+} (row c). For the motility assay, the medium contained different Hg^{2+} concentrations. The chemotaxis assay loaded different Hg^{2+} concentrations on the filter paper. **(D)** Effects of different Hg^{2+} concentrations on biofilm formation in *P. stutzeri* 273 analyzed by crystal violet staining (left panel). Quantification shown in right panel.

Hg^{2+} (**Figures 3C–E**). There are 18 differentially expressed genes (DEGs), 15 DEGs or 24 DEGs under the terms "flagellar assembly" (**Figure 3C**), "bacterial chemotaxis" (**Figure 3D**) and "two-component system involved in the regulation of flagella and chemotaxis" (**Figure 3E**), respectively. Down-regulation of chemotaxis and two-component system implies that signal transduction of *P. stutzeri* 273 was strictly controlled in response to mercury stress as described previously (Liu et al., 2015). Notably, many down-regulated genes overlapped with different terms, such as PS273GM_RS08465 and PS273GM_RS08525 were classified as both "flagellar assembly" and "bacterial chemotaxis," and PS273GM_RS08525 belongs to all three pathways, which strongly suggests that these three pathways are closely correlated. We then verified the reliability of the transcriptomic data by qRT-PCR analysis. In total, we selected five genes (*flgG*, *fliC*, *motA*, *cheY*, and *flgB*) that belong to "flagellar assembly," "bacterial chemotaxis" or "two-component system" for validation. We consistently observed similar trends between qRT-PCR and

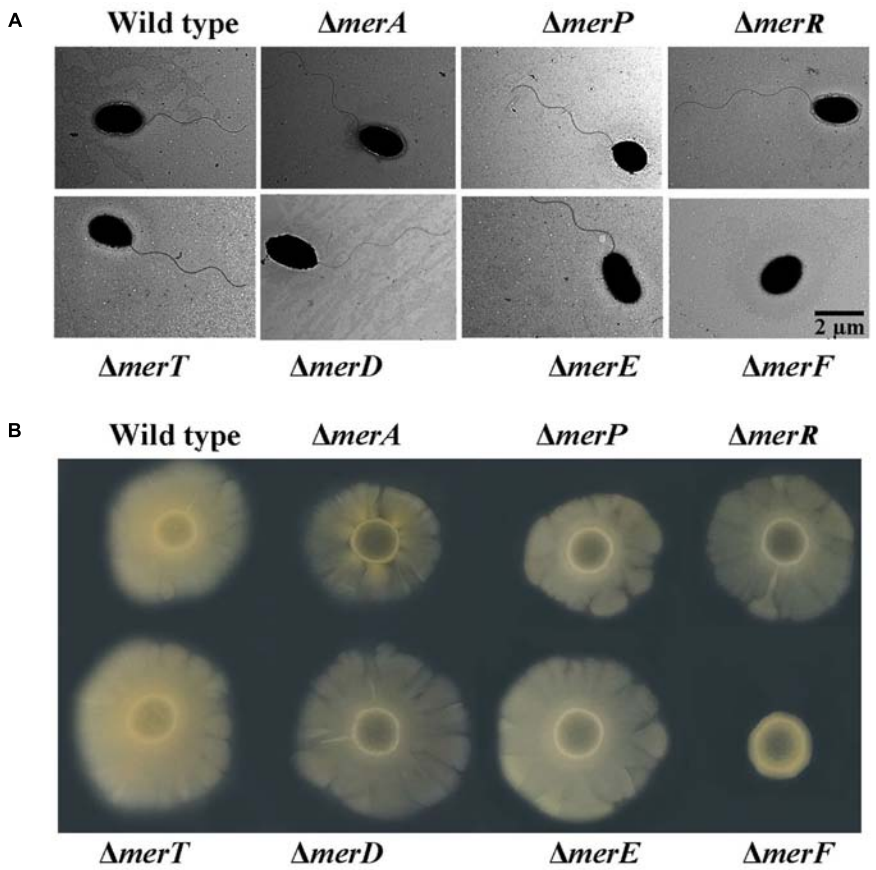

FIGURE 5 | Morphology and motility assays in wild type and different deletion mutants of genes within the *mer* gene cluster. **(A)** Flagellar formation in *P. stutzeri* 273 wild type and mutants (Δ*merA*, Δ*merP*, Δ*merR*, Δ*merT*, Δ*merD*, Δ*merE*, and Δ*merF*) by TEM. **(B)** Motility assays of *P. stutzeri* 273 wild type and mutants (Δ*merA*, Δ*merP*, Δ*merR*, Δ*merT*, Δ*merD*, Δ*merE*, and Δ*merF*) on agar plate.

RNA-seq results, which support the validity of our RNA-seq data (Supplementary Figure S2).

Different Mercury Concentrations on Physiological Development in *P. stutzeri* 273

Because many DEGs involved in "bacterial chemotaxis" or "two-component system" are associated with flagellar formation, we examined the effects of different mercury concentrations on flagella formation in *P. stutzeri* 273 by TEM. Consistent with our transcriptome profile results, flagellar formation in *P. stutzeri* 273 was dramatically inhibited with increased Hg^{2+} concentration (**Figure 4A**). In the condition without mercury stress, we could observe one intact polar flagellum in all cells (**Figure 4A**, left panel). However, most cells formed only abnormal flagella when exposed to Hg^{2+}, and the flagellar abnormal ratio and severity were Hg^{2+}-concentration dependent (**Figure 4A**, middle and right panels). So, we then examined the protein expression of flagellin (FliC), the typical symbol protein for detecting flagella formation, using western blot (Ammendola et al., 2016). The results showed that FliC expression gradually decreased with increased Hg^{2+} concentration (**Figure 4B**). These results confirm that Hg^{2+} affects bacterial flagella development as shown in **Figure 4A**. Because flagella formation is closely related to bacterial motility, chemotaxis and biofilm formation (Stelmack et al., 1999; Kearns, 2010), we then examined these features of *P. stutzeri* 273 in the absence or presence of Hg^{2+}. *P. stutzeri* 273 is a strong motile bacterium, and it swarms in 0.5–1.0% agar plate with a similar speed (Supplementary Figure S3). However, cell motility was significantly inhibited when amended with 20 μM Hg^{2+}. This inhibition became more evident when the concentration of Hg^{2+} increased to 50 μM (**Figure 4C**, row a). The bacterial chemotaxis system, which helps bacteria find optimal conditions for growth and survival, decreased toward the Hg^{2+} gradient (**Figure 4C**, row b). Consistent with the result of **Figure 4B**, the bacteria totally lost the motility ability when removing *fliC* from the chromosome regardless the absence or presence of mercury stress (**Figure 4C**, row c). Considering the close relationship among bacterial flagellar formation, motility, chemotaxis, and biofilm formation (Dressaire et al., 2015), we examined biofilm formation of *P. stutzeri* 273 when exposed to Hg^{2+} environment. As expected, the biofilm formation of *P. stutzeri* 273 was dramatically inhibited in the presence of 20 μM or 50 μM Hg^{2+} (**Figure 4D**). This result indicates that

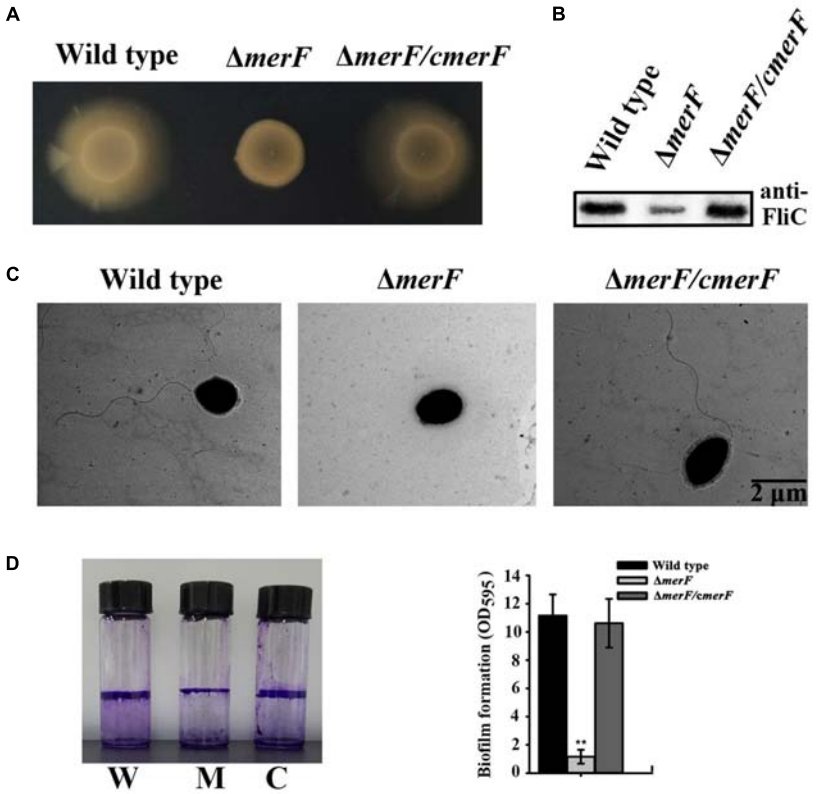

FIGURE 6 | MerF determines flagellar formation and motility of *P. stutzeri* 273. **(A)** Motility assays of *P. stutzeri* 273 wild type, *merF* deletion mutant Δ*merF* and its complementation strain Δ*merF*/*cmerF* on agar plate. **(B)** Western blot analysis of FliC protein expression in *P. stutzeri* 273 wild type, *merF* deletion mutant Δ*merF* and its complementation strain Δ*merF*/*cmerF*. **(C)** Flagella formation in *P. stutzeri* 273 wild type, *merF* deletion mutant Δ*merF* and its complementation strain Δ*merF*/*cmerF*. **(D)** Comparison of biofilm formation in *P. stutzeri* 273 wild type (labeled with W), *merF* deletion mutant Δ*merF* (labeled with M) and its complementation strain Δ*merF*/*cmerF* (labeled with C) by crystal violet staining (left panel). Quantification shown in right panel.

P. stutzeri 273 physiologically adapted to the mercury stress by down-regulating motility and positive chemotaxis.

MerF Determines Flagellar Formation and Motility of *P. stutzeri* 273

Mer operon plays key roles in mercury resistance. But, our results suggest that mercury stress correlates with bacterial physiology. We next examined the possible relationship between *mer* genes and bacterial physiological development. First, we checked the morphology of wild type and *mer*-related gene deletion mutants of *P. stutzeri* 273 via TEM. Surprisingly, the mutant with *merF* deletion (Δ*merF*) could not form flagella compared with wild type and other mutants (**Figure 5A**). The mutant Δ*merF* completely lost motile capability on the agar plate, while wild type and other mutants showed normal motile phenotype (**Figure 5B**). To further elucidate these novel functions of MerF, we constructed a complement of Δ*merF* (Δ*merF*/*cmerF*). We detected bacterial motility and flagella/biofilm formation. As expected, the complementation of *merF* restored the capabilities of motility (**Figure 6A**), flagella formation (**Figures 6B,C**) and biofilm formation (**Figure 6D**). These results demonstrate that MerF is a key factor to determine flagella formation in *P. stutzeri* 273.

Considering the important role of MerF for flagella development, motility and biofilm formation, we searched for homologs in the NCBI database. Interestingly, MerF homologs of *P. stutzeri* 273 exist in many prevalent pathogens, including some bacterial strains belong to *P. aeruginosa*, *Vibrio cholera*, *Enterobacter cloacae*, *Vibrio shilonii,* and *Enterobacter hormaechei* (**Figure 7A**). Moreover, MerF homologs in these other bacterial strains not only show high identity but also share sveral conserved domains with MerF in *P. stutzeri* 273 (**Figure 7B**).

DISCUSSION

The extremely broad phenotypic and genotypic diversity of *P. stutzeri* has proven an ideal model system for biochemical characterization of bioremediation and yielded significant advances in this area (Chen et al., 2011). *P. stutzeri* 273 is a marine bacterium isolated from sediments of the East China Sea, an environment existing different heavy metals (Yuan et al., 2004). Bacteria possess an exceptional ability to adapt to their environment, and their genetic and physiological flexibility enables them to develop a variety of survival mechanisms

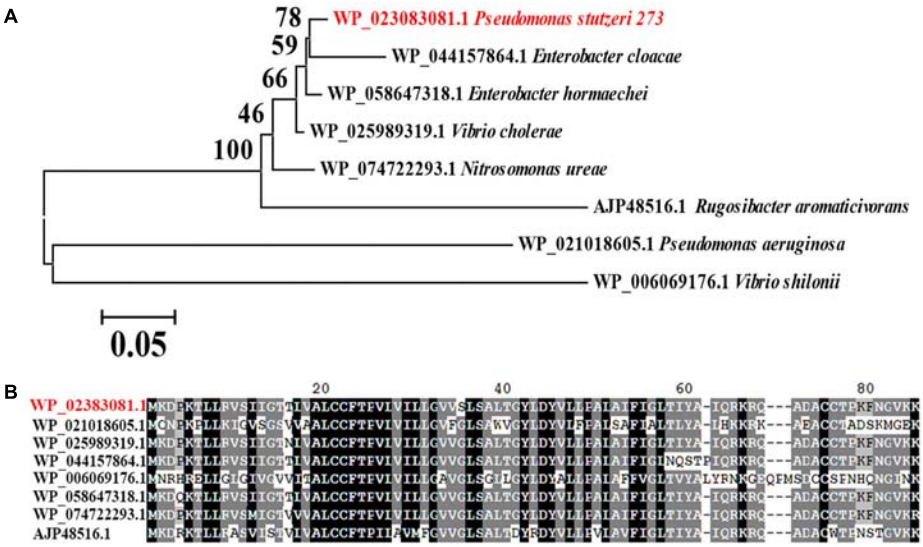

FIGURE 7 | Phylogenetic and conservation analyses of MerF. **(A)** The consensus phylogenetic tree of MerF in *P. stutzeri* 273 with other related MerF obtained from GenBank (accession numbers are indicated before the species name) constructed by the neighbor-joining method. Numbers above the branches are bootstrap values based on 1000 replicates. **(B)** Amino acid sequence alignment of MerF of *P. stutzeri* 273 (WP_023083081.1) with other MerF existing in different pathogenic bacterial strains (WP_021018605.1, *Pseudomonas aeruginosa*; WP_025989319.1, *Vibrio cholera*; WP_044157864.1, *Enterobacter cloacae*; WP_006069176.1, *Vibrio shilonii*; WP_058647318.1, *Enterobacter hormaechei*; WP_074722293.1, *Nitrosomonas ureae*; AJP48516.1, *Rugosibacter aromaticivorans*).

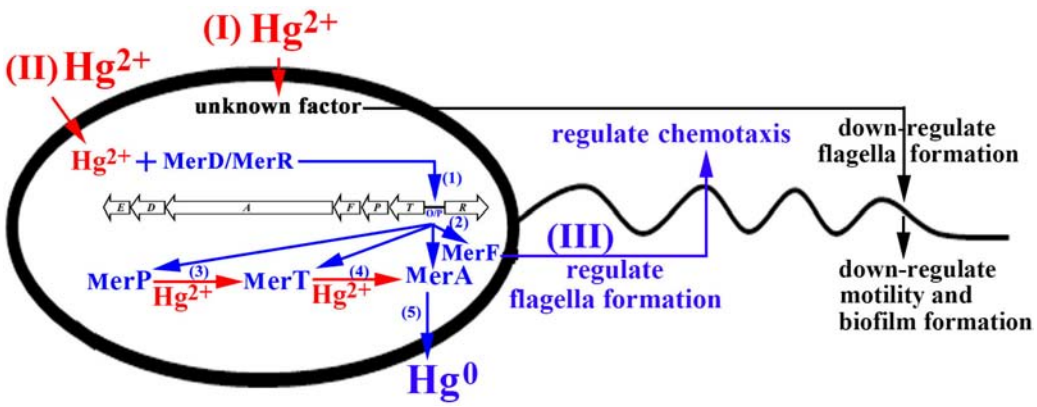

FIGURE 8 | Proposed model of genetic and physiological adaptations of marine bacterium *P. stutzeri* 273 to mercury stress. With the functional *mer* gene cluster in *P. stutzeri* 273, while sensing toxic levels of Hg^{2+}, an unknown factor begins to down-regulate flagella/biofilm formation to decrease bacterial motility for passive adaptation to mercury stress (I). (II) Meanwhile, Hg^{2+} enters into the cell and interacts with MerD or MerR to bind *mer* operator/promoter (O/P) region for activating the expression of the *mer* gene cluster (step 1); With the activation of the *mer* gene cluster, MerP/MerT/MerA/MerF are produced in cells (step 2); the Hg^{2+} existing in the cells binds with MerP and then transfers to MerT (step 3). MerT subsequently transfers Hg^{2+} to MerA and converts toxic Hg^{2+} to non-toxic Hg^0 (step 4). (III) MerF regulates flagella formation and chemotaxis to promote bacterial motility for positive adaptation to mercury stress.

(Mathema et al., 2011). Several gene loci involved in resistance to different heavy metals exist in the genome of *P. stutzeri* 273, such as mercury, cadmium and copper (Wu et al., 2017). Specifically, *P. stutzeri* 273 possesses strong mercury resistance and removal capabilities and there is a *mer* gene cluster located in the chromosome (**Figure 1**). *P. stutzeri* 273 also produces exopolysaccharide EPS273, which effectively inhibited both biofilm formation of *P. aeruginosa* PAO1 and biofouling in the marine environment (Wu et al., 2016). Together with our present discoveries, we deduce that *P. stutzeri* 273 has evolved different strategies to respond to the harsh conditions and compete with other microbes for survival. Overall, we propose *P. stutzeri* 273 will be an ideal candidate to study the adaptation and evolution of marine bacteria to the harsh environment.

In most mercury resistance bacteria, MerR tightly controls the expression of the whole *mer* gene cluster; however, the exact function of the other potential regulatory protein MerD remains unresolved. MerD may function as either an activator (Nucifora et al., 1989) or a repressor of the *mer* operon

(Mukhopadhyay et al., 1991). In *P. stutzeri* 273, MerR and MerD were demonstrated to be a repressor and an activator in the absence of Hg^{2+} (**Figure 2C**, left panel), respectively. MerR functions as an activator only in the presence of low concentration of Hg^{2+} (such as 20 μM) (**Figure 2C**, middle panel), however, MerD acts as an activator in both low and high concentrations of Hg^{2+} (**Figure 2C**, middle and right panels). In the presence of mercury stress, MerR and MerD might cooperate to regulate the expression of the *mer* gene cluster as described previously (Champier et al., 2004). We are still not clear the exact action mechanisms of MerR and MerD, which need further elucidation in the future.

Bacteria maintain an uneasy relationship with metal ions and alter their physiological behavior to minimize or nullify the toxicity of metals when residing in such regions or encountering such conditions (Singh et al., 2014). Bacteria can sense metal stress through a receptor and signal(s) using two-component regulatory systems and transmitting information to flagellar motors, which move them in the required direction by the chemotaxis system (Bren and Eisenbach, 2000). Here, we consistently demonstrated using transcriptional profiles that most genes involved in bacterial flagellar assembly, chemotaxis and corresponding two-component system of *P. stutzeri* 273 were dramatically down-regulated when challenged with 50 μM Hg^{2+} (**Figures 3B–D**). Correspondingly, Hg^{2+} significantly altered bacterial physiology development including flagella formation, motility, chemotaxis, and biofilm formation (**Figure 4**).

The question remains why bacteria undergo such physiological responses under mercuric stress. Many metals have no known beneficial function and can be quite toxic, even at low levels. Given our experimental conditions in the presence of Hg^{2+}, *P. stutzeri* 273 could only remove mercury near their living microenvironment. However, some amounts of Hg^{2+} still remained in the media, which the bacterial chemotaxis system could sense. Therefore, the optimal bacterial response will decrease motility to avoid more mercuric stress exposure. So, bacteria down-regulate flagella development to reduce motility under these harsh conditions. This is consistent with our finding that flagellum biosynthesis is inhibited by stressful environmental conditions including metal stress due to flagellum biosynthesis which requires significant cellular resources (Soutourina et al., 2002). The results in this study extend our knowledge of the regulatory mechanisms of the bacterial flagellar system and the complex mechanisms governing bacterial motility in response to heavy metal challenges.

While we understand the transformation of toxic Hg^{2+} to non-toxic Hg^{0} mediated by *mer* genes from a genetic perspective, the roles of *mer* genes playing in bacterial physiological development to cope with the mercuric stress remain elusive. Surprisingly, *merF* deletion from the chromosome of *P. stutzeri* 273 led to defective flagella formation (**Figure 5A**) and decreased swarming motility (**Figure 5B**) and biofilm formation (**Figure 6D**), while *merF* complement could restore these disabled functions (**Figures 6A–D**). MerF was reported to have 81 residues, two transmembrane helices and 20% sequence identity with two-thirds of the N-terminal of MerT (116 residues and three transmembrane helices) (Wilson et al., 2000). Previous studies propose that MerF is a mercuric ion transport protein possessing similar functions as MerT and MerC (Wilson et al., 2000). Thus, our findings discovered the connection between the *mer* related gene and bacterial flagella formation. MerF exists in many strains of pathogens, including *P. aeruginosa*, *Vibrio cholera,* and *Enterobacter cloacae*. This finding strongly suggests that MerF homologs in these pathogens may also regulate flagella and biofilm formation. Due to the importance of flagella formation, motility and biofilm formation in pathogenic infection (Chaban et al., 2015; Al-Wrafy et al., 2017), our study provides novel candidates to target some pathogen containing *merF*. Based on the novel MerF function we identified, we hypothesize that *mer* genes have gradually increased their gene complements and functional diversity. We further propose that *mer* evolution has progressed by sequential recruitment of novel functions over evolutionary time (Barkay et al., 2003).

Taken together, we propose a model for the mercury-adapted lifestyle of the marine bacterium *P. stutzeri* 273 which adopts both passive and active strategies to respond to mercury stress (**Figure 8**). We also propose that the *mer* gene cluster in *P. stutzeri* 273 is representative of that found in the genomes of bacteria living in marine environment contaminated by mercury, and this bacterium might be a good candidate to understand bacterial adaptation mechanisms to mercury stress and *mer* genes evolution in marine microbes.

AUTHOR CONTRIBUTIONS

RZ and CS conceived and designed the experiments. RZ performed the experiments. RZ, SW, NM, and CS analyzed the data. RZ, SW, and CS wrote the paper.

FUNDING

This work was supported by Taishan Young Scholar Foundation of Shandong Province (No. tsqn20161051), AoShan Talents Program supported by Qingdao National Laboratory for Marine Science and Technology (No. 2015ASTP), Natural Science Outstanding Youth Fund of Shandong Province (JQ201607), and "100-Talent Project" of the Chinese Academy of Sciences for CS. The plasmid pEX18Gm was kindly provided by Luyan Ma of the Institute of Microbiology, Chinese Academy of Sciences.

ACKNOWLEDGMENTS

We thank Dr. Brandi Mattson from the professional editing group "Life Science Editors" for the helpful comments on the manuscript.

SUPPLEMENTARY MATERIAL

The Supplementary Material for this article can be found online at: https://www.frontiersin.org/articles/10.3389/fmicb.2018.00682/full#supplementary-material

REFERENCES

Al-Wrafy, F., Brzozowska, E., Gorska, S., and Gamian, A. (2017). Pathogenic factors of *Pseudomonas aeruginosa* - the role of biofilm in pathogenicity and as a target for phage therapy. *Postepy. Hig. Med. Dosw.* 71, 78–91. doi: 10.5604/01.3001.0010.3792

Ammendola, S., D'Amico, Y., Chirullo, B., Drumo, R., Civardelli, D., Pasquali, P., et al. (2016). Zinc is required to ensure the expression of flagella and the ability to form biofilms in *Salmonella enterica* sv *Typhimurium*. *Metallomics* 8, 1131–1140. doi: 10.1039/c6mt00108d

Barkay, T., Miller, S. M., and Summers, A. O. (2003). Bacterial mercury resistance from atoms to ecosystems. *FEMS Microbiol. Rev.* 27, 355–384. doi: 10.1016/S0168-6445(03)00046-9

Boyd, E. S., and Barkay, T. (2012). The mercury resistance operon: from an origin in a geothermal environment to an efficient detoxification machine. *Front. Microbiol.* 3:349. doi: 10.3389/Fmicb.2012.00349

Bren, A., and Eisenbach, M. (2000). How signals are heard during bacterial chemotaxis: protein-protein interactions in sensory signal propagation. *J. Bacteriol.* 182, 6865–6873. doi: 10.1128/Jb.182.24.6865-6873.2000

Bundeleva, I. A., Shirokova, L. S., Pokrovsky, O. S., Bénézeth, P., Ménez, B., Gérard, E., et al. (2014). Experimental modeling of calcium carbonate precipitation by cyanobacterium *Gloeocapsa* sp. *Chem. Geol.* 374, 44–60. doi: 10.1016/j.chemgeo.2014.03.007

Chaban, B., Hughes, H. V., and Beeby, M. (2015). The flagellum in bacterial pathogens: for motility and a whole lot more. *Semin. Cell Dev. Biol.* 46, 91–103. doi: 10.1016/j.semcdb.2015.10.032

Champier, L., Duarte, V., Michaud-Soret, I., and Coves, J. (2004). Characterization of the MerD protein from *Ralstonia metallidurans* CH34: a possible role in bacterial mercury resistance by switching off the induction of the *mer* operon. *Mol. Microbiol.* 52, 1475–1485. doi: 10.1111/j.1365-2958.2004.04071.x

Chen, M., Yan, Y. L., Zhang, W., Lu, W., Wang, J., Ping, S. Z., et al. (2011). Complete genome sequence of the type strain *Pseudomonas stutzeri* CGMCC 1.1803. *J. Bacteriol.* 193, 6095–6095. doi: 10.1128/Jb.06061-11

Dash, H. R., and Das, S. (2012). Bioremediation of mercury and the importance of bacterial *mer* genes. *Int. Biodeter. Biodegr.* 75, 207–213. doi: 10.1016/j.ibiod.2012.07.023

Dietrich, G. J., Dietrich, M., Kowalski, R. K., Dobosz, S., Karol, H., Demianowicz, W., et al. (2010). Exposure of rainbow trout milt to mercury and cadmium alters sperm motility parameters and reproductive success. *Aquat. Toxicol.* 97, 277–284. doi: 10.1016/j.aquatox.2009.12.010

Dressaire, C., Moreira, R. N., Barahona, S., de Matos, A. P. A., and Arraiano, C. M. (2015). BolA is a transcriptional switch that turns off motility and turns on biofilm development. *MBio* 6:e02352-14. doi: 10.1128/mBio.02352-14

Gadd, G. M. (2010). Metals, minerals and microbes: geomicrobiology and bioremediation. *Microbiology* 156, 609–643. doi: 10.1099/mic.0.037143-0

Han, Z., Yan, H., Zhao, H., Zhou, S., Han, M., Meng, X., et al. (2014). Bio-precipitation of calcite with preferential orientation induced by *Synechocystis* sp. PCC6803. *Geomicrobiol. J.* 31, 884–899. doi: 10.1080/01490451.2014.907379

Hong, L., Sharp, M. A., Poblete, S., Bieh, R., Zamponi, M., Szekely, N., et al. (2014). Structure and dynamics of a compact state of a multidomain protein, the mercuric ion reductase. *Biophys. J.* 107, 393–400. doi: 10.1016/j.bpj.2014.06.013

Kearns, D. B. (2010). A field guide to bacterial swarming motility. *Nat. Rev. Microbiol.* 8, 634–644. doi: 10.1038/nrmicro2405

Kime, D. E. (1995). The effects of pollution on reproduction in fish. *Rev. Fish Biol. Fish.* 5, 52–95. doi: 10.1007/Bf01103366

Larkin, M. A., Blackshields, G., Brown, N. P., Chenna, R., McGettigan, P. A., McWilliam, H., et al. (2007). Clustal W and clustal X version 2.0. *Bioinformatics* 23, 2947–2948. doi: 10.1093/bioinformatics/btm404

Lee, K.-J., Kim, J.-A., Hwang, W., Park, S.-J., and Lee, K.-H. (2013). Role of capsular polysaccharide (CPS) in biofilm formation and regulation of CPS production by quorum-sensing in *Vibrio vulnificus*. *Mol. Microbiol.* 90, 841–857. doi: 10.1111/mmi.12401

Liu, P. L., Chen, X., Huang, Q. Y., and Chen, W. L. (2015). The role of CzcRS two-component systems in the heavy metal resistance of *Pseudomonas putida* X4. *Int. J. Mol. Sci.* 16, 17005–17017. doi: 10.3390/ijms160817005

Mathema, V. B., Thakuri, B. C., and Sillanpaa, M. (2011). Bacterial *mer* operon-mediated detoxification of mercurial compounds: a short review. *Arch. Microbiol.* 193, 837–844. doi: 10.1007/s00203-011-0751-4

Morby, A. P., Hobman, J. L., and Brown, N. L. (1995). The role of cysteine residues in the transport of mercuric ions by the Tn501 mert and merp mercury-resistance proteins. *Mol. Microbiol.* 17, 25–35. doi: 10.1111/j.1365-2958.1995.mmi_17010025.x

Mukhopadhyay, D., Yu, H. R., Nucifora, G., and Misra, T. K. (1991). Purification and functional-characterization of MerD - a coregulator of the mercury resistance operon in Gram-negative bacteria. *J. Biol. Chem.* 266, 18538–18542.

Nucifora, G., Silver, S., and Misra, T. K. (1989). Down regulation of the mercury resistance operon by the most promoter-distal gene *merD*. *Mol. Gen. Genet.* 220, 69–72. doi: 10.1007/BF00260858

Petrus, A. K., Rutner, C., Liu, S., Wang, Y., Wiatrowski, H. A., and Kostka, J. E. (2015). Mercury reduction and methyl mercury degradation by the soil bacterium *Xanthobacter autotrophicus* Py2. *Appl. Environ. Microbiol.* 81, 7833–7838. doi: 10.1128/aem.01982-15

Radin, J. N., Gaddy, J. A., Gonzalez-Rivera, C., Loh, J. T., Algood, H. M., and Cover, T. L. (2013). Flagellar localization of a *Helicobacter pylori* autotransporter protein. *MBio* 4:e00613–12. doi: 10.1128/mBio.00613-12

Schue, M., Glendinning, K. J., Hobman, J. L., and Brown, N. L. (2008). Evidence for direct interactions between the mercuric ion transporter (MerT) and mercuric reductase (MerA) from the Tn501mer operon. *Biometals* 21, 107–116. doi: 10.1007/s10534-007-9097-4

Singh, A. K., Dhanjal, S., and Cameotra, S. S. (2014). Surfactin restores and enhances swarming motility under heavy metal stress. *Colloid Surf. B Biointerfaces* 116, 26–31. doi: 10.1016/j.colsurfb.2013.12.035

Sone, Y., Nakamura, R., Pan-Hou, H., Itoh, T., and Kiyono, M. (2013). Role of MerC, MerE, MerF, MerT, and/or MerP in resistance to mercurials and the transport of mercurials in *Escherichia coli*. *Biol. Pharm. Bull.* 36, 1835–1841. doi: 10.1248/bpb.b13-00554

Sone, Y., Uraguchi, S., Takanezawa, Y., Nakamura, R., Pan-Hou, H., and Kiyono, M. (2017). Cysteine and histidine residues are involved in *Escherichia coli* Tn21 MerE methylmercury transport. *FEBS Open Bio.* 7, 1994–1999. doi: 10.1002/2211-5463.12341

Soutourina, O. A., Krin, E., Laurent-Winter, C., Hommais, F., Danchin, A., and Bertin, P. N. (2002). Regulation of bacterial motility in response to low pH in *Escherichia coli*: the role of H-NS protein. *Microbiology* 148, 1543–1551. doi: 10.1099/00221287-148-5-1543

Steele, R. A., and Opella, S. J. (1997). Structures of the reduced and mercury-bound forms of MerP, the periplasmic protein from the bacterial mercury detoxification system. *Biochemistry* 36, 6885–6895. doi: 10.1021/bi9631632

Stelmack, P. L., Gray, M. R., and Pickard, M. A. (1999). Bacterial adhesion to soil contaminants in the presence of surfactants. *Appl. Environ. Microbiol.* 65, 163–168.

Tamura, K., Stecher, G., Peterson, D., Filipski, A., and Kumar, S. (2013). MEGA6: molecular evolutionary genetics analysis version 6.0. *Mol. Biol. Evol.* 30, 2725–2729. doi: 10.1093/molbev/mst197

Vetriani, C., Chew, Y. S., Miller, S. M., Yagi, J., Coombs, J., Lutz, R. A., et al. (2005). Mercury adaptation among bacteria from a deep-sea hydrothermal vent. *Appl. Environ. Microbiol.* 71, 220–226. doi: 10.1128/AEM.71.1.220-226.2005

Wahba, H. M., Stevenson, M. J., Mansour, A., Sygusch, J., Wilcox, D. E., and Omichinski, J. G. (2017). Structural and biochemical characterization of organotin and organolead compounds binding to the organomercurial lyase MerB provide new insights into its mechanism of carbon-metal bond cleavage. *J. Am. Chem. Soc.* 139, 910–921. doi: 10.1021/jacs.6b11327

Wang, M. H., Lee, J. S., and Li, Y. (2017). Global proteome profiling of a marine copepod and the mitigating effect of ocean acidification on mercury toxicity after multigenerational exposure. *Environ. Sci. Technol.* 51, 5820–5831. doi: 10.1021/acs.est.7b01832

Weller-Stuart, T., Toth, I., De Maayer, P., and Coutinho, T. (2017). Swimming and twitching motility are essential for attachment and virulence of *Pantoea ananatis* in onion seedlings. *Mol. Plant Pathol.* 18, 734–745. doi: 10.1111/mpp.12432

Wilson, J. R., Leang, C., Morby, A. P., Hobman, J. L., and Brown, N. L. (2000). MerF is a mercury transport protein: different structures but a common mechanism for mercuric ion transporters? *FEBS Lett.* 472, 78–82. doi: 10.1016/S0014-5793(00)01430-7

Wu, S., Zheng, R., Sha, Z., and Sun, C. (2017). Genome sequence of *Pseudomonas stutzeri* 273 and identification of the exopolysaccharide EPS273 biosynthesis locus. *Mar. Drugs* 15:218. doi: 10.3390/md15070218

Wu, S. M., Liu, G., Jin, W. H., Xiu, P. Y., and Sun, C. M. (2016). Antibiofilm and anti-infection of a marine bacterial exopolysaccharide against *Pseudomonas aeruginosa*. *Front. Microbiol.* 7:102. doi: 10.3389/fmicb.2016.00102

Yuan, C. G., Shi, J. B., He, B., Liu, J. F., Liang, L. N., and Jiang, G. B. (2004). Speciation of heavy metals in marine sediments from the East China Sea by ICP-MS with sequential extraction. *Environ. Int.* 30, 769–783. doi: 10.1016/j.envint.2004.01.001

Zhu, Y., Ma, N., Jin, W., Wu, S., and Sun, C. (2017). Genomic and transcriptomic insights into calcium carbonate biomineralization by marine actinobacterium *Brevibacterium linens* BS258. *Front. Microbiol.* 8:602. doi: 10.3389/fmicb.2017.00602

Conflict of Interest Statement: The authors declare that the research was conducted in the absence of any commercial or financial relationships that could be construed as a potential conflict of interest.

frontiers in Microbiology

ORIGINAL RESEARCH
published: 25 May 2018
doi: 10.3389/fmicb.2018.01098

Temperature-Dependent Gene Expression in *Yersinia ruckeri*: Tracking Specific Genes by Bioluminescence During *in Vivo* Colonization

*Jessica Mendez, Desirée Cascales, Ana I. Garcia-Torrico and Jose A. Guijarro**

Área de Microbiología, Departamento de Biología Funcional, Facultad de Medicina, Instituto de Biotecnología de Asturias, Universidad de Oviedo, Oviedo, Spain

Yersinia ruckeri is a bacterium causing fish infection processes at temperatures below the optimum for growth. A derivative *Tn5* transposon was used to construct a library of *Y. ruckeri* mutants with transcriptional fusions between the interrupted genes and the promoterless *luxCDABE* and *lacZY* operons. *In vitro* analysis of β-galactosidase activity allowed the identification of 168 clones having higher expression at 18°C than at 28°C. Among the interrupted genes a SAM-dependent methyltransferase, a diguanylated cyclase, three genes involved in legionaminic acid synthesis and three transcriptional regulators were defined. In order to determine, via bioluminescence emission, the *in vivo* expression of some of these genes, two of the selected mutants were studied. In one of them, the *acrR* gene coding a repressor involved in regulation of the AcrAB-TolC expulsion pump was interrupted. This mutant was found to be highly resistant to compounds such as chloramphenicol, tetracycline, and ciprofloxacin. Although *acrR* mutation was not related to virulence in *Y. ruckeri,* this mutant was useful to analyze *acrR* expression in fish tissues *in vivo*. The other gene studied was *osmY* which is activated under osmotic stress and is involved in virulence. In this case, complemented mutant was used for experiments with fish. *In vivo* analysis of bioluminescence emission by these two strains showed higher values for *acrR* in gut, liver and adipose tissue, whereas *osmY* showed higher luminescence in gut and, at the end of the infection process, in muscle tissue. Similar results were obtained in *ex vivo* assays using rainbow trout tissues. The results indicated that this kind of approach was useful for the identification of genes related to virulence in *Y. ruckeri* and also for the *in vivo* and *in vitro* studies of each of the selected genes.

Keywords: *Yersinia ruckeri*, temperature regulated genes, bioluminescence, *acrR, osmY*

OPEN ACCESS

Edited by:
Daniela De Biase, Sapienza Università di Roma, Italy

Reviewed by:
Jack Christopher Leo, University of Oslo, Norway
Jesus L. Romalde, Universidade de Santiago de Compostela, Spain

****Correspondence:***
Jose A. Guijarro
jaga@uniovi.es

Specialty section:
This article was submitted to Microbial Physiology and Metabolism, a section of the journal Frontiers in Microbiology

Received: *20 December 2017*
Accepted: *08 May 2018*
Published: *25 May 2018*

Citation:
Mendez J, Cascales D, Garcia-Torrico AI and Guijarro JA (2018) Temperature-Dependent Gene Expression in Yersinia ruckeri: Tracking Specific Genes by Bioluminescence During in Vivo Colonization. Front. Microbiol. 9:1098. doi: 10.3389/fmicb.2018.01098

INTRODUCTION

Yersinia ruckeri is the etiological agent of "Enteric red mouth disease" of salmonids which causes important economic losses in the aquaculture industry. The bacterium is distributed worldwide and four serotypes were defined (Romalde et al., 1993). The most virulent is serotype O1 which has two biotypes 1 and 2 (Davies and Frerichs, 1989). Most outbreaks are caused by biotype 1,

but in recent years biotype 2 has been associated with outbreaks in different parts of the world (Arias et al., 2007; Calvez et al., 2014).

A key environmental stress factor in outbreaks of most bacterial fish diseases in fish farms is water temperature. In some cases, outbreaks occur when water temperature drops to a certain value, as in the case of "Cold water vibriosis" (Enger et al., 1991) and "Cold water disease" (Cipriano and Holt, 2005). In other diseases, such as "lactococcosis," outbreaks are related to an increase in water temperature (Vendrell et al., 2006). Interestingly, a remarkable number of bacterial diseases in aquaculture, particularly those of freshwater, occurred at temperatures below the optimum for growth of the infecting bacteria (Guijarro et al., 2015). Bacterial genes activated under these conditions were identified in fish pathogens. Indeed, in *Flavobacterium psychrophilum*, Hesami et al. (2011) defined a set of genes that were up-regulated at 8°C versus 20°C by using suppression subtractive hybridization. In the same way, in *Lactococcus garvieae* several genes linked to virulence were up-regulated at 18°C versus 37°C (Aguado-Urda et al., 2013). In *Aeromonas hydrophila* a MALDI-TOF analysis of the extracellular products showed that a serine-metalloprotease, S-layer, flagellins and proteins related to the type III secretion system were up-regulated at 25°C versus 37°C (Yu et al., 2007). The two-component system PhoP-PhoQ of *Edwardsiella tarda* responds to changes in environmental temperature by activating type III and type VI secretion systems, both associated with virulence of the bacterium (Srinivasa Rao et al., 2003, 2004; Zheng et al., 2005; Wang et al., 2009; Chakraborty et al., 2010). In spite of these studies, little is known about the temperature-regulated virulence factors in fish-associated bacterial pathogens and even less about the systems involved in their regulation.

Y. ruckeri has an optimal growth temperature of 28°C but outbreaks of disease occur at temperatures around 18°C. Virulence of *Y. ruckeri* is multifactorial and different genes were described as being involved in pathogenesis (Fernández et al., 2007a; Tobback et al., 2007; Kumar et al., 2015). Expression of some of these genes was higher at 18°C than at 28°C (Fernández et al., 2004). Thus, the expression of the *traH-N* operon encoding a putative type IV secretion system (Méndez et al., 2009), YhlA hemolysin (Fernández et al., 2007b), Yrp1protease (Méndez and Guijarro, 2013) and ruckerbactin, a catecholate siderophore iron acquisition system were up-regulated at 18°C versus 28°C (Fernández et al., 2004). Therefore, the temperature-dependent modulation of virulence genes in *Y. ruckeri* tends to optimize the expression of these in conditions mimicking those encountered in the host.

As opposed to human pathogenic *Yersinia* species in which virulence factors are induced at temperatures near the optimal for bacterial growth, there is no study related to how *Y. ruckeri* regulates virulence gene expression at temperatures below the optimum for growth. The results of previous studies carried out in *Y. ruckeri* (Fernández et al., 2004; Méndez and Guijarro, 2013), showed the need for the present investigation, whose goal was the selection and identification of *Y. ruckeri* genes expressed preferentially at 18°C versus 28°C due to their potential role as virulence factors. Using transcriptional fusions between *Y. ruckeri* promoters and *lux-lac* operons inserted in the *Tn5* transposon, 168 clones having higher β-galactosidase activity at 18°C than at 28°C in an EMB medium were selected. Two of them, carrying *Tn5 lux-lac* insertions in the *acrR* and *osmY* genes, a repressor of the AcrAB-TolC system and a gene induced under osmotic shock, respectively, were further characterized both *in vitro* and *in vivo*. This study presents a useful, practical approach for the identification and further analysis of genes involved in virulence and for the determination of their expression both *in vitro* and *in vivo*.

MATERIALS AND METHODS

Bacterial Strains, Plasmids, and Culture Conditions

E. coli strains (**Table 1**) were routinely grown in 2x TY (16 g/L tryptone, 10 g/L yeast extract, 5 g/L NaCl) broth and 2% agar, and *Y. ruckeri* strains (**Table 1**) in nutrient broth (NB) or nutrient 1.5% agar (NA) from VWR International and Tryptic Soy Broth (TSB) and Tryptic Soy 1.5% agar (TSA) from Merck. Liquid cultures were incubated at 37°C for *E. coli* and at 18°C and 28°C for *Y. ruckeri* in orbital shakers at 250 rpm. Growth was monitored by determining the OD_{600}. In order to detect changes in the β-galactosidase activity, EMB from Merck was used. This is a differential microbiological medium useful to distinguish between organisms that ferment lactose (β-galactosidase positive) and those that do not (β-galactosidase negative). The lactose fermenters would produce dark colonies whereas the non-fermenters would form translucent or pink ones. When required, the following compounds were added to the media: 10 μg/mL erythromycin, 0.1 μg/mL cefotaxime, 50 μg/mL kanamycin, 50 μg/mL streptomycin, or 100 μg/mL ampicillin, all from Sigma-Aldrich Co.

Construction of Mini-*Tn5 lux-lac Km2* Transposon

Construction of pUT mini-*Tn5 lux-lac Km2* (**Table 1**) was initiated by utilizing the pUT mini-*Tn5 Km2* vector (de Lorenzo et al., 1990). First, a 6 Kb SphI DNA fragment harboring the *lacZY* operon lacking the promoter and terminator was removed by enzymatic digestion from the pIVET8 plasmid (Mahan et al., 1995) (**Table 1**) and ligated to the pUT vector, previously digested with the same enzyme and dephosphorylated. The ligation mixture was introduced in *E. coli* S17-1λ*pir* by electroporation. Transformed cells were selected on 2x TY media supplemented with ampicillin. The correct orientation of the *lacZY* operon was defined by DNA sequencing using the Lacsec primer (Supplementary Table S1). Once the pUT mini-*Tn5 lac Km2* vector was obtained, a 5.8 Kb NotI DNA fragment containing the *luxCDABE* operon was removed from the pCS26PAC vector (Bjarnason et al., 2003) and ligated into the NotI restriction size located at the 5′end of the *lacZY* operon in the pUT mini-*Tn5 lac Km2* vector. The ligation mixture was introduced by electroporation in *E. coli* S17-1λ*pir* and clones were selected on 2x TY media containing ampicillin. Random clones were used

TABLE 1 | Characteristics of the strains and plasmids used in this work.

Strain or plasmid	Relevant properties	Source or reference
Strains		
E. coli		
S17-1λpir	λ(pir) hsdR pro thi RP4-2 Tc::mu Km::Tn7	Simon et al., 1983
DH5 αλpir	F'/endA1 hsdR17 (rk-mk+) supE44 thi-1 recA1 gyrA (Nal^R) λ (pir)	Woodcock et al., 1989
Y. ruckeri		
150	Strain of serotype O1, biotype 1 isolated from an outbreak in trout.	J. L. Larsen, (Denmark)
150CTX	Strain 150 cultured in presence of cefotaxime	This work
150 *acrR*$^-$	*acrR*::mini-Tn5 *luxlac* Km2, Km^r	This work
150 *acrR*$^+$	*acrR*$^-$ con pGBM5::*acrR*	This work
150 *osmY*$^-$	*osmY*::mini-Tn5 *luxlac* Km2, Km^r	This work
150 *osmY*$^+$	*osmY*$^-$ harboring pGBM5::*osmY*	This work
150 *osmY*$^{++}$	*osmY*$^-$ harboring pGBM5::*osmY-ytjA*	This work
150 β1T.B2	Mini Tn5-luxlac mutant cultured in presence of cefotaxime	This work
Plasmids		
pCS26Pac	Km^r, *luxCDABE*	Bjarnason et al., 2003
pGBM5	Spc^r/Sm^r, promoter lac	Manen et al., 1997
pIVET8	Ap^r, oriR6K, mob+, cat-lacZY promotorless	Mahan et al., 1995
pUC19	Ap^r, cloning vector	Pharmacia
pUT mini-Tn5 Km2	Ap^r, oriR6K, mobRP4, tnp, mini-Tn5 Km2 (Km^r)	de Lorenzo et al., 1990
pUT mini-Tn5 *lac* Km2	pUT mini-Tn5 Km2 harboring *trpAlacZY* genes without promoter or transcription termination sequences	This work
pUT mini-Tn5 *luxlac* Km2	pUT mini-Tn5 Km2, harboring *luxABCDE* and *trpAlacZY* tandem genes without promoter	This work

for plasmid purification and further analysis by PCR and DNA sequencing in order to select those carrying the *lux* operon in the 5′-3′orientation with respect to *lacZY* and kanamycin-resistant genes. The obtained plasmid was named pUT mini-*Tn5 lux-lac Km2* (**Table 1**).

In brief, pUT mini-*Tn5 lux-lac Km2* plasmid was transferred from *E. coli* S17-1λ*pir* to *Y. ruckeri* 150 by conjugation. To do that, 500 μl of donor and 4 mL of recipient strains in exponential growth phase (OD_{600}, 0.6) were washed twice by centrifugation and resuspended in 10 mL of MilliQ water. Then, the suspension was filtered through a 0.45 μm pore membrane that was transferred onto a 2x TY medium and incubated for 4 h at 28°C. After incubation, the bacteria were resuspended in 2 mL of NB medium and aliquots of 50 μL were spread onto NA medium containing kanamycin (resistance to which was conferred by the transposon) and erythromycin or cefotaxime, antibiotics to which *Y. ruckeri* 150 is intrinsically resistant. After incubation at 28°C for 48 h, each selected transconjugant was transferred to a microtiter plate well containing 100 μL of NB medium with kanamycin and erythromycin and incubated for 48 h at 28°C. Triplicates of each plate were generated by using a Steer replicator, a multiple inoculator composed of 96 specifically spaced inoculating rods corresponding in position to the wells of a microtiter plate, and after incubation, glycerol was added to each well at a final proportion of 30%. Plates were kept at −80°C until use.

In order to determine the insertion pattern of the *Tn5 lux-lac Km2* transposon, 28 randomly selected insertion mutants were analyzed by Southern blot after digestion of the genomic DNA with SphI, using the *km* gene as a probe (Supplementary Table S1). Probe labeling, hybridization, and development were performed with the DIG DNA labeling and detection kit from Roche, following the manufacturer's instructions. After hybridization, high-stringency washes of the membrane was carried out to remove the *km* probe and plasmid insertion events were analyzed in the same membrane using as a probe the *bla* gene previously amplified by PCR from the pUT mini-*Tn5 lux-lac Km2* vector (**Table 1**). Transposon stability was assessed by repeated subculture of some mutants in non-selective TSB. After 3 days subculture, the numbers of cultivable cells on TSA with and without kanamycin were determined. The percentages of kanamycin-resistant bacteria were determined in relation to total cells.

Selection and Identification of Promoters by Using β-Galactosidase Activity as a Marker

In order to identify clones harboring transcriptional fusions between the *lacZY* operon and *Y. ruckeri* genes induced at 18°C, the library of transconjugants was replicated twice onto plates containing EMB medium supplemented with kanamycin. One of these plates was incubated at 18°C and the other one at 28°C for 40 and 24 h, respectively. After that, both replicas were analyzed to select those colonies having higher β-galactosidase activity, indicated by the colony having a more intense color, at 18°C than at 28°C. Clones of interest were submitted to a second screening in the same conditions and then kept at −80°C until use.

To identify the *Tn5 lux-lac Km2* transposon insertion site in the selected clones, genomic DNA from each clone was digested with PstI, XbaI, or SphI and then ligated into the pUC19 plasmid previously digested with the corresponding

enzyme and dephosphorylated. The resulting ligation mixture was electroporated into *E. coli* S17-1λ*pir* and clones of interest were further selected on 2x TY medium with ampicillin and kanamycin. These clones carried a DNA fragment harboring the kanamycin resistance gene from the transposon followed by a DNA fragment of variable length from the DNA located at the 3′position of the transposon insertion site. These fragments were sequenced using the TDKm6 primer (Supplementary Table S1) present at the end of the kanamycin resistance gene sequence and analyzed by RAST and BlastX programs.

Complementation and Phenotypic Characterization of *acrR* and *osmY* Mutants

Complementation of *acrR* and *osmY* mutants was carried out by using plasmid pGBM5 (**Table 1**). *acrR*, *osmY*, and *osmY* and the adjacent gene *ytjA* (osmY^{++}) were PCR amplified using the primers acrR-F/acrR-R, osmy-F/osmy-R and osmY-F/osmY-R2, respectively (Supplementary Table S1). All primers contained BamHI and PstI site at one end in order to clone the PCR-generated fragment into the BamHI-PstI restriction sites of the pGBM5 plasmid. The ligation mixture was introduced into *E. coli* DH5α λ*pir* and transformants were selected on 2x TY medium with streptomycin. Restriction enzyme analysis, as well as PCR amplification of the generated plasmids, confirmed the correct structure and presence of the genes of interest. Constructions were transferred by electroporation to the respective mutants, and the appropriate clones were selected on TSA medium with kanamycin and streptomycin.

Susceptibility tests to antimicrobial agents and detergents were carried out in microtiter plates using twofold serial dilutions. Triplicate wells containing 5×10^4 cells of each strain and the respective compound to be tested were incubated at 18°C for 24 h. The MIC was determined for each compound. The experiments were carried out in triplicate. The compounds assayed and the ranges of concentration were: acriflavine and chloramphenicol 0.02–40.96 μg/mL; ciprofloxacin 0.02–1.28 μg/mL; tetracycline 0.02–10.24 μg/mL; SDS and Triton X-100, 0.0015–25.6%.

To determine the effect of n-hexane and bile salts on bacterial growth 10 μL of a bacterial suspension of 10^8 cfu/mL were deposited onto TSA medium in glass plates. After 10 min, the culture medium was covered with a 3 mm layer of n-hexane and plates were incubated at 18°C for 72 h. The effect of bile salts was assessed by spotting 10 μL of 10-fold serially diluted bacterial culture onto TSA media supplemented with 4% (w/v) bile salts in a proportion of 85:15 sodium cholate and sodium deoxycholate that, according to Denton et al. (1974), corresponds with that found in the rainbow trout gut.

For motility assays, 2 μl of overnight cultures of each strain were spotted onto TSA medium containing lactose 0.5% and 0.3% or 0.6% of agar; and in NA with 0.6% agar and different concentrations of glucose and lactose (glucose 0.25%, glucose 0.5%, lactose 0.75%, and lactose 0.5% + glucose 0.25%). Plates were incubated at 18 and 28°C for 3 days.

Real-Time PCR Validation

Total RNA was extracted from two biological replicates of *Y. ruckeri* 150 grown at the early stationary phase ($OD_{600} \approx 1.1$) in TSB at 28°C and 18°C. The cultures were fixed using RNA^{TM} Protect Bacterial Reagent (Qiagen Inc.) in a ratio of 1 mL of reagent per 0.5 mL of bacterial culture. Centrifugation was used to pellet the cells and RNA was extracted in RNase-/DNase-free water using the High Pure RNA Isolation Kit (Roche). After three treatments with RNase-free DNase (Ambion) to eliminate DNA contamination, total RNA was quantified using micro-spectrophotometry (Nanodrop ND-1000, Nanodrop Technologies, EEUU). The RNA quality was estimated using an Agilent 2100 Bioanalyzer and RNA samples with an RNA Integrity Number (RIN) above 9.5 were selected.

cDNA synthesis was performed from 1 μg of total RNA using the High Capacity cDNA Reverse Transcription Kit (Applied Biosystems, United States) and random primers according to the manufacturer's instructions. Samples in which reverse transcriptase had not been added were used as negative controls. The cDNAs were subsequently quantified by real-time PCR amplification on an ABI PRISM 7900 Sequence Detection System (Applied Biosystems) with primers specifics to the *yrp1* (Yrp1-qF: 5′-TGCGCAAACCAATAT CAGCG-3′; Yrp1-qR: 5′-TGCGCAAACCAATATCAGCG-3′), *acrR* (AcrR-qF: 5′-CGTGCTTATATCACCGGCCT-3′; AcrR-qR: 5′-AGGCATTGCGCGATCATTTC-3′), *osmY* (Osmy-qF: 5′-CGGTTAGCGAATATGCCGGT-3′; OsmY-qR: 5′-ACAAAACCACGCCATCGGTA-3′) and 16S (16S-F: 5′-TTTG TTGCCAGCACGTAATGGT-3′; and 16S-R: 5′-GCGAGTT CGCTTCACTTTGTATCT-3′) genes and using the SYBR Green PCR Master Mix (Applied Biosystems, United States).

Expression level results were standardized relative to the transcription level of the housekeeping gene 16S rRNA for each isolate. The relative change in the *yrp1*, *acrR*, and *osmY* was calculated as the ratio of reference target using the $\Delta\Delta$Ct, where Ct is the cycle threshold. Real-time PCR was carried out on two independent biological replicates each containing three technical replicates. The results are represented as the mean ± SD.

Virulence Determination

For rapid virulence screening of mutant strains in the genes coding for AcrR, OsmY, hypothetical protein OEU24935.1, polymyxin resistance ArnC, hypothetical protein OEU21186.1, esterase YqiA and UDP-*N*-acetylglucosamine 4,6-deshydratase, a total of 10 fish, average weight 6–8 g, were intraperitoneally injected with 0.1 mL of 10^3 cfu/mL of each mutant.

For virulence determination of *acrR*$^-$ and *osmY*-strains, 15 rainbow trout fry distributed in three groups were intraperitoneally injected with 0.1 mL of 10^7 cfu/mL of each strain. The fish were kept in 70 L tanks at 18°C and mortalities were recorded each day for a week and compared with those produced by the parental strain. The data were analyzed with Chi-square test. $P < 0.05$ was considered statistically significant.

LD_{50} experiments by intraperitoneal injection with the parental, *acrR* mutant and *acrR*$^+$ complemented strains were carried out as described by Fernández et al. (2002). The doses

injected ranged from 10 to 10^8 cfu per fish and mortalities were followed up to 7 days. The LD_{50} values were calculated by the method of Reed and Muench (1938). Bath infection was carried out by immersion of the fish for 1 h in 10 L dechlorinated water containing a final concentration of 10^7 cfu/mL of the different strains. The fish were then transferred to 70 L tanks and mortalities were followed up to 7 days. In both challenges, dead fish were withdrawn every day and samples from internal organs were spread onto TSA medium. After 48 h of incubation at 28°C several colonies of the predominant bacteria were identified by PCR in order to confirm that they corresponded to the previously injected strain.

All the experiments carried out with fish were authorized and supervised by the Ethics Committee of Oviedo University.

Real-Time Visualization of *Y. ruckeri* Promoter Expression

Three groups of 30 fish weighing from 8 to 10 g were infected with *Y. ruckeri acrR*$^-$ and *osmY*$^{++}$ strains. The *acrR*$^-$ strain was used in both intraperitoneal and immersion infection experiments. Thus, one group of 30 fish was infected by intraperitoneal injection using 10^6 cfu per fish and another group of 30 individuals was kept in a 10 L tank of dechlorinated water in contact with the *acrR* mutant at a concentration of 10^7 cfu/mL for 1 h. Infection challenge using *osmY*$^{++}$ was only carried out by intraperitoneal injection following the procedure used for *acrR*. After infection, fish were transferred to tanks containing 70 L of dechlorinated water at 18°C. At 24 h intervals over a 7-day period, fish were euthanized by overdose of ethylene glycol monophenyl ether, dissected and analyzed with IVIS Imaging System (Xenogen) to monitor the bacterial progression and expression of *acrR* and *osmY* genes in the fish organs. Each experiment was repeated twice to ensure data accuracy.

To analyze gene expression using different rainbow trout tissues, each strain was spread on plates containing TSA medium for confluent growth. Then, fish tissues were deposited onto the medium. Plates were incubated at 18°C overnight and luminescence analyzed by Ivis Lumina.

RESULTS

Development of a Vector to Generate a Dual Reporter *lux-lac* Transcriptional Fusion Library in *Y. ruckeri*

To create an appropriate dual reporter cassette for the analysis of differential gene expression in *Y. ruckeri* and also in other Gram-negative bacteria, we have modified the original pUT mini-*Tn5 Km2* plasmid, a *λpir*-dependent delivery vector. Inside the mini-*Tn5 Km2* transposon and at the 5′end of the kanamycin gene, the promoterless *luxCDABE* operon from *Photorhabdus luminescens* (Meighen and Szittner, 1992) and *lacZY* genes from the pIVET8 plasmid (Mahan et al., 1995) were inserted (**Figure 1A**). The resulting plasmid, named pUT-mini *Tn5 lux-lac Km2*, was transferred by conjugation from *E. coli* S17*λpir* to *Y. ruckeri* 150. Since the latter lacks the Pir protein necessary for the replication of the pUT plasmid, transconjugants must have randomly integrated the transposon (*Tn5 lux-lac Km2*) into their genomes. Insertion of the mini *Tn5 lux-lac Km2* transposon into the *Y. ruckeri* genome generated, in many cases, transcriptional fusions between the promoter of the interrupted gene by the transposon and the *lux-lac* cassette (**Figure 1B**). In that way, the capture of promoters transcribing the *lux-lac* fusions was useful to determine *in vitro* and *in vivo* promoter regulation of different genes under specific conditions.

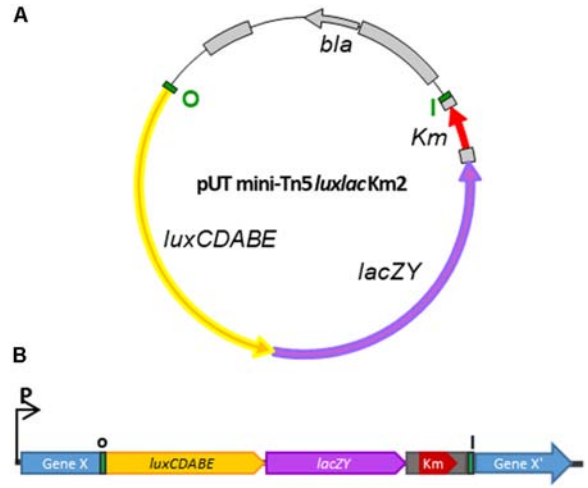

FIGURE 1 | Schematic representation of the generation of a library of *Y. ruckeri* mutants by transposition. **(A)** Plasmid pUT mini-*Tn5 lux-lac Km2* carrying the modified mini-*Tn5* transposon harboring the *luxCDABE* and *lacZY* operons without promoters. **(B)** Transcriptional fusion between a putative *Y. ruckeri* chromosomal promoter and the *lux-lac* fusion operons generated after mini-*Tn5 lux-lac* insertion. *Bla*, resistance ampicillin; *Km*, resistance kanamycin; I-O terminal inverted *Tn5* sequences.

A library of 14,724 individual *Y. ruckeri* transconjugants harboring *Tn5 lux-lac Km2* insertions was generated. To determine if the transposon insertion in the genome of each cell was a random, plasmid-independent and unique event as it was previously described (Herrero et al., 1990), 28 kanamycin-resistant colonies were arbitrarily selected and subjected to Southern blot analysis. Each of the clones analyzed showed a single hybridizing fragment of a particular size when the kanamycin gene was used as a probe (Supplementary Figure S1A) indicating that the transposon insertion occurred randomly and only one time in the *Y. ruckeri* genome. When the ampicillin gene present in the plasmid was used as a probe not a single transconjugant showed a hybridizing signal (Supplementary Figure S1B). These results are consistent with those found by other authors.

Characterization and Identification of Temperature-Regulated Promoters by Using *lux-lac* Reporters

Y. ruckeri transconjugants were screened at 18° and 28°C for differential β-galactosidase activity in EMB medium (**Figure 2A**). A total of 168 clones (1.14%) displaying higher β-galactosidase

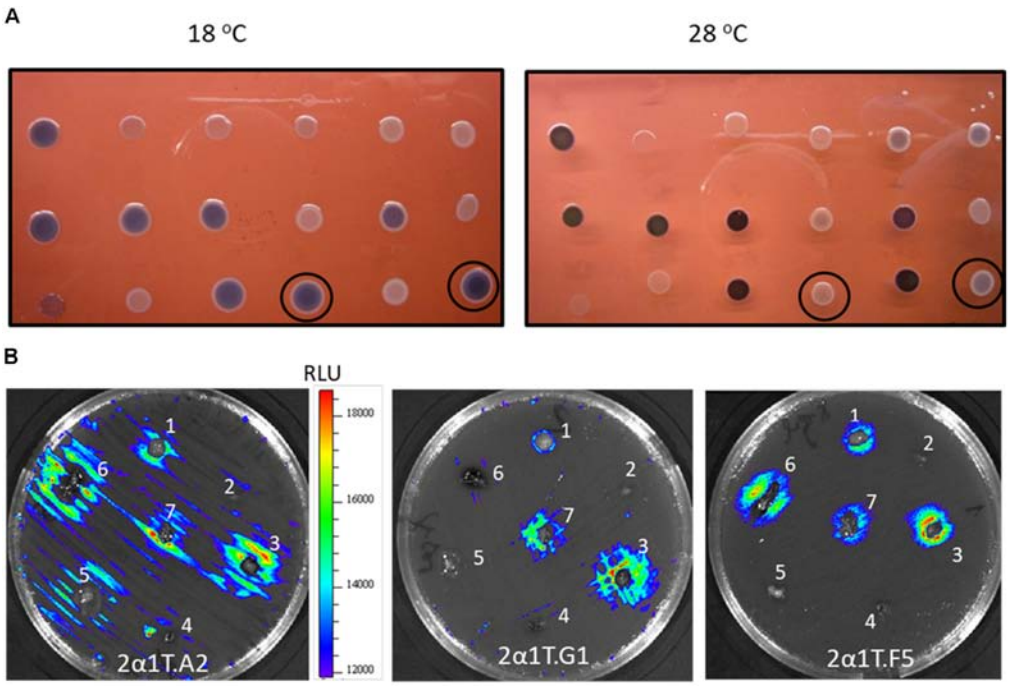

FIGURE 2 | Temperature differential gene expression of *Y. ruckeri* clones containing the *Tn5-lux-lac* transposon insertion. **(A)** β-galactosidase activity on EMB medium after incubation at 18°C and 28°C. Circled colonies represent two examples of differential expression depending on the temperature. **(B)** Bioluminescence emission by different *Y. ruckeri* clones after 24 h of incubation at 18°C in the presence of different rainbow trout (*O. mykiss*) organs which were distributed on the surface of TSA plates: brain (1); heart (2); liver (3); spleen (4); adipose tissue (5); gut (6); gills (7), 2B. Bar indicating the correlation between luminescence (RLU) and color.

activity, indicated by a more intense purple-black color at 18°C than at 28°C in the experimental conditions, were selected. Analysis of these clones by an Ivis Lumina apparatus showed that there was correspondence between the light emission level and β-galactosidase activity in most cases (data not shown).

The transposon insertion sites were mapped for 33 out of 168 selected clones and the identified genes are shown in **Table 2**. The growth culture patterns of several temperature-regulated mutants were similar to each other and also to the parental strain, indicating that the energy cost resulting from the differential expression of the *lux-lac* operons, both present in a single copy in the chromosome, had no major effect on the bacterial physiology (data not shown). For two clones, the existence of a linear correlation between cell number, in the range of 10^2 and 10^7 cfu, and luminescence with R^2 values of 0.9593 and 0.9865, respectively, was also determined.

In order to determine whether or not luminescence signals were useful in analyzing *Y. ruckeri* gene expression *ex vivo*, different randomly selected mutants were confluent spread on TSA medium. Tissue sections of several rainbow trout organs were deposited onto the culture and after 24 h of incubation at 18°C differences in the light emission displayed by the bacteria surrounding the different tissues were observed (**Figure 2B**). Thus, the gene interrupted in the 2a1T.A2 mutant showed highest light emission in liver, gills and gut tissues, whereas 2a1T.G1 and 2a1T.F5 mutants displayed the highest light emission in gills and liver, and gut and liver, respectively (**Figure 2B**).

Virulence determination was assessed in several of the selected mutants. Using intraperitoneal injection, 7 days post infection the parental strain produced 70% mortality, whereas mortalities for the selected mutants were: AcrR regulator, 80%; hyperosmotic protein OsmY, 0%; Hypothetical protein OEU24935.1, 30%; polymyxin resistance ArnC, 50%; Hypothetical protein OEU21186.1, 60%; Esterase YqiA, 50%; and UDP-*N*-acetylglucosamine 4,6-deshydratase, 0%.

Analysis of the Mutations in the Temperature-Regulated Genes *acrR* and *osmY*

In order to check if the strategy developed to identify temperature-regulated genes allowed us to select the appropriate clones, two of the mutants harboring transcriptional fusions between the *acrR* and *osmY* promoters and the *lux-lac* operons were chosen for further analysis. The *acrR* mutant was selected because it was found to be as virulent as the parental strain, whereas the *osmY* mutant was attenuated. In this way, each of them was useful for the *in vivo* monitoring of the infection process: the *acrR* mutant as a positive control and the *osmY* mutant to confirm its attenuation in virulence which should revert with the introduction of *osmY* gene *in trans*.

First, the differences in β-galactosidase activity displayed by the two mutants in EMB at 18°C in relation to 28°C

TABLE 2 | Products of *Y. ruckeri* interrupted genes by the *Tn5-lux-lac* transposon.

Gene product	Accession number	Gene product	Accession number	Gene product	Accession number
Metalloprotease Yrp1	CAC39217.1	Galactose/methyl galactoside import ATP-binding protein	OEU26755.1	Tn7-like transposition protein	OEU24391.1
Diguanylate cyclase	OEU26487.1	Glycogen phosphorylase	OEU26568.1	ADP-ribosyltransferase exoenzyme family protein	KGA50131.1
Glycosyltransferase	OEU24749.1	4-alpha-glucanotransferase	OEU26314.1	PsiF repeat protein	EEQ00620.1
SAM-dependent methyltransferase	OEU24750.1	UDP-*N*-acetylglucosamine 4,6-dehydratase	OEU25693.1	Putative esterase (YqiA)	AJI94468.1
Serine/threonine protein kinase (anti-sigma regulatory factor)	OEU26573.1	D-Glycero-D-manno-heptose 1-phosphate guanosyltransferase	OEU25698.1	Hypothetical protein	OEU24382.1
Response regulator (YsrR)	OEU25024.1	O-antigen polymerase	ABY48117.1	Hypothetical protein	OEU24387.1
DNA-binding transcriptional repressor AcrR	OEU24368.1	O-acyltransferase	OEU26581.1	Hypothetical protein	KGA49879.1
Osmotically inducible protein OsmY	OEU26500.1	Putative peptidoglycan deacetylase	OEU25943.1	Hypothetical protein	OEU24935.1
Co/Mg/Ni transporter	OEU26742.1	Antitoxin of toxin-antitoxin stability system	OEU25145.1	Hypothetical protein	EEP98349.1
MFS transporter	OEU26751.1	Cell division protein (DamX)	EEP98349.1	Hypothetical protein	OEU25186.1
Phosphoporin PhoE	OEU26976.1	Polymyxin resistance protein ArnC	OEU24187.1	Hypothetical protein	OEU24718.1

were quantified by the Miller method using *o*-nitrophenyl-β-D-galactopyranoside (ONPG) as a substrate. The results confirmed that both genes, *acrR* and *osmY*, were highly expressed at 18°C (2860.6 ± 158.3 and 786.6 ± 42.1 Miller units, respectively) in relation to 28°C (1439.8 ± 11.9 and 583.4 ± 15.4 Miller units). Moreover, in order to confirm the upregulation of *acrR* and *osmY* genes at 18°C compared to 28°C (used as a reference), SYBR Green qPCR was carried out using *yrp1* as positive control of expression at 18°C. According to the qRT-PCR analysis, *yrp1*, *acrR* and *osmY* transcription increased about three times at 18°C compared to 28°C (Supplementary Figure S2).

Once the higher expression of *acrR* and *osmY* genes at low temperature had been corroborated, their implication in the physiology and virulence of *Y. ruckeri* was investigated.

Phenotypic Characterization and Virulence Determination of the *acrR* Mutant and Complemented Strain *acrR*$^+$

The *acrR* gene from *Y. ruckeri* encodes for a 216 amino acid protein belonging to the TetR transcriptional repressor family, with high identity (80%) with the AcrR protein from *Y. pestis* (EFA48822.1) among other bacteria. This protein is a repressor which modulates the expression of the *acrAB* operon, which is located upstream and in the opposite direction of the *acrR* gene in the *Y. ruckeri* genome (Supplementary Figure S3). Binding of AcrR to the operator region located between the *acrR* and *acrAB* genes (Supplementary Figure S3) represses, in *E. coli*, both the expression of the *acrAB* operon, thus preventing its excessive expression, and also its own expression (Deng et al., 2013).

The AcrAB is part of the AcrAB-TolC pump involved in the expulsion of different toxic compounds from bacteria. Thus, as expected, the *acrR* mutant strain was more resistant than the parental strain to the antibiotics ciprofloxacin, chloramphenicol, tetracycline and also to acriflavine (**Table 3**). In the same way, the mutant strain turned out to be highly resistant to hexane, whereas the parental strain was sensitive (data not shown). The complemented mutant *acrR*$^+$ presented a similar phenotype to the parental strain, although it was a little more sensitive to the effect of all the antibiotics (**Table 3**). However, no differences were found between the parental and mutant strains in the sensitivity to detergents such as SDS and Triton X100. Interestingly, both strains were found to be resistant to bile salts when they were added at 4% to TSA medium, whereas the *acrR*$^+$ strain was highly sensitive (**Figure 3**).

The *acrR*$^-$ mutant developed bigger colonies that the parental and *acrR*$^+$ complemented strains when they were grown in TSA medium containing lactose 0.5% (**Figure 4**). The reason is that in this medium, when the percentage of agar was lowered to 0.3% or 0.6%, the *acrR* mutant showed swimming and swarming motility, respectively. However, no motility at all was observed for the parental and complemented *acrR*$^+$ strains (**Figure 4**). Since TSA medium contains 0.25% glucose, a medium free of sugar such as NA was used to define the role of different carbohydrates in *acrR*$^-$ motility. Thus, when 0.25% glucose was added to

TABLE 3 | Effect of different compounds over *Y. ruckeri acrR* derivate strains.

Compound	*P*	*acrR*$^-$	*acrR*$^+$
Acriflavine	10,24	20,48	10,24
Ciprofloxacin	0,08	0,32	0,04
Chloramphenicol	5,12	10,24	2,56
Tetracycline	0,32	0,64	0,16
Triton X-100	12,8	12,8	ND
SDS	12,8	12,8	ND

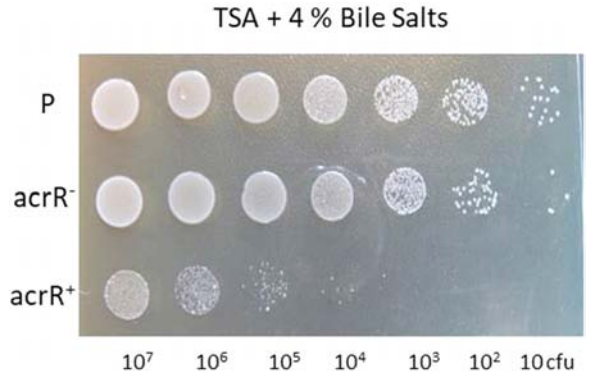

FIGURE 3 | Involvement of the AcrR regulator in resistance to bile salts in *Y. ruckeri*. Ten microliters of 10-fold (diluted series) dilutions of *Y. ruckeri* strain cultures (corresponding to a range from 10^7 to 10 cfu) were spotted onto TSA medium containing 4% bile salts and incubated at 18°C for 72 h. Parental (P), *acrR* mutant (*acrR*$^-$), and complemented *acrR*$^-$ (*acrR*$^+$) strains.

this medium, no motility was observed in any strain, just as occurred in TSA medium (data not shown). However, when the percentage of glucose in NA medium was increased to 0.5%, all the strains showed motility (**Figure 4**). Other sugars such as galactose, lactose and arabinose did not induced motility in any strain when added to NA medium at 0.5% or 0.75% (data not shown). Nevertheless, the presence in the media of glucose at 0.25% and lactose at 0.5% only resulted in the motility of the *acrR*$^-$ strain, as occurred when the TSA supplemented with 0.5% lactose was used (**Figure 4**). All of these results can be explained by the β-galactosidase activity displayed by the *acrR* mutant that hydrolyses the lactose of the culture medium to glucose and galactose. Neither the parental strain nor the *acrR*$^+$ strain can use lactose, the first because of the lack of *lacZY* genes in the genome and the second as a consequence of the transcriptional repression of the *acrR* promoter, exercised by the overexpression of AcrR encoding in the plasmid used for complementation.

No clear differences in mortality were detected when parental and *acrR* mutant strains were administered (10^6 cfu/fish) by intraperitoneal injection in three groups of five fish (data not shown). For this reason LD_{50} experiments were carried out. The results obtained confirmed that there were no significant differences between the parental (LD_{50} 6.3×10^2 cfu) and mutant strains (LD_{50} 3.8×10^2 cfu). Similarly, when the infection process was carried out by immersion, 90% of fish died 8 days post infection regardless of the strain inoculated. These results clearly indicate that the inactivation of the *acrR* gene in *Y. ruckeri* has no effect on virulence.

Phenotypic Characterization and Virulence Determination of the *osmY* Mutant and Complemented Strains *osmY*$^+$ and *osmY*$^{++}$

One of the selected clones presented the transposon inserted into an ORF encoding a 204 amino acid protein homolog to the OsmY protein of *E. coli*. The *Y. ruckeri* OsmY protein, according to Blast(p) program, has two BON conserved domains related to osmotic shock cell protection (pfam04972) (Yeats and Bateman, 2003; Zheng et al., 2015). *osmY* is flanked at the 5′end by the factor 3 encoding gene, involved in the release of the peptide chain, and at the opposite end by a gene encoding a 53 amino acid peptide containing the YtjA domain typical of many bacterial membrane proteins (NCBI accession number, COG5487). This genetic structure also appears in other *Yersinia* species as well as in *E. coli* K12, *Salmonella* Typhimurium and *Shigella flexneri*.

Growth curves in TSB medium of the *osmY* mutant and complemented *osmY*$^+$ and *osmY*$^{++}$ (*osmY*+*ytjA*) strains were

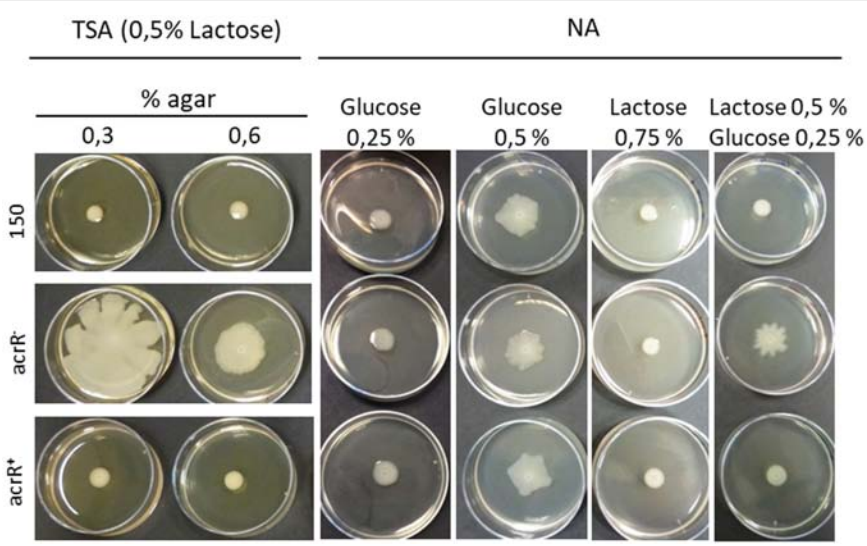

FIGURE 4 | Effect of sugars on the motility of *Y. ruckeri*. Parental, *acrR*$^-$ and *acrR*$^+$ strains were spotted onto TSA media containing lactose 0.5% and 0.3% or 0.6% of agar; and in NA with 0.6% agar and different sugar percentages. Note that all the strains display motility when 0.5% glucose is present in the medium.

similar to that of the parental strain (data not shown). Interestingly, when NaCl (1.5%) was added to TSB medium, up-regulation of the *osmY* gene was observed via bioluminescence emission, showing the relation between this gene and osmotic stress (Supplementary Figure S4).

As was inferred in previous experiments described above, the *osmY* mutant was found to be attenuated in virulence. Thus, injection experiments carried out with 10^6 cfu per fish of parental and *osmY* mutant resulted in 93.3% mortality and 16.6% (p-value 0.0165), respectively, at 7 days post infection. When $osmY^+$ and $osmY^{++}$ strains were injected, partial virulence recovery reaching 40% (p-value 0.0183) fish mortality was observed, but only for the latter.

In Vivo and *ex Vivo* Analysis of *acrR* and *osmY* Promoters

Transcriptional fusion between the *acrR* promoter and the *lux* operon was used for *in vivo* analysis of the infection process. Fish were infected both by injection or immersion and the light emitted by bacteria through fish tissues was monitored every 24 h by using the Ivis-Lumina system. Both models of infection began to produce luminescence 48 h post infection. At that time, high light intensity was located mainly in the liver, in the gut and in the adipose tissue (**Figure 5A**). A similar result was found when the *acrR* mutant was confluent grown on TSA plates containing different trout tissues. As can be observed in **Figure 5B**, maximum luminescence emitted by the *acrR* mutant corresponded to liver, just as was seen *in vivo,* although light was also detected in the gut. Interestingly, no luminescence was detected in the adipose tissue. *Yersinia ruckeri* $acrR^+$ did not showed bioluminescence in presence of any fish tissue (**Figure 5C**).

As expected, according to the virulence attenuation, at LD_{50} doses no light emission was detected at any time post infection when fish were intraperitoneally injected with the *osmY* mutant and $osmY^+$ strains and further examined under Ivis-Lumina equipment (data not shown). However, when the $osmY^{++}$ complemented strain was used, *osmY* expression was highly detected in the gut (**Figure 6A**), although in many cases high levels of expression in the muscle tissue were found at the end of the infection process, in dead fish (**Figure 6B**). A similar result was found when rainbow trout tissues were deposited onto TSA media, previously inoculated with *Y. ruckeri* $osmY^{++}$ strain for confluent growth. Thus, the highest luminescence intensity after 24 h of incubation was observed in bacteria surrounding the muscle (**Figure 6C**).

DISCUSSION

In this study, a novel mini *Tn5* transposon plasmid, pUT-mini *Tn5 lux-lac Km2*, was constructed on the backbone of pUT *Tn5*

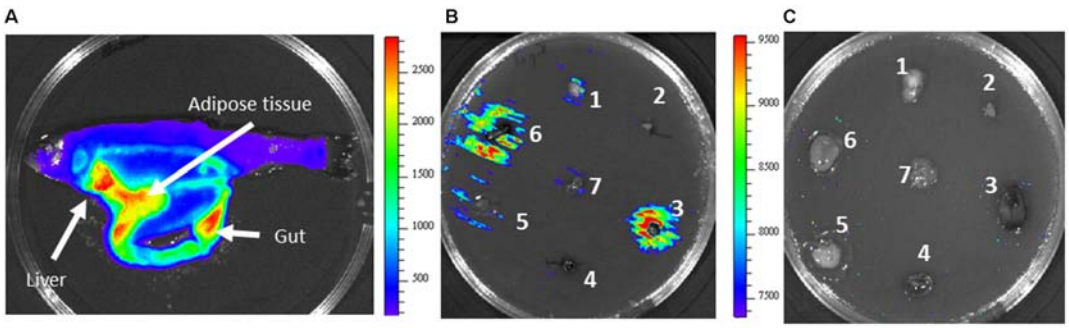

FIGURE 5 | *In vivo* and *in vitro* bioluminescence emission by *Y. ruckeri* $acrR^-$ and $acrR^+$ strains. **(A)** Fish imaged at 4 days post infection carried out by intraperitoneal injection with the $acrR^-$ strain. Bioluminescence imaging of $acrR^-$ **(B)** and $acrR^+$ **(C)** strains in presence of different fish tissues deposited on TSA plates previously inoculated with the corresponding strain. Brain (1), heart (2), liver (3), spleen (4), adipose tissue (5), gut (6), gills (7). Color bar shows RLU level.

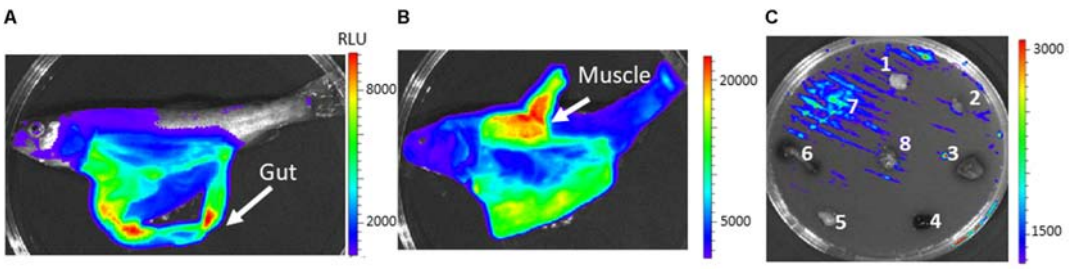

FIGURE 6 | *In vivo* and *in vitro* bioluminescence emission by *Y. ruckeri* $osmY^{++}$ strain. Fish intraperitoneally infected with the $osmY^{++}$ strain were visualized at 3 days **(A)** and 4 days **(B)** post infection. *In vitro* expression of *osmY* in response to different fish tissues deposited on TSA plates **(C)**. Brain (1), heart (2), liver (3), spleen (4), adipose tissue (5), gut (6), muscle (7), gills (8). Color bar shows RLU level.

Km2 plasmid (de Lorenzo et al., 1990). The main advantage of mutagenesis with this transposon is that its insertion in the bacterial genome not only results in a knockout mutation but also may lead to the production of transcriptional fusions between the promoterless *luxCDABE* and *lacZY* operons and the promoter of the interrupted gene. This study demonstrated that the *Tn5 lux-lac Km2* transposon was integrated randomly into the genome of *Y. ruckeri* and was stable in the absence of selective pressure. Additionally, it was confirmed that expression of *lux-lac* reporter genes has no effect on the growth rate of *Y. ruckeri*.

A library of *Y. ruckeri Tn5 lux-lac Km2* mutants was screened, via detection of β-galactosidase activity on EMB medium, for differential expression depending on temperature. Thus, a total of 168 clones showed higher expression at 18°C, the temperature at which outbreaks occurred, than at the optimal growth temperature (28°C). In 33 of those clones the gene interrupted was identified (**Table 2**). Interestingly, one of the selected genes was the *yrp1*, encoding for the metalloprotease Yrp1 (CAC39217.1) (Fernández et al., 2002, 2003). This gene has already been reported to be regulated by temperature, its expression being more active at 18°C than at 28°C (Fernández et al., 2002). Additionally, up to three different genes disrupted by the transposon encode for proteins involved in the synthesis of legionaminic acid (OEU25698.1, OEU25693.1, ABY48117.1), which strongly supports the involvement of temperature in the regulation of this process (Welch and LaPatra, 2016; Cascales et al., 2017). All of this strongly suggests that the strategy aimed at selecting promoters whose activity is regulated by temperature (highly expressed at 18°C in relation to 28°C) was the appropriate one. The selected mutants were grouped according to specific functions:

One group of mutants presented transposon insertions in genes related to response to environmental changes. Among them, the *yfiN* gene encoding the diguanylate cyclase (OEU26487.1) involved in the synthesis of cyclic di-GMP, a bacterial second messenger related to the control of many bacterial cellular functions such as changes from the transition between sessile and motile bacterial states (Römbling et al., 2013) and virulence (Raterman et al., 2013; Xu et al., 2016). Two other mutants presented transposon insertion in a putative operon of two genes encoding for a glycosyltransferase (OEU24749.1) and a SAM-dependent methyltransferase (OEU24750.1). Both kinds of enzymes have been previously linked to virulence in bacteria such as *Haemophilus parasuis* (Zhou et al., 2016), *Mycobacterium tuberculosis* (Berney et al., 2015), and *Klebsiella pneumoniae* (Ye et al., 2016). Three transcriptional regulators were also found. One of them encodes for a serine/threonine kinase (OEU26573.1) homologous to the anti-sigma factor RsbW from *Y. frederiksenii* which is involved in stress response through modulation of the sigma B factor (Hughes and Mathee, 1998). Another was the regulator YsrR (OEU25024.1), a member of the two component regulatory system YsrRS that in *Y. enterocolitica* is involved in the regulation of the type III secretion system Ysa-YsP (Walker and Miller, 2004). The third was the AcrR regulator (OEU24368.1), which represses the AcrAB-TolC pump expulsion system (Deng et al., 2013) involved in resistance to toxic compounds. This gene as well as *osmY* (OEU26500.1), a gene induced under osmotic stress, were further analyzed in this work.

Molecular exchanges between bacteria and their environment is mediated by multiple and complex systems. Three genes were selected in relation to this process: *mgtE* (OEU26742.1) involved in the transport of magnesium, cobalt and nickel and the genes encoding for a MSF family transporter (OEU26751.1) and the PhoE phosphoporin (OEU26976.1). All of them have been previously linked to virulence (Osorio et al., 2004; Andersson and Hughes, 2010; Chen et al., 2013; Coffey et al., 2014).

Another group of interrupted genes has a relationship with transport and the metabolism of sugars. Such is the case of *mglA*, a component of an ABC transport system (OEU26755.1) involved in galactose uptake (Harayama et al., 1983); a gene coding a glycogen phosphorylase (OEU26568.1) and another one, *malQ* (OEU26314.1) which forms part of *malPQ* operon involved in the uptake and degradation of maltodextrin which is the preferential carbon source in *E. coli* (Boos and Shuman, 1998). In *V. cholera*, it has been described that *malQ* plays a role in the virulence of the bacterium (Lang et al., 1994).

A major group of selected genes had a relationship with the bacterial membrane and wall. Thus, the interrupted genes of three different clones form part of a cluster encoding for proteins involved in the synthesis of legionaminic acid, a component of the LPS structure. The encoded proteins correspond with a UDP-*N*-acetylglucosamine 4,6-dehydratase (OEU25693.1), a D-glycerol-D-mano-heptosa-1-phosphate guanosyltransferase (OEU25698.1) and an *O*-antigen polymerase (ABY48117.1). This cluster is only present in *Y. ruckeri* serotype O1 (Welch and LaPatra, 2016; Cascales et al., 2017), and vaccination with a strain carrying a deletion of the second gene of the cluster encoding for the *nab2* gene, a nonulosonic acid biosynthesis gene (*nab* gene), resulted in absence of protection against yersiniosis infection, showing the importance of this cluster for ERM bacterin vaccine efficiency (Welch and LaPatra, 2016). According to this and to data reported from other bacteria such as *Legionella pneumophila* (Lüneberg et al., 1998) and *Campylobacter jejuni* (Zebian et al., 2016), it is possible that legionaminic acid is involved in the virulence of *Y. ruckeri*. Additional selected genes related to the cellular wall were an *O*-acyltransferase and a polysaccharide deacetylase which are probably involved in peptidoglycan biosynthesis. Two other genes with higher expression at 18°C than at 28°C are those encoding an *O*-acyltransferase (OEU26581.1) and a putative deacetylase (OEU25943.1) probably involved in peptidoglycan synthesis. In *Streptococcus iniae* the polysaccharide deacetylase Pdi is involved in virulence in the hybrid striped bass model and is necessary for survival in whole fish blood.

Another identified gene was related to antitoxin StbD (OUE25145.1) from the StbD/E toxin-antitoxin system (TA). TA systems are related to multiple functions in bacteria and, recently, some authors have suggested that they could in some cases be directly or indirectly related to infection processes in bacteria (Lobato-Márquez et al., 2016).

A mutant in the *damX* gene coding for a protein involved in cell division (EEP98349.1) was also isolated. In *S. typhi* (Leclerc

et al., 1998) and *E. coli* (Khandige et al., 2016) this gene was necessary for full virulence.

Other two selected mutants had interrupted the gene encoding the ArnC protein (OEU24187.1), which confers resistance to polymyxin, an antibiotic used in the therapy of multidrug-resistant Gram-negative bacterial infections (Evans et al., 1999), and a gene encoding a protein similar to the protein TnsC (OEU24391.1), which is part of the transposition machinery of the *Tn7* transposon. This kind of transposon is widespread in bacteria and facilitates the accumulation of mobile DNA within the *att*Tn*7* site in the chromosome leading to the formation of genomic islands (Parks and Peters, 2007).

PsiF (EEQ00620.1) is an inducible protein under phosphate starvation (Metcalf et al., 1990). Its expression is under the control of the PhoB-PhoR two-component system which is involved in virulence, motility and biofilm formation, among others (Lamarche et al., 2008). The selection at outbreak temperature of the gene coding PsiF in *Y. ruckeri* could be related to a response of the bacterium to phosphate limitation during the infection process.

An interesting selected gene is that encoding an ADP-ribosyltransferase exoenzyme (KGA50131.1). A large number of these enzymes are toxins involved in covalent modification of host proteins leading to a pathological manifestation. That is the case for different toxin produced by the genus *Clostridium* (Stiles et al., 2014), the SpvB virulence factor of *Salmonella enterica* (Lesnick et al., 2001) and A toxin of *Pseudomonas aeruginosa* (Wick et al., 1990), among others.

Some of the identified genes encode for hypothetical proteins. It is the case of the gene encoding for the hypothetical protein OEU2487.1 harboring a PDDEXK_7 domain characteristic of nucleases involved in DNA restriction methylation-dependent. The encoding gene forms part of an operon together with a gene coding for and AAA type ATPase involved in DNA repair. In the same way, the gene coding for the hypothetic protein KGA49879.1 seems to be part of an operon related to sugar metabolism. Additionally, the gene encoding for the hypothetical protein OEU24382.1 probably forms part of an operon with the gene encoding for a GTP pyrophosphokinase, homolog to RelA/SpoT, which is associated with virulence in different pathogenic bacteria (Klinkenberg et al., 2010; Nguyen et al., 2011; Zhu et al., 2016).

Finally, mention should be made of the gene encoding the esterase YqiA (AJI94468.1), which forms part of an operon including three other genes encoding for an ADP-ribose pyrophosphatase, a membrane protein and an cAMP phosphodiesterase involved in different cellular process, including the expression of virulence factors in *V. cholera* (Skorupski and Taylor, 1997) and *V. vulnificus* (Jeong et al., 2001; Choi et al., 2002).

Role of *acrR* and *osmY* Genes and Their Expression During Infection

As expected, the absence of the *acrR* gene in *Y. ruckeri* resulted in an increase in the resistance to a wide variety of toxic compounds that are extruded by the AcrAB-TolC system, including chloramphenicol or tetracycline as well as n-hexane, among others. Epidemiological data indicate that in *Y. ruckeri,* tetracycline resistance genes also confer resistance to oxytetracycline, a compound used in the treatment of red mouth disease (Balta et al., 2010). According to the study of Balta et al. (2010) 47.6% of isolated oxytetracycline-resistant *Y. ruckeri* strains harbored the *tetA* and *tetB* genes. In the other strains, resistance to oxytetracycline could be related to an increase in the AcrAB-TolC system activity, resulting from a simple *acrR* mutation which would be further selected during antibiotic treatments.

Bile salts induce the expression of the *E. coli* AcrAB-TolC system (Rosenberg et al., 2003). Although the expression of this pump is subject to complex regulation, it is activated by compounds which come into contact with the bacteria. In this way, *Y. ruckeri*, as an intestinal pathogen, is highly resistant to bile salts given that 4% of these compounds allowed the growth of both parental and *acrR*$^{-}$ strains. Interestingly, the complemented *acrR* strain was more sensitive to bile salts as well as to tetracycline, ciprofloxacin and chloramphenicol than the parental and mutant strains. This indicates that in the complemented strain the AcrAB pump is highly repressed by AcrR, which in turn suggests that the AcrAB pump is involved in the expulsion of bile salts from *Y. ruckeri*.

It has been previously reported that in *E. coli*, AcrR is involved in swimming and swarming motilities, both mediated by flagella, and necessary to evade toxic compounds (Inoue et al., 2007; Kim et al., 2016). In this sense, it seems that the role of AcrR goes beyond the repression of the AcrAB-TolC system. However, our data indicate that the increase in motility detected for the *Y. ruckeri acrR* mutant strain was not a consequence of this mutation, but of the presence in the culture media of a minimum proportion of 0.5% of glucose, part of which originated from lactose degradation. Thus, in the presence of 0.5% glucose, the parental, *acrR* mutant and complemented strains displayed motility. In *Y. ruckeri*, this relationship between glucose and motility seems to be specific since other sugars did not produce any effect on motility. In *Salmonella* Typhimurium and *E. coli*, the presence of glucose in the medium was necessary for swarming, probably because it provides the energy needed for the process (Harshey, 1994; Inoue et al., 2007; Kim et al., 2016). However, gliding motility in *Clostridium perfringens* is repressed by sugars such as glucose, lactose and galactose (Mendez et al., 2008) and swarming motility in *Pseudomonas aeruginosa* is limited by the presence of glucose (Shrout et al., 2006), indicating that effect of glucose in the motility of bacteria is species-specific.

In spite of being a gene regulated by temperature, *acrR* was not involved in the infection process when *Y. ruckeri* was infected either by intraperitoneal via or by bath immersion. Different studies indicate that the interruption of the AcrAB-TolC system resulted in virulence attenuation of *S.* Typhimurium (Lacroix et al., 1996), *Klebsiella pneumoniae* (Padilla et al., 2010), *Enterobacter cloacae* (Perez et al., 2012), *Francisella tularensis* (Bina et al., 2008) and the fish pathogen *E. tarda* (Hou et al., 2009). However, there are some exceptions to this, such as the case of *Y. pestis* in which the AcrAB does not play an essential role in the pathogenic process (Lister et al., 2012), something that also seems to occur in *Y. ruckeri*.

Although its role is still unknown, induction of the *osmY* gene of *Y. ruckeri* in presence of NaCl confirms the relation between this gene and osmotic stress, as occurred in *E. coli* (Yim and Villarejo, 1992; Yim et al., 1994). The fact that mutation of the *osmY* gene resulted in a decrease in the virulence of the bacterium showed its importance in the development of the infection process. Perhaps the role it plays has to do with a response to the high molarities present in the fish gut. In any case, not only is the *osmY* gene involved in the stress response, but also the adjacent one, *ytjA*, given that complementation of the *osmY* mutant strain with both *osmY* and *ytjA* genes was necessary to achieve partial virulence recovery. There are not much data on the role and involvement of *osmY* in bacterial virulence but some indirect relationship was found in *S.* Typhimurium (Bader et al., 2003). Zheng et al. (2015) suggested that *osmY* could play a role during the initial period of infection where the bacterium has to survive osmotic gut stress. This gene was also linked to the infection processes caused by *Cronobacter sakazakii* (Ye et al., 2015) and *E. coli* (Dong and Schellhorn, 2009).

Using the *lux* operon as reporter gene, it was possible to follow the *acrR* and *osmY* gene expression in different fish tissues. Interestingly, *in vivo* experiments showed that light emission of *acrR* was higher in gut, liver and adipose tissue, where toxic compounds are usually accumulated, whereas *osmY* showed higher levels of light in the gut, probably mediated by the osmotic stress generated in the bacterium in this organ. Nevertheless, the high level of luminescence detected after septicaemia in muscle tissue in many of the fish analyzed indicates that *osmY* expression could depend on the infection state.

These results are in agreement with those obtained on plates using rainbow trout tissues. Therefore, maximum luminescence resulting from *acrR* promoter activity was also detected in gut and liver, although, adipose tissue did not give a high level of light probably because this tissue, once out of the fish, was rapidly altered by fatty acid oxidation. In the same way, the *osmY* gene showed the highest light emission in muscle tissue. Bioluminescence-based bacterial reporter genes are useful to identify and study *in vitro* and *in vivo* gene regulation (Méndez and Guijarro, 2013; van Zyl et al., 2015). This result, together with that obtained using randomly selected clones cultivated in the presence of rainbow trout tissues, indicates that plate assays seem to be useful to determine *Y. ruckeri* differential gene expression in trout tissues. This approach allows the number of fish used in the experiments to be reduced, thus making the analyses easier and faster.

AUTHOR CONTRIBUTIONS

DC performed most of the experiments and analysis of results. AG-T participated in some of the experiments and analysis of results. JM participated in experimental design, experimental work, and critically revised the results. JG participated in experimental design, data analysis, and wrote the paper. DC, JM, AG-T, and JG drafted the first version of the manuscript. All authors reviewed the final version of the manuscript.

FUNDING

This research was supported by the AGL2012-35808 and AGL2015-66018-R grants from the Ministerio de Economía y Competitividad of Spain. Desiree Cascales and Ana Isabel Garcia were the recipients of FPU and FPI fellowships, respectively.

SUPPLEMENTARY MATERIAL

The Supplementary Material for this article can be found online at: https://www.frontiersin.org/articles/10.3389/fmicb.2018.01098/full#supplementary-material

REFERENCES

Aguado-Urda, M., Gibello, A., Blanco, M., del, M., Fernández-Garayzábal, J. F., López-Alonso, V., et al. (2013). Global transcriptome analysis of *Lactococcus garvieae* strains in response to temperature. *PLoS One* 8:e79692. doi: 10.1371/journal.pone.0079692

Andersson, D. I., and Hughes, D. (2010). Antibiotic resistance and its cost: is it possible to reverse resistance? *Natl. Rev. Microbiol.* 8, 260–271. doi: 10.1038/nrmicro2319

Arias, C. R., Olivares-Fuster, O., Hayden, K., Shoemaker, C. A., Grizzle, J. M., and Klesius, P. H. (2007). U.S. department of agriculture, agricultural research service, aquatic animal health research laboratory, post office box 952, Auburn, Alabama, 36830, USA First report of *Yersinia ruckeri* biotype 2 in the USA. *J. Aquat. Anim. Health* 19, 35–40. doi: 10.1577/H06-011.1

Bader, M. W., Navarre, W. W., Shiau, W., Nikaido, H., Frye, J. G., McClelland, M., et al. (2003). Regulation of *Salmonella typhimurium* virulence gene expression by cationic antimicrobial peptides: *Salmonella* response to antimicrobial peptides. *Mol. Microbiol.* 50, 219–230. doi: 10.1046/j.1365-2958.2003.03675.x

Balta, F., Sandalli, C., Kayis, S., and Ozgumus, O. B. (2010). Molecular analysis of antimicrobial resistance in *Yersinia ruckeri* strains isolated from rainbow trout (*Oncorhynchus mykiss*) grown in commercial fish farms in Turkey. *Bull. Eur. Assoc. Fish Pathol.* 30, 211–219.

Berney, M., Berney-Meyer, L., Wong, K. W., Chen, B., Chen, M., Kim, J., et al. (2015). Essential roles of methionine and S-adenosylmethionine in the autarkic lifestyle of *Mycobacterium tuberculosis*. *Proc. Natl. Acad. Sci. U.S.A.* 112, 10008–10013. doi: 10.1073/pnas.1513033112

Bina, X. R., Lavine, C. L., Miller, M. A., and Bina, J. E. (2008). The AcrAB RND efflux system from the live vaccine strain of *Francisella tularensis* is a multiple drug efflux system that is required for virulence in mice. *FEMS Microbiol. Lett.* 279, 226–233. doi: 10.1111/j.1574-6968.2007.01033.x

Bjarnason, J., Southward, C. M., and Surette, M. G. (2003). Genomic profiling of iron-responsive genes in *Salmonella enterica* serovar Typhimurium by high-throughput screening of a random promoter library. *J. Bacteriol.* 185, 4973–4982. doi: 10.1128/JB.185.16.4973-4982.2003

Boos, W., and Shuman, H. (1998). Maltose/maltodextrin system of *Escherichia coli*: transport, metabolism, and regulation. *Microbiol. Mol. Biol. Rev.* 62, 204–229.

Calvez, S., Gantelet, H., Blanc, G., Douet, D. G., and Daniel, P. (2014). *Yersinia ruckeri* biotypes 1 and 2 in France: presence and antibiotic susceptibility. *Dis. Aquat. Organ.* 109, 117–126. doi: 10.3354/dao02725

Cascales, D., Guijarro, J. A., García-Torrico, A. I., and Méndez, J. (2017). Comparative genome analysis reveals important genetic differences among serotype O1 and serotype O2 strains of *Y. ruckeri* and provides insights into host adaptation and virulence. *Microbiologyopen* 6:e460. doi: 10.1002/mbo3.460

Chakraborty, S., Li, M., Chatterjee, C., Sivaraman, J., Leung, K. Y., and Mok, Y.-K. (2010). Temperature and Mg+ sensing by a Novel PhoP-PhoQ two-component

system for regulation of virulence in *Edwardsiella tarda*. *J. Biol. Chem.* 285, 38876–38888. doi: 10.1074/jbcM110.179150

Chen, S., Wang, H., Katzianer, D. S., Zhong, Z., and Zhu, J. (2013). LysR family activator-regulated major facilitator superfamily transporters are involved in *Vibrio cholerae* antimicrobial compound resistance and intestinal colonization. *Int. J. Antimicrob. Agents* 41, 188–192. doi: 10.1016/j.ijantimicag.2012.10.008

Choi, H. K., Park, N. Y., Kim, D.-I., Chung, H. J., Ryu, S., and Choi, S. H. (2002). Promoter analysis and regulatory characteristics of *vvh*BA encoding cytolytic hemolysin of *Vibrio vulnificus*. *J. Biol. Chem.* 277, 47292–47299. doi: 10.1074/jbc.M206893200

Cipriano, R. C., and Holt, R. A. (2005). *Flavobacterium psychrophilum, Cause of Bacterial Cold Water Disease and Rainbow Trout Fry Syndrome*. Fish Disease Leaflet No. 86. Kearneysville, WV: United States Department of the Interior.

Coffey, B. M., Akhand, S. S., and Anderson, G. G. (2014). MgtE is a dual-function protein in *Pseudomonas aeruginosa*. *Microbiology* 160, 1200–1213. doi: 10.1099/mic.0.075275-0

Davies, R. L., and Frerichs, G. N. (1989). Morphological and biochemical differences among isolates of *Yersinia ruckeri* obtained from wide geographical areas. *J. Fish Dis.* 12, 357–365. doi: 10.1111/j.1365-2761.1989.tb00324.x

de Lorenzo, V., Herrero, M., Jakubzik, U., and Timmis, K. N. (1990). Mini Tn5 transposon derivatives for insertion mutagenesis, promoter probing, and chromosomal insertion of cloned DNA in gram-negative eubacteria. *J. Bacteriol.* 172, 6568–6572. doi: 10.1128/jb.172.11.6568-6572.1990

Deng, W., Li, C., and Xie, J. (2013). The underling mechanism of bacterial TetR/AcrR family transcriptional repressors. *Cell. Signal.* 25, 1608–1613. doi: 10.1016/j.cellsig.2013.04.003

Denton, J. E., Yousef, M. K., Yousef, I. M., and Kuksis (1974). Bile acid composition of rainbow trout, *Salmo gairdneri*. *Lipids* 9, 945–951. doi: 10.1007/BF02533816

Dong, T., and Schellhorn, H. E. (2009). Global effect of RpoS on gene expression in pathogenic *Escherichia coli* O157:H7 strain EDL933. *BMC Genomics* 10:349. doi: 10.1186/1471-2164-10-349

Enger, O., Husevag, B., and Goksoyr, J. (1991). Seasonal variation in presence of *Vibrio salmonicida* and total bacterial counts in Norwegian fish- farm water. *Can. J. Microbiol.* 37, 618–623. doi: 10.1139/m91-105

Evans, M. E., Feola, D. J., and Rapp, R. P. (1999). Polymyxin B sulfate and colistin: old antibiotics for emerging multiresistant gram-negative bacteria. *Ann. Pharmacother.* 33, 960–967. doi: 10.1345/aph.18426

Fernández, L., Lopez, J. R., Secades, P., Menendez, A., Marquez, I., and Guijarro, J. A. (2003). *In vitro* and *in vivo* studies of the Yrp1 protease from *Yersinia ruckeri* and its role in protective immunity against enteric red mouth disease of salmonids. *Appl. Environ. Microbiol.* 69, 7328–7335. doi: 10.1128/AEM.69.12.7328-7335.2003

Fernández, L., Marquez, I., and Guijarro, J. A. (2004). Identification of specific *in vivo*-induced (*ivi*) genes in *Yersinia ruckeri* and analysis of ruckerbactin, a catecholate siderophore iron acquisition system. *Appl. Environ. Microbiol.* 70, 5199–5207. doi: 10.1128/AEM.70.9.5199-5207.2004

Fernández, L., Méndez, J., and Guijarro, J. A. (2007a). Molecular virulence mechanisms of the fish pathogen *Yersinia ruckeri*. *Vet. Microbiol.* 125, 1–10. doi: 10.1016/j.vetmic.2007.06.013

Fernández, L., Prieto, M., and Guijarro, J. A. (2007b). The iron- and temperature-regulated haemolysin YhlA is a virulence factor of *Yersinia ruckeri*. *Microbiology* 153, 483–489. doi: 10.1099/mic.0.29284-0

Fernández, L., Secades, P., Lopez, J. R., Márquez, I., and Guijarro, J. A. (2002). Isolation and analysis of a protease gene with an ABC transport system in the fish pathogen *Yersinia ruckeri*: insertional mutagenesis and involvement in virulence. *Microbiology* 148, 2233–2243. doi: 10.1099/00221287-148-7-2233

Guijarro, J. A., Cascales, D., García-Torrico, A. I., García-Domínguez, M., and Méndez, J. (2015). Temperature-dependent expression of virulence genes in fish-pathogenic bacteria. *Front. Microbiol.* 6:700. doi: 10.3389/fmicb.2015.00700

Harayama, S., Bollinger, J., Iino, T., and Hazelbauer, G. L. (1983). Characterization of the *mgl* operon of *Escherichia coli* by transposon mutagenesis and molecular cloning. *J. Bacteriol.* 153, 408–415.

Harshey, R. M. (1994). Bees aren't the only ones: swarming in gram-negative bacteria. *Mol. Microbiol.* 13, 389–394. doi: 10.1111/j.1365-2958.1994.tb00433.x

Herrero, M., de Lorenzo, V., and Timmis, K. N. (1990). Transposon vectors containing non-antibiotic resistance selection markers for cloning and stable chromosomal insertion of foreign genes in Gram-negative bacteria. *J. Bacteriol.* 172, 6557–6567. doi: 10.1128/jb.172.11.6557-6567.1990

Hesami, S., Metcalf, D. S., Lumsden, J. S., and Macinnes, J. I. (2011). Identification of cold-temperature-regulated genes in *Flavobacterium psychrophilum*. *Appl. Environ. Microbiol.* 77, 1593–1600. doi: 10.1128/AEM.01717-10

Hou, J., Hu, Y., Zhang, M., and Sun, L. (2009). Identification and characterization of the AcrR/AcrAB system of a pathogenic *Edwardsiella tarda* strain. *J. Gen. Appl. Microbiol.* 55, 191–199. doi: 10.2323/jgam.55.191

Hughes, K. T., and Mathee, K. (1998). The anti-sigma factors. *Annu. Rev. Microbiol.* 52, 231–286. doi: 10.1146/annurev.micro.52.1.231

Inoue, T., Shingaki, R., Hirose, S., Waki, K., Mori, H., and Fukui, K. (2007). Genome-wide screening of genes required for swarming motility in *Escherichia coli* K-12. *J. Bacteriol.* 189, 950–957. doi: 10.1128/JB.01294-06

Jeong, H. S., Jeong, K. C., Choi, H. K., Park, K.-J., Lee, K.-H., Rhee, J. H., et al. (2001). Differential expression of *Vibrio vulnificus* elastase gene in a growth phase-dependent manner by two different types of promoters. *J. Biol. Chem.* 276, 13875–13880. doi: 10.1074/jbc.M010567200

Khandige, S., Asferg, C. A., Rasmussen, K. J., Larsen, M. J., Overgaard, M., Andersen, T. E., et al. (2016). DamX controls reversible cell morphology switching in uropathogenic *Escherichia coli*. *mBio* 7:e00642-16. doi: 10.1128/mBio.00642-16

Kim, Y. J., Im, S. Y., Lee, J. O., and Kim, O. B. (2016). Potential swimming motility variation by AcrR in *Escherichia coli*. *J. Microbiol. Biotechnol.* 26, 1824–1828. doi: 10.4014/jmb.1607.07058

Klinkenberg, L. G., Lee, J., Bishai, W. R., and Karakousis, P. C. (2010). The stringent response is required for full virulence of *Mycobacterium tuberculosis* in guinea pigs. *J. Infect. Dis.* 202, 1397–1404. doi: 10.1086/656524

Kumar, G., Menanteau-Ledouble, S., Saleh, M., and El-Matbouli, M. (2015). *Yersinia ruckeri*, the causative agent of enteric redmouth disease in fish. *Vet. Res.* 46, 103–123. doi: 10.1186/s13567-015-0238-4

Lacroix, F. J., Cloeckaert, A., Grépinet, O., Pinault, C., Popoff, M. Y., Waxin, H., et al. (1996). *Salmonella typhimurium acrB*-like gene: identification and role in resistance to biliary salts and detergents and in murine infection. *FEMS Microbiol. Lett.* 135, 161–167. doi: 10.1111/j.1574-6968.1996.tb07983.x

Lamarche, M. G., Wanner, B. L., Crepin, S., and Harel, J. (2008). The phosphate regulon and bacterial virulence: a regulatory network connecting phosphate homeostasis and pathogenesis. *FEMS Microbiol. Rev.* 32, 461–473. doi: 10.1111/j.1574-6976.2008.00100.x

Lang, H., Jonson, G., Holmgren, J., and Palva, E. T. (1994). The maltose regulon of *Vibrio cholerae* affects production and secretion of virulence factors. *Infect. Immun.* 62, 4781–4788.

Leclerc, G. J., Tartera, C., and Metcalf, E. S. (1998). Environmental regulation of *Salmonella typhi* invasion-defective mutants. *Infect. Immun.* 66, 682–691.

Lesnick, M. L., Reiner, N. E., Fierer, J., and Guiney, D. G. (2001). The *Salmonella spvB* virulence gene encodes an enzyme that ADP-ribosylates actin and destabilizes the cytoskeleton of eukaryotic cells. *Mol. Microbiol.* 39, 1464–1470. doi: 10.1046/j.1365-2958.2001.02360.x

Lister, I. M., Raftery, C., Mecsas, J., and Levy, S. B. (2012). *Yersinia pestis acrAB*-tolC in antibiotic resistance and virulence. *Antimicrob. Agents Chemother.* 56, 1120–1123. doi: 10.1128/AAC.05338-11

Lobato-Márquez, D., Díaz-Orejas, R., and García-del Portillo, F. (2016). Toxin-antitoxins and bacterial virulence. *FEMS Microbiol. Rev.* 40, 592–609. doi: 10.1093/femsre/fuw022

Lüneberg, E., Zähringer, U., Knirel, Y. A., Steinmann, D., Hartmann, M., Steinmetz, I., et al. (1998). Phase-variable expression of lipopolysaccharide contributes to the virulence of *Legionella pneumophila*. *J. Exp. Med.* 188:49. doi: 10.1084/jem.188.1.49

Mahan, M. J., Tobias, J. W., Slauch, J. M., Hanna, P. C., Collier, R. J., and Mekalanos, J. J. (1995). Antibiotic-based selection for bacterial genes that are specifically induced during infection of a host. *Proc. Natl. Acad. Sci. U.S.A.* 92, 669–673. doi: 10.1073/pnas.92.3.669

Manen, D., Pougeon, M., Damay, P., and Geiselmann, J. (1997). A sensitive reporter gene system using bacterial luciferase based on a series of plasmid cloning vectors compatible with derivatives of pBR322. *Gene* 186, 197–200. doi: 10.1016/S0378-1119(96)00702-0

Meighen, E. A., and Szittner, R. B. (1992). Multiple repetitive elements and organization of the lux operons of luminescence terrestrial bacteria. *J. Bacteriol.* 174, 5371–5381. doi: 10.1128/jb.174.16.5371-5381.1992

Méndez, J., Fernandez, L., Menendez, A., Reimundo, P., Perez-Pascual, D., Navais, R., et al. (2009). A chromosomally located *traHIJKCLMN* operon

encoding a putative Type IV secretion system is involved in the virulence of *Yersinia ruckeri*. *Appl. Environ. Microbiol.* 75, 937–945. doi: 10.1128/AEM.01377-08

Méndez, J., and Guijarro, J. A. (2013). *In vivo* monitoring of *Yersinia ruckeri* in fish tissues: progression and virulence gene expression. *Environ. Microbiol. Rep.* 5, 179–185. doi: 10.1111/1758-2229.12030

Mendez, M., Huang, I. H., Ohtani, K., Grau, R., Shimizu, T., and Sarker, M. R. (2008). Carbon catabolite repression of type IV pilus-dependent gliding motility in the anaerobic pathogen *Clostridium perfringens*. *J. Bacteriol.* 190, 48–60. doi: 10.1128/JB.01407-07

Metcalf, W. W., Steed, P. M., and Wanner, B. L. (1990). Identification of phosphate starvation-inducible genes in *Escherichia coli* K-12 by DNA sequence analysis of *psi::lacZ*(Mu d1) transcriptional fusions. *J. Bacteriol.* 172, 3191–3200. doi: 10.1128/jb.172.6.3191-3200.1990

Nguyen, D., Joshi-Datar, A., Lepine, F., Bauerle, E., Olakanmi, O., Beer, K., et al. (2011). Active starvation responses mediate antibiotic tolerance in biofilms and nutrient-limited bacteria. *Science* 334, 982–986. doi: 10.1126/science.1211037

Osorio, C. G., Martinez-Wilson, H., and Camilli, A. (2004). The *ompU* paralogue vca1008 is required for virulence of *Vibrio cholera*. *J. Bacteriol.* 186, 5167–5171. doi: 10.1128/JB.186.15.5167-5171.2004

Padilla, E., Llobet, E., Domenech-Sanchez, A., Martinez-Martinez, L., Bengoechea, J. A., and Alberti, S. (2010). *Klebsiella pneumoniae* AcrAB efflux pump contributes to antimicrobial resistance and virulence. *Antimicrob. Agents Chemother.* 54, 177–183. doi: 10.1128/AAC.00715-09

Parks, A. R., and Peters, J. E. (2007). Transposon *Tn7* is widespread in diverse bacteria and forms genomic islands. *J. Bacteriol.* 189, 2170–2173. doi: 10.1128/JB.01536-06

Perez, A., Poza, M., Fernandez, A., Fernandez Mdel, C., Mallo, S., Merino, M., et al. (2012). Involvement of the AcrAB-TolC efflux pump in the resistance, fitness, and virulence of *Enterobacter cloacae*. *Antimicrob. Agents Chemother.* 56, 2084–2090. doi: 10.1128/AAC.05509-11

Raterman, E. L., Shapiro, D. D., Stevens, D. J., Schwartz, K. J., and Welch, R. A. (2013). Genetic analysis of the role of *yfiR* in the ability of *Escherichia coli* CFT073 to control cellular cyclic dimeric GMP levels and to persist in the urinary tract. *Infect. Immun.* 81, 3089–3098. doi: 10.1128/IAI.01396-12

Reed, L. J., and Muench, H. (1938). A simple method of estimating fifty per cent endpoints. *Am. J. Epidemiol.* 27, 493–497. doi: 10.1093/oxfordjournals.aje.a118408

Romalde, J. L., Magariños, B., Barja, J. L., and Toranzo, A. E. (1993). Antigenic and molecular characterization of *Yersinia ruckeri* proposal for a new intraspecies classification. *Syst. Appl. Microbiol.* 16, 411–419. doi: 10.1016/S0723-2020(11)80274-2

Römbling, U., Galperin, M. Y., and Gomelsky, M. (2013). Cyclic di-GMP: the first 25 years of a universal bacterial second messenger. *Microbiol. Mol. Biol. Rev.* 77, 1–52. doi: 10.1128/MMBR.00043-12

Rosenberg, E. Y., Bertenthal, D., Nilles, M. L., Bertrand, K. P., and Nikaido, H. (2003). Bile salts and fatty acids induce the expression of *Escherichia coli* AcrAB multidrug efflux pump through their interaction with Rob regulatory protein: binding of bile salts to Rob regulates AcrAB expression. *Mol. Microbiol.* 48, 1609–1619. doi: 10.1046/j.1365-2958.2003.03531.x

Shrout, J. D., Chopp, D. L., Just, C. L., Hentzer, M., Givskov, M., and Parsek, M. R. (2006). The impact of quorum sensing and swarming motility on *Pseudomonas aeruginosa* biofilm formation is nutritionally conditional. *Mol. Microbiol.* 62, 1264–1277. doi: 10.1111/j.1365-2958.2006.05421.x

Simon, R., Priefer, U., and Pühler, A. (1983). A broad host range mobilization system for *in vivo* genetic engineering: transposon mutagenesis in gram negative bacteria. *Nat. Biotechnol.* 1, 784–791. doi: 10.1038/nbt1183-784

Skorupski, K., and Taylor, R. K. (1997). Cyclic AMP and its receptor protein negatively regulate the coordinate expression of cholera toxin and toxin-coregulated pilus in *Vibrio cholera*. *Proc. Natl. Acad. Sci. U.S.A.* 94, 265–270. doi: 10.1073/pnas.94.1.265

Srinivasa Rao, P. S., Lim, T. M., and Leung, K. Y. (2003). Functional genomic approach to the identification of virulence genes involved in *Edwardsiella tarda* pathogenesis. *Infect. Immun.* 71, 1343–1351. doi: 10.1128/IAI.71.3.1343-1351.2003

Srinivasa Rao, P. S., Yamada, Y., Tan, Y. P., and Leung, K. Y. (2004). Use of proteomics to identify novel virulence determinants that are requires for *Edwardsiella tarda* pathogenesis. *Mol. Microbiol.* 53, 573–586. doi: 10.1111/j.1365-2958.2004.04123.x

Stiles, B. G., Pradhan, K., Fleming, J. M., Samy, R. P., Barth, H., and Popoff, M. R. (2014). *Clostridium* and *Bacillus* binary enterotoxins: bad for the bowels, and eukaryotic being. *Toxin* 6, 2626–2656. doi: 10.3390/toxins6092626

Tobback, E., Decostere, A., Hermans, K., Haesebrouck, F., and Chiers, K. (2007). *Yersinia ruckeri* infections in salmonid fish. *J. Fish Dis.* 30, 257–268. doi: 10.1111/j.1365-2761.2007.00816.x

van Zyl, W. F., Deane, S. M., and Dicks, L. M. (2015). Reporter systems for *in vivo* tracking of lactic acid bacteria in animal model studies. *Gut Microbes* 6, 291–299. doi: 10.1080/19490976.2015.1086058

Vendrell, D., Balcázar, J. L., Ruiz-Zarzuela, I., de Blas, I, Gironés, O., and Múzquiz, J. L. (2006). *Lactococcus garvieae* in fish: a review. *Comp. Immunol. Microbiol. Infect. Dis.* 29, 177–198. doi: 10.1016/j.cimid2006.06.003

Walker, K. A., and Miller, V. L. (2004). Regulation of the Ysa type III secretion system of *Yersinia enterocolitica* by YsaE/SycB and YsrS/YsrR. *J. Bacteriol.* 186, 4056–4066. doi: 10.1128/JB.186.13.4056-4066.2004

Wang, X., Wang, Q., Xiao, J., Liu, Q., Wu, H., Xu, L., et al. (2009). *Edwardsiella tarda* T6SS component *evpP* is regulated by *esrB* and iron, and plays essential roles in the invasion of fish. *Fish Shellfish Inmunol.* 27, 469–477. doi: 10.1016/j.fsi.2009.06.013

Welch, T. J., and LaPatra, S. (2016). *Yersinia ruckeri* lipopolysaccharide is necessary and sufficient for eliciting a protective immune response in rainbow trout (*Oncorhynchus mykiss*, Walbaum). *Fish Shellfish Immunol.* 49, 420–426. doi: 10.1016/j.fsi.2015.12.037

Wick, M. J., Hamood, A. N., and Iglewski, B. H. (1990). Analysis of the structure-function relationship of *Pseudomonas aeruginosa* exotoxin A. *Mol. Microbiol.* 4, 527–535. doi: 10.1111/j.1365-2958.1990.tb00620.x

Woodcock, D. M., Crowther, P. J., Doherty, J., Jefferson, S., De Cruz, E., Noyer-Weidner, M., et al. (1989). Quantitative evaluation of *Escherichia coli* host strains for tolerance to cytosine methylation in plasmid and phage recombinants. *Nucleic Acids Res.* 17, 3469–3478. doi: 10.1093/nar/17.9.3469

Xu, M., Yang, X., Yang, X.-A., Zhou, L., Liu, T.-Z., Fan, Z., et al. (2016). Structural insights into the regulatory mechanism of the *Pseudomonas aeruginosa* YfiBNR system. *Protein Cell* 7, 403–416. doi: 10.1007/s13238-016-0264-7

Ye, M., Tu, J., Jiang, J., Bi, Y., You, W., Zhang, Y., et al. (2016). Clinical and genomic analysis of liver abscess-causing *Klebsiella pneumoniae* identifies new liver abscess-associated virulence genes. *Front. Cell. Infect. Microbiol.* 6:165. doi: 10.3389/fcimb.2016.00165

Ye, Y., Gao, J., Jiao, R., Li, H., Wu, Q., Zhang, J., et al. (2015). The membrane proteins involved in virulence of *Cronobacter sakazakii* virulent G362 and attenuated L3101 isolates. *Front. Microbiol.* 6:1238. doi: 10.3389/fmicb.2015.01238

Yeats, C., and Bateman, A. (2003). The BON domain: a putative membrane-binding domain. *Trends Biochem. Sci.* 28, 352–355. doi: 10.1016/S0968-0004(03)00115-4

Yim, H. H., Brems, R. L., and Villarejo, M. (1994). Molecular characterization of the promoter of *osmY*, an *rpoS*-dependent gene. *J. Bacteriol.* 176, 100–107. doi: 10.1128/jb.176.1.100-107.1994

Yim, H. H., and Villarejo, M. (1992). *osmY*, a new hyperosmotically inducible gene, encodes a periplasmic protein in *Escherichia coli*. *J. Bacteriol.* 174, 3637–3644. doi: 10.1128/jb.174.11.3637-3644.1992

Yu, H. B., Kaur, R., Lim, S., Wang, X. H., and Leung, K. Y. (2007). Characterization of extracellular proteins produced by *Aeromonas hydrophila* AH-1. *Proteomics* 7, 436–449. doi: 10.1002/pmic.200600396

Zebian, N., Merkx-Jacques, A., Pittock, P. P., Houle, S., Dozois, C. M., Lajoie, G. A., et al. (2016). Comprehensive analysis of flagellin glycosylation in *Campylobacter jejuni* NCTC 11168 reveals incorporation of legionaminic acid and its importance for host colonization. *Glycobiology* 26, 386–397. doi: 10.1093/glycob/cwv104

Zheng, J., Tung, S. L., and Leung, K. Y. (2005). Regulation of a type III and putative secretion system in *Edwardsiella tarda* by EsrC is under the control of a two-component system EsrA-EsrB. *Infect. Immun.* 73, 4127–4137. doi: 10.1128/IAI.73.7.4127-4137.2005

Zheng, X., Ji, Y., Weng, X., and Huang, X. (2015). RpoS-dependent expression of OsmY in *Salmonella enterica* serovar Typhi: activation under stationary phase and SPI-2-inducing conditions. *Curr. Microbiol.* 70, 877–882. doi: 10.1007/s00284-015-0802-1

Zhou, Q., Feng, S., Zhang, J., Jia, A., Yang, K., Xing, K., et al. (2016). Two glycosyltransferase genes of *Haemophilus parasuis* SC096 implicated in lipooligosaccharide biosynthesis, serum resistance, adherence, and invasion. *Front. Cell. Infect. Microbiol.* 6:100. doi: 10.3389/fcimb.2016.00100

Zhu, J., Zhang, T., Su, Z., Li, L., Wang, D., Xiao, R., et al. (2016). (p)ppGpp synthetases regulate the pathogenesis of zoonotic *Streptococcus suis*. *Microbiol. Res.* 191, 1–11. doi: 10.1016/j.micres.2016.05.007

Conflict of Interest Statement: The authors declare that the research was conducted in the absence of any commercial or financial relationships that could be construed as a potential conflict of interest.

frontiers in Microbiology

ORIGINAL RESEARCH
published: 29 May 2018
doi: 10.3389/fmicb.2018.01121

Homeostasis of Second Messenger Cyclic-di-AMP Is Critical for Cyanobacterial Fitness and Acclimation to Abiotic Stress

*Marco Agostoni[1,2†], Alshaé R. Logan-Jackson[2,3], Emily R. Heinz[2], Geoffrey B. Severin[4], Eric L. Bruger[3†], Christopher M. Waters[1,3] and Beronda L. Montgomery[1,2,3,4]**

[1] Cell and Molecular Biology Graduate Program, Michigan State University, East Lansing, MI, United States, [2] Department of Energy Plant Research Laboratory, Michigan State University, East Lansing, MI, United States, [3] Department of Microbiology and Molecular Genetics, Michigan State University, East Lansing, MI, United States, [4] Department of Biochemistry and Molecular Biology, Michigan State University, East Lansing, MI, United States

OPEN ACCESS

Edited by:
Conor P. O'Byrne,
National University of Ireland Galway,
Ireland

Reviewed by:
Iris Maldener,
Universität Tübingen, Germany
Juan Carlos Alonso,
Centro Nacional de Biotecnología (CNB), Spain
Ronan Sulpice,
National University of Ireland Galway,
Ireland

***Correspondence:**
Beronda L. Montgomery
montg133@msu.edu

†Present address:
Marco Agostoni,
California Institute for Quantitative Biosciences, University of California, Berkeley, Berkeley, CA, United States
Eric L. Bruger,
Department of Biological Sciences, University of Idaho, Moscow, ID, United States

Specialty section:
This article was submitted to Microbial Physiology and Metabolism, a section of the journal Frontiers in Microbiology

Received: 22 January 2018
Accepted: 11 May 2018
Published: 29 May 2018

Citation:
Agostoni M, Logan-Jackson AR, Heinz ER, Severin GB, Bruger EL, Waters CM and Montgomery BL (2018) Homeostasis of Second Messenger Cyclic-di-AMP Is Critical for Cyanobacterial Fitness and Acclimation to Abiotic Stress. Front. Microbiol. 9:1121. doi: 10.3389/fmicb.2018.01121

Second messengers are intracellular molecules regulated by external stimuli known as first messengers that are used for rapid organismal responses to dynamic environmental changes. Cyclic di-AMP (c-di-AMP) is a relatively newly discovered second messenger implicated in cell wall homeostasis in many pathogenic bacteria. C-di-AMP is synthesized from ATP by diadenylyl cyclases (DAC) and degraded by specific c-di-AMP phosphodiesterases (PDE). C-di-AMP DACs and PDEs are present in all sequenced cyanobacteria, suggesting roles for c-di-AMP in the physiology and/or development of these organisms. Despite conservation of these genes across numerous cyanobacteria, the functional roles of c-di-AMP in cyanobacteria have not been well-investigated. In a unique feature of cyanobacteria, phylogenetic analysis indicated that the broadly conserved DAC, related to CdaA/DacA, is always co-associated in an operon with genes critical for controlling cell wall synthesis. To investigate phenotypes regulated by c-di-AMP in cyanobacteria, we overexpressed native DAC (*sll0505*) and c-di-AMP PDE (*slr0104*) genes in the cyanobacterium *Synechocystis* sp. PCC 6803 (hereafter *Synechocystis*) to increase and decrease intracellular c-di-AMP levels, respectively. DAC- and PDE-overexpression strains, showed abnormal aggregation phenotypes, suggesting functional roles for regulating c-di-AMP homeostasis *in vivo*. As c-di-AMP may be implicated in osmotic responses in cyanobacteria, we tested whether sorbitol and NaCl stresses impacted expression of *sll0505* and *slr0104* or intracellular c-di-AMP levels in *Synechocystis*. Additionally, to determine the range of cyanobacteria in which c-di-AMP may function, we assessed c-di-AMP levels in two unicellular cyanobacteria, i.e., *Synechocystis* and *Synechococcus elongatus* PCC 7942, and two filamentous cyanobacteria, i.e., *Fremyella diplosiphon* and *Anabaena* sp. PCC 7120. C-di-AMP levels responded differently to abiotic stress signals in distinct cyanobacteria strains, whereas salt stress uniformly impacted another second messenger cyclic di-GMP in cyanobacteria. Together, these results suggest regulation of c-di-AMP homeostasis in cyanobacteria and implicate a role for the second messenger in maintaining cellular fitness in response to abiotic stress.

Keywords: abiotic stresses, c-di-AMP, c-di-GMP, cyanobacteria, ionic stress, osmotic stress, salt stress, second messengers

INTRODUCTION

Cyanobacteria comprise a group of highly diverse, oxygenic photosynthetic bacteria that respond to a range of abiotic and biotic signals in their environment, from light that has direct impacts on photosynthesis and productivity to osmotic and saline stresses. These organisms are highly abundant in many ecosystems (Garcia-Pichel et al., 2003) and as carbon, and sometimes nitrogen fixers, contribute significantly to global carbon and nitrogen cycles. Second messengers are critical intracellular molecules that are regulated in response to specific external stimuli known as first messengers. Control of second messenger homeostasis is used frequently to initiate physiological changes that occur in microorganisms as a part of environmental acclimation. A range of second messengers have been identified that play key roles in regulating environmentally-controlled physiological responses in cyanobacteria (Agostoni and Montgomery, 2014). Among second messengers, cyanobacteria commonly rely on cyclic nucleotide signaling molecules such as cyclic AMP (i.e., cAMP) (Ohmori et al., 1988, 2001, 2002; Katayama and Ohmori, 1997; Terauchi and Ohmori, 1999, 2004; Ohmori and Okamoto, 2004; Okamoto et al., 2004; Imashimizu et al., 2005) and cyclic GMP (i.e., cGMP) (Ochoa De Alda et al., 2000; Cadoret et al., 2005). However, dicyclic nucleotides such as cyclic dimeric GMP (hereafter, cyclic di-GMP or c-di-GMP) have only recently been reported in these organisms. In cyanobacteria, c-di-GMP has roles in acclimation to light, phototaxis, and cellular aggregation (Savakis et al., 2012; Agostoni et al., 2013, 2016; Enomoto et al., 2014, 2015; Angerer et al., 2017).

The second messenger cyclic dimeric AMP (hereafter, cyclic di-AMP or c-di-AMP) is a relatively newly discovered cyclic dinucleotide (Romling, 2008; Witte et al., 2008; Fu et al., 2016; Jenal et al., 2017; Krasteva and Sondermann, 2017). Cyclic di-AMP is synthesized by diadenylyl cyclase (DAC; PF02457) from two molecules of ATP and degraded by specific phosphodiesterase (PDE) enzymes into pApA (Corrigan and Grundling, 2013). Cyclic di-AMP and its functional roles *in vivo* have been studied primarily in Gram-positive bacteria. In Gram-positive species, the regulation of c-di-AMP homeostasis has been associated with a range of responses. Cyclic di-AMP levels impact growth (Witte et al., 2013; Rismondo et al., 2016; Whiteley et al., 2017), sporulation (Oppenheimer-Shaanan et al., 2011; Mehne et al., 2014; Zheng et al., 2015; Raguse et al., 2017), virulence (Bai et al., 2013; Cho and Kang, 2013; Du et al., 2014; Yang et al., 2014; Dey et al., 2015), biofilm formation related to host–microbe interactions (Townsley et al., 2018), and DNA repair damage responses or the coordination of DNA damage response and stress homeostasis (Bejerano-Sagie et al., 2006; Witte et al., 2008; Gándara and Alonso, 2015; Gándara et al., 2017; Raguse et al., 2017), among other phenotypes in a range of Gram-positive strains. A role for c-di-AMP in growth and virulence has also been observed for the Gram-negative *Borrelia burgdorferi* and *Chlamydia trachomatis* (Barker et al., 2013; Ye et al., 2014). Additionally, c-di-AMP has been implicated in cellular responses to abiotic stresses in multiple Gram-positive bacteria (Dengler et al., 2013; Bowman et al., 2016; Zhu et al., 2016).

Whereas numerous roles for c-di-AMP have been documented in Gram positive bacteria, limited insights into the roles of this molecule in other bacteria have been reported. Notably, cyanobacteria have recently been reported to contain c-di-AMP synthesis genes (Agostoni and Montgomery, 2014) and c-di-AMP accumulation has recently been reported in *Synechococcus elongatus* sp. PCC 7942 (Rubin et al., 2018). All sequenced cyanobacteria possess at least one DAC, with some exceptions of strains that carry two DACs (Agostoni and Montgomery, 2014). Unlike those DAC proteins reported in many bacteria which include a DAC domain with fusions to other regulatory domains, the DACs of cyanobacteria generally contain only the cyclase enzymatic domain. Additionally, two specific c-di-AMP PDEs have been discovered in bacteria: one containing a DHH-DHHA1 domain (Romling, 2008; Corrigan and Grundling, 2013), a class which is likely not present in cyanobacteria; the other with a domain architecture similar to the 7TM_7TMR_HD protein family (Huynh et al., 2015). The 7TM_7TMR_HD is more common than DHH-DHHA1 domain-containing PDEs in bacteria and it is also present in cyanobacterial genomes (Huynh et al., 2015; Huynh and Woodward, 2016).

Recently, an assessment of regulons of riboswitches involved in binding the second messenger c-di-AMP suggested a function of c-di-AMP in regulating the synthesis of osmoprotectants under abiotic stress in cyanobacteria (Nelson et al., 2013). The addition of organic solutes, which are not permeable to the bacterial cell, to cellular growth medium induces osmotic stress. Although salt stress is often referred to as osmotic stress (Hagemann, 2011), salt stress specifically results in reduced water availability due to dissolved ions that concomitantly induce osmotic stress (Pade and Hagemann, 2015). Thus, salt stress includes both ionic stress and secondary osmotic stress. The primary signals induced in response to salt and osmotic stress in cyanobacteria are still being elucidated (Pade and Hagemann, 2015). However, a role for two component histidine kinase Hik33 in responses to osmotic and salt stress in cyanobacteria has been noted (Mikami et al., 2002; Marin et al., 2003; Paithoonrangsarid et al., 2004; Shoumskaya et al., 2005). The primary abiotic stress can also induce secondary signals, including second messengers. In cyanobacteria, the second messenger Ca^{2+} is involved in organismal responses to environmental osmotic and salt changes (Torrecilla et al., 2001). The recognition that potential c-di-AMP binding riboswitches may be involved in osmoprotectant production in response to osmotic stress in cyanobacteria suggests a potential role for c-di-AMP in cellular responses to abiotic stress.

In this study, we investigated the activity of DAC and PDE enzymes in the moderately halotolerant freshwater unicellular cyanobacterium *Synechocystis*, the potential for abiotic stresses to alter intracellular c-di-AMP levels, and the impact of altering c-di-AMP homeostasis on the physiology and survival of this organism. Furthermore, we assessed the impacts of osmotic and salt stresses on modulating c-di-AMP homeostasis in several additional

cyanobacteria, including another freshwater unicellular strain *Synechococcus elongatus* PCC 7942 (hereafter *Synechococcus*) for which c-di-AMP has been recently implicated in nighttime survival (Rubin et al., 2018), and two filamentous freshwater strains *Fremyella diplosiphon* [also known as *Tolypothrix* sp. PCC 7601 (Yerrapragada et al., 2015)], and *Anabaena* sp. PCC 7120 (hereafter *Anabaena*, also known as *Nostoc* sp. PCC 7120) to more broadly understand the modulation of c-di-AMP homeostasis across a range of cyanobacteria.

MATERIALS AND METHODS

Plasmid Construction in *Synechocystis*

Intracellular levels of c-di-AMP in *Synechocystis* were targeted for increase by overexpressing the native DAC protein Sll0505 or reduction by overexpressing the native PDE protein Slr0104. The open reading frame of native genes encoding the DAC and PDE enzymes were constitutively overexpressed under the control of the *apcE* (*slr0335*) promoter using the self-replicating plasmid pRL1342 (Wolk et al., 2007; GenBank: AF403427.1). Promoters were added to the DAC- or PDE-encoding genes by overlap PCR using primers indicated in **Table 1**. The genes were amplified from genomic DNA with PrimeSTAR Max DNA polymerase (Clontech Laboratory, Inc.) using primers that encoded *Xho*I and *BamH*I restriction sites (**Table 1**). The promoter-gene fusion product and pRL1342 were restricted with *Xho*I and *BamH*I and the cleaved products ligated using DNA Ligation Kit, Mighty Mix (Takara). After transformation of the ligation mix into *E. coli* DH5α competent cells (Life Technologies, Inc.), transformants were selected on LB agar containing chloramphenicol at 50 μg mL^{-1} (w/v). The DNA sequences of isolated plasmids were confirmed by Sanger sequencing. The plasmid was then inserted into *Synechocystis* by triparental mating as previously described (Agostoni et al., 2016).

Culture Conditions

Axenic cultures of *Synechocystis*, *F. diplosiphon*, *Synechococcus*, and *Anabaena* were grown at 28°C in BG-11 (Allen, 1968) containing 20 mM HEPES at pH 8.0 (hereafter BG-11/HEPES) with the indicated antibiotic when needed. *F. diplosiphon* strain SF33, a shortened-filament mutant strain that displays wild-type (WT) pigmentation (Cobley et al., 1993), was used as the WT *F. diplosiphon* strain. Cultures (25 ml) in 250 ml glass flasks were adapted to fluorescent white light (WL; Philips F32T8/TL741/ALTO) at 15 μmol m^{-2} s^{-1} with shaking at 175 rpm for at least a week. Growth rate of the WT, overexpression (OE) DAC, and OE PDE strains was estimated by optical density at 750 nm (OD_{750}) every day for strains grown under WL (Philips F32T8/TL741/ALTO) at 35 μmol m^{-2} s^{-1} with shaking at 175 rpm. A secondary analysis of growth was conducted on BG-11 plates containing 1% (w/v) agar. A 1:10 dilution series of cells growing homogenously in liquid culture was plated for each strain with the initial cultures at an OD_{750} of 0.6. Aliquots of 10 μL of the dilutions up to 1:10,000 were plated and the plates incubated under 15 μmol m^{-2} s^{-1} of WL.

Abiotic Stresses and c-di-AMP/c-di-GMP Quantification

Cells were grown to an optical density at 750 nm (OD_{750}) of 1 and transferred to new 250 ml flasks with BG-11/HEPES medium containing 0.2 M sorbitol for the osmotic stress, or 0.2 M NaCl for the ionic stress, except for halophile *Synechocystis* for which the NaCl concentration was 0.6 M. As a control, BG-11/HEPES medium without sorbitol or NaCl added was utilized. Cells were maintained under osmotic or salt stress for 24 h. After 24 h, c-di-AMP and c-di-GMP were quantified as described (Massie et al., 2012; Agostoni et al., 2013; Barker et al., 2013). In brief, c-di-AMP and c-di-GMP were quantified by UPLC-MS/MS. Prior to analysis, an aliquot of each sample was dried under vacuum to remove extraction buffer and the pellet was resuspended in an equal volume of water. A 10-μl volume of the resuspended sample was analyzed together with an eight-point standard curve of purified c-di-AMP or c-di-GMP (Biolog). C-di-AMP and c-di-GMP concentrations determined for samples were normalized to total soluble protein content from an equal volume of cells from which second messengers were extracted as previously described (Agostoni et al., 2013; Zhu et al., 2016). Growth over time of WT, OE DAC and OE PDE *Synechocystis* stains in the presence of sorbitol (0.5 M) or NaCl (0.6 M) was measured using OD_{750} as described above.

Quantitative Reverse Transcriptase PCR (qRT-PCR) and RT-PCR in *Synechocystis*

For RNA extraction, *Synechocystis* cells from a 10 ml aliquot of culture were collected 24 h after the osmotic stress or after subculturing. RNA was isolated using Trizol reagent essentially as described (Seib and Kehoe, 2002; Singh and Montgomery, 2013a). Total RNA extracted was treated with a TURBO DNA-free kit (Ambion, Austin, TX, United States). cDNA synthesis was performed as described (Pattanaik and Montgomery, 2010) with 0.5 μg of total RNA using the Reverse Transcription System (Promega Corporation, Madison, WI, United States). Control reactions were conducted in which no reverse transcriptase (No RT) was added to the reaction mixtures. Gene *rnpB* (RNase P subunit B), the expression of which is not altered by nutrient or salt stress (Kloft et al., 2005; Zhang et al., 2007; Wang et al., 2014), was used as an internal control. RT cycling parameters were denaturing at 95°C for 20 s, 40 cycles of denaturation at 95°C for 3 s and annealing/extension at 60°C for 30 s, followed by melt-curve analysis starting at 60°C and ending at 95°C for 15 min. **Table 1** shows primers used for qRT-PCR and RT-PCR.

Genome Comparisons

Phylogenetic analyses of multiple conserved DAC domain sequences (PF02457) from 83 finished cyanobacterial genomes present in the IMG database were performed using SeaView4 software (Galtier et al., 1996). Multiple alignments of amino

TABLE 1 | Primers used in this study.

	Forward primer (5′-3′)[a]	Reverse primer (5′-3′)	Purpose
OE*sll0505_npapcE*	CGCG**CTCGAG**TTAAAACTGCATTATCAG	CTGTCAATGGCGACTCCCCGATTGAGGAAA	DAC cloning
OE*sll0505*	TTTCCTCAATCGGGGAGTCGCCATTGACAG	CGC**GGATCC**TCATTTTTTGTCGTT	DAC cloning
OE*slr0104_npapcE*	CGCG**CTCGAG**TTAAAACTGCATTATCAG	GGCAAAAATTGCTTTCATTGGATTTCATTATCTCCC	PDE cloning
OE*slr0104*	GGGAGATAATGAAATCCAATGAAAGCAATTTTTGCC	CTC**GGATCC**CTAAAATCTGGTGGTG	PDE cloning
sll0504	ACCGGATGAACGACGAAATTA	TAGACAATCCTGGCGCAATAG	RT-PCR/qRT-PCR
sll0505	GGAGTCGCCATTGACAGTAA	TCCTCGGAAACGACAATACAA	RT-PCR/qRT-PCR
sll0506	CCGGATTTGGACCAGCA	TCCTTTAATTCCCGCCGTAG	RT-PCR/qRT-PCR
slr0104	CGCCCAACTCAAACAAGAAAG	GTTGCTGCTCCAGGGTAAA	RT-PCR/qRT-PCR
rnpB	GTGAGGACAGTGCCACAGAA	GGCAGGAAAAAGACCAACCT	qRT-PCR

[a]*Bold text indicates sequence of restriction site.*

acid sequences were generated using MUSCLE (Edgar, 2004). Phylogenetic trees were inferred using maximum likelihood-based method 100 bootstraps, and the Jones-Taylor-Thornton model (Jones et al., 1992). The likelihood log was −23144.7.

Cell Lysis Assay

The cell lysis assay was conducted by pelleting 7 mL of cells that had been grown in BG-11/HEPES medium under WL at 15 μmol m^{-2} s^{-1} as described above and diluted to an OD_{750} of 0.4 and incubated for an additional 24 h. Pelleted cells were then resuspended in 4 mL of CelLytic^{TM} B (Millipore Sigma, St. Louis, MO, United States) containing 10 μg/mL (w/v) lysozyme and shaken on a vortexer for 30 min. After this period, samples were centrifuged at 10,000 × *g* at room temperature for 5 min. The level of cellular lysis was estimated based on measuring absorbance at 660 nm of the chlorophyll released into the supernatant (Mehta et al., 2015). Chlorophyll absorbance values were standardized relative to total soluble protein content of cells.

Statistical Analysis

Experiments were conducted with at least three independent biological replicates. Statistical significance was determined via Student's *t*-test or via one way analysis of variance (ANOVA) with Fisher *post hoc* test using OpenStat statistical software (version 10.01.08; W. G. Miller http://www.Statprograms4U.com). Statistical analyses were performed utilizing 95% confidence intervals ($p < 0.05$).

RESULTS

Bioinformatic and Evolutionary Analyses of c-di-AMP Synthesis Genes in Cyanobacteria

Nearly all sequenced cyanobacteria assessed contain one copy of the c-di-AMP synthesis gene DAC, with the exception of *Cyanothece* sp. PCC 7424, *Cyanothece* sp. PCC 7822, *Gloeobacter kilaueensis* JS1, and *Gloeobacter violaceus* PCC 7421, which each carry two copies (Agostoni and Montgomery, 2014). Notably, DACs from cyanobacteria lack additional sensor domains (Agostoni and Montgomery, 2014), in contrast to DACs from other bacteria that contain domains involved in multimerization or in regulating enzymatic activity (Corrigan and Grundling, 2013; Commichau et al., 2015). The genus *Gloeobacter,* which represents primordial cyanobacteria (Turner et al., 1999), possesses both DACs suggesting that c-di-AMP signaling was present early during the evolution of this phylum. Phylogenetic analysis based on amino acid sequences of DACs in cyanobacteria (**Figure 1**) indicated that DACs have been vertically transferred as the typology of the tree is similar to one generated based on phylogenetic diversity of cyanobacterial genomes (Shih et al., 2013). For cyanobacterial species with two DACs, one of the two copies is extremely divergent from that of all the other DACs found in species with just one copy (**Figure 1**, indicated as "2^{nd} DAC"). The diverged copy of DAC is related to other unknown or hypothetical DAC enzyme-encoding genes that contain a DisA-N domain, which may indicate a novel class of DAC enzymes.

Cyanobacteria exhibit a conserved operon structure for the DAC gene related to *cdaA*/*dacA* that is found broadly across distinct strains. The Diaminopimelate Decarboxylase (DAPDC or *lysA*) and Undecaprenyl Pyrophosphate Synthase (UPS or *uppS*) genes are always downstream and upstream, respectively, from the DAC gene which is conserved across cyanobacteria (**Figure 2A**). It appears that the grouping of these three genes in an operon is a unique feature of cyanobacteria, as this arrangement is absent in non-cyanobacterial species. In species with two DACs, only one DAC is found in this gene arrangement (data not shown). DAPDC catalyzes the last step in the biosynthesis of the amino acid lysine, i.e., conversion of the peptidoglycan precursor DAP to lysine (Bukhari and Taylor, 1971a,b). UPS is a prenyltransferase that catalyzes the production of undecaprenyl pyrophosphate, which is critical as a lipid carrier for peptidoglycan synthesis (Apfel et al., 1999). Thus, both neighboring genes appear to be implicated in peptidoglycan synthesis. In *Synechocystis*, there is a 42 bp intergenic region between the DAPDC gene (*sll0504*) and DAC gene (*sll0505*), whereas the DAC overlaps with the UPS gene (*sll0506*). We decided to verify whether the three genes were co-transcribed. RT-PCR analyses of amplicons of portions of the mRNA indicated that the three genes can be transcribed together in a single operon in *Synechocystis* (**Figure 2B**, lane 6), suggesting that they may be involved in similar or related functions in the organism.

FIGURE 1 | Phylogenetic analysis based on multiple putative functionally conserved DAC sequences. For the species with two DACs (see gray line for the second rare DAC), the gene identification number was added. Red asterisks indicate four species investigated in this study.

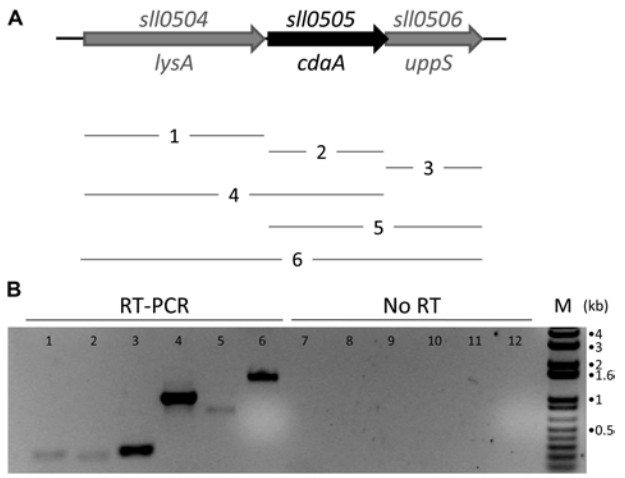

FIGURE 2 | Genomic context and RT-PCR analyses of conserved DAC-containing operon in *Synechocystis*. **(A)** Genomic context of conserved DAC (*sll0505*) in *Synechocystis*. Lines (1–6) below genomic region indicate PCR products amplified from cDNA in panel B. RT-PCR of DAPDC (*sll0504*), DAC (*sll0505*), and UPS (*sll0506*) in *Synechocystis*. **(B)** RT-PCR analyses of transcripts produced from the DAC genomic region in *Synechocystis*: Lanes 1 and 7, DAPDC; Lanes 2 and 8, DAC; Lanes 3 and 9, UPS; Lanes 4 and 10, DAPDC and DAC; Lanes 5 and 11, DAC and UPS; Lanes 6 and 12, DAPDC, DAC, and UPS. Lanes 1–6, RT-PCR reactions; Lanes 7–12, no RT negative control reactions. M, molecular marker. RNA was isolated from cells grown at 35 μmol m^{-2} s^{-1} white light.

Overexpression of Native DAC-Encoding *sll0505* and PDE-Encoding *slr0104* Genes in *Synechocystis*

In *Synechocystis* there is only one DAC (PF02457, *sll0505*), which is related to *cdaA*/*dacA*, and one c-di-AMP PDE (PF07698, *slr0104,* belonging to the 7TM_7TMR_HD family), which is related to *pgpH*. In many bacteria c-di-AMP is essential for survival (Commichau et al., 2015), and in accordance with this observation, we were not able to produce a mutant completely lacking *sll0505* in *Synechocystis* (data not shown). We, thus, decided to overexpress the c-di-AMP DAC and PDE native enzymes in *Synechocystis* to investigate their activity *in vivo*. Quantitative RT-PCR showed increased accumulation of the mRNA for DAC and PDE genes in the DAC and PDE overexpression strains, respectively (**Figure 3**). The DAC strain exhibited an ∼40-fold increase in the level of DAC mRNA accumulation compared to WT (**Figure 3A**), whereas the PDE strain had a more than 200-fold increase in PDE mRNA levels compared to WT (**Figure 3B**).

Quantification of c-di-AMP levels in the DAC and PDE overexpression strains was conducted to assess whether these two native enzymes could modulate intracellular levels of c-di-AMP (**Figure 4**). The levels of c-di-AMP in the DAC overexpression strain were significantly altered, i.e., 1.7-fold higher ($p < 0.05$), compared to the WT strain. Whereas this is lower than might be anticipated based on gene expression data, some bacterial strains which overaccumulate DAC mRNA show no upregulation of intracellular c-di-AMP levels suggesting possible negative feedback mechanisms on DAC activity in some cases (Savage et al., 2015). The levels of c-di-AMP in the PDE overexpression *Synechocystis* strain were on average half as much as the WT strain, although this level was not significantly different. To assess whether the overexpression of the DAC and c-di-AMP-specific PDE were specific to affecting c-di-AMP levels, we assessed levels of another second messenger c-di-GMP. We observed no difference in c-di-GMP levels between WT, DAC-overexpression strain, and c-di-AMP PDE overexpression strain (data not shown).

Previously, it has been observed that c-di-AMP homeostasis is fundamental for optimal growth, with either lower than normal levels or overaccumulation relative to WT resulting in defects in growth (Corrigan et al., 2013; Mehne et al., 2013; Ye et al., 2014; Gundlach et al., 2015; Rubin et al., 2018). Our overexpressing strains both exhibited a lag in growth compared to WT in BG-11/HEPES medium (**Figure 5A**). Additionally, WT grew homogenously in the medium, whereas DAC and PDE strains formed distinct aggregates in the late part of the growth curve analysis (**Figure 5B**). This aggregation may impact analysis of growth by measuring culture optical density. Thus, we also assessed growth using dilution-based colony growth assays on agar plates. In this assay, we similarly observed that the OE DAC and OE PDE strains exhibited impaired growth relative to WT (**Figure 5C**).

Given the association of the c-di-AMP synthesis gene with other genes associated with peptidoglycan synthesis or modification and the cellular aggregation phenotypes, c-di-AMP accumulation in cells may impact cell wall synthesis or modification. We, thus, tested for alterations in cell wall properties for the OE strains relative to WT by conducting lysozyme sensitivity assays. Both the OE DAC strain and OE PDE strain had increased sensitivity to lysozyme treatment relative to WT, as measured by chlorophyll release into the supernatant (**Figure 6**).

Osmotic and Salt Stresses Impact c-di-AMP Levels in Multiple Cyanobacteria

Based on the observation that c-di-AMP-binding riboswitches have a putative role in osmoprotectant synthesis and transport in cyanobacteria (Nelson et al., 2013), c-di-AMP could be critical for osmotic or salt stress responses in these organisms. Osmoprotectants have recognized roles in cellular responses to both osmotic and salt stresses (Bougouffa et al., 2014). Thus, we quantified changes in DAC and PDE mRNA levels in WT under osmotic and salt stresses, the latter of which induces both osmotic and ionic stress. After 24 h of osmotic or salt stress, levels of DAC and PDE mRNA decreased compared to non-stress, control conditions although differences were not statistically significant (**Figure 3**). The DAC mRNA levels decreased to 0.3- and 0.7-fold relative to WT under sorbitol and salt stress, respectively (**Figure 3A**). Similarly, the PDE mRNA levels decreased to 0.5- and 0.7-fold relative to WT under sorbitol and salt stress, respectively (**Figure 3B**).

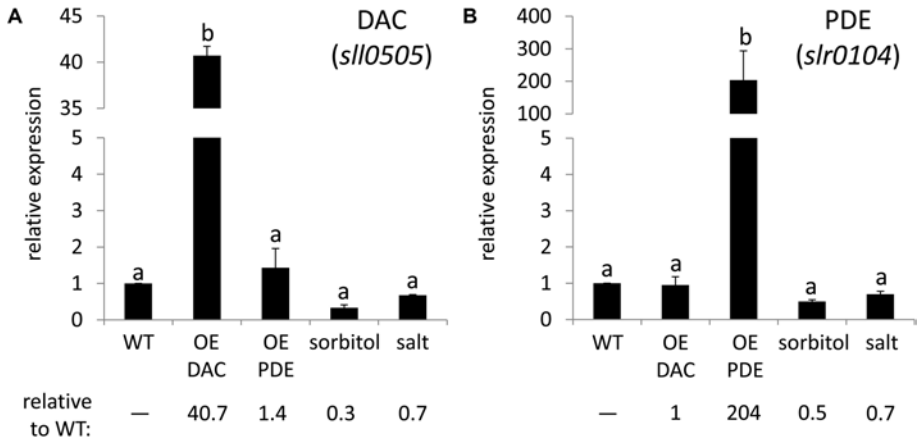

FIGURE 3 | Quantitative reverse transcriptase PCR (qRT-PCR) analysis of the expression of DAC and PDE genes in *Synechocystis*. **(A)** DAC and **(B)** PDE genes were analyzed for strains grown under 35 μmol m^{-2} s^{-1} white light. Wild-type (WT), overexpression of DAC (*sll0505*) in WT (OE DAC), overexpression of PDE (*slr0104*) in WT (OE PDE), WT under sorbitol stress (sorbitol, 0.2 M sorbitol), WT under salt stress (salt, 0.6 M NaCl). The transcript level of the *rnpB* gene was used as an internal control for each sample. Bars represent averages (± standard deviations). Bars marked with different letters are significantly different ($p < 0.05$). Numbers below graphs represent fold difference relative to WT grown under non-stress conditions.

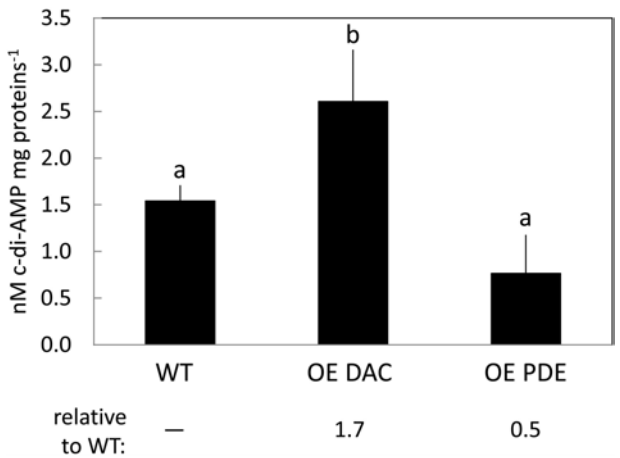

FIGURE 4 | Cyclic di-AMP levels in *Synechocystis* in replete BG-11/HEPES medium under white light. WT, wild-type; OE DAC, strain overexpressing the native DAC (*sll0505*); OE PDE, strain overexpressing the native PDE (*slr0104*). Bars represent averages (± standard deviations). Bars marked with different letters are significantly different ($p < 0.05$). Numbers below graphs represent fold difference relative to WT.

To determine whether these stresses influence intracellular c-di-AMP levels and whether stress-induced changes occur in cyanobacteria beyond *Synechocystis*, we exposed *Synechocystis* and three additional species of cyanobacteria to sorbitol or salt stress for 24 h. Two were unicellular cyanobacteria, moderately halotolerant *Synechocystis* (Reed et al., 1985) and salt-sensitive *Synechococcus* (Kaku et al., 2000), and two were filamentous cyanobacteria, highly salt-sensitive *Anabaena* (Rai and Tiwari, 2001) and salt-sensitive *F. diplosiphon* (Singh and Montgomery, 2013b). C-di-AMP levels were threefold higher under sorbitol-induced osmotic stress in *Synechocystis*. By comparison, there was no significant difference in intracellular levels of c-di-AMP in another unicellular strain *Synechococcus* in response to osmotic stress (**Figure 7A**). In the filamentous cyanobacterium *F. diplosiphon*, c-di-AMP levels were much higher than for the other cyanobacterial strains and increased ∼2-fold under osmotic stress, whereas sorbitol treatment did not result in an increase in c-di-AMP under our conditions in *Anabaena* (**Figure 7A**). Changes in the intracellular concentration of c-di-AMP occur during osmotic stress in *Synechocystis* and *F. diplosiphon*. We also investigated whether c-di-AMP levels varied in these four cyanobacterial species under salt stress (**Figure 7A**). Under salt stress, c-di-AMP levels were not impacted in unicellular strains, whereas levels were lower in *F. diplosiphon* and higher in *Anabaena* in the presence of salt.

In cyanobacteria, biofilm formation is a protective mechanism against salt stress (Jittawuttipoka et al., 2013). We previously demonstrated that induction of biofilm formation is under the control of c-di-GMP in *Synechocystis* (Agostoni et al., 2016). To investigate whether c-di-GMP is elevated under salt stress conditions that are associated with cyanobacterial biofilm formation, we quantified c-di-GMP levels in response to treatment with salt. Indeed, c-di-GMP levels increased in all four species after 24 h of salt stress (**Figure 7B**). In contrast to stress caused by salt, the levels of c-di-GMP did not vary in *Synechocystis*, *Synechococcus*, and *Anabaena* under sorbitol stress (**Figure 7B**). However, c-di-GMP levels significantly increased under sorbitol stress in *F. diplosiphon* (**Figure 7B**). Taken together, these analyses suggest that c-di-AMP responds to osmotic and salt stress, although generally an increase in c-di-AMP levels is associated with sorbitol-induced osmotic stress (if there is a response). By contrast, levels of c-di-GMP primarily respond to ionic rather than osmotic stress across cyanobacterial species, with an increase in c-di-GMP levels observed in all tested strains in response to salt stress. The distinct responses of these cyanobacterial strains to salt and osmotic stresses may reflect

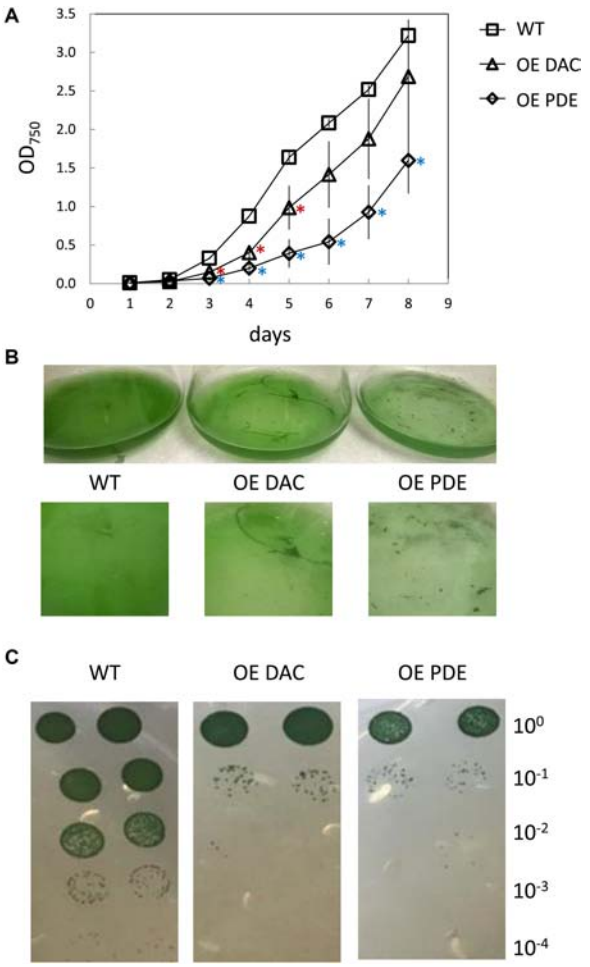

FIGURE 5 | Growth curve of *Synechocystis* wild-type (WT), strain overexpressing diadenylyl cyclase (OE DAC), and strain overexpressing c-di-AMP phosphodiesterase (OE PDE). **(A)** All strains were grown in BG-11/HEPES under 35 μmol m^{-2} s^{-1} white light. Data points represent averages (± standard deviations). *$p < 0.05$ with red asterisks indicating comparison between OE DAC and WT and blue asterisks comparing OE PDE and WT. **(B)** Picture of representative WT, OE DAC, and OE PDE cultures. **(C)** Images of WT, OE DAC, and OE PDE growth as measured by spotting of cells (10 μL) of a 1:10 serial dilution on BG-11/HEPES plates containing 1% (w/v) agar under white light. Cells were initially at an OD_{750} of 0.6 in the undiluted culture and cells diluted up to 1:10,000-fold.

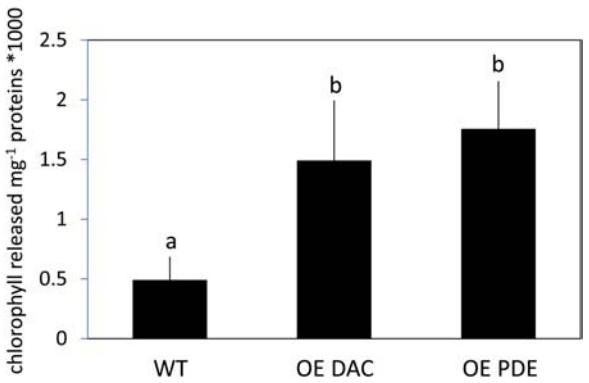

FIGURE 6 | Comparison of lysozyme-dependent lysis of *Synechocystis* wild-type (WT), strain overexpressing diadenylyl cyclase (OE DAC), and strain overexpressing c-di-AMP phosphodiesterase (OE PDE). All strains were grown in BG-11/HEPES under 15 μmol m^{-2} s^{-1} white light. Cells were treated with 10 μg mL^{-1} lysozyme for 30 min. Cellular lysis was measured based on chlorophyll released from cells at measured by absorbance at 660 nm in the supernatant after centrifugation. Bars represent averages (± standard deviations). Bars marked with different letters are significantly different ($p < 0.05$).

their distinct sensitivities to salt (Reed et al., 1985; Kaku et al., 2000; Rai and Tiwari, 2001; Singh and Montgomery, 2013b), as well as other aspects of their unique ecological histories. However, the production of c-di-AMP in a range of cyanobacterial species is evident.

Given that at least osmotic stress results in an alteration of intracellular c-di-AMP levels in *Synechocystis*, we queried whether strains with overexpression of DAC or PDE genes exhibited altered growth responses due to applied abiotic stresses. In these analyses, we reduced the intensity of white light to which cells were exposed (compared to results shown in **Figure 5**) due to the noted combined detrimental effect of multiple stresses such as high light and salt on cyanobacterial growth (Lu and Zhang, 2000). We first noted that, although not directly comparable due to changing multiple factors, growth under lower light (i.e., ~15 μmol m^{-2} s^{-1}) resulted in a significant impairment only of the OE PDE strain compared to WT compared to growth under higher white light (i.e., 35 μmol m^{-2} s^{-1}). Additionally, OE DAC and OE PDE cells exposed to low light lacked a major lag in growth relative to WT that was observed at higher white light levels (compare **Figure 5A** and **Figure 8A**). Osmotic stress conditions had minor effects, with only the OE PDE strain having statistically significant, transiently improved growth relative to WT (**Figure 8B**). However, both OE PDE and OE DAC strains exhibited an impairment in growth relative to WT in the presence of salt (**Figure 8C**). The significant changes in growth under salt in the OE DAC and OE PDE strains relative to WT were associated with altered intracellular c-di-AMP levels. The OE DAC strain exhibited significantly higher intracellular c-di-AMP levels compared to WT, whereas c-di-AMP levels in the OE PDE strain were below detection when strains were grown in the presence of NaCl (**Figure 9**).

DISCUSSION

Given that the genus *Gloeobacter*, which is considered the most primordial of extant cyanobacteria (Rippka et al., 1974), possesses two DAC enzymes, in contrast with the majority of cyanobacterial species that have only have one DAC enzyme, we speculate that cyanobacteria initially contained two DAC enzymes and that during evolution the second DAC was lost. Since the conserved DAC, DAPDC and the UPS cassette (i.e., *lysA-cdaA-uppS* operon) is extremely conserved among cyanobacteria, uniquely, and both the DAC and UPS have associations with peptidoglycan synthesis, these three genes together likely play a

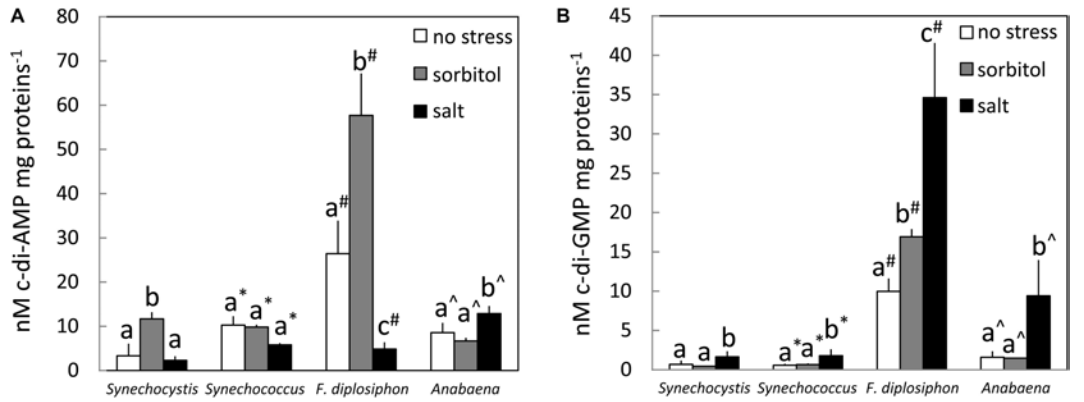

FIGURE 7 | Cyclic di-AMP and cyclic di-GMP levels under sorbitol and salt stresses. **(A)** Cyclic di-AMP and **(B)** cyclic di-GMP levels normalized to total proteins were determined for *Synechocystis* sp. PCC 6803 (*Synechocystis*), *Synechococcus elongatus* sp. PCC 7942 (*Synechococcus*), *Fremyella diplosiphon* (*F. diplosiphon*), and *Anabaena* sp. PCC 7120 (*Anabaena*) grown under 35 μmol m^{-2} s^{-1} white light. Bars represent averages (± standard deviations). Bars marked with different letters indicate a significant difference ($p < 0.05$) for comparisons made within each species.

critical role in controlling cell wall synthesis across cyanobacteria. This is a role consistent with prior studies which indicated that c-di-AMP metabolism impacts cell wall structure or stability in multiple, largely pathogenic, bacteria (Commichau et al., 2017). However, the conserved operon structure suggest an important and well-conserved function for c-di-AMP in peptidoglycan-dependent processes in cyanobacteria.

We were able to strongly increase transcript accumulation of DAC and PDE in *Synechocystis* using overexpression plasmids and demonstrate a significant impact on intracellular c-di-AMP levels in the OE DAC strain in BG-11 and significant impacts on c-di-AMP homeostasis in both the OE DAC and OE PDE strains grown in the presence of salt. Higher or lower levels of c-di-AMP are both detrimental to normal growth in *Bacillus subtilis*, *Listeria monocytogenes, Borrelia burgdorferi,* and *Staphylococcus aureus* (Corrigan et al., 2011; Dengler et al., 2013; Mehne et al., 2013; Witte et al., 2013; Ye et al., 2014). Also, reduced levels of c-di-AMP have been recently shown to impact cyanobacterial growth in a *Synechococcus* strain in which *cdaA* was deleted (Rubin et al., 2018). In *B. subtilis* the differences in growth rates between WT and a strain with strong accumulation of c-di-AMP were attributed to aberrant cell morphologies (Mehne et al., 2013). Given that the *cdaA* gene is next to a gene encoding GlmM that is essential for peptidoglycan synthesis in *B. subtilis*, the observed aberrant cell morphologies may be due to disruptions in c-di-AMP regulation of peptidogylan synthesis in the mutant compared to WT (Mehne et al., 2013). Mutation of the *S. aureus* PDE GdpP resulted in increased peptidoglycan cross-linking which was detrimental to growth (Corrigan et al., 2011).

Here, *Synechocystis* strains with overexpression of either DAC or PDE grew slower than WT. Notably, the DAC and PDE overexpression strains formed aggregates later in the growth analysis compared to WT which grew homogenously in the medium throughout. These phenotypes may be related to the observed changes in cell morphology or cell wall integrity of c-di-AMP mutants in several bacteria (Corrigan et al., 2011; Bai et al., 2013; Mehne et al., 2013; Witte et al., 2013; Zhang and He, 2013; Tang et al., 2015). Indeed, the DAC and PDE overexpression strains exhibited increased sensitivity to lysozyme as compared to the WT parent strain. The results for the OE PDE strain are in accordance with prior analyses showing that decreased c-di-AMP levels have previously been implicated in cell wall sensitivity and altered cell lysis for a number of bacteria (Luo and Helmann, 2011; Witte et al., 2013). On the other hand, the increased sensitivity observed for the OE DAC strain may be associated with the fact that the DAC/*cdaA* gene is in an operon with genes associated with cell wall synthesis/modification. Specifically, the role of the DADPC gene in crosslinking of peptidoglycan corresponds to prior associations of c-di-AMP levels with peptidoglycan cross-linking (Luo and Helmann, 2011). Thus, the altered phenotype of the OE DAC strain could be related to associated impacts of altering c-di-AMP accumulation on peptidoglycan crosslinking, which in turn could alter cellular responses to lysozyme.

Cyclic di-AMP homeostasis is critical in replete BG-11 medium. Additionally, the regulation of DAC and PDE genes in osmotic and salt stress, especially the latter, appears to contribute to cell fitness. Whereas WT has impaired growth in both stresses, changes in intracellular c-di-AMP homeostasis is important for cellular responses to salt stress as both the DAC and PDE OE strains, which have significantly higher and lower c-di-AMP levels in the presence of salt, respectively, exhibited impaired growth over time in the presence of NaCl-induced stress.

Osmotic and ionic stresses are common in natural ecosystems (Williams, 1987; Kaushal et al., 2005; Durack et al., 2012; Canedo-Arguelles et al., 2013; El-Akhal et al., 2013) and identifying the mechanisms by which cyanobacteria can tolerate osmotic and ionic stresses is critical. Species able to maintain osmotic equilibrium under these conditions will prove most beneficial for use in cyanobacterial mass cultivation (Hagemann, 2011). There is still a lack of knowledge on the mechanisms used by cyanobacteria to specifically sense and respond to osmotic and ionic stresses. Experiments described here show that sorbitol is an important factor in the regulation of c-di-AMP homeostasis,

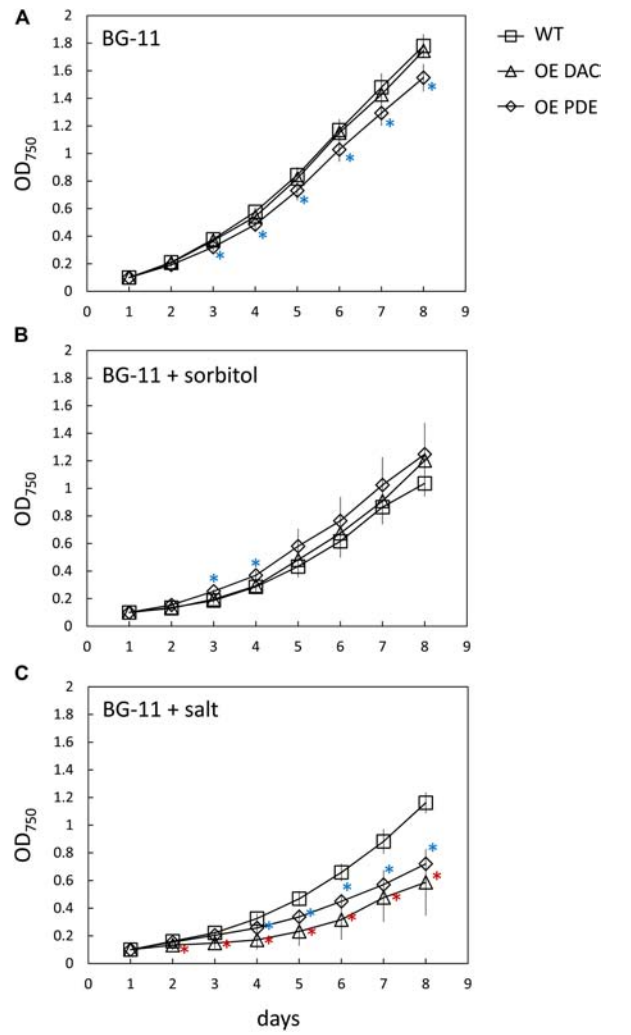

FIGURE 8 | Growth curve of *Synechocystis* wild-type (WT), strain overexpressing diadenylyl cyclase (OE DAC), and strain overexpressing c-di-AMP phosphodiesterase (OE PDE) under low white light and in presence of abiotic stresses. All strains were grown in BG-11/HEPES under 15 μmol m^{-2} s^{-1} white light in **(A)** BG-11 medium, **(B)** sorbitol-induced osmotic stress (0.5 M sorbitol), or **(C)** salt stress (0.6 M NaCl). Data points represent averages (± standard deviations). *$p < 0.05$ with red asterisks indicating comparison between OE DAC and WT and blue asterisks comparing OE PDE and WT.

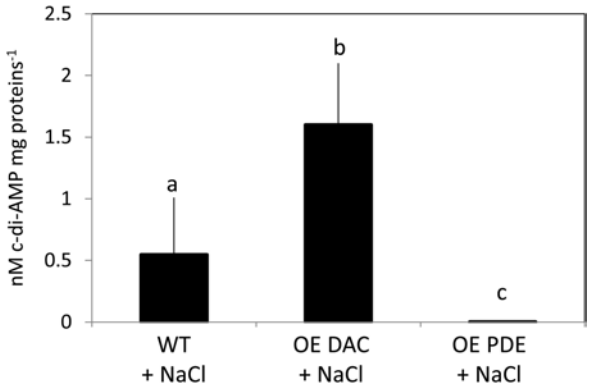

FIGURE 9 | Cyclic di-AMP levels in *Synechocystis* in replete BG-11/HEPES medium containing 0.6 M NaCl under low white light at 15 μmol m^{-2} s^{-1}. WT, wild-type; OE DAC, strain overexpressing the native DAC (*sll0505*); OE PDE, strain overexpressing the native PDE (*slr0104*). Bars represent averages (± standard deviations). Bars marked with different letters are significantly different ($p < 0.05$).

whereas salt is a critical factor to regulate c-di-AMP synthesis and c-di-GMP homeostasis. Prior studies with Gram-positive bacteria have implicated c-di-AMP as critical during osmotic stress, based on the identification of a potassium transporter and a regulator of a K^+ transporter as c-di-AMP receptors (Corrigan et al., 2011, 2013; Bai et al., 2014; Moscoso et al., 2015). Also, regulation of c-di-AMP levels have been associated with salt sensitivity in Gram-positive strains (Smith et al., 2012; Dengler et al., 2013). Notably, a study on c-di-AMP-binding riboswitches implicated c-di-AMP-dependent regulation of the synthesis and transport of osmoprotectants in cyanobacteria as critical for stress responses, such as osmotic or salt stresses, in these organisms (Nelson et al., 2013). Our results suggest a role in response to salt stress in *Synechocystis*. Determining the molecular mechanisms of c-di-AMP and c-di-GMP signaling networks during cyanobacterial adaptation is necessary to understand how cyanobacteria survive in stressful and fluctuating environments and ensure improved biomass and product yields under osmotic and ionic stresses to improve applications and fundamental research in solving environmental problems.

AUTHOR CONTRIBUTIONS

MA and BM: conceived and designed the experiments. MA, AL-J, EH, GS, and EB: performed the experiments and contributed to data analysis. MA and BM: drafted the article. MA, AL-J, CW, and BM: critically revised the article.

FUNDING

This work was supported by the National Science Foundation (Grant No. MCB-1243983 to BM), the Michigan State University Discretionary Funding Initiative (Funding I.D. No. MSU-DFI 70222 to BM), the National Institutes of Health (Grant Nos. GM109259 and AI130554 to CW) and support to Marco Agostoni from the United States Department of Energy (Chemical Sciences, Geosciences and Biosciences Division, Office of Basic Energy Sciences, Office of Science, Grant No. DE-FG02-91ER20021 to BM). Participation of AL-J was additionally made possible by a predoctoral training award from Grant No. T32-GM110523 from National Institute of General Medical Sciences of the National Institutes of Health and Alliance for Graduate Education and Professoriate (AGEP) Scholar Awards from the MSU Graduate School. The contents of this publication are solely the responsibility of the authors and do not necessarily represent the official views of the NIGMS or NIH.

REFERENCES

Agostoni, M., Koestler, B. J., Waters, C. M., Williams, B. L., and Montgomery, B. L. (2013). Occurrence of cyclic di-GMP-modulating output domains in cyanobacteria: an illuminating perspective. *mBio* 4:e00451-13. doi: 10.1128/mBio.00451-13

Agostoni, M., and Montgomery, B. L. (2014). Survival strategies in the aquatic and terrestrial world: the impact of second messengers on cyanobacterial processes. *Life* 4, 745–769. doi: 10.3390/life4040745

Agostoni, M., Waters, C. M., and Montgomery, B. L. (2016). Regulation of biofilm formation and cellular buoyancy through modulating intracellular cyclic di-GMP levels in engineered cyanobacteria. *Biotechnol. Bioeng.* 113, 311–319. doi: 10.1002/bit.25712

Allen, M. M. (1968). Simple conditions for growth of unicellular blue-green algae on plates. *J. Phycol.* 4, 1–4. doi: 10.1111/j.1529-8817.1968.tb04667.x

Angerer, V., Schwenk, P., Wallner, T., Kaever, V., Hiltbrunner, A., and Wilde, A. (2017). The protein Slr1143 is an active diguanylate cyclase in *Synechocystis* sp. PCC 6803 and interacts with the photoreceptor Cph2. *Microbiology* 163, 920–930. doi: 10.1099/mic.0.000475

Apfel, C. M., Takacs, S., Fountoulakis, M., Stieger, M., and Keck, W. (1999). Use of genomics to identify bacterial undecaprenyl pyrophosphate synthetase: cloning, expression, and characterization of the essential uppS gene. *J. Bacteriol.* 181, 483–492.

Bai, Y., Yang, J., Eisele, L. E., Underwood, A. J., Koestler, B. J., Waters, C. M., et al. (2013). Two DHH subfamily 1 proteins in *Streptococcus pneumoniae* possess cyclic Di-AMP phosphodiesterase activity and affect bacterial growth and virulence. *J. Bacteriol.* 195, 5123–5132. doi: 10.1128/jb.00769-13

Bai, Y., Yang, J., Zarrella, T. M., Zhang, Y., Metzger, D. W., and Bai, G. (2014). Cyclic di-AMP impairs potassium uptake mediated by a cyclic di-AMP binding protein in *Streptococcus pneumoniae*. *J. Bacteriol.* 196, 614–623. doi: 10.1128/jb.01041-13

Barker, J. R., Koestler, B. J., Carpenter, V. K., Burdette, D. L., Waters, C. M., Vance, R. E., et al. (2013). STING-dependent recognition of cyclic di-AMP mediates type I interferon responses during *Chlamydia trachomatis* infection. *mBio* 4:e00018-13. doi: 10.1128/mBio.00018-13

Bejerano-Sagie, M., Oppenheimer-Shaanan, Y., Berlatzky, I., Rouvinski, A., Meyerovich, M., and Ben-Yehuda, S. (2006). A checkpoint protein that scans the chromosome for damage at the start of sporulation in *Bacillus subtilis*. *Cell* 125, 679–690. doi: 10.1016/j.cell.2006.03.039

Bougouffa, S., Radovanovic, A., Essack, M., and Bajic, V. B. (2014). DEOP: a database on osmoprotectants and associated pathways. *Database* 2014:bau100. doi: 10.1093/database/bau100

Bowman, L., Zeden, M. S., Schuster, C. F., Kaever, V., and Gründling, A. (2016). New insights into the cyclic Di-adenosine monophosphate (c-di-AMP) degradation pathway and the requirement of the cyclic dinucleotide for acid stress resistance in *Staphylococcus aureus*. *J. Biol. Chem.* 291, 26970–26986. doi: 10.1074/jbc.M116.747709

Bukhari, A. I., and Taylor, A. L. (1971a). Genetic analysis of diaminopimelic acid- and lysine-requiring mutants of *Escherichia coli*. *J. Bacteriol.* 105, 844–854.

Bukhari, A. I., and Taylor, A. L. (1971b). Mutants of *Escherichia coli* with a growth requirement for either lysine or pyridoxine. *J. Bacteriol.* 105, 988–998.

Cadoret, J.-C., Rousseau, B., Perewoska, I., Sicora, C., Cheregi, O., Vass, I., et al. (2005). Cyclic nucleotides, the photosynthetic apparatus and response to a UV-B stress in the cyanobacterium *Synechocystis* sp. PCC 6803. *J. Biol. Chem.* 280, 33935–33944.

Canedo-Arguelles, M., Kefford, B. J., Piscart, C., Prat, N., Schafer, R. B., and Schulz, C. J. (2013). Salinisation of rivers: an urgent ecological issue. *Environ. Pollut.* 173, 157–167. doi: 10.1016/j.envpol.2012.10.011

Cho, K. H., and Kang, S. O. (2013). Streptococcus pyogenes c-di-AMP phosphodiesterase. GdpP, influences SpeB processing and virulence. *PLoS One* 8:e69425. doi: 10.1371/journal.pone.0069425

Cobley, J. G., Zerweck, E., Reyes, R., Mody, A., Seludounson, J. R., Jaeger, H., et al. (1993). Construction of shuttle plasmids which can be efficiently mobilized from *Escherichia coli* into the chromatically adapting cyanobacterium, *Fremyella diplosiphon*. *Plasmid* 30, 90–105. doi: 10.1006/plas.1993.1037

Commichau, F. M., Dickmanns, A., Gundlach, J., Ficner, R., and Stülke, J. (2015). A jack of all trades: the multiple roles of the unique essential second messenger cyclic di-AMP. *Mol. Microbiol.* 97, 189–204. doi: 10.1111/mmi.13026

Commichau, F. M., Gibhardt, J., Halbedel, S., Gundlach, J., and Stülke, J. (2017). A delicate connection: c-di-AMP affects cell integrity by controlling osmolyte transport. *Trends Microbiol.* 26, 175–185. doi: 10.1016/j.tim.2017.1009.1003

Corrigan, R. M., Abbott, J. C., Burhenne, H., Kaever, V., and Grundling, A. (2011). c-di-AMP Is a new second messenger in *Staphylococcus aureus* with a role in controlling cell size and envelope stress. *PLoS Pathog.* 7:e1002217. doi: 10.1371/journal.ppat.1002217

Corrigan, R. M., Campeotto, I., Jeganathan, T., Roelofs, K. G., Lee, V. T., and Gründling, A. (2013). Systematic identification of conserved bacterial c-di-AMP receptor proteins. *Proc. Natl. Acad. Sci. U.S.A.* 110, 9084–9089. doi: 10.1073/pnas.1300595110

Corrigan, R. M., and Grundling, A. (2013). Cyclic di-AMP: another second messenger enters the fray. *Nat. Rev. Microbiol.* 11, 513–524. doi: 10.1038/nrmicro3069

Dengler, V., Mccallum, N., Kiefer, P., Christen, P., Patrignani, A., Vorholt, J. A., et al. (2013). Mutation in the c-di-AMP cyclase dacA affects fitness and resistance of methicillin resistant *Staphylococcus aureus*. *PLoS One* 8:e73512. doi: 10.1371/journal.pone.0073512

Dey, B., Dey, R. J., Cheung, L. S., Pokkali, S., Guo, H., Lee, J.-H., et al. (2015). A bacterial cyclic dinucleotide activates the cytosolic surveillance pathway and mediates innate resistance to tuberculosis. *Nat. Med.* 21, 401–406. doi: 10.1038/nm.3813

Du, B., Ji, W., An, H., Shi, Y., Huang, Q., Cheng, Y., et al. (2014). Functional analysis of c-di-AMP phosphodiesterase, GdpP, in *Streptococcus suis* serotype 2. *Microbiol. Res.* 169, 749–758. doi: 10.1016/j.micres.2014.01.002

Durack, P. J., Wijffels, S. E., and Matear, R. J. (2012). Ocean salinities reveal strong global water cycle intensification during 1950 to 2000. *Science* 336, 455–458. doi: 10.1126/science.1212222

Edgar, R. C. (2004). MUSCLE: multiple sequence alignment with high accuracy and high throughput. *Nucleic Acids Res.* 32, 1792–1797. doi: 10.1093/nar/gkh340

El-Akhal, M. R., Rincon, A., Coba De La Pena, T., Lucas, M. M., El Mourabit, N., Barrijal, S., et al. (2013). Effects of salt stress and rhizobial inoculation on growth and nitrogen fixation of three peanut cultivars. *Plant Biol.* 15, 415–421. doi: 10.1111/j.1438-8677.2012.00634.x

Enomoto, G., Ni-Ni-Win, Narikawa, R., and Ikeuchi, M. (2015). Three cyanobacteriochromes work together to form a light color-sensitive input system for c-di-GMP signaling of cell aggregation. *Proc. Natl. Acad. Sci. U.S.A.* 112, 8082–8087. doi: 10.1073/pnas.1504228112

Enomoto, G., Nomura, R., Shimada, T., Ni-Ni Win, Narikawa, R., and Ikeuchi, M. (2014). Cyanobacteriochrome SesA is a diguanylate cyclase that induces cell aggregation in *Thermosynechococcus*. *J. Biol. Chem.* 289, 24801–24809. doi: 10.1074/jbc.M114.583674

Fu, T., Zhao, Y., and Xi, J. (2016). A new second messenger: bacterial c-di-AMP. *Crit. Rev. Eukaryot. Gene Expr.* 26, 309–316. doi: 10.1615/CritRevEukaryotGeneExpr.2016016642

Galtier, N., Gouy, M., and Gautier, C. (1996). SeaView and Phylo_win: two graphic tools for sequence alignment and molecular phylogeny. *Comput. Appl. Biosci.* 12, 543–548. doi: 10.1093/bioinformatics/12.6.543

Gándara, C., and Alonso, J. C. (2015). DisA and c-di-AMP act at the intersection between DNA-damage response and stress homeostasis in exponentially growing *Bacillus subtilis* cells. *DNA Repair* 27, 1–8. doi: 10.1016/j.dnarep.2014.12.007

Gándara, C., De Lucena, D. K. C., Torres, R., Serrano, E., Altenburger, S., Graumann, P. L., et al. (2017). Activity and in vivo dynamics of *Bacillus subtilis* DisA are affected by RadA/Sms and by Holliday junction-processing proteins. *DNA Repair* 55, 17–30. doi: 10.1016/j.dnarep.2017.05.002

Garcia-Pichel, F., Belnap, J., Neuer, S., and Schanz, F. (2003). Estimates of global cyanobacterial biomass and its distribution. *Algol. Stud.* 109, 213–227. doi: 10.1127/1864-1318/2003/0109-0213

Gundlach, J., Mehne, F. M., Herzberg, C., Kampf, J., Valerius, O., Kaever, V., et al. (2015). An essential poison: synthesis and degradation of cyclic di-AMP in *Bacillus subtilis*. *J. Bacteriol.* 197, 3265–3274. doi: 10.1128/jb.00564-15

Hagemann, M. (2011). Molecular biology of cyanobacterial salt acclimation. *FEMS Microbiol. Rev.* 35, 87–123. doi: 10.1111/j.1574-6976.2010.00234.x

Huynh, T. N., Luo, S., Pensinger, D., Sauer, J. D., Tong, L., and Woodward, J. J. (2015). An HD-domain phosphodiesterase mediates cooperative hydrolysis of c-di-AMP to affect bacterial growth and virulence. *Proc. Natl. Acad. Sci. U.S.A.* 112, E747–E756. doi: 10.1073/pnas.1416485112

Huynh, T. N., and Woodward, J. J. (2016). Too much of a good thing: regulated depletion of c-di-AMP in the bacterial cytoplasm. *Curr. Opin. Microbiol.* 30, 22–29. doi: 10.1016/j.mib.2015.12.007

Imashimizu, M., Yoshimura, H., Katoh, H., Ehira, S., and Ohmori, M. (2005). NaCl enhances cellular cAMP and upregulates genes related to heterocyst development in the cyanobacterium, *Anabaena* sp. strain PCC 7120. *FEMS Microbiol. Lett.* 252, 97–103. doi: 10.1016/j.femsle.2005.08.035

Jenal, U., Reinders, A., and Lori, C. (2017). Cyclic di-GMP: second messenger extraordinaire. *Nat. Rev. Microbiol.* 15, 271–284. doi: 10.1038/nrmicro.2016.190

Jittawuttipoka, T., Planchon, M., Spalla, O., Benzerara, K., Guyot, F., Cassier-Chauvat, C., et al. (2013). Multidisciplinary evidences that *Synechocystis* PCC6803 exopolysaccharides operate in cell sedimentation and protection against salt and metal stresses. *PLoS One* 8:e55564. doi: 10.1371/journal.pone.0055564

Jones, D. T., Taylor, W. R., and Thornton, J. M. (1992). The rapid generation of mutation data matrices from protein sequences. *Comput. Appl. Biosci.* 8, 275–282. doi: 10.1093/bioinformatics/8.3.275

Kaku, N., Hibino, T., Tanaka, Y., Ishikawa, H., Araki, E., Takabe, T., et al. (2000). Effects of overexpression of *Escherichia coli* katE and bet genes on the tolerance for salt stress in a freshwater cyanobacterium *Synechococcus* sp. PCC 7942. *Plant Sci.* 159, 281–288.

Katayama, M., and Ohmori, M. (1997). Isolation and characterization of multiple adenylate cyclase genes from the cyanobacterium *Anabaena* sp. strain PCC 7120. *J. Bacteriol.* 179, 3588–3593. doi: 10.1128/jb.179.11.3588-3593.1997

Kaushal, S. S., Groffman, P. M., Likens, G. E., Belt, K. T., Stack, W. P., Kelly, V. R., et al. (2005). Increased salinization of fresh water in the northeastern United States. *Proc. Natl. Acad. Sci. U.S.A.* 102, 13517–13520. doi: 10.1073/pnas.0506414102

Kloft, N., Rasch, G., and Forchhammer, K. (2005). Protein phosphatase PphA from *Synechocystis* sp. PCC 6803: the physiological framework of PII-P dephosphorylation. *Microbiology* 151, 1275–1283. doi: 10.1099/mic.0.27771-0

Krasteva, P. V., and Sondermann, H. (2017). Versatile modes of cellular regulation via cyclic dinucleotides. *Nat. Chem. Biol.* 13, 350–359. doi: 10.1038/nchembio.2337

Lu, C., and Zhang, J. (2000). Role of light in the response of PSII photochemistry to salt stress in the cyanobacterium *Spirulina platensis*. *J. Exp. Bot.* 51, 911–917. doi: 10.1093/jxb/51.346.911

Luo, Y., and Helmann, J. D. (2011). Analysis of the role of *Bacillus subtilis* σM in β-lactam resistance reveals an essential role for c-di-AMP in peptidoglycan homeostasis. *Mol. Microbiol.* 83, 623–639. doi: 10.1111/j.1365-2958.2011.07953.x

Marin, K., Suzuki, I., Yamaguchi, K., Ribbeck, K., Yamamoto, H., Kanesaki, Y., et al. (2003). Identification of histidine kinases that act as sensors in the perception of salt stress in *Synechocystis* sp. PCC 6803. *Proc. Natl. Acad. Sci. U.S.A.* 100, 9061–9066. doi: 10.1073/pnas.1532302100

Massie, J. P., Reynolds, E. L., Koestler, B. J., Cong, J. P., Agostoni, M., and Waters, C. M. (2012). Quantification of high-specificity cyclic diguanylate signaling. *Proc. Natl. Acad. Sci. U.S.A.* 109, 12746–12751. doi: 10.1073/pnas.1115663109

Mehne, F. M., Schröder-Tittmann, K., Eijlander, R. T., Herzberg, C., Hewitt, L., Kaever, V., et al. (2014). Control of the diadenylate cyclase CdaS in *Bacillus subtilis*: an autoinhibitory domain limits cyclic di-AMP production. *J. Biol. Chem.* 289, 21098–21107. doi: 10.1074/jbc.M114.562066

Mehne, F. M. P., Gunka, K., Eilers, H., Herzberg, C., Kaever, V., and Stulke, J. (2013). Cyclic di-AMP homeostasis in *Bacillus subtilis*: both lack and high level accumulation of the nucleotide are detrimental for cell growth. *J. Biol. Chem.* 288, 2004–2017. doi: 10.1074/jbc.M112.395491

Mehta, K. K., Evitt, N. H., and Swartz, J. R. (2015). Chemical lysis of cyanobacteria. *J. Biol. Eng.* 9:10. doi: 10.1186/s13036-015-0007-y

Mikami, K., Kanesaki, Y., Suzuki, I., and Murata, N. (2002). The histidine kinase Hik33 perceives osmotic stress and cold stress in *Synechocystis* sp. PCC 6803. *Mol. Microbiol.* 46, 905–915.

Moscoso, J. A., Schramke, H., Zhang, Y., Tosi, T., Dehbi, A., Jung, K., et al. (2015). Binding of cyclic di-AMP to the *Staphylococcus aureus* sensor kinase KdpD occurs via the universal stress protein domain and downregulates the expression of the Kdp potassium transporter. *J. Bacteriol.* 198, 98–110. doi: 10.1128/jb.00480-15

Nelson, J. W., Sudarsan, N., Furukawa, K., Weinberg, Z., Wang, J. X., and Breaker, R. R. (2013). Riboswitches in eubacteria sense the second messenger c-di-AMP. *Nat. Chem. Biol.* 9, 834–839. doi: 10.1038/nchembio.1363

Ochoa De Alda, J. A. G., Ajlani, G., and Houmard, J. (2000). *Synechocystis* strain PCC 6803 *cya2*, a prokaryotic gene that encodes a guanylyl cyclase. *J. Bacteriol.* 182, 3839–3842. doi: 10.1128/jb.182.13.3839-3842.2000

Ohmori, M., Ikeuchi, M., Sato, N., Wolk, P., Kaneko, T., Ogawa, T., et al. (2001). Characterization of genes encoding multi-domain proteins in the genome of the filamentous nitrogen-fixing cyanobacterium *Anabaena* sp. strain PCC 7120. *DNA Res.* 8, 271–284.

Ohmori, M., Ohmori, K., and Hasunuma, K. (1988). Rapid change in cyclic 3′, 5′-AMP concentration triggered by a light-off or light-on signal in *Anabaena cylindrica*. *Arch. Microbiol.* 150, 203–204. doi: 10.1007/BF00425163

Ohmori, M., and Okamoto, S. (2004). Photoresponsive cAMP signal transduction in cyanobacteria. *Photochem. Photobiol. Sci.* 3, 503–511. doi: 10.1039/b401623h

Ohmori, M., Terauchi, K., Okamoto, S., and Watanabe, M. (2002). Regulation of cAMP-mediated photosignaling by a phytochrome in the cyanobacterium *Anabaena cylindrica*. *Photochem. Photobiol.* 75, 675–679. doi: 10.1562/0031-8655(2002)075<0675:ROCMPB>2.0.CO;2

Okamoto, S., Kasahara, M., Kamiya, A., Nakahira, Y., and Ohmori, M. (2004). A phytochrome-like protein AphC triggers the cAMP signaling induced by far-red light in the cyanobacterium *Anabaena* sp. strain PCC7120. *Photochem. Photobiol.* 80, 429–433. doi: 10.1562/0031-8655(2004)080<0429:APPATT>2.0.CO;2

Oppenheimer-Shaanan, Y., Wexselblatt, E., Katzhendler, J., Yavin, E., and Ben-Yehuda, S. (2011). c-di-AMP reports DNA integrity during sporulation in *Bacillus subtilis*. *EMBO Rep.* 12, 594–601. doi: 10.1038/embor.2011.77

Pade, N., and Hagemann, M. (2015). Salt acclimation of cyanobacteria and their application in biotechnology. *Life* 5, 25–49. doi: 10.3390/life5010025

Paithoonrangsarid, K., Shoumskaya, M. A., Kanesaki, Y., Satoh, S., Tabata, S., Los, D. A., et al. (2004). Five histidine kinases perceive osmotic stress and regulate distinct sets of genes in *Synechocystis*. *J. Biol. Chem.* 279, 53078–53086. doi: 10.1074/jbc.M410162200

Pattanaik, B., and Montgomery, B. L. (2010). FdTonB is involved in the photoregulation of cellular morphology during complementary chromatic adaptation in *Fremyella diplosiphon*. *Microbiology* 156, 731–741. doi: 10.1099/mic.0.035410-0

Raguse, M., Torres, R., Seco, E. M., Gándara, C., Ayora, S., Moeller, R., et al. (2017). *Bacillus subtilis* DisA helps to circumvent replicative stress during spore revival. *DNA Repair* 59, 57–68. doi: 10.1016/j.dnarep.2017.09.006

Rai, A. K., and Tiwari, S. P. (2001). NO_3– nutrition and salt tolerance in the cyanobacterium *Anabaena* sp. PCC 7120 and mutant strains. *J. Appl. Microbiol.* 86, 991–998. doi: 10.1046/j.1365-2672.1999.00788.x

Reed, R. H., Richardson, D. L., and Stewart, W. D. P. (1985). Na^+ uptake and extrusion in the cyanobacterium *Synechocystis* PCC 6714 in response to hypersaline treatment. Evidence for transient changes in plasmalemma Na^+ permeability. *Biochim. Biophys. Acta* 814, 347–355. doi: 10.1016/0005-2736(85)90455-9

Rippka, R., Waterbury, J., and Cohen-Bazire, G. (1974). A cyanobacterium which lacks thylakoids. *Arch. Microbiol.* 100, 419–436. doi: 10.1007/bf00446333

Rismondo, J., Gibhardt, J., Rosenberg, J., Kaever, V., Halbedel, S., and Commichau, F. M. (2016). Phenotypes associated with the essential diadenylate cyclase CdaA and its potential regulator CdaR in the human pathogen *Listeria monocytogenes*. *J. Bacteriol.* 198, 416–426. doi: 10.1128/jb.00845-15

Romling, U. (2008). Great times for small molecules: c-di-AMP, a second messenger candidate in Bacteria and Archaea. *Sci. Signal.* 1:pe39. doi: 10.1126/scisignal.133pe39

Rubin, B. E., Huynh, T. N., Welkie, D. G., Diamond, S., Simkovsky, R., Pierce, E. C., et al. (2018). High-throughput interaction screens illuminate the role of c-di-AMP in cyanobacterial nighttime survival. *PLoS Genet.* 14:e1007301. doi: 10.1371/journal.pgen.1007301

Savage, C. R., Arnold, W. K., Gjevre-Nail, A., Koestler, B. J., Bruger, E. L., Barker, J. R., et al. (2015). Intracellular concentrations of *Borrelia burgdorferi* cyclic di-AMP are not changed by altered expression of the cdaA synthase. *PLoS One* 10:e0125440. doi: 10.1371/journal.pone.0125440

Savakis, P., De Causmaecker, S., Angerer, V., Ruppert, U., Anders, K., Essen, L. O., et al. (2012). Light-induced alteration of c-di-GMP level controls motility of

Synechocystis sp, PCC 6803. *Mol. Microbiol.* 85, 239–251. doi: 10.1111/j.1365-2958.2012.08106.x

Seib, L. O., and Kehoe, D. M. (2002). A turquoise mutant genetically separates expression of genes encoding phycoerythrin and its associated linker peptides. *J. Bacteriol.* 184, 962–970. doi: 10.1128/jb.184.4.962-970.2002

Shih, P. M., Wu, D. Y., Latifi, A., Axen, S. D., Fewer, D. P., Talla, E., et al. (2013). Improving the coverage of the cyanobacterial phylum using diversity-driven genome sequencing. *Proc. Natl. Acad. Sci. U.S.A.* 110, 1053–1058. doi: 10.1073/pnas.1217107110

Shoumskaya, M. A., Paithoonrangsarid, K., Kanesaki, Y., Los, D. A., Zinchenko, V. V., Tanticharoen, M., et al. (2005). Identical Hik-Rre systems are involved in perception and transduction of salt signals and hyperosmotic signals but regulate the expression of individual genes to different extents in *Synechocystis*. *J. Biol. Chem.* 280, 21531–21538. doi: 10.1074/jbc.M412174200

Singh, S. P., and Montgomery, B. L. (2013a). Distinct salt-dependent effects impair *Fremyella diplosiphon* pigmentation and cellular shape. *Plant Signal. Behav.* 8:e24713. doi: 10.4161/psb.24713

Singh, S. P., and Montgomery, B. L. (2013b). Salinity impacts photosynthetic pigmentation and cellular morphology changes by distinct mechanisms in *Fremyella diplosiphon*. *Biochem. Biophys. Res. Commun.* 33, 84–89. doi: 10.1016/j.bbrc.2013.02.060

Smith, W. M., Pham, T. H., Lei, L., Dou, J., Soomro, A. H., Beatson, S. A., et al. (2012). Heat resistance and salt hypersensitivity in *Lactococcus lactis* due to spontaneous mutation of llmg_1816 (gdpP) induced by high-temperature growth. *Appl. Environ. Microbiol.* 78, 7753–7759. doi: 10.1128/aem.02316-12

Tang, Q., Luo, Y., Zheng, C., Yin, K., Ali, M. K., Li, X., et al. (2015). Functional analysis of a c-di-AMP-specific phosphodiesterase MsPDE from *Mycobacterium smegmatis*. *Int. J. Biol. Sci.* 11, 813–824. doi: 10.7150/ijbs.11797

Terauchi, K., and Ohmori, M. (1999). An adenylate cyclase, cyal, regulates cell motility in the cyanobacterium *Synechocystis* sp. PCC 6803. *Plant Cell Physiol.* 40, 248–251.

Terauchi, K., and Ohmori, M. (2004). Blue light stimulates cyanobacterial motility via a cAMP signal transduction system. *Mol. Microbiol.* 52, 303–309. doi: 10.1111/j.1365-2958.2003.03980.x

Torrecilla, I., Leganés, F., Bonilla, I., and Fernández-Piñas, F. (2001). Calcium transients in response to salinity and osmotic stress in the nitrogen-fixing cyanobacterium *Anabaena* sp. PCC7120, expressing cytosolic apoaequorin. *Plant Cell Environ.* 24, 641–648. doi: 10.1046/j.0016-8025.2001.00708.x

Townsley, L., Yannarell, S. M., Huynh, T. N., Woodward, J. J., and Shank, E. A. (2018). Cyclic di-AMP acts as an extracellular signal that impacts *Bacillus subtilis* biofilm formation and plant attachment. *mBio* 9:e00341-18. doi: 10.1128/mBio.00341-18

Turner, S., Pryer, K. M., Miao, V. P. W., and Palmer, J. D. (1999). Investigating deep phylogenetic relationships among cyanobacteria and plastids by small submit rRNA sequence analysis. *J. Eukaryot. Microbiol.* 46, 327–338. doi: 10.1111/j.1550-7408.1999.tb04612.x

Wang, J., Zhang, X., Shi, M., Gao, L., Niu, X., Te, R., et al. (2014). Metabolomic analysis of the salt-sensitive mutants reveals changes in amino acid and fatty acid composition important to long-term salt stress in *Synechocystis* sp. PCC 6803. *Funct. Integr. Genomics* 14, 431–440. doi: 10.1007/s10142-014-0370-7

Whiteley, A. T., Garelis, N. E., Peterson, B. N., Choi, P. H., Tong, L., Woodward, J. J., et al. (2017). c-di-AMP modulates *Listeria monocytogenes* central metabolism to regulate growth, antibiotic resistance and osmoregulation. *Mol. Microbiol.* 104, 212–233. doi: 10.1111/mmi.13622

Williams, W. D. (1987). Salinization of rivers and streams: an important environmental hazard. *Ambio* 16, 180–185.

Witte, C. E., Whiteley, A. T., Burke, T. P., Sauer, J. D., Portnoy, D. A., and Woodward, J. J. (2013). Cyclic di-AMP is critical for *Listeria monocytogenes* growth, cell wall homeostasis, and establishment of infection. *mBio* 4:e00282-13. doi: 10.1128/mBio.00282-13

Witte, G., Hartung, S., Büttner, K., and Hopfner, K.-P. (2008). Structural biochemistry of a bacterial checkpoint protein reveals diadenylate cyclase activity regulated by DNA recombination intermediates. *Mol. Cell* 30, 167–178. doi: 10.1016/j.molcel.2008.02.020

Wolk, C. P., Fan, Q., Zhou, R., Huang, G., Lechno-Yossef, S., Kuritz, T., et al. (2007). Paired cloning vectors for complementation of mutations in the cyanobacterium *Anabaena* sp. strain PCC 7120. *Arch. Microbiol.* 188, 551–563. doi: 10.1007/s00203-007-0276-z

Yang, J., Bai, Y., Zhang, Y., Gabrielle, V. D., Jin, L., and Bai, G. (2014). Deletion of the cyclic di-AMP phosphodiesterase gene (cnpB) in *Mycobacterium tuberculosis* leads to reduced virulence in a mouse model of infection. *Mol. Microbiol.* 93, 65–79. doi: 10.1111/mmi.12641

Ye, M., Zhang, J. J., Fang, X., Lawlis, G. B., Troxell, B., Zhou, Y., et al. (2014). DhhP, a cyclic di-AMP phosphodiesterase of *Borrelia burgdorferi*, is essential for cell growth and virulence. *Infect. Immun.* 82, 1840–1849. doi: 10.1128/iai.00030-14

Yerrapragada, S., Shukla, A., Hallsworth-Pepin, K., Choi, K., Wollam, A., Clifton, S., et al. (2015). Extreme sensory complexity encoded in the 10-Megabase draft genome sequence of the chromatically acclimating cyanobacterium *Tolypothrix* sp. PCC 7601. *Genome Announc.* 3:e00355-15. doi: 10.1128/genomeA.00355-15

Zhang, L., and He, Z. G. (2013). Radiation-sensitive gene A (RadA) targets DisA, DNA integrity scanning protein A, to negatively affect cyclic Di-AMP synthesis activity in *Mycobacterium smegmatis*. *J. Biol. Chem.* 288, 22426–22436. doi: 10.1074/jbc.M113.464883

Zhang, P., Sicora, C. I., Vorontsova, N., Allahverdiyeva, Y., Battchikova, N., Nixon, P. J., et al. (2007). FtsH protease is required for induction of inorganic carbon acquisition complexes in *Synechocystis* sp. PCC 6803. *Mol. Microbiol.* 65, 728–740. doi: 10.1111/j.1365-2958.2007.05822.x

Zheng, C., Ma, Y., Wang, X., Xie, Y., Ali, M. K., and He, J. (2015). Functional analysis of the sporulation-specific diadenylate cyclase CdaS in *Bacillus thuringiensis*. *Front. Microbiol.* 6:908. doi: 10.3389/fmicb.2015.00908

Zhu, Y., Pham, T. H., Nhiep, T. H. N., Vu, N. M. T., Marcellin, E., Chakrabortti, A., et al. (2016). Cyclic-di-AMP synthesis by the diadenylate cyclase CdaA is modulated by the peptidoglycan biosynthesis enzyme GlmM in *Lactococcus lactis*. *Mol. Microbiol.* 99, 1015–1027. doi: 10.1111/mmi.13281

Conflict of Interest Statement: The authors declare that the research was conducted in the absence of any commercial or financial relationships that could be construed as a potential conflict of interest.

The reviewer RS and handling Editor declared their shared affiliation.

frontiers in Microbiology

ORIGINAL RESEARCH
published: 22 June 2018
doi: 10.3389/fmicb.2018.01340

Absence of Curli in Soil-Persistent *Escherichia coli* Is Mediated by a C-di-GMP Signaling Defect and Suggests Evidence of Biofilm-Independent Niche Specialization

Yinka M. Somorin[1†], Tara Vollmerhausen[1], Nicholas Waters[1], Leighton Pritchard[2], Florence Abram[1], Fiona Brennan[3] and Conor O'Byrne[1]*

[1] Discipline of Microbiology, School of Natural Sciences, College of Science, National University of Ireland, Galway, Ireland, [2] The James Hutton Institute, Dundee, United Kingdom, [3] Soil and Environmental Microbiology, Teagasc, Johnstown Castle, Ireland

OPEN ACCESS

Edited by:
Manuel Simões,
Universidade do Porto, Portugal

Reviewed by:
Timothy James Wells,
The University of Queensland, Australia
Jeri D. Barak,
University of Wisconsin–Madison, United States

***Correspondence:**
Conor O'Byrne
conor.obyrne@nuigalway.ie

†Present address:
Yinka M. Somorin,
School of Pharmacy, Queen's University Belfast, Belfast, United Kingdom

Specialty section:
This article was submitted to Microbial Physiology and Metabolism, a section of the journal Frontiers in Microbiology

Received: 27 February 2018
Accepted: 31 May 2018
Published: 22 June 2018

Citation:
Somorin YM, Vollmerhausen T, Waters N, Pritchard L, Abram F, Brennan F and O'Byrne C (2018) Absence of Curli in Soil-Persistent Escherichia coli Is Mediated by a C-di-GMP Signaling Defect and Suggests Evidence of Biofilm-Independent Niche Specialization. Front. Microbiol. 9:1340. doi: 10.3389/fmicb.2018.01340

Escherichia coli is commonly viewed as a gastrointestinal commensal or pathogen although an increasing body of evidence suggests that it can persist in non-host environments as well. Curli are a major component of biofilm in many enteric bacteria including *E. coli* and are important for adherence to different biotic and abiotic surfaces. In this study we investigated curli production in a unique collection of soil-persistent *E. coli* isolates and examined the role of curli formation in environmental persistence. Although most soil-persistent *E. coli* were curli-positive, 10% of isolates were curli-negative (17 out of 170). Curli-producing *E. coli* (COB583, COB585, and BW25113) displayed significantly more attachment to quartz sand than the curli-negative strains. Long-term soil survival experiments indicated that curli production was not required for long-term survival in live soil (over 110 days), as a curli-negative mutant BW25113Δ*csgB* had similar survival compared to wild type BW25113. Mutations in two genes associated with c-di-GMP metabolism, *dgcE* and *pdeR*, correlated with loss of curli in eight soil-persistent strains, although this did not significantly impair their survival in soil compared to curli-positive strains. Overall, the data indicate that curli-deficient and biofilm-defective strains, that also have a defect in attachment to quartz sand, are able to reside in soil for long periods of time thus pointing to the possibility that niches may exist in the soil that can support long-term survival independently of biofilm formation.

Keywords: curli, biofilm, soil, c-di-GMP, RpoS, *Escherichia coli*

INTRODUCTION

Escherichia coli is commonly associated with the gastrointestinal tract of humans, warm-blooded animals, and reptiles (Berg, 1996; Gordon and Cowling, 2003), and its presence in the external environment is often used as an indication of recent fecal contamination. This niche specificity underpins its use as an indicator of fecal contamination in the environment. Nevertheless, *E. coli*

has been isolated from various sources outside of its primary habitat (Ishii et al., 2006; Chiang et al., 2011; Byappanahalli et al., 2012) and it persists and grows in external environments such as subtropical waters and sediments (Anderson et al., 2005). In fact, some *E. coli* linages have been reported to exhibit primarily a non-host lifestyle (Walk et al., 2009). Brennan et al. (2010) reported that *E. coli* are capable of long-term colonization and persistence in an lysimeters that had not been exposed to fecal material during a 10-year period prior to their isolation. These soil-persistent *E. coli* strains are genetically diverse and possess unique growth and metabolic characteristics that suggest adaptation to soil conditions (Brennan et al., 2013). When *E. coli* enters the soil, there is rapid decline in the population, but a part of the population is able to persist due to inherent physiological properties or has an ability to colonize favorable niches in the environment (Ogden et al., 2001).

While it has been shown that the general stress response regulator, RpoS, is important for long-term persistence of *E. coli* in soil (Somorin et al., 2016), the exact mechanisms for their survival in the soil environment remain unclear. Some genetic factors are known to enhance bacterial survival in the different environments. For example, flagellin was identified to help *Pseudomonas aeruginosa* to adhere to soil amoeba and persist in soil (DeFlaun et al., 1990). A functional flagellum was shown to be important for attachment and colonization of infant mouse bowels by *Vibrio cholerae* (Attridge and Rowley, 1983). Exopolysaccharides and type 1 aggregative adherence fimbriae were found to support *in vivo* colonization of germ-free mice and biofilm formation in *E. coli* O104:H4 (Al Safadi et al., 2012). More recently, Yad fimbriae were demonstrated to promote *E. coli* adherence to plants, animal cells and promote persistence in the environment (Larsonneur et al., 2016). Production of biofilm enhances the survival of *Salmonella* in a dry and nutrient-depleted environment (Vestby et al., 2009) and of *E. coli* in soil (Truhlar et al., 2015). Biofilm has also been shown to promote the persistence of *E. coli* on fresh produce (Annous et al., 2009) and in food processing environments (Silagyi et al., 2009; Maal-Bared et al., 2013). Curli form a major component of biofilm in many enteric bacteria including *E. coli* (Barnhart and Chapman, 2006; Yaron and Römling, 2014). Curli are crucial for adherence to plant and animal tissues, plastic and stainless steel by *E. coli* and Salmonella (Patel et al., 2011; Fink et al., 2012; Yaron and Römling, 2014; Carter et al., 2016). Although curli are important for attachment of *E. coli* to biotic and abiotic surfaces, little is known about their contribution to persistence in a soil environment. Brombacher et al. (2003) previously reported that presence of curli enhanced retention of *E. coli* in sand columns, however, curli production in *Salmonella* spp. did not have an impact on their retention in sand (Salvucci et al., 2009).

Since biofilm formation is thought to play an important role in the survival of *E. coli* in the environment (Vogeleer et al., 2014), it was hypothesized that environmentally adapted *E. coli* would retain the capacity to produce biofilms. However, three out of five soil-persistent *E. coli* strains in our previous study were unable to produce biofilms in microtiter plates (Somorin et al., 2016). This raises questions about the ability of these soil-persistent *E. coli* to produce the extracellular matrices (ECM) that make up biofilm. Curli fimbriae are proteinaceous fibers which consist of over 85% by mass of the ECM produced by *E. coli* (McCrate et al., 2013), but it is unknown whether they are important for long-term soil persistence. This study investigated a unique collection of phylogenetically diverse, long-term soil-persistent *E. coli* isolates to investigate the prevalence of curli-negative strains and understand the role of curli and attachment in soil persistence. A significant subset of soil-persistent strains were found not to produce curli and the basis for this phenotype was investigated further. Some of these curli-deficient strains were found to carry mutations in genes involved in c-di-GMP metabolism, which are known to influence curli expression (Sommerfeldt et al., 2009; Lindenberg et al., 2013). This present study shows that curli are important for attachment of *E. coli* to sand but are dispensable for soil survival, and suggests that *E. coli* may occupy niches within the soil environment that does not rely on biofilm formation.

MATERIALS AND METHODS

Bacterial Strains Used and Growth Conditions

Long-term soil-persistent *E. coli* strains, which were isolated from leachates obtained from lysimeter units (Brennan et al., 2010) and belonging to distinct phylogenetic groups were used in this study (Supplementary Table S1). Some of these strains have been previously described (Brennan et al., 2010; Somorin et al., 2016). Two commensal strains (SE11 and SE15) and a well-studied laboratory strain (BW25113) were used for comparative purposes. The mutant strains from the BW25113 background were obtained from the Coli Genetic Stock Centre (Yale, United States) and the kanamycin resistance cassette used in constructing the mutants was removed by FLP-FRT recombination, and removal of the cassette was confirmed by plating on Luria-Bertani (LB) agar with 50 μg ml^{-1} kanamycin (LBKan).

The PdeR^{E620K} point mutation was created in BW25113 using homologous recombination by λ-red-recombinase using pKOBEGA with a single-stranded DNA oligonucleotide (5′-AATCTTCAGGTGATCGCCGAAGGCGTCAAAAGCGCCAAGGAAGATGCTTTTTTAACCAAG-3′) (Costantino and Court, 2003). An additional 13 bp silent mutations were introduced to enable detection of recombinants by PCR. PdeR^{E620K} mutations were selected based on color morphology after being grown on CR-YESCA at 28°C for 48 h. The introduction of the PdeR^{E620K} point mutation was confirmed by sequencing the *pdeR* PCR product (using primers: Forward, 5′-TTATGCGCGCTTCAGATAG-3′; Reverse, 5′-CATAAACCTGCGAGTGGCG-3′).

Congo Red Assay

Curli production was determined in the strains by Congo Red assay as previously described (Zhou et al., 2013). Congo Red agar plates was made by preparing yeast extract and Casamino acid agar (YESCA; 1 g L^{-1} yeast extract, 10 g L^{-1} casamino acids, 20 g L^{-1} agar) and after autoclaving, filter sterilized Congo

Red (50 μg ml^{-1} final concentration; Sigma) and filter sterilized Brilliant Blue G (10 μg ml^{-1} final concentration; Sigma) were added. *E. coli* strains were grown in LB broth and incubated at 37°C overnight. Five microliters of the overnight culture of each strain was spotted on the center of a thick Congo Red agar plate. The plates were incubated at 28°C for 48 h. Images were captured with Canon CanoScan 9000F MKII Flatbed Scanner at 600 dpi.

Western Blot for CsgA, RpoS, and CsgD

Protein extraction and western blot analysis was used to analyze bacteria-associated curli as previously described (Zhou et al., 2013). For CsgA, whole-cell samples from YESCA plates were resuspended in 1 ml of Potassium phosphate (KPi) buffer and normalized to OD_{600nm} of 1.0. Each pellet resulting from 150 μl of normalized cell suspension was resuspended in 70 μl of 100% Hexafluoroisopropanol (HFIP) to dissociate the curli subunits and the HFIP was removed by vacuum concentration (Concentrator plus; Eppendorf) at 45°C for 30 min. The dried cell pellets were resuspended in SDS-PAGE loading buffer and boiled at 95°C for 10 min. An equal amount of protein from each sample was separated using a 15% SDS–PAGE gels at 100 V for 1 h. After electrophoresis, proteins were blotted onto a polyvinylidene difluoride (PVDF) membrane using a semidry system (Jencons, United Kingdom) at 3 V for 1 h. A blocking step with 5% (w/v) skim milk in Tris-buffered saline with 0.05% Tween 20 (TBST) was performed, and the membrane was incubated in 5,000-fold diluted anti-CsgA antibody (gift from Matt Chapman) in the blocking solution. Blots were washed in TBST three times for 10 min each and incubated in 10,000-fold diluted goat anti-rabbit IgG conjugated with horseradish peroxidase (Santa Cruz). After washing three times in TBST, the blot was developed with Amersham ECL Prime Western Blotting Detection (GE Healthcare), prior to exposure to photographic film and CsgA bands observed following development of the film in a Kodak X-ray developer. CsgD and RpoS were detected using a similar approach except that there was no HFIP treatment involved. CsgD was detected using anti-CsgD antibody (gift from Shinya Sugimoto) diluted 2,000-fold in SignalBoost Immunoreaction Enhancer Solution 1 (Merck Millipore) and anti-rabbit IgG HRP (Santa Cruz) diluted 20,000-fold in SignalBoost Immunoreaction Enhancer Solution 2 (Merck Millipore). RpoS was resolved on 10% gel and detected by 5,000-fold diluted mouse monoclonal anti-RpoS antibody (Santa Cruz) and 3,000-fold diluted anti-mouse IgG HRP (Santa Cruz).

Bioinformatics

All nucleotide sequences for *E. coli* K-12 MG1655 were obtained from the EcoCyc *E. coli* database[1]. Nucleotide sequences of *E. coli* SE11, SE15, BW25113, and W3110 were retrieved from the National Centre for Biotechnology Information (NCBI) database with GenBank Accession numbers AP009240.1, AP009378.1, CP009273.1, and AP009048.1, respectively. Unassembled genomic sequences of the soil-persistent *E. coli* were provided by F. P. Brennan (unpublished data). Nucleotide sequences of the genes of interest were extracted from the contigs of the soil-persistent strains using Geneious R8 (Biomatters), the nucleotide sequences were translated to amino acid sequences and multiple sequence alignment was performed using Clustal Omega (Sievers et al., 2011). For the graphical representation of the sequence alignments, ClustalW in BioEdit v7.2.5 (Ibis Bioscience, United States) was used. The phylogenetic analysis was performed using kSNP3.0 (Gardner et al., 2015) to construct an alignment-free SNP-based phylogeny from the eight curli negative strains (Sequence data available at BioProject Accession # PRJNA420620) and representatives from all of the Clermont 2013 phylogroups (Clermont et al., 2013), using a *k* value of 31. The accession numbers for these strains can be found in Supplementary Table S2. The resulting parsimony tree was visualized with FigTree v1.4.3 and annotated using Inkscape.

[1]https://ecocyc.org/

Overexpression of PdeR, DgcE, and Curli Expression

The curli-positive and curli-negative soil strains were transformed with pCAB18 plasmid (IPTG-inducible low copy number vector carrying the *P*tac promoter, Amp^R) carrying wild type *pdeR* (pCAB18-*pdeR*; gift from Regine Hengge). The transformed strains were grown on Congo Red-containing Yeast Extract and Casamino acid agar (CR-YESCA) with IPTG (10 μM) and ampicillin (100 μg ml^{-1}) at 28°C for 48 h to induce overexpression of PdeR. CsgD protein expression was determined in the strains overexpressing PdeR grown on YESCA, as described above. Wild type DgcE from *E. coli* BW25113 was cloned into TOPO-XL-PCR (Invitrogen). Transformed curli-negative soil strains with pCR-XL-TOPO-*dgcE* were grown on CR-YESCA at 28°C for 48 h.

Soil Survival Assay

Survival of *E. coli* BW25113 and its corresponding Δ*rpoS*, Δ*csgA*, Δ*csgB*, and Δ*csgD* mutants in silty loam soil was determined as described by Somorin et al. (2016). Silty loam soil, which had no detectable background levels of *E. coli*, was sieved with a 2-mm sieve and 1 g weighed into a series of 15 ml tubes. Equal cell numbers were first washed in PBS and then inoculated into separate soil samples (to give 1×10^7 CFU g^{-1} of soil), inverted 10 times by hand, slightly capped to allow air exchange, and incubated at 15°C. As a control, 50 μl of sterile PBS was added to 1 g of silty loam soil. The experiment was set up in triplicate. Inoculated soils were destructively sampled at different time intervals to determine the survival of the wild type and mutant strains. For cell recovery, 2 ml of PBS was added to each tube containing soil sample, capped and mixed by inverting the tube three times and vortexed for 2 × 20 s. The resulting soil slurry was allowed to settle for 2 min and 20 μl of the supernatant liquid was collected and serially diluted. Ten microliters of all dilutions were plated in triplicate on MacConkey agar (Sigma) and incubated at 37°C overnight. Colonies were counted to enumerate the viable cells at each time-point.

Sand Attachment Assay

Sand attachment assay was conducted according to the method described by Hinsa et al. (2003). *E. coli* cells were grown for 24 h

on LB agar at 28°C. Colonies were scraped off with a loop and resuspended in 5 ml PBS. OD_{600nm} was measured and normalized in LB without salt (LBns) to give a starting population of 10^6 CFU ml^{-1}. Quartz sand was pre-weighed into 1.5 ml tubes and sterilized by autoclaving. Then, 0.5 g of sterilized quartz sand (Sigma) was added to wells of a 96-well plate and 1 ml of the inoculated LBns was added to each well. Plates were incubated static in the dark at 28°C for 48 h. After incubation, the LBns in each well was removed, serially diluted, and plated out to determine planktonic cell count. For biofilm cell count, sand in the 96-well plate was pipetted into pre-weighed 1.5 ml tubes and 500 µl of PBS was used to wash the sand five times to remove unattached cells. All liquid was removed and tubes were re-weighed. Then 500 µl of PBS was added and the tubes were vortexed for 30 s, sonicated (4 min, 100% power) and vortexed again for 30 s. The liquid fraction was then serially diluted and plated onto LB agar to determine the biofilm count. The bacterial cell counts were normalized to the weight of the sand.

Statistical Analysis

The Student's *t*-test was used when comparing means from two samples whereas one-way Analysis of variance (ANOVA) was used when comparing means from three or more samples. Statistical comparisons among the means in ANOVA were compared using Duncan Multiple Range Test at 5% probability level. Error bars on graphs indicate standard deviations from the means. Differences in soil survival and sand attachment were investigated using GraphPad Prism 6.

RESULTS

Curli Production Varies Among Soil-Persistent *E. coli*

Curli production was determined in five soil persistent strains using a Congo Red (CR) assay as previously described (Zhou et al., 2013). CR binding among soil-persistent *E. coli* revealed the formation of red colonies on CR-YESCA for COB583 and COB585 whereas COB584, COB586, and COB587 formed white or pale pink colonies (**Figure 1**). Human commensal *E. coli* isolates, SE11 and SE15, were used for comparison purposes and both stained red on CR-YESCA agar indicating curli production. *E. coli* BW25113, which was used as the positive control, was red while the negative control, *E. coli* BW25113Δ*csgA*, was white, confirming that the red staining was dependent on curli production. These data suggested that three of the soil strains (COB584, COB586, and COB587) were not expressing curli under these growth conditions, a finding that is consistent with the inability of these strains to produce biofilm (Somorin et al., 2016). The morphology of the macrocolonies in the curli-positive strains varied from red, dry and rough (rdar) morphotype (as in COB583, SE11, SE15) which suggests the cells produced curli and cellulose (Bokranz et al., 2005) to brown-red, dry with large rings (as in COB585 and BW25113) (**Figure 1**), which suggests the macrocolonies produced curli only (Bokranz et al., 2005). Preliminary screening of COB584, COB586, and COB587 for cellulose production on agar plates containing Calcoflour white, showed that COB584 and COB587 produced cellulose but not COB586 (data not shown). When the total collection of 170 soil-persistent *E. coli* isolates was analyzed, 153 (90%) were curli-positive and 17 (10%) were curli-negative (Supplementary Table S3).

Curli Transcriptional Regulator CsgD and Curli Major Subunit CsgA Are Not Expressed in Curli-Negative Soil-Persistent *E. coli*

To understand the reason for the loss of curli production in the three soil-persistent *E. coli* strains (COB584, COB586, and COB587) unable to produce biofilm (Somorin et al., 2016), the expression of the major curli subunit CsgA, which is essential for curli production, was investigated. Western blotting analysis showed that these three curli-negative strains did not express CsgA, whereas the curli-positive strains COB583 and COB585 did (**Figure 2A**). Since the expression of curli is regulated by RpoS, the ability of the curli-negative strains to express RpoS under the curli-inducing condition (YESCA agar at 28°C for 48 h) was investigated. All the curli-positive and curli-negative strains expressed RpoS under this condition (**Figure 2B**). Since RpoS regulation of curli expression occurs through the curli transcriptional regulator CsgD, which activates the transcription of *csgBAC* operon, the ability of the strains to express CsgD on YESCA agar was determined. CsgD was also not expressed in the curli-negative *E. coli* COB584, COB586, and COB587 but was expressed in all the curli-positive strains (**Figure 2C**). This suggests that the loss of curli in these strains was caused by the absence of CsgD and suggests some defect in regulation upstream of CsgD in the curli production regulatory pathway.

Sequence Analyses Reveal That Mutations in the GGDEF Domain of DgcE and in the EAL Domain of PdeR Are Associated With the Curli-Negative Phenotype

Computational analysis of whole-genome sequence data for genes with known roles in curli production (RpoS, phosphodiesterase PdeR, diguanylate cyclase DgcM, DNA binding transcriptional activator MlrA, transcriptional dual regulator CsgD, minor curli subunit CsgB, major curli subunit CsgA, DNA-Binding protein Dps, chaperone protein DnaK, transcriptional regulator OmpR, catabolite repressor/activator protein Cra, small regulatory RNA RydC, small regulatory RNA RprA, and the *csgD* promoter region preceding *csgB*) was used to identify alleles that might impact curli production in the three curli-negative soil-persistent *E. coli* strains. RpoS was 100% conserved in the curli-positive (COB583 and COB585) as well as curli-negative *E. coli* (COB584, COB586 and COB587) while both the *csgB* and the *csgD* promoter sequences were 100% identical in them (data not shown). There were amino acid substitutions in MlrA in *E. coli* COB585 but none in the three curli-negative or the other curli-positive strains (COB583, SE11, SE15 and BW25113) compared to the reference

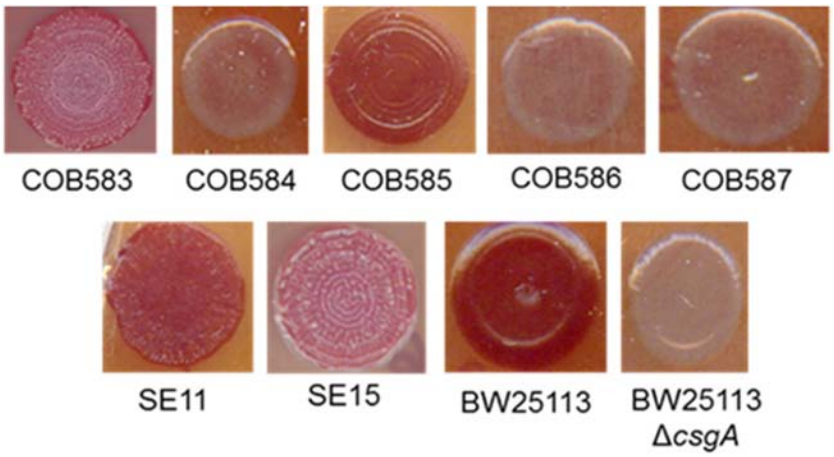

FIGURE 1 | Curli production among soil-persistent *Escherichia coli*. Macrocolonies of soil-persistent, commensal and control strains were grown on Congo Red-containing Yeast Extract and Casamino acid (CR-YESCA) agar at 28°C for 48 h. *E. coli* BW25113 was used as the positive control and *E. coli* BW25113 Δ*csgA* was the negative control.

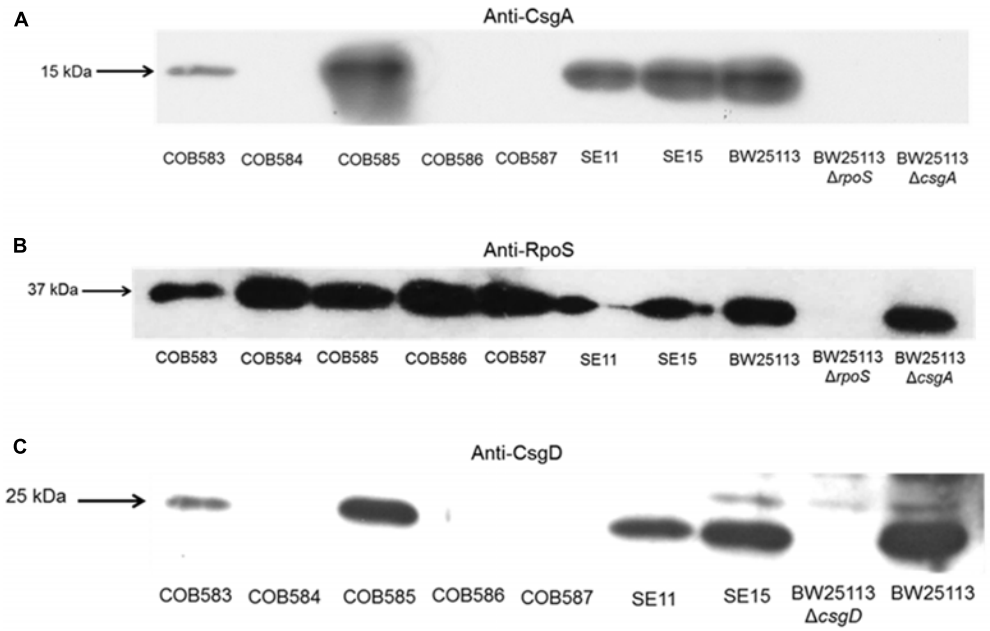

FIGURE 2 | CsgA and CsgD are not expressed in curli-negative soil-persistent *Escherichia coli* strains. Cells of soil-persistent, commensal and control strains were grown on Yeast Extract and Casamino acid (YESCA) agar at 28°C for 48 h. Protein extraction and western blotting was done for determining the expression of CsgA **(A)**, RpoS **(B)**, and CsgD **(C)**.

sequence (*E. coli* K-12 W3110) (data not shown). Although soil-persistent *E. coli* COB585 and commensal strain SE15 had some amino acid substitutions in many of these regulators of curli production when compared to the reference strain, they both retained the ability to produce curli. The same amino acid substitution, Threonine (T) to Alanine (A) at codon 98 (T98A), was found in DgcM in the three curli-negative strains, relative to the reference sequence. However, other soil-persistent *E. coli* with the same allele (T98A) in *dgcM* were curli-positive (data not shown). Strikingly, analysis of the phosphodiesterase PdeR (formerly named YciR) coding sequence, regarded as the "trigger switch" for *E. coli* biofilm (Lindenberg et al., 2013), revealed a point mutation at nucleotide 1858 (1858G > A) (**Figure 3A**), which resulted in an amino acid change from Glutamate (E) to Lysine (K) at codon 620 (E620K) in the three curli-negative strains (**Figure 3B**). The mutation (E620K) occurred in the EAL domain of the phosphodiesterase PdeR, which is important for the catalytic activity of PdeR. Multiple sequence alignment of the gene encoding the cyclic-di-GMP diguanylate cyclase (*dgcE*) revealed a single base deletion

(1456delC) in the three curli-negative strains (**Figure 3C**) that led to a frameshift mutation in the amino acid sequence of DgcE (H486fs), resulting in a stop codon at codon 490 (**Figure 3D**). These mutations in *pdeR* and *dgcE* were found uniquely in the three curli-negative soil-persistent *E. coli* strains thus suggesting a causative role in the curli-deficient phenotype.

Analysis of the sequences of the remaining 165 soil-persistent *E. coli* in the collection, which were obtained from different soil lysimeters, showed that the same *dgcE* and *pdeR* mutations were found in five additional soil-persistent *E. coli* strains. Interestingly, these five additional strains (Lys 34, 35, 45, 52, and 53) neither expressed CsgD nor produced curli (**Figure 4**), thus confirming that these mutations in *dgcE* and *pdeR* are associated with the loss of curli production at least on this growth medium. These eight curli-negative soil-persistent *E. coli* strains belonged to phylogenetic group B1 and clustered closely, although not all soil-persistent *E. coli* strains belonging to phylogenetic group B1 were curli-negative (**Figure 5**). Scanning Electron Microscopy (SEM) of the cells grown under the same conditions as previous experiments showed rough and wrinkled surfaces on the colonies of COB583, COB585, and BW25113, which correlates with curli production in those strains (data not shown). This wrinkled surface was absent in the curli-negative soil-persistent strains and the BW25113Δ*csgA* used as negative control.

Complementation of *dgcE* Restores Curli Production in Curli-Negative Soil Isolates

To determine the relative importance of the two mutations identified on curli expression we endeavored to separate the alleles into separate strains. Attempts to cross wild type alleles of *dgcE* and *pdeR* into the soil strains proved technically difficult because of the low transformation efficiencies. Instead, we complemented the curli-deficient soil strains with plasmids carrying wild type copies of these two genes. The *dgcE* gene *in trans* fully restored the curli-expressing rdar morphotype on CR-YESCA medium (**Figure 6A**). In contrast, a wild type copy of *pdeR* had no significant effect on the curli expression in the curli-deficient strains (COB58, 586, and 587) (**Figure 6B**). This result was not unexpected as this phosphodiesterase has a negative influence on the expression of curli through its inhibition of MlrA (Lindenberg et al., 2013). Indeed, the negative effect of the *pdeR* gene on curli expression was clearly seen in COB583 and COB585, where it repressed curli expression (**Figure 6C** and Supplementary Figure S1).

In an attempt to understand the contribution of the $PdeR^{E620K}$ mutation to the curli-negative phenotype of the soil strains, this allele was introduced to the K-12 strain BW25113 by allelic exchange, selecting for any recombinants that displayed reduced Congo Red staining. One BW25113 transformant was identified that had a slight reduction in CR staining and was subsequently confirmed by sequence analysis to carry the $PdeR^{E620K}$ allele (**Figure 6D**). Hence, this allele appears to confer an intermediate curli expression phenotype, at least in this genetic background. Taken together these results suggest the frameshift mutation in *dgcE* ($DgcE^{H486fs}$) had the dominant effect on the loss of curli in the soil-persistent strains, with a lesser contribution from the $PdeR^{E620K}$ allele.

Curli Enhances the Attachment of *E. coli* to Quartz Sand but Are Not Required for Long-Term Persistence in Soil

Although our previous study showed that there was no difference in survival between curli-positive or negative strains (Somorin et al., 2016), the contribution of curli to soil survival was analyzed in *E. coli* BW25113 using mutants with deletion in genes required for curli production. It was observed that deletion of curli subunit genes did not significantly impair soil survival in the initial 50 days in soil as seen in BW25113Δ*rpoS* (**Figure 7**). There was a small but significant defect in the survival of BW25113Δ*csgA* ($p = 0.0084$, Student's *t*-test) and BW25113Δ*csgD* ($p = 0.0012$, Student's *t*-test) after 113 days in soil but BW25113Δ*csgB* was not significantly different ($p > 0.05$; Student's *t*-test) from the wild type BW25113. Since CsgB is essential for curli formation in *E. coli* (Barnhart and Chapman, 2006), this result suggested that curli are not required for long-term soil survival in this genetic background. Although the differences observed between the wildtype BW25113 and its corresponding Δ*csgA* and Δ*csgD* mutants were statistically significant at two time points (92 days and 113 days), these differences were very small and not likely to be biologically meaningful.

Since curli enhances biofilm production in soil-persistent *E. coli* in microtiter plates, we investigated whether curli were important for attachment to an environmentally relevant surface using quartz sand. All curli-negative *E. coli* strains had significantly ($p < 0.05$, one-way ANOVA) higher planktonic cell counts than curli-positive *E. coli* indicating that fewer cells attached to the sand (**Figure 8A**). Conversely, in the same experimental setup, curli-positive strains were significantly ($p < 0.05$, one-way ANOVA) more attached to quartz sand than BW25113 Δ*csgA* and other curli-negative strains (**Figure 8B**). Attachment for the curli-positive strains was between 10- and 100-fold greater than for the curli-negative strains. There was no significant difference between the attachment of the curli negative strains ($p > 0.05$; one-way ANOVA). Complementation of curli-negative soil-persistent *E coli* with wild type DgcE, which restored curli production ability, significantly reduced planktonic cell counts and increased adhesion to quartz sand (**Figures 8C,D**). Together these data indicate that curli promote attaching to quartz sand and show that all the curli-defective soil-persistent *E. coli* strains identified in this study display reduced attachment.

DISCUSSION

Many studies have described curli fimbriae as being important for *E. coli* to attach to biotic and abiotic surfaces such as glass, stainless steel, and polystyrene (Cookson et al., 2002; Uhlich et al., 2009; Carter et al., 2016), but little is known about the role of curli production for soil persistence. Previously, we showed that soil-persistent *E. coli* strains varied in their ability to produce biofilm in a 96-well micro-titer plate assay (Somorin et al., 2016). In this study, we established that impaired biofilm formation

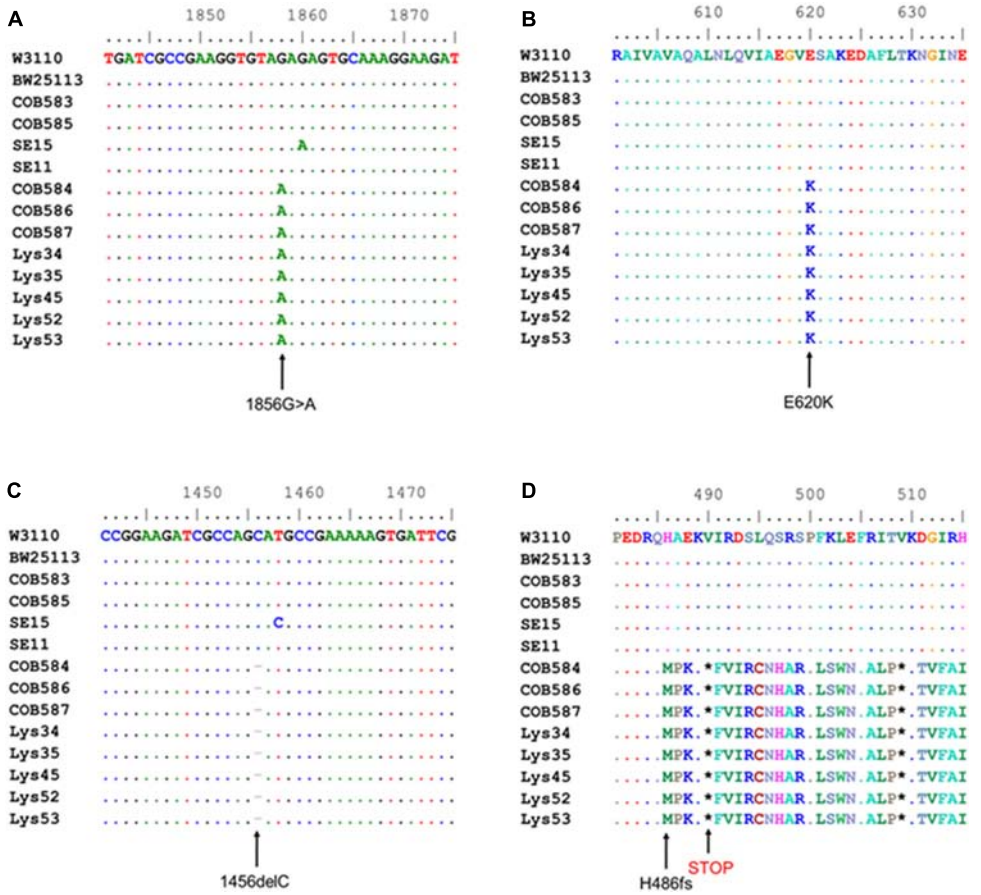

FIGURE 3 | Multiple sequence alignment shows mutations in cyclic-di-GMP metabolism genes in curli-negative soil-persistent *Escherichia coli*. Multiple sequence alignment of nucleotide sequences in cyclic di-GMP phosphodiesterase-encoding gene (*pdeR*) among 170 soil-persistent strains in our collection shows a point mutation (1858G > A) **(A)** which led to an amino acid change in the PdeR protein sequence (E620K) in COB584, COB586 and COB587 and five additional soil-persistent strains **(B)**. Alignment of the nucleotide sequence in diguanylate cyclase (*dgcE*) reveals a deletion (1456delC) **(C)** which results in a frameshift mutation at amino acid residue 486 in the protein sequence (H486fs) and a STOP codon at position 490 **(D)**. Multiple sequence alignment was performed using ClustalW in BioEdit v7.2.5).

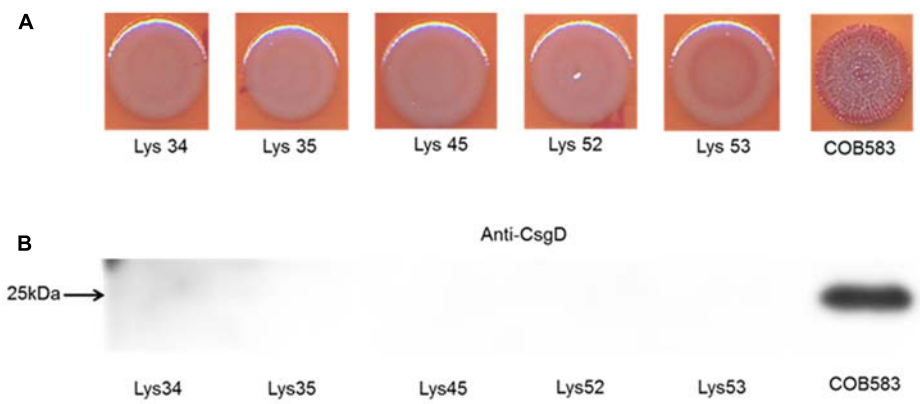

FIGURE 4 | Five additional soil-persistent *Escherichia coli* with mutations in *dgcE* and *pdeR* were curli-negative. **(A)** Macrocolonies of additional soil-persistent *E. coli* with the same mutations in the nucleotide sequences of diguanylate cyclase (*dgcE*) and phosphodiesterase (*pdeR*) (*E. coli* Lys34, Lys35, Lys45, Lys52, Lys53) with positive control strain (COB583) were grown on Congo Red-containing Yeast Extract and Casamino acid (CR-YESCA) agar at 28°C for 48 h. **(B)** Western blotting was done for determining the expression of CsgD under the same conditions described above.

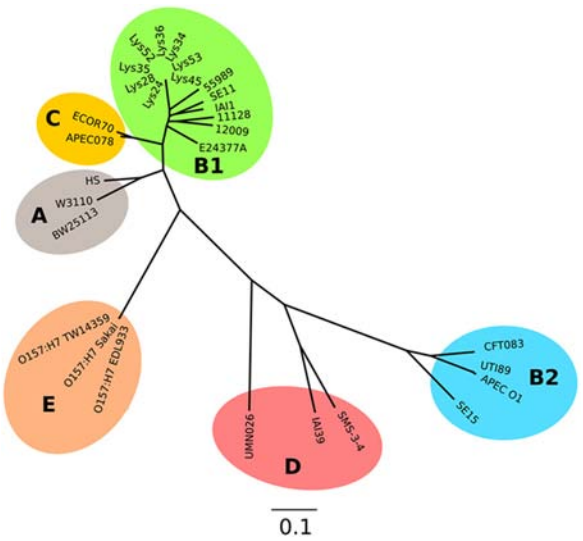

FIGURE 5 | Parsimony tree of whole-genome SNPs shows relatedness of the curli-negative strains with other known *E. coli* strains. Phylogeny generated with kSNP3 using sequence data indicated in Supplementary Table S2. Non-curli producing strains form a distinct cluster within the B1 phylogroup.

was associated with a lack of curli production, and subsequently investigated the role of curli and attachment in soil survival.

Production of curli correlated with a higher level of biofilm production (Somorin et al., 2016) and attachment to a component of many soils (quartz sand) (**Figure 8**). Curli production has been shown to contribute to survival in manure-amended soil (Truhlar et al., 2015). Our data show that loss of biofilm/attachment does not affect long-term soil persistence, suggesting that some *E. coli* may occupy non-biofilm niches in the soil. The heterogeneity in curli production may reflect the genetic diversity of *E. coli* lineages present in the soil, perhaps suggesting that they have evolved to occupy different localized niches in the soil, with some of the niches not requiring the ability to retain curli. Evidence supporting this hypothesis comes from a study by Truhlar et al. (2015), which showed that the population of *E. coli* curli producers was maintained at a higher level when manure was spread on the surface of the soil than when it was injected into the soil. The selection for retention of curli on the soil surface was proposed to be based on a need for protective biofilm to help overcome UV radiation and desiccation, which would not be encountered below the soil surface (Truhlar et al., 2015).

Curli production by *E. coli* and *Salmonella* promotes macrocolony formation, community behavior and colonization of host plant and animal tissues (Gophna et al., 2001; Pande et al., 2016). Curli enhanced the attachment of *E. coli* O157:H7 to plants and stainless steel whereas mutants not producing curli showed reduced colonization of these surfaces (Carter et al., 2016). Protection against toxic metals that may be present in soil, such as mercury, is an additional benefit curli confers on *E. coli* in the environment (Hidalgo et al., 2010). Although it was hypothesized that biofilm production would increase survival of *E. coli* in the soil environment, we tested five soil-persistent *E. coli* with unknown curli status (as at then) and found that biofilm production did not confer increased soil survival (Somorin et al., 2016). This suggests that biofilm production does not provide any advantage for survival in soil under the conditions we tested. In this study, two curli-deficient mutants (BW25113Δ*csgD* and BW25113Δ*csgA*) showed a small decrease in survival compared to the wild type BW25113 at the last time two points of the assay, whereas the curli-deficient mutant (BW25113Δ*csgB*) showed no significant difference in survival compared to the wild type, suggesting soil survival is independent of the ability to produce curli (**Figure 7**). *E. coli* generally has an intrinsic ability to survive for long periods outside the host despite being thought to be primarily a gastrointestinal commensal (Ishii et al., 2006; Chiang et al., 2011; Byappanahalli et al., 2012). The finding that soil survival is independent of curli production agrees with our earlier observation that curli-positive soil-persistent *E. coli* showed no significant increase in survival compared to curli-negative soil-persistent strains (Somorin et al., 2016). The perception that persistence in the soil might depend on attachment to soil particles is challenged by our findings, thereby giving an important new insight into the lifestyle of *E. coli* outside the host.

It is possible to speculate that the soil may be exerting some selective pressures on the regulatory networks of curli production, leading to the loss of curli biosynthesis. Indeed Ravva et al. (2014) showed that exposure of *E. coli* O157:H7 to soil increased the curli-deficient subpopulation recovered from the soil. This could be because curli production is not strictly needed for long-term survival in the soil as curli-negative strains are still able to survive long-term in the soil (Somorin et al., 2016). The poor attachment of the curli-negative strains to sand (**Figure 8B**) suggests that loss of curli may also reduce biofilm formation on soil particles and could act as a strategy for environmental dissemination, allowing *E. coli* to colonize new environments and potentially new hosts. Previous studies have described that *E. coli* biofilm usually contains two subpopulations, matrix-encased and non-matrix-encased *E. coli* cells; where the non-matrix-encased cells produce no curli and are more susceptible to stress (DePas et al., 2013). The non-matrix-encased cells, which are flagellated, are considered the main agents of biofilm dispersal, giving rise to the idea that the loss of curli production observed in some of the soil-persistent *E. coli* strains may have evolved to maintain an easily dispersible population.

Although the majority of the soil-persistent *E. coli* produced curli, 10% of the strains were curli-deficient under the conditions tested. The loss of curli in the initial three curli-negative strains tested (COB584, COB586 and COB587) was not attributable to the loss of RpoS, since Western blotting showed that RpoS is expressed and functional in all of them (**Figure 2**; Somorin et al., 2016). It has previously been reported that prophage insertions into transcriptional factor *mlrA* abolished curli and biofilm production in some *E. coli* O157:H7 isolates (Uhlich et al., 2013) and non-O157 STEC (Chen et al., 2013). Truncation of *csgB* by an insertional element IS1 has also been shown to eliminate curli production in *E. coli* O78:K80 (La Ragione

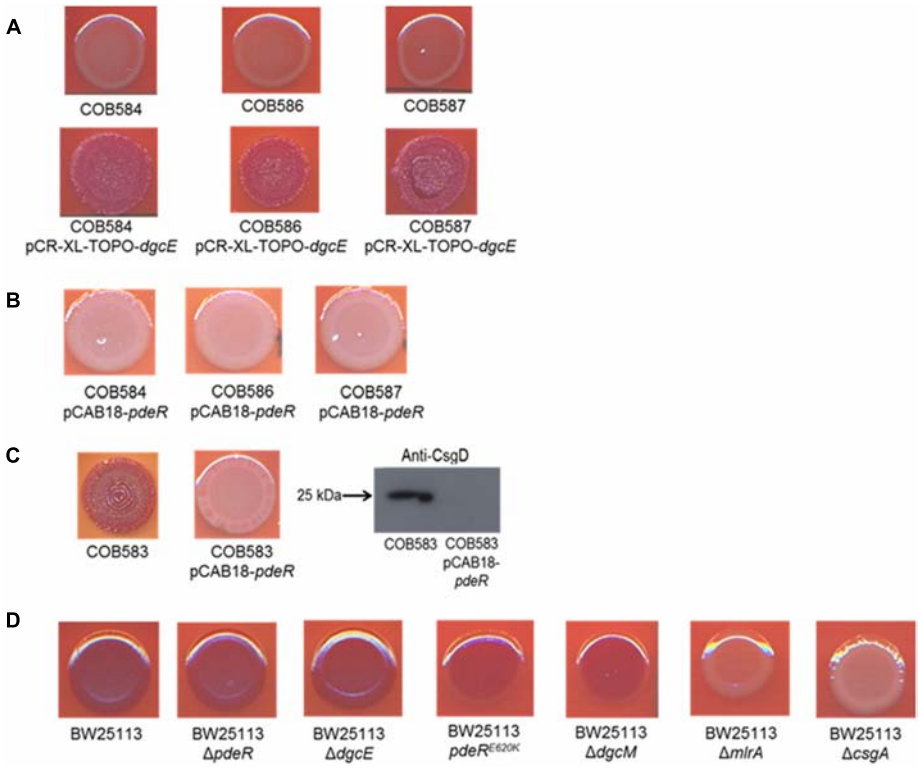

FIGURE 6 | Complementation of curli-negative soil-persistent *Escherichia coli* with **(A)** wildtype DgcE restored curli production, and **(B)** PdeR had no effect on curli production. Curli-negative *E. coli* were transformed with pCR-XL-TOPO plasmid carrying wildtype *dgcE*, and pCAB18 plasmid carrying wildtype *pdeR*, grown on Congo Red-containing Yeast Extract and Casamino acid agar (CR-YESCA) at 28°C for 48 h. **(C)** Curli production in curli-positive soil-persistent *E. coli* with wildtype *pdeR* reduced curli production and CsgD protein. **(D)** Curli production among BW25113 deletion mutants grown on CR-YESCA at 28°C for 48 h.

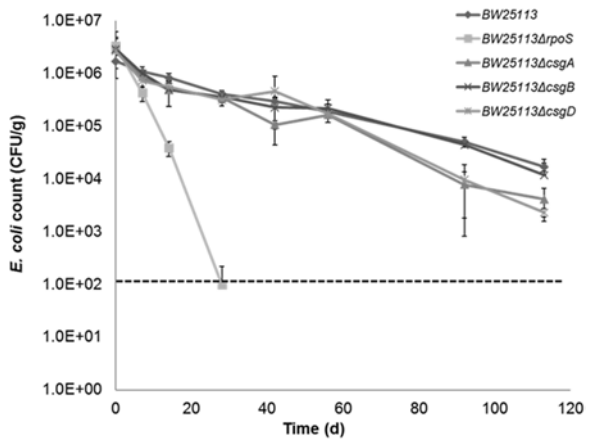

FIGURE 7 | Curli are not required for *Escherichia coli* to survive in soil. Soil survival was performed by inoculating wildtype and mutants into live soil and incubated at 15°C. Dashed line represents detection limit of soil survival assay.

et al., 1999). These previously mentioned mutations were not observed in this present study. Bioinformatic analyses of some of the main genes required for curli production (such as *csgD*, *csgB*, *csgA* and *csgD* promoters) revealed wild type alleles in the strains lacking curli production. The presence of wild type curli subunit genes in *E. coli* strains do not always result in curli production and this has been reported by several authors in *E. coli* (Dyer et al., 2007; Truhlar et al., 2015), *Salmonella* spp. (De Oliveira et al., 2014) and *Enterobacter sakazakii* (Zogaj et al., 2003).

PdeR and DgcE have been identified as key regulators of curli biosynthesis (Pesavento et al., 2008; Lindenberg et al., 2013) and these two mutations (PdeR^{E620K} and DgcE^{H486fs}) correlated with the inability to produce curli (and the rdar colony morphology) in COB584, COB586 and COB587 (**Figures 1**, **3**). The same mutations were found in five additional soil-persistent strains (Lys34, Lys35, Lys45, Lys52, Lys53) (**Figure 3**). All eight of these curli-negative strains belong to phylogenetic group (B1) and were isolated from two distinct lysimeters containing Rathangan soil (COB584, COB586, COB587, Lys34, Lys35, Lys45 were from Lysimeter 12; Lys52 and Lys53 were from Lysimeter 19). These two mutations are very unlikely to arise independently in separate strains in different lysimeters. The ancestor of these strains may have been introduced to the soil (or arose in the soil) over a decade or more ago. These eight strains were unable to express CsgD and hence unable to produce curli (**Figures 1**, **4**). The conserved signature GGDEF motif, which is required for diguanylate cyclase (DGC) activity and therefore cyclic-di-GMP (c-di-GMP)

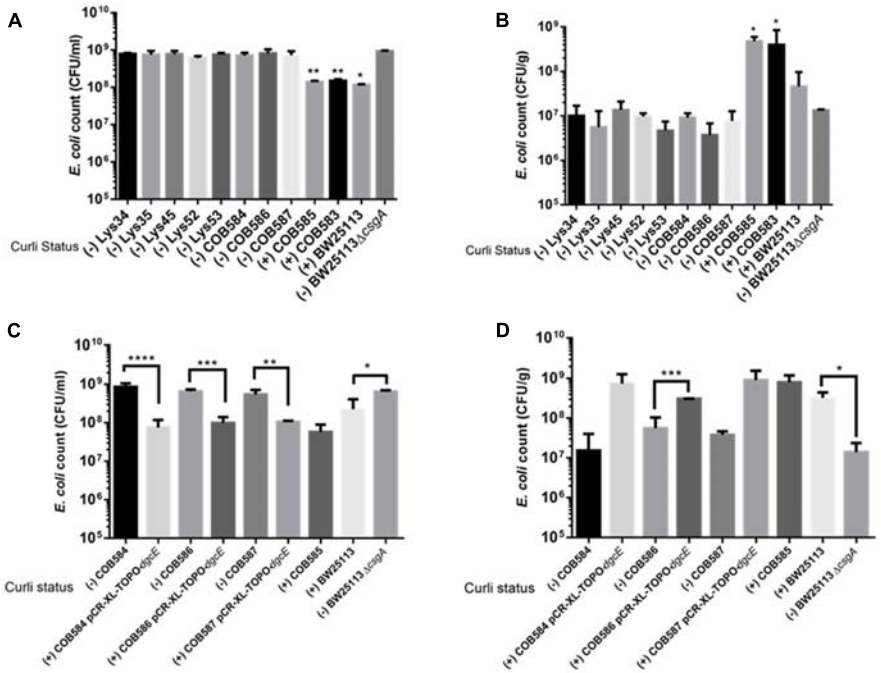

FIGURE 8 | Curli-positive *Escherichia coli* attach better to quartz sand than curli-negative *E. coli.* Attachment of *E. coli* strains to quartz sand was determined after 28°C at 48 h. Planktonic cell counts **(A,C)** and biofilm cell counts **(B,D)** were determined under same condition for the wildtype and for *dgcE*-complemented curli-negative strains. Multiple comparison of the means using one-way ANOVA shows significant differences (represented by asterisks) between the curli-positive and curli-negative strains. $*p < 0.05$; $**p < 0.01$; $***p < 0.001$; $****p < 0.0001$.

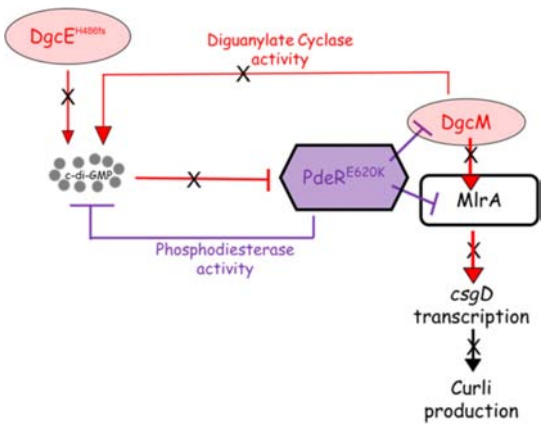

FIGURE 9 | Proposed model for curli inhibition in some of the soil-persistent *Escherichia coli*. The mutated diguanylate cyclase DgcE (H486fs) in the curli-negative strains is predicted to be unable to produce sufficient cyclic di-GMP (c-di-GMP) to relieve the inhibition of MlrA-DgcM by mutated phosphodiesterase PdeR (E620K). In this state, the mutated PdeR is not able to sense c-di-GMP and thus retains the inhibition of DgcM and MlrA. This renders DgcM unable to act as transcriptional regulator to interact with MlrA and as a DGC to add to the local c-di-GMP pool, thereby inhibiting *csgD* transcription and curli production.

synthesis, is disrupted by the frameshift mutation in DgcE in the eight PdeR^{E620K} strains, which is likely to limit their capacity to synthesize c-di-GMP via DgcE, and in turn making PdeR unable to trigger curli and biofilm production in them (Lindenberg et al., 2013). The fact that the *dgcE* frameshift mutation could be fully complemented *in trans* in the soil strains, restoring curli production (**Figure 6**), suggests that this mutation produces the dominant effect. Unsurprisingly the presence of a plasmid expressing wild type PdeR did not restore curli production in the curli-deficient soil strains as this phosphodiesterase acts negatively in modulating the activity of the MlrA transcriptional regulator (Lindenberg et al., 2013). Indeed, this plasmid repressed curli production in COB583 and COB585, curli-expressing soil persistent strains. Considering these data, it seems possible that the *pdeR* mutation (E620K) arose first in the ancestor of these curli-deficient soil strains, producing a reduced curli phenotype and that subsequently curli production was lost entirely when the *dgcE* frameshift mutation was acquired.

The proposed model explaining the basis for the loss of curli in the eight strains bearing the DgcE^{H486fs} and PdeR^{E620K} mutations is summarized in **Figure 9**. This model, which is based on the current model describing regulation of curli production in *E. coli* (Lindenberg et al., 2013), seeks to explain the loss of CsgD expression (**Figures 2**, **4**), which in turn prevents the transcription of *csgBAC* and thereby blocks curli production. In wild type cells, c-di-GMP binds PdeR causing it to dissociate from the PdeR-MlrA-DgcM complex, which in turn allows DgcM to form productive interactions with MlrA, stimulating its activity as a transcriptional regulator and as a DGC to produce more local c-di-GMP to further prevent the inhibitory activity of PdeR.

The *dgcE* mutation is predicted to result in a drop in the local c-di-GMP pool, which is insufficient to dissociate PdeR from the PdeR-MlrA-DgcM complex. The *pdeR* mutation probably affects the affinity of PdeR for c-di-GMP (because the E620K change results in a charge change in a region that is very close to the active site) and this exacerbates the effect of the reduced pool of c-di-GMP. This is suggested by the reduction in CR binding that was observed when the E620K mutation was introduced into *pdeR* in BW25113. This model will need to be tested further to fully understand the mechanism behind the curli inhibition in these strains. It will be important to measure c-di-GMP levels in these curli-negative strains to determine if reduced c-di-GMP level correlates with the curli-negative phenotype. Secondly, it will be important to establish the effect of the E620K change in PdeR on the binding and hydrolysis of c-di-GMP. The interaction of the mutated PdeR with DgcM and MlrA from these strains should also be investigated, which would likely provide further insights into the regulation of the trigger mechanism.

Analysis of the EAL domains from different bacterial species showed that active EALs have glutamate (E) at codon 620 (E620) (Supplementary Figure S2). This suggests that E620 may play some role in the catalytic activity of PDEs, in addition to the previously identified conserved glutamate residue (equivalent to glutamate (E) at codon 617 in PdeR) in other functional phosphodiesterases (Rao et al., 2008). $PdeR^{E620K}$ may be unable to play its role in c-di-GMP metabolism since the E620 of PdeR is possibly involved in its catalytic activity. Tchigvintsev et al. (2010) showed that the second guanine base of c-di-GMP interacts electrostatically with conserved glutamate at codon 706 (E706) in TBD1265 of *Thiobacillus denitrificans* (equivalent to E620 in PdeR of *E. coli*). Rao et al. (2008) observed that although mutation of E355 in RocR of *P. aeruginosa* (equivalent to E620 in *E. coli* PdeR) plays a minor role in catalysis of c-di-GMP, the distal location of the residue makes it likely to play an important role in maintaining the conformational structure required for c-di-GMP binding. Amino acid residues distal to active site residues have been shown to play crucial roles in enhancing the catalytic activity of enzymes through structure stabilization (Rajagopalan et al., 2002; He et al., 2015). Based on this, $PdeR^{E620K}$ may cause structural changes making it difficult for the conserved residue E617 to be catalytically active. This assumption becomes important since the eight curli-negative strains in this study retained all the conserved residues previously reported to be important for PDE activity of PdeR (Römling et al., 2013). E620 is conserved in all *E. coli* PdeR searched in the National Center for Biotechnology Information (NCBI) database and no strain had K620 in its PdeR (data not shown). This tight conservation of E620 in EAL domains of different bacteria suggests a possible role for them in regulating curli production.

CONCLUSION

This study identified a significant number of soil dwelling *E. coli* strains that do not produce either curli or biofilm and have a defect in attachment to quartz sand, yet are able to reside in this habitat for long periods of time. This shows that inability to produce biofilm does not compromise the ability of *E. coli* to inhabit a soil environment. For eight of the curli-defective strains identified in this study, the loss of curli was attributed to a defect in c-di-GMP signaling that leads to a failure to express the curli regulator CsgD. The data also highlight residue 620 of the phosphodiesterase PdeR as being critical for its normal activity. Finally, the results suggest that dissemination of *E. coli* in the environment could be facilitated by the loss of curli production.

AUTHOR CONTRIBUTIONS

YS and CO conceived the study. YS performed Congo Red Assay, western blotting, genomic comparison, SEM, soil survival, and statistical analysis. TV performed sand attachment assay and constructed mutants. NW and LP performed phylogenetic analysis. FA and FB provided the soil-persistent *E. coli* isolates used in the study. YS, TV, and CO wrote the manuscript, with contributions from NW, LP, FA, and FB. All authors reviewed the manuscript and approved the final draft of the manuscript.

FUNDING

This work was supported by an NUI Galway College of Science PhD Fellowship and Thomas Crawford Hayes Research awards to YS.

ACKNOWLEDGMENTS

We thank Matthew Chapman for anti-CsgA antibody, Shinya Sugimoto for anti-CsgD antibody and Regine Hengge for the pCAB18-*pdeR* plasmid used in this study. We are grateful to Jörgen Johansson and members of the Bacterial Stress Response Group for helpful discussions and critical reading of the manuscript.

SUPPLEMENTARY MATERIAL

The Supplementary Material for this article can be found online at: https://www.frontiersin.org/articles/10.3389/fmicb.2018.01340/full#supplementary-material

REFERENCES

Al Safadi, R., Abu-Ali, G. S., Sloup, R. E., Rudrik, J. T., Waters, C. M., Eaton, K. A., et al. (2012). Correlation between in vivo biofilm formation and virulence gene expression in *Escherichia coli* O104:H4. *PLoS One* 7:e41628. doi: 10.1371/journal.pone.004162

Anderson, K. L., Whitlock, J. E., and Harwood, V. J. (2005). Persistence and differential survival of fecal indicator bacteria in subtropical waters and sediments. *Appl. Environ. Microbiol.* 71, 3041–3048. doi: 10.1128/AEM.71.6.3041-3048.2005

Annous, B. A., Smith, J. L., Fratamico, P. M., and Somolon, E. B. (2009). "Biofilms in fresh fruit and vegetables," in *Biofilms in the Food and Beverage Industries*, eds

P. M. Fratamico, B. A. Annous, and N. W. Gunther (Cambridge: Woodhead Publishing), 517–535. doi: 10.1533/9781845697167.4.517

Attridge, S. R., and Rowley, D. (1983). The Role of the flagellum in the adherence of *Vibrio cholerae*. *J. Infect. Dis.* 147, 864–872. doi: 10.1093/infdis/147.5.864

Barnhart, M. M., and Chapman, M. R. (2006). Curli biogenesis and function. *Annu. Rev. Microbiol.* 60, 131–147. doi: 10.1146/annurev.micro.60.080805.142106

Berg, R. (1996). The indigenous gastrointestinal microflora. *Trends Microbiol.* 4, 430–435. doi: 10.1016/0966-842X(96)10057-3

Bokranz, W., Wang, X., Tschäpe, H., and Römling, U. (2005). Expression of cellulose and curli fimbriae by *Escherichia coli* isolated from the gastrointestinal tract. *J. Med. Microbiol.* 54, 1171–1182. doi: 10.1099/jmm.0.46064-0

Brennan, F. P., Grant, J., Botting, C. H., O'Flaherty, V., Richards, K. G., and Abram, F. (2013). Insights into the low-temperature adaptation and nutritional flexibility of a soil-persistent *Escherichia coli*. *FEMS Microbiol. Ecol.* 84, 75–85. doi: 10.1111/1574-6941.12038

Brennan, F. P., O'Flaherty, V., Kramers, G., Grant, J., and Richards, K. G. (2010). Long-term persistence and leaching of *Escherichia coli* in temperate maritime soils. *Appl. Environ. Microbiol.* 76, 1449–1455. doi: 10.1128/AEM.02335-09

Brombacher, E., Dorel, C., Zehnder, A. J., and Landini, P. (2003). The curli biosynthesis regulator CsgD co-ordinates the expression of both positive and negative determinants for biofilm formation in *Escherichia coli*. *Microbiology* 149, 2847–2857. doi: 10.1099/mic.0.26306-0

Byappanahalli, M. N., Yan, T., Hamilton, M. J., Ishii, S., Fujioka, R. S., Whitman, R. L., et al. (2012). The population structure of *Escherichia coli* isolated from subtropical and temperate soils. *Sci. Total Environ.* 41, 273–279. doi: 10.1016/j.scitotenv.2011.12.041

Carter, M. Q., Louie, J. W., Feng, D., Zhong, W., and Brandl, M. T. (2016). Curli fimbriae are conditionally required in *Escherichia coli* O157:H7 for initial attachment and biofilm formation. *Food Microbiol.* 57, 81–89. doi: 10.1016/j.fm.2016.01.006

Chen, C.-Y., Hofmann, C. S., Cottrell, B. J., Strobaugh, T. P., Paoli, G. C., Nguyen, L.-H., et al. (2013). Phenotypic and genotypic characterization of biofilm forming capabilities in non-O157 Shiga toxin-producing *Escherichia coli* strains. *PLoS One* 8:e84863. doi: 10.1371/journal.pone.0084863

Chiang, S. M., Dong, T., Edge, T. A., and Schellhorn, H. E. (2011). Phenotypic diversity caused by differential RpoS activity among environmental *Escherichia coli*. *Appl. Environ. Microbiol.* 77, 7915–7923. doi: 10.1128/AEM.05274-11

Clermont, O., Christenson, J. K., Denamur, E., and Gordon, D. M. (2013). The clermont *Escherichia coli* phylo-typing method revisited: improvement of specificity and detection of new phylo-groups. *Environ. Microbiol. Rep.* 5, 58–65. doi: 10.1111/1758-2229.12019

Costantino, N., and Court, D. L. (2003). Enhanced levels of λ Red-mediated recombinants in mismatch repair mutants. *Proc. Natl. Acad. Sci. U.S.A.* 100, 15748–15753. doi: 10.1073/pnas.2434959100

Cookson, A. L., Cooley, W. A., and Woodward, M. J. (2002). The role of type 1 and curli fimbriae of Shiga toxin-producing *Escherichia coli* in adherence to abiotic surfaces. *Int. J. Med. Microbiol.* 292, 195–205. doi: 10.1078/1438-4221-00203

De Oliveira, D. C., Fernandes Júnior, A., Kaneno, R., Silva, M. G., Araújo Júnior, J. P., Silva, N. C., et al. (2014). Ability of *Salmonella* spp. to produce biofilm is dependent on temperature and surface material. *Foodborne Pathog. Dis.* 11, 478–483. doi: 10.1089/fpd.2013.1710

DeFlaun, M. F., Tanzer, A. S., McAteer, A. L., Marshall, B., and Levy, S. B. (1990). Development of an adhesion assay and characterization of an adhesion-deficient mutant of *Pseudomonas fluorescens*. *Appl. Environ. Microbiol.* 56, 112–119.

DePas, W. H., Hufnagel, D. A., Lee, J. S., Blanco, L. P., Bernstein, H. C., Fisher, S. T., et al. (2013). Iron induces bimodal population development by *Escherichia coli*. *Proc. Natl. Acad. Sci. U.S.A.* 110, 2629–2634. doi: 10.1073/pnas.1218703110

Dyer, J. G., Sriranganathan, N., Nickerson, S. C., and Elvinger, F. (2007). Curli production and genetic relationships among *Escherichia coli* from cases of bovine mastitis. *J. Dairy Sci.* 90, 193–201. doi: 10.3168/jds.S0022-0302(07)72620-6

Fink, R. C., Black, E. P., Hou, Z., Sugawara, M., Sadowsky, M. J., and Diez-Gonzalez, F. (2012). Transcriptional responses of *Escherichia coli* K-12 and O157:H7 associated with lettuce leaves. *Appl. Environ. Microbiol.* 78, 1752–1764. doi: 10.1128/AEM.07454-11

Gardner, S. N., Slezak, T., and Hall, B. G. (2015). kSNP3.0: SNP detection and phylogenetic analysis of genomes without genome alignment or reference genome. *Bioinformatics* 31, 2877–2878. doi: 10.1093/bioinformatics/btv271

Gophna, U., Barlev, M., Seijffers, R., Oelschlager, T. A., and Ron, E. Z. (2001). Curli fibers mediate internalization of *Escherichia coli* by eukaryotic cells. *Infect. Immun.* 69, 2659–2665. doi: 10.1128/IAI.69.4.2659-2665.2001

Gordon, D. M., and Cowling, A. (2003). The distribution and genetic structure of *Escherichia coli* in Australian vertebrates: host and geographic effects. *Microbiology* 149, 3575–3586. doi: 10.1099/mic.0.26486-0

He, D., Chiou, J., Zeng, Z., Liu, L., Chen, X., Zeng, L., et al. (2015). Residues distal to the active site contribute to enhanced catalytic activity of variant and hybrid β-lactamases derived from CTX-M-14 and CTX-M-15. *Antimicrob. Agents Chemother.* 59, 5976–5983. doi: 10.1128/AAC.04920-14

Hidalgo, G., Chen, X., Hay, A. G., and Lion, L. W. (2010). Curli produced by *Escherichia coli* PHL628 provide protection from Hg(II). *Appl. Environ. Microbiol.* 76, 6939–6941. doi: 10.1128/AEM.01254-10

Hinsa, S. M., Espinosa-Urgel, M., Ramos, J. L., and O'Toole, G. A. (2003). Transition from reversible to irreversible attachment during biofilm formation by *Pseudomonas fluorescens* WCS365 requires an ABC transporter and a large secreted protein. *Mol. Microbiol.* 49, 905–918. doi: 10.1046/j.1365-2958.2003.03615.x

Ishii, S., Ksoll, W. B., Hicks, R. E., and Sadowsky, M. J. (2006). Presence and growth of naturalized *Escherichia coli* in temperate soils from Lake Superior watersheds. *Appl. Environ. Microbiol.* 72, 612–621. doi: 10.1128/AEM.72.1.612-621.2006

La Ragione, R. M., Collighan, R. J., and Woodward, M. J. (1999). Non-curliation of *Escherichia coli* O78:K80 isolates associated with IS1 insertion in csgB and reduced persistence in poultry infection. *FEMS Microbiol. Lett.* 175, 247–253. doi: 10.1111/j.1574-6968.1999.tb13627.x

Larsonneur, F., Martin, F. A., Mallet, A., Martinez-Gil, M., Semetey, V., Ghigo, J.-M., et al. (2016). Functional analysis of *Escherichia coli* Yad fimbriae reveals their potential role in environmental persistence. *Environ. Microbiol.* 18, 5228–5248. doi: 10.1111/1462-2920.13559

Lindenberg, S., Klauck, G., Pesavento, C., Klauck, E., and Hengge, R. (2013). The EAL domain protein YciR acts as a trigger enzyme in a c-di-GMP signalling cascade in *E. coli* biofilm control. *EMBO J.* 32, 2001–2014. doi: 10.1038/emboj.2013.120

Maal-Bared, R., Bartlett, K. H., Bowie, W. R., and Hall, E. R. (2013). Phenotypic antibiotic resistance of *Escherichia coli* and *E. coli* O157 isolated from water, sediment and biofilms in an agricultural watershed in British Columbia. *Sci. Total Environ.* 443, 315–323. doi: 10.1016/j.scitotenv.2012.10.106

McCrate, O. A., Zhou, X., Reichhardt, C., and Cegelski, L. (2013). Sum of the parts: composition and architecture of the bacterial extracellular matrix. *J. Mol. Biol.* 425, 4286–4294. doi: 10.1016/j.jmb.2013.06.022

Ogden, L. D., Fenlon, D. R., Vinten, A. J., Lewis, D., and Ogden, I. (2001). The fate of *Escherichia coli* O157 in soil and its potential to contaminate drinking water. *Int. J. Food Microbiol.* 66, 111–117. doi: 10.1016/S0168-1605(00)00508-0

Pande, V. V., McWhorter, A. R., and Chousalkar, K. K. (2016). *Salmonella enterica* isolates from layer farm environments are able to form biofilm on eggshell surfaces. *Biofouling* 32, 699–710. doi: 10.1080/08927014.2016.1191068

Patel, J., Sharma, M., and Ravishakar, S. (2011). Effect of curli expression and hydrophobicity of *Escherichia coli* O157:H7 on attachment to fresh produce surfaces. *J. Appl. Microbiol.* 110, 737–745. doi: 10.1111/j.1365-2672.2010.04933.x

Pesavento, C., Becker, G., Sommerfeldt, N., Possling, A., Tschowri, N., Mehlis, A., et al. (2008). Inverse regulatory coordination of motility and curli-mediated adhesion in *Escherichia coli*. *Genes Dev.* 22, 2434–2446. doi: 10.1101/gad.475808

Rajagopalan, P. T., Lutz, S., and Benkovic, S. J. (2002). Coupling interactions of distal residues enhance dihydrofolate reductase catalysis: mutational effects on hydride transfer rates. *Biochemistry* 41, 12618–12628. doi: 10.1021/bi026369d

Rao, F., Yang, Y., Qi, Y., and Liang, Z.-X. (2008). Catalytic mechanism of cyclic di-GMP-specific phosphodiesterase: a study of the EAL domain-containing RocR from *Pseudomonas aeruginosa*. *J. Bacteriol.* 190, 3622–3631. doi: 10.1128/JB.00165-08

Ravva, S. V., Sarreal, C. Z., and Mandrell, R. E. (2014). Strain differences in fitness of *Escherichia coli* O157:H7 to resist protozoan predation and survival in soil. *PLoS One* 9:e102412. doi: 10.1371/journal.pone.0102412

Römling, U., Galperin, M. Y., and Gomelsky, M. (2013). Cyclic di-GMP: the first 25 years of a universal bacterial second messenger. *Microbiol. Mol. Biol. Rev.?* 77, 1–52. doi: 10.1128/MMBR.00043-12

Salvucci, A. E., Zhang, W., Morales, V. L., Cakmak, M. E., Hay, A. G., and Steenhuis, T. S. (2009). The impact of biofilm-forming potential and tafi production on transport of environmental *Salmonella* through unsaturated porous media. *Biologia* 64, 460–464. doi: 10.2478/s11756-009-0102-y

Sievers, F., Wilm, A., Dineen, D., Gibson, T. J., Karplus, K., Li, W., et al. (2011). Fast, scalable generation of high-quality protein multiple sequence alignments using Clustal Omega. *Mol. Syst. Biol.* 7:539. doi: 10.1038/msb.2011.75

Silagyi, K., Kim, S. H., Martin Lo, Y., and Wei, C. I. (2009). Production of biofilm and quorum sensing by *Escherichia coli* O157:H7 and its transfer from contact surfaces to meat, poultry, ready-to-eat deli, and produce products. *Food Microbiol.* 26, 514–519. doi: 10.1016/j.fm.2009.03.004

Sommerfeldt, N., Possling, A., Becker, G., Pesavento, C., Tschowri, N., and Hengge, R. (2009). Gene expression patterns and differential input into curli fimbriae regulation of all GGDEF/EAL domain proteins in *Escherichia coli*. *Microbiology* 155, 1318–1331. doi: 10.1099/mic.0.024257-0

Somorin, Y., Abram, F., Brennan, F., and O'Byrne, C. (2016). The general stress response is conserved in long-term soil-persistent strains of *Escherichia coli*. *Appl. Environ. Microbiol.* 82, 4628–4640. doi: 10.1128/AEM.01175-16

Tchigvintsev, A., Xu, X., Singer, A., Chang, C., Brown, G., Proudfoot, M., et al. (2010). Structural insight into the mechanism of c-di-GMP hydrolysis by EAL domain phosphodiesterases. *J. Mol. Biol.* 402, 524–538. doi: 10.1016/j.jmb.2010.07.050

Truhlar, A. M., Salvucci, A. E., Walter, M. T., Warnick, L. D., Hay, A. G., and Steenhuis, T. S. (2015). Effects of manure-application practices on curli production by *Escherichia coli* transported through soil. *Environ. Sci. Technol.* 49, 2099–2104. doi: 10.1021/es5053039

Uhlich, G. A., Chen, C. Y., Cottrell, B. J., Hofmann, C. S., Dudley, E. G., Strobaugh, T. P., et al. (2013). Phage insertion in mlrA and variations in rpoS limit curli expression and biofilm formation in *Escherichia coli* serotype O157: H7. *Microbiology* 159, 1586–1596. doi: 10.1099/mic.0.066118-0

Uhlich, G. A., Gunther, N. W., Bayles, D. O., and Mosier, D. A. (2009). The CsgA and Lpp proteins of an *Escherichia coli* O157:H7 strain affect HEp-2 cell invasion, motility, and biofilm formation. *Infect. Immun.* 77, 1543–1552. doi: 10.1128/IAI.00949-08

Vestby, L. K., Møretrø, T., Ballance, S., Langsrud, S., and Nesse, L. L. (2009). Survival potential of wild type cellulose deficient *Salmonella* from the feed industry. *BMC Vet. Res.* 5:43. doi: 10.1186/1746-6148-5-43

Vogeleer, P., Tremblay, Y. D. N., Mafu, A. A., Jacques, M., and Harel, J. (2014). Life on the outside: role of biofilms in environmental persistence of Shiga-toxin producing *Escherichia coli*. *Front. Microbiol.* 5:317. doi: 10.3389/fmicb.2014.00317

Walk, S. T., Alm, E. W., Gordon, D. M., Ram, J. L., Toranzos, G. A., Tiedje, J. M., et al. (2009). Cryptic lineages of the genus *Escherichia*. *Appl. Environ. Microbiol.* 75, 6534–6544. doi: 10.1128/AEM.01262-09

Yaron, S., and Römling, U. (2014). Biofilm formation by enteric pathogens and its role in plant colonization and persistence. *Microb. Biotechnol.* 7, 496–516. doi: 10.1111/1751-7915.12186

Zhou, Y., Smith, D. R., Hufnagel, D. A., and Chapman, M. R. (2013). Experimental manipulation of the microbial functional amyloid called curli. *Methods Mol. Biol.* 966, 53–75. doi: 10.1007/978-1-62703-245-2_4

Zogaj, X., Bokranz, W., Nimtz, M., and Römling, U. (2003). Production of cellulose and curli fimbriae by members of the family *Enterobacteriaceae* isolated from the human gastrointestinal tract. *Infect. Immun.* 71, 4151–4158. doi: 10.1128/IAI.71.7.4151-4158.2003

Conflict of Interest Statement: The authors declare that the research was conducted in the absence of any commercial or financial relationships that could be construed as a potential conflict of interest.

frontiers in Microbiology

ORIGINAL RESEARCH
published: 04 July 2018
doi: 10.3389/fmicb.2018.01479

Transgenerational Epigenetic Inheritance Under Environmental Stress by Genome-Wide DNA Methylation Profiling in Cyanobacterium

*Lang Hu[1,2], Peng Xiao[1], Yongguang Jiang[1], Mingjie Dong[1], Zixi Chen[3], Hui Li[1], Zhangli Hu[1], Anping Lei[1] and Jiangxin Wang[1,2]**

[1] Shenzhen Key Laboratory of Marine Bioresource and Eco-environmental Science, Shenzhen Engineering Laboratory for Marine Algal Biotechnology, Guangdong Provincial Key Laboratory for Plant Epigenetics, College of Life Sciences and Oceanography, Shenzhen University, Shenzhen, China, [2] Nanshan District Key Lab for Biopolymers and Safety Evaluation, College of Materials Science and Engineering, Shenzhen University, Shenzhen, China, [3] Laboratory of Synthetic Microbiology, School of Chemical Engineering and Technology, Tianjin University, Tianjin, China

OPEN ACCESS

Edited by:
Daniela De Biase,
Sapienza Università di Roma, Italy

Reviewed by:
Igor Kovalchuk,
University of Lethbridge, Canada
Xuefeng Lu,
Qingdao Institute of Bioenergy and Bioprocess Technology (CAS), China

***Correspondence:**
Jiangxin Wang
jxwang@szu.edu.cn

Specialty section:
This article was submitted to Microbial Physiology and Metabolism, a section of the journal Frontiers in Microbiology

Received: 29 March 2018
Accepted: 13 June 2018
Published: 04 July 2018

Citation:
Hu L, Xiao P, Jiang Y, Dong M, Chen Z, Li H, Hu Z, Lei A and Wang J (2018) Transgenerational Epigenetic Inheritance Under Environmental Stress by Genome-Wide DNA Methylation Profiling in Cyanobacterium. Front. Microbiol. 9:1479. doi: 10.3389/fmicb.2018.01479

Epigenetic modifications such as DNA methylation are well known as connected with many important biological processes. Rapid accumulating evidence shows environmental stress can generate particular defense epigenetic changes across generations in eukaryotes. This transgenerational epigenetic inheritance in animals and plants has gained interest over the last years. Cyanobacteria play very crucial role in the earth, and as the primary producer they can adapt to nearly all diverse environments. However, few knowledge about the genome wide epigenetic information such as methylome information in cyanobacteria, especially under any environment stress, was reported so far. In this study we profiled the genome-wide cytosine methylation from a model cyanobacterium *Synechocystis* sp. PCC 6803, and explored the possibility of transgenerational epigenetic process in this ancient single-celled prokaryote by comparing the DNA methylomes among normal nitrogen medium cultivation, nitrogen starvation for 72 h and nitrogen recovery for about 12 generations. Our results shows that DNA methylation patterns in nitrogen starvation and nitrogen recovery are much more similar with each other, significantly different from that of the normal nitrogen. This study reveals the difference in global DNA methylation pattern of cyanobacteria between normal and nutrient stress conditions and reports the evidence of transgenerational epigenetic process in cyanobacteria. The results of this study may contribute to a better understanding of epigenetic regulation in prokaryotic adaptation to and survive in the ever changing environment.

Keywords: cyanobacteria, adaptation, environmental stress, DNA methylation, transgenerational epigenetic inheritance

INTRODUCTION

Epigenetic modifications, heritable chemical additions to DNA or histones which are associated with gene expression but do not alter the primary DNA sequence, are well known as connected with many important processes (Law and Jacobsen, 2010). DNA methylation is one of the most important epigenetic modifications and catalyzed by DNA-specific methyltransferase which transfers methyl group from general substrate, *S*-adenosylmethionine, to specific DNA sequences. This epigenetic modification is usually related to regulation of gene expression, genomic imprinting, X chromosome inactivation, chromosome stability and so on in eukaryotes (Feng et al., 2010).

DNA methylation mainly refers to 5-methylcytosine (thereafter m^5C) in eukaryotes. In mammals most m^5C exist within CG context, and methyltransferases DNMT3 and DNMT1 are responsible for establishment and maintenance of the DNA methylation, respectively. In higher plants, m^5C could exist in CG, CHG, and CHH context. Establishment of the methylation is conducted by methyltransferase DRM2, and two methyltransferases, MET1 and CMT3, are involved in maintenance of the methylation in higher plants (Chan et al., 2005; Law and Jacobsen, 2010). Bisulfite can convert cytosine into uracil but cannot alter m^5C (Patterson et al., 2011). The whole genome bisulfite sequencing (thereafter WGBS) technology has been widely used in exploring the global pattern of m^5C in eukaryotes (i.e., Lister et al., 2009; Carvalho et al., 2012). In addition, m^4C can also show partially resistance to the bisulfite-mediated deamination, therefore WGBS indeed could be used to identify both m^5C and m^4C (Vilkaitis and Klimasauskas, 1999).

Besides methylation by DNA methyltransferases, demethylation could also influence the global DNA methylation pattern in mammals and plants. Deaminases (Aid/Apobec), glycosylase (Mbd4), thymine DNA glycosylase (Tdg), and unidentified apyrimidinic lyase are needed for active demethylation in mammals, while bifunctional 5-methylcytosine glycosylases (DME/ROS1) are needed for active demethylation in higher plants (Ikeda and Kinoshita, 2009).

In bacteria, besides m^5C, N6-methyladenine (m^6A) and N4-methylcytosine (m^4C) also exist. Unlike in mammals and plants, DNA methylation in bacteria is believed to be part of the restriction/modification system, which prevents bacteria from being self-digested (Wilson and Murray, 1991). Taking *Escherichia coli* genome as an example, three DNA methyltransferase genes exist, one of which is clustered with its cognate restriction enzyme gene and the other two encode solitary methyltransferases. In bacteria, DNA methyltransferases may also have other physiological significances. The methyltransferase, Dam, involves in distinguishing newly synthesized DNA from the old DNA (Palmer and Marinus, 1994) and takes part in DNA repair (Pukkila et al., 1983). In *Caulobacter crescentus*, the methyltransferase CcrM acts as a regulator for cell cycle (Reisenauer et al., 1999). Single molecule real-time (SMRT) sequencing technology could be used to directly detect m^6A and m^4C with high degree of accuracy and sensitivity (Flusberg et al., 2010). With this technology, many bacterial and archaeal species were investigated for their global m^6A and m^4C distribution patterns (Clark et al., 2012; Fang et al., 2012; Murray et al., 2012; Lluch-Senar et al., 2013; Blow et al., 2016). Besides SMRT sequencing, WGBS has also been applied into bacterial such as *E. coli* to determine the global m^5C distribution (Kahramanoglou et al., 2012).

As an ancient group of photosynthetic bacteria, cyanobacteria plays very crucial role in the earth as the primary producer in the ecosystem. They could be found in many diverse ecological habitats, and survive under adverse environments such as deserts, polar region, and hot springs (Whitton and Potts, 2000; Stomp et al., 2007). Some cyanobacteria species may form water bloom, threatening the health of human (Catherine et al., 2013). Based on sequence homology, some methyltransferase encoding genes have been identified in cyanobacteria. For example, there are nine genes possibly encoding DNA methyltransferase in *Anabaena* sp. PCC 7120 (Matveyev et al., 2001). Type II restriction/modification system and solitary methyltransferase genes were also predicted in *N. punctiforme* genome (Meeks et al., 2001). In *Synechocystis* sp. PCC 6803 (thereafter *Synechocystis*), a model cyanobacterium, three genes encoding solitary methyltransferases, *mbpA*, *sll0729,* and *synMI*, exist (Kaneko et al., 1995, 1996; Scharnagl et al., 1998). Some limited DNA methylation studies have also been conducted in cyanobacteria. Restriction analysis and quantitative estimation of methylated bases in filamentous and unicellular cyanobacterial DNA shows the presence of methyladenine in the GATC sequence (Padhy et al., 1988). Enzyme digestion experiments in two *Anabaena* species indicates that DNA from both species is methylated, but that no gross change in methylation occurs during heterocyst formation (Adams, 1988). Recently, global DNA methylation pattern study has been conducted in *Synechocystis* and more methyltransferases were identified (Hagemann et al., 2018).

Many studies have reported external environment stress could influence the epigenetic processes in eukaryotes (Gao et al., 2010; Lira-Medeiros et al., 2010; Kou et al., 2011; Menzel et al., 2011; Navarro-Martin et al., 2011; Yu et al., 2013). Furthermore, rapid accumulating evidence shows that environmental stress could generate particular defense epigenetic changes across generations in eukaryotes (Hauser et al., 2011; Heard and Martienssen, 2014; Skinner, 2014). This transgenerational epigenetic inheritance has gained interest over the last years and addressed the importance of transgenerational inheritance for adaptation to ever changing environment and for practical applications. For instance, in *Oryza sativa* L., it has been reported chronic nitrogen deficiency could induce global change in DNA methylation in leaf-tissue of the stressed plant, and part of the change could be stably inherited to its non-stress suffered progenies and improve the resistance to nitrogen deficiency in progenies (Kou et al., 2011). In contrast, in bacteria few studies concerned about the influence of external environment on global DNA methylation pattern, much less the defense transgenerational epigenetic inheritance.

While nutrients are important to microbes, seasonal depletion and repletion of nutrients in the environment are common in

nature. In some habitats, nitrogen, one of the most important essential nutrients, is seriously scarce for cyanobacteria to survive (Elser et al., 1990; Vitousek and Howarth, 1991; Conley et al., 2009; Thomas et al., 2015). However, cyanobacteria have evolved sophisticated mechanisms to cope with the nitrogen deficiency. For example, most cyanobacteria could utilize various alternative forms of nitrogen source under nitrogen deficiency (Flores and Herrero, 2005). Moreover, some cyanobacteria could biologically fix nitrogen from air (Wolk, 1996). Considering that DNA methyltransferase is widespread in this group (Kaneko et al., 1995, 1996; Scharnagl et al., 1998; Matveyev et al., 2001; Meeks et al., 2001), it is possible for cyanobacteria to deal with the stress through defense alteration in DNA methylation as in plant (Kou et al., 2011). However, knowledge about the whole-genome DNA methylation in cyanobacteria is still poor, and defense epigenetic modifications such as DNA methylation in this group, especially under any environment stress, remain a mystery.

In this study, DNA from a model single-celled model cyanobacterium *Synechocystis* cultured under normal nitrogen (sample as NC), nitrogen starved for 72 h (N72), and nitrogen recovered (NR) which was derived from N72 but thereafter NR for 12 days was bisulfite converted for next generation sequencing, and the DNA methylation patterns were compared among the three samples. Questions proposed to answer are: (i) whether widely spread mC exists in *Synechocystis*? (ii) whether the DNA methylation could be influenced by nutrient depletion or not? and (iii) if influenced whether the altered pattern is inheritable and how? Results indicate that nitrogen deficiency stress can induce DNA methylation alternations, and gives the evidence of transgenerational epigenetic process, inheritance of DNA methylation pattern from N72 to NR, in cyanobacteria. Our current data will contribute to a better understanding of the biological function, epigenetic adaptation to ever changing environment, and even the evolution of DNA methylation in prokaryotes.

MATERIALS AND METHODS

Strains and Culture Conditions

Synechocystis sp. PCC 6803 (thereafter *Synechocystis*) was provided kindly by Professor Weiwen Zhang in Tianjin University, China. All cells were cultured autotrophically at a constant photon flux density of 30 μmol photons m^{-2} s^{-1} on a rotary shaker at 30°C. The BG11 medium which contains 1.5 g L^{-1} $NaNO_3$ (Rippka et al., 1979), N^0 BG11 medium (modified BG11 containing no $NaNO_3$), and $N^{1/3}$ BG11 medium (modified BG11 containing only 0.5 g L^{-1} $NaNO_3$) were used.

Nitrogen Starvation and Nitrogen Recovery

Synechocystis cells were cultured in BG11 medium, and when OD_{730} reached to 0.8 cells were collected as normal nitrogen sample (NC). Some cells taken from NC were transferred into N^0 BG11 medium with $OD_{730} = 0.8$ and starved for 72 h, then cells were collected as nitrogen starved sample (N72). Some cells derived from N72 were transferred back into BG11 medium and cultured for 6 days with initial $OD_{730} = 0.05$. After 6 days some cells were collected and retransferred into BG11 medium with initial $OD_{730} = 0.05$ for another cultivation of 6 days. Finally, cells were collected as nitrogen recovery sample (NR). Cells for whole genome bisulfite sequencing were all stored in −80°C before processing.

Extraction of Genomic DNA

Genomic DNA was extracted as described previously (Hu et al., 2015). Briefly, cells were digested with proteinase K (Thermo Fisher Scientific, United States). Lysate was then extracted with mix of phenol (Sinopharm, China) and chloroform (Sinopharm, China). RNA was removed with RNase A (Thermo Fisher Scientific, United States) and DNA was precipitated with isopropanol (Sinopharm, China).

Extraction of RNA and qRT-PCR

Cells were grinded in liquid nitrogen and then extracted with Trizol (Thermo Fisher Scientific, United States). Genomic DNA was removed by gDNA eraser (Takara, Japan). cDNAs were synthesized using SuperScript VILO™ Master Mix Kit (Thermo Fisher Scientific, United States). The qRT-PCR was conducted on QuantStudio™ 6 flex (Thermo Fisher Scientific, United States). A total of 10 μL qRT-PCR reaction solution was set, containing 5 μL SYBR Premix Ex Taq (Tli RNaseH Plus) (Takara, Japan), 0.2 μL ROX reference dye (Takara, Japan), 200 nM primers, and 10 ng cDNA. The qRT-PCR procedure was set as follows: initial denaturation step of 95°C for 20 s, 40 cycles of 95°C for 10 s, 60°C for 20 s, followed by a melt curve stage. Relative expression of the target genes was determined using $2^{-\Delta\Delta CT}$ method (Livak and Schmittgen, 2001). The gene *rnpB* was used as internal reference. Means and SDs were calculated from three biological replicates. Primers used were listed in **Supplementary Table S1**.

Growth in Limited Nitrogen

Cells were cultured in $N^{1/3}$ BG11 with initial $OD_{730} = 0.05$. OD_{730} was measured every 2 days. Three biological replicates were set. The specific growth rate was calculated as follows:

$$\mu = \frac{\ln OD_2 - \ln OD_1}{T_2 - T_1}$$

In the formula, μ represents the specific growth rate for the first 18 days. T_2 and T_1 represent day 18 and day 0, and the OD_2 and OD_1 represent OD_{730} at day 18 and day 0, respectively. Significant difference in specific growth rate was tested by using *t*-test with the software IBM SPSS Statistics 20.0 (SPSS Inc., Chicago, IL, United States).

Whole Genome Bisulfite Sequencing

Whole genome bisulfite sequencing was conducted by Novogene Company (China). Briefly, sample DNA spiked with λ phage genome DNA was fragmented into 200–300 bp with ultrasonication (Covaris S220 System, Thermo Fisher Scientific, United States). Barcodes were ligated to the DNA fragments,

and then bisulfite converted with EZ DNA Methylation Gold Kit (Zymo Research, United States). The bisulfite conversion was conducted according to the protocol provided by the kit. λ phage genome DNA was included to help assess the methylation rate (bisulfite conversion rate). The constructed library was quantified with Qubit 2.0 (Thermo Fisher Scientific, United States), and diluted to 1 ng μL^{-1}. The length of the inserted fragment of the library was checked with Agilent 2100 Bioanalyzer system (Agilent). In order to ensure the quality of the library, the effective concentration of the library is kept to ≥2 nM. Sequencing of clustering of the index-coded DNA fragments was conducted on Hiseq sequencer (Illumina, United States) with PE125 sequencing strategy.

Quality Control of Sequencing

Reads were first pre-processed through in-house perl scripts, and the software Trimmomatic was used for the raw data trimming. The Trimmomatic processing parameters were set as follows: SLIDING WINDOW was set to 4:15. Both LEADING and TRAILING were set to 3. ILLUMINACLIP:adapter.fa:2:30:7:1:true was applied. Clean reads were retrieved as follows: Firstly, reads were scanned for adapter sequence and those reads with adapter sequences were filtered out. Then percentage of undefined bases (N bases) in each read was calculated, and the reads with undefined base percentage higher than 5% were also removed. Lastly, those reads with low quality (PHRED score ≤ 20, and percentage of the low quality bases ≥ 50%) were removed. The remaining reads were considered as clean reads, and all subsequent analyses were based on clean reads.

Details such as data size, read length, sequencing depth, median coverage and so on can be found in results section.

Reads Mapping to the Reference Genome and Identification of Sites for Methylcytosine

Bismark software (Krueger and Andrews, 2011) was used to perform the alignment of reads to the reference genome (NCBI Bioproject ID: PRJNA80481). To identify the sites for methylcytosine, we treated the sum of methylated reads as a binomial random variable with methylation rate (bisulfite conversion rate), and the fdr q-value of each mC candidate was calculated with R script. Only sites with ≥5× coverage and fdr q-value ≤ 0.05 were used in analyses.

To calculate methylation level of mC sites, we first calculated the uncorrected methylation level for each cytosine site, and then corrected it with bisulfite non-conversion rate. The uncorrected methylation level for each cytosine site was calculated as follows:

$$ML_{(\text{uncorrected})} = \frac{\text{reads}_{(\text{mC})}}{\text{reads}_{(\text{mC})} + \text{reads}_{(\text{C})}}$$

In the formula, $ML_{(uncorrected)}$ represents the uncorrected methylation level for the given site. The $reads_{(mC)}$ and $reads_{(C)}$ represent the reads with mC and reads with mC or cytosine in the given site, respectively.

Then uncorrected methylation level was further corrected with the bisulfite non-conversion rate and the corrected methylation level for each cytosine site was calculated as follows:

$$ML = \frac{ML_{(\text{uncorrected})} - R}{1 - R}$$

In the formula, ML represents the corrected methylation level and R represents the bisulfite non-conversion rate.

Differentially Methylated Regions Analysis

Differentially methylated regions (DMRs) were identified using sliding-window approach with the software package swDMR[1]. The window length was set to 200 bp, and the step length was set to 40 bp. Fisher test was conducted to interrogate DMRs. Those genes located in DMRs are defined as differentially methylated genes.

KEGG Enrichment Analysis of DMR-Related Genes

KEGG is a database resource for understanding high-level functions and utilities of the biological system (Kanehisa et al., 2008). KOBAS software package was used to test the statistical enrichment of DMR-related genes in KEGG pathways (Wu et al., 2006).

Comparison of Methylome Data With the Published Transcriptomic Results

Krasikov et al. (2012) investigated the global gene expression in *Synechocystis* at 0, 6, 12, 24, and 96 h during nitrogen starvation with microarrays. Their transcriptome data can be retrieved from the URL[2]. We therefore investigated the correlation between our DNA methylation data of N72 and their transcriptome data at 96 h after nitrogen starvation by comparing their differentially expressed genes (DEG) with the DMR-related genes found in our study.

RESULTS

Whole-Genome Methylation Landscape in *Synechocystis*

Our sequencing data has been deposited in NCBI with Bioproject ID PRJNA445519[3]. About 1.5, 1.76, and 2.06 Gb clean data with read length longer than 125 bp were generated for NC, N72, and NR, respectively, and the sequencing depth reached 380×. The bisulfite conversion rate was 99.72, 99.70, and 99.71% for NC, N72, and NR, respectively, showing almost complete bisulfite conversion. The unique mapped reads accounted for 75.61, 81.05, and 71.79% of the clean reads in NC, N72, and NR, respectively, resulting in a median coverage of 163 reads per base.

[1] https://github.com/xflicsu/swDMR

[2] http://dx.doi.org/10.1111/j.1399-3054.2012.01585.x

[3] https://www.ncbi.nlm.nih.gov/

As shown in **Table 1**, the overall methylation levels of the three samples were similar. 1.35, 1.34, and 1.48% of cytosines were methylated for NC, N72, and NR, respectively. About 3.0% CG, 0.9% CHG, and 1.0% CHH were methylated comprising the DNA methylation in each of the samples. In total, 96,961 sites for methylcytosine (thereafter mC sites) were identified in the *Synechocystis* genome, including 62,415, 18,057, and 16,489 in CHH, CG, and CHG context (H represents any nucleotide except guanine), respectively. For all the three samples CHH was always the most preferred context by mC site, followed by CG and CHG, e.g., mC sites in CHH, CG, and CHG context accounted for about 63, 21, and 16% of the total sites, respectively (**Supplementary Table S2**). Interestingly, large difference in the number of mC site was found between samples despite their similar overall methylation level (**Supplementary Table S2**). Under normal nitrogen 79,801 mC sites were found, but the number decreased to 56,914 after nitrogen starvation for 72 h. Interestingly, after 12 days of nitrogen recovery, the number of the site (58,884) was still close to that under nitrogen starvation, much less than under normal nitrogen.

We also notice that methylation site ratio (sites for methylcytosine vs. plasmid nucleotides) differs among plasmids and chromosome. For instance, the methylation site ratio of mC site in CG, CHG, and CHH context in pSYSG_M was about 6.3, 4.4, and 16.5%, respectively, vs. only about 0.4, 0.4, and 1.3% in chromosome (**Supplementary Figure S1**). More extreme, there were no mC detected in pSYSA_M.

Significant Transgenerational Epigenetic Inheritance in Cyanobacterium

To look into the details of the similar numbers of mC site in NR and N72, Venn diagram was drawn. As shown in **Figure 1A**, after nitrogen starvation 32,745 mC sites (32,488 plus 257) which had been found in NC disappeared and 9,858 new sites (5,392 plus 4466) were induced. Relatively small change in mC site occurred after cells were transferred from nitrogen deficiency to nitrogen recovery, with 5,589 sites (5,392 plus 197) disappearing and 7,559 sites (7,302 plus 257) newly induced. There were 47,056 (46,859 plus 197) overlapped sites between NC and N72, 51,325 (46,859 plus 4,466) between N72 and NR, and 47,116 (46,859 plus 257) between NR and NC. Of these overlapped sites, 46,859 were detected in all the three samples, and these sites were possibly less susceptible to the nitrogen treats than other mC sites. Of the 9,858 sites newly induced by nitrogen starvation stress, more than 45% (4,466 sites) were preserved in NR. On the other hand, of the 32,745 mC sites which had been found in NC but disappeared in N72, NR only regain about 1% (257 sites). These indicated that the profile of mC sites in NR was much more similar with N72 than NC.

Considering the similar overall methylation level among the three samples (**Table 1**) and the decreased numbers of mC sites in NR and N72, mC sites in NR and N72 must have higher methylation level than those in NC. Analysis of methylation level of mC sites confirmed this, and further supported the similarity in methylation pattern between NR and N72. Compared with NC, mC site in N72 showed median-increased but variability-decreased methylation level distribution (**Figure 2**). Furthermore, similar methylation level distributions were found for mC site in N72 and that in NR (**Figure 2**). With regard to site context, we found the median of methylation level was much higher in CG context than in non-CG context (CHG and CHH context).

Methylated Genes

All mC sites were annotated in this study, and we found a total of 3,503 genes containing mC, unexpectedly as high as 95% of all genes in *Synechocystis*. There were 3,444, 3,307, and 3,320 genes with mC in NC, N72, and NR, respectively (**Supplementary Table S3**). As shown in **Figure 1B**, after nitrogen starvation 170 genes (109 plus 61) lost mC while 33 new genes (15 plus 18) acquired mC sites. In addition, 74 genes (59 plus 15) lost and 87 genes (61 plus 26) acquired mC sites further after cells were transferred from nitrogen deficiency to nitrogen recovery.

We further investigated the methylation level of mC sites within each functional region, i.e., gene body, intergenic region (region between genes), upstream region (promoter and 5′ UTR) and downstream region (3′ UTR). As shown in **Supplementary Figure S2** no obvious difference in methylation level distribution could be found between functional regions.

Methylation in Transposable Elements

Transposable elements (TEs) are hyper-variable in cyanobacterial genomes, and it could work as a new perspective to further explore the diversity of cyanobacteria in the ever changing environment (Lin et al., 2011; Wang et al., 2015). We investigated the methylation of mC sites exclusively within TEs (thereafter TE-type mC sites). In total, 497 TE-type mC sites were detected in 107 TEs. In NC there were 338 distributed in 95 TEs, and after nitrogen starvation the sites decreased to 150 distributed in 65 TEs. After nitrogen was recovered 130 TE-type mC sites were found within 64 TEs (**Supplementary Figure S3**).

We also investigated the methylation level of the TE-type mC site. Similarly, TE-type mC sites showed increased median methylation level except those in CG context after nitrogen

TABLE 1 | Proportion of 5-methylcytosines under normal nitrogen (NC), nitrogen starvation (N72), and nitrogen recovery (NR).

Samples	Proportion of methylated CG (%)	Proportion of methylated CHG (%)	Proportion of methylated CHH (%)	Proportion of all mC (%)
NC	3.05	0.90	1.03	1.35
N72	3.02	0.90	1.03	1.34
NR	3.15	1.00	1.16	1.48

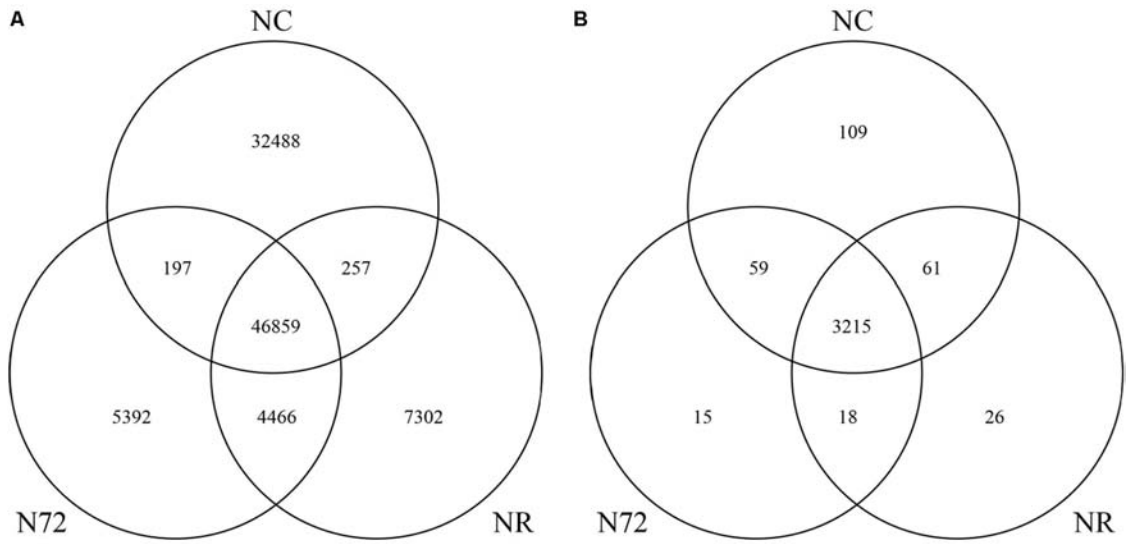

FIGURE 1 | Venn diagram showing the overlapped mC sites **(A)** and the overlapped genes with methylcytosine **(B)** among normal nitrogen (NC), nitrogen starvation (N72), and nitrogen recovery (NR).

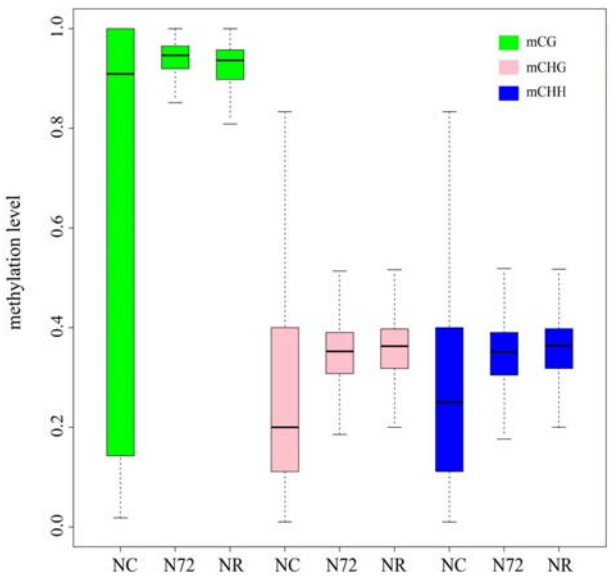

FIGURE 2 | Box plot showing the methylation level of sites for methylcytosine under normal nitrogen (NC), nitrogen starvation (N72), and nitrogen recovery (NR). Distribution of methylation level in nitrogen starvation (N72) is similar with that in nitrogen recovery (NR) rather than in normal nitrogen (NC).

starvation. Even so, TE-type mC sites have distinct nitrogen starvation-response pattern, i.e., a much wider methylation level range were found for TE-type mC sites except those in CHG context after nitrogen starvation, as opposed to what we had showed when mC sites of all types were taken into account (**Figure 2** and **Supplementary Figure S4**). Additionally, we found methylation level distribution differed between N72 and NR at TE-type mC sites in CG and CHH context, namely the median methylation levels at these two TE-type sites were much higher in NR than in N72 (**Supplementary Figure S4**).

Differentially Methylated Region Analysis

Due to the large difference in pattern of DNA methylation between N72 and NC, the DMRs were analyzed. After nitrogen deficiency a total of 1,194 genes were found in DMRs, with 1,042 genes in hyper-methylated regions and 152 genes in hypo-methylated regions. By KEGG enrichment analysis, we found the genes in hyper-methylated regions were mainly enriched in biosynthesis of antibiotics, biosynthesis of secondary metabolites, microbial metabolism in diverse environments, and metabolic pathways. On the other hand, the genes in hypo-methylated regions were mainly enriched in porphyrin and chlorophyll metabolism, streptomycin biosynthesis and carbon metabolism (**Supplementary Figure S5**).

DNA Methylation and Gene Expression

The photosynthesis system, which is sensitive to nitrogen starvation and other environmental stresses, was down-regulated by most stresses (Qiao et al., 2013). Six photosynthetic genes (*psbL*, *psbB*, *psbE*, *psbK*, *atpA*, and *psaA*) were checked for their methylation status. *psbL* and *psbE* contained no or few mC sites whereas the other four contained many hyper-methylated mC sites (**Figure 3**). For all the six genes, the three samples showed similar methylation pattern (**Figure 3**). We also measured the expression of the six genes mentioned above. As shown in **Figure 4**, for all the six genes the expression was down-regulated upon nitrogen deficiency, and almost restored to normal expression level after nitrogen was recovered, regardless of the similarity in DNA methylation among three samples.

We also investigated the correlation between our DNA methylation data of N72 and the published transcriptome data at

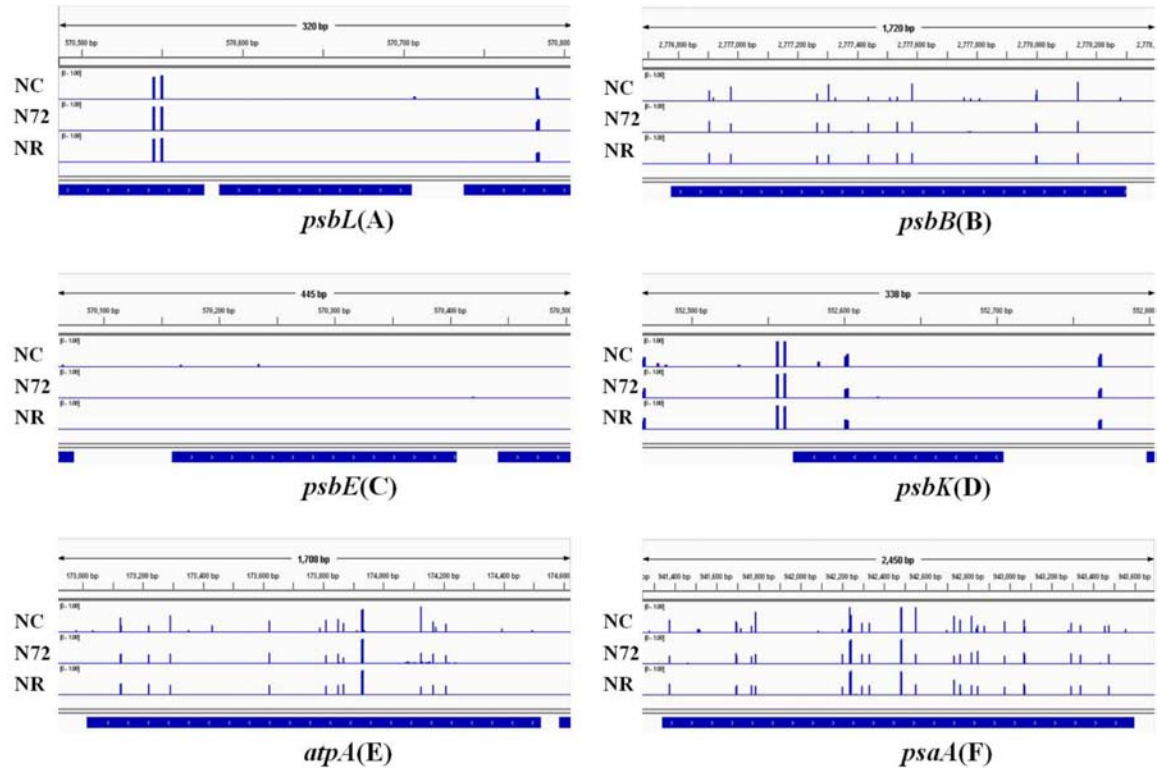

FIGURE 3 | DNA methylation status of six photosynthesis related genes under normal nitrogen (NC), nitrogen starvation (N72), and nitrogen recovery (NR). Gene body and 100 bp gene-flanking regions at upstream and downstream were covered. DNA methylation status of *psbL* is shown in **(A)**, *psbB* in **(B)**, *psbE* in **(C)**, *psbK* in **(D)**, *atpA* in **(E)**, and *psaA* in **(F)**. Height of blue bars represents the methylation level of each site for methylcytosine. No obvious difference in methylation was found among the three samples.

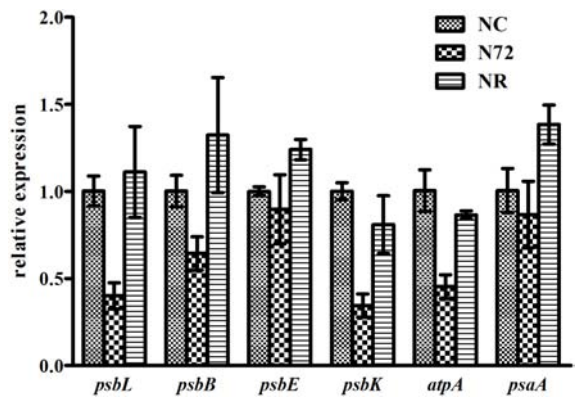

FIGURE 4 | Gene expressions under normal nitrogen (NC), nitrogen starvation (N72), and nitrogen recovery (NR). *rnpB* was used as internal reference. Data represent means ± SDs from three biological replicates. Expressions of all the six genes were down-regulated under nitrogen deficiency and almost restored to normal expression level when nitrogen was recovered.

96 h after nitrogen starvation (Krasikov et al., 2012). Our DMRs-related genes whose expression can be identified in the data were shown in Supplementary Data Sheet S1. Of the 1,042 genes in hyper-methylated regions, expression of 987 genes was identified in their transcriptome data, including 488 genes with down-regulated expression, 493 genes with up-regulated expression, and 6 genes with no changed expression. Likewise, of the 152 genes in hypo-methylated regions, 134 genes were found to express, including 64 genes with down-regulated expression, and 70 genes with up-regulated expression.

Growth of NC and NR Under Limited Nitrogen

To explore whether the transgenerational epigenetic modifications could benefit NR when encountering next time limited nitrogen resource, we recultured NC and NR in limited nitrogen ($N^{1/3}$ BG11), and compared their growth. Specific growth rates of NC and NR in $N^{1/3}$ BG11 were shown in **Supplementary Figure S6**. The specific growth rate was $0.194 \pm 0.002\ d^{-1}$ for NC, vs. $0.196 \pm 0.001\ d^{-1}$ for NR. Even though slightly higher growth rate seemed in NR, no statistically significant difference could be found ($p > 0.05$).

DISCUSSION

With SMRT sequencing, many methylomes were explored in bacterial. At first, Clark et al. (2012) introduced plasmids containing cloned distinct DNA methyltransferases into *E. coli*

mutant lacking endogenous DNA methyltransferases, and examined the methylation status of the plasmids. Then they investigated the methylation status of six bacterial genomes with the same technology, including *Geobacter metallireducens* GS-15, *Chromohalobacter salexigens*, *Vibrio breoganii* 1C-10, *Bacillus cereus* ATCC 10987, *Campylobacter jejuni* subsp. jejuni 81-176, and *C. jejuni* NCTC 11168 (Murray et al., 2012). Finally, Blow et al. (2016) investigated DNA modifications among 230 diverse bacterial and archaeal species and found lots of reproducibly methylated target motifs. All these studies have been largely limited to m^6A and m^4C due to the weak and somewhat diffuse SMRT signal generated by m^5C (Flusberg et al., 2010). The first genome-wide study of m^5C at base resolution was carried out by applying WGBS into *E. coli* and found cytosine methylation may take part in regulation of gene expression in stationary phase as a regulator (Kahramanoglou et al., 2012). With respect to cyanobacteria, SMRT sequencing showed the existence of m^6A in *Microcystis* (Zhao et al., 2017), and Hagemann et al. (2018) profiled the global DNA methylation (including m^6A, m^4C, and m^5C) in *Synechocystis* by using combination of SMRT sequencing and WGBS, which indicated 5-methylcytosine and m^4C in *Synechocystis* were in the context of m^5CGATCG and GGm^4CC, respectively. All these studies were conducted to determine the specificity of methyltransferases.

In our study, the CG methylation indeed corresponds to the m^5CGATCG, and CHG and CHH methylations comprise the GGm^4CC. Considering the methylation level change of CHG obviously differed from that of CHH in TEs (**Supplementary Figure S4**), we proposed the differential influence of bases downstream the methyltransferase target motif (GGm^4CC), and therefore distinguished CHG from CHH. A similar situation for the differential influence of base outside of the target motif was found in *E. coli* K12 of mid-exponential phase, where the methylation level for CmCCWGG was lower than [ATG]mCCWGG (mCCWGG was the methyltransferase target motif) (Kahramanoglou et al., 2012). Due to the partially resistance of m^4C to the bisulfite-mediated deamination, the methylation level of GGm^4CC context is much lower than that of m^5CGATCG (Hagemann et al., 2018). Consistent with this, our study also showed the methylation level of mCG methylation was higher than those of mCHG and mCHH.

Some features in *Synechocystis* were also identified in this study. Firstly, we found about 3.0% CG, 0.9% CHG, and 1.0% CHH were methylated in *Synechocystis*, which is different from chordata (31.1–80.3% CG, 0.17–1.22% CHG, and 0.12–0.91% CHH were methylated) and magnoliophyta (22.3–59.4% CG, 5.92–20.9% CHG, and 1.51–3.25% CHH were methylated) (Cokus et al., 2008; Feng et al., 2010), but similar with the eukaryotic microalga *Chlamydomonas reinhardtii* (5.4% CG, 2.6% CHG, and 2.5% CHH were methylated) (Feng et al., 2010). Then, we found no obvious differences in methylation level distribution among functional regions, which maybe implies that there is no preference of hyper/hypo-methylation to a certain functional region in *Synechocystis*. In contrast, in eukaryotic microalga *Chlorella variabilis*, CG within gene body is universally methylated while CG within promoter region is seldom methylated (Zemach et al., 2010). These differences are maybe due to the lack of nucleosomal structure and different protein factors in *Synechocystis*. It is also reported that hyper-methylated CG in nucleosome linkers is involved in nucleosome positioning and chromatin compaction (Huff and Zilberman, 2014).

In eukaryotes (Lindahl, 1981; Bird, 2002) and some bacteria such as *E. coli* (Roberts et al., 1985; Kahramanoglou et al., 2012; Militello et al., 2014) and *Helicobacter pylori* (Kumar et al., 2012, 2018) there are evidence for the regulation role of DNA methylation on gene expression. However, when the correlation between our DNA methylation data of N72 and the published transcriptome data at 96 h after nitrogen starvation (Krasikov et al., 2012) was investigated, neither preference of hyper-methylated region to down-regulated expression nor preference of hypo-methylated region to up-regulated expression were found, we therefore speculate that there was probably no correlation between methylation status and gene expression in *Synechocystis*. Also, we found the expression of some photosynthesis-related genes seem to be independent of their methylation status in *Synechocystis*.

With applying methylation sensitive amplified polymorphism analysis to *Oryza sativa* L, Kou, H.P. has proved a whole-generation nitrogen deficiency stress (10 or 20 mg L^{-1} nitrogen) could induce methylation alteration in the leaf-tissue of the stressed plants (Kou et al., 2011). In addition, with multiple electrophoresis-based polymorphism analysis techniques Yu et al. (2013) reported that nitrogen addition stress could also induced alterations in cytosine methylation patterns in natural populations of *Leymus chinensis*. However, these electrophoresis technology-based studies cannot provide the details about methylation change at base resolution. To investigate whether DNA methylation in bacterial could be influenced by surrounding environment, and if influenced, whether the altered DNA methylation pattern is inheritable, we compared the global DNA methylation among normal nitrogen (NC), nitrogen starvation (N72), and nitrogen recovery (NR) in the model cyanobacteria, *Synechocystis*. After 72 h of nitrogen deficiency about 40% mC sites were demethylated, but the methylation level of the remaining mC sites increased, which results in the almost unchanged overall methylation level. Because most *Synechocystis* cells can become dormant and survive as long as 45 days under nitrogen deficiency (lab observation), the altered DNA methylation pattern in N72 reflects the cellular response to nitrogen deficiency rather than the death or enrichment of some subpopulation. Conclusion can therefore be drawn that in cyanobacteria, environment stress could induce alternations in global DNA methylation pattern through reducing the number of mC sites but increasing the methylation level of the remaining mC sites.

The similar DNA methylation pattern in NR and N72 is interesting. Considering the cell doubling time for *Synechocystis* is about 23 h, cells in NR sample have already propagated

for about 12 generations since being transferred into normal nitrogen, i.e., one cell propagates for 12 times and becomes into 4,096 cells. However, NR regained only 1% of mC sites which demethylated after nitrogen deficiency and preserved about 45% of mC sites induced by nitrogen deficiency. Furthermore, mC sites in NR preserved high levels of methylation as those in N72. All these implied that the altered DNA methylation pattern induced by nitrogen deficiency stress could be partly inheritable even though the environment stress was removed, which demonstrates the environmental memory of epigenetic modifications in cyanobacteria, as in higher plants (Henderson and Jacobsen, 2007).

Environmental stress could generate particular defense epigenetic changes across generations in plants (Holeski et al., 2012), and in *Oryza sativa* L, alteration in DNA methylation induced by nitrogen deficiency stress could contribute the resistance to the nitrogen stress (20 mg L^{-1} nitrogen) for the non-stress suffered progenies which inherited the altered methylation pattern (Kou et al., 2011). The physiological significance of mC in bacterial genomes has raised enigmatic questions during several decades (Sanchez-Romero et al., 2015). Even though slightly higher growth rate seemed in NR cells, no significant growth difference between NC and NR can be found when being recultured in nitrogen limited condition. Considering that nitrogen deficiency stress lasts only 72 h, we speculate DNA methylation alteration in NR is not enough to increase the adaptation to nutrient limitation significantly. In the future examination of growth and genome-wide DNA methylation of *Synechocystis* having suffered nitrogen deficiency repeatedly or long term of nitrogen deficiency would provide more information. Furthermore, due to WGBS used in this study could not cover N^6-methyladenine, combination of SMRT sequencing and WGBS will therefore be needed for more comprehensive understanding of epigenetic adaptation to the ever changing environment in *Synechocystis*.

In summary, we confirmed the widely spread mC methylation and response of DNA methylation to nutrient depletion in *Synechocystis*. What's more, we verified the modified DNA methylation pattern could be partly inheritable in cyanobacteria. The results of this study might provide a primer to explore the wealth of information on the epigenetic transgenerational inheritance in prokaryotes.

AUTHOR CONTRIBUTIONS

JW contributed to conception and design of the study. LH, MD, PX, ZC, and YJ performed the experiments. LH, AL, and PX performed the statistical analysis. JW and LH wrote the first draft of the manuscript. JW, LH, and PX wrote the sections of the manuscript. YJ, MD, ZC, HL, and ZH contributed to manuscript revision. All authors read and approved the submitted version.

FUNDING

This work was supported by Guangdong Innovation Research Team Fund (2014ZT05S078), the Natural Science Foundation of SZU (#827–000081), the National Natural Science Foundation of China (31670116), and the Shenzhen Grant Plan for Science & Technology (JCYJ20160308095910917), used for the design of the study, data collection, data analysis, interpretation of data, and in writing the manuscript, respectively.

SUPPLEMENTARY MATERIAL

The Supplementary Material for this article can be found online at: https://www.frontiersin.org/articles/10.3389/fmicb.2018.01479/full#supplementary-material

FIGURE S1 | Methylation site ratio (sites for methylcytosine vs. plasmid nucleotides) of chromosomes and plasmids under normal nitrogen **(A)**, nitrogen starvation **(B)**, and nitrogen recovery **(C)**. No methylcytosine was detected in pSYSA_M, and pSYSG_M had the highest methylation site ratios in all the three samples.

FIGURE S2 | Box plot showing methylation level of sites for methylcytosine within gene body, intergenic region, upstream, and downstream region under normal nitrogen (NC), nitrogen starvation (N72), and nitrogen recovery (NR). No obvious difference in distribution of methylation level among different functional regions could be found.

FIGURE S3 | Venn diagram showing overlapped mC sites exclusively within transposable elements (TEs) **(A)** and overlapped TEs with mC sites **(B)** among normal nitrogen (NC), nitrogen starvation (N72), and nitrogen recovery (NR).

FIGURE S4 | Box plot showing methylation level of mC sites exclusively within TEs under normal nitrogen (NC), nitrogen starvation (N72), and nitrogen recovery (NR). Sites for methylcytosine under nitrogen starvation have higher-median and wider-range methylation level than those under normal nitrogen.

FIGURE S5 | The KEGG pathway enrichments of genes in hyper-methylated regions **(A)** and genes hypo-methylated regions **(B)** after nitrogen starvation.

FIGURE S6 | Specific growth rates of NC sample and NR sample re-cultured in $N^{1/3}$ BG11. Data represent means ± SDs from three biological replicates. The difference between the two samples was not significant ($p > 0.05$).

TABLE S1 | Primers used in this study.

TABLE S2 | Numbers and proportions of mC sites in each context under normal nitrogen (NC), nitrogen starvation (N72), and nitrogen recovery (NR).

TABLE S3 | Numbers and proportions of genes with mC sites under normal nitrogen (NC), nitrogen starvation (N72), and nitrogen recovery (NR).

REFERENCES

Adams, D. G. (1988). Isolation and restriction analysis of DNA from heterocysts and vegetative cells of cyanobacteria. *J. Gen. Microbiol.* 134, 2943–2949. doi: 10.1099/00221287-135-1-219

Bird, A. (2002). DNA methylation patterns and epigenetic memory. *Genes Dev.* 16, 6–21. doi: 10.1101/gad.947102

Blow, M. J., Clark, T. A., Daum, C. G., Deutschbauer, A. M., Fomenkov, A., Fries, R., et al. (2016). The epigenomic landscape of prokaryotes. *PLoS Genet.* 12:e1005854. doi: 10.1371/journal.pgen.1005854

Carvalho, R. H., Haberle, V., Hou, J., van Gent, T., Thongjuea, S., van Ijcken, W., et al. (2012). Genome-wide DNA methylation profiling of non-small cell lung carcinomas. *Epigenetics Chromatin* 5:9. doi: 10.1186/1756-8935-5-9

Catherine, Q., Susanna, W., Isidora, E. S., Mark, H., Aurelie, V., and Jean-Francois, H. (2013). A review of current knowledge on toxic benthic freshwater cyanobacteria–ecology, toxin production and risk management. *Water Res.* 47, 5464–5479. doi: 10.1016/j.watres.2013.06.042

Chan, S. W., Henderson, I. R., and Jacobsen, S. E. (2005). Gardening the genome: DNA methylation in *Arabidopsis thaliana*. *Nat. Rev. Genet.* 6, 351–360. doi: 10.1038/nrg1601

Clark, T. A., Murray, I. A., Morgan, R. D., Kislyuk, A. O., Spittle, K. E., Boitano, M., et al. (2012). Characterization of DNA methyltransferase specificities using single-molecule, real-time DNA sequencing. *Nucleic Acids Res.* 40:e29. doi: 10.1093/nar/gkr1146

Cokus, S. J., Feng, S., Zhang, X., Chen, Z., Merriman, B., Haudenschild, C. D., et al. (2008). Shotgun bisulphite sequencing of the *Arabidopsis* genome reveals DNA methylation patterning. *Nature* 452, 215–219. doi: 10.1038/nature06745

Conley, D. J., Paerl, H. W., Howarth, R. W., Boesch, D. F., Seitzinger, S. P., Havens, K. E., et al. (2009). Controlling eutrophication: Nitrogen and phosphorus. *Science* 323, 1014–1015. doi: 10.1126/science.1167755

Elser, J. J., Marzolf, E. R., and Goldman, C. R. (1990). Phosphorus and nitrogen limitation of phytoplankton growth in the fresh- water of North-America. *Can. J. Fish. Aquat. Sci.* 47, 1468–1477. doi: 10.1139/f90-165

Fang, G., Munera, D., Friedman, D. I., Mandlik, A., Chao, M. C., Banerjee, O., et al. (2012). Genome-wide mapping of methylated adenine residues in pathogenic *Escherichia coli* using single-molecule real-time sequencing. *Nat. Biotechnol.* 30, 1232–1239. doi: 10.1038/nbt.2432

Feng, S., Cokus, S. J., Zhang, X., Chen, P. Y., Bostick, M., Goll, M. G., et al. (2010). Conservation and divergence of methylation patterning in plants and animals. *Proc. Natl. Acad. Sci. U.S.A.* 107, 8689–8694. doi: 10.1073/pnas.1002720107

Flores, E., and Herrero, A. (2005). Nitrogen assimilation and nitrogen control in cyanobacteria. *Biochem. Soc. Trans.* 33(Pt 1), 164–167. doi: 10.1042/BST0330164

Flusberg, B. A., Webster, D. R., Lee, J. H., Travers, K. J., Olivares, E. C., Clark, T. A., et al. (2010). Direct detection of DNA methylation during single-molecule, real-time sequencing. *Nat. Methods* 7, 461–465. doi: 10.1038/nmeth.1459

Gao, L., Geng, Y., Li, B., Chen, J., and Yang, J. (2010). Genome-wide DNA methylation alterations of *Alternanthera philoxeroides* in natural and manipulated habitats: Implications for epigenetic regulation of rapid responses to environmental fluctuation and phenotypic variation. *Plant Cell Environ.* 33, 1820–1827. doi: 10.1111/j.1365-3040.2010.02186.x

Hagemann, M., Gartner, K., Scharnagl, M., Bolay, P., Lott, S. C., Fuss, J., et al. (2018). Identification of the DNA methyltransferases establishing the methylome of the cyanobacterium *Synechocystis* sp. PCC 6803. *DNA Res.* doi: 10.1093/dnares/dsy006 [Epub ahead of print].

Hauser, M. T., Aufsatz, W., Jonak, C., and Luschnig, C. (2011). Transgenerational epigenetic inheritance in plants. *Biochim. Biophys. Acta* 1809, 459–468. doi: 10.1016/j.bbagrm.2011.03.007

Heard, E., and Martienssen, R. A. (2014). Transgenerational epigenetic inheritance: myths and mechanisms. *Cell* 157, 95–109. doi: 10.1016/j.cell.2014.02.045

Henderson, I. R., and Jacobsen, S. E. (2007). Epigenetic inheritance in plants. *Nature* 447, 418–424. doi: 10.1038/nature05917

Holeski, L. M., Jander, G., and Agrawal, A. A. (2012). Transgenerational defense induction and epigenetic inheritance in plants. *Trends Ecol. Evol.* 27, 618–626. doi: 10.1016/j.tree.2012.07.011

Hu, L., Kong, R., and Xu, X. (2015). Autumnal increase in proportion of toxic *Microcystis* in Lake Taihu depends more on temperature adaptability than on effects of toxigenicity. *J. Appl. Microbiol.* 119, 744–752. doi: 10.1111/jam.12868

Huff, J. T., and Zilberman, D. (2014). Dnmt1-independent CG methylation contributes to nucleosome positioning in diverse eukaryotes. *Cell* 156, 1286–1297. doi: 10.1016/j.cell.2014.01.029

Ikeda, Y., and Kinoshita, T. (2009). DNA demethylation: a lesson from the garden. *Chromosoma* 118, 37–41. doi: 10.1007/s00412-008-0183-3

Kahramanoglou, C., Prieto, A. I., Khedkar, S., Haase, B., Gupta, A., Benes, V., et al. (2012). Genomics of DNA cytosine methylation in *Escherichia coli* reveals its role in stationary phase transcription. *Nat. Commun.* 3:886. doi: 10.1038/ncomms1878

Kanehisa, M., Araki, M., Goto, S., Hattori, M., Hirakawa, M., Itoh, M., et al. (2008). KEGG for linking genomes to life and the environment. *Nucleic Acids Res.* 36, D480–D484. doi: 10.1093/nar/gkm882

Kaneko, T., Sato, S., Kotani, H., Tanaka, A., Asamizu, E., Nakamura, Y., et al. (1996). Sequence analysis of the genome of the unicellular cyanobacterium *Synechocystis* sp. strain PCC 6803. II. Sequence determination of the entire genome and assignment of potential protein-coding regions (supplement). *DNA Res.* 3, 185–209. doi: 10.1093/dnares/3.3.185

Kaneko, T., Tanaka, A., Sato, S., Kotani, H., Sazuka, T., Miyajima, N., et al. (1995). Sequence analysis of the genome of the unicellular cyanobacterium *Synechocystis* sp. strain PCC 6803. I. Sequence features in the 1 Mb region from map positions 64% to 92% of the genome. *DNA Res.* 2, 153–166. doi: 10.1093/dnares/2.4.153

Kou, H. P., Li, Y., Song, X. X., Ou, X. F., Xing, S. C., Ma, J., et al. (2011). Heritable alteration in DNA methylation induced by nitrogen-deficiency stress accompanies enhanced tolerance by progenies to the stress in rice (*Oryza sativa* L.). *J. Plant Physiol.* 168, 1685–1693. doi: 10.1016/j.jplph.2011.03.017

Krasikov, V., Aguirre von Wobeser, E., Dekker, H. L., Huisman, J., and Matthijs, H. C. (2012). Time-series resolution of gradual nitrogen starvation and its impact on photosynthesis in the cyanobacterium *Synechocystis* PCC 6803. *Physiol. Plant.* 145, 426–439. doi: 10.1111/j.1399-3054.2012.01585.x

Krueger, F., and Andrews, S. R. (2011). Bismark: a flexible aligner and methylation caller for Bisulfite-Seq applications. *Bioinformatics* 27, 1571–1572. doi: 10.1093/bioinformatics/btr167

Kumar, R., Mukhopadhyay, A. K., Ghosh, P., and Rao, D. N. (2012). Comparative transcriptomics of *H. pylori* strains AM5, SS1 and their *hpyAVIBM* deletion mutants: possible roles of cytosine methylation. *PLoS One* 7:e42303. doi: 10.1371/journal.pone.0042303

Kumar, S., Karmakar, B. C., Nagarajan, D., Mukhopadhyay, A. K., Morgan, R. D., and Rao, D. N. (2018). N4-cytosine DNA methylation regulates transcription and pathogenesis in *Helicobacter pylori*. *Nucleic Acids Res.* 46, 3429–3445. doi: 10.1093/nar/gky195

Law, J. A., and Jacobsen, S. E. (2010). Establishing, maintaining and modifying DNA methylation patterns in plants and animals. *Nat. Rev. Genet.* 11, 204–220. doi: 10.1038/nrg2719

Lin, S., Haas, S., Zemojtel, T., Xiao, P., Vingron, M., and Li, R. (2011). Genome-wide comparison of cyanobacterial transposable elements, potential genetic diversity indicators. *Gene* 473, 139–149. doi: 10.1016/j.gene.2010.11.011

Lindahl, T. (1981). DNA methylation and control of gene expression. *Nature* 290, 363–364. doi: 10.1038/290363b0

Lira-Medeiros, C. F., Parisod, C., Fernandes, R. A., Mata, C. S., Cardoso, M. A., and Ferreira, P. C. (2010). Epigenetic variation in mangrove plants occurring in contrasting natural environment. *PLoS One* 5:e10326. doi: 10.1371/journal.pone.0010326

Lister, R., Pelizzola, M., Dowen, R. H., Hawkins, R. D., Hon, G., Tonti-Filippini, J., et al. (2009). Human DNA methylomes at base resolution show widespread epigenomic differences. *Nature* 462, 315–322. doi: 10.1038/nature08514

Livak, K. J., and Schmittgen, T. D. (2001). Analysis of relative gene expression data using real-time quantitative PCR and the $2^{-\Delta\Delta C_T}$ Method. *Methods* 25, 402–408. doi: 10.1006/meth.2001.1262

Lluch-Senar, M., Luong, K., Llorens-Rico, V., Delgado, J., Fang, G., Spittle, K., et al. (2013). Comprehensive methylome characterization of *Mycoplasma genitalium* and *Mycoplasma pneumoniae* at single-base resolution. *PLoS Genet.* 9:e1003191. doi: 10.1371/journal.pgen.1003191

Matveyev, A. V., Young, K. T., Meng, A., and Elhai, J. (2001). DNA methyltransferases of the cyanobacterium *Anabaena* PCC 7120. *Nucleic Acids Res.* 29, 1491–1506. doi: 10.1093/nar/29.7.1491

Meeks, J. C., Elhai, J., Thiel, T., Potts, M., Larimer, F., Lamerdin, J., et al. (2001). An overview of the genome of *Nostoc punctiforme*, a multicellular, symbiotic cyanobacterium. *Photosynth. Res.* 70, 85–106. doi: 10.1023/A:1013840025518

Menzel, S., Bouchnak, R., Menzel, R., and Steinberg, C. E. (2011). Dissolved humic substances initiate DNA-methylation in cladocerans. *Aquat. Toxicol.* 105, 640–642. doi: 10.1016/j.aquatox.2011.08.025

Militello, K. T., Mandarano, A. H., Varechtchouk, O., and Simon, R. D. (2014). Cytosine DNA methylation influences drug resistance in *Escherichia coli* through increased *sugE* expression. *FEMS Microbiol. Lett.* 350, 100–106. doi: 10.1111/1574-6968.12299

Murray, I. A., Clark, T. A., Morgan, R. D., Boitano, M., Anton, B. P., Luong, K., et al. (2012). The methylomes of six bacteria. *Nucleic Acids Res.* 40, 11450–11462. doi: 10.1093/nar/gks891

Navarro-Martin, L., Vinas, J., Ribas, L., Diaz, N., Gutierrez, A., Di Croce, L., et al. (2011). DNA methylation of the gonadal aromatase (*cyp19a*) promoter is involved in temperature-dependent sex ratio shifts in the European sea bass. *PLoS Genet.* 7:e1002447. doi: 10.1371/journal.pgen.1002447

Padhy, R. N., Hottat, F. G., Coene, M. M., and Hoet, P. P. (1988). Restriction analysis and quantitative estimation of methylated bases of filamentous and unicellular cyanobacterial DNAs. *J. Bacteriol.* 170, 1934–1939. doi: 10.1128/jb.170.4.1934-1939.1988

Palmer, B. R., and Marinus, M. G. (1994). The *dam* and *dcm* strains of *Escherichia coli*–a review. *Gene* 143, 1–12. doi: 10.1016/0378-1119(94)90597-5

Patterson, K., Molloy, L., Qu, W., and Clark, S. (2011). DNA methylation: Bisulphite modification and analysis. *J. Vis. Exp.* 56:3170. doi: 10.3791/3170

Pukkila, P. J., Peterson, J., Herman, G., Modrich, P., and Meselson, M. (1983). Effects of high levels of DNA adenine methylation on methyl-directed mismatch repair in *Escherichia coli*. *Genetics* 104, 571–582.

Qiao, J., Huang, S., Te, R., Wang, J., Chen, L., and Zhang, W. (2013). Integrated proteomic and transcriptomic analysis reveals novel genes and regulatory mechanisms involved in salt stress responses in *Synechocystis* sp. PCC 6803. *Appl. Microbiol. Biotechnol.* 97, 8253–8264. doi: 10.1007/s00253-013-5139-8

Reisenauer, A., Kahng, L. S., McCollum, S., and Shapiro, L. (1999). Bacterial DNA methylation: a cell cycle regulator? *J. Bacteriol.* 181, 5135–5139.

Rippka, R., Deruelles, J., Waterbury, J. B., Herdman, M., and Stanier, R. Y. (1979). Generic assignment, strain histories of pure cultures of cyanobacteria. *J. Gen. Microbiol.* 111, 1–61. doi: 10.1099/00221287-111-1-1

Roberts, D., Hoopes, B. C., McClure, W. R., and Kleckner, N. (1985). IS10 transposition is regulated by DNA adenine methylation. *Cell* 43, 117–130. doi: 10.1016/0092-8674(85)90017-0

Sanchez-Romero, M. A., Cota, I., and Casadesus, J. (2015). DNA methylation in bacteria: from the methyl group to the methylome. *Curr. Opin. Microbiol.* 25, 9–16. doi: 10.1016/j.mib.2015.03.004

Scharnagl, M., Richter, S., and Hagemann, M. (1998). The cyanobacterium *Synechocystis* sp. strain PCC 6803 expresses a DNA methyltransferase specific for the recognition sequence of the restriction endonuclease PvuI. *J. Bacteriol.* 180, 4116–4122.

Skinner, M. K. (2014). Environmental stress and epigenetic transgenerational inheritance. *BMC Med.* 12:153. doi: 10.1186/s12916-014-0153-y

Stomp, M., Huisman, J., Voros, L., Pick, F. R., Laamanen, M., Haverkamp, T., et al. (2007). Colourful coexistence of red and green picocyanobacteria in lakes and seas. *Ecol. Lett.* 10, 290–298. doi: 10.1111/j.1461-0248.2007.01026.x

Thomas, R. Q., Brookshire, E. N., and Gerber, S. (2015). Nitrogen limitation on land: How can it occur in earth system models? *Glob. Chang. Biol.* 21, 1777–1793. doi: 10.1111/gcb.12813

Vilkaitis, G., and Klimasauskas, S. (1999). Bisulfite sequencing protocol displays both 5-methylcytosine and N4-methylcytosine. *Anal. Biochem.* 271, 116–119. doi: 10.1006/abio.1999.4116

Vitousek, P. M., and Howarth, R. W. (1991). Nitrogen limitation on land and in the sea: How can it occur? *Biogeochemistry* 13, 87–115. doi: 10.1007/BF00002772

Wang, J., Chen, L., Chen, Z., and Zhang, W. (2015). RNA-seq based transcriptomic analysis of single bacterial cells. *Integr. Biol.* 7, 1466–1476. doi: 10.1039/c5ib00191a

Whitton, B. A., and Potts, M. (eds) (2000). "The ecology of cyanobacteria: their diversity in time and space," in *Ecology of Cyanobacteria Their Diversity in Time & Space*, (Berlin: Springer).

Wilson, G. G., and Murray, N. E. (1991). Restriction and modification systems. *Annu. Rev. Genet.* 25, 585–627. doi: 10.1146/annurev.ge.25.120191.003101

Wolk, C. P. (1996). Heterocyst formation. *Annu. Rev. Genet.* 30, 59–78. doi: 10.1146/annurev.genet.30.1.59

Wu, J., Mao, X., Cai, T., Luo, J., and Wei, L. (2006). KOBAS server: a web-based platform for automated annotation and pathway identification. *Nucleic Acids Res.* 34, W720–W724. doi: 10.1093/nar/gkl167

Yu, Y., Yang, X., Wang, H., Shi, F., Liu, Y., Liu, J., et al. (2013). Cytosine methylation alteration in natural populations of *Leymus chinensis* induced by multiple abiotic stresses. *PLoS One* 8:e55772. doi: 10.1371/journal.pone.0055772

Zemach, A., McDaniel, I. E., Silva, P., and Zilberman, D. (2010). Genome-wide evolutionary analysis of eukaryotic DNA methylation. *Science* 328, 916–919. doi: 10.1126/science.1186366

Zhao, L., Li, L., Gan, N., Humbert, J.-F., and Song, L. (2017). "Insight on the genomics and epigenetics of Microcystis," in *Proceedings of the XIX International Botanical Congress Abstract Book I, T5-15-0 4* (Bratislava: International Association for Plant Taxonomy).

Conflict of Interest Statement: The authors declare that the research was conducted in the absence of any commercial or financial relationships that could be construed as a potential conflict of interest.

frontiers in Microbiology

ORIGINAL RESEARCH
published: 15 August 2018
doi: 10.3389/fmicb.2018.01739

The Culture Environment Influences Both Gene Regulation and Phenotypic Heterogeneity in *Escherichia coli*

*Ashley Smith[1,2], Agnieszka Kaczmar[1,2], Rosemary A. Bamford[1,2], Christopher Smith[2], Simona Frustaci[1], Andrea Kovacs-Simon[2], Paul O'Neill[2], Karen Moore[2], Konrad Paszkiewicz[2], Richard W. Titball[2] and Stefano Pagliara[1,2]**

[1] Living Systems Institute, University of Exeter, Exeter, United Kingdom, [2] Biosciences, University of Exeter, Exeter, United Kingdom

Microorganisms shape the composition of the medium they are growing in, which in turn has profound consequences on the reprogramming of the population gene-expression profile. In this paper, we investigate the progressive changes in pH and sugar availability in the medium of a growing *Escherichia coli* (*E. coli*) culture. We show how these changes have an effect on both the cellular heterogeneity within the microbial community and the gene-expression profile of the microbial population. We measure the changes in gene-expression as *E. coli* moves from lag, to exponential, and finally into stationary phase. We found that pathways linked to the changes in the medium composition such as ribosomal, tricarboxylic acid cycle (TCA), transport, and metabolism pathways are strongly regulated during the different growth phases. In order to quantify the corresponding temporal changes in the population heterogeneity, we measure the fraction of *E. coli* persisters surviving different antibiotic treatments during the various phases of growth. We show that the composition of the medium in which β-lactams or quinolones, but not aminoglycosides, are dissolved strongly affects the measured phenotypic heterogeneity within the culture. Our findings contribute to a better understanding on how the composition of the culture medium influences both the reprogramming in the population gene-expression and the emergence of phenotypic variants.

Keywords: phenotypic heterogeneity, *Escherichia coli*, persisters, metabolism, bacterial physiology, antibiotics, gene-expression profiling, KEGG pathways

OPEN ACCESS

Edited by:
Daniela De Biase, Sapienza Università di Roma, Italy

Reviewed by:
Bei-Wen Ying, University of Tsukuba, Japan
Peter Adrian Lund, University of Birmingham, United Kingdom

***Correspondence:**
Stefano Pagliara
s.pagliara@exeter.ac.uk

Specialty section:
This article was submitted to Microbial Physiology and Metabolism, a section of the journal Frontiers in Microbiology

Received: *11 March 2018*
Accepted: *11 July 2018*
Published: *15 August 2018*

Citation:
Smith A, Kaczmar A, Bamford RA, Smith C, Frustaci S, Kovacs-Simon A, O'Neill P, Moore K, Paszkiewicz K, Titball RW and Pagliara S (2018) The Culture Environment Influences Both Gene Regulation and Phenotypic Heterogeneity in Escherichia coli. Front. Microbiol. 9:1739. doi: 10.3389/fmicb.2018.01739

INTRODUCTION

Within isogenic populations there may be substantial cell-to-cell heterogeneity in terms of metabolic activity (Nikolic et al., 2013; Şimşek and Kim, 2018), growth rate (Kotte et al., 2014), substrate assimilation (Sheik et al., 2016), compound secretion (Veening et al., 2008), virulence (Arnoldini et al., 2014), and resistance to stress (Balaban et al., 2004). This heterogeneity has been observed across all the domains of life and arises from the inherent random nature of biochemical reactions (Elowitz et al., 2002; Kaern et al., 2005; Lidstrom and Konopka, 2010). Phenotypic heterogeneity may allow some individual cells to survive shifts in the environmental conditions,

and thus permitting the population to withstand fluctuating environments (Balaban et al., 2004; Ackermann, 2015; Venturelli et al., 2015; Schreiber et al., 2016; Bódi et al., 2017). It has also been suggested that phenotypic heterogeneity can accelerate evolutionary adaptation to different environmental challenges (Beaumont et al., 2009; New et al., 2014). The culture environment in turn affects the population transcriptome. For instance, pH has been shown to regulate genes involved in catabolism and transport (Hayes et al., 2006), whereas glucose-lactose diauxie induces the downregulation of amino acid biosynthesis and aerobic metabolism genes (Chang et al., 2002). Additionally, changes in gene-expression levels in response to nutritional changes are strongly linked to growth rate and cell size (Weart et al., 2007; Scott et al., 2010; Chien et al., 2012; Yao et al., 2012). Moreover, it has been suggested that a reduction in cell size increases the heterogeneity in gene-expression within the population (Kaern et al., 2005).

However, only a small subpopulation of bacteria shows observable physiological variations, such as growth rate that is more than twofold different than the remainder of the population (Lidstrom and Konopka, 2010). Therefore, the identification and study of such small subpopulations can be challenging but can be simplified by analyzing the functional consequences of a given case of phenotypic heterogeneity (Ackermann, 2015).

For example, persister cells are a small proportion of a clonal microbial population that can survive otherwise lethal doses of antibiotics and resume growth shortly after removing the antibiotic (Hansen et al., 2008; Lewis, 2010; Maisonneuve et al., 2013), but without acquiring genetic changes that confer antibiotic resistance. In this paper we used persister cell formation as a proxy for phenotypic heterogeneity. Persister cells have been observed across all the domains of life (Lewis, 2010; Hangauer et al., 2017; Megaw and Gilmore, 2017) and are believed to contribute to the survival of bacteria in biofilms exposed to antibiotics (LaFleur et al., 2006; Lewis, 2010) and to chronic infections in immunosuppressed hosts (Mulcahy et al., 2010; Maisonneuve and Gerdes, 2014).

Persisters can form stochastically as a result of fluctuations in gene-expression (Amato et al., 2013). However, a variety of environmental factors favor persister formation, including subinhibitory concentrations of antibiotics (Amato et al., 2013), nutrient limitation (Vega et al., 2012), intra-species interactions (Bernier et al., 2013), starvation (Fung et al., 2010), and in the case of pathogens, interactions with the host (Helaine et al., 2014). Amato et al. (2013) showed that diauxic growth contributes to persister cell formation, whereas another study by the same group showed that nutrient transitions contributed to persister formation within bacterial biofilms (Amato and Brynildsen, 2014). Keren et al. reported that the number of ampicillin or ofloxacin persisters increased from lag to stationary phase (Keren et al., 2004a). However, the temporal windows when there are substantial increases in the formation of persisters to different antibiotics during growth of *Escherichia coli* (*E. coli*) on lysogeny broth (LB) have yet to be defined. Moreover, gene-expression profiling has been carried out on both exponential and stationary phase *E. coli* O157 growing on 3-(*N*-morpholino)propanesulfonic acid (MOPS) minimal medium supplemented with 0.1% glucose (Bergholz et al., 2007). However, the changes in the transcriptome throughout the growth cycle of *E. coli* K12 growing in LB remain to be determined, despite this being an experimental model system employed in microbiology, biotechnology, and molecular biology.

In this paper, we report the changes in sugar levels and pH and the associated reprogramming in gene-expression during the transitions between the different phases of *E. coli* growth. We then investigate the phenotypic heterogeneity within the *E. coli* population throughout the growth cycle by using persister formation, in response to ampicillin, gentamicin, or ofloxacin as a proxy for studying cellular heterogeneity. Our findings will be instrumental for investigations into the mechanisms underlying microbial survival in transitioning environments and provide key transcriptomic data for a commonly used model in many bacterial studies.

MATERIALS AND METHODS

Chemicals and Culture Preparation

All chemicals were purchased from Fisher Scientific or Sigma-Aldrich unless otherwise stated. LB medium (10 g/L tryptone, 5 g/L yeast extract, and 10 g/L NaCl, Melford) and LB agar plates (LB with 15 g/L agar) were used for planktonic growth and enumeration of colony-forming units (CFUs), respectively. *E. coli* BW25113 was purchased from Dharmacon (GE Healthcare). A single colony of *E. coli* BW25113 was grown in 200 ml fresh LB in a shaking incubator at 200 rpm and 37°C for 17 h (**Supplementary Figure S1A**). After 17 h incubation, the culture was diluted 1:1000 in fresh LB and growth was measured hourly by taking three aliquots that were then centrifuged (13,000 *g* for 5 min), the supernatant was removed, the pellet was resuspended in phosphate-buffered saline (PBS), and serial dilutions were plated on LB agar for CFU counts (**Supplementary Figures S1B,C,H**). This experiment allowed us to determine that the culture was in stationary phase at t = 17 h (left axis in **Supplementary Figure S2**). In order to avoid introducing any bias in our measurements (Luidalepp et al., 2011), we used the same LB autoclaving conditions in all our assays. The relatively small error bars in our measurements and in other recent reports (Orman and Brynildsen, 2016; Radzikowski et al., 2016) demonstrate the suitability of autoclaved LB for these microbiological assays.

Characterizing the Bacterial Environment

A culture was prepared as described above and eighty-one 100 μl aliquots were added to individual wells of a 96-well plate (three technical replicates in biological triplicates for each of the nine time points were investigated). The remaining wells were filled with fresh LB for blank measurements. The plate was placed in a preheated (37°C) Infinite® 200 PRO plate reader (TECAN) shaking at 200 rpm. To quantify bacterial growth in this assay, optical density at 595 nm (OD_{595}) was measured hourly in nine selected wells for each time point. Bacterial growth measured via the plate reader method (right axis in **Supplementary Figure S2**) was comparable to that measured via

CFU counts in cultures growing in 200 ml flasks (left axis in **Supplementary Figure S2**). To quantify the amount of reducing sugars, preheated (100°C) Benedict's reagent (Sigma-Aldrich) was then added to the same wells according to the manufacturer's instructions and absorbance at 490 nm was measured after 15 min incubation. The absolute sugar concentration was determined by extrapolation through a standard curve of known glucose concentration (**Supplementary Figure S3**). This was obtained by adding glucose in MilliQ water at concentrations of 125, 250, 500, or 1000 μM in triplicate in a 96-well plate. Preheated (100°C) Benedict's reagent was then added to the same wells and the absorbance at 490 nm was measured after a 15 min incubation. The average reading from three wells containing only MilliQ water was subtracted from the readings of the glucose containing wells. These blank subtracted readings are reported in **Supplementary Figure S3** together with a linear regression fitting of the experimental data. In order to measure the culture pH, the probe of a PH-100 ATC pH meter (with an accuracy of pH 0.01, Voltcraft) was immersed in a separate culture prepared as described above and the pH was recorded hourly. The measurements were taken in at least three biological replicates.

Transcriptomic and qPCR Analysis

A culture was prepared as described above. Immediately after dilution (0 h), 500 μl aliquots were taken from the overnight (17 h) culture and 1, 2, 3, 3.5, 4, 4.5, 5, 6, or 7 h after dilution in fresh LB (1:1000) and were incubated at 200 rpm and 37°C as described above. The RNA of the cells contained in each aliquot was stabilized using RNAprotect Bacteria Reagent (Qiagen). Extraction was performed with RNeasy Mini Kit (Qiagen) and DNA removal with DNase I (RNase-free, Ambion), using the recommended protocols. RNA concentration and purity were determined using a 2100 Bioanalyzer (Agilent). cDNA libraries from all samples with an RNA integrity number (RIN) greater than eight were prepared and then sequenced using Illumina HiSeq 2500. The paired reads were trimmed and sequencing adaptors were removed using fastq-mcf. RNA ERCC spike-in control sequences were removed using bowtie version 1.0.0, and the remaining reads were aligned to the reference genome using tophat2 version 2.1.0. The gene-expression was quantified using HTseq-count. DESeq2 v1.6.3 was used to normalize the raw transcript reads for all genes by using the median-ratio normalization method and for library size (Love et al., 2014). To reduce the number of false-positive results, the $\log_2$ fold changes were shrunk toward zero for lowly expressed genes and the adjusted *p*-values were calculated using a false discovery rate (FDR) of 0.1. We then determined the $\log_2$ fold change in the normalized transcript reads for each gene at different time points, relative to the normalized transcript reads in the overnight stationary phase sample (t = 17 h). In order to identify the variables that best differentiate the data, as well as to determine how well-clustered the replicates were, we performed principal component analysis (PCA) using DESeq2 and a built-in R method (prcomp) on the top 500 expressed genes. These genes were normalized using a regularized log transform prior to PCA to allow better visualization of the trends and clusters that may otherwise remain hidden. The data shown represent the first (PC1) and second principal components (PC2). The clustering of the time point replicates indicates a high level of reproducibility in our data. During the three different growth phases the top 10% of upregulated and downregulated genes, based on their $\log_2$ fold change, were identified and goseq was used to identify overrepresented pathways in the Kyoto Encyclopedia of Genes and Genomes (KEGG) (Ogata et al., 1999; Kanehisa et al., 2016, 2017). In order to check the results, qPCR was performed on the same aliquots on a StepOnePlus™ Real-Time PCR System for selected genes. Both RNA-seq and qPCR measurements were performed in biological triplicates.

MIC Determination

The minimum inhibitory concentration (MIC) of the employed antibiotics against *E. coli* BW25113 was determined using a 96-well plate method. *E. coli* was grown for 17 h in LB containing different concentrations of ampicillin (0.5–512 μg ml^{-1}), ofloxacin (0.0625–64 μg ml^{-1}), or gentamicin (0.125–128 μg ml^{-1}) and the OD_{595} was measured hourly. The MICs were measured as the lowest concentrations at which the OD_{595} was the same as the control (bacteria-free LB) and were determined as 5, 4, and 0.125 μg ml^{-1} for ampicillin, gentamicin, and ofloxacin, respectively.

Persister Enumeration

A culture was prepared as described above and during mid-exponential phase (t = 3 h after dilution) the respective antibiotics were added to the culture to reach a concentration of 25 × MIC, with persister levels typically not varying above this concentration of antibiotics (Johnson and Levin, 2013). Every 30 min an aliquot was taken from the treated culture, centrifuged (13,000 *g* for 5 min), re-suspended in PBS, and plated on LB agar plates. The plates were incubated and CFUs were determined the following day. For each antibiotic, the fraction of persister cells plateaued after 3 h of treatment, as previously reported (Johnson and Levin, 2013), confirming that we were studying persister subpopulations rather than antibiotic-tolerant populations (Brauner et al., 2016).

In order to enumerate persisters based on the effect of different antibiotics during the various phases of growth, a culture was prepared as described above (**Supplementary Figures S1A,B**). Nine 500 μl aliquots were withdrawn from the growing culture hourly (**Supplementary Figures S1C,E**). Three of them were used for untreated controls, the aliquots were centrifuged (13,000 *g* for 5 min), supernatant was removed, the pellet was resuspended in PBS, and serial dilutions were plated on LB agar (**Supplementary Figure S1H**). Three aliquots were supplied with 500 μl LB (1:1 dilution) containing 50 × MIC of one of the three above specified antibiotics (final concentration 25 × MIC) and were returned to the shaking incubator (**Supplementary Figure S1F**). After 3 h, these aliquots were centrifuged, the supernatant was removed, and the pellet was re-suspended in PBS. Serial dilutions were then performed and plated on LB agar (**Supplementary Figure S1I**). Three aliquots were injected with 10 μl of one of the three above specified antibiotics to reach a final concentration of 25 × MIC and returned to the shaking

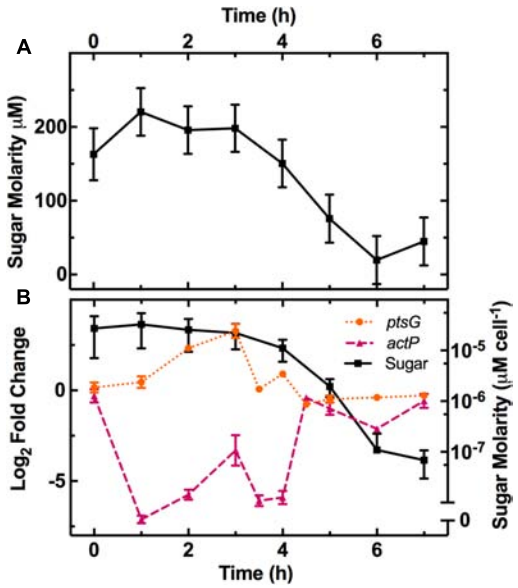

FIGURE 1 | Characterization of the physical changes in the bacterial environment. **(A)** Dependence of the concentration of reducing sugars in the culture on the time elapsed from dilution in LB medium of an overnight *E. coli* culture. **(B)** Dependence of sugar concentration per cell (squares, right axis) and the expression of the glucose (*ptsG*, circles, left axis) and acetate (*actP*, triangles, left axis) related genes on time elapsed from dilution in LB medium. Gene-expression is reported as the $\log_2$ fold change with respect to the measurements on the overnight samples (t = 17 h). Data and error bars are the mean and standard error of the mean (SEM) calculated on measurements obtained in biological triplicate.

incubator (**Supplementary Figure S1G**). After 3 h these aliquots were centrifuged, the supernatant was removed, the pellet was re-suspended in PBS, serially diluted and plated on LB agar (**Supplementary Figure S1J**).

RESULTS

Nutritional and Chemical Environment of a Growing *E. coli* Culture

We investigated how the sugar content and the pH of the growth medium changed over time. Notably, both quantities are known to affect the outcome of antibiotic treatment (Allison et al., 2011; Cama et al., 2014). The measured concentration of fermentable sugars in the LB medium we employed was 163 ± 35 μM. A previous study found that LB contained less than 100 μM fermentable sugars by using a genetic approach based on a *hemA* deletion mutant unable to grow in the absence of fermentable sugars (Sezonov et al., 2007). This discrepancy could be due to the different sources of LB and the different techniques used to quantify the sugar concentrations. This further emphasizes the added value of carrying out the simple assay described in Section 3.2 to quantify the concentration of fermentable sugars during bacterial growth.

After *E. coli* inoculation into LB medium, we measured the remaining sugar concentration at various intervals throughout the growth cycle (**Figure 1A**). We calculated the corresponding concentration of sugar available per bacterium (squares in **Figure 1B**) by dividing the measured sugar concentration by the measured number of bacteria in the culture (full symbols in **Supplementary Figure S2**, left axis). This revealed a one order of magnitude decrease in the sugar available per bacterium between 3 and 6 h after inoculation, when the culture transitioned from exponential to stationary growth-phase.

We also measured the pH of the culture throughout the growth cycle (**Supplementary Figure S4**). The pH decreased from 6.8 and reached it's most acidic value of 6.2 during the exponential phase at t = 4 h, then rose up to a maximum of 7.0 during the stationary phase at t = 7 h. We explain this finding by considering that the culture environment is acidified by the excretion of acetate during aerobic fermentation, resulting from bacterial growth on carbohydrates during exponential phase (Kleman and Strohl, 1994). However, upon exhaustion of these carbohydrates, the bacteria use alternative carbon sources such as amino acids and other gluconeogenic substrates (Sezonov et al., 2007), resulting in the production and excretion of ammonia that increases the culture pH. Losen et al. (2004) did not observe the same growth-phase dependence for the pH of a growing *E. coli* culture. However, their assay was performed using a different *E. coli* strain (ATCC 53323) and different culture conditions including a different LB supplier, a one order of magnitude smaller LB volume and a one order of magnitude higher inoculum concentration. All together, our data complement our existing knowledge on the changes occurring in the medium composition during *E. coli* growth in LB (Losen et al., 2004; Sezonov et al., 2007).

Changes in Gene-Expression During the Growth Cycle

The gene-expression profile of bacterial populations is profoundly affected by changes in the culture (Hua et al., 2004; Bergholz et al., 2007; Klumpp and Hwa, 2015; Vital et al., 2015). However, to the best of our knowledge, this is the first study reporting the progressive reprogramming of the gene-expression profile of *E. coli* growing in LB throughout the different phases of growth.

In order to study the effect of the changing nutritional or chemical environment of the culture on the population transcriptome, we measured gene-expression profile in aliquots taken at different stages of growth in biological triplicates. **Supplementary Table S1** reports, for each gene, the mean and SEM of the normalized transcript reads measured in the samples taken at t = 17 h post inoculation. **Supplementary Table S1** also reports the mean and SEM of the $\log_2$ fold change in normalized transcript reads in the samples taken at t = 0, 1, 2, 3, 3.5, 4, 4.5, 5, 6, or 7 h post inoculation relative to the t = 17 h sample. The mean relative error, averaged on the relative errors for the transcript reads of all genes at t = 17 h, is 24%, thus confirming good reproducibility across biological replicates. Indeed, this corresponds to a $\log_2$ fold change of 0.31, whereas in comparison, the average absolute $\log_2$ fold change in gene-expression at t = 2 h relative to t = 17 h is 1.9. We further confirmed the changes in

gene-expression of selected genes using qPCR (**Supplementary Figure S5**).

The PCA allowed clustering of the transcriptome profiles measured from the different biological replicates at each time point (**Figure 2A**), demonstrating good reproducibility of our cultures grown in shake flasks without the need for fermenter cultivation (Chang et al., 2002). The transcriptomes from adjacent time points clustered close to each other forming a nearly complete cycle, with the transcriptome measured at t = 0 being close to that measured at t = 7 h. Similarly, a cyclic transcriptional response of *E. coli* to acid adaptation was previously reported (Stincone et al., 2011). Furthermore, the transcriptomes measured at t = 0 and t = 1 h are simultaneously similar in terms of PC2 but different in terms of PC1 (**Figure 2B**), suggesting that part of the transcriptome rapidly adapts to changes in the nutritional environment. The population transcriptome then becomes increasingly different in PC1 (circles in **Figure 2B**). This suggests that the regulation of the genes used for PC1 analysis allows the culture to progressively adapt to an environment unfavorable for growth, as explained in the discussion below. On the other hand, the PC2 variance reveals that the transcriptomes at t = 3.5 and t = 4 h differ the most from the transcriptome at t = 0 h. The PC2 variance for the t = 0 h transcriptome is instead similar to that of the t = 7 h transcriptome, a trend similar to the temporal dependence of the average division rate (**Supplementary Figure S6**) and a mirror image of the trend in pH (**Supplementary Figure S4**). This suggests that the regulation of the genes used in the PC2 analysis governs the cell division and metabolism machineries, which in turn drive the changes in the environmental pH. This is, to the best of our knowledge, the first time PCA is carried out on the transcriptome of an *E. coli* culture throughout its growth cycle.

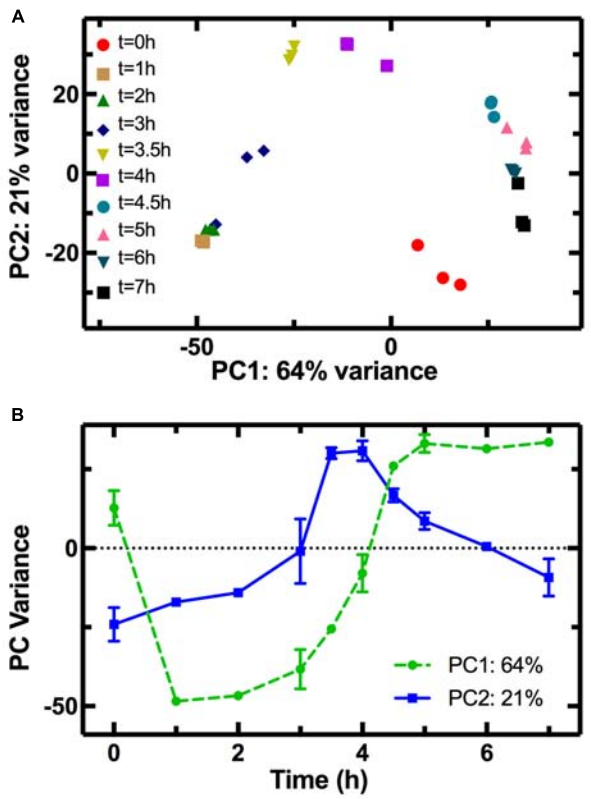

FIGURE 2 | Principal component analysis (PCA) of the transcriptome at different stages of growth. **(A)** Correlation between the first (PC1) and second (PC2) principal components of the transcriptome of samples taken in biological triplicate at different time points during *E. coli* growth in LB. The clustering of transcriptomes from the same time points confirms the reproducibility of our measurements. Furthermore, adjacent time points clustered close to each other forming a nearly complete cycle, the transcriptome measured at t = 0 being close to that measured at t = 7 h. **(B)** The temporal dependence of PC1 (circles) resembles that of *E. coli* growth (**Figure 3A**) suggesting that genes used for PC1 may play a role in adaptation to the exhaustion of nutrients, whereas the temporal dependence of PC2 (squares) resembles that of the culture pH (**Supplementary Figure S4**) suggesting that these genes may be involved in the adaptation to pH changes.

The decrease in sugar levels in the medium parallels the regulation of a set of genes including *ptsG*, a glucose-specific phosphotransferase (Luli and Strohl, 1990), and the dedicated acetate uptake system *actP* (Luli and Strohl, 1990; **Figure 1B**). Expression of *ptsG* increases during the lag phase (circles in **Figure 1B**) when fresh medium is added to the culture and then decreases as the sugar concentration per bacterium decreases after t = 3 h (squares in **Figure 1B**). Bergholz et al. did not investigate gene-expression profile during lag phase but reported a similar downregulation of *ptsG* with a -3 $\log_2$ fold change between 4.5 and 5 h growth. In comparison, *actP* expression rapidly decreases between t = 0 h to t = 1 h as fresh medium is added to the culture before increasing at t = 4 h as sugars are metabolized and acetate becomes available in the environment (triangles in **Figure 1B**) as previously reported (Bergholz et al., 2007).

The growth curve in **Figure 3A** shows the three characteristic phases of growth: lag phase between t = 0 h and t = 2 h, exponential phase from t = 2 h to t = 5 h, and stationary phase from t = 5 h onward. We considered gene regulation during each of these phases based on the $\log_2$ fold change in transcript levels at t = 2 h relative to t = 0 h, t = 5 h relative to t = 2 h, and t = 7 h relative to t = 5 h, respectively. Furthermore, for each growth phase we grouped the top 10% of upregulated genes, from the 4313 genes analyzed. Then for each KEGG pathway we determined the number of genes that were in the top 10% group. We then used goseq to calculate the probability of this number occurring when compared to the total number of genes in the pathway (p-value in **Figure 3**). For example, the KEGG pathway "Microbial metabolism in diverse environments" has 201 associated genes. Therefore, in the top 10% group of the upregulated genes from all pathways one would expect to find 20 genes associated to this KEGG pathway. However, in the top 10% group of upregulated genes during exponential phase, we identified 54 genes from the "Microbial metabolism in diverse environments" pathway. Therefore, this pathway was overrepresented in the 10% group of upregulated genes during exponential phase with a p-value

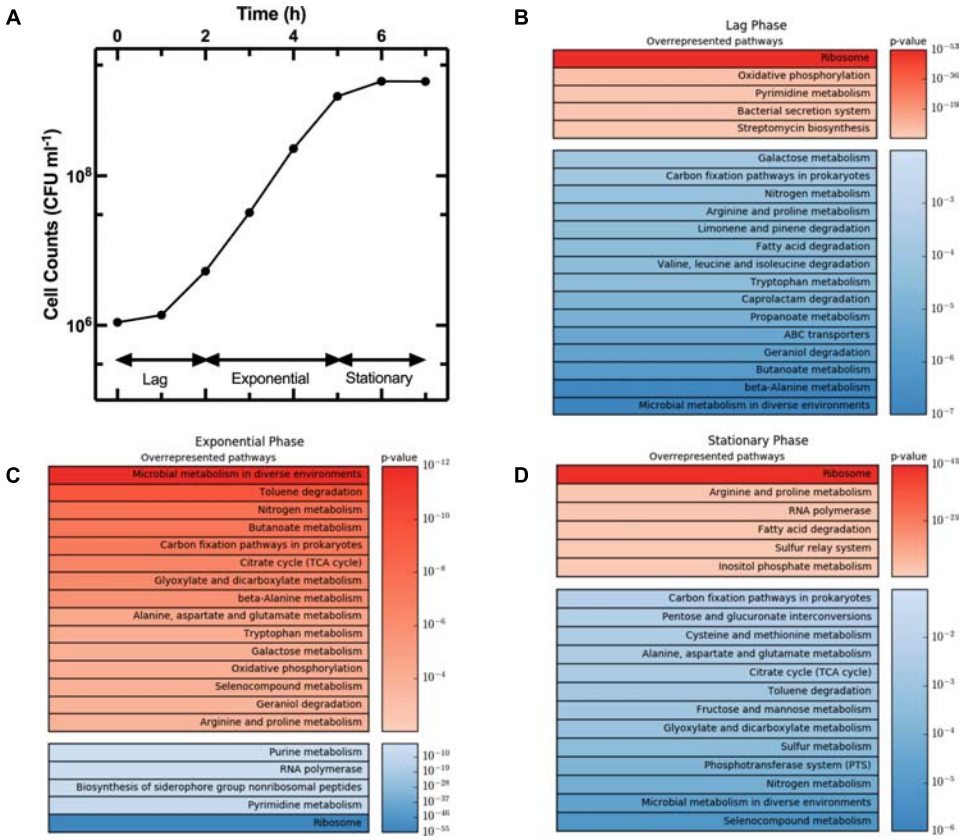

FIGURE 3 | Regulation of KEGG pathways during different phases of the growth cycle. **(A)** Growth phases of an *E. coli* culture. **(B–D)** Heat map tables of the top twenty overrepresented KEGG pathways during lag, exponential, and stationary phase, respectively. Each top table reports upregulated genes (in red) while each bottom table reports downregulated pathways (in blue). Pathways were ranked by significance of their *p*-values. Both growth and gene-expression profile measurements were performed in biological triplicate. In **(A)** data and error bars are the mean and SEM of measurements. Error bars are small compared to the corresponding mean values and are hidden behind some of the data points.

of 1.12×10^{-12}. We repeated this process for the top 10% downregulated genes, before ranking all the KEGG pathways by *p*-value, and reported the top 20 overrepresented pathways for the up- and downregulated genes (in red and blue, respectively, in **Figure 3**) during lag phase (**Figure 3B**), exponential phase (**Figure 3C**), and stationary phase (**Figure 3D**). **Supplementary Table S2** reports the *p*-value and number of genes in each of these pathways for lag, exponential, and stationary phase. We could not directly compare our results with previously reported datasets (Weber et al., 2005; Bergholz et al., 2007) because these studies did not employ the KEGG database. Therefore, we report below the expression of strongly regulated genes for each growth phase and discuss our findings in the context of data reported in previous studies investigating either persisters or the influence of the medium composition on gene regulation.

The average expression dynamics for the whole transcriptome (dashed line in **Figure 4**) remained relatively constant throughout the different phases of growth. However, unlike previous reports (Chang et al., 2002), we found significant changes in the expression of several pathways during the lag phase (t = 0 to t = 2 h). Metabolism pathways were strongly downregulated (**Figure 3B** bottom table and **Supplementary Table S2**) and in particular the most overrepresented of these KEGG pathways was "Microbial metabolism in diverse environments." This pathway was previously found to play a key role in *Klebsiella pneumoniae* adaptation to cold or heat shocks (Tripathy et al., 2014). Among the 10 most downregulated genes, we found *astA* (−13.0 $\log_2$ fold change, squares in **Figure 4A**), *astB*, and *astC* in the AST pathway controlling arginine degradation; *gadA* and *gadB* controlling glutamate decarboxylase activity (De Biase et al., 1999); the biofilm regulator *bssR*; and the aldehyde dehydrogenase *aldB*. These genes were then all strongly induced during the exponential phase (between 8 and 10 $\log_2$ fold).

Among the upregulated pathways (**Figure 3B** top table and **Supplementary Table S2**), "Ribosome" was the most overrepresented indicating induction of the translation machinery. Furthermore, among the 10 most upregulated genes, we found *yghG* (7.9 $\log_2$ fold change, circles in **Figure 4A**) and *yghF* that were induced at t = 1 h and have previously been linked to type II secretion (Kim et al., 2017); *borD* encoding a

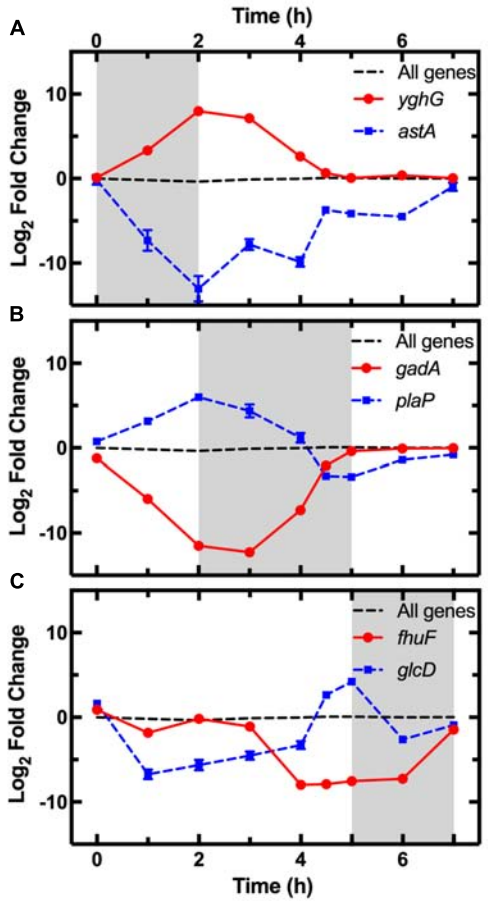

FIGURE 4 | Pattern of expression of the top most upregulated and downregulated genes during each phase. Expression profiles of the most upregulated (circles) and downregulated (squares) genes between t = 0–2 h **(A)**, t = 2–5 h **(B)**, and t = 5–7 h **(C)** from dilution in LB medium of an overnight *E. coli* culture. Gene expression is reported as the $\log_2$ fold change with respect to the measurements on the overnight samples (t = 17 h). The average expression dynamics for the whole transcriptome (dashed line) remains relatively constant throughout the different phases of growth. The expression dynamics for all the 4373 analyzed genes is reported in **Supplementary Table S1**. Data and error bars are the mean and SEM of measurements obtained on biological triplicates. Error bars are hidden behind some of the data points.

prophage lipoprotein; *proV*, *proW*, and *proX* also induced at t = 1 h, encoding parts of an ABC transporter for the uptake of glycine, betaine, and proline; *iraM* induced at t = 1 h and encoding an anti-adapter protein that inhibits RpoS proteolysis; and *stpA* encoding a DNA-binding protein. *yghG*, *yghF*, *borD*, *iraM*, and *stpA* were then strongly downregulated (between −6 and −8 $\log_2$ fold) during exponential phase. Notably, gene-expression profiling during the lag phase was not reported in a previous transcriptomic study carried out on *E. coli* O157 (Bergholz et al., 2007).

During the exponential growth phase (t = 2 h to t = 5 h) there was an extensive reprogramming of gene-expression. The "Ribosome" pathway was the most overrepresented in the top 10% downregulated genes, indicating repression of the translation machinery at the transition between exponential and stationary phase (t = 5 h) in response to the depletion of nutrients in the culture conditions. This was reflected in the measured division rate (**Supplementary Figure S6**). Among the 10 most downregulated genes, we found *plaP* (−9.4 $\log_2$ fold change, squares in **Figure 4B**) encoding a putrescine importer required for the induction of pili-driven motility, in accordance with the reported low motility of exponentially growing *E. coli* (Amsler et al., 1993); *cspA* encoding a cold shock protein; *fhuF* encoding an iron reductase protein; *lpxT* encoding the lipid A 1-diphosphate synthase; *fecA* encoding an outer membrane receptor in the Fe^{3+} dicitrate transport system; and the above discussed *yghF*. *fhuF* and *plaP* were then upregulated by a factor of 6 and 2 $\log_2$ fold, respectively, during stationary phase.

Metabolism related pathways were upregulated with "Microbial metabolism in diverse environments" now being the most overrepresented KEGG pathway (**Figure 3C** top table). Among the 10 most upregulated genes, we found *gadA* (11.1 $\log_2$ fold change, circles in **Figure 4B**), *gadB*, *gadC*, and *gadE* that were induced at t = 4 h and whose upregulation at the transition between exponential and stationary phase have previously been reported (De Biase et al., 1999; Weber et al., 2005; Bergholz et al., 2007); *glcD* and *glcE* induced at t = 3.5 h, encoding a subunit of the glycolate oxidase; *narU* induced at t = 3 h, encoding a nitrate and nitrite inner membrane transporter; *aldB* already discussed above; and *tnaC* discussed below. *glcD*, *glcE*, and *tnaC* were then downregulated during the stationary phase. The *tnaC* gene is part of the *tnaCAB* operon that regulates tryptophan catabolism and is comprised of a 24 residue upstream peptide TnaC, the tryptophanase TnaA, and the low affinity tryptophan permease TnaB (Konan and Yanofsky, 1997). TnaA is responsible for the breakdown of tryptophan, which is utilized by *E. coli* as an energy source to produce pyruvate, ammonia, and indole (Luli and Strohl, 1990). Interestingly, as the sugars were depleted in the culture, we observed an increase in expression of the *tnaCAB* operon (**Supplementary Table S1**). This was in accordance with a previous proteomic study carried out on *E. coli* K12 BW25113 growing on minimal medium (Soufi et al., 2015), suggesting a correlation between tryptophan related gene and protein expression. Furthermore, Gaimster and Summers (2015) observed an increase in *tnaA* expression in a growing *E. coli* culture, correlating this to an increase in the concentration of extracellular indole (Gaimster et al., 2014). Finally, we also observed an upregulation of transport genes including *ompF* and *lamB* encoding two of the major *E. coli* outer membrane porins (**Supplementary Table S1**), which was not previously observed (Bergholz et al., 2007).

Metabolism related pathways were downregulated as the population entered stationary phase (t = 5 h to t = 7 h) with "Microbial metabolism in diverse environments" now being the most overrepresented KEGG pathway (**Figure 3D** bottom table). This coincided with the previously mentioned reduction in sugar availability (**Figure 1B**). Almost all of the genes in the phosphoenolpyruvate (PEP)-dependent phosphotransferase system (PTS) pathway, a major bacterial mechanism for the accumulation of carbohydrates (Shimizu, 2013), were

downregulated as the bacteria moved from late-exponential to stationary phase (**Figure 3D**). The downregulation of the PTS pathway may cause reduced levels of glycolysis intermediates such as fructose 1,6-bisphosphate (FDP), which in *E. coli* results in the activation of *cra* and the subsequent transcriptional repression of *pfkA* and *pykF* (Shimizu, 2013). Both *pykF* and *pfkA* were downregulated as the culture transitioned from exponential to stationary phase (**Supplementary Figure S7**) resulting in the downregulation of the TCA cycle (**Figure 3D**). This is in agreement with a previous transcriptomic study carried out on *E. coli* O157, reporting a downregulation of the tricarboxylic acid (TCA) cycle pathway after t = 4.5 h compared to t = 3 h growth on minimal medium (Bergholz et al., 2007). Similarly, we found agreement between Bergholz's data and ours on the downregulation of the sulfur metabolism pathway, sulfur being present in LB and instrumental for the biosynthesis of the amino acids cysteine and methionine (Sekowska et al., 2000).

Among the 10 most downregulated genes were *glcD* (−5.1 $\log_2$ fold change, squares in **Figure 4C**), *glcE*, *glcA*, and *glcB*; *ansB* encoding L-asparaginase 2; *fumB* encoding a fumarate hydratase; and *adiY* encoding a transcriptional regulator. *glcD*, *glcE*, *glcA*, and *glcB* were further downregulated during the lag phase. Finally, genes encoding transporters including *ompF* and *lamB*, were also downregulated as previously reported (Chang et al., 2002).

The "Ribosome" pathway was the most overrepresented in the top 10% upregulated genes. However, the mean expression of all the 48 genes in this pathway was downregulated by a factor of 2.8 $\log_2$ fold at t = 7 h compared to t = 2 h. Among the 10 most upregulated genes, we identified *fhuF* (6.1 $\log_2$ fold change, circles in **Figure 4C**); *astA*, *astC*, and *astE* in the AST pathway, that were induced at t = 6 h; *prpB* induced at t = 4 h, encoding the 2-methylisocitrate lyase; *bfd* encoding bacterioferritin-associated ferredoxin; *rmf* induced at t = 4 h, encoding a ribosome modulation factor; *ynfM* encoding an inner membrane transporter; *sodA* induced at t = 6 h, encoding a superoxide dismutase, previously associated with the emergence of metabolic heterogeneity during nutrient starvation (Şimşek and Kim, 2018); and *obgE* encoding the essential GTPase ObgE/CgtA. In the AST pathway, *rmf*, *ynfM*, and *prpB* were then strongly downregulated (between −5 and −10 $\log_2$ fold) during lag phase. Furthermore, a major regulator of the stress response in bacteria, particularly their entry into stationary phase, is the sigma factor *rpoS* controlling the expression of approximately 10% of genes in *E. coli* (Weber et al., 2005). Our data shows that *rpoS* expression increases rapidly as the culture enters stationary phase (**Supplementary Figure S8**), in accordance with previously reported data (2.4 and 2.8 $\log_2$ fold change, respectively, between t = 4 h and 5 h from inoculation) (Bergholz et al., 2007). Bergholz, et al. also reported that the most highly upregulated gene during the transition to stationary phase was *acs*, which encodes acetyl CoA synthetase, confirming the data reported in a separate study on *E. coli MG1655* (Baev et al., 2006). Similarly, between t = 4 h and t = 4.5 h from inoculation, we observe a 7.4 $\log_2$ fold change in the expression of *acs* and 4.7 $\log_2$ fold change of *aceB* expression, in accordance with Bergholz, et al. who reported a 5.4 $\log_2$ fold change for *aceB* during the same temporal window. These data suggest that at least some *E. coli* responses to changes in growth medium are conserved across evolutionary distance and are not specific to the growth medium employed. All together, our data on the reprogramming of the culture gene-expression during the transitions between the different growth phases (**Figures 3**, **4** and **Supplementary Tables S1**, **S2**) will be relevant for studying the responses of microbial communities to environmental changes.

Growth Stage Dependent Persister Formation

We then studied the growth cycle dependence of phenotypic heterogeneity within the population by measuring persistence to antibiotics as a phenotypic proxy. We used three antibiotics with distinct modes of action: ampicillin, gentamicin, and ofloxacin. Specifically, ampicillin is a β-lactam that binds to the penicillin-binding proteins located inside the bacterial cell wall. It inhibits the last stage of bacterial cell wall synthesis leading to lysis mediated by autolytic enzymes. Gentamicin is an aminoglycoside that works by irreversibly binding to the 30S subunit of the bacterial ribosome, thereby interrupting protein synthesis. Ofloxacin is a second-generation fluoroquinolone that acts on DNA gyrase and topoisomerase IV, and thus altering the control of DNA supercoiling and inhibiting normal cell division (Aldred et al., 2014).

To investigate the growth-dependent heterogeneity of the response to each antibiotic, we performed two different treatments (see **Supplementary Figure S1**): three culture aliquots were injected with antibiotic and fresh LB (**Supplementary Figure S1F**), while three other aliquots were injected with antibiotic only (**Supplementary Figure S1G**). In both cases, the final antibiotic concentration was 25× the antibiotic MIC. For each time point and each antibiotic treatment, we then calculated the ratio between the measured number of persisters in the culture relative to the total number of bacteria in the culture (**Figure 3A**), defining this as the persister fraction. We finally normalized each persister fraction dataset to their maximum values.

When gentamicin was added to the culture aliquots with fresh LB, the fraction of persisters showed a 3.4 $\log_{10}$ fold increase between t = 3 h and t = 4 h, before remaining relatively constant for the remainder of the growth cycle (**Figure 5A**). When only gentamicin was added to the culture aliquots the fraction of persisters showed a similar pattern, except for a shift of 1 h, with a 3.6 $\log_{10}$ fold increase between t = 2 h and t = 3 h (**Figure 5B**).

When ofloxacin was added to the culture aliquots with fresh LB, there was a small increase in the persister fraction during the lag phase (**Figure 5C**). However, the persister fraction showed a 2.6 $\log_{10}$ fold increase during the exponential phase (between t = 2 h and t = 4 h) when only ofloxacin was added to the culture aliquots (**Figure 5D**).

When ampicillin was added to the culture aliquots with fresh LB, we measured a 2 $\log_{10}$ fold increase in the persister fraction

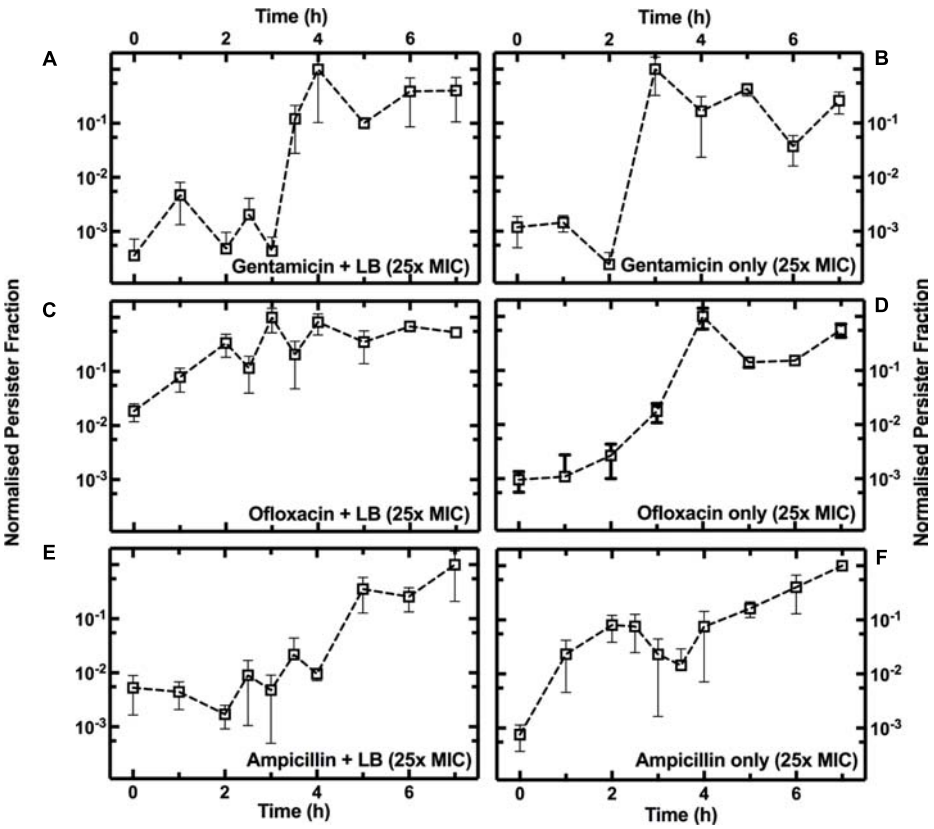

FIGURE 5 | Growth phase dependence of the fraction of persisters to gentamicin, ofloxacin, or ampicillin. Temporal dependence of the normalized fraction of persisters to treatment either with gentamicin **(A)**, ofloxacin **(C)**, or ampicillin **(E)**, with the addition of fresh LB, or with antibiotics only [**(B,D,F)**, respectively]. At $t = 0$ an overnight *E. coli* culture was diluted 1:1000 in LB medium and the culture growth started. Each data set is normalized to its maximum persister fraction. Data and error bars are the mean and SEM of measurements obtained at least on biological and technical triplicates.

during the stationary phase (**Figure 5E**). When only ampicillin was added to the culture aliquots, we measured a 1.5 $\log_{10}$ fold increase in the fraction of persister cells during the lag phase ($t = 1$ h, **Figure 5F**).

Growth-dependent bacterial susceptibility has recently been reported (Greulich et al., 2015). Here, we demonstrate that as the composition of the medium in the culture environment changes, the microbial population becomes increasingly heterogeneous in response to the treatment to antibiotics with different modes of action.

Furthermore, antibiotic susceptibility and persister assays are often carried out by supplementing antibiotics with fresh LB medium (Wu et al., 2015; Orman and Brynildsen, 2016). We demonstrate that in the case of gentamicin, the addition of fresh LB medium does not substantially affect the dependence of persister fraction on growth phase. Indeed, it has recently been demonstrated that nutrient-rich environments do not increase susceptibility to antibiotics that irreversibly bind to the 30S subunit of the bacterial ribosome (Greulich et al., 2015). On the contrary, we observed that the formation of persisters to β-lactams and quinolones is strongly affected by the medium composition, suggesting that this should be carefully considered when screening for antibiotics against persister cells.

DISCUSSION

Within an isogenic population, there is inherent phenotypic heterogeneity which allows an adaptive response to an ever-changing extracellular environment (Balaban et al., 2004; Ryall et al., 2012; Nikolic et al., 2013; Kotte et al., 2014). For example, within a growing isogenic population of bacteria there are multiple growth phenotypes present, from exponentially growing to slow growing, or dormant bacteria (Ryall et al., 2012; Kotte et al., 2014). Persister cells are an example of a phenotype which differs from the majority of cells in a clonal population in terms of growth rate (Lewis, 2010; Maisonneuve et al., 2013), motility, gene expression, and cell size (Ryall et al., 2012). Furthermore, persister cells can be generated in response to a number of environmental conditions (Keren et al., 2004b; Vega et al., 2012; Bernier et al., 2013; Helaine et al., 2014), including nutrient limitation (Fung et al., 2010; Maisonneuve and Gerdes, 2014) and nutrient transitions (Amato et al., 2013) that also generate a variety of other bacterial responses (Lidstrom and Konopka, 2010).

Therefore, we utilized the persister phenotype as a proxy for changes in population-wide heterogeneity throughout the *E. coli* growth cycle where the environmental conditions are

constantly changing. We observed homogeneity in response to all antibiotics during lag phase with very few persisters to any of the tested antibiotics. However, the different persister fractions observed in response to the different antibiotics further emphasize the phenotypic heterogeneity within the population during the exponential and stationary phases. In fact, population based heterogeneity allows rapid response to alterations in the nutritional environment; it is only when the environment becomes favorable to a given subpopulation that they are able to dominate the whole population-level response (Lidstrom and Konopka, 2010). Indeed, within the growth cycle we observed changes in both nutrient availability (**Figure 1**) and pH (**Supplementary Figure S4**).

These changes in the culture medium also influenced the population transcriptome during the same temporal windows where we measured notable increases in the fraction of persisters. We observed upregulation of carbon fixation pathways and tryptophan metabolism (**Figure 3C**), potentially as a result of an increase in the concentration of extracellular indole (Gaimster et al., 2014). Indole has also been linked to persister cell formation (Vega et al., 2012, 2013) and the induced expression of a variety of drug exporters (Meng and Bennett, 1992; Balaban et al., 2004). Moreover, *ompF* and *lamB*, encoding two of the major outer membrane porins that have been associated with drug uptake (Ziervogel and Roux, 2013; Lin et al., 2014; Cama et al., 2015) were also upregulated at the whole population level during exponential phase (**Supplementary Table S1**).

In comparison, during stationary phase we observed a clear downregulation of metabolism related pathways (**Figure 3D**). The downregulation of the TCA cycle as the population moves from exponential to stationary phase (**Figure 3D**) results in the excretion of acetate into the extracellular environment and its subsequent utilization (**Figure 1**; Luli and Strohl, 1990; Shimizu, 2013). Kotte et al. (2010) modeled population adaptation to different nutrients *in silico*, showing that as glucose levels reduce, cells are predicted to utilize their natively produced acetate. This ability to adapt to nutrient availability appears to be a result of metabolic flux at the single-cell level (Kotte et al., 2010; Kochanowski et al., 2013) and results in the diversification of growing and non-growing phenotypes, such as persisters (Kotte et al., 2014). Indeed, we measured an increase in persister fraction in response to all three antibiotics as the available sugars become limited (**Figure 1**). However, each type of antibiotic reveals different levels of heterogeneity suggesting that different biological pathways underlie persistence to different antibiotics.

We also found that the outcome of antibiotic treatment is strongly influenced by the composition of the medium containing the antibiotic. In fact, the addition of antibiotics and fresh LB alters the native culture environment and causes a reduction in the number of persisters (**Figure 5**), reducing phenotypic heterogeneity within the *E. coli* community.

One of the current limitations within our knowledge of persister bacteria is that their transcriptome has been examined only after treatment with antibiotics (Keren et al., 2004b) owing to the lack of biomarkers to isolate persisters from the majority of susceptible cells before antibiotic challenge. However, antibiotic treatment is known to alter the bacterial transcriptome (Lewis, 2010). Our current study identifies molecular pathways that are strongly regulated at the whole population level when the environment changes and, coincidentally, the fraction of persisters within the population increases. Some of the identified pathways such as tryptophan metabolism and TCA cycle (Vega et al., 2012; Kotte et al., 2014), have indeed previously been associated with persisters. However, it is noteworthy that our approach measures the mean transcriptomic response of the whole population. Therefore, our measurements do not allow us to determine whether the pathways that we have identified are also strongly regulated in the minority of persister cells. Indeed, the differential response of persisters could be masked by that of the majority of susceptible cells. Considering that cell-to-cell variation increases with increasing mean gene-expression (Silander et al., 2012), these comprehensive data sets provide well defined culturing time points, medium compositions, and putative pathways that could be investigated with single-cell approaches (Henry and Brynildsen, 2016; Bamford et al., 2017) to determine molecular pathways that are differentially regulated in persisters compared to the majority of susceptible cells.

Our approach could easily be extended to investigate the dynamics of phenotypic heterogeneity in different microbial communities such as bacterial biofilms (Domka et al., 2007), natural yeast and fungal populations (LaFleur et al., 2010; Holland et al., 2014), or cancer cells (Hangauer et al., 2017) responding to a variety of environmental cues.

AUTHOR CONTRIBUTIONS

SP developed the project and designed the research. AS, AK, RB, CS, SF, and AK-S performed the experiments. PO, KM, and KP carried out sequencing. All authors analyzed and discussed the data. AS and SP wrote the paper.

FUNDING

This work was supported by a Royal Society Research Grant (RG140203), a Wellcome Trust Strategic Seed Corn Fund (WT097835/Z/11/Z), and a start up Grant from the University of Exeter awarded to SP. AS acknowledges support from the BBSRC through a SWBio-DTP studentship (BB/M009122/1). KP, KM, and PO would like to acknowledge support from the following awards: Wellcome Trust Institutional Strategic Support Fund (WT097835MF), Wellcome Trust Multi User Equipment Award (WT101650MA), and Medical Research Council Clinical Infrastructure Funding (MR/M008924/1). This work was partly supported by BBSRC award BB/1024631/1 to RT.

SUPPLEMENTARY MATERIAL

The Supplementary Material for this article can be found online at: https://www.frontiersin.org/articles/10.3389/fmicb.2018.01739/full#supplementary-material

REFERENCES

Ackermann, M. (2015). A functional perspective on phenotypic heterogeneity in microorganisms. *Nat. Rev. Microbiol.* 13, 497–508. doi: 10.1038/nrmicro3491

Aldred, K. J., Kerns, R. J., and Osheroff, N. (2014). Mechanism of quinolone action and resistance. *Biochemistry* 53, 1565–1574. doi: 10.1021/bi5000564

Allison, K. R., Brynildsen, M. P., and Collins, J. J. (2011). Metabolite-enabled eradication of bacterial persisters by aminoglycosides. *Nature* 473, 216–220. doi: 10.1038/nature10069

Amato, S. M., and Brynildsen, M. P. (2014). Nutrient transitions are a source of persisters in *Escherichia coli* biofilms. *PLoS One* 9:e93110. doi: 10.1371/journal.pone.0093110

Amato, S. M., Orman, M. A., and Brynildsen, M. P. (2013). Metabolic control of persister formation in *Escherichia coli*. *Mol. Cell* 50, 475–487. doi: 10.1016/j.molcel.2013.04.002

Amsler, C. D., Cho, M., and Matsumura, P. (1993). Multiple factors underlying the maximum motility of *Escherichia coli* as cultures enter post-exponential growth. *J. Bacteriol.* 175, 6238–6244. doi: 10.1128/jb.175.19.6238-6244.1993

Arnoldini, M., Vizcarra, I. A., Peña-Miller, R., Stocker, N., Diard, M., Vogel, V., et al. (2014). Bistable expression of virulence genes in *Salmonella* leads to the formation of an antibiotic-tolerant subpopulation. *PLoS Biol.* 12:e1001928. doi: 10.1371/journal.pbio.1001928

Baev, M. V., Baev, D., Radek, A. J., and Campbell, J. W. (2006). Growth of *Escherichia coli* MG1655 on LB medium: determining metabolic strategy with transcriptional microarrays. *Appl. Microbiol. Biotechnol.* 71, 323–328. doi: 10.1007/s00253-006-0392-8

Balaban, N. Q., Merrin, J., Chait, R., Kowalik, L., and Leibler, S. (2004). Bacterial persistence as a phenotypic switch. *Science* 305, 1622–1625. doi: 10.1126/science.1099390

Bamford, R. A., Smith, A., Metz, J., Glover, G., Titball, R. W., and Pagliara, S. (2017). Investigating the physiology of viable but non-culturable bacteria by microfluidics and time-lapse microscopy. *BMC Biol.* 15:121. doi: 10.1186/s12915-017-0465-4

Beaumont, H. J. E., Gallie, J., Kost, C., Ferguson, G. C., and Rainey, P. B. (2009). Experimental evolution of bet hedging. *Nature* 462, 90–93. doi: 10.1038/nature08504

Bergholz, T. M., Wick, L. M., Qi, W., Riordan, J. T., Ouellette, L. M., and Whittam, T. S. (2007). Global transcriptional response of *Escherichia coli* O157:H7 to growth transitions in glucose minimal medium. *BMC Microbiol.* 7:97. doi: 10.1186/1471-2180-7-97

Bernier, S. P., Lebeaux, D., DeFrancesco, A. S., Valomon, A., Soubigou, G., Coppée, J. Y., et al. (2013). Starvation, together with the SOS response, mediates high biofilm-specific tolerance to the fluoroquinolone ofloxacin. *PLoS Genet.* 9:e1003144. doi: 10.1371/journal.pgen.1003144

Bódi, Z., Farkas, Z., Nevozhay, D., Kalapis, D., Lázár, V., Csörgő, B., et al. (2017). Phenotypic heterogeneity promotes adaptive evolution. *PLoS Biol.* 15:e2000644. doi: 10.1371/journal.pbio.2000644

Brauner, A., Fridman, O., Gefen, O., and Balaban, N. Q. (2016). Distinguishing between resistance, tolerance and persistence to antibiotic treatment. *Nat. Rev. Microbiol.* 14, 320–330. doi: 10.1038/nrmicro.2016.34

Cama, J., Bajaj, H., Pagliara, S., Maier, T., Braun, Y., Winterhalter, M., et al. (2015). Quantification of fluoroquinolone uptake through the outer membrane channel ompf of *Escherichia coli*. *J. Am. Chem. Soc.* 137, 13836–13843. doi: 10.1021/jacs.5b08960

Cama, J., Chimerel, C., Pagliara, S., Javer, A., and Keyser, U. F. (2014). A label-free microfluidic assay to quantitatively study antibiotic diffusion through lipid membranes. *Lab Chip* 14, 2303–2308. doi: 10.1039/c4lc00217b

Chang, D., Smalley, D. J., and Conway, T. (2002). Gene expression profiling of *Escherichia coli* growth transitions: an expanded stringent response model. *Mol. Microbiol.* 45, 289–306. doi: 10.1046/j.1365-2958.2002.03001.x

Chien, A.-C., Hill, N. S., and Levin, P. A. (2012). Cell size control in bacteria. *Curr. Biol.* 22, R340–R349. doi: 10.1016/j.cub.2012.02.032

De Biase, D., Tramonti, A., Bossa, F., and Visca, P. (1999). The response to stationary-phase stress conditions in *Escherichia coli*: role and regulation of the glutamic acid decarboxylase system. *Mol. Microbiol.* 32, 1198–1211. doi: 10.1046/j.1365-2958.1999.01430.x

Domka, J., Lee, J., Bansal, T., and Wood, T. K. (2007). Temporal gene-expression in *Escherichia coli* K-12 biofilms. *Environ. Microbiol.* 9, 332–346. doi: 10.1111/j.1462-2920.2006.01143.x

Elowitz, M., Levine, A., Siggia, E., and Swain, P. (2002). Stochastic gene expression in a single cell. *Science* 297, 1183–1186. doi: 10.1126/science.1070919

Fung, D. K. C., Chan, E. W. C., Chin, M. L., and Chan, R. C. Y. (2010). Delineation of a bacterial starvation stress response network which can mediate antibiotic tolerance development. *Antimicrob. Agents Chemother.* 54, 1082–1093. doi: 10.1128/AAC.01218-09

Gaimster, H., Cama, J., Hernández-Ainsa, S., Keyser, U. F., and Summers, D. K. (2014). The indole pulse: a new perspective on indole signalling in *Escherichia coli*. *PLoS One* 9:e93168. doi: 10.1371/journal.pone.0093168

Gaimster, H., and Summers, D. (2015). Regulation of indole signalling during the transition of *E. coli* from exponential to stationary phase. *PLoS One* 10:e0136691. doi: 10.1371/journal.pone.0136691

Greulich, P., Scott, M., Evans, M. R., and Allen, R. J. (2015). Growth-dependent bacterial susceptibility to ribosome-targeting antibiotics. *Mol. Syst. Biol.* 11:796. doi: 10.15252/msb.20145949

Hangauer, M. J., Viswanathan, V. S., Ryan, M. J., Bole, D., Eaton, J. K., Matov, A., et al. (2017). Drug-tolerant persister cancer cells are vulnerable to GPX4 inhibition. *Nature* 551, 247–250. doi: 10.1038/nature24297

Hansen, S., Lewis, K., and Vulić, M. (2008). Role of global regulators and nucleotide metabolism in antibiotic tolerance in *Escherichia coli*. *Antimicrob. Agents Chemother.* 52, 2718–2726. doi: 10.1128/AAC.00144-08

Hayes, E. T., Wilks, J. C., Sanfilippo, P., Yohannes, E., Tate, D. P., Jones, B. D., et al. (2006). Oxygen limitation modulates pH regulation of catabolism and hydrogenases, multidrug transporters, and envelope composition in *Escherichia coli* K-12. *BMC Microbiol.* 6:89. doi: 10.1186/1471-2180-6-89

Helaine, S., Cheverton, A., Watson, K., Faure, L., Matthews, S., and Holden, D. (2014). Internalization of *Salmonella* by macrophages induces formation of nonreplicating persisters. *Science* 343, 204–208. doi: 10.1126/science.1244705

Henry, T. C., and Brynildsen, M. P. (2016). Development of persister-FACSeq: a method to massively parallelize quantification of persister physiology and its heterogeneity. *Sci. Rep.* 6:25100. doi: 10.1038/srep25100

Holland, S. L., Reader, T., Dyer, P. S., and Avery, S. V. (2014). Phenotypic heterogeneity is a selected trait in natural yeast populations subject to environmental stress. *Environ. Microbiol.* 16, 1729–1740. doi: 10.1111/1462-2920.12243

Hua, Q., Yang, C., Oshima, T., Mori, H., and Shimizu, K. (2004). Analysis of gene expression in *Escherichia coli* in response to changes of growth-limiting nutrient in chemostat cultures. *Appl. Environ. Microbiol.* 70, 2354–2366. doi: 10.1128/AEM.70.4.2354-2366.2004

Johnson, P. J. T., and Levin, B. R. (2013). Pharmacodynamics, population dynamics, and the evolution of persistence in *Staphylococcus aureus*. *PLoS Genet.* 9:e1003123. doi: 10.1371/journal.pgen.1003123

Kaern, M., Elston, T. C., Blake, W. J., and Collins, J. J. (2005). Stochasticity in gene expression: from theories to phenotypes. *Nat. Rev. Genet.* 6, 451–464. doi: 10.1038/nrg1615

Kanehisa, M., Furumichi, M., Tanabe, M., Sato, Y., and Morishima, K. (2017). KEGG: new perspectives on genomes, pathways, diseases and drugs. *Nucleic Acids Res.* 45, D353–D361. doi: 10.1093/nar/gkw1092

Kanehisa, M., Sato, Y., Kawashima, M., Furumichi, M., and Tanabe, M. (2016). KEGG as a reference resource for gene and protein annotation. *Nucleic Acids Res.* 44, D457–D462. doi: 10.1093/nar/gkv1070

Keren, I., Kaldalu, N., Spoering, A., Wang, Y., and Lewis, K. (2004a). Persister cells and tolerance to antimicrobials. *FEMS Microbiol. Lett.* 230, 13–18. doi: 10.1016/S0378-1097(03)00856-5

Keren, I., Shah, D., Spoering, A., Kaldalu, N., and Lewis, K. (2004b). Specialized persister cells and the mechanism of multidrug tolerance in *Escherichia coli*. *J. Bacteriol.* 186, 8172–8180.

Kim, S., Jeong, H., Kim, E. Y., Kim, J. F., Lee, S. Y., and Yoon, S. H. (2017). Genomic and transcriptomic landscape of *Escherichia coli* BL21(DE3). *Nucleic Acids Res.* 45, 5285–5293. doi: 10.1093/nar/gkx228

Kleman, G. L., and Strohl, W. R. (1994). Acetate metabolism by *Escherichia coli* in high-cell-density fermentation. *Appl Environ. Microbiol.* 60, 3952–3958.

Klumpp, S., and Hwa, T. (2015). Bacterial growth: global effects on gene expression, growth feedback and proteome partition. *Curr. Opin. Biotechnol.* 28, 96–102. doi: 10.1016/j.copbio.2014.01.001

Kochanowski, K., Volkmer, B., Gerosa, L., Haverkorn van Rijsewijk, B. R., Schmidt, A., and Heinemann, M. (2013). Functioning of a metabolic flux sensor in *Escherichia coli*. *Proc. Natl. Acad. Sci. U.S.A.* 110, 1130–1135. doi: 10.1073/pnas.1202582110

Konan, K. V., and Yanofsky, C. (1997). Regulation of the *Escherichia coli* tna operon: nascent leader peptide control at the tnaC stop codon. *J. Bacteriol.* 179, 1774–1779. doi: 10.1128/jb.179.5.1774-1779.1997

Kotte, O., Volkmer, B., Radzikowski, J. L., and Heinemann, M. (2014). Phenotypic bistability in *Escherichia coli*'s central carbon metabolism. *Mol. Syst. Biol.* 10:736. doi: 10.15252/msb.20135022

Kotte, O., Zaugg, J. B., and Heinemann, M. (2010). Bacterial adaptation through distributed sensing of metabolic fluxes. *Mol. Syst. Biol.* 6, 1–9. doi: 10.1038/msb.2010.10

LaFleur, M. D., Kumamoto, C. A., and Lewis, K. (2006). Candida albicans biofilms produce antifungal-tolerant persister cells. *Antimicrob. Agents Chemother.* 50, 3839–3846. doi: 10.1128/AAC.00684-06

LaFleur, M. D., Qi, Q., and Lewis, K. (2010). Patients with long-term oral carriage harbor high-persister mutants of Candida albicans. *Antimicrob. Agents Chemother.* 54, 39–44. doi: 10.1128/AAC.00860-09

Lewis, K. (2010). Persister cells. *Annu. Rev. Microbiol.* 64, 357–372. doi: 10.1146/annurev.micro.112408.134306

Lidstrom, M. E., and Konopka, M. C. (2010). The role of physiological heterogeneity in microbial population behavior. *Nat. Chem. Biol.* 6, 705–712. doi: 10.1038/nchembio.436

Lin, X. M., Yang, M. J., Li, H., Wang, C., and Peng, X. X. (2014). Decreased expression of LamB and Odp1 complex is crucial for antibiotic resistance in *Escherichia coli*. *J. Proteomics* 98, 244–253. doi: 10.1016/j.jprot.2013.12.024

Losen, M., Frölich, B., Pohl, M., and Büchs, J. (2004). Effect of oxygen limitation and medium composition on *Escherichia coli* fermentation in shake-flask cultures. *Biotechnol. Prog.* 20, 1062–1068. doi: 10.1021/bp034282t

Love, M. I., Huber, W., and Anders, S. (2014). Moderated estimation of fold change and dispersion for RNA-seq data with DESeq2. *Genome Biol.* 15, 1–21. doi: 10.1186/s13059-014-0550-8

Luidalepp, H., Jõers, A., Kaldalu, N., and Tenson, T. (2011). Age of inoculum strongly influences persister frequency and can mask effects of mutations implicated in altered persistence. *J. Bacteriol.* 193, 3598–3605. doi: 10.1128/JB.00085-11

Luli, G. W., and Strohl, W. R. (1990). Comparison of growth, acetate production, and acetate inhibition of *Escherichia coli* strains in batch and fed-batch fermentations. *Appl. Environ. Microbiol.* 56, 1004–1011.

Maisonneuve, E., Castro-Camargo, M., and Gerdes, K. (2013). (p)ppGpp controls bacterial persistence by stochastic induction of toxin-antitoxin activity. *Cell* 154, 1140–1150. doi: 10.1016/j.cell.2013.07.048

Maisonneuve, E., and Gerdes, K. (2014). Molecular mechanisms underlying bacterial persisters. *Cell* 157, 539–548. doi: 10.1016/j.cell.2014.02.050

Megaw, J., and Gilmore, B. F. (2017). Archaeal persisters: persister cell formation as a stress response in *Haloferax volcanii*. *Front. Microbiol.* 8:1589. doi: 10.3389/fmicb.2017.01589

Meng, S. Y., and Bennett, G. N. (1992). Nucleotide sequence of the *Escherichia coli* cad operon: a system for neutralization of low extracellular pH. *J. Bacteriol.* 174, 2659–2669. doi: 10.1128/jb.174.8.2659-2669.1992

Mulcahy, L. R., Burns, J. L., Lory, S., and Lewis, K. (2010). Emergence of *Pseudomonas aeruginosa* strains producing high levels of persister cells in patients with cystic fibrosis. *J. Bacteriol.* 192, 6191–6199. doi: 10.1128/JB.01651-09

New, A. M., Cerulus, B., Govers, S. K., Perez-Samper, G., Zhu, B., Boogmans, S., et al. (2014). Different levels of catabolite repression optimize growth in stable and variable environments. *PLoS Biol.* 12:e1001764. doi: 10.1371/journal.pbio.1001764

Nikolic, N., Barner, T., and Ackermann, M. (2013). Analysis of fluorescent reporters indicates heterogeneity in glucose uptake and utilization in clonal bacterial populations. *BMC Microbiol.* 13:258. doi: 10.1186/1471-2180-13-258

Ogata, H., Goto, S., Sato, K., Fujibuchi, W., Bono, H., and Kanehisa, M. (1999). KEGG: Kyoto encyclopedia of genes and genomes. *Nucleic Acids Res.* 27, 29–34. doi: 10.1093/nar/27.1.29

Orman, M. A., and Brynildsen, M. P. (2016). Persister formation in *Escherichia coli* can be inhibited by treatment with nitric oxide. *Free Radic. Biol. Med.* 93, 145–154. doi: 10.1016/j.freeradbiomed.2016.02.003

Radzikowski, J. L., Vedelaar, S., Siegel, D., Ortega, ÁD., Schmidt, A., and Heinemann, M. (2016). Bacterial persistence is an active σS stress response to metabolic flux limitation. *Mol. Syst. Biol.* 12:882. doi: 10.15252/msb.20166998

Ryall, B., Eydallin, G., and Ferenci, T. (2012). Culture history and population heterogeneity as determinants of bacterial adaptation: the adaptomics of a single environmental transition. *Microbiol. Mol. Biol. Rev.* 76, 597–625. doi: 10.1128/MMBR.05028-11

Schreiber, F., Littmann, S., Lavik, G., Escrig, S., Meibom, A., Kuypers, M. M. M., et al. (2016). Phenotypic heterogeneity driven by nutrient limitation promotes growth in fluctuating environments. *Nat. Microbiol.* 1, 1–7. doi: 10.1038/nmicrobiol.2016.55

Scott, M., Gunderson, C. W., Mateescu, E. M., Zhang, Z., and Hwa, T. (2010). Interdependence of cell growth origins and consequences. *Science* 330, 1099–1102. doi: 10.1126/science.1192588

Sekowska, A., Kung, H., and Danchin, A. (2000). Sulfur metabolism in *Escherichia coli* and related bacteria: facts and fiction. *J. Mol. Microbiol. Biotechnol.* 2, 145–177.

Sezonov, G., Joseleau-Petit, D., and D'Ari, R. (2007). *Escherichia coli* physiology in Luria-Bertani broth. *J. Bacteriol.* 189, 8746–8749. doi: 10.1128/JB.01368-07

Sheik, A. R., Muller, E. E. L., Audinot, J. N., Lebrun, L. A., Grysan, P., Guignard, C., et al. (2016). In situ phenotypic heterogeneity among single cells of the filamentous bacterium Candidatus *Microthrix parvicella*. *ISME J.* 10, 1274–1279. doi: 10.1038/ismej.2015.181

Shimizu, K. (2013). Regulation systems of bacteria such as *Escherichia coli* in response to nutrient limitation and environmental stresses. *Metabolites* 4, 1–35. doi: 10.3390/metabo4010001

Silander, O. K., Nikolic, N., Zaslaver, A., Bren, A., Kikoin, I., Alon, U., et al. (2012). A genome-wide analysis of promoter-mediated phenotypic noise in *Escherichia coli*. *PLoS Genet.* 8:e1002443. doi: 10.1371/journal.pgen.1002443

Şimşek, E., and Kim, M. (2018). The emergence of metabolic heterogeneity and diverse growth responses in isogenic bacterial cells. *ISME J.* 12, 1199–1209. doi: 10.1038/s41396-017-0036-2

Soufi, B., Krug, K., Harst, A., and Macek, B. (2015). Characterization of the *E. coli* proteome and its modifications during growth and ethanol stress. *Front. Microbiol.* 6:103. doi: 10.3389/fmicb.2015.00103

Stincone, A., Daudi, N., Rahman, A. S., Antczak, P., Henderson, I., Cole, J., et al. (2011). A systems biology approach sheds new light on *Escherichia coli* acid resistance. *Nucleic Acids Res.* 39, 7512–7528. doi: 10.1093/nar/gkr338

Tripathy, S., Sen, R., Padhi, S. K., Mohanty, S., and Maiti, N. K. (2014). Upregulation of transcripts for metabolism in diverse environments is a shared response associated with survival and adaptation of *Klebsiella pneumoniae* in response to temperature extremes. *Funct. Integr. Genomics* 14, 591–601. doi: 10.1007/s10142-014-0382-3

Veening, J. W., Igoshin, O. A., Eijlander, R. T., Nijland, R., Hamoen, L. W., and Kuipers, O. P. (2008). Transient heterogeneity in extracellular protease production by *Bacillus subtilis*. *Mol. Syst. Biol.* 4, 1–15. doi: 10.1038/msb.2008.18

Vega, N. M., Allison, K. R., Khalil, A. S., and Collins, J. J. (2012). Signaling-mediated bacterial persister formation. *Nat. Chem. Biol.* 8, 431–433. doi: 10.1038/nchembio.915

Vega, N. M., Allison, K. R., Samuels, A. N., Klempner, M. S., and Collins, J. J. (2013). *Salmonella* typhimurium intercepts *Escherichia coli* signaling to enhance antibiotic tolerance. *Proc. Natl. Acad. Sci. U.S.A.* 110, 14420–14425. doi: 10.1073/pnas.1308085110

Venturelli, O. S., Zuleta, I., Murray, R. M., and El-Samad, H. (2015). Population diversification in a yeast metabolic program promotes anticipation of environmental shifts. *PLoS Biol.* 13:e1002042. doi: 10.1371/journal.pbio.1002042

Vital, M., Chai, B., Østman, B., Cole, J., Konstantinidis, K. T., and Tiedje, J. M. (2015). Gene expression analysis of *E. coli* strains provides insights into the role of gene regulation in diversification. *ISME J.* 9, 1130–1140. doi: 10.1038/ismej.2014.204

Weart, R. B., Lee, A. H., Chien, A. C., Haeusser, D. P., Hill, N. S., and Levin, P. A. (2007). A metabolic sensor governing cell size in bacteria. *Cell* 130, 335–347. doi: 10.1016/j.cell.2007.05.043

Weber, H., Polen, T., Heuveling, J., Wendisch, V. F., and Hengge, R. (2005). Genome-wide analysis of the general stress response network in *Escherichia coli*: σ S -dependent genes, promoters, and sigma factor selectivity. *J. Bacteriol.* 187, 1591–1603. doi: 10.1128/JB.187.5.1591-1603.2005

Wu, N., He, L., Cui, P., Wang, W., Yuan, Y., Liu, S., et al. (2015). Ranking of persister genes in the same *Escherichia coli* genetic background demonstrates varying importance of individual persister genes in tolerance to different antibiotics. *Front. Microbiol.* 6:1003. doi: 10.3389/fmicb.2015.01003

Yao, Z., Davis, R. M., Kishony, R., Kahne, D., and Ruiz, N. (2012). Regulation of cell size in response to nutrient availability by fatty acid biosynthesis in *Escherichia coli*. *Proc. Natl. Acad. Sci. U.S.A.* 109, E2561–E2568. doi: 10.1073/pnas.1209742109

Ziervogel, B. K., and Roux, B. (2013). The binding of antibiotics in OMPF porin. *Structure* 21, 76–87. doi: 10.1016/j.str.2012.10.014

Conflict of Interest Statement: The authors declare that the research was conducted in the absence of any commercial or financial relationships that could be construed as a potential conflict of interest.

frontiers in Microbiology

ORIGINAL RESEARCH
published: 20 August 2018
doi: 10.3389/fmicb.2018.01933

Melatonin Minimizes the Impact of Oxidative Stress Induced by Hydrogen Peroxide in *Saccharomyces* and Non-conventional Yeast

Jennifer Vázquez[1], Karlheinz Grillitsch[2], Günther Daum[3], Albert Mas[1], María-Jesús Torija[1] and Gemma Beltran[1]*

[1] Oenological Biotechnology Research Group, Department of Biochemistry and Biotechnology, Faculty of Oenology, University of Rovira i Virgili, Tarragona, Spain, [2] Austrian Centre of Industrial Biotechnology, Graz, Austria, [3] Institute of Biochemistry, Graz University of Technology, Graz, Austria

OPEN ACCESS

Edited by:
John P. Morrissey, University College Cork, Ireland

Reviewed by:
Giuseppe Spano, University of Foggia, Italy
Matthias Sipiczki, University of Debrecen, Hungary
Rodrigo Ledesma-Amaro, Imperial College London, United Kingdom

***Correspondence:**
María-Jesús Torija
mjesus.torija@urv.cat

Specialty section:
This article was submitted to Microbial Physiology and Metabolism, a section of the journal Frontiers in Microbiology

Received: *08 May 2018*
Accepted: *30 July 2018*
Published: *20 August 2018*

Citation:
Vázquez J, Grillitsch K, Daum G, Mas A, Torija M-J and Beltran G (2018) Melatonin Minimizes the Impact of Oxidative Stress Induced by Hydrogen Peroxide in Saccharomyces and Non-conventional Yeast. Front. Microbiol. 9:1933. doi: 10.3389/fmicb.2018.01933

Melatonin (*N*-acetyl-5-methoxytryptamine) is synthesized from tryptophan by *Saccharomyces cerevisiae* and non-conventional yeast species. Antioxidant properties have been suggested as a possible role of melatonin in a *S. cerevisiae* wine strain. However, the possible antioxidant melatonin effect on non-*Saccharomyces* species and other strains of *S. cerevisiae* must be evaluated. The aim of this study was to determine the antioxidant capacity of melatonin in eight *S. cerevisiae* strains and four non-conventional yeasts (*Torulaspora delbrueckii*, *Metschnikowia pulcherrima*, *Starmerella bacillaris,* and *Hanseniaspora uvarum*). Therefore, the ROS formation, lipid peroxidation, catalase activity, fatty acid composition, and peroxisome proliferation were investigated. The results showed that the presence of melatonin increases peroxisome accumulation and slightly increases the catalase activity. When cells grown in the presence of melatonin were exposed to oxidative stress induced by H_2O_2, lower ROS accumulation and lipid peroxidation were observed in all tested strains. Therefore, the increased catalase activity that was a consequence of oxidative stress was lower in the presence of melatonin. Moreover, the presence of MEL modulates cell FA composition, increasing oleic and palmitoleic acids and leading to higher UFA/SFA ratios, which have been previously related to a higher tolerance to H_2O_2. These findings demonstrate that melatonin can act as an antioxidant compound in both *S. cerevisiae* and non-*Saccharomyces* yeasts.

Keywords: *Torulaspora delbrueckii*, *Metschnikowia pulcherrima*, *Starmerella bacillaris*, *Hanseniaspora uvarum*, ROS, TBARS, catalase, peroxisomes

INTRODUCTION

Melatonin (*N*-acetyl-5-methoxytryptamine) (MEL) is not only known as a neurohormone in vertebrates, but it is as well considered as a ubiquitous molecule that is present in most living organisms (Hardeland and Poeggeler, 2003). Sprenger et al. (1999) were the first authors to associate the production of MEL with *Saccharomyces cerevisiae*. Later, other reports showed high

quantities of MEL being produced by *S. cerevisiae*, and by other non-conventional yeast species such as *Torulaspora delbrueckii* and *Zygosaccharomyces bailii* (Rodriguez-Naranjo et al., 2011; Vigentini et al., 2015). Although only limited information is available on MEL biosynthesis in organisms other than vertebrates, the pathway in yeasts is thought to be similar to the synthetic route described in vertebrates. Four enzymes are involved in the conversion of tryptophan into serotonin and *N*-acetylserotonin intermediates and finally into MEL (Mas et al., 2014).

The functions of MEL have been extensively studied in mammals and animals, and they are primarily related to the regulatory mechanisms involved in circadian rhythms. However, the role of MEL in yeasts still needs to be elucidated. Recently, we have reported that MEL is able to act as antioxidant compound in one commercial wine strain of *S. cerevisiae* (Vázquez et al., 2017). As is the case in humans, MEL might protect various biomolecules from damages caused by free radicals by acting as a direct scavenger, detoxifying reactive oxygen and nitrogen species (Reiter et al., 2001, 2016; Anisimov et al., 2006), and indirectly increasing the activities of antioxidant defense systems. It could also act by stimulating the synthesis of other important intracellular antioxidants such as glutathione peroxidase and superoxide dismutase (Antolín et al., 1996; Rodriguez et al., 2004).

Oxidative stress is the outcome of an imbalance between the presence of reactive oxygen species (ROS) and the capacity of cells to detoxify these reactive intermediates of molecular oxygen, or to repair the resulting damage. ROS are constantly generated during normal metabolism, and they exert physiological actions. However, when produced in excess, ROS cause detrimental effects and can damage cell macromolecules, such as DNA, lipids or proteins (Gutteridge and Halliwell, 2000; Halliwell, 2006). Among these targets of ROS, lipid peroxidation leads to one of the most damaging consequences for cells when unsaturated lipids are converted into polar lipid hydroperoxides because it allows the propagation of free radical reactions that could affect membrane integrity and even result in cell death (Howlett and Avery, 1997; Ayala et al., 2014). However, ROS formation is accompanied by an increase in yeast antioxidant defenses, with the aim of protecting the cells against noxious ROS. One system for neutralizing the excessive ROS formation in cells is to degrade them with antioxidant enzymes, such as catalase, glutathione peroxidase, and superoxide dismutase. By contrast, non-enzymatic systems, such as glutathione, glutaredoxins, and thioredoxins repair or remove the products of oxidative damage (Jamieson, 1998; Costa and Moradas-Ferreira, 2001; Auchère et al., 2008; Herrero et al., 2008).

Due to its high fermentation capacity, *S. cerevisiae* is the yeast that is traditionally used in the biotechnology, food and beverage industries. However, non-*Saccharomyces* yeasts are now gaining higher interests for industries; in fact, several studies have demonstrated that the presence of non-conventional yeasts during winemaking process can contribute to the aroma profile, sensory complexity and color stability (Jolly et al., 2014). During these industrial processes, yeasts are involved in different stages that can lead to oxidative stress for the cells, which could negatively affect yeast performance (Pretorius, 2000; Gómez-Pastor et al., 2012; Pérez-Gallardo et al., 2013). Thus, protective treatments against oxidative damage with natural antioxidants may have important biotechnological implications.

The goal of this study was to evaluate the possible antioxidant effect of MEL on different yeast species. To this end, we evaluated ROS production, lipid peroxidation and intracellular catalase activity in sixteen yeast strains of different species. We evaluated the response to oxidative stress induced by H_2O_2 and analyzed the possible protective activity of MEL supplementation.

MATERIALS AND METHODS

Yeast Strains and Experimental Conditions

The yeast strains used in this study were eight *S. cerevisiae* and eight non-*Saccharomyces*. The *S. cerevisiae* strains included three laboratory strains (BY4741, BY4742, and Sigma 1278b from EUROSCARF collection, Frankfurt, Germany), three commercial wine strains [QA23®, uvaferm HPS® and the hybrid VIN7 (*S. cerevisiae* x *S. kudriavzevii* AWRI1539®)] and two commercial strains for animal nutrition (Levucell® SC20 and SB20). The non-*Saccharomyces* species included two wine strains of *T. delbrueckii* [BIODIVA® (TdB) and Tdp], two wine strains of *Metschnikowia pulcherrima* [FLAVIA® (MpF) and Mpp], two wine strains of *Starmerella bacillaris* (Cz4 and Cz11), and two wine strains of *Hanseniaspora uvarum* (Hu4 and Hu35). The commercial *Saccharomyces* and non-*Saccharomyces* strains QA23, Uvaferm HPS, SC20, SB20, FLAVIA, and BIODIVA were provided by Lallemand S.A. (Montreal, QC, Canada), and VIN7 was provided by AWRI (Glen Osmond, SA, Australia). The other six non-*Saccharomyces* strains (Tdp, Mpp, Cz4, Cz11, Hu4, and Hu35) were isolated from natural musts from Priorat Appellation of Origin (Catalonia, Spain) (Padilla et al., 2016). The Tdp, Mpp, Cz4, and Hu4 were deposited in the Spanish Type Culture Collection (CECT) as CECT 13135, CECT 13131, CECT 13129, and CECT 13130, respectively.

All commercial strains were provided as active dry yeast and rehydrated according to the manufacturer's instructions. For all experiments, precultures for biomass propagation were prepared in YPD liquid medium [2% (w/v) glucose, 2% (w/v) peptone, and 1% (w/v) yeast extract (PanReac, Barcelona, Spain)] and incubated for 24 h at 28°C with orbital shaking (120 rpm). Yeast cells were subsequently inoculated into 50 mL of YPD broth (initial population 5×10^3 cells/mL) with and without supplementation of 5 μM MEL (two flasks for each condition) and grown until cells reached the initial exponential phase at 28°C with orbital shaking at 120 rpm. Sublethal oxidative stress was then induced in one flask of each condition with 2 mM of H_2O_2 for 1 h to generate the following four conditions: Control and MEL (without stress); and H_2O_2 and MEL H_2O_2 (with stress). The MEL and H_2O_2 concentrations were chosen from our previous study in the QA23 strain (Vázquez et al., 2017). Three biological replicates were tested for each condition.

Determination of Reactive Oxygen Species (ROS)

The effect of H_2O_2 (2 mM) with and without MEL (5 μM) on the intracellular ROS was evaluated in the sixteen yeast strains. Furthermore, ascorbic acid (25 μM), a well-known antioxidant, was used as positive control (Saffi et al., 2006). ROS was detected using dihydrorhodamine 123 (DHR 123; Sigma-Aldrich), according to the method used by Vázquez et al. (2017). In brief, the cells were stained with 10 μg DHR 123 per mL of cell culture for 15 min at 120 rpm in the dark. Cells were then washed twice with phosphate-buffered saline (PBS, pH 7.4), and the fluorescence intensity was measured by flow cytometry. The captured files were processed using WinMDI 2.9 software (Joseph Trotter, Salk Institute for Biological Studies, La Jolla, CA, United States) and the ROS were represented as the mean fluorescence index (MFI) and calculated according to Boettiger et al. (2001) as follows: [(geometric mean of the positive fluorescence) – (geometric mean of the control)]/(geometric mean of the control).

Thiobarbituric Acid Reacting Substances (TBARS)

The degree of lipid peroxidation was measured in unstressed and stressed cells with and without MEL supplementation in terms of TBARS content (Buege and Aust, 1978; Aust, 1994). Following a treatment using 2 mM of H_2O_2 for 1 h, 1×10^7 yeast cells from each condition were mechanically homogenized over three cycles of alternating sonication and liquid nitrogen (10/10 s). The samples were then mixed with 250 μL of trichloroacetic acid (10% v/v), incubated 15 min on ice, and after centrifugation at 2200 *g* for 15 min at 4°C, 200 μL of the supernatant was mixed with 200 μL thiobarbituric acid (6.7 g/L). These samples were then incubated in a boiling water bath for 10 min and cooled at room temperature. Finally, the absorbance was measured at 532 nm with a microplate reader (Omega POLARstar, BMG LABTECH GmbH, Ortenberg, Germany). The TBARS content was estimated by referring to a standard curve prepared with 1,1,3,3-tetramethoxypropane and the results were expressed as nmol of TBARS per mg of protein.

Catalase Activity

The catalase activity was evaluated in unstressed and stressed cells with and without MEL. First, 1×10^7 yeast cells were suspended in PBS (50 mM, pH 7.0) with one tablet of protease inhibitor per 10 mL of extraction solution (cOmplete™; Roche), and they were disrupted using glass beads with six cycles alternating cooling and shaking (30/30 s) and centrifuged at 14.000 rpm for 2 min. The assay was performed according to the method described by Aebi (1984). In brief, cells extracts were exposed to 10 mM of H_2O_2, and the decrease in absorbance at 240 nm due to H_2O_2 decomposition was monitored for 4 min, with measurements every 30 s at constant temperature (25°C) using a microplate reader (Omega POLARstar, BMG LABTECH GmbH, Ortenberg, Germany). The catalase activity was expressed as units of catalase per mg of protein. One unit of catalase activity decomposes 1 mmol of H_2O_2 per min.

Protein Estimation

The total protein levels were determined using the Bradford method (Bradford, 1976) by spectrophotometric determination at 545 nm, with bovine serum albumin (BSA, Sigma-Aldrich) as a standard. The absorbance was measured in an Omega POLARstar microplate reader spectrophotometer.

Yeast Viability After Stress Exposure

As in our previous study with *S. cerevisiae* (Vázquez et al., 2017), the viability of non-*Saccharomyces* strains after exposure to stress (MEL H_2O_2, ASC H_2O_2, and H_2O_2) in comparison with cells without stress (Control and MEL) was evaluated by a microplate assay. 96-well plates were prepared by dispensing 250 μL of YPD broth inoculated with cells of each condition to obtain an initial OD_{600} of 0.005. The microplate was incubated at 28°C and the optical density at 600 nm was measured every 30 min during 30 h using a microplate reader (Omega POLARstar, BMG LABTECH GmbH, Ortenberg, Germany).

Analysis of Fatty Acid Composition

The composition of fatty acids (FAs) of QA23 and TdB strains was analyzed in cells which were untreated and treated with 5 μM of MEL in absence of stress (Control and MEL) and 18 h after the oxidative stress (2 mM H_2O_2) was applied to allow the cells to respond to this stress (MEL H_2O_2 and H_2O_2). Yeast cells homogenates were obtained from 50 mL of total cells pellets using glass beads and a Disruptor Genie® (Scientific Industries, Inc., NY, United States) for 10 min at 4°C. Proteins from the homogenates were then precipitated with 10% (v/v) trichloroacetic acid and quantified with de Folin phenol reagent (Lowry et al., 1951). The total lipids were extracted from cell fractions corresponding to 1 mg of total cell protein according to the method by Folch et al. (1957). The FA composition was determined by gas liquid chromatography (GLC) according to Rußmayer et al. (2015). In brief, the total FAs from lipid extracts were first converted to methyl esters by methanolysis with sulfuric acid (2.5% in methanol (v/v); 80°C for 90 min) and then extracted twice with light petroleum and water (3:1; v/v) by shaking on a Vibrax orbital shaker® (IKA, Staufen, Germany) for 30 min. Finally, FAs were separated by GLC on a Hewlett-Packard 6890 gas-chromatograph (Agilent Technologies, CA, United States) using an HP-INNOWax capillary column (15 m × 0.25 mm × 0.50 μm film thickness) with helium as a carrier gas. Identification was done by comparison with a commercial FA methyl ester standard mix (NuCheck, Inc., MN, United States) and quantification using the pentadecanoic acid (C15:0, Sigma-Aldrich) as an internal standard. Two biological replicates were set up for each strain and two analytical replicates were performed for each biological replicate.

Western Blot (Immunoblot) Analysis

The immunological characterization of QA23 and TdB strain homogenates from the four conditions (Control, MEL, MEL

H_2O_2, and H_2O_2) was performed by Western blot analysis as described by Haid and Suissa (1983). In brief, the cells were disrupted with glass beads using a Disruptor Genie® (Scientific Industries, Inc., NY, United States) at 4°C for 10 min and centrifuged at 4°C at 500 *g* for 5 min. After TCA precipitation of supernatants, protein samples were separated by sodium dodecyl sulfate polyacrylamide gel electrophoresis (SDS-PAGE, 12.5%), and later transferred to the nitrocellulose sheets according to standard procedures (Laemmli, 1970). Finally, a western blot analysis was performed using a primary rabbit antibody against Fox1p protein (multifunctional β-oxidation protein from peroxisomal membranes), a marker of peroxisomes organelles. Immunoreactive bands were visualized using a peroxidase-conjugated secondary antibody according to the manufacturer's instructions (SuperSignal™, Pierce Chemical Company, IL, United States). The cytosolic protein GAPDH (glyceraldehyde-3-phosphate dehydrogenase) was used as a loading control, and isolated peroxisomes from *S. cerevisiae* were the positive control. The identified bands were quantified using ImageJ software (National Institutes of Health, MD, United States) and normalized to positive control.

Data Analysis

The data were subjected to one-way analysis of variance (ANOVA) and Tukey's *post hoc* test to evaluate the effect of each treatment. The results were considered statistically significant at a *p*-value less than 0.05 (IBM SPSS Inc, XLSTAT Software).

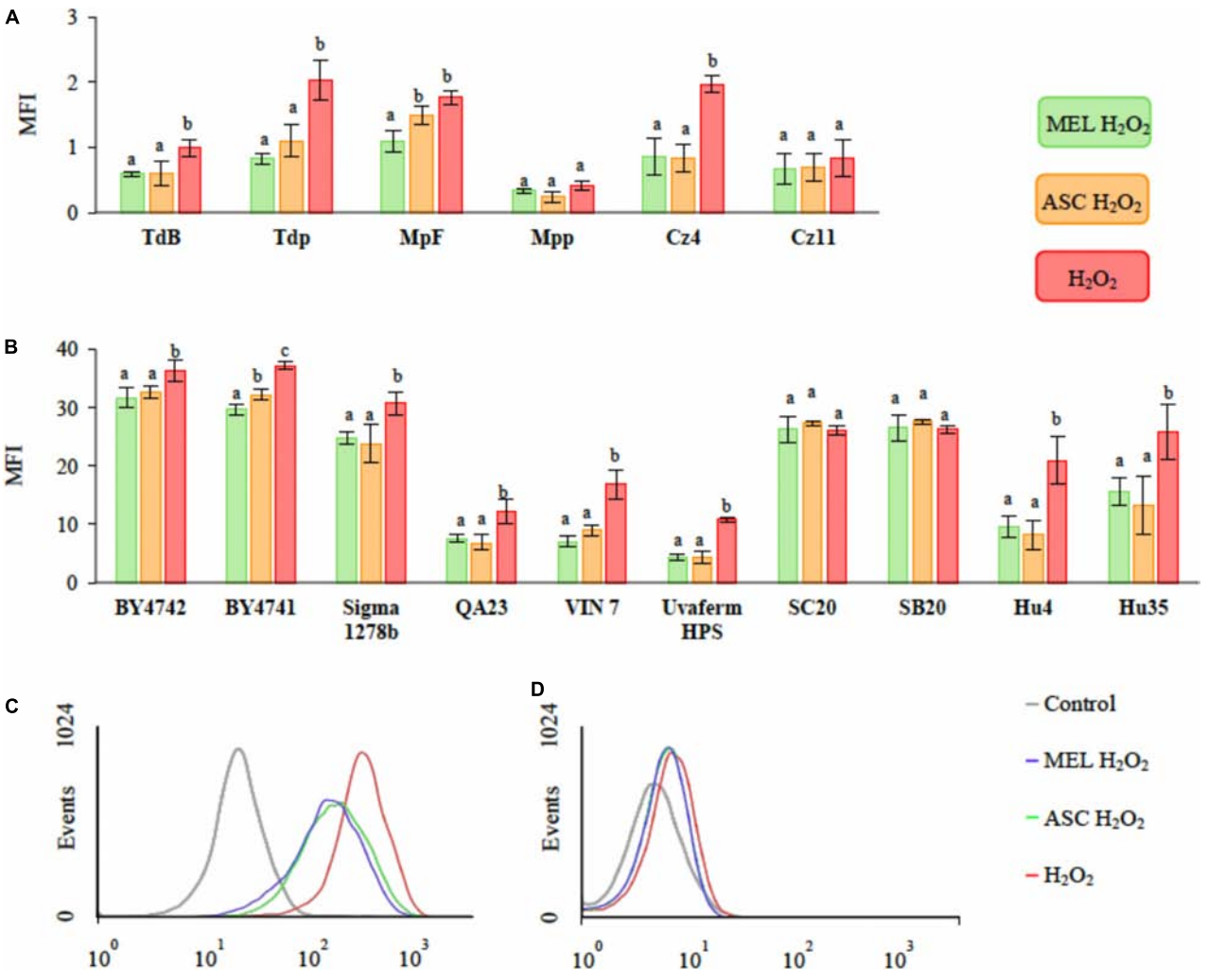

FIGURE 1 | Melatonin (MEL, 5 μM) effect on ROS accumulation as evaluated in sixteen yeast strains under oxidative stress that was induced with 2 mM of H_2O_2. Cells without MEL and H_2O_2 were used as negative control, cells with 2 mM of H_2O_2 were used as the positive control and cells treated with ascorbic acid (25 μM) served as the positive antioxidant control. **(A)** The mean fluorescence index (MFI) of the *T. delbrueckii* (TdB and Tdp), *M. pulcherrima* (MpF and Mpp), and *C. zemplinina* (Cz4 and Cz11) strains. **(B)** The MFI of the *S. cerevisiae* (BY4742, BY4741, Sigma 1278b, QA23, VIN 7, SC20, SB20, and Uvaferm HPS) and *H. uvarum* (Hu4 and Hu35) strains. **(A,B)** Different letters indicate significant differences between conditions within each strain, $p < 0.05$. **(C,D)** Flow cytometry histogram profiles expressed as the number of events in VIN 7 **(C)** and Cz4 **(D)** with MEL (5 μM) or ascorbic acid (ASC, 25 μM) and with 2 mM of H_2O_2.

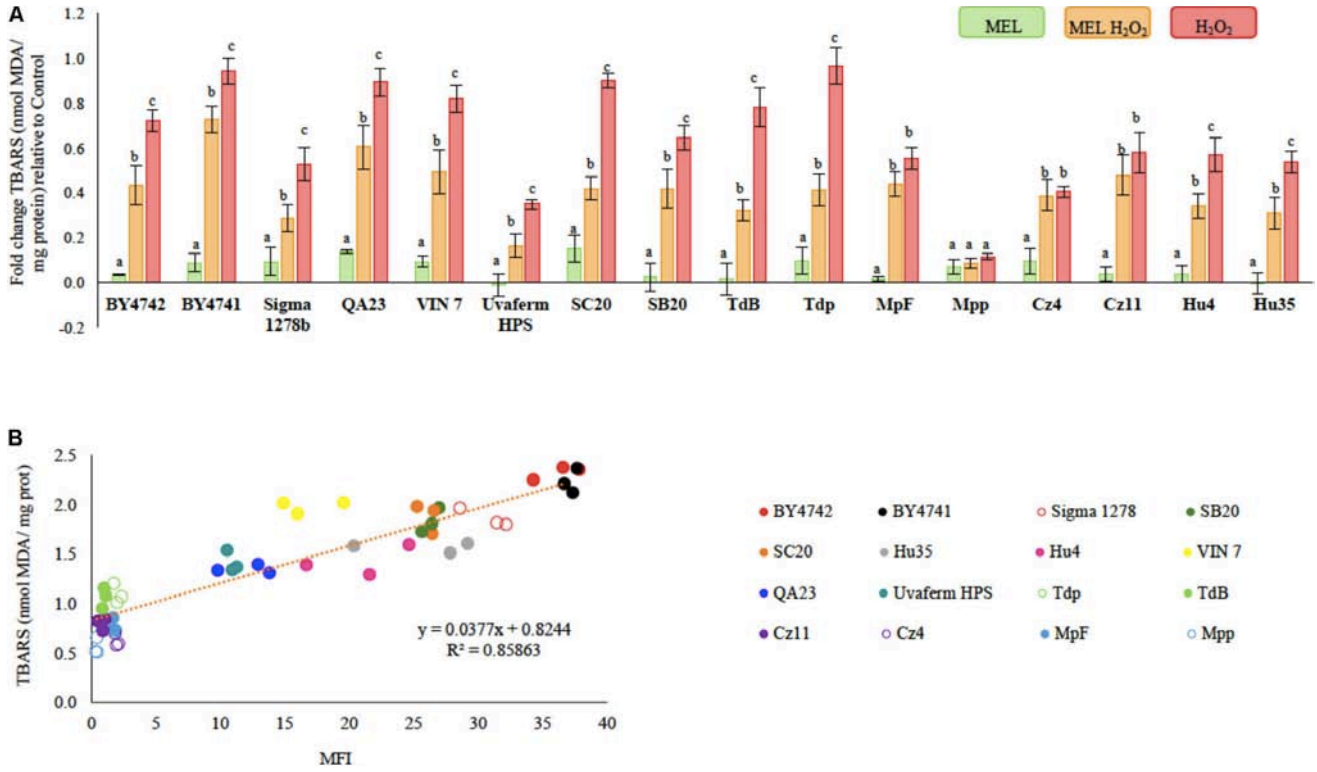

FIGURE 2 | (A) Lipid peroxidation in unstressed and stressed yeast cells with 2 mM of H_2O_2, growing with and without 5 μM of melatonin (MEL). The strains analyzed (n = 3 of each strain) were *S. cerevisiae* (BY4742, BY4741, Sigma 1278b, QA23, VIN 7, SC20, SB20, and uvaferm HPS), *T. delbrueckii* (TdB and Tdp), *M. pulcherrima* (MpF and Mpp), *C. zemplinina* (Cz4 and Cz11), and *H. uvarum* (Hu4 and Hu35). Error bars represent ± SD of n = 3 by ANOVA. Different letters indicate significant differences between conditions within each strain, $p < 0.05$. **(B)** The correlation between ROS accumulation (MFI, **Figure 1**) and lipid peroxidation (TBARS, **Supplementary Table S1**) in the sixteen strains (n = 3 of each strain) after stress exposure with H_2O_2 (2 mM).

RESULTS

Reactive Oxygen Species (ROS)

To evaluate the possible role of MEL as an antioxidant agent in the *Saccharomyces* and non-*Saccharomyces* species, the intracellular ROS levels were measured in stressed cells with and without 5 μM of MEL (Vázquez et al., 2017). Stressed cells with 2 mM of H_2O_2 and without MEL were used as positive control and cells without stress and without MEL were used as a negative control. Cells treated with 25 μM of ascorbic acid were used as positive antioxidant control (**Figure 1**). The results showed that cells that had been exposed to oxidative stress (2 mM H_2O_2) exhibited an increase in the total ROS. However, the ROS accumulation was species-dependent, with *M. pulcherrima*, *S. bacillaris* and *T. delbrueckii* exhibiting the lowest levels of endogenous ROS (**Figures 1A,D**). By contrast, the *Saccharomyces* and *H. uvarum* strains presented the highest levels of ROS (**Figures 1B,C**). For the *S. cerevisiae* strains, clear differences were observed between the wine strains and laboratory and animal nutrition strains, with the wine strains exhibiting the lower levels of endogenous ROS. The antioxidant effects of MEL were very similar to those of ascorbic acid for most investigated strains. However, there were few cases in which none of the antioxidants had any protective effect (*S. cerevisiae* strains SC20 and SB20, *M. pulcherrima* Mpp and *S. bacillaris* Cz11 (**Figure 1**).

Lipid Peroxidation

The effect of MEL on oxidative damage in the membranes was evaluated in all yeasts by measuring the lipid peroxides in the TBA derivative form (**Figure 2A**). Most strains studied here suffered from a significant increase in lipid peroxidation after stress exposure, with the Mpp strain being the only one in which its lipid peroxidation was not affected by H_2O_2. In fact, the lipid peroxidation results were positively correlated with ROS accumulation (**Figure 2B**, R^2 = 0.85863). Thus, the *M. pulcherrima*, *S. bacillaris*, and *T. delbrueckii* strains, which showed lower ROS accumulation, also exhibited lower lipid peroxidation and vice versa. Strains with higher ROS accumulation showed higher lipid peroxidation (**Figure 2B**). The positive effect of MEL supplementation was clearly observed under stress conditions (**Figure 2A**, MEL H_2O_2), in which MEL seems to protect *Saccharomyces*, *T. delbrueckii*, and *H. uvarum* cells against H_2O_2 damage by decreasing lipid peroxidation. In *M. pulcherrima* and *S. bacillaris*, no MEL effect was observed on lipid peroxidation. However, no significant differences were observed in the lipid peroxidation between unstressed cells with or without MEL, although in some strains, there was

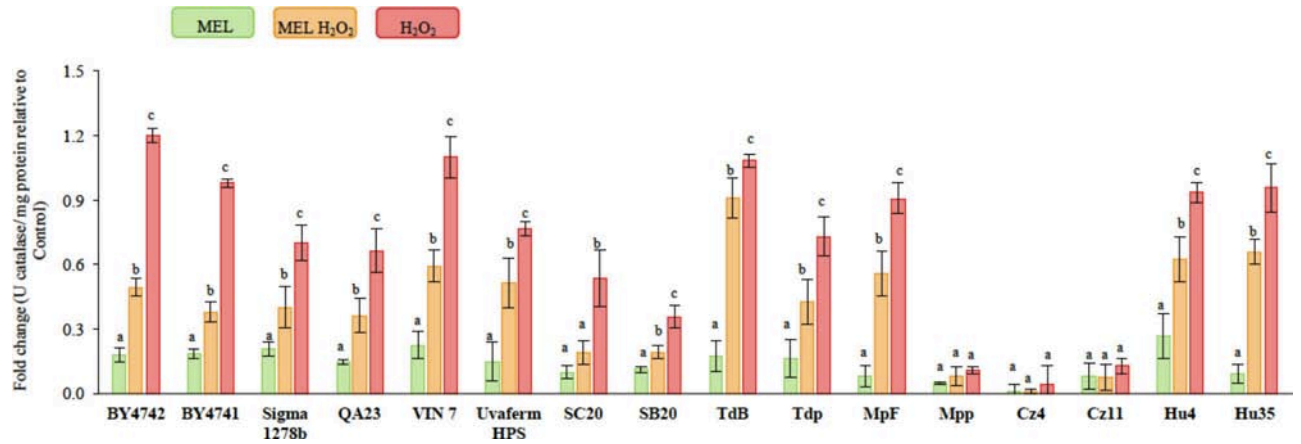

FIGURE 3 | Catalase activity in unstressed and stressed yeast cells with 2 mM of H_2O_2, growing with and without 5 μM of melatonin (MEL). The strains used were: *S. cerevisiae* (BY4742, BY4741, Sigma 1278b, QA23, VIN 7, SC20, SB20, and uvaferm HPS), *T. delbrueckii* (TdB and Tdp), *M. pulcherrima* (MpF and Mpp), *C. zemplinina* (Cz4 and Cz11), and H. uvarum (Hu4 and Hu35). The error bars represent ± SD of $n = 3$ by ANOVA. Different letters indicate significant differences between conditions within each strain, $p < 0.05$.

an increasing trend in lipid peroxidation in presence of MEL (**Figure 2A** and **Supplementary Table S1**, Control and MEL).

Catalase Activity

To further study the role of MEL in yeasts, the effect of its supplementation (5 μM MEL) on catalase activity was evaluated in unstressed and stressed cells (**Figure 3**). The control condition (without stress and without MEL) for non-conventional yeasts showed higher catalase activity than did the *Saccharomyces* species (**Supplementary Table S1**). When MEL was added in absence of stress, the catalase activity of *Saccharomyces*, *T. delbrueckii*, and *H. uvarum* slightly increased (**Figure 3** and **Supplementary Table S1**). However, when cells were exposed to H_2O_2, the catalase activity clearly increased in all the strains except for Mpp and *S. bacillaris* (**Figure 3**). However, this activity was significantly reduced when the cells had been grown in the presence of MEL before the stress was applied (**Figure 3** and **Supplementary Table S1**). Under these stress conditions, no numeric correlation was found between the catalase activity and ROS accumulation or TBARS assay (data not shown).

Effect of Melatonin on Cell Growth Viability After Oxidative Stress Exposure

To evaluate the effect of MEL on the growth of non-*Saccharomyces* strains after stress exposure, cells were reinoculated in YPD, and growth was followed during 30 h (**Figure 4**). In the absence of stress, similar growth curves were observed for both conditions (with and without MEL).

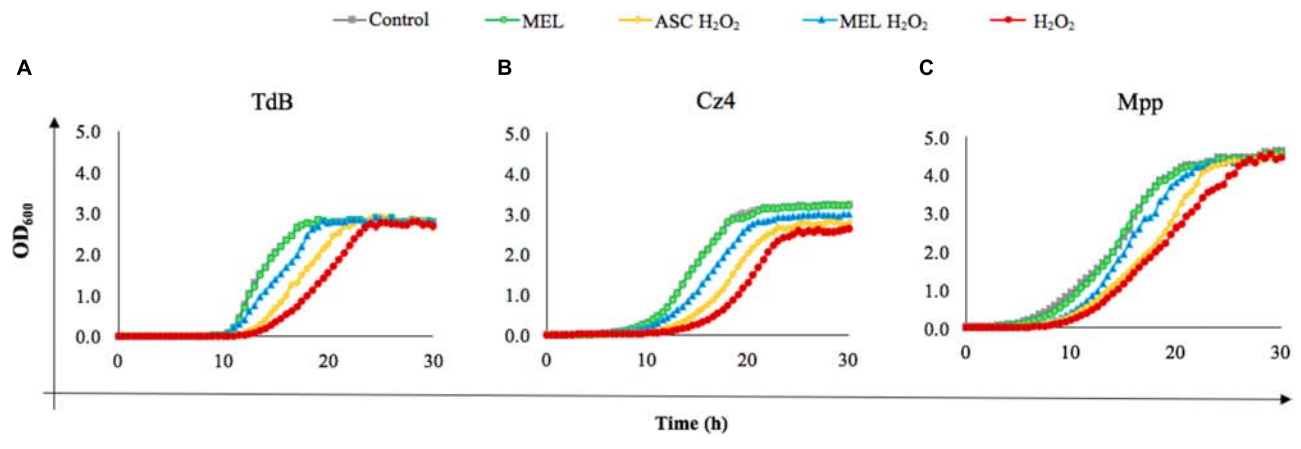

FIGURE 4 | Melatonin effect on cell growth viability after oxidative stress exposure (2 mM of H_2O_2) in three non-*Saccharomyces* yeast (**A**, *T. delbrueckii* TdB strain; **B**, *S. bacillaris* Cz4 strain; and **C**, *M. pulcherrima* Mpp strain). Stress was applied in early exponential phase. H_2O_2, stressed cells; MEL H_2O_2, stressed cells in presence of 5 μM of MEL; ASC H_2O_2, stressed cells in presence of 25 μM of ascorbic acid. Two conditions were considered as controls. Control, unstressed cells; MEL, unstressed cells in presence of 5 μM of MEL.

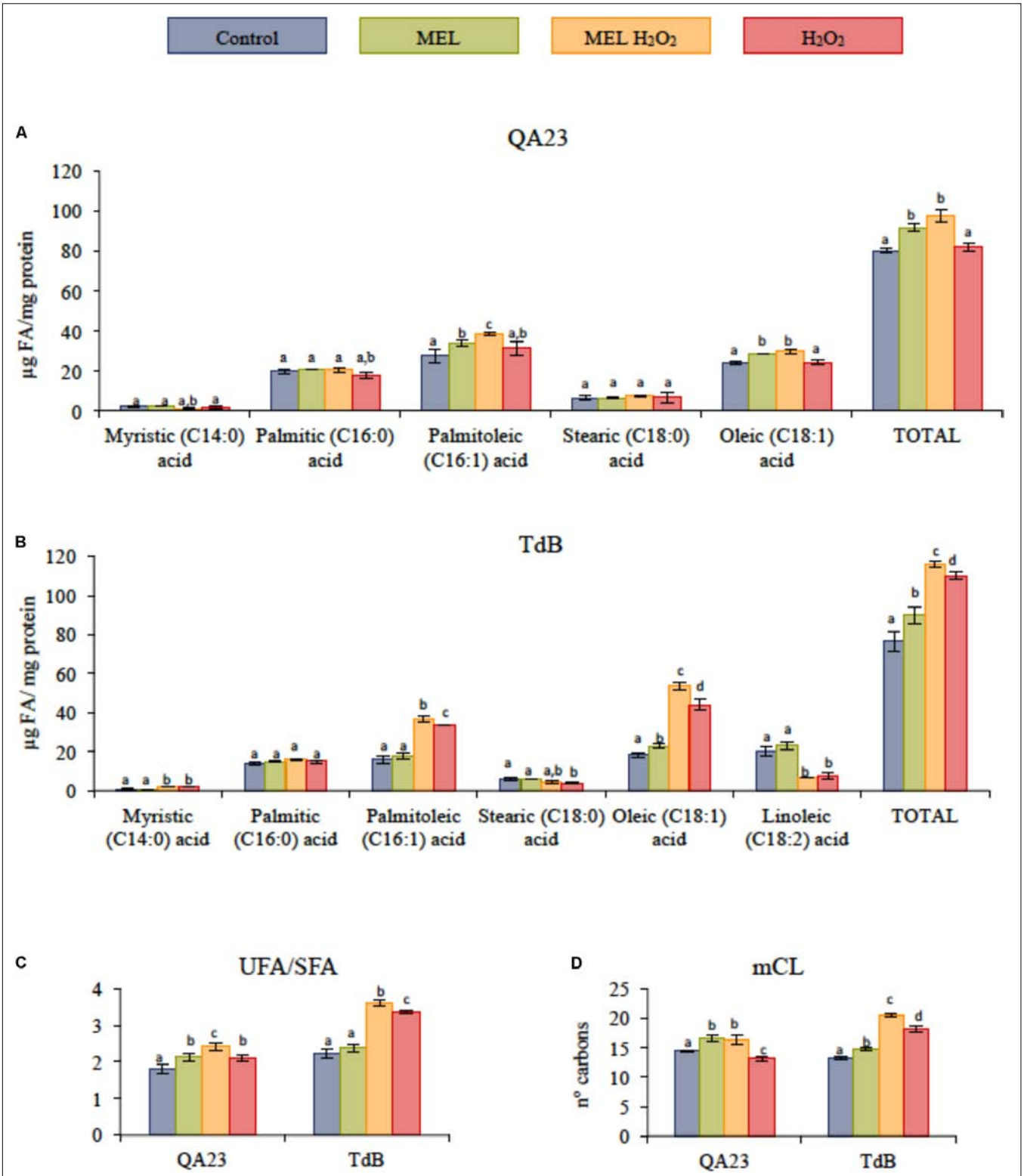

FIGURE 5 | Fatty acid (FA) composition of unstressed and stressed yeast cells with 2 mM of H_2O_2, growing with and without 5 µM of melatonin (MEL). **(A)** FA of QA23 strain. **(B)** FA of TdB strain. **(C)** Unsaturated to saturated FA ratio (UFA/SFA) of both strains. UFA/SFA ratio was defined as follows: (C16:1 + C18:1 + C18:2)/(C14:0 + C16:0 + C18:0). **(D)** Medium length chain of FA of both strains. mCL was calculated as follows: Σ(%FA × N° FA carbons)/100. Different letters in superscripts indicate significant differences between conditions for each studied compound **(A,B)** or for each strain **(C,D)** ($P < 0.05$).

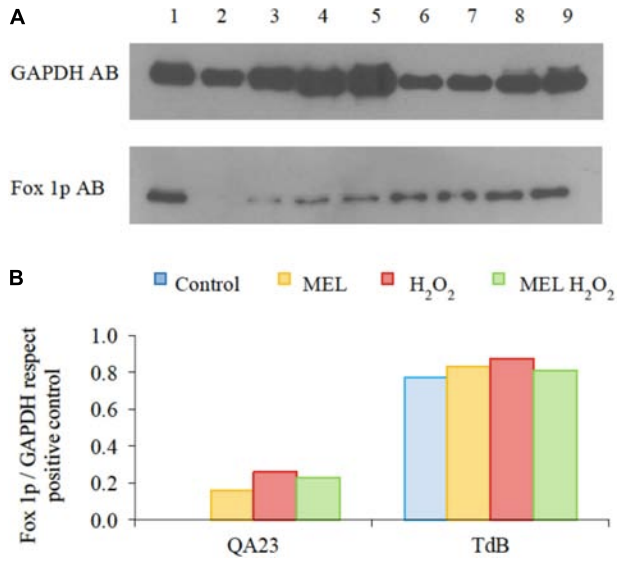

FIGURE 6 | Western blot analysis of homogenates analyzed with antibody against peroxisome marker Fox1p using antibody GAPDH antibody as the loaded protein control. **(A)** Isolated peroxisomes from *S. cerevisiae* were used as the positive control (1). Homogenates from *S. cerevisiae* QA23 (2–5) and *T. delbrueckii* TdB (6–9) in cells without treatment (Control: 2 and 6), cells without stress and 5 μM of melatonin (MEL, 3 and 7), cells with 2 mM H_2O_2 (4 and 8) and cells with 2 mM H_2O_2 and 5 μM of MEL (5 and 9). **(B)** Fox1p/GAPDH quantification from the bands identified in **A** was normalized to the positive control.

In contrast, under oxidative stress, viability of all strains was significantly affected; the presence of MEL was able to greatly enhance cell growth in non-*Saccharomyces* strains, recovering, in general, a growth curve similar to non-stressed cells. In addition, the effect of 5 μM of MEL was higher than that of 25 μM of ascorbic acid.

Changes in FA Composition

The effect of MEL on FA content under the four experimental conditions (Control, MEL, MEL H_2O_2, and H_2O_2, **Figure 5**) was tested in two strains (QA23 and TdB). In general, the total FA content increased mainly due to a higher content of monounsaturated fatty acids (MUFAs), such as oleic and palmitoleic acids (**Figures 5A,B**). In *S. cerevisiae* QA23 strain, the highest content of FA was found under melatonin conditions, whereas in the TdB strain, under stress conditions. Similar results were observed in unsaturated to saturated FA ratio (UFA/SFA) and percentage of medium chain length (mCL), being the MEL H_2O_2, the condition with the highest UFA/SFA ratio in both strains (**Figures 5C,D**). On the other hand, TdB strain presented also linoleic acid in its lipid composition, which significantly decreased after stress exposure.

Analysis of Peroxisome Proliferation

A western blot analysis using the direct antibody against Fox1p, a multifunctional β-oxidation protein from the peroxisomal membranes, was performed with QA23 and TdB homogenates, with and without stress exposure, and in the presence or absence of MEL. As shown in **Figures 6A,B**, the enrichment of Fox1p was higher in *T. delbrueckii* than in *S. cerevisiae* under both stressed and unstressed conditions. Under the control condition, Fox1p was undetectable in *S. cerevisiae,* but its detection increased in the presence of H_2O_2. Instead, *T. delbrueckii* showed a high number of peroxisomes independent of stress exposure. MEL induced the proliferation of peroxisomes in the absence of stress, especially in *S. cerevisiae*. Under stress conditions, MEL seemed to decrease the peroxisomes accumulation slightly in both species.

DISCUSSION

The role of MEL in cells has been extensively studied in humans and other organisms (Hardeland and Poeggeler, 2003; Tan et al., 2015) and its antioxidant capacity is one of the most important biological activities described to date. *S. cerevisiae* synthetizes MEL from tryptophan during alcoholic fermentation (Mas et al., 2014), but very little information is available on MEL biosynthesis and its bioactive functions in yeast. Recently, we reported that MEL is able to act as an antioxidant compound in a wine *S. cerevisiae* strain (Vázquez et al., 2017); however, its antioxidant role in other *Saccharomyces* strains and other non-conventional yeast species is still unknown. Therefore, sixteen strains from five different yeast species were used to evaluate if the protective effect of MEL against oxidative stress is provided due to intra or interspecific response.

As expected, ROS formation was positively correlated with lipid peroxidation. Exposure to oxidative stress has been reported to cause an increase in intracellular ROS that resulted in a loss of membrane integrity due to the peroxidation of unsaturated fatty acids by ROS because the polyunsaturated fatty acids (PUFAs) are more prone to oxidation than MUFAs (Ayala et al., 2014; Johansson et al., 2016). However, in our study, the non-*Saccharomyces* species that include PUFAs as native constituent in their biological membranes (*T. delbrueckii, M. pulcherrima*, and *S. bacillaris*) (Rozès et al., 1992), have exhibited higher resistance to oxidative stress together with lower ROS formation and lower lipid peroxidation. Cipak et al. (2008) reported that even if a PUFA-producing *S. cerevisiae* yeast was initially more sensitive to oxidative stress than the wild-type strain, this transgenic strain became more resistant to H_2O_2 after some time of cultivation had passed, indicating that there was an adaptation to the endogenous oxidative stress due to the presence of PUFAs. The authors hypothesized that the presence of those PUFAs during aerobic growth generated low but significant levels of lipid peroxidation products (specifically 4-hydroxynonenal, or HNE), even in the absence of exogenous stress, which can act as a signaling molecule to activate the stress response and prepare the cells for subsequent stresses (Chen et al., 2006; Cipak et al., 2008). At sublethal concentrations, the accumulation of lipid peroxidation products stimulates the defense network, triggering the early response enzymes (antioxidative and detoxifying enzymes) and induces an adaptive response to cope with the forthcoming oxidative stress (Chen et al., 2006). A similar stress response mechanism might explain

the higher resistance to oxidative stress of these yeast species of our study that characteristically contained membranes rich in PUFAs. Nevertheless, a decrease of PUFAs and an increase of MUFAs after stress were observed in these species, which could be a mechanism of non-*Saccharomyces* yeasts to better resist oxidative stress without compromising membrane integrity.

The results obtained here show that under unfavorable conditions that affect the redox balance, *Saccharomyces*, *T. delbrueckii*, and *H. uvarum* clearly take advantage of MEL supplementation in the growth medium, reducing the toxic effects of H_2O_2 (decreasing the ROS levels and lipid peroxidation). These results are in accordance with several studies in humans (Tesoriere et al., 1999; Taysi et al., 2003; Ündeğer et al., 2004) and with our previous studies with a wine *S. cerevisiae* strain (Vázquez et al., 2017) in which the protective action of MEL might be attributed to its ability to scavenge ROS particles and consequently prevent cellular damage. MEL is able to act as a direct free radical scavenger and as an indirect antioxidant, detoxifying for numerous ROS including H_2O_2, hydroxyl radical ($^{\cdot}OH$), peroxyl radicals ($ROO^{\cdot}$), singlet oxygen ($^1O_2$), and also reactive nitrogen species (RNS) (Romero et al., 2014). Moreover, MEL was able to enhance cell recovery in non-*Saccharomyces* strains after being exposed to oxidative stress in early exponential phase, while this effect was observed in late exponential phase for QA23 strain in a previous study (Vázquez et al., 2017). This early improvement of cell viability after stress in non-*Saccharomyces* strains could be related to the different lipid composition of their membranes compared to *S. cerevisiae* strains (submitted manuscript). Indeed, the presence of MEL in stressed cells increased the total FA levels, specifically, the MUFAs, leading to higher UFA/SFA ratios, which have been previously related to a higher tolerance to H_2O_2 (Serrazanetti et al., 2015). Oleic acid has been reported as a membrane fluidity sensor, and it seems to be the most important UFA for counteracting the toxic nature of ethanol by increasing the membrane stability and antagonizing the fluidity caused by ethanol (You et al., 2003). Furthermore, palmitoleic acid is induced by stress in high-density fermentations, and it has a protective function against damage (Mannazzu et al., 2008; Ding et al., 2009).

Catalases are clearly important for proper resistance toward H_2O_2. However, the role of catalases enzymes in yeasts is not fully understood. Catalase A is located in the peroxisome and is primarily responsible for detoxifying H_2O_2 formed by acyl-CoA oxidase during β-oxidation, whereas the physiological role of the cytosolic catalase T is less clear. However, the expression of *CTT1* gene, which encodes this enzyme, is regulated by oxidative and osmotic stress (Jamieson, 1998; Krantz et al., 2004). The process of β-oxidation is exclusively housed by peroxisomes in yeast. Here, peroxisomal oxidases, such as Pox1p/Fox1p pass electrons directly to oxygen to generate H_2O_2, which is decomposed into water and oxygen by catalase A with concomitant release of energy as heat. β-oxidation per se does not depend on a functional peroxisomal catalase (Hiltunen et al., 2003).

Non-conventional yeasts showed slightly higher catalase activity than *Saccharomyces* strains under the control condition (without stress or MEL). Cipak et al. (2008) uncovered related PUFA production with an increase in the catalase activity, pinpointing cytosolic catalase T as essential for the survival of cells against oxidative stress, and peroxisomal catalase A as important for adapting to this stress. Therefore, higher catalase activity in non-*Saccharomyces* strains prior to stress occurs can also be induced as a response to the presence of PUFA in the membrane composition, resulting in a faster adaptation and a better tolerance to the stress. Although the catalase activity increased in the presence of oxidative stress with H_2O_2, no direct correlation between catalase activity and ROS or lipid peroxidation was observed in our results, suggesting that catalase, which is a primary enzymatic defense, is quickly activated in presence of H_2O_2 with the aim of avoiding cellular damage neutralizing ROS. Furthermore, this finding could indicate that other antioxidant primary defenses such as superoxide dismutase and glutathione peroxidase (no determined in this study), which rapidly sense and respond to oxidative stress, may also be contributing to the maintainance of the ROS concentrations at a basal level (Jamieson, 1998; Costa and Moradas-Ferreira, 2001; Moradas-Ferreira and Costa, 2013).

Moreover, MEL supplementation increased catalase activity in the *Saccharomyces*, *T. delbrueckii*, and *H. uvarum* strains. Together with our previous results in the QA23 strain (Vázquez et al., 2017) in which we also observed that MEL slightly increased the ROS amount as well as the mRNA levels of *CTT1* and *CTA1* (genes encoding catalase T and catalase A, respectively) and other enzymes involved in primary defense, these current results seem to confirm the role of MEL as a prooxidant that prepares the cells to better endure subsequent stress. As expected, the catalase activity was even higher in cells exposed to H_2O_2. When cells exposed to H_2O_2 were pretreated with MEL, catalase activity significantly decreased. Similar results were obtained by Saffi et al. (2006), but using L-ascorbic acid as an antioxidant and paraquat as an oxidative agent. The authors hypothesized that the reduced catalase activity caused by the presence of L-ascorbic acid could indicate that L-ascorbic acid has sequestered part of the ROS generated by paraquat, thereby reducing the need for catalase biosynthesis. Therefore, the presence of antioxidant compounds such as MEL would reduce the amount of ROS when an oxidative stress is applied and would modulate the catalase levels in yeast cells.

Peroxisomes play important roles in yeast metabolism, mostly in the β-oxidation of fatty acids and in the degradation of toxic hydrogen peroxide via catalase and other antioxidant enzymes (Hiltunen et al., 2003; Schrader and Fahimi, 2006). The amount of peroxisomes in the cell (proliferation or degradation) is modulated in response to nutritional and environmental stimuli. Our results showed higher peroxisome proliferation in cells under stress coinciding with higher catalase activities, indicating a direct relationship between both parameters. In fact, the responses to oxidative stress in *S. cerevisiae* seem to be co-regulated, similar to the increase of ROS and lipid peroxidation, which activates the proliferation of peroxisomes. The observed increase in the peroxisome proliferation comes hand with elevated catalase activity. To shed cellular organelles from harmful ROS, yeasts sequester ROS in peroxisomes, an organelle specialized and perfectly enzymatically equipped for

detoxification of harmful molecules, such as H_2O_2. In fact, peroxisomes are considered a source of oxidative stress due to the generation of ROS in its respiratory pathway. However, peroxisomes can also respond to oxidative stress and ROS when they are generated at other intra- or extracellular locations, protecting the cell against oxidative damage (Schrader and Fahimi, 2006). Higher amounts of peroxisomes were observed in TdB strain (together with higher amounts of catalase activity and lower ROS levels), in comparison to QA23. Although several authors have described *T. delbrueckii* as Crabtree positive, its respiratory metabolism makes greater contribution to the overall metabolism than in *Saccharomyces* (Alves-Araújo et al., 2007; Merico et al., 2007). Moreover, genes encoding for peroxisomal β-oxidation in *S. cerevisiae* are repressed by glucose, even in the presence of both oleate and oxygen, which are two inducers of the peroxisomes proliferation (Hiltunen et al., 2003; Schrader and Fahimi, 2006). Therefore, this higher peroxisomal activity of TdB strain, even before stress, together with the lower levels of ROS, indicates that *T. delbrueckii* (TdB strain) could have established a sophisticated strategy to maintain an equilibrium between the production and scavenging of ROS. Peroxisome proliferation was induced by MEL, even without stress and primarily in *S. cerevisiae* (QA23 strain). Those results suggest a possible role of MEL as pro-oxidant because it seems capable to prepare the cells to better endure a later oxidative stress, as observed by Vázquez et al. (2017).

Our results indicate that MEL presents antioxidant properties against hydrogen peroxide stress in all the studied yeasts. To the best of our knowledge, the antioxidant effect of MEL in non-*Saccharomyces* yeasts was not previously investigated. Furthermore, in terms of antioxidant properties, MEL is comparable to vitamin C (Reiter et al., 2007), and its effect was even higher under our conditions, because after stress exposure, cell viability was higher and ROS reduction similar with MEL than with ascorbic acid, but at lower MEL concentration.

The knowledge of the role of MEL in yeast will help to understand its synthesis and to obtain MEL-overproducing strains, which could have important biotechnological implications, such as diminishing cellular oxidative stress during the biotechnological production of yeast starters (Gamero-Sandemetrio et al., 2015). Moreover, a better characterization of this antioxidant mechanism could favor its use as potential therapeutic target for several oxidative stress-related diseases (Halliwell, 2006; Gutteridge and Halliwell, 2010; Escoté et al., 2012).

CONCLUSION

In conclusion, the present results provide a significant advance in our understanding of the *in vivo* antioxidant activity of MEL in *Saccharomyces* and non-*Saccharomyces* species. MEL can serve to mitigate oxidative stress and oxidative damage by leading to a decrease in the intracellular ROS content and lipid peroxidation under unfavorable conditions. Furthermore, MEL previously activated catalase activity, reducing the need of its biosynthesis against future oxidative redox changes. Therefore, MEL could be acting at different levels in yeast to reduce the oxidative stress damage: (1) as an antioxidant that directly scavenges ROS, (2) indirectly stimulating the antioxidant enzyme production, (3) by modulating FA composition of membranes, and (4) by increasing the effectiveness of peroxisome functions, which would further decrease lipid peroxidation. Thus, protective treatment with MEL could minimize the oxidative stress suffered by active dry yeast during the biomass propagation and dehydration but also increase the replicative lifespan of yeasts, particularly important in re-pitching practices. On the other hand, MEL synthesis by yeast during wine production could confer cells higher ability to adapt and endure the hostile environment of the winemaking process (low dissolved oxygen concentration, low pH, high osmolarity, ethanol toxicity, nutrient starvation, and non-optimal temperature) and counteract the oxidant effects of ethanol. Thus, the effect of MEL on yeast under stresses present in wine or yeast biomass production should be elucidated.

AUTHOR CONTRIBUTIONS

JV designed, performed, and analyzed the experiments, discussed the results, and wrote the manuscript. KG and GD helped in the design and discussion of the peroxisome proliferation analysis and the revision of the manuscript. AM, GB, and M-JT designed the experiments, discussed the results, and wrote the manuscript.

ACKNOWLEDGMENTS

The authors thank the Ministry of Economy and Competitiveness, Spain (Projects AGL2013-47300-C3-1-R and AGL2016-77505-C3-3-R), for its financial support. JV is grateful for the pre-doctoral fellowship from the University of Rovira i Virgili, and thanks to Braulio Esteve-Zarzoso and Verónica Sempere for generously helping with the catalase tuning assay, and Nicolas Rozès for helping with the data analysis.

SUPPLEMENTARY MATERIAL

The Supplementary Material for this article can be found online at: https://www.frontiersin.org/articles/10.3389/fmicb.2018.01933/full#supplementary-material

REFERENCES

Aebi, H. (1984). [13] Catalase *in vitro*. *Methods Enzymol.* 105, 121–126. doi: 10.1016/S0076-6879(84)05016-3

Alves-Araújo, C., Pacheco, A., Almeida, M. J., Spencer-Martins, I., Leão, C., and Sousa, M. J. (2007). Sugar utilization patterns and respiro-fermentative metabolism in the baker's yeast *Torulaspora delbrueckii*. *Microbiology* 153, 898–904. doi: 10.1099/mic.0.2006/003475-0

Anisimov, V. N., Popovich, I. G., Zabezhinski, M. A., Anisimov, S. V., Vesnushkin, G. M., and Vinogradova, I. A. (2006). Melatonin as antioxidant, geroprotector and anticarcinogen. *Biochim. Biophys. Acta* 1757, 573–589. doi: 10.1016/j.bbabio.2006.03.012

Antolín, I., Rodríguez, C., Saínz, R. M., Mayo, J. C., Uría, H., Kotler, M. L., et al. (1996). Neurohormone melatonin prevents cell damage: effect on gene expression for antioxidant enzymes. *FASEB J.* 10, 882–890. doi: 10.1096/fasebj.10.8.8666165

Auchère, F., Santos, R., Planamente, S., Lesuisse, E., and Camadro, J. M. (2008). Glutathione-dependent redox status of frataxin-deficient cells in a yeast model of Friedreich's ataxia. *Hum. Mol. Genet.* 17, 2790–2802. doi: 10.1093/hmg/ddn178

Aust, S. D. (1994). Thiobarbituric acid assay reactants. *Methods Toxicol.* 1, 367–374. doi: 10.1016/B978-0-08-092440-3.50036-1

Ayala, A., Muñoz, M. F., and Arguelles, S. (2014). Lipid peroxidation: production, metabolism, and signaling mechanisms of malondialdehyde and 4-hydroxy-2-nonenal. *Oxid. Med. Cell. Longev.* 2014:360438. doi: 10.1155/2014/360438

Boettiger, D., Huber, F., Lynch, L., and Blystone, S. (2001). Activation of alpha(v)beta3-vitronectin binding is a multistage process in which increases in bond strength are dependent on Y747 and Y759 in the cytoplasmic domain of beta3. *Mol. Biol. Cell* 12, 1227–1237. doi: 10.1091/mbc.12.5.1227

Bradford, M. M. (1976). A rapid and sensitive method for the quantitation of microgram quantities of protein utilizing the principle of protein-dye binding. *Anal. Biochem.* 72, 248–254. doi: 10.1016/0003-2697(76)90527-3

Buege, J. A., and Aust, S. D. (1978). Microsomal lipid peroxidation. *Methods Enzymol.* 52, 302–310. doi: 10.1016/S0076-6879(78)52032-6

Chen, Z.-H., Yoshida, Y., Saito, Y., Noguchi, N., and Niki, E. (2006). Adaptive response induced by lipid peroxidation products in cell cultures. *FEBS Lett.* 580, 479–483. doi: 10.1016/j.febslet.2005.12.045

Cipak, A., Jaganjac, M., Tehlivets, O., Kohlwein, S. D., and Zarkovic, N. (2008). Adaptation to oxidative stress induced by polyunsaturated fatty acids in yeast. *Biochim. Biophys. Acta* 1781, 283–287. doi: 10.1016/j.bbalip.2008.03.010

Costa, V., and Moradas-Ferreira, P. (2001). Oxidative stress and signal transduction in *Saccharomyces cerevisiae*: insights into ageing, apoptosis and diseases. *Mol. Aspects Med.* 22, 217–246. doi: 10.1016/S0098-2997(01)00012-7

Ding, M. Z., Tian, H. C., Cheng, J. S., and Yuan, J. S. (2009). Inoculum size-dependent interactive regulation of metabolism and stress response of *Saccharomyces cerevisiae* revealed by comparative metabolomics. *J. Biotechnol.* 144, 279–286. doi: 10.1016/j.jbiotec.2009.09.020

Escoté, X., Miranda, M., Menoyo, S., Rodríguez-Porrata, B., Carmona-Gutíerrez, D., Jungwirth, H., et al. (2012). Resveratrol induces antioxidant defence via transcription factor Yap1p. *Yeast* 29, 251–263. doi: 10.1002/yea.2903

Folch, J., Lees, M., and Stanley, S. G. H. (1957). A simple method for the isolation and purification of total lipids from animal tissues. *J. Biol. Chem.* 226, 497–509.

Gamero-Sandemetrio, E., Torrellas, M., Rábena, M. T., Gómez-Pastor, R., Aranda, A., and Matallana, E. (2015). Food-grade argan oil supplementation in molasses enhances fermentative performance and antioxidant defenses of active dry wine yeast. *AMB Express* 5:75. doi: 10.1186/s13568-015-159-7

Gómez-Pastor, R., Pérez-Torrado, R., and Matallana, E. (2012). Modification of the TRX2 gene dose in *Saccharomyces cerevisiae* affects hexokinase 2 gene regulation during wine yeast biomass production. *Appl Microbiol Biotechnol.* 94, 773–787. doi: 10.1007/s00253-011-3738-9

Gutteridge, J. M. C., and Halliwell, B. (2000). Free radicals and antioxidants in the year 2000: a historical look to the future. *Ann. N. Y. Acad. Sci.* 899, 136–147. doi: 10.1111/j.1749-6632.2000.tb06182.x

Gutteridge, J. M. C., and Halliwell, B. (2010). Antioxidants: molecules, medicines, and myths. *Biochem. Biophys. Res. Commun.* 393, 561–564. doi: 10.1016/j.bbrc.2010.02.071

Haid, A., and Suissa, M. (1983). [13] Immunochemical identification of membrane proteins after sodium dodecyl sulfate-polyacrylamide gel electrophoresis. *Methods Enzymol.* 96, 192–205. doi: 10.1016/S0076-6879(83)96017-2

Halliwell, B. (2006). Reactive species and antioxidants. Redox biology is a fundamental theme of aerobic life. *Plant Physiol.* 141, 312–322. doi: 10.1104/pp.106.077073

Hardeland, R., and Poeggeler, B. (2003). Non-vertebrate melatonin. *J. Pineal Res.* 34, 233–241. doi: 10.1034/j.1600-079X.2003.00040.x

Herrero, E., Ros, J., Bellí, G., and Cabiscol, E. (2008). Redox control and oxidative stress in yeast cells. *Biochim. Biophys. Acta* 1780, 1217–1235. doi: 10.1016/j.bbagen.2007.12.004

Hiltunen, J. K., Mursula, A. M., Rottensteiner, H., Wierenga, R. K., Kastaniotis, A. J., and Gurvitz, A. (2003). The biochemistry of peroxisomal β-oxidation in the yeast *Saccharomyces cerevisiae*. *FEMS Microbiol. Rev.* 27, 35–64. doi: 10.1016/S0168-6445(03)00017-2

Howlett, N. G., and Avery, S. V. (1997). Induction to lipid peroxidation during heavy metal stress in *Saccharomyces cerevisiae* and influence of plasma membrane fatty acid unsaturation. *Appl. Environ. Microbiol.* 63, 2971–2976.

Jamieson, D. J. (1998). Oxidative stress responses of the yeast *Saccharomyces cerevisiae*. *Yeast* 14, 1511–1527. doi: 10.1002/(SICI)1097-0061(199812)14:16<1511::AID-YEA356>3.0.CO;2-S

Johansson, M., Chen, X., Milanova, S., Santos, C., and Petranovic, D. (2016). PUFA-induced cell death is mediated by Yca1p-dependent and -independent pathways, and is reduced by vitamin C in yeast. *FEMS Yeast Res.* 16:fow007. doi: 10.1093/femsyr/fow007

Jolly, N. P., Varela, C., and Pretorius, I. S. (2014). Not your ordinary yeast: non-Saccharomyces yeasts in wine production uncovered. *FEMS Yeast Res.* 14, 215–237. doi: 10.1111/1567-1364.12111

Krantz, M., Nordlander, B., Valadi, H., Johansson, M., Gustafsson, L., and Hohmann, S. (2004). Anaerobicity prepares. *Society* 3, 1381–1390. doi: 10.1128/EC.3.6.1381

Laemmli, U. K. (1970). Cleavage of structural proteins during the assembly of the head of bacteriophage T4. *Nature* 227, 680–685. doi: 10.1038/227680a0

Lowry, O. H., Rosebrough, N. J., Farr, A. L., and Randall, R. J. (1951). Protein measurement with the Folin phenol reagent. *J. Biol. Chem.* 193, 265–275.

Mannazzu, I., Angelozzia, D., Belviso, S., Budroni, M., Farris, G. A., Goffrini, P., et al. (2008). Behaviour of *Saccharomyces cerevisiae* wine strains during adaptation to unfavourable conditions of fermentation on synthetic medium: cell lipid composition, membrane integrity, viability and fermentative activity. *Int. J. Food Microbiol.* 121, 84–91. doi: 10.1016/j.ijfoodmicro.2007.11.003

Mas, A., Guillamon, J. M., Torija, M. J., Beltran, G., Cerezo, A. B., Troncoso, A. M., et al. (2014). Bioactive compounds derived from the yeast metabolism of aromatic amino acids during alcoholic fermentation. *Biomed Res. Int.* 2014:898045. doi: 10.1155/2014/898045

Merico, A., Sulo, P., Piškur, J., and Compagno, C. (2007). Fermentative lifestyle in yeasts belonging to the Saccharomyces complex. *FEBS J.* 274, 976–989. doi: 10.1111/j.1742-4658.2007.05645.x

Moradas-Ferreira, P., and Costa, V. (2013). Adaptive response of the yeast *Saccharomyces cerevisiae* to reactive oxygen species: defences, damage and death. *Redox Rep.* 5, 277–285. doi: 10.1179/135100000101535816

Padilla, B., García-Fernández, D., González, B., Izidoro, I., Esteve-Zarzoso, B., Beltran, G., et al. (2016). Yeast biodiversity from DOQ priorat uninoculated fermentations. *Front. Microbiol.* 7:930. doi: 10.3389/fmicb.2016.00930

Pérez-Gallardo, R. V., Briones, L. S., Díaz-Pérez, A. L., Gutiérrez, S., Rodríguez-Zavala, J. S., and Campos-García, J. (2013). Reactive oxygen species production induced by ethanol in *Saccharomyces cerevisiae* increases because of a dysfunctional mitochondrial iron-sulfur cluster assembly system. *FEMS Yeast Res.* 13, 804–819. doi: 10.1111/1567-1364.12090

Pretorius, I. S. (2000). Tailoring wine yeast for the new millennium: novel approaches to the ancient art of winemaking. *Yeast* 16, 675–729. doi: 10.1002/1097-0061(20000615)16:8<675::AID-YEA585>3.0.CO;2-B

Reiter, R. J., Mayo, J. C., Tan, D. X., Sainz, R. M., Alatorre-Jimenez, M., and Qin, L. (2016). Melatonin as an antioxidant: under promises but over delivers. *J. Pineal Res.* 253–278. doi: 10.1111/jpi.12360

Reiter, R. J., Tan, D. X., Manchester, L. C., and Qi, W. (2001). Biochemical reactivity of melatonin with reactive oxygen and nitrogen species: a review of the evidence. *Cell Biochem. Biophys.* 34, 237–256. doi: 10.1385/CBB:34:2:237

Reiter, R. J., Tan, D. X., Terron, M. P., Flores, L. J., and Czarnocki, Z. (2007). Melatonin and its metabolites: new findings regarding their production and their radical scavenging actions. *Acta Biochim. Pol.* 54, 1–9.

Rodriguez, C., Mayo, J. C., Sainz, R. M., Antolín, I., Herrera, F., Martín, V., et al. (2004). Regulation of antioxidant enzymes: a significant role for melatonin. *J. Pineal Res.* 36, 1–9. doi: 10.1046/j.1600-079X.2003.00092.x

Rodriguez-Naranjo, M. I., Gil-Izquierdo, A., Troncoso, A. M., Cantos-Villar, E., and Garcia-Parrilla, M. C. (2011). Melatonin is synthesised by yeast during

alcoholic fermentation in wines. *Food Chem.* 126, 1608–1613. doi: 10.1016/j.foodchem.2010.12.038

Romero, A., Ramos, E., De Los Ríos, C., Egea, J., Del Pino, J., and Reiter, R. J. (2014). A review of metal-catalyzed molecular damage: protection by melatonin. *J. Pineal Res.* 56, 343–370. doi: 10.1111/jpi.12132

Rozès, N., Garcia-Jares, C., Larue, F., and Lonvaud-Funel, A. (1992). Differentiation between fermenting and spoliage yeasts in wine by total free fatty acid analysis. *J. Sci. Food Agric.* 59, 351–357. doi: 10.1002/jsfa.2740590312

Rußmayer, H., Buchetics, M., Gruber, C., Valli, M., Grillitsch, K., Modarres, G., et al. (2015). Systems-level organization of yeast methylotrophic lifestyle. *BMC Biol.* 13:80. doi: 10.1186/s12915-015-0186-5

Saffi, J., Sonego, L., Varela, Q. D., and Salvador, M. (2006). Antioxidant activity of L-ascorbic acid in wild-type and superoxide dismutase deficient strains of *Saccharomyces cerevisiae*. *Redox Rep.* 11, 179–184. doi: 10.1179/135100006x116691

Schrader, M., and Fahimi, H. D. (2006). Peroxisomes and oxidative stress. *Biochim. Biophys. Acta* 1763, 1755–1766. doi: 10.1016/j.bbamcr.2006.09.006

Serrazanetti, D. I., Patrignani, F., Russo, A., Vannini, L., Siroli, L., Gardini, F., et al. (2015). Cell membrane fatty acid changes and desaturase expression of *Saccharomyces bayanus* exposed to high pressure homogenization in relation to the supplementation of exogenous unsaturated fatty acids. *Front. Microbiol.* 6:1105. doi: 10.3389/fmicb.2015.01105

Sprenger, J., Hardeland, R., Fuhrberg, B., and Han, S. (1999). Melatonin and other 5-methoxylated lndoles in yeast: presence in high concentrations and dependence on tryptophan availability. *Cytologia* 64, 209–213. doi: 10.1508/cytologia.64.209

Tan, D. X., Manchester, L. C., Esteban-Zubero, E., Zhou, Z., and Reiter, R. J. (2015). Melatonin as a potent and inducible endogenous antioxidant: synthesis and metabolism. *Molecules* 20, 18886–18906. doi: 10.3390/molecules201018886

Taysi, S., Koc, M., Büyükokuroğlu, M. E., Altinkaynak, K., and Sahin, Y. N. (2003). Melatonin reduces lipid peroxidation and nitric oxide during irradiation-induced oxidative injury in the rat liver. *J. Pineal Res.* 34, 173–177. doi: 10.1034/j.1600-079X.2003.00024.x

Tesoriere, L., D'Arpa, D., Conti, S., Giaccone, V., Pintaudi, A. M., and Livrea, M. A. (1999). Melatonin protects human red blood cells from oxidative hemolysis: new insights into the radical-scavenging activity. *J. Pineal Res.* 27, 95–105. doi: 10.1111/j.1600-079X.1999.tb00602.x

Ündeğer, Ü, Giray, B., Zorlu, A. F., Öge, K., and Başaran, N. (2004). Protective effects of melatonin on the ionizing radiation induced DNA damage in the rat brain. *Exp. Toxicol. Pathol.* 55, 379–384. doi: 10.1078/0940-2993-00332

Vázquez, J., González, B., Sempere, V., Mas, A., Torija, M. J., and Beltran, G. (2017). Melatonin reduces oxidative stress damage induced by hydrogen peroxide in *Saccharomyces cerevisiae*. *Front. Microbiol.* 8:1066. doi: 10.3389/fmicb.2017.01066

Vigentini, I., Gardana, C., Fracassetti, D., Gabrielli, M., Foschino, R., Simonetti, P., et al. (2015). Yeast contribution to melatonin, melatonin isomers and tryptophan ethyl ester during alcoholic fermentation of grape musts. *J. Pineal Res.* 58, 388–396. doi: 10.1111/jpi.12223

You, K. M., Rosenfield, C., and Knipple, D. C. (2003). Ethanol tolerance in the yeast *Saccharomyces cerevisiae* is dependent on cellular oleic acid content. *Appl. Environ. Microbiol.* 69, 1499–1503. doi: 10.1128/AEM.69.3.1499

Conflict of Interest Statement: The authors declare that the research was conducted in the absence of any commercial or financial relationships that could be construed as a potential conflict of interest.

frontiers in Microbiology

ORIGINAL RESEARCH
published: 21 August 2018
doi: 10.3389/fmicb.2018.01932

Ethanol Dehydrogenase I Contributes to Growth and Sporulation Under Low Oxygen Condition via Detoxification of Acetaldehyde in *Metarhizium acridum*

Erhao Zhang[1,2,3], *Yueqing Cao*[1,2,3]* *and Yuxian Xia*[1,2,3]*

[1] School of Life Sciences, Chongqing University, Chongqing, China, [2] Chongqing Engineering Research Center for Fungal Insecticides, Chongqing, China, [3] Key Laboratory of Gene Function and Regulation Technologies under Chongqing Municipal Education Commission, Chongqing, China

OPEN ACCESS

Edited by:
Daniela De Biase,
Sapienza Università di Roma, Italy

Reviewed by:
Octavio Loera,
Universidad Autónoma Metropolitana, Mexico
Juan Carlos Aon,
GlaxoSmithKline, United States

***Correspondence:**
Yueqing Cao
yueqingcao@cqu.edu.cn
Yuxian Xia
yuxianxia@cqu.edu.cn

Specialty section:
This article was submitted to Microbial Physiology and Metabolism, a section of the journal Frontiers in Microbiology

Received: *07 June 2018*
Accepted: *30 July 2018*
Published: *21 August 2018*

Citation:
Zhang E, Cao Y and Xia Y (2018) Ethanol Dehydrogenase I Contributes to Growth and Sporulation Under Low Oxygen Condition via Detoxification of Acetaldehyde in Metarhizium acridum. Front. Microbiol. 9:1932. doi: 10.3389/fmicb.2018.01932

The entomopathogenic fungi encounter hypoxic conditions in both nature and artificial culture. Alcohol dehydrogenases (ADHs) are a group of oxidoreductases that occur in many organisms. Here we demonstrate that an alcohol dehydrogenase I, *MaADH1*, in the locust-specific fungal pathogen, *Metarhizium acridum*, functions in acetaldehyde detoxification mechanism under hypoxic conditions in growth and sporulation. The *MaADH1* was highly expressed in sporulation stage under hypoxic conditions. Compared with a wild-type strain, the Δ*MaADH1* mutant showed inhibited growth and sporulation under hypoxic conditions, but no impairment under normal conditions. Under hypoxic conditions, Δ*MaADH1* mutant produced significant decreased alcohol, but significant increased acetaldehyde compared to wild type. *M. acridum* was sensitive to exogenous acetaldehyde, exhibiting an inhibited growth and sporulation with acetaldehyde added in the medium. MaADH1 did not affect virulence. Our results indicated that the *MaADH1* was critical to growth and sporulation under hypoxic stress by detoxification of acetaldehyde in *M. acridum*.

Keywords: ethanol dehydrogenase, conidiation, growth, entomopathogenic fungi, hypoxic condition

INTRODUCTION

Entomopathogenic fungi are one of the widespread organisms belonging to different systematic groups. About 1000 species of these fungi have been recorded as insect pathogens (Fang et al., 2012). Entomopathogenic fungi are distributed throughout the world, from the plateaus to the plains, and from the deserts to the swamps (Zimmermann, 2007). Hence entomopathogenic fungi are exposed to a variety of environmental stresses, including hypoxia, heat, UV radiation, etc. (Ortiz-Urquiza and Keyhani, 2015). However, altitude has no impact on the presence of entomopathogenic fungi even in a range up to 5200 m where oxygen was only 50% of the sea level value (Peacock, 1998; Quesada-Moraga et al., 2007; Sun and Liu, 2008). *Beauveria* and *Metarhizium* had been reported in Nepal and Tibet, where the oxygen availability was only 70% of the normal

atmospheric levels value (Peacock, 1998; Yubak Dhoj et al., 2008; Freed et al., 2011), showing their ability to adapt to a wide range of oxygen levels. Thus, entomopathogenic fungi can grow and produce conidia under hypoxic conditions in nature, and they likely have mechanisms to sense and respond to hypoxic stress.

Entomopathogenic fungi are one of the most promising agents for biological control of pest insects. Some species have been developed to biopesticide products. Up to 2016 September, 51 commercial fungal biopesticide products from 58 countries around the world are available, which are mostly based on the aerial conidia for at least 12 species of insect fungi (de Faria and Wraight, 2007; Muñiz-Paredes et al., 2017). As a microbial pesticide, *M. acridum* was used for locust and grasshopper control in Africa, Australia and Asia (Hunter et al., 2001; Lomer et al., 2001; Peng et al., 2008). Aerial conidia of entomopathogenic fungi produced in solid culture are of lipophilic nature, a superb property for developing an oil-based formulation suitable for ultra-low volume (ULV) application in arid environments (Bateman et al., 1993; Burges, 1998; Lomer et al., 2001). As aerobic organisms of entomopathogenic fungi, aeration is an important factor for aerial conidia production (Muñiz-Paredes et al., 2017). However, the solid-state fermentation has some disadvantages, such as oxygen limitation due to poor diffusion of oxygen in solid substrate especially for mass production (Bartlett and Jaronski, 1998; Mienda et al., 2011). Therefore, aeration has a strong impact on the fungal growth and conidiation (Rahardjo et al., 2005). The increase of dissolved oxygen (DO) during sporulation in the liquid culture results in an increased blastospore production compared to normal condition (Issaly et al., 2005). In solid culture, conidia production was increased significantly under higher oxygen (26% O_2) compared to normal oxygen condition (21% O_2) (Tlecuitl-Beristain et al., 2010). Normally, entomopathogenic fungi encounter the challenges of hypoxic stress in nature or in artificial culture. However, up to now, the regulation mechanisms of hypoxic stress tolerance have not been explored in entomopathogenic fungi.

Alcohol dehydrogenases (ADHs) are a group of oxidoreductases that occur in many organisms facilitating the conversion between alcohols and aldehydes with the reduction of NAD+. Alcohol dehydrogenases are widespread in the animals, plants, fungi and bacteria. However, the ADH type and number varied in different species. For example, there are five ADH members (ADH1, ADH2, ADH3, ADH4, and ADH5), three in *Saccharomyces cerevisiae* (ADH1, ADH2, and ADH3) (de Smidt et al., 2008), two in *Aspergillus nidulans* (ADH1 and ADH3) (Reid and Fewson, 1994), and one in *Mucor circinelloides* (ADH1) (Rangel-Porras et al., 2005).

The functions of ADH members vary within the ADH family. In *Thermoanaerobacter ethanolicus*, three ADHs play different roles during ethanol formation (Zhou et al., 2017). In yeast, ADH1 is responsible for ethanol production from acetaldehyde and NADH, contributing to fungal growth in the presence of alcohol (Plapp et al., 2013). Yeast ADH2 converts the ethanol accumulating to acetaldehyde under anaerobic conditions (de Smidt et al., 2008). In plant pathogenic fungus *Fusarium oxysporum*, ADH1 disruption impaired growth under hypoxic conditions, diminished production of ethanol and affected the fungal disease development in tomato plants (Corrales Escobosa et al., 2011). In *A. fumigatus*, ADH could be induced by hypoxic condition, and influence fungal growth and pathogenesis (Grahl et al., 2011).

The *ADH* genes widely exist in the insect pathogenic fungi of *Metarhizium, Beauveria,* and *Cordyceps*. Few past studies were reported on the function of alcohol dehydrogenase in entomopathogenic fungi. In *M. anisopliae*, *ADH1* is expressed during infection process and required for virulence (Callejas-Negrete et al., 2015). In this study, we explored the function of the *MaADH1* gene by targeted disruption in *M. acridum*. Our results showed that Δ*MaADH1* had inhibited growth and sporulation under hypoxic conditions, while it had no impairment under normal oxygen conditions. When oxygen level was low, Δ*MaADH1* mutant produced decreased alcohol and increased acetaldehyde compared to wild type. Exogenous acetaldehyde had similar inhibition on sporulation as deletion of *MaADH1* in *M. acridum*. These data suggested that *MaADH1* was involved in hypoxic stress tolerance and contributed to conidiation under low oxygen condition.

MATERIALS AND METHODS

Organisms and Culture Conditions

Metarhizium acridum CQMa102 is wild type strain that was obtained from China General Microbiological Culture Collection Center (CGMCC, No. 0877). The fungal strains were propagated in 1/4 SDAY medium, consisting of 1% dextrose, 0.25% mycological peptone, 0.5% yeast extract, and 2% agar (w/v). *Escherichia coli* DH5α (DingGuo, Beijing, China) was used for routine cloning.

Semi-Quantitative Reverse Transcription (qRT)-PCR and qRT-PCR

Total RNAs were extracted from WT mycelia grown for 14 and 20 h days on plate, conidia (growing for 3 days), germinated conidia, appressoria formed on locust wing, and hyphal bodies grown for 5 days in hemolymph of infected locusts (Luo et al., 2013). Appressorium induction and hyphal body collection were performed as described previously (He and Xia, 2009). Total RNAs were extracted using TRIzol reagent (Invitrogen, United States). For first strand cDNA synthesis, 1 μg total RNA was applied with an oligo-dT primer using the PrimeScript^{TM} RT Master Mix (TaKaRa, Dalian, China). Semi-quantitative RT-PCR and qRT-PCR were performed using primers ADH1-EF and ADH1-ER. cDNA synthesis and qRT-PCR were performed using the method described by Luo et al. (2013). All PCR amplifications were conducted in triplicate, the glyceraldehyde-3-phosphate dehydrogenase gene (gpd) was used as an internal control. Transcript ratios of target gene were evaluated using the $2^{-\Delta\Delta CT}$ method (Livak and Schmittgen, 2001). Primer sequences are listed in **Supplementary Table S1**.

MaADH1 Deletion, Complementation, and Over-Expression

The *MaADH1* gene was disrupted by homologous recombination. About 1 kb upstream and 1 kb downstream sequences of *MaADH1* open reading frame (ORF) were amplified with primer pairs LF/LR and RF/RR from *M. acridum* genomic DNA. Amplification fragments were inserted into pK2-pB (Luo et al., 2013) separated by a selection marker Bar cassette. The recombinant plasmid was transformed into *M. acridum* with *Agrobacterium tumefaciens* according to Fang et al. (2004). Transformants were screened by PCR with primers L1/PR and BF/R1 and confirmed by Southern blot. A plasmid for complementation was generated using primers HF/HR to amplify the entire *MaADH1* gene including 2 kb of the *MaADH1* promoter, the coding sequence, and the terminator. The amplified fragment was inserted into pK2-EGFP-Sur containing the chorimuron ethyl resistance gene Sur (Luo et al., 2013). The pK2-Sur-ADH1-EGFP construct was transformed into the Δ*MaADH1*. Transformants were screened on Czapek-dox plates supplemented with 20 μg/ml chorimuron ethyl (Sigma, Bellefonte, PA, United States) and confirmed by DNA blots. Primers used for transformants construction are listed in **Supplementary Table S1**.

Growth Under Different Oxygen Condition

To examine the role of MaADH1 on fungal growth under different DO condition, WT, Δ*MaADH1,* and complemented strain (CP) were grown in liquid culture under normal dissolved-oxygen and low DO condition, respectively. Conidia were inoculated into 1/4 SDY liquid medium with a concentration of 1×10^5 conidia/ml in 50 ml centrifuge tubes. Centrifuge tubes were sealed with ventilated films for normal oxygen condition. To get lower DO, 20 μl liquid CO_2 was added in the culture mixture to obtain about 18% oxygen concentration at the initial time of growth (80% of normal oxygen level), then the tubes were sealed with caps and shaken at 250 rpm at 28°C. The fungal cultures were collected by centrifugation every 12 h during a 5-day growing period. The pellets were weighed and compared among fungal strains. The transcription of *MaADH1* and ADHs enzyme activity were also determined in these samples. Total RNAs were extracted from these fungal cultures for transcription level analysis of *MaADH1* by qRT-PCR as described above. The DO in liquid culture was detected with DO electrode (Mettler Toledo, Inpro6000, Switzerland).

ADH Activity Assay

The ADH activity assays were performed in reaction mixtures containing 25 μl cell-free fractions, 1.0 ml semicarbazide buffer (pH 8.7), 1.5 mM NAD+ solutions and 10 mM ethanol. The reduction of NAD+ was monitored by the increased absorbance at 340 nm. One unit of enzyme activity was defined as the amount of enzyme catalyzing the reduction of 1 μmol NAD+ per min at 25°C. Specific activity was expressed as units (U) per mg of protein. Protein concentration was determined using the BCA protein assay kit (Beyotime, China)

Sporulation Determination

Sporulation under hypoxic condition was determined in liquid medium and on solid rice grain. Fungal strains were grown in liquid medium under hypoxic condition as described above. After growing for 3 days, the fungal culture was collected and filtered with four layers of lens tissue to remove mycelia. Blastospore concentration in filtered solution was determined by hemocytometer under microscope. Two-stage technique was applied in solid-state fermentation, which involves submerged liquid fermentation and solid substrate fermentation. Rice grains were soaked in water for 5 h, and then were autoclaved after removing water. Three-day fungal culture grown in liquid 1/4 SDY medium (1×10^6 spore/ml) under normal condition was mixed thoroughly with grains to a final concentration of 10% (V/W). The mixture was then filled into sealed glass tubes (diameter: 3.5 cm, height: 11 cm), and then fermented at 28°C for 14 days to produce conidia. The rice grains were shaken once every 2 days to prevent the grains sticking together. Fermented rice (0.25 g) was soaked in 1 ml H_2O, and vortexed to wash off the conidia from rice grains. Conidia number was determined by hemocytometer under microscope.

Alcohol and Acetaldehyde Determination

Alcohol and acetaldehyde determination was performed as described previously with minor modifications (Bernt and Gutmann, 1974; Rotariu et al., 2004). Fungal growth in liquid 1/4 SDY under hypoxic condition were as described above. The cultures were collected every 12 h during a 5-day growing period and then centrifuged to collect the supernatant. For alcohol determination, supernatant of 25 μl was mixed thoroughly with 1.0 ml semicarbazide buffer (pH 8.7) and 25 μl NAD+ solutions (Solarbio, Beijing, China). Alcohol dehydrogenase solution (5 μl) sourced from *S. cerevisiae* (Solarbio, Beijing, China) was added to the mixture and then incubated at 25°C for 30 min. The absorbance of the reaction mixture was read at 340 nm. Standard curve was generated using 0–0.04% (v/v) ethanol solutions.

For acetaldehyde determination, 25 μl of sample solution was added to a tube containing 300 μl Tris–HCl buffer (1 M, pH 8.0) and 25 μl NAD+ solutions (1 mM). Acetaldehyde dehydrogenase (E.C 1.2.1.5) (5 μl) was added to the mixture and then incubated at 25°C for 30 min. The absorbance of the reaction mixture was read at 340 nm. Standard curve was generated using 0–0.04% (v/v) acetaldehyde solutions prepared with phosphate buffer pH 9.0 containing 0.1 M KCl.

Effect of Acetaldehyde on Fungal Growth

To investigate the effects of acetaldehyde on fungal growth, wild type strain was grown in liquid or solid medium containing 0.01 or 0.1% acetaldehyde. For liquid culture, conidia were inoculated in 1/4 SDY in a 50 ml centrifuge tube at a final concentration of 1×10^5 conidia/ml, and then shaken at 28°C with 250 rpm for 4 days. Blastospore production was determined daily. For culture on plate, conidia (1×10^6 conidia/ml) were spotted or spread on 1/4 SDAY plate and grown for 14 days. Conidia production

was determined every 3 days as described previously (Liu et al., 2010). The phenotype of fungal colonies was shown on 6th day of growth.

Germination, Stress Tolerance, and Bioassay

Germination rate was determined on normal medium (1/4 SDAY) and host insect wing [*Locusta migratoria manilensis* (Meyen)] as described previously (Liu et al., 2010).

Tolerance to heat and ultraviolet radiation was determined according to Liu et al. (2010). IT_{50} (time for 50% inhibition in germination rate by heat or UV irradiation) was compared among WT, Δ*MaADH1*, and the CP.

Bioassay was performed using fifth instar nymphs of *L. migratoria* as described previously (Cao et al., 2012). Conidia suspensions (5 μl) were topically inoculated on pronotum (1×10^7 conidia/ml liquid paraffin oil). Half-lethal time (LT_{50}) was calculated and compared between WT and Δ*MaADH1*.

Data Analysis

Conidiation production, enzyme activity, ethanol, and acetaldehyde concentration, germination rate, IT_{50} and LT_{50}, were statistically analyzed using one-way analysis of variance model (SPSS 16.0; SPSS Inc., Chicago, IL, United States). Tukey's honestly significant difference test was used to separate means at $p = 0.05$.

RESULTS

Gene Cloning and Molecular Characterization

The full length of cDNA of *MaADH1* is 1062 bp (Accession number KX021843). It encodes a predicted protein of 353 amino acids residues, with a deduced molecular weight of 37 KDa and a pI of 7.61. The SignalP 3.0 program revealed no signal sequence, suggesting that MaADH1 is a cell-bound protein. MaADH1 contains typical ethanol dehydrogenase structural domains including NAD+ binding domain, Zn^{2+} binding site and ADH1 activity domain (**Supplementary Figure S1A**). Phylogenic analysis indicated that MaADH1 protein was closely related to ADH1 from the entomopathogenic fungi *M. anisopliae* (identity 94%) and *Beauveria bassiana* (identity 73%) (**Supplementary Figure S1B**).

MaADH1 Is Induced in Hypoxic Condition

The concentration of DO in culture fluctuated around the value of 21% under normal condition during growth period (**Figure 1A**). Under low oxygen condition, DO in culture was about 18% at the initial time and then gradually decreased along with the fungal growth. However, DO in Δ*MaADH1* culture was slightly higher than WT and CP strains (**Figure 1A**). In 1/4 SDY liquid medium, the *MaADH1* had significantly increased transcription under low DO condition, with up to 10 times higher as compared to normal oxygen condition (**Figure 1B**). Transcription of *MaADH1* gene was drastically increased after 2 days of growth under hypoxic condition, while normal oxygen condition had slight effect on *MaADH1* transcription in this period (**Figure 1B**). Blastospores were produced substantially in liquid media during this period. These results demonstrated that *MaADH1* might have a function in sporulation, especially sporulation under hypoxic condition.

Alcohol dehydrogenases enzyme activities were also determined in *M. acridum* under low and normal DO conditions. ADH activity showed a similar trend as the transcription results of *MaADH1* (**Figure 1C**). The specific activity of ADHs was significantly increased under low DO condition compared to aerobic condition. The ADH enzyme activity increased from 1st day and reached to peak value of 40.5 ± 1.5 U/mg after growing for 2.5 days under hypoxic condition, almost 2 times higher than that under aerobic condition (21.5 ± 0.9 U/mg). A drastic decrease in ADHs activity was found at 3.5 days under aerobic condition, showing about 50% decrease compared to the peak value, while a 20% decrease was found at 3.5 day under hypoxic condition (**Figure 1C**). However, compared to transcription results of *MaADH1*, ADH enzyme activity did not have such drastic difference between normal and hypoxic condition (10 times versus 2 times increase) (**Figure 1C**). We supposed that this was due to the total ADH activity we determined in this study, and some other ADH members might require different biochemical conditions to measure the activity or have relative higher activity under normal oxygen condition, thus obscuring the difference in total ADH activity under normal and hypoxic condition.

MaADH1 Is Highly Expressed in Sporulation

The expression of *MaADH1* at different stages of the life cycle and under low DO condition in liquid culture was analyzed by semi-quantitative RT-PCR and qRT-PCR. On 1/4 SDAY plate, the *MaADH1* was highly transcribed in sporulation stage (3-day culture on plate) and poorly transcribed in mycelium, appressorium and hyphal body formation stages (**Figures 2A,B**). Consistent with the transcription results, MaADH1-EGFP fusion expression showed that the fungus had strong green fluorescence in sporulation stage on the 3rd day grown on plate, while weak or no signal was found in mycelia, germ tubes, appressorium and hyphal body (**Figure 2C**).

MaADH1 Contributes Fungal Growth and Conidiation Under Low Oxygen Condition

Targeted gene disruption of *MaADH1* was generated by homologous recombination (**Supplementary Figure S2A**). Correct integration events in transformants of the deletion and subsequent complementation mutants were confirmed by Southern blotting (**Supplementary Figure S2B**). To examine the role of *MaADH1* in fungal growth, biomass of fungal strains in liquid culture was analyzed under normal dissolved-oxygen and low DO condition, respectively. Results showed that biomass of Δ*MaADH1* had no significant difference compared with WT and CP under normal oxygen condition (**Figure 3A**), while decreased

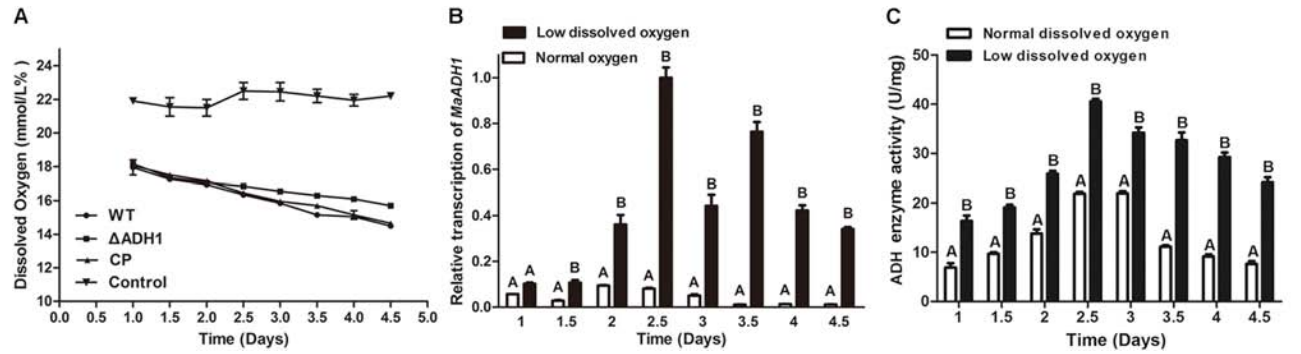

FIGURE 1 | Transcription and enzyme activity. **(A)** Dissolved oxygen under normal and low oxygen condition. **(B)** Relative expression of *MaADH1* under hypoxic condition and normal condition. **(C)** ADH activity at different growth time under hypoxic condition and normal condition. A, B indicate significant difference at $p < 0.01$.

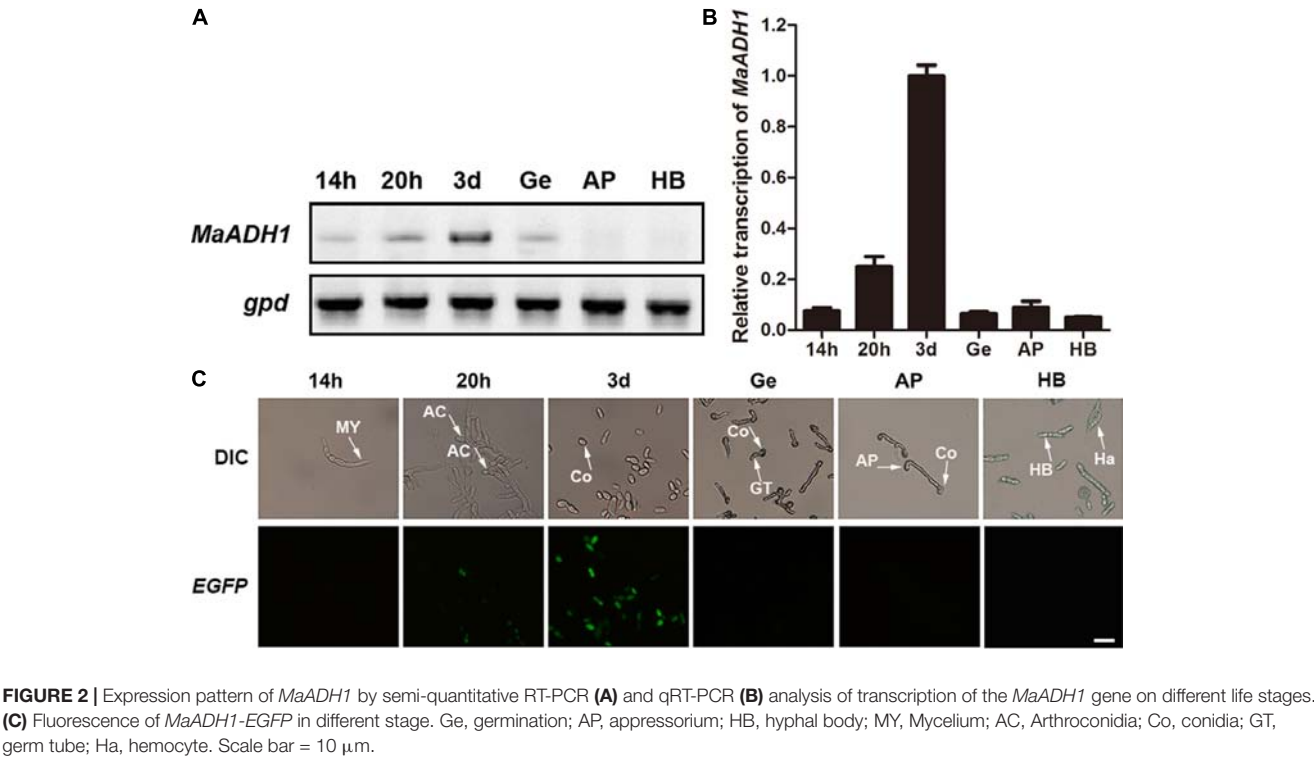

FIGURE 2 | Expression pattern of *MaADH1* by semi-quantitative RT-PCR **(A)** and qRT-PCR **(B)** analysis of transcription of the *MaADH1* gene on different life stages. **(C)** Fluorescence of *MaADH1-EGFP* in different stage. Ge, germination; AP, appressorium; HB, hyphal body; MY, Mycelium; AC, Arthroconidia; Co, conidia; GT, germ tube; Ha, hemocyte. Scale bar = 10 μm.

significantly after growing for 3 days under low oxygen condition (**Figures 3B,C**). The pellet of Δ*MaADH1* fungal culture was obviously less than WT and CP strains (**Figure 3D**). These results indicated that *MaADH1* affected growth of *M. acridum* in liquid medium under low DO condition.

Conidiation of fungal strains on rice grains under low oxygen condition showed that rice grains in both WT and CP strains groups were covered with dark green conidia, while grains of Δ*MaADH1* group were covered with light-green conidia (**Figure 4A**). Microscopic analysis revealed that more white mycelia were found on rice surface in Δ*MaADH1* group compared to WT (**Figure 4A**). Quantitative conidiation analysis showed that Δ*MaADH1* had significantly decreased conidia production, almost 50% less than wild type strain, suggesting that *MaADH1* also contributed to aerial conidiation in *M. acridum* under hypoxic condition (**Figure 4B**). Sporulation in liquid culture exhibited the same decreased trend as on rice grains in Δ*MaADH1* under hypoxic condition (**Figures 4C,D**).

MaADH1 did not affect conidia germination, heat and UV stress tolerance, and virulence (data not shown).

MaADH1 Regulates Acetaldehyde Metabolism in *M. acridum*

Alcohol dehydrogenases constitute a large family of enzymes responsible for the reversible oxidation of alcohols to aldehydes with the concomitant reduction of NAD+ or NADP+. To

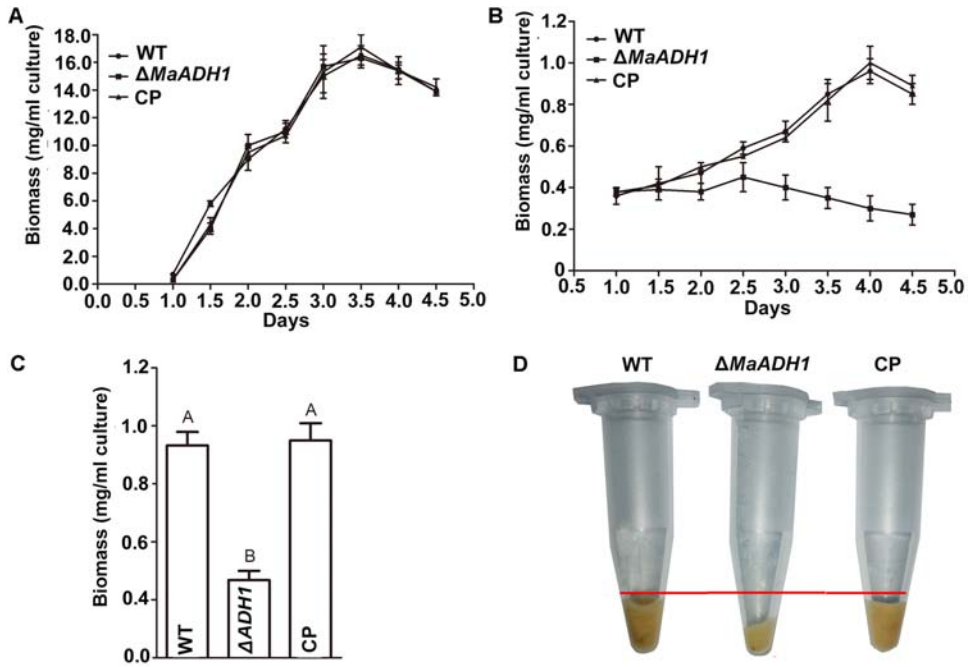

FIGURE 3 | Biomass analysis. **(A)** Time course study of dry weight under normal oxygen condition. **(B)** Biomass under low dissolved-oxygen condition. Dry weight **(C)** and pellets **(D)** on 3rd day under low dissolved-oxygen condition. Error bars are standard deviations of three trials. A, B indicate significant difference at $p < 0.01$.

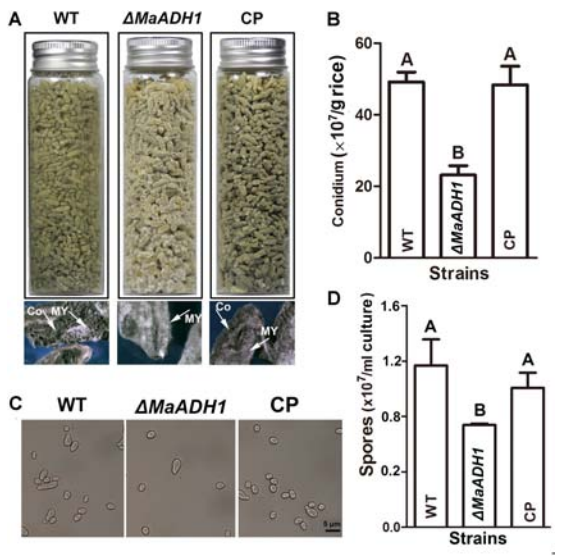

FIGURE 4 | Sporulation under hypoxic conditions. **(A)** Conidiation after growing on rice under hypoxic condition for 12 days. CO: conidium; MY: mycelia. **(B)** Quantification of conidiation on rice. **(C)** Sporulation in liquid medium under hypoxic condition **(D)** Quantitative sporulation in liquid medium under hypoxic condition. All experiments were repeated at least three times. Error bars, SD. A, B indicate significant difference at $p < 0.01$.

further explore the roles of *MaADH1* under low oxygen condition, the ethanol and acetaldehyde in the liquid culture were measured. Compared to wild type, the Δ*MaADH1* culture had significant decreased alcohol concentration (about 0.005% in Δ*MaADH1* versus to 0.008% in WT) (**Figure 5A**) and significant increased concentration of acetaldehyde (about 0.01% in Δ*MaADH1* versus to 0.002% in WT) (**Figure 5B**). Considering the inhibited growth results of Δ*MaADH1*, it could be speculated that acetaldehyde accumulation in the culture was toxic to *M. acridum*.

Acetaldehyde Affected Conidiation in *M. acridum*

To further analysis the influence of acetaldehyde on growth and sporulation, wild type strain was inoculated on 1/4 SDAY plate and in liquid media containing acetaldehyde (0.01 or 0.1%, v/v). Results showed that acetaldehyde inhibited the growth of *M. acridum* at concentrations of both 0.1 and 0.01% on plate (**Figure 6A**) or in liquid medium (**Figure 6B**), suggesting the acetaldehyde accumulation caused by *MaADH1* deletion was sufficient to inhibit fungal growth. Compared to control, sporulation production was decreased significantly both in liquid (**Figure 6C**) and on solid medium (**Figure 6D**) containing acetaldehyde, showing about 50% decrease during the inspection period. These results suggested that acetaldehyde had negative effect on sporulation in *M. acridum*.

DISSCUSSION

In this study, we identified an *ADH1* gene from the entomopathogenic fungus *M. acridum*, also explored its function in sporulation and growth under low or normal

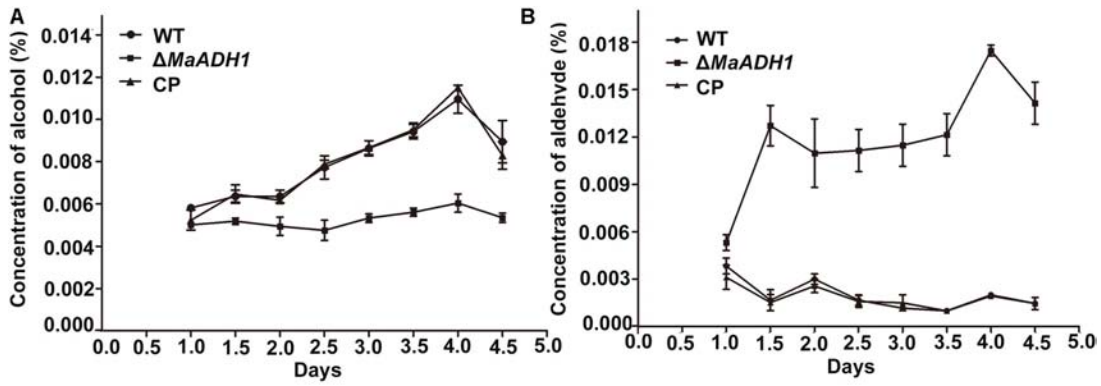

FIGURE 5 | Alcohol and acetaldehyde production under low oxygen condition. Concentration of alcohol **(A)** and acetaldehyde **(B)** in liquid medium at the different cultural time. Error bars are standard deviations of three trials.

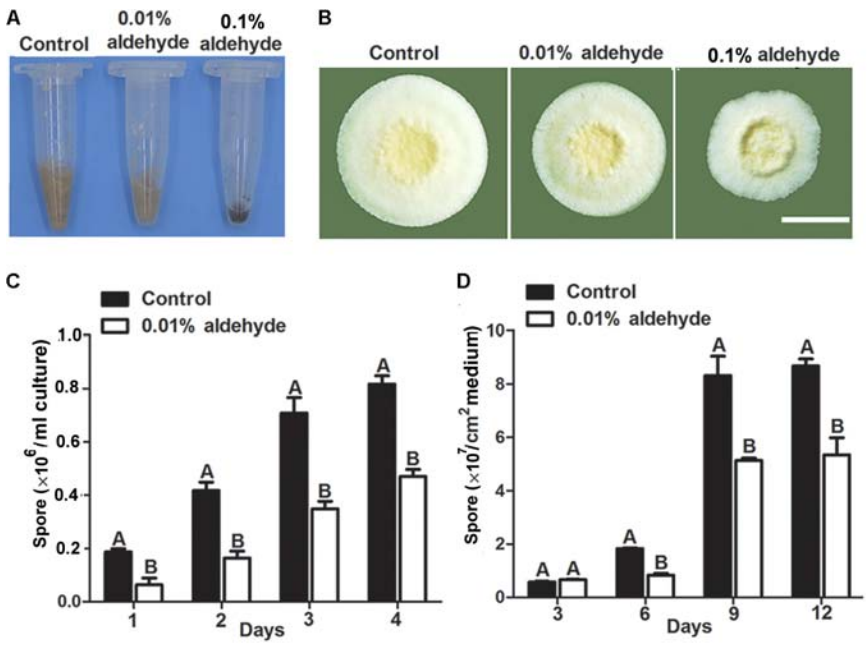

FIGURE 6 | Effect of aldehyde on conidiation under normal condition. **(A)** Sporulation in the 1/4 SDA liquid culture medium containing aldehyde **(B)** Conidiation on 1/4 SDAY solid medium with aldehyde. **(C)** Sporulation quantification in liquid medium with 0.01% aldehyde **(D)** Sporulation quantification on solid medium with 0.01% aldehyde. All experiments were repeated at least three times. Error bars, SD. A, B indicate significant difference at $p < 0.01$.

oxygen condition. Our results showed that the *MaADH1* gene contributed to growth and sporulation under low oxygen condition via detoxification of acetaldehyde. However, this gene was not involved in virulence and UV/heat stress tolerance in *M. acridum*.

MaADH1 mainly accounted for conversion from acetaldehyde to ethanol under hypoxic condition in *M. acridum*. Similar as reported in some other fungi (Leskovac et al., 2002; Rangel-Porras et al., 2005), The *MaADH1* had an up-regulated transcription and increased enzyme activity under low oxygen condition, suggesting its role under micro-oxygen conditions. Our data revealed a decrease in ethanol production and an increase in acetaldehyde production in Δ*MaADH1* culture, indicating a block in ethanol production from acetaldehyde under hypoxic condition when the *MaADH1* gene was impaired. This physiological function was consistent with earlier reports in some fungi, such as *S. cerevisiae* (Leskovac et al., 2002; de Smidt et al., 2008), *Candida maltose* (Lin et al., 2010), *F. oxysporum* (Corrales Escobosa et al., 2011), *M. anisopliae* (Callejas-Negrete et al., 2015), and *M. circinelloides* (Rangel-Porras et al., 2005).

ADH1 is an enzyme strategy to detoxify acetaldehyde under low oxygen condition in *M. acridum*. Acetaldehyde is an inhibitor of a wide range of metabolic activities and is toxic to fungi (Aranda and del Olmo, 2004). Acetaldehyde at high concentrations can even stop yeast cell growth (Stanley et al., 1993). Consistence to these reports, our results showed

that acetaldehyde had strong adverse effect on growth in *M. acridum* (**Figure 5**). ADH1 is a fermentative enzyme to catalyze the transformation of acetaldehyde to ethanol, reducing the accumulation of acetaldehyde in cells. In our study, deletion of the *MaADH1* gene resulted in accumulation of acetaldehyde (reach to a concentration of 0.01%) in culture (**Figure 5**) and inhibited growth and sporulation. The inhibition effect was in accordance with that of exogenous acetaldehyde (at a concentration of 0.01%) on the growth of wild type strain (**Figure 6**). It is therefore reasonably supposed that MaADH1 played a major role in overcoming acetaldehyde toxicity in the liquid or solid-state fermentation in *M. acridum*.

The ability to sense and respond to changes in oxygen is essential for the survival of prokaryotic and eukaryotic organisms (Giaccia et al., 2004). Our data showed that fungal blastospore production in liquid culture appeared to be clearly related to the DO concentration. Sporulation was significantly decreased with low DO concentration (**Figure 3**). These results were in accordance with the previous report in *M. flavoviride* (Issaly et al., 2005). Ethanol could be detected when oxygen was depleted in part of the solid medium (Oostra et al., 2001), which also agreed to our data (**Figure 5**). Therefore, microbes would develop a strategy to decrease the adverse effect of hypoxic condition. As a group of fermentative enzymes, ADHs might play a role in this process. The physiological functions vary among different ADH members. In *Thermoanaerobacter ethanolicus*, AdhE primarily functions in acetaldehyde production, and AdhB has high activity for ethanol production, but does not contribute to acetaldehyde production (Zhou et al., 2017). In yeast, ADH1 and ADH2 are responsible for the inverse conversion between ethanol and acetaldehyde (de Smidt et al., 2008). Therefore, ADHs members might coordinate to overcome the hypoxic stress. Our data revealed that *MaADH1* was induced in conidiation process under low oxygen condition, showing a much higher transcription compared to normal oxygen condition (**Figure 2**). This has also been reported in other ADH members in *A. fumigatus* (Grahl et al., 2011). Oxygen limitation has been the major concern in fungal solid-state fermentation (Bartlett and Jaronski, 1998; Mienda et al., 2011). Disruption of *MaADH1* resulted in decreased conidiation on rice grain (**Figure 4**), suggesting a role of *MaADH1* under hypoxic condition. Better understanding the regulation mechanisms and comprehensive utilization of ADH members in engineered strain construction could improve the fungal fermentation, especially in high density fermentation.

ADH1 did not contribute to virulence in *M. acridum*. The infection process of entomopathogenic fungi involves attachment of conidia to the insect cuticle, germination of conidia, development of appressorium, formation of the penetration peg to penetrate the insects' cuticle and killing the host insect by the growth of invasive hyphae in hemolymph and toxin produced by the fungi (Clarkson and Charnley, 1996). Our results revealed that ADH1 had very low transcription during germination and almost no transcription in appressoria and hyphal bodies. Accordingly, no fluorescence was detected in hyphal bodies and appressoria for ADH1-EGFP fused expression in *M. acridum*, suggesting ADH1 did not involve in pathogenicity process. Bioassay results against locusts were in accordance with the transcription profiles of *MaADH1*, showing no contribution of ADH1 to virulence (data now shown). However, our results were not consistent with the findings in *M. anisopliae*, which ADH1 is expressed during insect colonization and required for full virulence (Callejas-Negrete et al., 2015). ADH1 is also involved in virulence in plant pathogenic fungus *F. oxysporum* (Corrales Escobosa et al., 2011) and human pathogenic fungus *C. albicans* (Ku et al., 2017) and *A. fumigatus* (Grahl et al., 2011). This variation in ADH1 function illustrates that ADH1 might have distinct roles for a pathogenic fungi during interactions with host organisms.

In summary, our results demonstrated that the function of MaADH1 was to convert acetaldehyde to alcohol and eliminate side effect of acetaldehyde on fungal growth and sporulation under hypoxic conditions. Further better understanding the function and regulation of the *MaADH1* may potentially help to improve high density fermentation in entomopathogenic fungi.

AUTHOR CONTRIBUTIONS

EZ conducted the main experiment and wrote the manuscript. YX and YC conceived and designed the experiments. EZ and YC analyzed the data. YX and YC provided technical oversight and critical manuscript review and editing.

FUNDING

This work was supported by the National Science and Technology Major Project of China (2017YFD0201208) and National Science Foundation of China (31272090).

SUPPLEMENTARY MATERIAL

The Supplementary Material for this article can be found online at: https://www.frontiersin.org/articles/10.3389/fmicb.2018.01932/full#supplementary-material

REFERENCES

Aranda, A., and del Olmo, M. L. (2004). Exposure of *Saccharomyces cerevisiae* to acetaldehyde induces sulfur amino acid metabolism and polyamine transporter genes, which depend on Met4p and Haa1p transcription factors, respectively. *Appl. Environ. Microbiol.* 70, 1913–1922. doi: 10.1128/AEM.70.4.1913-1922.2004

Bartlett, M. C., and Jaronski, S. T. (1998). "Mass production of entomogenous fungi for biological Control of insects," in *Fungi in Biological Control Systems,* ed. M. N. Burge, 61–85. Manchester: Manchester University Press.

Bateman, R. P., Carey, M., Moore, D., and Prior, C. (1993). The enhanced infectivity of *Metarhizium flavoviride* in oil formulations to desert locusts at low humidities. *Ann. Appl. Biol.* 122, 145–152. doi: 10.1111/j.1744-7348.1993.tb04022.x

Bernt, E., and Gutmann, I. (1974). "Ethanol determination with alcohol dehydrogenase and NAD," in *Methods of Enzymatic Analysis*, Vol. 3, ed. H. A. Bergmeyer (Weinheim: Verlag Chemie), 1499–1502.

Burges, H. D. (1998). "Formulation of mycoinsecticides," in *Formulation of Microbial Biopesticides: Beneficial Microorganisms, Nematodes and Seed Treatments*, ed. H. D. Burges (Dordrecht: Kluwer Academic Publisher), 132–185. doi: 10.1007/978-94-011-4926-6

Callejas-Negrete, O. A., Torres-Guzman, J. C., Padilla-Guerrero, I. E., Esquivel-Naranjo, U., Padilla-Ballesteros, M. F., Garcia-Tapia, A., et al. (2015). The Adh1 gene of the fungus *Metarhizium anisopliae* is expressed during insect colonization and required for full virulence. *Microbiol. Res.* 172, 57–67. doi: 10.1016/j.micres.2014.11.006

Cao, Y., Zhu, X., Jiao, R., and Xia, Y. (2012). The *Magas1* gene is involved in pathogenesis by affecting penetration in *Metarhizium acridum*. *J. Microbiol. Biotechnol.* 22, 889–893. doi: 10.4014/jmb.1111.11055

Clarkson, J. M., and Charnley, A. K. (1996). New insights into the mechanisms of fungal pathogenesis in insects. *Trends Microbiol.* 4, 197–203. doi: 10.1016/0966-842X(96)10022-6

Corrales Escobosa, A. R., Rangel Porras, R. A., Meza Carmen, V., Gonzalez Hernandez, G. A., Torres Guzman, J. C., Wrobel, K., et al. (2011). *Fusarium oxysporum* Adh1 has dual fermentative and oxidative functions and is involved in fungal virulence in tomato plants. *Fungal Genet. Biol.* 48, 886–895. doi: 10.1016/j.fgb.2011.06.004

de Faria, M., and Wraight, S. P. (2007). Mycoinsecticides and mycoacaricides: a comprehensive list with worldwide coverage and international classification of formulation types. *Biol. Control.* 43, 237–256. doi: 10.1016/j.biocontrol.2007.08.001

de Smidt, O., du Preez, J. C., and Albertyn, J. (2008). The alcohol dehydrogenases of *Saccharomyces cerevisiae*: a comprehensive review. *FEMS Yeast Res.* 8, 967–978. doi: 10.1111/j.1567-1364.2008.00387.x

Fang, W., Azimzadeh, P., and St Leger, R. J. (2012). Strain improvement of fungal insecticides for controlling insect pests and vector-borne diseases. *Curr. Opin. Microbiol.* 15, 232–238. doi: 10.1016/j.mib.2011.12.012

Fang, W., Zhang, Y., Yang, X., Zheng, X., Duan, H., Li, Y., et al. (2004). *Agrobacterium tumefaciens*-mediated transformation of *Beauveria bassiana* using an herbicide resistance gene as a selection marker. *J. Invertebr. Pathol.* 85, 18–24. doi: 10.1016/j.jip.2003.12.003

Freed, S., Jin, F. L., and Ren, S. X. (2011). Determination of genetic variability among the isolates of *Metarhizium anisopliae* var. anisopliae from different geographical origins. *World J. Microbiol. Biot.* 27, 359–370. doi: 10.1007/s11274-010-0466-8

Giaccia, A. J., Simon, M. C., and Johnson, R. (2004). The biology of hypoxia: the role of oxygen sensing in development, normal function, and disease. *Genes Dev.* 18, 2183–2194. doi: 10.1101/gad.1243304

Grahl, N., Puttikamonkul, S., Macdonald, J. M., Gamcsik, M. P., Ngo, L. Y., Hohl, T. M., et al. (2011). In vivo hypoxia and a fungal alcohol dehydrogenase influence the pathogenesis of invasive pulmonary *Aspergillosis*. *PLoS Pathog.* 7:e1002145. doi: 10.1371/journal.ppat.1002145

He, M., and Xia, Y. (2009). Construction and analysis of a normalized cDNA library from *Metarhizium anisopliae* var. acridum germinating and differentiating on *Locusta migratoria* wings. *FEMS Microbiol. Lett.* 291, 127–135. doi: 10.1111/j.1574-6968.2008.01447.x

Hunter, D. M., Milner, R. J., and Spurgin, P. A. (2001). Aerial treatment of the Australian plague locust, *Chortoicetes terminifera* (Orthoptera:Acrididae) with *Metarhizium anisopliae* (Deuteromycotina: Hyphomycetes). *Bull. Entomol. Res.* 91, 93–99.

Issaly, N., Chauveau, H., Aglevor, F., Fargues, J., and Durand, A. (2005). Influence of nutrient, pH and dissolved oxygen on the production of *Metarhizium flavoviride* Mf189 blastospores in submerged batch culture. *Process Biochem.* 40, 1425–1431. doi: 10.1016/j.procbio.2004.06.029

Ku, M., Baek, Y. U., Kwak, M. K., and Kang, S. O. (2017). *Candida albicans* glutathione reductase downregulates Efg1-mediated cyclic AMP/protein kinase A pathway and leads to defective hyphal growth and virulence upon decreased cellular methylglyoxal content accompanied by activating alcohol dehydrogenase and glycolytic enzymes. *Biochim. Biophys. Acta* 1861, 772–788. doi: 10.1016/j.bbagen.2016.10.010

Leskovac, V., Trivić, S., and Peričin, D. (2002). The three zinc-containing alcohol dehydrogenases from baker's yeast, *Saccharomyces cerevisiae*. *FEMS Yeast Res.* 2, 481–494. doi: 10.1111/j.1567-1364.2002.tb00116.x

Lin, Y., He, P., Wang, Q., Lu, D., Li, Z., Wu, C., et al. (2010). The alcohol dehydrogenase system in the xylose-fermenting yeast *Candida maltosa*. *PLoS One* 5:e11752. doi: 10.1371/journal.pone.0011752

Liu, J., Cao, Y., and Xia, Y. (2010). Mmc, a gene involved in microcycle conidiation of the entomopathogenic fungus *Metarhizium anisopliae*. *J. Invertebr. Pathol.* 105, 132–138. doi: 10.1016/j.jip.2010.05.012

Livak, K. J., and Schmittgen, T. D. (2001). Analysis of relative gene expression data using real-time quantitative PCR and the 2-ΔΔCT method. *Methods* 25, 402–408. doi: 10.1006/meth.2001.1262

Lomer, C. J., Bateman, R. P., Johnson, D. L., Langewald, J., and Thomas, M. (2001). Biological control of locusts and grasshoppers. *Annu. Rev. Entomol.* 46, 667–702. doi: 10.1146/annurev.ento.46.1.667

Luo, S., He, M., Cao, Y., and Xia, Y. (2013). The tetraspanin gene MaPls1 contributes to virulence by affecting germination, appressorial function and enzymes for cuticle degradation in the entomopathogenic fungus, *Metarhizium acridum*. *Environ. Microbiol.* 15, 2966–2979. doi: 10.1111/1462-2920.12166

Mienda, B. S., Idi, A., and Umar, A. (2011). Microbiological features of solid state fermentation and its applications - An overview. *Res. J. Biotech.* 2, 21–26.

Muñiz-Paredes, F., Miranda-Hernández, F., and Loera, O. (2017). Production of conidia by entomopathogenic fungi: from inoculants to final quality tests. *World J. Microbiol. Biotechnol.* 33:57. doi: 10.1007/s11274-017-2229-2

Oostra, J., le Comte, E. P., van den Heuvel, J. C., Tramper, J., and Rinzema, A. (2001). Intra-particle oxygen diffusion limitation in solid-state fermentation. *Biotechnol. Bioeng.* 75, 13–24. doi: 10.1002/bit.1159

Ortiz-Urquiza, A., and Keyhani, N. O. (2015). Stress response signaling and virulence: insights from entomopathogenic fungi. *Curr. Genet.* 61, 239–249. doi: 10.1007/s00294-014-0439-9

Peacock, A. J. (1998). ABC of oxygen: oxygen at high altitude. *BMJ* 1998, 1063–1066. doi: 10.1136/bmj.317.7165.1063

Peng, G. X., Wang, Z. K., Yin, Y. P., Zeng, D. Y., and Xia, Y. X. (2008). Field trials of *Metarhizium anisopliae* var. acridum (Ascomycota:Hypocreales) against oriental migratory locusts, *Locusta migratoria* manilensis (Meyen) in Northern China. *Crop Prot.* 27, 1244–1250. doi: 10.1016/j.cropro.2008.03.007

Plapp, B. V., Lee, A. T., Khanna, A., and Pryor, J. M. (2013). Bradykinetic alcohol dehydrogenases make yeast fitter for growth in the presence of allyl alcohol. *Chem. Biol. Interact.* 202, 104–110. doi: 10.1016/j.cbi.2012.11.010

Quesada-Moraga, E., Navas-Cortes, J. A., Maranhao, E. A., Ortiz-Urquiza, A., and Santiago-Alvarez, C. (2007). Factors affecting the occurrence and distribution of entomopathogenic fungi in natural and cultivated soils. *Mycol. Res.* 111, 947–966. doi: 10.1016/j.mycres.2007.06.006

Rahardjo, Y. S., Sie, S., Weber, F. J., Tramper, J., and Rinzema, A. (2005). Effect of low oxygen concentrations on growth and alpha-amylase production of *Aspergillus oryzae* in model solid-state fermentation systems. *Biomol. Eng.* 21, 163–172. doi: 10.1016/j.bioeng.2005.01.001

Rangel-Porras, R. A., Meza-Carmen, V., Martinez-Cadena, G., Torres-Guzman, J. C., Gonzalez-Hernandez, G. A., Arnau, J., et al. (2005). Molecular analysis of an NAD-dependent alcohol dehydrogenase from the zygomycete *Mucor circinelloides*. *Mol. Genet. Genomics* 274, 354–363. doi: 10.1007/s00438-005-0025-4

Reid, M. F., and Fewson, C. A. (1994). Molecular characterization of microbial alcohol dehydrogenases. *Crit. Rev. Microbiol.* 20, 13–56. doi: 10.3109/10408419409113545

Rotariu, L., Arvinte, A., Litescu, S. C., and Bala, C. (2004). Fast enzymatic method for acetaldehyde determination in wine quality control. *Univ. Ann. Bucharest Chem* 13, 105–110.

Stanley, G. A., Douglas, N. G., Every, E. J., Tzanatos, T., and Pamment, N. B. (1993). Inhibition and stimulation of yeast growth by acetaldehyde. *Biotechnol. Lett.* 15, 1199–1204. doi: 10.1007/BF00130297

Sun, B. D., and Liu, X. Z. (2008). Occurrence and diversity of insect-associated fungi in natural soils in China. *Appl. Soil Ecol.* 39, 100–108. doi: 10.1016/j.apsoil.2007.12.001

Tlecuitl-Beristain, S., Viniegra-Gonzalez, G., Diaz-Godinez, G., and Loera, O. (2010). Medium selection and effect of higher oxygen concentration pulses on *Metarhizium anisopliae* var. lepidiotum conidial production and quality. *Mycopathologia* 169, 387–394. doi: 10.1007/s11046-009-9268-7

Yubak Dhoj, G. C., Kellar, S., Nagel, P., and Kafle, L. (2008). Virulence of *Metarhizium anisopliae* and *Beauveria bassiana* against common white grubs in Nepal. *Formosan Entomol.* 28, 11–20.

Zhou, J., Shao, X., Olson, D. G., Murphy, S. J., Tian, L., and Lynd, L. R. (2017). Determining the roles of the three alcohol dehydrogenases (AdhA, AdhB and AdhE) in *Thermoanaerobacter ethanolicus* during ethanol formation. *J. Ind. Microbiol. Biotechnol.* 44, 745–757. doi: 10.1007/s10295-016-1896-6

Zimmermann, G. (2007). Review on safety of the entomopathogenic fungus *Metarhizium anisopliae*. *Biocontrol. Sci. Technol.* 17, 879–920. doi: 10.1080/09583150701593963

Conflict of Interest Statement: The authors declare that the research was conducted in the absence of any commercial or financial relationships that could be construed as a potential conflict of interest.

frontiers in Microbiology

ORIGINAL RESEARCH
published: 19 September 2018
doi: 10.3389/fmicb.2018.02158

A *GRX1* Promoter Variant Confers Constitutive Noisy Bimodal Expression That Increases Oxidative Stress Resistance in Yeast

*Jian Liu[1], Delphine Lestrade[2], Sevan Arabaciyan[1], Julien Cescut[2], Jean-Marie François[1,2] and Jean-Pascal Capp[1]**

[1] *Laboratoire d'Ingénierie des Systèmes Biologiques et des Procédés, UMR CNRS 5504, UMR INRA 792, Institut National des Sciences Appliquées de Toulouse, Université de Toulouse, Toulouse, France,* [2] *Toulouse White Biotechnology, UMS INRA 1337, UMS CNRS 3582, Institut National des Sciences Appliquées de Toulouse, Toulouse, France*

Higher noise in the expression of stress-related genes was previously shown to confer better resistance in selective conditions. Thus, evolving the promoter of such genes toward higher transcriptional noise appears to be an attractive strategy to engineer microbial strains with enhanced stress resistance. Here we generated hundreds of promoter variants of the *GRX1* gene involved in oxidative stress resistance in *Saccharomyces cerevisiae* and created a yeast library by replacing the native *GRX1* promoter by these variants at the native locus. An outlier clone with very strong increase in noise (6-times) at the same mean expression level as the native strain was identified whereas the other noisiest clones were only 3-times increased. This variant provides constitutive bimodal expression and consists in 3 repeated but differently mutated copies of the *GRX1* promoter. In spite of the multi-factorial oxidative stress-response in yeast, replacement of the native promoter by this variant is sufficient alone to confer strongly enhanced resistance to H_2O_2 and cumene hydroperoxide. New replacement of this variant by the native promoter in the resistant strain suppresses the resistance. This work shows that increasing noise of target genes in a relevant strategy to engineer microbial strains toward better stress resistance. Multiple promoter replacement could synergize the effect observed here with the sole *GRX1* promoter replacement. Finally this work suggests that combining several mutated copies of the target promoter could allow enhancing transcriptional-mediated noise at higher levels than mutating a single copy by providing constitutive bimodal and highly heterogeneous expression distribution.

Keywords: stochastic gene expression, *Saccharomyces cerevisiae*, single-cell analysis, bimodal expression, noise, phenotypic heterogeneity

OPEN ACCESS

Edited by:
John P. Morrissey, University College Cork, Ireland

Reviewed by:
Nuno Pereira Mira, Instituto de Bioengenharia e Biociências (IBB), Portugal
Olin Silander, Massey University, New Zealand

***Correspondence:**
Jean-Pascal Capp
capp@insa-toulouse.fr

Specialty section:
This article was submitted to Microbial Physiology and Metabolism, a section of the journal Frontiers in Microbiology

Received: *16 May 2018*
Accepted: *23 August 2018*
Published: *19 September 2018*

Citation:
Liu J, Lestrade D, Arabaciyan S, Cescut J, François JM and Capp JP (2018) A GRX1 Promoter Variant Confers Constitutive Noisy Bimodal Expression That Increases Oxidative Stress Resistance in Yeast. Front. Microbiol. 9:2158. doi: 10.3389/fmicb.2018.02158

INTRODUCTION

The stochastic nature of the chemical reactions governing gene expression and the small number of molecules involved in this process create cell-to-cell variations in the mRNA and protein contents (McAdams and Arkin, 1999), even among clonal cells and in homogeneous environments. This phenomenon called gene expression noise affects all genes but the level of noise depends on the gene function, suggesting a positive selection during evolution (Newman et al., 2006). For

instance, noise minimization arises for genes coding for housekeeping proteins and complex-forming proteins (Fraser et al., 2004) while genes involve in stress response exhibit higher levels of noise (Newman et al., 2006).

The first modern studies of gene expression noise in bacteria and yeast (Elowitz et al., 2002; Blake et al., 2003; Raser and O'Shea, 2004) were rapidly followed by experimental evidences of its adaptive role in stressful environments or during nutritional shift (Blake et al., 2006; Smith et al., 2007; Acar et al., 2008; Fraser and Kaern, 2009; Ito et al., 2009; Lidstrom and Konopka, 2010; Ackermann, 2013; New et al., 2014; Venturelli et al., 2015; Wang et al., 2015). Since the pioneering work from Blake et al. (2006), several cases of stress resistance linked to phenotypic heterogeneity conferred by expression noise have been described in *Saccharomyces cerevisiae* (Smith et al., 2007; Rotem et al., 2010; Liu et al., 2015). It is assumed that this represents a bet-hedging strategy which allows subpopulations to be "pre-adapted" to variable selective conditions.

As modulation of noise for stress-related genes appears to modify the ability of a population to adapt, whether gene expression noise is under selection or not has been questioned (Richard and Yvert, 2014). Also stress-related genes and genes coding for trans-membrane transporters are expressed with higher noise than other genes (Bar-Even et al., 2006; Newman et al., 2006; Zhang et al., 2009; Lehner, 2010), suggesting that this phenomenon contributes to adaptation to changing environments (Liu et al., 2016). On the contrary, housekeeping and essential genes that are supposed to require stable expression to provide stable properties are expressed with lower noise (Newman et al., 2006; Lehner, 2008). Finally, gene order and chromosome organization seem to be highly linked to reduction of noise: for instance, clustering of essential genes in the genome seems to indicate negative selection on noise (Batada and Hurst, 2007), suggesting again that the level of noise is under selection and that reduction or increase of noise can be acquired by various genetic and epigenetic ways.

Many genetic determinants in promoters play a role in the generation of noise in eucaryotes (Sanchez et al., 2013), especially transcription factor (TF) binding sites (Murphy et al., 2007; Octavio et al., 2009; To and Maheshri, 2010; Sharon et al., 2014) and TATA box (Raser and O'Shea, 2004; Blake et al., 2006; Hornung et al., 2012). Also, promoter with nucleosome binding sites harbors ON vs. OFF alternative states and thus produces bursts of mRNA production which generate cell-to-cell variability in gene expression (Sanchez and Golding, 2013). Promoters containing poly-nucleosome-disfavoring sequences have lower noise due to higher transcription burst frequency (Sharon et al., 2014). The impact of these genetic determinants on noise has been mostly studied by several works aiming at modifying promoter sequences either rationally or randomly (Murphy et al., 2007, 2010; Hornung et al., 2012; Carey et al., 2013; Sharon et al., 2014). These strategies helped to decipher the origin of noise but they have never been used to generate promoter variants of stress-related genes that might enhance resistance to specific stresses by producing higher noise in their expression.

In yeast, oxidative stress is one of the most studied because of its importance in many basic (aging) and industrial processes. Especially, reactive oxygen species (ROS) are generated by various mechanisms in bioprocessing using yeast and can limit the efficiency of its use in biotechnological applications (Wiseman, 2005; Fu et al., 2014; Landi et al., 2015). It is also one of the most complex stresses with 37 protective enzymes that are up-regulated in response to ROS exposure in yeast (Morano et al., 2012). Among this family, the glutathione-dependent disulfide oxidoreductases (glutaredoxins) such as Grx1 are part of the glutaredoxin system where glutaredoxins are oxidized by substrates, and reduced non-enzymatically by glutathione (Luikenhuis et al., 1998; Collinson et al., 2002; Collinson and Grant, 2003). Especially, elevated gene dosage of *GRX1* confers resistance to peroxides including hydrogen peroxide (H_2O_2), tert-butyl hydroperoxide and cumene hydroperoxide in yeast (Collinson et al., 2002). This suggests that increasing expression noise of this gene would produce a higher resistant subpopulation with increased Grx1 levels that could favor survival and growth upon challenging the yeast culture with an oxidative stress.

Thus the purpose of this work was to evaluate the hypothesis that resistance of yeast strains to oxidative stress could be improved by modifying the expression variability of *GRX1* without changing its mean expression. To this end, we generated hundreds of *S. cerevisiae GRX1* promoter variants and identified an evolved yeast clone that harbors a candidate variant that strongly enhances noise without changing the mean expression level and which was associated with increased resistance to H_2O_2 and cumene hydroperoxide. We furthermore found that this promoter variant conferred a bimodal expression profile that was lost upon replacement with the native promoter in the evolved strain. Altogether, this work shows that varying the noise level in the expression of a gene implicated a given stress could be alternative strategy to readily isolate evolved population with higher resistance to this given stress.

MATERIALS AND METHODS

Yeast Strains and Growth Conditions

The yeast strain *GRX1-GFP-HIS3MX6* was purchased from Thermo Ficher Scientific. All the primers used in this study are listed in **Supplementary Table 1**. To create the *GRX1-GFP-tdTomato-kanR* strain, a PCR fragment containing tdTomato-kanR and homologies to *GFP-HIS3MX6* was amplified with primers C1 and C2 from pfa6a-tdTomato-kanR (constructed in our lab) and transformed to the *GRX1-GFP-HIS3MX6* strain.

All the strains were grown in liquid YPD medium containing 20 g/L glucose (Sigma), 10 g/L peptone (Euromedex) and 10 g/L yeast extraction (Euromedex). When needed, 20 g/L agar (Euromedex) was added to make solid plates. YNB-URA$^-$ plates [20 g/L glucose (Sigma), 20 g/L agar (Euromedex), 1.71 g/L yeast nitrogen base without amino acids and nitrogen (Euromedex), 5 g/L ammonium sulfate (Sigma), and 0.77 g/L CSM-URA$^-$ (Euromedex)] or 5-FOA plate [20 g/L glucose (Sigma), 20 g/L agar (Euromedex), 1.71 g/L yeast nitrogen base without amino acids and nitrogen (Euromedex), 5 g/L ammonium sulfate (Sigma), 0.79 g/L CSM-URA$^-$ (Euromedex), and 1 g/L 5-FOA (Euromedex)] were used to select transformants.

Generation of the *GRX1* Promoter Variants Library

The PCR fragment containing the *GRX1* promoter (400 bp core sequence) and its flanking sequence (about 300 bp) was amplified from the genomic DNA of the *GRX1-GFP-HIS3MX6* strain with primers C3 and C4. This fragment was cloned into the plasmid pfa6a-GFP-kanR through EcoRI and SalI (now named pfa6a-GRX1).

The GeneMorph II Random Mutagenesis Kit (Agilent) was used to amplify the *GRX1* core promoter with random mutations from pfa6a-GRX1 with primers C5 and C6 following the standard protocol of the manufacturer (a total of 50 cycles of amplification was applied). The purified PCR product was used as primers to amplify the rest of the plasmids by the Phusion DNA polymerase (NEB). The final product was digested by DpnI, purified, and then transformed to DH5α (NEB) following the standard protocol of the manufacturer (a total of 10^5 transformants were obtained and pooled together). 14 transformants were isolated and sequenced to estimate mutation frequencies.

The *GRX1* promoter in the *GRX1-GFP-tdTomato-kanR* strain was first replaced by a PCR fragment containing *URA3* which was amplified from the plasmid pJRL2-TATA-CFP (Addgene) with primers C7 and C8. Then *URA3* was replaced by the fragments of pfa6a-GRX1 containing a variant promoter which was cut from the pooled plasmids by EcoRI and SalI through 5-FOA selection (a total of 10^5 transformants were obtained and pooled together).

Screening of Single Clones Containing *GRX1* Promoter Variants and Cell Sorting

Single cells from the library were isolated by the MoFlo Astrios EQ cell sorter with the Summit v6.3 software (Beckman Coulter, Brea, CA, United States). Cultures at stationary phase were diluted 20 times and grown at 30°C with vigorous shaking (200 rpm) for 6 h before cell sorting (final OD≈2). Cultures were spun down at 3,000 *g* for 5 min at 4°C. Growth media was removed, and cells were re-suspended in ice-cold PBS. The SmartSampler and microplate holder were kept at 4°C during cell sorting. Cell sorting was carried out with a 70 μm nozzle and 60 psi operating pressure. The sorting speed was kept at around 30,000 events per second. The single mode for the sort mode and 0.5 drop for the droplet envelope were chosen. Based on the FSC-Area vs. SSC-Area (488 nm laser) plot and the FSC-Height vs. FSC-Area (488 nm laser) plot, single cells with similar cell size and granularity were first selected. Then based on the histogram of the GFP-tdTomato fluorescence (560 nm laser, 614/20 filter), single cells of which the fluorescence lied in the middle 50% of the population were sorted to single wells of a 96 well plate with 200 μL YPD per well. Finally, a total of 4 plates were obtained.

The plates were kept in an incubator (30 h, 700 rpm, and 70% humidity) for 48 h till stationary phase. They were diluted 20 times and grown to exponential phase (6 h) to measure the expression profile of *GRX1-GFP-tdTomao* of each clone by MACSQuant® VYB with the MACSQuantify™ Software (Miltenyi Biotec, Germany). A total of 10^5 cells were analyzed for each clone, and the fsc files were exported and analyzed by R program (v3.2) with the Bioconductor packages (v3.0). A norm2Filter filter was applied on FSC-A/SSC-A to select homogeneous cells regarding size, shape, and cellular complexity. The GFP-tdTomato fluorescence (Channel Y2-A) was transformed with the log function. Then the mean GRX1-GFP-tdTomato fluorescence value and its noise (the square of the coefficient of variance) was calculated and exported. All the figures were drawn based on the transformed data. Experiments were repeated three times.

To analyze the dynamics of bimodality recovering in the bimodal clone, the BY4741 strain was used as a negative (non-fluorescent) control and for calibrations. Both strains were grown overnight at 30°C in YPD medium and diluted 10 times in the morning. After 6 h, 10^6 cells around each peak in the bimodal clone were sorted simultaneously with MoFlo Astrios EQ (Beckman Coulter, Brea, CA, United States). The unimodality of the sorted cells was checked and they were then grown at 30°C in YPD medium. The recovery of bimodality was followed with MACSQuant VYB (Miltenyi Biotec, Germany).

Promoter Swapping

The *GRX1* promoter variant of the outlier clone was first replaced by *URA3* as described above and then replaced by the native promoter cloned by PCR. To study each mutated copy identified in the *GRX1* promoter variant of the outlier clone, the core promoter of *GRX1* from this outlier was amplified by PCR with primers C5 and C6. The purified PCR product was used as primers to amplify the plasmid pfa6a-GRX1. The final product was digested by DpnI, purified and transformed to DH5α. The plasmids extracted from 10 clones were sequenced. Each of the three mutated copies was identified as a single copy in different clones. Then the promoters with a single mutated core sequence were cut from the plasmid and replaced the *URA3* fragment as described above. The expression profile of all these strains was verified by MACSQuant® VYB with the MACSQuantify™ Software, and all the data were analyzed by R program as described above. Experiments were repeated three times.

Resistance to the Oxidative Reagents

Overnight cultures were diluted to *OD* = 0.2 and cells grown in YPD medium until late exponential phase (7 h). Then they were diluted 100-times in YPD cultures with different concentrations of oxidative reagents [H_2O_2 (Sigma, 0–9 mM) or cumene hydroperoxide (Sigma, 0–160 μM)]. The OD of each culture was measured after 30 h. The residual growth was calculated as the OD with a specific concentration of one reagent divided by the OD in YPD. For experimental growth time course in 5.5 mM H_2O_2 or without H_2O_2, OD was followed during 35 h to draw the growth curve. All these experiments were repeated at least three times.

For the spot assays, overnight cultures were diluted to *OD* = 0.2 and grown in YPD medium until late exponential phase (7 h). All the final cultures were adjusted to OD 1, then 10 μL of each culture was dropped on YPD plates containing either 4.5 mM H_2O_2, 2 mM diamide, 2 mM tert-butyl hydroperoxide, or 1 g/L furfural. All the plate were kept at 30 h for 2 days. All these experiments were repeated at least three times.

RESULTS

Random Mutagenesis of the *GRX1* Promoter and Library Construction

The *GRX1* gene was chosen to evaluate our hypothesis because it is one of the most expressed oxidative-stress response genes in non-selective conditions (Newman et al., 2006), and hence this should facilitate measurement of its expression noise level using flow cytometry experiments. However, we found that the fluorescence conferred by a fusion protein Grx1-GFP (Newman et al., 2006) was not satisfactorily distinct from the fluorescence background of a yeast population that do not bear this fusion protein (**Supplementary Figure 1**). Therefore, we decided to create a double fluorescent marker with tdTomato added in C-terminal which allowed us to obtain a distribution that does not overlap the control population (**Supplementary Figure 1**).

We then considered that we had the necessary brightness to evaluate the effects of *GRX1* promoter mutations in a wide range of expression distribution. These variants were obtained after three rounds of error-prone PCR on the 400 bp *GRX1* promoter. Sequencing of 14 clones showed that 2.73 ± 1.49 mutations were present per promoter with "G–A" and "C–T" representing about half of the mutations (frequencies are given in the **Supplementary Table 2**). Then we first created a library in *Escherichia coli* before integrating it in replacement of the native promoter in the *S. cerevisiae* laboratory strain BY4741. The strategy consisted in replacing the native promoter by the auxotrophic marker *URA3*, and then replacing *URA3* by the variants using the classical recombination procedure in yeast. We finally obtained a library *S. cerevisiae* clones, with each of them containing potentially a mutated version of the *GRX1* promoter. Clones were distributed in 96-well plates and analyzed by high-throughput flow cytometry to measure their mean and noise levels (**Supplementary Table 3**). We found the expected correlation where decreased mean is associated to increased noise, but very interestingly, we identified an outlier clone that exhibited a noise level approximatively 2-times higher than the second noisiest clone (0.0383 vs. 0.0204) (**Figure 1A**).

Sequencing and Expression Profile of the *GRX1* Promoter Variant With the Highest Noise

This outlier clone was further analyzed in comparison with the native promoter in exponential and stationary phase (**Figure 1B**). In both phases, its mean expression level was the same as the one conferred by the native promoter, but its noise level was increased about 6-times ($p < 0.01$). The mean expression levels were increased in stationary phase, associated with an increased noise for the mutated promoter. Moreover, when examining the expression profiles by flow cytometry, a bimodal distribution was clearly visible both exponential and stationary phase while the native promoter conferred unimodal expression (**Figure 1C**). The peak corresponding to the low-expressers is slightly above the fluorescence background, showing that expression is weak but high enough to be above the threshold of detection in this subpopulation (**Supplementary Figure 2**). The slight increase in mean expression in stationary phase is noticeable for both the

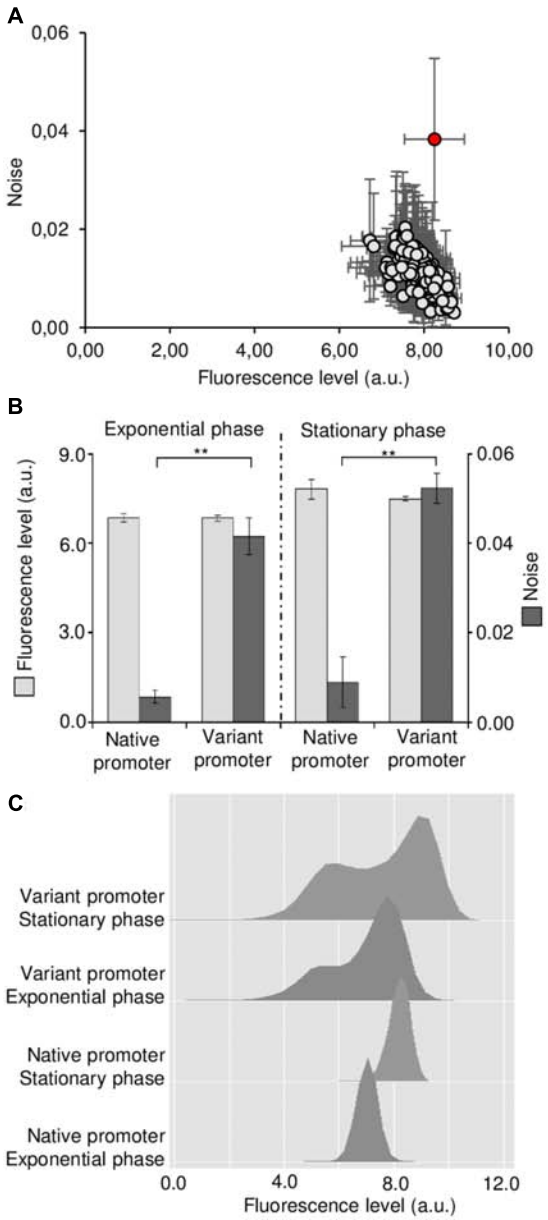

FIGURE 1 | Identification of a *GRX1* promoter variant conferring constitutive bimodal expression profile. **(A)** Mean expression and noise levels of about 200 *S. cerevisiae* clones each containing a variant version of the *GRX1* promoter (*pGRX1*) at its original locus. The outlier clone with the highest noise is highlighted in red. Results are the mean of three independent experiments with standard deviation. **(B)** Mean expression (light gray) and noise (dark gray) levels conferred by the native and the noisiest *pGRX1* variant in exponential (left) or stationary (right) phase. Results are the mean of three independent experiments with standard deviation. A significant statistical difference is represented by (**) when $p < 0.01$ in *T*-test. **(C)** Expression profiles conferred by the native and the noisiest variant *pGRX1* in exponential or stationary phase.

A

B

Mutation	TF binding site	Position	Effect
T to C	Gcr1p (CWTCC)	-233 (F) on the Reapeat1	add
G to C	Ace2p (ACCAGC)	-252 (F) on the Reapeat3	add
G to C	Hac1p (CCAGC)	-251 (F) on the Reapeat3	add
A to G	Cbf1p (RTCACRTG)	-157 (R) on theReapeat3	delete
A to G	Gcn4p (CACGTG)	-159 (F) on theReapeat3	delete
A to G	Met4p (TCACGTG)	-157 (R) on theReapeat3	delete
A to G	Pho4p (CACGTK)	-157 (F) on theReapeat3	delete

C

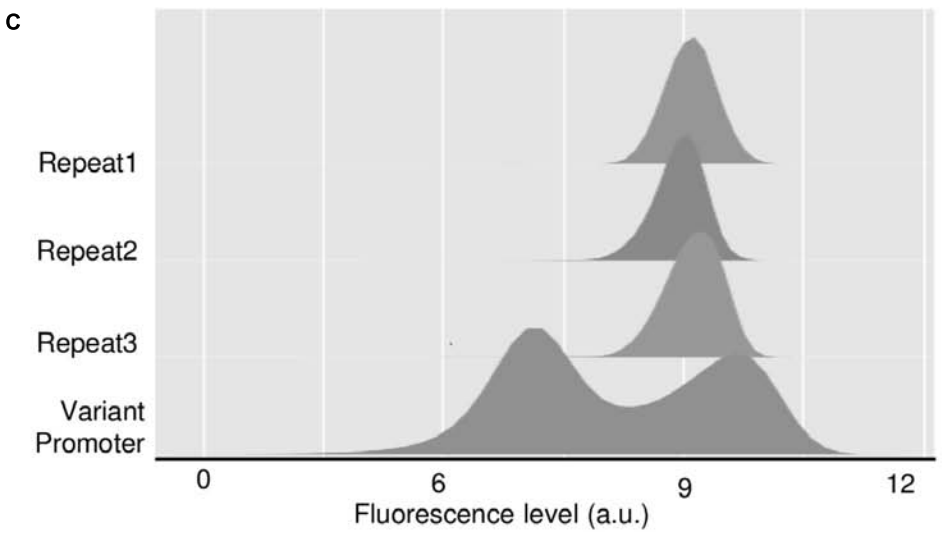

FIGURE 2 | Characterization of the noisiest *GRX1* promoter variant. **(A)** Schematic representation of the noisiest variant *pGRX1* variant and the downstream encoded gene: three repeated but differently mutated copies of *pGRX1* (blue) separated by few codons of the beginning of the *GRX1* ORF (yellow), the *GRX1* (yellow), GFP (green), and tdTomato (red) ORF. **(B)** Effects of the mutations in *pGRX1* that add or delete transcription factor (TF) binding sites. For each mutation (first column), the consensus TF binding site is given (second column) with the site of the mutation highlighted in red, the position of the mutation, the modified repeat and the modified strand (F for Forward, R for Reverse) (third column) and the effect of the mutation on the TF binding site (addition or deletion) (fourth column). **(C)** Expression profiles conferred by the noisiest variant *pGRX1* and each of the mutated repeat that constitutes this variant *pGRX1*.

native and the mutated promoters, but for the latter only the peak with the highest expression moved to higher expression levels. This logically led to increased noise in stationary phase because the population as a whole becomes even more heterogeneous. We also followed the dynamics of recovering of the bimodal profile after cell sorting of either the low-expressing cells or the high-expressing cells. Growth of these subpopulations in non-selective media showed that bimodality was restored after 16 h

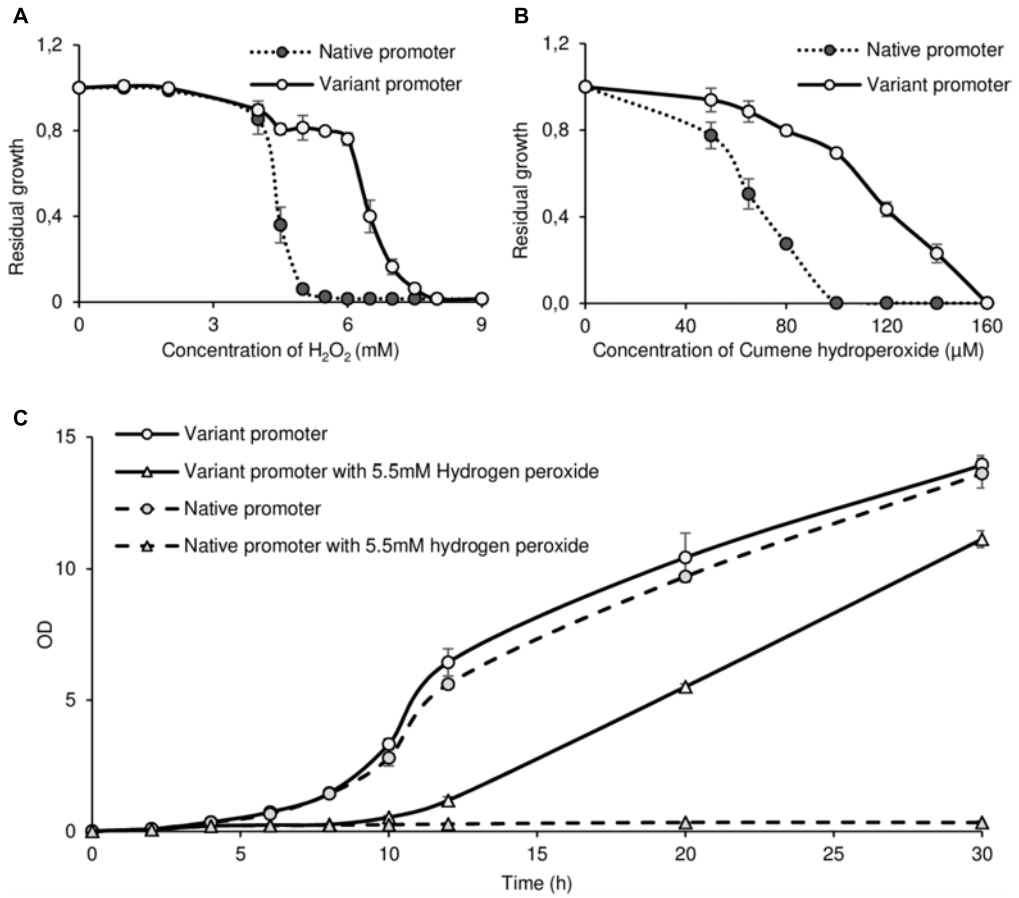

FIGURE 3 | The constitutive bimodal expression pattern produced by the noisiest *GRX1* promoter variant confers oxidative stress resistance. **(A,B)** Residual growth of strains containing either the native or the noisiest *pGRX1* variant in rich medium after 30 h in increasing H_2O_2 **(A)** or cumene hydroperoxide **(B)** concentrations. Residual is defined as the OD after 30 h in non-selective rich medium divided by the OD after 30 h in rich medium containing H_2O_2 or cumene hydroperoxide. **(C)** Example of growth curves of strains containing either the native or the noisiest *pGRX1* variant in rich medium containing or not 5.5 mM H_2O_2. All results are the mean of three independent experiments with standard deviation.

in both cases (**Supplementary Figure 3**), showing that the two states are highly reversible and epigenetic in nature, and that and the switching rate seems to be the same for both subpopulations.

Sequencing of the mutated promoter revealed an expected structure with three successive repeats of the *GRX1* each mutated differently (**Figure 2A**, see **Supplementary Figure 4** for the full sequence). These copies were numbered repeat 1, 2, and 3 from 5' to 3'. Repeat 1, 2, and 3 contained two mutations, one mutation and one deletion, and four mutations, respectively. Some of these mutations suppress or create TF binding sites, mainly in repeat 3 (**Figure 2B**). Moreover, few codons of the beginning of the ORF are present at the junction between repeats 1 and 2, and between repeats 2 and 3, and correspond to the sequence of the reverse primer initially used to amplify the promoter sequence (**Supplementary Figure 4**). Moreover 7 nucleotides were added at the junctions, suggesting that this extremely rare junctional event occurred in the cell during the process of library construction and transformation.

To decipher whether one or two or three repeats were needed to confer bimodality, we cloned each repeat independently to replace the native promoter. None of the three copies was able to confer bimodality by its own (**Figure 2C**). They all provided very similar unimodal expression distribution, showing that only the combinatorial action of several repeats is able to modify the expression profile. Interestingly, despite the relatively homogenous distribution conferred by each repeat independently, the bimodal distribution given by the three repeats cover a wide range of expression levels, from cells in the auto-fluorescence background to cells expressing *GRX1* at far higher levels than the highest levels given by a unique repeat.

The Noisiest *GRX1* Promoter Variant Improves H_2O_2 and Cumene Hydroperoxide Resistance

Given our initial hypothesis, we tested a possible increase in oxidative stress resistance in this strain. As *GRX1* overexpression confers resistance to peroxides in yeast (Collinson et al., 2002), we grew the control strain containing the native promoter and the strain containing the mutated promoter in a wide

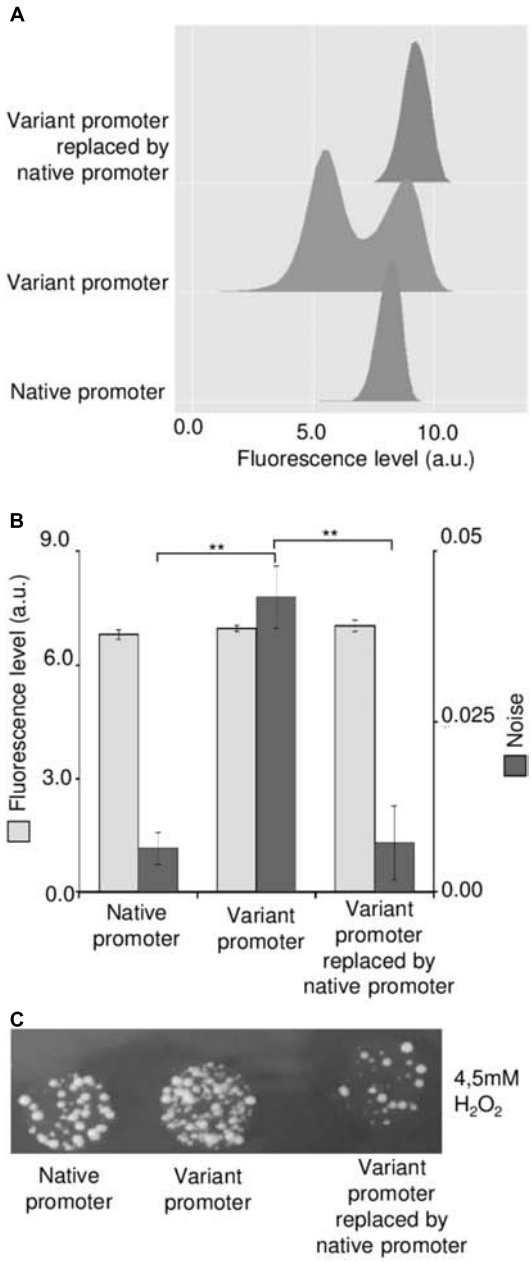

FIGURE 4 | New replacement of the *pGRX1* variant in the resistant strain by the native promoter suppresses bimodality and oxidative stress resistance. **(A)** Expression profiles conferred by the native *pGRX1*, the noisiest *pGRX1* variant or the native *pGRX1* after replacement of noisiest *pGRX1* variant in the resistant strain. **(B)** Mean expression (light gray) and noise (dark gray) levels conferred by the native *pGRX1*, the noisiest *pGRX1* variant, or the native *pGRX1* after replacement of noisiest *pGRX1* variant in the resistant strain. Results are the mean of three independent experiments with standard deviation. A significant statistical difference is represented by (**) when $p < 0.01$ in *T*-test. **(C)** Spot assay in 4.5 mM H_2O_2 with strains containing the native *pGRX1*, the noisiest *pGRX1* variant or the native *pGRX1* after replacement of noisiest *pGRX1* variant in the resistant strain.

range of hydrogen peroxide (H_2O_2) and cumene hydroperoxide concentrations. These compounds represent typical inorganic and organic peroxides, respectively. When considering the residual growth in each concentration (OD after 30 h in peroxide-containing medium divided by OD after 30 h in control medium), a strong increase in resistance is observed for both compounds: from 4.5 to 7 mM H_2O_2 (**Figure 3A**) and from 50 to 140 μM cumene hydroperoxide (**Figure 3B**).

A representative growth curve in H_2O_2 shows that while both strains grew similarly in the non-selective medium, only the mutated promoter allowed growth in 5.5 mM H_2O_2 (**Figure 3C**). The same phenomenon is observed from 5 to 7 mM H_2O_2 and from 100 to 140 μM cumene hydroperoxide where no growth was observed with the native promoter. Another example of growth curves without or with 100 μM cumene hydroperoxide in given in **Supplementary Figure 5**. Spot assays were also performed with 4.5 mM H_2O_2 in rich medium and showed better growth with the mutated promoter both with cells in exponential and in stationary phase (**Supplementary Figure 6**), confirming the increased resistance observed in liquid medium. Other compounds producing oxidative stress response were tested in spot assays: diamide 2 mM, tert-butyl hydroperoxide 2 mM, and furfural 1 g/L where the strains did not show any difference (**Supplementary Figure 6**).

Bimodality and Oxidative Stress Resistance Is Specifically Conferred by This Promoter Variant of *GRX1*

To go further in deciphering the origins of the increased *GRX1* expression variability by distinguishing *cis*- and possible *trans*-effects (in other words to check that it is only due to the mutated promoter or to the combined effect of mutations in *cis* and *trans*), we decided to replace the promoter variant in the resistant strain by the native one. As shown in **Figure 4A**, we found that the bimodal expression was only produced by the mutated promoter since the expression profile returned to unimodality with the native promoter. In addition, the noise level decreased at the level of the original strain while the mean expression level was very slightly increased after swapping in the resistant strain (**Figure 4B**). This promoter swapping was also associated with the suppression of the resistance of the strain to H_2O_2 (**Figure 4C**).

DISCUSSION

Several works showed an increased stress resistance conferred by higher expression noise in *Saccharomyces cerevisiae* (Smith et al., 2007; Rotem et al., 2010; Liu et al., 2015). Especially, we previously observed that the increased expression variability conferred by a natural yeast promoter variant isolated from an oenological strain provided a clear benefit in the face of an environmental stress compared to its lab strain counterpart (Liu et al., 2015). This modulation of gene expression noise was partly due to promoter modifications. As other works revealed the possibility to get a wide range of mean and/or noise levels by random mutagenesis of promoter sequences (Hornung et al., 2012), we hypothesized that such mutagenesis of promoters related to stress-response should allow identification of interesting variants that could improve stress resistance.

More precisely, this work aimed at obtaining promoters variants of the oxidative stress-related gene *GRX1* in *Saccharomyces cerevisiae* that confer higher noise at equal mean and testing the phenotypic consequences in terms of oxidative stress resistance.

We succeeded in obtaining a strain with enhanced oxidative stress resistance by this targeted (gene-specific) approach. This approach is original for stress resistance improvement because it targets specific genes while classical evolutionary engineering protocols do not. It allows better control of (and knowledge on) the intracellular events leading to increased resistance, even for multi-factorial stress responses. Moreover, contrary to other controlled strategies such as gene overexpression, modifying the expression profile of target genes without modifying their expression mean allows that there is no consumption and mobilization of energy resources to overexpress this gene when it is useless (which could be deleterious to the strain behavior in non-selective conditions). Finally, higher gene expression variability allows the pre-existence of a subpopulations with these higher levels of expression that are "pre-adapted" to the onset of stress, and cells to reach these higher levels more quickly when stress appears, which would limit cell death.

Previous works aiming at mutating target promoters to study mean–noise relationships did not identify outlier mutants in this relationship (Hornung et al., 2012). Here we found a clone harboring such a highly increased noise and bimodal expression profile at equal mean compared to the native promoter (×4 while our second noisiest was only 2-times increased), suggesting that this clone undergone an original genetic event. Indeed this noisiest clone contained a *GRX1* promoter structure consisting in three repeated by differently mutated copies of the promoter. In spite of the unknown process that led to this original structure, it reveals that promoter engineering that consists in combining several mutated copies of a promoter of interest could be a way to strongly increase noise, especially by producing bimodal expression, while mutating only a single copy does not allow such strong modification of the noise level.

Interestingly, we recently showed that bimodality in gene expression can be instigated by DNA context, inducing conditions and strain background from the same promoter sequence (Liu et al., 2018). In fact, many phenomena, especially gene regulatory networks topologies (To and Maheshri, 2010; Venturelli et al., 2012), cell signaling (Biggar and Crabtree, 2001; Paliwal et al., 2007; Birtwistle et al., 2012) or TFs dynamics, binding and regulation (Kelemen et al., 2010; Pelet et al., 2011), have a major impact on bimodality. Nevertheless, only few works showed *cis*-effects on bimodality. For instance, the spatial distribution of activator and repressor binding sites has been shown to influence gene expression to become monostable or bistable in yeast (Kelemen et al., 2010). The expression profile depends on the spatial distribution of the binding sites of the repressors along the DNA (Kelemen et al., 2010). Chromatin remodeling is another determinant of this bimodal expression behavior in yeast (Pelet et al., 2011). It seems that only a fraction of the population remodel chromatin to allow for efficient transcription at low stress levels. Genomic regions undergoing frequent chromatin remodeling such as subtelomeres also frequently display bimodal and stochastic gene expression in response to environmental stimuli (Halme et al., 2004; Domergue et al., 2005; Choi et al., 2008). Also, variegated expression of cell adhesion genes localized in subtelomeric domains may enhance the survival or virulence of fungal cells (Halme et al., 2004; Domergue et al., 2005). Interestingly, nucleoid-binding proteins in *Escherichia coli* were recently proposed to also contribute to regulation of bimodal expression of virulence genes leading to opposing bacterial fates (Leh et al., 2017). All these previous observations suggest that modification of the TF binding sites distribution, number and affinity together with modification of nucleosome occupancy and positioning are all responsible for the transition from unimodal to bimodal expression mode in our *GRX1* promoter variant.

Moreover, many bimodal expression profiles have been studied on artificial inducible systems where bimodality was produced in specific inducting conditions, rendering extrapolation to strain engineering rather difficult. On non-artificial systems, bimodality has been mostly studied in the context of nutritional and stress response in *S. cerevisiae*. Especially, downstream targets harbor bimodal expression only in specific ranges of stimulus concentrations in the galactose regulatory network (Acar et al., 2005; Venturelli et al., 2012) or the high-osmolarity glycerol (HOG) pathway (Pelet et al., 2011), suggesting that this expression mode could have been selected for at least in certain stressful conditions thanks to an adaptive benefit for the population through a bet-hedging strategy. Here we showed that it is possible to obtain promoter variants that constitutively drive noisy bimodal expression from a unimodal native promoter. This avoids the need for specific inducer or repressor and precise control of growth conditions, and shows that bet-hedging in a very wide range of gene expression could be counter-intuitively not detrimental in optimal growth conditions while being highly in beneficial in selective conditions. Indeed, the sole replacement of the native promoter by the variant conferring this basal bimodal profile of stress-response genes is sufficient alone to allow better resistance in stressful conditions.

While oxidative stress response involves 37 different enzymes in *S. cerevisiae*, modifying expression variability of *GRX1* alone produced phenotypic effects here, suggesting that combining the same strategy for several genes involved in the same stress response could produce additive or even synergistic effects. To engineer strains of interest toward even higher resistance, either the same variant could be placed upstream other genes involved in resistance to the same stress (here for instance the *GRX2* gene which is a paralog of *GRX1)*, or the same strategy of generating noisier promoter variants could be applied to these other genes to reach an optimal effect from their native promoters.

Compared to *in vivo* evolution methods using turbidostat or chemostat culture that can take approximately between few months and a year, the method presented here could be much more efficient and save time for strain improvement. Moreover, in these "classical" methods, a strong constraint must be defined *a priori*, while it is not needed to define here such constraints at the outset but to choose/identify a target gene linked to a given

stress or to a specific metabolic function. This may seem easier especially when the constraint for *in vivo* evolution is difficult to implement. In conclusion, this work shows that varying expression noise of a gene linked to a relevant biotechnology trait such as oxidative or osmotic stress could be an alternative strategy in reverse engineering of industrial strains.

AUTHOR CONTRIBUTIONS

JL, J-MF, and J-PC conceived and designed the experiments. JL, DL, SA, and J-PC acquired, analyzed or interpreted the data. JL and J-PC wrote the manuscript.

FUNDING

This work was supported in part by the Toulouse White Biotechnology consortium (pre-competitive financial support Robustrain) and by the Institut Carnot 3BCar (consolidation project CYTOM).

SUPPLEMENTARY MATERIAL

The Supplementary Material for this article can be found online at: https://www.frontiersin.org/articles/10.3389/fmicb.2018.02158/full#supplementary-material

REFERENCES

Acar, M., Becskei, A., and Van Oudenaarden, A. (2005). Enhancement of cellular memory by reducing stochastic transitions. *Nature* 435, 228–232. doi: 10.1038/nature03524

Acar, M., Mettetal, J. T., and Van Oudenaarden, A. (2008). Stochastic switching as a survival strategy in fluctuating environments. *Nat. Genet.* 40, 471–475. doi: 10.1038/ng.110

Ackermann, M. (2013). Microbial individuality in the natural environment. *ISME J.* 7, 465–467. doi: 10.1038/ismej.2012.131

Bar-Even, A., Paulsson, J., Maheshri, N., Carmi, M., O'Shea, E., Pilpel, Y., et al. (2006). Noise in protein expression scales with natural protein abundance. *Nat. Genet.* 38, 636–643. doi: 10.1038/ng1807

Batada, N. N., and Hurst, L. D. (2007). Evolution of chromosome organization driven by selection for reduced gene expression noise. *Nat. Genet.* 39, 945–949. doi: 10.1038/ng2071

Biggar, S. R., and Crabtree, G. R. (2001). Cell signaling can direct either binary or graded transcriptional responses. *EMBO J.* 20, 3167–3176. doi: 10.1093/emboj/20.12.3167

Birtwistle, M. R., Rauch, J., Kiyatkin, A., Aksamitiene, E., Dobrzynski, M., Hoek, J. B., et al. (2012). Emergence of bimodal cell population responses from the interplay between analog single-cell signaling and protein expression noise. *BMC Syst. Biol.* 6:109. doi: 10.1186/1752-0509-6-109

Blake, W. J., Balazsi, G., Kohanski, M. A., Isaacs, F. J., Murphy, K. F., Kuang, Y., et al. (2006). Phenotypic consequences of promoter-mediated transcriptional noise. *Mol. Cell.* 24, 853–865. doi: 10.1016/j.molcel.2006.11.003

Blake, W. J., KAErn, M., Cantor, C. R., and Collins, J. J. (2003). Noise in eukaryotic gene expression. *Nature* 422, 633–637. doi: 10.1038/nature01546

Carey, L. B., Van Dijk, D., Sloot, P. M., Kaandorp, J. A., and Segal, E. (2013). Promoter sequence determines the relationship between expression level and noise. *PLoS Biol.* 11:e1001528. doi: 10.1371/journal.pbio.1001528

Choi, J. K., Hwang, S., and Kim, Y. J. (2008). Stochastic and regulatory role of chromatin silencing in genomic response to environmental changes. *PLoS One* 3:e3002. doi: 10.1371/journal.pone.0003002

Collinson, E. J., and Grant, C. M. (2003). Role of yeast glutaredoxins as glutathione S-transferases. *J. Biol. Chem.* 278, 22492–22497. doi: 10.1074/jbc.M301387200

Collinson, E. J., Wheeler, G. L., Garrido, E. O., Avery, A. M., Avery, S. V., and Grant, C. M. (2002). The yeast glutaredoxins are active as glutathione peroxidases. *J. Biol. Chem.* 277, 16712–16717. doi: 10.1074/jbc.M111686200

Domergue, R., Castano, I., De Las Penas, A., Zupancic, M., Lockatell, V., Hebel, J. R., et al. (2005). Nicotinic acid limitation regulates silencing of Candida adhesins during UTI. *Science* 308, 866–870. doi: 10.1126/science.1108640

Elowitz, M. B., Levine, A. J., Siggia, E. D., and Swain, P. S. (2002). Stochastic gene expression in a single cell. *Science* 297, 1183–1186. doi: 10.1126/science.1070919

Fraser, D., and Kaern, M. (2009). A chance at survival: gene expression noise and phenotypic diversification strategies. *Mol. Microbiol.* 71, 1333–1340. doi: 10.1111/j.1365-2958.2009.06605.x

Fraser, H. B., Hirsh, A. E., Giaever, G., Kumm, J., and Eisen, M. B. (2004). Noise minimization in eukaryotic gene expression. *PLoS Biol.* 2:e137. doi: 10.1371/journal.pbio.0020137

Fu, Z., Verderame, T. D., Leighton, J. M., Sampey, B. P., Appelbaum, E. R., Patel, P. S., et al. (2014). Exometabolome analysis reveals hypoxia at the up-scaling of a *Saccharomyces cerevisiae* high-cell density fed-batch biopharmaceutical process. *Microb Cell Fact.* 13:32. doi: 10.1186/1475-2859-13-32

Halme, A., Bumgarner, S., Styles, C., and Fink, G. R. (2004). Genetic and epigenetic regulation of the FLO gene family generates cell-surface variation in yeast. *Cell* 116, 405–415. doi: 10.1016/S0092-8674(04)00118-7

Hornung, G., Bar-Ziv, R., Rosin, D., Tokuriki, N., Tawfik, D. S., Oren, M., et al. (2012). Noise-mean relationship in mutated promoters. *Genome Res.* 22, 2409–2417. doi: 10.1101/gr.139378.112

Ito, Y., Toyota, H., Kaneko, K., and Yomo, T. (2009). How selection affects phenotypic fluctuation. *Mol. Syst. Biol.* 5:264. doi: 10.1038/msb.2009.23

Kelemen, J. Z., Ratna, P., Scherrer, S., and Becskei, A. (2010). Spatial epigenetic control of mono- and bistable gene expression. *PLoS Biol.* 8:e1000332. doi: 10.1371/journal.pbio.1000332

Landi, C., Paciello, L., De Alteriis, E., Brambilla, L., and Parascandola, P. (2015). High cell density culture with *S. cerevisiae CEN.PK*113-5D for IL-1beta production: optimization, modeling, and physiological aspects. *Bioprocess Biosyst. Eng.* 38, 251–261. doi: 10.1007/s00449-014-1264-8

Leh, H., Khodr, A., Bouger, M. C., Sclavi, B., Rimsky, S., and Bury-Mone, S. (2017). Bacterial-chromatin structural proteins regulate the bimodal expression of the locus of enterocyte effacement (LEE) pathogenicity island in Enteropathogenic *Escherichia coli*. *mBio* 8:e00773-17. doi: 10.1128/mBio.00773-17

Lehner, B. (2008). Selection to minimise noise in living systems and its implications for the evolution of gene expression. *Mol. Syst. Biol.* 4:170. doi: 10.1038/msb.2008.11

Lehner, B. (2010). Conflict between noise and plasticity in yeast. *PLoS Genet.* 6:e1001185. doi: 10.1371/journal.pgen.1001185

Lidstrom, M. E., and Konopka, M. C. (2010). The role of physiological heterogeneity in microbial population behavior. *Nat. Chem. Biol.* 6, 705–712. doi: 10.1038/nchembio.436

Liu, J., Arabaciyan, S., Francois, J. M., and Capp, J. P. (2018). Bimodality of gene expression from yeast promoter can be instigated by DNA context, inducing conditions and strain background. *FEMS Yeast Res.* 18:foy047. doi: 10.1093/femsyr/foy047

Liu, J., Francois, J. M., and Capp, J. P. (2016). Use of noise in gene expression as an experimental parameter to test phenotypic effects. *Yeast* 33, 209–216. doi: 10.1002/yea.3152

Liu, J., Martin-Yken, H., Bigey, F., Dequin, S., Francois, J. M., and Capp, J. P. (2015). Natural yeast promoter variants reveal epistasis in the generation of transcriptional-mediated noise and its potential benefit in stressful conditions. *Genome Biol. Evol.* 7, 969–984. doi: 10.1093/gbe/evv047

Luikenhuis, S., Perrone, G., Dawes, I. W., and Grant, C. M. (1998). The yeast *Saccharomyces cerevisiae* contains two glutaredoxin genes that are required for protection against reactive oxygen species. *Mol. Biol. Cell* 9, 1081–1091. doi: 10.1091/mbc.9.5.1081

McAdams, H. H., and Arkin, A. (1999). It's a noisy business! Genetic regulation at the nanomolar scale. *Trends Genet.* 15, 65–69. doi: 10.1016/S0168-9525(98)01659-X

Morano, K. A., Grant, C. M., and Moye-Rowley, W. S. (2012). The response to heat shock and oxidative stress in *Saccharomyces cerevisiae*. *Genetics* 190, 1157–1195. doi: 10.1534/genetics.111.128033

Murphy, K. F., Adams, R. M., Wang, X., Balazsi, G., and Collins, J. J. (2010). Tuning and controlling gene expression noise in synthetic gene networks. *Nucleic Acids Res.* 38, 2712–2726. doi: 10.1093/nar/gkq091

Murphy, K. F., Balazsi, G., and Collins, J. J. (2007). Combinatorial promoter design for engineering noisy gene expression. *Proc. Natl. Acad. Sci. U.S.A.* 104, 12726–12731. doi: 10.1073/pnas.0608451104

New, A. M., Cerulus, B., Govers, S. K., Perez-Samper, G., Zhu, B., Boogmans, S., et al. (2014). Different levels of catabolite repression optimize growth in stable and variable environments. *PLoS Biol.* 12:e1001764. doi: 10.1371/journal.pbio.1001764

Newman, J. R., Ghaemmaghami, S., Ihmels, J., Breslow, D. K., Noble, M., Derisi, J. L., et al. (2006). Single-cell proteomic analysis of *S. cerevisiae* reveals the architecture of biological noise. *Nature* 441, 840–846. doi: 10.1038/nature04785

Octavio, L. M., Gedeon, K., and Maheshri, N. (2009). Epigenetic and conventional regulation is distributed among activators of FLO11 allowing tuning of population-level heterogeneity in its expression. *PLoS Genet.* 5:e1000673. doi: 10.1371/journal.pgen.1000673

Paliwal, S., Iglesias, P. A., Campbell, K., Hilioti, Z., Groisman, A., and Levchenko, A. (2007). MAPK-mediated bimodal gene expression and adaptive gradient sensing in yeast. *Nature* 446, 46–51. doi: 10.1038/nature05561

Pelet, S., Rudolf, F., Nadal-Ribelles, M., De Nadal, E., Posas, F., and Peter, M. (2011). Transient activation of the HOG MAPK pathway regulates bimodal gene expression. *Science* 332, 732–735. doi: 10.1126/science.1198851

Raser, J. M., and O'Shea, E. K. (2004). Control of stochasticity in eukaryotic gene expression. *Science* 304, 1811–1814. doi: 10.1126/science.1098641

Richard, M., and Yvert, G. (2014). How does evolution tune biological noise? *Front. Genet.* 5:374. doi: 10.3389/fgene.2014.00374

Rotem, E., Loinger, A., Ronin, I., Levin-Reisman, I., Gabay, C., Shoresh, N., et al. (2010). Regulation of phenotypic variability by a threshold-based mechanism underlies bacterial persistence. *Proc. Natl. Acad. Sci. U.S.A.* 107, 12541–12546. doi: 10.1073/pnas.1004333107

Sanchez, A., Choubey, S., and Kondev, J. (2013). Regulation of noise in gene expression. *Annu. Rev. Biophys.* 42, 469–491. doi: 10.1146/annurev-biophys-083012-130401

Sanchez, A., and Golding, I. (2013). Genetic determinants and cellular constraints in noisy gene expression. *Science* 342, 1188–1193. doi: 10.1126/science.1242975

Sharon, E., Van Dijk, D., Kalma, Y., Keren, L., Manor, O., Yakhini, Z., et al. (2014). Probing the effect of promoters on noise in gene expression using thousands of designed sequences. *Genome Res.* 24, 1698–1706. doi: 10.1101/gr.168773.113

Smith, M. C., Sumner, E. R., and Avery, S. V. (2007). Glutathione and Gts1p drive beneficial variability in the cadmium resistances of individual yeast cells. *Mol. Microbiol.* 66, 699–712. doi: 10.1111/j.1365-2958.2007.05951.x

To, T. L., and Maheshri, N. (2010). Noise can induce bimodality in positive transcriptional feedback loops without bistability. *Science* 327, 1142–1145. doi: 10.1126/science.1178962

Venturelli, O. S., El-Samad, H., and Murray, R. M. (2012). Synergistic dual positive feedback loops established by molecular sequestration generate robust bimodal response. *Proc. Natl. Acad. Sci. U.S.A.* 109, E3324–E3333. doi: 10.1073/pnas.1211902109

Venturelli, O. S., Zuleta, I., Murray, R. M., and El-Samad, H. (2015). Population diversification in a yeast metabolic program promotes anticipation of environmental shifts. *PLoS Biol.* 13:e1002042. doi: 10.1371/journal.pbio.1002042

Wang, J., Atolia, E., Hua, B., Savir, Y., Escalante-Chong, R., and Springer, M. (2015). Natural variation in preparation for nutrient depletion reveals a cost-benefit tradeoff. *PLoS Biol.* 13:e1002041. doi: 10.1371/journal.pbio.1002041

Wiseman, A. (2005). Avoidance of oxidative-stress perturbation in yeast bioprocesses by proteomic and genomic biostrategies? *Lett. Appl. Microbiol.* 40, 37–43. doi: 10.1111/j.1472-765X.2004.01624.x

Zhang, Z., Qian, W., and Zhang, J. (2009). Positive selection for elevated gene expression noise in yeast. *Mol. Syst. Biol.* 5:299. doi: 10.1038/msb.2009.58

Conflict of Interest Statement: The authors declare that the research was conducted in the absence of any commercial or financial relationships that could be construed as a potential conflict of interest.

frontiers in Microbiology

ORIGINAL RESEARCH
published: 24 September 2018
doi: 10.3389/fmicb.2018.02267

NsrR1, a Nitrogen Stress-Repressed sRNA, Contributes to the Regulation of *nblA* in *Nostoc* sp. PCC 7120

Isidro Álvarez-Escribano, Agustín Vioque and Alicia M. Muro-Pastor*

Instituto de Bioquímica Vegetal y Fotosíntesis, Consejo Superior de Investigaciones Científicas and Universidad de Sevilla, Seville, Spain

Small regulatory RNAs (sRNAs) are currently considered as major post-transcriptional regulators of gene expression in bacteria. The interplay between sRNAs and transcription factors leads to complex regulatory networks in which both transcription factors and sRNAs may appear as nodes. In cyanobacteria, the responses to nitrogen availability are controlled at the transcriptional level by NtcA, a CRP/FNR family regulator. In this study, we describe an NtcA-regulated sRNA in the cyanobacterium *Nostoc* sp. PCC 7120, that we have named NsrR1 (nitrogen stress repressed RNA1). We show sequence specific binding of NtcA to the promoter of NsrR1. Prediction of possible mRNA targets regulated by NsrR1 allowed the identification of *nblA*, encoding a protein adaptor for phycobilisome degradation under several stress conditions, including nitrogen deficiency. We demonstrate specific interaction between NsrR1 and the 5′-UTR of the *nblA* mRNA, that leads to decreased expression of *nblA*. Because both NsrR1 and NblA are under transcriptional control of NtcA, this regulatory circuit constitutes a coherent feed-forward loop, involving a transcription factor and an sRNA.

Keywords: regulatory RNA, cyanobacteria, NtcA, feed-forward loop, post-transcriptional regulation

OPEN ACCESS

Edited by:
Daniela De Biase, Università degli Studi di Roma La Sapienza, Italy

Reviewed by:
Rakefet Schwarz, Bar-Ilan University, Israel
Patrick Jean-Adrien Videau, Southern Oregon University, United States
Tanya Soule, Purdue University Fort Wayne, United States

****Correspondence:***
Agustín Vioque
vioque@us.es

Specialty section:
This article was submitted to Microbial Physiology and Metabolism, a section of the journal Frontiers in Microbiology

Received: *25 May 2018*
Accepted: *05 September 2018*
Published: *24 September 2018*

Citation:
Álvarez-Escribano I, Vioque A and Muro-Pastor AM (2018) NsrR1, a Nitrogen Stress-Repressed sRNA, Contributes to the Regulation of nblA in Nostoc sp. PCC 7120. Front. Microbiol. 9:2267. doi: 10.3389/fmicb.2018.02267

INTRODUCTION

Small non-coding RNAs (sRNAs) are important players in bacterial regulatory networks. Most often, this type of molecules exert its function at the post-transcriptional level by fine-tuning responses to different environmental situations (Wagner and Romby, 2015). The interplay between transcription factors and small RNAs provides an additional level of control that, in many cases, results in feed-forward regulatory loops (coherent or incoherent) between a transcription factor, an sRNA and the regulated target (Mandin and Guillier, 2013; Nitzan et al., 2017).

Global nitrogen regulation in cyanobacteria is controlled by NtcA, a protein that belongs to the CRP/FNR family of transcriptional regulators (Herrero et al., 2001). Direct transcriptional regulation mediated by NtcA is operated by binding to conserved sequences (first defined as $GTAN_8TAC$, later re-defined as $GTN_{10}AC$) in the promoters of the regulated genes (Luque et al., 1994; Mitschke et al., 2011; Picossi et al., 2014; Giner-Lamia et al., 2017). NtcA has been described to act either as an activator or as a repressor of transcription, depending on the location of the binding site with respect to the regulated transcriptional start site (TSS) (Mitschke et al., 2011; Picossi et al., 2014). Most NtcA-activated promoters contain an NtcA binding site centered around position −41.5 with respect to the TSS (like Class II CRP-activated promoters). In contrast, NtcA-repressed genes bear NtcA binding sites that overlap critical elements of the promoter, including the −35 box,

the −10 box or the TSS. Therefore, the mechanism of repression by NtcA involves interference with RNA polymerase binding. Similar to the case of other CRP-family regulators, NtcA has been shown to regulate expression of several sRNAs (Mitschke et al., 2011; Brenes-Álvarez et al., 2016) including NsiR4 (nitrogen-stress inducible RNA 4), which is involved in nitrogen assimilation control via regulation of the key enzyme glutamine synthetase (Klähn et al., 2015).

Non-diazotrophic cyanobacteria respond to nutrient deprivation by a process called chlorosis, involving degradation of photosynthetic pigments, including the phycobilisomes (PBS) (Grossman et al., 1993a,b). Degradation of PBS protects the photosynthetic apparatus under exposure to high light and also provides amino acids as a source of nitrogen under nitrogen deficiency. NblA (non-bleaching phenotype) is a protein adaptor involved in PBS degradation by targeting phycobiliproteins to a proteolytic complex (Karradt et al., 2008; Sendersky et al., 2014). The *nblA* gene is induced under stress situations that promote PBS degradation (Collier and Grossman, 1994). *nblA* has multiple promoters and is subject to complex regulation that includes transcription induction by NtcA under nitrogen deprivation (Luque et al., 2001; Mitschke et al., 2011) and regulation by FurA under iron deficiency (González et al., 2016). Although heterocystous cyanobacteria are ultimately able to overcome nitrogen deprivation by fixation of atmospheric nitrogen, their transient response to nitrogen deprivation also includes induction of the *nblA* gene and partial degradation of PBS (Baier et al., 2004; Karradt et al., 2008).

We have previously carried out a differential RNA-Seq-based genome-wide identification of TSSs in the heterocystous cyanobacteria *Nostoc* sp. PCC 7120 (also known as *Anabaena* sp. PCC 7120), which included a description of transcriptional responses corresponding to the NtcA regulon (Mitschke et al., 2011). Based on the RNA-Seq data, we have also conducted a global approach to the identification of conserved, potentially regulatory small non-coding RNAs (sRNAs) in *Nostoc* sp. PCC 7120. This work has lead to the prediction and verification of several phylogenetically conserved sRNAs, including nitrogen-regulated and heterocyst-specific sRNAs (Brenes-Álvarez et al., 2016).

In this work, we show transcription of a small, nitrogen-regulated RNA, which we have named NsrR1 (nitrogen stress-repressed RNA 1), in *Nostoc* sp. PCC 7120. The promoter of NsrR1 contains a putative NtcA binding site, whose position, overlapping the −10 box, is suggestive of NtcA-mediated repression. We demonstrate sequence specific binding of purified NtcA to the promoter of *nsrR1*. Phylogenetic analysis reveals that sequences encoding orthologs of NsrR1 and the nearby NtcA binding site overlapping the −10 box are conserved among heterocystous cyanobacteria. Computational target prediction for NsrR1 identified *nblA* mRNA as possibly interacting with NsrR1 and therefore being subjected to post-transcriptional regulation by this sRNA. Here, we verify that NsrR1 regulates expression of NblA by its interaction with the 5′-UTR of *nblA* mRNA, therefore participating in an NtcA-operated coherent feed-forward regulatory loop.

MATERIALS AND METHODS

Strains and Growth Conditions

Cultures of wild-type and the different mutant strains of *Nostoc* sp. PCC 7120 (**Supplementary Table S1**) were bubbled with an air/CO_2 mixture (1% v/v) and grown photoautotrophically at 30°C in BG11 medium (Rippka et al., 1979) containing ferric citrate instead of ammonium ferric citrate, lacking $NaNO_3$ and containing 6 mM NH_4Cl, 10 mM $NaHCO_3$, and 12 mM *N*-tris(hydroxymethyl)methyl-2-aminoethanesulfonic acid-NaOH buffer (pH 7.5). Nitrogen deficiency was induced by removal of combined nitrogen. Occasionally, 17.6 mM $NaNO_3$ was used as nitrogen source. Solid media were solidified with 1% Difco Agar. Mutant strains were grown in the presence of appropriate antibiotics at the following concentrations: streptomycin (Sm) and spectinomycin (Sp), 2–3 μg/ml each (liquid medium) or 5 μg/ml each (solid medium), neomycin (Nm), 5 μg/ml (liquid medium) or 25 μg/ml (solid medium).

Escherichia coli strains (**Supplementary Table S1**) were grown in LB medium, supplemented with appropriate antibiotics (Sambrook and Russell, 2001).

Generation of NsrR1 Mutant Strains

To generate a strain lacking NsrR1 (Δ*nsrR1*), two overlapping fragments encompassing flanking sequences around NsrR1 were amplified by PCR using as template genomic DNA with oligonucleotides 170 and 171 and oligonucleotides 172 and 173, respectively (see **Supplementary Table S2** for oligonucleotide sequences and description). The resulting products were then used as templates for a third PCR with oligonucleotides 170 and 173 resulting in the fusion of both fragments and the deletion of the sequences encoding NsrR1. The fragment was cloned into pSpark (Canvax Biotech), rendering pSAM319 and its sequence was verified by sequencing (Eurofins Genomics) (see **Supplementary Table S3** for plasmids description). After digestion with BamHI at the sites provided by oligonucleotides 170 and 173, the fragment was cloned into BamHI-digested *sacB*-containing $SmSp^R$ vector pCSRO (Merino-Puerto et al., 2010), rendering pSAM325, which was transferred to *Nostoc* sp. strain PCC 7120 by conjugation (Elhai and Wolk, 1988) with selection for resistance to Sm and Sp. Cultures of the exconjugants obtained were used to select for clones resistant to 5% sucrose (Cai and Wolk, 1990), and individual sucrose resistant colonies were checked by PCR. Clones lacking the deleted region were named Δ*nsrR1*.

To establish controlled expression of NsrR1 in *Nostoc*, the *nsrR1* gene was placed under control of the *petE* promoter, which mediates Cu^{2+}-regulated transcription (Buikema and Haselkorn, 2001) and was cloned in a self-replicating plasmid. The *petE* promoter of *Nostoc* sp. PCC 7120 (genomic coordinates 278185 to 277848) was amplified with oligonucleotides 186 and 299 and fused to the *nsrR1* fragment amplified with oligonucleotides 184 and 185 by a third PCR using the two fragments as templates and oligonucleotides 184 and 299. The product was cloned into pSpark, rendering pSAM329 and its sequence was verified. After digestion with ClaI and XhoI at the sites provided by

oligonucleotides 299 and 184, the fragment was cloned into pSAM221, rendering pIAE17. pIAE17 was introduced into the Δ*nsrR1* strain by conjugation as described above.

Whole Cell Spectra

Wild type or Δ*nsrR1* cells were grown under standard conditions in the presence of NH_4^+ or subjected to nitrogen deficiency for the number of hours indicated in each case. Spectra of the different cultures where taken between 500 and 750 nm on a JASCO V-650 spectrophotometer and normalized for chlorophyll content by the absorbance at 680 nm after subtraction of absorbance at 750 nm. Absorbance at 635 nm and 680 nm were used to estimate phycocyanin and chlorophyll content, respectively.

Computing Methods

The predicted sequences of NsrR1 and its putative homologs were obtained from Brenes-Álvarez et al. (2016) and multiple sequence alignment was generated with T-Coffee (Notredame et al., 2000) at the EMBL-EBI web server (Li et al., 2015).

Target prediction of NsrR1 was performed using CopraRNA (Wright et al., 2013, 2014) with the NsrR1 homologs of *Nostoc* sp. PCC 7120, *Anabaena cylindrica* PCC 7122, *Anabaena variabilis* ATCC 29413 (recently renamed *Trichormus variabilis* NIES-23), *Cylindrospermum stagnale* PCC 7417, *Nodularia spumigena* CCY9414, '*Nostoc azollae*' 0708, *Nostoc punctiforme* PCC 73102, *Nostoc* sp. PCC 7524, *Rivularia* sp. PCC 7116, *Nostoc* sp. PCC 7107, and *Calothrix* sp. PCC 7507.

The interaction between NsrR1 and the *nblA* mRNA of diverse cyanobacteria was analyzed with IntaRNA (Mann et al., 2017).

RNA Isolation and Northern Blot Analysis

RNA samples were isolated from cells collected at different times after removing combined nitrogen from the media. Total RNA was isolated using hot phenol as described (Mohamed and Jansson, 1989) with modifications (Brenes-Álvarez et al., 2016). Northern blot hybridization was performed as previously described (Muro-Pastor et al., 1999; Steglich et al., 2008). Strand specific ^{32}P-labeled probes for Northern blot were prepared with Taq DNA polymerase using a PCR fragment (oligonucleotides 158 and 159) as template in a reaction with α-^{32}P-dCTP and one single oligonucleotide as primer (corresponding to the complementary strand of the sRNA or mRNA to be detected). Hybridization signals were quantified on a Cyclone Storage Phosphor System with Optiquant software.

Expression and Purification of NtcA and NblA Proteins, EMSA Assays, and Western Blot

To produce His-tagged NtcA protein, the *ntcA* gene was amplified using *Nostoc* DNA as template and primers 343 and 344, and the PCR product was cloned in vector pET-28a (+) (Novagen) using NcoI and XhoI, producing plasmid pSAM334 (see **Supplementary Table S3** for plasmids description). Plasmid pSAM334, containing the *ntcA* gene fused to a sequence encoding a His_6-tag under a T7 polymerase-dependent promoter, was transferred by electroporation to *E. coli* BL21-(DE3)-RIL, in which the gene encoding T7 RNA polymerase is under the control of an isopropyl-β-D-1-thiogalactopyranoside (IPTG)-regulated promoter. A 25-ml pre-inoculum of this strain was grown overnight in LB medium supplemented with chloramphenicol and kanamycin and used to inoculate 275 ml of the same medium. The culture was incubated at 37°C until OD_{600} = 0.6. Recombinant NtcA expression was induced by addition of 1 mM IPTG. After 4 h at 37°C, cells were collected and resuspended in 20 mM sodium phosphate buffer (pH 7.2) containing 500 mM NaCl, 20 mM imidazole and 1 mM phenylmethylsulfonyl fluoride (6 ml/g of cells). Cells were broken by sonication and after centrifugation at 15,000 × *g* (15 min, 4°C), the His_6-NtcA protein was purified from the supernatant by chromatography through a 1-ml HisTrap HP column (GE Healthcare), using imidazole to elute the retained proteins. Samples obtained after purification were subjected to SDS-PAGE to assess purity and 10% glycerol was added to fractions before storage at −20°C.

A similar procedure was followed for expression and purification of NblA using oligonucleotides 358 and 359 for cloning of the *nblA* gene in pET-28a (+), rendering pIAE32. In this case, an additional purification step was carried out by size-exclusion chromatography in a HiLoad 16/60 Superdex 75 column (Pharmacia) using 20 mM sodium phosphate buffer (pH 7.2) containing 150 mM NaCl. A total amount of 3.5 mg of purified protein was used in seven subcutaneous injections of a rabbit to produce antibodies in the 'Animal Production and Experimentation Center', Universidad de Sevilla (Seville, Spain). Antiserum was recovered at several times up to 5 months after the first injection and stored at −80°C until used. Antibodies specific for NblA were purified from the serum by affinity chromatography on immobilized His-tagged NblA using the AminoLink Plus® Immobilization Kit (Thermo Fisher).

Electrophoresis mobility shift assays (EMSA) were carried out as described (Muro-Pastor et al., 1999) with a 295-bp PCR fragment amplified with oligonucleotides 153 and 183 and encompassing positions −239 to +50 with respect to the TSS of *nsrR1*. A mutated version of the same DNA fragment was obtained by overlap-extension PCR using mutagenic complementary oligonucleotides 418 and 419 and flanking oligonucleotides 153 and 183.

For Western blot analysis, *E. coli* cells were resuspended in SDS-PAGE loading buffer and the proteins fractionated on 15% SDS-PAGE. Antibodies against NblA (see above), GFP (Roche) and *E. coli* GroEL (Sigma-Aldrich) were used. The ECL Plus immunoblotting system (GE Healthcare) was used to detect the different antibodies using anti-rabbit (Sigma-Aldrich) or anti-mouse (Bio-Rad) horse-radish peroxidase conjugated secondary antibodies.

Reporter Assays for *in vivo* Verification of Targets

For the experimental target verification in *E. coli*, we used the reporter system described (Urban and Vogel, 2007) and the superfolder GFP (sfGFP) plasmid pXG10-SF (Corcoran et al., 2012). The 5′-UTR of *nblA*, from the TSS at position −106 with respect to the initiation codon (coordinates 5407397)

to 60 nucleotides within the coding region, containing the predicted NsrR1 interaction sequence, was amplified from genomic DNA using primers 253 and 254. The information about the TSS was taken from Mitschke et al. (2011). The corresponding PCR product was cloned into the vector pXG-10-SF using NsiI and NheI, resulting in a translational fusion of a truncated NblA protein with sfGFP (plasmid pIAE11, **Supplementary Table S4**). For NsrR1 expression in *E. coli*, the *nsrR1* gene was amplified from genomic DNA using primers 197 (5′-phosphorylated) and 198. The PCR product was digested with XbaI and fused to a plasmid backbone that was amplified from pZE12-luc with primers PLlacOB and PLlacOD and digested with XbaI, rendering pAVN1 (**Supplementary Table S5**).

For the mutagenesis of NsrR1 and the 5′-UTR of *nblA*, plasmids like those harboring the native versions were constructed using, in addition to the above-mentioned oligonucleotides, overlapping PCR with primers containing the desired changes (**Supplementary Tables S2, S4, S5**). Positions for mutations were selected on the basis of lowered hybridization energies predicted by IntaRNA (Mann et al., 2017). For testing various combinations of both plasmids, these were introduced into *E. coli* DH5α. Plasmid pJV300 was used as a control expressing an unrelated RNA. Fluorescence measurements were done by flow cytometry or with a microplate reader (Varioskan) using liquid cultures from eight individual colonies of each combination of plasmids, as described previously (Wright et al., 2013).

In vitro Synthesis and Labeling of RNA

RNA transcripts were generated *in vitro* with MEGAscript High Yield Transcription Kit (AM1333, Ambion). The DNA templates for the transcription of NsrR1 (wild type or Mut-63 variant) and *nblA* 5′-UTR RNA (wild type and variant Comp-63) were generated by PCR with a forward primer that includes a T7 promoter sequence and three extra Gs upstream the 5′-end of the coded RNA, and a reverse primer matching the 3′ end of the RNA (**Supplementary Tables S2, S6**). The *nblA* 5′-UTR fragment extends from the TSS at position -106 to 60 nucleotides downstream the translational start. After transcription, RNAs were treated with DNase I and purified by phenol and chloroform extraction, ethanol-precipitated at −20°C, and washed with 70% ethanol.

For end labeling, 100 pmol of wild type or mutated variants of NsrR1 RNA was dephosphorylated with one unit of rAPid Alkaline Phosphatase (Roche) at 37°C for 1 h in a 20 μl reaction, followed by purification and precipitation as above. 20 pmol of dephosphorylated RNA was 5′-labeled in a 15 μl reaction with 2 μl of [γ-^{32}P] ATP (10 mCi/ml, 3,000 Ci/mmol) and 15 units of polynucleotide kinase (Thermo) for 1 h at 37°C. Unincorporated nucleotides were removed with G-25 spin columns and the labeled RNAs were purified on a denaturing 8% polyacrylamide gel. The labeled RNA was visualized with a Cyclone Storage Phosphor System and the RNA bands excised and eluted overnight at 4°C in 300 μl of 20 mM Tris-HCl (pH 7.5), 0.25 M sodium acetate, 0.25% SDS, 1 mM EDTA. The eluate was ethanol-precipitated at −20°C, washed with 70% ethanol and resuspended in water.

In vitro Structure Probing and Footprinting

0.1 pmol of labeled NsrR1 RNA was mixed in 7 μl with different amounts of unlabelled *nblA* 5′-UTR RNA, denatured for 1 min at 95°C and chilled on ice for 5 min, followed by addition of 1 μl of 1 mg/ml yeast RNA (Ambion AM7118) and 1 μl of 10x structure buffer (Ambion). The samples were incubated further for 15 min at 37°C.

For RNase treatment, 1 μl of 0.01 U/ml RNAse T1 (Ambion AM2283) or 1 μl of 0.01 U/ml RNAse A was added and the samples incubated for 15 min at room temperature. Reactions were stopped by addition of 20 μl of inactivation/precipitation buffer (Ambion) and incubation at −20°C for 15 min. The precipitate was washed with 70% ethanol and resuspended in 3–7 μl of denaturing formamide loading buffer.

Lead acetate treatment was performed by the addition of 1 μl of 25 mM lead(II) acetate (Sigma) and incubation for 1 min at 37°C. Reactions were stopped by addition of 1 μl 0.1 M EDTA and 22 μl of inactivation/precipitation buffer (Ambion) and incubation at −20°C for 15 min. The precipitate was washed with 70% ethanol and resuspended in 3–7 μl of denaturing formamide loading buffer.

Alkaline ladder was obtained by incubating 0.2 pmol of 5′-labeled RNA at 95°C for 3 min in 7.5 μl of alkaline hydrolysis buffer (Ambion) containing 1.5 μg of yeast RNA (Ambion AM7118). Reactions were stopped by the addition of 15 μl of denaturing formamide loading buffer.

RNase T1 G ladders were obtained by incubating 0.1 pmol of 5′-labeled RNA and 1 μl of 1 mg/ml yeast RNA (Ambion AM7118) in 9 μl sequencing buffer (Ambion) for 10 min at 50°C, followed by the addition of 1 μl of 0.1 U/ml RNAse T1 (Ambion AM2283) and incubation at room temperature for 15 min. Reactions were stopped by the addition of 20 μl of inactivation/precipitation buffer (Ambion) and incubation at −20°C for 15 min. The precipitate was washed with 70% ethanol and resuspended in 3–7 μl of denaturing formamide loading buffer.

All samples were run on 10% polyacrylamide, 7 M urea gels and bands visualized with a Cyclone Storage Phosphor System.

RESULTS

Identification of NsrR1 (Nitrogen Stress-Regulated RNA 1) in *Nostoc* sp. PCC 7120

A nitrogen stress-responsive TSS was identified by differential RNA-Seq at position 2050703f of the *Nostoc* sp. PCC 7120 chromosome, in the 710-bp intergenic region between two annotated open reading frames (*alr1709* and *all1710*). Transcription from this TSS is significantly repressed in the absence of combined nitrogen ($\log_2$ fold-change = −2.1) (Mitschke et al., 2011). Another RNA-Seq experiment available

for *Nostoc* sp. PCC 7120 also showed nitrogen-regulated transcription in the intergenic region between *alr1709* and *all1710* (Flaherty et al., 2011).

Furthermore, a recent approach to the global identification of phylogenetically conserved small non-coding RNAs in *Nostoc* sp. PCC 7120 (Brenes-Álvarez et al., 2016) identified a putative conserved small RNA transcribed from the TSS at position 2050703f to a predicted Rho-independent terminator that ends at position 2050814f (Ionescu et al., 2010). We named the predicted sRNA NsrR1 (nitrogen stress-repressed RNA 1), not to be confused with the previously described NsiR1 (Ionescu et al., 2010). A schematic representation of the *nsrR1* genomic region in *Nostoc* sp. PCC 7120 is shown in **Figure 1A**. Sequences putatively encoding homologs of NsrR1 were found in the genomes of heterocystous strains and two unicellular strains that are phylogenetically close to the heterocystous strains, but not in more distantly related cyanobacteria (Brenes-Álvarez et al., 2016). The alignment of the corresponding sequences allows the identification of putative Rho-independent transcriptional terminators in all cases, suggesting transcription of a phylogenetically conserved small RNA (**Figure 1B**).

To determine whether a small non-coding RNA was in fact transcribed in this region, Northern blot hybridization was performed using a strand specific DNA probe that covered the intergenic region between *alr1709* and *all1710* shown in **Figure 1A**.

Figure 2A shows expression of a small RNA of about 110 nt, consistent with RNA-Seq data and the prediction for transcriptional terminators. Upon removal of combined nitrogen, transcription was strongly repressed (90% after 9 h without nitrogen, **Supplementary Figure S1**). In the *ntcA* mutant strain repression was significantly lower at all time points (**Figure 2A** and **Supplementary Figure S1**), suggesting transcriptional repression operated by NtcA. The observation that repression, although to a lower extent, took place in the *ntcA* mutant strain suggests that NtcA is not the only component repressing *nsrR1*. Transcription of NsrR1 seemed de-repressed in the wild-type after 24 h of nitrogen stress, a situation in which heterocysts have already differentiated and atmospheric nitrogen is being fixed so that nitrogen stress is alleviated. We have also analyzed the time-course of NsrR1 transcription upon ammonium addition to cells that were stably growing with nitrate or dinitrogen as nitrogen sources. In both cases addition of ammonium led to de-repression of NsrR1 expression (**Supplementary Figure S2**). De-repression was faster upon ammonium addition to cells growing in the presence of nitrate (**Supplementary Figure S2A**) than upon ammonium addition to cells growing without a source of combined nitrogen (**Supplementary Figure S2B**).

NtcA Binds to the Promoter of NsrR1

Cyanobacterial nitrogen-responsive promoters are in many cases directly regulated by binding of the global nitrogen regulator NtcA. We have compared the promoter of NsrR1 from *Nostoc* sp. PCC 7120 with the sequences upstream from the homologs shown in **Figure 1B**. In all cases a putative

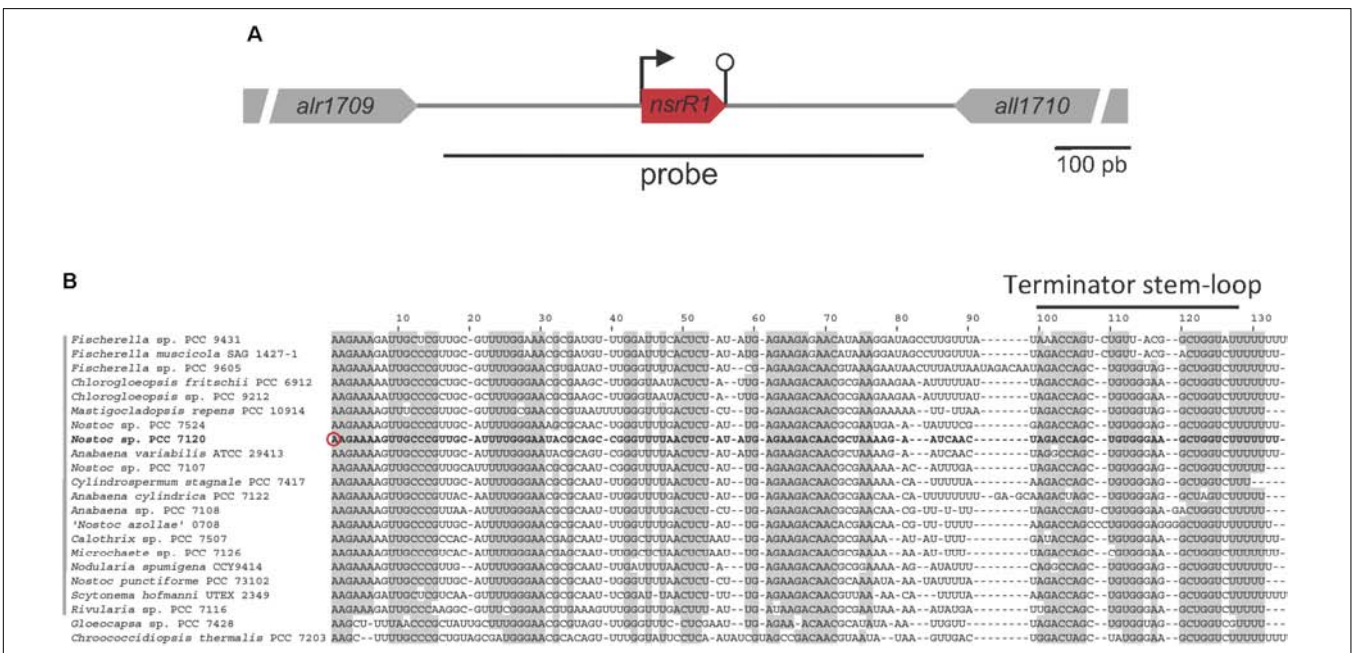

FIGURE 1 | The nitrogen-stress repressed RNA 1 (NsrR1) in cyanobacteria. **(A)** Schematic representation of the region encoding NsrR1 in *Nostoc* sp. PCC 7120. The two flanking annotated open reading frames are indicated together with the region used as a probe in Northern blots (black line under the scheme). The bent arrow represents the transcriptional start at position 2050703f, and the stem-loop represents the transcriptional terminator. **(B)** Alignment of NsrR1 homologs identified in Brenes-Álvarez et al. (2016). The sequence from *Nostoc* sp. PCC 7120 is shown in bold. The verified TSS in *Nostoc* sp. PCC 7120 (Mitschke et al., 2011) is marked with a red circle and the terminator stem-loops with a black bar. Heterocystous strains are indicated with a gray bar on the left. Shadowed nucleotides indicate more than 90% conservation of the sequence.

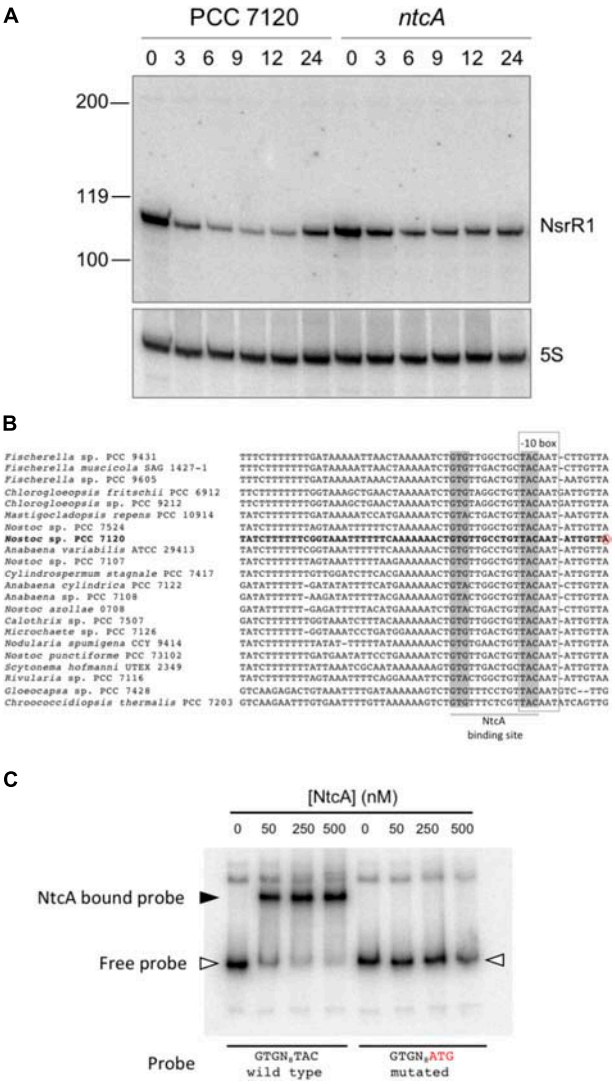

FIGURE 2 | Transcription of NsrR1 is regulated by NtcA.
(A) Nitrogen-responsive expression of NsrR1 in *Nostoc* sp. PCC 7120 and its *ntcA* mutant derivative CSE2. Expression was analyzed in cells grown in the presence of ammonium and transferred to medium containing no source of combined nitrogen (N_2) for the number of hours indicated. The upper panel shows hybridization to the NsrR1 probe. The lower panel shows hybridization to a probe for 5S RNA used as loading and transfer control. Size markers are indicated on the left. **(B)** Comparison of promoter sequences upstream of *nsrR1* homologs encoded in cyanobacterial genomes. The verified TSS in *Nostoc* sp. PCC 7120 (Mitschke et al., 2011) is marked with a red circle. Putative NtcA binding sites (highlighted in gray) and –10 boxes (framed) are indicated. **(C)** Electrophoretic mobility shift assays showing binding of purified His-tagged NtcA protein to a DNA fragment containing the wild type promoter of NsrR1 from *Nostoc* sp. PCC 7120 or a mutated version altered in the positions indicated in red. The position of retarded DNA fragments is indicated with a black triangle, whereas the free fragments are indicated with empty triangles.

NtcA binding motif ($GTRN_8TAC$) partially overlaps the −10 box (**Figure 2B**), suggesting NtcA might directly repress transcription of NsrR1 by binding to these sequences. EMSA assays were performed with purified histidine-tagged NtcA and a DNA fragment extending from −239 to +50 with respect to the TSS of NsrR1 that included the putative NtcA binding sequence. A retarded band was observed that was not detected when the NtcA binding sequence was mutated (TAC changed to ATG) (**Figure 2C**). These results demonstrate sequence-specific binding of NtcA to sequences overlapping the −10 box of the promoter region of NsrR1. These observations are compatible with direct repression of transcription from the NsrR1 promoter by NtcA, although some other mechanism must be responsible for the additional repression that is still observed in the *ntcA* mutant upon nitrogen depletion (**Figure 2A**). **Supplementary Figure S3** shows a comparison of the position of the NtcA binding site in the promoter of *nsrR1* and in three previously described NtcA-repressed promoters.

NsrR1 Interacts With *nblA* mRNA 5′-UTR

To identify possible mRNAs regulated by NsrR1, we have used the CopraRNA algorithm, that considers folding, energy of hybridization and phylogenetic conservation of the sRNA (Wright et al., 2013, 2014) (**Table 1**). Among the 20 best targets predicted by CopraRNA, *nblA* is the gene with a known function that has the highest score (p-value = 8.45×10^{-7}). NsrR1 is predicted to interact with the 5′-UTR of *nblA* mRNA (**Figure 3A**). A potential interaction between NsrR1 and the 5′-UTR of *nblA* mRNA is conserved in many cyanobacteria that contain NsrR1 (**Supplementary Figure S4**). Although the exact position in the 5′-UTR predicted to interact with NsrR1 is not conserved, in most cases it is very close or overlapping the putative Shine-Dalgarno sequence.

To verify the interaction between NsrR1 and the mRNA of *nblA*, we used a heterologous reporter assay (Corcoran et al., 2012), in which the shortest 5′-UTR of *nblA*, corresponding to transcription from position −106 (Mitschke et al., 2011) plus 60 nucleotides of the coding sequence of *nblA* were fused to the gene for sfGFP and co-expressed with NsrR1 or with a control RNA in *E. coli*. According to CopraRNA, the predicted interacting region (**Figure 3A**) was located very close to the translation initiation region of *nblA* and therefore was predicted to affect translation of the mRNA. Accumulation of GFP protein was measured in cells bearing different combinations of plasmids. Cells carrying the *nblA*::sf*gfp* translational fusion showed significant GFP fluorescence, as well as GFP protein determined by Western blot (**Figure 3B**), demonstrating that the translation initiation region of *nblA* was functional in *E. coli*. The GFP fluorescence of cells bearing the *nblA*::sf*gfp* fusion (and the amount of GFP protein) decreased to about 50% of the control when NsrR1 was co-expressed, indicating a direct interaction between NsrR1 and the 5′-UTR of *nblA*, which affects translation (**Figures 3B,C**). To verify the interaction at the predicted site, two different point mutations were introduced in NsrR1 in the middle of the predicted helix between NsrR1 and the 5′-UTR of *nblA* (nucleotide 63, C to G; nucleotide 66, C to G). Compensatory mutations were introduced in the corresponding positions of the 5′-UTR of *nblA* (nucleotide 89, G to C; nucleotide

TABLE 1 | CopraRNA prediction of candidate mRNAs that interact with NsrR1.

fdr	*p*-value	Locus tag	Annotation
2.63×10^{-05}	6.11×10^{-09}	*all1871*	Unknown
1.58×10^{-03}	**8.45×10^{-07}**	***asr4517***	***nblA***
1.58×10^{-03}	1.10×10^{-06}	*all1043*	Hypothetical protein
7.46×10^{-02}	9.11×10^{-05}	*all7229*	Unknown
7.46×10^{-02}	1.04×10^{-04}	*asr2666*	Hypothetical protein
9.92×10^{-02}	1.61×10^{-04}	*alr3099*	GCN5-related *N*-acetyltransferase
9.97×10^{-02}	1.85×10^{-04}	*all4613*	Acetohydroxy acid synthase; *IlvG*
0.110	2.63×10^{-04}	*alr4291*	Photosystem II CP43 protein
0.110	2.92×10^{-04}	*alr5103*	LL-Diaminopimelate aminotransferase apoenzyme
0.110	3.04×10^{-04}	*alr2079*	Cl- channel, voltage gated
0.110	3.05×10^{-04}	*alr3594*	Response regulator receiver domain protein (*CheY*)
0.136	4.40×10^{-04}	*alr4814*	Hypothetical protein
0.136	4.51×10^{-04}	*all3970*	Endonuclease III
0.136	4.75×10^{-04}	*all3794*	Tryptophan synthase beta subunit
0.141	5.23×10^{-04}	*all0330*	GAF sensor signal transduction histidine kinase
0.162	6.40×10^{-04}	*all7229*	Unknown
0.165	6.92×10^{-04}	*all1228*	Hypothetical protein
0.165	7.26×10^{-04}	*alr0309*	Hypothetical protein
0.305	1.43×10^{-03}	*alr4953*	Hypothetical protein
0.305	1.49×10^{-03}	*alr4696*	Class I peptide chain release factor

CopraRNA (Wright et al., 2013, 2014) was implemented at the Freiburg RNA Tools Server with default options. NsrR1 from Nostoc sp. PCC 7120 was used as reference together with the NsrR1 sequences from Anabaena cylindrica PCC 7122, Anabaena variabilis ATCC 29413 (recently renamed Trichormus variabilis NIES-23), Cylindrospermum stagnale PCC 7417, Nodularia spumigena CCY9414, 'Nostoc azollae' 0708, Nostoc punctiforme PCC 73102, Nostoc sp. PCC 7524, Rivularia sp. PCC 7116, Nostoc sp. PCC 7107, and Calothrix sp. PCC 7507. The nblA gene studied in this work is shown in bold. Only the 20 genes with the highest scores are shown.

86, G to C). Mutation of either one of those nucleotides in NsrR1 drastically reduced the interaction between NsrR1 and the 5′-UTR of *nblA*, as suggested by the absence of fluorescence reduction with respect to control (**Figures 3C,D**). When the mutated version of the sRNA was combined with the mutated version of the mRNA containing the compensatory change, base pairing was restored and again a significant fluorescence reduction was observed. These data support a direct interaction of NsrR1 with the 5′-UTR of the *nblA* mRNA and its effect on translation of NblA.

In addition, we have studied the interaction between NsrR1 and the *nblA* mRNA by *in vitro* footprinting analysis. ^{32}P-labeled NsrR1 was incubated with unlabeled *nblA* mRNA (a fragment extending from positions −106 to +60 with respect to the start of the coding sequence) and probed with RNase T1 (**Figure 4A**) or lead(II) acetate (**Figure 4B**). When wild type NsrR1 RNA and *nblA* mRNA were used, a footprint was detected between positions 58 and 67 of NsrR1, in agreement with the bioinformatic prediction (**Figure 3A**). This footprint was not observed with the mutant version of *nblA* mRNA (Comp-63). However, when the mutant version of NsrR1 RNA (Mut-63) was used, only the mutant *nblA* mRNA (Comp-63) generated a footprint, but not the wild type *nblA* mRNA. These *in vitro* results are therefore in agreement with the *in vivo* results obtained in *E. coli* with the GFP fusion analysis.

We have also performed *in vitro* structure probing analysis of NsrR1 (**Supplementary Figure S5**). The NsrR1 region involved in interaction with *nblA* mRNA is predicted to be single stranded, according to the pattern of sensitivity to RNase T1, RNase A, and lead(II) acetate (**Figure 4** and **Supplementary Figure S5**).

nblA Expression Is Reduced by NsrR1 in *Nostoc* sp. PCC 7120

Transcription of NsrR1 is only partially (and transiently) repressed upon nitrogen step down. Therefore, to study *in vivo* in *Nostoc* the possible effect of NsrR1 on *nblA* expression, we have generated a mutant strain lacking NsrR1 (Δ*nsrR1*) by deleting the DNA region containing *nsrR1* through homologous recombination. Cells lacking NsrR1 have no apparent phenotype under normal growth conditions. Furthermore, there is no growth difference with respect to wild-type cells in medium containing nitrate, ammonia, or lacking a nitrogen source (**Supplementary Figure S6**). A complemented strain (Δ*nsrR1* + P_{petE}::*nsrR1*) in which NsrR1 expression is under control of the Cu^{2+}-inducible *petE* promoter (Buikema and Haselkorn, 2001) was generated, releasing NsrR1 expression from nitrogen control and allowing Cu^{2+}-controlled expression instead.

nblA is transcribed from five TSS, three of them induced in response to nitrogen deprivation (Mitschke et al., 2011) (see a scheme in **Figure 5A**). Northern blot hybridization confirmed the NtcA dependent induction of transcription from three of the *nblA* promoters (**Figure 5B**). We have compared *nblA* expression between the Δ*nsrR1* and the Δ*nsrR1* + P_{petE}::*nsrR1* strains during several hours after nitrogen step down (so

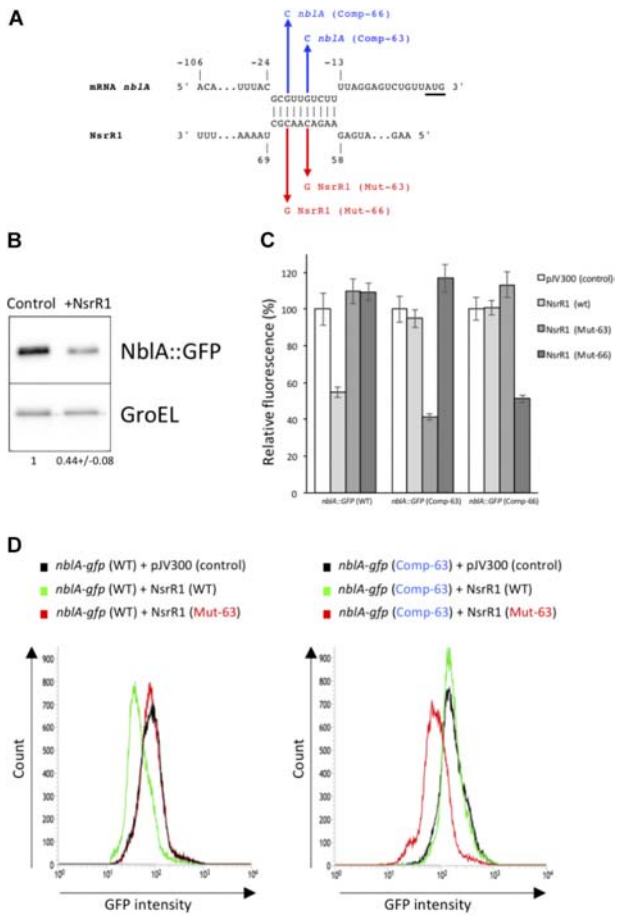

FIGURE 3 | Verification of NsrR1 interaction with the 5′-UTR of *nblA* using an *in vivo* reporter system. **(A)** Predicted interaction between NsrR1 and the 5′-UTR of *nblA* according to CopraRNA (Wright et al., 2013, 2014). *nblA* nucleotides are numbered with respect to the start of the coding sequence (AUG codon is underlined). Mutations introduced in NsrR1 at position 63 (C to G, Mut-63) or 66 (C to G, Mut-66) and the corresponding compensatory mutations in *nblA* 5′-UTR position –18 (G to C, Comp-63) or –21 (G to C, Comp-66) are indicated in red and blue, respectively. **(B)** Accumulation of GFP protein in *E. coli* DH5α cultures bearing an *nblA*::sf*gfp* fusion combined with plasmid pJV300 (encoding a control RNA) or a plasmid encoding NsrR1. Western blots were carried out using antibodies against GFP or GroEL. Numbers at the bottom of the image indicate relative GFP levels with respect to control after normalization with GroEL (average of two experiments). **(C)** Fluorescence measurements of *E. coli* DH5α cultures with various combinations of plasmids expressing different versions of NsrR1 or *nblA*::sf*gfp* fusions. Plasmid pJV300 (encoding a control RNA) was used as control. The data are presented as the mean ± standard deviation of cultures from eight independent colonies after subtraction of fluorescence in cells bearing pXG-0. **(D)** FACS-based reporter assays. *E. coli* DH5α cells carrying combinations of plasmids bearing wild-type and mutated version Mut-63 of NsrR1 and wild type or mutated version Comp-63 of *nblA*::sf*gfp* were grown to stationary phase and subjected to flow cytometry analysis. Data were acquired on 50,000 cells per sample.

that transcription of *nblA* is induced) and Cu^{2+} addition (to induce transcription of NsrR1 from the *petE* promoter in strain Δ*nsrR1* + P_{petE}::*nsrR1*) (**Figure 5C**). Under these conditions transcription of all three N-regulated *nblA* transcripts was induced in the Δ*nsrR1* strain in response to nitrogen deficiency. However, accumulation of the three transcripts was strongly reduced in the strain that produced NsrR1 from the *petE* promoter (**Figure 5C**). After 8 h in the absence on combined nitrogen the amount of *nblA* mRNA (adding all three transcripts together) in the Δ*nsrR1* strain is about fourfold higher than in the Δ*nsrR1* + P_{petE}::*nsrR1* strain (**Supplementary Figure S7**), indicating that NsrR1 has a significant negative effect on the accumulation of *nblA* mRNA in *Nostoc*.

To analyze the accumulation of NblA protein in the different strains, we have generated antibodies against recombinant purified *Nostoc* NblA protein. Unfortunately, although these antibodies could detect NblA in Western blots of extracts from *E. coli* cells overproducing NblA (**Supplementary Figure S8**), they were, however, unable to detect NblA in extracts of *Nostoc* under conditions of full induction of *nblA* expression. Similarly, a histidine-tagged version of NblA could not be detected in *Nostoc* using commercial anti-His antibodies. Lack of detection of NblA with either antibodies could likely be due to the presence of very low levels of NblA in cyanobacterial cells. In fact, it has been suggested that NblA is itself degraded by the cellular degradation machinery (Baier et al., 2014; Sendersky et al., 2014).

To assess possible effects of the Δ*nsrR1* mutation on pigment content, whole cell spectra were taken of cells growing in the presence of NH_4^+ or 24 and 48 h after removal of combined nitrogen. Δ*nsrR1* mutant cells have lower phycocyanin content in all cases, even in the presence of NH_4^+ (**Figure 6**). Phycocyanin content was further reduced in both strains by nitrogen starvation but while in the wild type strain it is similar at 24 and 48 h, in the Δ*nsrR1* mutant strain the reduction is stronger at 48 h than at 24 h (**Figure 6B**).

DISCUSSION

Small regulatory RNAs are important players in the operation of regulatory effects exerted by classical transcription factors. In *E. coli*, every major transcription factor regulates transcription of one or several regulatory RNAs that, in turn, operate post-transcriptional regulation. FNR and CRP, the best studied members of the CRP/FNR family, are known to regulate the expression of several small regulatory RNAs, including CRP-induced CyaR (Papenfort et al., 2008; De Lay and Gottesman, 2009), CRP-repressed Spot 42 (Beisel and Storz, 2011) or FNR-induced FnrS (Durand and Storz, 2010), all of them contributing to the regulatory effects exerted by these two transcriptional regulators.

In response to nitrogen deficiency, expression of many cyanobacterial genes is regulated, either positively or negatively, by the global nitrogen regulator NtcA, a CRP-family regulator. In many cases the mechanism underlying such regulation seems to be direct activation or repression of gene expression, as deduced from the presence of consensus NtcA binding sites in the respective promoters. However, in cases where no obvious sequence elements can be identified as responsible for the observed regulation, the mechanism is assumed to be indirect. Transcriptomic analyses identifying NtcA-regulated

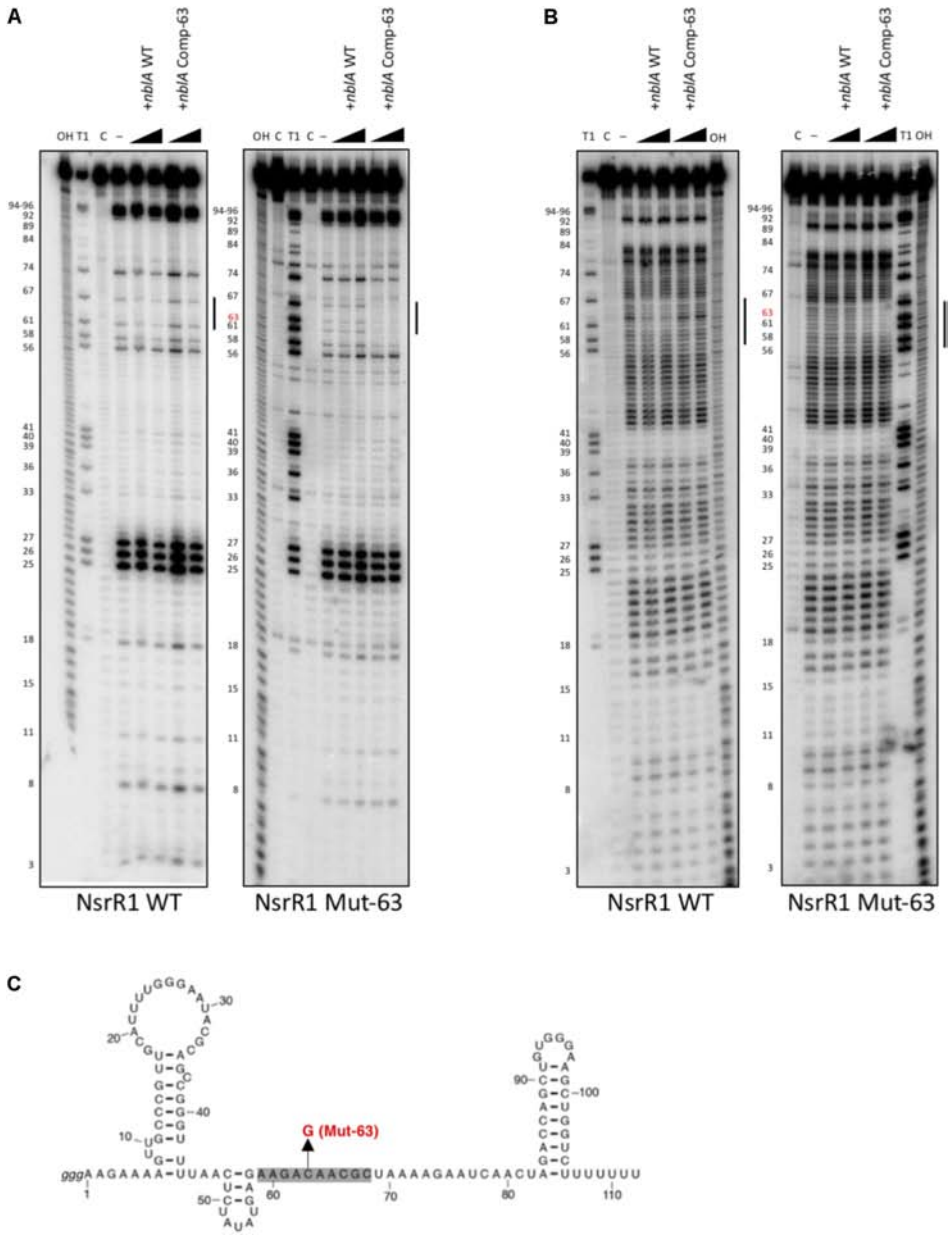

FIGURE 4 | *In vitro* footprinting assay of the NsrR1/*nblA* 5′-UTR interaction. **(A)** RNase T1 footprinting of the interaction between wild type NsrR1 (left) or mutant C63G (Mut-63, right) with wild type and compensatory mutant (Comp-63) of the *nblA* 5′-UTR. **(B)** Pb(II) footprinting of the interaction between wild type NsrR1 (left) or mutant C63G (right) with wild type and compensatory mutant (Comp-63) of the *nblA* 5′-UTR. Two concentrations of *nblA* RNA were used (100 and 200 nM). The protected area is indicated by vertical bars in **(A,B)**. NsrR1 was 5′ end-labeled. C, untreated control; OH, alkaline ladder; T1, RNase T1 ladder. Nucleotide positions of NsrR1 are shown on the left. **(C)** Secondary structure model of NsrR1 from *Nostoc* sp. PCC 7120 based on structure probing (**Supplementary Figure S5**). The area protected by *nblA* RNA is shaded. The nucleotide changed in Mut-63 is also indicated.

non-coding RNAs suggest this type of molecules might also be involved in NtcA-mediated post-transcriptional regulation (Mitschke et al., 2011; Brenes-Álvarez et al., 2016). A feed-forward coherent regulatory loop involving NtcA and a nitrogen-regulated sRNA has been recently described in *Synechocystis* sp. PCC 6803. In this unicellular strain NtcA operates transcriptional regulation of the genes encoding glutamine synthetase and its inactivating factors IF7 and IF17, and also regulates transcription of NsiR4 (nitrogen stress inducible RNA 4), that modulates translation of IF7 (Klähn et al., 2015). A similar loop has been described for RpaB, that operates direct transcriptional regulation of several genes encoding proteins of the photosystem I and of PsrR1 (photosynthesis regulatory RNA 1), a high light-responsive small RNA that post-transcriptionally regulates translation of some of those photosystem I-related proteins (Georg et al., 2014). These regulatory loops, like the case of

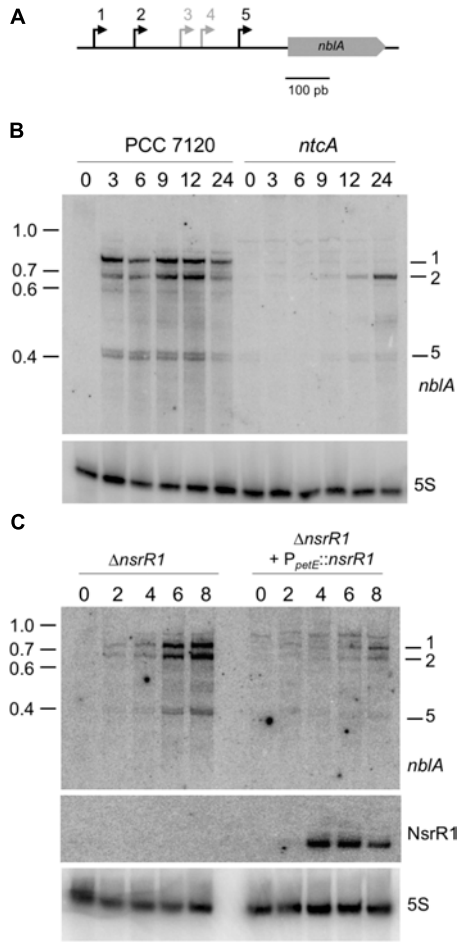

FIGURE 5 | Nitrogen-regulated transcripts of *nblA* and their regulation by NsrR1 in *Nostoc* sp. PCC 7120. **(A)** Schematic representation of the five transcriptional start sites (bent arrows) previously defined for *nblA* (Mitschke et al., 2011), with the nitrogen-regulated transcriptional starts (1, 2, and 5) indicated in black. **(B)** Identification by Northern hybridization of the transcripts originated from nitrogen-regulated transcriptional starts in *Nostoc* sp. PCC 7120 and its *ntcA* mutant derivative CSE2. Expression was analyzed in cells grown in the presence of ammonium and transferred to medium containing no source of combined nitrogen for the number of hours indicated. The upper panel shows hybridization to the *nblA* probe. The lower panel shows hybridization to a probe for 5S RNA used as loading and transfer control. Size markers (kb) are indicated on the left. Transcripts corresponding to TSS 1, 2, and 5 are indicated. **(C)** Nitrogen-regulated expression of *nblA* in strains with altered levels of NsrR1. Expression was analyzed in a mutant strain lacking NsrR1 (Δ*nsrR1*) and in the same strain complemented with a plasmid bearing *nsrR1* under control of the Cu^{2+}-regulated promoter of the *petE* gene. Cells were grown in the presence of ammonium in medium lacking Cu^{2+} (to prevent expression of the *petE* promoter) and transferred to medium containing no source of combined nitrogen and 1.5 μM Cu^{2+} for the number of hours indicated. The upper panel shows hybridization to the *nblA* probe. The middle panel shows hybridization to the probe for NsrR1 indicated in **Figure 1A**. The lower panel shows hybridization to a probe for 5S RNA used as loading and transfer control.

PmgR1 (photomixotrophic growth RNA 1), a sRNA that acts downstream of PmgA and is involved in regulation of glycogen accumulation (de Porcellinis et al., 2016), point to a relevant role of small regulatory RNAs in the regulation of cyanobacterial metabolism.

Here, we describe NsrR1, a small RNA whose transcription is regulated in response to nitrogen limitation in *Nostoc* sp. PCC 7120. Repression of NsrR1 transcription is at least partially operated by NtcA, as deduced from Northern analysis in the *ntcA* mutant and binding assays with purified NtcA protein (**Figure 2**). The observation that repression by NtcA is only partial suggests participation of some other regulator(s) integrating different signal(s). In this context, expression of NsrR1 might be additionally regulated by another repressor, perhaps in the CRP family. Conservation of a T immediately upstream of the $GTN_{10}AC$ conserved NtcA binding sequence suggests possible binding of an unidentified CRP-like regulator (Forcada-Nadal et al., 2014). In contrast to the wide distribution observed for some cyanobacterial sRNAs such as Yfr1 (Voss et al., 2007; Brenes-Álvarez et al., 2016), NsrR1 homologs are only found in the genomes from heterocystous cyanobacteria (and closely related unicellular strains), suggesting its possible function might be specifically related to some particular metabolic trait in this group of organisms.

Phycobilisomes account for a large amount of the total protein, and therefore nitrogen, in cyanobacterial cells. In unicellular cyanobacteria unable to fix N_2, recycling of phycobiliproteins as a source of amino acids is an adaptive response to lack of available combined nitrogen, prior to cessation of growth. In heterocystous cyanobacteria, that are ultimately able to overcome nitrogen deficiency by nitrogen fixation, transcription of *nblA* is induced as a transient response to nitrogen deprivation but the extension of PBS degradation is much lower than in unicellular strains (Maldener et al., 1991; Baier et al., 2004). Using an *in vivo* reporter system established in *E. coli* we demonstrate a direct interaction between NsrR1 and the 5′-UTR of *nblA*, leading to reduced expression of an NblA::sfGFP fusion in the presence of NsrR1. Unfortunately, we have not succeeded in detecting the NblA protein in extracts from *Nostoc* sp. PCC 7120, and therefore cannot assess directly the effects of NsrR1 overexpression on NblA accumulation at the protein level. Antibodies generated and purified against NblA from *Nostoc* sp. PCC 7120 detected NblA when expressed in *E. coli* (**Supplementary Figure S8**) but not in cyanobacterial extracts, probably because of limited amount of NblA in these cells.

We have also demonstrated reduced accumulation of *nblA* transcripts in strains of *Nostoc* sp. PCC 7120 that over-express NsrR1 (**Figure 5** and **Supplementary Figure S7**), which can be a consequence of the interaction of these two RNA molecules leading to reduced translation of NblA. Interaction of NsrR1 at the predicted region in the 5′-UTR of *nblA* has been verified by *in vitro* footprinting experiments (**Figure 4**). The predicted region targeted is located close to the translation initiation and is therefore common to all five possible *nblA* 5′-UTRs. Thus, although transcriptional regulation of *nblA* might be operated by different regulators integrating different signals, all possible transcripts would be susceptible to additional post-transcriptional regulation by NsrR1 and therefore the accumulation of NblA protein would be ultimately under

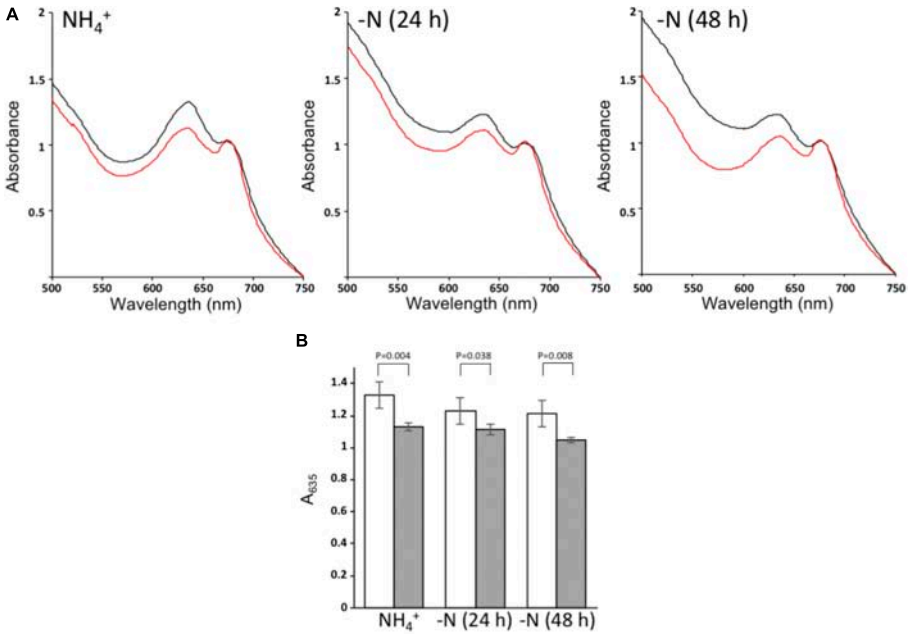

FIGURE 6 | Whole cell absorption spectra. **(A)** Absorption spectra of wild type cells (black) or Δ*nsrR1* cells (red) growing in the presence of NH_4^+ (left) or after 24 h (center) or 48 h (right) of nitrogen depletion, normalized by the chlorophyll content (A_{680}). **(B)** Normalized A_{635} of cultures from wild type cells (white) or Δ*nsrR1* cells (gray) growing in the presence of NH_4^+, or after 24 h or 48 h of nitrogen depletion. Error bars represent the standard error of four experiments. *p*-values (unpaired *t*-test) are indicated for the comparison of wild type and Δ*nsrR1* cells at each time point.

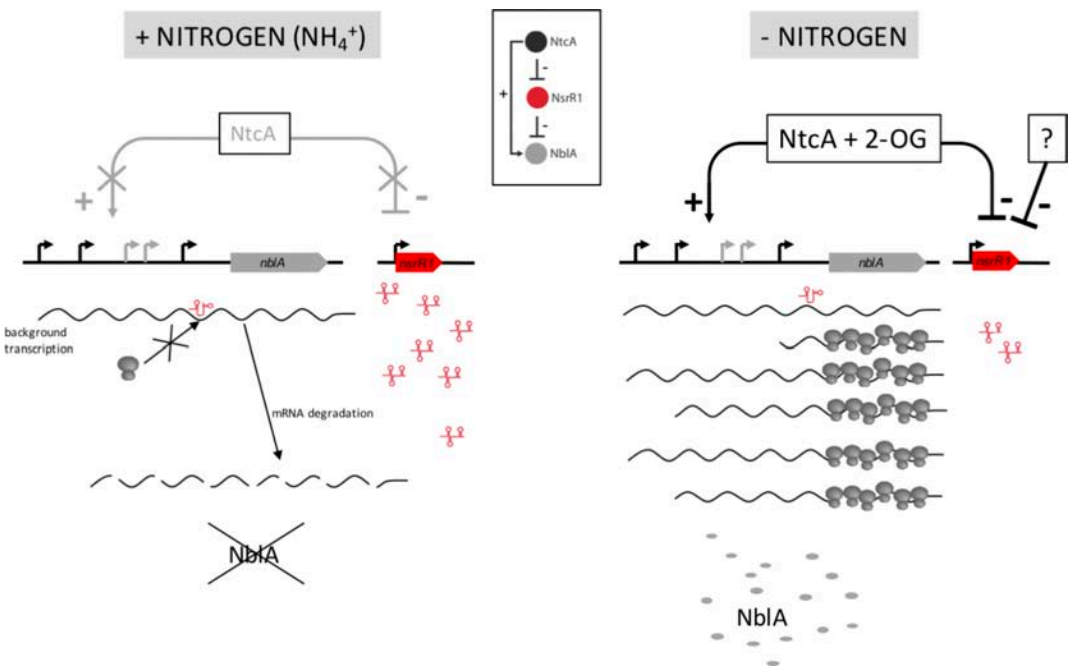

FIGURE 7 | Model for the function of NsrR1 in *nblA* regulation. Under nitrogen sufficient conditions **(Left)** intracellular 2-oxoglutarate (2-OG) concentration is low and NtcA cannot activate transcription of *nblA*, while NsrR1 is expressed at high levels. Therefore, under these conditions NsrR1 is in excess of any small amount of *nblA* mRNA that could be present due to background transcription. Binding of NsrR1 to the mRNA blocks translation, resulting in degradation of the mRNA and preventing any production of NblA protein under nitrogen sufficient conditions. When the nitrogen source is removed **(Right)** 2-OG concentration increases and NtcA can activate transcription of *nblA*, while *nsrR1* is partially repressed. As a result, there is not enough NsrR1 RNA to repress translation of an excess of *nblA* transcripts and NblA protein can accumulate. Inset: Scheme of a type 4 feed-forward loop (Nitzan et al., 2017) as applied to the NtcA-NsrR1-NblA regulatory circuit.

control of nitrogen limitation. The reduced accumulation of *nblA* mRNAs in the presence of NsrR1 can be attributed to destabilization of the mRNA when translation is inhibited. A more direct mechanistic effect of NsrR1 on mRNA stability, recruitment of a ribonuclease for instance, cannot be excluded.

The presence of NsrR1 in ammonium growing cells would suppress transcriptional noise due to leaky transcription initiation of *nblA*, reducing background production of NblA that would have undesirable consequences on phycobilisome stability. In fact, RNA-Seq and primer extension assays (Mitschke et al., 2011) indicate above-background transcription of *nblA* from promoters 2, 4, and 5 in ammonium growing cells, that is not readily detectable in the less sensitive Northern blot experiments (**Figure 5**). Another protein directly involved in PBS degradation, NblB, has been shown to be present under nitrogen sufficient conditions in *Synechococcus elongatus* (Levi et al., 2018). The RNA-Seq data available for *Nostoc* sp. PCC 7120 (Flaherty et al., 2011; Mitschke et al., 2011) suggest that in this organism *nblB* is also expressed constitutively. Therefore, it would be of utmost importance to avoid any background accumulation of NblA under nitrogen sufficient conditions that, together with NblB, would compromise PBS stability. In addition, the presence of NsrR1 would lead to a delay in NblA production after NtcA induction of *nblA* transcription due to a threshold effect (Levine and Hwa, 2008), creating a delay in the onset of phycobilisome degradation and providing stability by avoiding an inappropriate response under fluctuating environmental conditions. Controlled degradation of PBS, although not essential for adaptation to transient nitrogen deficiency in N_2-fixing strains, might be an advantage in natural environments subjected to changes in different factors such as light intensity or availability of other nutrients.

The changes detected in pigment content between wild type and Δ*nsrR1* mutant cells agree with the proposed repression of NblA accumulation by NsrR1, and with our model of regulation (**Figure 7**). We speculate that the slightly, but significant, lower phycobilin/chlorophyll ratio of the Δ*nsrR1* mutant compared with wild type (**Figure 6B**) when growing in the presence of NH_4^+ is due to background expression of *nblA* in the absence of NsrR1, resulting in reduced phycobilin stability. After 48 h of nitrogen depletion heterocysts are fully functional and nitrogen status should be more similar to NH_4^+ growing cells. In fact, in wild type cells the phycocyanin/chlorophyll ratio is stabilized while in the Δ*nsrR1* it drops further, suggesting extended presence of NblA in the absence of NsrR1.

The regulatory circuit we propose (**Figure 7**) represents a type 4 coherent feed-forward loop (Alon, 2007; Nitzan et al., 2017). This type of loop, in which a transcription factor is the top regulator, provides a delayed increase in the level of the target protein (NblA in this case) when the transcription factor (NtcA in this case) is activated, and an accelerated decrease in target protein level when the transcription factor is deactivated (Beisel and Storz, 2011). Dual regulation at the transcriptional and post-transcriptional levels should provide strict control of the levels of the NblA proteolytic adaptor. In addition, because the top regulator (NtcA) is itself subjected to differential accumulation in heterocysts (Olmedo-Verd et al., 2006; Sandh et al., 2014), the feed-forward loop is likely reinforced in heterocysts *vs.* vegetative cells. Higher amounts of NtcA in heterocysts could promote stronger transcription of *nblA*. The combination of increased transcription of *nblA* with low levels of NsrR1 (affecting its translation) would lead to increased amounts of NblA protein producing faster PBS degradation specifically in developing heterocysts.

AUTHOR CONTRIBUTIONS

IÁ-E contributed to the acquisition, analysis, or interpretation of the data. AM-P and AV contributed to the acquisition, analysis, interpretation of the data, and writing of the manuscript.

FUNDING

This work was supported by grants BFU2013-48282-C2-1-P from Ministerio de Economía y Competitividad, and BFU2016-74943-C2-1-P from Agencia Estatal de Investigación (AEI), Ministerio de Economía, Industria y Competitividad, both co-financed by FEDER. IÁ-E is the recipient of a predoctoral contract from Ministerio de Economía y Competitividad, Spain (BES-2014-068488).

ACKNOWLEDGMENTS

We thank M. Isabel Muro-Pastor (IBVF-CSIC) for help with protein purification, Jörg Vogel (University of Würzburg) for providing plasmids for the analysis of interactions in *E. coli*, and Alicia Orea (IBVF-CSIC) for technical assistance with flow cytometry.

SUPPLEMENTARY MATERIAL

The Supplementary Material for this article can be found online at: https://www.frontiersin.org/articles/10.3389/fmicb.2018.02267/full#supplementary-material

REFERENCES

Alon, U. (2007). Network motifs: theory and experimental approaches. *Nat. Rev. Genet.* 8, 450–461. doi: 10.1038/nrg2102

Baier, A., Winkler, W., Korte, T., Lockau, W., and Karradt, A. (2014). Degradation of phycobilisomes in *Synechocystis* sp. PCC6803: evidence for essential formation of an NblA1/NblA2 heterodimer and its codegradation by A Clp protease complex. *J. Biol. Chem.* 289, 11755–11766. doi: 10.1074/jbc.M113.520601

Baier, K., Lehmann, H., Stephan, D. P., and Lockau, W. (2004). NblA is essential for phycobilisome degradation in *Anabaena* sp. strain PCC 7120 but not for development of functional heterocysts. *Microbiology* 150, 2739–2749. doi: 10.1099/mic.0.27153-0

Beisel, C. L., and Storz, G. (2011). The base-pairing RNA spot 42 participates in a multioutput feedforward loop to help enact catabolite repression in *Escherichia coli*. *Mol. Cell* 41, 286–297. doi: 10.1016/j.molcel.2010.12.027

Brenes-Álvarez, M., Olmedo-Verd, E., Vioque, A., and Muro-Pastor, A. M. (2016). Identification of conserved and potentially regulatory small RNAs in heterocystous cyanobacteria. *Front. Microbiol.* 7:48. doi: 10.3389/fmicb.2016.00048

Buikema, W. J., and Haselkorn, R. (2001). Expression of the *Anabaena hetR* gene from a copper-regulated promoter leads to heterocyst differentiation under repressing conditions. *Proc. Natl. Acad. Sci. U.S.A.* 98, 2729–2734. doi: 10.1073/pnas.051624898

Cai, Y. P., and Wolk, C. P. (1990). Use of a conditionally lethal gene in *Anabaena* sp. strain PCC 7120 to select for double recombinants and to entrap insertion sequences. *J. Bacteriol.* 172, 3138–3145. doi: 10.1128/jb.172.6.3138-3145.1990

Collier, J. L., and Grossman, A. R. (1994). A small polypeptide triggers complete degradation of light-harvesting phycobiliproteins in nutrient-deprived cyanobacteria. *EMBO J.* 13, 1039–1047. doi: 10.1002/j.1460-2075.1994.tb06352.x

Corcoran, C. P., Podkaminski, D., Papenfort, K., Urban, J. H., Hinton, J. C., and Vogel, J. (2012). Superfolder GFP reporters validate diverse new mRNA targets of the classic porin regulator, MicF RNA. *Mol. Microbiol.* 84, 428–445. doi: 10.1111/j.1365-2958.2012.08031.x

De Lay, N., and Gottesman, S. (2009). The crp-activated small noncoding regulatory RNA CyaR (RyeE) links nutritional status to group behavior. *J. Bacteriol.* 191, 461–476. doi: 10.1128/JB.01157-08

de Porcellinis, A. J., Klahn, S., Rosgaard, L., Kirsch, R., Gutekunst, K., Georg, J., et al. (2016). The non-coding RNA Ncr0700/PmgR1 is required for photomixotrophic growth and the regulation of glycogen accumulation in the cyanobacterium *Synechocystis* sp. PCC 6803. *Plant. Cell Physiol.* 57, 2091–2103. doi: 10.1093/pcp/pcw128

Durand, S., and Storz, G. (2010). Reprogramming of anaerobic metabolism by the FnrS small RNA. *Mol. Microbiol.* 75, 1215–1231. doi: 10.1111/j.1365-2958.2010.07044.x

Elhai, J., and Wolk, C. P. (1988). Conjugal transfer of DNA to cyanobacteria. *Methods Enzymol.* 167, 747–754. doi: 10.1016/0076-6879(88)67086-8

Flaherty, B. L., Van Nieuwerburgh, F., Head, S. R., and Golden, J. W. (2011). Directional RNA deep sequencing sheds new light on the transcriptional response of *Anabaena* sp. strain PCC 7120 to combined-nitrogen deprivation. *BMC Genomics* 12:332. doi: 10.1186/1471-2164-12-332

Forcada-Nadal, A., Forchhammer, K., and Rubio, V. (2014). SPR analysis of promoter binding of *Synechocystis* PCC6803 transcription factors NtcA and CRP suggests cross-talk and sheds light on regulation by effector molecules. *FEBS Lett.* 588, 2270–2276. doi: 10.1016/j.febslet.2014.05.010

Georg, J., Dienst, D., Schurgers, N., Wallner, T., Kopp, D., Stazic, D., et al. (2014). The small regulatory RNA SyR1/PsrR1 controls photosynthetic functions in cyanobacteria. *Plant Cell* 26, 3661–3679. doi: 10.1105/tpc.114.129767

Giner-Lamia, J., Robles-Rengel, R., Hernández-Prieto, M. A., Muro-Pastor, M. I., Florencio, F. J., and Futschik, M. E. (2017). Identification of the direct regulon of NtcA during early acclimation to nitrogen starvation in the cyanobacterium *Synechocystis* sp. PCC 6803. *Nucleic Acids Res.* 45, 11800–11820. doi: 10.1093/nar/gkx860

González, A., Bes, M. T., Peleato, M. L., and Fillat, M. F. (2016). Expanding the role of FurA as essential global regulator in cyanobacteria. *PLoS One* 11:e0151384. doi: 10.1371/journal.pone.0151384

Grossman, A. R., Schaefer, M. R., Chiang, G. G., and Collier, J. L. (1993a). Environmental effects on the light-harvesting complex of cyanobacteria. *J. Bacteriol.* 175, 575–582. doi: 10.1128/jb.175.3.575-582.1993

Grossman, A. R., Schaefer, M. R., Chiang, G. G., and Collier, J. L. (1993b). The phycobilisome, a light-harvesting complex responsive to environmental conditions. *Microbiol. Rev.* 57, 725–749.

Herrero, A., Muro-Pastor, A. M., and Flores, E. (2001). Nitrogen control in cyanobacteria. *J. Bacteriol.* 183, 411–425. doi: 10.1128/JB.183.2.411-425.2001

Ionescu, D., Voss, B., Oren, A., Hess, W. R., and Muro-Pastor, A. M. (2010). Heterocyst-specific transcription of NsiR1, a non-coding RNA encoded in a tandem array of direct repeats in cyanobacteria. *J. Mol. Biol.* 398, 177–188. doi: 10.1016/j.jmb.2010.03.010

Karradt, A., Sobanski, J., Mattow, J., Lockau, W., and Baier, K. (2008). NblA, a key protein of phycobilisome degradation, interacts with ClpC, a HSP100 chaperone partner of a cyanobacterial Clp protease. *J. Biol. Chem.* 283, 32394–32403. doi: 10.1074/jbc.M805823200

Klähn, S., Schaal, C., Georg, J., Baumgartner, D., Knippen, G., Hagemann, M., et al. (2015). The sRNA NsiR4 is involved in nitrogen assimilation control in cyanobacteria by targeting glutamine synthetase inactivating factor IF7. *Proc. Natl. Acad. Sci. U.S.A.* 112, E6243–E6252. doi: 10.1073/pnas.1508412112

Levi, M., Sendersky, E., and Schwarz, R. (2018). Decomposition of cyanobacterial light harvesting complexes: NblA-dependent role of the bilin-lyase homolog NblB. *Plant J.* 94, 813–821. doi: 10.1111/tpj.13896

Levine, E., and Hwa, T. (2008). Small RNAs establish gene expression thresholds. *Curr. Opin. Microbiol.* 11, 574–579. doi: 10.1016/j.mib.2008.09.016

Li, W., Cowley, A., Uludag, M., Gur, T., McWilliam, H., Squizzato, S., et al. (2015). The EMBL-EBI bioinformatics web and programmatic tools framework. *Nucleic Acids Res.* 43, W580–W584. doi: 10.1093/nar/gkv279

Luque, I., Flores, E., and Herrero, A. (1994). Molecular mechanism for the operation of nitrogen control in cyanobacteria. *EMBO J.* 13, 2862–2869. doi: 10.1002/j.1460-2075.1994.tb06580.x

Luque, I., Zabulon, G., Contreras, A., and Houmard, J. (2001). Convergence of two global transcriptional regulators on nitrogen induction of the stress-acclimation gene nblA in the cyanobacterium *Synechococcus* sp. PCC 7942. *Mol. Microbiol.* 41, 937–947.

Maldener, I., Lockau, W., Cai, Y., and Wolk, C. P. (1991). Calcium-dependent protease of the cyanobacterium *Anabaena*: molecular cloning and expression of the gene in *Escherichia coli*, sequencing and site-directed mutagenesis. *Mol. Gen. Genet.* 225, 113–120. doi: 10.1007/BF00282649

Mandin, P., and Guillier, M. (2013). Expanding control in bacteria: interplay between small RNAs and transcriptional regulators to control gene expression. *Curr. Opin. Microbiol.* 16, 125–132. doi: 10.1016/j.mib.2012.12.005

Mann, M., Wright, P. R., and Backofen, R. (2017). IntaRNA 2.0: enhanced and customizable prediction of RNA-RNA interactions. *Nucleic Acids Res.* 45, W435–W439. doi: 10.1093/nar/gkx279

Merino-Puerto, V., Mariscal, V., Mullineaux, C. W., Herrero, A., and Flores, E. (2010). Fra proteins influencing filament integrity, diazotrophy and localization of septal protein SepJ in the heterocyst-forming cyanobacterium *Anabaena* sp. *Mol. Microbiol.* 75, 1159–1170. doi: 10.1111/j.1365-2958.2009.07031.x

Mitschke, J., Vioque, A., Haas, F., Hess, W. R., and Muro-Pastor, A. M. (2011). Dynamics of transcriptional start site selection during nitrogen stress-induced cell differentiation in *Anabaena* sp. PCC7120. *Proc. Natl. Acad. Sci. U.S.A.* 108, 20130–20135. doi: 10.1073/pnas.1112724108

Mohamed, A., and Jansson, C. (1989). Influence of light on accumulation of photosynthesis-specific transcripts in the cyanobacterium *Synechocystis* 6803. *Plant. Mol. Biol.* 13, 693–700. doi: 10.1007/BF00016024

Muro-Pastor, A. M., Valladares, A., Flores, E., and Herrero, A. (1999). The *hetC* gene is a direct target of the NtcA transcriptional regulator in cyanobacterial heterocyst development. *J. Bacteriol.* 181, 6664–6669.

Nitzan, M., Rehani, R., and Margalit, H. (2017). Integration of bacterial small RNAs in regulatory networks. *Annu. Rev. Biophys.* 46, 131–148. doi: 10.1146/annurev-biophys-070816-034058

Notredame, C., Higgins, D. G., and Heringa, J. (2000). T-Coffee: a novel method for fast and accurate multiple sequence alignment. *J. Mol. Biol.* 302, 205–217. doi: 10.1006/jmbi.2000.4042

Olmedo-Verd, E., Muro-Pastor, A. M., Flores, E., and Herrero, A. (2006). Localized induction of the *ntcA* regulatory gene in developing heterocysts of *Anabaena* sp. strain PCC 7120. *J. Bacteriol.* 188, 6694–6699. doi: 10.1128/JB.00509-06

Papenfort, K., Pfeiffer, V., Lucchini, S., Sonawane, A., Hinton, J. C., and Vogel, J. (2008). Systematic deletion of *Salmonella* small RNA genes identifies CyaR, a conserved CRP-dependent riboregulator of OmpX synthesis. *Mol. Microbiol.* 68, 890–906. doi: 10.1111/j.1365-2958.2008.06189.x

Picossi, S., Flores, E., and Herrero, A. (2014). ChIP analysis unravels an exceptionally wide distribution of DNA binding sites for the NtcA transcription factor in a heterocyst-forming cyanobacterium. *BMC Genomics* 15:22. doi: 10.1186/1471-2164-15-22

Rippka, R., Deruelles, J., Waterbury, J. B., Herdman, M., and Stanier, R. Y. (1979). Generic assignments, strain stories and properties of pure cultures of cyanobacteria. *J. Gen. Microbiol.* 111, 1–61.

Sambrook, J., and Russell, D. W. (2001). *Molecular Cloning: A Laboratory Manual*. New York, NY: Cold Spring Harbor Laboratory Press.

Sandh, G., Ramstrom, M., and Stensjo, K. (2014). Analysis of the early heterocyst Cys-proteome in the multicellular cyanobacterium *Nostoc punctiforme* reveals novel insights into the division of labor within diazotrophic filaments. *BMC Genomics* 15:1064. doi: 10.1186/1471-2164-15-1064

Sendersky, E., Kozer, N., Levi, M., Garini, Y., Shav-Tal, Y., and Schwarz, R. (2014). The proteolysis adaptor, NblA, initiates protein pigment degradation by interacting with the cyanobacterial light-harvesting complexes. *Plant J.* 79, 118–126. doi: 10.1111/tpj.12543

Steglich, C., Futschik, M. E., Lindell, D., Voss, B., Chisholm, S. W., and Hess, W. R. (2008). The challenge of regulation in a minimal photoautotroph: non-coding RNAs in *Prochlorococcus*. *PLoS Genet.* 4:e1000173. doi: 10.1371/journal.pgen.1000173

Urban, J. H., and Vogel, J. (2007). Translational control and target recognition by *Escherichia coli* small RNAs *in vivo*. *Nucleic Acids Res.* 35, 1018–1037. doi: 10.1093/nar/gkl1040

Voss, B., Gierga, G., Axmann, I. M., and Hess, W. R. (2007). A motif-based search in bacterial genomes identifies the ortholog of the small RNA Yfr1 in all lineages of cyanobacteria. *BMC Genomics* 8:375. doi: 10.1186/1471-2164-8-375

Wagner, E. G., and Romby, P. (2015). Small RNAs in bacteria and archaea: who they are, what they do, and how they do it. *Adv. Genet.* 90, 133–208. doi: 10.1016/bs.adgen.2015.05.001

Wright, P. R., Georg, J., Mann, M., Sorescu, D. A., Richter, A. S., Lott, S., et al. (2014). CopraRNA and IntaRNA: predicting small RNA targets, networks and interaction domains. *Nucleic Acids Res.* 42, W119–W123. doi: 10.1093/nar/gku359

Wright, P. R., Richter, A. S., Papenfort, K., Mann, M., Vogel, J., Hess, W. R., et al. (2013). Comparative genomics boosts target prediction for bacterial small RNAs. *Proc. Natl. Acad. Sci. U.S.A.* 110, E3487–E3496. doi: 10.1073/pnas.1303248110

Conflict of Interest Statement: The authors declare that the research was conducted in the absence of any commercial or financial relationships that could be construed as a potential conflict of interest.

frontiers in Microbiology

MINI REVIEW
published: 16 October 2018
doi: 10.3389/fmicb.2018.02495

Sodium Acetate Responses in *Saccharomyces cerevisiae* and the Ubiquitin Ligase Rsp5

*Akaraphol Watcharawipas, Daisuke Watanabe and Hiroshi Takagi**

Division of Biological Science, Graduate School of Science and Technology, Nara Institute of Science and Technology, Nara, Japan

Recent studies have revealed the feasibility of sodium acetate as a potentially novel inhibitor/stressor relevant to the fermentation from neutralized lignocellulosic hydrolysates. This mini-review focuses on the toxicity of sodium acetate, which is composed of both sodium and acetate ions, and on the involved cellular responses that it elicits, particularly via the high-osmolarity glycerol (HOG) pathway, the Rim101 pathway, the P-type ATPase sodium pumps Ena1/2/5, and the ubiquitin ligase Rsp5 with its adaptors. Increased understanding of cellular responses to sodium acetate would improve our understanding of how cells respond not only to different stimuli but also to composite stresses induced by multiple components (e.g., sodium and acetate) simultaneously. Moreover, unraveling the characteristics of specific stresses under industrially related conditions and the cellular responses evoked by these stresses would be a key factor in the industrial yeast strain engineering toward the increased productivity of not only bioethanol but also advanced biofuels and valuable chemicals that will be in demand in the coming era of bio-based industry.

Keywords: ***Saccharomyces cerevisiae*, ubiquitin ligase, Rsp5, sodium acetate responses, P-type ATPase sodium pumps, Ena1/2/5**

OPEN ACCESS

Edited by:
John P. Morrissey,
University College Cork, Ireland

Reviewed by:
Paola Branduardi,
Università degli studi di Milano Bicocca, Italy
Gianluca Bleve,
Istituto di Scienze delle Produzioni Alimentari (ISPA), Italy

***Correspondence:**
Hiroshi Takagi
hiro@bs.naist.jp

Specialty section:
This article was submitted to Microbial Physiology and Metabolism, a section of the journal Frontiers in Microbiology

Received: *21 July 2018*
Accepted: *28 September 2018*
Published: *16 October 2018*

Citation:
Watcharawipas A, Watanabe D and Takagi H (2018) Sodium Acetate Responses in Saccharomyces cerevisiae and the Ubiquitin Ligase Rsp5. Front. Microbiol. 9:2495. doi: 10.3389/fmicb.2018.02495

INTRODUCTION

The budding yeast *Saccharomyces cerevisiae* is an important microorganism for the production of alcoholic beverages, bread, and bioethanol, as well as other biochemicals due to its well-known ability during the fermentation process. *S. cerevisiae* cells possess relatively high ethanol productivity, and strong gassing power required for making dough, as well as produce distinct flavor for alcoholic beverages and bakery products (Shima and Takagi, 2009; Sasano et al., 2012a; Shiroma et al., 2014; Arshad et al., 2017). They also have lower nutrient requirement for growth and higher acid tolerance than lactic acid bacteria, which make them potentially useful for lactic acid production (Sugiyama et al., 2014). In the last decades, there has been increased interest in using *S. cerevisiae* for the production of other high value-added chemicals, e.g., isobutanol, branch-chain alcohols, amino acids, β-glucan, and lactic acids (Baek et al., 2017; Generoso et al., 2017; Mongkontanawat et al., 2018; Takpho et al., 2018). To meet these demands, researchers have considered the feasibility of using yeast cells in the presence of numerous stress conditions, e.g., weak acids, freeze-thaw, high sugar contents, oxidative treatment, and high temperature (Nakagawa et al., 2013; Sugiyama et al., 2014; Kitichantaropas et al., 2016), as well as several growth and/or fermentation inhibitors derived from feedstock biomass (Sasano et al., 2012b; Ishida et al., 2017; Jayakody et al., 2018). Thus, understanding the cellular responses of yeast in adaptation to these harsh conditions will be a key to improving yeast strains for future industrial applications.

Second-generation production of fuels and chemicals e.g., bioethanol involves the utilization of lignocellulosic biomasses such as rice straw, wheat straw, bagasse, corn fiber, and corn stover as a feedstock. These materials are comprised of 40–50% cellulose, 20–30% hemicellulose, and 10–25% lignin (Anwar et al., 2014). To release sugars (monosaccharides/disaccharides) from these biomasses, several hydrolytic processes with acid/base or enzyme are employed (Limayem and Ricke, 2012). However, not only sugars, but also growth/fermentation inhibitors including furfural, 5-hydroxymethylfurfural, vanillin, glycolaldehyde, and acetate are generated (Iwaki et al., 2013; Jonsson and Martin, 2016; Jayakody et al., 2017). In contrast to other inhibitors that can be reduced by the optimization of hydrolytic processes, acetate released from highly acetylated hemicellulose tentatively exists in lignocellulosic hydrolylates over 10 g/L at pH 5-6 (Palmqvist and Hahn-Hagerdal, 2000; Klinke et al., 2004; Almeida et al., 2007). Many studies have shown that acetate exerts an inhibitory effect on the growth and fermentation ability of *S. cerevisiae* cells (Pampulha and Loureiro-Dias, 1989; Larsson et al., 1999; Bellissimi et al., 2009). In addition, recent studies have demonstrated that acetate in the presence of sodium exerts higher growth inhibition than that in the presence of potassium (Pena et al., 2013), and sodium acetate exhibits higher cellular toxicity than sodium chloride at equal molar concentration, suggesting a synergistic inhibitory role of sodium and acetate (Watcharawipas et al., 2017). In terms of application, these findings underscore the importance of sodium acetate stress in the growth and fermentation from neutralized lignocellulosic hydrolysates.

SODIUM AND ACETATE STRESSES: TOXICITY AND ADAPTIVE MECHANISMS FOR YEAST CELLS

Acetic acid is a weak organic acid with low lipophilicity (p*K*a = 4.75). It can enter yeast cells either by passive diffusion across the plasma membrane or facilitated diffusion via the aquaglyceroporin channel Fps1 (Mollapour and Piper, 2007). At the cytosolic pH, acetic acid dissociates to acetate anions and protons in the cytoplasm, causing intracellular acidification and growth inhibition due to the perturbation of cytosolic pH homeostasis, which affects several cellular activities including signal transduction, metabolic functions, protein interaction, and cell division (Dechant et al., 2010; Young et al., 2010; Orij et al., 2012; Ullah et al., 2012; Stratford et al., 2013; Fernandez-Nino et al., 2015). Therefore, removing excess protons from the cells by the plasma membrane H^+-ATPase Pma1 and collecting protons inside the vacuole by the vacuolar proton pump V-ATPase are suggested to be necessary for normal cytosolic pH maintenance and cell growth recovery under acetic acid stress conditions (Martinez-Munoz and Kane, 2008; Ullah et al., 2012; Stratford et al., 2013; Smardon and Kane, 2014). Moreover, the released acetate anions also negatively affect yeast cells by increasing the internal turgor pressure that leads to cell growth inhibition (Mollapour et al., 2008). In addition, the depletion of intracellular ATP pools is postulated to occur as a result of the ATP utilization by the plasma membrane H^+-ATPase Pma1 and the vacuolar proton pump V-ATPase to pump protons out of the cells and into the vacuole, respectively (Ullah et al., 2013). Acetic acid also negatively affects the uptake of some nutrients, including glucose, tryptophan, histidine, lysine, leucine, uracil, and phosphate, which is possibly caused by either the reduction of intracellular ATP required for mediating the nutrient uptake or the downregulation of the involving genes such as *HXT1*, *HXT3*, *BAP2,* and *GAP1* genes (Kawahata et al., 2006; Ding et al., 2013). Moreover, programmed cell death was also triggered by high concentrations of acetic acid (Ludovico et al., 2002).

To cope with these cellular toxicities from acetic acid stress, *S. cerevisiae* utilizes the high-osmolarity glycerol (HOG) pathway to transduce acetic acid responses (Mollapour and Piper, 2006). The Hog1 mitogen-activated protein kinase (MAPK) phosphorylates Fps1, which triggers its ubiquitination, endocytosis, and degradation in the vacuole, thereby rendering yeast cells resistant to acetic acid (Mollapour and Piper, 2007). In addition to Hog1, the acetic acid-responsive transcriptional activator Haa1 also plays a pivotal role in acetic acid responses (Mira et al., 2011). Haa1 functions by regulating the transcription of various genes via the Haa1-responsive element (HRE) in their promoter regions (Mira et al., 2011). These genes belong to the so-called Haa1 regulon, and include *TPO2*, *TPO3*, *SAP30*, *HRK1*, *SPI1*, and *YGP1*. The drug:H^+ antiporters Tpo2 and Tpo3 are reported to play an important role in intracellular acetate anion extrusion (Fernandes et al., 2005). It has also been suggested that the component of Rpd3L histone deacetylase complex Sap30 and the protein kinase Hrk1 are crucial for decreasing intracellular acetate contents (Mira et al., 2010). The cell wall proteins Spi1 and Ygp1 have been suggested to replenish the yeast cell wall to prevent the re-entry of acetic acid by direct diffusion (Fernandes et al., 2005; Simoes et al., 2006; Mira et al., 2011). In addition, it was shown that both laboratory and industrial strains of *S. cerevisiae* constitutively expressing *HAA1* exhibited significantly improved cell growth and initial fermentation rates under acetic acid stress (Tanaka et al., 2012; Inaba et al., 2013). Therefore, molecular breeding of industrial yeast strains lacking *FPS1* or overexpressing *HAA1* could be regarded as a promising strategy for improving acetic acid tolerance in yeast cells.

On the other hand, the pH of lignocellulosic hydrolysates after pretreatment can be increased up to the range of 5 to 6 due to neutralization (Guo and Olsson, 2014; Wilkinson et al., 2016; Bazoti et al., 2017). Under this pH condition, which is higher than the p*K*a of acetic acid (4.75), acetic acid molecules are largely present as acetate anions with lower toxicity (Mollapour et al., 2009). However, the counter ions of acetic acid (e.g., sodium) play an important role in the toxicity of acetate at higher pH (Pena et al., 2013; Watcharawipas et al., 2017). Sodium ions inhibit the growth of yeast cells via two phenomena: (i) a high concentration of sodium causes a hyperosmotic environment that induces the loss of cytoplasmic water from yeast cells (Hohmann, 2002); (ii) a high concentration of sodium increases intracellular sodium and decreases intracellular potassium contents, interfering proper cation homeostasis in yeast cells (Arino et al., 2010). At high concentrations, sodium enters the cells mainly by displacing potassium through transporters

that include: (i) the high-affinity potassium transport Trk1/Trk2 system (Haro and Rodriguez-Navarro, 2002); (ii) the non-specific cation transport system named NSC1 for non-specific cation channels (Gomez et al., 1996); and (iii) the sodium-dependent phosphate transport Pi-Na^+ symporter Pho89 (Martinez and Persson, 1998; Serrano et al., 2002). High cytoplasmic sodium levels have been shown to negatively affect the 3′,5′-bisphosphate nucleotidase gene *HAL2* (Murguia et al., 1996), whereas proper intracellular potassium concentrations have been suggested to be necessary for several enzyme functions (Lapathitis and Kotyk, 1998).

The primary way that yeast cells cope with sodium stress is by maintaining intracellular contents and osmolarity. Hog1 phosphorylates the basic leucine-zipper transcriptional factor Sko1, leading to the upregulation of a subset of defensive genes that include the stress-inducible methylglyoxal reductase gene *GRE2*, the antioxidant peroxyredoxin gene *AHP1*, and the sodium pump gene *ENA1* (Proft and Serrano, 1999; Proft and Struhl, 2002). Ion homeostasis also involves the post-translational regulation of the sodium/proton antiporter Nha1 and the potassium channel Tok1 mediated by Hog1 phosphorylation (Proft and Struhl, 2004). To maintain suitable cytoplasmic sodium levels, surplus amounts of sodium must either be extruded through the plasma membrane by active transport via the sodium/proton antiporter Nha1 and the P-type ATPase sodium pumps Ena system or sequestered in the vacuole by the activity of Nhx1 and Vnx1, the two sodium/proton antiporters located in endosomal and vacuolar membranes, respectively (Nass et al., 1997; Cagnac et al., 2007). Additionally, the basal task of Hog1 is to increase the accumulation of glycerol as a compatible solute in response to hyperosmotic stress induced by high sodium concentration through: (i) the upregulation of glycerol biosynthesis genes *GPD1*, *GPP1*, and *GPP2* as well as the active glycerol uptake system Stl1 (Rep et al., 2000; Ferreira et al., 2005; Petelenz-Kurdziel et al., 2013); (ii) an increase of glycolytic enzyme phosphofructo-2-kinase activity (Dihazi et al., 2004); (iii) the limiting of the aquaglyceroporin channel Fps1 activity that exports glycerol (Lee et al., 2013). Besides HOG signaling, the alkaline pH-sensing Rim101 pathway also plays a role in intracellular sodium homeostasis. At alkaline pH after being C-terminally processed, the alkaline pH transcription factor Rim101 enters the nucleus to control the transcription of alkaline-responsive genes such as *ENA1* (Lamb et al., 2001; Serrano et al., 2002). In general, Rim101 and Hog1 act as the independent pathways to regulate the transcription of *ENA1*. Interestingly, a recent study showed that although Hog1, not Rim101, is predominantly required for controlling the transcription of *ENA1* under sodium chloride stress conditions, Rim101 is indispensable and has a potentially novel role in the post-translational regulation of Ena1 trafficking to the plasma membrane (Marques et al., 2015). However, detailed molecular mechanisms need to be further elucidated. In addition, previous studies also showed that Rim101 is required for tolerance to propionic acid stress due to its involvement in the transcriptional responses of *KNH1*, which encodes a protein that functions in the synthesis of cell wall β-1,6-glucan; *CWP1*, which encodes a mannoprotein that links to the β-1,3- and β-1,6-glucan in the cell wall; *BAG7*, which encodes a Rho GTPase-activating protein that plays a role in the synthesis of β-1,3-glucan by stimulating Rho1; and *YIL029c*, which encodes a protein with unknown function (Mira et al., 2009). Yeast cells lacking *RIM101* also exhibit impaired vacuole acidification, leading to acidic cytosolic pH under propionic acid stress (Mira et al., 2009). Taken together, these findings suggested that both the HOG and the Rim101 pathways potentially participate in the cellular responses to composite stress from a salt and weak acid — in this case, sodium and acetate.

THE E3 UBIQUITIN LIGASE Rsp5 AND ITS ADAPTORS

Rsp5 (Reverses Spt^- phenotype protein 5) is the sole orthologue of the human Nedd4 E3 ubiquitin ligases in *S. cerevisiae*, and plays important roles in regulating physiological processes in cells — including intracellular trafficking, signal transduction, and quality control of the plasma membrane and cytosolic proteins (Dunn and Hicke, 2001; Hiraishi et al., 2009; Jarmoszewicz et al., 2012; Shiga et al., 2014) — through the interaction and ubiquitination of diverse substrate proteins. Rsp5 is composed of the N-terminal calcium-dependent phospholipid membrane binding (C2) domain, three substrate-recognizing WW domains (commonly referred to two conserved tryptophan residues in the domains), and the C-terminal catalytic ubiquitin ligase (HECT) domain (Rotin and Kumar, 2009).

The essential role of Rsp5 is attributed to its activity in the regulation of the *OLE1* gene expression via ubiquitination-mediated proteolytic processing of the transcriptional activators Spt23 and Mga2 that localize at the endoplasmic reticulum (ER) (Zhang et al., 1999; Hoppe et al., 2000; Shcherbik et al., 2003, 2004). Rsp5 is known to downregulate various plasma membrane transporters for nutrients and ions as well as receptors. This downregulation contributes both to protein quality control mechanisms in which the plasma membrane proteins are misfolded (e.g., in response to heat stress) and regulatory mechanisms in which the transporters are endocytosed to restrict their activity or receptors are degraded for their desensitization. For example, the ubiquitination by Rsp5 mediates the endocytosis of the general amino acid permease Gap1 in response to the shifting from a poor nitrogen source to ammonium ions (Springael et al., 1999) and in response to environmental stresses such as ethanol, hydrogen peroxide, high temperature, and lithium chloride (Hoshikawa et al., 2003; Shiga et al., 2014). Our previous studies also suggest that Rsp5 participates in the maintenance of stress-induced abnormal proteins through degradation or repair process (Haitani et al., 2006; Haitani and Takagi, 2008; Hiraishi et al., 2009). It has been shown that Gap1 remains stable on the plasma membrane under ethanol stress in the stress-hypersensitive $rsp5^{A401E}$ mutant (Hoshikawa et al., 2003; Shiga et al., 2014). On the other hand, constitutive inactivation and endocytosis of Gap1 was effectively mediated by the $rsp5^{T357A/K764E}$ mutant (Haitani et al., 2009). Interestingly, a novel mechanism, in which Rsp5 is dephosphorylated and activated when a rich nitrogen source is supplied and vice

versa, was also proposed to involve the regulation of Gap1 ubiquitination (Sasaki and Takagi, 2013).

Moreover, the endocytosis of the maltose permease Mal61, the hexose transporter Hxt6/7, the uracil permease Fur4, the tryptophan permease Tat2, the zinc transporter Zrt1, and the divalent cation transporter Smf1 is regulated via the ubiquitination by Rsp5 in response to various stimuli (Galan et al., 1996; Hein and Andre, 1997; Krampe et al., 1998; Medintz et al., 1998; Beck et al., 1999; Gitan and Eide, 2000; Sullivan et al., 2007; Nikko and Pelham, 2009). The internalization of the pheromone receptor Ste2 after pheromone sensing is also controlled by the ubiquitination mediated by Rsp5 as a part of its desensitization (Dunn and Hicke, 2001). In addition, Rsp5 ubiquitin ligase activity has been shown to be important for fluid phase endocytosis (Dunn and Hicke, 2001). Recently, the plasma membrane H^+-ATPase Pma1 was shown to be mono-ubiquitinated by Rsp5, leading to its internalization and vacuolar degradation, in response to the loss of V-ATPase activity (Smardon and Kane, 2014), suggesting that Rsp5 plays a role in the regulation of cytosolic pH homeostasis in yeast cells. In summary, Rsp5 plays important physiological roles in various cellular processes. However, our knowledge of the role of Rsp5 in regulation of the monovalent cation transporters Ena1/2/5 is still limited.

To catalyze the ubiquitination on a particular substrate, Rsp5 has to interact with the substrate through the interaction between the WW domains of Rsp5 and the PY motifs consisting of short peptide sequences (XPXY) located in the substrate. However, most of the Rsp5 substrates do not contain the PY motifs (Gupta et al., 2007), suggesting the requirement of PY-motifs containing adaptor proteins. The evidence supporting the existence of the Rsp5 adaptors originates from the identification of Bsd2 and Tre1/2, which contain the PY motifs, as the proteins required for the ubiquitination of the divalent cation transporter Smf1 (Liu et al., 1997; Hettema et al., 2004; Stimpson et al., 2006). In addition, Bsd2, but not Tre1/2, is found to be crucial for ubiquitination and trafficking of the precursor of the vacuolar enzyme polyphosphatase Phm5 (Hettema et al., 2004). This suggests that combination of adaptors can also affect the substrate specificity by Rsp5 (Watanabe et al., 2015). In addition, many Rsp5 adaptor proteins have been identified, including Bul1/2 (Soetens et al., 2001; Liu et al., 2007), Ear1 and its homologue Ssh4 (Leon et al., 2008), as well as the arrestin-related trafficking adaptor (ART) protein family members, which consist of Art1 to Art9 (Lin et al., 2008; **Table 1**).

PROSPECTIVE ROLES OF Rsp5 AND ITS ADAPTORS IN SODIUM ACETATE RESPONSES

We can summarize our understanding of the cellular responses to sodium acetate as follows. Previous studies have shown that acetate stress in the presence of sodium at pH 6.8 exhibits a growth-inhibitory effect and triggers Hog1 MAPK

TABLE 1 | Lists of Rsp5 adaptor proteins, conserved domains, and their locations.

Adaptor protein	Conserved domain	Location
Bsd2	TM	Golgi-endosome
Tre1/2	TM, TFR dimer, PA	Golgi-endosome
Ear1/Ssh4	TM, B30.2/SPRY	Golgi-endosome
Bul1/2	Bul1 N-terminus, Bul1 C-terminus	Plasma membrane, Golgi-endosome
Bul3	Bul1 N-terminus	-ND-
Art1	Arrestin N-terminus	Plasma membrane
Art2	Arrestin C-terminus	Plasma membrane
Art3	Arrestin N-terminus, Arrestin C-terminus	-ND-
Art4	Arrestin N-terminus, Arrestin C-terminus	Plasma membrane
Art5	Arrestin C-terminus	Plasma membrane
Art6	Arrestin C-terminus	-ND-
Art7	Arrestin N-terminus, Arrestin C-terminus	-ND-
Art8	Arrestin C-terminus	Plasma membrane
Art9 (Rim8)	Arrestin N-terminus, Arrestin C-terminus	Plasma membrane
Art10	-ND-	-ND-

TM, Predicted transmembrane domain; TFR dimer, Transferrin receptor-like dimerization domain; PA, protease-associated domain; B30.2/SPRY, B30.2 and/or SP1a/RYanodine receptor domain; and ND, Not determined (Information was obtained from Saccharomyces Genome Database (SGD) and Lauwers et al., 2010).

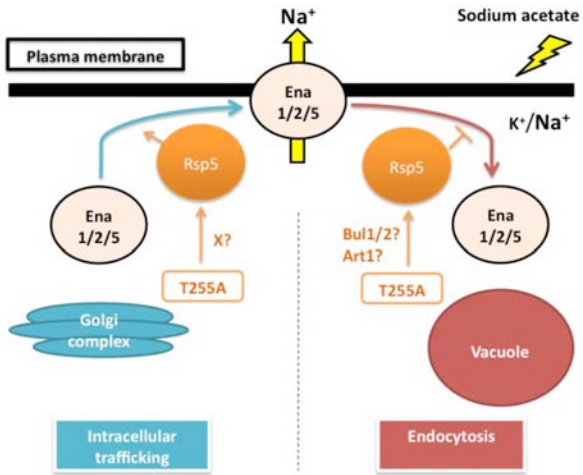

FIGURE 1 | Sodium acetate responses by yeast cells: hypothesized role of Rsp5 in regulating the sodium pumps Ena1/2/5. Sodium acetate triggers the increased accumulation of intracellular sodium. In this model, Rsp5 is hypothesized to play a post-translational regulatory role in either intracellular trafficking of Ena1/2/5 from the Golgi complex to the plasma membrane or endocytosis of Ena1/2/5 from the plasma membrane to the vacuole. The T255A mutation might either promote the intracellular trafficking of Ena1/2/5 through an unidentified factor (X) or inhibit the endocytosis of Ena1/2/5 via Bul1/2 or Art1 adaptor proteins, thereby enhancing the sodium extruding activity of Ena1/2/5 on the plasma membrane under sodium acetate stress conditions.

phosphorylation, which leads to upregulation of the *GPD1* mRNA level and thereby increased accumulation of intracellular glycerol (Mollapour and Piper, 2006; Mollapour et al., 2009). Our study also found that disruption of *HOG1* conferred sodium acetate sensitivity on yeast cells, but did not significantly affect the accumulation of intracellular sodium in yeast cells under sodium acetate stress conditions, suggesting that Hog1 mediated sodium acetate responses via other components e.g., glycerol (Watcharawipas et al., 2017). Thus, these studies indicate that one of the sodium acetate responses at higher pH is to increase intracellular osmolarity via the accumulation of glycerol, which allows the cells to counteract the loss of cytoplasmic water. Our recent study also revealed that the full acquisition of tolerance to sodium acetate is essentially dependent on the Rim101 pathway, since the disruption of *RIM8*, *RIM20*, and *RIM101* causes sodium acetate sensitivity on yeast cells (Watcharawipas et al., 2017). Moreover, we found that yeast cells lacking *RIM8* showed an increased accumulation of intracellular sodium content under sodium acetate stress conditions (Watcharawipas et al., 2017) similar to that observed under sodium chloride stress conditions (Marques et al., 2015), supporting the finding that the Rim101 pathway is crucial for the proper transport and accumulation of Ena1 on the plasma membrane (Marques et al., 2015). However, whether the Rim101 pathway has a principal role in regulating the transcription of *ENA1* in the presence of sodium acetate still needs to be clarified. This might also explain why the disruption of *HOG1* did not affect the intracellular sodium level under sodium acetate stress conditions. Thus, these results suggest that the HOG signaling and the Rim101 pathway independently play important roles in the sodium acetate responses in *S. cerevisiae* cells. Further investigation showed that the triple disruption of *ENA1/2/5*, which is downstream of the HOG and Rim101 pathways, confers sodium acetate sensitivity and increases the intracellular sodium accumulation in yeast cells under sodium acetate stress (Watcharawipas et al., 2017). Previous studies also show that the copy number of P-type ATPase sodium extrusion pump *ENA1/2/5* genes is associated with acetate tolerance in the presence of sodium (Gilbert et al., 2009; Pena et al., 2013). Another study shows that the sodium/proton antiporters Nha1, Nhx1, and Vnx1 located at the plasma membrane, endosome, and vacuole, respectively, are involved in the cellular adaptation under sodium acetate stress at initial growth phase (Yang et al., 2010). Thus, these studies underscore the great importance of the Ena1/2/5 sodium pumps for the realization of sodium acetate tolerance, and imply that, at the very least, the sodium acetate responses involve the extrusion of sodium out of the cells or the sequestration of sodium inside the vacuole in the presence of acetate. Importantly, the intracellular sodium accumulation in the presence of sodium and acetate is higher than that in the presence of sodium and chloride, indicating the synergistic inhibitory effect of acetate anions (Watcharawipas et al., 2017). It would be intriguing to further investigate whether the acetate anions negatively impact the Ena1/2/5 activity.

The physiological importance of Rsp5 in the sodium acetate responses has been suggested by the sodium acetate sensitivity of *rsp5*^{L733S} (*rsp5-1*) and *rsp5*^{A401E}, which have defects in the catalytic HECT domain and the WW3 domain, respectively (Watcharawipas et al., 2017). Recently, Wijayanti et al. (2015) found that Thr255Ala, an amino acid substitution in the WW1 domain, renders yeast cells the tolerance to sodium acetate with higher initial growth rate. Intriguingly, the changed threonine residue (Thr255) is conserved among the WW domains of Nedd4-family ubiquitin ligases and has corresponding positions at Thr357 in WW2 and Thr413 in WW3 of Rsp5. These threonine residues are also the putative phosphorylation sites which may play an important role in the substrate specificity of Rsp5 (Sasaki and Takagi, 2013; Watanabe et al., 2015). Interestingly, the Thr255Ala variant causes lower intracellular sodium accumulation than wild-type cells under sodium acetate stress. This sodium level difference is canceled by the triple deletion of *ENA1/2/5*, suggesting that the *rsp5*^{T255A} mutant positively affects the sodium extruding activity through Ena1/2/5. Generally, Rsp5 post-translationally controls several plasma membrane proteins under various conditions. Thus, it is possible that Rsp5 might affect either Ena1/2/5 trafficking to the plasma membrane or Ena1/2/5 endocytosis. However, Ena1/2/5 does not have the PY motifs. For this reason, it is hypothesized that adaptor proteins are required for mediating the regulation of Ena1/2/5 by Rsp5. The Rsp5 adaptors Rim8, Bul1/2 and Art1 have been shown to be important for the sodium acetate tolerance in yeast cells. However, the Rsp5-Rim8 interaction and Rim8 mono-ubiquitination by Rsp5 are dispensable for sodium acetate tolerance (Watcharawipas et al., 2017). It would be intriguing to further examine the roles of Bul1/2 or Art1 in sodium acetate responses (**Figure 1**).

CONCLUSION

In this mini-review, we discuss the current understanding of sodium acetate stress as a composite stress of sodium and acetate, which may be able to influence each other. Thus, the cellular responses involve not only individual responses to sodium or to acetate, but also integrated actions to combat the effects of both. In addition, we shed light on a potentially important link—namely, that the protein ubiquitination system mediated by the E3 ubiquitin ligase Rsp5 possesses an important role in selectively regulating intracellular sodium homeostasis under sodium acetate stress, potentially through the P-type ATPases Ena1/2/5 and Rsp5 adaptor proteins. Further investigations will uncover the evolutionarily conserved role of Nedd4-family ubiquitin ligases, and will also benefit industrial applications through an improved understanding of their related stress conditions.

AUTHOR CONTRIBUTIONS

AW, DW, and HT analyzed the data and drafted the manuscript. AW prepared the figure and table. HT coordinated the manuscript preparation. All authors reviewed and approved the final version of manuscript.

REFERENCES

Almeida, J. R. M., Modig, T., Petersson, A., Hahn-Hagerdal, B., Liden, G., and Gorwa-Grauslund, M. F. (2007). Increased tolerance and conversion of inhibitors in lignocellulosic hydrolysates by *Saccharomyces cerevisiae*. *J. Chem. Technol. Biotechnol.* 82, 340–349. doi: 10.1002/jctb.1676

Anwar, Z., Gulfraz, M., and Irshad, M. (2014). Agro-industrial lignocellulosic biomass a key to unlock the future bio-energy: a brief review. *J. Radiat. Res. Appl. Sci.* 7, 163–173. doi: 10.1016/j.jrras.2014.02.003

Arino, J., Ramos, J., and Sychrova, H. (2010). Alkali metal cation transport and homeostasis in yeasts. *Microbiol. Mol. Biol. Rev.* 74, 95–120. doi: 10.1128/MMBR.00042-09

Arshad, M., Hussain, T., Iqbal, M., and Abbas, M. (2017). Enhanced ethanol production at commercial scale from molasses using high gravity technology by mutant *S. cerevisiae*. *Braz. J. Microbiol.* 48, 403–409. doi: 10.1016/j.bjm.2017.02.003

Baek, S. H., Kwon, E. Y., Bae, S. J., Cho, B. R., Kim, S. Y., and Hahn, J. S. (2017). Improvement of D-lactic acid production in *Saccharomyces cerevisiae* under acidic conditions by evolutionary and rational metabolic engineering. *Biotechnol. J.* 12:1700015. doi: 10.1002/biot.201700015

Bazoti, S. F., Golunski, S., Pereira Siqueira, D., Scapini, T., Barrilli, E. T., Alex Mayer, D., et al. (2017). Second-generation ethanol from non-detoxified sugarcane hydrolysate by a rotting wood isolated yeast strain. *Bioresour. Technol.* 244, 582–587. doi: 10.1016/j.biortech.2017.08.007

Beck, T., Schmidt, A., and Hall, M. N. (1999). Starvation induces vacuolar targeting and degradation of the tryptophan permease in yeast. *J. Cell Biol.* 146, 1227–1237. doi: 10.1083/jcb.146.6.1227

Bellissimi, E., van Dijken, J. P., Pronk, J. T., and van Maris, A. J. (2009). Effects of acetic acid on the kinetics of xylose fermentation by an engineered, xylose-isomerase-based *Saccharomyces cerevisiae* strain. *FEMS Yeast Res.* 9, 358–364. doi: 10.1111/j.1567-1364.2009.00487.x

Cagnac, O., Leterrier, M., Yeager, M., and Blumwald, E. (2007). Identification and characterization of Vnx1p, a novel type of vacuolar monovalent cation/H + antiporter of *Saccharomyces cerevisiae*. *J. Biol. Chem.* 282, 24284–24293. doi: 10.1074/jbc.M703116200

Dechant, R., Binda, M., Lee, S. S., Pelet, S., Winderickx, J., and Peter, M. (2010). Cytosolic pH is a second messenger for glucose and regulates the PKA pathway through V-ATPase. *EMBO J.* 29, 2515–2526. doi: 10.1038/emboj.2010.138

Dihazi, H., Kessler, R., and Eschrich, K. (2004). High osmolarity glycerol (HOG) pathway-induced phosphorylation and activation of 6-phosphofructo-2-kinase are essential for glycerol accumulation and yeast cell proliferation under hyperosmotic stress. *J. Biol. Chem.* 279, 23961–23968. doi: 10.1074/jbc.M312974200

Ding, J., Bierma, J., Smith, M. R., Poliner, E., Wolfe, C., Hadduck, A. N., et al. (2013). Acetic acid inhibits nutrient uptake in *Saccharomyces cerevisiae*: auxotrophy confounds the use of yeast deletion libraries for strain improvement. *Appl. Microbiol. Biotechnol.* 97, 7405–7416. doi: 10.1007/s00253-013-5071-y

Dunn, R., and Hicke, L. (2001). Domains of the Rsp5 ubiquitin-protein ligase required for receptor-mediated and fluid-phase endocytosis. *Mol. Biol. Cell* 12, 421–435. doi: 10.1091/mbc.12.2.421

Fernandes, A. R., Mira, N. P., Vargas, R. C., Canelhas, I., and Sa-Correia, I. (2005). *Saccharomyces cerevisiae* adaptation to weak acids involves the transcription factor Haa1p and Haa1p-regulated genes. *Biochem. Biophys. Res. Commun.* 337, 95–103. doi: 10.1016/j.bbrc.2005.09.010

Fernandez-Nino, M., Marquina, M., Swinnen, S., Rodriguez-Porrata, B., Nevoigt, E., and Arino, J. (2015). The cytosolic pH of individual *Saccharomyces cerevisiae* cells is a key factor in acetic acid tolerance. *Appl. Environ. Microbiol.* 81, 7813–7821. doi: 10.1128/AEM.02313-15

Ferreira, C., van Voorst, F., Martins, A., Neves, L., Oliveira, R., Kielland-Brandt, M. C., et al. (2005). A member of the sugar transporter family, Stl1p is the glycerol/H + symporter in *Saccharomyces cerevisiae*. *Mol. Biol. Cell.* 16, 2068–2076. doi: 10.1091/mbc.e04-10-0884

Galan, J. M., Moreau, V., Andre, B., Volland, C., and Haguenauer-Tsapis, R. (1996). Ubiquitination mediated by the Npi1p/Rsp5p ubiquitin-protein ligase is required for endocytosis of the yeast uracil permease. *J. Biol. Chem.* 271, 10946–10952. doi: 10.1074/jbc.271.18.10946

Generoso, W. C., Brinek, M., Dietz, H., Oreb, M., and Boles, E. (2017). Secretion of 2,3-dihydroxyisovalerate as a limiting factor for isobutanol production in *Saccharomyces cerevisiae*. *FEMS Yeast Res.* 17:fox029. doi: 10.1093/femsyr/fox029

Gilbert, A., Sangurdekar, D. P., and Srienc, F. (2009). Rapid strain improvement through optimized evolution in the cytostat. *Biotechnol. Bioeng.* 103, 500–512. doi: 10.1002/bit.22272

Gitan, R. S., and Eide, D. J. (2000). Zinc-regulated ubiquitin conjugation signals endocytosis of the yeast ZRT1 zinc transporter. *Biochem. J.* 346, 329–336. doi: 10.1042/bj3460329

Gomez, M. J., Luyten, K., and Ramos, J. (1996). The capacity to transport potassium influences sodium tolerance in *Saccharomyces cerevisiae*. *FEMS Microbiol. Lett.* 135, 157–160. doi: 10.1016/0378-1097(95)00441-6

Guo, Z., and Olsson, L. (2014). Physiological response of *Saccharomyces cerevisiae* to weak acids present in lignocellulosic hydrolysate. *FEMS Yeast Res.* 14, 1234–1248. doi: 10.1111/1567-1364.12221

Gupta, R., Kus, B., Fladd, C., Wasmuth, J., Tonikian, R., Sidhu, S., et al. (2007). Ubiquitination screen using protein microarrays for comprehensive identification of Rsp5 substrates in yeast. *Mol. Syst. Biol.* 3:116. doi: 10.1038/msb4100159

Haitani, Y., Nakata, M., Sasaki, T., Uchida, A., and Takagi, H. (2009). Engineering of the yeast ubiquitin ligase Rsp5: isolation of a new variant that induces constitutive inactivation of the general amino acid permease Gap1. *FEMS Yeast Res.* 9, 73–86. doi: 10.1111/j.1567-1364.2008.00460.x

Haitani, Y., Shimoi, H., and Takagi, H. (2006). Rsp5 regulates expression of stress proteins via post-translational modification of Hsf1 and Msn4 in *Saccharomyces cerevisiae*. *FEBS Lett.* 580, 3433–3438. doi: 10.1016/j.febslet.2006.05.016

Haitani, Y., and Takagi, H. (2008). Rsp5 is required for the nuclear export of mRNA of HSF1 and MSN2/4 under stress conditions in *Saccharomyces cerevisiae*. *Genes Cells* 13, 105–116. doi: 10.1111/j.1365-2443.2007.01154.x

Haro, R., and Rodriguez-Navarro, A. (2002). Molecular analysis of the mechanism of potassium uptake through the TRK1 transporter of *Saccharomyces cerevisiae*. *Biochim. Biophys. Acta* 1564, 114–122. doi: 10.1016/S0005-2736(02)00408-X

Hein, C., and Andre, B. (1997). A C-terminal di-leucine motif and nearby sequences are required for $NH4^+$-induced inactivation and degradation of the general amino acid permease, Gap1p, of *Saccharomyces cerevisiae*. *Mol. Microbiol.* 24, 607–616. doi: 10.1046/j.1365-2958.1997.3771735.x

Hettema, E. H., Valdez-Taubas, J., and Pelham, H. R. (2004). Bsd2 binds the ubiquitin ligase Rsp5 and mediates the ubiquitination of transmembrane proteins. *EMBO J.* 23, 1279–1288. doi: 10.1038/sj.emboj.7600137

Hiraishi, H., Shimada, T., Ohtsu, I., Sato, T., and Takagi, H. (2009). The yeast ubiquitin ligase Rsp5 down-regulates the alpha subunit of nascent polypeptide-associated complex Egd2 under stress conditions. *FEBS J.* 276, 5287–5297. doi: 10.1111/j.1742-4658.2009.07226.x

Hohmann, S. (2002). Osmotic stress signaling and osmoadaptation in yeasts. *Microbiol. Mol. Biol. Rev.* 66, 300–372. doi: 10.1128/mmbr.66.2.300-372.2002

Hoppe, T., Matuschewski, K., Rape, M., Schlenker, S., Ulrich, H. D., and Jentsch, S. (2000). Activation of a membrane-bound transcription factor by regulated ubiquitin/proteasome-dependent processing. *Cell* 102, 577–586. doi: 10.1016/S0092-8674(00)00080-5

Hoshikawa, C., Shichiri, M., Nakamori, S., and Takagi, H. (2003). A non-conserved Ala401 in the yeast Rsp5 ubiquitin ligase is involved in degradation of Gap1 permease and stress-induced abnormal proteins. *Proc. Natl. Acad. Sci. U.S.A.* 100, 11505–11510. doi: 10.1073/pnas.1933153100

Inaba, T., Watanabe, D., Yoshiyama, Y., Tanaka, K., Ogawa, J., Takagi, H., et al. (2013). An organic acid-tolerant HAA1-overexpression mutant of an industrial bioethanol strain of *Saccharomyces cerevisiae* and its application to the production of bioethanol from sugarcane molasses. *AMB Express* 3, 1–7. doi: 10.1186/2191-0855-3-74

Ishida, Y., Nguyen, T. T. M., and Izawa, S. (2017). The yeast ADH7 promoter enables gene expression under pronounced translation

repression caused by the combined stress of vanillin, furfural, and 5-hydroxymethylfurfural. *J. Biotechnol.* 252, 65–72. doi: 10.1016/j.jbiotec.2017.04.024

Iwaki, A., Ohnuki, S., Suga, Y., Izawa, S., and Ohya, Y. (2013). Vanillin inhibits translation and induces messenger ribonucleoprotein (mRNP) granule formation in *Saccharomyces cerevisiae*: application and validation of high-content, image-based profiling. *PLoS One* 8:e61748. doi: 10.1371/journal.pone.0061748

Jarmoszewicz, K., Lukasiak, K., Riezman, H., and Kaminska, J. (2012). Rsp5 ubiquitin ligase is required for protein trafficking in *Saccharomyces cerevisiae* COPI mutants. *PLoS One* 7:e39582. doi: 10.1371/journal.pone.0039582

Jayakody, L. N., Ferdouse, J., Hayashi, N., and Kitagaki, H. (2017). Identification and detoxification of glycolaldehyde, an unattended bioethanol fermentation inhibitor. *Crit. Rev. Biotechnol.* 37, 177–189. doi: 10.3109/07388551.2015.1128877

Jayakody, L. N., Turner, T. L., Yun, E. J., Kong, I. I., Liu, J. J., and Jin, Y. S. (2018). Expression of Gre2p improves tolerance of engineered xylose-fermenting *Saccharomyces cerevisiae* to glycolaldehyde under xylose metabolism. *Appl. Microbiol. Biotechnol.* 102, 8121–8133. doi: 10.1007/s00253-018-9216-x

Jonsson, L. J., and Martin, C. (2016). Pretreatment of lignocellulose: formation of inhibitory by-products and strategies for minimizing their effects. *Bioresour. Technol.* 199, 103–112. doi: 10.1016/j.biortech.2015.10.009

Kawahata, M., Masaki, K., Fujii, T., and Iefuji, H. (2006). Yeast genes involved in response to lactic acid and acetic acid: acidic conditions caused by the organic acids in *Saccharomyces cerevisiae* cultures induce expression of intracellular metal metabolism genes regulated by Aft1p. *FEMS Yeast Res.* 6, 924–936. doi: 10.1111/j.1567-1364.2006.00089.x

Kitichantaropas, Y., Boonchird, C., Sugiyama, M., Kaneko, Y., Harashima, S., and Auesukaree, C. (2016). Cellular mechanisms contributing to multiple stress tolerance in *Saccharomyces cerevisiae* strains with potential use in high-temperature ethanol fermentation. *AMB Express* 6:107. doi: 10.1186/s13568-016-0285-x

Klinke, H. B., Thomsen, A. B., and Ahring, B. K. (2004). Inhibition of ethanol-producing yeast and bacteria by degradation products produced during pre-treatment of biomass. *Appl. Microbiol. Biotechnol.* 66, 10–26. doi: 10.1007/s00253-004-1642-2

Krampe, S., Stamm, O., Hollenberg, C. P., and Boles, E. (1998). Catabolite inactivation of the high-affinity hexose transporters Hxt6 and Hxt7 of *Saccharomyces cerevisiae* occurs in the vacuole after internalization by endocytosis. *FEBS Lett.* 441, 343–347. doi: 10.1016/S0014-5793(98)01583-X

Lamb, T. M., Xu, W., Diamond, A., and Mitchell, A. P. (2001). Alkaline response genes of *Saccharomyces cerevisiae* and their relationship to the RIM101 pathway. *J. Biol. Chem.* 276, 1850–1856. doi: 10.1074/jbc.M008381200

Lapathitis, G., and Kotyk, A. (1998). Univalent cation fluxes in yeast. *Biochem. Mol. Biol. Int.* 44, 371–380.

Larsson, S., Palmqvist, E., Hahn-Hagerdal, B., Tengborg, C., Stenberg, K., Zacchi, G., et al. (1999). The generation of fermentation inhibitors during dilute acid hydrolysis of softwood. *Enzyme Microb. Technol.* 24, 151–159. doi: 10.1016/S0141-0229(98)00101-X

Lauwers, E., Erpapazoglou, Z., Haguenauer-Tsapis, R., and Andre, B. (2010). The ubiquitin code of yeast permease trafficking. *Trends Cell Biol.* 20, 196–204. doi: 10.1016/j.tcb.2010.01.004

Lee, J., Reiter, W., Dohnal, I., Gregori, C., Beese-Sims, S., Kuchler, K., et al. (2013). MAPK Hog1 closes the *S. cerevisiae* glycerol channel Fps1 by phosphorylating and displacing its positive regulators. *Genes Dev.* 27, 2590–2601. doi: 10.1101/gad.229310.113

Leon, S., Erpapazoglou, Z., and Haguenauer-Tsapis, R. (2008). Ear1p and Ssh4p are new adaptors of the ubiquitin ligase Rsp5p for cargo ubiquitylation and sorting at multivesicular bodies. *Mol. Biol. Cell* 19, 2379–2388. doi: 10.1091/mbc.E08-01-0068

Limayem, A., and Ricke, S. C. (2012). Lignocellulosic biomass for bioethanol production: current perspectives, potential issues and future prospects. *Prog. Energy Combust. Sci.* 38, 449–467. doi: 10.1016/j.pecs.2012.03.002

Lin, C. H., MacGurn, J. A., Chu, T., Stefan, C. J., and Emr, S. D. (2008). Arrestin-related ubiquitin-ligase adaptors regulate endocytosis and protein turnover at the cell surface. *Cell* 135, 714–725. doi: 10.1016/j.cell.2008.09.025

Liu, J., Sitaram, A., and Burd, C. G. (2007). Regulation of copper-dependent endocytosis and vacuolar degradation of the yeast copper transporter, Ctr1p, by the Rsp5 ubiquitin ligase. *Traffic* 8, 1375–1384. doi: 10.1111/j.1600-0854.2007.00616.x

Liu, X. F., Supek, F., Nelson, N., and Culotta, V. C. (1997). Negative control of heavy metal uptake by the *Saccharomyces cerevisiae* BSD2 gene. *J. Biol. Chem.* 272, 11763–11769. doi: 10.1074/jbc.272.18.11763

Ludovico, P., Rodrigues, F., Almeida, A., Silva, M. T., Barrientos, A., and Corte-Real, M. (2002). Cytochrome c release and mitochondria involvement in programmed cell death induced by acetic acid in *Saccharomyces cerevisiae*. *Mol. Biol. Cell* 13, 2598–2606. doi: 10.1091/mbc.E01-12-0161

Marques, M. C., Zamarbide-Fores, S., Pedelini, L., Llopis-Torregrosa, V., and Yenush, L. (2015). A functional Rim101 complex is required for proper accumulation of the Ena1 Na^+-ATPase protein in response to salt stress in *Saccharomyces cerevisiae*. *FEMS Yeast Res.* 15:fov017. doi: 10.1093/femsyr/fov017

Martinez, P., and Persson, B. L. (1998). Identification, cloning and characterization of a derepressible Na^+-coupled phosphate transporter in *Saccharomyces cerevisiae*. *Mol. Gen. Genet.* 258, 628–638. doi: 10.1007/s004380050776

Martinez-Munoz, G. A., and Kane, P. (2008). Vacuolar and plasma membrane proton pumps collaborate to achieve cytosolic pH homeostasis in yeast. *J. Biol. Chem.* 283, 20309–20319. doi: 10.1074/jbc.M710470200

Medintz, I., Jiang, H., and Michels, C. A. (1998). The role of ubiquitin conjugation in glucose-induced proteolysis of Saccharomyces maltose permease. *J. Biol. Chem.* 273, 34454–34462. doi: 10.1074/jbc.273.51.34454

Mira, N. P., Becker, J. D., and Sa-Correia, I. (2010). Genomic expression program involving the Haa1p-regulon in *Saccharomyces cerevisiae* response to acetic acid. *OMICS* 14, 587–601. doi: 10.1089/omi.2010.0048

Mira, N. P., Henriques, S. F., Keller, G., Teixeira, M. C., Matos, R. G., Arraiano, C. M., et al. (2011). Identification of a DNA-binding site for the transcription factor Haa1, required for *Saccharomyces cerevisiae* response to acetic acid stress. *Nucleic Acids Res.* 39, 6896–6907. doi: 10.1093/nar/gkr228

Mira, N. P., Lourenco, A. B., Fernandes, A. R., Becker, J. D., and Sa-Correia, I. (2009). The RIM101 pathway has a role in *Saccharomyces cerevisiae* adaptive response and resistance to propionic acid and other weak acids. *FEMS Yeast Res.* 9, 202–216. doi: 10.1111/j.1567-1364.2008.00473.x

Mollapour, M., and Piper, P. W. (2006). Hog1p mitogen-activated protein kinase determines acetic acid resistance in *Saccharomyces cerevisiae*. *FEMS Yeast Res.* 6, 1274–1280. doi: 10.1111/j.1567-1364.2006.00118.x

Mollapour, M., and Piper, P. W. (2007). Hog1 mitogen-activated protein kinase phosphorylation targets the yeast Fps1 aquaglyceroporin for endocytosis, thereby rendering cells resistant to acetic acid. *Mol. Cell. Biol.* 27, 6446–6456. doi: 10.1128/MCB.02205-06

Mollapour, M., Shepherd, A., and Piper, P. W. (2008). Novel stress responses facilitate *Saccharomyces cerevisiae* growth in the presence of the monocarboxylate preservatives. *Yeast* 25, 169–177. doi: 10.1002/yea.1576

Mollapour, M., Shepherd, A., and Piper, P. W. (2009). Presence of the Fps1p aquaglyceroporin channel is essential for Hog1p activation, but suppresses Slt2(Mpk1)p activation, with acetic acid stress of yeast. *Microbiology* 155, 3304–3311. doi: 10.1099/mic.0.030502-0

Mongkontanawat, N., Wasikadilok, N., Phuangborisut, S., Chanawanno, T., and Khunphutthiraphi, T. (2018). β-Glucan production of *Saccharomyces cerevisiae* by using malva nut juice production wastewater. *Int. Food Res. J.* 25, 499–503.

Murguia, J. R., Belles, J. M., and Serrano, R. (1996). The yeast HAL2 nucleotidase is an in vivo target of salt toxicity. *J. Biol. Chem.* 271, 29029–29033. doi: 10.1074/jbc.271.46.29029

Nakagawa, Y., Seita, J., Komiyama, S., Yamamura, H., Hayakawa, M., and Iimura, Y. (2013). A new simple method for isolating multistress-tolerant semidominant mutants of *Saccharomyces cerevisiae* by one-step selection under lethal hydrogen peroxide stress condition. *Biosci. Biotechnol. Biochem.* 77, 224–228. doi: 10.1271/bbb.120533

Nass, R., Cunningham, K. W., and Rao, R. (1997). Intracellular sequestration of sodium by a novel Na^+/H^+exchanger in yeast is enhanced by mutations in the plasma membrane H^+-ATPase. *J. Biol. Chem.* 272, 26145–26152. doi: 10.1074/jbc.272.42.26145

Nikko, E., and Pelham, H. R. (2009). Arrestin-mediated endocytosis of yeast plasma membrane transporters. *Traffic* 10, 1856–1867. doi: 10.1111/j.1600-0854.2009.00990.x

Orij, R., Urbanus, M. L., Vizeacoumar, F. J., Giaever, G., Boone, C., Nislow, C., et al. (2012). Genome-wide analysis of intracellular pH reveals quantitative control of cell division rate by pHc in *Saccharomyces cerevisiae*. *Genome Biol.* 13, 1–15. doi: 10.1186/gb-2012-13-9-r80

Palmqvist, E., and Hahn-Hagerdal, B. (2000). Fermentation of lignocellulosic hydrolysates. II: inhibitors and mechanisms of inhibition. *Bioresour. Technol.* 74, 25–33. doi: 10.1016/S0960-8524(99)00161-3

Pampulha, M. E., and Loureiro-Dias, M. C. (1989). Combined effect of acetic acid, pH and ethanol on intracellular pH of fermenting yeast. *Appl. Microbiol. Biotechnol.* 31, 547–550. doi: 10.1007/BF00270792

Pena, P. V., Glasker, S., and Srienc, F. (2013). Genome-wide overexpression screen for sodium acetate resistance in *Saccharomyces cerevisiae*. *J. Biotechnol.* 164, 26–33. doi: 10.1016/j.jbiotec.2012.12.005

Petelenz-Kurdziel, E., Kuehn, C., Nordlander, B., Klein, D., Hong, K. K., Jacobson, T., et al. (2013). Quantitative analysis of glycerol accumulation, glycolysis and growth under hyper osmotic stress. *PLoS Comput. Biol.* 9:e1003084. doi: 10.1371/journal.pcbi.1003084

Proft, M., and Serrano, R. (1999). Repressors and upstream repressing sequences of the stress regulated ENA1 gene in *Saccharomyces cerevisiae*: bZIP protein Sko1p confers HOG-dependent osmotic regulation. *Mol. Cell. Biol.* 19, 537–546. doi: 10.1128/MCB.19.1.537

Proft, M., and Struhl, K. (2002). Hog1 kinase converts the Sko1-Cyc8-Tup1 repressor complex into an activator that recruits SAGA and SWI/SNF in response to osmotic stress. *Mol. Cell* 9, 1307–1317. doi: 10.1016/S1097-2765(02)00557-9

Proft, M., and Struhl, K. (2004). MAP kinase-mediated stress relief that precedes and regulates the timing of transcriptional induction. *Cell* 118, 351–361. doi: 10.1016/j.cell.2004.07.016

Rep, M., Krantz, M., Thevelein, J. M., and Hohmann, S. (2000). The transcriptional response of *Saccharomyces cerevisiae* to osmotic shock. *J. Biol. Chem.* 275, 8290–8300. doi: 10.1074/jbc.275.12.8290

Rotin, D., and Kumar, S. (2009). Physiological functions of the HECT family of ubiquitin ligases. *Nat. Rev. Mol. Cell Biol.* 10, 398–409. doi: 10.1038/nrm2690

Sasaki, T., and Takagi, H. (2013). Phosphorylation of a conserved Thr357 in yeast Nedd4-like ubiquitin ligase Rsp5 is involved in downregulation of the general amino acid permease Gap1. *Genes Cells* 18, 459–475. doi: 10.1111/gtc.12049

Sasano, Y., Haitani, Y., Hashida, K., Ohtsu, I., Shima, J., and Takagi, H. (2012a). Enhanement of the proline and nitric oxide synthetic pathway improves fermentation ability under multiple baking-associated stress conditions in industrial baker's yeast. *Microb. Cell Fact.* 11:40. doi: 10.1186/1475-2859-11-40

Sasano, Y., Watanabe, D., Ukibe, K., Inai, T., Ohtsu, I., Shimoi, H., et al. (2012b). Overexpression of the yeast transcription activator Msn2 confers furfural resistance and increases the initial fermentation rate in ethanol production. *J. Biosci. Bioeng.* 113, 451–455. doi: 10.1016/j.jbiosc.2011.11.017

Serrano, R., Ruiz, A., Bernal, D., Chambers, J. R., and Arino, J. (2002). The transcriptional response to alkaline pH in *Saccharomyces cerevisiae*: evidence for calcium-mediated signalling. *Mol. Microbiol.* 46, 1319–1333. doi: 10.1046/j.1365-2958.2002.03246.x

Shcherbik, N., Kee, Y., Lyon, N., Huibregtse, J. M., and Haines, D. S. (2004). A single PXY motif located within the carboxyl terminus of Spt23p and Mga2p mediates a physical and functional interaction with ubiquitin ligase Rsp5p. *J. Biol. Chem.* 279, 53892–53898. doi: 10.1074/jbc.M410325200

Shcherbik, N., Zoladek, T., Nickels, J. T., and Haines, D. S. (2003). Rsp5p is required for ER bound Mga2p120 polyubiquitination and release of the processed/tethered transactivator Mga2p90. *Curr. Biol.* 13, 1227–1233. doi: 10.1016/s0960-9822(03)00457-3

Shiga, T., Yoshida, N., Shimizu, Y., Suzuki, E., Sasaki, T., Watanabe, D., et al. (2014). Quality control of plasma membrane proteins by *Saccharomyces cerevisiae* Nedd4-like ubiquitin ligase Rsp5p under environmental stress conditions. *Eukaryot. Cell* 13, 1191–1199. doi: 10.1128/EC.00104-14

Shima, J., and Takagi, H. (2009). Stress-tolerance of baker's-yeast (*Saccharomyces cerevisiae*) cells: stress-protective molecules and genes involved in stress tolerance. *Biotechnol. Appl. Biochem.* 53, 155–164. doi: 10.1042/BA20090029

Shiroma, S., Jayakody, L. N., Horie, K., Okamoto, K., and Kitagaki, H. (2014). Enhancement of ethanol fermentation in *Saccharomyces cerevisiae* sake yeast by disrupting mitophagy function. *Appl. Environ. Microbiol.* 80, 1002–1012. doi: 10.1128/AEM.03130-13

Simoes, T., Mira, N. P., Fernandes, A. R., and Sa-Correia, I. (2006). The SPI1 gene, encoding a glycosylphosphatidylinositol-anchored cell wall protein, plays a prominent role in the development of yeast resistance to lipophilic weak-acid food preservatives. *Appl. Environ. Microbiol.* 72, 7168–7175. doi: 10.1128/AEM.01476-06

Smardon, A. M., and Kane, P. M. (2014). Loss of vacuolar H^+-ATPase activity in organelles signals ubiquitination and endocytosis of the yeast plasma membrane proton pump Pma1p. *J. Biol. Chem.* 289, 32316–32326. doi: 10.1074/jbc.M114.574442

Soetens, O., De Craene, J. O., and Andre, B. (2001). Ubiquitin is required for sorting to the vacuole of the yeast general amino acid permease, Gap1. *J. Biol. Chem.* 276, 43949–43957. doi: 10.1074/jbc.M102945200

Springael, J. Y., Galan, J. M., Haguenauer-Tsapis, R., and Andre, B. (1999). $NH4^+$-induced down-regulation of the *Saccharomyces cerevisiae* Gap1p permease involves its ubiquitination with lysine-63-linked chains. *J. Cell Sci.* 112, 1375–1383.

Stimpson, H. E., Lewis, M. J., and Pelham, H. R. (2006). Transferrin receptor-like proteins control the degradation of a yeast metal transporter. *EMBO J.* 25, 662–672. doi: 10.1038/sj.emboj.7600984

Stratford, M., Nebe-von-Caron, G., Steels, H., Novodvorska, M., Ueckert, J., and Archer, D. B. (2013). Weak-acid preservatives: pH and proton movements in the yeast *Saccharomyces cerevisiae*. *Int. J. Food Microbiol.* 161, 164–171. doi: 10.1016/j.ijfoodmicro.2012.12.013

Sugiyama, M., Akase, S. P., Nakanishi, R., Horie, H., Kaneko, Y., and Harashima, S. (2014). Nuclear localization of Haa1, which is linked to its phosphorylation status, mediates lactic acid tolerance in *Saccharomyces cerevisiae*. *Appl. Environ. Microbiol.* 80, 3488–3495. doi: 10.1128/AEM.04241-13

Sullivan, J. A., Lewis, M. J., Nikko, E., and Pelham, H. R. B. (2007). Multiple interactions drive adaptor-mediated recruitment of the ubiquitin ligase Rsp5 to membrane proteins in vivo and in vitro. *Mol. Biol. Cell* 18, 2429–2440. doi: 10.1091/mbc.E07-01-0011

Takpho, N., Watanabe, D., and Takagi, H. (2018). High-level production of valine by expression of the feedback inhibition-insensitive acetohydroxyacid synthase in *Saccharomyces cerevisiae*. *Metab. Eng.* 46, 60–67. doi: 10.1016/j.ymben.2018.02.011

Tanaka, K., Ishii, Y., Ogawa, J., and Shima, J. (2012). Enhancement of acetic acid tolerance in *Saccharomyces cerevisiae* by overexpression of the HAA1 gene, encoding a transcriptional activator. *Appl. Environ. Microbiol.* 78, 8161–8163. doi: 10.1128/AEM.02356-12

Ullah, A., Chandrasekaran, G., Brul, S., and Smits, G. J. (2013). Yeast adaptation to weak acids prevents futile energy expenditure. *Front. Microbiol.* 4:142. doi: 10.3389/fmicb.2013.00142

Ullah, A., Orij, R., Brul, S., and Smits, G. J. (2012). Quantitative analysis of the modes of growth inhibition by weak organic acids in *Saccharomyces cerevisiae*. *Appl. Environ. Microbiol.* 78, 8377–8387. doi: 10.1128/AEM.02126-12

Watanabe, D., Murai, H., Tanahashi, R., Nakamura, K., Sasaki, T., and Takagi, H. (2015). Cooperative and selective roles of the WW domains of the yeast Nedd4-like ubiquitin ligase Rsp5 in the recognition of the arrestin-like adaptors Bul1 and Bul2. *Biochem. Biophys. Res. Commun.* 463, 76–81. doi: 10.1016/j.bbrc.2015.05.025

Watcharawipas, A., Watanabe, D., and Takagi, H. (2017). Enhanced sodium acetate tolerance in *Saccharomyces cerevisiae* by the Thr255Ala mutation of the ubiquitin ligase Rsp5. *FEMS Yeast Res.* 17:fox083. doi: 10.1093/femsyr/fox083

Wijayanti, I., Watanabe, D., Oshiro, S., and Takagi, H. (2015). Isolation and functional analysis of yeast ubiquitin ligase Rsp5 variants that alleviate the toxicity of human α-synuclein. *J. Biochem.* 157, 251–260. doi: 10.1093/jb/mvu069

Wilkinson, S., Greetham, D., and Tucker, G. A. (2016). Evaluation of different lignocellulosic biomass pretreatments by phenotypic microarray-based metabolic analysis of fermenting yeast. *Biofuel Res. J.* 3, 357–365. doi: 10.18331/brj2016.3.1.5

Yang, S., Land, M. L., Klingeman, D. M., Pelletier, D. A., Lu, T.-Y. S., Martin, S. L., et al. (2010). Paradigm for industrial strain improvement identifies sodium acetate tolerance loci in *Zymomonas mobilis* and *Saccharomyces cerevisiae*. *Proc. Natl. Acad. Sci. U.S.A.* 107, 10395–10400. doi: 10.1073/pnas.0914506107

Young, B. P., Shin, J. J. H., Orij, R., Chao, J. T., Li, S. C., Guan, X. L., et al. (2010). Phosphatidic acid is a pH biosensor that links membrane biogenesis to metabolism. *Science* 329, 1085–1088. doi: 10.1126/science.1191026

Zhang, S., Skalsky, Y., and Garfinkel, D. J. (1999). MGA2 or SPT23 is required for transcription of the D9 fatty acid desaturase gene, OLE1, and nuclear membrane integrity in *Saccharomyces cerevisiae*. *Genetics* 151, 473–483.

Conflict of Interest Statement: The authors declare that the research was conducted in the absence of any commercial or financial relationships that could be construed as a potential conflict of interest.

frontiers in Microbiology

REVIEW
published: 13 November 2018
doi: 10.3389/fmicb.2018.02700

Resistance of *Listeria monocytogenes* to Stress Conditions Encountered in Food and Food Processing Environments

*Florentina Ionela Bucur[1], Leontina Grigore-Gurgu[1], Peter Crauwels[2], Christian U. Riedel[2] and Anca Ioana Nicolau[1]**

[1] Faculty of Food Science and Engineering, Dunarea de Jos University of Galati, Galati, Romania, [2] Institute of Microbiology and Biotechnology, Ulm University, Ulm, Germany

Listeria monocytogenes is a human food-borne facultative intracellular pathogen that is resistant to a wide range of stress conditions. As a consequence, *L. monocytogenes* is extremely difficult to control along the entire food chain from production to storage and consumption. Frequent and recent outbreaks of *L. monocytogenes* infections illustrate that current measures of decontamination and preservation are suboptimal to control *L. monocytogenes* in food. In order to develop efficient measures to prevent contamination during processing and control growth during storage of food it is crucial to understand the mechanisms utilized by *L. monocytogenes* to tolerate the stress conditions in food matrices and food processing environments. Food-related stress conditions encountered by *L. monocytogenes* along the food chain are acidity, oxidative and osmotic stress, low or high temperatures, presence of bacteriocins and other preserving additives, and stresses as a consequence of applying alternative decontamination and preservation technologies such high hydrostatic pressure, pulsed and continuous UV light, pulsed electric fields (PEF). This review is aimed at providing a summary of the current knowledge on the response of *L. monocytogenes* toward these stresses and the mechanisms of stress resistance employed by this important food-borne bacterium. Circumstances when *L. monocytogenes* cells become more sensitive or more resistant are mentioned and existence of a cross-resistance when multiple stresses are present is pointed out.

Keywords: acidity, temperature, oxidative stress, osmolarity, high pressure, UV light, pulsed electric fields, bacteriocins

OPEN ACCESS

Edited by:
Conor P. O'Byrne, National University of Ireland Galway, Ireland

Reviewed by:
Stephan Schmitz-Esser, Iowa State University, United States
Francisco Diez-Gonzalez, University of Georgia, United States

****Correspondence:***
Anca Ioana Nicolau
anca.nicolau@ugal.ro

Specialty section:
This article was submitted to Microbial Physiology and Metabolism, a section of the journal Frontiers in Microbiology

Received: *31 July 2018*
Accepted: *23 October 2018*
Published: *13 November 2018*

Citation:
Bucur FI, Grigore-Gurgu L, Crauwels P, Riedel CU and Nicolau AI (2018) Resistance of Listeria monocytogenes to Stress Conditions Encountered in Food and Food Processing Environments. Front. Microbiol. 9:2700. doi: 10.3389/fmicb.2018.02700

INTRODUCTION

Along the food chain, bacteria are constantly exposed to a wide range of stress factors, which affect their activity and viability. These stresses are either intrinsic to the food matrix or extrinsic factors intentionally applied to preserve food or imposed onto the organisms upon consumption by the host (Ruiz et al., 2017). *L. monocytogenes* is an important food-borne pathogen (Schlech et al., 1983)

that frequently causes food recalls[1,2] and disease outbreaks with significant case numbers and a mortality rate of 20–30%[3] worldwide (Buchanan et al., 2017). This organism is known for its ability to survive or even to replicate under a wide range of environmental stress conditions (Gandhi and Chikindas, 2007; Ferreira et al., 2014; Gahan and Hill, 2014). Resistance to stress supports colonization and persistence of *L. monocytogenes* in various niches along the food chain and thus formation of reservoirs for contamination (Berrang et al., 2010; Leong et al., 2014, 2015; Bolocan et al., 2016). Moreover, it ultimately contributes to the ability of this bacterium to infect humans (Sleator et al., 2009).

The stresses encountered by *L. monocytogenes* in foods include those that are a consequence of various methods of preservation, including traditional ones as acidic pH due to fermentation by e.g., lactic acid bacteria (LAB), and osmotic stress by increased salt concentrations and more contemporary ones as using of growth inhibitors including bacteriocins and other food preservatives (Leroy and de Vuyst, 2004; Albarracín et al., 2011; Johnson et al., 2017). It should be mentioned that bacteriocins, which are small antimicrobial peptides, may either be naturally produced by bacteria used for food fermentation or can be added exogenously as a preserving additive. On the other hand, there are measures of food preservation that are rather technical in nature and are designed either to kill pathogens and spoilage microorganism at the processing stage [thermal treatments and its alternatives high pressure, pulsed electric fields (PEF), radiation] or even to protect foods during their storage (low temperatures/refrigeration, low oxygen concentrations, presence of protective gases in the surrounding atmosphere) (Morris et al., 2007; Rascon Escajeda et al., 2018).

The same stress may occur on several occasions along the food chain. For example, *L. monocytogenes* may be exposed to pH and osmotic stress first in the food matrix as consequence of fermentation or food preservation and subsequently in the host gastrointestinal tract. In this respect, it is of importance that resistance to different stresses is interconnected. For example incubation of *L. monocytogenes* at low temperatures enhances its resistance to high salt concentrations (Schmid et al., 2009). Likewise, osmotic stress in *L. monocytogenes* can lead to cross-protection against other causes of injury, including heat, ethanol, acidity, alkalinity, and oxidative stress (Melo et al., 2015). This is, at least partially explained by the fact that the stress signal received by the two component systems *liaRS*, *lisRK*, *cesRK*, *agrCA*, and *virRS*, which have been demonstrated to play a role in the stress response (Kang et al., 2015; Pöntinen et al., 2015, 2017), converge on the level of SigB, which is the alternative sigma factor σ^B that controls the general stress response in *L. monocytogenes* and other Gram-positive bacteria (Kazmierczak et al., 2003; Chaturongakul and Boor, 2006; Abram et al., 2008). For *L. monocytogenes*, SigB has been shown to be involved in the resistance to acidity (Wemekamp-Kamphuis et al., 2004b), osmotic stress (Fraser et al., 2003), cold and freezing stress (Becker et al., 2000), oxidative stress (Chaturongakul and Boor, 2004), and high hydrostatic pressure (Wemekamp-Kamphuis et al., 2004b). Appropriate resistance mechanisms are triggered by activation of σ^B-dependent promoters (Van Schaik and Abee, 2005). The extremely high tolerance to stressful conditions makes *L. monocytogenes* a major concern in food processing and a suitable model organism to study resistance mechanisms to stress conditions encountered in food and food processing environments.

Some of the mechanisms (and consequences) of resistance of *L. monocytogenes* have been expertly reviewed previously (Doyle et al., 2001; Tasara and Stephan, 2006; Thévenot et al., 2006; Gandhi and Chikindas, 2007; Lungu et al., 2009; NicAogáin and O'Byrne, 2016). However, most of these reviews focus on osmotic, pH, and temperature stress. With the present review we aim at providing a summary of the current knowledge on resistance and associated mechanisms of *L. monocytogenes* with a clear focus on stressful conditions that arise from traditional or alternative methods of food processing, preservation and decontamination. While we will touch upon stresses reviewed elsewhere (acidic pH, osmolarity, high and low temperatures, oxidative stress), we will also discuss resistance of *L. monocytogenes* to other stress conditions that have not gained as much attention (bacteriocins, pulsed or continuous UV radiation or visible light, electrical fields, high pressure). A deeper understanding of the mechanisms used by *L. monocytogenes* to survive and proliferate in food products may help food specialists to design efficient preservation methods that will extend shelf lives and provide a better protection of consumers against this pathogen while at the same time maintain the sensory and nutritional properties of the food products.

RESISTANCE OF *L. monocytogenes* TO STRESS DURING FOOD PROCESSING AND STORAGE

Resistance to Thermal Stress

Thermal treatments and temperature control are strategies that have been applied in food production and preservation for centuries to prevent or limit contamination and outgrowth of food-borne pathogens. However, the efficacy of thermal treatments against *L. monocytogenes* is limited by the intrinsic ability of this pathogen to survive and actively replicate at temperatures between −0.4 and 45°C (Chaturongakul et al., 2008; Chan and Wiedmann, 2009).

Resistance to Thermal Treatments

Mild thermal treatments (<100°C) are largely applied in food processing in order to inactivate vegetative microbial cells of food-spoilage bacteria and food-borne pathogens. Such treatments ensure food safety and prolonged shelf life as long as food products are properly packed and adequately stored (Van Boekel et al., 2010). Despite these benefits, thermal treatments can have a negative impact on the quality of food affecting the

[1]https://www.theguardian.com/business/2018/jul/06/uk-supermarkets-recall-frozen-vegetables-over-bacteria-fears (Accessed 31.07.2018)

[2]https://www.fda.gov/AJAX/All/ (Accessed 31.07.2018)

[3]http://www.who.int/csr/don/02-may-2018-listeriosis-south-africa/en/ (Accessed 10.10.2018)

nutritional value and sensory properties (Hardy et al., 1999). However, the main concern with thermal processing of foods remains the ability of sublethally injured pathogenic bacteria to recover and grow during post-processing storage. This is of particular relevance for *L. monocytogenes* with its ability to grow in a wide temperature range (Sörqvist, 1993; Mackey et al., 1994). Although *L. monocytogenes* does not manifest an extraordinary resistance to high temperatures, it was shown to be more heat tolerant than other non-spore-forming pathogens such as *Salmonella* and *E. coli* (Abdel Karem and Mattar, 2001; Huang, 2004; Sallami et al., 2006). Factors that influence the resistance of *L. monocytogenes* to heat vary among strains, bacterial cells' age, test and growth conditions, previous environmental stresses, or food components (Doyle et al., 2001).

L. monocytogenes has been shown to survive the minimum high-temperature, short-time treatment imposed by U.S. Food and Drug Administration (71.7°C, 15 s) in the case of milk collected from deliberately contaminated cows. Early studies raised the possibility that polymorphonuclear leukocytes present in milk may have a protective effect on *L. monocytogenes* during heat treatments residing inside these cells (Fleming et al., 1985; Doyle et al., 1987). However, subsequent reports showed that, in naturally contaminated milk, *L. monocytogenes* was not able to resist temperatures greater than 67.5°C combined with a holding time of 16.2 s (Farber et al., 1988). Nevertheless, the conditions associated with dairy products seem to influence the resistance of *L. monocytogenes* to heat treatments. For instance, Casadei and colleagues showed that limited access to essential nutrients in butter and the physical structure of this food could induce a starvation state in *L. monocytogenes* cells correlated with cross-resistance to other types of stress. In this case *L. monocytogenes* Scott A grown within this food matrix was four times more resistant to a treatment at 60°C than the same strain grown in TSB broth (Casadei et al., 1998). Furthermore, *L. monocytogenes* was shown to survive relatively high temperatures in heat-treated meat (Farber et al., 1989; Gaze et al., 1989; Murphy et al., 2003), egg products (Bartlett and Hawke, 1995; Monfort et al., 2012) and vegetables such as mushrooms and peas (Mazzotta, 2001a).

Resistance of *L. monocytogenes* strains to heat can vary significantly among serotypes (Sörqvist, 1994). In one study, strains belonging to serotype 1/2a showed relatively low tolerance to heat (up to 2 log CFU/mL), while strains representing serotypes 1/2b and 4b exhibited an extensive variability (from undetectable to 4 log CFU/mL). The highest heat tolerance was recorded for a serotype 7 strain (5 log CFU/mL) (Shen et al., 2014).

L. monocytogenes cells exposed to sublethal stresses prior to thermal challenge can become considerably more heat resistant. Shen and colleagues found that exposure of *L. monocytogenes* to a temperature of 48°C for 30 min led to heat stress adaptation among bacterial cells. Moreover, subjection to this mild stress for a short period of time did not affect the capacity of growing (Shen et al., 2014). Salt was also shown to potentiate the ability of *L. monocytogenes* to withstand thermal treatments (Jørgensen et al., 1995). For instance, the $D_{63°C}$ value, which is the time required to kill 90% of bacteria when exposed to the temperature of 63°C, for Scott A strain inoculated in egg products with 10% NaCl increased approximately 6 times in comparison with that of the same strain processed in egg products without salt (Bartlett and Hawke, 1995). This may be due to the protective effect of decreased water activity in the growth medium (Shebuski et al., 2000). Acidity is another factor that can influence bacteria's thermotolerance. Acid-adaptation in fruit juices was shown to substantially increase the resistance of *L. monocytogenes* to subsequent heat treatment (Mazzotta, 2001b). Also, *L. monocytogenes* displays an increased heat tolerance and a significantly increased $D_{60°C}$ value (2.2 min) in stationary compared to exponential growth phase (0.6 min) (Jørgensen et al., 1999).

At the molecular level, the response of *L. monocytogenes* to 48°C involves the expression of genes belonging to specific heat-shock regulons, namely class I and class III heat-shock genes, and genes of the SigB-dependent class II stress response. The upregulation of *recA* expression, an activator of SOS response implicated in DNA repair could be also observed (Van der Veen et al., 2007). Class I heat-shock genes (*grpE*, *dnaK*, *dnaJ*, *groEL,* and *groES*) encode for heat-shock proteins (HSPs) that act as intra-cellular chaperones whose expression is increased when denatured proteins accumulate in cytoplasm (**Figure 1Ba**). The role of HSPs is to stabilize and assemble partially unfolded proteins, preventing their aggregation under stress conditions. Under physiological growth conditions at ambient temperature, expression of class I heat-shock genes is controlled by the HrcA repressor (**Figure 1Aa**), which in turn is encoded by the first gene of the *dnaK* operon (Hendrick and Hartl, 1993; Hanawa et al., 2000; Hartl and Hayer-Hartl, 2002). Class III heat-shock genes encode for ATP-dependent proteases (ClpC, ClpP, and ClpE) required for degradation of misfolded proteins under stress conditions including high temperature (**Figure 1Bb**). These proteases are negatively regulated by the CtsR repressor (**Figure 1Ab**), which is the product of the first gene of the *clpC* operon (Nair et al., 2000). The ClpL protease was recently found to play a considerable role in the elevated temperature tolerance of *L. monocytogenes* AT3E. This finding was observed upon curing the strain from plasmid pLM58, which harbors *clpL*, resulting in a strain with reduced heat resistance. Moreover, insertion of *clpL* increased the resistance of a heat-sensitive *L. monocytogenes* strain (Pöntinen et al., 2017).

Resistance to Low Temperatures

L. monocytogenes is considered a psychrotolerant bacterium due to its ability to grow at temperatures as low as −0.4°C (Chan and Wiedmann, 2009). This tolerance to cold stress is responsible for the frequent detection of *L. monocytogenes* in refrigerated food products, especially meat, poultry, and seafood (Tasara and Stephan, 2006). Low temperatures result in decreased metabolic rates and changes in membrane composition, expression of cold shock proteins (Csps), and uptake of cryoprotective compounds (Phadtare et al., 1999; Neunlist et al., 2005; Cordero et al., 2016).

The alterations in the membrane in response to cold stress comprise a reduced chain length of fatty acids, an increase in the concentration of unsaturated fatty acids, and altered ratios of *iso*- and *anteiso*-branched fatty acids (Püttman et al., 1993; Russell et al., 1995; Neunlist et al., 2005). These changes maintain fluidity

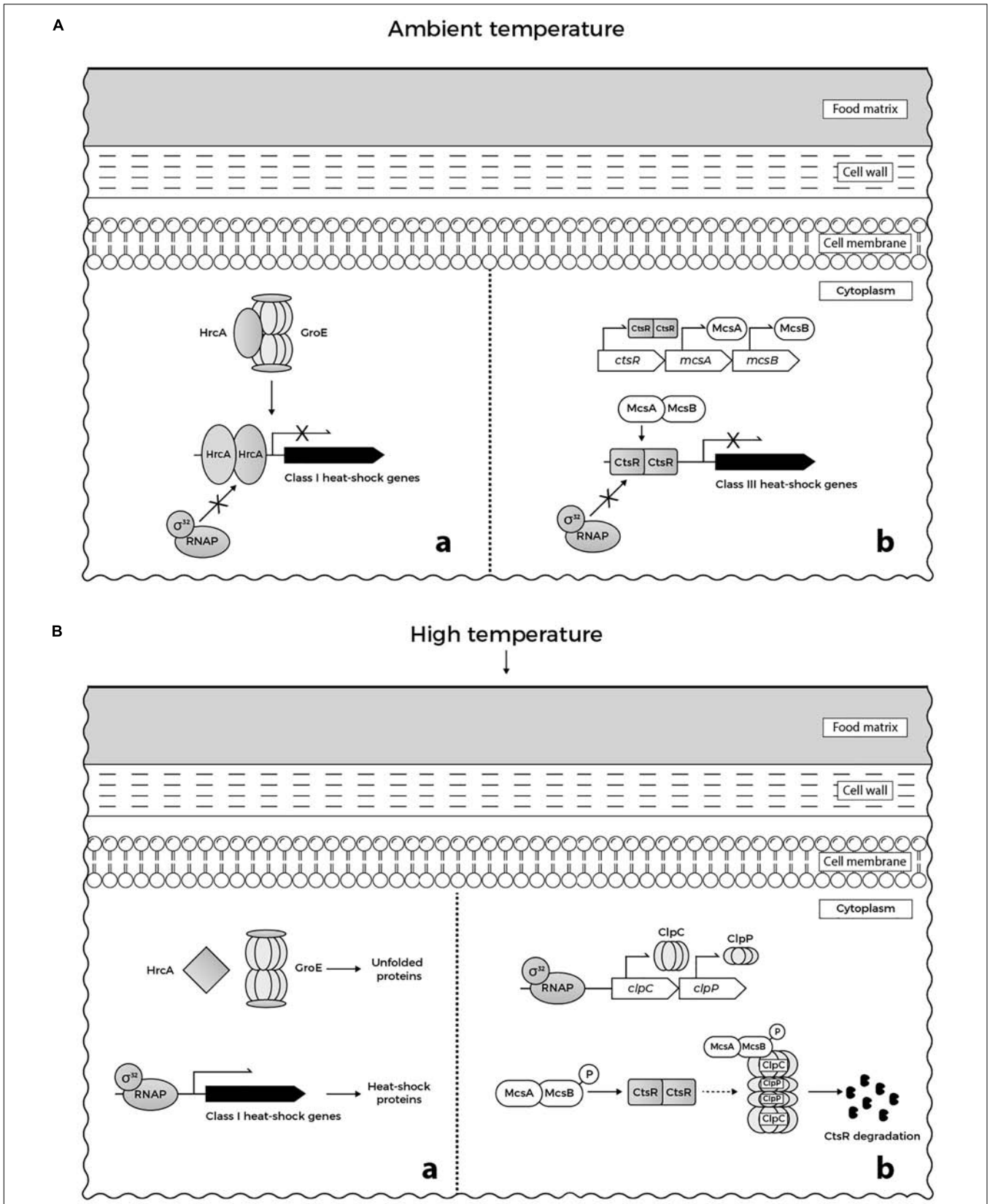

FIGURE 1 | Continued

FIGURE 1 | (A) Regulation of heat-shock genes in *L. monocytogenes* under ambient temperature in food matrices: **(a)** GroE chaperonine ensures the adequate folding of HrcA repressor. When folded correctly, the repressor binds to its target promoters, preventing expression of class I heat-shock genes. **(b)** McsB (tyrosine kinase) and its co-activator McsA (zinger finger protein) are involved in the regulation of CtsR repressor activity. CtsR, stabilized by McsA, binds to its target promoters, preventing expression of class III heat-shock genes. **(B)** Regulation of heat-shock genes in *L. monocytogenes* under heat stress in food matrices: **(a)** GroE is titrated by unfolded proteins that accumulate in cytoplasm and cannot interact with HrcA. When denatured upon heat stress, misfolded HrcA is unable to bind to the target DNA. Consequently, RNA polymerase-σ^{32} binds to the target promoters allowing the transcription of class I heat shock genes. **(b)** Similarly, CtsR undergoes heat-induced conformational changes that prevent its interaction with the target promoters. This allows binding of RNA polymerase-σ^{32} to the promoters of *clp* genes inducing the transcription of *clpC* and *clpP*. Following temperature-dependent autophosphorylation, McsB, assisted by McsA, targets CtsR to degradation by ClpCP protease (based on Krüger et al., 2001; Roncarati and Scarlato, 2017; Roncarati and Scarlato, 2018).

of the membrane at low temperatures and prevent formation of a gel-like state that may result in leakage of cytoplasmic content (Beales, 2004).

Csps are small proteins (65–70 amino acids long) with a highly conserved structure. They bind to single-stranded nucleic acid molecules *via* their ribonucleoprotein binding motifs RNP1 and RNP2 (Horn et al., 2007). This stabilizes the conformation of the nucleic acid and prevents degradation (Barria et al., 2013). Thus, Csps act as molecular chaperones that facilitate replication, transcription, and translation at low temperatures (Lee et al., 2012). CspA, CspB, and CspD contribute to resistance to low temperatures albeit with different importance (Schmid et al., 2009). Interestingly, they also seem to be involved in the resistance to osmotic stress (Schmid et al., 2009). The ferritin-like protein (Flp) was highly induced in response to cold shock suggesting it is involved in response to cold stress (Hébraud and Guzzo, 2000). Chan et al. (2007) determined the cold shock regulon by genome-wide expression analysis and could show that expresion of 105 and 170 genes was increased during growth on 4°C vs. 37°C in logarithmic- and stationary-phase with an overlap of 30 genes including *cspL*. Of these 30 genes, many are involved in membrane and cell wall function, lipid metabolism, transcription or translation.

Another mechanism of *L. monocytogenes* to counteract cold stress is the import of osmolytes such as glycine betaine, carnitine, γ-butyrobetaine, proline betaine, and 3-dimethylsulphoniopropionate as cryoprotectants. In the above mentioned genome-wide transcriptional analysis, the *opuCABCD* operon, which encodes a carnitine transporter, and *gbuC* encoding the substrate binding protein of a glycine betaine transporter showed increased expression in exponential growth phase at 4°C compared to 37°C (Chan et al., 2007). Similarly, expression of *opuCA* and *betL* were increased after exposure of *L. monocytogenes* S1 to cold and freezing stress as shown by quantitative RT-PCR (Miladi et al., 2016). This confirmed previous observations showing that Gbu-mediated betaine uptake improves growth under cold stress and uptake of betaine via BetL and OpuC transport betaine slightly improves cryotolerance (Angelidis and Smith, 2003). In the same study, OpuC was shown to be the main carnitine transporter, which provided markedly higher resistance to cold stress than betaine uptake.

Resistance to Acidity

Acidification is a method of food preservation widely applied to dairy, meat and vegetable products for centuries and is primarily achieved by fermentation by bacteria either present in the raw food or added as starter cultures (Hill et al., 2017). The preserving effect is achieved, on the one hand, by the metabolic end products, which are weak organic acids (e.g., acetate, lactate) that have anti-microbial activity, and, on the other hand, by inhibition of microbial growth at low pH (Caplice and Fitzgerald, 1999).

Both planktonic and surface attached cells of *L. monocytogenes* display adaptive acid tolerance response (ATR), i.e., bacteria pre-exposed to mild acid stress (pH 5.0) showed higher survival to subsequent challenge at a lower pH (3.0) compared to untreated bacteria (Davis et al., 1996; Chorianopoulos et al., 2011). The extent of ATR may be influenced by the structural properties of the food matrices. For example, *L. monocytogenes* grown on the surface of meat product slices formulated with potassium lactate and sodium diacetate exhibited higher resistance to a pH of 1.5 than the same bacteria exposed to the same pH in homogenates of the meat product (Skandamis et al., 2012). Similar observations were made for *L. monocytogenes* incubated on tomato, lettuce or in culture media for 5 days at 5°C. Bacteria incubated on vegetables were more tolerant to exposure to acidic conditions induced by lactic acid, acetic acid or hydrochloric acid than those kept in tryptic soy broth under the same conditions (Poimenidou et al., 2016).

L. monocytogenes has several mechanisms to maintain its internal pH (pH_i) under acid stress (**Table 1**) including the F_0F_1-ATPase (Cotter et al., 2000), the glutamatic acid decarboxylase (GAD; Feehily et al., 2014), and the arginine and agmatine deiminases (ADI and AgDI; Lund et al., 2014). The F_0F_1-ATPase is involved in ATR initiation during mild pH stress (Mclaughlin and Rees, 2009). The GAD system confers resistance to more severe acidic conditions (pH < 4.5; Karatzas et al., 2012) and has also been shown to be activated as result of reduced oxygen availability associated with food atmosphere packaging (Francis et al., 2007; Sewell et al., 2015). It is comprised of two proteins, a cytoplasmic glutamate decarboxylase (GadA or GadB) and a glutamate/GABA antiporter (GadC) located in the cytoplasmic membrane (Cotter et al., 2005). The role of the GAD system is to increase pH_i by converting extracellular glutamate to Γ-aminobutyrate (GABA) in an enzymatic reaction that reduces the intracellular proton concentration (Cotter et al., 2001). The ADI and AgDI systems are both involved in the response of *L. monocytogenes* to extreme acidity (Ryan et al., 2009; Soares and Knuckley, 2016). ADI imports arginine molecules from the extracellular environment, converting them to ornithine, CO_2, ammonia (NH_3), and ATP. NH_3 is then protonated to ammonium (NH_4), which increases pH_i (Cotter and Hill, 2003).

TABLE 1 | Genes involved in the acidity resistance of *L. monocytogenes* (data retrieved from two databases, The Universal Protein Resource (UniProt) and The National Center of Biotechnology Information (NCBI), respectively).

Response mechanisms	Genes involved in the response mechanisms	Encoded proteins/enzymes	Class of proteins/enzymes	Location of proteins/enzymes
F_0F_1-ATPase	*atpA2* (*lmo2531*)	ATP synthase F1 sector, subunit alfa 2	EC 3.6.3.14 Hydrolase H(+)-transporting two-sector ATPase	Plasma membrane Proton-transporting ATP synthase complex, catalytic core F(1)
	atpB (*lmo2535*)	ATP synthase F0 sector, subunit alfa		Integral component of membrane Plasma membrane Proton-transporting ATP synthase complex, coupling factor F(o)
	atpC (*lmo2528*)	ATP synthase F1 sector, epsilon subunit		Plasma membrane ATP synthase complex, catalytic core F(1)
	atpD2 (lmo2529)	ATP synthase F1 sector, beta 2 subunit		Plasma membrane ATP synthase complex, catalytic core F(1)
	*atp*E (*lmo2534*)	ATP synthase F(0) sector, subunit c		Integral component of membrane Plasma membrane ATP synthase complex, coupling factor F(o)
	atpF (*lmo2533*)	ATP synthase F(0) sector, subunit b		Integral component of membrane Plasma membrane Proton-transporting ATP synthase complex, coupling factor F(o)
	atpG (*lmo2530*)	ATP synthase F1 sector, gamma subunit		Plasma membrane Proton-transporting ATP synthase complex, catalytic core F(1)
	atpH (*lmo2532*)	ATP synthase F(1) sector, delta subunit		Integral component of membrane Proton-transporting ATP synthase complex, catalytic core F(1)
Glutamate decarboxylase activity (GAD) system	*gadA* (*lmo0447*)	Glutamate decarboxylase alpha (GAD-alpha)	EC 4.1.1.15 Decarboxylase, lyase	Cytoplasm
	gadB (*lmo2363*)	Glutamate decarboxylase beta (GAD-beta)		
	gadC (*lmo2362*)	Putative glutamate:gamma-aminobutyrate antiporter		Cell inner membrane; Multi-pass membrane protein
Arginine deiminase (ADI) system	*arcA* (*lmo0043*)	Arginine deiminase	EC 3.5.3.6 Hydrolase	Cytoplasm
	arcB (*lmo0036*)	Ornithine carbamoyltransferase	EC 2.1.3.3 Transferase	Cytosol
	arcC (*lmo0039*)	Carbamate kinase	EC 2.7.2.2 Phosphotransferases with a carboxy group as acceptor	Cytosol
Agmatine deiminase (AgDI) system	*aguA1* (*lmo0038*)	Agmatine deiminases 1	EC 3.5.3.12 Agmatine iminohydrolase 1	Cytoplasm
	aguA2 (*lmo0040*)	Putative agmatine deiminase 2		
	ptcA (*lmo0036*)	Putrescine carbamoyltransferase	EC 2.1.3.6 Carbamoyltransferase	Cytoplasm
	aguC (*lmo0039*)	Carbamate kinase	EC 2.7.2.2 Transferases	Cytosol
	lmo0037	Agmatine/ putrescine antiporter associated with agmatine catabolism		Integral component of membrane

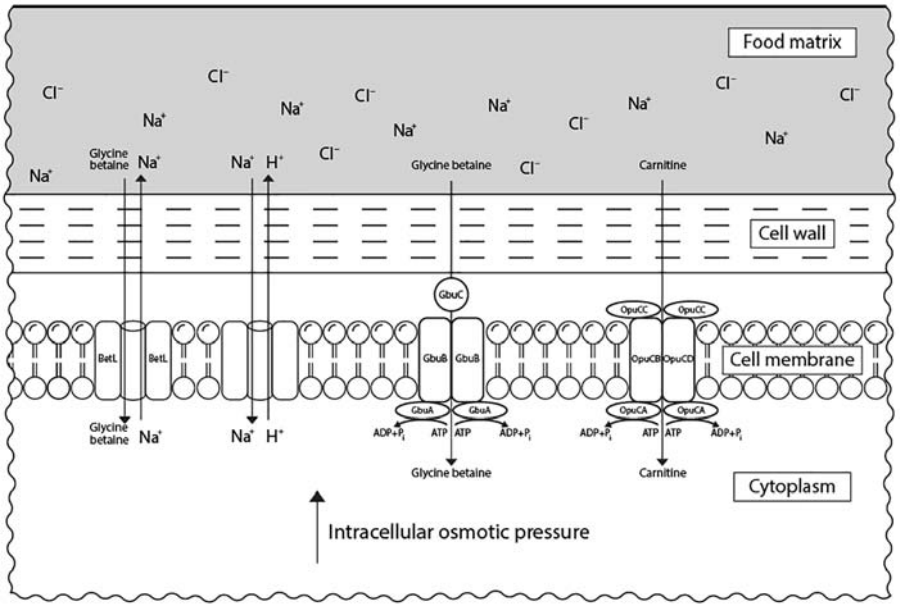

FIGURE 2 | Transport systems of compatible solutes in *L. monocytogenes* associated with its resistance to osmotic stress in food matrices. Under salt stress, *L. monocytogenes* accumulates compatible solutes (carnitine and glycine betaine) *via* specific transport systems from the external medium (food matrix). Carnitine is transported via OpuCABCD system, while glycine betaine can be accumulated via both GbuABC and BetL systems. The presence of compatible solutes in cytoplasm leads to an increase in the intracellular osmotic pressure which restores cell turgor.

The same is true for AgDI, which converts agmatine into putrescine and NH_3 (Chen et al., 2011).

Resistance to Osmotic Stress

Osmotic stress in food is mostly the result of increased concentrations of salts or sugars that are added to improve the sensory properties and as preserving agents to increase the shelf life of seafood, cheese, salami, pickles, jams, or syrups (Burgess et al., 2016). The presence and concentration of these additives determine water activity (Duché et al., 2002b) and affect bacterial cells by challenging the osmotic balance between cytoplasm and extracellular environment (Bae et al., 2012).

In response to elevated concentrations of salt, *L. monocytogenes* accumulates osmolytes, known also as compatible solutes, such as carnitine and glycine betaine in the cytoplasm to reduce osmotic pressure and water loss (Duché et al., 2002a). Besides their property to keep turgor pressure under control, compatible solutes were also shown to stabilize enzymes' structure and function during stress (Lippert and Galinski, 1992). This mechanism is mediated by an increased expression of genes encoding for proteins involved in the transport of the respective compatible solutes (Cacace et al., 2010; Bae et al., 2012). These are the main carnitine transport system encoded by *opuCABCD* operon, the glycine betaine porter II system, encoded by *gbuABC*, and the sodium-motive-force-dependent glycine betaine uptake system, encoded by *betL* (Chan et al., 2007; **Figure 2**). L-carnitine is present in raw meat in relevant quantities (Vermassen et al., 2016), while glycine betaine is found in vegetables (e.g., sugar beet, spinach, cereals) (Sleator et al., 1999). OpuCABCD couples ATP hydrolysis to osmolyte transport across the cytoplasmic membrane (Wemekamp-Kamphuis et al., 2004a). This system is formed of OpuCA that hydrolyses ATP providing the energy for transport of the substrate by a complex consisting of the two transmembrane proteins OpuCB and OpuCD and a solute-binding protein OpuCC (Fraser et al., 2000). While BetL is involved in the primary response of *L. monocytogenes* to salt, GbuABC seems to administer the capacity of this bacterium to tolerate such stress during a long-term exposure (Sleator et al., 2003b).

In response to osmotic stress, *L. monocytogenes* can also adjust expression levels of genes other than those associated with osmolytes accumulation. For example, growth of *L. monocytogenes* under salt stress resulted in increased expression of genes for Csps, especially *cspA* and *cspD*, promoting also adaptation to cold stress. The chaperone activity of these proteins is thought to facilitate the repair of DNA lesions, since NaCl has been shown to induce DNA breaks (Dmitrieva et al., 2004; Schmid et al., 2009). On the other hand, Bae and colleagues showed that presence of salt in the growth medium led to a decreased expression of genes associated with carbohydrate PTS systems in *L. monocytogenes* including those related to uptake of β-glucoside, galactitol, fructose, and cellobiose. This suggests a possible connection between a significantly lower growth rate and reduced uptake of carbohydrates under osmotic stress (Bae et al., 2012).

While accumulation of compatible solutes plays the main role in *L. monocytogenes*' survival to hyper-osmotic shock, a potential response of this bacterium to hypo-osmotic conditions may be mediated by mechanosensitive channels. Bacterial

mechanosensitive ion channels regulate turgor pressure by assisting efflux of osmolytes (Perozo and Rees, 2003). So far, genes for two putative mechanosensitive channels have been identified in *L. monocytogenes*. The *lmo2064* gene shows significant homology to *mscL* from *E. coli*, which encodes for a large-conductance mechanosensitive channel (MscL). Additionally, lmo1013 is similar to mscS of Streptococcus pneumoniae encoding for a small-conductance mechanosensitive channel (MscS) (Sleator et al., 2003a; Renier et al., 2012). After subjection to osmotic downshock, *L. monocytogenes* cells have been shown to release almost instantaneously betaine and L-carnitine, which may be linked to the activity of these channels (Verheul et al., 1997a).

Resistance to Bacteriocins

Bacteriocins are antimicrobial peptides produced by a wide range of LAB and are mostly active against Gram-positive bacteria including *L. monocytogenes* (Cotter et al., 2013; Chikindas et al., 2018). Bacteriocins are natural and safe food additives for a wide range of food products including fruits, vegetables, dairy products, and meat, that are either produced *in situ* by LAB used for food fermentation or added exogenously (Silva et al., 2018). Most bacteriocins are highly specific for their target organisms and kill their targets by inhibiting growth, disruption of membrane homeostasis and pore formation (Zhang and Gallo, 2016).

The only bacteriocin approved as preserving additive in food is nisin, which belongs to the class I bacteriocins and has a broad activity against various Gram-positive bacteria (Cleveland et al., 2001). Nisin is widely used in dairy and meat products with the purpose to inhibit the growth of food-borne pathogens including *L. monocytogenes* and *Clostridium botulinum* (Gharsallaoui et al., 2016). The antimicrobial activity of this bacteriocin is mediateded by two mechanisms. Nisin inhibits the cell wall biosynthesis by binding and sequestering lipid II, which is an essential carrier molecule for peptidoglycan building blocks. Moreover, nisin-lipid II complexes form pores in the membrane leading to permeabilization (Wiedemann et al., 2001).

Resistance of *L. monocytogenes* to nisin has been associated with a series of changes in the cytoplasmic membrane composition aiming to prevent the peptide from crossing this barrier. The studies conducted on nisin-resistant (Nis^r) cells noticed a reduction in the content of phospholipids with particular emphasis on phosphatidylglycerol and diphosphatidylglycerol, major components correlated with the interaction between nisin and membrane (Ming and Daeschel, 1995; Verheul et al., 1997b). In addition, it was indicated an increase in the proportion of straight-chain fatty acids to the detriment of branched-chain fatty acids, changes that result in a less fluid and, in the same time, more rigid cell membrane (Ming and Daeschel, 1993). The alterations in the cell wall of Nis^r strains of *L. monocytogenes* have been also investigated. The resistance of Nis^r cells to the degradation action of lysozyme and their sensitivity to benzylpenicillin and ampicillin suggested compositional changes that occurred at the level of this cellular component (Crandall and Montville, 1998). One example could be the D-alanine esterification of teichoic acids (Vadyvaloo et al., 2004). However, a recent transcriptomic analysis of *L. monocytogenes* survival cells following the exposure to a high nisin concentration reported the downregulation of *dltA* and *dltB*, implying that D-alanine residues are not involved in the elevated resistance to this bacteriocin. The study also emphasized the expression regulation of two cell-wall associated genes: downregulation of *lmo2714* encoding for a peptidoglycan anchored protein and upregulation of *lmo2522* encoding for a cell wall-binding protein with possible implication in nisin tolerance (Wu et al., 2018).

In *L. monocytogenes*, nisin resistance is directly mediated by VirR (Grubaugh et al., 2018), the response regulator of the VirRS two component system previously described to be involved in resistance to stress (Mandin et al., 2005). However, in the case of nisin an ABC-transporter encoded by *virAB* seems to be responsible in perception of the stressor instead of the VirS receptor histidine kinase (Grubaugh et al., 2018). VirR mediates the resistance to nisin and other stresses of the cell envelop by regulating the *dltABCD* operon (Kang et al., 2015) that is responsible for modification of lipoteichoic acids (Abachin et al., 2002). Other two component systems that were shown to be involved in resistance to nisin are LiaRS and LisRK (Cotter et al., 2002; Collins et al., 2012; Bergholz et al., 2013). Genes/operons and their products regulated by these TCS with a reported role in resistance to nisin are *lmo2229* (Gravesen et al., 2004; Collins et al., 2012), *telA* (Collins et al., 2010b), *mprF* (Thedieck et al., 2006), *anrAB* (Collins et al., 2010a), and *dltABCD* (Abachin et al., 2002). With the exception of *telA*, all these genes have a known role in metabolism/biosynthesis of components of the membrane or cell wall. Similar to e.g., resistance to pH or salt stress, nisin resistance can also be induced by other stresses, e.g., increased salt concentrations (Bergholz et al., 2013).

Recently, a number of class II bacteriocins with activity against *L. monocytogenes* have been isolated and characterized including pediocins, sakacin P, leucocins, enterococin, mesentericin Y105, garvicin, linocin M18, and others (Eppert et al., 1997; Tosukhowong et al., 2012; Perez et al., 2014; Ovchinnikov et al., 2016; Ríos et al., 2018). *L. monocytogenes* and other bacteria are able to develop resistance to bacteriocins. Natural resistance is observed with a frequency of 1–8% depending on the bacteriocin and the *L. monocytogenes* strain tested (Macwana and Muriana, 2012). Consistent with the receptors and mechanisms of action of bacteriocins, resistant strains show altered expression or mutations in certain phosphotransferase systems (PTSs) (Vadyvaloo et al., 2002, 2004; Tymoszewska et al., 2017). For instance, a spontaneous leucocin-resistant mutant of *L. monocytogenes* B73 was lacking a putative IIAB subunit of a mannose PTS (Ramnath et al., 2000). Furthermore, pediocin PA-1-resistant *L. monocytogenes* 412 mutants overexpressed gene fragments associated with a β-glucoside-specific PTS (Gravesen et al., 2000). Similar results of other studies suggest that resistance of *L. monocytogenes* to class IIa bacteriocins is correlated with a general mechanism consisting of a lack in EII subunits of mannose PTS and a compensatory upregulation of the β-glucoside PTS genes (Dalet et al., 2001; Gravesen et al., 2002).

RESISTANCE OF *L. monocytogenes* TO STRESS DURING PROCESSING AND DECONTAMINATION USING ALTERNATIVE TECHNOLOGIES

In recent years, a number of novel technologies are applied by the industry for production and preservation of minimally processed foods and diminish the impact of chemical substances on the environment. Consequently this results in new stress conditions encountered by *L. monocytogenes*.

Resistance to High Hydrostatic Pressure

High pressure processing (HPP) is a technology used in food preservation as an alternative to thermal treatments, aiming to destroy food spoilage microorganisms and food-borne pathogens (Huang et al., 2014). Depending on the food and spoilage organisms, pressures applied for sterilization are usually between 250 and 700 MPa. Bacterial cells subjected to HPP treatments display morphological and physiological changes that may be reversible depending on pressure and holding time. Primary effects of HPP are an increase in the permeability of the cell membrane, the disruption of the protein structure and function, and, as a consequence, inhibition of the metabolism, replication, and transcription (Huang et al., 2014).

The effect of HPP on survival of *L. monocytogenes* was tested under various settings in different food products including cheese (Tomasula et al., 2014), fruit juice (Alpas and Bozoglu, 2003), jams (Préstamo et al., 1999), whole milk (Hayman et al., 2007), and RTE cooked meat products (Hereu et al., 2012). Overall, the results of these studies indicate that resistance of *L. monocytogenes* to HPP varies depending on the strain. For instance, when pressured with 350 MPa at 20°C, *L. monocytogenes* EGD-e displayed only 1.0 log CFU/mL reduction and was more resistant to this HPP treatment than LO28 strain (1.8 log CFU/mL reduction) and ScottA strain (3.2 log CFU/mL reduction) (Van Boeijen et al., 2008). In addition, the type, composition and matrix of food products have an impact on the resistance of bacteria to HPP. Vitamins, amino acids, and cations (Ca^{2+}, Mg^{2+}) may have protective effects. For example, Mg^{2+} is known to stabilize ribosome structure and Ca^{2+} strengthens the outer membrane (Niven et al., 1999). Also, elevated salt concentrations in a food product may induce uptake of compatible solutes, which in turn stabilize cells during HPP (Abe, 2007). In line with this, a mutant deficient in synthesis of the compatible solute proline showed increased sensitivity to HPP (Considine et al., 2011)

The effect of HPP on *L. monocytogenes* was investigated on the global transcriptomic level by microarray analysis with subsequent RT-PCR on some target genes (Bowman et al., 2008). This indicated that mRNA levels were reduced globally with increasing intensity and duration of the treatment. Nevertheless, HPP induced expression of genes associated with DNA repair, transcription, translation, cell division, protein secretion, motility, chemotaxis, and membrane and cell wall biosynthesis. On the other hand, reduced expression was observed for genes involved in carbohydrates' uptake, energy metabolism and virulence. Surprisingly, HPP seemed to reduce expression of the general stress sigma factor SigB and part of the SigB regulon. One of the genes showing highest induction by HPP was *cspL* encoding a cold-shock protein. This suggests that HPP also induces cross-resistance to other stresses. For example, HPP resistance in semi-skimmed milk was higher than in buffer and the resistant isolate was also more resistant to heat, acid, and oxidative stress (Karatzas and Bennik, 2002).

Mutations in CtsR, a class III stress genes repressor (Nair et al., 2000), have been linked to spontaneous resistance of *L. monocytogenes* cells to HPP. Mutants with a stable resistance showed point mutations, insertions or deletions in the *ctsR* gene that negatively affected its activity. This loss in *ctsR* function in HPP resistant variants of *L. monocytogenes* was accompanied by increased expression of *clpB*, *clpC*, *clpE*, and *clpP* (Karatzas et al., 2003; Van Boeijen et al., 2010). Clp proteases have a clear role in degradation of misfolded or damaged proteins preventing their potentially harmful accumulation in bacterial cells (Krüger et al., 2000; Tomoyasu et al., 2001). Since protein denaturation is one of the consequences of HPP treatment (Moreirinha et al., 2016) increased Clp protease activity is in line with increased HPP tolerance in *L. monocytogenes*. However, isolation of resistant mutants that do not display these changes indicates that there may be other unknown mechanisms conferring resistance to HPP (Karatzas et al., 2005). Moreover, Chen et al. (2009) reported that different levels of HPP resistance among *L. monocytogenes* strains are not based on *ctsR* gene mutations.

*L. mononcytogene*s ScottA and a spontaneous HPP resistant isolate of this strain were shown to be more resistant to HPP in stationary compared to exponential growth phase (Karatzas and Bennik, 2002). Moreover, it seems that cells in stationary phase of growth do not exhibit the highest resistance to HPP treatment. *L. monocytogenes* cells found in long-term-survival phase showed even higher HPP tolerance, as transition back to log and stationary phases resulted in less survivors after pressurization. This phenomenon has been attributed to a change in cell morphology from rods to cocci that results in cytoplasmic condensation and, implicitly, reduction of intracellular water activity (Wen et al., 2009).

Resistance to UV-Light

Another more recent method of food decontamination, included under the umbrella of alternative technologies, is pulsed or continuous UV-light, which kills microorganisms found on the surface of food products as result of cross-contamination occurring during processing procedures such as cutting, slicing or packing (Gómez-López et al., 2007). Although approved by the United States and Food and Drug Administration (USFDA) for food application in 1996, the safety of this technology regarding the potential of permanent microbial inactivation still remains under question.

The bactericidal effect of UV light is caused by DNA damage as a consequence of the formation of photoproducts including cyclobutane-pyrimidine dimers (CPDs), pyrimidine 6-4 pyrimidone photoproducts (6-4PPs), and their Dewar isomers (Rastogi et al., 2010). Other mechanisms of bacteria inactivation caused by UV light are the photophysical and photothermal

effects resulting in leakage of cellular content following the absorption of the high energy light pulses (Gómez-López et al., 2007). The efficacy of UV treatment in decontamination of food surfaces depends on a number of factors including the food product, distance and position of the product to the light source, energy level given by number and frequency of the light pulses, level of contamination and others (Gómez-López et al., 2007). The potential of UV-C light in *L. monocytogenes* inactivation was shown to be lower on fruits with smooth surface (apples and pears) compared to fruits with a rougher surface (cantaloupe, strawberry or raspberry) (Adhikari et al., 2015). UV light is also used as disinfection procedure to improve hygiene in food processing environments (Bintsis et al., 2000). The presence of organic materials such as food debris on stainless steel surfaces appeared to protect *L. monocytogenes* cells against UV-C radiation (Bernbom et al., 2011).

Several studies have been conducted in order to investigate the efficacy of *L. monocytogenes* inactivation by pulsed UV-light on/within various food matrices. A maximum of inactivation of *L. monocytogenes* ScottA on the skin side of salmon filets was achieved with 180 pulses of UV light of 5.6 J/cm^2 at a distance of 8 cm for 60 s and efficacy was markedly lower on the muscle side (Ozer and Demirci, 2006). Similarly, the best inactivation rates of the same strain on chicken frankfurters was obtained with 180 pulses in 60 s at UV energy of 1.27/cm^2 (Keklik et al., 2009).

L. monocytogenes has been reported to be more resistant to UV-light than other pathogens, such as *E. coli* (Beauchamp and Lacroix, 2012). However, very little is known regarding specific mechanisms of UV resistance in *L. monocytogenes*. Sublethal challenge with other stresses does not induce cross-resistance to UV light and UV resistance does not seem to depend on SigB, the general stress sigma factor of *L. monocytogenes* (Gayán et al., 2015). Global gene expression analysis of the response to both pulsed light (PL) and continuous ultraviolet treatment was conducted in *L. monocytogenes* 10403S (Uesugi et al., 2016). Although the overall amplitude of the changes in gene expression was low, a number of genes encoding for stress proteins, motility and transcriptional regulators were induced by UV exposure. However, no increased expression was observed for *lmo0588*. This gene encodes for a (putative) photolyase. This protein plays an important role in photoreactivation, which is the recovery of bacteria sublethally injured by UV light due to subsequent exposure of visible light (Gómez-López et al., 2007). During photoreactivation, photolyase binds and repairs the pyrimidine DNA lesions using light energy absorbed by its chromophores (Sinha and Häder, 2002). In fact, an increase in viability was observed for a UV-treated *L. monocytogenes* serotype 1/2b after incubation in daylight for only 90 min followed by storage under dark (Lasagabaster and Martínez de Marañón, 2017).

Resistance to Pulsed Electric Fields

Pulsed electric fields (PEF) processing is another non-thermal alternative technology for decontamination mainly used in liquid foods processing and thus is not limited to inactivation on the surface of a product. The treatment consists of short, highly intense pulses of electric fields applied to the products in order to achieve the inactivation of unwanted microorganisms (Góngora-Nieto et al., 2002). The inactivating effects of PEF are destabilization and, depending on the strength of the PEF, irreversible damage of the cytoplasmic membrane with formation of micropores and leakage of cytoplasmic content (Góngora-Nieto et al., 2002). Similar to HPP and UV light but unlike conventional thermal food processing technologies, such as pasteurization, this method is less detrimental to food matrices and better in preserving the sensory and nutritional characteristics of the product (Toepfl et al., 2007). The efficacy of inactivation by PEF is determined by a number of factors related to the process (strength, duration, frequency of the pulses, temperature, etc.), the food product (composition, conductivity, pH, etc.) and the microorganisms to be inactivated (species, growth phase, etc.) (Wouters et al., 2001).

In general, Gram-positive organisms are believed to be more resistant to PEF than Gram-negative bacteria, presumably due to the thicker cell wall and stiffening (lipo)teichoic acids (Lado and Yousef, 2002). For example, *L. monocytogenes* proved to be more PEF tolerant than *Salmonella enteritidis* and *E. coli* when treated in melon and watermelon juices (Mosqueda-Melar et al., 2007). Thus, PEF alone is probably not the method of choice for inactivation of *L. monocytogenes*. It has been recommended to combine PEF with other methods such as ozone (Unal et al., 2001), mild heat (Fleischman et al., 2004) or plants infusions with antimicrobial properties (Rivas et al., 2016) to decontaminate food products at risk for contamination with *L. monocytogenes*. Low inactivation rates were observed for *L. monocytogenes* in a Spanish vegetable-based beverage and this was attributed to the neutral pH of the product (Selma et al., 2006). In fact, in buffer inactivation rates of *L. monocytogenes* by PFE were higher at acidic pH (Álvarez et al., 2002; Gómez et al., 2005; Saldaña et al., 2009). Further data in buffered systems or culture media indicated that resistance to PEF was increased in stationary growth phase and in media with reduced water activities (Álvarez et al., 2002; Lado and Yousef, 2003) suggesting a cross-resistance with other stresses.

Besides membrane disruption, PEF was suggested to affect bacterial cells by denaturation of the membrane-bound proteins as result of localized overheating caused by the capacity of the formed pores to conduct electricity (Simpson et al., 1999). This might imply an involvement of chaperones in the response of *L. monocytogenes* to PEF. One study compared the expression levels of three major molecular chaperones, namely GroEL, GroES, and DnaJ, in a resistant and a sensitive *L. monocytogenes* strain treated with a sublethal PFE challenge and found a transient reduction in expression of these chaperones in the sensitive strain (Lado et al., 2004).

Somolinos and colleagues have shown no difference in the resistance to PEF processing between *L. monocytogenes* EGD-e and its isogenic Δ*sigB* mutant suggesting that SigB is not involved in the repair mechanism of injured cells as shown for thermal treatment of the same strains. Also, unlike heat challenge, mild acid shock applied to *L. monocytogens* cells did not increase the resistance to subsequent PEF treatment (Somolinos et al., 2010).

Resistance to Oxidative Stress

Under oxidative stress (bacterial) cells encounter high concentrations of oxygen radicals (Suo et al., 2014). This disturbs the normal redox state of cells leading to cell death due to the oxidative damage of proteins, lipids and nucleic acids. Bacteria use reduction pathways that repair damage of susceptible amino acids (cysteine and methionine) induced by reactive oxygen (ROS) or reactive chlorine species (RCS). ROS are a group of compounds containing oxygen on different redox states such as hydrogen peroxide, hydroxyl radical or peroxyl radical. In bacteria, these compounds activate enzymes such as superoxide dismutases (SOD), catalases, peroxidases and efflux pumps to counteract oxidative stress (Dröge, 2003; Archambaud et al., 2006).

Recently, Harter and colleagues revealed the presence of a novel stress survival islet (SSI-2) in *L. monocytogenes* ST121 and other strains isolated from food and food processing environments. The SSI-2 consists of two genes *lin*0464 and *lin*0465 (PfpI protease), that are upregulated after 10 min of exposure to oxidative stress. Lin0464 seems to be a positive gene regulator of *lin0465*, because the time frame of increased transcription of *lin0465* is longer compared to that of *lin0464* and because the constitutive expression of *lin0464* has no effect on the survival rate in Δ*lin0465* mutant. Under alkaline or oxidative stress encountered in food processing environments, the expression of both genes offers *L. monocytogenes* ST121 the possibility to adapt and survive, an independent response mechanism from the alternative sigma factor (Harter et al., 2017).

Even if SigB is the main regulator of stress genes, its role in the oxidative stress resistance is controversial. A number of authors (Ferreira et al., 2001; Oliver et al., 2010) provided experimental data suggesting that, in *L. monocytogenes,* oxidative stress protection is conferred by σ^B since Δ*sigB* mutant cells are sensitive to this stress. Other studies suggested that *sigB* expression is harmful for stationary-phase *L. monocytogenes* (EGD-e and 10403S) cells grown aerobically, under oxidative stress conditions mediated by hydrogen peroxide. Furthermore, Δ*sigB* mutant proved, besides oxidative stress resistance, a stronger catalase activity upon addition of 30% H_2O_2, compared to the wild type. Interestingly, no difference was observed in the transcription of the catalase gene between the Δ*sigB* mutant and the wild type (Boura et al., 2016). All these discrepancies within the role of *sigB* in oxidative stress response may be explained by variation between strains (Moorhead and Dykes, 2003), oxidative agents tested, differences in growth phase, and oxygen tension of the culture (Boura et al., 2016).

In *L. monocytogenes*, the resistance to oxidative stress was also correlated with biofilm formation (Suo et al., 2012). Four genes related to oxidative stress, *kat*, *perR* (peroxide operon regulator), *sigB* and *recA* (recombinase A) were upregulated in a Δ*sod* mutant, which produced more ROS than the wild-type *L. monocytogenes* 4b G (Suo et al., 2014). Also, a Δ*perR L. monocytogenes* mutant showed increased sensitivity to hydrogen peroxide stress. Moreover, catalase activity in these cells increased to a toxic level resulting in smaller colonies and changes in cell morphology compared to the wild type (Rea et al., 2005).

The anti-oxidative *kat* gene acts synergistically with *sod* gene (superoxide dismutase), both being involved in the protection against toxic effects of hydrogen peroxide and superoxide anion radicals (Suo et al., 2012). The *sodA* gene encodes for MnSOD, a cytosolic SOD enzyme which uses manganese in the catalytic reactions. Archambaud and colleagues reported that, during stationary phase, *L. monocytogenes* MnSOD activity is downregulated by phosphorylation at serine/threonine residues. MnSOD activity increases only when dephosphorylation is performed, condition that facilitates its secretion in the bacterial culture media via SecA2 pathway (Archambaud et al., 2006).

Other genes involved in the response to oxidative stress are *fri*, *gltB,* and *gltC*. Based on its iron-binding activity, *fri*-encoded ferritin detoxifies oxidative agents (Dussurget et al., 2005; Olsen et al., 2005). Huang and colleagues introduced a role of *glt*B and *glt*C gene products in oxidative stress and *L. monocytogenes* biofilm formation. GltC is a member of LysR-type transcriptional regulator and *gltB* encodes for a glutamate synthase regulated by GltC. Experiments with *gltB* and *gltC* mutants revealed a reduced ability to form biofilm and an increased sensitivity to oxidative stress (Huang et al., 2013).

CONCLUSION

L. monocytogenes is able to use diverse mechanisms to survive various stress conditions encountered in food matrices. This explains the efforts made by scientists to understand these mechanisms in order to develop more efficient methods to reduce *L. monocytogenes* occurrence in food and food related environments. With the present review, we aim at providing an overview of the current knowledge on food-related stress and stress resistance of *L. monocytogenes*. As observed for many other organisms, *L. monocytogenes* employs different survival mechanisms for the same stress or use the same mechanism for different stresses (heat-shock genes are expressed when *L. monocytogenes* is subjected to heat stress, HPP or PEF; cold-shock genes are expressed and osmolytes transport systems are activated when *L. monocytogenes* encounters cold or osmotic stress). However, compared to other organisms, the large number of mechanisms also increases the possibilities of this organism for cross-resistance.

The ongoing trend toward healthier, minimally processed food products with unaltered sensory and nutritional properties demands new strategies for food preservation, while no compromises are accepted for food safety. Alternative treatments (e.g., high pressure, pulsed electrical field, UV light), have yielded promising results, but their application often allows to *L. monocytogenes* recovery. However, current data also suggest that combinations of these techniques with e.g., natural preserving additives such as bacteriocins may be feasible solutions. Nevertheless, the effects on and resistance of *L. monocytogenes* to such combinations of stresses need to be investigated.

AUTHOR CONTRIBUTIONS

FB and LG-G drafted the manuscript and all authors revised and contributed to its final version.

FUNDING

This study was funded within the ERA-IB2 consortium "SafeFood" (ID: ERA-IB-16- 247 014) by grants of the Executive Agency for Higher Education, Research, Development and Innovation Funding in Romania to AN (International and European Cooperation – 250 Subprogramme 3.2 – Horizon 2020 – Contract No. 15/2017) and by the German Ministry for Education and Research to CR (Grant No. 031B0268). The activity of FB was partially funded by the Doctoral School of Mechanical and Industrial Engineering belonging to "Dunarea de Jos" University of Galati.

ACKNOWLEDGMENTS

We thankfully acknowledge Cornel Leuştean for providing professional technical support for graphical representation of the molecular mechanisms.

REFERENCES

Abachin, E., Poyart, C., Pellegrini, E., Milohanic, E., Fiedler, F., Berche, P., et al. (2002). Formation of D-alanyl-lipoteichoic acid is required for adhesion and virulence of *Listeria monocytogenes*. *Mol. Microbiol.* 43, 1–14. doi: 10.1046/j.1365-2958.2002.02723.x

Abdel Karem, H., and Mattar, Z. (2001). Heat resistance and growth of *Salmonella enteritidis*, *Listeria monocytogenes* and *Aeromonas hydrophila* in whole liquid egg. *Acta Microbiol. Pol.* 50, 27–35.

Abe, F. (2007). Exploration of the effects of high hydrostatic pressure on microbial growth, physiology and survival: perspectives from piezophysiology. *Biosci. Biotechnol. Biochem.* 71, 2347–2357. doi: 10.1271/bbb.70015

Abram, F., Starr, E., Karatzas, K. A. G., Matlawska-Wasowska, K., Boyd, A., Wiedmann, M., et al. (2008). Identification of components of the sigma B regulon in *Listeria monocytogenes* that contribute to acid and salt tolerance. *Appl. Environ. Microbiol.* 74, 6848–6858. doi: 10.1128/AEM.00442-08

Adhikari, A., Syamaladevi, R. M., Killinger, K., and Sablani, S. S. (2015). Ultraviolet-C light inactivation of *Escherichia coli* O157:H7 and *Listeria monocytogenes* on organic fruit surfaces. *Int. J. Food Microbiol.* 210, 136–142. doi: 10.1016/j.ijfoodmicro.2015.06.018

Albarracín, W., Sánchez, I. C., Grau, R., and Barat, J. M. (2011). Salt in food processing; usage and reduction: a review. *Int. J. Food Sci. Technol.* 46, 1329–1336. doi: 10.1111/j.1365-2621.2010.02492.x

Alpas, H., and Bozoglu, F. (2003). Efficiency of high pressure treatment for destruction of *Listeria monocytogenes* in fruit juices. *FEMS Immunol. Med. Microbiol.* 35, 269–273. doi: 10.1016/S0928-8244(02)00446-7

Álvarez, I., Pagán, R., Raso, J., and Condón, S. (2002). Environmental factors influencing the inactivation of *Listeria monocytogenes* by pulsed electric fields. *Lett. Appl. Microbiol.* 35, 489–493. doi: 10.1046/j.1472-765X.2002.01221.x

Angelidis, A. S., and Smith, G. M. (2003). Role of the glycine betaine and carnitine transporters in adaptation of *Listeria monocytogenes* to chill stress in defined medium. *Appl. Environ. Microbiol.* 69, 7492–7498. doi: 10.1128/AEM.69.12.7492-7498.2003

Archambaud, C., Nahori, M.-A., Pizarro-Cerda, J., Cossart, P., and Dussurget, O. (2006). Control of *Listeria* superoxide dismutase by phosphorylation. *J. Biol. Chem.* 281, 31812–31822. doi: 10.1074/jbc.M606249200

Bae, D., Liu, C., Zhang, T., Jones, M., Peterson, S. N., and Wang, C. (2012). Global gene expression of *Listeria monocytogenes* to salt stress. *J. Food Prot.* 75, 906–912. doi: 10.4315/0362-028X.JFP-11-282

Barria, C., Malecki, M., and Arraiano, C. M. (2013). Bacterial adaptation to cold. *Microbiology* 159(Pt 12), 2437–2443. doi: 10.1099/mic.0.052209-0

Bartlett, F. M., and Hawke, A. E. (1995). Heat resistance of *Listeria monocytogenes* Scott A and HAL 957E1 in various liquid egg products. *J. Food Prot.* 58, 1211–1214. doi: 10.4315/0362-028X-58.11.1211

Beales, N. (2004). Adaptation of microorganisms to cold temperatures, weak acid preservatives, low pH, and osmotic stress: a review. *Compr. Rev. Food Sci. Food Saf.* 3, 1–20. doi: 10.1111/j.1541-4337.2004.tb00057.x

Beauchamp, S., and Lacroix, M. (2012). Resistance of the genome of *Escherichia coli* and *Listeria monocytogenes* to irradiation evaluated by the induction of cyclobutane pyrimidine dimers and 6-4 photoproducts using gamma and UV-C radiations. *Radiat. Phys. Chem.* 81, 1193–1197. doi: 10.1016/j.radphyschem.2011.11.007

Becker, L. A., Evans, S. N., Hutkins, R. W., and Benson, A. K. (2000). Role of σB in adaptation of *Listeria monocytogenes* to growth at low temperature. *J. Bacteriol.* 182, 7083–7087. doi: 10.1128/JB.182.24.7083-7087.2000

Bergholz, T. M., Tang, S., Wiedmann, M., and Boor, K. J. (2013). Nisin resistance of *Listeria monocytogenes* is increased by exposure to salt stress and is mediated via LiaR. *Appl. Environ. Microbiol.* 79, 5682–5688. doi: 10.1128/AEM.01797-13

Bernbom, N., Vogel, B. F., and Gram, L. (2011). *Listeria monocytogenes* survival of UV-C radiation is enhanced by presence of sodium chloride, organic food material and by biofilm formation. *Int. J. Food Microbiol.* 147, 69–73. doi: 10.1016/j.ijfoodmicro.2011.03.009

Berrang, M. E., Meinersmann, R. J., Frank, J. F., and Ladely, S. R. (2010). Colonization of a newly constructed commercial chicken further processing plant with *Listeria monocytogenes*. *J. Food Prot.* 73, 286–291. doi: 10.4315/0362-028X-73.2.286

Bintsis, T., Litopoulou-Tzanetaki, E., and Robinson, R. K. (2000). Existing and potential applications of ultraviolet light in the food industry – a critical review. *J. Sci. Food Agric.* 80, 637–645. doi: 10.1002/(SICI)1097-0010(20000501)80:6

Bolocan, A. S., Nicolau, A. I., Álvarez-Ordóñez, A., Borda, D., Oniciuc, E. A., Stessl, B., et al. (2016). Dynamics of *Listeria monocytogenes* colonisation in a newly-opened meat processing facility. *Meat Sci.* 113, 26–34. doi: 10.1016/j.meatsci.2015.10.016

Boura, M., Keating, C., Royet, K., Paudyal, R., O'Donoghue, B., O'Byrne, C. P., et al. (2016). Loss of SigB in *Listeria monocytogenes* strains EGD-e and 10403S confers hyperresistance to hydrogen peroxide in stationary phase under aerobic conditions. *Appl. Environ. Microbiol.* 82, 4584–4591. doi: 10.1128/AEM.00709-16

Bowman, J. P., Bittencourt, C. R., and Ross, T. (2008). Differential gene expression of *Listeria monocytogenes* during high hydrostatic pressure processing. *Microbiology* 154(Pt 2), 462–475. doi: 10.1099/mic.0.2007/010314-0

Buchanan, R. L., Gorris, L. G. M., Hayman, M. M., Jackson, T. C., and Whiting, R. C. (2017). A review of *Listeria monocytogenes*: an update on outbreaks, virulence, dose-response, ecology, and risk assessments. *Food Control* 75, 1–13. doi: 10.1016/j.foodcont.2016.12.016

Burgess, C. M., Gianotti, A., Gruzdev, N., Holah, J., Knøchel, S., Lehner, A., et al. (2016). The response of foodborne pathogens to osmotic and desiccation stresses in the food chain. *Int. J. Food Microbiol.* 221, 37–53. doi: 10.1016/j.ijfoodmicro.2015.12.014

Cacace, G., Mazzeo, M. F., Sorrentino, A., Spada, V., Malorni, A., and Siciliano, R. A. (2010). Proteomics for the elucidation of cold adaptation mechanisms in *Listeria monocytogenes*. *J. Proteomics* 73, 2021–2030. doi: 10.1016/j.jprot.2010.06.011

Caplice, E., and Fitzgerald, G. F. (1999). Food fermentations: role of microorganisms in food production and preservation. *Int. J. Food Microbiol.* 50, 131–149. doi: 10.1016/S0168-1605(99)00082-3

Casadei, M. A., de Matos, R. E., Harrison, S. T., and Gaze, J. E. (1998). Heat resistance of *Listeria monocytogenes* in dairy products as affected by the growth medium. *J. Appl. Microbiol.* 84, 234–239. doi: 10.1046/j.1365-2672.1998.00334.x

Chan, Y. C., Raengpradub, S., Boor, K. J., and Wiedmann, M. (2007). Microarray-based characterization of the *Listeria monocytogenes* cold regulon in log- and stationary-phase cells. *Appl. Environ. Microbiol.* 73, 6484–6498. doi: 10.1128/AEM.00897-07

Chan, Y. C., and Wiedmann, M. (2009). Physiology and genetics of *Listeria monocytogenes* survival and growth at cold temperatures. *Crit. Rev. Food Sci. Nutr.* 49, 237–253. doi: 10.1080/10408390701856272

Chaturongakul, S., and Boor, K. J. (2004). RsbT and RsbV contribute to σB-dependent survival under environmental, energy, and intracellular stress conditions in *Listeria monocytogenes*. *Appl. Environ. Microbiol.* 70, 5349–5356. doi: 10.1128/AEM.70.9.5349-5356.2004

Chaturongakul, S., and Boor, K. J. (2006). σB activation under environmental and energy stress conditions in *Listeria monocytogenes*. *Appl. Environ. Microbiol.* 72, 5197–5203. doi: 10.1128/AEM.03058-05

Chaturongakul, S., Raengpradup, S., Wiedmann, M., and Boor, K. J. (2008). Modulation of stress and virulence in *Listeria monocytogenes*. *Trends Microbiol.* 16, 388–396. doi: 10.1016/j.tim.2008.05.006

Chen, H., Neetoo, H., Ye, M., and Joerger, R. D. (2009). Differences in pressure tolerance of *Listeria monocytogenes* strains are not correlated with other stress tolerances and are not based on differences in CtsR. *Food Microbiol.* 26, 404–408. doi: 10.1016/j.fm.2009.01.007

Chen, J., Cheng, C., Xia, Y., Zhao, H., Fang, C., Shan, Y., et al. (2011). *Lmo0036*, an ornithine and putrescine carbamoyltransferase in *Listeria monocytogenes*, participates in arginine deiminase and agmatine deiminase pathways and mediates acid tolerance. *Microbiology* 157(Pt 11), 3150–3161. doi: 10.1099/mic.0.049619-0

Chikindas, M. L., Weeks, R., Drider, D., Chistyakov, V. A., and Dicks, L. M. T. (2018). Functions and emerging applications of bacteriocins. *Curr. Opin. Biotechnol.* 49, 23–28. doi: 10.1016/j.copbio.2017.07.011

Chorianopoulos, N., Giaouris, E., Grigoraki, I., Skandamis, P., and Nychas, G. (2011). Effect of acid tolerance response (ATR) on attachment of *Listeria monocytogenes* Scott A to stainless steel under extended exposure to acid or/and salt stress and resistance of sessile cells to subsequent strong acid challenge. *Int. J. Food Microbiol.* 145, 400–406. doi: 10.1016/j.ijfoodmicro.2011.01.001

Cleveland, J., Montville, T. J., Nes, I. F., and Chikindas, M. L. (2001). Bacteriocins: safe, natural antimicrobials for food preservation. *Int. J. Food Sci. Technol.* 71, 1–20. doi: 10.1016/S0168-1605(01)00560-8

Collins, B., Guinane, C. M., Cotter, P. D., Hill, C., and Ross, P. R. (2012). Assessing the contributions of the lias histidine kinase to the innate resistance of *Listeria monocytogenes* to nisin, cephalosporins, and disinfectants. *Appl. Environ. Microbiol.* 78, 2923–2929. doi: 10.1128/AEM.07402-11

Collins, B., Curtis, N., Cotter, P. D., Hill, C., and Ross, R. P. (2010a). The ABC transporter AnrAB contributes to the innate resistance of *Listeria monocytogenes* to nisin, bacitracin, and various β-lactam antibiotics. *Antimicrob. Agents Chemother.* 54, 4416–4423. doi: 10.1128/AAC.00503-10

Collins, B., Joyce, S., Hill, C., Cotter, P. D., and Ross, R. P. (2010b). TelA contributes to the innate resistance of *Listeria monocytogenes* to nisin and other cell wall-acting antibiotics. *Antimicrob. Agents Chemother.* 54, 4658–4663. doi: 10.1128/AAC.00290-10

Considine, K. M., Sleator, R. D., Kelly, A. L., Fitzgerald, G. F., and Hill, C. (2011). A role for proline synthesis and transport in *Listeria monocytogenes* barotolerance. *J. Appl. Microbiol.* 110, 1187–1194. doi: 10.1111/j.1365-2672.2011.04982.x

Cordero, N., Maza, F., Navea-Perez, H., Aravena, A., Marquez-Fontt, B., Navarrete, P., et al. (2016). Different transcriptional responses from slow and fast growth rate strains of *Listeria monocytogenes* adapted to low temperature. *Front. Microbiol.* 7:229. doi: 10.3389/fmicb.2016.00229

Cotter, P. D., Gahan, C. G. M., and Hill, C. (2000). Analysis of the role of the *Listeria monocytogenes* F0F1-ATPase operon in the acid tolerance response. *Int. J. Food Microbiol.* 60, 137–146. doi: 10.1016/S0168-1605(00)00305-6

Cotter, P. D., Gahan, C. G. M., and Hill, C. (2001). A glutamate decarboxylase system protects *Listeria monocytogenes* in gastric fluid. *Mol. Microbiol.* 40, 465–475. doi: 10.1046/j.1365-2958.2001.02398.x

Cotter, P. D., Guinane, C. M., and Hill, C. (2002). The LisRK signal transduction system determines the sensitivity of *Listeria monocytogenes* to nisin and cephalosporins. *Antimicrob. Agents Chemother.* 46, 2784–2790. doi: 10.1128/AAC.46.9.2784-2790.2002

Cotter, P. D., and Hill, C. (2003). Surviving the acid test: responses of Gram-positive bacteria to low pH. *Microbiol. Mol. Biol. Rev.* 67, 429–453. doi: 10.1128/MMBR.67.3.429

Cotter, P. D., Ross, R. P., and Hill, C. (2013). Bacteriocins - a viable alternative to antibiotics? *Nat. Rev. Microbiol.* 11, 95–105. doi: 10.1038/nrmicro2937

Cotter, P. D., Ryan, S., Gahan, C. G. M., and Hill, C. (2005). Presence of GadD1 glutamate decarboxylase in selected *Listeria monocytogenes* strains is associated with an ability to grow at low pH. *Appl. Environ. Microbiol.* 71, 2832–2839. doi: 10.1128/AEM.71.6.2832

Crandall, A. D., and Montville, T. J. (1998). Nisin resistance in *Listeria monocytogenes* ATCC 700302 is a complex phenotype. *Appl. Environ. Microbiol.* 64, 231–237.

Dalet, K., Cenatiempo, Y., Cossart, P., and Héchard, Y. (2001). A σ54-dependent PTS permease of the mannose family is responsible for sensitivity *Listeria monocytogenes* to mesentericin Y105. *Microbiology* 147, 3263–3269. doi: 10.1099/00221287-147-12-3263

Davis, M. J., Coote, P. J., and O'Byrne, C. P. (1996). Acid tolerance in *Listeria monocytogenes*: the adaptive acid tolerance response (ATR) and growth-phase-dependent acid resistance. *Microbiology* 142, 2975–2982. doi: 10.1099/13500872-142-10-2975

Dmitrieva, N. I., Cai, Q., and Burg, M. B. (2004). Cells adapted to high NaCl have many DNA breaks and impaired DNA repair both in cell culture and *in vivo*. *Proc. Natl. Acad. Sci. U.S.A.* 101, 2317–2322. doi: 10.1073/pnas.0308463100

Doyle, M. E., Mazzotta, A. S., Wang, T., Wiseman, D. W., and Scott, V. N. (2001). Heat resistance of *Listeria monocytogenes*. *J. Food Prot.* 64, 410–429. doi: 10.4315/0362-028X-64.3.410

Doyle, M. P., Glass, K. A., Beery, J. T., Garcia, G. A., Pollard, D. J., and Schultz, R. D. (1987). Survival of *Listeria monocytogenes* in milk during high-temperature, short-time pasteurization. *Appl. Environ. Microbiol.* 53, 1433–1438.

Dröge, W. (2003). ""Oxidative stress and aging"," in *Hypoxia. Advances in Experimental Medicine and Biology*, Vol. 543, eds R. C. Roach, P. D. Wagner, and P. H. Hackett (Boston, MA: Springer), 191–200. doi: 10.1007/978-1-4419-8997-0_14

Duché, O., Trémoulet, F., Glaser, P., and Labadie, J. (2002a). Salt stress proteins induced in *Listeria monocytogenes*. *Appl. Environ. Microbiol.* 68, 1491–1498. doi: 10.1128/AEM.68.4.1491

Duché, O., Trémoulet, F., Namane, A., and Labadie, J. (2002b). A proteomic analysis of the salt stress response of *Listeria monocytogenes*. *FEMS Microbiol. Lett.* 215, 183–188.

Dussurget, O., Dumas, E., Archambaud, C., Chafsey, I., Chambon, C., Hebraud, M., et al. (2005). *Listeria monocytogenes* ferritin protects against multiple stresses and is required for virulence. *FEMS Microbiol. Lett.* 250, 253–261. doi: 10.1016/j.femsle.2005.07.015

Eppert, I., Valdés-Stauber, N., Götz, H., Busse, M., and Scherer, S. (1997). Growth reduction of *Listeria* spp. caused by undefined industrial red smear cheese cultures and bacteriocin-producing *Brevibacterium* lines as evaluated in situ on soft cheese. *Appl. Environ. Microbiol.* 63, 4812–4817.

Farber, J. M., Hughes, A., Holley, R., and Brown, B. (1989). Thermal resistance of *Listeria monocytogenes* in sausage meat. *Acta Microbiol. Hung.* 36, 273–275.

Farber, J. M., Sanders, G. W., Speirs, J. I., D'Aoust, J.-Y., Emmons, D. B., and McKellar, R. (1988). Thermal resistance of *Listeria monocytogenes* in inoculated and naturally contaminated raw milk. *Int. J. Food Microbiol.* 7, 277–286. doi: 10.1016/0168-1605(88)90054-2

Feehily, C., Finnerty, A., Casey, P. G., Hill, C., Gahan, C. G. M., O'Byrne, C. P., et al. (2014). Divergent evolution of the activity and regulation of the glutamate decarboxylase systems in *Listeria monocytogenes* EGD-e and 10403S: roles in virulence and acid tolerance. *PLoS One* 9:e112649. doi: 10.1371/journal.pone.0112649

Ferreira, A., O'Byrne, C. P., and Boor, K. J. (2001). Role of σB in heat, ethanol, acid, and oxidative stress resistance and during carbon starvation in *Listeria monocytogenes*. *Appl. Environ. Microbiol.* 67, 4454–4457. doi: 10.1128/AEM.67.10.4454-4457.2001

Ferreira, V., Wiedmann, M., Teixeira, P., and Stasiewicz, M. J. (2014). *Listeria monocytogenes* persistence in food-associated environments: epidemiology, strain characteristics, and implications for public health. *J. Food Prot.* 77, 150–170. doi: 10.4315/0362-028X.JFP-13-150

Fleischman, G. J., Ravishankar, S., and Balasubramaniam, V. M. (2004). The inactivation of *Listeria monocytogenes* by pulsed electric field (PEF) treatment in a static chamber. *Food Microbiol.* 21, 91–95. doi: 10.1016/s0740-0020(03)00015-7

Fleming, D. W., Cochi, S. L., MacDonald, K. L., Brondum, J., Hayes, P. S., Plikaytis, B. D., et al. (1985). Pasteurized milk as a vehicle of infection in an outbreak of listeriosis. *N. Engl. J. Med.* 312, 404–407. doi: 10.1056/NEJM198502143120704

Francis, G. A., Scollard, J., Meally, A., Bolton, D. J., Gahan, C. G. M., Cotter, P. D., et al. (2007). The glutamate decarboxylase acid resistance mechanism affects survival of *Listeria monocytogenes* LO28 in modified atmosphere-packaged foods. *J. Appl. Microbiol.* 103, 2316–2324. doi: 10.1111/j.1365-2672.2007.03466.x

Fraser, K. R., Harvie, D., Coote, P. J., and O'Byrne, C. P. (2000). Identification and characterization of an ATP binding cassette L-Carnitine transporter in *Listeria monocytogenes*. *Appl. Environ. Microbiol.* 66, 4696–4704. doi: 10.1128/AEM.66.11.4696-4704.2000

Fraser, K. R., Sue, D., Wiedmann, M., Boor, K., and O'Byrne, C. P. (2003). Role of σB in regulating the compatible solute uptake systems of *Listeria monocytogenes*: osmotic induction of *opuC* is σB dependent. *Appl. Environ. Microbiol.* 69, 2015–2022. doi: 10.1128/AEM.69.4.2015-2022.2003

Gahan, C. G., and Hill, C. (2014). *Listeria monocytogenes*: survival and adaptation in the gastrointestinal tract. *Front. Cell. Infect. Microbiol.* 4:9. doi: 10.3389/fcimb.2014.00009

Gandhi, M., and Chikindas, M. L. (2007). *Listeria*: a foodborne pathogen that knows how to survive. *Int. J. Food Microbiol.* 113, 1–15. doi: 10.1016/j.ijfoodmicro.2006.07.008

Gayán, E., Serrano, M. J., Pagán, R., Álvarez, I., and Condón, S. (2015). Environmental and biological factors influencing the UV-C resistance of *Listeria monocytogenes*. *Food Microbiol.* 46, 246–253. doi: 10.1016/j.fm.2014.08.011

Gaze, J. E., Brown, G. D., Gaskell, D. E., and Banks, J. G. (1989). Heat resistance of *Listeria monocytogenes* in homogenates of chicken, beef steak and carrot. *Food Microbiol.* 6, 251–259. doi: 10.1016/S0740-0020(89)80006-1

Gharsallaoui, A., Oulahal, N., Joly, C., and Degraeve, P. (2016). Nisin as a food preservative: part 1: physicochemical properties, antimicrobial activity, and main uses. *Crit. Rev. Food Sci. Nutr.* 56, 1262–1274. doi: 10.1080/10408398.2013.763765

Gómez, N., García, D., Álvarez, I., Condón, S., and Raso, J. (2005). Modelling inactivation of *Listeria monocytogenes* by pulsed electric fields in media of different pH. *Int. J. Food Microbiol.* 103, 199–206. doi: 10.1016/j.ijfoodmicro.2004.11.033

Gómez-López, V. M., Ragaert, P., Debevere, J., and Devlieghere, F. (2007). Pulsed light for food decontamination: a review. *Trends Food Sci. Technol.* 18, 464–473. doi: 10.1016/j.tifs.2007.03.010

Góngora-Nieto, M. M., Sepúlveda, D. R., Pedrow, P., Barbosa-Cánovas, G. V., and Swanson, B. G. (2002). Food processing by pulsed electric fields: treatment delivery, inactivation level, and regulatory aspects. *Food Sci. Technol.* 35, 375–388. doi: 10.1006/fstl.2001.0880

Gravesen, A., Kallipolitis, B., Holmstrøm, K., Høiby, P. E., Ramnath, M., and Knøchel, S. (2004). pbp2229-mediated nisin resistance mechanism in *Listeria monocytogenes* confers cross-protection to class IIa bacteriocins and affects virulence gene expression. *Appl. Environ. Microbiol.* 70, 1669–1679. doi: 10.1128/AEM.70.3.1669

Gravesen, A., Ramnath, M., Rechinger, K. B., Andersen, N., Jänsch, L., Héchard, Y., et al. (2002). High-level resistance to class IIa bacteriocins is associated with one general mechanism in *Listeria monocytogenes*. *Microbiology* 148, 2361–2369. doi: 10.1099/00221287-148-8-2361

Gravesen, A., Warthoe, P., Knøchel, S., and Thirstrup, K. (2000). Restriction fragment differential display of pediocin-resistant *Listeria monocytogenes* 412 mutants shows consistent overexpression of a putative β-glucoside-specific PTS system. *Microbiology* 146, 1381–1389. doi: 10.1099/00221287-146-6-1381

Grubaugh, D., Regeimbal, J. M., Ghosh, P., Zhou, Y., Lauer, P., Dubensky, T. W., et al. (2018). The VirAB ABC transporter is required for VirR regulation of *Listeria monocytogenes* virulence and resistance to nisin. *Infect. Immun.* 86, e901–e917. doi: 10.1128/IAI.00901-17

Hanawa, T., Kai, M., Kamiya, S., and Yamamoto, T. (2000). Cloning, sequencing, and transcriptional analysis of the dnak heat shock operon of *Listeria monocytogenes*. *Cell Stress Chaperones* 5, 21–29. doi: 10.1379/1466-1268(2000)005<0021:CSATAO>2.0.CO;2

Hardy, J., Parmentier, M., and Fanni, J. (1999). Functionality of nutrients and thermal treatments of food. *Proc. Nutr. Soc.* 58, 579–585. doi: 10.1017/s0029665199000762

Harter, E., Wagner, E. M., Zaiser, A., Halecker, S., Wagner, M., and Rychli, K. (2017). Stress survival Islet 2, predominantly present in *Listeria monocytogenes* strains of sequence type 121, is involved in the alkaline and oxidative stress responses. *Appl. Environ. Microbiol.* 83:e00827-17. doi: 10.1128/AEM.00827-17

Hartl, F. U., and Hayer-Hartl, M. (2002). Molecular chaperone in the cytosol: from nascent chain to folded protein. *Science* 295, 1852–1858. doi: 10.1126/science.1068408

Hayman, M. M., Anantheswaran, R. C., and Knabel, S. J. (2007). The effects of growth temperature and growth phase on the inactivation of *Listeria monocytogenes* in whole milk subject to high pressure processing. *Int. J. Food Microbiol.* 115, 220–226. doi: 10.1016/j.ijfoodmicro.2006.10.019

Hébraud, M., and Guzzo, J. (2000). The main cold shock protein of *Listeria monocytogenes* belongs to the family of ferritin-like proteins. *FEMS Microbiol. Lett.* 190, 29–34. doi: 10.1016/S0378-1097(00)00310-4

Hendrick, J. P., and Hartl, F. U. (1993). Molecular chaperone functions of heat shock proteins. *Annu. Rev. Biochem.* 62, 349–384. doi: 10.1146/annurev.bi.62.070193.002025

Hereu, A., Dalgaard, P., Garriga, M., Aymerich, T., and Bover-Cid, S. (2012). Modeling the high pressure inactivation kinetics of *Listeria monocytogenes* on RTE cooked meat products. *Innov. Food Sci. Emerg. Technol.* 16, 305–315. doi: 10.1016/j.ifset.2012.07.005

Hill, D., Sugrue, I., Arendt, E., Hill, C., and Stanton, C. (2017). Recent advances in microbial fermentation for dairy and health [version 1; referees:3 approved]. *F1000Res.* 6:751. doi: 10.12688/f1000research.10896.1

Horn, G., Hofweber, R., Kremer, W., and Kalbitzer, H. R. (2007). Structure and function of bacterial cold shock proteins. *Cell. Mol. Life Sci.* 64, 1457–1470. doi: 10.1007/s00018-007-6388-4

Huang, H. W., Lung, H. M., Yang, B. B., and Wang, C. Y. (2014). Responses of microorganisms to high hydrostatic pressure processing. *Food Control* 40, 250–259. doi: 10.1016/j.foodcont.2013.12.007

Huang, L. (2004). Thermal resistance of *Listeria monocytogenes*, *Salmonella heidelberg*, and *Escherichia coli* O157:H7 at elevated temperatures. *J. Food Prot.* 67, 1666–1670. doi: 10.4315/0362-028x-67.8.1666

Huang, Y., Suo, Y., Shi, C., Szlavik, J., Shi, X. M., and Knøchel, S. (2013). Mutations in *gltB* and *gltC* reduce oxidative stress tolerance and biofilm formation in *Listeria monocytogenes* 4b G. *Int. J. Food Microbiol.* 163, 223–230. doi: 10.1016/j.ijfoodmicro.2013.02.023

Johnson, E. M., Jung, D. Y., Jin, D. Y., Jayabalan, D. R., Yang, D. S. H., and Suh, J. V. (2017). Bacteriocins as food preservatives: challenges and emerging horizons. *Crit. Rev. Food Sci. Nutr.* 7, 1–25. doi: 10.1080/10408398.2017.1340870

Jørgensen, F., Hansen, T. B., and Knøchel, S. (1999). Heat shock-induced thermotolerance in *Listeria monocytogenes* 13-249 is dependent on growth phase, pH and lactic acid. *Food Microbiol.* 16, 185–194. doi: 10.1006/fmic.1998.0222

Jørgensen, F., Stephens, P. J., and Knøchel, S. (1995). The effect of osmotic shock and subsequent adaptation on the thermotolerance and cell morphology of *Listeria monocytogenes*. *J. Appl. Bacteriol.* 79, 274–281. doi: 10.1111/j.1365-2672.1995.tb03137.x

Kang, J., Wiedmann, M., Boor, K. J., and Bergholz, T. M. (2015). VirR-mediated resistance of *Listeria monocytogenes* against food antimicrobials and cross-protection induced by exposure to organic acid salts. *Appl. Environ. Microbiol.* 81, 4553–4562. doi: 10.1128/AEM.00648-15

Karatzas, K. A. G., and Bennik, M. H. J. (2002). Characterization of a *Listeria monocytogenes* Scott A isolate with high tolerance towards high hydrostatic pressure. *Appl. Environ. Microbiol.* 68, 3183–3189. doi: 10.1128/AEM.68.7.3183

Karatzas, K. A. G., Suur, L., and O'Byrne, C. P. (2012). Characterization of the intracellular glutamate decarboxylase system: analysis of its function, transcription, and role in the acid resistance of various strains of *Listeria monocytogenes*. *Appl. Environ. Microbiol.* 78, 3571–3579. doi: 10.1128/AEM.00227-12

Karatzas, K. A. G., Valdramidis, V. P., and Wells-Bennik, M. H. J. (2005). Contingency locus in *ctsR* of *Listeria monocytogenes* Scott A: a strategy for occurrence of abundant piezotolerant isolates within clonal populations. *Appl. Environ. Microbiol.* 71, 8390–8396. doi: 10.1128/AEM.71.12.8390-8396.2005

Karatzas, K. A. G., Wouters, J. A., Gahan, C. G. M., Hill, C., Abee, T., and Bennik, M. H. J. (2003). The CtsR regulator of *Listeria monocytogenes* contains a variant glycine repeat region that affects piezotolerance, stress resistance, motility and virulence. *Mol. Microbiol.* 49, 1227–1238. doi: 10.1046/j.1365-2958.2003.03636.x

Kazmierczak, M. J., Mithoe, S. C., Boor, K. J., and Wiedmann, M. (2003). *Listeria monocytogenes* σB regulates stress response and virulence functions. *J. Bacteriol.* 185, 5722–5734. doi: 10.1128/JB.185.19.5722

Keklik, N. M., Demirci, A., and Puri, V. M. (2009). Inactivation of *Listeria monocytogenes* on unpackaged and vacuum-packaged chicken frankfurters using pulsed UV-light. *J. Food Sci.* 74, 431–439. doi: 10.1111/j.1750-3841.2009.01319.x

Krüger, E., Witt, E., Ohlmeier, S., Hanschke, R., and Hecker, M. (2000). The Clp proteases of *Bacillus subtilis* are directly involved in degradation of misfolded proteins. *J. Bacteriol.* 182, 3259–3265. doi: 10.1128/jb.182.11.3259-3265.2000

Krüger, E., Zühlke, D., Witt, E., Ludwig, H., and Hecker, M. (2001). Clp-mediated proteolysis in Gram-positive bacteria is autoregulated by the stability of a repressor. *EMBO J.* 20, 852–863. doi: 10.1093/emboj/20.4.852

Lado, B. H., Bomser, J. A., Dunne, C. P., and Yousef, A. E. (2004). Pulsed electric field alters molecular chaperone expression and sensitizes *Listeria monocytogenes* to heat. *Appl. Environ. Microbiol.* 70, 2289–2295. doi: 10.1128/AEM.70.4.2289

Lado, B. H., and Yousef, A. E. (2002). Alternative food-preservation technologies: efficacy and mechanisms. *Microbes Infect.* 4, 433–440. doi: 10.1016/S1286-4579(02)01557-5

Lado, B. H., and Yousef, A. E. (2003). Selection and identification of a *Listeria monocytogenes* target strain for pulsed electric field process optimization. *Appl. Environ. Microbiol.* 69, 2223–2229. doi: 10.1128/AEM.69.4.2223

Lasagabaster, A., and Martínez de Marañón, I. (2017). Comparative study on the inactivation and photoreactivation response of *Listeria monocytogenes* seafood isolates and a *Listeria innocua* surrogate after pulsed light treatment. *Food Bioproc. Tech.* 10, 1931–1935. doi: 10.1007/s11947-017-1972-6

Lee, J. H., Jeong, K. W., and Kim, Y. M. (2012). Purification and structural characterization of cold shock protein from *Listeria monocytogenes*. *Bull. Korean Chem. Soc.* 33, 2508–2512. doi: 10.5012/bkcs.2012.33.8.2508

Leong, D., Alvarez-Ordóñez, A., and Jordan, K. (2014). Monitoring occurrence and persistence of *Listeria monocytogenes* in foods and food processing environments in the Republic of Ireland. *Front. Microbiol.* 5:436. doi: 10.3389/fmicb.2014.00436

Leong, D., Alvarez-Ordóñez, A., Zaouali, S., and Jordan, K. (2015). Examination of *Listeria monocytogenes* in seafood processing facilities and smoked salmon in the Republic of Ireland. *J. Food Prot.* 78, 2184–2190. doi: 10.4315/0362-028X.JFP-15-233

Leroy, F., and de Vuyst, L. (2004). Lactic acid bacteria as functional starter cultures for the food fermentation industry. *Trends Food Sci. Technol.* 15, 67–78. doi: 10.1016/j.tifs.2003.09.004

Lippert, K., and Galinski, E. A. (1992). Enzyme stabilization by ectoine-type compatible solutes: protection against heating, freezing and drying. *Appl. Microbiol. Biotechnol.* 37, 61–65. doi: 10.1007/BF00174204

Lund, P., Tramonti, A., and De Biase, D. (2014). Coping with low pH: molecular strategies in neutralophilic bacteria. *FEMS* 38, 1091–1125. doi: 10.1111/1574-6976.12076

Lungu, B., Ricke, S. C., and Johnson, M. G. (2009). Growth, survival, proliferation and pathogenesis of *Listeria monocytogenes* under low oxygen or anaerobic conditions: a review. *Anaerobe* 15, 7–17. doi: 10.1016/j.anaerobe.2008.08.001

Mackey, B. M., Boogard, E., Hayes, C. M., and Baranyi, J. (1994). Recovery of heat-injured *Listeria monocytogenes*. *Int. J. Food Microbiol.* 22, 227–237. doi: 10.1016/0168-1605(94)90174-0

Macwana, S., and Muriana, P. M. (2012). Spontaneous bacteriocin resistance in *Listeria monocytogenes* as a susceptibility screen for identifying different mechanisms of resistance and modes of action by bacteriocins of lactic acid bacteria. *J. Microbiol. Methods* 88, 7–13. doi: 10.1016/j.mimet.2011.09.009

Mandin, P., Fsihi, H., Dussurget, O., Vergassola, M., Milohanic, E., Toledo-Arana, A., et al. (2005). VirR, a response regulator critical for *Listeria monocytogenes* virulence. *Mol. Microbiol.* 57, 1367–1380. doi: 10.1111/j.1365-2958.2005.04776.x

Mazzotta, A. S. (2001a). Heat resistance of *Listeria monocytogenes* in vegetables: evaluation of blanching processes. *J. Food Prot.* 64, 385–387. doi: 10.4315/0362-028x-64.3.385

Mazzotta, A. S. (2001b). Thermal inactivation of stationary-phase and acid-adapted *Escherichia coli* O157:H7, *Salmonella*, and *Listeria monocytogenes* in fruit juices. *J. Food Prot.* 64, 315–320. doi: 10.4315/0362-028X-64.3.315

Mclaughlin, J., and Rees, C. E. D. (2009). "Genus I. *Listeria*," in *Bergey's Manual of Systematic Bacteriology*, 2nd Edn, eds P. De Vos, G. M. Garrity, D. Jones, N. R. Krieg, W. Ludwig, F. A. Rainey, et al. (New York, NY: Springer), 244–257.

Melo, J., Andrew, P. W., and Faleiro, M. L. (2015). *Listeria monocytogenes* in cheese and the dairy environment remains a food safety challenge: the role of stress responses. *Food Res. Int.* 67, 75–90. doi: 10.1016/j.foodres.2014.10.031

Miladi, H., Elabed, H., Ben Slama, R., Rhim, A., and Bakhrouf, A. (2016). Molecular analysis of the role of osmolyte transporters *opuCA* and *betL* in *Listeria monocytogenes* after cold and freezing stress. *Arch. Microbiol.* 199, 259–265. doi: 10.1007/s00203-016-1300-y

Ming, X., and Daeschel, M. A. (1993). Nisin resistance of foodborne bacteria and the specific resistance responses of *Listeria monocytogenes* Scott A. *J. Food Prot.* 56, 944–948. doi: 10.4315/0362-028X-56.11.944

Ming, X., and Daeschel, M. A. (1995). Correlation of cellular phospholipid content with nisin resistance of *Listeria monocytogenes* Scott A. *J. Food Prot.* 58, 416–420. doi: 10.4315/0362-028X-58.4.416

Monfort, S., Sagarzazu, N., Gayán, E., Raso, J., and Álvarez, I. (2012). Heat resistance of *Listeria* species to liquid whole egg ultrapasteurization treatment. *J. Food Eng.* 111, 478–481. doi: 10.1016/j.jfoodeng.2012.02.014

Moorhead, S. M., and Dykes, G. A. (2003). The role of the *sigB* gene in the general stress response of *Listeria monocytogenes* varies between a strain of serotype 1/2a and a strain of serotype 4c. *Curr. Microbiol.* 46, 461–466. doi: 10.1007/s00284-002-3867-6

Moreirinha, C., Almeida, A., Saraiva, J. A., and Delgadillo, I. (2016). High-pressure processing effects on foodborne bacteria by mid-infrared spectroscopy analysis. *LWT Food Sci. Technol.* 73, 212–218. doi: 10.106/j.lwt.2016.05.041

Morris, C., Brody, A. L., and Wicker, L. (2007). Non-thermal food processing/preservation technologies: a review with packaging implications. *Packag. Technol. Sci.* 20, 275–286. doi: 10.1002/pts.789

Mosqueda-Melar, J., Raybaudi-Massilia, R. M., and Martín-Belloso, O. (2007). Influence of treatment time and pulse frequency on *Salmonella enteritidis*, *Escherichia coli* and *Listeria monocytogenes* populations inoculated in melon and watermelon juices treated by pulsed electric fields. *Int. J. Food Microbiol.* 117, 192–200. doi: 10.1016/j.ijfoodmicro.2007.04.009

Murphy, R. Y., Duncan, L. K., Driscoll, K. H., Marcy, J. A., and Beard, B. L. (2003). Thermal inactivation of *Listeria monocytogenes* on ready-to-eat Turkey breast meat products during postcook in-package pasteurization with hot water. *J. Food Prot.* 66, 1618–1622. doi: 10.4315/0362-028X-66.9.1618

Nair, S., Derré, I., Msadek, T., Gaillot, O., and Berche, P. (2000). CtsR controls class III heat shock gene expression in the human pathogen *Listeria monocytogenes*. *Mol. Microbiol.* 35, 800–811. doi: 10.1046/j.1365-2958.2000.01752.x

Neunlist, M. R., Federighi, M., Laroche, M., Sohier, D., Delattre, G., Jacquet, C., et al. (2005). Cellular lipid fatty acid pattern heterogeneity between reference and recent food isolates of *Listeria monocytogenes* as a response to cold stress. *Antonie van Leeuwenhoek J. Microbiol.* 88, 199–206. doi: 10.1007/s10482-005-5412-7

NicAogáin, K., and O'Byrne, C. P. (2016). The role of stress and stress adaptations in determining the fate of the bacterial pathogen *Listeria monocytogenes* in the food chain. *Front. Microbiol.* 7:1856. doi: 10.3389/fmicb.2016.01865

Niven, G. W., Miles, C. A., and Mackey, B. M. (1999). The effects of hydrostatic pressure on ribosome conformation in *Escherichia coli*: an in vivo study using differential scanning calorimetry. *Microbiology* 145, 419–425. doi: 10.1099/13500872-145-2-419

Oliver, H. F., Orsi, R. H., Wiedmann, M., and Boor, K. J. (2010). *Listeria monocytogenes* σB has a small core regulon and a conserved role in virulence but makes differential contributions to stress tolerance across a diverse collection of strains. *Appl. Environ. Microbiol.* 76, 4216–4232. doi: 10.1128/AEM.00031-10

Olsen, K. N., Larsen, M. H., Gahan, C. G. M., Kallipolitis, B., Wolf, X. A., Rea, R., et al. (2005). The Dps-like protein Fri of *Listeria monocytogenes* promotes stress tolerance and intracellular multiplication in macrophage-like cells. *Microbiology* 151(Pt 3), 925–933. doi: 10.1099/mic.0.27552-0

Ovchinnikov, K. V., Chi, H., Mehmeti, I., Holo, H., Nes, I. F., and Diep, D. B. (2016). Novel group of leaderless multipeptide bacteriocins from Gram-positive bacteria. *Appl. Environ. Microbiol.* 82, 5216–5224. doi: 10.1128/AEM.01094-16

Ozer, N. P., and Demirci, A. (2006). Inactivation of *Escherichia coli* O157:H7 and *Listeria monocytogenes* inoculated on raw salmon fillets by pulsed UV-light treatment. *Int. J. Food Sci. Technol.* 41, 354–360. doi: 10.1111/j.1365-2621.2005.01071.x

Perez, R. H., Zendo, T., and Sonomoto, K. (2014). Novel bacteriocins from lactic acid bacteria (LAB): various structures and applications. *Microb. Cell Fact.* 13(Suppl. 1):S3. doi: 10.1186/1475-2859-13-S1-S3

Perozo, E., and Rees, D. C. (2003). Structure and mechanism in prokaryotic mechanosensitive channels. *Curr. Opin. Struct. Biol.* 13, 432–442. doi: 10.1016/s0959-440x(03)00106-4

Phadtare, S., Alsina, J., and Inouye, M. (1999). Cold-shock response and cold-shock proteins. *Curr. Opin. Microbiol.* 2, 175–180. doi: 10.1016/S1369-5274(99)80031-9

Poimenidou, S. V., Chatzithoma, D., Nychas, G., and Skandamis, N. (2016). Adaptive response of *Listeria monocytogenes* to heat, salinity and low pH, after habituation on cherry tomatoes and lettuce leaves. *PLoS One* 11:e0165746. doi: 10.1371/journal.pone.0165746

Pöntinen, A., Lindström, M., Skurnik, M., and Korkeala, H. (2017). Screening of the two-component-system histidine kinases of *Listeria monocytogenes* EGD-e. LiaS is needed for growth under heat, acid, alkali, osmotic, ethanol and oxidative stresses. *Food Microbiol.* 65, 36–43. doi: 10.1016/j.fm.2017.01.018

Pöntinen, A., Markkula, A., Lindström, M., and Korkeala, H. (2015). Two-component-system histidine kinases involved in growth of *Listeria monocytogenes* EGD-e at low temperatures. *Appl. Environ. Microbiol.* 81, 3994–4004. doi: 10.1128/AEM.00626-15

Préstamo, G., Sanz, P. D., Fonberg-Broczek, M., and Arroyo, G. (1999). High pressure response of fruit jams contaminated with *Listeria monocytogenes*. *Lett. Appl. Microbiol.* 28, 313–316. doi: 10.1046/j.1365-2672.1999.00531.x

Püttman, M., Ade, N., and Hof, H. (1993). Dependence of fatty acid composition of *Listeria* spp on growth temperature. *Res. Microbiol.* 144, 279–283. doi: 10.1016/0923-2508(93)90012-Q

Ramnath, M., Beukes, M., Tamura, K., and Hastings, J. (2000). Absence of a putative mannose-specific phosphotransferase system enzyme IIAB component in a leucocin A-resistant strain of *Listeria monocytogenes*, as shown by two-dimensional sodium dodecyl sulfate polyacrylamide gel electrophoresis. *Appl. Environ. Microbiol.* 66, 3098–3101. doi: 10.1128/AEM.66.7.3098-3101.2000

Rascon Escajeda, L. F., Cruz Hernandez, M., Rodriguez Jasso, R. M., Charles Rodriguez, A. V., Robledo Olivo, A., Contreras Esquivel, J. C., et al. (2018). Discussion between alternative processing and preservation technologies and their application in beverages: a review. *J. Food Process. Preserv.* 42, 1–15. doi: 10.1111/jfpp.13322

Rastogi, R. P., Richa, K. A., Tyagi, M. B., and Sinha, R. P. (2010). Molecular mechanisms of ultraviolet radiation-induced DNA damage and repair. *J. Nucleic Acids* 2010:592980. doi: 10.4061/2010/592980

Rea, R., Hill, C., and Gahan, C. G. M. (2005). *Listeria monocytogenes* perR mutants display a small-colony phenotype, increased sensitivity to hydrogen peroxide, and significantly reduced murine virulence. *Appl. Environ. Microbiol.* 71, 8314–8322. doi: 10.1128/AEM.71.12.8314-8322.2005

Renier, S., Micheau, P., Talon, R., Hébraud, M., and Desvaux, M. (2012). Subcellular localization of extracytoplasmic proteins in monoderm bacteria: rational secretomics-based strategy for genomic and proteomic analyses. *PLoS One* 7:e42982. doi: 10.1371/journal.pone.0042982

Ríos, C. N. S., Chalón, M. C., Navarro, S. A., and Bellomio, A. (2018). Pediocin-like bacteriocins: new perspectives on mechanism of action and immunity. *Curr. Genet.* 64, 345–351. doi: 10.1007/s00294-017-0757-9

Rivas, A., Sansano, S., Pérez, M. C. P., Martinez, A., and Rodrigo, D. (2016). "Antimicrobial effect of *Stevia rebaudiana* bertoni against *Listeria monocytogenes* in a beverage processed by pulsed electric fields (PEFs): combined effectiveness," in *1st World Congress on Electroporation and Pulsed Electric Fields in Biology, Medicine and Food & Environmental Technologies*, Vol. 53, eds T. Jarm and P. Kramar (Singapore: Springer), 43–46. doi: 10.1007/978-981-287-817-5_10

Roncarati, D., and Scarlato, V. (2017). Regulation of heat-shock genes in bacteria: from signal sensing to gene expression output. *FEMS Microbiol. Rev.* 41, 549–574. doi: 10.1093/femsre/fux015

Roncarati, D., and Scarlato, V. (2018). The interplay between two transcriptional repressors and chaperones orchestrates *Helicobacter pylori* heat-shock response. *Int. J. Mol. Sci.* 19:E1702. doi: 10.3390/ijms19061702

Ruiz, L., Aertsen, A., Nguyen-The, C., Gänzle, M. G., and Alvarez-Ordóñez, A. (2017). Editorial: industrial and host associated stress responses in food microbes. Implications for food technology and food safety. *Front. Microbiol.* 8:1522. doi: 10.3389/fmicb.2017.01522

Russell, N. J., Evans, R. I., ter Steeg, P. F., Hellemons, J., Verheul, A., and Abee, T. (1995). Membranes as a target for stress adaptation. *Int. J. Food Microbiol.* 28, 255–261. doi: 10.1016/0168-1605(95)00061-5

Ryan, S., Begley, M., Gahan, C. G. M., and Hill, C. (2009). Molecular characterization of the arginine deiminase system in *Listeria monocytogenes*: regulation and role in acid tolerance. *Environ. Microbiol.* 11, 432–445. doi: 10.1111/j.1462-2920.2008.01782.x

Saldaña, G., Puértolas, E., López, N., García, D., Álvarez, I., and Raso, J. (2009). Comparing the PEF resistance and occurrence of sublethal injury on different strains of *Escherichia coli*, *Salmonella typhimurium*, *Listeria monocytogenes* and *Staphylococcus aureus* in media of pH 4 and 7. *Innov. Food Sci. Emerg. Technol.* 10, 160–165. doi: 10.1016/j.ifset.2008.11.003

Sallami, L., Marcotte, M., Naim, F., Quattara, B., Leblanc, C., and Saucier, L. (2006). Heat inactivation of *Listeria monocytogenes* and *Salmonella enterica* serovar Typhi in a typical bologna matrix during an industrial cooking-cooling cycle. *J. Food Prot.* 69, 3025–3030. doi: 10.4315/0362-028x-69.12.3025

Schlech, W. F. III, Lavigne, P. M., Bortolussi, R. A., Allen, A. C., Haldane, E. V., Wort, A. J., et al. (1983). Epidemic listeriosis-Evidence for transmission by food. *N. Engl. J. Med.* 308, 203–206. doi: 10.1056/NEJM198301273080407

Schmid, B., Klumpp, J., Raimann, E., Loessner, M. J., Stephan, R., and Tasara, T. (2009). Role of cold shock proteins in growth of *Listeria monocytogenes* under cold and osmotic stress conditions. *Appl. Environ. Microbiol.* 75, 1621–1627. doi: 10.1128/AEM.02154-08

Selma, M. V., Salmerón, M. C., Valero, M., and Fernández, P. S. (2006). Efficacy of pulsed electric fields for *Listeria monocytogenes* inactivation and control in horchata. *J. Food Saf.* 26, 137–149. doi: 10.1111/j.1745-4565.2006.00038.x

Sewell, D., Allen, S. C. H., and Phillips, C. A. (2015). Oxygen limitation induces acid tolerance and impacts simulated gastro-intestinal transit in *Listeria monocytogenes* J0161. *Gut Pathog.* 7, 1–5. doi: 10.1186/s13099-015-0058-0

Shebuski, J. R., Vilhelmsson, O., and Miller, K. J. (2000). Effects of low water activity on the thermal tolerance of *Staphylococcus aureus*. *J. Food Prot.* 63, 1277–1281. doi: 10.4315/0362-028X-63.9.1277

Shen, Q., Jangam, P. M., Soni, K. A., Nannapaneni, R., Schilling, W., and Silva, J. L. (2014). Low, medium, and high heat tolerant strains of *Listeria monocytogenes* and increased heat stress resistance after exposure to sublethal heat. *J. Food Prot.* 77, 1298–1307. doi: 10.4315/0362-028x.jfp-13-423

Silva, C. C. G., Silva, S. P. M., and Ribeiro, S. C. (2018). Application of bacteriocins and protective cultures in dairy food preservation. *Front. Microbiol.* 9:594. doi: 10.3389/fmicb.2018.00594

Simpson, R. K., Whittington, R., Earnshaw, R. G., and Russell, N. J. (1999). Pulsed high electric field causes 'all or nothing' membrane damage in *Listeria monocytogenes* and *Salmonella typhimurium*, but membrane H^+-ATPase is not a primary target. *Int. J. Food Microbiol.* 48, 1–10. doi: 10.1016/S0168-1605(99)00022-7

Sinha, R. P., and Häder, D. P. (2002). UV-induced DNA damage and repair: a review. *Photochem. Photobiol. Sci.* 1, 225–236. doi: 10.1039/b201230h

Skandamis, P. N., Gounadaki, A. S., Geornaras, I., and Sofos, J. N. (2012). Adaptive acid tolerance response of *Listeria monocytogenes* strains under planktonic and immobilized growth conditions. *Int. J. Food Microbiol.* 159, 160–166. doi: 10.1016/j.ijfoodmicro.2012.07.027

Sleator, R. D., Gahan, C. G., Abee, T., and Hill, C. (1999). Identification and disruption of BetL, a secondary glycine betaine transport system linked to the salt tolerance of *Listeria monocytogenes* LO28. *Appl. Environ. Microbiol.* 65, 2078–2083.

Sleator, R. D., Watson, D., Hill, C., and Gahan, C. G. M. (2009). The interaction between *Listeria monocytogenes* and the host gastrointestinal tract. *Microbiology* 155, 2463–2475. doi: 10.1099/mic.0.030205-0

Sleator, R. D., Gahan, C. G. M., and Hill, C. (2003a). A postgenomic appraisal of osmotolerance in *Listeria monocytogenes*. *Appl. Environ. Microbiol.* 69, 1–9. doi: 10.1128/AEM.69.1.1-9.2003

Sleator, R. D., Wood, J. M., and Hill, C. (2003b). Transcriptional regulation and posttranslational activity of the betaine transporter BetL in *Listeria monocytogenes* are controlled by environmental salinity. *J. Bacteriol.* 185, 7140–7144. doi: 10.1128/JB.185.24.7140-7144.2003

Soares, C. A., and Knuckley, B. (2016). Mechanistic studies of the agmatine deiminase from *Listeria monocytogenes*. *Biochem. J.* 473, 1553–1561. doi: 10.1042/BCJ20160221

Somolinos, M., Espina, L., Pagán, R., and Garcia, D. (2010). *sigB* absence decreased *Listeria monocytogenes* EGD-e heat resistance but not its pulsed electric fields resistance. *J. Food Microbiol.* 141, 32–38. doi: 10.1016/j.ijfoodmicro.2010.04.023

Sörqvist, S. (1993). Heat resistance of *Listeria monocytogenes* by two recovery media used with and without cold preincubation. *J. Appl. Bacteriol.* 74, 428–432. doi: 10.1111/j.1365-2672.1993.tb05150.x

Sörqvist, S. (1994). Heat resistance of different serovars of *Listeria monocytogenes*. *J. Appl. Bacteriol.* 76, 383–388. doi: 10.1111/j.1365-2672.1994.tb01644.x

Suo, Y., Huang, Y., Liu, Y., Shi, C., and Shi, X. (2012). The expression of superoxide dismutase (SOD) and a putative ABC transporter permease is inversely correlated during biofilm formation in *Listeria monocytogenes* 4b G. *PLoS One* 7:e48467. doi: 10.1371/journal.pone.0048467

Suo, Y., Liu, Y., Zhou, X., Huang, Y., Shi, C., Matthews, K., et al. (2014). Impact of *sod* on the expression of stress-related genes in *Listeria monocytogenes* 4b G with/without paraquat treatment. *J. Food Sci.* 79, M1745–M1749. doi: 10.1111/1750-3841.12545

Tasara, T., and Stephan, R. (2006). Cold stress tolerance of *Listeria monocytogenes*: a review of molecular adaptive mechanisms and food safety implications. *J. Food Prot.* 69, 1473–1484. doi: 10.4315/0362-028X-69.6.1437

Thedieck, K., Hain, T., Mohamed, W., Tindall, B. J., Nimtz, M., Chakraborty, T., et al. (2006). The MprF protein is required for lysinylation of phospholipids in listerial membranes and confers resistance to cationic antimicrobial peptides (CAMPs) on *Listeria monocytogenes*. *Mol. Microbiol.* 62, 1325–1339. doi: 10.1111/j.1365-2958.2006.05452.x

Thévenot, D., Dernburg, A., and Vernozy-Rozand, C. (2006). An updated review of *Listeria monocytogenes* in the pork meat industry and its products. *J. Appl. Microbiol.* 101, 7–17. doi: 10.1111/j.1365-2672.2006.02962.x

Toepfl, S., Heinz, V., and Knorr, D. (2007). High intensity pulsed electric fields applied for food preservation. *Chem. Eng. Prog.* 46, 537–546. doi: 10.1016/j.cep.2006.07.011

Tomasula, P. M., Renye, J. A., Van Hekken, D. L., Tunick, M. H., Kwoczak, R., Toht, M., et al. (2014). Effect of high-pressure processing on reduction of *Listeria monocytogenes* in packaged Queso Fresco. *J. Dairy Sci.* 97, 1281–1295. doi: 10.3168/jds.2013-7538

Tomoyasu, T., Mogk, A., Langen, H., Goloubinoff, P., and Bukau, B. (2001). Genetic dissection of the roles of chaperones and proteases in protein folding and degradation in the *Escherichia coli* cytosol. *Mol. Microbiol.* 40, 397–413. doi: 10.1046/j.1365-2958.2001.02383.x

Tosukhowong, A., Zendo, T., Visessanguan, W., Roytrakul, S., Pumpuang, L., Jaresitthikunchai, J., et al. (2012). Garvieacin Q, a novel class II bacteriocin from *Lactococcus garvieae* BCC 43578. *Appl. Environ. Microbiol.* 78, 1619–1623. doi: 10.1128/AEM.06891-11

Tymoszewska, A., Diep, D. B., Wirtek, P., and Aleksandrzak-Piekarczyk, T. (2017). The non-lantibiotic bacteriocin garvicin Q targets Man-PTS in a broad spectrum of sensitive bacterial genera. *Sci. Rep.* 7:8359. doi: 10.1038/s41598-017-09102-7

Uesugi, A. R., Hsu, L. C., Worobo, R. W., and Moraru, C. I. (2016). Gene expression analysis for *Listeria monocytogenes* following exposure to pulsed light and continuous ultraviolet light treatments. *Food Sci. Technol.* 68, 579–588. doi: 10.1016/j.lwt.2016.01.007

Unal, R., Kim, J.-G., and Yousef, A. E. (2001). Inactivation of *Escherichia coli* O157:H7, *Listeria monocytogenes*, and *Lactobacillus leichmannii* by combinations of ozone and pulsed electric field. *J. Food Prot.* 64, 777–782. doi: 10.4315/0362-028x-64.6.777

Vadyvaloo, V., Arous, S., Gravesen, A., Héchard, Y., Chauhan-Haubrock, R., Hastings, J. W., et al. (2004). Cell-surface alterations in class IIa bacteriocin-resistant *Listeria monocytogenes* strains. *Microbiology* 150, 3025–3033. doi: 10.1099/mic.0.27059-0

Vadyvaloo, V., Hastings, J. W., van der Merwe, M. J., and Rautenbach, M. (2002). Membranes of class IIa bacteriocin-resistant *Listeria monocytogenes* cells contain increased levels of desaturated and short-acyl-chain phosphatidylglycerols. *Appl. Environ. Microbiol.* 68, 5223–5230. doi: 10.1128/AEM.68.11.5223

Van Boeijen, I. K. H., Chavaroche, A. A. E., Valderrama, W. B., Moezelaar, R., Zwietering, M. H., and Abee, T. (2010). Population diversity of *Listeria monocytogenes* LO28: phenotypic and genotypic characterization of variants resistant to high hydrostatic pressure. *Appl. Environ. Microbiol.* 76, 2225–2233. doi: 10.1128/AEM.02434-09

Van Boeijen, I. K. H., Moezelaar, R., Abee, T., and Zwietering, M. H. (2008). Inactivation kinetics of three *Listeria monocytogenes* strains under high hydrostatic pressure. *J. Food Prot.* 71, 2007–2013. doi: 10.4315/0362-028X-71.10.2007

Van Boekel, M., Fogliano, V., Pellegrini, N., Stanton, C., Scholz, G., Lalljie, S., et al. (2010). A review on the beneficial aspects of food processing. *Mol. Nutr. Food Res.* 54, 1215–1247. doi: 10.1002/mnfr.200900608

Van der Veen, S., Hain, T., Wouters, J. A., Hossain, H., de Vos, W. M., Abee, T., et al. (2007). The heat-shock response of *Listeria monocytogenes* comprises genes involved in heat shock, cell division, cell wall synthesis, and the SOS response. *Microbiology* 153, 3593–3607. doi: 10.1099/mic.0.2007/006361-0

Van Schaik, W., and Abee, T. (2005). The role of σB in the stress response of Gram-positive bacteria-targets for food preservation and safety. *Curr. Opin. Biotechnol.* 16, 218–224. doi: 10.1016/j.copbio.2005.01.008

Verheul, A., Glaasker, E., Poolman, B., and Abee, T. (1997a). Betaine and L-carnitine transport by *Listeria monocytogenes* ScottA in response to osmotic signals. *J. Bacteriol.* 179, 6979–6985. doi: 10.1128/jb.179.22.6979-6985.1997

Verheul, A., Russell, N. J., van'T Hof, R., Rombouts, F. M., and Abee, T. (1997b). Modifications of membrane phospholipid composition in nisin-resistant *Listeria monocytogenes* Scott A. *Appl. Environ. Microbiol.* 63, 3451–3457.

Vermassen, A., Dordet-Frisoni, E., de la Foye, A., Micheau, P., Laroute, V., Leroy, S., et al. (2016). Adaptation of *Staphylococcus xylosus* to nutrients and osmotic stress in a salted meat model. *Front. Microbiol.* 7:87. doi: 10.3389/fmicb.2016.00087

Wemekamp-Kamphuis, H. H., Sleator, R. D., Wouters, J. A., Hill, C., and Abee, T. (2004a). Molecular and physiological analysis of the role of osmolyte transporters BetL, Gbu, and OpuC in growth of *Listeria monocytogenes* at low temperatures. *Appl. Environ. Microbiol.* 70, 2912–2918. doi: 10.1128/AEM.70.5.2912

Wemekamp-Kamphuis, H. H., Wouters, J. A., de Leeuw, P. P. L. A., Hain, T., Chakraborty, T., and Abee, T. (2004b). Identification of sigma factor σB-controlled genes and their impact on acid stress, high hydrostatic pressure, and freeze survival in *Listeria monocytogenes* EGD-e. *Appl. Environ. Microbiol.* 70, 3457–3466. doi: 10.1128/AEM.70.6.3457-3466.2004

Wen, J., Anantheswaran, R. C., and Knabel, S. J. (2009). Changes in barotolerance, thermotolerance, and cellular morphology throughout the life cycle of *Listeria monocytogenes*. *Appl. Environ. Microbiol.* 75, 1581–1588. doi: 10.1128/AEM.01942-08

Wiedemann, I., Breukink, E., van Kraaij, C., Kuipers, O. P., Bierbaum, G., de Kruijff, B., et al. (2001). Specific binding of nisin to the peptidoglycan precursor lipid II combines pore formation and inhibition of cell wall biosynthesis for potent antibiotic activity. *J. Biol. Chem.* 276, 1772–1779. doi: 10.1074/jbc.M006770200

Wouters, P. C., Alvarez, I., and Raso, J. (2001). Critical factors determining inactivation kinetics by pulsed electric field food processing. *Trends Food Sci. Technol.* 12, 112–121. doi: 10.1016/S0924-2244(01)00067-X

Wu, S., Yu, P.-L., Wheeler, D., and Flint, S. (2018). Transcriptomic study on persistence and survival of *Listeria monocytogenes* following lethal treatment with nisin. *J. Glob. Antimicrob. Resist.* 15, 25–31. doi: 10.1016/j.jgar.2018.06.003

Zhang, L.-J., and Gallo, R. L. (2016). Antimicrobial peptides. *Curr. Biol.* 26, R14–R19. doi: 10.1016/j.cub.2015.11.017

Zühlke, D., Witt, E., Ludwig, H., and Hecker, M. (2001). Clp-mediated proteolysis in Gram-positive bacteria is autoregulated by the stability of a repressor. *EMBO J.* 20, 852–863. doi: 10.1093/emboj/20.4.852

Conflict of Interest Statement: The authors declare that the research was conducted in the absence of any commercial or financial relationships that could be construed as a potential conflict of interest.

frontiers in Microbiology

ORIGINAL RESEARCH
published: 15 November 2018
doi: 10.3389/fmicb.2018.02869

The Glutaminase-Dependent Acid Resistance System: Qualitative and Quantitative Assays and Analysis of Its Distribution in Enteric Bacteria

*Eugenia Pennacchietti[1], Chiara D'Alonzo[1], Luca Freddi[2], Alessandra Occhialini[2] and Daniela De Biase[1]**

[1] Department of Medico-Surgical Sciences and Biotechnologies, Laboratory Affiliated to the Istituto Pasteur Italia-Fondazione Cenci Bolognetti, Sapienza University of Rome, Latina, Italy, [2] Institut de Recherche en Infectiologie de Montpellier, CNRS, University of Montpellier, Montpellier, France

OPEN ACCESS

Edited by:
Christian Sohlenkamp, Universidad Nacional Autónoma de México, Mexico

Reviewed by:
Kimon Andreas Karatzas, University of Reading, United Kingdom
Fabian Moritz Commichau, Georg-August-Universität Göttingen, Germany
Diana Ximena Sahonero-Canavesi, Royal Netherlands Institute for Sea Research (NIOZ), Netherlands

***Correspondence:**
Daniela De Biase
daniela.debiase@uniroma1.it

Specialty section:
This article was submitted to Microbial Physiology and Metabolism, a section of the journal Frontiers in Microbiology

Received: 27 August 2018
Accepted: 08 November 2018
Published: 15 November 2018

Citation:
Pennacchietti E, D'Alonzo C, Freddi L, Occhialini A and De Biase D (2018) The Glutaminase-Dependent Acid Resistance System: Qualitative and Quantitative Assays and Analysis of Its Distribution in Enteric Bacteria. Front. Microbiol. 9:2869. doi: 10.3389/fmicb.2018.02869

Neutralophilic bacteria have developed several strategies to overcome the deleterious effects of acid stress. In particular, the amino acid-dependent systems are widespread, with their activities overlapping, covering a rather large pH range, from 6 to <2. Recent reports showed that an acid resistance (AR) system relying on the amino acid glutamine (AR2_Q), the most readily available amino acid in the free form, is operative in *Escherichia coli*, *Lactobacillus reuteri,* and some *Brucella* species. This system requires a glutaminase active at acidic pH and the antiporter GadC to import *L*-glutamine and export either glutamate (the glutamine deamination product) or GABA. The latter occurs when the deamination of glutamine to glutamate, via acid-glutaminase (YbaS/GlsA), is coupled to the decarboxylation of glutamate to GABA, via glutamate decarboxylase (GadB), a structural component of the glutamate-dependent AR (AR2) system, together with GadC. Taking into account that AR2_Q could be widespread in bacteria and that until now assays based on ammonium ion detection were typically employed, this work was undertaken with the aim to develop assays that allow a straightforward identification of the acid-glutaminase activity in permeabilized bacterial cells (qualitative assay) as well as a sensitive method (quantitative assay) to monitor in the pH range 2.5–4.0 the transport of the relevant amino acids *in vivo*. The qualitative assay is colorimetric, rapid and reliable and provides several additional information, such as co-occurrence of AR2 and AR2_Q in the same bacterial species and assessment of the growth conditions that support maximal expression of glutaminase at acidic pH. The quantitative assay is HPLC-based and allows to concomitantly measure the uptake of glutamine and the export of glutamate and/or GABA via GadC *in vivo* and depending on the external pH. Finally, an extensive bioinformatic genome analysis shows that the gene encoding the glutaminase involved in AR2_Q is often nearby or in operon arrangement with the genes coding for GadC and GadB. Overall, our results indicate that AR2_Q is likely to be of prominent importance in the AR of enteric bacteria and that it modulates the enzymatic as well as antiport activities depending on the imposed acidic stress.

Keywords: acid stress, *Escherichia coli*, GadC antiporter, glutamine, GABA, rapid assay, HPLC

INTRODUCTION

By definition, neutralophilic microorganisms are those that best grow in the pH range 5–8 (Krulwich et al., 2011). However, during their lifecycle they can be exposed, transiently or for prolonged periods, to acidic conditions (Lund et al., 2014). An increase in extracellular proton concentration such as that found in some areas of the animal host, i.e., the pH $\leq$ 2.5 in the stomach and, intracellularly, the pH 4.5–5.5 in the phagolysosome, typically challenges the microorganisms, regardless of whether they are pathogens or not. Moreover, many organic acids are used as food preservative (Hazan et al., 2004; Theron and Lues, 2010) and their production is a common strategy adopted by food-fermenting bacteria to exert a control of other microbial species in food matrices (Ross et al., 2002; Krulwich et al., 2011) and/or in the distal gut (Flint et al., 2008). Thus, perceiving and responding to an acidic environment is important in microbial physiology because it ensures survival in a microbial community and in the host (Krulwich et al., 2011; Lund et al., 2014).

The acid-protecting systems discovered to date allow the microorganisms to counteract the deleterious effect resulting from an intracellular increase of protons which negatively affect the transmembrane potential, by dissipating it, the activity of many enzymes, and the folding of proteins. In other words, acids can be a threat to microbial vitality. On the other hand, it should also be recalled that the acidic pH is a cue that triggers virulence trait in pathogenic microorganisms (Porte et al., 1999; Vandal et al., 2009; De Biase and Lund, 2015).

In Gram-positive and Gram-negative neutralophilic bacteria protection from acidic stress is provided by many systems each acting in a precise pH-range and having specific requirements to function. The pH range of activity of these systems is such that they effectively protect from the life-threatening effects of the exposure to acid stress in a rather large pH range, from pH 6 to pH 2.5 or lower (Kanjee and Houry, 2013; Lund et al., 2014). Among the strategies adopted to face the acid encounter, the amino acid-dependent systems have been shown to be quite widespread in enteric bacteria exposed to harsh acid. In particular, the glutamate-dependent acid resistance (GDAR; also named AR2) system is extremely powerful: it provides the most effective protection to the bacterial cells exposed to a pH $\leq$ 2.5, up to some hours (Lin et al., 1996).

This system is operative in *Escherichia coli*, as well as in many other bacteria (De Biase and Pennacchietti, 2012; Occhialini et al., 2012; Damiano et al., 2015). It relies on the activity of the pyridoxal 5′-phosphate (PLP)-dependent enzyme glutamate decarboxylase (two isoforms, GadA and GadB, are present in *E. coli*, whereas in other microorganisms only one glutamate decarboxylase, GadB, occurs) and on the activity of the plasma membrane antiporter GadC, which imports glutamate (Glu) and export its decarboxylation product, i.e., γ-aminobutyrate (GABA; **Figure 1A**). Both, the decarboxylase and the antiporter are maximally active in the pH range 4.0–5.5 and are inactive at pH $\geq$ 6.5 (De Biase et al., 1996; Capitani et al., 2003; Gut et al., 2006; Ma et al., 2012; Grassini et al., 2015). Strikingly, in both proteins, i.e., GadB and GadC, the C-terminal tail of each polypeptide chain is responsible for self-inhibition at pH $\geq$ 6.5 (Gut et al., 2006; Pennacchietti et al., 2009; Ma et al., 2012, 2013). Moreover, while the only known physiological substrate of *E. coli* GadA/B is Glu (Fonda, 1972), GadC is able to import glutamine (Gln) in addition to Glu (Ma et al., 2012, 2013; Tsai et al., 2013). It was elegantly shown that GadC provides a "selective transport path" for Gln, Glu and GABA, according to their overall net charge, and this is instrumental to avoid further proton stress to the cell. Specifically, GadC allows the influx of Glu^0 and Gln^0 and the efflux of Glu^0 or $GABA^+$ (Ma et al., 2013; Tsai et al., 2013) (**Figure 1B**). In particular, the Glu^0(or $Gln^0)_{in}/GABA^+_{out}$ pH-dependent activity of GadC is responsible for pumping out positive charges, is positively affected by a positive membrane potential, and decreases when the membrane potential is negative or nil (Ma et al., 2013; Tsai et al., 2013).

The ability of GadC to import Gln, in exchange for Glu or GABA, provided the first evidence that glutamine can be a physiological substrate for GadC (Ma et al., 2012). This finding was reinforced by the same authors who demonstrated that *E. coli* possesses a glutamine-dependent AR system relying on the availability of extracellular glutamine, typically in the free form in many food sources, and on the enzyme YbaS, a glutaminase active in the acidic pH range (Lu et al., 2013) (**Figure 1C**). The glutamine-dependent AR system was therefore renamed AR2_Q, as it shares GadC with the AR2 system (Lund et al., 2014).

Recent reports have demonstrated the occurrence of an AR2_Q in other bacteria than *E. coli* (Lu et al., 2013), such as *Lactobacillus reuteri* (Teixeira et al., 2014) and some *Brucella* species (Freddi et al., 2017). In all these species, the AR2_Q provides protection to extreme acid stress, i.e., pH 2.5, to the same extent as the powerful system depending on Glu (AR2), provided that glutamine was available extracellularly.

Until now the activity of the acid glutaminase, YbaS, was measured by detecting ammonia production either directly, through an ammonium ion electrode (Lu et al., 2013), or indirectly, using a coupled assay with glutamate dehydrogenase (Brown et al., 2008). This work was therefore undertaken with the aim to develop assays that allow, on one hand, a rapid and reliable identification of acid-glutaminase activity in permeabilized bacterial cells (qualitative assay) and, on the other hand, a sensitive HPLC-based method for the detection of extracellular Gln, Glu, and GABA levels *in vivo* (quantitative assay). The latter assay allowed also to show that, in the pH range 2.5–4.0, *E. coli* modulates the enzymatic as well as the antiport activities depending on the imposed acidic stress. Moreover, by means of an extensive bioinformatic analysis it was possible to show that the gene coding for the acid-glutaminase is often found nearby, likely in an operon arrangement, with the genes coding for GadC and GadB, thus suggesting that AR2_Q is as widespread in bacteria, mostly Gram-negative and enteric, as AR2.

MATERIALS AND METHODS

Materials

Restriction enzymes, alkaline phosphatase, and ampicillin were obtained from Roche. The DNA Blunt T/A ligase and Taq-Q5 High-Fidelity DNA polymerase were from New England Biolabs. Plasmid DNA preparation and DNA extraction from

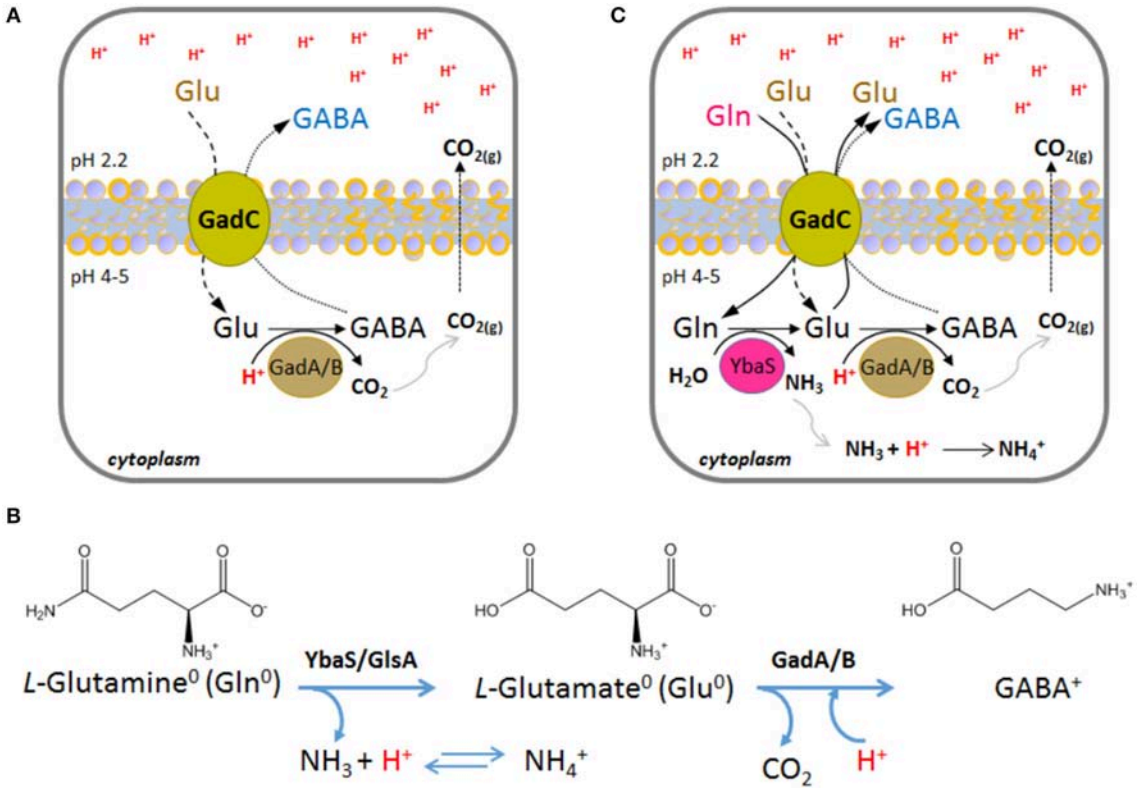

FIGURE 1 | Schematic representation of the enzymatic reactions and transport activity in the AR2 and AR2_Q systems in *Escherichia coli*. **(A)** A typical situation where the AR2 comes into action is when the drop of the extracellular pH to below 2.5 leads, as a consequence, to the decrease of the intracellular pH to below 5. This activates the GadC-mediated import of Glu^0 (if available extracellularly) and the export of $GABA^+$, the latter generated by the intracellular proton-consuming activity of GadA/B. **(B)** Chemical structures and net charge of the species imported and exported by GadC, according to (Ma et al., 2013; Tsai et al., 2013). The reactions and the enzymes involved are shown. **(C)** A situation where the AR2_Q can be operative is when the extracellular pH drops below 2.5 and, as a consequence, the intracellular pH decreases to below 5. This activates the GadC-mediated import of Gln^0 (when available extracellularly) and the export of Glu^0 (arising from Gln deamination) or $GABA^+$ (arising from Glu decarboxylation). In AR2_Q, protons are taken up during ammonium ion formation and during GABA synthesis. According to previous reports (Ma et al., 2013; Tsai et al., 2013), GadC can export either Glu^0 or $GABA^+$, depending on the cellular need to buffer the cytosol and effectively consume protons.

agarose gel were carried out using PureYield™ Plasmid miniprep system (Promega) and QIAEX II Gel Extraction Kit (Qiagen), respectively.

Ingredients for bacterial growth were from Difco. Bromocresol green was from Fluka; L-Glutamic acid, L-Glutamine, D,L-Norvaline, sodium acetate, sodium chloride, Triton X-100, GABA, and other reagents, if not otherwise stated, were from Sigma–Aldrich. Super gradient grade methanol for HPLC was from VWR. 2-*o*-phthalaldehyde (OPA) was from Agilent Technologies. Oligonucleotide synthesis and DNA sequencing services were by MWG Biotech.

Bacterial Strains, Plasmids and Growth Conditions

The bacterial strains, plasmids, and oligonucleotides used in this work are listed in **Table S1**. *E. coli* K12 strain MG1655 and its isogenic mutant derivatives Δ*ybaS*, Δ*gadC*, and Δ*gadAB* as well as the complemented strains were reported elsewhere or prepared as part of this work (Occhialini et al., 2012; Freddi et al., 2017; **Table S1**).

Depending on the experiments to be carried out, the *E. coli* strains were grown in the following media at 37°C: LB broth (Luria Bertani), pH 7.4; LBG, pH 5.0 (LB acidified to pH 5.0 with HCl and supplemented with 0.4% glucose); LB-MOPS, pH 8.0 (LB buffered at pH 8.0 with 100 mM morpholinepropanesulfonic acid, MOPS); LBG-MOPS, pH 8.0 (as LB-MOPS, pH 8.0, and supplemented with 0.4% glucose). All the *Brucella* strains were grown on TS (Tryptic Soy, Difco) agar and broth at 37°C in a biosafety level laboratory L3 in the respect of the legislation (BSL3 confinement; IRIM Montpellier). *Yersinia ruckeri* was grown in NB (Nutrient Broth, Difco) at 25°C. When required, the antibiotics ampicillin, kanamycin, and chloramphenicol were added at the concentration of 100, 25, and 34 μg/ml, respectively.

Construction and Complementation of *E. coli* Δ*ybas* Mutant Strains

The Δ*ybaS* mutant strain was obtained from *E. coli* using the one-step gene inactivation procedure described by Datsenko and Wanner (2000), plasmid pKD13 as template for amplification of the kanamycin cassette (Kan^R) and the *ybaS*-specific

oligonucleotide pair Δ*ybaS*_for(P1)/Δ*ybaS*_rev(P4) listed in **Table S1**. The insertion of the Kan^R cassette, replacing the *ybaS* gene, was checked by PCR using the primer pair k1/*ybaS*_rev (**Table S1**).

To complement *E. coli* Δ*ybaS*, plasmids pBBR-*ybaS_Ec*(long), pBBR-*ybaS_Ec*, and pBBR-*glsA_Bm* were used. The construction of these plasmids is described in section Cloning of the *E. coli ybaS* gene in plasmid pBBR1MCS and in **Table S1**.

Cloning of the *E. coli ybaS* Gene in Plasmid pBBR1MCS

In order to assess the influence of the *yba*S promoter on the expression of this gene as directed by plasmid pBBR1MCS, the construct pBBR-*ybaS_Ec*, derived from the previously described pBBR-*ybaS_Ec*(long) (Freddi et al., 2017 and **Table S1)**, was generated. Briefly, the 110 bp promoter region of *E. coli ybaS* was removed by digesting pBBR-*ybaS_Ec*(long) with the restriction enzymes *Xho*I-*Bam*HI, cutting at 159 and 49 bp from the *ybaS* ATG start codon, respectively (Petersen and Moller, 2000). The restriction site for *Bam*HI was introduced as part of the synthetic gene preparation of *ybaS_Ec*(long) (Freddi et al., 2017) by replacing the CA in sequence GGCACC with an AT, thereby yielding the sequence GGATCC recognized by *Bam*HI. After restriction with *Xho*I-*Bam*HI, the plasmid was filled-in using Taq-Q5 High-Fidelity DNA polymerase (New England Biolabs) and religated with Blunt T/A ligase (New England Biolabs). The newly generated plasmid, named pBBR-*ybaS_Ec*, was sequenced on both strands (MWG Biotech).

Rapid Glutaminase Assay ("GlsAssay")

The "GlsAssay" solution consists of 1 g/L *L*-Glutamine, 0.05 g/L bromocresol green, 90 g/L NaCl, and 3 ml/L Triton X-100 dissolved in distilled water brought to pH 3.1 with KOH. At this pH the starting solution is yellow. The reagent is stable for up to 3 month when stored at 4°C.

It is possible to perform the "GlsAssay" in two ways: (a) from bacterial colonies taken directly from an agar plate or (b) from bacterial cultures grown overnight in liquid media.

GlsAssay From Colonies on Plate

One centimeter (in length) of confluent bacterial colonies or 5 independent colonies (1–4 × 10^8 cells) were resuspended in 500 μl physiological saline solution (0.9% NaCl in water), to achieve a suspension of 0.2–1.0 × 10^9 cells/ml. The suspension was centrifuged at 14,000 rpm for 5 min, the supernatant was discarded and the pellet resuspended in 150 μl of the "GlsAssay" solution by vigorous vortexing or pipetting. After incubation for 2 h at 37°C, the change in color from yellow (negative, -) to green (positive, +) or blue (strongly positive, ++) was assessed by eye (see **Figure S2**).

GlsAssay From Liquid Culture

To set up this assay, bacterial cells were grown at 37°C overnight in 1–2 ml of different media at different pH (i.e., LB, pH 7.4; LBG, pH 5.0; LB-MOPS, pH 8.0; LBG-MOPS, pH 8.0). After 24 h, the cells were harvested by centrifugation at 4,000 rpm for 20 min, resuspended in an isovolume of physiological saline solution and again centrifuged. The latter two steps were repeated one more time. The cell density was then measured and adjusted to an OD_{600} = 2.0 by adding saline solution, where required. 500 μl of each sample at OD_{600} = 2.0, (which corresponds to 0.2–1.0 × 10^9 cells/ml) were centrifuged at 14,000 rpm for 5 min and the pellet resuspended by vigorous vortexing or pipetting in 150 μl of "GlsAssay" solution. Following the incubation at 37°C for 30 min, 2 h or overnight, the change in color was assessed by eye, as described above.

Acid Resistance (AR) Assay and Cell Viability

Acid Resistance Assay

Depending on the experiment to be performed and for comparison with previous studies (De Biase et al., 1999; Lu et al., 2013), bacteria were grown to the stationary phase for a total of 24 h at 37°C in different media (LB, pH 7.4; LBG, pH 5.0; LB-MOPS, pH 8.0; LBG-MOPS, pH 8.0). The following day the cultures were diluted 1:1000 (except for cultures grown in LBG-MOPS, which were diluted 1:4000) in pre-warmed EG medium, pH 2.2, with/without glutamine (1–3 mM). The acid challenge was carried out for 2 h (t = 2 h) at 37°C (without shaking). At this time point, 20 μl of each samples were diluted in physiological saline solution (1:50) and bacteria (20 μl) were plated out and incubated overnight (15–18 h) at 37°C. Only for bacteria challenged in EG without glutamine, plating at t = 2 h was without dilution. The percentage of survival was calculated comparing the bacterial counts at t = 2 h with the bacterial count at time 0 (t = 0). At least three independent experiments (in duplicate) were performed for each strain/condition.

Cell Viability Assay

For the purpose of the HPLC assay described in section HPLC Analysis of Glutamine, Glutamate, and GABA in spent media, cell viability was carried out. It consisted in checking the bacterial counts following incubation for 1 h at pHs less extreme than that used for AR assay, i.e., pH 2.5, pH 3.1, pH 3.5, and pH 4.0, and always in the presence of 3 mM Gln.

HPLC Analysis of Glutamine, Glutamate and GABA in Spent Media

In order to assess the contribution of *ybaS*/*glsA*, *gadAB*, and *gadC* genes to glutamine metabolism and transport in *E. coli* in acidic media, a HPLC-based method to detect simultaneously the three amino acids in the spent media was developed.

Sample Preparation

Few colonies of each bacterial strain, from freshly streaked LB Agar plates, were inoculated in 2 ml of LBG-MOPS pH 8.0 and grown for 24 h at 37°C. Following growth, each culture was harvested by centrifugation, washed twice with an isovolume (2 ml) of physiological saline solution and finally adjusted to OD_{600} = 4.0 (2.0 × 10^9 cells/ml). 400-μl aliquots of each culture (now at an identical OD_{600}) were then centrifuged and resuspended in EG medium (adjusted with 6N HCl to the indicated pH) containing 3 mM glutamine. At time 0 and after 1 h of incubation at 37°C, the cells were spun down by

centrifugation at 4°C for 3–5 min at 10,000 rpm and 100 μl-aliquots of the supernatant (spent medium) were transferred into a clean tube and stored at 4°C for subsequent HPLC analysis, which was always within 3 days from sample collection. A 3.5-μl aliquot from each sample was then added of 10 μL of 0.2 mM Norvaline (internal standard) and HPLC-grade water to reach a final volume of 100 μl.

HPLC Conditions

HPLC analysis was performed on an Agilent 1260 series system (Agilent Technologies, USA) equipped with a quaternary pump and a fluorescence detector. GABA, Gln, Glu and the internal standard, Norvaline, were separated under a mix of isocratic and gradient elution using an Agilent Poroshell 120 HPH-C18, 4.6 × 150 mm, 2.7 μm LC column (Agilent Technologies) and an Agilent InfinityLab Poroshell UHPLC-C18 guard column (4.6 × 5 mm, 2.7 μm particle size). The mobile phase consisted of Solvent A (50 mM Sodium Acetate buffer: Methanol; 50:50, v/v) adjusted to pH 4.18 with HCl and Solvent B (100% Methanol). Prior to methanol addition, all solutions were filtered through a 0.2-μm nitrocellulose Whatman filters (Ø 47 mm).

Pre-column derivatization of standard amino acids and samples with *o*-phtalaldehyde (OPA) reagent solution (Agilent, 10 mg/ml) was set to be carried out automatically in the HPLC autosampler. Briefly, the derivatization was performed with a programmable automatic injector (Agilent) by mixing 80 μL of sample (or standard solution) with 8 μl of OPA. After 1 min at RT, a 80-μl aliquot of the derivatized sample was directly injected into the HPLC column equilibrated with Solvent A. The elution was carried out at RT and a flow rate of 1 ml/min with the following programme: from 0 to 18 min in 100% Solvent A (isocratic step), from 18.1 to 25 min gradient step to attain 100% Solvent B. The column was then washed for 7 min at 100% Solvent B and equilibrated back into 100% Solvent A with a 4-min gradient step and kept in the same solvent for 10 min, ready for the next injection. The fluorescence detector was set at an excitation wavelength of 240 nm and an emission wavelength of 450 nm according to Perucho et al. (2015).

Using the above HPLC programme, Gln, Glu, GABA, and Norvaline displayed the following retention times: Gln, 2.75 ± 0.02 min; Glu, 4.46 ± 0.06 min; GABA, 12.15 ± 0.20 min; Norvaline, 23.42 ± 0.05 min. The software used for analysis and peak integration was OpenLab (Agilent). Sample peak areas were typically measured by the automatic integration system, though in some circumstances a manual correction of the baseline was required. In order to quantify the amino acids concentrations, the peak area was compared to a calibration curve standard.

Preparation of Stock and Working Solutions

300 mM stock solutions of either GABA or Gln or Glu or norvaline were prepared in HPLC-grade water, aliquoted out and stored at 4°C. Working solutions (10 μM) were prepared weekly (every 3 days for norvaline) by diluting the stock solutions either in HPLC-grade water or in EG medium pH 2.5, aliquoted out and stored at 4°C until use.

Bioinformatics

In order to verify the presence of the *ybaS*/*glsA* gene in the genomes of bacterial species potentially capable of employing GadC to import glutamine for AR2_Q, i.e., possessing *gadBC* operon (alike *E. coli*, *B. microti*, and *L. reuteri*), a Protein Cluster search (https://www.ncbi.nlm.nih.gov/proteinclusters/) using "glutaminase" as search word we performed.

Eighty Protein Clusters were retrieved, 35 of which were excluded because unrelated to the acid-glutaminase, i.e., because they referred to the "pyridoxal 5'-phosphate synthase glutaminase subunit PdxT." In addition to this, all the Protein clusters that included proteins shorter than 200 amino acids or longer than 400 amino acids were also excluded because these proteins share little sequence identity with the reference proteins (*E. coli* YbaS, *B. microti* GlsA) and much different in size. This led to restrict the analysis to 20 protein clusters for a total of 1,584 genomes. When possible, redundant genomes were removed.

In checking all the genomes, the above selection criterion (i.e. occurrence of the *gadBC* operon) was made less restrictive by taking into account also those organisms (and genomes) that did not possess GadB (therefore lack the AR2 system) though still possessed a GadC antiporter, making the AR2_Q system still likely to occur. However, in the latter case only those organisms in which the *gadC* and *ybaS*/*glsA* genes were in close proximity were considered.

All the genomes of interest were therefore searched using the Bacterial Bioinformatics Resource Center PATRIC (https://www.patricbrc.org/) in order to obtain information on the localization of the relevant genes in the genome, their orientation and relative distances, also in a visual way. For completeness of information, when available, fully sequenced genomes were selected among a given species.

Statistical Analysis

Data from AR assays were analyzed via "two-way ANOVA" using the Bonferroni test (as available in the GraphPad Prism software suite, version v5.0a). Data were expressed as means of three independent experiments with standard deviations. Differences were considered statistically significant when $P < 0.05$.

RESULTS

The "GlsAssay" Provides a Rapid and Reliable Screening of Acid-Glutaminase Activity

In recent reports, it was shown that the Rice test (Rice et al., 1993), a colorimetric assay initially performed on *E. coli*, allows to reliably distinguish amongst *Brucella* strains (and their mutant derivatives) those possessing an active GadB (positive to the Rice test) from those having the relevant gene inactivated by mutations and therefore with an AR2 not functional (negative to the Rice test) (Occhialini et al., 2012; Damiano et al., 2015). The acid assay solution is hypertonic (9% of NaCl), cell-permeabilizing (0.3% of Triton X-100) and unbuffered, so that it allows to detect the GadB activity in bacterial cells because the color of the pH indicator (bromocresol green) in the assay

solution turns from yellow to green and then to blue, as protons are consumed (i.e., pH increases) during the decarboxylation of L-Glutamic acid present in the assay solution.

It was therefore hypothesized that an assay solution as above, but in which *L*-Glutamine (Gln) replaces *L*-Glutamic acid (Glu) would allow to detect the activity of the acid-glutaminase (which is named YbaS in *E. coli* and GlsA in *Brucella* spp. and other bacteria) in a similar way as the Rice test allows the detection of GadB activity. The new assay was named "GlsAssay" (hereafter GlsAssay). According to the working hypothesis (see arrow in **Figure 2A**), the pH indicator bromocresol green in the unbuffered solution of the GlsAssay should change color upon pH increase due to the formation of ammonium ion (NH_4^+) from ammonia NH_3 (which at acidic pH remains in solution) during the deamination of glutamine into glutamate by YbaS/GlsA. Moreover, if the GadB activity is present in the bacterial strain under analysis, the glutamine-derived glutamate should feed GadB, which is also active at acidic pH, to yield GABA and a further increase in pH, as monitored by a change in color into blue (**Figure 2A**).

The optimal conditions for GlsAssay were: a starting pH of the assays solution in the range 2.8–3.1 (**Figure S1A**), a density of liquid culture at $OD_{600} = 2.0$ ($0.2–1.0 \times 10^9$ cells/ml), and an incubation at 37°C of 2 h (**Figure S1B**, picture framed in red). At this time point there was a full development of the color which did not change even after an overnight incubation. More cells can be used, i.e., up to twice as much, though this might lead the negative control strain (*E. coli* Δ*ybaS*) to yield a greenish-yellow color, because of the likely alkalinizing effect of too many cells permeabilized in 150 μl of the unbuffered GlsAssay solution (**Figure S1B**, left panels).

In **Figure 2** are summarized the key features of the GlsAssay. In particular, in **Figure 2B** a comparison of the GlsAssay with the Rice test is provided. This shows that the *E. coli* Δ*gadA*-Δ*gadB* mutant (devoid of glutamate decarboxylase activity) was, as expected, yellow at the Rice test, because this test uses *L*-glutamic acid and therefore cannot detect the glutaminase activity. However, *E. coli* Δ*gadA*-Δ*gadB* in the GlsAssay gave a green color because the presence of glutamine in the GlsAssay solution allows to detect the YbaS activity, which is clearly not affected by the Δ*gadA*-Δ*gadB* mutation. The green color detected in the absence of GadA/B, even after a prolonged incubation, suggested that the pH increase as well as the buffering of the ammonium ion and the glutamate formed during Gln deamination do not allow the solution to go much above pH 4.0–4.5, at which pH the bromocresol green is indeed in the green-absorbing form. In **Figure 2C** it is shown that *E. coli* Δ*ybaS* was yellow and therefore negative, as hypothesized, and that the color developed with the GlsAssay after 2 h remained yellow even when the incubation was prolonged to an overnight (**Figure 2C** middle panel).

Overall, it is possible to conclude that the GlsAssay allows to detect the presence of acid-glutaminase activity (samples 3 and 4 in **Figure 2B** lower panel), clearly not detectable when glutamate is used as substrate (i.e., Rice test; samples 3 and 4 in **Figure 2B**, upper panel) and gives a negative results (i.e., yellow) when the strain to be assayed does not possess the gene coding for the acid-glutaminase YbaS/GlsA (Δ*ybaS*), even after an overnight incubation (sample 3 in **Figure 2C**, middle panel). The wild type *E. coli* strain and its Δ*ybaS* derivative strain complemented with a plasmid carrying the *ybaS* gene from *E. coli* gave the expected blue color (samples 1 and 4 in **Figure 2C**), which was the result of an additive effect of the YbaS and GadA/B activities in these strains. The blue color obtained with these strains is clearly arising from the more effective irreversible proton consumption carried out by GadB and the consumption of glutamate, which result in an increase of the pH to above 5.0, where the bromocresol green is blue-absorbing (**Figure 2A**).

Finally, it was tested if the GlsAssay could be rendered even faster by using as starting material colonies picked directly from a plate (see section GlsAssay From Colonies on Plate) rather than bacteria from a liquid culture. Indeed **Figure 2C** (bottom panel) shows that the assay was equally effective regardless of whether the bacteria came from colonies picked on a plate or from a liquid culture. **Figure S2** schematically summarizes the steps of the GlsAssay, starting either from colonies on plate or from liquid cultures, and how to interpret the results according to the scheme provided in **Figure 2A**.

The GlsAssay Allows to Screen the Best Growth Conditions for the Expression of the Acid-Glutaminase

As it can be noticed in **Figure 2C** and **Figure S1B**, during the setting up of the GlsAssay, the strain *E. coli* Δ*ybaS*/pBBR-*glsA_Bm* was also assayed (in the rightmost test tube). This strain was tested to assess for the ability of the *glsA* gene of *Brucella microti* to complement for the mutation in *E. coli* Δ*ybaS*. Indeed *B. microti glsA* was shown to be involved in the AR2_Q of this microorganism and the *E. coli ybaS* gene was demonstrated to complement for the *glsA* mutation in *B. microti* (Freddi et al., 2017). Complementation of *E. coli* Δ*ybaS* with the plasmid pBBR-*glsA_Bm* gave different results depending on the medium in which the bacteria were grown prior to the GlsAssay (to detect GlsA activity) and the AR2_Q assay. According to the intensity of the green in *E. coli* Δ*gadA*-Δ*gadB* (sample n. 2 in **Figure 2C**, **Figure S3A**), the endogenous acid-glutaminase activity in *E. coli* increased when the pH of the medium in which the bacteria were grown prior to perform the assay was increased (from 5 to 8.0) and when glucose was present. However, while the plasmid carrying *ybaS* from *E. coli* (*ybaS_Ec*) could restore the expected phenotype in the GlsAssay (i.e., blue; sample n. 4 in **Figure 2C** and **Figure S1B**) and in the AR2_Q assay (**Figure 3** and **Figure S3B**), regardless of the medium tested, the strain carrying the plasmid with the *glsA* gene of *B. microti* (*glsA_Bm*) gave positive results only when the bacteria were cultivated in LBG-MOPS, pH 8.0, prior to performing the GlsAssay (sample 5 in **Figure 2C** vs. **Figure S3A**) and the AR2_Q assay (**Figure 3**, **Figure S3B**). Also, in the latter case the recovery of the AR phenotype in the *E. coli* Δ*ybaS* carrying the *glsA* gene from *B. microti* was only partial, though significant (i.e., more than 5 logs).

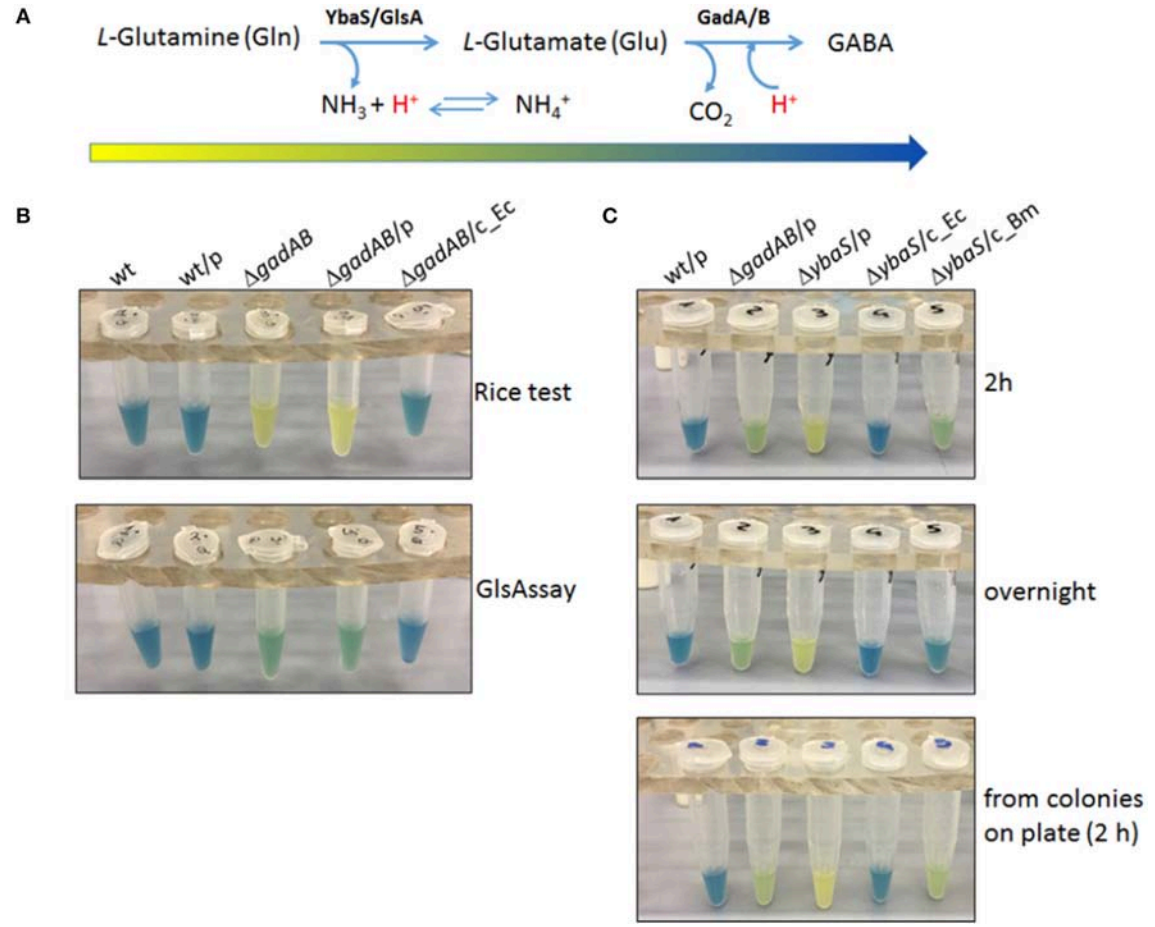

FIGURE 2 | The GlsAssay in *Escherichia coli* K12 MG1655. **(A)** Working hypothesis of the GlsAssay based on the substrates and the enzymes involved. The arrow that begins yellow and ends blue corresponds to the approximate change in color that is expected to occur as the GlsAssay develops, using Gln as starting molecule. **(B)** Preliminary controls. Comparison between the Rice test performed using glutamic acid (upper panel) and the GlsAssay performed using glutamine (lower panel). The strains used were: *E. coli* wild type (wt); wt/pBBR (wt/p); Δ*gadA*-Δ*gadB* (Δ*gadAB*); Δ*gadA*-Δ*gad*/pBBR (Δ*gadAB*/p); Δ*gadA*-Δ*gad*/pBBR_*gadBC* (Δ*gadAB*/c_Ec). The presence of the empty plasmid pBBR1MCS (p) had no effect on the outcome of both tests. The strains were grown for 24 h in LBG pH 5.0, typically used for AR2 assay and Rice test in *E. coli* (Occhialini et al., 2012; Damiano et al., 2015). The GlsAssay was carried out at 37°C overnight. **(C)** Optimized conditions of GlsAssay as described in Materials and Methods (section Rapid Glutaminase Assay ("GlsAssay") and in **Figure S2**). The assay was carried out on the strains: wt/pBBR (wt/p); Δ*gadA*-Δ*gadB*/pBBR (Δ*gadAB*/p); Δ*ybaS*/pBBR (Δ*ybaS*/p); Δ*ybaS*/pBBR-*ybaS_Ec* (Δ*ybaS*/c_Ec); Δ*ybaS*/pBBR-*glsA_Bm* (Δ*ybaS*/c_Bm). The incubation time is shown on the right. p, plasmid pBBR1MCS; c, complemented strain with the missing gene.

Thus, the GlsAssay on the strain *E. coli* Δ*gadA*-Δ*gadB* confirmed that the growth in LBG-MOPS, pH 8.0 was optimal for endogenous YbaS expression and activity, as already reported by Lu et al. (2013). In addition to this, the GlsAssay allowed to demonstrate that the overexpression of the *glsA* gene of *B. microti* could restore the missing activity in the *E. coli* Δ*ybaS* mutant (**Figure 2C**, **Figure S3A**) and that this resulted in recovery of the AR2_Q phenotype (**Figure 3**, **Figure S3B**) only when the overnight growth of *E. coli* Δ*ybaS*/pBBR-*glsA_Bm* was carried out in LBG-MOPS, pH 8.0. This represented a key finding because when using media at lower pH, the recovery of the AR2_Q phenotype turned out to be negative or unsatisfactory (**Figure S3B**).

Notably, the AR phenotype of the *E. coli* Δ*gadA*-Δ*gadB* mutant in the presence of glutamine was always nil (**Figure 3**, **Figure S3B**). Thus, this mutant, though possessing a fully functional *ybaS* gene, is acid-sensitive in the presence of glutamine. This findings points out to the importance of the integrity of the *ybaS* and *gadBC* genes for the full development of a AR2_Q phenotype in *E. coli* and in this respect these results are different from those obtained in *B. microti*, *L. reuteri* and a pathogenic strain of *E. coli* (Lu et al., 2013; Teixeira et al., 2014; Freddi et al., 2017), where the AR2_Q system (i.e. YbaS/GlsA + GadC) seems to be sufficient to protect from extreme acid stress, i.e., pH $\leq$ 2.5. The assay conditions, i.e., higher number of cells and higher Gln levels used in pathogenic *E. coli* and *L. reuteri* (Lu et al., 2013; Teixeira et al., 2014), and the GlsA-GadC over-expression in the *B. microti* strain (Freddi et al., 2017) assayed may well explain the discrepancy.

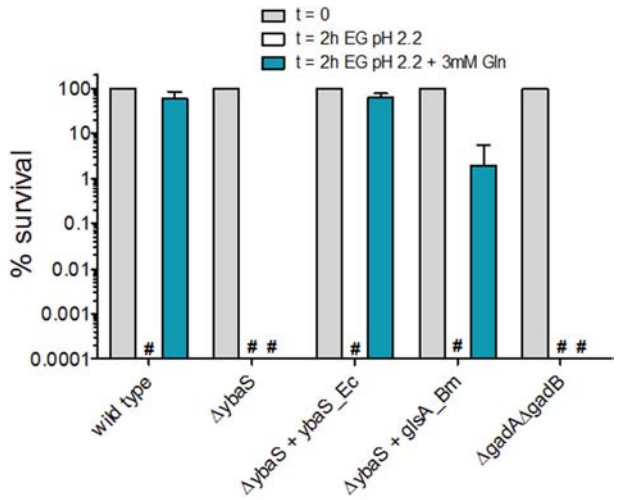

FIGURE 3 | Effect of Gln addition to EG minimal medium at pH 2.2 on the survival of *E. coli* MG1655 and its isogenic mutant strains. Residual viability of stationary-phase cultures of the indicated strains, diluted 1:4000 in EG pH 2.2 and incubated (statically) for 2 h at 37°C. Following the acid challenge, viability was expressed as % CFU/ml on a $\log_{10}$ scale, compared to bacteria present at time zero. The data represent the mean (SD) of 3–6 independent experiments. The hashtag indicates no survivors detected. The complemented strains carried the relevant gene cloned into plasmid pBBR1MCS. For consistency, the empty plasmid was also carried by the mutant strains.

A Quantitative HPLC Assay Allows to Monitor the pH-Dependent Uptake of Glutamine and the Export of Glutamate and GABA *in vivo*

As far as *E. coli* is concerned, the above observation on the acid-sensitive phenotype of the *E. coli* Δ*gadA*-Δ*gadB* mutant is not fully in line with a previous report (Lu et al., 2013). On the other hand, the GlsAssay in the present report (**Figure 2**) as well as previous data (Lu et al., 2013) confirmed that YbaS was still active in *E. coli*Δ*gadA*-Δ*gadB*. In order to understand the origin of the acid-sensitive phenotype of *E. coli* Δ*gadA*-Δ*gadB* and to show how Gln uptake is linked to Glu and/or GABA export *in vivo*, a HPLC-based method was developed. This method allowed to quantitatively assay Gln, Glu and GABA in samples (i.e. supernatants) from bacterial cells exposed for 1 h at 37°C to pH 2.5, 3.1, 3.5, and 4.0 in minimal medium EG containing 3 mM Gln.

The details of the protocol used are provided in Materials and Methods (section HPLC Analysis of Glutamine, Glutamate and GABA in Spent Media) and reported schematically in **Figure S4**. This method allows the quantitation of Gln, Glu, and GABA starting from a few microliters of the acidic medium to which the bacteria were exposed, as reported in section Sample Preparation. Briefly, bacteria (3×10^8 cells, which correspond to at least 10–20 times more cells than in the AR assay in **Figure 3**) were incubated for 1 h at 37°C in EG medium containing 3 mM Gln at pH 2.5, 3.1, 3.5, and 4.0, respectively. After incubation, an aliquot of samples was kept aside to assay the amino acids by HPLC, while another aliquot was immediately plated to perform a bacterial count that provided information on cell viability (**Figure S5**).

The results of the quantitation using the HPLC, shown in **Figure 4**, indicated that depending on the pH and the genotype the cells had different behaviors.

The results shown in **Figure 4** provided the following indications:

(i) in *E. coli* wild-type, the cells consumed Gln and released mainly GABA, only at the most acidic pH tested (i.e., 2.5 and 3.1), while the content of Glu in the medium increased in the sample incubated at pH 3.5, where GABA decreases significantly. At pH 4.0 Gln was very little consumed and, accordingly, Glu and GABA levels were low. This observation was in line with the hypothesis that turning off the transport path provided by GadC *in vivo* is more likely to happen in the lower pH range, with respect to what has been reported in the *in vitro* studies employing reconstituted proteoliposomes (Richard and Foster, 2004; Ma et al., 2012).

(ii) in *E. coli* Δ*ybaS*, the cells were unable to use Gln, which was entirely found in the medium, regardless of the pH. Trace amounts of Glu and GABA were detected. A possible explanation for this finding is that some intracellular Glu was converted by GadA/B (still functional in the Δ*ybaS* mutant) into GABA, which was then exported in exchange for some Gln entering in the cell via GadC (which is expected to be functional in the *ybaS* mutant). The observed trace amounts of Glu and GABA are unlikely to originate from cells lysis because the viability (at least in the samples at pH 3.5 and 4.0) was close to 100% after 1 h of incubation (**Figure S5**) and therefore it is unlikely to be the explanation for the Glu and GABA levels detected in all the samples tested.

(iii) in *E. coli* Δ*gadA*-Δ*gadB*, both decarboxylases are not present, while GadC (Occhialini et al., 2012) and YbaS are functional. The cells used Gln and exported significant amounts of Glu. Maximal Gln consumption was observed at pH 3.1–3.5 (**Figure 4**, left bottom graph), suggesting that this pH is indeed the optimal external pH for GadC, to export Glu (pI 3.25). Notably under the conditions for the HPLC dosage, survival of *E. coli* Δ*gadA*-Δ*gadB* was observed though full AR was not recovered (**Figure S5** vs. **Figure 3**), thus confirming that the discrepancy between the results in **Figure 3** and those published by others (Lu et al., 2013) can be reasonably explained by the starting number of bacteria used in the AR assay.

(iv) in *E. coli* Δ*gadC*, the cells did not import Gln, but some Glu and very little GABA were detected in the medium, though in this case Glu was detected mainly at pH 4.0 with respect to the lower pHs, thus suggesting that another transporter, otherwise silent or less active when GadC is present, was involved in this activity, maybe compensating for the lack of GadC. The observed Glu and traces of GABA are unlikely to originate from cells lysis because the viability (at least in the samples at pH 3.5 and 4.0) was above 70% after 1 h of incubation (**Figure S5**) and therefore cell death cannot be the explanation for the low levels of Glu and GABA detected in all the samples tested. Furthermore, cell lysis would release YbaS and GadA/B

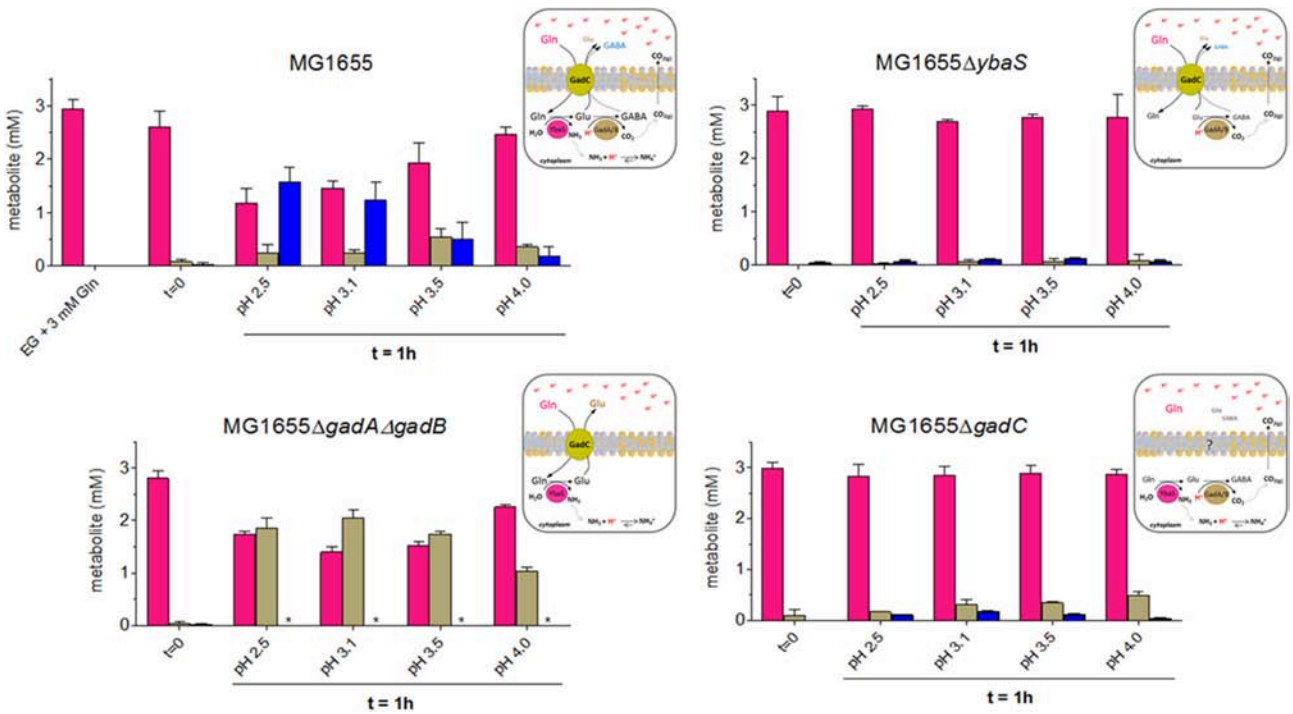

FIGURE 4 | HPLC analysis of Gln, Glu and GABA levels in EG medium at different pHs and from the different mutant strains derived from wild type *E. coli* MG1655. Following the protocol described in Materials and Methods (Section HPLC Analysis of Glutamine, Glutamate and GABA in Spent Media), and represented graphically in **Figure S4**, bacteria were incubated for 1 h at 37°C. Each spent medium was analyzed by HPLC for glutamine (magenta), glutamate (light dove) and GABA (blue) content. Each panel is accompanied by a schematic representation of the cellular context that provides a possible explanation for the observed findings. *means GABA not detected.

which would consume Gln (just as in the GlsAssay) to GABA. However, GABA was hardly detected, which points to the fact that the transport activity by live cells was indeed measured.

In light of these HPLC data, it was concluded that when Gln was available extracellularly at acidic pH, the *E. coli* wild-type cells preferred to export GABA at pH below 3.1, whereas they exported Glu when exposed to a pH less extreme (3.1–3.5), to finally reduce the export activity of both molecules when the pH was above 4.0. The latter can be most likely attributed to a significantly lower activity of intracellular YbaS and GadA/B (at an external pH of 4 the cytoplasm is expected to be $\geq$ 6.0) and of GadC at the level of the membrane. The results with the *gadC* mutant provided strong evidence that in the absence of GadC, Gln remained in the medium and was not taken up by the cells; under acidic conditions, GadC is thus the only membrane protein allowing Gln influx. The absence of YbaS had a similar effect, i.e., Gln mostly in the extracellular medium, thus confirming that YbaS is the only glutaminase that allows the deamination of Gln to yield Glu in the acidic pH range. The striking phenotype of the Δ*gadA*-Δ*gadB E. coli* mutant confirmed that GadC is indeed operative in this mutant by importing Gln and exporting Glu, as already suggested by *in vitro* studies using proteoliposomes (Ma et al., 2013; Tsai et al., 2013). However, this did not compensate for the absence of GadA/B, because under the "classical" assay conditions used for measuring the AR phenotype in *E. coli* (Lin et al., 1995, 1996; De Biase et al., 1999) Δ*gadA*-Δ*gadB* showed a strongly acid-sensitive phenotype at pH $\leq$ 2.5 (**Figure 3**).

In the Genomes of Many Enteric Bacteria the *glsA* Gene Is Adjacent to the *gadB* and *gadC* Genes

The previous reports on the glutamine/acid-glutaminase-dependent AR system (Lu et al., 2013; Teixeira et al., 2014; Freddi et al., 2017) and the results presented above suggested that there is a strong functional link between the AR systems using Gln (AR2_Q) and Glu (AR2). However, the location of the genes *ybaS*, *glsA*, and *gls3* in the genomes of *E. coli*, *B. microti*, and *L. reuteri*, respectively, turned out to be different: the gene coding for the acid-glutaminase can be either far from *gadBC* (as in *E. coli*), or immediately downstream the *gadBC* genes with which it constitutes an operon (as in *B. microti*) or preceding the *gadCB* genes, again in a likely operon arrangement (as in *L. reuteri*).

The functional link between the glutamine and glutamate AR systems suggested that the arrangement of these genes in *E. coli* could be an exception rather than a rule and that *ybaS*/*glsA* gene more typically is near the *gadB* and *gadC* genes, as in *B. microti* and *L. reuteri*. Moreover, it was previously shown that *gadB* and *gadC* are adjacent in many orally-acquired microorganisms and typically constitute an operon (De Biase and Pennacchietti,

2012). Starting from all the above-mentioned observations and findings, an extensive search for *ybaS*/*glsA* in all those bacteria possessing a *gadBC* operon was carried out. This was performed using the procedure described in section Bioinformatics in Materials and Methods. The results are reported in full in **Table S2** and **Figure S6**, whereas in **Figure 5** and **Table 1** are provided the key information. **Figure 5** in particular shows only eleven representative members out of the over 70 species that constitute the 5 groups (in roman numbers, from I to V) that were identified (**Figure S6** and **Table S2**).

Briefly, it was found that the typical gene arrangements were the following: (1) *ybaS*/*glsA* distant from *gadBC* (group I, which included *E. coli*); (2) *glsA* immediately following *gadBC* (groups IIa, which included *B. microti*, and IIb); (3) *glsA* immediately downstream *gadC*, while *gadB*(*C*) is either downstream or, more frequently, distantly located (group III); (4) *glsA* downstream *gadB*, while *gadC* is either immediately downstream or 1–2 genes downstream (group IV); (5) *glsA* preceeding *gadC*, while *gadB* is close (group V, which included *L. reuteri*).

Having this list in hands, it was decided to assess the usefulness of the GlsAssay in microorganisms other than *E. coli*, which was used to set up the assay. Using the conditions of the GlsAssay from colonies on plate described in Materials and Methods, many *Brucella* species with the *glsA* gene functional/not functional were tested because their AR2_Q phenotype was already reported and the occurrence of a functional *glsA* gene and the co-presence of functional *gadB* also known (Freddi et al., 2017). In addition *Proteus mirabilis* (group I), *Yersinia ruckeri* and *Yersinia enterocolitica* (group IIa), *Morganella morganii* (group IIb), *Bacteroides fragilis* (group IV) and *Salmonella* typhimurium LT2 (negative at the bioinformatic analysis) were assayed. As shown in **Figure 6**, all the strains tested gave the expected results at the GlsAssay, as based on the presence of intact/mutated/absent relevant genes. Other strains were tested and the results of the GlsAssay confirmed that they had or not a functional acid-glutaminase, in line with the results of the bioinformatic analysis (data not shown).

DISCUSSION

The ability to sense and respond to an acid stress is central to ensure that bacteria transiting through the extremely acidic stomach compartment will eventually reach and colonize the gut, in which some areas like the colon are also acidic (De Biase and

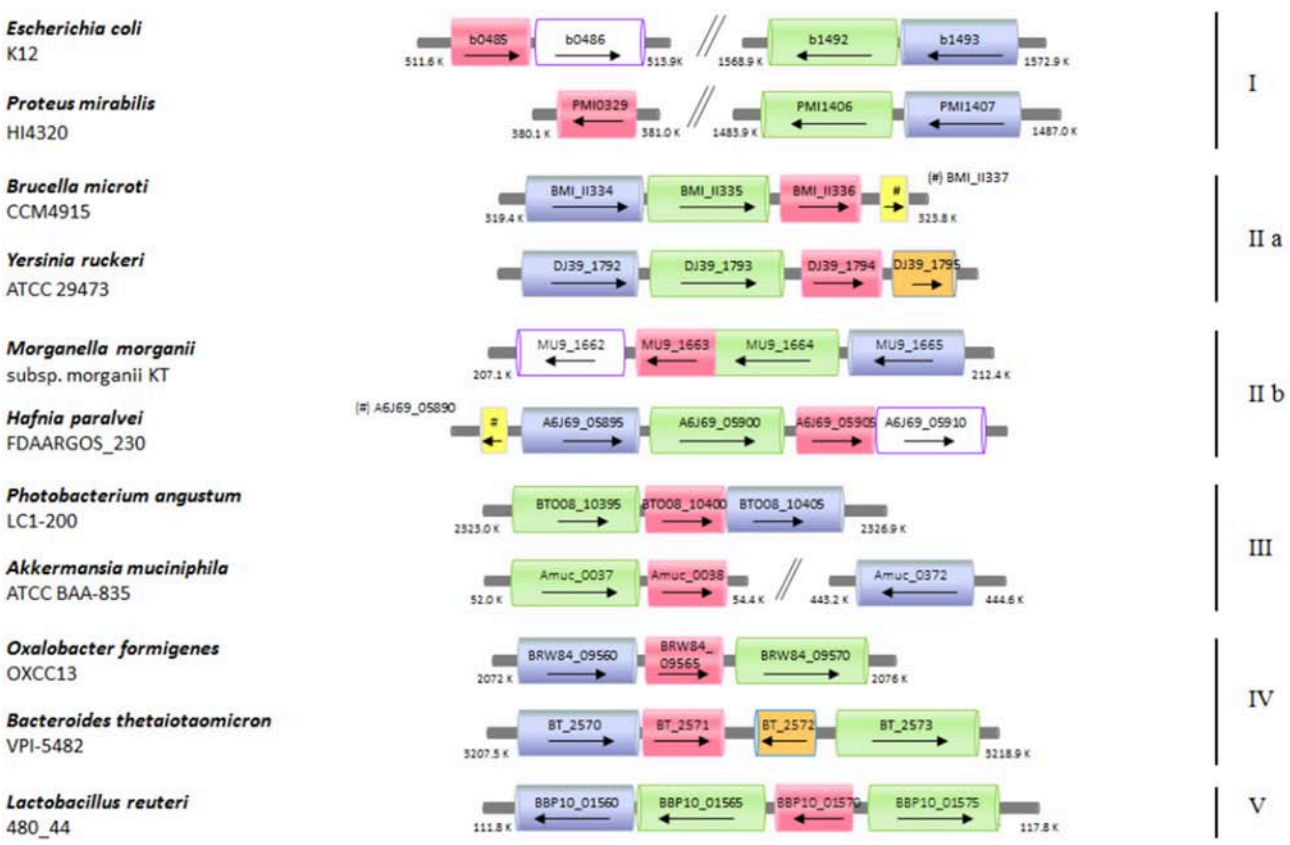

FIGURE 5 | Schematic representation of the distribution of the genes coding for *ybaS*/*glsA*, *gadB*, and *gadC* in different bacterial genomes. Selected bacterial species and strains, where a potentially functional AR2_Q system occurs, are shown. The arrow lengths and the relative distances are proportional to the gene lengths and distances between adjacent genes, respectively. The corresponding locus tags are shown within each arrow. The homologous genes are represented in different colors: *ybaS*/*glsA*, in magenta; *gadC*, in green; *gadB*, in blu; *ybaT*, in white with violet contour; *hdeA*/*B* (periplasmic chaperone) in yellow; putative potassium channel, in orange. The genes with putative functions are dashed in the same color as that of the genes with an assigned function.

TABLE 1 | Bacteria species possessing a potentially functional glutamine-dependent AR system.

Colors of the relevant genes in **Figure 5** and **Figure S6**			*gadB*		*gadC*		*glsA*	
[a]**Species and Strains**	[d]**Phylum**	**First isolated**[e]	**aa**	***gadB* PATRIC ID or RefSeq locus tag**	**aa**	***gadC* PATRIC ID or RefSeq locus tag**	**aa**	***glsA* PATRIC ID or RefSeq locus tag**
[b,c]*Achromobacter piechaudii* (–) ATCC 43553	PROTEOBAC (beta)	Human	391/73	HMPREF0004_2599/ 2600	437	HMPREF0004_2601	311	HMPREF0004_2602
Acidovorax (–) sp 202149	PROTEOBAC (beta)	Human	459	BMF38_06800	514	BMF38_06795	313	BMF38_08290
Akkermansia muciniphila (–) ATCC BAA-835	VERRUCO	Human and animals	466	Amuc_0372	494	Amuc_0037	327	Amuc_0038
Alistipes shahii (–) WAL 8301 (1)	BACTEROID	Human	471	ALI_03190	509	ALI_03010	327	ALI_03000
Bacteroides fragilis (–) NCTC 9343(2)	BACTEROID	Mammals	480	BF0393	411 532	BF0392 BF0487	321	BF0394
Bacteroides thetaiotaomicron (–) VPI-5482 (2a)	BACTEROID	Mammals	481	BT2570	570	BT_2573	321	BT_2571
Barnesiella intestinihominis (–) YIT 11860	BACTEROID	Human	480	HMPREF9448_00311	504	HMPREF9448_00315	320	HMPREF9448_00312
Bordetella avium (–) 197N	PROTEOBAC (beta)	Birds	466	BAV2797	491	BAV2795	312	BAV2794
Brucella microti (–) CCM4915 (3)	PROTEOBAC (alpha)	Common vole	464	BMI_II334	485	BMI_II335	317	BMI_II336
Clostridium perfringens (+) str. 13	FIRMICUTES	soil	464	CPE2058	472	CPE2060	305	CPE1995
Desulfovibrio desulfuricans (–) subsp. desulfuricans str. ATCC 27774	PROTEOBAC (alpha)	Sheep *Ovis aries*	468	Ddes_0045	495 499	Ddes_0046 Ddes_0047	310	Ddes_00484
Edwardsiella tarda (–) EIB202 (4)	PROTEOBAC (gamma)	Fish, humans, chickens and other animals	464	ETAE 2868	526	ETAE_2867	295	ETAE_0268
Enterobacter (–) sp R4-368	PROTEOBAC (gamma)	Jatropha	461	H650_09405	508	H650_09400	308	H650_03370
Enterobacteriaceae bacterium (–) 9_2_54FAA	PROTEOBAC (gamma)	Human	466	HMPref0864_03641	529	HMPref0864_03640	312	HMPref0864_03639
Enterococcus malodoratus (+) *ATCC 43197*	FIRMICUTES	Gouda cheese	466 458	I585_01385 I585_04429	503 475 492	I585_01386 I585_02954 I585_04428	312	I585_02953
Enterovibrio calviensis (–) 1F_211(5)	PROTEOBAC (gamma)	Seawater	459	Figl1190606.3.peg579	518	Figl1190606.3.peg578	313	Figl1190606.3.peg577
Escherichia albertii (–) KF1	PROTEOBAC (gamma)	Human	466	EAKF1_ch0011	511	EAKF1_ch0012	310	EAKF1_ch0947
Escherichia coli (–) *K12* MG1655 (6)	PROTEOBAC (gamma)	Human	466	b1493	511	b1492	310	b0485
Escherichia fergusonii (–) ATCC35469	PROTEOBAC (gamma)	Human	466 466	EFER_2817 EFER_1575	511	EFER_1577	315	EFER_2818
Eubacterium limosum (+) KIST612	FIRMICUTES	Sheep	472	ELI_0972	545	ELI_0973	313	ELI_2455

(Continued)

TABLE 1 | Continued

Colors of the relevant genes in **Figure 5** and **Figure S6**			gadB		gadC		glsA	
[a]**Species and Strains**	[d]**Phylum**	**First isolated**[e]	**aa**	***gadB* PATRIC ID or RefSeq locus tag**	**aa**	***gadC* PATRIC ID or RefSeq locus tag**	**aa**	***glsA* PATRIC ID or RefSeq locus tag**
Fusobacterium nucleatum (–) subsp. animalis, strain KCOM 1279 [7]	FUSOBACT	Subgingival dental plaque, periimplantitis	459	RN98_06450	479	RN98_06445	304	RN98_03350
Grimontia indica (–) AK16	PROTEOBAC (gamma)	Water	459	D515_2780	519	D515_2781	312	D515_2782
Hafnia paralvei (–) strain FDAARGOS_230	PROTEOBAC (gamma)	Human	466	A6J69_05895	529	A6J69_05900	312	A6J69_05905
Izhakiella capsodis (–) strain N6PO6	PROTEOBAC (gamma)	mirid bug, *Capsodes infuscatus*	466	SAMN05216516_101630	516	SAMN05216516_101631	318	SAMN05216516_101632
Lactobacillus reuteri (+) strain 480_44	FIRMICUTES	*Mus musculus*	468	BBP10_01560	510 517	BBP10_01565 BBP10_01575	306	BBP10_01570
Mesorhizobium soli (–) strain JCM 19897	PROTEOBAC (alpha)	Forestal soil	464	C7I85_04950	517	C7I85_04945	314	C7I85_04940
Morganella morganii (–) subsp. morganii KT	PROTEOBAC (gamma)	Human	460	MU9_1665	493	MU9_1664	309	MU9_1663
Obesumbacterium proteus (–) strain DSM2777	PROTEOBAC (gamma)	Feces of wild boar	466	DSM2777_06325	515	DSM2777_06320	312	DSM2777_06315
Odoribacter splanchnicus (–) DSM 20712	BACTEROID	Human, abdominal abscess	465	Odosp_1307	538	Odosp_0380	321	Odosp_0379
Oxalobacter formigenes (–) *OXCC13* strain OXCC13	PROTEOBAC (beta)	Human	465	BRW84_09560	524	BRW84_09570	316	BRW84_09565
Parabacteroides merdae (–) ATCC 43184	BACTEROID	Human	479	PARMER_03646	526	PARMER_03642	321	PARMER_03645
Paraburkholderia xenovorans (–) LB400 [8]	PROTEOBAC (beta)	Contaminated soil	461 461	Bxe_A3826 Bxe_C0551	506 506	Bxe_A3825 Bxe_C0552	304	Bxe_B1127
Photobacterium angustum (–) LC1-200	PROTEOBAC (gamma)	Seawater	466	BTO08_10405	505	BTO08_10395	314	BTO08_10400
Photobacterium damselae (–) subsp. damselae strain KC-Na-1	PROTEOBAC (gamma)	Skin lesions on damselfish	466	CAY62_11315	508	CAY62_11305	319	CAY62_11310
Proteus mirabilis (–) HI4320	PROTEOBAC (gamma)	Human	463	PMI1407	517	PMI1407	308	PMI0329
Providencia alcalifaciens (–) Dmel2 [9]	PROTEOBAC (gamma)	Fruit fly, *Drosophila melanogaster*	466 391	OO9_16601 OO9_18596	512 518	OO9_16606 OO9_18591	311	OO9_18586
Pseudomonas psychrophila (–) strain BS3667 [10]	PROTEOBAC (gamma)	Petroleum sludge	465	SAMN04490201_1375	525	SAMN04490201_1373	314	SAMN04490201_1374
Serratia fonticola (–) strain DSM 4576	PROTEOBAC (gamma)	Human	466 466	WN53_13795 WN53_24805	512 512	WN53_13800 WN53_24810	307	WN53_03050
Shewanella halifaxensis (–) HAW-EB4	PROTEOBAC (gamma)	Sediment	464	Shal_3043	504	Shal_2708	311	Shal_2709

(Continued)

TABLE 1 | Continued

Colors of the relevant genes in **Figure 5** and **Figure S6**			*gadB*		*gadC*		*glsA*	
[a]Species and Strains	[d]Phylum	First isolated[e]	aa	*gadB* PATRIC ID or RefSeq locus tag	aa	*gadC* PATRIC ID or RefSeq locus tag	aa	*glsA* PATRIC ID or RefSeq locus tag
Shigella flexneri (–) 2a str. 301 (11)	PROTEOBAC (gamma)	Human	486 466	SF310_0690 SF301_3206	486 511	SF301_0691 SF301_3205	310	SF301_2702
Tannerella (–) sp. 6_1_58FAA_CT1	BACTEROID	Human	480	HMPREF1033_20619	509	HMPREF1033_20622	321	HMPREF1033_20620
Wohlfahrtiimonas chitiniclastica (–) SH04	PROTEOBAC (gamma)	Fly, *Chrysomya megacephala*	458	F387_10770	489 479	F387_00701 F387_01771	307	F387_00700
Yersinia enterocolitica (–) 8081(12)	PROTEOBAC (gamma)	Human	466	YE3693	518	YE3692	313	YE3691
Yersinia ruckeri (–) 29473	PROTEOBAC (gamma)	Fish	467	DJ39_1792	531	DJ39_1793	312	DJ39_1794

*[a]The species and strains reported in the list are the most representative. The number near each species links to the list (provided below) of all the genomes where the same gene arrangement has been found. They are: [(1)]A. indistinctus 17126; A. putredinis DMS 17216; A. finegoldii DMS242 (but missing gadB)–[(2)]B. oleiciplenus YIT 12058; B. massiliensis B84634; B. vulgatus; B. dorei [(2a)]B. caccae ATCC 43185; B. stercoris ATCC 43183; B. cellulosilyticus WH2; B. intestinalis; B. fluxus–[(3)]B. inopinata BO1; Brucella sp. Br2 09RB8910; B. ceti L2/15; B. pinnipedialis BCCN06-44 – [(4)]E. ictaluri 93-146–[(5)]E. norvegicus.–[(6)] E. coli 12264 (O76:H⁻); E. coli 50588 (O8:H⁻); E. coli DEC14D; E. coli E101; E. coli M718; E. coli STEC_94C – [(7)]Fusobacterium nucleatum subsp. polymorphum strain ChDC F30; Fusobacterium periodonticum strain KCOM 1263–[(8)] the locus tags are of genes located on different chromosome, as indicated by the lettering A, B, and C preceding each number –[(9)]Providencia burhodogranariea DSM 19968 possesses gadBC and glsA but far apart–[(10)]P. fragi P121–[(11)]S. boydii; S. boydii Sb227; S. dysenteriae 1617; S. dysenteriae 225-75; S. dysenteriae CD_74_112–[(12)]Y. frederiksenii ATCC 33641; Y. intermedia ATCC 29909; Y. kristensenii ATCC 33638; Y. kristensenii ATCC 43969. [b]In light gray are shown the species for which the genome sequence is not complete. For this reason in **Figure 5** and **Figure S6** the position of the genes in the genome (K, in kilobases) is not shown. [c](–) Gram–negative bacterium; (+) Gram–positive bacterium [d]BACTEROID, Bacteroidetes; FIRMICUTES, Firmicutes; FUSOBACT, Fusobacteria; PROTEOBAC, Proteobacteria [(alpha), Alphaproteobacteria; (beta), Betaproteobacteria; (gamma), Gammaproteobacteria]; VERRUCO, Verrucomicrobia. [e]The species that are recognized as enteric are shown with a gray background. The coloring of the genes and of the corresponding column in the Table are according to those used in **Figure 5** and **Figure S6**.*

Pennacchietti, 2012; Lund et al., 2014; De Biase and Lund, 2015). However, the ability to tolerate an high concentration of acids is also of great interest in biotechnology where, through adaptive evolution, microorganisms are rendered more and more tolerant to acids which build up either as part of their same production or as a consequence of the metabolic activities of microbial cell factories involved in the synthesis of valuable chemicals (Raab and Lang, 2011; Liu et al., 2015).

Amongst the most efficient acid resistance (AR) mechanisms in bacteria, the amino acid-dependent systems are quite widespread in Gram-negative and Gram-positive bacteria, including pathogenic ones (De Biase and Pennacchietti, 2012; Feehily and Karatzas, 2013; Lund et al., 2014; De Biase and Lund, 2015). In addition to the glutamate- and arginine-dependent AR systems (also named AR2 and AR3, respectively), more recently the glutamine-dependent AR system (AR2_Q) has received attention, because it was found to be functional not only in *E. coli*, but also in some *Brucella* species isolated from the environment and in the wildlife and in *L. reuteri* (Lu et al., 2013; Teixeira et al., 2014; Freddi et al., 2017). This system is as effective as the AR2, with which it shares the GadC antiporter, which is therefore a key structural element of both systems. Notably, as compared to glutamate, glutamine is an amino acid more readily available in the free form in various food sources as well as in the human body, and represents the major form through which nitrogen is transported in an organic form between cells (Lu et al., 2013; Xiao et al., 2016; Kim and Kim, 2017).

In addition to GadC, a key structural component of the AR2_Q is the enzyme glutaminase YbaS (Lu et al., 2013). In *E. coli* there are two glutaminases, one (YbaS) active in the acidic pH range (i.e., pH 4–6) and one (YneH) active in the neutral-alkaline pH range (i.e., 6.0–8). Notably, the gene coding for GlsA, the *Brucella* homolog of YbaS, is located immediately downstream the *gadBC* genes of the AR2, with which it constitutes an operon together with the downstream *hdeA* gene (coding for a periplasmic chaperone), also involved in AR in *E. coli* (Kern et al., 2007; Tapley et al., 2010; Hong et al., 2012).

Herein, a further characterization of the mechanism of action of the AR2_Q system was undertaken with multiple aims. First, to develop qualitative and quantitative assays as convenient alternatives to those currently used, and second to dissect the pH-dependent transport mechanism oparated by GadC. Finally, through an extensive bioinformatic analysis it was attempted to establish the distribution of AR2_Q in bacteria.

The qualitative assay was named GlsAssay: it is an inexpensive, simple to perform, fast, reliable and sensitive colorimetric assay that allows to test for the expression and functionality of the *ybaS*/*gls*A gene product under acidic conditions and to detect if also GadB (i.e., a component of the AR2) is present and active. This is very easily assessed by observing whether the color developed with the assay remains green (even after a prolonged incubation), which indicates that only the YbaS/GlsA enzyme is present and active, or turns into blue, which points to an additive effect of the proton-consuming activity of GadB, the

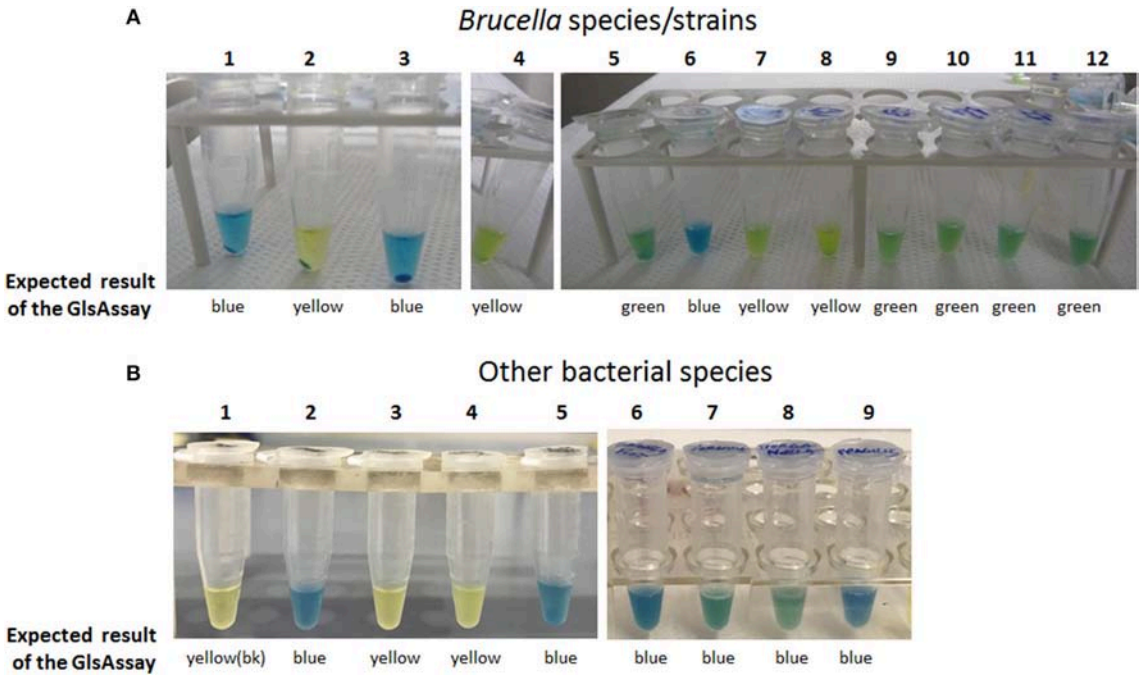

FIGURE 6 | The GlsAssay tested on different bacterial species/strains. **(A)** The GlsAssay was performed starting form colonies on TS plate of the following *Brucella* species/strains: (1) *B. microti* CCM4915 (wild type), (2) *B. microti* CCM4915 Δ*glsA*, (3) *B. microti* CCM4915 Δ*glsA* carrying plasmid pBBR-*glsA_Bm*, (4) *B. abortus* ATCC23448 (wild type), (5) *B. abortus* ATCC23448 carrying plasmid pBBR-*glsA_Bm,* (6) *B. inopinata* BO1, (7) *B. melitensis* 16M, (8) *B. ovis* ATCC25840, (9) *B. neotomae* 5K33, (10) *B. suis* 1330, (11) *B. suis* S4, (12) *B. canis* RM16/66. **(B)** The GlsAssay was performed starting form liquid cultures (picture on the left) or from colonies (picture on the right) of the following bacterial species*:* (1) GlsAssay solution (blank), (2) *E. coli* MG1655 wild type, (3) *E. coli*Δ*ybaS*, (4) *Salmonella* typhimurium LT2, (5) *Yersinia ruckeri* ATCC29473, (6) *Shigella flexneri* CIP52.36, (7) *Yersinia enterocolitica*, (8) *Morganella morganii* morganii CIP A236, (9) *Bacteroides fragilis* CIP77.16. The incubation was carried out at 37°C for 2–3 h.

enzyme glutamate decarboxylase that works under acidic pH conditions too (Rice et al., 1993; Occhialini et al., 2012; Damiano et al., 2015). The results reported herein clearly show that in a physiological background the GlsAssay allows the detection of the acid-glutaminase as well as the co-occurrence of the decarboxylation of glutamate, thus suggesting that intracellularly YbaS/GlsA and GadB work in concert in the bacterial species under analysis.

Even though very informative, the GlsAssay does not provide any information on the *in vivo* uptake of glutamine and which are the molecules released in the extracellular medium (glutamate, GABA or both) depending on the pH of the imposed acid stress. The reports published to date (Lu et al., 2013; Teixeira et al., 2014; Freddi et al., 2017) have dealt only marginally with this point, which is a key point to understand, because the bacterial response to acidic pH involves a number of acid-protecting system, each working at the best within a specific pH range. In other words, the previous reports suggest that in *E. coli* the amino acid glutamine is converted into GABA (via GadA/B activity), but there was no attempt to link this to the pH of the extracellular medium and to quantify the exported substrate(s). On the other hand, we know that GadC, when reconstituted into proteoliposomes, is indeed capable of exporting either glutamate or GABA in exchange for glutamine (Ma et al., 2012, 2013; Tsai et al., 2013). Thus, to evaluate if glutamine is effectively imported by GadC and exported as glutamate and/or GABA, it was necessary to develop an assay that allowed to measure the extracellular levels of these three amino acids at the same time. It should also be reminded that the glutaminase activity was previously detected both *in vivo* and *in vitro* by measuring ammonia production either directly (i.e., using an ammonium ion selective electrode meter) or indirectly (i.e., through a coupled assay using glutamate dehydrogenase) (Brown et al., 2008; Lu et al., 2013), but without any mention on the fate of glutamate arising from glutamine deamination. The results obtained in this work indicate that the AR2 systems (i.e., AR2_Q and AR2) are extremely versatile and that, when Gln is provided extracellularly, GadC exports either GABA, as result of the intracellular activity of the glutaminase YbaS/GlsA and the decarboxylase GadA/B, or glutamate, when only Ybas/GlsA is operative, or both, depending on the acid stress to which the cells are exposed. Overall, the extracellular levels of Glu and GABA reflect the intracellular activity of the two enzymes: GABA is the major product when the acid stress imposed is harsh (pH 2.5), whereas glutamate increases when the extracellular pH is above 3.0. At an extracellular pH > 4.0, the levels of both molecules are low and this clearly reflects the decrease of the intracellular activity of the two enzymes as well as the turning off of the transport channel of GadC, in line with previous studies (Richard and Foster, 2004; Ma et al., 2012). Therefore, this work shows for the first time the pH-dependent

turning off of GadC *in vivo* in the pH range 2.5–4.0 and how this membrane protein provides the key path through which GABA and/or Glu are exported in the medium, depending on the extracellular pH, when Gln is supplied. At pH > 4.0 other systems and membrane proteins are expected (and known) to work (Kanjee and Houry, 2013; Lund et al., 2014; Tramonti et al., 2017).

One of the key findings of this work is that the *glsA* gene in many bacteria is strongly associated with the *gadB* and *gadC* genes. A previous study highlighted that *gadB* and *gadC* lie next to/near each other (De Biase and Pennacchietti, 2012) and a recently published computational study confirmed the correctness of those observations (Bradley et al., 2018). In the present work, for the first time, this association is shown to be extended to the *glsA* gene too. Indeed, in four out of the five groups shown in **Figure 5** and **Figure S6**, the *glsA* gene was typically found close to both *gadB* and *gadC* or at least to one of them. This observation comes from the scrutiny of over 1,500 genomes and opens very interesting perspectives, in particular with regards to the relevance of the AR2_Q system (i.e., glutamine-dependent), as compared to the much more characterized AR2 system (glutamate-dependent). This hypothesis, supported by the results of the GlsAssay performed on several strains (**Figure 6**), needs to be confirmed with more detailed studies aimed at demonstrating the occurrence of a glutamine/glutaminase-dependent AR system in the bacterial species listed in **Table 1**, many of which are of great interest. Nonetheless, the results of the bioinformatic analysis (**Table 1**, **Table S2**, and **Figure 5**, **Figure S6**), do provide a strong indication that the glutamine-dependent AR system is likely to occur and be operative in many bacterial species. With the exception of the Gram-positive *Clostridium perfringens* and *Eubacterium limosum* in group I, *Enterococcus malodoratus* in group III, and *Lactobacillus reuteri* in group V, all the other bacterial species belong to the Gram-negatives. Moreover, most of them (70%) are enteric (with an equal distribution between pathogenic and beneficial bacteria), with some notable exceptions of bacteria isolated from soil or seawater (**Table 1**). This points to a prominent role of the glutamine-dependent AR system in the physiology of bacteria in the gut and in providing an effective mechanism to protect from the extreme acid stress encountered during the transit through the stomach before reaching the gut (Giannella et al., 1972; Martinsen et al., 2005; Beasley et al., 2015). Most of the species belong to the phyla Proteobacteria (approximately 70%) and Bacteroidetes (approximately 20%), with the remainder including four species belonging to the phylum Firmicutes (that also represent the Gram-positives), two species belonging to Fusobacteria and one species belonging to Verrucomicrobia (*Akkermansia muciniphila*). A preliminary observation, restricted to nine genera belonging to the *Enterobacteriaceae* (Djoko et al., 2017), is also in line with the more comprehensive analysis presented in this work.

A notable finding of the bioinformatic analysis is that some genes in one or more groups are frequently found associated to *glsA*, *gadB*, and *gadC*. These include: the homologs of *E. coli hdeA* and *ybaT* genes, and a gene coding for a putative voltage gated-potassium channel.

The *hdeA* gene was already known to be involved in protection from acid stress in Gram-negative bacteria as it encodes a periplasmic acid-induced chaperone (Kern et al., 2007; Tapley et al., 2010; Hong et al., 2012). This gene was found adjacent to or in between the genes of interest in some members of group II (*Brucella microti*, *Enterobacteriaceae bacterium*, and *Hafnia paralvei*) and in one member of group III (*Bordetella avium*).

The *ybaT* gene is encountered in some members of group I (i.e., *Escherichia coli*, *E. albertii*, *Shigella flexneri, S. boydii, S. dysenteriae*), whereas it is strongly associated to the other three genes in members of group IIb. The present as well as a previous work (Lu et al., 2013) have shown that GadC is the key membrane protein involved in the import of glutamine under acid stress. Also, the substrate specificity of the *ybaT* gene product still needs to be established conclusively, though *ybaT* does not seem to code for a membrane protein playing a key role in AR2_Q. A recent report suggests that the increased expression of *ybaS* and *ybaT* during a copper stress under acidic pH and in the presence of Gln, may counteract the inhibition of the GOGAT enzyme (i.e., glutamate synthase) which occurs under these conditions, thereby overcoming the block of Glu synthesis through this important enzyme (Djoko et al., 2017). Overall, the role of the *ybaT* gene product is still elusive and requires further investigations.

Finally, a gene coding for a "putative" voltage gated-potassium channel was frequently found in some bacterial species, mostly belonging to the phylum Bacteroidetes. In particular *Odoribacter splanchnicus* (in group III), most of the members of group IV, except for *Oxalobacter formigens*, and *Yersinia ruckeri* (in group IIa). These proteins are K^+-selective and assigned to the Voltage-gated Ion Channel (VIC) Superfamily. A clear function in AR was never reported for these proteins, however the studies on GadC using proteoliposomes and those on the AR2_Q system in *L. reuteri* do point to a role of potassium entry in positively affecting the antiport activity in GadC and AR in general (Ma et al., 2013; Tsai et al., 2013; Teixeira et al., 2014). The role of potassium channels in bacteria is largely unknown, however it is well known that K^+ is an important cellular cation, for which glutamate represents the major counterion (McLaggan et al., 1994) and that extracellular K^+ (together with Na^+) strongly stimulates the activation of the EvgS sensor kinase of the two component system EvgAS that confers acid resistance to *E. coli* (Eguchi and Utsumi, 2014). A strong link between acidic pH in the activity of potassium channels was demonstrated to be physiologically important in *Corynebacterium glutamicum*, where bacteria respond to a decrease in extracellular pH by decreasing the membrane potential through the influx of K^+ via the ClgK channel, which contributes to maintaining the electrochemical membrane potential constant (Follmann et al., 2009). More recently, the role of acidic pH in the activity of potassium channels was elegantly shown in a structural study on KcsA (a K^+ channel from *Streptomyces lividans*) (Tilegenova et al., 2017). In general, the literature on bacterial potassium channels is scarce however, the bioinformatic analysis carried out in the present work

suggests that there is much more to be understood on the link between acid stress and K^+ transport in bacteria, in particular in Bacteroidetes that are common inhabitants of the human gut.

Overall, the bioinformatic search for the co-occurrence of the *glsA* gene and *gadBC* genes (regardless if distantly located or adjacent) failed to identify a significant number of Gram–positive bacteria, i.e., only 5 out of the over 70 species included in **Table 1**, some of which are listed in the footnotes to avoid redundancy. The reason for this is still unclear and will need further studies.

In conclusion, a rapid method for the detection of the glutaminase activity in bacteria was developed in this work. This method can easily find utilization in routine analysis in laboratories and be used for phenotypic screening. Moreover, the HPLC-based analysis provides a tool for studying the pH-dependent activity of GadC in different bacteria. Finally, the bioinformatic study strongly supports of the widespread occurrence of the glutamine/glutaminase-dependent AR system in many bacterial species, including those that are part of the human gut microbiome. This latter finding is particularly important taking into account that Gln is the most abundant amino acid in systemic circulation (0.6 mM) and that it represents an important microbial metabolite in the distal gut (Matsumoto et al., 2012; Mariño et al., 2017).

AUTHOR CONTRIBUTIONS

DB designed the study. EP, CD, LF, and AO carried out the experiments. EP and DB analyzed the data and performed the bioinformatic analysis. DB and EP drafted the manuscript. All authors contributed to the critical discussion of the results and to the final drafting of the manuscript. The manuscript in the present version was read and approved by all the authors.

FUNDING

This work was supported by Sapienza University of Rome and in part by a grant (PTR540) from Pasteur Institute Paris to DB. Work performed at the Montpellier Laboratory (AO and LF) was supported by a grant (1329-485) from the German Federal Institute for Risk Assessment. EP and LF were recipient of a post-doctoral fellowship (assegno di ricerca) from Sapienza University of Rome and doctoral fellowship from the foundation Infectiopôle Sud, respectively.

ACKNOWLEDGMENTS

We thank Dr. Daniela Bastianelli for constructing the *E. coli* Δ*ybaS* mutant strain. We thank Dr. Josè A. Guijarro (Universidad de Oviedo) for kindly providing the strain *Y. ruckeri* ATCC29473 to test with the GlsAssay. The authors are grateful to Dr. Stephan Köhler (IRIM, Montpellier) and Dr. Dirk Hofreuter (BFR, Berlin) for critically reading the manuscript.

SUPPLEMENTARY MATERIAL

The Supplementary Material for this article can be found online at: https://www.frontiersin.org/articles/10.3389/fmicb.2018.02869/full#supplementary-material

REFERENCES

Beasley, D. E., Koltz, A. M., Lambert, J. E., Fierer, N., and Dunn, R. R. (2015). The evolution of stomach acidity and its relevance to the human microbiome. *PLoS ONE* 10:e0134116. doi: 10.1371/journal.pone.0134116

Bradley, P. H., Nayfach, S., and Pollard, K. S. (2018). Phylogeny-corrected identification of microbial gene families relevant to human gut colonization. *PLoS Comput. Biol.* 14:e1006242. doi: 10.1371/journal.pcbi.1006242

Brown, G., Singer, A., Proudfoot, M., Skarina, T., Kim, Y., Chang, C., et al. (2008). Functional and structural characterization of four glutaminases from *Escherichia coli* and *Bacillus subtilis*. *Biochemistry* 47, 5724–5735. doi: 10.1021/bi800097h

Capitani, G., De Biase, D., Aurizi, C., Gut, H., Bossa, F., and Grutter, M. G. (2003). Crystal structure and functional analysis of *Escherichia coli* glutamate decarboxylase. *EMBO J.* 22, 4027–4037. doi: 10.1093/emboj/cdg403

Damiano, M. A., Bastianelli, D., Al Dahouk, S., Kohler, S., Cloeckaert, A., De Biase, D., et al. (2015). Glutamate decarboxylase-dependent acid resistance in *Brucella* spp.: distribution and contribution to fitness under extremely acidic conditions. *Appl. Environ. Microbiol.* 81, 578–586. doi: 10.1128/AEM.02928-14

Datsenko, K. A., and Wanner, B. L. (2000). One-step inactivation of chromosomal genes in *Escherichia coli* K-12 using PCR products. *Proc. Natl. Acad. Sci. U.S.A.* 97, 6640–6645. doi: 10.1073/pnas.120163297

De Biase, D., and Lund, P. A. (2015). The *Escherichia coli* acid stress response and its significance for pathogenesis. *Adv. Appl. Microbiol.* 92, 49–88. doi: 10.1016/bs.aambs.2015.03.002

De Biase, D., and Pennacchietti, E. (2012). Glutamate decarboxylase-dependent acid resistance in orally acquired bacteria: function, distribution and biomedical implications of the gadBC operon. *Mol. Microbiol.* 86, 770–768. doi: 10.1111/mmi.12020

De Biase, D., Tramonti, A., Bossa, F., and Visca, P. (1999). The response to stationary-phase stress conditions in *Escherichia coli*: role and regulation of the glutamic acid decarboxylase system. *Mol. Microbiol.* 32, 1198–1211. doi: 10.1046/j.1365-2958.1999.01430.x

De Biase, D., Tramonti, A., John, R. A., and Bossa, F. (1996). Isolation, overexpression, and biochemical characterization of the two isoforms of glutamic acid decarboxylase from *Escherichia coli*. *Protein Expr. Purif.* 8, 430–438. doi: 10.1006/prep.1996.0121

Djoko, K. Y., Phan, M. D., Peters, K. M., Walker, M. J., Schembri, M. A., and McEwan, A. G. (2017). Interplay between tolerance mechanisms to copper and acid stress in *Escherichia coli*. *Proc. Natl. Acad. Sci. U.S.A.* 114, 6818–6823. doi: 10.1073/pnas.1620232114

Eguchi, Y., and Utsumi, R. (2014). Alkali metals in addition to acidic pH activate the EvgS histidine kinase sensor in *Escherichia coli*. *J. Bacteriol.* 196, 3140–3149. doi: 10.1128/JB.01742-14

Feehily, C., and Karatzas, K. A. (2013). Role of glutamate metabolism in bacterial responses towards acid and other stresses. *J. Appl. Microbiol.* 114, 11–24. doi: 10.1111/j.1365-2672.2012.05434.x

Flint, H. J., Bayer, E. A., Rincon, M. T., Lamed, R., and White, B. A. (2008). Polysaccharide utilization by gut bacteria: potential for new insights from genomic analysis. *Nat. Rev. Microbiol.* 6, 121–131. doi: 10.1038/nrmicro1817

Follmann, M., Becker, M., Ochrombel, I., Ott, V., Kramer, R., and Marin, K. (2009). Potassium transport in corynebacterium glutamicum is facilitated by the putative channel protein CglK, which is essential for pH homeostasis and growth at acidic pH. *J. Bacteriol.* 191, 2944–2952. doi: 10.1128/JB.00074-09

Fonda, M. (1972). Glutamate decarboxylase. Substrate specificity and inhibition by carboxylic acids. *Biochemistry* 11, 1304–1309. doi: 10.1021/bi00757a029

Freddi, L., Damiano, M. A., Chaloin, L., Pennacchietti, E., Al Dahouk, S., Kohler, S., et al. (2017). The glutaminase-dependent system confers extreme acid

resistance to new species and atypical strains of brucella. *Front. Microbiol.* 8:2236. doi: 10.3389/fmicb.2017.02236

Giannella, R. A., Broitman, S. A., and Zamcheck, N. (1972). Gastric acid barrier to ingested microorganisms in man: studies *in vivo* and *in vitro*. *Gut* 13, 251–256. doi: 10.1136/gut.13.4.251

Grassini, G., Pennacchietti, E., Cappadocio, F., Occhialini, A., and De Biase, D. (2015). Biochemical and spectroscopic properties of Brucella microti glutamate decarboxylase, a key component of the glutamate-dependent acid resistance system. *FEBS Open Bio* 5, 209–218. doi: 10.1016/j.fob.2015.03.006

Gut, H., Pennacchietti, E., John, R. A., Bossa, F., Capitani, G., De Biase, D., et al. (2006). *Escherichia coli* acid resistance: pH-sensing, activation by chloride and autoinhibition in GadB. *EMBO J.* 25, 2643–2651. doi: 10.1038/sj.emboj.7601107

Hazan, R., Levine, A., and Abeliovich, H. (2004). Benzoic acid, a weak organic acid food preservative, exerts specific effects on intracellular membrane trafficking pathways in *Saccharomyces cerevisiae*. *Appl. Environ. Microbiol.* 70, 4449–4457. doi: 10.1128/AEM.70.8.4449-4457.2004

Hong, W., Wu, Y. E., Fu, X., and Chang, Z. (2012). Chaperone-dependent mechanisms for acid resistance in enteric bacteria. *Trends Microbiol.* 20, 328–335. doi: 10.1016/j.tim.2012.03.001

Kanjee, U., and Houry, W. A. (2013). Mechanisms of acid resistance in *Escherichia coli*. *Annu Rev. Microbiol.* 67, 65–81. doi: 10.1146/annurev-micro-092412-155708

Kern, R., Malki, A., Abdallah, J., Tagourti, J., and Richarme, G. (2007). *Escherichia coli* HdeB is an acid stress chaperone. *J. Bacteriol.* 189, 603–610. doi: 10.1128/JB.01522-06

Kim, M. H., and Kim, H. (2017). The roles of glutamine in the intestine and its implication in intestinal diseases. *Int. J. Mol. Sci.* 18:1051. doi: 10.3390/ijms18051051

Krulwich, T. A., Sachs, G., and Padan, E. (2011). Molecular aspects of bacterial pH sensing and homeostasis. *Nat. Rev. Microbiol.* 9, 330–343. doi: 10.1038/nrmicro2549

Lin, J., Lee, I. S., Frey, J., Slonczewski, J. L., and Foster, J. W. (1995). Comparative analysis of extreme acid survival in *Salmonella typhimurium*, *Shigella flexneri*, and *Escherichia coli*. *J. Bacteriol.* 177, 4097–4104. doi: 10.1128/jb.177.14.4097-4104.1995

Lin, J., Smith, M. P., Chapin, K. C., Baik, H. S., Bennett, G. N., and Foster, J. W. (1996). Mechanisms of acid resistance in enterohemorrhagic *Escherichia coli*. *Appl. Environ. Microbiol.* 62, 3094–3100.

Liu, Y., Tang, H., Lin, Z., and Xu, P. (2015). Mechanisms of acid tolerance in bacteria and prospects in biotechnology and bioremediation. *Biotechnol. Adv.* 33, 1484–1492. doi: 10.1016/j.biotechadv.2015.06.001

Lu, P., Ma, D., Chen, Y., Guo, Y., Chen, G. Q., Deng, H., et al. (2013). L-glutamine provides acid resistance for *Escherichia coli* through enzymatic release of ammonia. *Cell Res.* 23, 635–644. doi: 10.1038/cr.2013.13

Lund, P., Tramonti, A., and De Biase, D. (2014). Coping with low pH: molecular strategies in neutralophilic bacteria. *FEMS Microbiol. Rev.* 38, 1091–1125. doi: 10.1111/1574-6976.12076

Ma, D., Lu, P., and Shi, Y. (2013). Substrate selectivity of the acid-activated glutamate/gamma-aminobutyric acid (GABA) antiporter GadC from *Escherichia coli*. *J. Biol. Chem.* 288, 15148–15153. doi: 10.1074/jbc.M113.474502

Ma, D., Lu, P., Yan, C., Fan, C., Yin, P., Wang, J., et al. (2012). Structure and mechanism of a glutamate-GABA antiporter. *Nature* 483, 632–636. doi: 10.1038/nature10917

Mariño, E., Richards, J. L., McLeod, K. H., Stanley, D., Yap, Y. A., Knight, J., et al. (2017). Gut microbial metabolites limit the frequency of autoimmune T cells and protect against type 1 diabetes. *Nat. Immunol.* 18, 552–562. doi: 10.1038/ni.3713

Martinsen, T. C., Bergh, K., and Waldum, H. L. (2005). Gastric juice: a barrier against infectious diseases. *Basic Clin. Pharmacol. Toxicol.* 96, 94–102. doi: 10.1111/j.1742-7843.2005.pto960202.x

Matsumoto, M., Kibe, R., Ooga, T., Aiba, Y., Kurihara, S., Sawaki, E., et al. (2012). Impact of intestinal microbiota on intestinal luminal metabolome. *Sci. Rep.* 2:233. doi: 10.1038/srep00233

McLaggan, D., Naprstek, J., Buurman, E. T., and Epstein, W. (1994). Interdependence of K+ and glutamate accumulation during osmotic adaptation of *Escherichia coli*. *J. Biol. Chem.* 269, 1911–1917.

Occhialini, A., Jimenez de Bagues, M. P., Saadeh, B., Bastianelli, D., Hanna, N., De Biase, D., et al. (2012). The glutamic acid decarboxylase system of the new species *Brucella microti* contributes to its acid resistance and to oral infection of mice. *J. Infect. Dis.* 206, 1424–1432. doi: 10.1093/infdis/jis522

Pennacchietti, E., Lammens, T. M., Capitani, G., Franssen, M. C., John, R. A., Bossa, F., et al. (2009). Mutation of His465 alters the pH-dependent spectroscopic properties of Escherichia coli glutamate decarboxylase and broadens the range of its activity toward more alkaline pH. *J. Biol. Chem.* 284, 31587–31596. doi: 10.1074/jbc.M109.049577

Perucho, J., Gonzalo-Gobernado, R., Bazan, E., Casarejos, M. J., Jimenez-Escrig, A., Asensio, M. J., et al. (2015). Optimal excitation and emission wavelengths to analyze amino acids and optimize neurotransmitters quantification using precolumn OPA-derivatization by HPLC. *Amino Acids* 47, 963–973. doi: 10.1007/s00726-015-1925-1

Petersen, C., and Moller, L. B. (2000). Control of copper homeostasis in Escherichia coli by a P-type ATPase, CopA, and a MerR-like transcriptional activator, CopR. *Gene* 261, 289–298. doi: 10.1016/S0378-1119(00)00509-6

Porte, F., Liautard, J. P., and Kohler, S. (1999). Early acidification of phagosomes containing *Brucella suis* is essential for intracellular survival in murine macrophages. *Infect. Immun.* 67, 4041–4047.

Raab, A. M., and Lang, C. (2011). Oxidative versus reductive succinic acid production in the yeast saccharomyces cerevisiae. *Bioengineered Bugs* 2, 120–123. doi: 10.4161/bbug.2.2.14549

Rice, E. W., Johnson, C. H., Dunnigan, M. E., and Reasoner, D. J. (1993). Rapid glutamate decarboxylase assay for detection of *Escherichia coli*. *Appl. Environ. Microbiol.* 59, 4347–4349.

Richard, H., and Foster, J. W. (2004). Escherichia coli glutamate- and arginine-dependent acid resistance systems increase internal pH and reverse transmembrane potential. *J. Bacteriol.* 186, 6032–6041. doi: 10.1128/JB.186.18.6032-6041.2004

Ross, R. P., Morgan, S., and Hill, C. (2002). Preservation and fermentation: past, present and future. *Int. J. Food Microbiol.* 79, 3–16. doi: 10.1016/S0168-1605(02)00174-5

Tapley, T. L., Franzmann, T. M., Chakraborty, S., Jakob, U., and Bardwell, J. C. (2010). Protein refolding by pH-triggered chaperone binding and release. *Proc. Natl. Acad. Sci. U.S.A.* 107, 1071–1076. doi: 10.1073/pnas.0911610107

Teixeira, J. S., Seeras, A., Sanchez-Maldonado, A. F., Zhang, C., Su, M. S., and Ganzle, M. G. (2014). Glutamine, glutamate, and arginine-based acid resistance in *Lactobacillus reuteri*. *Food Microbiol.* 42, 172–180. doi: 10.1016/j.fm.2014.03.015

Theron, M. M., and Lues, J. F. R. (2010). *Organic Acids and Food Preservation*. Boca Raton, FL: Taylor and Francis.

Tilegenova, C., Cortes, D. M., and Cuello, L. G. (2017). Hysteresis of KcsA potassium channel's activation– deactivation gating is caused by structural changes at the channel's selectivity filter. *Proc. Natl. Acad. Sci. U.S.A.* 114, 3234–3239. doi: 10.1073/pnas.1618101114

Tramonti, A., De Santis, F., Pennacchietti, E., and De Biase, D. (2017). The yhiM gene codes for an inner membrane protein involved in GABA export in *Escherichia coli*. *AIMS Microbiol.* 3, 71–87. doi: 10.3934/microbiol.2017.1.71

Tsai, M. F., McCarthy, P., and Miller, C. (2013). Substrate selectivity in glutamate-dependent acid resistance in enteric bacteria. *Proc. Natl. Acad. Sci. U.S.A.* 110, 5898–5902. doi: 10.1073/pnas.1301444110

Vandal, O. H., Roberts, J. A., Odaira, T., Schnappinger, D., Nathan, C. F., and Ehrt, S. (2009). Acid-susceptible mutants of *Mycobacterium tuberculosis* share hypersusceptibility to cell wall and oxidative stress and to the host environment. *J. Bacteriol.* 191, 625–631. doi: 10.1128/JB.00932-08

Xiao, D., Zeng, L., Yao, K., Kong, X., Wu, G., and Yin, Y. (2016). The glutamine-alpha-ketoglutarate (AKG) metabolism and its nutritional implications. *Amino Acids* 48, 2067–2080. doi: 10.1007/s00726-016-2254-8

Conflict of Interest Statement: The authors declare that the research was conducted in the absence of any commercial or financial relationships that could be construed as a potential conflict of interest.

frontiers in Microbiology

ORIGINAL RESEARCH
published: 16 November 2018
doi: 10.3389/fmicb.2018.02689

Comparative Transcriptomics Highlights New Features of the Iron Starvation Response in the Human Pathogen *Candida glabrata*

*Médine Benchouaia[1†], Hugues Ripoche[1†], Mariam Sissoko[1†], Antonin Thiébaut[1†], Jawad Merhej[1], Thierry Delaveau[1], Laure Fasseu[1], Sabrina Benaissa[1], Geneviève Lorieux[1], Laurent Jourdren[2], Stéphane Le Crom[3], Gaëlle Lelandais[4], Eduardo Corel[3] and Frédéric Devaux[1]**

[1] Sorbonne Université, CNRS, Institut de Biologie Paris-Seine, UMR 7238, Laboratoire de Biologie Computationnelle et Quantitative, Paris, France, [2] École Normale Supérieure, PSL Research University, CNRS, Inserm U1024, Institut de Biologie de l'École Normale Supérieure, Plateforme Génomique, Paris, France, [3] Sorbonne Université, CNRS, Institut de Biologie Paris-Seine, UMR 7138, Évolution, Paris, France, [4] UMR 9198, Institute for Integrative Biology of the Cell, CEA, CNRS, Université Paris-Sud, UPSay, Gif-sur-Yvette, France

OPEN ACCESS

Edited by:
John P. Morrissey,
University College Cork, Ireland

Reviewed by:
Cécile Neuvéglise,
Institut National de la Recherche Agronomique (INRA), France
Sandra Paiva,
University of Minho, Portugal
Gary Moran,
Trinity College, Dublin, Ireland

***Correspondence:**
Frédéric Devaux
frederic.devaux@upmc.fr

[†] These authors have contributed equally to this work

Specialty section:
This article was submitted to Microbial Physiology and Metabolism, a section of the journal Frontiers in Microbiology

Received: 13 July 2018
Accepted: 22 October 2018
Published: 16 November 2018

Citation:
Benchouaia M, Ripoche H, Sissoko M, Thiébaut A, Merhej J, Delaveau T, Fasseu L, Benaissa S, Lorieux G, Jourdren L, Le Crom S, Lelandais G, Corel E and Devaux F (2018) Comparative Transcriptomics Highlights New Features of the Iron Starvation Response in the Human Pathogen Candida glabrata. Front. Microbiol. 9:2689. doi: 10.3389/fmicb.2018.02689

In this work, we used comparative transcriptomics to identify regulatory outliers (ROs) in the human pathogen *Candida glabrata*. ROs are genes that have very different expression patterns compared to their orthologs in other species. From comparative transcriptome analyses of the response of eight yeast species to toxic doses of selenite, a pleiotropic stress inducer, we identified 38 ROs in *C. glabrata*. Using transcriptome analyses of *C. glabrata* response to five different stresses, we pointed out five ROs which were more particularly responsive to iron starvation, a process which is very important for *C. glabrata* virulence. Global chromatin Immunoprecipitation and gene profiling analyses showed that four of these genes are actually new targets of the iron starvation responsive Aft2 transcription factor in *C. glabrata*. Two of them (*HBS1* and *DOM34b*) are required for *C. glabrata* optimal growth in iron limited conditions. In *S. cerevisiae*, the orthologs of these two genes are involved in ribosome rescue by the NO GO decay (NGD) pathway. Hence, our results suggest a specific contribution of NGD co-factors to the *C. glabrata* adaptation to iron starvation.

Keywords: yeast, Aft, ChIP-seq, NO GO decay, evolution

INTRODUCTION

Candidemia are systemic infections caused by different *Candida* yeast species. They are responsible for high mortality rates (40–50%) in immunocompromised patients, despite the existing treatments (Pfaller and Diekema, 2007). These last 20 years, *Candida glabrata* has become the second leading cause of candidemia, behind the extensively studied *Candida albicans* (Pfaller et al., 2014). Although they have similar names, *C. glabrata* and *C. albicans* are very different species (Brunke and Hube, 2013). *C. glabrata*, in evolutionary terms, is more closely related to the model yeast *Saccharomyces cerevisiae* than to *C. albicans* (Dujon et al., 2004). It actually belongs to the *Nakaseomyces* clade. In contrast to *C. albicans*, *C. glabrata* is a haploid. It is less susceptible to the azole compounds which are commonly used to treat candidemia and can rapidly develop high-level resistance

(Pfaller and Diekema, 2007). Moreover, it has evolved distinct invasive strategies and unique transcriptional responses to stress compared to other pathogenic fungi. For instance, *Candida glabrata* is able to survive and multiply in macrophages by escaping or inhibiting most of the phagolysosome anti-microbial weapons (Kaur et al., 2007; Seider et al., 2011, 2014; Kasper et al., 2015). Identifying the specificities of *C. glabrata* is therefore a key issue to understand its virulence and eventually find efficient treatments.

One obvious way to find *C. glabrata* particularities is comparative genomics (Gabaldon and Carrete, 2015). The comparison of *C. glabrata* and *S. cerevisiae* genomes indicated that *C. glabrata* has lost some genes involved in galactose, phosphate, nitrogen, and sulfur metabolisms (Roetzer et al., 2011). These gene losses resulted in auxotrophy for nicotinic acid, pyridoxine, and thiamine (Dujon et al., 2004; Domergue et al., 2005). These features were hypothesized to be related to the pathogenic nature of *C. glabrata*. However, the sequencing of five more *Nakaseomyces* species, including two species found in human patients and three, non-pathogenic, environmental species, showed that most of these changes were actually shared by both pathogenic and non-pathogenic *Nakaseomyces* species (Gabaldon et al., 2013). This study identified the amplification of the *EPA* genes, which encode for glycosyl-phosphatidylinositol (GPI)-anchored cell wall proteins involved in cell adhesion, stress responses and recognition by the innate immune system (Cormack et al., 1999; De Las Penas et al., 2003, 2015; Domergue et al., 2005; Juarez-Cepeda et al., 2015; Vitenshtein et al., 2016) as the main genomic feature correlating with virulence in this clade (Gabaldon et al., 2013; Gabaldon and Carrete, 2015).

Besides gene gains and losses, phenotypic diversity can also arise from gene regulation divergence (Romero et al., 2012; Roy and Thompson, 2015; Thompson et al., 2015; Johnson, 2017). Hence, numerous cases have been described in which changes in the *cis*- or *trans*- regulatory elements of otherwise conserved genes can lead to the emergence of new functions (Romero et al., 2012; Thompson et al., 2015). For instance, the evolution of pregnancy in mammals was associated with transcriptional network rewiring driven by transposable elements (Lynch et al., 2011, 2015). In yeasts, the loss of an AT rich *cis*-regulatory element in the promoters of oxidative phosphorylation and mitochondrial ribosomal protein genes following a Whole Genome Duplication event (WGD) allowed for the appearance of a respiro-fermentative life style in extent post-WGD species (Ihmels et al., 2005; Habib et al., 2012; Thompson et al., 2013). Comparative transcriptomics (i.e., the comparison of gene expression profiles in different species) has been extensively used in yeasts to identify changes in gene regulation that accompanied the appearance of new physiological properties (Ihmels et al., 2005; Lavoie et al., 2010; Wapinski et al., 2010), to achieve model phylogeny for regulatory evolution (Roy et al., 2013; Thompson et al., 2013) or to predict transcriptional regulatory networks in non-model species (Koch et al., 2017). In the present work, we used comparative transcriptomics to identify regulatory outliers (ROs) in *C. glabrata* and in seven other yeast species. ROs are genes that have very different expression profiles from their orthologs in the other species. To find them, we designed REGULOUT, a program which automatically identifies genes with unique profiles among their group of orthologs (i.e., orthogroups). We applied REGULOUT to comparative transcriptome analyses of the response of eight yeast species to toxic doses of selenite, a pleiotropic stress inducer. From these data, REGULOUT identified 38 ROs in *C. glabrata*. Using transcriptome analyses of the *C. glabrata* response to five different stresses, we pointed out five *C. glabrata* ROs which were more particularly responsive to iron starvation, a process which is very important for *C. glabrata* virulence (Nevitt and Thiele, 2011; Srivastava et al., 2014). Global chromatin Immunoprecipitation (ChIP-seq) and gene profiling analyses showed that these five genes were under the control of the iron starvation responsive transcription factor Aft2 and that four of them were actually *C. glabrata* specific Aft2 targets as compared to *S. cerevisiae*. Phylogenetic analyses of the promoter sequences of these four genes suggest that their control by Aft2 was fixed after the WGD. Interestingly, the amount of Aft motifs in the promoters of those genes was particularly high in the *Nakaseomyces* sub-clade including the three potentially pathogenic species sequenced to date (namely *C. glabrata*, *Candida bracarensis* and *Candida nivariensis*), as compared with the non-pathogenic *Nakaseomyces* sub-clade or with the *Saccharomyces* genus. Among these four genes, two (*HBS1* and *DOM34b*) were required for optimal growth of *C. glabrata* in iron limited conditions. In *S. cerevisiae*, the orthologs of these two genes are involved in ribosome rescue by the NO GO decay (NGD) pathway. Hence, our results demonstrate the power of comparative functional genomics to identify novel regulatory systems in non-model species and suggest a specific contribution of NGD co-factors to the *C. glabrata* strategy for its adaptation to iron starvation.

MATERIALS AND METHODS

Strains and Growth Conditions

For comparative transcriptomic analyses, we used the following strains: *Saccharomyces cerevisiae* S288C, *Candida glabrata* CBS138, *Lachancea kluyveri* CBS3082, *Lachancea thermotolerans* CBS6340, *Kluyveromyces lactis* CBS2359, *Candida albicans* SC5315, *Debaryomyces hansenii* CBS767, *Yarrowia lipolytica* CLIB122. All strains were grown in rich media at 30°C (YPD: 1% bacto peptone, 1% yeast extract, 2% glucose) on a rotating shaker (150 rpm), except the halophilic yeast *D. hansenii* which was grown in YPD supplemented with 0.5 M NaCl.

For *C. glabrata* mutant strain construction, we used the HTL background (*his3-*, *trp1-*, *leu2-*) (Schwarzmuller et al., 2014). The tagging of *DOM34a*, *DOM34b*, *HBS1*, and *MAK16b* with TAP tag was performed by PCR and homologous recombination as described in Merhej et al. (2015). The tagging cassette was PCR amplified from the pBS1479 plasmid (Puig et al., 2001). The tagging of *AFT2* with a myc epitope was performed exactly as described (Merhej et al., 2015) using the myc-His cassette from the Longtine's collection (Longtine et al., 1998). The *AFT2* deleted strain was obtained from the Schwarzmuller et al. (2014) collection. The *MAK16b* deleted strain was obtained by PCR and homologous recombination as described previously

(Merhej et al., 2015). The *HBS1*, *DOM34a*, and *DOM34b* deletion mutants were obtained by a two steps PCR process using large homologous regions as described previously (Schwarzmuller et al., 2014). For all deletions, we used the *TRP1* deletion cassette from the Longtine's collection (Longtine et al., 1998). For all constructs, the positive clones were selected by growth on CSM-TRP media, except for the *AFT2-MYC* tagged construct which was screened on CSM-HIS media (2% glucose, 0.67% yeast nitrogen base, recommended amounts of CSM-HIS or CSM-TRP from MP Bio). The proper insertion of the cassettes at the targeted genomic loci and the absence of wild type versions of the targeted gene was controlled by PCR. All primers used in this study are available in **Supplementary File S1**.

Multispecies Transcriptome Analyses: Basic Experimental Set Up and RNA Extractions

For each species, we first determined the dose of selenite required for a 100% decrease of the growth rate in exponential phase. The results were: 0.5 mM for *C. albicans*, *D. hansenii*, *K. lactis*, and *L. kluyveri*, 1 mM for *C. glabrata*, 5 mM for *L. thermotolerans*, 10 mM for *S. cerevisiae* and *Y. lipolytica*. Next, we performed kinetic experiments in which the cells were grown in YPD (or YPD + salt for *D. hansenii* as indicated above) at 30°C until they reach an optical density (OD) at 600 nm of 0.6–0.7. Then, we split the cultures in two: one sub-culture received a mock treatment while the second was treated by the indicated amount of selenite (sodium selenite from sigma, stock solution prepared at 0.2 M in water). This step defines time zero. Every 10 min from time 10 to time 80 min, 20 mL of each culture were collected and flash-frozen in 30 mL of cold (−80°C) absolute ethanol. The cells were centrifuged (5 min, 4,000 rpm), washed with cold (4°C) distilled sterilized water, centrifuged again and cell pellets were stored at −80°C. In parallel to sample collection, the OD of the two cultures was measured every 30 min for 3 h to assess the impact of the selenite treatment on the growth rate. For each species, 6–10 independent kinetic series were generated. Only the four series which were the closest to the 100% decrease of growth rate as compared to the mock treated cultures were used for RNA extraction and microarray analyses. RNAs were extracted using the RNeasy kit (Qiagen) following the protocol provided by the supplier. The quality of the RNA extracts was checked on agarose gels prior to reverse transcription.

Multispecies Transcriptome Analyses: Microarray Design, Microarray Experiments, Data Analyses

Agilent 8x60k custom microarrays were designed for each species (array express accession numbers: A-MEXP-2402, A-MEXP-2365, A-MTAB-642 to 647). For probes design, we used the Teolenn software version 2.0.1 (Jourdren et al., 2010). The genome sequences and ORFs positions used to create probe sequences were downloaded from the Genolevures website. Only the coding sequences were used for probe design, introns and intergenic regions were not considered. The masked genomes (i.e., without repeated sequences) required for Teolenn were created using RepeatMasker version open-3.2.8 with the "-pa 4 -species fungi -xsmall" arguments. The main features of the design are summarized in **Supplementary File S2**. There were no probe replicates on the arrays but each ORF was covered by eight different probes in average. For microarray experiments, 1 μg of total RNA was used for fluorescent cDNA synthesis according to the amino-allyl protocol (Merhej et al., 2015). The cDNAs were labeled with Cy3 and Cy5 and hybridization was performed as previously described (Merhej et al., 2015). Four biologically independent experiments were performed for each condition, using dye switch. After overnight hybridization and washing, the slides were scanned using a 2-micron Agilent microarray scanner. The images were analyzed using the feature extraction software (Agilent Technologies) and normalized using global LOESS (Lemoine et al., 2006). The mean of the four biological replicates was calculated. A gene was considered as being induced (repressed) if its mean Log_2(fold change) value was more than 0.75 (less than −0.75) and if its expression variation was considered as being statistically significant using the LIMMA package with a cut-off *p*-value of 0.01 (Ritchie et al., 2015) for at least two consecutive time points. The complete microarray data are available at Array express database under the accession numbers: E-MTAB-7022, E-MTAB-7023, E-MTAB-7044 to 7047, E-MTAB-7049 and E-MTAB-7053. The processed dataset is available in **Supplementary Table T1**.

REGULOUT

REGULOUT is a python program which takes as an input a multispecies expression matrix and the repartition of the genes in orthogroups. There are two parameters which need to be set up by the user: the minimal size of the orthogroups to be used and the Euclidian distance cut-off to be applied. Then REGULOUT calculates, for each orthogroup reaching the defined minimal size, the pairwise distances between the expression profiles of the genes belonging to the orthogroup. In a next step, REGULOUT defines as ROs all the genes which minimal pairwise distance in their orthogroup is equal to or higher than the minimal distance cut-off. As an output, REGULOUT provides a text file with the name of the ROs, their minimal distance in their orthogroup, the ID number and the size of their orthogroup. It also generates automatically PNG files with the expression profiles of the orthogroups in which at least one RO has been identified. REGULOUT can be freely downloaded from www.lcqb.upmc.fr/REGULOUT/, together with a tutorial and the input data sets used in this study. More precisely, the input files used in this article were the expression matrix for all species and the composition of yeast orthogroups taken from the PhylomeDB database (Huerta-Cepas et al., 2014). The distribution of the sizes of the orthogroups is available in **Supplementary File S3**. The minimal size of the orthogroups to be used was set up to 8 to work mostly with genes which were conserved in all the eight yeast species that were considered. The impact of this filter on the number of expression profiles analyzed by REGULOUT is indicated in **Supplementary File S2**. The minimal distance cut-off was set up at 3, which corresponded to the 75 percentile of all the possible pairwise distances in the dataset. From the raw output of REGULOUT (440 genes), we filtered out the

genes which were defined as ROs based on expression variations that were poorly reproducible (p-value > 0.01). Because the Euclidian distance that we used is very sensitive to stochastic variations for genes with a large amplitude in their expression changes, we also removed from the RO list the genes belonging to orthogroups in which all the members had the same directionality in their expression variations (see **Supplementary File S4** for an illustration). The filtered REGULOUT output contained 289 ROs which are listed in **Supplementary Table T2**.

Multi-Stress Transcriptome Analyses in *C. glabrata*

All cultures were conducted in a rotating shaker at 30°C in YPD (glucose 2%, yeast extract 1%, bacto peptone 1%). Stress conditions used were: 1 mM for sodium selenite, 1 M for NaCl, 2 mM for cadmium chloride, 5 mM for iron sulfate or 0.5 mM for bathophenanthroline disulfonate (BPS). Stressed and mock-treated cells were collected as described above, 20 min and 40 min after treatment. RNA extractions, microarray hybridization and data normalization were performed as described above. For the *aft2Δ* versus wild type comparisons, the stress concentrations were the same as above but the cells were collected only 30 min after treatment. The complete microarray data are available at Array express database under the accession numbers: E-MTAB-7023, E-MTAB-7042, and E-MTAB-7043.

Chromatin Immunoprecipitation and High-Throughput Sequencing (ChIP-Seq)

For Aft2 ChIP experiments, myc-tagged strains were grown in YPD until exponential phase (OD = 0.8), they were then treated by 0.5 mM of BPS for 60 min. Cross-linking of the cells and ChIP were performed as described previously (Merhej et al., 2016). The parental HTL (untagged strain) was grown and processed the same way to provide the mock-IP samples. Sequencing of the IPs, Input DNAs and mock IPs samples and primary data analyses (quality controls and mapping of the reads) were performed as described previously (Merhej et al., 2016). Peak calling was performed with the bpeaks software, using both the Input DNA and the mock IP as references (Merhej et al., 2014). For peak calling using the Input DNA as reference, the bpeaks parameters were T1 = 1, T2 = 6, T3 = 1, T4 = 0.7. For peak calling using the Mock IP as reference, the bpeaks parameters were T1 = 1, T2 = 6, T3 = 1, and T4 = 0. Only the peaks that were found in both analyses were kept for further processing. These peaks were then manually checked on a genome browser (Thorvaldsdottir et al., 2013) to discard artifactual peaks (e.g., peaks centered on a tRNA locus, peaks perfectly overlapping a highly expressed ORF) which would have escaped the bpeaks filter. Peaks located outside of a promoter region (i.e., between convergent ORF or inside ORFs) were also discarded from the final list presented in **Supplementary Table T3**. For DNA motif prediction, DNA sequences of ChIP peaks were retrieved from their genomic locations (BED file) using the "getfasta" function from the BEDTOOLS suite (Quinlan and Hall, 2010). These genomic sequences were used as inputs for the peak-motif tool to search for regulatory motifs (Thomas-Chollier et al., 2012). An additional filtering step was added to the standard peak motif procedure to discard low complexity motifs (e.g., CCCCCCC). The list of Aft targets from *S. cerevisiae* was obtained from Yeastract (Teixeira et al., 2018) and completed by the "regulation" pages of the SGD[1], taking all the documented regulatory interactions using DNA binding or expression evidences and keeping only the targets which were found in relevant growth conditions (i.e., metal stress conditions). The raw ChIP-seq data can be downloaded from the GEO database with the accession number GSE116077.

Bioinformatics Analyses: Gene Ontology, Hierarchical Clustering, Promoter Sequence Analyses

Gene ontology (GO) analyses were performed using the GO term finder tool at the Candida Genome Database[2] for *C. albicans*, *C. glabrata*, and *D. hansenii* (with the names of the *C. albicans* orthologs), at the Saccharomyces Genome Database for *S. cerevisiae*, the two *Lachancea* species, *K. lactis* and *Y. lipolytica* (using the names of the *S. cerevisiae* orthologs). The hierarchical clustering of **Figure 2** was performed using Mev with Euclidian distance, optimization of gene leaf order and average linkage. For phylogenetic analyses of the promoter sequences, we downloaded the promoter sequences (i.e., 500 base pairs upstream of the ATG) from the Genome Resources for Yeast Chromosomes database (GRYC[3]), except for the *Saccharomyces* sequences which were taken from the www.saccharomycessensustricto.org website (Scannell et al., 2011) and for the *Kazachstania Africana* sequences which were downloaded from the NCBI website. The sequences used can be found in **Supplementary Files S5–S8**.

Western Blot Analyses

The cells were grown in YPD at 30°C until they reach an OD at 600 nm of 0.6–0.7. Then, we split the cultures in two: one sub-culture received a mock treatment while the second was treated by 0.5 mM BPS. This step defines time zero. At 30, 60, and 90 min, 10 mL of each culture were collected and centrifuged (5 min, 4,000 rpm), washed with cold (4°C) distilled sterilized water, centrifuged again and cell pellets were stored at −80°C. Proteins were separated on 10% SDS-polyacrylamide gel electrophoresis (SDS-PAGE). Proteins were then transferred to Whatman® Protan® BA83 nitrocellulose membrane (GE Healthcare). Immunoblotting of the protein A-tagged proteins was performed with a rabbit IgG-HRP polyclonal antibody (PAP; code Z0113; Dako), which has a high affinity for Protein A. The membrane was stripped by boiling 30 min in 62.5 mM Tris-HCl pH 6.8, SDS 2% and 4 mM DTT, followed by 10 washes in PBS-Tween (0.1%). Then, immunoblotting of the ribosomal protein Rpl3, used as a loading and transfer control, was performed using 1:10000 rabbit IgG Anti-Rpl3 [gift from M. Garcia: refer to (Delaveau et al., 2016)] and 1:15000 anti-rabbit IgG-HRP

[1] www.yeastgenome.org
[2] www.candidagenome.org
[3] http://gryc.inra.fr/

(Promega) as primary and secondary antibodies, respectively. Detection of the signals was performed using G:BOX Chemi XT4 (Syngene) following incubation with UptiLightTM HRP blot chemiluminescent ECL substrate (Interchim).

Growth Assays

Growth assays were performed in 96 well plates using a TECAN Sunrise machine. Exponential phase growing cultures of the strains to be tested were diluted to OD = 0.1 in a 50 mL sterile Falcon tube. The 96 well plate was filled with 90 μL of the cultures. Then, 10 μL of BPS 0.5 mM stock solution (iron starvation conditions, final concentration 0.05 mM) or 10 μL of sterile water (mock treatment) were added to each well to reach a final culture volume of 100 μL. Cell growth at 30°C was followed for 24 h. The slope of the linear part of the log(OD) = f(t) curve was extracted and used as the growth rate of each culture in exponential phase. Two technical replicates were made in each plate.

RESULTS

Identifying Regulatory Outliers From Comparative Transcriptomics Data

The starting point of this study consisted in analyzing and comparing the response of eight yeast species (*S. cerevisiae*, *C. glabrata*, *L. kluyveri*, *L. thermotolerans*, *K. lactis*, *C. albicans*, *D. hansenii*, and *Y. lipolytica*) to the stress caused by detrimental doses of selenite. These eight species were chosen because they span the whole Hemiascomycetes tree and because of their high-quality genome annotation at the time when we started the study (Genolevures et al., 2009). Selenite was chosen because it was shown to induce both iron starvation and oxidative stress responses in *S. cerevisiae* (Salin et al., 2008; Herrero and Wellinger, 2015), two stress conditions that *C. glabrata* is facing when invading the human body and being internalized by the cells of the innate immune system (Nevitt and Thiele, 2011; Brunke and Hube, 2013). A key challenge in comparative transcriptomics is to set up the growth conditions to make the physiological state of the different species as similar as possible and to minimize irrelevant differences in gene expression (Kuo et al., 2010; Thompson et al., 2013). To do so, we adjusted the selenite doses used for each species to obtain the same 100% increase in the generation time. Then, RNA samples were collected at eight time points after selenite exposure and compared to the RNAs extracted from a control culture mock-treated for the same duration using microarrays. Four replicates were performed for each species and each time point. **Supplementary Table T1** provides the average $\log_2$ of the expression ratios between treated and untreated cells for each measured gene in each species for the eight time points, together with a statistical assessment of the significance of the gene expression variations.

As *a posteriori* validation of our approach, we examined the expression patterns of genes from the general Environmental Stress Response (ESR), which were shown to be highly conserved among the species we studied (Gasch et al., 2000, 2004; Gasch, 2007; Roy et al., 2013; Thompson et al., 2013). We observed that the induction of genes encoding proteasomal subunits and the repression of genes from the Ribosome Biogenesis (Ribi) regulon were consistent between the different species (**Supplementary File S9**). This was a good indication that the eight species were encountering physiologically similar stress conditions. To identify ROs from these 44,723 expression profiles, we designed a program called REGULOUT (**Figure 1**, left panel). REGULOUT takes as input files the expression profiles obtained in the different species and a table describing the orthology relationships between genes (i.e., the names of the genes composing each orthogroup). For each orthogroup taken independently, it calculates all the pairwise distances between the expression profiles of all the genes belonging to the orthogroup. Then, it looks for genes which minimal distance value in the orthogroup is higher than a distance cut-off set up by the user. Those genes with special expression profiles are the so-called "ROs." The key parameters for REGULOUT are the minimal distance that the user accepts to define a RO and the minimal number of genes for an orthogroup to be considered in the analysis. We applied REGULOUT to our data with parameters corresponding to genes conserved in most of our yeast species (i.e., minimal orthogroup size = 8) and to a minimal distance cut-off equal to the 75 percentile of all the calculated pairwise distances (i.e., $d = 3$). With this criterion, we identified a total of 289 ROs in the eight species, ranging from 6 in *L. thermotolerans* up to 87 in *C. albicans* (**Figure 1** and **Supplementary Table T2**). Careful examination of the corresponding expression profiles led us to distinguish three different situations: directional ROs, quantitative ROs and timing-related ROs. Directional ROs are unique in the directionality of their regulation (i.e., up-regulation, down-regulation or unchanged expression). This is exemplified by the *DOM34* orthogroup in **Figure 1** (right panel). In this example, the expression of one *C. glabrata* member (*CAGL0B04675g*) is strongly induced by selenite while its paralog in *C. glabrata* and its orthologs in the seven other species show unchanged or reduced expression. The quantitative ROs have the same directionality of regulation than other members of the orthogroup, but with much larger amplitude. This is exemplified by the *HBS1/SKI7* orthogroup in the right panel of **Figure 1**. *HBS1* is induced by selenite in *C. albicans*, *D. hansenii*, *L. kluyveri*, and *C. glabrata*, but the induction of the *C. glabrata* gene *CAGL0G02255g* is sufficiently higher than its orthologs to be considered as a RO by REGULOUT. The timing-related ROs have the same directionality and range of regulation than some of their orthologs, but with a different timing. This is exemplified by the *GCV1* orthogroup in **Figure 1** (right panel). *GCV1* is induced in several species following selenite exposure but the pattern of early and transient induction is unique to the *S. cerevisiae* member of this group (*YDR019c*).

Gene ontology analyses indicated that only a few GO terms were enriched in the RO lists of the different species (**Supplementary File S10**). These include genes of the arginine biosynthesis pathway (*ARG3*, *ARG4*, *ARG5,6*, *ARG8*, *CPA1*, *CPA2*), which were much more strongly induced by selenite

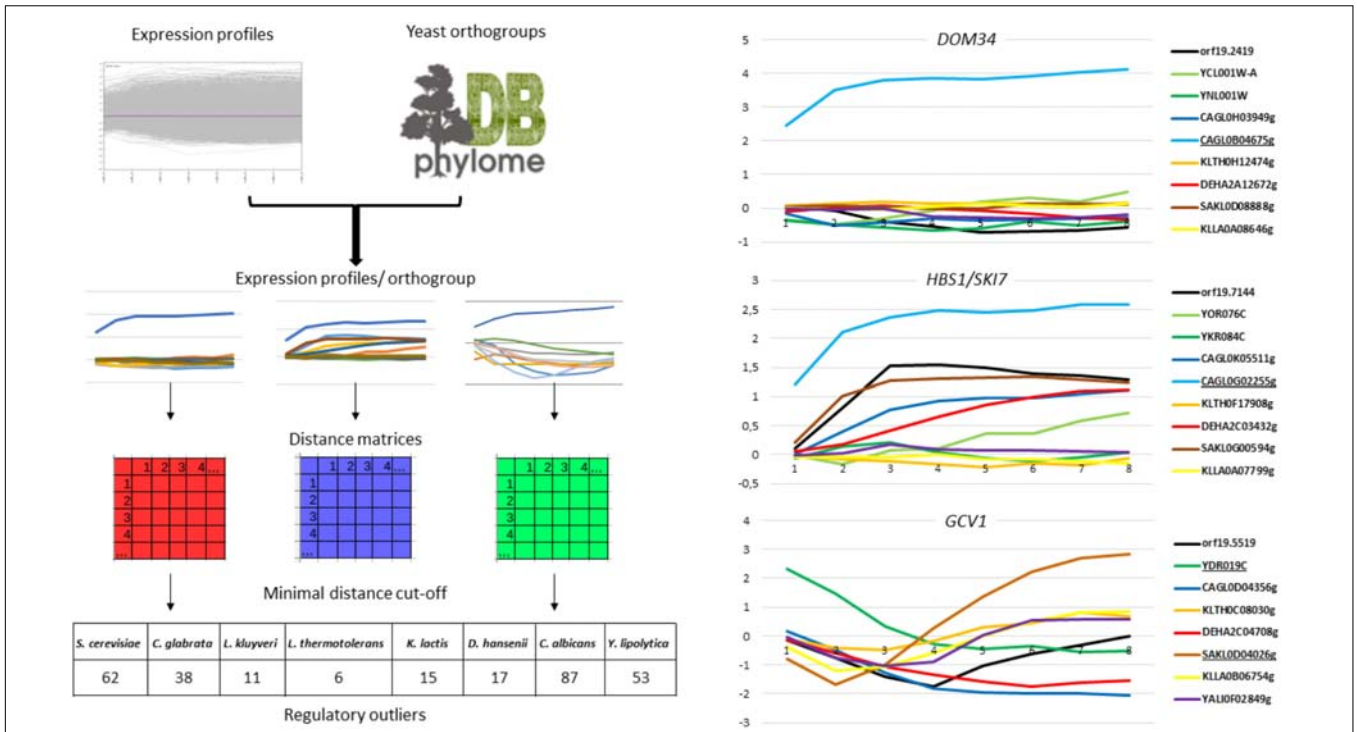

FIGURE 1 | Rationale and outputs of REGULOUT. **(Left)** This scheme summarizes the rationale of REGULOUT. The table at the bottom indicates the number of regulatory outliers identified for each species with the parameters indicated in the material and methods. **(Right)** Expression profiles [Log_2(selenite/mock treatment expression ratio)] as a function of time (1 unit = 10 min) for three orthogroup (*DOM34*, *HBS1/SKI7,* and *GCV1*). The names of the genes in the orthogroup are indicated at the right of each graph. The names of the regulatory outliers are underlined. The colors are: blue for *C. glabrata*, green for *S. cerevisiae*, black for *C. albicans*, orange for *L. thermotolerans*, red for *D. hansenii*, brown for *L. kluyveri*, yellow for *K. lactis*. The phylome DB logo was taken from the phylome DB database website (Huerta-Cepas et al., 2014).

in *C. albicans* than in any other species, and orthologs for the two main actors of a ribosome disassembly pathway named NGD (*DOM34* and *HBS1*), which were specifically induced in *C. glabrata*. Also, several amino-acid metabolism genes (*ARG3*, *HIS1*, *HIS4*, *HIS7*, *CPA1*, *LYS12, MET6, TRP3*) had special expression patterns in *C. glabrata*. This was already noticed in a previous comparative transcriptomics study analyzing the heat shock stress response in eight yeast species (Roy et al., 2013).

Five ROs in *C. glabrata* Are Induced in Iron Starvation Conditions

As mentioned above, selenite triggers several stress responses (iron starvation, oxidative stress response, DNA damage…) (Pinson et al., 2000; Salin et al., 2008; Perez-Sampietro et al., 2016) and therefore the ROs identified from the selenite comparative transcriptomics data may actually respond to different physiological signals and pathways. We were more particularly interested in identifying ROs in *C. glabrata* which would be linked to the iron starvation response. With this goal in mind, we focused on the 38 *C. glabrata* ROs and took advantage of transcriptome data analyzing the response of *C. glabrata* to five different stress conditions (osmotic stress, iron excess, cadmium, BPS or selenite treatments), which were obtained in the frame of another project (unpublished data). For the present work, we only extracted the data for the *C. glabrata* ROs (**Supplementary Table T4**). We then clustered them according to their expression profiles in these five stress conditions (**Figure 2**). Doing so, we could point out a group of five ROs which showed early and strong induction in response to the two iron starvation conditions (namely BPS and selenite treatments) and unchanged or slightly increased expression in response to osmotic and iron excess stresses. This group included the *C. glabrata* orthologs of the *S. cerevisiae* genes encoding the Grx3 glutaredoxin (*CAGL0L11990g*), the Mmt2 mitochondrial iron transporter (*CAGL0E06006g*), the Mak16 ribosome biogenesis factor encoding (*CAGL0F00715g*) and the Dom34 and Hbs1 translation surveillance factors (*CAGL0B04675g* and *CAGL0G02255g*). For the sake of simplicity, we will call the *C. glabrata* genes by the name of their *S. cerevisiae* orthologs in the rest of the article. For *DOM34* and *MAK16*, two paralogs exist in *C. glabrata*. In these cases, the BPS and selenite inducible versions will be called *MAK16b* and *DOM34b* and the versions with unchanged or repressed expression patterns will be called *MAK16a* (*CAGL0G06248g*) and *DOM34a* (*CAGL0H03949g*). Among these five ROs, three were directional ones (*GRX3*, *DOM34b* and *MAK16b*), meaning that they were induced by selenite only in *C. glabrata*, and two were quantitative ROs (*HBS1* and *MMT2*), meaning that they were also induced in other species, but to a lesser extent than in *C. glabrata* (**Supplementary File S11**).

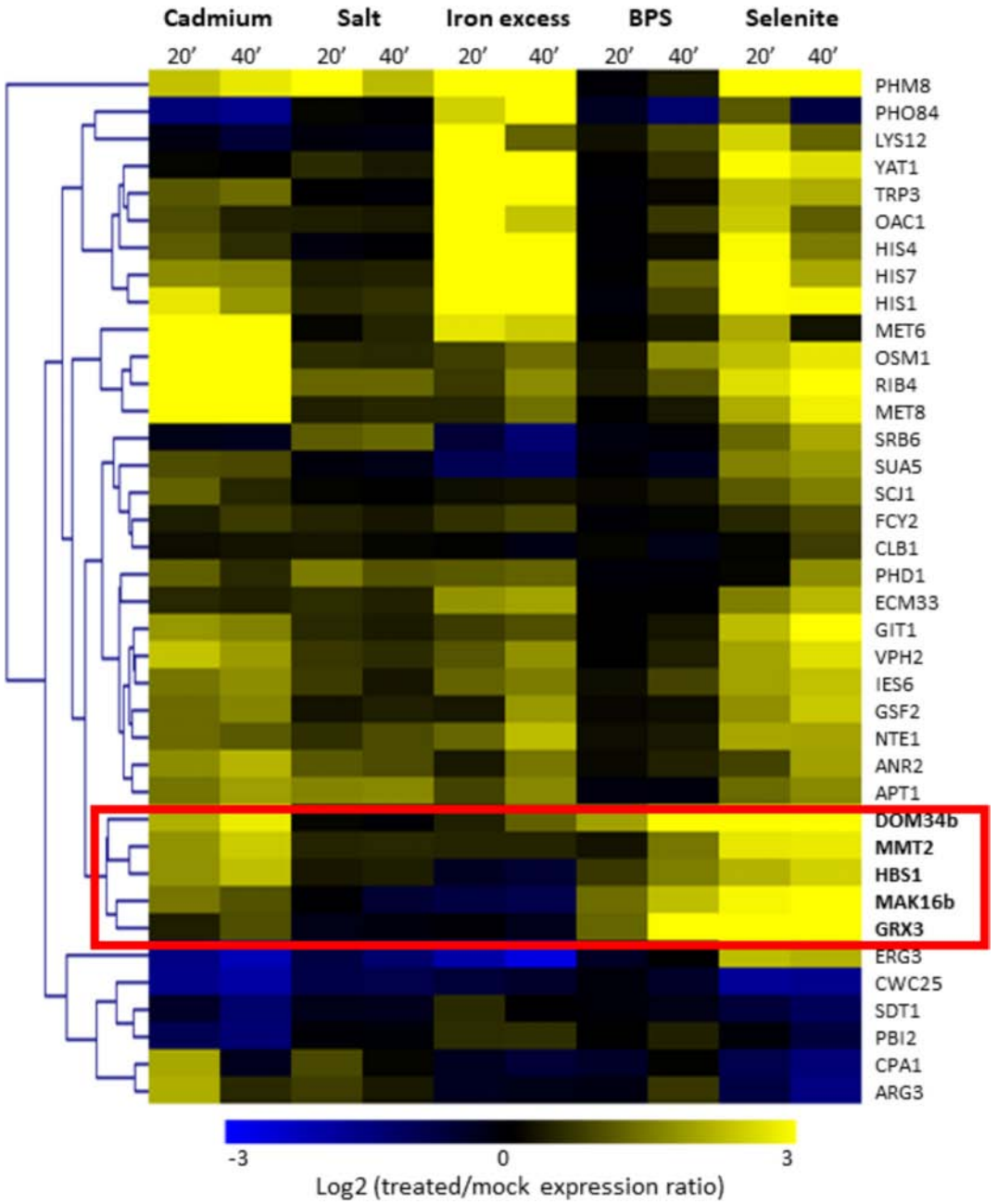

FIGURE 2 | Hierarchical clustering of the 38 *C. glabrata* ROs based on their expression profiles in response to different stress conditions. Expression profiles [Log_2(stressed cells/mock treatment expression ratio)] are represented by a color code (scale at the bottom). Two duration times of treatment were used (20 min and 40 min). The names of the genes are based on the names of their closest homologs in *S. cerevisiae*. A group of genes which is more particularly induced in iron limited conditions (BPS and selenite) has been highlighted by a red box.

GRX3, *DOM34b*, *HBS1*, and *MAK16b* Are New Targets of the Aft2 Transcription Factor in *C. glabrata*

Interestingly enough, these five genes were also induced by cadmium in *C. glabrata* (**Figure 2**). In the model yeast *S. cerevisiae*, BPS and selenite trigger an iron starvation transcriptional response which is controlled by the two paralogous transcription factors Aft1 and Aft2 (Blaiseau et al., 2001; Rutherford et al., 2001, 2003; Courel et al., 2005; Salin et al., 2008; Perez-Sampietro and Herrero, 2014; Perez-Sampietro et al., 2016). However, only the Aft2 regulon is reproducibly induced by cadmium, while most of the Aft1 regulon remains unchanged or is even repressed (Fauchon et al., 2002; Caetano et al., 2015). The expression profiles of the five ROs identified in **Figure 2**

hence suggested that their particular stress regulation pattern in *C. glabrata* could be due to Aft2.

The Aft2 regulon was not previously deciphered in *C. glabrata*. Then, to test our hypothesis, we conducted genome-wide chromatin immunoprecipitation (ChIP-seq) on a Aft2 myc-tagged strain in iron starvation conditions induced by BPS treatment. ChIP-seq analyses identified 63 promoters bound by Aft2, corresponding to 88 potential gene targets (**Supplementary Table T3** and **Figure 3**, left panel). Sequence analyses of the ChIP peaks identified the ACACCC motif as being the most enriched in the Aft2 bound locus, being present in 80% of the target promoters (**Figure 3**, left panel). This motif is identical to the consensus previously identified for Aft2 in *S. cerevisiae* (Courel et al., 2005; Conde e Silva et al., 2009). GO analyses revealed an enrichment in genes involved in iron homeostasis (p-value = 5.15e-08) and oxidative stress response (p-value = 0.00276) (**Figure 3**, left panel). More specifically, Aft2 targeted genes belonging to the iron homeostasis category were involved in the reductive iron uptake pathway (*FRE8*, *FET4*), the siderophore iron uptake pathway (*SIT1*), the intracellular iron transport (*MRS4*, *SMF3*, *CCC1*, *MMT2*) and the iron–sulfur cluster biogenesis and assembly pathway (*ISU1*, *ISU2*, *ISD11*, *NFS1*, *YAH1*). In connection with redox homeostasis, Aft2 bound the promoters of the genes encoding the reductases *HBN1*, *OSM1*, *YHB1*, *RNR1*, *RNR2,* and *ERG4,* the superoxide dismutases *SOD1* and *SOD2*, the catalase *CTA1* and the peroxiredoxin AHP1. Interestingly, Aft2 also targets genes involved in autophagy (*ATG8*, *ATG19*, and *ATG41*), which may be consistent with the recent finding that mitophagy is triggered by iron starvation in *C. glabrata* (Nagi et al., 2016).

Then we compared the set of targets identified in *C. glabrata* with those of Aft2 and Aft1 in *S. cerevisiae* (**Figure 3**, left panel). Half of the *C. glabrata* Aft2 targets were also targets of Aft1 and/or Aft2 in *S. cerevisiae* (**Figure 3**, left panel). Among these conserved targets is *MMT2,* which was consistent with our observation that *MMT1* and *MMT2* are also induced by selenite in *S. cerevisiae* (**Supplementary File S11**). Reciprocally, 50% of the Aft2 targets were specific to *C. glabrata* ("specific" meaning here as compared to *S. cerevisiae*). Among these *C. glabrata* "specific" Aft2 targets were *GRX3*, *DOM34b*, *HBS1*, and *MAK16b*.

To measure the impact of Aft2 on the expression of its potential targets, we performed transcriptome analyses comparing the *aft2Δ* and wild type strains grown either in optimal conditions (YPD), iron starvation caused by BPS or by selenite, and cadmium exposure. Twenty-four of the 63 promoters bound by Aft2 (38%) were associated to a gene which showed a significant decrease of expression in the *aft2Δ* cells in at least one growth condition. Reciprocally, among the 30 genes which were the most reproducibly affected by *AFT2* deletion, 23 (77%) were directly targeted by Aft2 according to our ChIP-seq results (**Figure 3**, right panel). Among the seven genes which showed changed expression but no binding in ChIP-seq, only one had a potential connection with iron homeostasis (*MET8*, encoding a ferrochelatase) but remarkably six of them (the exception being *GCV1*) had an Aft2 binding motif in the 500 bp upstream of their ATG (data not shown). These differences in expression were observed only in stress conditions and not in optimal growth conditions (except for *AFT2* itself, which was constitutively deleted in the mutant strain). The four new targets of interest (*GRX3*, *DOM34b*, *HBS1,* and *MAK16b*) showed decreased expression in the *aft2Δ* strain in all three stress conditions, but with different ranges (**Figure 3**, right panel). Hence, our results demonstrate that the increase of expression of *GRX3*, *DOM34b*, *HBS1,* and *MAK16b* in *C. glabrata* is controlled by Aft2.

DOM34b and *HBS1* Are Required for Optimal Growth in Iron Starvation Conditions

This regulation of *MAK16b*, *DOM34b,* and *HBS1* by Aft2 in *C. glabrata* was particularly intriguing because none of the processes they are contributing to in the model yeast *S. cerevisiae*, namely ribosome biogenesis for Mak16, Dom34 and Hbs1 and ribosome rescue pathway for Dom34 and Hbs1, were directly connected to the transcriptional regulation of iron homeostasis.

Therefore, we assessed the physiological impact of these new regulatory interactions. First, we wanted to know if the increase that we observed at the mRNA level for *DOM34b, MAK16b,* and *HBS1* in iron starvation conditions was translated to the protein level. We constructed *C. glabrata* strains with genomic TAP-tagged versions of *DOM34b, MAK16b,* and *HBS1*. A strain tagged for *DOM34a* was also constructed as a control for a gene which is not induced by stress at the mRNA level. We performed Western blot analyses on these four strains grown in presence or absence of BPS. We observed a clear and fast induction of Dom34b, Mak16b, and Hbs1 in response to stress, which was perfectly mimicking what was observed at the mRNA level (**Figure 4**, left panel and **Supplementary Files S12, S13**). In contrast, Dom34a displayed unchanged expression levels, as expected.

Second, we assessed the importance of *MAK16b*, *DOM34b*, and *HBS1* in the adaptation to iron starved conditions. We constructed strains deleted for these three genes. We included in our phenotypic analyses strains deleted for *DOM34a* and for *AFT2*. The growth rates of these strains in exponential phase were measured in presence or absence of 0.05 mM BPS and compared to the growth rate of the isogenic wild type strain (**Figure 4**, right panel). Two independent clones were tested for each strain. All mutant strains had similar growth rates compared to the wild type in standard growth conditions (**Figure 4**, upper right panel). In presence of BPS, the *dom34aΔ*, *mak16bΔ* and *aft2Δ* strains did not show any growth defect (**Figure 4**, bottom right panel). In contrast, the *dom34bΔ* and *hbs1Δ* mutants had a decreased fitness in iron starvation conditions.

The Regulation of *DOM34b* and *HBS1* by Iron Starvation Probably Arose From the Whole Genome Duplication (WGD)

As mentioned above, in post-WGD species such as *S. cerevisiae* and *C. glabrata*, there are two Aft transcription factors: Aft2 having a preference for the ACACCC motif and Aft1 being more likely associated to TGCACCC (Courel et al., 2005; Conde e Silva et al., 2009; Goncalves et al., 2014; Srivastava

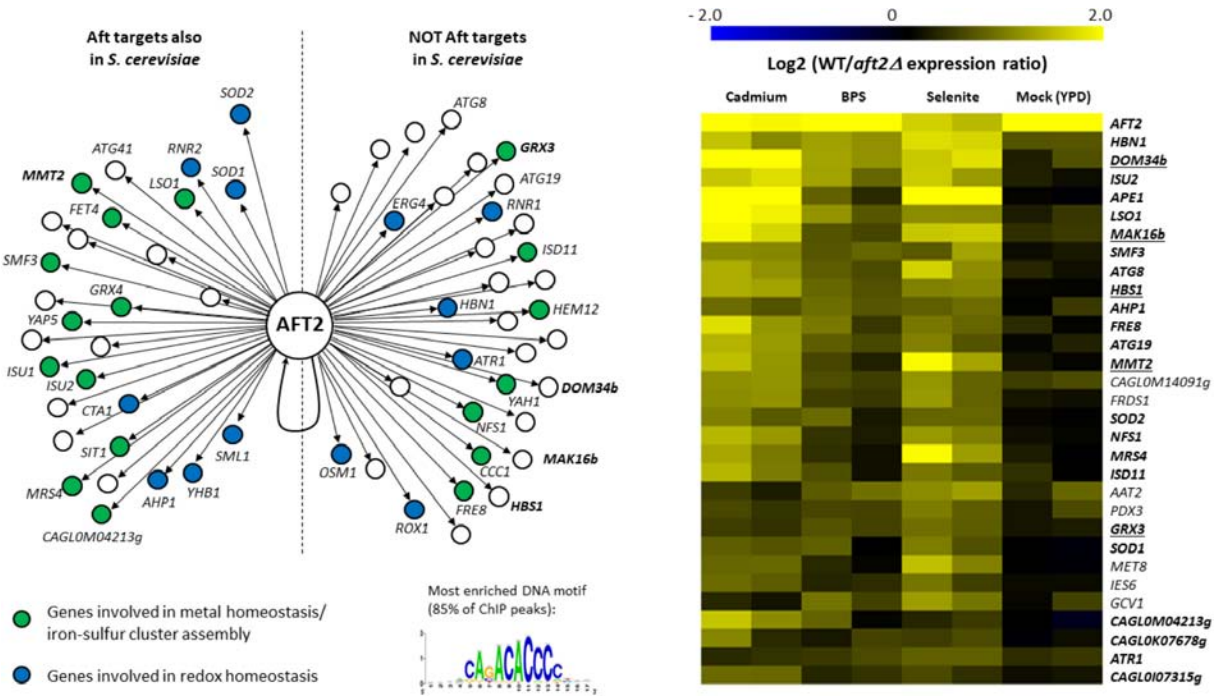

FIGURE 3 | The Aft2 regulon in *C. glabrata*. **(Left)** The 63 Aft2 target promoters, as defined by ChIP-seq (**Supplementary Table T3**), were separated in two groups: target promoters which ortholog is also an Aft target in *S. cerevisiae* and target promoters which ortholog has not been identified as an Aft target in *S. cerevisiae*. Only the names of the genes which are discussed in the main text are indicated. The names of the five ROs of interest are in bold. The targets are colored according to the two main GO terms enriched among Aft2 targets: blue = redox homeostasis, green = iron metabolism. The most enriched DNA motif among all ChIP-peaks is indicated at the bottom right. **(Right)** Transcriptomic comparison of gene expression between the wild type and the *aft2Δ* mutant in four growth conditions. The 30 most affected genes are represented here. The names of genes which were also targeted by Aft2 in our ChIP-seq experiment are in bold. The names of the five ROs of interest have been underlined. The results of two biologically independent replicates are indicated for each growth condition. The complete results are available in **Supplementary Table T5**.

et al., 2015; Gerwien et al., 2016; this work). Besides post-WGD species, the role of the Aft transcription factors in the control of the iron regulon is apparently conserved in the whole *Saccharomycetaceae* family, together with their DNA binding preference for PuGACCC motifs (Conde e Silva et al., 2009; Goncalves et al., 2014). To assess the evolution of the regulation of *DOM34b* and *HBS1* by Aft2 and iron starvation that we characterized in *C. glabrata*, we analyzed the promoter sequences of the orthologs and ohnologs of these two genes in several post- and pre-WGD yeast species spanning the *Saccharomycetaceae* tree, looking for ACACCC (Aft2-like) and GCACCC (Aft1-like) motifs on both DNA strands (**Figure 5** and **Supplementary Files S5, S6, S14**).

In post-WGD species, the evolution of the *DOM34* orthogroup is complex and different situations were observed. In some species (e.g., *Candida glabrata* and its three most related *Nakaseomyces* species, but also *Naumovozyma castellii*, *Kazachstania Africana*, and *Saccharomyces uvarum*) the two ohnologs *DOM34a* and *DOM34b* were retained. In others (e.g., *Tetrapisispora blattae*, *Candida castellii*, *Nakaseomyces bacillisporus*) only one copy remained and reciprocal BLAST or synteny analyses could not indicate without ambiguity if it corresponded to the *DOM34a* or *DOM34b* paralog in the other species. Finally, in most *Saccharomyces* species, one of the two ohnologs was split in two or more ORFs by non-coding insertions (e.g., *YCL001w-a* and *YCL001w-b* in *S. cerevisiae*) and is probably on its way to pseudogenization. Promoter analyses indicated a clear enrichment for Aft motifs in the *DOM34b* lineage of the post-WGD species compared to the *DOM34a* lineage or to the *DOM34* orthologs in the pre-WGD species (**Figure 5**). However, this enrichment is heterogeneous. It is particularly obvious in *C. glabrata* and its close relatives *C. bracarensis*, *N. delphensis*, and *C. nivariensis*, in which the position of one of the Aft2-like motif is particularly well-conserved while the rest of the promoter sequence largely diverged (**Supplementary File S15**). In contrast, there is a loss of the Aft motif enrichment in the *Saccharomyces* species, which seems to be correlated to the pseudogenization of one of the two ohnologs.

A similar pattern was observed for *HBS1*: there is a clear enrichment for Aft motif in the *HBS1* lineage of post-WGD species compared with its *SKI7* ohnolog or with the *SKI7/HBS1* orthologs in pre-WGD species (**Supplementary File S14**). Again, this enrichment in post-WGD species was heterogeneous with, for instance, a clear conservation in the *C. glabrata* sub-clade of the *Nakaseomyces* genus but no Aft motifs in promoters of the *HBS1* versions in the two other *Nakaseomyces* species *C. castellii* and *N. bacillisporus*.

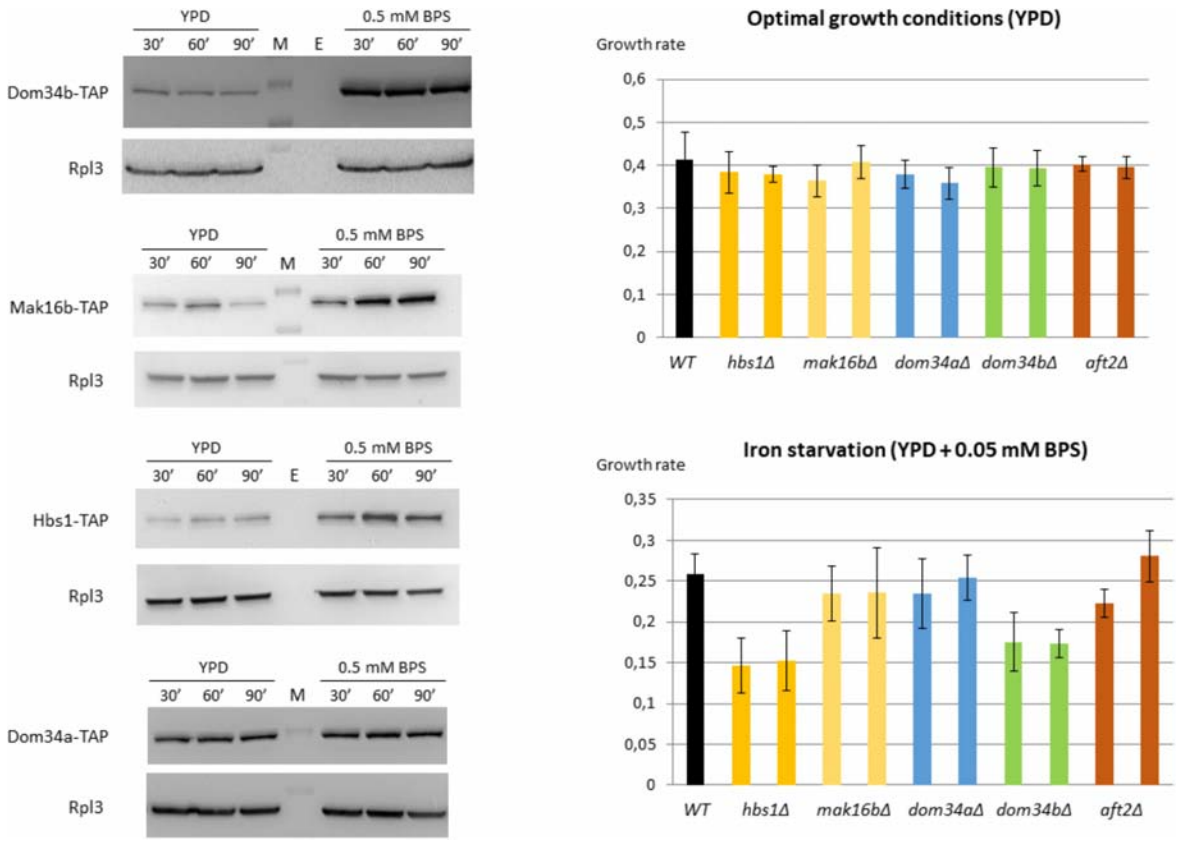

FIGURE 4 | Protein expression levels and fitness analyses in iron starvation conditions. **(Left)** Western blot analyses of the Dom34b-TAP, Hbs1-TAP, Mak16b-TAP, and Dom34a-TAP strains grown in YPD or in YPD + 0.5 mM BPS. Cells were collected 30, 60, and 90 min after the start of BPS or mock treatments. The signal obtained for the Rpl3 ribosomal protein was used as a loading control. Full gel pictures are available in **Supplementary File S12**. A quantification of the Western blot signals from two biologically independent replicates is available in **Supplementary File S13**. **(Right)** Growth rates in exponential phase of different strains in YPD (upper) or in YPD + 0.05 mM BPS (lower). Two independent clones were tested for each mutant strains. The values are the average of six measurements: three independent biological replicates with two technical replicates for each of them.

This phylogenetic analysis strongly suggests that the Aft motifs were fixed in the promoters of *DOM34b* and *HBS1* after the whole genome duplication, in a process equivalent to a neo-functionalization event. Then their evolution varied from strong conservation in some species to disappearance in others, possibly reflecting different selection pressures exerted on this new regulation. Yet, it is very important to remember that the presence of an Aft motif does not imply that the motif is active and that the corresponding gene is under Aft regulation. Still, the high conservation of the position of Aft motifs in the promoter of *DOM34b* in *C. glabrata* and its three most related species, while the rest of the promoter diverged, strongly suggests that this motif is under positive selection in these species and then that the regulation that we characterized here for *C. glabrata* is also active in these three species (**Supplementary File S15**).

DISCUSSION

In this study, we designed a program, called REGULOUT, for the identification of conserved genes with divergent expression profiles from comparative transcriptomics datasets. The inputs of REGULOUT are multispecies gene expression profiles on one hand and the composition of orthogroups on the other. Hence, REGULOUT can be applied to any group of species for which this information is available. The output of REGULOUT is strongly influenced by the distance cut-off chosen and the type of distance used but also by the way the orthogroups were defined and by the stress conditions which were tested. Hence, the label of "ROs" that we introduced in this article is more a technical concept than a straightforward biological feature and REGULOUT should be used as a fast way to sort out lists of potentially interesting cases and not as a tool for gene annotation. We applied REGULOUT to transcriptomics data obtained from eight yeast species responding to the stress caused by detrimental doses of selenite. To assess the power of REGULOUT in highlighting new, biologically meaningful, regulations, we investigated further the 38 ROs identified in the human pathogen *C. glabrata* and we focused on those which were more particularly induced by stress conditions associated to iron starvation.

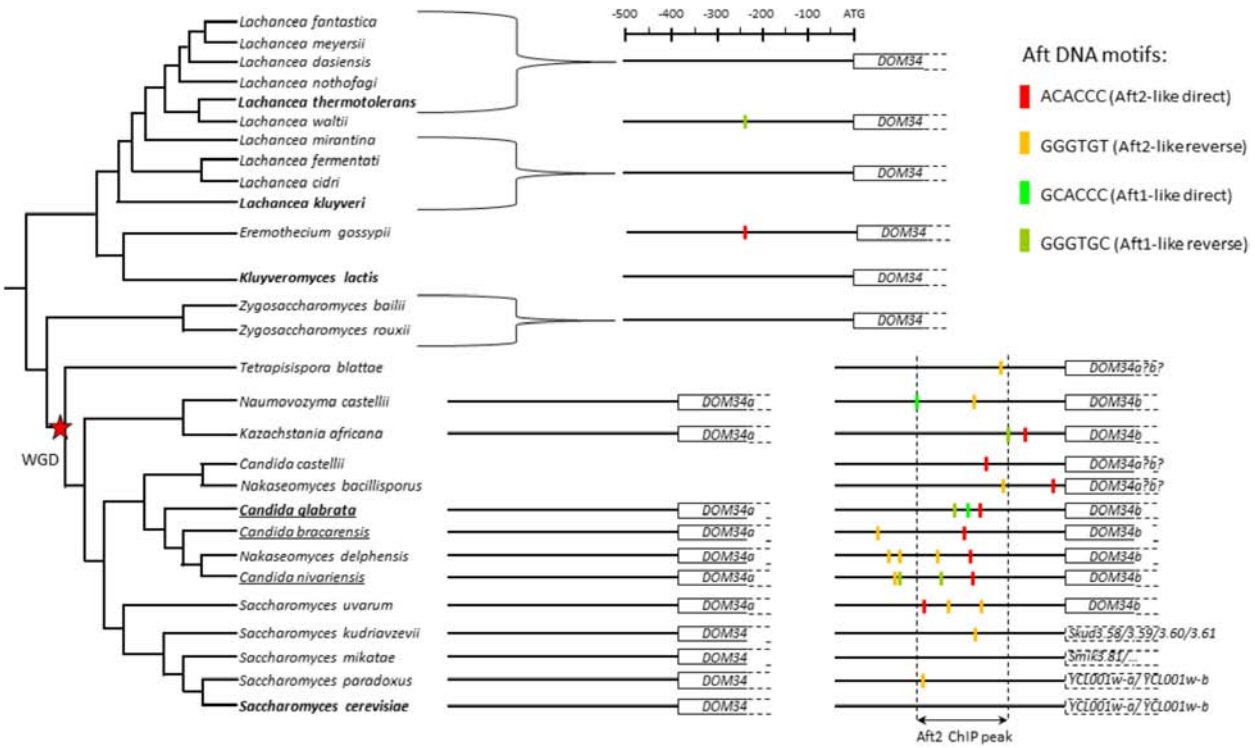

FIGURE 5 | Analyses of the promoters of the *DOM34* orthogroup in 28 *Saccharomycetaceae* species. The tree is a schematic representation of the phylogeny of the species inspired from Vakirlis et al. (2016) for the *Lachancea* species and from Shen et al. (2016) for all the other species. The Whole Genome Duplication (WGD) is indicated by a red star. The positions of the Aft sites in the promoters of the genes are indicated by colored boxes (color code is on the upper right part). The boundaries of the Aft2 ChIP peak in the *C. glabrata DOM34b* gene are indicated by dashed vertical lines. The ORFs in the *DOM34b* lineage of the *Saccharomyces* genus (lower right part of the tree) are interrupted ORFs probably corresponding to pseudogenes. The names of the three pathogenic *Nakaseomyces* species are underlined. The sequences used for this analysis can be found in **Supplementary File S5**.

Iron acquisition is a critical challenge for most microorganisms and a key virulence factor for many fungal pathogens (reviewed in Bairwa et al., 2017; Gerwien et al., 2018). Iron acquisition genes are required for the survival of *C. glabrata* in the macrophages, its adhesion to epithelial cells and for its virulence in animal models (Nevitt and Thiele, 2011; Seider et al., 2014; Srivastava et al., 2014; Brunke et al., 2015). In *S. cerevisiae*, the iron starvation transcriptional response is controlled by the two paralogous transcription factors Aft1 and Aft2. Aft1 activates the expression of genes involved in iron uptake at the plasma membrane (e.g., *FET3*, *FTR1*, *ATX1*, *FRE1-3*, *SIT1*, . . .) and genes involved in the cytoplasmic adaptation to low iron conditions, especially the *CTH1* and *CTH2* genes encoding RNA binding proteins involved in the selective degradation of mRNAs encoding iron consuming proteins (Puig et al., 2005, 2008). Aft2 shares some targets with Aft1 but also specifically activates the expression of genes encoding, for instance, the vacuolar iron transporter Smf3 and the mitochondrial iron transporter Mrs4 (Rutherford et al., 2003; Courel et al., 2005; Martinez-Pastor et al., 2017).

Previous studies have shown that many aspects of the iron homeostasis regulation in *C. glabrata* resemble what had been shown in *S. cerevisiae*. Like *S. cerevisiae*, *C. glabrata* strongly depends on the reductive pathway and siderophore uptake for extracellular iron acquisition (Nevitt and Thiele, 2011; Srivastava et al., 2014; Gerwien et al., 2016). Low affinity iron transport mediated by the Fet4 protein also exists in *C. glabrata* (Srivastava et al., 2014; Gerwien et al., 2016). We showed here that *FET4* is targeted by Aft2 but the sole deletion of *AFT2* had no impact on its induction by BPS, selenite or cadmium (**Supplementary Tables T3, T5**). The key genes of the iron regulon in *S. cerevisiae* are also induced by iron starvation in *C. glabrata* (Srivastava et al., 2015; Gerwien et al., 2016; Nagi et al., 2016). *C. glabrata* Aft1 plays a major role in the up-regulation of membrane iron uptake and is itself induced by iron starvation (Srivastava et al., 2015; Gerwien et al., 2016). Moreover, the enrichment of Cth2 motif in the 3′UTR of genes from the *C. glabrata* iron regulon suggests that the post-transcriptional negative regulation of iron consuming genes is also active in this species (Gerwien et al., 2016). In this work, we showed that the role of Aft2 in the control of intracellular iron trafficking and homeostasis is globally conserved. Especially, the two main specific targets of Aft2 in *S. cerevisiae*, *MRS4* and *SMF3* (Courel et al., 2005), were also regulated by this factor in *C. glabrata* (**Figure 3**). As in *S. cerevisiae* (Blaiseau et al., 2001; Rutherford et al., 2001), the *aft2Δ* mutant exhibited no particular growth defect in response to stress in *C. glabrata* (Srivastava et al., 2014; Gerwien et al., 2016; **Figure 4** of this work).

However, several important differences in iron homeostasis control have also been observed between *C. glabrata* and other model yeast species. For instance, the deletion of the *C. glabrata* ferric reductase encoding genes *FRE8* and *FRE6* does not seem to impact the *C. glabrata* extracellular iron uptake or extracellular ferric reduction activities, in contrast to what has been shown in *S. cerevisiae* and *C. albicans* (Gerwien et al., 2017). Still, these two genes are induced by iron starvation (Nagi et al., 2016; Gerwien et al., 2017) and regulated by Aft2 (this work) and Aft1 (Gerwien et al., 2017), respectively. Moreover, iron starvation was shown to induce the expression of the autophagy genes *ATG32*, *ATG11,* and *ATG8* (Srivastava et al., 2015; Nagi et al., 2016) and to trigger mitophagy in *C. glabrata* but not in *S. cerevisiae* (Nagi et al., 2016; reviewed in Fukuda and Kanki, 2018). We showed here that the iron starvation induction of *ATG8* is under the control of Aft2 (**Figure 3**). Of note, *ATG32* and *ATG11* are required for *C. glabrata* dissemination in mice and survival in macrophages, respectively (Roetzer et al., 2010; Nagi et al., 2016).

REGULOUT pointed out *GRX3*, *MAK16b*, *DOM34b*, and *HBS1* as being particularly responsive to selenite exposure in *C. glabrata*. Further analyses showed that in *C. glabrata* these four genes were also sensitive to BPS and cadmium treatment, but not to iron excess or osmotic stress (**Figure 2**). We investigated the regulatory mechanisms underlying these expression patterns and found that the stress response of these four genes is under the control of Aft2 in *C. glabrata* (**Figure 3**). Our analyses of the evolution of the promoter sequences of the *DOM34* and *HBS1* orthogroups in 14 post-WGD and 14 pre-WGD yeast species revealed enrichment for Aft-like DNA binding motifs in the *DOM34b* and *HBS1* orthologs but neither in the pre-WGD orthologs nor in the *DOM34a* and *SKI7* ohnologs (**Figure 5**). This strongly suggests that this regulation appeared after the whole genome duplication and was subsequently lost in *Saccharomyces cerevisiae*. This is consistent with previous, more global, observations that duplicated genes are often differentially expressed and evolve divergent regulatory patterns (Gu et al., 2004; Conant and Wolfe, 2006; Tirosh and Barkai, 2007; Wapinski et al., 2007; Thompson et al., 2013), with one of the paralogs retaining the ancestral expression profile while the regulation of the other copy evolves more rapidly (Gu et al., 2005). This can be achieved by changes in the transcription factors that regulate the paralogs (Wapinski et al., 2010; Perez et al., 2014; Pougach et al., 2014), by loss and/or gain of different *cis*-regulatory elements in their promoters (Papp et al., 2003; Zhang et al., 2004; Ihmels et al., 2005) or by a combination of both mechanisms. The latter scenario might be the one at work in our case. Indeed, based on the observation that the Aft transcription factor of the pre-WGD species *K. lactis* fulfills the Aft1 but not the Aft2 functions, it was proposed that the mitochondrial and vacuolar control of iron homeostasis by Aft2 appeared as a neo-functionalization event after the WGD and the duplication of the Aft ancestral gene (Conde e Silva et al., 2009). Then, the acquisition of Aft2 regulation by *DOM34b* and *HBS1* would be concomitant to the emergence of the specific role of this transcription factor. Among the post-WGD species, the enrichment of Aft motifs in the promoters of the *DOM34b* and *HBS1* was especially clear in the *Nakaseomyces* sub-lineage which contains *C. glabrata* and two other potential human pathogens (*C. bracarensis* and *C. nivariensis*) (Gabaldon et al., 2013) (**Figure 5** and **Supplementary File S14**), as compared to the other *Nakaseomyces* sub-clade or to the *Saccharomyces* genus. A similar pattern was also observed for *GRX3/4*, which showed a dramatic enrichment of Aft motifs in the promoters of the *GRX3* lineage in the *C. glabrata* sub-clade (**Supplementary File S16**). *C. glabrata*, *C. bracarensis*, *C. nivariensis* and their non-pathogenic relative *N. delphensis* were also the only yeast species to have two *MAK16* orthologs, with the promoter of the *MAK16b* paralog being enriched in Aft DNA motifs (**Supplementary File S17**). Hence, the presence of two *DOM34*, *GRX3/4* and *MAK16* orthologs and the co-regulation of *DOM34b*, *HBS1*, *GRX3*, and *MAK16b* by Aft2 may be a specificity of this *Nakaseomyces* sub-clade, which is enriched in hosts of the human body (three species out of four). To go further in the characterization of this regulation, it would be interesting to determine the actual contribution of the different Aft motifs in the promoters of the genes by site-directed mutagenesis.

Why were these new regulations fixed in *C. glabrata* and lost in *S. cerevisiae*? In other terms, how could these four genes contribute to iron homeostasis in *C. glabrata*? In *S. cerevisiae*, the cytosolic monothiol glutaredoxins Grx3 and Grx4 play a central role in communicating the mitochondrial iron status to Aft1 and Aft2 (Ojeda et al., 2006; Pujol-Carrion et al., 2006; Kumanovics et al., 2008). In iron replete cells, the mitochondrial Fe–S clusters biogenesis is very active and Fe–S clusters are exported to the cytosol where Grx3 and Grx4 form Fe–S bridged homodimers which has the capacity to transfer its Fe–S cluster to Aft1 and Aft2, therefore decreasing their DNA binding affinity by favoring the formation of Fe/S bridged Aft homodimers (Kumanovics et al., 2008; Ueta et al., 2012; Poor et al., 2014; Chi et al., 2018). This role of Grx3/4 proteins in the regulation of iron homeostasis is conserved from yeasts to humans (Li et al., 2012; Labbe et al., 2013; Jacques et al., 2014; Banci et al., 2015; Encinar del Dedo et al., 2015). It may seem counter-intuitive that *C. glabrata* Aft2 induces the expression of a protein which would negatively control its activity. However, besides its role in the regulation of Aft1/2, Grx3 (and its ohnolog Grx4) also makes important contributions to the oxidative stress response and to the cytosolic and nuclear Fe–S cluster protein assembly (Molina et al., 2004; Herrero et al., 2010; Muhlenhoff et al., 2010; Pujol-Carrion and de la Torre-Ruiz, 2010; Vall-Llaura et al., 2016; Pujol-Carrion and Torre-Ruiz, 2017).

In *S. cerevisiae*, *MAK16* was initially identified in a screen for the maintenance of the killer virus double stranded RNA genome (Wickner and Leibowitz, 1979; Icho et al., 1986). Later on, genetic, biochemical and cryoEM analyses showed that Mak16 is actually involved in the biogenesis of the 60S ribosomal particles (Ohtake and Wickner, 1995; Capowski and Tracy, 2003; Pellett and Tracy, 2006; Altvater et al., 2012; Kater et al., 2017; Zhou et al., 2018). *MAK16* is an essential gene, conserved from yeast to human (Kaback et al., 1984; Wickner et al., 1987). As mentioned above, *C. glabrata* and its three most closely related *Nakaseomyces* species (*C. nivariensis*, *N. delphensis* and *C. bracarensis*) have two *MAK16* paralogs, which we named here *MAK16a* and *MAK16b*. *MAK16b* was obviously not essential

in *C. glabrata* since the *mak16b*Δ mutant cells grew at wild type rates in YPD (**Figure 4**). As all members of the ribosome biogenesis (RiBi) regulon, *MAK16* was repressed by stress in all the species we examined (**Supplementary File S11**). This was also true for *MAK16a* in *Candida glabrata*, which was consistently repressed by selenite and by all the other stresses that we tested (**Supplementary File S11**, unpublished data). Then, the dramatic induction of *MAK16b* by selenite, cadmium and BPS, and its regulation by Aft2, is particularly intriguing. The sole link that can be made between Mak16 proteins and stress responses based on the literature is the fact that they were proposed to form an atypical class of glutathione-*S* transferases (GSTs) (McGoldrick et al., 2005). GSTs are enzymes which assist the cell in the defense against reactive oxygen species (reviewed in Kalinina et al., 2014). Moreover, glutathione plays a key role in iron sensing by Grx3/4 and in iron–sulfur cluster assembly (Muhlenhoff et al., 2010; Kumar et al., 2011; Ueta et al., 2012; Martinez-Pastor et al., 2017; Cardenas-Rodriguez et al., 2018). Still, this annotation of *MAK16* orthologs as GSTs only relies on immunological criteria, i.e., the Mak16 protein of the trematode *Schistosoma mansoni* was probed by an anti-serum against purified *S. mansoni* GSTs (Milhon et al., 2000), and an actual GST activity was never proven for these proteins. Moreover, the fact that the deletion of *MAK16b* does not alter the growth of *C. glabrata* in iron starvation conditions makes its actual contribution to the iron homeostasis in this species questionable.

In contrast to *MAK16b*, *DOM34b*, and *HBS1* were required for optimal growth in iron starvation conditions, suggesting a role for these genes in the adaptation to iron limitation in *C. glabrata* (**Figure 4**). Dom34 and Hbs1 are also highly conserved proteins which are found in all eukaryotes, but they are not essential in yeasts. In *S. cerevisiae*, Dom34 and Hbs1, together with the general translation termination factor Rli1, were initially described as being responsible for a translation surveillance pathway called NGD, which rescues and recycles the ribosomes that stall before translation is completed (Doma and Parker, 2006; Passos et al., 2009; Simms et al., 2014; see Buskirk and Green, 2017; Simms et al., 2017, for recent reviews). Later on, the NGD co-factors were shown to be involved in ribosome biogenesis (Kispal et al., 2005; Yarunin et al., 2005; Cole et al., 2009; Lebaron et al., 2012; Strunk et al., 2012) and in the re-activation of hibernating ribosomes prior to quiescence exit (van den Elzen et al., 2014). Dom34 and Hbs1 also have a role in preventing ectopic translation of mRNA 3′ untranslated regions (Guydosh and Green, 2014), that is especially important in conditions in which the activity of Rli1 in regular translation termination is impaired (Young et al., 2015). In *S. cerevisiae*, the expression of *DOM34* and *HBS1* is not regulated by stress and these proteins have not been connected to the regulation of iron homeostasis. So, what could be the functional meaning of the strong induction of *DOM34b* and *HBS1* by BPS, selenite and cadmium in *C. glabrata*? Actually, a quite direct connection can be made between iron starvation and the Dom34-Hbs1 co-factor Rli1. Indeed, Rli1 is an essential Fe–S cluster containing protein (Paul et al., 2015). This iron–sulfur cluster is required for most of Rli1 functions and is very sensitive to redox stress (Kispal et al., 2005; Yarunin et al., 2005; Alhebshi et al., 2012). As a consequence, the number of unrecycled ribosomes in 3′UTRs

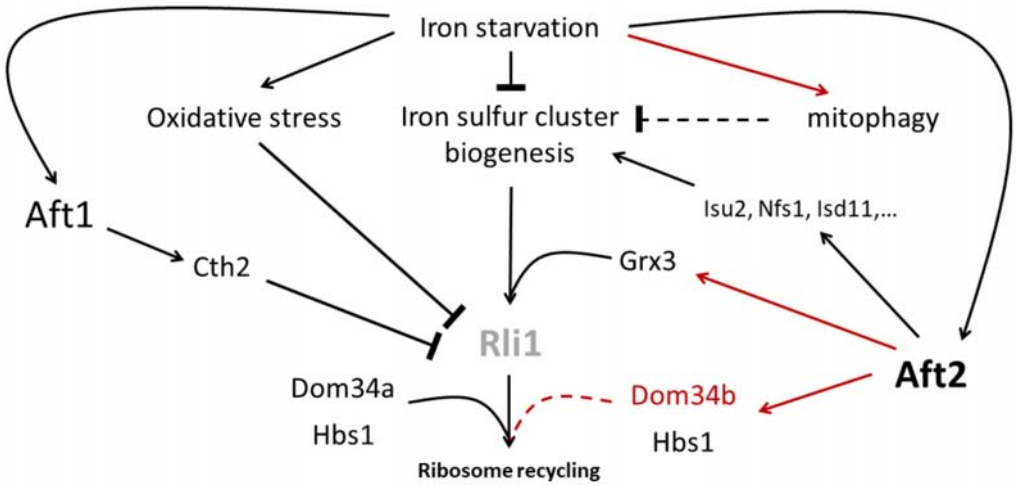

FIGURE 6 | Hypothetical working model for the role of Dom34b and Hbs1 in iron starvation adaptation of *C. glabrata*. Iron starvation alters the functioning of the essential iron–sulfur cluster containing Rli1 in ribosome recycling at many levels: 1- by reducing the iron–sulfur cluster biogenesis potential, 2- by generating oxidative stress which was shown to strongly alter Rli1 activity, 3- by inducing the expression of the Cth2 RNA binding protein which targets part of the Rli1 mRNAs for degradation and 4- specifically in *C. glabrata*, by inducing mitophagy, which may reduce the mitochondrial biogenesis of iron–sulfur clusters. However, iron starvation also triggers the activation of Aft2 which may compensate the decreased activity of Rli1 by overexpressing 1- components of the mitochondrial core iron–sulfur cluster biogenesis machinery; 2- the glutaredoxin Grx3 which is involved in the delivery of iron–sulfur clusters to Rli1 in the cytosol and 3- the Dom34b and Hbs1 ribosome rescue factors, which, together with the constitutively expressed paralog Dom34a, may contribute to increase the ribosome recycling activity of Rli1. In this scheme, the red lines indicate the regulations which are specific to *C. glabrata* as compared to *S. cerevisiae*. The dashed lines indicate hypothetical activities which have not yet been supported by experimental data (namely: an impact of mitophagy on iron–sulfur cluster biogenesis and a role of Dom34b and Dom34a in ribosome rescue in *C. glabrata*).

increases upon treatment with oxidizing agents, such as diamide, which targets iron–sulfur cluster proteins (Guydosh and Green, 2014). Some authors even called Rli1 the "Achilles' heel" of the cells in oxidizing conditions and hypothesized that Rli1 dysfunction is the main cause of cell death in acute oxidative stress (Alhebshi et al., 2012).

Hence, iron starvation is likely to alter the essential Rli1 activity in ribosome rescue at many levels (**Figure 6**). Indeed, iron starvation has been shown to render yeast cells more sensitive to oxidative stress (Blaiseau et al., 2001; Matsuo et al., 2017). Moreover, the Fe–S cluster biogenesis, which takes place in the mitochondria, obviously depends on the iron supply (reviewed in Outten and Albetel, 2013). Finally, in *S. cerevisiae* and in *C. glabrata*, iron starvation provokes the Aft1-mediated overexpression of the RNA binding protein Cth2 which targets the Rli1 mRNA to degradation pathways (Puig et al., 2001, 2005; Gerwien et al., 2016). These effects may be particularly and specifically amplified in *C. glabrata* due to the active mitophagy triggered by iron limitation conditions (Nagi et al., 2016), which may also alter mitochondrial Fe–S cluster biogenesis. Thus, it is tempting to hypothesize that the transcriptional induction of *DOM34b* and *HBS1* would be a *C. glabrata* strategy to better cope with the decreased Rli1 activity caused by iron starvation (**Figure 6**). Interestingly enough, such a transcriptional up-regulation of *DOM34* and *HBS1* to compensate Rli1's defects has already been described in human erythroblasts (Mills et al., 2016). When differentiating in red blood cells, erythroblasts face a difficult challenge: they completely get rid of their mitochondria and hence lose the capacity of producing iron–sulfur clusters, while having to maintain an active translation of hemoglobin, and therefore an active ribosome rescue process, in the last differentiation stages. They do so by transiently overexpressing Pelota (the human equivalent for *DOM34*) and HBS1L (the human ortholog of *HBS1*), which compensates for the progressive loss of active Rli1 (ABCE1 in Human) (Mills et al., 2016). Then, the hypothetical model that we propose for C. *glabrata* (**Figure 6**) would be analog to what was described for human erythroblasts. Of note, the induction of *GRX3* by Aft2 can also take place in this model, because Grx3 is involved in the transfer of the Fe–S cluster for the biogenesis of cytosolic and nuclear Fe–S proteins, such as Rli1 (Muhlenhoff et al., 2010) (**Figure 6**). This model is also consistent with our observation that in *C. glabrata* Aft2 targets several components of the core iron–sulfur cluster machinery. Obviously, many experiments, which go far beyond the scope of this study, will be required to test this working model. Especially, the actual contribution of Hbs1, Dom34a and Dom34b to ribosome rescue in *C. glabrata*, the precise role of Grx3 in the *C. glabrata* iron starvation response and the potential link between the regulation of these genes by Aft2 and the iron starvation-triggered mitophagy in *C. glabrata* will need to be thoroughly investigated.

AUTHOR CONTRIBUTIONS

MS, HR, and EC made the REGULOUT script and identified the ROs. LJ and SLC designed the microarrays. GeL, SB, and FD performed the multispecies microarray experiments. GaL, AT, and FD analyzed the microarray experiments. MB, LF, and TD built the strains and performed the Western blot analyzes. MB and LF made the growth assays in 96-well plates. AT and JM performed the multistress *C. glabrata* microarrays experiments. MB and AT performed the transcriptome analyses of the *aft2D* mutant strain. AT performed the ChIP experiments, the peak calling and the *cis*-regulatory motif enrichment analyzes. FD did the phylogenetic analyzes of the promoters, conceived the whole project, interpreted the results and wrote the manuscript.

FUNDING

This work was funded by the Agence Nationale pour la Recherche (CANDIHUB project, grant number ANR-14-CE14-0018-02 and STRUDYEV project, grant number ANR-10-JCJC-1603) and by the Emergence program of Université Pierre et Marie Curie (2009 session).

ACKNOWLEDGMENTS

We are grateful to Marc Lemaire, Dominique Sanglard, Christophe D'enfert, Cecile Neuveglise, Cecile Fairhead, and Gilles Fischer for providing strains. We thank Gilles Fischer, Cécile Neuveglise, and Julianna Silva Bernardes for useful discussions. We thank Mathilde Garcia for critical reading of the manuscript. We are grateful to the Array express database staff for their valuable help in the submission of the transcriptome data.

SUPPLEMENTARY MATERIAL

The Supplementary Material for this article can be found online at: https://www.frontiersin.org/articles/10.3389/fmicb.2018.02689/full#supplementary-material

REFERENCES

Alhebshi, A., Sideri, T. C., Holland, S. L., and Avery, S. V. (2012). The essential iron-sulfur protein Rli1 is an important target accounting for inhibition of cell growth by reactive oxygen species. *Mol. Biol. Cell* 23, 3582–3590. doi: 10.1091/mbc.E12-05-0413

Altvater, M., Chang, Y., Melnik, A., Occhipinti, L., Schutz, S., Rothenbusch, U., et al. (2012). Targeted proteomics reveals compositional dynamics of 60S pre-ribosomes after nuclear export. *Mol. Syst. Biol.* 8:628. doi: 10.1038/msb.2012.63

Bairwa, G., Hee Jung, W., and Kronstad, J. W. (2017). Iron acquisition in fungal pathogens of humans. *Metallomics* 9, 215–227. doi: 10.1039/c6mt00301j

Banci, L., Ciofi-Baffoni, S., Gajda, K., Muzzioli, R., Peruzzini, R., and Winkelmann, J. (2015). N-terminal domains mediate [2Fe-2S] cluster transfer from glutaredoxin-3 to anamorsin. *Nat. Chem. Biol.* 11, 772–778. doi: 10.1038/nchembio.1892

Blaiseau, P. L., Lesuisse, E., and Camadro, J. M. (2001). Aft2p, a novel iron-regulated transcription activator that modulates, with Aft1p, intracellular iron use and resistance to oxidative stress in yeast. *J. Biol. Chem.* 276, 34221–34226. doi: 10.1074/jbc.M104987200

Brunke, S., and Hube, B. (2013). Two unlike cousins: *Candida albicans* and C. glabrata infection strategies. *Cell. Microbiol.* 15, 701–708. doi: 10.1111/cmi.12091

Brunke, S., Quintin, J., Kasper, L., Jacobsen, I. D., Richter, M. E., Hiller, E., et al. (2015). Of mice, flies–and men? Comparing fungal infection models for large-scale screening efforts. *Dis. Model. Mech.* 8, 473–486. doi: 10.1242/dmm.019901

Buskirk, A. R., and Green, R. (2017). Ribosome pausing, arrest and rescue in bacteria and eukaryotes. *Philos. Trans. R. Soc. Lond. B Biol. Sci.* 372:20160183. doi: 10.1098/rstb.2016.0183

Caetano, S. M., Menezes, R., Amaral, C., Rodrigues-Pousada, C., and Pimentel, C. (2015). Repression of the low affinity iron transporter Gene FET4: a novel mechanism against cadmium toxicity orchestrated by YAP1 via ROX1. *J. Biol. Chem.* 290, 18584–18595. doi: 10.1074/jbc.M114.600742

Capowski, E. E., and Tracy, J. W. (2003). Ribosomal RNA processing and the role of SmMAK16 in ribosome biogenesis in *Schistosoma mansoni*. *Mol. Biochem. Parasitol.* 132, 67–74. doi: 10.1016/j.molbiopara.2003.08.006

Cardenas-Rodriguez, M., Chatzi, A., and Tokatlidis, K. (2018). Iron-sulfur clusters: from metals through mitochondria biogenesis to disease. *J. Biol. Inorg. Chem.* 23, 509–520. doi: 10.1007/s00775-018-1548-6

Chi, C. B., Tang, Y., Zhang, J., Dai, Y. N., Abdalla, M., Chen, Y., et al. (2018). Structural and biochemical insights into the multiple functions of yeast Grx3. *J. Mol. Biol.* 430, 1235–1248. doi: 10.1016/j.jmb.2018.02.024

Cole, S. E., LaRiviere, F. J., Merrikh, C. N., and Moore, M. J. (2009). A convergence of rRNA and mRNA quality control pathways revealed by mechanistic analysis of nonfunctional rRNA decay. *Mol. Cell.* 34, 440–450. doi: 10.1016/j.molcel.2009.04.017

Conant, G. C., and Wolfe, K. H. (2006). Functional partitioning of yeast co-expression networks after genome duplication. *PLoS Biol.* 4:e109. doi: 10.1371/journal.pbio.0040109

Conde e Silva, N., Goncalves, I. R., Lemaire, M., Lesuisse, E., Camadro, J. M., and Blaiseau, P. L. (2009). KlAft, the *Kluyveromyces lactis* ortholog of Aft1 and Aft2, mediates activation of iron-responsive transcription through the PuCACCC Aft-type sequence. *Genetics* 183, 93–106. doi: 10.1534/genetics.109.104364

Cormack, B. P., Ghori, N., and Falkow, S. (1999). An adhesin of the yeast pathogen *Candida glabrata* mediating adherence to human epithelial cells. *Science* 285, 578–582. doi: 10.1126/science.285.5427.578

Courel, M., Lallet, S., Camadro, J. M., and Blaiseau, P. L. (2005). Direct activation of genes involved in intracellular iron use by the yeast iron-responsive transcription factor Aft2 without its paralog Aft1. *Mol. Cell. Biol.* 25, 6760–6771. doi: 10.1128/MCB.25.15.6760-6771.2005

De Las Penas, A., Pan, S. J., Castano, I., Alder, J., Cregg, R., and Cormack, B. P. (2003). Virulence-related surface glycoproteins in the yeast pathogen Candida glabrata are encoded in subtelomeric clusters and subject to RAP1- and SIR-dependent transcriptional silencing. *Genes Dev.* 17, 2245–2258. doi: 10.1101/gad.1121003

De Las Penas, A., Juarez-Cepeda, J., Lopez-Fuentes, E., Briones-Martin-Del-Campo, M., Gutierrez-Escobedo, G., and Castano, I. (2015). Local and regional chromatin silencing in *Candida glabrata*: consequences for adhesion and the response to stress. *FEMS Yeast Res.* 15:fov056. doi: 10.1093/femsyr/fov056

Delaveau, T., Davoine, D., Jolly, A., Vallot, A., Rouviere, J. O., Gerber, A., et al. (2016). Tma108, a putative M1 aminopeptidase, is a specific nascent chain-associated protein in *Saccharomyces cerevisiae*. *Nucleic Acids Res.* 44, 8826–8841. doi: 10.1093/nar/gkw732

Doma, M. K., and Parker, R. (2006). Endonucleolytic cleavage of eukaryotic mRNAs with stalls in translation elongation. *Nature* 440, 561–564. doi: 10.1038/nature04530

Domergue, R., Castano, I., De Las Penas, A., Zupancic, M., Lockatell, V., Hebel, J. R., et al. (2005). Nicotinic acid limitation regulates silencing of *Candida adhesins* during UTI. *Science* 308, 866–870. doi: 10.1126/science.1108640

Dujon, B., Sherman, D., Fischer, G., Durrens, P., Casaregola, S., Lafontaine, I., et al. (2004). Genome evolution in yeasts. *Nature* 430, 35–44. doi: 10.1038/nature02579

Encinar del Dedo, J., Gabrielli, N., Carmona, M., Ayte, J., and Hidalgo, E. (2015). A cascade of iron-containing proteins governs the genetic iron starvation response to promote iron uptake and inhibit iron storage in fission yeast. *PLoS Genet* 11:e1005106. doi: 10.1371/journal.pgen.1005106

Fauchon, M., Lagniel, G., Aude, J. C., Lombardia, L., Soularue, P., Petat, C., et al. (2002). Sulfur sparing in the yeast proteome in response to sulfur demand. *Mol. Cell.* 9, 713–723. doi: 10.1016/S1097-2765(02)00500-2

Fukuda, T., and Kanki, T. (2018). Mechanisms and physiological roles of mitophagy in yeast. *Mol. Cells* 41, 35–44.

Gabaldon, T., Martin, T., Marcet-Houben, M., Durrens, P., Bolotin-Fukuhara, M., Lespinet, O., et al. (2013). Comparative genomics of emerging pathogens in the *Candida glabrata* clade. *BMC Genomics* 14:623. doi: 10.1186/1471-2164-14-623

Gabaldon, T., and Carrete, L. (2015). The birth of a deadly yeast: tracing the evolutionary emergence of virulence traits in *Candida glabrata*. *FEMS Yeast Res.* 16:fov110 doi: 10.1093/femsyr/fov110

Gasch, A. P., Spellman, P. T., Kao, C. M., Carmel-Harel, O., Eisen, M. B., Storz, G., et al. (2000). Genomic expression programs in the response of yeast cells to environmental changes. *Mol. Biol. Cell* 11, 4241–4257. doi: 10.1091/mbc.11.12.4241

Gasch, A. P., Moses, A. M., Chiang, D. Y., Fraser, H. B., Berardini, M., and Eisen, M. B. (2004). Conservation and evolution of cis-regulatory systems in ascomycete fungi. *PLoS Biol.* 2:e398. doi: 10.1371/journal.pbio.0020398

Gasch, A. P. (2007). Comparative genomics of the environmental stress response in ascomycete fungi. *Yeast* 24, 961–976. doi: 10.1002/yea.1512

Genolevures, C., Souciet, J. L., Dujon, B., Gaillardin, C., Johnston, M., Baret, P. V., et al. (2009). Comparative genomics of protoploid Saccharomycetaceae. *Genome Res.* 19, 1696–1709. doi: 10.1101/gr.091546.109

Gerwien, F., Safyan, A., Wisgott, S., Hille, F., Kaemmer, P., Linde, J., et al. (2016). A novel hybrid iron regulation network combines features from pathogenic and nonpathogenic yeasts. *mBio* 7:e01782-16. doi: 10.1128/mBio.01782-16

Gerwien, F., Safyan, A., Wisgott, S., Brunke, S., Kasper, L., and Hube, B. (2017). The fungal pathogen *Candida glabrata* does not depend on surface ferric reductases for iron acquisition. *Front. Microbiol.* 8:1055. doi: 10.3389/fmicb.2017.01055

Gerwien, F., Skrahina, V., Kasper, L., Hube, B., and Brunke, S. (2018). Metals in fungal virulence. *FEMS Microbiol. Rev.* 42:fux050. doi: 10.1093/femsre/fux050

Goncalves, I. R., Conde e Silva, N., Garay, C. L., Lesuisse, E., Camadro, J. M., and Blaiseau, P. L. (2014). The basis for evolution of DNA-binding specificity of the Aft1 transcription factor in yeasts. *Genetics* 196, 149–160. doi: 10.1534/genetics.113.157693

Gu, X., Zhang, Z., and Huang, W. (2005). Rapid evolution of expression and regulatory divergences after yeast gene duplication. *Proc. Natl. Acad. Sci. U.S.A.* 102, 707–712. doi: 10.1073/pnas.0409186102

Gu, Z., Rifkin, S. A., White, K. P., and Li, W. H. (2004). Duplicate genes increase gene expression diversity within and between species. *Nat. Genet.* 36, 577–579. doi: 10.1038/ng1355

Guydosh, N. R., and Green, R. (2014). Dom34 rescues ribosomes in 3′ untranslated regions. *Cell* 156, 950–962. doi: 10.1016/j.cell.2014.02.006

Habib, N., Wapinski, I., Margalit, H., Regev, A., and Friedman, N. (2012). A functional selection model explains evolutionary robustness despite plasticity in regulatory networks. *Mol. Syst. Biol.* 8:619. doi: 10.1038/msb.2012.50

Herrero, E., Belli, G., and Casa, C. (2010). Structural and functional diversity of glutaredoxins in yeast. *Curr. Protein Pept. Sci* 11, 659–668. doi: 10.2174/138920310794557637

Herrero, E., and Wellinger, R. E. (2015). Yeast as a model system to study metabolic impact of selenium compounds. *Microb. Cell* 2, 139–149. doi: 10.15698/mic2015.05.200

Huerta-Cepas, J., Capella-Gutierrez, S., Pryszcz, L. P., Marcet-Houben, M., and Gabaldon, T. (2014). PhylomeDB v4: zooming into the plurality of evolutionary histories of a genome. *Nucleic Acids Res.* 42:D897–D902. doi: 10.1093/nar/gkt1177

Icho, T., Lee, H. S., Sommer, S. S., and Wickner, R. B. (1986). Molecular characterization of chromosomal genes affecting double-stranded RNA replication in *Saccharomyces cerevisiae*. *Basic Life Sci.* 40, 165–171. doi: 10.1007/978-1-4684-5251-8_13

Ihmels, J., Bergmann, S., Gerami-Nejad, M., Yanai, I., McClellan, M., Berman, J., et al. (2005). Rewiring of the yeast transcriptional network through the evolution of motif usage. *Science* 309, 938–940. doi: 10.1126/science.1113833

Jacques, J. F., Mercier, A., Brault, A., Mourer, T., and Labbe, S. (2014). Fra2 is a co-regulator of Fep1 inhibition in response to iron starvation. *PLoS One* 9:e98959. doi: 10.1371/journal.pone.0098959

Johnson, A. D. (2017). The rewiring of transcription circuits in evolution. *Curr. Opin. Genet. Dev.* 47, 121–127. doi: 10.1016/j.gde.2017.09.004

Jourdren, L., Duclos, A., Brion, C., Portnoy, T., Mathis, H., Margeot, A., et al. (2010). Teolenn: an efficient and customizable workflow to design high-quality probes for microarray experiments. *Nucleic Acids Res.* 38:e117. doi: 10.1093/nar/gkq110

Juarez-Cepeda, J., Orta-Zavalza, E., Canas-Villamar, I., Arreola-Gomez, J., Perez-Cornejo, G. P., Hernandez-Carballo, C. Y., et al. (2015). The EPA2 adhesin encoding gene is responsive to oxidative stress in the opportunistic fungal pathogen *Candida glabrata*. *Curr. Genet.* 61, 529–544. doi: 10.1007/s00294-015-0473-2

Kaback, D. B., Oeller, P. W., Yde Steensma, H., Hirschman, J., Ruezinsky, D., Coleman, K. G., et al. (1984). Temperature-sensitive lethal mutations on yeast chromosome I appear to define only a small number of genes. *Genetics* 108, 67–90.

Kalinina, E. V., Chernov, N. N., and Novichkova, M. D. (2014). Role of glutathione, glutathione transferase, and glutaredoxin in regulation of redox-dependent processes. *Biochemistry* 79, 1562–1583.

Kasper, L., Seider, K., and Hube, B. (2015). Intracellular survival of *Candida glabrata* in macrophages: immune evasion and persistence. *FEMS Yeast Res.* 15:fov042. doi: 10.1093/femsyr/fov042

Kater, L., Thoms, M., Barrio-Garcia, C., Cheng, J., Ismail, S., Ahmed, Y. L., et al. (2017). Visualizing the assembly pathway of nucleolar Pre-60S ribosomes. *Cell* 171: 1599.e14–1610.e14. doi: 10.1016/j.cell.2017.11.039

Kaur, R., Ma, B., and Cormack, B. P. (2007). A family of glycosylphosphatidylinositol-linked aspartyl proteases is required for virulence of *Candida glabrata*. *Proc. Natl. Acad. Sci. U.S.A.* 104, 7628–7633. doi: 10.1073/pnas.0611195104

Kispal, G., Sipos, K., Lange, H., Fekete, Z., Bedekovics, T., Janaky, T., et al. (2005). Biogenesis of cytosolic ribosomes requires the essential iron-sulphur protein Rli1p and mitochondria. *EMBO J.* 24, 589–598. doi: 10.1038/sj.emboj.7600541

Koch, C., Konieczka, J., Delorey, T., Lyons, A., Socha, A., Davis, K., et al. (2017). Inference and evolutionary analysis of genome-scale regulatory networks in large phylogenies. *Cell Syst.* 4, 543.e8–558.e8. doi: 10.1016/j.cels.2017.04.010

Kumanovics, A., Chen, O. S., Li, L., Bagley, D., Adkins, E. M., Lin, H., et al. (2008). Identification of FRA1 and FRA2 as genes involved in regulating the yeast iron regulon in response to decreased mitochondrial iron-sulfur cluster synthesis. *J. Biol. Chem.* 283, 10276–10286. doi: 10.1074/jbc.M801160200

Kumar, C., Igbaria, A., D'Autreaux, B., Planson, A. G., Junot, C., Godat, E., et al. (2011). Glutathione revisited: a vital function in iron metabolism and ancillary role in thiol-redox control. *EMBO J.* 30, 2044–2056. doi: 10.1038/emboj.2011.105

Kuo, D., Tan, K., Zinman, G., Ravasi, T., Bar-Joseph, Z., and Ideker, T. (2010). Evolutionary divergence in the fungal response to fluconazole revealed by soft clustering. *Genome Biol.* 11:R77. doi: 10.1186/gb-2010-11-7-r77

Labbe, S., Khan, M. G., and Jacques, J. F. (2013). Iron uptake and regulation in *Schizosaccharomyces pombe*. *Curr. Opin. Microbiol.* 16, 669–676. doi: 10.1016/j.mib.2013.07.007

Lavoie, H., Hogues, H., Mallick, J., Sellam, A., Nantel, A., and Whiteway, M. (2010). Evolutionary tinkering with conserved components of a transcriptional regulatory network. *PLoS Biol.* 8:e1000329. doi: 10.1371/journal.pbio.1000329

Lebaron, S., Schneider, C., van Nues, R. W., Swiatkowska, A., Walsh, D., Bottcher, B., et al. (2012). Proofreading of pre-40S ribosome maturation by a translation initiation factor and 60S subunits. *Nat. Struct. Mol. Biol.* 19, 744–753. doi: 10.1038/nsmb.2308

Lemoine, S., Combes, F., Servant, N., and Le Crom, S. (2006). Goulphar: rapid access and expertise for standard two-color microarray normalization methods. *BMC Bioinformatics* 7:467. doi: 10.1186/1471-2105-7-467

Li, H., Mapolelo, D. T., Randeniya, S., Johnson, M. K., and Outten, C. E. (2012). Human glutaredoxin 3 forms [2Fe-2S]-bridged complexes with human BolA2. *Biochemistry* 51, 1687–1696. doi: 10.1021/bi2019089

Longtine, M. S., McKenzie, A. III, Demarini, D. J., Shah, N. G., Wach, A., Brachat, A., et al. (1998). Additional modules for versatile and economical PCR-based gene deletion and modification in *Saccharomyces cerevisiae*. *Yeast* 14, 953–961. doi: 10.1002/(SICI)1097-0061(199807)14:10<953::AID-YEA293>3.0.CO;2-U

Lynch, V. J., Leclerc, R. D., May, G., and Wagner, G. P. (2011). Transposon-mediated rewiring of gene regulatory networks contributed to the evolution of pregnancy in mammals. *Nat. Genet.* 43, 1154–1159. doi: 10.1038/ng.917

Lynch, V. J., Nnamani, M. C., Kapusta, A., Brayer, K., Plaza, S. L., Mazur, E. C., et al. (2015). Ancient transposable elements transformed the uterine regulatory landscape and transcriptome during the evolution of mammalian pregnancy. *Cell Rep.* 10, 551–561. doi: 10.1016/j.celrep.2014.12.052

Martinez-Pastor, M. T., Perea-Garcia, A., and Puig, S. (2017). Mechanisms of iron sensing and regulation in the yeast *Saccharomyces cerevisiae*. *World J. Microbiol. Biotechnol.* 33:75. doi: 10.1007/s11274-017-2215-8

Matsuo, R., Mizobuchi, S., Nakashima, M., Miki, K., Ayusawa, D., and Fujii, M. (2017). Central roles of iron in the regulation of oxidative stress in the yeast *Saccharomyces cerevisiae*. *Curr. Genet.* 63, 895–907. doi: 10.1007/s00294-017-0689-4

McGoldrick, S., O'Sullivan, S. M., and Sheehan, D. (2005). Glutathione transferase-like proteins encoded in genomes of yeasts and fungi: insights into evolution of a multifunctional protein superfamily. *FEMS Microbiol. Lett.* 242, 1–12. doi: 10.1016/j.femsle.2004.10.033

Merhej, J., Frigo, A., Le Crom, S., Camadro, J. M., Devaux, F., and Lelandais, G. (2014). bPeaks: a bioinformatics tool to detect transcription factor binding sites from ChIPseq data in yeasts and other organisms with small genomes. *Yeast* 31, 375–391. doi: 10.1002/yea.3031

Merhej, J., Delaveau, T., Guitard, J., Palancade, B., Hennequin, C., Garcia, M., et al. (2015). Yap7 is a transcriptional repressor of nitric oxide oxidase in yeasts, which arose from neofunctionalization after whole genome duplication. *Mol. Microbiol.* 96, 951–972. doi: 10.1111/mmi.12983

Merhej, J., Thiebaut, A., Blugeon, C., Pouch, J., Ali Chaouche Mel, A., Camadro, J. M., et al. (2016). A network of paralogous stress response transcription factors in the human pathogen *Candida glabrata*. *Front. Microbiol.* 7:645. doi: 10.3389/fmicb.2016.00645

Milhon, J. L., Albert, T. J., Vande Waa, E. A., O'Leary, K. A., Jackson, R. N., Kessler, M. A., et al. (2000). SmMAK16, the *Schistosoma mansoni* homologue of MAK16 from yeast, targets protein transport to the nucleolus. *Mol. Biochem. Parasitol.* 108, 225–236. doi: 10.1016/S0166-6851(00)00221-8

Mills, E. W., Wangen, J., Green, R., and Ingolia, N. T. (2016). Dynamic regulation of a ribosome rescue pathway in erythroid cells and platelets. *Cell Rep.* 17, 1–10. doi: 10.1016/j.celrep.2016.08.088

Molina, M. M., Belli, G., de la Torre, M. A., Rodriguez-Manzaneque, M. T., and Herrero, E. (2004). Nuclear monothiol glutaredoxins of *Saccharomyces cerevisiae* can function as mitochondrial glutaredoxins. *J. Biol. Chem.* 279, 51923–51930. doi: 10.1074/jbc.M410219200

Muhlenhoff, U., Molik, S., Godoy, J. R., Uzarska, M. A., Richter, N., Seubert, A., et al. (2010). Cytosolic monothiol glutaredoxins function in intracellular iron sensing and trafficking via their bound iron-sulfur cluster. *Cell Metab.* 12, 373–385. doi: 10.1016/j.cmet.2010.08.001

Nagi, M., Tanabe, K., Nakayama, H., Ueno, K., Yamagoe, S., Umeyama, T., et al. (2016). Iron-depletion promotes mitophagy to maintain mitochondrial integrity in pathogenic yeast *Candida glabrata*. *Autophagy* 12, 1259–1271. doi: 10.1080/15548627.2016.1183080

Nevitt, T., and Thiele, D. J. (2011). Host iron withholding demands siderophore utilization for *Candida glabrata* to survive macrophage killing. *PLoS Pathog* 7:e1001322. doi: 10.1371/journal.ppat.1001322

Ohtake, Y., and Wickner, R. B. (1995). Yeast virus propagation depends critically on free 60S ribosomal subunit concentration. *Mol. Cell. Biol.* 15, 2772–2781. doi: 10.1128/MCB.15.5.2772

Ojeda, L., Keller, G., Muhlenhoff, U., Rutherford, J. C., Lill, R., and Winge, D. R. (2006). Role of glutaredoxin-3 and glutaredoxin-4 in the iron regulation of the Aft1 transcriptional activator in *Saccharomyces cerevisiae*. *J. Biol. Chem.* 281, 17661–17669. doi: 10.1074/jbc.M602165200

Outten, C. E., and Albetel, A. N. (2013). Iron sensing and regulation in *Saccharomyces cerevisiae*: ironing out the mechanistic details. *Curr. Opin. Microbiol.* 16, 662–668. doi: 10.1016/j.mib.2013.07.020

Papp, B., Pal, C., and Hurst, L. D. (2003). Evolution of cis-regulatory elements in duplicated genes of yeast. *Trends Genet.* 19, 417–422. doi: 10.1016/S0168-9525(03)00174-4

Passos, D. O., Doma, M. K., Shoemaker, C. J., Muhlrad, D., Green, R., Weissman, J., et al. (2009). Analysis of Dom34 and its function in no-go decay. *Mol. Biol. Cell* 20, 3025–3032. doi: 10.1091/mbc.E09-01-0028

Paul, V. D., Muhlenhoff, U., Stumpfig, M., Seebacher, J., Kugler, K. G., Renicke, C., et al. (2015). The deca-GX3 proteins Yae1-Lto1 function as adaptors recruiting

the ABC protein Rli1 for iron-sulfur cluster insertion. *eLife* 4:e08231. doi: 10.7554/eLife.08231

Pellett, S., and Tracy, J. W. (2006). Mak16p is required for the maturation of 25S and 5.8S rRNAs in the yeast *Saccharomyces cerevisiae*. *Yeast* 23, 495–506. doi: 10.1002/yea.1368

Perez-Sampietro, M., and Herrero, E. (2014). The PacC-family protein Rim101 prevents selenite toxicity in *Saccharomyces cerevisiae* by controlling vacuolar acidification. *Fungal Genet. Biol.* 71, 76–85. doi: 10.1016/j.fgb.2014.09.001

Perez-Sampietro, M., Serra-Cardona, A., Canadell, D., Casas, C., Arino, J., and Herrero, E. (2016). The yeast Aft2 transcription factor determines selenite toxicity by controlling the low affinity phosphate transport system. *Sci. Rep.* 6:32836. doi: 10.1038/srep32836

Perez, J. C., Fordyce, P. M., Lohse, M. B., Hanson-Smith, V., DeRisi, J. L., and Johnson, A. D. (2014). How duplicated transcription regulators can diversify to govern the expression of nonoverlapping sets of genes. *Genes Dev.* 28, 1272–1277. doi: 10.1101/gad.242271.114

Pfaller, M. A., and Diekema, D. J. (2007). Epidemiology of invasive candidiasis: a persistent public health problem. *Clin. Microbiol. Rev.* 20, 133–163. doi: 10.1128/CMR.00029-06

Pfaller, M. A., Andes, D. R., Diekema, D. J., Horn, D. L., Reboli, A. C., Rotstein, C., et al. (2014). Epidemiology and outcomes of invasive candidiasis due to non-albicans species of Candida in 2,496 patients: data from the prospective antifungal therapy (PATH) registry 2004-2008. *PLoS One* 9:e101510. doi: 10.1371/journal.pone.0101510

Pinson, B., Sagot, I., and Daignan-Fornier, B. (2000). Identification of genes affecting selenite toxicity and resistance in *Saccharomyces cerevisiae*. *Mol. Microbiol.* 36, 679–687. doi: 10.1046/j.1365-2958.2000.01890.x

Poor, C. B., Wegner, S. V., Li, H., Dlouhy, A. C., Schuermann, J. P., Sanishvili, R., et al. (2014). Molecular mechanism and structure of the *Saccharomyces cerevisiae* iron regulator Aft2. *Proc. Natl. Acad. Sci. U.S.A.* 111, 4043–4048. doi: 10.1073/pnas.1318869111

Pougach, K., Voet, A., Kondrashov, F. A., Voordeckers, K., Christiaens, J. F., Baying, B., et al. (2014). Duplication of a promiscuous transcription factor drives the emergence of a new regulatory network. *Nat. Commun.* 5:4868. doi: 10.1038/ncomms5868

Puig, O., Caspary, F., Rigaut, G., Rutz, B., Bouveret, E., Bragado-Nilsson, E., et al. (2001). The tandem affinity purification (TAP) method: a general procedure of protein complex purification. *Methods* 24, 218–229. doi: 10.1006/meth.2001.1183

Puig, S., Askeland, E., and Thiele, D. J. (2005). Coordinated remodeling of cellular metabolism during iron deficiency through targeted mRNA degradation. *Cell* 120, 99–110. doi: 10.1016/j.cell.2004.11.032

Puig, S., Vergara, S. V., and Thiele, D. J. (2008). Cooperation of two mRNA-binding proteins drives metabolic adaptation to iron deficiency. *Cell Metab.* 7, 555–564. doi: 10.1016/j.cmet.2008.04.010

Pujol-Carrion, N., Belli, G., Herrero, E., Nogues, A., and de la Torre-Ruiz, M. A. (2006). Glutaredoxins Grx3 and Grx4 regulate nuclear localisation of Aft1 and the oxidative stress response in *Saccharomyces cerevisiae*. *J. Cell Sci.* 119, 4554–4564. doi: 10.1242/jcs.03229

Pujol-Carrion, N., and de la Torre-Ruiz, M. A. (2010). Glutaredoxins Grx4 and Grx3 of *Saccharomyces cerevisiae* play a role in actin dynamics through their Trx domains, which contributes to oxidative stress resistance. *Appl. Environ. Microbiol.* 76, 7826–7835. doi: 10.1128/AEM.01755-10

Pujol-Carrion, N., and Torre-Ruiz, M. A. (2017). Physical interaction between the MAPK Slt2 of the PKC1-MAPK pathway and Grx3/Grx4 glutaredoxins is required for the oxidative stress response in budding yeast. *Free Radic. Biol. Med.* 103, 107–120. doi: 10.1016/j.freeradbiomed.2016.12.023

Quinlan, A. R., and Hall, I. M. (2010). BEDTools: a flexible suite of utilities for comparing genomic features. *Bioinformatics* 26, 841–842. doi: 10.1093/bioinformatics/btq033

Ritchie, M. E., Phipson, B., Wu, D., Hu, Y., Law, C. W., Shi, W., et al. (2015). limma powers differential expression analyses for RNA-sequencing and microarray studies. *Nucleic Acids Res.* 43:e47. doi: 10.1093/nar/gkv007

Roetzer, A., Gratz, N., Kovarik, P., and Schuller, C. (2010). Autophagy supports *Candida glabrata* survival during phagocytosis. *Cell. Microbiol.* 12, 199–216. doi: 10.1111/j.1462-5822.2009.01391.x

Roetzer, A., Gabaldon, T., and Schüller, C. (2011) From *Saccharomyces cerevisiae* to *Candida glabrata* in a few easy steps: important adaptations for an opportunistic pathogen. *FEMS Microbiol. Lett.* 314, 1–9. doi: 10.1111/j.1574-6968.2010.02102.x

Romero, I. G., Ruvinsky, I., and Gilad, Y. (2012). Comparative studies of gene expression and the evolution of gene regulation. *Nat. Rev. Genet.* 13, 505–516. doi: 10.1038/nrg3229

Roy, S., Wapinski, I., Pfiffner, J., French, C., Socha, A., Konieczka, J., et al. (2013). Arboretum: reconstruction and analysis of the evolutionary history of condition-specific transcriptional modules. *Genome Res.* 23, 1039–1050. doi: 10.1101/gr.146233.112

Roy, S., and Thompson, D. (2015). Evolution of regulatory networks in *Candida glabrata*: learning to live with the human host. *FEMS Yeast Res.* 15:fov087. doi: 10.1093/femsyr/fov087

Rutherford, J. C., Jaron, S., Ray, E., Brown, P. O., and Winge, D. R. (2001). A second iron-regulatory system in yeast independent of Aft1p. *Proc. Natl. Acad. Sci. U.S.A.* 98, 14322–14327. doi: 10.1073/pnas.261381198

Rutherford, J. C., Jaron, S., and Winge, D. R. (2003). Aft1p and Aft2p mediate iron-responsive gene expression in yeast through related promoter elements. *J. Biol. Chem.* 278, 27636–27643. doi: 10.1074/jbc.M300076200

Salin, H., Fardeau, V., Piccini, E., Lelandais, G., Tanty, V., Lemoine, S., et al. (2008). Structure and properties of transcriptional networks driving selenite stress response in yeasts. *BMC Genomics* 9:333. doi: 10.1186/1471-2164-9-333

Scannell, D. R., Zill, O. A., Rokas, A., Payen, C., Dunham, M. J., Eisen, M. B., et al. (2011). The Awesome power of yeast evolutionary genetics: new genome sequences and strain resources for the *Saccharomyces* sensu stricto Genus. *G3* 1, 11–25. doi: 10.1534/g3.111.000273

Schwarzmuller, T., Ma, B., Hiller, E., Istel, F., Tscherner, M., Brunke, S., et al. (2014). Systematic phenotyping of a large-scale *Candida glabrata* deletion collection reveals novel antifungal tolerance genes. *PLoS Pathog* 10:e1004211. doi: 10.1371/journal.ppat.1004211

Seider, K., Brunke, S., Schild, L., Jablonowski, N., Wilson, D., Majer, O., et al. (2011). The facultative intracellular pathogen *Candida glabrata* subverts macrophage cytokine production and phagolysosome maturation. *J. Immunol.* 187, 3072–3086. doi: 10.4049/jimmunol.1003730

Seider, K., Gerwien, F., Kasper, L., Allert, S., Brunke, S., Jablonowski, N., et al. (2014). Immune evasion, stress resistance, and efficient nutrient acquisition are crucial for intracellular survival of *Candida glabrata* within macrophages. *Eukaryot. Cell* 13, 170–183. doi: 10.1128/EC.00262-13

Shen, X. X., Zhou, X., Kominek, J., Kurtzman, C. P., Hittinger, C. T., and Rokas, A. (2016). Reconstructing the backbone of the saccharomycotina yeast phylogeny using genome-scale data. *G3* 6, 3927–3939. doi: 10.1534/g3.116.034744

Simms, C. L., Hudson, B. H., Mosior, J. W., Rangwala, A. S., and Zaher, H. S. (2014). An active role for the ribosome in determining the fate of oxidized mRNA. *Cell Rep.* 9, 1256–1264. doi: 10.1016/j.celrep.2014.10.042

Simms, C. L., Thomas, E. N., and Zaher, H. S. (2017). Ribosome-based quality control of mRNA and nascent peptides. *Wiley Interdiscip. Rev. RNA* 8:e1366. doi: 10.1002/wrna.1366

Srivastava, V. K., Suneetha, K. J., and Kaur, R. (2014). A systematic analysis reveals an essential role for high-affinity iron uptake system, haemolysin and CFEM domain-containing protein in iron homoeostasis and virulence in *Candida glabrata*. *Biochem. J.* 463, 103–114. doi: 10.1042/BJ20140598

Srivastava, V. K., Suneetha, K. J., and Kaur, R. (2015). The mitogen-activated protein kinase CgHog1 is required for iron homeostasis, adherence and virulence in *Candida glabrata*. *FEBS J.* 282, 2142–2166. doi: 10.1111/febs.13264

Strunk, B. S., Novak, M. N., Young, C. L., and Karbstein, K. (2012). A translation-like cycle is a quality control checkpoint for maturing 40S ribosome subunits. *Cell* 150, 111–121. doi: 10.1016/j.cell.2012.04.044

Teixeira, M. C., Monteiro, P. T., Palma, M., Costa, C., Godinho, C. P., Pais, P., et al. (2018). Yeastract: an upgraded database for the analysis of transcription regulatory networks in *Saccharomyces cerevisiae*. *Nucleic Acids Res.* 46:D348–D353. doi: 10.1093/nar/gkx842

Thomas-Chollier, M., Herrmann, C., Defrance, M., Sand, O., Thieffry, D., and van Helden, J. (2012). RSAT peak-motifs: motif analysis in full-size ChIP-seq datasets. *Nucleic Acids Res.* 40:e31. doi: 10.1093/nar/gkr1104

Thompson, D., Regev, A., and Roy, S. (2015). Comparative analysis of gene regulatory networks: from network reconstruction to evolution. *Annu. Rev. Cell Dev. Biol.* 31, 399–428. doi: 10.1146/annurev-cellbio-100913-012908

Thompson, D. A., Roy, S., Chan, M., Styczynsky, M. P., Pfiffner, J., French, C., et al. (2013). Evolutionary principles of modular gene regulation in yeasts. *eLife* 2:e00603. doi: 10.7554/eLife.00603

Thorvaldsdottir, H., Robinson, J. T., and Mesirov, J. P. (2013). Integrative Genomics Viewer (IGV): high-performance genomics data visualization and exploration. *Brief. Bioinform.* 14, 178–192. doi: 10.1093/bib/bbs017

Tirosh, I., and Barkai, N. (2007). Comparative analysis indicates regulatory neofunctionalization of yeast duplicates. *Genome Biol.* 8:R50. doi: 10.1186/gb-2007-8-4-r50

Ueta, R., Fujiwara, N., Iwai, K., and Yamaguchi-Iwai, Y. (2012). Iron-induced dissociation of the Aft1p transcriptional regulator from target gene promoters is an initial event in iron-dependent gene suppression. *Mol. Cell. Biol.* 32, 4998–5008. doi: 10.1128/MCB.00726-12

Vakirlis, N., Sarilar, V., Drillon, G., Fleiss, A., Agier, N., Meyniel, J. P., et al. (2016). Reconstruction of ancestral chromosome architecture and gene repertoire reveals principles of genome evolution in a model yeast genus. *Genome Res.* 26, 918–932. doi: 10.1101/gr.204420.116

Vall-Llaura, N., Reverter-Branchat, G., Vived, C., Weertman, N., Rodriguez-Colman, M. J., and Cabiscol, E. (2016). Reversible glutathionylation of Sir2 by monothiol glutaredoxins Grx3/4 regulates stress resistance. *Free Radic. Biol. Med.* 96, 45–56. doi: 10.1016/j.freeradbiomed.2016.04.008

van den Elzen, A. M., Schuller, A., Green, R., and Seraphin, B. (2014). Dom34-Hbs1 mediated dissociation of inactive 80S ribosomes promotes restart of translation after stress. *EMBO J.* 33, 265–276. doi: 10.1002/embj.201386123

Vitenshtein, A., Charpak-Amikam, Y., Yamin, R., Bauman, Y., Isaacson, B., Stein, N., et al. (2016). NK Cell recognition of *Candida glabrata* through binding of NKp46 and NCR1 to fungal ligands Epa1, Epa6, and Epa7. *Cell Host Microbe* 20, 527–534. doi: 10.1016/j.chom.2016.09.008

Wapinski, I., Pfeffer, A., Friedman, N., and Regev, A. (2007). Natural history and evolutionary principles of gene duplication in fungi. *Nature* 449, 54–61. doi: 10.1038/nature06107

Wapinski, I., Pfiffner, J., French, C., Socha, A., Thompson, D. A., and Regev, A. (2010). Gene duplication and the evolution of ribosomal protein gene regulation in yeast. *Proc. Natl. Acad. Sci. U.S.A.* 107, 5505–5510. doi: 10.1073/pnas.0911905107

Wickner, R. B., and Leibowitz, M. J. (1979). Mak mutants of yeast: mapping and characterization. *J. Bacteriol.* 140, 154–160.

Wickner, R. B., Koh, T. J., Crowley, J. C., O'Neil, J., and Kaback, D. B. (1987). Molecular cloning of chromosome I DNA from *Saccharomyces cerevisiae*: isolation of the MAK16 gene and analysis of an adjacent gene essential for growth at low temperatures. *Yeast* 3, 51–57. doi: 10.1002/yea.320030108

Yarunin, A., Panse, V. G., Petfalski, E., Dez, C., Tollervey, D., and Hurt, E. C. (2005). Functional link between ribosome formation and biogenesis of iron-sulfur proteins. *EMBO J.* 24, 580–588. doi: 10.1038/sj.emboj.7600540

Young, D. J., Guydosh, N.R., Zhang, F., Hinnebusch, A.G., and Green, R. (2015) Rli1/ABCE1 recycles terminating ribosomes and controls translation reinitiation in 3′UTRs in vivo. *Cell* 162, 872–884. doi: 10.1016/j.cell.2015.07.041

Zhang, Z., Gu, J., and Gu, X. (2004). How much expression divergence after yeast gene duplication could be explained by regulatory motif evolution? *Trends Genet* 20, 403–407.

Zhou, D., Zhu, X., Zheng, S., Tan, D., Dong, M. Q., and Ye, K. (2018). Cryo-EM structure of an early precursor of large ribosomal subunit reveals a half-assembled intermediate. *Protein Cell.* doi: 10.1007/s13238-018-0526-7 [Epub ahead of print].

Conflict of Interest Statement: The authors declare that the research was conducted in the absence of any commercial or financial relationships that could be construed as a potential conflict of interest.

frontiers in Microbiology

ORIGINAL RESEARCH
published: 20 November 2018
doi: 10.3389/fmicb.2018.02786

Investigation of the Role That NADH Peroxidase Plays in Oxidative Stress Survival in Group B *Streptococcus*

*Michelle L. Korir[1], Rebecca A. Flaherty[1], Lisa M. Rogers[2], Jennifer A. Gaddy[2,3,4], David M. Aronoff[2,4,5] and Shannon D. Manning[1]**

[1] Department of Microbiology and Molecular Genetics, Michigan State University, East Lansing, MI, United States, [2] Division of Infectious Diseases, Department of Medicine, Vanderbilt University Medical Center, Nashville, TN, United States, [3] Tennessee Valley Healthcare Systems, Department of Veterans Affairs, Nashville, TN, United States, [4] Department of Pathology, Microbiology, and Immunology, Vanderbilt University Medical Center, Nashville, TN, United States, [5] Department of Obstetrics and Gynecology, Vanderbilt University Medical Center, Nashville, TN, United States

Macrophages play an important role in defending the host against infections by engulfing pathogens and containing them inside the phagosome, which consists of a harsh microbicidal environment. However, many pathogens have developed mechanisms to survive inside macrophages despite this challenge. Group B *Streptococcus* (GBS), a leading cause of sepsis and meningitis in neonates, is one such pathogen that survives inside macrophages by withstanding phagosomal stress. Although a few key intracellular survival factors have been identified, the mechanisms by which GBS detoxifies the phagosome are poorly defined. Transcriptional analysis during survival inside macrophages revealed strong upregulation of a putative NADH peroxidase (*npx*) at 1 and 24 h post-infection. A deletion mutant of *npx* (Δ*npx*) was more susceptible to killing by a complex *in vitro* model of multiple phagosomal biochemical/oxidant stressors or by hydrogen peroxide alone. Moreover, compared to an isogenic wild type GBS strain, the Δ*npx* strain demonstrated impaired survival inside human macrophages and a reduced capacity to blunt macrophage reactive oxygen species (ROS) production. It is therefore likely that Npx plays a role in survival against ROS production in the macrophage. A more thorough understanding of how GBS evades the immune system through survival inside macrophages will aid in development of new therapeutic measures.

Keywords: group B *Streptococcus*, *Streptococcus agalactiae*, macrophages, oxidative stress, intracellular survival

OPEN ACCESS

Edited by:
Conor P. O'Byrne, National University of Ireland Galway, Ireland

Reviewed by:
Johanna Rivera, Albert Einstein College of Medicine, United States
Aoife Boyd, National University of Ireland Galway, Ireland

***Correspondence:**
Shannon D. Manning
mannin71@msu.edu

Specialty section:
This article was submitted to Microbial Physiology and Metabolism, a section of the journal Frontiers in Microbiology

Received: *18 May 2018*
Accepted: *30 October 2018*
Published: *20 November 2018*

Citation:
Korir ML, Flaherty RA, Rogers LM, Gaddy JA, Aronoff DM and Manning SD (2018) Investigation of the Role That NADH Peroxidase Plays in Oxidative Stress Survival in Group B Streptococcus. Front. Microbiol. 9:2786. doi: 10.3389/fmicb.2018.02786

INTRODUCTION

Group B *Streptococcus* (GBS; *Streptococcus agalactiae*) is well-known for its ability to cause adverse pregnancy outcomes and severe neonatal infections. Moreover, GBS can cause infections in the elderly as well as immunocompromised individuals (Johri et al., 2006). In neonatal infections, GBS can ascend the maternal vaginal tract, cross the extraplacental membranes and cause an infection *in utero*. Alternatively, the baby can become infected while passing through the birth canal by inhaling GBS when present in vaginal secretions (Katz and Bowes, 1988; Doran and Nizet, 2004). Despite the use of prevention strategies like intrapartum antibiotic prophylaxis, which have been successful in reducing the incidence of

neonatal infections overall, the current rates of neonatal infections have plateaued over the years, indicating the need for alternative therapies and preventative measures (Verani et al., 2010; Russell et al., 2017).

Macrophages play an important role in defending the host from invading pathogens. In the pregnant uterus, both maternally-derived decidual macrophages and fetally-derived placental macrophages play roles in maintaining maternal immune tolerance to the fetus while helping defend against pathogens that may infect and traverse the extraplacental (fetal) membranes to infect the baby *in utero* (Heikkinen et al., 2003; Petroff et al., 2003; Kim et al., 2012). Upon recognition by a macrophage, a pathogen is typically phagocytosed and contained inside a phagosome that, through a maturation process, becomes highly microbicidal, consisting of reactive oxygen and nitrogen species, antimicrobial peptides, heavy metals, low nutrients, and acidic pH (Flannagan et al., 2012). Previous studies have reported that GBS is capable of withstanding this extreme environment and can persist inside the fully mature phagolysosome for an extended period of time without inhibiting phagosome maturation (Valentin-weigand et al., 1996; Cornacchione et al., 1998; Cumley et al., 2012; Korir et al., 2016). This ability to survive inside macrophages may explain its ability to cross host cell barriers, effectively evade the immune system, and persistently colonize women, even after antibiotic treatment.

An important aspect of the highly microbicidal environment GBS endures inside the macrophage is the production of reactive oxygen species (ROS). ROS can also be produced as a by product during metabolism and represent a source of endogenous ROS; therefore many bacteria require ways to inactivate or detoxify ROS (Cabiscol et al., 2000). The amount of ROS produced by the NOX2 NADPH oxidase in macrophages during the ROS burst, however, is significantly higher, inducing oxidative stress to kill invading pathogens (Slauch, 2011). ROS can target and damage lipids, proteins, DNA, and RNA, making it particularly harmful to the cell (Cabiscol et al., 2000). Despite being catalase negative, GBS has been shown to survive exposure to high levels of hydrogen peroxide (H_2O_2), a type of ROS (Poyart et al., 2001; Cumley et al., 2012; Korir et al., 2016). Moreover, the ability to withstand a combination of phagosomal stressors, including H_2O_2, varied among strains of different sequence types (STs). Specifically, strains belonging to ST-17, considered to be a hypervirulent lineage, were better able to survive compared to strains of other lineages (Korir et al., 2016). One mechanism that GBS uses to defend against ROS is superoxide dismutase, which aids in detoxification of superoxide by converting it to O_2 and H_2O_2 (Poyart et al., 2001); however, the mechanism by which GBS detoxifies H_2O_2 has yet to be examined. GBS also produces glutathione as well as a carotenoid pigment, both of which have been shown to protect against oxidative damage (Liu et al., 2004; Janowiak and Griffith, 2005).

In this study, we sought to address the extent to which a putative NADH peroxidase, encoded by *npx*, fosters GBS survival within the macrophage and the ability to withstand ROS. These studies demonstrate that expression of *npx* is highly upregulated during survival inside macrophages and that Npx plays a role in defending against oxidative stress and is important for reducing ROS production inside macrophages.

MATERIALS AND METHODS

Bacterial Strains and Growth Conditions

The GBS strain used in this study was GB00112, a strain isolated from a vaginal rectal screen of a woman who had recently given birth (Manning et al., 2008) and was classified as sequence type (ST)-17 using multilocus sequence typing. This strain has previously been examined by our group for host cell attachment and intracellular survival in macrophages (Korir et al., 2014, 2016). Isogenic mutants of this strain, including a *npx* deletion mutant (Δ*npx*) harboring the empty vector (GB02168), a complemented *npx* mutant harboring a plasmid containing the *npx* locus, referred to as Δ*npx*:*npx* (GB02169), and the parental strain harboring the empty vector alone (GB02139) also were used in this study. Bacterial strains were grown on Todd-Hewitt agar (THA) plates or in Todd-Hewitt broth (THB) at 37°C. Derivatives harboring the pLZ12 plasmid were grown in media supplemented with 3 μg/mL chloramphenicol. *E. coli* DH5α strains used for the mutation and complementation process were grown in LB broth or agar supplemented with either 150 μg/mL erythromycin or 20 μg/mL chloramphenicol when necessary.

Cell Culture

THP-1 monocyte-like cells (ATCC TIB-202) were cultured in RPMI medium with 2 mM L-glutamine (Gibco), 10% fetal bovine serum (FBS; Atlanta Biologicals), and 1% penicillin/streptomycin (Gibco) at 37°C with 5% carbon dioxide. THP-1 cells were differentiated into macrophages by incubation with 100 nM phorbol 12-myristate 13-acetate (PMA; Sigma) in RPMI medium with 2% FBS for 24 h as described (Schwende et al., 1996).

Macrophage Survival Assays

Intracellular survival assays were described previously (Korir et al., 2016). Briefly, GBS strains were grown to mid-log phase in THB. PMA treated THP-1 macrophages were then infected with GBS strains at a multiplicity of infection (MOI) of 10:1 in RPMI for 1 h. Extracellular bacteria were killed by first washing any unattached bacteria and adding RPMI supplemented with 2% FBS, 100 μg/ml gentamicin (Gibco), and 5 μg/ml penicillin G (Sigma) to the wells. At the indicated time points, intracellular bacteria were enumerated by lysing the macrophages with 0.1% Triton-X (Sigma), and serially diluting and plating lysates to calculate CFUs. Survival was normalized to the total amount of bacteria present in the well after the 1 h infection period (final inoculum). In a separate series of experiments, the macrophages were treated with 500 μM apocynin or 0.1% DMSO as a negative control for 30 min prior to infection with GBS to inhibit production of ROS; the macrophages remained in the medium containing apocynin or DMSO for the duration of the experiment. The number of bacteria surviving intracellularly with apocynin treatment was normalized to survival in DMSO.

Generation of GBS Competent Cells and Construction of Isogenic Bacterial Mutant Strains

Group B *Streptococcus* electrocompetent cells were generated as previously described with modification (Framson et al., 1997). GBS was grown in THB with 0.5 M sucrose and a sublethal, but inhibitory concentration of glycine to early log phase (OD = 0.25) in shaking conditions. The culture was then pelleted at 4°C, the supernatant removed, and the pellet washed with ice cold 0.625 M sucrose solution. The culture was pelleted again and resuspended in 0.625 M sucrose and stored at −80°C.

The *npx* gene was deleted using the thermosensitive plasmid pG$^+$host5 as previously described (Al Safadi et al., 2011; Parker et al., 2017). The 5′ and 3′ flanking regions of *npx* were amplified using the primer sets *npx*-P1/*npx*-P2 for 5′ and *npx*-P3/*npx*-P4 for 3′ regions (**Table 1**). The two amplified flanking regions were combined in a crossover PCR, resulting in a single PCR product of the deletion sequence. The PCR product and the pG$^+$host5 plasmid were digested with *BamH*I and *Kpn*I then ligated to create pG$^+$host5Δ*npx*. This plasmid was electroporated into GB112 competent cells and transformants were selected by growth on 2 μg/ml erythromycin at 28°C. Cells in which the plasmid integrated into the chromosome via homologous recombination were selected for by growth on erythromycin at 42°C. Colonies that grew at 42°C were then grown in broth without antibiotic selection at 28°C for several passages to allow for excision of the plasmid. The cultures were then plated and single colonies were tested for erythromycin susceptibility and screened for gene deletion using PCR with primers *npx*-P5 and *npx*-P6. Deletion was confirmed by sequencing.

Complementation of the *npx* deletion was done using the pLZ12 plasmid under control of the *rofA* constitutive promoter (Neely et al., 2003). The coding sequence of *npx* was amplified using the *npx*-pLZ12 primer set (**Table 1**). The PCR product and the pLZ12-rofApro plasmid were digested with *BamH*I and *Pst*I and ligated to create npx-pLZ12. The plasmid was electroporated into GBS competent cells and transformants were selected by growth on 3 μg/ml chloramphenicol.

TABLE 1 | Oligonucleotide primers used to generate GBS mutagenesis and complementation vectors.

Primer name	Sequence (5′ to 3′)
npx-P1[a]	CCGC**GGATCC**CCAAAGCCCCAGATTTTGCTG
npx-P2[b]	CCCATCCACTAAACTTAACAAAGAGGATTGGGCTATGCGA
npx-P3[b]	TGTTTAAGTTTAGTGGATGGGACCATAAAGTCGGTCTCAGCA
npx-P4[c]	GGG**GGTACC**TTAGACCCCATTATGAGGCTGC
npx-P5	CTAAGGCTGCGTCTAACCGT
npx-P6	TGCTGTAGCTATTGCAGCGT
npx-pLZ12-F2[a]	CGC**GGAT**CCAGGAGGACAGCTATGACAGAAAAATATGTA
npx-pLZ12-R2[d]	AAAA**CTGCAG**CTATTCGCATAGCCCAATCC

[a]BamHI restriction site is shown in bold. [b]Complementary sequences for P2 and P3 sets are underlined. [c]KpnI restriction site is shown in bold. [d]PstI restriction site is shown in bold.

RNA Isolation and RT-PCR

RNA isolation, cDNA synthesis and RT-PCR were performed as described previously (Korir et al., 2014; Korir, 2016). Briefly, RNA samples were collected from bacterial culture in liquid medium by adding two volumes of RNAprotect Bacteria Reagent (Qiagen) or from bacteria inside macrophages by washing the cells twice with PBS then adding 1 ml RNAprotect Bacteria Reagent directly to the cells. RNA was then extracted using the RNeasy minikit (Qiagen) using the "Enzymatic Lysis, Proteinase K Digestion, and Mechanical Disruption of Bacteria" protocol in the RNAprotect handbook. Residual genomic DNA was removed using the Turbo DNA-free kit (Ambion). The iScript Select cDNA synthesis kit was used to synthesize cDNA using random primers. As a control to test for DNA contamination, samples were processed without reverse transcriptase. RT-PCR analysis was performed using the iQ SYBR Supermix (Bio-Rad) and gene specific primers (**Table 2**). Relative fold change in gene expression was calculated using the $2^{-\Delta\Delta Ct}$ method and relative transcript level was calculated using $2^{-\Delta Ct}$ method; *gyrA* was used as the internal control for both (Schmittgen and Livak, 2008).

H_2O_2 Quantification

Bacterial cultures were incubated at 37°C with the indicated concentrations of H_2O_2 in sodium phosphate buffer for 1 h in a 96 well plate. Buffer with bacteria alone (no H_2O_2 added) and buffer with H_2O_2 but without cultures, were included as controls. After 1 h, the bacteria were pelleted and supernatants were transferred to a new 96 well plate. The amount of H_2O_2 remaining in the supernatants was determined using the Fluorimetric Hydrogen Peroxide Assay Kit (Sigma) according to the manufacturer's directions. The concentration of H_2O_2 was calculated by comparing fluorescence readings from the samples to a standard curve. Percent detoxification was calculated by normalizing data to the H_2O_2 controls without bacterial cultures.

Survival in H_2O_2 and Multiple Stress Medium

The ability of GBS to survive phagosomal stress was described in our prior study (Korir et al., 2016). Briefly, GBS cultures were exposed to either 5 mM H_2O_2 alone, 5 mM H_2O_2 in sodium phosphate buffer at pH 4.5, or a multiple stress medium, which consisted of 1.5 mM H_2O_2, 3 mM $NaNO_2$, 100 μM $CuCl_2$, and 100 μg/ml lysozyme in acidic sodium phosphate buffer (pH 4.5) for 1 h then diluted and plated to enumerate viable bacteria. Percent survival was calculated by normalizing viable bacteria in the treated sample to the untreated samples.

TABLE 2 | Oligonucleotide primers used for RT-PCR.

Gene	Forward primer (5′ to 3′)	Reverse primer (5′ to 3′)
gyrA	CGGGACACGTACAGGCTACT	CGATACGAGAAGCTCCCACA
npx	GACCGCCTTCCCTGATTCAT	TAGCAGTTGTTGGGGCAGG
ahpC	GCGGATGTATTGAGCAGCAC	GATCCAGACGGTGTCATCCA
tpx	GCATTTGTTAACGCGTGCAG	CAGCATTAATCGCCGCTTCG

Human Placental Macrophage Isolation

Placental tissue was collected from non-laboring women who delivered healthy, full term infants by Caesarian section. De-identified tissue samples were provided by the Cooperative Human Tissue Network, which is funded by the National Cancer Institute. Placental macrophages were isolated according to our previously published methods (Tetz et al., 2015).

Ethics Statement

This study was carried out in accordance with the recommendations of the Vanderbilt University Institutional Review Board. All placentae were obtained fully de-identified by the Cooperative Human Tissue Network. This protocol was approved by the Institutional Review Board (Approval No. 131607), which determined that our studies did not qualify as "human subject" research. The study did not involve interaction or intervention with a human subject and the specimens were stripped of identifiable information prior to the investigator receiving the samples.

ROS Production in Placental Macrophages

The level of ROS produced by human placental macrophages after GBS infection was quantified as described in our prior study (Korir et al., 2016). Briefly, macrophages were labeled with 10 μM Carboxyl H2DCF-DA using the manufacturer's recommendations (Invitrogen), washed and infected with GBS using a MOI of 50:1. ROS was also induced using 200 ng/mL PMA as a positive control, while ROS production was measured 30 min after infection and was normalized as percent of the untreated control. The 30 min time point was chosen based on data generated in our prior study (Korir et al., 2016) and to prevent the induction of a cytotoxic response.

Statistical Analysis

GraphPad Prism version 5 was used for all statistical analyses. Comparisons across multiple groups or with two parameters were analyzed using one-way or two-way ANOVA respectively using Bonferroni post-tests where appropriate. Comparisons with $P \leq 0.05$ were accepted as statistically significant.

RESULTS

NADH Peroxidase Is Highly Upregulated in GBS During Intracellular Survival

In a previous study, we determined that a ST-17 isolate, GB00112, was capable of surviving inside human THP-1 macrophages significantly longer than a ST-12 isolate (Korir et al., 2016). This same strain was used for RNA sequencing (data not shown) to identify factors that are upregulated during intracellular survival relative to growth in medium alone (Korir, 2016). Significant upregulation of locus GB112_04315 (*npx*), which encodes a putative NADH peroxidase (Npx), was confirmed to be highly upregulated at both 1 and 24 h post-infection (**Figure 1**). Furthermore, a BLAST search of 252 published GBS genomes with full *npx* coverage showed a high (98.9–100% identity) level of homology across strains.

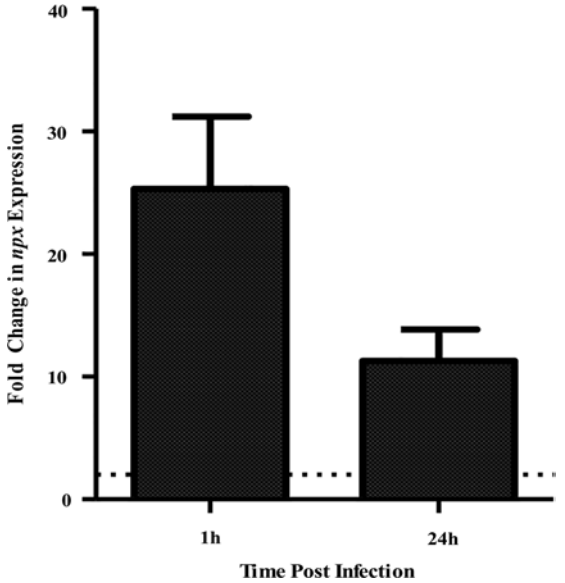

FIGURE 1 | Expression of *npx* at 1 and 24 h survival inside PMA-treated human macrophages tested using qPCR. Fold change in expression was calculated relative to gene expression during growth in RPMI medium alone for 1 h. Dotted line indicates twofold change in gene expression. Data shown is average ± SD of three separate biological replicates.

The Role of Npx in H_2O_2 Survival

The presumed function of NADH peroxidases is to detoxify endogenously produced H_2O_2, such as that produced during aerobic growth, metabolism, or through dismutation of superoxide (La Carbona et al., 2007). Because they could also detoxify exogenous sources of H_2O_2, including those that occur during the ROS burst in macrophages, we sought to determine the role of Npx in survival against H_2O_2 stress. To do this, a deletion mutant was constructed in the ST-17, GB00112 strain background and complementation was performed *in trans* using the pLZ12 plasmid containing the constitutive *rofA* promoter (Neely et al., 2003) controlling the wild type (WT) allele of *npx*.

To examine the ability of Δ*npx* to withstand high levels of endogenously produced H_2O_2, we compared the level of growth in complex medium (THB), which consists of glucose as the main carbon source, to that of growth in medium with glycerol as the sole carbon source. H_2O_2 is produced in lactic acid bacteria during glycerol metabolism through α-glycerophosphate oxidation (Whittenbury, 1964; Koditschek and Umbreit, 1969). Growth was very similar for all three strains when grown on glucose (**Figure 2A**); however, Δ*npx* showed a higher level of growth in glycerol compared to the WT strain. The Δ*npx*:*npx* strain had a level of growth that was between the mutant and WT indicating incomplete complementation under higher oxidative stress conditions (**Figure 2B**).

The GBS genome also encodes two other putative peroxidases: a thiol peroxidase (*tpx*) and an alkylhydroperoxide reductase

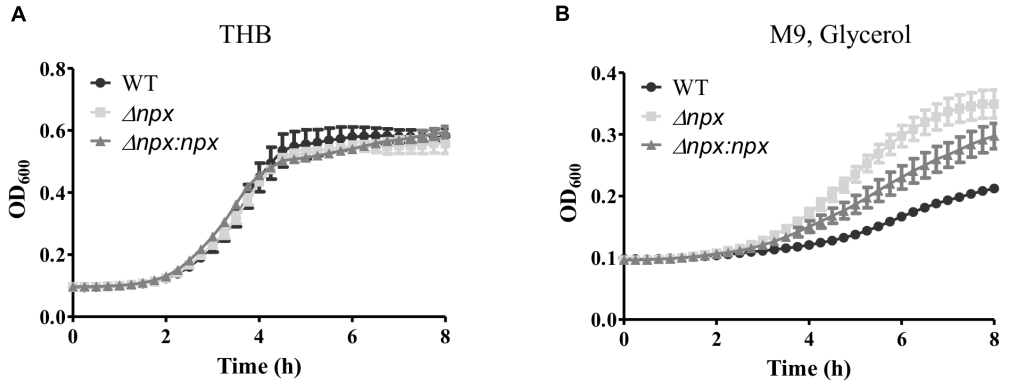

FIGURE 2 | Growth of GBS utilizing different carbon sources. GBS strains were grown in either **(A)** THB, which contains glucose as the main carbon source or **(B)** M9 medium using glycerol as the sole carbon source. Cultures were grown in 96 well plates and OD_{600} was read every 15 min using Bio Tek Cytation 3 plate reader. Data shown is representative of three separate biological replicates. Error bars represent SD of six technical replicates.

(*ahpC*), both of which could also contribute to ROS detoxification in the cell (Glaser et al., 2002). Therefore, we hypothesized that one or both of these genes could be overexpressed in the Δ*npx* strain to compensate for the loss of Npx. Indeed, such overexpression could allow for more rapid detoxification of the endogenously produced H_2O_2 during growth on glycerol, thereby resulting in a higher level of growth in the mutant. To test this hypothesis, we collected RNA at various stages of growth in medium containing glycerol as the sole carbon source and examined gene expression of *ahpC* and *tpx*. Since the strains exhibited different growth rates over time, samples were collected based on OD_{600} rather than time of growth to ensure cells were in the same growth phase at time of collection. Expression of *ahpC* was significantly lower in Δ*npx* compared to the WT around mid-log phase (OD_{600} 0.4 and 0.6) but was similar to WT expression at early and late log phase (**Figure 3A**). Expression of *tpx* was higher in Δ*npx* relative to WT levels at all times except OD_{600} 0.4, although the difference was not significant at OD_{600} 0.6 (**Figure 3B**). For each replicate performed, the fold-change value in gene expression varied slightly between replicates, however, the overall trends were the same. It is also important to note that the discrepancy between maximum OD_{600} in **Figure 2B** and OD_{600} values reported in **Figure 3** are due to slightly different growth conditions. Cultures were grown in 96-well plates for **Figure 2B**, which results in a lower maximum OD_{600} compared to growth in tubes with much larger volumes for **Figure 3**. Despite the difference in maximum OD_{600} reached during culture, all strains exhibited similar growth patterns relative to the others (data not shown).

We next examined the ability of these strains to survive in the presence of an exogenous source of H_2O_2 by incubating the culture in 5 mM H_2O_2 and determining the level of survival after 1 h. The *npx* mutant was significantly more susceptible to killing in the presence of H_2O_2 relative to the WT (**Figure 4A**). Surprisingly, this phenotype was not complemented in Δ*npx*:*npx*

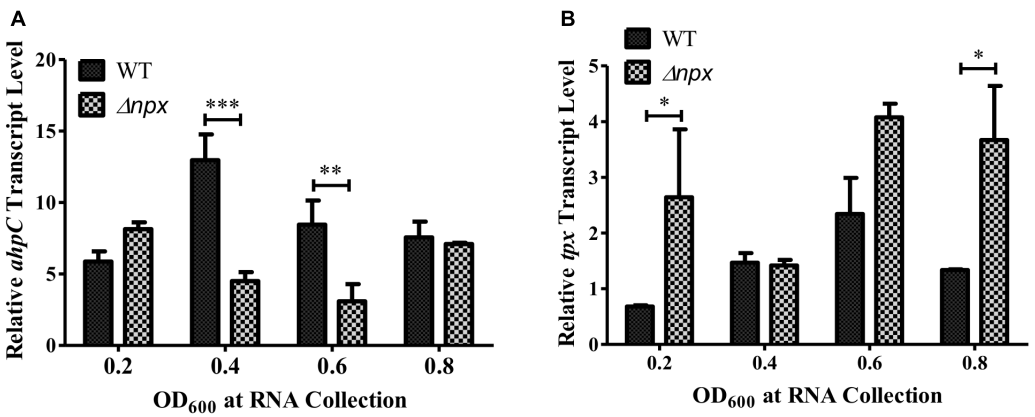

FIGURE 3 | Peroxidase expression during growth in M9 with glycerol as the sole carbon source. RNA was collected at the indicated time points and relative transcript levels of **(A)** *ahpC* or **(B)** *tpx* was determined using *gyrA* as the internal control gene. Data shown is representative of two separate biological replicates. Error bars and statistical analysis shown were done using three technical replicates (*$P < 0.05$, **$P < 0.01$, ***$P < 0.001$).

despite this strain showing similar phenotypes to the WT strain in other experiments (**Figures 5**, **6**). In our previous study, we reported that the ability of this ST-17 WT stain to survive H_2O_2 exposure was rescued when H_2O_2 stress was combined with low pH exposure (pH = 4.5) (Korir et al., 2016). Therefore, we next examined survival of these strains in the presence of both 5 mM H_2O_2 and pH 4.5. Consistent with our previous results, the survival of the WT was restored in the combined stress. Interestingly, both Δ*npx* and Δ*npx*:*npx* showed reduced survival in the combined stress relative to the WT; however, their survival rate was very similar to that of the WT in H_2O_2 alone (**Figure 4A**).

To further explore the mechanism of how Npx aids in survival against H_2O_2, we determined how well GBS was able to detoxify exogenous H_2O_2 by measuring the level of H_2O_2 present in the medium before and after incubation. No significant difference in H_2O_2 detoxification was detected between Δ*npx* and WT in any H_2O_2 concentration examined. However, the complemented *npx* mutant detoxified H_2O_2 at a significantly higher rate than Δ*npx* and WT at 10 μM H_2O_2 (**Figure 4B**).

Contribution of Npx to GBS Survival in the Presence of Phagosomal Stressors

Since *npx* was initially found to be upregulated during macrophage survival, we next examined the role that Npx plays in the survival of GBS inside macrophages. We first examined the ability of these strains to survive in our previously developed multiple stress medium that consists of a number of stressors found in the phagosome, including acidic pH, H_2O_2, NO, Cu^{2+}, and lysozyme (Korir et al., 2016). The Δ*npx* strain was more susceptible to killing by this medium relative to the WT, while this phenotype was partially rescued in the Δ*npx*:*npx* strain (**Figure 5A**). Next, the ability of these strains to survive inside PMA treated THP-1 human macrophages was determined at 1 h (**Figure 5B**) and 24 h (**Figure 5C**) post-infection. At both time points, Δ*npx* showed a slight, but insignificant decrease in ability to survive. Although the Δ*npx*:*npx* strain survived similarly when compared to the WT, it had a significantly enhanced ability to survive compared to Δ*npx*.

Because GBS is capable of inhibiting the ROS burst in macrophages (Korir et al., 2016), we examined ROS production by human placental macrophages 30 min post-infection with our GBS strains. Consistent with previous results, the WT significantly reduced ROS production relative to the untreated control as well as the positive control, indicating inhibition of the ROS burst. Although there was no significant difference between WT and Δ*npx,* the Δ*npx* strain did not significantly reduce ROS production relative to the negative control as observed in the WT. Importantly, Δ*npx* did not *induce* a ROS burst as was observed with the induced positive control, suggesting it was still capable of partially inhibiting the ROS burst. The WT phenotype was fully restored in the complemented strain (**Figure 6A**).

Finally, we sought to determine how the macrophage oxidative burst impacts intracellular survival by examining the ability of GBS to survive inside macrophages that were pretreated with either DMSO as a negative control or apocynin, an inhibitor of ROS production in phagocytic cells (Stolk et al., 1994). To highlight the specific impact of apocynin on intracellular survival, survival in apocynin treated macrophages was normalized to survival in control macrophages. At 1 h post-infection, apocynin treatment did not reduce survival of any strains relative to the DMSO negative control, while at 24 h post-infection, apocynin treatment reduced survival to approximately 25% of the DMSO negative control for all three strains. Overall, apocynin treatment had a similar impact on survival of all three strains (**Figure 6B**). It is important to note that no difference in survival was observed in the WT (P = 0.15), Δ*npx* (P = 0.30), or Δ*npx*:*npx* (P = 0.31) strains when grown in RPMI and 500 mM apocynin after 24 h compared to DMSO and performed in triplicate.

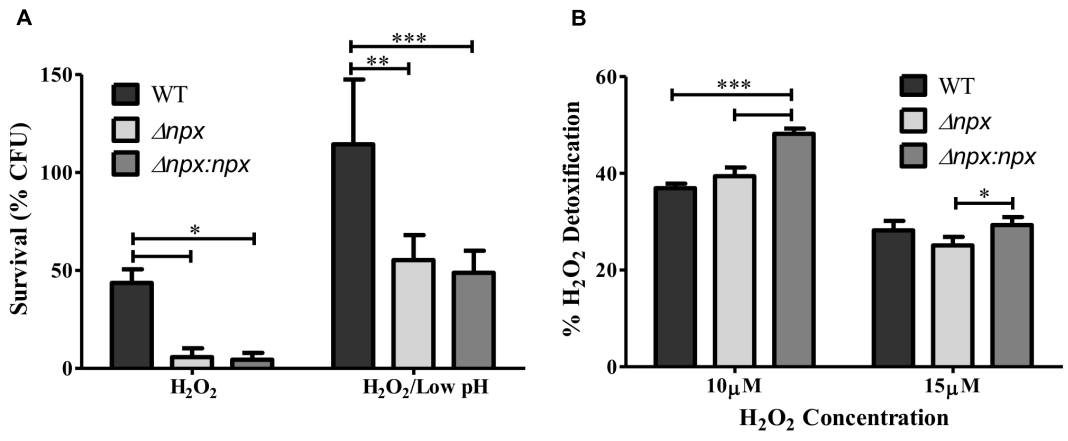

FIGURE 4 | Role of the *npx* locus in response to H_2O_2. **(A)** Survival of GBS after 1 h exposure to 5 mM H_2O_2 alone or in combination with pH 4.5. Survival is expressed as the percent of CFU after exposure relative to the untreated control. **(B)** The level of H_2O_2 detoxification by GBS at two different H_2O_2 concentrations. Percent detoxification was calculated by normalizing the amount of H_2O_2 remaining after incubation with GBS to the amount of H_2O_2 in the culture free control. Data shown is average ± SD of three separate biological replicates (*P < 0.05, **P < 0.01, ***P < 0.001).

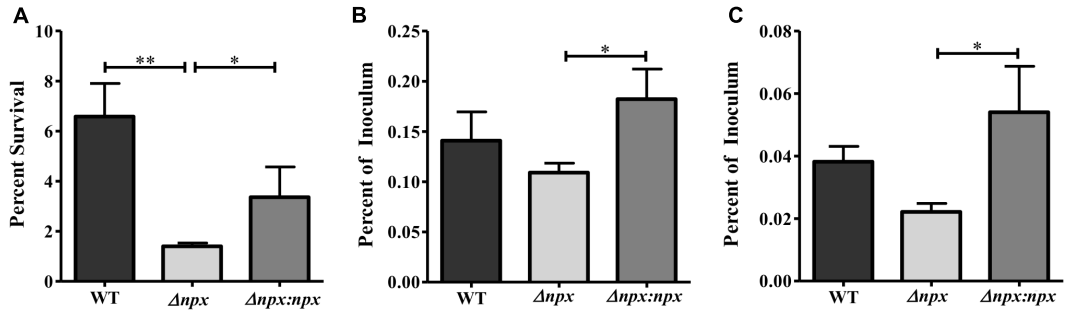

FIGURE 5 | The role of the *npx* locus in surviving phagosomal stress. **(A)** Survival of GBS in a multiple stress medium consisting of acidic pH (pH 4.5), H_2O_2, NO, lysozyme, and Cu^{2+}. Survival was calculated by normalizing the number of CFUs after treatment to the untreated control. **(B,C)** Survival of GBS inside PMA treated THP-1 human macrophages after 1 h **(B)** and 24 h **(C)**. The number of intracellular bacteria was normalized to the total amount of bacteria in the well after the initial infection period. Data shown is representative of three separate biological replicates. Error bars and statistical analysis shown were done using three technical replicates (*$P < 0.05$, **$P < 0.01$).

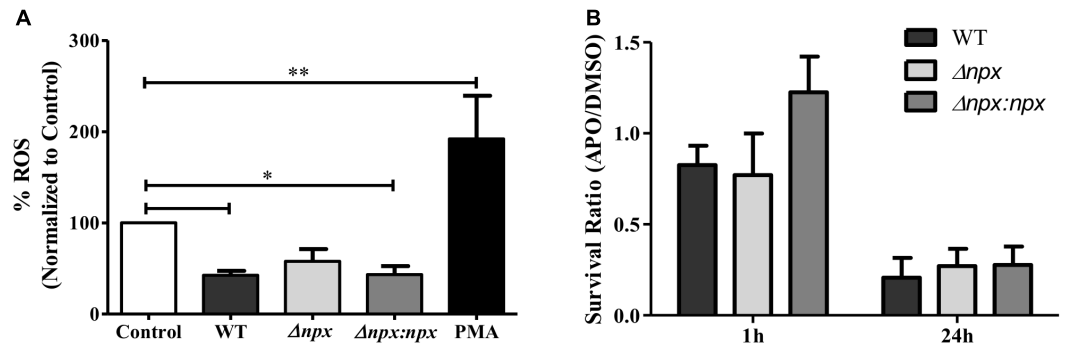

FIGURE 6 | Association between *npx* and the ROS burst in macrophages. **(A)** ROS production in placental macrophages was measured 30 min after exposure to medium alone (control), GBS, or 200 ng/ml PMA as a positive control. ROS production was normalized to the untreated control. **(B)** Intracellular survival of GBS strains was determined at 1 and 24 h post-infection. Macrophages were treated with either DMSO (negative control) or apocynin (APO) 30 min prior to infection. Survival in APO is shown as a ratio relative to survival in DMSO. Data shown is average ± SD of three separate biological replicates (*$P < 0.05$, **$P < 0.01$).

DISCUSSION

Macrophages play an important role in establishing immune tolerance during pregnancy as well as immune defense against invading pathogens. However, pathogens with the ability to survive inside these macrophages can evade immune system clearing and cross host cell barriers undetected inside these important immune cells. Therefore, it is essential to have a better understanding of how these pathogens remain inside macrophages in order to develop new therapeutics to eliminate this intracellular threat.

Here, as well as in previous studies, GBS has been shown to withstand high levels of oxidative stress as well as inhibit the ROS burst in macrophages (Poyart et al., 2001; Cumley et al., 2012; Korir et al., 2016). The ability of GBS to resist oxidative damage by the ROS burst is in part due to superoxide dismutase; however, GBS is catalase negative and therefore, requires other ways to detoxify H_2O_2. In this study we identified a putative NADH peroxidase to be highly upregulated during intracellular survival and demonstrated that *npx* contributes to the mechanism employed by GBS to withstand H_2O_2 as well as inhibiting the ROS burst. However, it is likely not the only factor contributing to H_2O_2 survival as the *npx* mutant showed a higher level of growth with endogenous H_2O_2 stress relative to the WT, was still able to detoxify H_2O_2 at levels similar to that of the WT, and was not completely killed by H_2O_2 stress or macrophages. The *npx* mutant also inhibited the ROS burst but not to the same extent as the WT. Indeed, a significant reduction in ROS relative to the uninduced control was observed in the WT but not in Δ*npx*. Genome sequencing shows that the GBS genome also encodes a thiol peroxidase (*tpx*) and an alkylhydroperoxide reductase (*ahpC*) that could contribute to H_2O_2 detoxification (Glaser et al., 2002), though the role of these two genes in ROS defense requires further investigation for their involvement in this mechanism. Our results, which were performed in duplicate and revealed similar expression trends by growth stage in glycerol, show that *tpx* was expressed at higher levels in Δ*npx* relative to the WT. Hence, *tpx* expression may be upregulated in the Δ*npx* background to compensate for the loss of Npx function during increased production of H_2O_2 through endogenous sources. This finding suggests that Tpx does indeed function to aid in ROS detoxification, however, further studies

are required to draw any conclusions on the function of Tpx and confirm these differences. Additional studies are also needed to determine whether each strain varies in the level of phagocytic uptake.

We have shown that Npx plays a role in survival against exogenous sources of H_2O_2. However, the exact mechanism by which it does this has yet to be determined. NADH peroxidases have been shown to detoxify H_2O_2 by converting it to H_2O in a NADH dependent manner; however, when we examined reduction of H_2O_2 in the presence of Δ*npx* vs. WT as a measure of detoxification, we observed no significant difference. This result could in part be due to the low concentration of H_2O_2 used this assay. At such low concentrations, it is possible that other enzymes present in GBS were able to detoxify the H_2O_2 and that Npx was not needed or induced in the WT. When higher concentrations were used in this assay, however, it was difficult to see reduced levels of H_2O_2 in the presence of WT GBS vs. the untreated control (data not shown). Future work will require the use of purified protein with H_2O_2 in kinetic assays similar to that done with purified NADH peroxidase from *Enterococcus faecalis* (Parsonage et al., 1993) in order to determine if Npx does indeed directly detoxify H_2O_2.

In a few of our experiments, we observed either lack of complementation or incomplete complementation despite seeing complementation in other experiments. Upon further examination of the genome sequence of the WT strain (GB00112), we identified a gene immediately downstream of *npx*, which could potentially be within the same operon as *npx*. This gene, GB112_04310, is annotated as a hypothetical protein. Because certain peroxidases require reductases in order to recycle the enzyme (Poole, 2005), it is possible that this hypothetical protein may serve as a reductase for Npx or play a role in activating the reductase. Although we designed our deletion mutant to limit polar effects as much as possible, there is a chance that deletion of *npx* negatively impacted GB112_04310 expression. In this case, it is possible that the plasmid-expressed Npx may not have been getting recycled for further enzymatic activity in our complemented strain. This hypothesis is supported by our finding that the Δ*npx* phenotypes without complementation were observed in conditions with higher concentrations of H_2O_2 such as during growth with glycerol as the sole carbon source or when high concentrations of H_2O_2 were directly added to the culture. Hence, it is possible that all available Npx was used before adequate amounts of the H_2O_2 was removed, and Npx was unable to be recycled to continue removing H_2O_2. Further exploration of this possible operon, the catalytic activity of Npx, and the function of GB112_04310, however, is required for confirmation.

Although *npx* was highly expressed during survival inside THP-1 macrophages, we did not observe a significant reduction in survival in the *npx* mutant relative to the WT. This discrepancy could be due, in part, to other peroxidases compensating for the loss of *npx* or the type of cells used. Although THP-1 cells have been used in a number of studies and there are many advantages of using cell lines, they do not replicate the conditions as well as primary cells or *in vivo* models would (Kaur and Dufour, 2012; Chanput et al., 2014). Future work will therefore need to examine this mutant using both primary cell lines that produce a robust ROS response and in animal models to determine how loss of *npx* impacts GBS virulence. Evaluating the role of this gene in different strain backgrounds will also be important, particularly given our finding that different strains vary in their ability to survive inside THP-1 cells (Korir et al., 2016).

A previous study that examined survival of GBS inside J774 murine macrophages found that apocynin treatement did not affect GBS survival through 9 h post-infection (Cumley et al., 2012). Consistent with this finding, we did not observe reduced survival at 1 h; however, a significant reduction in survival was observed at 24 h post-infection. The difference between our current findings and the previous study could be due to timing differences as we did not sample between 1 and 24 h, which could represent a limitation. Indeed, these two time points were chosen solely based on the methodology utilized and differences observed in our prior study (Korir et al., 2016). We had hypothesized that inhibiting the ROS burst would increase the ability of GBS to survive intracellularly, yet our unexpected results show a reduction in intracellular survival. This finding suggests that either: (1) the ROS burst or something influenced by the ROS burst is needed for long term survival in macrophages; or (2) the long term inhibition of ROS production is negatively impacting the macrophages themselves. Although we examined cell permeabilization as a measure of cell death, we did not observe a difference with apocynin (data not shown). It is therefore clear that the mechanism of ROS inhibition requires further investigation.

We previously demonstrated that the WT strain, GB00112 could inhibit ROS production during infection of human placental macrophages (Korir et al., 2016), yet the mechanism by which GBS does this in macrophages has yet to be determined. It could involve rapid detoxification of ROS as it is being produced, the inhibition of the NOX2 NADPH oxidase, or a combination of the two. In this study, we showed that the *npx* mutant strain was still capable of inhibiting ROS production in human placental macrophages, but to a lesser extent than that of both the WT and the complemented mutant; differences between the strains, however, were not statistically significant. Nonetheless, this finding suggests that, although Npx is not necessary for ROS inhibition, it is involved in full ROS inhibition. Because the proposed function of NADH peroxidases is to directly detoxify H_2O_2, the possible mechanism of ROS inhibition by Npx is in detoxification of the generated ROS. However, we were unable to observe differences in H_2O_2 detoxification abilities between the mutant and WT, and thus, it is difficult to deduce the exact role that Npx plays in ROS inhibition without further investigation.

In *E. faecalis*, the well-characterized *npr* gene, which also encodes a NADH peroxidase, has 23% homology to the GBS *npx* examined in this study. Congruent with the current findings, an *E. faecalis npr* mutant had similar growth to the WT under normal growth conditions, but was more susceptible to killing by H_2O_2 as well as macrophages (La Carbona et al., 2007). Since NADH peroxidases have been found in other Firmicutes

members (Sakamoto and Komagata, 1996), they likely represent a conserved mechanism for survival in the presence of intracellular H_2O_2 and ROS stress.

In summary, this study defines Npx as a key factor that allows GBS to survive oxidative and phagosomal stress, and contributes to the inhibition of the ROS burst in human macrophages. Additional studies should focus on determining the exact mechanism by which Npx contributes to these important virulence traits and understanding the role that other genes play in withstanding oxidative stress as well as other stressors (e.g., nitric oxide). Understanding the mechanism that GBS uses to survive phagosomal stress remains largely unknown and requires further study in order to define new ways to treat and prevent GBS infections.

AUTHOR CONTRIBUTIONS

MK, JG, DA, and SM contributed to the concepts and design of the study. MK, RF, and LR performed the experiments. MK, RF, and SM analyzed the data. MK and SM drafted the manuscript. All authors contributed to and edited the final version of the manuscript.

FUNDING

This work was supported by grants from the National Institutes of Health (AI134036, HD090061), U.S. Department of Veterans Affairs (CDA-2 1IK2BX001701 to JG), and the March of Dimes Foundation (DA).

ACKNOWLEDGMENTS

The authors would like to thank Dr. Agnes Rosenau for providing the pG$^+$host5 plasmid and Dr. Melody Neely for providing the pLZ12 plasmid. The authors would also like to thank Heather Blankenship for assisting with the *npx* genome analysis. A portion of these findings were included in Dr. Michelle Korir's Ph.D. dissertation from Michigan State University (Korir, 2016).

REFERENCES

Al Safadi, R., Mereghetti, L., Salloum, M., Lartigue, M.-F., Virlogeux-Payant, I., Quentin, R., et al. (2011). Two-component system RgfA/C activates the fbsB gene encoding major fibrinogen-binding protein in highly virulent CC17 clone group *B Streptococcus*. *PLoS One* 6:e14658. doi: 10.1371/journal.pone.0014658

Cabiscol, E., Tamarit, J., and Ros, J. (2000). Oxidative stress in bacteria and protein damage by reactive oxygen species. *Int. Microbiol.* 3, 3–8. doi: 10.2436/im.v3i1.9235

Chanput, W., Mes, J. J., and Wichers, H. J. (2014). THP-1 cell line: an in vitro cell model for immune modulation approach. *Int. Immunopharmacol.* 23, 37–45. doi: 10.1016/J.INTIMP.2014.08.002

Cornacchione, P., Scaringi, L., Fettucciari, K., Rosati, E., Sabatini, R., Orefici, G., et al. (1998). Group B streptococci persist inside macrophages. *Immunology* 93, 86–95. doi: 10.1046/j.1365-2567.1998.00402.x

Cumley, N. J., Smith, L. M., Anthony, M., and May, R. C. (2012). The CovS/CovR acid response regulator is required for intracellular survival of group *B Streptococcus* in macrophages. *Infect. Immun.* 80, 1650–1661. doi: 10.1128/IAI.05443-11

Doran, K. S., and Nizet, V. (2004). Molecular pathogenesis of neonatal group B streptococcal infection: no longer in its infancy. *Mol. Microbiol.* 54, 23–31. doi: 10.1111/j.1365-2958.2004.04266.x

Flannagan, R. S., Jaumouillé, V., and Grinstein, S. (2012). The cell biology of phagocytosis. *Annu. Rev. Pathol.* 7, 61–98. doi: 10.1146/annurev-pathol-011811-132445

Framson, P. E., Nittayajarn, A., Merry, J., Youngman, P., Framson, P. E., Nittayajarn, A., et al. (1997). New genetic techniques for group B streptococci: high-efficiency transformation, maintenance of temperature-sensitive pWV01 plasmids, and mutagenesis with Tn917. *Appl. Environ. Microbiol.* 63, 3539–3547.

Glaser, P., Rusniok, C., Buchrieser, C., Chevalier, F., Frangeul, L., Msadek, T., et al. (2002). Genome sequence of *Streptococcus agalactiae*, a pathogen causing invasive neonatal disease. *Mol. Microbiol.* 45, 1499–1513. doi: 10.1046/j.1365-2958.2002.03126.x

Heikkinen, J., Mottonen, M., Komi, J., Alanen, A., and Lassila, O. (2003). Phenotypic characterization of human decidual macrophages. *Clin. Exp. Immunol.* 131, 498–505. doi: 10.1046/j.1365-2249.2003.02092.x

Janowiak, B. E., and Griffith, O. W. (2005). Glutathione synthesis in *Streptococcus agalactiae*: one protein accounts for gamma-glutamylcysteine synthetase and glutathione synthetase activities. *J. Biol. Chem.* 280, 11829–11839. doi: 10.1074/jbc.M414326200

Johri, A. K., Paoletti, L. C., Glaser, P., Dua, M., Sharma, P. K., Grandi, G., et al. (2006). Group *B Streptococcus*: global incidence and vaccine development. *Nat. Rev. Microbiol.* 4, 932–942. doi: 10.1038/nrmicro1552

Katz, V., and Bowes, W. A. (1988). Perinatal group B streptococcal infections across intact amniotic membranes. *J. Reprod. Med.* 33, 445–449.

Kaur, G., and Dufour, J. M. (2012). Cell lines: valuable tools or useless artifacts. *Spermatogenesis* 2, 1–5. doi: 10.4161/spmg.19885

Kim, S. Y., Romero, R., Tarca, A. L., Bhatti, G., Kim, C. J., Lee, J., et al. (2012). Methylome of fetal and maternal monocytes and macrophages at the feto-maternal interface. *Am. J. Reprod. Immunol.* 68, 8–27. doi: 10.1111/j.1600-0897.2012.01108.x

Koditschek, L. K., and Umbreit, W. W. (1969). a-Glycerophosphate oxidase in *Streptococcus faecium* F 24. *J. Bacteriol.* 98, 1063–1068.

Korir, M. L. (2016). *Variation in Host-Pathogen Interactions Among Genetically Diverse Strains of Group B Streptococcus*. dissertation, Michigan State University, East Lansing, MI.

Korir, M. L., Knupp, D., LeMerise, K., Boldenow, E., Loch-Caruso, R., Aronoff, D. M., et al. (2014). Association and virulence gene expression vary among serotype III group *B Streptococcus* isolates following exposure to decidual and lung epithelial cells. *Infect. Immun.* 82, 4587–4595. doi: 10.1128/IAI.02181-14

Korir, M. L., Laut, C., Rogers, L. M., Plemmons, J. A., Aronoff, D. M., and Manning, S. D. (2016). Differing mechanisms of surviving phagosomal stress among group *B Streptococcus* strains of varying genotypes. *Virulence* 0, 1–14. doi: 10.1080/21505594.2016.1252016

La Carbona, S., Sauvageot, N., Giard, J. C., Benachour, A., Posteraro, B., Auffray, Y., et al. (2007). Comparative study of the physiological roles of three peroxidases (NADH peroxidase, Alkyl hydroperoxide reductase and Thiol peroxidase) in oxidative stress response, survival inside macrophages and virulence of *Enterococcus faecalis*. *Mol. Microbiol.* 66, 1148–1163. doi: 10.1111/j.1365-2958.2007.05987.x

Liu, G. Y., Doran, K. S., Lawrence, T., Turkson, N., Puliti, M., Tissi, L., et al. (2004). Sword and shield: linked group B streptococcal beta-hemolysin/cytolysin and carotenoid pigment function to subvert host phagocyte defense. *Proc. Natl. Acad. Sci. U.S.A.* 101, 14491–14496. doi: 10.1073/pnas.0406143101

Manning, S. D., Lewis, M. A., Springman, A. C., Lehotzky, E., Whittam, T. S., and Davies, H. D. (2008). Genotypic diversity and serotype distribution of group *B Streptococcus* isolated from women before and after delivery. *Clin. Infect. Dis.* 46, 1829–1837. doi: 10.1086/588296

Neely, M. N., Lyon, W. R., Runft, D. L., and Caparon, M. (2003). Role of RopB in growth phase expression of the SpeB cysteine protease of *Streptococcus pyogenes*. *J. Bacteriol.* 185, 5166–5174. doi: 10.1128/JB.185.17.5166

Parker, R. E., Knupp, D., Al Safadi, R., Rosenau, A., and Manning, S. D. (2017). Contribution of the RgfD quorum sensing peptide to rgf regulation and host cell association in group *B Streptococcus*. *Genes* 8, 1–15. doi: 10.3390/genes8010023

Parsonage, D., Miller, H., Ross, R. P., and Claiborne, A. (1993). Purification and analysis of streptococcal NADH peroxidase expressed in *Escherichia coli*. *J. Biol. Chem.* 268, 3161–3167.

Petroff, M. G., Chen, L., Phillips, T. A., Azzola, D., Sedlmayr, P., and Hunt, J. S. (2003). B7 family molecules are favorably positioned at the human maternal-fetal interface. *Biol. Reprod.* 68, 1496–1504. doi: 10.1095/biolreprod.102.010058

Poole, L. B. (2005). Bacterial defenses against oxidants: mechanistic features of cysteine-based peroxidases and their flavoprotein reductases. *Arch. Biochem. Biophys.* 433, 240–254. doi: 10.1016/j.abb.2004.09.006

Poyart, C., Pellegrini, E., Gaillot, O., Boumaila, C., Baptista, M., and Trieu-cuot, P. (2001). Contribution of Mn-cofactored superoxide dismutase (SodA) to the virulence of *Streptococcus agalactiae*. *Infect. Immun.* 68, 5098–5106. doi: 10.1128/IAI.69.8.5098

Russell, N. J., Seale, A. C., O'Sullivan, C., Le Doare, K., Heath, P. T., Lawn, J. E., et al. (2017). Risk of early-onset neonatal group B streptococcal disease with maternal colonization worldwide: systematic review and meta-analyses. *Clin. Infect. Dis.* 65, S152–S159. doi: 10.1093/cid/cix655

Sakamoto, M., and Komagata, K. (1996). Aerobic growth of and activities of NADH oxidase and NADH peroxidase in lactic acid bacteria. *J. Ferment. Bioeng.* 82, 210–216. doi: 10.1016/0922-338X(96)88810-6

Schmittgen, T. D., and Livak, K. J. (2008). Analyzing real-time PCR data by the comparative CT method. *Nat. Protoc.* 3, 1101–1108. doi: 10.1038/nprot.2008.73

Schwende, H., Fitzke, E., Ambs, P., and Dieter, P. (1996). Differences in the state of differentiation of THP-1 cells induced by phorbol ester and 1,25-dihydroxyvitamin D3. *J. Leukoc. Biol.* 59, 555–561. doi: 10.1002/jlb.59.4.555

Slauch, J. M. (2011). How does the oxidative burst of macrophages kill bacteria? Still an open question. *Mol. Microbiol.* 80, 580–583. doi: 10.1111/j.1365-2958.2011.07612.x

Stolk, J., Hiltermann, T. J., Dijkman, J. H., and Verhoeven, A. J. (1994). Characteristics of the inhibition of NADPH oxidase activation in neutrophils by apocynin, a methoxy-substituted catechol. *Am. J. Respir. Cell Mol. Biol.* 11, 95–102. doi: 10.1165/ajrcmb.11.1.8018341

Tetz, L. M., Aronoff, D. M., and Loch-Caruso, R. (2015). Mono-ethylhexyl phthalate stimulates prostaglandin secretion in human placental macrophages and THP-1 cells. *Reprod. Biol. Endocrinol.* 13, 1–8. doi: 10.1186/s12958-015-0046-8

Valentin-weigand, P., Benkel, P., Rohde, M., and Chhatwal, G. S. (1996). Entry and intracellular survival of group B Streptococci in J774 macrophages. *Infect. Immun.* 64, 2467–2473.

Verani, J. R., McGee, L., and Schrag, S. J. (2010). Prevention of perinatal group B streptococcal disease. *MMWR Recomm. Rep.* 51, 1–22.

Whittenbury, R. (1964). Hydrogen peroxide formation and catalase activity in the lactic acid bacteria. *J. Gen. Microbiol.* 35, 13–26. doi: 10.1099/00221287-35-1-13

Conflict of Interest Statement: The authors declare that the research was conducted in the absence of any commercial or financial relationships that could be construed as a potential conflict of interest.

The reviewer AB and handling Editor declared their shared affiliation at time of review.

frontiers in Microbiology

ORIGINAL RESEARCH
published: 22 November 2018
doi: 10.3389/fmicb.2018.02656

A New Role of OmpR in Acid and Osmotic Stress in *Salmonella* and *E. coli*

Smarajit Chakraborty[1†] *and Linda J. Kenney*[1,2,3,4,5*]

[1] *Mechanobiology Institute, National University of Singapore, Singapore, Singapore,* [2] *Department of Biochemistry, National University of Singapore, Singapore, Singapore,* [3] *Departments of Microbiology and Immunology, University of Illinois at Chicago, Chicago, IL, United States,* [4] *Bioengineering, University of Illinois at Chicago, Chicago, IL, United States,* [5] *Jesse Brown Veterans Administration Medical Center, Chicago, IL, United States*

OPEN ACCESS

Edited by:
Daniela De Biase, Università degli Studi di Roma La Sapienza, Italy

Reviewed by:
Peter Adrian Lund, University of Birmingham, United Kingdom
Sylvie Rimsky, INSERM U1050 Centre Interdisciplinaire de Recherche en Biologie, France
Samantha Miller, University of Aberdeen, United Kingdom

***Correspondence:**
Linda J. Kenney
kenneyl@uic.edu

†Present address:
*Smarajit Chakraborty, Fat Metabolism and Stem Cell Group, Laboratory of Metabolic Medicine, Singapore Bioimaging Consortium, A*STAR, Singapore, Singapore*

Specialty section:
This article was submitted to Microbial Physiology and Metabolism, a section of the journal Frontiers in Microbiology

Received: *16 July 2018*
Accepted: *17 October 2018*
Published: *22 November 2018*

Citation:
Chakraborty S and Kenney LJ (2018) A New Role of OmpR in Acid and Osmotic Stress in Salmonella and E. coli. Front. Microbiol. 9:2656. doi: 10.3389/fmicb.2018.02656

Bacteria survive and respond to diverse environmental conditions and during infection inside the host by systematic regulation of stress response genes. *E. coli* and *S.* Typhimurium can undergo large changes in intracellular osmolality (up to 1.8 Osmol/kg) and can tolerate cytoplasmic acidification to at least pH_i 5.6. Recent analyses of single cells challenged a long held view that bacteria respond to extracellular acid stress by rapid acidification followed by a rapid recovery. It is now appreciated that both *S.* Typhimurium and *E. coli* maintain an acidic cytoplasm through the actions of the outer membrane protein regulator OmpR via its regulation of distinct signaling pathways. However, a comprehensive comparison of OmpR regulons between *S.* Typhimurium and *E. coli* is lacking. In this study, we examined the expression profiles of wild-type and *ompR* null strains of the intracellular pathogen *S.* Typhimurium and a commensal *E. coli* in response to acid and osmotic stress. Herein, we classify distinct OmpR regulons and also identify shared OmpR regulatory pathways between *S.* Typhimurium and *E. coli* in response to acid and osmotic stress. Our study establishes OmpR as a key regulator of bacterial virulence, growth and metabolism, in addition to its role in regulating outer membrane proteins.

Keywords: single cells, fluorescence microscopy, two-component regulatory systems, EnvZ, OmpR, GltA, acid stress, osmotic stress

INTRODUCTION

Eukaryotic cells maintain strict pH homeostasis between pH 7.0–7.4 by ion transport mechanisms and a high buffering capacity of the cytosol (see (Madshus, 1988; Casey et al., 2010) for reviews). Recent advances in fluorophores, imaging technology and the ability to examine single cell behavior has led to a new view of the bacterial response to acid and osmotic stress (Chakraborty et al., 2015, 2017). Unlike eukaryotes, it is now appreciated that bacteria can survive and respond to

Abbreviations: BCECF-AM, 2′,7′-Bis-(2-Carboxyethyl)-5-(and-6)Carboxyfluorescein, AcetoxymethylEster); CAD, cadaverine decarboxylation system; cF, 5 (and 6-)-carboxyfluorescein; FRET, fluorescence resonance energy transfer; GAD, glutamine decarboxylation system; min, minutes; pH_e, extracellular pH; pH_i, intracellular pH; qRT-PCR, quantitative real-time polymerase chain reaction; RT, room temperature; SPI-2, *S.* Typhimurium pathogenicity island 2; Spt-PALM, single particle tracking photoactivatable localization microscopy; TCRS, two-component regulatory systems; TTSS, type three secretion systems.

diverse environmental conditions both inside and outside of the host by systematic regulation of stress response genes (Boor, 2006; Krulwich et al., 2011). The long held view was that Gram negative bacteria such as *E. coli* and *S.* Typhimurium were neutralophiles, i.e., they maintain their intracellular pH between 7.2 and 7.8 (see Slonczewski et al., 2009; De Biase and Lund, 2015 for reviews). For strong acids and pH values down to ∼5.0, it was reported that the periplasm rapidly equilibrated with the external medium, but the cytoplasm showed only transient acidification before returning to its normal pH of ∼7.4 (Wilks and Slonczewski, 2007; Slonczewski et al., 2009). In contrast, recent studies in single cells using fluorescence microscopy and the pH-sensitive fluorophore BCECF-AM reported that *E. coli* and *S.* Typhimurium were acidified in response to both acid and osmotic stress and acidification was maintained for > 90 min (Chakraborty et al., 2017). *In vivo* measurements of *S.* Typhimurium inside macrophage vacuoles using a FRET DNA biosensor termed the I-switch, also reported prolonged acidification (Chakraborty et al., 2015). The mechanism is now established: the global regulator OmpR (best known for its regulation of outer membrane proteins) plays a central role in the bacterial response to acid and osmotic stress (Stincone et al., 2011; Quinn et al., 2014; Chakraborty et al., 2015, 2017), resulting in a substantial reprograming of the bacterial transcriptome. The observation that the cytoplasm was acidified as a consequence of both acid and osmotic stress (Chakraborty et al., 2017), also explains why previous studies reported that acid-induced genes were also induced in response to osmotic stress (De Biase et al., 1999; Kitko et al., 2010).

Environmental stress pathways in bacteria, including acid and osmotic stress, are regulated by two-component regulatory systems (TCRS). These TCRSs employ a sensor histidine kinase, which is most often embedded in the cytoplasmic membrane. The second component is a response regulator, which usually functions as a transcription factor that binds DNA and regulates transcription. The two components communicate via a series of phosphorylation reactions involving autophosphorylation of the kinase on a conserved histidine residue, followed by phosphoryl transfer to an aspartate on the response regulator. The EnvZ/OmpR TCRS is best known for its role in regulating expression of outer membrane porins OmpF and OmpC in response to osmotic stress (Walthers et al., 2005; Anand and Kenney, unpublished).

In most cases, the signaling process by histidine kinases is not well understood. However, in the case of the EnvZ kinase, previous studies using hydrogen-deuterium exchange mass spectrometry established that the sensor was a seventeen amino acid peptide that flanked the phosphorylated histidine (Wang et al., 2012). It was surprising that the sensor was located in the cytoplasm and the cytoplasmic domain alone (EnvZc) was capable of sensing without being in the membrane (Wang et al., 2012), although the presence of the transmembrane domains increased the dynamic range of the response (Ghosh et al., 2017). These studies provided a new view of cytoplasmic signaling by histidine kinases (Wang et al., 2012; Foo et al., 2015a), which led to the proposal that intracellular acid stress was a driver of metabolic reprogramming in response to both acid and osmotic stress (Chakraborty et al., 2015, 2017). More recently, others have shown that additional histidine kinases are capable of intracellular signaling, although most studies are still lacking in mechanistic detail (Eguchi and Utsumi, 2014; Choi and Groisman, 2016; Sen et al., 2017).

During acid stress in *S.* Typhimurium and *E. coli*, OmpR contributes to cytoplasmic acidification by repressing the *cadC/BA* operon (Chakraborty et al., 2015, 2017). CadC is in the OmpR subfamily of response regulators and normally it activates transcription of *cadBA*. CadA is a lysine decarboxylase, which consumes a proton during decarboxylation. The product, cadaverine, is then transported out of the cell by the CadB antiporter. Repression of *cadC/BA* by OmpR thus prevents neutralization. Because the pH optima of the CAD system is 6.1–6.5 (Cheeseman and Fuller, 1968), it is the most important acid stress system when *S.* Typhimurium is in the vacuole during infection inside the host (Chakraborty et al., 2015).

OmpR also promotes acidification in response to osmotic stress, but different pathways are involved. In *S.* Typhimurium, OmpR represses the alternative stationary phase sigma factor, *rpoS,* relieving RpoS repression of *yghA*. YghA is a putative oxidoreductase that is predicted to produce protons (Chakraborty et al., 2017). In *E. coli*, the intracellular pH was less acidic and OmpR regulated different pathways. In *E. coli*, OmpR represses *speF*, the ornithine decarboxylation system, which has a higher pH optimum of 7 (Vivijs et al., 2016) compared to the glutamate and arginine decarboxylation systems (pH optima 4 and 5, respectively) (Bearson et al., 2009). Normally, ornithine decarboxylase decarboxylates arginine, consumes protons and produces putrescine, which allows for recovery from acidification. Repression of *speF* by OmpR prevents recovery at high osmolality (Chakraborty et al., 2017).

In *E. coli* MG1655, whole-genome expression profiling identified acid-responsive genes including: chaperones, regulators and genes involved in metabolism (e.g., glutamine decarboxylase) and some genes associated with the cell envelope. (Tucker et al., 2002). In another study, the *E. coli* response to mild and strong acidic conditions was compared, revealing a complex transcriptional program that was dependent on OmpR and the switch between aerobic and anaerobic growth (Stincone et al., 2011). OmpR was connected to genes involved in pyruvate metabolism and glycolysis, signal transduction and transport and some components of the glutamate decarboxylation (GAD) system. Direct OmpR targets were not identified, most likely because OmpR regulation of acid stress pathways occurs most commonly via repression of transcription, which has less precise DNA recognition requirements (Chakraborty et al., 2015, 2017). Identification of OmpR binding sites by sequence gazing is difficult, because OmpR has a high non-specific DNA binding component, and makes more phosphate backbone contacts and fewer DNA base contacts than other response regulators (Rhee et al., 2008). Since OmpR showed distinct and differential regulation in response to exogenous stresses, in the present work, we set out to elucidate a comprehensive network of OmpR regulons. We compared the gene expression profiles of wild-type and *ompR* null strains between the pathogen *S.* Typhimurium and a non-pathogenic *E. coli*

in response to both acid and osmotic stress. Our analysis of OmpR-regulated genes indicates that it drives a major reprogramming in bacteria in response to acid and osmotic stress.

MATERIALS AND METHODS

Bacterial Strains and Growth Conditions

Salmonella enterica serovar Typhimurium 14028s and *E. coli* MG1655 were used throughout this study. To determine the acid and osmotic stress response, bacterial strains were grown in a modified N-minimal medium (MgM), buffered with either 100 mM Tris (pH 7.2 ± 15% (w/v) sucrose) or 100 mM MES (pH 5.6), containing 7.5 mM $(NH_4)_2SO_4$, 5 mM KCl, 0.5 mM K_2SO_4, 1 mM KH_2PO_4, 10 mM $MgCl_2$, 2 mM glucose, and 0.1% Casamino acids. To obtain the growth profiles, cultures of *S.* Typhimurium and *E. coli* in Luria Broth (LB) were grown overnight and sub-cultured (1:100) in 5 ml of MgM pH 7.2 for 24 h. The cultures were then sub-cultured (1:50) in either MgM pH 5.6 or pH 7.2 and incubated for an additional 10 h. The optical density at 600 nm was measured hourly and plotted as a function of time ($n = 3$). The doubling time (Td) was determined by the exponential curve fitting function to generate an equation in the form $y = Ae^{Bx}$, where A, B are numbers and x is the time between doubling of $y(A_{600nm})$. The equation simplifies to $Td = ln2/B = 0.693/B$.

RNA Isolation and qRT-PCR

Wild-type strains of *E. coli* and *S.* Typhimurium were grown in MgM pH 7.2 for 24 h, then sub-cultured (1:50) in MgM pH 5.6, 7.2, and 7.2 with 15% (w/v) sucrose for 5–6 h until the optical density at 600 nm was ∼0.6. Total RNA was isolated, followed by cDNA synthesis and quantification. The mRNA expression level of the target genes was normalized relative to 16S rRNA.

Construction of a *gltA* Mutant and Over-Expression Strain

The chromosomal copy of *gltA* from wild-type or an *ompR* null strain of *S.* Typhimurium and *E. coli* was replaced by *tetRA* using λ-Red recombination techniques (Karlinsey, 2007). The *gltA* over-expressed strains were generated by cloning *gltA* into plasmid pMPMA5omega placed under control of the arabinose-inducible pBAD promoter by using primer pairs: *gltA* EcoR1#1F and *gltA* HindIII#1R. The primers used are listed in **Supplementary Table S5**.

Fluorescence Measurements of BCECF in *S.* Typhimurium and *E. coli*

Cultures of *S.* Typhimurium and *E. coli* were pre-incubated with 20 μM BCECF-AM for 60 min before the shift to acidic pHe 5.6, neutral pHe 7.2, or high osmolality pHe 7.2 plus 15% (w/v) sucrose as described in Chakraborty et al. (2015, 2017). Cells were placed on microscope slides (Marienfeld) coated with 1% (w/v) agarose and images were analyzed by ImageJ version 1.42.

Microarray

100 ng of total RNA was labeled with Low Input Quick AMP WT Labeling Kit (Agilent; One-color) following the manufacturer's instructions. Briefly, 100 ng of total RNA was converted into double-stranded cDNA by priming with an oligo-dT primer containing the recognition site for T7 RNA polymerase. *In vitro* transcription with T7 RNA polymerase was used to produce cyanine 3-CTP labeled cRNA. 600 ng of labeled cRNA was hybridized onto an Agilent SurePrint HD GE 8X15 Microarray (*E. coli*) or Agilent SurePrint G3 custom GE 8X60 Microarray (*S.* Typhimurium) for 17 h at 65°C, 10 rpm in an Agilent hybridization oven. After hybridization, the microarray slide was washed in gene expression buffer 1 (Agilent wash buffer kit) for 1 min at RT and another minute in gene expression buffer 2 (Agilent wash buffer kit) at 37°C before scanning on an Agilent High Resolution Microarray Model C Scanner. The results of gene expression profiles are accessible on the Gene Expression Omnibus (GEO) platform with accession number Microarray data GEO submission GSE106629.

Data Analysis

DAVID Functional Annotation was used to identify gene clusters, which measures relationships among the annotation terms based on the degrees of their co-association genes to different groups. The "Category" column in **Supplementary Table S2B** represents the original database or resource where the term originates. DAVID consists of a total of 14 annotation categories, which are all collected in the DAVID knowledgebase such as Gene ontology, Biological process, Molecular function, Cellular component, KEGG pathway, Biocarta pathway, Up keywords, BBID pathway, SMART domain, NIH genetic association, UNIPROT sequence feature, KOG ontology, NCBI OMIM and the Interpro domain. The Kyoto Encyclopedia of Genes and Genome (KEGG) is one such database. The next column in **Supplementary Table S2B**, "Term," represents the pathway maps to facilitate biological interpretation in a network context. "Count" signifies the number of genes involved in the process. The *P*-value indicates the threshold of EASE Score, a modified Fisher Exact *P*-Value, for gene-enrichment analysis. Fisher Exact *P*-Value = 0 represents perfect enrichment. *P*-Value ≤ 0.05 is considered to be strongly enriched. "Benjamini" is one of the multiple testing correction techniques used to control family-wide false discovery rate. Functional Annotation Clustering integrates the same techniques of Kappa statistics to measure the degree of the common genes between two annotations. Based on Kappa statistics, more common genes are likely to be grouped together in one cluster. Thus, the presence of genes in more than one cluster represents multiple functions or association between two networks. The non-cluster category in **Supplementary Table S2B** represents multiple genes having varying biological functions, which cannot be put under one single cluster. The non-cluster generally represents the total pool of genes. Significance analysis was performed using Student's *t*-test with Benjamini-Horchberg False Discovery Rate (FDR) correction and fold change analysis. The comparison involving 3 conditions was analyzed with the

Analysis of Variance (ANOVA) with FDR correction, followed by a *post hoc* testing (Turkey HSD test) and fold change analysis.

Atomic Force Microscopy

A 703 base pair (bp) region from the *gltA* promoter was gel-purified using the QIAquick Gel Extraction Kit (Qiagen) by using primer pairs *gltA* F and *gltA* R for *S.* Typhimurium (−689 bp to + 14 bp) and for *E. coli* (−694 bp to + 9 bp), respectively. A glutaraldehyde-modified mica surface was prepared as described in Chakraborty et al. (2017). Ten nanograms of the *gltA* regulatory region was incubated with 30 nM OmpR for 15 min at RT. This mixture was then deposited on the mica for 15 min. Images were acquired on a Bruker Dimension FastScan AFM system using the tapping mode with a silicon nitride cantilever (FastScan C, Bruker). Raw AFM images were processed using Gwyddion software[1].

RESULTS

Acid Stress Does Not Affect Cell Growth

We were interested in understanding the role of OmpR in the acid stress response. To address this, we first examined whether loss of OmpR led to a growth defect during acid stress. In **Figure 1**, the growth profiles of *S.* Typhimurium and *E. coli* wild-type and isogenic *ompR* null strains at neutral and acid pH were compared. At neutral pH, the growth of the wild-type and the *ompR* null strain of *S.* Typhimurium was nearly identical (Δ*ompR* Td = 94% of wild-type, **Figure 1C**). At acid pH, the growth of the *ompR* null strain was similar to the wild-type growth at neutral pH. However, the wild-type strain grew more slowly (Td = 87% of Td at neutral pH, **Figure 1C**) at acid pH (top panel). In *E. coli* the differences were similar to *S.* Typhimurium, although the Tds were all slightly faster (**Figures 1B,C**). Under these growth conditions, we previously measured the intracellular pH of wild-type *S.* Typhimurium (pH_i = 6.15) and *E. coli* (pH_i = 6.55) after 90 min exposure to pH_e 5.6 (see **Supplementary Table S1**). Thus, acid stress has only minor effects on *S.* Typhimurium and *E. coli* growth.

Acid Stress Does Not Affect *ompR* Transcript Levels

Because cytoplasmic acidification during acid and osmotic stress was dependent upon OmpR, we first examined whether *ompR* was up-regulated during these stress conditions (**Figure 2**). We measured the *ompR* transcript levels by quantitative real-time polymerase chain reaction (qRT-PCR) in *S.* Typhimurium and *E. coli* after growth in acid or at high osmolality and compared *ompR, ompC* and *ompF* levels in the wild-type strains. The levels of *ompR* were insensitive to an acid pH shift, but increased at high osmolality in *S.* Typhimurium (2.3-fold) and in *E. coli* (1.8-fold) (**Figure 2**). The known *ompR*-regulated transcripts responded as predicted: *ompC* levels increased in response to acid pH, but were even higher at high osmolality, whereas *ompF* was repressed under acid stress compared to neutral pH. At high osmolality, *ompF* levels decreased in *S.* Typhimurium and *E. coli*, but *ompF* levels in *E. coli* were similar at acid and neutral pH (**Figure 2**). The observation that *ompR* transcripts did not change in acid pH was consistent with our previous studies, where we counted OmpR molecules by PALM imaging of an OmpR-PAmCherry photoactivatable fluorescent protein fusion. There was no difference in OmpR molecules in acidic conditions compared to neutral pH in *S.* Typhimurium (Liew et al., unpublished), and in *E. coli,* OmpR numbers were slightly lower at acid pH (Foo et al., 2015b) (see section "Discussion").

Identification of the OmpR Acid Stress Regulon

In order to identify OmpR-dependent pathways induced during acid stress, gene expression profiles between wild-type and an *ompR* null strain of *S.* Typhimurium and *E. coli* were compared. Genes with statistically significant differential expression were required to meet two criteria: a fold change (FC) ≥ 2 and a *P*-value of ≤ 0.05, as determined by the Student's *t*-test (**Figure 3**). The OmpR acid stress regulon was considerably more extensive in *E. coli* compared to *S.* Typhimurium, where a higher number of OmpR affected genes were apparent (1360 vs. 240). In *S.* Typhimurium, more acid-sensitive genes (78%) were positively regulated by OmpR (**Figure 3A**), i.e., they were down-regulated when OmpR was absent. In contrast, *E. coli* was poised in the opposite direction, i.e., OmpR repressed the majority of the acid-responsive genes (71%). As shown in **Figure 3B**, it was evident that there was significant divergence between *S.* Typhimurium and *E. coli* OmpR acid stress regulons, as only 25 targets were common to both organisms. These 25 genes represented <2% of the overall OmpR response in *E. coli*, but were ∼10% of the *S.* Typhimurium OmpR-dependent acid stress response (**Figures 3B,C**).

We used the UniProt Gene Ontology (GO) annotation program to represent the normal molecular function and biological processes of the 25 common targets (**Supplementary Table S2A**). As intracellular acidification in wild-type *S.* Typhimurium and *E. coli* did not result in significant growth defects (**Figure 1**), we searched for biosynthetic and metabolic pathways and/or for pathways that might prevent accumulation of metabolites or toxins in order to support growth at acid pH. To gain insight into the metabolic functions, significantly differentiated genes were matched with the BioCyc Database collection (PGDB) (Keseler et al., 2011). The OmpR overlapping targets revealed three genes (*dacC, gltA and adhP*) involved in metabolic pathways (**Figure 3D**). DacC is a D-alanyl-D-alanine carboxypeptidase that was activated by OmpR (3.7-fold) (see section "Discussion"). OmpR down-regulated the citrate synthase *gltA* (2.9-fold), which synthesizes citrate from oxaloacetate and acetyl-CoA. A previous report showed that the expression of *gltA* was inversely proportional to the cell growth rate in *E. coli* (Park et al., 1994). In another study *S.* Typhimurium *gltA* was shown to catalyze the accumulation of 2-methylcitrate, which is deleterious to cell growth (Horswill et al., 2001). In both *S.* Typhimurium and *E. coli,* over-expression of *gltA* resulted in growth defects (**Figures 1A,B**), as evident by the increased

[1]http://gwyddion.net/

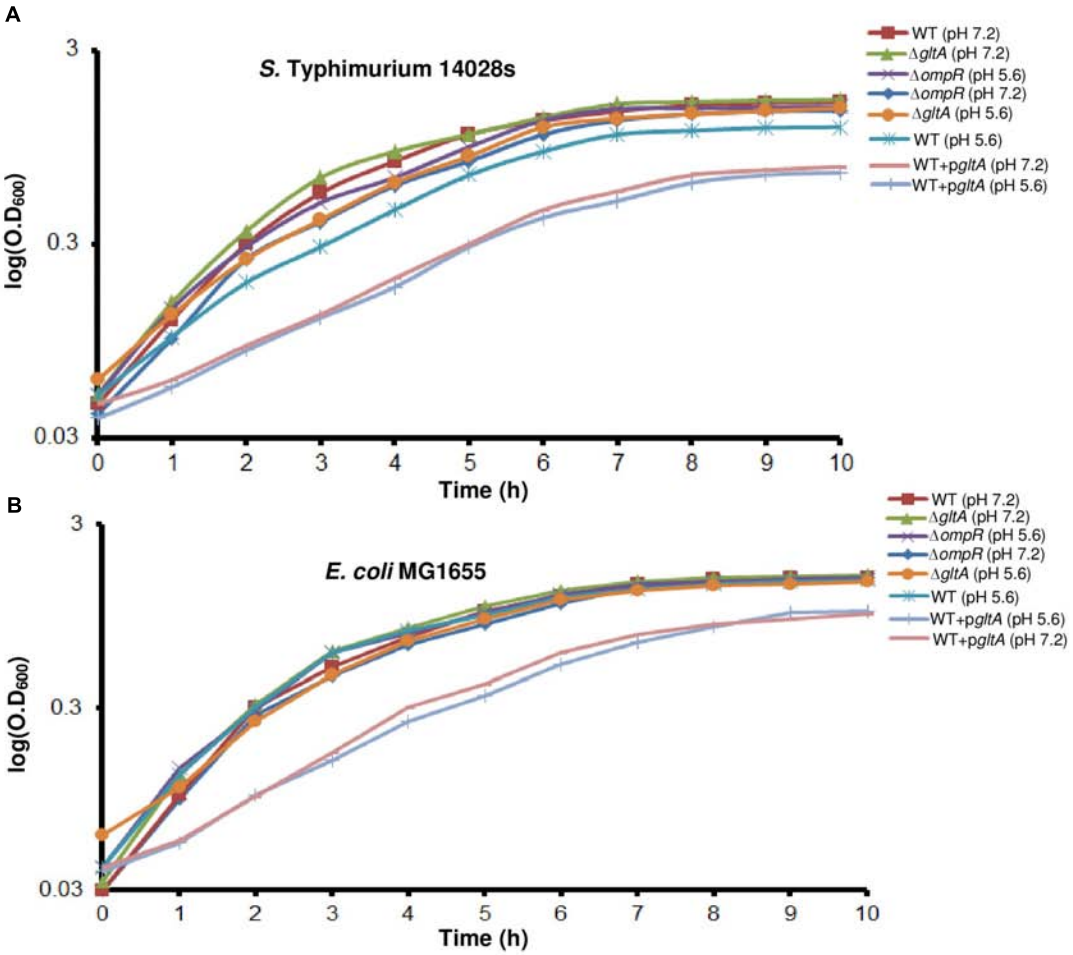

C

S. Typhimurium 14028s	Td (h)	*E. coli* MG1655	Td (h)
WT (pH 5.6)	1.77±0.15	WT (pH 5.6)	1.67±0.15
WT (pH 7.2)	1.54±0.11	WT (pH 7.2)	1.46±0.17
Δ*ompR* (pH 5.6)	1.51±0.15	Δ*ompR* (pH 5.6)	1.45±0.12
Δ*ompR* (pH 7.2)	1.45±0.13	Δ*ompR* (pH 7.2)	1.38±0.14
Δ*gltA* (pH 5.6)	1.59±0.12	Δ*gltA* (pH 5.6)	1.49±0.11
Δ*gltA* (pH 7.2)	1.41±0.08	Δ*gltA* (pH 7.2)	1.36±0.10
WT+p*gltA* (pH 5.6)	2.39±0.20	WT+p*gltA* (pH 5.6)	2.26±0.25
WT+p*gltA* (pH 7.2)	2.36±0.18	WT+p*gltA* (pH 7.2)	2.23±0.19

FIGURE 1 | The effect of acid pH on growth curves of *S.* Typhimurium and *E. coli.* Wild-type, an *ompR* null mutant, a *gltA* null mutant and a *gltA* over-expressed strain of **(A)** Overnight cultures of *S.* Typhimurium and **(B)** *E. coli* grown in LB were sub-cultured (1:100) in MgM pH 7.2 for 24 h. The cultures were then sub-cultured again (1:50) in MgM pH 5.6 or pH 7.2 for an additional 10 h as described in Materials and Methods. The optical density at 600 nm ($O.D._{600}$) was measured hourly to monitor bacterial growth ($n = 3$). Strains in which *gltA* was over-expressed exhibited growth defects at neutral and acid pH compared to the wild-type and *ompR* null strains in both *S.* Typhimurium and *E. coli*. The error bars were removed to make the graphs legible. **(C)** The doubling time (Td) was plotted as determined from the exponential curve fitting function as described in Materials and Methods. Error bars represent the mean ± standard deviation ($n = 3$).

doubling times (Td) at acidic (∼25%) and neutral pH (∼34%) (**Figure 1C**). Thus, OmpR repression of *gltA* contributes to optimum growth when *S.* Typhimurium and *E. coli* are acidified. A systems biology approach also identified *gltA* as being down-regulated in response to acid stress (Stincone et al., 2011). Cluster analysis of the common targets in *S.* Typhimurium and *E. coli* identified shared functions such as membrane transport (*tppB, ompC, ompR, potC, potD, ygbE*), biosynthesis of antibiotics and secondary metabolites (*adhP, gltA, gcvH, dacC, pepB*) and others (see **Supplementary Table S2B** for the full list).

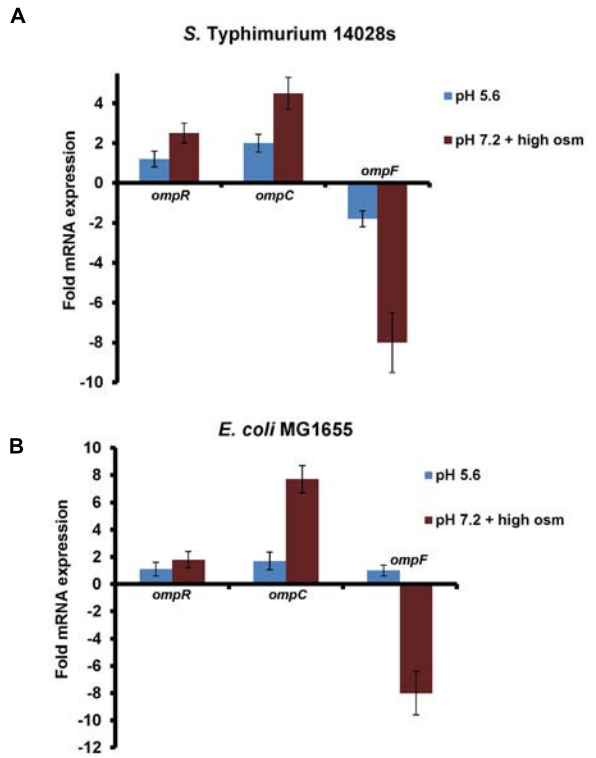

FIGURE 2 | *ompR* transcription in *S*. Typhimurium and *E. coli* is insensitive to pH, but increases slightly at high osmolality. **(A)** The mRNA levels of *ompR*, *ompC* and *ompF* at pH_e 5.6 and pH_e 7.2 plus 15% (w/v) sucrose were compared to pH_e 7.2 by qRT-PCR in the wild-type *S*. Typhimurium and **(B)** *E. coli* strains. The mRNA expression level of the target genes was normalized relative to 16S rRNA. Error bars represent the mean ± standard deviation (n = 3).

Analysis of the OmpR Osmotic Stress Regulon

In repsonse to osmotic stress, the cytoplasm of both *E. coli* and *S*. Typhimurium was acidified in an OmpR-dependent manner. However, acidification was not as pronounced as during acid stress and the pathways involved were distinct (Chakraborty et al., 2015, 2017). We therefore examined the OmpR regulon in response to osmotic stress. At high osmolality, the number of OmpR-regulated genes was similar between *E. coli* (875) and *S*. Typhimurium (764) (**Figure 4A**). Sixty six OmpR targets that were sensitive to changes in osmolality were overlapping, comprising ∼8–9% of the total OmpR response in either *S*. Typhimurium or *E. coli* (**Figure 4B**).

Uniprot GO was used to list the functions of the 66 common OmpR targets (**Supplementary Table S3A**). Interestingly, genes encoding nitrate reductase such as *narZ* (95-fold), *narW* (71-fold) and *narV* (38-fold) showed the highest decrease in the *ompR* null strain compared to the wild-type, indicating that they were strongly activated (directly or indirectly) by OmpR (**Figure 4C**). Growth inhibition by accumulation of nitrate during osmotic stress has been reported in the sulfate-reducing bacterium *Desulfovibrio vulgaris* (He et al., 2010). Thus, up-regulation of nitrate reductase is a possible mechanism employed by wild-type *S*. Typhimurium and *E. coli* to relieve nitrate toxicity at high osmolality. PGDB analysis of the overlapping targets identified 18 genes involved in various metabolic functions (**Figure 4D**). Cluster analysis identified eight major clusters linked to biological processes, including: nitrate metabolism, membrane transport, biosynthesis of metabolites and amino acids and transcriptional regulation (**Supplementary Table S3B**).

Common OmpR Targets in Acid and Osmotic Stress

We next identified the OmpR targets that were involved in response to both acid and osmotic stress. In *S*. Typhimurium, 52 genes were common OmpR targets responsive to both stress pathways (**Figure 5A**), and in *E. coli,* 325 genes were common (**Figure 5B**). Out of these, nine genes were common to the OmpR regulons of *S*. Typhimurium and *E. coli* (**Figure 5C**). Three of the nine genes were again the well-known OmpR targets, *ompC*, *ompF* and *tppB* (Goh et al., 2004). Five genes were of unknown function (**Figure 5D** and **Supplementary Table S4A**). These nine genes were grouped into the membrane transport cluster (**Supplementary Table S4B**).

PGDB analysis identified *gltA* as the sole OmpR target involved in metabolism (**Figure 5E**). Thus, OmpR repression of *gltA* appears to play a major role in supressing growth defects upon intracellular acidification in wild-type *S*. Typhimurium and *E. coli* in response to both acid and osmotic stress. To determine if *gltA* was involved in intracellular acidification, we measured the pH_i of *gltA* null strains and strains of *S*. Typhimurium and *E. coli* in which *gltA* was over-expressed in response to both acid and osmotic stress. The *gltA* null strains were fully capable of cytoplasmic acidification and the pH_i was similar to the wild-type in both *S*. Typhimurium and *E. coli* (**Figures 6A–D**). Similarly, in the Δ*ompR/gltA* null strains, the pH was similar to the pH of the *ompR* null strain. This was not surprising, because citrate synthase (*gltA*) is not known to be involved in proton exchange. In contrast, the *gltA* over-expressed strains exhibited a slightly higher intracellular pH (∼0.1 pH unit) compared to the wild-type strains.

To determine whether *gltA* repression was the result of direct interaction by OmpR, we used AFM to visualize OmpR binding to P*gltA*. OmpR was added to a solution buffered to the measured pH_i of *S*. Typhimurium or *E. coli,* as determined from previous experiments (Chakraborty et al., 2017). Addition of OmpR at pH 6.1 (*S*. Typhimurium) or at pH 6.5 (*E. coli*) increased the proportion of DNA-OmpR protein complexes (**Figure 7A**), as evident by an increase in the relative height (white foci). OmpR binding to the *gltA* promoter was increased at acid pH ompared to the addition of OmpR at neutral pH (**Figures 7A,B**). Thus, OmpR represses *gltA* during acidification via a direct interaction at its promoter to enable optimum growth in both *S*. Typhimurium and *E. coli*. In previous studies, we also determined that there was no visible effect of acid pH on OmpR (pH 6.1–7.1) in the absence of

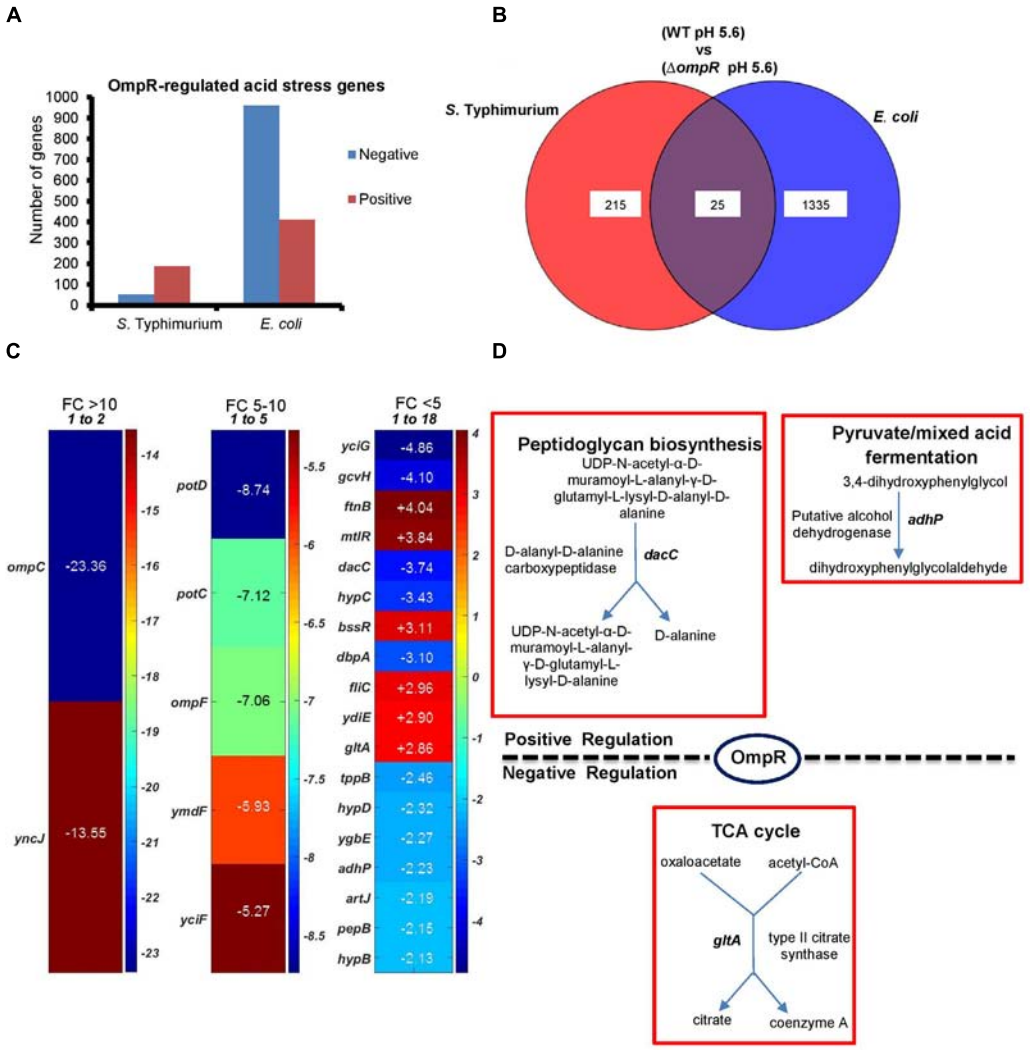

FIGURE 3 | Comparison of the *ompR* acid stress regulons of *S.* Typhimurium and *E. coli.* **(A)** The number of OmpR regulated genes (≥ 2-fold change; *P*-value ≤ 0.05) in *S.* Typhimurium and *E. coli* are shown in response to acid stress. **(B)** Overlap of OmpR acid stress targets between *S.* Typhimurium and *E. coli*. **(C)** A heat map shows the differential expression profiles of common OmpR targets separated into three groups based on the fold change, i.e., *ompC* was the most highly downregulated-regulated gene at –23.36. A positive number indicates OmpR repression. The fold change represents the expression level of an *ompR* null strain compared to the wild-type in *S.* Typhimurium or *E. coli* during acid stress. The color scale represents the average fold change ($n = 3$). **Supplementary Table S2** provides a detailed description of the overlapping genes. Data processing was performed using MATLAB 6.1 (MathWorks Inc., Natick, MA, United States). **(D)** Enzymatic reactions and pathways of the common OmpR targets involved in metabolism are shown using PGDB analysis (*EcoSal Plus* doi: 10.1128/ecosalplus.ESP-0009-2014). Similar algorithms and software tools were used for the remaining microarray analyses.

DNA (Chakraborty et al., 2017) (see **Supplementary Figure S1**).

Comparison of Osmolytes in the OmpR *S.* Typhimurium Transcriptome- Salt *vs.* Sucrose

Our previous data showed that the local unfolding and ensemble behavior of EnvZc was comparable in the presence of either sucrose or salt as the osmolyte (Wang et al., 2012). We were curious whether there were separate effects of osmolytes depending on whether the osmolyte was ionic or non-ionic. We therefore analyzed the effect of salt by adding 400 mM NaCl to N-minimal medium (MgM) at pH_e 5.6 (976 mOsmol/kg). We compared OmpR-dependent pathways induced by acid, sucrose and salt stress from the expression profiles of wild-type and the *ompR* null strain of *S.* Typhimurium (**Figure 8**). Salt stress resulted in the highest number of differentially expressed genes (947) compared to acid (240) and sucrose (764) stress (**Figure 8A**). There was moderate overlap of these three responses, as 120 genes were common OmpR targets, but >50% of these were uncharacterized genes. This core regulon represented ∼13% of the OmpR response to salt stress (**Figures 8B,C**). It was noteworthy that half of the most

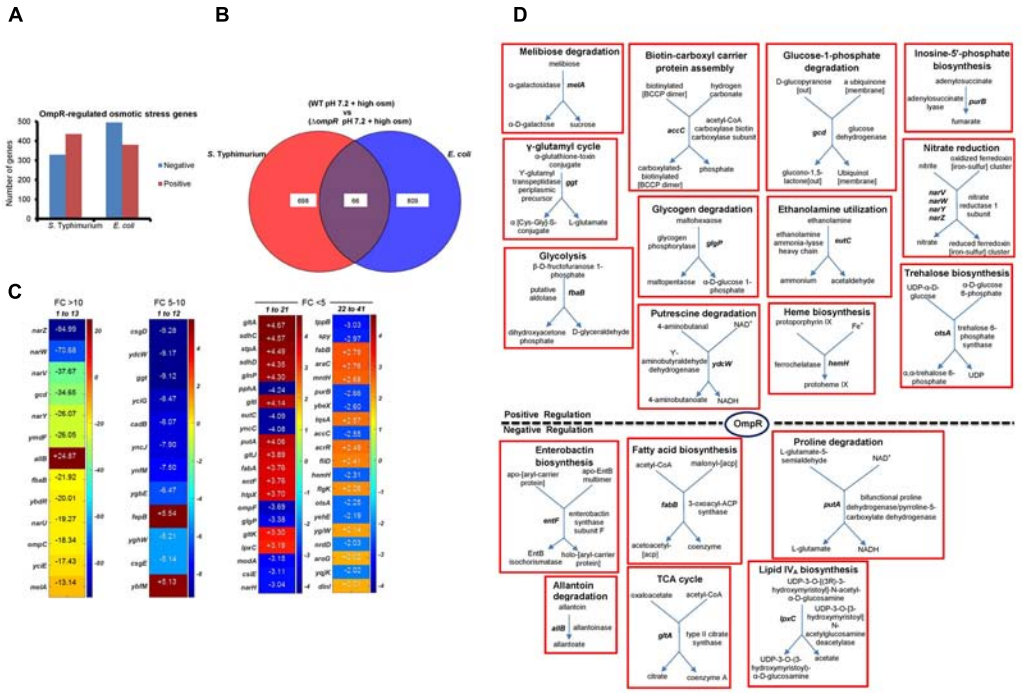

FIGURE 4 | Analysis of OmpR osmotic stress-sensitive targets in *S*. Typhimurium and *E. coli*. **(A)** The number of differentially expressed (≥ 2-fold change; *P*-value ≤ 0.05) OmpR-affected genes in *S*. Typhimurium and *E. coli* are indicated. **(B)** Overlapping OmpR targets between *S*. Typhimurium and *E. coli* during osmotic stress are shown. **(C)** A heat map representing the expression profiles of the overlapping OmpR targets are grouped based on their fold change. The color scale represents the average fold change of *ompR* null strain compared to the wild-type in *S*. Typhimurium ($n = 3$). **Supplementary Table S3** details a description of the overlapping genes. **(D)** Metabolic maps of overlapping OmpR targets involved in cellular processes are shown.

highly expressed genes (fold change >10) were SPI-2 or SPI-2 co-regulated genes, which enable *S*. Typhimurium to survive the high osmolality and low pH of the macrophage vacuole (Chakraborty et al., 2015). Apart from *ssrA* and *ssrB*, none of the other SPI-2 genes have been shown to be direct targets of OmpR regulation (Lee et al., 2000; Feng et al., 2003, 2004), although many of them are directly regulated by SsrB (Feng et al., 2004; Walthers et al., 2007, 2011). PGDB analysis of the 120 OmpR common targets revealed only nine genes involved in metabolism (**Figure 8D**), and most of these were degradative pathways. Interestingly, *gltA* was the only OmpR-repressed target that was sensitive to acid, sucrose and salt stress in *S*. Typhimurium (**Figure 8D**) and in *E. coli* during acid and sucrose stress (**Figure 5D**). Our findings suggest that in both *S*. Typhimurium, *S*. Typhi (Perkins et al., 2013) and *E. coli*, OmpR repression of *gltA* plays a major role in maintaining optimum cell growth during stress.

DISCUSSION

OmpR Is an Important Global Regulator of the Bacterial Response to Acid/Osmotic Stress

Bacteria encounter diverse environmental conditions both inside and outside of the host. TCRSs play a major role in sensing these varied environmental cues and subsequently modulate gene expression in response to stress. In a previous study, we established that the cytoplasmic domain alone of the sensor kinase EnvZ sensed cytoplasmic signals to activate its downstream target OmpR without being in the membrane (Wang et al., 2012). It was then logical that **cytoplasmic** acidification of *S*. Typhimurium occurred during macrophage infection (Chakraborty et al., 2015) and during *in vitro* acid and osmotic stress (Chakraborty et al., 2017). Cytoplasmic acidification was completely dependent on the OmpR response regulator, but did not require known OmpR-regulated genes such as *ompC*, *ompF*, or *ssaC* (a SPI-2 structural gene). To elucidate the OmpR regulatory networks, we performed microarray analysis and compared the transcriptome of *ompR* null and wild-type strains of *S*. Typhimurium and *E. coli* during acid and osmotic stress. OmpR repressed distinct genes, depending on whether the stressor was acid or osmotic stress, as driven by differences in pH_i that ensued (Chakraborty et al., 2017). Thus, we were motivated to further understand the role of OmpR in the cellular stress response.

OmpR Down-Regulates a Metabolic Pathway That Produces Toxic Intermediates

A previous study proposed a program of gene expression of *E. coli* BW35113 during exposure to acid pH that involved the following

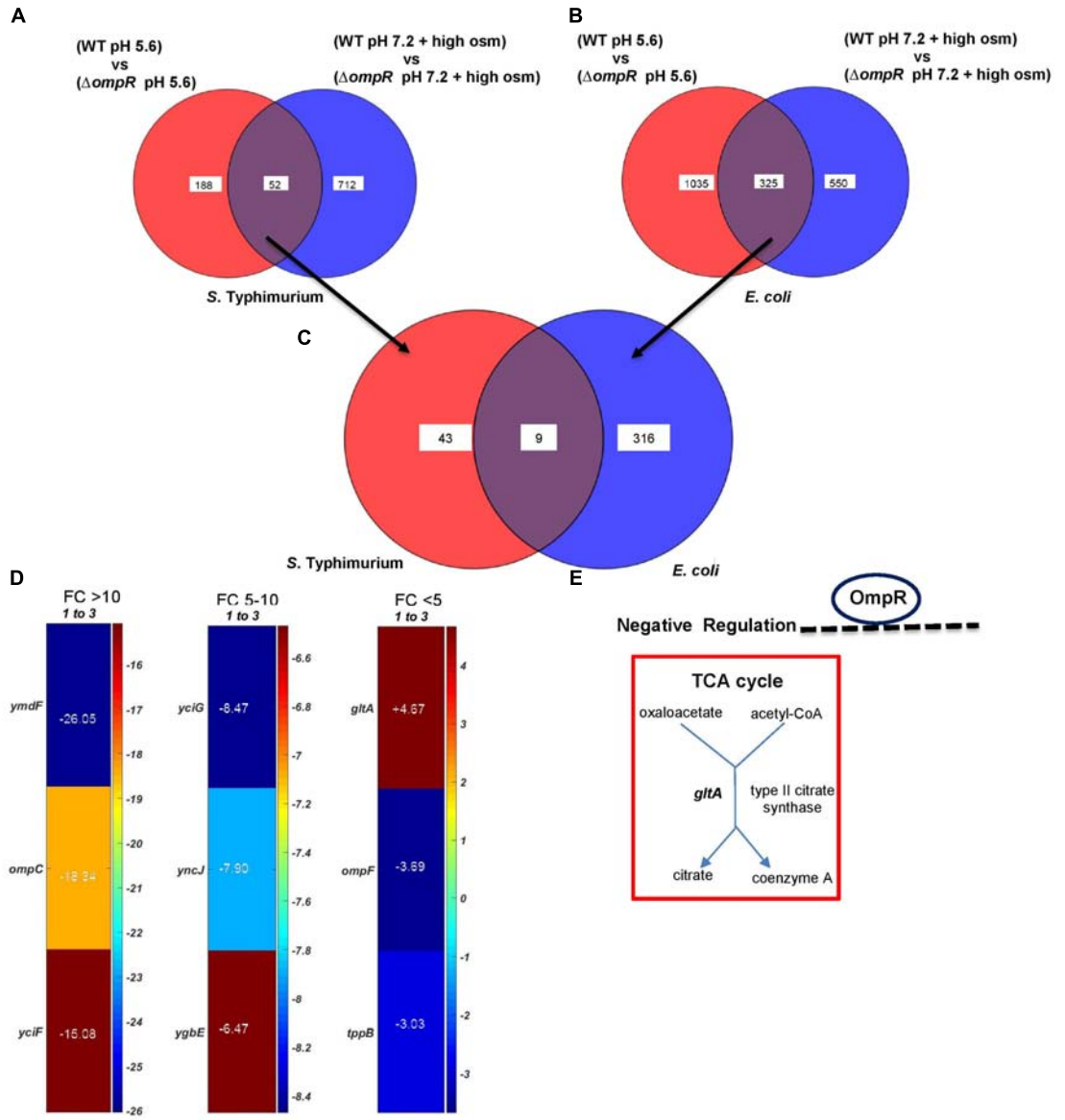

FIGURE 5 | Overlapping OmpR acid and osmotic stress targets. Common OmpR targets in **(A)** *S.* Typhimurium and **(B)** *E. coli* responsive to both acid and osmotic stress are shown. **(C)** Overlapping genes between **(A)** and **(B)** identifies nine common OmpR targets differentially expressed during both pH and osmolality shifts. **(D)** A heat map shows the expression profiles of the nine common OmpR targets. The color scale represents the average fold change of an *ompR* null strain of *S.* Typhimurium compared to the wild-type ($n = 3$). **Supplementary Table S4** provides a detailed description of the overlapping genes. **(E)** A metabolic map of *gltA* is shown.

metabolic switches: from utilizing glucose to gluconeogenesis and fatty acid synthesis, from aerobic to anaerobic growth and down–regulation of fumarate and up-regulation of formate and nitrate pathways (Stincone et al., 2011). In the present work, some of these same changes were evident in the response to acidification caused by osmotic stress, where *nar* (*ZWVY* and *U*) genes were highly up-regulated (**Figure 4C**), but fatty acid synthesis genes (*entF, fabB* and *lpxC*) were down-regulated. Common targets between *E. coli* and *S.* Typhimurium also included genes involved in carbohydrate degradation (*melA*, *gcd, ydcW, fbaB, and glgP*).

During acid stress, the OmpR overlapping targets revealed three genes in both *E. coli* and *S.* Typhimurium involved in metabolism, including: *dacC, gltA and adhP* (**Figure 3D**). DacC is a D-alanyl-D-alanine carboxypeptidase that was activated by OmpR (3.7-fold). Deletion of DacC (PBP6) had no detectible phenotype in *E. coli* (Broome-Smith and Spratt, 1982), but over-expression was reported to be toxic (Pedersen et al., 1998). In another study, *dacC* was shown to be essential for *E. coli* cell morphology and was regulated by BolA (Santos et al., 2002).

Nine common targets in the OmpR-dependent acid and osmotic stress response were identified. Three of these were

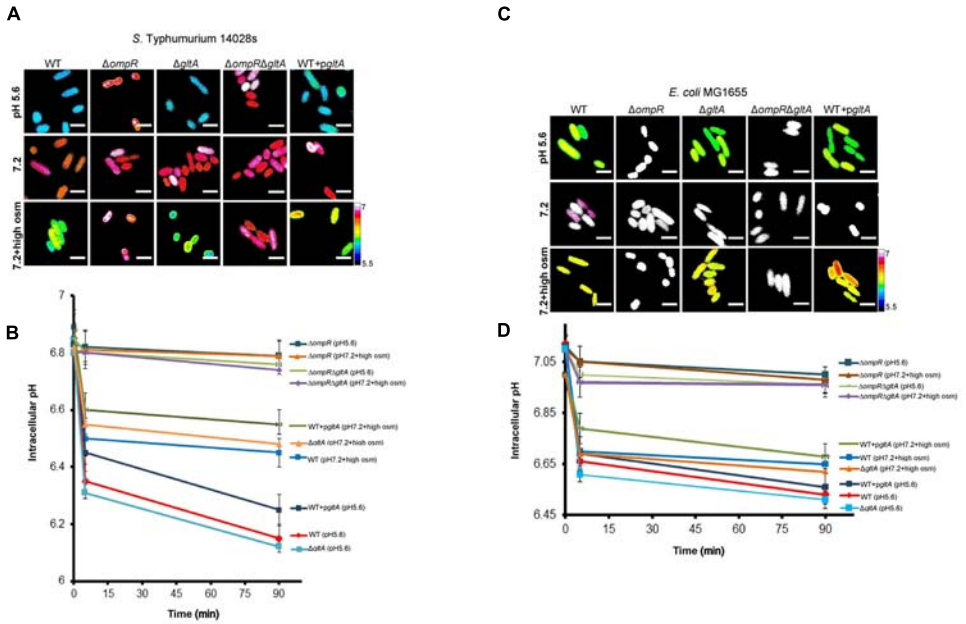

FIGURE 6 | GltA is not involved in intracellular acidification. *S*. Typhimurium and *E. coli* cultures were incubated with 20 μM BCECF for 60 min before imaging. Representative epifluorescence ratio images (R488/440) of emission channel 525 nm upon 488 and 440 nm excitation were obtained for wild type, an *ompR* null mutant, a *gltA* null mutant, an *ompR*/*gltA* null strain and a *gltA* over-expressed strain of **(A)** *S*. Typhimurium and **(C)** *E. coli* incubated at either acid pHe (5.6), pHe (7.2), or pHe (7.2) plus 15% (w/v) sucrose. Using ImageJ software, ratio images were color coded blue (ratio = 0.1) to white (ratio = 1). Scale bar, 3 μm. A plot of the intracellular pH of 50 cells of wild-type and mutants of **(B)** *S*. Typhimurium and **(D)** *E. coli* at each indicated time point. Error bars represent the mean ± s.e.m. (n = 3).

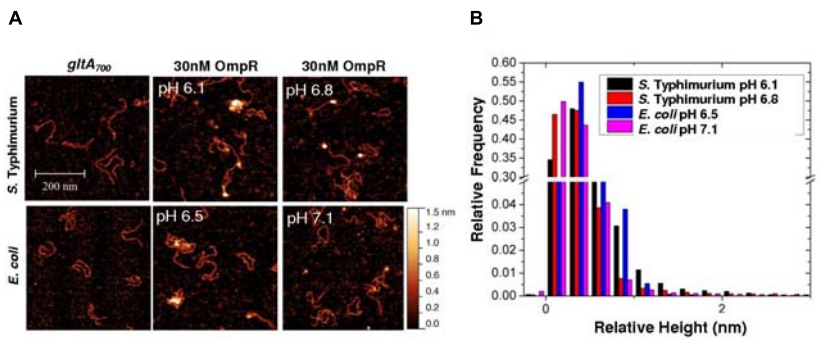

FIGURE 7 | OmpR binds to the *gltA* promoter. **(A)** AFM images of the 700 bp *gltA* promoter ($gltA_{700}$) from *S*. Typhimurium and *E. coli* (left panel) with 30 nM OmpR at either acidic (middle panel) or neutral pH (right panel). The pH corresponds to the relevant pH_i that was measured during acid stress (Chakraborty et al., 2015, 2017). **(B)** A relative height distribution histogram of the *gltA* promoter complexed with 30 nM OmpR at either acid or neutral pH. To obtain the relative height distribution histograms of OmpR-*gltA* complexes, a threshold was applied to filter the *gltA* contour from the background by a MATLAB code. The relative height, which is essentially the pixel values of the contour above the background, was plotted as a distribution histogram. A higher relative height indicates more OmpR bound to the DNA. The relative frequency indicates how often the relative height was observed in acid or neutal pH. The term relative height is used, as the apparent heights measured by AFM do not represent the true height (Lai et al., 2015). In the absence of DNA, OmpR was visible as pinpoint dots and was not aggregated (**Supplementary Figure S1**).

ompF, ompC and *tppB*, i.e., known OmpR-regulated genes. The fourth was *gltA*, which encodes citrate synthase, and converts oxaloacetate and acetyl-CoA into citrate (**Figures 3–6**). GltA controls the entry of metabolites into the TCA cycle, and it also appears to be the source of a toxic metabolite, 2-methylcitrate that can be a potent inhibitor of cell growth (Horswill et al., 2001). The *gltA* promoter is regulated by ArcA (Park et al., 1994) and in the present work we establish that OmpR binds to P*gltA* and represses its expression to ensure optimum growth. Over-expression of *gltA* resulted in growth defects in both *S*. Typhimurium and *E. coli* (**Figures 1**, **7**). OmpR regulation of *gltA* also appeared in a ChIP-seq analysis of *S*. Typhi (Perkins et al., 2013). A clearer picture will hopefully emerge when we understand the function of these unknown genes.

Although the remaining five common OmpR target genes are of unknown function, they include YmdF and YciG, annotated

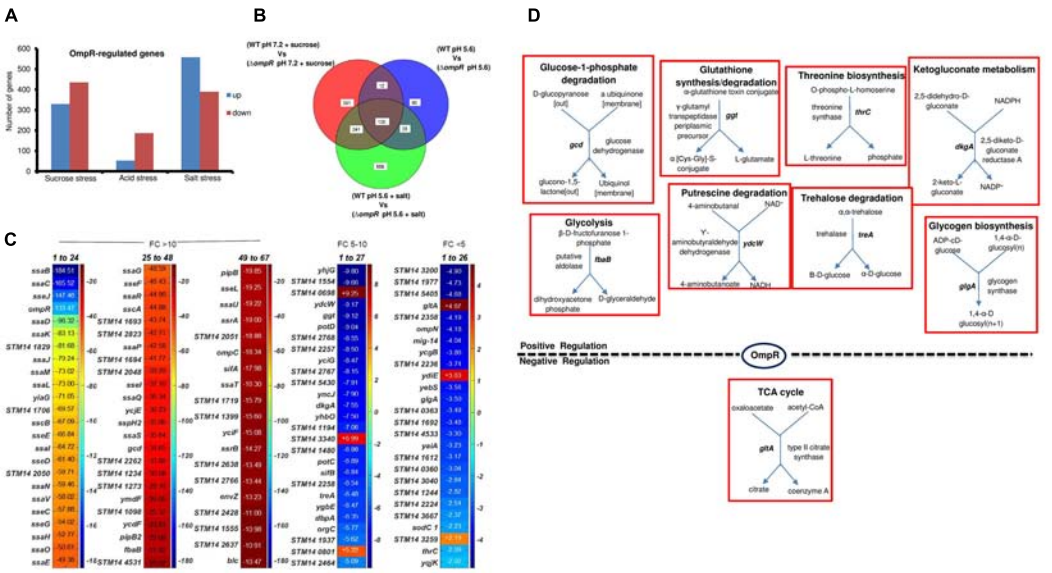

FIGURE 8 | Overlapping OmpR acid, sucrose, and salt stress targets **(A)** Statistically significant (≥ 2-fold change; *P*-value ≤ 0.05) OmpR targets differentially expressed in *S*. Typhimurium in response to acid, sucrose and salt stress are shown. **(B)** Overlapping OmpR targets are shown. **(C)** A heat map shows the expression profiles of the overlapping OmpR-regulated genes grouped based on differences in their fold change. The color scale represents the average fold change of an *ompR* null strain during sucrose stress (*n* = 3). **(D)** Metabolic overview of OmpR targets involved in cellular processes is shown.

as stress-induced proteins related to conidiation-specific protein 10 from *Neurospora*. YciF is highly conserved across the *Enterobacteriaciae,* and based on its structure, it was proposed to be a metal binding protein (Hindupur et al., 2006), and to function to protect the cell against oxidative damage. YciF was up-regulated in the OmpR response to acidification by acid or osmotic stress (**Figure 5**). It is annotated as being involved in the cellular response to DNA damage, as is *yciG*. YciF and YciG are in the *yciFGE-katN* operon, KatN is a non-heme catalase (Robbe-Saule et al., 2001). In *Salmonella*, YciF was reported to be under positive control of RpoS (Ibanez-Ruiz et al., 2000), yet our previous study showed that OmpR repressed *rpoS* during osmotic stress (Chakraborty et al., 2017), which would decrease *yciF* transcription. Our microarray results identify *yciF* as up-regulated by OmpR in both osmotic and acid stress (**Figure 5**). In *Salmonella*, *yciF* was reported to be regulated by bile, independently of *rpoS* (Prouty et al., 2004).

The *E. coli* Acid Stress Regulon Is Large

Our microarray results indicated that the OmpR-dependent response to acid stress in *E. coli* involved about six times as many genes as in *S*. Typhimurium (**Figure 3**). The involvement of 1360 genes in the OmpR-dependent *E. coli* MG1655 acid stress response (and 1538 genes in the total OmpR-independent acid stress response) was similar to a study of *E. coli* BW25113, in which 1871 genes were differentially expressed after a 15 min acid exposure (to pH 5.5) (Stincone et al., 2011). These two studies were in contrast to a ChIP-on-chip study using the *E. coli* K-12 strain CSH-50 (Quinn et al., 2014). In that study, only 144 OmpR-regulated acid stress genes were identified in CSH-50, i.e., only ∼10% compared to the 1360 genes that we identified in *E. coli* MG1655. In contrast, the response of *S*. Typhimurium was comparable between our study and the study by Quinn and colleagues: 240 vs. 212 acid stress genes (**Figure 3**; Quinn et al., 2014, respectively). Fifteen OmpR-regulated genes were common to *E. coli* CSH-50 and *S*. Typhimurium (Quinn et al., 2014), whereas in *E. coli* MG1655 and *S*. Typhimurium strain 14028, 25 genes were common (**Figure 3**). There was very little overlap between the common genes that we identified and the common genes identified by Dorman and co-workers (Quinn et al., 2014); although the few genes that were in common were again the known OmpR targets: *ompC*, *ompF* and the tripartite permease, *tppB*. These same targets appear in the common genes of the acid and osmotic stress responses of *S*. Typhimurium and *E. coli* (see **Figure 5**). CSH-50 is a proline and thiamine auxotroph, contains an insertion sequence in *fimE,* and is *rpsL* null (Miller, 1972; Blomfield et al., 1991). Thus, extensive genetic differences between *E. coli* K-12 CSH-50 and MG1655 likely explains the poor overlap between studies.

OmpR Numbers and pH Regulation

Our qRT-PCR results are in good agreement with our microarray; the *ompR* transcripts of both *S*. Typhimurium and *E. coli* were unchanged in acid pH, but were slightly up-regulated by ∼2-fold in response to osmotic stress (**Figure 2**). This result conflicts with a previous study that reported *ompR* transcripts in *S*. Typhimurium were ∼2.7-fold higher at pH 4.5 compared to pH 7 (Quinn et al., 2014). It may be that the lower pH examined (4.5 instead of 5.6), or differences in the culture media (EG-minimal medium instead of MGM) or the reference gene employed (*gmk*) might contribute to these discrepancies.

However, our finding that *ompR* transcripts did not change in acid stress (at pH 5.6) was entirely consistent with our use of super-resolution imaging to count OmpR molecules (Foo et al., 2015b; Liew et al., unpublished). OmpR molecules were counted in acid and neutral pH and the number of OmpR molecules was similar. We then used single particle tracking photoactivation localization microscopy (Spt-PALM) to monitor OmpR binding to DNA by measuring diffusion coefficients in acid and neutral pH. OmpR binding only increased by 5% in acid pH (Liew et al., unpublished). Previously, we have used AFM extensively to examine the role of pH in OmpR binding to DNA. OmpR binding affinity at the *ompC* and *cadB/A* promoters was increased in acid compared to neutral pH (Chakraborty et al., 2017). We propose that rather than increasing the number of OmpR molecules in acid pH, the OmpR binding affinity for DNA is pH-sensitive and increases in acid pH. In *E. coli* BW25113, it was reported that *ompR* transcripts were reduced by ∼50% in acid pH (Stincone et al., 2011). This was surprising, given the substantial role that OmpR plays in the acid stress response. In contrast, in the CSH-50 *E. coli* strain, *ompR* transcripts were unchanged between pH 7 and pH 4.5 (Quinn et al., 2014).

What Is the Cellular Response to Acid pH?

It was suggested that DNA topological changes at acid pH could drive OmpR binding to DNA and might be responsible for an increase in the number of OmpR-bound genes observed during acid stress (Cameron and Dorman, 2012). Previous studies used OmpR-dependent transcriptional fusions to *gfp* (including: *ompR-gfp* and *ssrA-gfp*) and reported that transcription was increased in the presence of novobiocin, which presumably reduces supercoiling. The authors concluded that DNA relaxation promoted OmpR binding to DNA, enhancing transcription (Cameron and Dorman, 2012). This was surprising, because we required supercoiled templates for OmpR transcription *in vitro* (D. Walthers and L.J. Kenney, unpublished observations). We used super-resolution microscopy to image a chromosomally-encoded OmpR-PAmCherry fusion protein during osmotic and acid stress (Foo et al., 2015b). We examined both the OmpR distribution and chromosomal compaction and discovered that the chromosome was actually more condensed during acidic conditions, rather than being more relaxed (Foo et al., 2015b; Liew et al., unpublished). This finding was recapitulated in a recent study of the nucleoid-associated protein H-NS (Gao et al., 2017).

A Caution Regarding C-Terminal Fusions to OmpR

ChIP-on-chip results with OmpR showed increased binding of OmpR at the *mgtC* promoter (Quinn et al., 2014), although microarray and qRT-PCR analysis of OmpR-regulated genes at acid pH did not identify *mgtC* as a target of OmpR regulation, nor did *mgtC* contribute to intracellular acidification (Chakraborty et al., 2015). A likely explanation for this discrepancy is that OmpR containing a 3XFLAG tag was employed in the ChIP-on-chip study, which also contained a D55E substitution (Quinn et al., 2014). It is well known that C-terminal tags to OmpR affect not only its DNA binding ability (Perkins et al., 2013), but also its specificity (Shimada et al., 2015), which may explain why it was observed that OmpR preferred relaxed DNA over supercoiled DNA. The D55E-3XFLAG-tagged OmpR also required concentrations > 1 μM to bind in electrophoretic mobility shift assays (Cameron and Dorman, 2012), even though the affinity of wildtype, unphosphorylated OmpR for the porin genes *ompF* and *ompC* is ∼150 nM (Head et al., 1998). In a recent study, OmpR targets were identified by SELEX (Shimada et al., 2015), but we were unable to validate the targets identified (Gao and Kenney, unpublished observations). Furthermore, different OmpR targets were identified depending on whether a C-terminal or N-terminal tag was employed (Shimada et al., 2015). Thus, extreme caution should be used when interpreting results using OmpR C-terminal fusions. A more likely explanation is that OmpR directly regulates *phoP*, in agreement with (Quinn et al., 2014), where OmpR was shown to bind to the *phoP* promoter. In turn, PhoP directly regulates *mgtC* and the reduced *mgtC* levels observed in the *ompR* null strain were likely due to reduced *phoP* levels. This type of indirect regulation has been observed in the OmpR regulation of the response regulator SsrB, which then regulates *sifA* (Walthers et al., 2011). It is also evident in the additional SPI-2 genes that are known SsrB targets (**Figure 8**).

Overall, this work revealed a large number of genes that are new targets of OmpR regulation during acid and osmotic stress. The challenge will be to determine whether these are direct effects or if they are mediated through OmpR regulation of an intermediating regulator, as we observed with the OmpR repression of the stationary phase sigma factor *rpoS* (Chakraborty et al., 2017).

AUTHOR CONTRIBUTIONS

SC performed the analysis and the experiments. SC and LK analyzed the data and wrote the manuscript.

FUNDING

Supported by VA IOBX-000372, NIH AI123640 to LK and an RCE in Mechanobiology from the Ministry of Education, Singapore.

ACKNOWLEDGMENTS

We thank Dr. Ricksen Winardhi, formerly of the MBI for contributing the *gltA* AFM images and Ong Hui Ting (MBI Microscopy Core) for assistance with microarray analysis.

SUPPLEMENTARY MATERIAL

The Supplementary Material for this article can be found online at: https://www.frontiersin.org/articles/10.3389/fmicb.2018.02656/full#supplementary-material

REFERENCES

Bearson, B. L., Lee, I. S., and Casey, T. A. (2009). *Escherichia coli* O157?: H7 glutamate- and arginine-dependent acid-resistance systems protect against oxidative stress during extreme acid challenge. *Microbiology* 155, 805–812. doi: 10.1099/mic.0.022905-0

Blomfield, I. C., McClain, M. S., Princ, J. A., Calie, P. J., and Eisenstein, B. I. (1991). Type 1 fimbriation and fimE mutants of *Escherichia coli* K-12. *J. Bacteriol.* 173, 5298–5307. doi: 10.1128/jb.173.17.5298-5307.1991

Boor, K. J. (2006). Bacterial stress responses: what doesn't kill them can make them stronger. *PLoS Biol.* 4:e23. doi: 10.1371/journal.pbio.0040023

Broome-Smith, J. K., and Spratt, B. G. (1982). Deletion of the penicillin-binding protein 6 gene of *Escherichia coli*. *J. Bacteriol.* 152, 904–906.

Cameron, A. D. S., and Dorman, C. J. (2012). A fundamental regulatory mechanism operating through OmpR and DNA topology controls expression of *Salmonella* pathogenicity islands SPI-1 and SPI-2. *PLoS Genet.* 8:e1002615. doi: 10.1371/journal.pgen.1002615

Casey, J. R., Grinstein, S., and Orlowski, J. (2010). Sensors and regulators of intracellular pH. *Nat. Rev. Mol. Cell Biol.* 11, 50–61. doi: 10.1038/nrm2820

Chakraborty, S., Mizusaki, H., and Kenney, L. J. (2015). A FRET-Based DNA biosensor tracks OmpR-dependent acidification of *Salmonella* during macrophage infection. *PLoS Biol.* 13:e1002116. doi: 10.1371/journal.pbio.1002116

Chakraborty, S., Winardhi, R. S., Morgan, L. K., Yan, J., and Kenney, L. J. (2017). Non-canonical activation of OmpR drives acid and osmotic stress responses in single bacterial cells. *Nat. Commun.* 8:1587. doi: 10.1038/s41467-017-02030-0

Cheeseman, G. C., and Fuller, R. (1968). Changes in the pH activity profile of the lysine decarboxylase during incubation of *Escherichia coli*. *J. Appl. Bacteriol.* 31, 253–258. doi: 10.1111/j.1365-2672.1968.tb00365.x

Choi, J., and Groisman, E. A. (2016). Acidic pH sensing in the bacterial cytoplasm is required for *Salmonella* virulence. *Mol. Microbiol.* 101, 1024–1038. doi: 10.1111/mmi.13439

De Biase, D., and Lund, P. A. (2015). The *Escherichia coli* acid stress response and its significance for pathogenesis. *Adv. Appl. Microbiol.* 92, 49–88. doi: 10.1016/bs.aambs.2015.03.002

De Biase, D., Tramonti, A., Bossa, F., and Visca, P. (1999). The response to stationary-phase stress conditions in *Escherichia coli*: role and regulation of the glutamic acid decarboxylase system. *Mol. Microbiol.* 32, 1198–1211. doi: 10.1046/j.1365-2958.1999.01430.x

Eguchi, Y., and Utsumi, R. (2014). Alkali metals in addition to acidic pH activate the EvgS histidine kinase sensor in *Escherichia coli*. *J. Bacteriol.* 196, 3140–3149. doi: 10.1128/JB.01742-14

Feng, X., Oropeza, R., and Kenney, L. J. (2003). Dual regulation by phospho-OmpR of ssrA/B gene expression in *Salmonella* pathogenicity island 2. *Mol. Microbiol.* 48, 1131–1143. doi: 10.1046/j.1365-2958.2003.03502.x

Feng, X., Walthers, D., Oropeza, R., and Kenney, L. J. (2004). The response regulator SsrB activates transcription and binds to a region overlapping OmpR binding sites at *Salmonella* pathogenicity island 2. *Mol. Microbiol.* 54, 823–835. doi: 10.1111/j.1365-2958.2004.04317.x

Foo, Y. H., Gao, Y., Zhang, H., and Kenney, L. J. (2015a). Cytoplasmic sensing by the inner membrane histidine kinase EnvZ. *Prog. Biophys. Mol. Biol.* 118, 119–129. doi: 10.1016/j.pbiomolbio.2015.04.005

Foo, Y. H., Spahn, C., Zhang, H., Heilemann, M., and Kenney, L. J. (2015b). Single cell super-resolution imaging of *E. coli* OmpR during environmental stress. *Integr. Biol.* 7, 1297–1308. doi: 10.1039/C5IB00077G

Gao, Y., Foo, Y. H., Winardhi, R. S., Tang, Q., Yan, J., and Kenney, L. J. (2017). Charged residues in the H-NS linker drive DNA binding and gene silencing in single cells. *Proc. Natl. Acad. Sci. U.S.A.* 114, 12560–12565. doi: 10.1073/pnas.1716721114

Ghosh, M., Wang, L. C., Ramesh, R., Morgan, L. K., Kenney, L. J., and Anand, G. S. (2017). Lipid-mediated regulation of embedded receptor kinases via parallel Allosteric Relays. *Biophys. J.* 112, 643–654. doi: 10.1016/j.bpj.2016.12.027

Goh, E. B., Siino, D. F., and Igo, M. M. (2004). The *Escherichia coli* tppB (ydgR) gene represents a new class of OmpR-regulated genes. *J. Bacteriol.* 186, 4019–4024. doi: 10.1128/JB.186.12.4019-4024.2004

Head, C. G., Tardy, A., and Kenney, L. J. (1998). Relative binding affinities of OmpR and OmpR-phosphate at the *ompF* and *ompC* regulatory sites. *J. Mol. Biol.* 281, 857–870. doi: 10.1006/jmbi.1998.1985

He, Q., He, Z., Joyner, D. C., Joachimiak, M., Price, M. N., Yang, Z. K., et al. (2010). Impact of elevated nitrate on sulfate-reducing bacteria: a comparative study of *Desulfovibrio vulgaris*. *ISME J.* 4, 1386–1397. doi: 10.1038/ismej.2010.59

Hindupur, A., Liu, D. Q., Zhao, Y. H., Bellamy, H. D., White, M. A., and Fox, R. O. (2006). The crystal structure of the *E-coli* stress protein YciF. *Protein Sci.* 15, 2605–2611. doi: 10.1110/Ps.062307706

Horswill, A. R., Dudding, A. R., and Escalante-Semerena, J. C. (2001). Studies of propionate toxicity in *Salmonella enterica* identify 2-methylcitrate as a potent inhibitor of cell growth. *J. Biol. Chem.* 276, 19094–19101. doi: 10.1074/jbc.M100244200

Ibanez-Ruiz, M., Robbe-Saule, V., Hermant, D., Labrude, S., and Norel, F. (2000). Identification of RpoS (sigma(S))-regulated genes in *Salmonella enterica* serovar typhimurium. *J. Bacteriol.* 182, 5749–5756. doi: 10.1128/JB.182.20.5749-5756.2000

Karlinsey, J. E. (2007). Lambda-Red genetic engineering in *Salmonella enterica* serovar Typhimurium. *Methods Enzymol.* 421, 199–209. doi: 10.1016/S0076-6879(06)21016-4

Keseler, I. M., Collado-Vides, J., Santos-Zavaleta, A., Peralta-Gil, M., Gama-Castro, S., Muniz-Rascado, L., et al. (2011). EcoCyc: a comprehensive database of *Escherichia coli* biology. *Nucleic Acids Res.* 39, D583–D590. doi: 10.1093/nar/gkq1143

Kitko, R. D., Wilks, J. C., Garduque, G. M., and Slonczewski, J. L. (2010). Osmolytes contribute to pH homeostasis of *Escherichia coli*. *PLoS One* 5:e10078. doi: 10.1371/journal.pone.0010078

Krulwich, T. A., Sachs, G., and Padan, E. (2011). Molecular aspects of bacterial pH sensing and homeostasis. *Nat. Rev. Microbiol.* 9, 330–343. doi: 10.1038/nrmicro2549

Lai, C.-Y., Santos, S., and Chiesa, M. (2015). General interpretation and theory of apparent height in dynamic atomic force microscopy. *RSC Adv.* 5, 80069–80075. doi: 10.1039/C5RA16695K

Lee, A. K., Detweiler, C. S., and Falkow, S. (2000). OmpR regulates the two-component system SsrA-SsrB in *Salmonella* pathogenicity island 2. *J. Bacteriol.* 182, 771–781. doi: 10.1128/JB.182.3.771-781.2000

Madshus, I. H. (1988). Regulation of intracellular pH in eukaryotic cells. *Biochem. J.* 250, 1–8. doi: 10.1042/bj2500001

Miller, J. H. (1972). *Experiments in Molecular Genetics*. New York, NY: Cold Spring Harb. Lab. Press. 433, 352–355.

Park, S. J., McCabe, J., Turna, J., and Gunsalus, R. P. (1994). Regulation of the citrate synthase (gltA) gene of *Escherichia coli* in response to anaerobiosis and carbon supply: role of the arcA gene product. *J. Bacteriol.* 176, 5086–5092. doi: 10.1128/jb.176.16.5086-5092.1994

Pedersen, L. B., Murray, T., Popham, D. L., and Setlow, P. (1998). Characterization of dacC, which encodes a new low-molecular-weight penicillin-binding protein in *Bacillus subtilis*. *J. Bacteriol.* 180, 4967–4973.

Perkins, T. T., Davies, M. R., Klemm, E. J., Rowley, G., Wileman, T., James, K., et al. (2013). ChIP-seq and transcriptome analysis of the OmpR regulon of *Salmonella enterica* serovars Typhi and Typhimurium reveals accessory genes implicated in host colonization. *Mol. Microbiol.* 87, 526–538. doi: 10.1111/mmi.12111

Prouty, A. M., Brodsky, I. E., Manos, J., Belas, R., Falkow, S., and Gunn, J. S. (2004). Transcriptional regulation of *Salmonella enterica* serovar Typhimurium genes by bile. *FEMS Immunol. Med. Microbiol.* 41, 177–185. doi: 10.1016/j.femsim.2004.03.002

Quinn, H. J., Cameron, A. D. S., and Dorman, C. J. (2014). Bacterial regulon evolution: distinct responses and roles for the identical OmpR proteins of *Salmonella* Typhimurium and *Escherichia coli* in the acid stress response. *PLoS Genet.* 10:e1004215. doi: 10.1371/journal.pgen.1004215

Rhee, E. J., Sheng, W., Morgan, L. K., Nolet, R., Liao, X., and Kenney, L. J. (2008). Amino acids important for DNA recognition by the response regulator OmpR. *J. Biol. Chem.* 283, 8664–8677. doi: 10.1074/jbc.M705550200

Robbe-Saule, V., Coynault, C., Ibanez-Ruiz, M., Hermant, D., and Norel, F. (2001). Identification of a non-haem catalase in *Salmonella* and its regulation by RpoS (σs). *Mol. Microbiol.* 39, 1533–1545. doi: 10.1046/j.1365-2958.2001.02340.x

Santos, J. M., Lobo, M., Matos, A. P. A., De Pedro, M. A., and Arraiano, C. M. (2002). The gene *bolA* regulates dacA (PBP5), dacC (PBP6) and ampC (AmpC), promoting normal morphology in *Escherichia coli*. *Mol. Microbiol.* 45, 1729–1740. doi: 10.1046/j.1365-2958.2002.03131.x

Sen, H., Aggarwal, N., Ishionwu, C., Hussain, N., Parmar, C., Jamshad, M., et al. (2017). Structural and functional analysis of the *Escherichia coli* acid-sensing histidine kinase, EvgS. *J. Bacteriol.* 199, e310–e317. doi: 10.1128/JB.00310-17

Shimada, T., Takada, H., Yamamoto, K., and Ishihama, A. (2015). Expanded roles of two-component response regulator OmpR in *Escherichia coli*: genomic SELEX search for novel regulation targets. *Genes Cells* 20, 915–931. doi: 10.1111/gtc.12282

Slonczewski, J. L., Fujisawa, M., Dopson, M., and Krulwich, T. A. (2009). Cytoplasmic pH measurement and homeostasis in bacteria and archaea. *Adv. Microb. Physiol.* 55, 1–79. doi: 10.1016/S0065-2911(09)05501-5

Stincone, A., Daudi, N., Rahman, A. S., Antczak, P., Henderson, I., Cole, J., et al. (2011). A systems biology approach sheds new light on *Escherichia coli* acid resistance. *Nucleic Acids Res.* 39, 7512–7528. doi: 10.1093/nar/gkr338

Tucker, D. L., Tucker, N., and Conway, T. (2002). Gene expression profiling of the pH response in *Escherichia coli*. *J. Bacteriol.* 184, 6551–6558. doi: 10.1128/JB.184.23.6551-6558.2002

Vivijs, B., Aertsen, A., and Michiels, C. W. (2016). Identification of genes required for growth of *Escherichia coli* MG1655 at moderately low pH. *Front. Microbiol.* 7:1672. doi: 10.3389/fmicb.2016.01672

Walthers, D., Carroll, R. K., Navarre, W. W., Libby, S. J., Fang, F. C., and Kenney, L. J. (2007). The response regulator SsrB activates expression of diverse *Salmonella* pathogenicity island 2 promoters and counters silencing by the nucleoid-associated protein H-NS. *Mol. Microbiol.* 65, 477–493. doi: 10.1111/j.1365-2958.2007.05800.x

Walthers, D., Go, A., and Kenney, L. J. (2005). "Regulation of porin gene expression by the two-component regulatory system EnvZ/OmpR," in *Bacterial and Eukaryotic Porins: Structure, Function, Mechanism*, ed. R. Benz (Weinheim: Wiley-VCH), 1–24.

Walthers, D., Li, Y., Liu, Y., Anand, G., Yan, J., and Kenney, L. J. (2011). *Salmonella enterica* response regulator SsrB relieves H-NS silencing by displacing H-NS bound in polymerization mode and directly activates transcription. *J. Biol. Chem.* 286, 1895–1902. doi: 10.1074/jbc.M110.164962

Wang, L. C., Morgan, L. K., Godakumbura, P., Kenney, L. J., and Anand, G. S. (2012). The inner membrane histidine kinase EnvZ senses osmolality via helix-coil transitions in the cytoplasm. *EMBO J.* 31, 2648–2659. doi: 10.1038/emboj.2012.99

Wilks, J. C., and Slonczewski, J. L. (2007). pH of the cytoplasm and periplasm of *Escherichia coli*: rapid measurement by green fluorescent protein fluorimetry. *J.Bacteriol.* 189, 5601–5607. doi: 10.1128/JB.00615-07

Conflict of Interest Statement: The authors declare that the research was conducted in the absence of any commercial or financial relationships that could be construed as a potential conflict of interest.

frontiers in Microbiology

ORIGINAL RESEARCH
published: 08 January 2019
doi: 10.3389/fmicb.2018.03265

Effect of Acetic Acid and Lactic Acid at Low pH in Growth and Azole Resistance of *Candida albicans* and *Candida glabrata*

*Andreia Lourenço, Nuno Alexandre Pedro, Sara Barbosa Salazar and Nuno Pereira Mira**

Department of Bioengineering, Institute for Bioengineering and Biosciences, Instituto Superior Técnico, University of Lisbon, Lisbon, Portugal

Successful colonization of the acidic vaginal niche by *C. glabrata* and *C. albicans* depends on their ability to cope with the presence of lactic and acetic acids produced by commensal microbiota. As such, the inhibitory effect of these acids at a low pH in growth of *C. glabrata* and *C. albicans* was investigated. The effect of the presence of these organic acids in tolerance of the two *Candida* species to azoles used in treatment of vaginal infections was also investigated including eventual synergistic effects. Under the different experimental conditions tested lactic acid exerted no significant inhibitory effect against *C. albicans* or *C. glabrata*, contrasting with the generalized impression that the production of this acid is on the basis of the protective effect exerted by vaginal lactobacilli. Differently, *C. glabrata* and *C. albicans* exhibited susceptibility to acetic acid, more prominent at lower pHs and stronger for the latter species. Synergism between acetic acid and azoles was observed both for *C. albicans* and *C. glabrata,* while lactic acid-azole synergism was only efficient against *C. albicans*. Altogether our *in vitro* results indicate that tolerance to acetic acid at a low pH may play a more relevant role than tolerance to lactic acid in determining competitiveness in the vaginal tract of *C. albicans* and *C. glabrata* including under azole stress. Treatment of vaginal candidiasis with azoles may depend on the level of acetic and lactic acids present and improvements could be achieved synergizing the azole with these acids.

Keywords: tolerance to acetic and lactic acids, vaginal candidiasis, Candida-bacteria interaction, *C. glabrata* and *C. albicans*, acetic and lactic acids

OPEN ACCESS

Edited by:
Daniela De Biase,
Sapienza University of Rome, Italy

Reviewed by:
Steven S. Witkin,
Weill Cornell Medicine, United States
Georgios Chamilos,
University of Crete, Greece

****Correspondence:***
Nuno Pereira Mira
nuno.mira@tecnico.ulisboa.pt

Specialty section:
This article was submitted to Microbial Physiology and Metabolism, a section of the journal Frontiers in Microbiology

Received: *20 July 2018*
Accepted: *14 December 2018*
Published: *08 January 2019*

Citation:
Lourenço A, Pedro NA, Salazar SB and Mira NP (2019) Effect of Acetic Acid and Lactic Acid at Low pH in Growth and Azole Resistance of Candida albicans and Candida glabrata. Front. Microbiol. 9:3265. doi: 10.3389/fmicb.2018.03265

INTRODUCTION

Candida species are known commensals of the human genito-urinary and gastro-intestinal tracts however, under certain conditions, the colonizing *Candida* population can overgrow resulting in superficial infections or, in more serious cases, in life threatening disseminated mycoses. Vaginal infections are the leading superficial infections caused by *Candida* spp. being *C. albicans* and *C. glabrata* the top ethiological causative species(e.g., Sobel et al., 1998; Goncalves et al., 2016; Sobel, 2016). Vulvovaginal candidiasis (VVC) is estimated to affect 70–75% of all women, half of them experiencing at least one episode of re-incidence (Sobel, 2016). In more severe cases, the infection becomes recurrent giving origin to recurrent vulvovaginal candidiasis (RVVC), a condition that is estimated to affect around 138 million of women worldwide (Sobel, 2016). The

high incidence and recurrence of vaginal candidiasis caused by *C. albicans* and *C. glabrata* results from these species being well-adapted to the vaginal environment rendering their eradication difficult (Sobel and Chaim, 1997; Sobel, 2007). A high adherence to vaginal epithelial cells mediated by specific adhesins, the ability to form biofilms on vaginal epithelium or in intra-uterine devices or the secretion of hydrolytic enzymes are among the factors attributed to vaginal pathogenicity of *Candida* spp. (Goncalves et al., 2016). High resilience to environmental stress and the natural increased resilience to azoles, the top therapeutic agents used in the treatment of superficial candidiasis, are distinguishable aspects of *C. glabrata* vaginal pathogenicity (Goncalves et al., 2016). The acidic environment of the vaginal tract (pH in the range of ∼4–4.5 (Aldunate et al., 2015) was suggested to contribute for the increased resilience to azoles of *C. glabrata* and *C. albicans* based on the demonstrated decreased efficacy of these drugs *in vitro* at acidic pHs (Danby et al., 2012; Kasper et al., 2015; Boikov et al., 2017; Spitzer and Wiederhold, 2018). In these studies the acidic pH of the vaginal tract was mimicked adjusting the pH of the medium with a strong acid, however, vaginal acidity results from the presence of lactic and acetic acid that are produced by epithelial cells and/or by the co-colonizing microbiota (Boskey et al., 1999, 2001; Aldunate et al., 2015). While organic acids are able to dissociate directly in the near neutral microbial cytosol due to the lipophilic properties of the undissociated acid form, chemical dissociation of strong acids results in the accumulation of protons in the environment which do not cross the cell envelope at a significantly extent due to their charge (Mira et al., 2010). This ability to dissociate directly inside microbial cells turns weak organic acids much more efficient as antimicrobials, comparing with strong acids (Mira et al., 2010). Besides inducing intracellular acidification, exposure to weak organic acids also results in internal accumulation of the negatively charged counter-ion leading to multiple deleterious effects for yeast cells that include, an increased turgor pressure, oxidative stress, depletion of ribosomal RNA, or of relevant cofactors, among others (Mira et al., 2010). Although much of these effects have been studied in the experimental model yeast *Saccharomyces cerevisiae*, more recent studies undertaken in *C. albicans* and in *C. glabrata* confirm similar toxicity mechanisms (Cottier et al., 2015, 2017; Bernardo et al., 2017; Cunha et al., 2017).

Although the presence of organic acids is largely recognized as an hallmark of vaginal health and a key factor in preventing overgrowth of pathogens, including of *Candida* spp. (Yan et al., 2009; Hickey et al., 2012), the eventual inhibitory effect of these molecules in inhibiting growth of *Candida* species has not been examined in a systematic and comparative manner including the study of eventual synergistic effects between the two acids. The effect exerted by these molecules in modulating tolerance of *Candida* spp. to azoles has also only been poorly studied. A study undertaken by Moosa et al. (2004) has shown that acetic acid (but not lactic acid) is able to potentiate the activity of fluconazole against *C. albicans*, however, in this work only one concentration of acetic or lactic acids has been used reflecting the concentration expected in vaginal secretions in healthy nonpregnant premenopausal women (Moosa et al., 2004). Differently, in our study we have used a range of concentrations of the two organic acids observed to occur in the vaginal tract under different conditions thus better reflecting the changing environment that *Candida* species are challenged in this infection site. Another distinctive aspect of our study is the use of other topical azoles besides fluconazole and also the focus on *C. glabrata* species and on the use of azole-resistant strains of this species which are herein shown to be sensitized in the presence of acetic acid.

MATERIALS AND METHODS

Strains and Growth Media

The strains used in this study are described in **Table 1**. The *Candida* strains used were batch-cultured at 30°C, with orbital agitation (250 rpm) in minimal medium (MM), in rich yeast peptone dextrose (YPD) or in RPMI. MM contains, per liter, 1.70 g yeast nitrogen base (YNB) without amino acids and $NH4^+$ (Difco Laboratories, Detroit, Mich.), 2.65 g $(NH_4)_2SO4$ (Merck Millipore) and glucose (10 or 2 g/L) (Merck Millipore, Darmstadt, Germany). YPD contains, per liter, 20 g glucose (Merck Millip3ore), 10 g yeast extract (HiMedia Laboratories, Mumbai, India) and 20 g peptone (HiMedia Laboratories). RPMI (Roswell Park Memorial Institute Medium) contains, per liter, 10.8 g RPMI-1640 synthetic medium (Sigma), 18 g glucose (Merck Millipore), and 34.5 g of MOPS (3-(N-morpholino) propanesulfonic acid, Sigma). When required the pH of the different growth media was adjusted using HCl or NaOH. All media were prepared in deionized water and sterilized by autoclaving for 15 min at 121°C and 1 atm, except RPMI that was sterilized by filtration. Solid media were obtained by supplementing the corresponding liquid growth medium with 20 g (per liter) of agar (Iberagar). The pH of the acetic and lactic acid stock solutions used were adjusted to pH 4.0 using NaOH 10 M and/or HCl. The stock solutions of the antifungals, clotrimazole, miconazole, fluconazole and tioconazole were prepared from the powder and using DMSO (Dimethyl sulfoxide, Sigma) as the solvent. All antifungals were purchased from Sigma.

Assessment of Susceptibility to Acetic and/or Lactic Acids

The susceptibility of *C. albicans* SC5314, *C. glabrata* CBS138 and *C. glabrata* BG2 to acetic and lactic acids was tested in 96-well microplates containing MM medium (having 1% or 0.2% glucose) either or not supplemented with acetic or lactic acids. Five concentrations of each acid were tested: 0.4, 4, 30, 45, and 75 mM for acetic acid and 80, 100, 120, 140, 160 mM for lactic acid. The media and the organic acids concentrations were adjusted to pH 4.5, 4, 3.5, and 3, always using HCl as the acidulant. Mid-exponential phase cells (OD_{600nm} of ∼0.8) cultivated in MM medium were used to inoculate the 96-microwell plates at an initial OD_{600nm} of 0.05. The inoculated plates were incubated at 30°C (using an agitation of 20 rpm or 200 rpm) for 24 h and growth was accompanied based on the increase in OD_{600nm}. The exact same experimental setting was used to assess susceptibility of the different *Candida* strains to acetic or lactic acids in RPMI medium (having 2 or 0.2%

TABLE 1 | Strains of *Candida* species used in this study.

Strain	Description	References
C. albicans SC5314	Reference strain	-
C. albicans VG216	Vaginal clinical isolate	This study
C. albicans VG485	Vaginal clinical isolate	This study
C. glabrata CBS138	Reference strain	Dujon et al., 2004
C. glabrata BG2	Vaginal clinical isolate	Fidel et al., 1996
C. glabrata VG99	Vaginal clinical isolate	Cunha et al., 2017
C. glabrata VG281	Vaginal clinical isolate	Cunha et al., 2017
C. glabrata VG216	Vaginal clinical isolate	Cunha et al., 2017
C. glabrata FFUL887	Azole-resistant clinical isolate harboring a gain-of-function CgPdr1 allele (K274Q substitution)	Salazar et al., 2018
C. glabrata FFUL667	Azole-resistant clinical isolate	Salazar et al., 2018
C. glabrata FFUL674	Azole-resistant clinical isolate harboring a gain-of-function CgPdr1 allele (I803T substitution)	Salazar et al., 2018
C. glabrata F15	Azole-resistant clinical isolate harboring a gain-of-function CgPdr1 allele (P927L substitution)	Vermitsky et al., 2006

glucose). For the synergistic assays the same experimental setting was used with the difference that the MM medium (at pH 4) was supplemented with both acetic and lactic acids (the same concentration range was used). All assays were performed in triplicates.

Assessment of Susceptibility to Azoles

Susceptibility of *C. glabrata* CBS138, *C. glabrata* BG2 and *C. albicans* SC5314 to clotrimazole, fluconazole, miconazole, and tioconazole in the presence of lactic or acetic acids was tested using a similar setup to the one described above. The concentrations of antifungals used were: 1, 5, 7.5, and 10 mg/L for clotrimazole; 30, 60, 64, and 128 mg/L for fluconazole; 0.05, 0.2, and 0.4 mg/L for miconazole and 0.1, 0.3, 0.45, and 0.6 mg/L for tioconazole. In all cases the stock solution of the antifungal was adjusted at pH 4. The concentrations of acetic acid tested were 4, 40, and 75 mM for acetic acid, while for lactic acid it were tested 80, 120, and 160 mM. Synergism between the two acids was only considered when the reduction in growth obtained in the medium supplemented with the organic acid and the azole drug was 50% higher than the inhibition registered when the cells were incubated with the compounds individually. In the case of fluconazole and clotrimazole it was also determined the MIC50 for the above referred *Candida* strains as well as for the clinical isolates *C. albicans* VG216, *C. albicans* VG485, *C. glabrata* FFUL887, *C. glabrata* VG99, *C. glabrata* VG216, *C. glabrata* VG281, *C. glabrata* 674, and *C. glabrata* 677. For this the microdilution method was used as recommended by EUCAST (Subcommittee on Antifungal Susceptibility Testing (AFST) of the ESCMID European Committee for Antimicrobial Susceptibility Testing (EUCAST) et al., 2003). All assays were performed in quadruplicates.

RESULTS

At a Low pH, C. glabrata and *C. albicans* Are Susceptible to Acetic Acid but Not to Lactic Acid

C. glabrata and *C. albicans* cells are challenged with acetic (1–120 mM) and lactic acids (∼120 mM) (Boskey et al., 1999, 2001; Aldunate et al., 2015) at a low pH in the acidic vaginal tract. Thus, we have monitored growth of these two pathogenic species in MM medium supplemented with increasing concentrations of the two organic acids (in the range of 4–75 mM for acetic acid and 80–160 mM for lactic acid) at pHs ranging from 3 to 4.5 (**Figure 1**). The reference strain *C. albicans* SC5314 and two *C. glabrata* laboratory strains: the reference strain CBS138 and BG2, used to study vaginal pathophysiology of *C. glabrata* (Fidel et al., 1996), were used. The results obtained clearly demonstrate that lactic acid exerts very little effect against the three strains tested, not even at the lower pH tested of 3 (**Figure 1**). Consistently, the number of viable *C. albicans* SC5314 and *C. glabrata* CBS138 recovered from cells cultivated for 24h in presence of 160 mM lactic acid at pH 4 was only slightly below the levels attained in control cells (**Figure S1**). Differently, in the presence of the higher concentrations of acetic acid tested (40 and 75 mM) a prominent reduction in growth of the two *Candida* species tested was observed, this being significantly more marked for *C. albicans* (**Figure 1**). As expected, the toxic effect of acetic acid was augmented with the reduction in pH (**Figure 1**). Consistent with the growth inhibition observed, a significant loss of cellular viability (of around 100-fold) was observed in the acetic acid stressed (75 mM at pH 4) *C. albicans* and *C. glabrata* populations (**Figure S1**). The inhibition in growth caused by acetic acid cannot be attributable to the acidification of the medium itself since acidification using the strong acid HCl as the acidulant agent did not led to growth inhibition for any of the strains tested (results not shown). Under the conditions that we have used no significant filamentation of *C. albicans* cells was observed (as assessed by microscopic observation of culture samples) (results not shown), in line with the previous demonstration that morphological yeast-hyphae transition does not occur at a significant extent in acidic pHs (Davis et al., 2000). The high tolerance of the two *C. glabrata* strains tested to acetic and lactic acids is in line with the described high resilience of this species to environmental stress (Jandric and Schuller, 2011). The vaginal strain *C. glabrata* BG2 showed higher tolerance against acetic acid than the reference strain CBS138, a trait that could be attributable to the development of efficient adaptive responses to cope with acetic acid stress at a low pH by vaginal *C. glabrata* strains (Cunha et al., 2017). The amount of glucose in the vaginal environment is low (around 0.5%) (Owen and Katz, 1999; Childers et al., 2016) and thus the phenotypic screening was repeated using the same mineral medium but having only 0.2% glucose (**Figure S2**). The results obtained were essentially the same as those shown in **Figure 1**, only being detectable a toxic effect against *C. albicans* and *C. glabrata* exerted by acetic acid (**Figure S2**). The same results were also obtained when RPMI was used (**Figure S3**). Since the vaginal environment is microaerophilic (Sosinska et al., 2008)

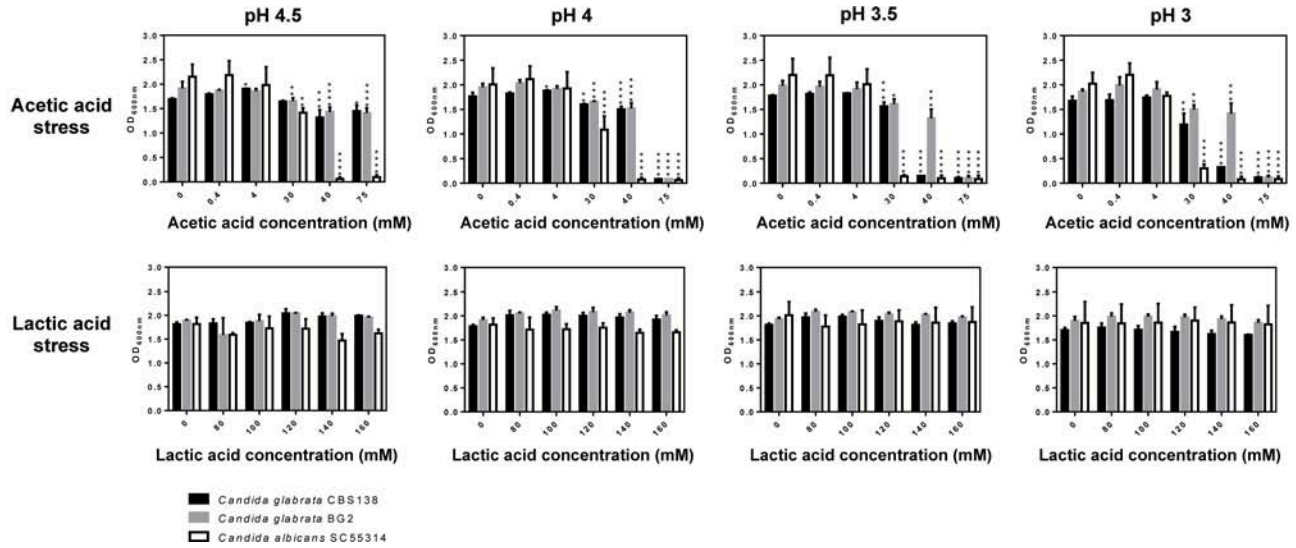

FIGURE 1 | Growth under aerophilic conditions of *C. albicans* (white bars), *C. glabrata* CBS138 (black bars) and *C. glabrata* BG2 (gray bars) in MM medium supplemented with the indicated concentrations of lactic or acetic acid at the pHs depicted in the figure. Statistical significance was calculated comparing growth of each strain in the presence and absence of acetic or lactic acids (**p*-value below 0.05; ***p*-value below 0.01; ****p*-value below 0.001; *****p*-value below 0.0001).

we have also examined the toxic effect imposed by acetic or lactic acids at a low pH in growth of *C. albicans* and *C. glabrata* under those conditions (**Figure 2** and **Figures S4, S5**). Although a generalized reduced growth in the O_2-limited setting was observed, the results obtained concerning the effect of acetic acid and the non-inhibition caused by lactic acid were similar (**Figure 2** and **Figures S4, S5**). We have also tested whether the increase in temperature from 30° to 37°C would change the pattern of acetic and lactic-susceptibilities observed, however, the results obtained at the two temperatures were identical (**Figure S6**).

At Low pH Lactic and Acetic Acids Do Not Synergistically Inhibit Growth of *Candida* spp.

Since acetic and lactic acids exist together in the vaginal tract, an eventual synergistic effect between these two acids in inhibiting growth of *C. albicans* and *C. glabrata* was hypothesized. To test this, the strains were cultivated under the same experimental conditions described above with the difference that this time both acetic and lactic acids were simultaneously added to the growth medium. The results obtained (shown in **Figure 3**) confirmed the lack of toxicity of lactic acid, while exposure to acetic acid resulted in growth inhibition, specially for concentrations above 40 mM (**Figure 3**). The hypothesized synergism between the two acids was not confirmed since the presence of lactic acid did not augmented the strong toxic effect exerted by acetic acid at pH 4. A similar result was also obtained in medium containing lower concentrations of glucose (0.2% instead of 1%) (results not shown) or under microaerophilic conditions (**Figure 3**).

The Presence of Acetic and Lactic Acids at Low pH Modulates Tolerance to Azoles in *C. albicans and C. glabrata*

Since vaginal candidiasis is typically treated using topical azoles we have tested whether the presence of acetic and lactic acids at a low pH could influence the activity of clotrimazole, miconazole, tioconazole, and fluconazole. For that, cells were cultivated in MM growth medium (having 1% glucose and adjusted at pH 4) supplemented with inhibitory concentrations of the different azoles and/or with acetic (**Figure 4**) or lactic (**Figure 5**) acids. Acetic acid synergized with clotrimazole and fluconazole in inhibiting growth of *C. glabrata* and *C. albicans* (**Figure 4** and **Figure S7**). It has to be pointed out, however, that for the *C. glabrata* BG2 strain the synergistic effect was only observed for the higher concentration of acetic acid tested, 75 mM, most likely due to the higher resilience of this strain to acetic acid. A synergistic effect with miconoazole and thioconazole was also observed but only against *C. albicans* (**Figure 4** and **Figure S7**). Lactic acid synergized with all the tested antifungals but only against *C. albicans* (**Figure 5** and **Figure S7**).

The observed synergistic effects between acetic and/or lactic acid with antifungals of clinical application prompted us to test whether the presence of the organic acids would alter the MIC level of the strains, as determined by the micro-dilution method recommended by EUCAST. Besides using reference, we have also used three *C. glabrata* vaginal strains (VG99, VG281, and VG216), two *C. albicans* vaginal strains (CaVG674 and CaVG677) and four previously documented *C. glabrata* azole-resistant strains (FFUL887, FFUL674, FFUL677, and F15) (Vermitsky et al., 2006; Salazar et al., 2018). The assays were conducted at two distinct pHs (4 and 7) to tackle the effect of the undissociated form of the acid in the eventual modulation of

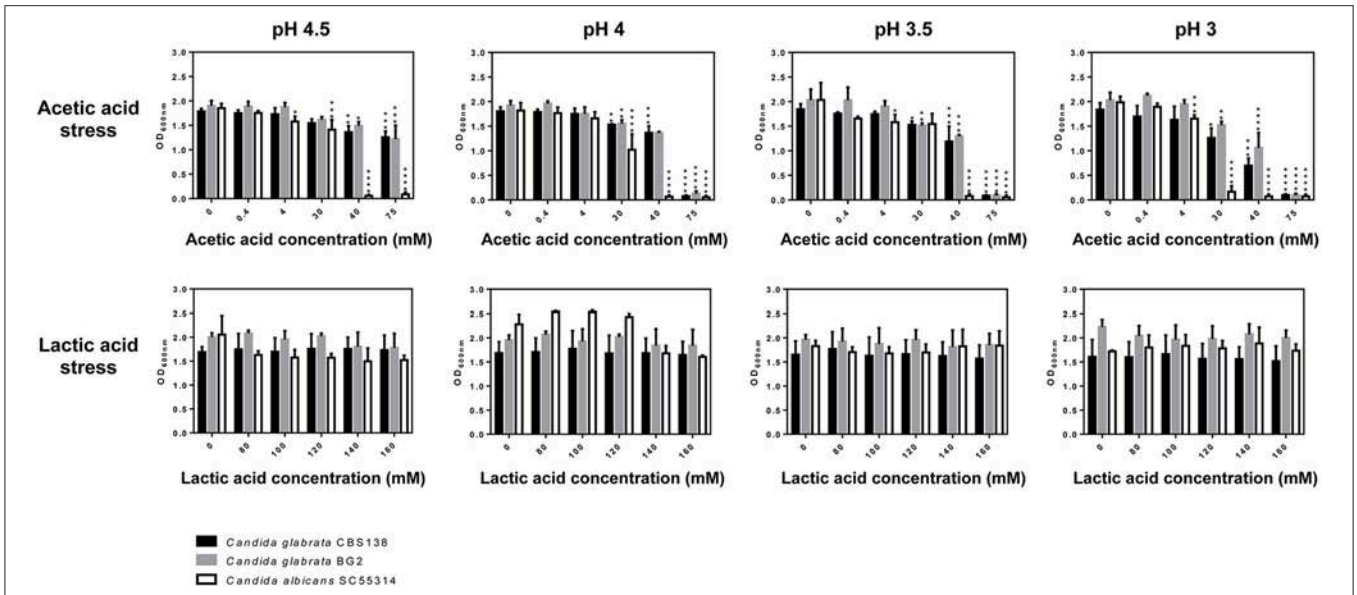

FIGURE 2 | Growth under microaerophilic conditions of *C. albicans* (white bars), *C. glabrata* CBS138 (black bars) and *C. glabrata* BG2 (gray bars) in MM medium supplemented with 0.2% glucose and with the indicated concentrations of lactic or acetic acid at the pHs depicted in the figure. Statistical significance was calculated comparing growth of each strain in the presence and absence of acetic or lactic acids (**p*-value below 0.05; ***p*-value below 0.01; ****p*-value below 0.001; *****p*-value below 0.0001).

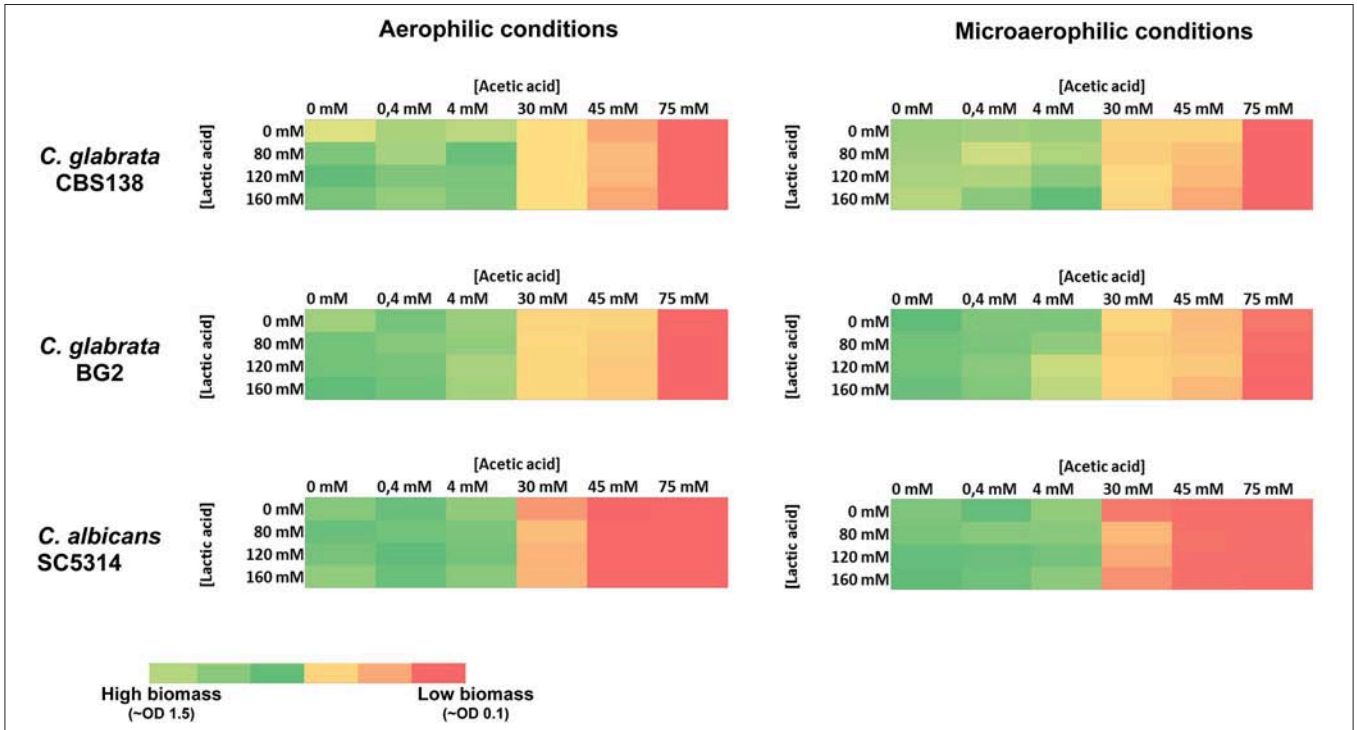

FIGURE 3 | Heat map representing the inhibitory effect of lactic and/or acetic acids against *C. albicans*, *C. glabrata* BG2 and *C. glabrata* CBS138 in MM medium (at pH 4). To assess an eventual synergistic effect of lactic and acetic acids in determining growth inhibition of *Candida* spp. growth of the different strains in MM medium (at pH4) in the presence of different concentrations of these organic acids was assessed based on the OD600nm after 24 h of incubation in the presence of the acids, which was used to build the heat-map depicted.

azole resistance of the strains. The results obtained confirm the previously reported reduction of fluconazole and clotrimazole efficacy in inhibiting growth of *C. albicans* and *C. glabrata* at acidic pHs when strong acids are used as acidulants (Danby et al., 2012), this being observed for all the strains tested (**Table 2**). In the presence of acetic acid at pH4 the susceptibility of

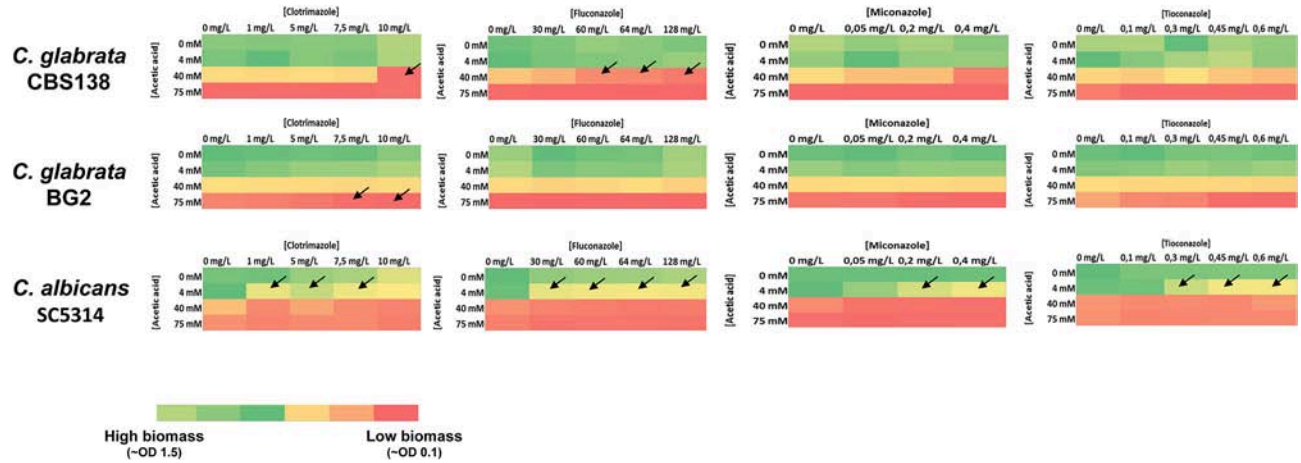

FIGURE 4 | Heat map representing the inhibitory effect of acetic acid and clotrimazole, fluconazole, miconazole, and tioconazole against *C. albicans*, *C. glabrata* BG2 and *C. glabrata* CBS138 in MM medium (at pH 4). To assess an eventual synergistic effect of acetic acids with the different azoles in determining growth inhibition of *Candida* spp., growth of the different strains in MM medium (at pH4) in the presence of different concentrations of acetic acid and of the different azoles was assessed based on the OD600nm after 24 h of incubation in the presence of the acids, as detailed in Materials and Methods. Synergism between acetic acid and an azole was only considered when growth inhibition achieved in the presence of the acid and of the azole was, at least, 50% higher the inhibition observed in the presence of the azole alone or of the acid alone. Conditions where the acid and an azole were found to synergize are represented by an arrow. Details on the results obtained in those conditions where azoles and acetic acid were found to synergize are provided in **Supplementary Figure S7** (**p*-value below 0.05; ***p*-value below 0.01; ****p*-value below 0.001; *****p*-value below 0.0001).

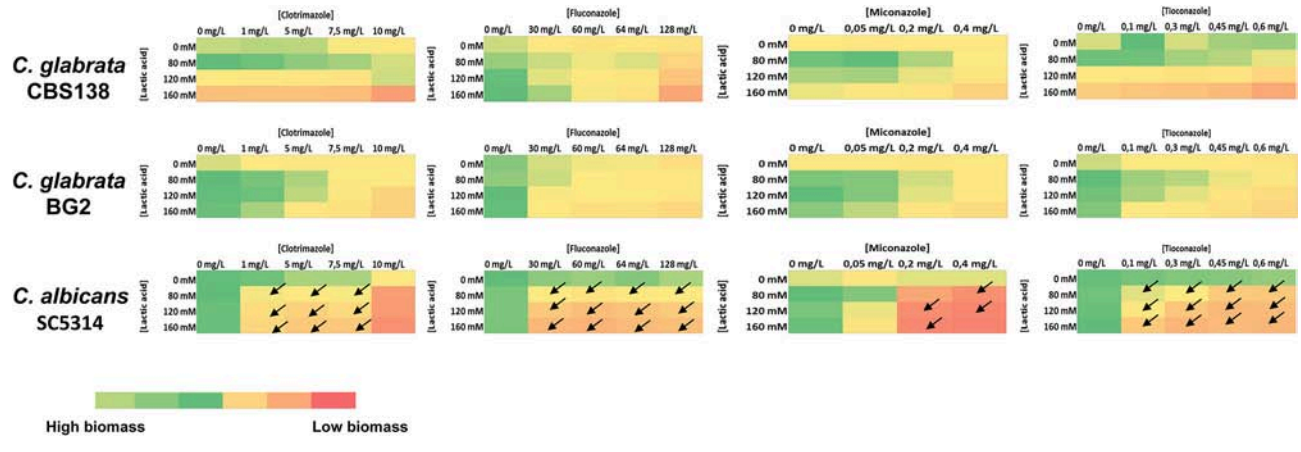

FIGURE 5 | Heat map representing the inhibitory effect of lactic acid and clotrimazole, fluconazole, miconazole, and tioconazole against *C. albicans*, *C. glabrata* BG2 and *C. glabrata* CBS138 in MM medium (at pH 4). To assess an eventual synergistic effect of lactic acid with the different azoles in determining growth inhibition of *Candida* spp., growth of the different strains in MM medium (at pH4) in the presence of different concentrations of acetic acid and of the different azoles was assessed based on the OD600nm after 24 h of incubation in the presence of the acids, as detailed in Materials and Methods. Synergism between lactic acid and an azole was only considered when growth inhibition achieved in the presence of the acid and of the azole was, at least, 50% higher the inhibition observed in the presence of the azole alone or of the acid alone. Conditions where the acid and an azole were found to synergize are represented by an arrow. Details on the results obtained in those conditions where azoles and lactic acid were found to synergize are provided in **Supplementary Figure S7**.

the more azole-susceptible strains (*C. glabrata* CBS138, BG2, VG281, VG99, and VG16 and *C. albicans* SC5314, CaVG674, and CaVG677) to fluconazole and clotrimazole was significantly enhanced being observed a prominent reduction in the MIC level of the strains (**Table 2**). Within the cohort of four azole-resistant *C. glabrata* strains herein examined, the F15 strain exhibited a prominent increase in susceptibility to fluconazole and clotrimazole (F15) in the presence of acetic acid (at pH 4) while for strains FFUL887 and FFUL677 a reduction in growth was also observed (**Figures 6A,B**), although this was not enough to cause a reduction in the MIC (**Table 2**). The observed increase in susceptibility of the strains to azoles in the presence of acetic acid correlated with their increased susceptibility to acetic acid alone (**Figures 6A,B**).

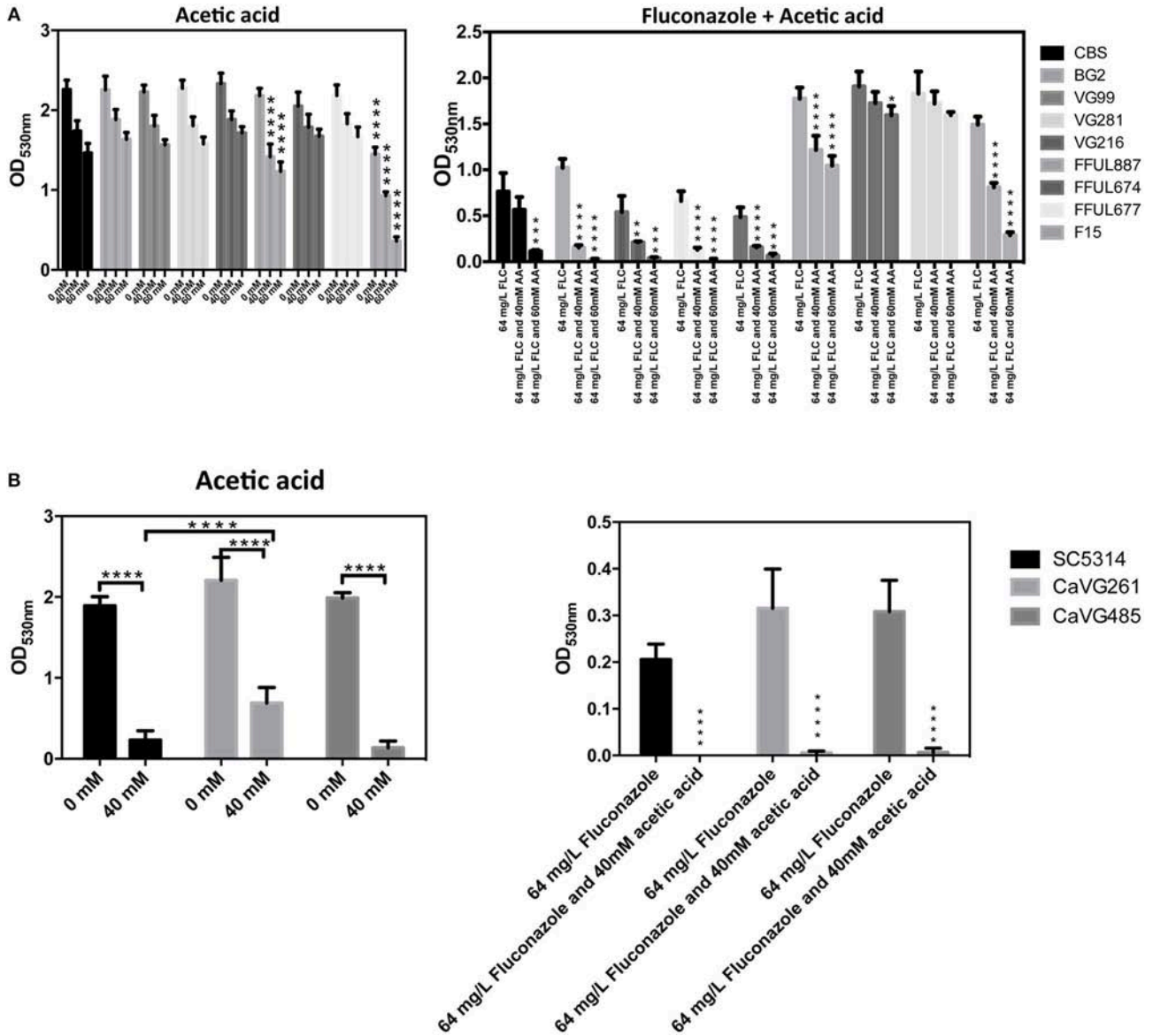

FIGURE 6 | Susceptibility of *C. glabrata* **(A)** and *C. albicans* **(B)** strains to acetic acid, to fluconazole or to a combination of fluconazole and acetic acid. This picture depicts the final OD600nm of cultures of the different strains used in our study after 24 h of cultivation in RPMI medium supplemented with acetic acid (40 or 60 mM, at pH 4) or in this same medium supplemented with fluconazole (64 mg/L) or with fluconazole and acetic acid (**p*-value below 0.05; ***p*-value below 0.01; ****p*-value below 0.001; *****p*-value below 0.0001).

DISCUSSION

The interest in the study of the effect on the physiology of *C. albicans* or *C. glabrata* of lactic and acetic acids at a low pH is boosted by the hypothesis that these organic acids play an important role in the control of the overgrowth of vaginal pathogens (Hickey et al., 2012; Aldunate et al., 2015; Petrova et al., 2015; Tachedjian et al., 2017). While various studies have demonstrated a prominent effect of lactic acid at a low pH in inactivating bacterial vaginal pathogens (O'hanlon et al., 2011, 2013), in the case of fungal species this topic has only been marginally investigated. Under the conditions that we have used, physiologically relevant concentrations of acetic acid significantly inhibited growth of *C. albicans* and *C. glabrata*, although at different extents since the latter species was considerably more tolerant. This particularly high susceptibility to acetic acid of *C. albicans* was observed both in lab (SC5314) and in two vaginal strains (**Figure 6**). Consistent with the idea that it is the undissociated form of acetic acid that induces toxicity against yeast cells, the decrease in pH (which favors the concentration of the undissociated form) led to a stronger inhibitory effect (**Figures 1**, **6B**). Differently, lactic acid exerted no significant effect in inhibiting growth of *C. albicans* or *C. glabrata*, not even at pH 3 that is already well below the acid pKa (∼3.9).

These results are in agreement with those obtained in prior studies that also reported an absence of lactic acid toxicity against *C. albicans* at acidic pHs (Moosa et al., 2004; Kasper et al., 2015). *C. albicans* was shown to consume lactic acid even when glucose is present in the growth medium and this was also hypothesized to occur for other short-chain fatty acids such as acetate (Childers et al., 2016). In the case of *C. glabrata* lactate and acetate utilization was shown (although lactate was clearly favored) and metabolization of these organic acids in the presence of glucose was also hypothesized (Ueno et al., 2011). More recently, co-consumption of glucose and acetic acid in *C. glabrata* was also shown, although this occurred only when cells were adapted and exponentially growing in the presence of the acid indicating that a prior adaptation response is required (Cunha et al., 2017). The ability of pathogenic *Candida* species to mobilize acetate or lactate even when glucose is present in the environment was suggested to favor virulence by contributing to improve metabolic versatility in infection niches often deprived of glucose such as the vaginal tract (Childers et al., 2016). In this context, it is reasonable to conceive that the low tolerance exhibited by *C. albicans* and *C. glabrata* to lactic acid could result from their rapid ability to fuel it for metabolization, while in the case of acetic acid this may occur at a much slower rate potentiating the toxic effects of the acid. Although *C. albicans* is equipped with an efficient lactate-uptake system also able to mediate acetate uptake (Vieira et al., 2010), and in *C. glabrata* transporters suggested to mediate acetate uptake have also been identified (Mota et al., 2015), at the acidic vaginal pH (close to or below the acids pKa) the entry of acetic and lactic acids is expected to occur by passive diffusion of the undissociated forms. As such, it is unlikely that the activity of these transport systems might play a significant role in modulating tolerance to those organic acids.

The observed lack of inhibitory effect of lactic acid against *C. albicans* and *C. glabrata* species suggests that the reported antimicrobial potential of supernatants obtained from vaginal lactobacilii cultures against *Candida* (e.g., Parolin et al., 2015) could result from other compounds present therein. In line with this hypothesis, metabolomic analysis of vaginal lactobacilii culture supernatants could not correlate the amount of lactic acid with the anti-candicidal potential of the supernatant, although this was encountered for other metabolites (Parolin et al., 2015). Further studies better characterizing the composition of these bacterial supernatants are required to clarify their inhibitory potential against *Candida* spp. The herein observed high toxicity of acetic acid against *C. albicans* and *C. glabrata* also indicates that mechanisms assuring tolerance of these yeast species to cope with this organic acid should play an important role to assure competitiveness and avoid exclusion from the vaginal tract, specially under dysbiosis conditions where the concentration of this organic acid increases prominently (∼120 mM) (Aldunate et al., 2015). In *C. glabrata* a few of those adaptive responses have been studied (Bernardo et al., 2017; Cunha et al., 2017) but in *C. albicans* this matter had not been thoroughly examined since the studies undertaken until so far examined responses using almost non-inhibitory conditions at pH 5.5, well above the acid pKa (Cottier et al., 2015, 2017). A particularly interesting aspect of these results would be to assess whether the competitiveness of *C. albicans*, compared to that of *C. glabrata*, in women with bacterial vaginosis, a condition known to increase acetic acid concentration. The metagenomic studies performed until so far of the vaginal micro- and myco- biomes do not allow the establishment of that correlation, either due to lack of identification at the species level or by only performing myco- or micro- biome analysis.

The effect exerted by the presence of acetic and lactic acids in modulating *C. albicans* and *C. glabrata* tolerance to azole drugs was another of the objectives of this work, this being a relevant interaction since these molecules may co-exist in the vaginal tract. It has been reported the reduced effect against *C. albicans* and *C. glabrata* of several antifungals belonging to different classes under acidic pHs using strong acids as the acidulants (Danby et al., 2012) and our study confirms these prior observations (**Table 2**). The presence of acetic acid improved the efficacy of all azoles tested against *C. albicans*—consistent with the results obtained by Moosa et al. (2004)-while for *C. glabrata* synergism was only observed for clotrimazole and fluconazole and this was strain-dependent. Against *C. glabrata* the synergistic effect was only observed for concentrations of acetic acid equal or above 40 mM (at pH 4), while for *C. albicans* this was observed even at 4 mM of acetic acid (at pH 4), a concentration within the range of those found in vaginal fluid even under eubiosis conditions (Boskey et al., 1999, 2001; Aldunate et al., 2015). This observation is consistent with the higher tolerance of the *C. glabrata* strains to acetic acid alone. Lactic acid improved efficacy of azoles only against *C. albicans* and at concentrations above 80 mM (at pH4), a value in line with those found in vaginal fluid (Boskey et al., 1999, 2001; Aldunate et al., 2015). Interestingly, this synergistic effect between azoles and lactic acid was not uncovered before in the study of Moosa et al. (2004), probably because in this work the authors have only used around 20 mM lactic acid, below concentrations reported to occur in vaginal fluid (Aldunate et al., 2015). One of the reported effects of undissociated organic acids (including of acetic acid) in yeast cells is the perturbation of the plasma membrane structure (Mira et al., 2010) which can thereby facilitate the entry of the azole drug into the yeast cells. Further studies are required to better investigate this synergistic effect between acetic and/or lactic acids and azoles in *Candida* spp. Another important feature of this interaction between organic acids and azoles is the previous demonstration that the combination of these two molecules has a fungicidal effect against *C. albicans* (Moosa et al., 2004), while when used alone the effect is only fungistatic.

One significant observation from our study is that the presence of acetic acid sensitized to azoles *C. glabrata* strains that were described to be resistant to these molecules, albeit not at the same extent since the effect was much more prominent for the F15 strain than for the other strains tested (**Figure 6A**). This sensitization effect correlated with the higher susceptibility of these strains to acetic acid (**Figure 6B**). The azole-resistance phenotype of all the *C. glabrata* strains used in our study results from them harboring different gain-of-function (GOF) mutations in the coding sequence of the transcriptional activator CgPdr1(Vermitsky et al., 2006 and our unpublished results;

TABLE 2 | MIC for fluconazole (FLC) and clotrimazole (CLTRI) in the presence or absence of acetic acid (AcA, 40, and 60 mM) for several *C. glabrata* and *C. albicans* strains.

Strain	pH 4						pH 7					
	MIC FLC (mg/mL)	MIC FLC (in the presence of 40 mM AcA) (mg/mL)	MIC FLC (in the presence of 60 mM AcA) (mg/mL)	MIC CLTRI (mg/mL)	MIC CLTRI (in the presence of 40 mM AcA) (mg/mL)	MIC CLTRI (in the presence of 60 mM AcA) (in mg/mL)	MIC FLC (in mg/mL)	MIC FLC (in the presence of 40 mM AcA) (in mg/mL)	MIC FLC (in the presence of 60 mM AcA) (in mg/mL)	MIC CLTRI (in mg/mL)	MIC CLTRI (in the presence of 40 mM AcA) (in mg/mL)	MIC CLTRI (in the presence of 60 mM AcA) (mg/mL)
C. glabrata												
C. glabrata CBS138	32	32	16	8	4	2	8	8	8	1	1	0.5
C. glabrata BG2	64	64	16	16	4	2	16	16	32	1	2	2
C. glabrata VG99	64	32	16	8	2	1	16	16	16	1	1	1
C. glabrata VG281	32	32	16	8	2	1	8	16	16	1	1	1
C. glabrata VG216	32	32	16	8	2	1	8	16	16	1	2	2
C. glabrata FFUL887 (FLC^R; K274Q GOF *CgPDR1* allele)	≥64	≥64	64	≥16	16	2	≥64	≥64	≥64	4	4	4
C. glabrata FFUL674 (FLC^R; unknown CgPdr1 GOF *CgPDR1* allele)	≥64	≥64	≥64	≥16	≥16	≥16	≥64	≥64	≥64	4	4	4
C. glabrata FFUL677 (FLC^R; unknown CgPdr1 GOF allele)	≥64	≥64	≥64	≥16	≥16	≥16	≥64	≥64	≥64	8	8	8
C. glabrata F15 (FLC^R; P927L GOF *CgPDR1* allele)	≥64	≥64	≤0.25	-	-	-	≥64	≥64	≥64	-	-	-
C. albicans												
C. albicans SC5314	0.5	≤0.25	-	0.1	≤0.0125	-	≤0.0125	≤0.25	-	≤0.00625	≤0.0125	-
C. albicans CaVG216	0.5	≤0.25	-	0.1	≤0.0125	-	0.025	≤0.25	-	≤0.00625	≤0.0125	-
C. albicans CaVG485	0.5	≤0.25	-	0.1	≤0.0125	-	0.025	≤0.25	-	≤0.00625	≤0.0125	-

The MIC was determined by the microdilution method, as recommended by EUCAST.

Salazar et al., 2018), an essential determinant of antifungal response in *C. glabrata*. Previously it had been suggested that the high susceptibility of FFUL887 and F15 strains to acetic acid may result from them expressing a CgPdr1 gain-of-function allele (Vermitsky et al., 2006; Salazar et al., 2018), which is in line with the results that we have obtained in the present work. Azole-resistant *C. albicans* strains were also found to be sensitized to fluconazole in the presence of acetic acid, however, in this case the molecular basis of the resistance phenotype of the strains was not investigated and thus no link with CaTac1 activity (the ortholog of CgPdr1) was made (Moosa et al., 2004). On the overall the results obtained in our work show that tolerance to acetic acid should play a relevant contributing role to assure competitiveness of *C. albicans* and *C. glabrata* in the vaginal tract, including under azole therapy. This should be a particularly relevant trait for successful colonization by *C. albicans*, which was found to be highly susceptible to this organic acid. The observed lack of effect of lactic acid in inhibiting growth of *C. albicans* and *C. glabrata* contrasts with the generalized idea that production of this organic acid by vaginal bacteria underlies a protective effect exerted against *Candida* species. It is also rendered clear that the levels of acetic and lactic acid in the vaginal tract may modulate susceptibility of *C. albicans* and *C. glabrata* to azoles used in treatment of vaginal infections, including those caused by some azole-resistant strains; this representing an important knowledge to improve therapeutic success.

AUTHOR CONTRIBUTIONS

AL, NP, and SS contributed to the phenotypic screenings conducted in the presence of organic acids under different conditions including in the presence of azoles. NPM coordinated and conceived the study, also having written the manuscript with contributions from NP and SS.

ACKNOWLEDGMENTS

This work was, in part, funded by FEDER through POCI-COMPETE 2020 and by Fundação para a Ciência e Tecnologia (contract PTDC/BIA-MIC/31515/2017, Project LactoCan-Fostering the development of new probiotic therapeutic approaches for the tretament of candidiasis through the exploration of lactobacilii-Candida interference mechanisms). Funding received by iBB–Institute for Bioengineering and Biosciences from FCT (UID/BIO/04565/2013), from Programa Operacional Regional de Lisboa 2020 (Project No. 007317) is also acknowledged. Professor Thomas Edlind is kindly acknowledged for sharing the *C. glabrata* F15 strain.

SUPPLEMENTARY MATERIAL

The Supplementary Material for this article can be found online at: https://www.frontiersin.org/articles/10.3389/fmicb.2018.03265/full#supplementary-material

REFERENCES

Aldunate, M., Srbinovski, D., Hearps, A. C., Latham, C. F., Ramsland, P. A., Gugasyan, R., et al. (2015). Antimicrobial and immune modulatory effects of lactic acid and short chain fatty acids produced by vaginal microbiota associated with eubiosis and bacterial vaginosis. *Front. Physiol.* 6:164. doi: 10.3389/fphys.2015.00164

Bernardo, R. T., Cunha, D. V., Wang, C., Pereira, L., Silva, S., Salazar, S. B., et al. (2017). The CgHaa1-regulon mediates response and tolerance to acetic acid stress in the human pathogen *Candida glabrata*. *G3 (Bethesda)* 7, 1–18. doi: 10.1534/g3.116.034660

Boikov, D. A., Locke, J. B., James, K. D., Bartizal, K., and Sobel, J. D. (2017). *In vitro* activity of the novel echinocandin CD101 at pH 7 and 4 against *Candida* spp. isolates from patients with vulvovaginal candidiasis. *J. Antimicrob. Chemother.* 72, 1355–1358. doi: 10.1093/jac/dkx008

Boskey, E. R., Cone, R. A., Whaley, K. J., and Moench, T. R. (2001). Origins of vaginal acidity: high D/L lactate ratio is consistent with bacteria being the primary source. *Hum. Reprod.* 16, 1809–1813. doi: 10.1093/humrep/16.9.1809

Boskey, E. R., Telsch, K. M., Whaley, K. J., Moench, T. R., and Cone, R. A. (1999). Acid production by vaginal flora *in vitro* is consistent with the rate and extent of vaginal acidification. *Infect. Immun.* 67, 5170–5175.

Childers, D. S., Raziunaite, I., Mol Avelar, G., Mackie, J., Budge, S., Stead, D., et al. (2016). The rewiring of ubiquitination targets in a pathogenic yeast promotes metabolic flexibility, host colonization and virulence. *PLoS Pathog.* 12:e1005566. doi: 10.1371/journal.ppat.1005566

Cottier, F., Tan, A. S., Xu, X., Wang, Y., and Pavelka, N. (2015). MIG1 regulates resistance of *Candida albicans* against the fungistatic effect of weak organic acids. *Eukaryot. Cell.* 14, 1054–1061. doi: 10.1128/EC.00129-15

Cottier, F., Tan, A. S. M., Yurieva, M., Liao, W., Lum, J., Poidinger, M., et al. (2017). The transcriptional response of *Candida albicans* to weak organic acids, carbon source, and MIG1 inactivation unveils a role for HGT16 in mediating the fungistatic effect of acetic acid. *G3 (Bethesda)* 7, 3597–3604. doi: 10.1534/g3.117.300238

Cunha, D. V., Salazar, S. B., Lopes, M. M., and Mira, N. P. (2017). Mechanistic insights underlying tolerance to acetic acid stress in vaginal *candida glabrata* clinical isolates. *Front. Microbiol.* 8:259. doi: 10.3389/fmicb.2017.00259

Danby, C. S., Boikov, D., Rautemaa-Richardson, R., and Sobel, J. D. (2012). Effect of pH on *in vitro* susceptibility of *Candida glabrata* and *Candida albicans* to 11 antifungal agents and implications for clinical use. *Antimicrob. Agents Chemother.* 56, 1403–1406. doi: 10.1128/AAC.05025-11

Davis, D., Wilson, R. B., and Mitchell, A. P. (2000). RIM101-dependent and-independent pathways govern pH responses in *Candida albicans*. *Mol. Cell. Biol.* 20, 971–978. doi: 10.1128/MCB.20.3.971-978.2000

Dujon, B., Sherman, D., Fischer, G., Durrens, P., Casaregola, S., Lafontaine, I., et al. (2004). Genome evolution in yeasts. *Nature* 430, 35–44. doi: 10.1038/nature02579

Fidel, P. L. Jr., Cutright, J. L., Tait, L., and Sobel, J. D. (1996). A murine model of *Candida glabrata* vaginitis. *J. Infect. Dis.* 173, 425–431.

Goncalves, B., Ferreira, C., Alves, C. T., Henriques, M., Azeredo, J., and Silva, S. (2016). Vulvovaginal candidiasis: epidemiology, microbiology and risk factors. *Crit. Rev. Microbiol.* 42, 905–927. doi: 10.3109/1040841X.2015.1091805

Hickey, R. J., Zhou, X., Pierson, J. D., Ravel, J., and Forney, L. J. (2012). Understanding vaginal microbiome complexity from an ecological perspective. *Transl. Res.* 160, 267–282. doi: 10.1016/j.trsl.2012.02.008

Jandric, Z., and Schuller, C. (2011). Stress response in *Candida glabrata*: pieces of a fragmented picture. *Fut. Microbiol.* 6, 1475–1484. doi: 10.2217/fmb.11.131

Kasper, L., Miramon, P., Jablonowski, N., Wisgott, S., Wilson, D., Brunke, S., et al. (2015). Antifungal activity of clotrimazole against *Candida albicans* depends on carbon sources, growth phase and morphology. *J. Med. Microbiol.* 64, 714–723. doi: 10.1099/jmm.0.000082

Mira, N. P., Teixeira, M. C., and Sa-Correia, I. (2010). Adaptive response and tolerance to weak acids in Saccharomyces cerevisiae: a genome-wide view. *OMICS* 14, 525–540. doi: 10.1089/omi.2010.0072

Moosa, M. Y. S., Sobel, J. D., Elhalis, H., Du, W., and Akins, R. A. (2004). Fungicidal activity of fluconazole against *Candida albicans* in a synthetic vagina-simulative medium. *Antimicrob. Agents Chemother.* 48, 161–167. doi: 10.1128/AAC.48.1.161-167.2004

Mota, S., Alves, R., Carneiro, C., Silva, S., Brown, A. J., Istel, F., et al. (2015). *Candida glabrata* susceptibility to antifungals and phagocytosis is modulated by acetate. *Front. Microbiol.* 6:919. doi: 10.3389/fmicb.2015.00919

O'hanlon, D. E., Moench, T. R., and Cone, R. A. (2011). In vaginal fluid, bacteria associated with bacterial vaginosis can be suppressed with lactic acid but not hydrogen peroxide. *BMC Infect. Dis.* 11:200. doi: 10.1186/1471-2334-11-200

O'hanlon, D. E., Moench, T. R., and Cone, R. A. (2013). Vaginal pH and microbicidal lactic acid when *lactobacilli* dominate the microbiota. *PLoS ONE* 8:e80074. doi: 10.1371/journal.pone.0080074

Owen, D. H., and Katz, D. F. (1999). A vaginal fluid simulant. *Contraception* 59, 91–95.

Parolin, C., Marangoni, A., Laghi, L., Foschi, C., Nahui Palomino, R. A., Calonghi, N., et al. (2015). Isolation of Vaginal *Lactobacilli* and Characterization of Anti-*Candida* Activity. *PLoS ONE* 10:e0131220. doi: 10.1371/journal.pone.0131220

Petrova, M. I., Lievens, E., Malik, S., Imholz, N., and Lebeer, S. (2015). *Lactobacillus* species as biomarkers and agents that can promote various aspects of vaginal health. *Front. Physiol.* 6:81. doi: 10.3389/fphys.2015.00081

Salazar, S. B., Wang, C., Münsterkötter, M., Okamoto, M., Takahashi-Nakaguchi, A., Chibana, H., et al. (2018). Comparative genomic and transcriptomic analyses unveil novel features of azole resistance and adaptation to the human host in *Candida glabrata*. *FEMS Yeast. Res* 18:fox079. doi: 10.1093/femsyr/fox079

Sobel, J. D. (2007). Vulvovaginal candidosis. *Lancet* 369, 1961–1971. doi: 10.1016/S0140-6736(07)60917-9

Sobel, J. D. (2016). Recurrent vulvovaginal candidiasis. *Am. J. Obstet. Gynecol.* 214, 15–21. doi: 10.1016/j.ajog.2015.06.067

Sobel, J. D., and Chaim, W. (1997). Treatment of Torulopsis glabrata vaginitis: retrospective review of boric acid therapy. *Clin. Infect. Dis.* 24, 649–652.

Sobel, J. D., Faro, S., Force, R. W., Foxman, B., Ledger, W. J., Nyirjesy, P. R., et al. (1998). Vulvovaginal candidiasis: epidemiologic, diagnostic, and therapeutic considerations. *Am. J. Obstet. Gynecol.* 178, 203–211.

Sosinska, G. J., De Groot, P. W. J., Teixeira De Mattos, M. J., Dekker, H. L., De Koster, C. G., Hellingwerf, K. J., et al. (2008). Hypoxic conditions and iron restriction affect the cell-wall proteome of *Candida albicans* grown under vagina-simulative conditions. *Microbiology* 154, 510–520. doi: 10.1099/mic.0.2007/012617-0

Spitzer, M., and Wiederhold, N. P. (2018). Reduced antifungal susceptibility of vulvovaginal *Candida* species at normal vaginal pH Levels: clinical implications. *J. Low Genit. Tract. Dis.* 22:152–8. doi: 10.1097/LGT.0000000000000383

Subcommittee on Antifungal Susceptibility Testing (AFST) of the ESCMID European Committee for Antimicrobial Susceptibility Testing (EUCAST) et al. 2003. Rodriguez-Tudela, J. L, Barchiest, F., Bille, J., Chryssanthou, E., Cuenta-Estrella, M., et al. (2003). EUCAST discussion documente E.Dis 7.1: Method for the determination of minimum inhibitory concentration (MIC) by broth dilution of fermentative yeasts. *Clin. Microbiol. Infect.* 14:398–405. doi: 10.1111/j.1469-0691.2007.01935.x

Tachedjian, G., Aldunate, M., Bradshaw, C. S., and Cone, R. A. (2017). The role of lactic acid production by probiotic *Lactobacillus* species in vaginal health. *Res. Microbiol.* 168, 782–792. doi: 10.1016/j.resmic.2017.04.001

Ueno, K., Matsumoto, Y., Uno, J., Sasamoto, K., Sekimizu, K., Kinjo, Y., et al. (2011). Intestinal resident yeast *Candida glabrata* requires Cyb2p-mediated lactate assimilation to adapt in mouse intestine. *PLoS ONE* 6:e24759. doi: 10.1371/journal.pone.0024759

Vermitsky, J. P., Earhart, K. D., Smith, W. L., Homayouni, R., Edlind, T. D., and Rogers, P. D. (2006). Pdr1 regulates multidrug resistance in *Candida glabrata*: gene disruption and genome-wide expression studies. *Mol. Microbiol.* 61, 704–722. doi: 10.1111/j.1365-2958.2006.05235.x

Vieira, N., Casal, M., Johansson, B., Maccallum, D. M., Brown, A. J., and Paiva, S. (2010). Functional specialization and differential regulation of short-chain carboxylic acid transporters in the pathogen *Candida albicans*. *Mol. Microbiol.* 75, 1337–1354. doi: 10.1111/j.1365-2958.2009.07003.x

Yan, D. H., Lu, Z., and Su, J. R. (2009). Comparison of main *lactobacillus* species between healthy women and women with bacterial vaginosis. *Chin. Med. J.* 122, 2748–2751. doi: 10.3760/cma.j.issn.0366-6999.2009.22.014

Conflict of Interest Statement: The authors declare that the research was conducted in the absence of any commercial or financial relationships that could be construed as a potential conflict of interest.

frontiers in Microbiology

ORIGINAL RESEARCH
published: 08 January 2019
doi: 10.3389/fmicb.2018.03196

Synergistic Impacts of Organic Acids and pH on Growth of *Pseudomonas aeruginosa*: A Comparison of Parametric and Bayesian Non-parametric Methods to Model Growth

Francesca M. L. Bushell[1,2†], *Peter D. Tonner*[3,4], *Sara Jabbari*[2,5], *Amy K. Schmid*[3,6] *and Peter A. Lund*[1,2*]

[1] School of Biosciences, University of Birmingham, Birmingham, United Kingdom, [2] Institute of Microbiology and Infection, University of Birmingham, Birmingham, United Kingdom, [3] Department of Biology, Duke University, Durham, NC, United States, [4] Statistical Engineering Division, National Institute of Standards and Technology, Gaithersburg, MD, United States, [5] School of Mathematics, University of Birmingham, Birmingham, United Kingdom, [6] Center for Genomics and Computational Biology, Duke University, Durham, NC, United States

OPEN ACCESS

Edited by:
Conor P. O'Byrne,
National University of Ireland Galway,
Ireland

Reviewed by:
Stanley Brul,
University of Amsterdam, Netherlands
Nuno Pereira Mira,
Instituto de Bioengenharia e Biociências (IBB), Portugal
Kimon Andreas Karatzas,
University of Reading,
United Kingdom

***Correspondence:**
Peter A. Lund
lundpa@gmail.com

†Present Address:
Francesca M. L. Bushell,
The Francis Crick Institute, London,
United Kingdom

Specialty section:
This article was submitted to Microbial Physiology and Metabolism, a section of the journal Frontiers in Microbiology

Received: 08 August 2018
Accepted: 10 December 2018
Published: 08 January 2019

Citation:
Bushell FML, Tonner PD, Jabbari S, Schmid AK and Lund PA (2019) Synergistic Impacts of Organic Acids and pH on Growth of Pseudomonas aeruginosa: A Comparison of Parametric and Bayesian Non-parametric Methods to Model Growth. Front. Microbiol. 9:3196. doi: 10.3389/fmicb.2018.03196

Different weak organic acids have significant potential as topical treatments for wounds infected by opportunistic pathogens that are recalcitrant to standard treatments. These acids have long been used as bacteriostatic compounds in the food industry, and in some cases are already being used in the clinic. The effects of different organic acids vary with pH, concentration, and the specific organic acid used, but no studies to date on any opportunistic pathogens have examined the detailed interactions between these key variables in a controlled and systematic way. We have therefore comprehensively evaluated the effects of several different weak organic acids on growth of the opportunistic pathogen *Pseudomonas aeruginosa*. We used a semi-automated plate reader to generate growth profiles for two different strains (model laboratory strain PAO1 and clinical isolate PA1054 from a hospital burns unit) in a range of organic acids at different concentrations and pH, with a high level of replication for a total of 162,960 data points. We then compared two different modeling approaches for the interpretation of this time-resolved dataset: parametric logistic regression (with or without a component to include lag phase) vs. non-parametric Gaussian process (GP) regression. Because GP makes no prior assumptions about the nature of the growth, this method proved to be superior in cases where growth did not follow a standard sigmoid functional form, as is common when bacteria grow under stress. Acetic, propionic and butyric acids were all more detrimental to growth than the other acids tested, and although PA1054 grew better than PAO1 under non-stress conditions, this difference largely disappeared as the levels of stress increased. As expected from knowledge of how organic acids behave, their

effect was significantly enhanced in combination with low pH, with this interaction being greatest in the case of propionic acid. Our approach lends itself to the characterization of combinatorial interactions between stressors, especially in cases where their impacts on growth render logistic growth models unsuitable.

Keywords: organic acid, Gaussian process, parametric (model-based) analysis, *Pseudomonas aeruginosa*, low pH, opportunistic pathogen

INTRODUCTION

Although bacterial stress responses are affected by the precise nature of the stress and the environment in which it occurs, detailed studies on the impact of systematically varying the factors that affect stress responses are rarely reported. While this is understandable from a pragmatic point of view, as varying parameters in several different factors requires multiple replicated experiments, it limits our understanding of these responses, and may mean that the conditions chosen under which to study them are not the most informative. Importantly, it also means that in many cases we lack both data and robust analytical tools that could reveal interactions between different factors, and how these might influence the ability of the organism to survive or grow in the stressful environment. This information is valuable both because it can lead to greater insights into the mechanism of the stress, and because it can have applied implications in (for example) optimizing strain construction and growth conditions for biotechnological processes, or designing effective strategies for removal of a particular organism or organisms. This latter point is particularly relevant given the pressing need to develop methods to reduce the use of antibiotics, and to treat organisms which may be resistant to multiple antibiotics.

A good example of infections which are difficult to treat are the opportunistic infections that can arise in open wounds, such as burns or skin ulcers. These often become colonized by bacteria or fungi that normally live harmlessly on the skin. Such infections are often hard to treat with antibiotics, particularly once they develop as biofilms. The two major organisms found in such infections are *Pseudomonas aeruginosa* and *Staphylococcus aureus*. The latter is the most common organism causing infection in burns, but infections caused by gram negative bacteria are the leading cause of mortality in burns patients (Branski et al., 2009; Williams et al., 2009; Høiby et al., 2010; Norbury et al., 2016). The increasing prevalence of bacteria resistant to multiple antibiotics in burns infections is associated with more surgical intervention and longer hospital stays for patients (van Langeveld et al., 2017). For this reason, alternative topical treatments are being sought for clinical use.

Organic acids (OAs) are generally more effective (at the same pH) than inorganic acids at preventing bacterial growth (Wolin, 1969; Cherrington et al., 1991; Hirshfield et al., 2003). This has led to their extensive use as preservatives in the food industry (Brul and Coote, 1999), and also to their increased use as topical agents to treat infected wounds, particularly burn wounds and diabetic ulcers (Phillips et al., 1968; Milner, 1992; Sloss et al., 1993; Nagoba et al., 2013b; Bjarnsholt et al., 2015; Halstead et al., 2015; Agrawal et al., 2017). Indeed, the use of vinegar (acetic acid) for its antibacterial properties has good historical precedents (Johnston and Gaas, 2006). The antibacterial action of OAs stems in part from their ability to diffuse freely across bacterial membranes in their uncharged state, and to then dissociate inside the bacterial cell (Salmond et al., 1984; Russell and Diez-Gonzalez, 1998; Hirshfield et al., 2003; Saparov et al., 2006; Slonczewski et al., 2009). Entry of OAs causes the proton gradient to partially collapse across the membrane, since the anion can combine with protons pumped out of the cell by the electron transport chain, then carry them back into the cell, bypassing the FoF1 ATPase (Sheu et al., 1975; Salmond et al., 1984). OAs also decrease the internal pH of the cell, although OAs are not chemiosmotic gradient uncouplers in the classical sense (Russell, 1992; Russell and Diez-Gonzalez, 1998). However, despite these effects, the toxicity of OAs does not correlate particularly well with their pKa (Sheu et al., 1975), suggesting that OA effects cannot be attributed solely to their impact on the proton gradient or the cell's internal pH. OA types vary depending on their structure in the extent to which they partition into the membrane, and the anions released when the OAs dissociate inside the cell may have different effects on cellular osmolarity and metabolism (Roe et al., 1998, 2002). The effect of OAs on growth of a given bacterial species can also vary with the particular strain chosen (King et al., 2010). Determining which OAs will be most effective against a particular bacterium therefore requires a systematic study on the combined impact of concentration and pH of several different OAs, and this needs to be done in more than one strain. However, such comprehensive comparisons have not been conducted to date for any bacterial species of which we are aware. As part of a larger investigation of the impact of OAs on the opportunistic pathogen *Pseudomonas aeruginosa,* we have therefore undertaken such a comparative study, investigating the combined effects of seven different OAs at three different concentrations and five different pH values for two different strains: a recent isolate from a burns unit, PA1054, and the strain PAO1, itself originally isolated from a wound but now used worldwide as a reference strain (Klockgether et al., 2010). These data then required analysis so that comparisons of the effects of the different factors and the interactions between them could be made in a statistically robust fashion.

Multifactorial studies into organismal behavior under stress require reproducible assays with easily measured outputs, the simplest of which are measurements of growth (or of a suitable proxy, such as optical density). In an ideal experiment, growth rates are monitored over time under a range of different conditions. Growth parameters are then extracted by fitting

the data to a suitable model, and they are compared in order to evaluate the relative importance of the different conditions. Typically, these parameters include the length of lag phase, maximum growth rate during logarithmic phase, and final carrying capacity. The carrying capacity is the maximum population density which can be reached in a growth experiment; in a logistical model this value is approached asymptotically over time. In experiments, it is represented by the optical density of the culture when it reaches stationary phase. As long as the growth of the organism can be fitted to a logistic or modified logistic equation, this approach is feasible (Zwietering et al., 1990; Baranyi and Roberts, 1994). Difficulties arise, however, when bacterial growth departs from simple logistic growth, as may happen when cells are growing under stress as the cell's resources may be partially reallocated from growth to repair stress-mediated damage or to ameliorate or compensate for non-optimal conditions in the cell (Darnell et al., 2017; Tonner et al., 2017). There is an extensive literature, largely based in food microbiology where theoretical predictions of growth are crucial for developing safe manufacturing and storage processes, on ways in which deviations from simple logistic growth can be modeled and statistically tested [reviewed in Peleg and Corradini (2011)]. However, although these methods can be quite successful, they generally require either an underlying assumption of parametric growth, some prior knowledge of how growth conditions may perturb this, or complex fitting procedures.

An alternative solution to this problem is to use Gaussian process (GP) regression models for data fitting (Tonner et al., 2017), as these can provide fits to any functional form without needing any prior assumptions about the way in which genetic and/or environmental perturbations affect growth, but instead rely on a process of learning growth behavior directly from the data. A version of this approach (called B-GREAT) was developed and implemented for modeling and determining the statistical differences between growth of wild type vs. mutated strains of the model archaeal species *Halobacterium salinarum*. The growth of a large collection of different yeast strains was also tested. In both organisms, B-GREAT was found to outperform four well-used parametric methods under a range of stress conditions (Tonner et al., 2017). B-GREAT could also be used to recover standard growth parameters with high accuracy when the growth curves showed a good fit to logistic growth. B-GREAT accurately estimated these parameters, especially for growth data of strains subjected to stress (Tonner et al., 2017). A further development of this model (FANOVA) incorporated functional analysis of variance, thus allowing the effects of different factors on growth, including their interaction, to be incorporated within a unified modeling framework (Darnell et al., 2017).

In this study we have compared two parametric methods (fitting to a simple logistic equation with or without a term for the lag phase) with a Bayesian hierarchical GP model of phenotypes, called *phenom*, for their accuracy in fits to the growth data and in statistical comparisons of the effects of variations in OA and pH on growth. The major novelty of *phenom*, compared to the previous B-GREAT and FANOVA growth models of which it is an extension, is that it allows direct analysis of the interaction term. Our data show the superiority of the GP regression method over logistic parametric models, particularly when high levels of stress lead to growth behavior that deviates from the expected sigmoid curve. Further, our analyses of the model output demonstrates that the different OA types can be split into two clear groups on the basis of the growth detriment that they cause, while confirming a very strong interaction between OA and pH in affecting bacterial growth.

MATERIALS AND METHODS

Strain Descriptions

Planktonic growth was measured for two strains of *Pseudomonas aeruginosa*: the widely used laboratory strain PAO1 (ATCC 15692), and *Pseudomonas aeruginosa* PA1054, a strain resistant to multiple antibiotics isolated from a patient in the burns unit at the Queen Elizabeth II hospital in Birmingham (Halstead et al., 2015).

Determination of Effects of Organic Acids on Planktonic Growth

P. aeruginosa strains were grown in M9 minimal medium supplemented with 0.4% (w/v) glucose and 0.2% (w/v) cas-amino acids (Fisher Scientific). All growth media were buffered with 100 mM MOPS and 100 mM MES (Burton et al., 2010). Growth kinetics were recorded using a CLARIOstar automated microplate reader (BMG Labtech). Bacteria were grown in clear, flat-bottomed 96 well Costar plates. The edges of the plate (rows A and H and columns 1 and 12) contained sterile media and were used to provide blanks, to test sterility, and to minimize any edge effects. No evidence of cross-contamination was seen in any experiments. 10× M9 salts (which had a starting pH of 5.8) were adjusted to a pH of 7, 6.5, 6, 5.5, or 5 using sodium hydroxide or hydrochloric acid. The salts were then diluted and autoclaved and supplements were added subsequently; this did not cause any significant change in pH. Control experiments (not shown) showed that variation in optical density measurements across the plate was negligible; nevertheless, to minimize any systematic bias, the relative position of the different conditions on plates was changed with each experiment. OAs were added to a final concentration of either 0 mM (control), 5, 10, or 20 mM: at these concentrations, addition of OAs had no significant effect on the measured pH of the buffered growth media. Each experiment was repeated on at least two different days, with a minimum of three independent biological replicates each day. Growth experiments were initiated from independent overnight cultures diluted to a starting OD_{600} of 0.05, with the appropriate media making up the final volume to 200 μl in each well. The plates were incubated in the plate reader at 37°C, with 300 rpm shaking continuously and rigorous 500 rpm shaking for 10 s prior to each read to reduce clumping. Plates were covered with an evaporation resistant lid, maintaining aerobic conditions whilst minimizing evaporation. The OD_{600} was recorded automatically every 15 min for a total of 24 h.

Modeling of Growth Curve Data: (1) Parametric Methods

The first method used a parametric approach to generate fits, $y(t)$, to the OD data measurements to either the simple three-parameter logistic growth equation (which requires estimation of the initial OD value, y_0, intrinsic growth rate, r, and carrying capacity, K):

$$y(t) = \frac{Ky_0 \exp(rt)}{K + y_0\left(\exp(rt) - 1\right)},$$

or to the four-parameter model of Baranyi and Roberts (1994), which incorporates a lag-time, λ, before the onset of exponential phase:

$$y(t) = \frac{Ky_0 \exp(r(t-\lambda))\left(1 - \exp(-rt) + \exp(-r(t-\lambda))\right)}{K + y_0 \exp(r(t-\lambda)) - y_0 \exp(-\lambda r)}.$$

The fitting was performed in (MATLAB., 2012) using the local minimiser *fminsearch* with the objective function given by the *L-2* norm of the absolute error vector. Fits were first performed for the logistic and Baranyi model against the original optical density data. For subsequent comparison with the *phenom* model, an appropriately scaled logistic model (scaled with initial value and log2 transform) was fitted to the data that was scaled for the *phenom* model analysis [as detailed below and in Tonner et al. (2017)]. The relative error (*L-2* norm of the absolute error scaled by the measured OD value at each data point) was used to assess goodness of fit. Failure to fit an accurate curve is reported when the maximum number of function evaluations is exceeded in MATLAB without tolerances being met (default options for *fminsearch* in MATLAB R2017b are used). Bad fits are reported when the relative error is >10 or when final carrying capacity is 1.5 times greater than the control condition of pH 7 with no added organic acid. Input data and model output are freely available at github.com/amyschmid/pseudomonas-organic-acids.

Modeling of Growth Curve Data: (2) Phenom Method

Data Pre-processing

Raw growth data were preprocessed prior to *phenom* modeling as follows. Any time points with missing data were removed prior to analysis. The first 5 time points of every growth curve was removed prior to analysis due to the variability of the growth instrument at these early time points. Data were log2 transformed, then normalized by polynomial regression as described in Tonner et al. (2017), such that the log2 OD values started at zero for all time series. Preprocessed data were standardized to mean = 0 and standard deviation = 1 for input to the *phenom* model. Standardization of model output data was then reverted to the original mean and standard deviation, but kept log2 transformed, for plotting and interpretation. Raw and preprocessed data are provided in the github repository for this study at github.com/amyschmid/pseudomonas-organic-acids.

Phenom Combinatorial Model

Data measured as $y(t, p, m)$ with pH p and molar acid concentration m was modeled with mean

$$\widehat{y}(t,p,m) = \begin{cases} \mu(t), & \text{if } p = 7 \text{ and } m = 0 \\ \mu(t) + \alpha_p(t), & \text{if } p \neq 7 \text{ and } m = 0 \\ \mu(t) + \beta_m(t), & \text{if } p = 7 \text{ and } m \neq 0 \\ \mu(t) + \alpha_p(t) + \beta_m(t) + (\alpha\beta)_{p,m}(t), & \text{otherwise,} \end{cases}$$

where $\mu(t)$ is the grand mean, $\alpha_p(t)$ is the independent effect of pH, $\beta_m(t)$ is the independent effect of acid concentration, and $(\alpha\beta)_{p,m}(t)$ is the interaction of pH and acid concentration. The variable of primary interest is $(\alpha\beta)_{p,m}(t)$, as this represents the impact of pH and acid relative to the independent effects of the two variables. Observations are assumed to be corrupted with Gaussian noise: $y(t,p,m) = \widehat{y}(t,p,m) + \epsilon$, $\epsilon \sim N(0, \sigma_y^2)$. This model (equation 1) corresponds to the null model, M_{null}.

Model Implementation

phenom is implemented using the STAN library, which provides efficient Hamiltonian Monte-Carlo sampling of the model posterior (Carpenter et al., 2017). Additional details of the *phenom* model will be published in a separate paper currently in preparation. Details of the *phenom* model and implementation are available at github.com/ptonner/phenom. *phenom* output data (carrying capacities, relmin values) are given in the **Supplementary Material** and at github.com/amyschmid/pseudomonas-organic-acids.

Post-hoc Analysis of *Phenom* Model Output

Model output was graphed using the R package ggplot2 (Wickham, 2009). *P*-values of significance reported throughout the text were determined using unpaired, two-sided Student's *t*-tests. All R code for *post-hoc* analysis of *phenom* model output is provided in an R markdown file via the github repository for this study github.com/amyschmid/pseudomonas-organic-acids.

RESULTS

Initial Analysis of Growth Curve Data

In order to determine the combined effects of pH and OA on growth of *P. aeruginosa*, we generated 1,680 independent growth curves, consisting of 162,960 data points after establishing optimal conditions for our experiments (**Figure S1**). The effects on planktonic growth of *P. aeruginosa* over 24 h were assessed under conditions varying by the nature of the strain, the specific OA used, the pH, and the concentration of the acid. A control with no added OA was included in every experiment to reduce the expected effects of day to day variation.

Visual inspection of growth curves showed both reduced growth and obvious deviations from normal logistic growth behavior, particularly when cells were grown under increasing levels of stress (a combination of low pH and high OA). As an example, the effects of different OAs at different pH but at the same concentration (arbitrarily chosen as 10 mM) are summarized in **Figure S2** for strain PAO1. This series of

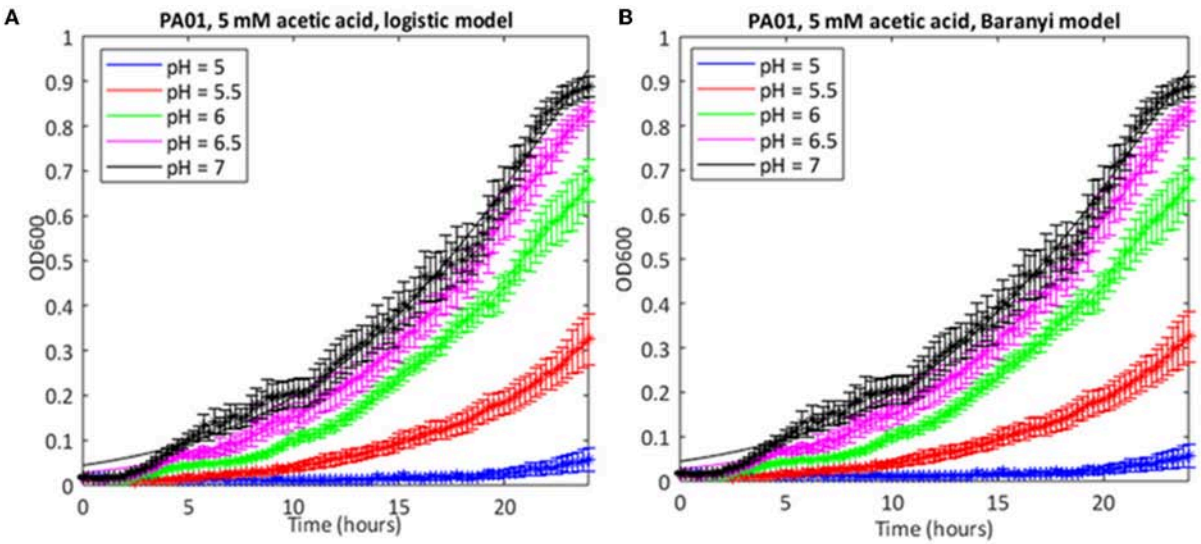

C

	Logistic			Baranyi			
pH	*r* (growth rate)	*K* (carrying capacity)	relative error	*r* (growth rate)	*K* (carrying capacity)	λ (lag time)	relative error
7	0.159	1.68	6.42	0.160	1.66	0.18	6.48
6.5	0.179	1.45	4.21	0.179	1.45	0.01	4.21
6	0.201	1.06	1.79	0.201	1.06	0.02	1.79
5.5	0.162	1.45	1.50	0.162	1.44	0.02	1.50
5	NF	NF	-	0.316	171	19.8	1.42

FIGURE 1 | Use of a simple logistic model to fit growth curve data of strain PAO1 in 5 mM acetic acid at varying pH. Six replicates were used to generate mean and SEM values for growth over 24 h, and best fit curves (shown as continuous lines) were generated using **(A)** the logistic growth curve or **(B)** the Baranyi method, encoded in MATLAB, as described in Materials and Methods. **(C)** Model parameters and error estimates generated by the two fitting protocols. NF, no fit could be obtained. All data given to three sig. figs.

graphs shows that the inhibitory effects of all the OAs at this specific concentration becomes greater as the pH of the medium decreases from 7 to 5, as expected, and that there is clear evidence of variation in the effects of the different OAs. However, these graphs also illustrate the difficulty of establishing the nature of the interactions between the different growth conditions, because of the large number of variables that were investigated. For this reason, we wished to find a way to extract simple growth parameters from the kinetic data, so that quantitative cross-condition and cross-strain comparisons could be made more easily. To do this, we turned to modeling of the growth curve data.

Comparison of Different Parametric Methods for Modeling Growth Curve Data

Because of the large number of growth curves generated in this study, we needed a method to estimate growth parameters where a mathematical model could be used repeatedly on a large dataset with minimal or no further input from the investigator. Initially, we used a model based on the logistic growth equation to fit the growth data, and implemented this in MATLAB. Estimates of the errors showed that in many cases, particularly where the stress level was relatively low, this approach yielded accurate fits to the observed data (**Supplementary Table 1**). Estimates of growth rates and carrying capacity could therefore be taken from these. As an example, the growth of PAO1 in 5 mM acetic acid at pH from 7 to 5 is shown in **Figure 1A**, together with growth parameter estimates, and estimates of the error in the curve fitting (see **Supplementary Table 1** for data from all conditions). The data show a clear step-wise increase in the inhibitory effect of acetic acid on both growth rate and carrying capacity as the pH of the solution drops from pH 7 to 5 (data are plotted using a linear y-axis to make this difference clearer). However, this method failed to find a fit when the pH of the growth medium was reduced to 5.

In many cases where the stress level was higher, the MATLAB routine failed to find a fit to the data using a logistic growth model (as defined in Materials and Methods). In some cases,

model fitting failed because the data deviated from the expected logistic form of the growth curve. For example, growth in 10 mM butyric and low pH is extremely poor (**Figure 2A**), but at higher pH values, the growth curve deviates from the sigmoid form, exhibiting diauxie. No fit could be found for most of these data using the logistic model. In other cases, it was possible to find a fit but the estimates of growth rate (nine cases) or carrying capacities (six cases) were anomalous, being one to three orders of magnitude greater than results derived from similar but less stressful conditions. Generally, these were cases where very little growth had occurred, and where the model was overly sensitive to small increases in initial optical density in fitting the data.

We attempted to improve the fits to the data using a Baranyi model, which accounts for a lag phase, a common feature of the growth of bacterial cultures (Baranyi and Roberts, 1994). In cases where both methods were able to find a good fit, the correlations between the parameter estimates was extremely high (Spearman's rank correlation coefficient >0.99, $p < 0.001$ for both carrying capacity and growth rate). In some cases, the Baranyi method was able to find a fit where the logistic model had failed. For example, for PA1054 growth in 5 mM acetic acid over the pH range 7 to 5, the logistic model was unable to generate a value for growth rate at pH 5 under these conditions, whereas the Baranyi model succeeded in fitting curves under all conditions (**Figure 3**). However, the number of failures was still high. From a total of 220 conditions tested, the logistic method failed to find a fit in a total of 28 cases (20 with PAO1, 8 with PA1054), and was considered to have generated a bad fit (as defined in Materials and Methods) in 30 additional cases (15 for PAO1 and 15 for PA1054). The Baranyi method failed in 17 cases (all PAO1), and generated a bad fit in a further 37 cases (19 PAO1 and 18 PA1054). We therefore turned to the use of the Bayesian non-parametric method *phenom* as an alternative method to estimate growth parameters.

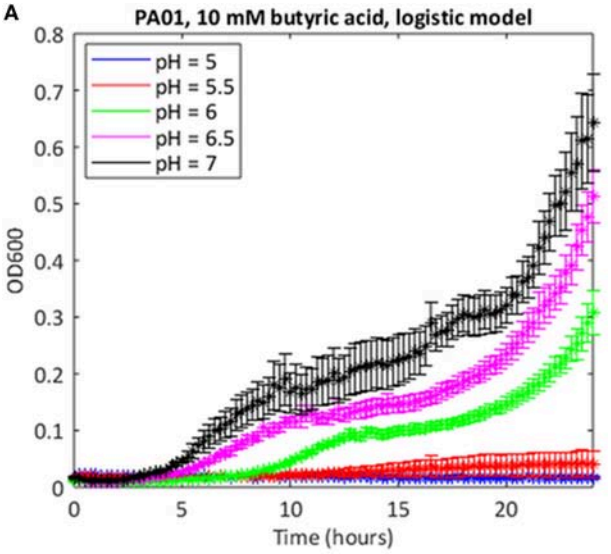

B

pH	*r* (growth rate)	*K* (carrying capacity)	relative error
7	NF	NF	NF
6.5	NF	NF	NF
6	NF	NF	NF
5.5	0.057	0.148	0.84
5	0.043	0.017	0.65

FIGURE 2 | Use of the simple logistic model to fit growth curve data of strain PAO1 in 10 mM butyric acid at varying pH. **(A)** Six replicates were used to generate mean and SEM values for growth over 24 h, and best fit curves were generated as in **Figure 1**. If a curve could not be generated, data points are shown but there is no continuous line. **(B)** Model parameters and error estimates generated by the fitting protocol: NF, no fit could be obtained.

Non-parametric *phenom* Outperforms Parametric Logistic Growth Models for Fitting Growth Curves With Non-canonical Functional Forms

Data from all growth curves were fitted using the *phenom* method described in Materials and Methods, and the results were compared with estimates from the logistic method described in the previous section. We observed that carrying capacity estimates were strongly and significantly correlated between the two models (Spearman's rank $\rho = 0.860$, $p \leq$ 2.2e-16, **Figure 4A**, **Supplementary Tables 1, 2**). However, this correlation is primarily driven by the fact that sum of squares error estimates for the goodness-of-fit of the logistic model to the data are low (i.e., good) for pH or OA conditions alone (**Figures 4B,C**, **Supplementary Table 1**). Erroneous fits to the data from the logistic model increase substantially under pH/OA combinatorial conditions, causing a sharp drop-off in the correlation of logistic carrying capacity estimates with those from *phenom* when cultures are grown under pH and OA combined. We observed that this error inflation in the logistic model fits is due either to inaccurate fits for growth curves that deviate from the sigmoid functional form, or a complete failure to fit the data (as described above and seen in **Figure 2**).

Together these data demonstrate that logistic models are suitable for fitting data when growth approximates a sigmoid function with canonical lag, log, and stationary phases. However, under many of the stress conditions of interest here, which often produce non-standard or flat growth curves, the *phenom* model is more appropriate and more accurate because it is agnostic to the functional form of the data. We therefore conducted all subsequent analysis of the growth data using *phenom*.

Growth of *P. aeruginosa* Is Significantly Impaired by Combinations of Organic Acid and pH Across Strains

To determine which OA/pH combinations were most effective in growth impairment for each of PAO1 and PA1054 strains, we first examined *phenom* model growth curve estimates (**Figure 5**, **Supplementary Table 3**). Each growth curve represents the mean of the model growth estimate given the data for a given OA/acid combination across all model terms combined (independent

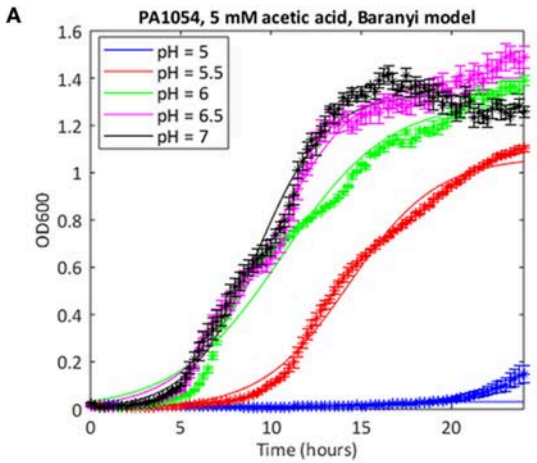

B

pH	*r* (growth rate)	*K* (carrying capacity)	λ (lag time)	relative error
7	0.524	1.33	0.01	3.06
6.5	0.425	1.41	0.01	8.04
6	0.344	1.30	0.002	17.2
5.5	0.412	1.07	0.03	3.84
5	0.652	0.03	0.03	6.99

FIGURE 3 | Use of Baranyi model can improve quality of curve fitting. **(A)** Growth curves of strain PA1054 grown in 5 mM acetic acid at varying pH, generated over 24 h, with best fit curves using the Baranyi growth curve model encoded in MATLAB, as described in Materials and Methods. **(B)** Model parameters and error estimates generated by the fitting protocol.

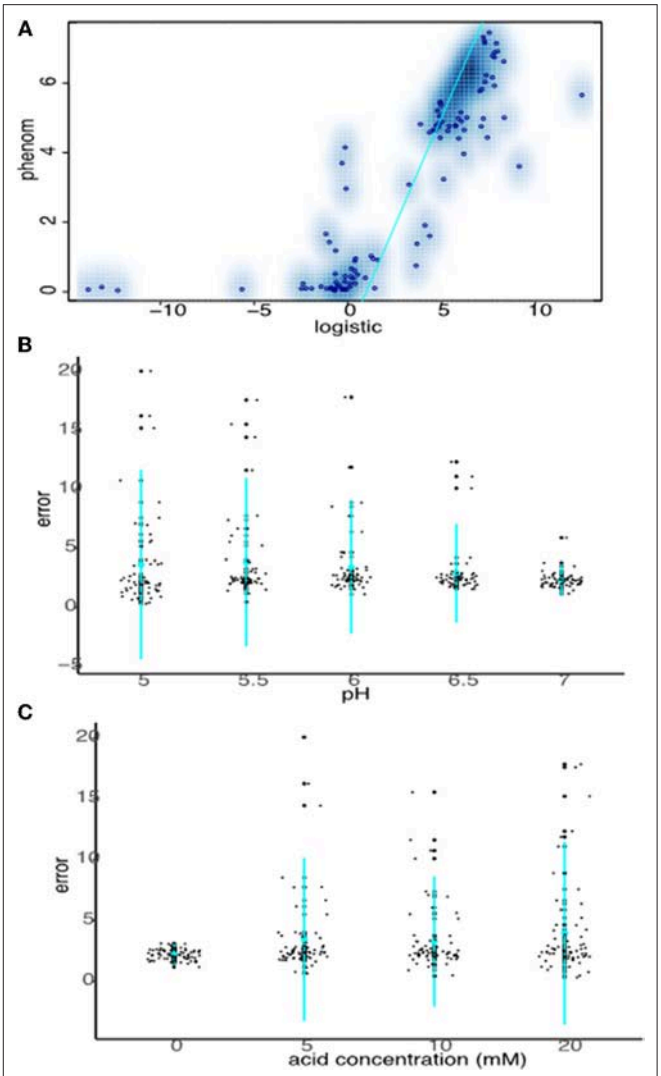

FIGURE 4 | Strong carrying capacity correlation between phenom and logistic models is driven by good logistic fits under non-stress conditions. **(A)** Scatterplot comparing carrying capacity estimates of logistic model carrying capacity estimates with those from the phenom model. Individual points represent the mean of log2 carrying capacity estimates across biological replicate samples for each pH/OA condition in each strain. Blue color density estimates surrounding point clouds represents the 2D kernel density estimate obtained via the smoothScatter() function in R. Cyan line represents the linear regression of the correlation. **(B)** Comparison of logistic model error fits to the data at given pH levels across acid concentrations. Individual points represent the error fit for a given pH/OA concentration combination. Cyan points represent the mean of the data for a given pH, lines represent the standard deviation. **(C)** As in **(B)**, except errors at each OA concentration across pH levels are shown.

effects on growth for each of OA and pH alone, the effect of OA/pH interaction, and the grand mean, see Methods). Regardless of the OA type used, we observed that PA1054 grew faster and reached a higher carrying capacity than PAO1 when OA concentration was low and pH was near neutral, with the exception of malic acid (**Figure 5**, **Figure S3**). However, growth was abolished under the strongest conditions of pH 5 and 20 mM OA, an effect that appeared indistinguishable between the two strains. At high OA concentration and low pH, some acids were more effective in growth inhibition than others. For example, acetic acid at pH 5.5 was completely bacteriostatic, whereas benzoic acid at the same concentrations had no effect on growth (**Figure 5**, **Figure S3**).

Across pH Levels, Some Organic Acids Have Significantly Stronger Bacteriostatic Effects Than Others Regardless of Strain Backgrounds

To quantify the statistical significance of the general trends observed by visual inspection of the growth function predictions from the model, we extracted carrying capacity estimates from the *phenom* model fits as a summary parameter (**Supplementary Table 2**). In general, the carrying capacity estimates reflect the observed trends in the differential effectiveness of OA/pH combinations on bacterial growth inhibition, suggesting that this is an informative summary metric for the growth estimates (compare **Figure 5** with **Figure 6A**). This correspondence is in contrast to the commonly used growth parameter of maximum specific growth rate (μmax), which has no meaning for growth curves with no slope, such as

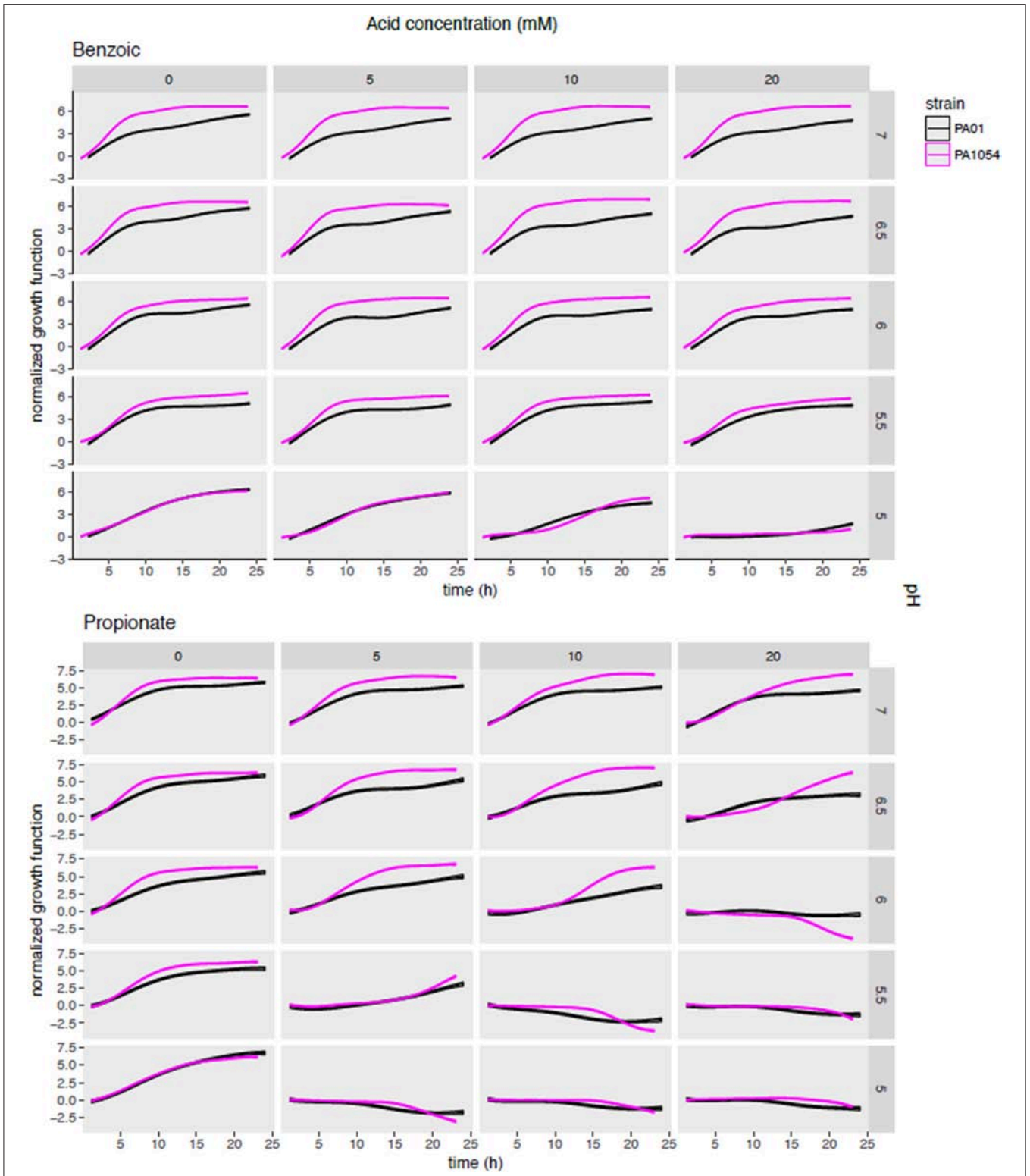

FIGURE 5 | Posterior predictions of growth functions across OA/pH combinations and strains. Each curve represents the growth curve mean (center line of each curve) and standard deviation (width of curve) for phenom growth fit. Each graph depicts a growth curve for each OA/pH combination. Time in hours (0–25) is given on the X-axis and log2 normalized growth function (see Methods) given on the Y-axis. Individual axis numbers are not shown for clarity of the figure, but each sub-graph shown has the same axis ranges. OA concentrations are arranged across the columns of the graph grid, and pH levels down the rows. Black lines represent growth of PAO1 strain, magenta represents PA1054. Results from only two OA types are shown for clarity, with the results from the remaining acids shown in **Figure S3**.

those observed for cultures in high OA and low pH conditions. Carrying capacities of cultures grown in the different OA types were ranked according to the strength of the growth impairment, as quantified by the mean carrying capacity across low pH levels ($\leq$6.0, acid concentration $\geq$5.0) and strains (**Figure 6B**). We found the ranking (from most active) to be as follows: propionic acid > butyric > acetic > citric > sorbic > malic > benzoic acid. We then categorized these OA types as "highly active" (propionic, butyric, acetic acids) or "weakly active" (citric, sorbic, malic, benzoic) based on this ranking. The order does not correlate with pKa or with whether the acid are mono-, di-, or tri-carboxylic. We chose to separate these categories between acetic and citric acid because the difference between the mean carrying capacities of these two OAs was larger than the difference between any other OAs that neighbor one another in the ranked list. Compared to weakly active OAs, cultures grown in highly active OAs had significantly lower carrying capacities in combination with low pH (pH $\leq$ 6, OA concentration $\geq$5 mM; $p \leq$ 1.121e-05; **Figures 6C,D**).

The quantitative effects of OA types on carrying capacities of PAO1 vs. PA1054 were consistent with our visual observations described above: in combinations of pH and OA that allowed for growth, PA1054 cultures reached significantly higher carrying capacities than those of PAO1 (p-value $\leq$ 5.096e-08; **Figure 6E**). In contrast, at growth limiting concentrations (OA $\geq$ 5 mM and pH $\leq$ 6), weakly active OAs appeared to be equally effective in limiting growth of PAO1 and PA1054 strains in combination with low pH (significance of carrying capacity differences between strains under growth limiting combinations for highly active OAs $p \leq$ 0.3858, weakly active OAs $p \leq$ 0.3968; **Figure 6F**). Taken together, these data show that, in terms of culture carrying capacity, and regardless of strain background, highly active OAs (propionic, butyric, acetic acids) may have more effective antimicrobial properties when combined with low pH than the other OAs tested here.

Relative to Either pH or Acid Alone, the Combinatorial Effects of Propionic Acid × pH Is Significantly More Growth Inhibitory Than any Other OA/pH Combination

To determine the synergistic effects on growth inhibition of combining OA and pH, and how this effect varies by strain and by OA type, we next examined the interaction term functions from the *phenom* model output, given by $(\alpha\beta)_{p,m}(t)$ (Methods, **Supplementary Table 4**). This function estimate captures the impact of the interaction between a given pH level and OA concentration relative to the independent effects of each of the two variables. We observed that the interaction term largely reflects the observations for carrying capacity in the sense that some OAs inhibit growth more effectively than others (**Figure 7**, **Figure S3**). For example, the only combination of conditions that were bacteriostatic for benzoic acid were at the highest acid concentration (20 mM) and lowest pH (5) (**Figure 7**).

The interaction term also reveals a synergistic effect on growth for certain OA × pH combinations that appeared different across the two strains. For example, malic acid at 20 mM + pH 5 and propionic acid at 20 mM, pH 6 appeared more effective in growth inhibition of PA1054 than PAO1 relative to either OA or pH alone (**Figure S3**). In contrast, 10 mM sorbic acid + pH 5.5 appeared more effective combination for inhibiting growth of PAO1 than PA1054.

Based on this observation, we used the minimum of the interaction term function ("relmin," **Supplementary Table 5**) as a novel growth metric to summarize and calculate the statistical significance of the combinatorial effects of OA × pH, with the ultimate aim of determining the most effective combination(s) (**Figure 8A**). Consistent with our observations for the interaction term across the growth curve, according to relmin, the propionic acid × pH combination more strongly inhibited the growth of PA1054 than PAO1 (**Figure 8A**), although this difference was not significant ($p \leq$ 0.1743; **Figure 8B**). Similarly, the difference between strains was not significantly different on malic ($p \leq$ 0.409) or sorbic ($p \leq$ 0.7803) acids across low pH levels. Indeed, the behaviors of PAO1 and PA1054 were not significantly different at growth limiting combinations of OA and pH across all conditions according to relmin (0.2444, **Figure 8C**). However, when both strains were considered together, we observed that growth was more strongly and significantly inhibited by the combination of propionic acid and low pH compared to any other OA × pH combination ($p \leq$ 0.02209; **Figure 8D**). Thus, combinatorial effects modeling has enabled us to correct for differences in growth in each of pH or OA conditions alone, providing an advantage (which will be relevant to any similar studies) over classical growth metrics, such as carrying capacity. Moreover, using relmin as a growth metric pinpointed propionic acid × low pH as a more effective antimicrobial strategy than any other combination of conditions tested.

DISCUSSION

The treatment of infections with antimicrobial agents in addition to or in combination with antibiotics is likely to increase in coming years. Strategies that minimize unnecessary antibiotic use are needed because so many organisms are becoming more resistant to all types of antibiotics (World Health Organization., 2014). There is also an ongoing need for antibacterial treatments that are effective in parts of the world where advanced health care is not available or is too expensive. OAs have a history of extensive use in the food industry, where they have long been known to have antibacterial and antifungal properties. In this context, weak OAs [principally acetic acid, though work with citric acid has also been reported (Nagoba et al., 1998, 2013a)] have been used on a small scale for many years to treat infections of wounds, such as burn wounds, diabetic ulcers, and post-operative wounds (Phillips et al., 1968; Milner, 1992; Sloss et al., 1993; Nagoba et al., 1997, 2013b; Ryssel et al., 2009; Bjarnsholt et al., 2015; Halstead et al., 2015; Agrawal et al., 2017). However, most of these publications are in the clinical literature and generally report single cases or small surveys. The evolution of high levels of resistance to OAs has not been reported [though resistance to benzoate under mild acid conditions has been

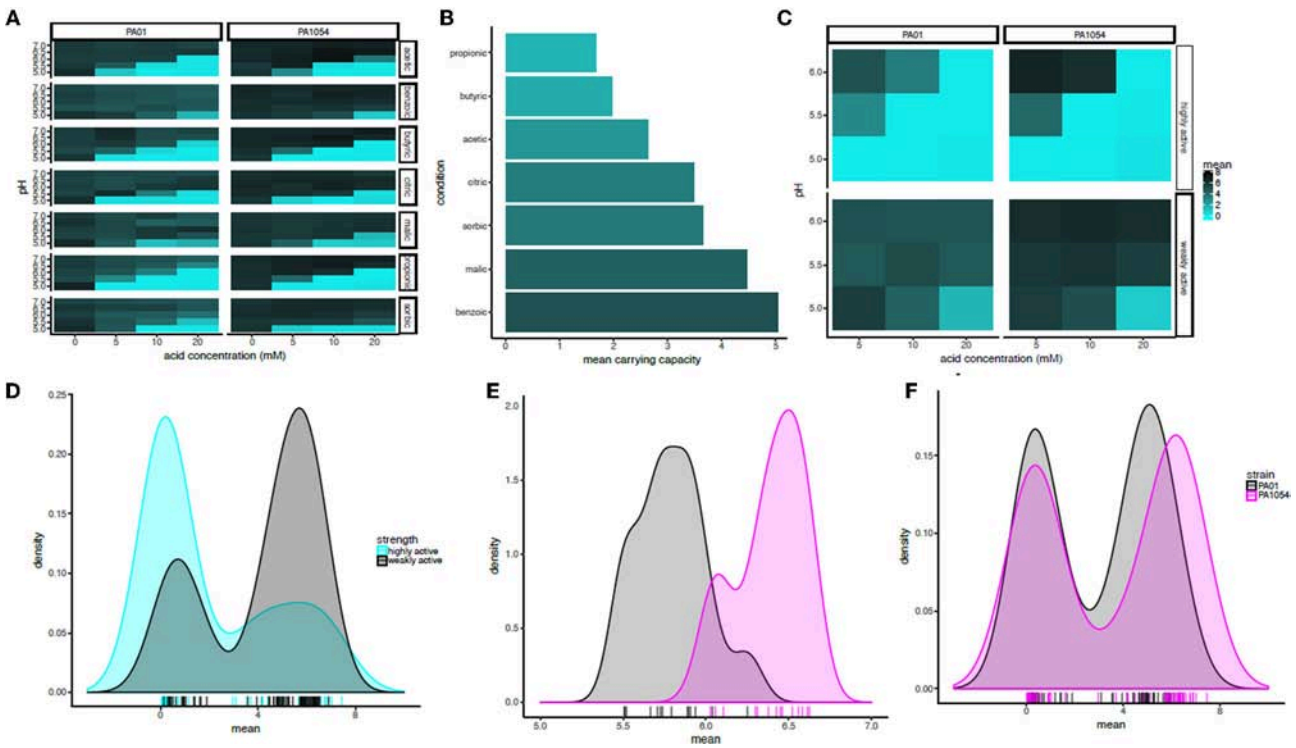

FIGURE 6 | In combination with pH at or below 6, acetic, butyric, and propionic acid impair growth significantly more strongly than the other acids regardless of strain background. **(A)** Heat map of mean carrying capacity estimates from the phenom model. In each heat map subpanel, OA concentrations are shown on the X-axis and pH levels on the Y-axis. In the heat map grid, PAO1 strain is given in the left column and PA1054 in the right. OA type is given in the rows. Brighter cyan intensity indicates a lower carrying capacity (see color legend at far right). **(B)** Bar graph rank ordering OA types in terms of mean carrying capacity across strains. OA types with the greatest bacteriostatic effect are shown at top, the weakest on the bottom. **(C)** Heat map of the mean effect on carrying capacity for highly active OA types (propionic, butyric, acetic), vs. weakly active (citric, sorbic, malic, benzoic). Carrying capacities were averaged across acids in each category at each pH and across strains. **(D)** Density histogram of carrying capacities for highly active OAs (cyan) vs. weakly active OAs (gray) at growth limiting concentrations. Each tick in the rug plot beneath the histograms represents an individual carrying capacity value at a given pH/OA combination in a given strain. **(E)** Density histograms of carrying capacities for cultures of PAO1 and PA1054 at concentrations of OA and pH levels that allow for growth. Ticks in rug plot represent individual carrying capacity values. **(F)** Density histograms of carrying capacities for cultures of PAO1 (black) and PA1054 (magenta) at growth limiting concentrations. Ticks in rug plot represent individual carrying capacity values.

studied using laboratory-based evolution in *E. coli* (Creamer et al., 2017)], which may therefore be another advantage of the use of these agents to treat infections. As far as we are aware, effects of OA concentration and pH, and the interactions between them, have not been reported for *P. aeruginosa,* one of the most common opportunistic pathogens of infected wounds (Williams et al., 2009; Norbury et al., 2016). . Indeed, information about the pH of the formulations used clinically is rarely given, although it can be calculated that many are used at a higher concentration and lower pH than we have used here (for example, a 5% (v/v) acetic acid solution, widely used in the literature cited above, will be 875 mM and have a pH of 2.91). This general lack of information prompted us to undertake the present study. Here, we have focussed on growth in a single defined medium and systematically evaluated the effectiveness of several OA types at stopping growth, including those widely used as food preservatives, paying particular attention to the interactions between pH and concentration. We have focused in this study on inhibition of growth rather than bactericidal action, which requires much higher concentrations of organic acids (FB, data not shown). Data on the effects of the different organic acids and conditions on biofilm formation and removal will be presented in a separate publication.

The combination of low pH and OAs are growth inhibitory for *P. aeruginosa*, as they are for many bacteria. Here we show that pH/OA treatment leads to growth behaviors which are very different from standard logistic growth, even at intermediate concentrations (**Figures 1**, **5**, **7**). In any study where stressors are being altered systematically, data about the impact of these changes should be captured so that comparisons are statistically robust, but our attempts to extract and compare growth parameters using logistic approaches were often not successful. The use of the Gaussian process regression-based method *phenom*, which makes no prior assumptions about the shape of the curve to which the data is being fitted, not only enabled us to generate estimates of growth parameters for all stress conditions, but also provided statistical measures of the significance of these conditions and the interactions between

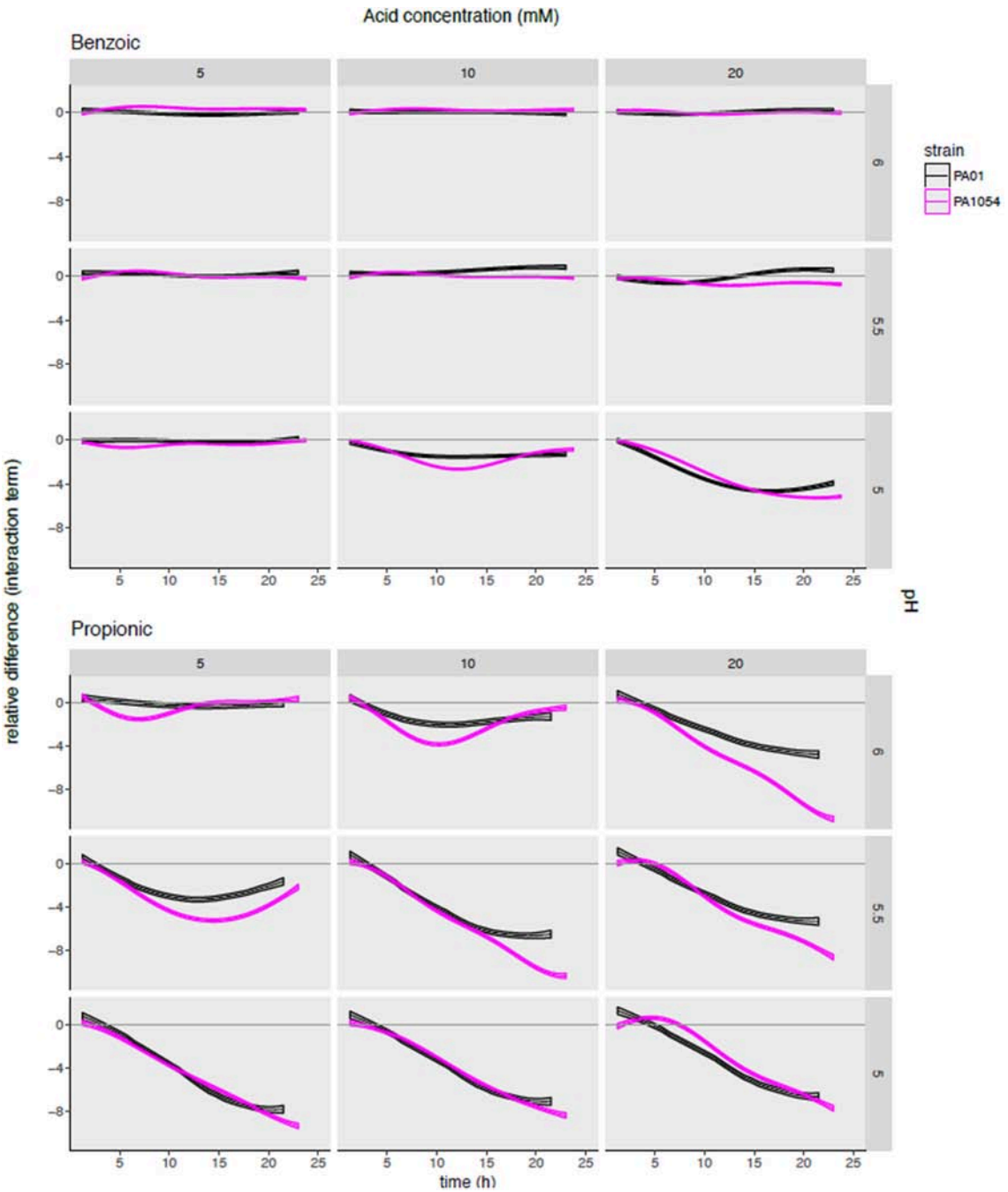

FIGURE 7 | Modeling the combinatorial effects of OA/pH together relative to either pH or OA treatment alone pinpoints effective conditions specific for inhibiting growth of each strain. Each subgraph in the grid plots the posterior predictions of the interaction term functions across each OA/pH combination and strain. Each curve represents the function mean (center line of each curve) and standard deviation (width of curve) for phenom interaction term function. Time in hours (0–25) is given on the X-axis, and the difference in log2 normalized growth compared to either pH or OA independently [i.e., independent effect of pH, $\alpha_p(t)$; and independent effect of OA, $\beta_m(t)$] is given on the Y-axis. Individual axis numbers are not shown for clarity of the figure, but each sub-graph shown has the same axis ranges. OA concentrations are arranged across the columns of the graph grid, and pH levels down the rows. Black lines represent growth of PAO1 strain, magenta represents PA1054. Results from only two OA types (most highly active and most weakly active) are shown for clarity, with the results from the remaining acids shown in **Figure S4**.

them. Under conditions of near to neutral pH and low or no added OA, parameters extracted using either approach correlated well, but our analysis clearly showed the superiority of *phenom* as stress levels increased and growth began to depart from logistic behavior. The different OAs varied in their effects on the two strains studied, with the laboratory strain PAO1 growing less well

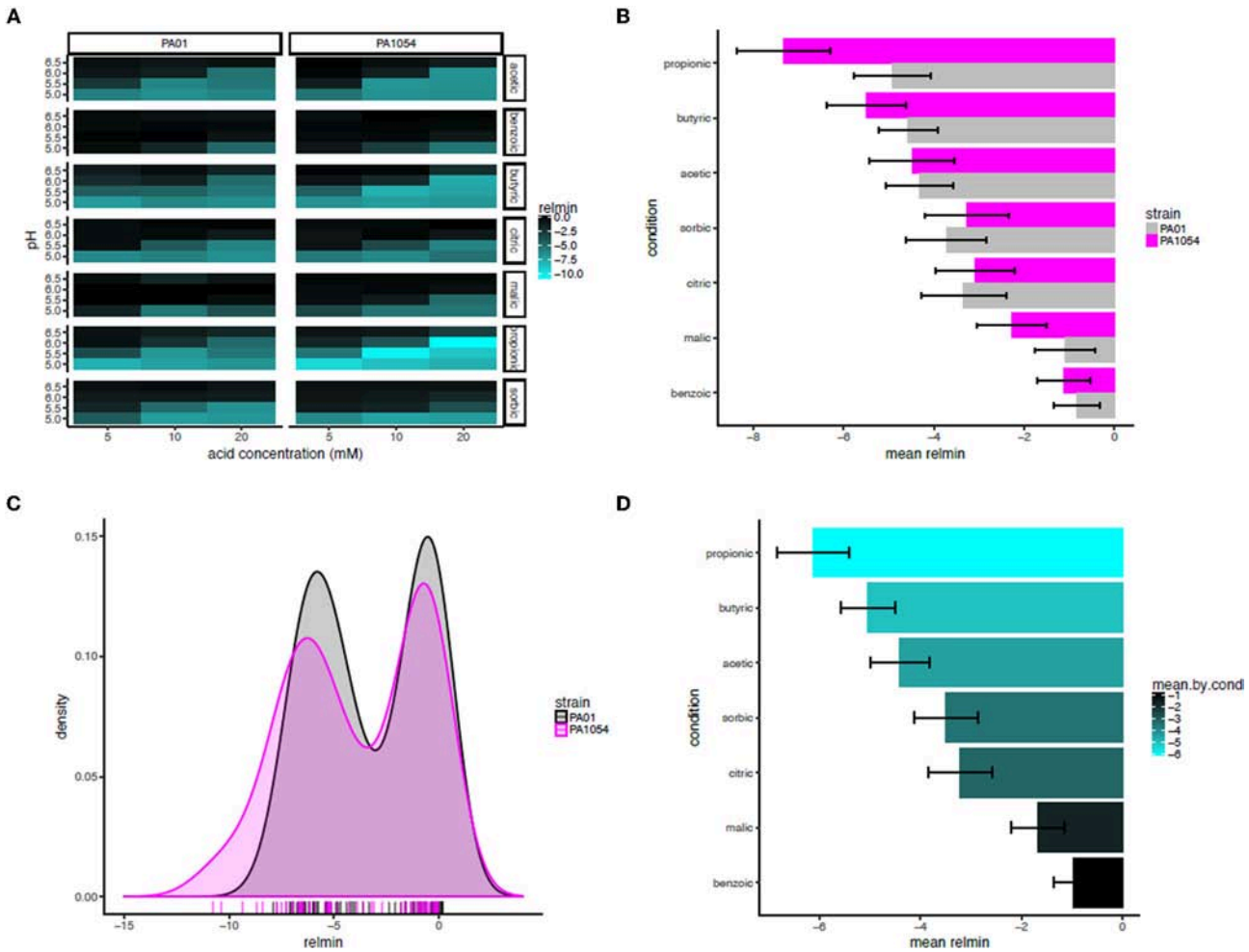

FIGURE 8 | Propionic acid in combination with low pH is the most effective antimicrobial treatment for both strains. **(A)** Heat map of mean minimum relative difference (interaction term) estimates from the phenom model. In each heatmap subpanel, OA concentrations are shown on the X-axis and pH levels on the Y-axis. In the heatmap grid, PAO1 strain is given in the left column and PA1054 in the right. OA type is given in the rows, abbreviated as follows: ac., acetic; ben., benzoic; bu., butyric; cit., citric; mal., malic; prop., propionic; sor., sorbic. Brighter cyan intensity indicates a lower minimum interaction term estimate (see color legend at far right). **(B)** Bar graph rank ordering OA types in terms of mean relative minimum in each strain. OA types with the greatest bacteriostatic effect are shown at top, the ones with the least effect on the bottom. Gray bars, PAO1; magenta bars, PA1054. **(C)** Density histograms of minimum interaction terms for cultures of PAO1 and PA1054 at growth limiting concentrations of OA and pH levels. Ticks in rug plot represent individual carrying capacity values. **(D)** Bar graph rank ordering and quantifying mean of relmin for each OA across strains and OA types. Brighter cyan intensity indicates a lower minimum interaction term estimate (see color legend at far right).

under non-stress conditions than the clinical isolate PA1054, but these differences disappeared as the stress levels increased. This observation implies that use of the laboratory strain to investigate effects of OA treatments on *P. aeruginosa* strains in general is statistically justified, although it would be desirable to extend this observation with a larger number of clinical isolates, such as exists in the international Pseudomonas reference panel (De Soyza et al., 2013). Among the OAs, acetic, propionic and butyric acid were all more inhibitory to growth than the other four acids tested (**Figure 6**).

One particular advantage of *phenom* compared to the previously developed B-GREAT method (Tonner et al., 2017) is that it provides an explicit decomposition of functional effects due to combinations of pH and OA as a function of time, thus enabling modeling of combinatorial effects on growth relative to either condition alone. This improves the B-GREAT method in two ways. First, the lengthscale of functional effects is estimated for each effect independently. This allows for greater flexibility in the shape of functions captured for each independent effect, while B-GREAT only considered a single, global lengthscale parameter. Second, by decomposing the functional effects into separate components, an explicit representation of the variance components is captured. This can be used for comparing overall impacts of independent experimental factors. B-GREAT had only a single variance hyperparameter for all effects combined. Our analysis showed that inhibition of growth increased both with increasing OA concentration and decreasing pH, and inspection of the summary metric relmin, which enables simple statistical

tests on combinatorial effects, showed that the most significant interaction between these two factors was seen in the case of propionic acid (**Figure 8**). The unpleasant smell of propionic acid may restrict its use in the clinic, but we found for all the highly active OAs that strong inhibition of growth was seen at lower concentrations and higher pH levels than those normally reported in clinical studies. Whether these conditions are also able to have an impact on biofilm formation and eradication, and their relationship to levels that are bactericidal, will be the subject of a separate paper.

We have not, in this study, attempted to address the mechanisms by which the different OAs may be acting to prevent bacterial growth. The link between pH and the bacteriostatic effect of weak OAs has long been known, and is thought to arise in part from the ability of OAs to cross the membrane in their dissociated state, and to subsequently ionize in the bacterial cytoplasm (Eklund, 1983; Salmond et al., 1984; Russell, 1992; Russell and Diez-Gonzalez, 1998; Foster, 1999; Hirshfield et al., 2003; Saparov et al., 2006; Slonczewski et al., 2009). As the proportion of OA that is undissociated and able to enter the cell will increase as the pH drops, so this effect will become more pronounced as the pH of the growth medium is lowered. This may then cause decreased cell growth for a variety of reasons including depression of cytoplasmic pH, toxicity of the anion, osmotic stress, and partial collapse of the trans-membrane proton gradient (Brul and Coote, 1999; Hirshfield et al., 2003; Carpenter and Broadbent, 2009; Trček et al., 2015). The fact that the impact of OAs on growth is not solely caused by the decreased pH can be seen by the poor correlation of the carrying capacity with the pKa of the different organic acids (**Table S1**), an effect which has been noted previously (Sheu et al., 1975, Heavin et al., 2009; van Beilen et al., 2014). It should be noted that some of the toxic effects of organic acids can be attributed to their dissociated forms (Eklund, 1983), and that in the experiments described in this study, there will still be substantial amounts of dissociated OA present, as even the lowest pH used is well above the pKa for any of the acids. In addition, OAs partition into membranes to different extents dependent on the nature of their aliphatic regions, which can in turn disrupt membrane function (Alakomi et al., 2000; van Beilen et al., 2014). But as our results here show, these partition coefficients for the different OAs also show no correlation with the impact of the OAs on growth (see **Table S1**). The poor ability of sorbic and benzoic acids to reduce *P. aeruginosa* growth was of particular interest given their widespread and effective use as food preservatives, but the mechanistic reasons for this remain to be explored. The overall impact of different OAs on growth presumably arises from the interaction of many effects, and in the absence of a complete understanding or a predictive model of these, experimental assessment on a case-by-case basis where the impacts of multiple parameters and the interactions between them are tested experimentally is still the best method to determine whether a given OA is a suitable choice for any given application.

This study establishes a reliable method for detecting such effects even when growth curves cannot be fitted by logistic models. This will be particularly useful in looking at the effects of combinations of different anti-microbial compounds at a range of dosage levels, as is now possible using automated high-throughput methods (Chevereau and Bollenbach, 2015; Brochado et al., 2018). Indeed, the use of approaches, such as the *phenom* method described here has considerable potential in any studies concerned with developing new treatments where combinations of compounds are used, as methods to robustly analyse drug combinations have long been sought (Greco et al., 1995; Twarog et al., 2016). The availability of a method that does not fail when growth behavior departs from standard models, and which can statistically account for the strength of interactions between multiple variables, will help searches of large "phenomics" experiments in which conditions studied will be clinically highly relevant, while also aiding the development of a deeper mechanistic understanding of the biological processes underlying the impacts of different stressors on growth.

AUTHOR CONTRIBUTIONS

PL and FB conceived the original study and designed the experiments. FB generated all the experimental data. FB, PL, AS, PT, and SJ analyzed the experimental data. FB, PL, AS, PT, and SJ wrote the paper.

ACKNOWLEDGMENTS

SJ gratefully acknowledges support from the Wellcome Trust (grant code: 1516ISSFFEL9) for funding a parameterisation workshop at the University of Birmingham (UK), the Biotechnology and Biological Sciences Research Council (grant code: BB/M021386/1) and the Medical Research Council (grant code: G1002093). AS gratefully acknowledges support from the National Science Foundation grants 1615685, 1642283, and 1651117. PT acknowledges support from the National Science Foundation Graduate Research Fellowship Program.

SUPPLEMENTARY MATERIAL

The Supplementary Material for this article can be found online at: https://www.frontiersin.org/articles/10.3389/fmicb.2018.03196/full#supplementary-material

REFERENCES

Agrawal, K. S., Sarda, A. V., Shrotriya, R., Bachhav, M., Puri, V., and Nataraj, G. (2017). Acetic acid dressings: finding the Holy Grail for infected wound management. *Indian J. Plast. Surg.* 50, 273–280. doi: 10.4103/ijps.IJPS_245_16

Alakomi, H. L., Skyttä, E., Saarela, M., Mattila-Sandholm, T., Latva-Kala, K., and Helander, I. M. (2000). Lactic acid permeabilizes gram-negative bacteria by disrupting the outer membrane. *Appl. Environ. Microbiol.* 66, 2001–2005. doi: 10.1128/AEM.66.5.2001-2005.2000

Baranyi, J., and Roberts, T. A. (1994). A dynamic approach to predicting bacterial growth in food. *Int. J. Food Microbiol.* 23, 277–294. doi: 10.1016/0168-1605(94)90157-0

Bjarnsholt, T., Alhede, M., Jensen, P. Ø., Nielsen, A. K., Johansen, H. K., Homøe, P., et al. (2015). Antibiofilm properties of acetic acid. *Adv. Wound Care (New Rochelle)* 4, 363–372. doi: 10.1089/wound.2014.0554

Branski, L. K., Al-Mousawi, A., Rivero, H., Jeschke, M. G., Sanford, A. P., and Herndon, D. N. (2009). Emerging infections in burns. *Surg. Infect. (Larchmt).* 10, 389–397. doi: 10.1089/sur.2009.024

Brochado, A. R., Telzerow, A., Bobonis, J., Banzhaf, M., Mateus, A., Selkrig, J., et al. (2018). Species-specific activity of antibacterial drug combinations. *Nature* 559, 259–263. doi: 10.1038/s41586-018-0278-9

Brul, S., and Coote, P. (1999). Preservative agents in foods. Mode of action and microbial resistance mechanisms. *Int. J. Food Microbiol.* 50, 1–17. doi: 10.1016/S0168-1605(99)00072-0

Burton, N. A., Johnson, M. D., Antczak, P., Robinson, A., and Lund, P. A. (2010). Novel aspects of the acid response network of *E. coli* K-12 are revealed by a study of transcriptional dynamics. *J. Mol. Biol.* 401, 726–742. doi: 10.1016/j.jmb.2010.06.054

Carpenter, B., Gelman, A., Hoffman, M. D., Lee, D., Goodrich, B., Betancourt, M., et al. (2017). Stan: a probabilistic programming language. *J. Stat. Softw.* 76:32. doi: 10.18637/jss.v076.i01

Carpenter, C. E., and Broadbent, J. R. (2009). External concentration of organic acid anions and pH: key independent variables for studying how organic acids inhibit growth of bacteria in mildly acidic foods. *J. Food Sci.* 74, R12–R15. doi: 10.1111/j.1750-3841.2008.00994.x

Cherrington, C. A., Hinton, M., Mead, G. C., and Chopra, I. (1991). Organic acids: chemistry, antibacterial activity and practical applications. *Adv. Microb. Physiol.* 32, 87–108. doi: 10.1016/S0065-2911(08)60006-5

Chevereau, G., and Bollenbach, T. (2015). Systematic discovery of drug interaction mechanisms. *Mol. Syst. Biol.* 11:807. doi: 10.15252/msb.20156098

Creamer, K. E., Ditmars, F. S., Basting, P. J., Kunka, K. S., Hamdallah, I. N., Bush, S. P., et al. (2017). Benzoate- and salicylate-tolerant strains of *Escherichia coli* K-12 lose antibiotic resistance during laboratory evolution. *Appl. Environ. Microbiol.* 83:e02736-16. doi: 10.1128/AEM.02736-16

Darnell, C. L., Tonner, P. D., Gulli, J. G., Schmidler, S. C., and Schmid, A. K. (2017). Systematic discovery of archaeal transcription factor functions in regulatory networks through quantitative phenotyping analysis. *mSystems* 2:e00032-17. doi: 10.1128/mSystems.00032-17

De Soyza, A., Hall, A. J., Mahenthiralingam, E., Drevinek, P., Kaca, W., Drulis-Kawa, Z., et al. (2013). Developing an international *Pseudomonas aeruginosa* reference panel. *Microbiologyopen* 2, 1010–1023. doi: 10.1002/mbo3.141

Eklund, T. (1983). The antimicrobial effect of dissociated and undissociated sorbic acid at different pH levels. *J. Appl. Bacteriol.* 54, 383–389.

Foster, J. W. (1999). when protons attack: microbial strategies of acid adaptation. *Curr. Opin. Microbiol.* 2, 170–174. doi: 10.1016/S1369-5274(99)80030-7

Greco, W. R., Bravo, G., and Parsons, J. C. (1995). The search for synergy: a critical review from a response surface perspective. *Pharmacol. Rev.* 47, 331–385.

Halstead, F. D., Rauf, M., Moiemen, N. S., Bamford, A., Wearn, C. M., Fraise, A. P., et al. (2015). The antibacterial activity of acetic acid against biofilm-producing pathogens of relevance to burns patients. *PLoS ONE* 10:e0136190. doi: 10.1371/journal.pone.0136190

Heavin, S. B., Brennan, O. M., Morrissey, J. P., and O'Byrne, C. P. (2009). Inhibition of *Listeria monocytogenes* by acetate, benzoate and sorbate: weak acid tolerance is not influenced by the glutamate decarboxylase system. *Lett. Appl. Microbiol.* 49, 179–185. doi: 10.1111/j.1472-765X.2009.02634.x

Hirshfield, I. N., Terzulli, S., and O'Byrne, C. (2003). Weak organic acids: a panoply of effects on bacteria. *Sci. Prog.* 86(Pt 4), 245–269. doi: 10.3184/003685003783238626

Høiby, N., Bjarnsholt, T., Givskov, M., Molin, S., and Ciofu, O. (2010). Antibiotic resistance of bacterial biofilms. *Int. J. Antimicrob. Agents* 35, 322–332. doi: 10.1016/j.ijantimicag.2009.12.011

Johnston, C. S., and Gaas, C. A. (2006). Vinegar: medicinal uses and antiglycemic effect. *MedGenMed* 8:61.

King, T., Lucchini, S., Hinton, J. C., and Gobius, K. (2010). Transcriptomic analysis of Escherichia coli O157:H7 and K-12 cultures exposed to inorganic and organic acids in stationary phase reveals acidulant- and strain-specific acid tolerance responses. *Appl. Environ. Microbiol.* 76, 6514–6528. doi: 10.1128/AEM.02392-09

Klockgether, J., Munder, A., Neugebauer, J., Davenport, C. F., Stanke, F., Larbig, K. D., et al. (2010). Genome diversity of *Pseudomonas aeruginosa* PAO1 laboratory strains. *J. Bacteriol.* 192, 1113–1121. doi: 10.1128/JB.01515-09

MATLAB. (2012). *MATLAB and Statistics Toolbox Release 8.1*. Natick, MA: The MathWorks, Inc.

Milner, S. M. (1992). Acetic acid to treat *Pseudomonas aeruginosa* in superficial wounds and burns. *Lancet* 340:61. doi: 10.1016/0140-6736(92)92483-V

Nagoba, B., Gandhi, R., Wadher, B., Rao, A., and Selkar, S. (2013a). Simple and effective approach for the treatment of traumatic wounds in non-diabetic patients: a prospective open study. *Int. Wound J.* 10, 585–589. doi: 10.1111/j.1742-481X.2012.01026.x

Nagoba, B. S., Deshmukh, S. R., Wadher, B. J., and Patil, S. B. (1997). Acetic acid treatment of pseudomonal postoperative wound infection. *J. Hosp. Infect.* 36, 243–244. doi: 10.1016/S0195-6701(97)90201-2

Nagoba, B. S., Gandhi, R. C., Wadher, B. J., Deshmukh, S. R., and Gandhi, S. P. (1998). Citric acid treatment of severe electric burns complicated by multiple antibiotic resistant *Pseudomonas aeruginosa*. *Burns* 24, 481–483. doi: 10.1016/S0305-4179(98)00052-7

Nagoba, B. S., Selkar, S. P., Wadher, B. J., and Gandhi, R. C. (2013b). Acetic acid treatment of pseudomonal wound infections–a review. *J. Infect. Public Health* 6, 410–415. doi: 10.1016/j.jiph.2013.05.005.

Norbury, W., Herndon, D. N., Tanksley, J., Jeschke, M. G., and Finnerty, C. C. (2016). Infection in burns. *Surg. Infect. (Larchmt).* 17, 250–255. doi: 10.1089/sur.2013.134

Peleg, M., and Corradini, M. G. (2011). Microbial growth curves: what the models tell us and what they cannot. *Crit. Rev. Food Sci. Nutr.* 51, 917–945. doi: 10.1080/10408398.2011.570463

Phillips, I., Lobo, A. Z., Fernandes, R., and Gundara, N. S. (1968). Acetic acid in the treatment of superficial wounds infected by *Pseudomonas aeruginosa*. *Lancet* 1, 11–14. doi: 10.1016/S0140-6736(68)90004-4

Roe, A. J., McLaggan, D., Davidson, I., O'Byrne, C., and Booth, I. R. (1998). Perturbation of anion balance during inhibition of growth of *Escherichia coli* by weak acids. *J. Bacteriol.* 180, 767–772.

Roe, A. J., O'Byrne, C., McLaggan, D., and Booth, I. R. (2002). Inhibition of Escherichia coli growth by acetic acid: a problem with methionine biosynthesis and homocysteine toxicity. *Microbiology* 148(Pt 7), 2215–2222. doi: 10.1099/00221287-148-7-2215

Russell, J. B. (1992). Another explanation for the toxicity of fermentation acids at low pH: anion accumulation versus uncoupling. *J. Appl. Bacteriol.* 72, 363–370. doi: 10.1111/j.1365-2672.1992.tb04990.x

Russell, J. B., and Diez-Gonzalez, F. (1998). The effects of fermentation acids on bacterial growth. *Adv. Microb. Physiol.* 39, 205–234. doi: 10.1016/S0065-2911(08)60017-X

Ryssel, H., Kloeters, O., Germann, G., Schäfer, T., Wiedemann, G., and Oehlbauer, M. (2009). The antimicrobial effect of acetic acid–an alternative to common local antiseptics? *Burns* 35, 695–700. doi: 10.1016/j.burns.2008.11.009

Salmond, C. V., Kroll, R. G., and Booth, I. R. (1984). The effect of food preservatives on pH homeostasis in *Escherichia coli*. *J. Gen. Microbiol.* 130, 2845–2850. doi: 10.1099/00221287-130-11-2845.

Saparov, S. M., Antonenko, Y. N., and Pohl, P. (2006). A new model of weak acid permeation through membranes revisited: does overton still rule? *Biophys. J.* 90, L86–88. doi: 10.1529/biophysj.106.084343

Sheu, C. W., Salomon, D., Simmons, J. L., Sreevalsan, T., and Freese, E. (1975). Inhibitory effects of lipophilic acids and related compounds on bacteria and mammalian cells. *Antimicrob. Agents Chemother.* 7, 349–363. doi: 10.1128/AAC.7.3.349

Slonczewski, J. L., Fujisawa, M., Dopson, M., and Krulwich, T. A. (2009). Cytoplasmic pH measurement and homeostasis in bacteria and archaea. *Adv. Microb. Physiol.* 55, 1–79, 317. doi: 10.1016/S0065-2911(09)05501-5

Sloss, J. M., Cumberland, N., and Milner, S. M. (1993). Acetic acid used for the elimination of *Pseudomonas aeruginosa* from burn and soft tissue wounds. *J. R. Army Med. Corps* 139, 49–51. doi: 10.1136/jramc-139-02-04

Tonner, P. D., Darnell, C. L., Engelhardt, B. E., and Schmid, A. K. (2017). Detecting differential growth of microbial populations with Gaussian process regression. *Genome Res.* 27, 320–333. doi: 10.1101/gr.210286.116

Trček, J., Mira, N. P., and Jarboe, L. R. (2015). Adaptation and tolerance of bacteria against acetic acid. *Appl. Microbiol. Biotechnol.* 99, 6215–6229. doi: 10.1007/s00253-015-6762-3

Twarog, N. R., Stewart, E., Hammill, C. V., and Shelat, A. A. (2016). BRAID: a unifying paradigm for the analysis of combined drug action. *Sci. Rep.* 6:25523. doi: 10.1038/srep25523

van Beilen, J. W., Teixeira de Mattos, M. J., Hellingwerf, K. J., and Brul, S. (2014). Distinct effects of sorbic acid and acetic acid on the electrophysiology and metabolism of *Bacillus subtilis*. *Appl. Environ. Microbiol.* 80, 5918–5926. doi: 10.1128/AEM.01391-14

van Langeveld, I., Gagnon, R. C., Conrad, P. F., Gamelli, R. L., Martin, B., Choudhry, M. A., et al. (2017). Multiple-drug resistance in burn patients: a retrospective study on the impact of antibiotic resistance on survival and length of stay. *J. Burn Care Res.* 38, 99–105. doi: 10.1097/BCR.0000000000000479

Wickham, H. (2009). *ggplot2: Elegant Graphics for Data Analysis* (Springer).

Williams, F. N., Herndon, D. N., Hawkins, H. K., Lee, J. O., Cox, R. A., Kulp, G. A., et al. (2009). The leading causes of death after burn injury in a single pediatric burn center. *Crit. Care* 13:R183. doi: 10.1186/cc8170

Wolin, M. J. (1969). Volatile fatty acids and the inhibition of *Escherichia coli* growth by rumen fluid. *Appl. Microbiol.* 17, 83–87.

World Health Organization. (2014). *Antimicrobial Resistance: Global Report on Surveillance*. Geneva: World Health Organization.

Zwietering, M. H., Jongenburger, I., Rombouts, F. M., and van 't Riet, K. (1990). Modeling of the bacterial growth curve. *Appl. Environ. Microbiol.* 56, 1875–1881.

Conflict of Interest Statement: The authors declare that the research was conducted in the absence of any commercial or financial relationships that could be construed as a potential conflict of interest.

frontiers in Microbiology

ORIGINAL RESEARCH
published: 09 January 2019
doi: 10.3389/fmicb.2018.03287

Overlap of Promoter Recognition Specificity of Stress Response Sigma Factors SigD and SigH in *Corynebacterium glutamicum* ATCC 13032

*Hana Dostálová[1], Tobias Busche[2†], Jiří Holátko[1], Lenka Rucká[1], Václav Štěpánek[1], Ivan Barvík[3], Jan Nešvera[1], Jörn Kalinowski[2] and Miroslav Pátek[1]**

[1] Institute of Microbiology of the CAS, v. v. i., Prague, Czechia, [2] Centrum für Biotechnologie, Universität Bielefeld, Bielefeld, Germany, [3] Institute of Physics, Faculty of Mathematics and Physics, Charles University, Prague, Czechia

OPEN ACCESS

Edited by:
Daniela De Biase, Sapienza University of Rome, Italy

Reviewed by:
Andreas Burkovski, Friedrich-Alexander-Universität Erlangen-Nürnberg, Germany
Saori Kosono, The University of Tokyo, Japan

***Correspondence:**
Miroslav Pátek
patek@biomed.cas.cz

†Present address:
Tobias Busche, Institute of Biology and Microbiology, Freie Universität Berlin, Berlin, Germany

Specialty section:
This article was submitted to Microbial Physiology and Metabolism, a section of the journal Frontiers in Microbiology

Received: *13 September 2018*
Accepted: *17 December 2018*
Published: *09 January 2019*

Citation:
Dostálová H, Busche T, Holátko J, Rucká L, Štěpánek V, Barvík I, Nešvera J, Kalinowski J and Pátek M (2019) Overlap of Promoter Recognition Specificity of Stress Response Sigma Factors SigD and SigH in Corynebacterium glutamicum ATCC 13032. Front. Microbiol. 9:3287. doi: 10.3389/fmicb.2018.03287

Corynebacterium glutamicum ATCC 13032 harbors five sigma subunits of RNA polymerase belonging to Group IV, also called extracytoplasmic function (ECF) σ factors. These factors σ^C, σ^D, σ^E, σ^H, and σ^M are mostly involved in stress responses. The role of σ^D consists in the control of cell wall integrity. The σ^D regulon is involved in the synthesis of components of the mycomembrane which is part of the cell wall in *C. glutamicum*. RNA sequencing of the transcriptome from a strain overexpressing the *sigD* gene provided 29 potential σ^D-controlled genes and enabled us to precisely localize their transcriptional start sites. Analysis of the respective promoters by both *in vitro* transcription and the *in vivo* two-plasmid assay confirmed that transcription of 11 of the tested genes is directly σ^D-dependent. The key sequence elements of all these promoters were found to be identical or closely similar to the motifs -35 GTAAC$^A/_G$ and -10 GAT. Surprisingly, nearly all of these σ^D-dependent promoters were also active to a much lower extent with σ^H *in vivo* and one (P*cg0607*) also *in vitro*, although the known highly conserved consensus sequence of the σ^H-dependent promoters is different (−35 GGAA$^T/_C$ and −10 GTT). In addition to the activity of σ^H at the σ^D-controlled promoters, we discovered separated or overlapping σ^A- or σ^B-regulated or σ^H-regulated promoters within the upstream region of 8 genes of the σ^D-regulon. We found that phenol in the cultivation medium acts as a stress factor inducing expression of some σ^D-dependent genes. Computer modeling revealed that σ^H binds to the promoter DNA in a similar manner as σ^D to the analogous promoter elements. The homology models together with mutational analysis showed that the key amino acids, Ala 60 in σ^D and Lys 53 in σ^H, bind to the second nucleotide within the respective -10 promoter elements (G**A**T and G**T**T, respectively). The presented data obtained by integrating *in vivo*, *in vitro* and *in silico* approaches demonstrate that most of the σ^D-controlled genes also belong to the σ^H-regulon and are also transcribed from the overlapping or closely located housekeeping (σ^A-regulated) and/or general stress (σ^B-regulated) promoters.

Keywords: *Corynebacterium glutamicum*, stress response, RNA-seq, *in vitro* transcription, sigma factor, promoter

INTRODUCTION

Most bacterial genes are transcribed by an RNA polymerase (RNAP) holoenzyme that includes a primary sigma subunit (σ factor) responsible for the transcription of housekeeping genes. In addition to the primary σ factor, a number of alternative sigma factors control various functions of the bacterial cells under specific nutritional, growth and environmental conditions. *Corynebacterium glutamicum* is a Gram-positive bacterium, which is applied in industrial biotechnology and also considered a model species for other corynebacteria as well as related actinobacterial genera such as *Mycobacterium* and *Rhodococcus*. The *C. glutamicum* genome encodes 7 σ factors: A primary σ^A, a primary-like σ^B and five σ factors of Group IV (Gruber and Gross, 2003) also called extracytoplasmic function (ECF) σ factors (σ^C, σ^D, σ^E, σ^H, and σ^M), which are involved in various stress responses.

Gene expression in bacteria is controlled by a complex regulatory network composed of protein transcription regulators, regulatory RNAs as well as low-molecular-weight metabolites. Sigma subunits of RNAP that are responsible for transcription initiation play an important role in this network. Groups of genes (σ factor regulons, called also sigmulons) controlled by different σ factors were found to constitute a modular network in *Pseudomonas aeruginosa* (Schulz et al., 2015). Individual separated sigmulons controlled by more than 25 σ factors display limited overlaps which probably allows this versatile bacterium to efficiently regulate cell processes and adapt to various environments as well as to the lifestyle of an opportunistic pathogen. The functions of the regulons of alternative σ factors in *P. aeruginosa* are significantly connected by the action of global transcriptional regulators which modulate transcription levels from the respective promoters (Binder et al., 2016). According to this hypothesis, modularity of regulatory networks may ensure rapid evolution (Binder et al., 2016). In contrast to previous notion concerning *P. aeruginosa*, considerable overlaps of σ factor regulons observed in many bacteria display regulatory redundancies and the ability to fine-tune responses to various environmental stimuli and combined stress conditions. Some genes belong to two or more sigmulons, since they are either transcribed from several promoters recognized by different alternative σ factors, or are transcribed with two or more different holoenzymes (RNAP core+σ) which drive transcription from the same promoter (Luo and Helmann, 2009). Microarray analysis revealed extensive coregulation of the genes involved in many cell processes, which are co-operatively controlled by four alternative σ factors (σ^B, σ^C, σ^H, and σ^L) in *Listeria monocytogenes* (Chaturongakul et al., 2011). Significant regulatory overlaps between the target genes of three σ factors (σ^M, σ^W, and σ^X) involved in cell surface stress responses were also found in *Bacillus subtilis* (Jordan et al., 2008). A single promoter of the *sigB* gene encoding an alternative σ in *Mycobacterium tuberculosis* was recognized by as many as three different ECF σ factors (σ^E, σ^H, and σ^L) (Dainese et al., 2006). Overlapping σ factor specificity in promoter recognition can be therefore considered to be a common feature of regulatory networks in bacteria.

Various types of stress conditions which bacteria encounter in the environment (e.g., heat, cell surface and oxidative stresses) often result in damaged proteins, which are then degraded by proteases or re-folded by chaperones during the stress response. Expression of some genes encoding proteases (*clpB*) and chaperones (*dnaK* and *dnaJ2*) was found to be activated by both σ^H (involved in heat and oxidative stress response) and σ^E (involved in cell surface stress response) in *C. glutamicum* (Šilar et al., 2016). The *clgR* gene encoding a heat-stress-responsive regulator was also found to be σ^H and σ^E-dependent (Šilar et al., 2016). ClgR controls expression of several genes involved in protein quality control, and the function of ECF σ factors and the transcriptional regulator is thus integrated into a network. The same σ^H/σ^E overlap was found in the transcription initiation of the *C. glutamicum sigB* gene, encoding the general stress response sigma factor σ^B (Dostálová et al., 2017). The possible activity of both σ^H and σ^M (involved in oxidative stress response) at the same *C. glutamicum* promoters was suggested, but has not yet been proven (Nakunst et al., 2007; Šilar et al., 2016; Dostálová et al., 2017), although the respective promoter consensus sequences seem very similar. Promoters of σ^C-regulated genes in *C. glutamicum* were found to be different from other promoters recognized by ECF σ factors, and σ^C regulon, which includes genes involved in the aerobic respiratory chain in *C. glutamicum*, seems to be separated from the other σ factor regulons (Toyoda and Inui, 2016).

Many stress response genes of *C. glutamicum* were found to be transcribed not only from stress promoters, but also from overlapping or closely located housekeeping promoters controlled by σ^A and/or σ^B (Engels et al., 2004; Ehira et al., 2009; Busche et al., 2012; Šilar et al., 2016). Such transcription of stress-response genes from multiple promoters also seems to be frequent in other bacteria (Seo et al., 2012; Cho et al., 2014). The activity of σ^A and/or σ^B under unstressed conditions probably ensures a basal level of expression of the respective genes which also play important roles in fast-growing bacterial cells.

We have recently found by using RNA-seq that σ^D-dependent genes are involved in the synthesis of components of the mycomembrane, which is a part of the cell wall in *C. glutamicum* ATCC 13032. The σ^D regulon, including 29 genes, thus contributes to the maintenance of cell wall integrity (Taniguchi et al., 2017). Similar group of σ^D-dependent genes was also detected in the strain *C. glutamicum* R using different techniques (Toyoda and Inui, 2018). In *C. glutamicum* R, the *sigD* overexpression conferred lysozyme resistance and the *lppS* gene (encoding L,D-transpeptidase) and probably some other σ^D-dependent genes were found to contribute to lysozyme resistance. No clear σ^D regulon induction was observed in this strain under any other stress conditions tested (treatment with sodium dodecyl sulfate, cetyl trimethylammonium bromide, ethambutol or ampicillin) (Toyoda and Inui, 2018).

Phenol was previously described to cause a significant oxidative stress at subtoxic concentrations. At higher concentrations, phenol affects bacterial cells by releasing cell wall components and causing non-specific increase in cell

permeability (Denyer, 1995). At the level of the cytoplasmic membrane, phenol induces a loss of structural integrity by the leakage of potassium ions and various organic compounds and can also displace phospholipid molecules in the cell envelope (Denyer, 1995). Such damage to the cell wall might induce a similar stress response as lysozyme treatment. However, effects of toxic aromatic compounds, such as phenol, vanillin and ferulic acid, which are degraded by *C. glutamicum* (Chen et al., 2016, 2017, 2018), on σ^D regulon induction have not yet been tested.

Although the number of precisely localized promoters driving expression of σ^D-dependent genes was not high, it was possible to propose their consensus sequence. Considering the difference between σ^D-controlled promoters and other promoter classes, the σ^D regulon seemed to also be an insulated gene group.

In this study, we discovered that nearly all of the σ^D-dependent promoters found in *C. glutamicum* ATCC 13032 are also to a much lower extent active with RNAP+σ^H, although the known highly conserved consensus sequence of the σ^H-dependent promoters differs from that of the σ^D-dependent promoters. We have found that phenol in the cultivation medium acts as a stress factor, inducing the expression of some σ^D-dependent genes. To achieve reliable results, we combined the genome-wide technique (RNA-seq) and single-promoter analysis (*in vitro* transcription and an *in vivo* two-plasmid system for the assignment of σ factors to genes/promoters). *In silico* homology modeling completed the different approaches to analyzing the sigma-promoter relationships.

MATERIALS AND METHODS

Bacterial Strains, Plasmids, Oligonucleotides and Growth Conditions

Escherichia coli DH5α (Hanahan, 1985) was cultivated aerobically in 500-ml flasks containing 70–100 ml of 2xYT medium (Green and Sambrook, 2012) at 37°C. Wild-type (WT) *C. glutamicum* ATCC 13032, its deletion derivative *C. glutamicum* Δ*sigD* (Taniguchi et al., 2017) and *C. glutamicum sigD*-overexpressing strain (Taniguchi et al., 2017) were used for DNA and RNA isolations, and as hosts for testing the activities of promoters cloned in the promoter-test vector pEPR1. *C. glutamicum* was cultivated aerobically in 500-ml flasks with 70–100 ml of complete 2xYT medium or in minimal CGXII medium (Keilhauer et al., 1993) at 30°C. Media were supplemented with antibiotics, when necessary: kanamycin (Km; 30 μg/ml), tetracycline (Tc; 10 μg/ml) or ampicillin (Ap; 100 μg/ml). The plasmid vectors used are listed in **Table 1**. The oligonucleotides used are listed in **Supplementary Table S1**.

DNA Manipulations

DNA isolation, PCR, cutting by restriction enzymes, ligation and transformation of *E. coli* were done using the standard techniques (Green and Sambrook, 2012). *C. glutamicum* cells were transformed by electroporation (van der Rest et al., 1999). DNA fragments for cloning promoters in pRLG770 and pEPR1 were assembled from the synthetized complementary oligonucleotides of around 75 nt in length, with overhangs ready for ligation. Their sequences are shown in **Supplementary Table S1**. Mutations in *sigH* were constructed using a Q5® Site-Directed Mutagenesis Kit (New England BioLabs® Inc.) according to the recommendations of the manufacturer. The specific oligonucleotide primers for mutagenesis were designed by NEBaseChanger™ v1.2.8 (New England BioLabs® Inc.).

RNA Isolation, cDNA Library Preparation and Sequencing

Corynebacterium glutamicum ATCC 13032 was cultivated in minimal medium CGXII with glucose (2%) or phenol (3.4 mM). The *sigD*-overexpressing *C. glutamicum* strain was used as described previously (Taniguchi et al., 2017). Total RNA was isolated from 3 biological replicates of *C. glutamicum* cells grown to the exponential phase using a Quick-RNA Miniprep Plus kit according to the manufacturer's instructions (Zymo Research). After additional DNase treatment, RNA samples were purified with an RNA Clean&Concentrator-5 kit (Zymo Research) and quantified with a DropSense 16 (Trinean). The quality of total RNA was controlled with an RNA 6000 Nano kit in an Agilent 2100 Bioanalyzer (Agilent Technologies). To construct the whole transcriptome cDNA library, 2.5 μg total RNA (RIN > 9) was used for the depletion of rRNA with a Ribo-Zero rRNA Removal Kit (Bacteria) according to manufacturer's instructions (Illumina). The rRNA removal was checked with an Agilent RNA Pico 6000 kit and the Agilent 2100 Bioanalyzer (Agilent Technologies). The mRNA obtained was converted to a cDNA library according to the TruSeq Stranded mRNA Sample Preparation guide (Illumina). The quality and quantity of the cDNA library was checked with an Agilent High Sensitivity DNA kit and the Agilent 2100 Bioanalyzer (Agilent Technologies). Sequencing was performed on an Illumina HiSeq 1500 using 70 bases read length (Illumina).

A primary 5′-end specific cDNA library was synthesized using 2 × 2.5 μg total RNA (RIN > 9) as described previously (Kranz et al., 2018). Briefly, after rRNA depletion and quality control, as described for the whole transcriptome cDNA libraries, a terminator 5′-phosphate-dependent exonuclease treatment (TEN, Illumina) was carried out to digest non-primary transcripts. The remaining non-digested non-primary transcripts were tagged by the ligation of the RNA 5′-index adapter 5′-CCCUACACGACGCUCUUCCGAUCGAG-**UACCCUAG** (index in bold) to the 5′-monophosphorylated ends. The primary 5′-triphosphate ends were converted to 5′-mono-phosphate by RNA 5′-polyphosphatase (RPP) treatment (Epicenter) to ligate the 5′-adapter to the 5′-ends of primary transcripts. Finally, reverse transcription with a stem-loop DNA adapter and library amplification was performed. The quality and quantity of the cDNA library was checked in the same way as for the whole transcriptome cDNA library. Prior to sequencing, primary 5′-end cDNA libraries were purified and size-selected for fragments approximately 100–1000 bases long via gel electrophoresis, and quantified again. Paired end sequencing was performed in an Illumina MiSeq using MiSeq Reagent Kits v3 with a read length of 2 × 75 bases (Illumina).

TABLE 1 | Plasmid vectors used in this study.

Plasmid	Characteristics	Source
pRLG770	*E. coli* vector, *rrnB* terminator, Ap^R, used for *in vitro* transcription analysis	Ross et al., 1990
pEPR1	*E. coli-C. glutamicum* promoter-test vector, Km^R, promoter-less *gfpuv* as a reporter	Knoppová et al., 2007
pEC-XT99A	*E. coli-C. glutamicum* expression vector, Tc^R, IPTG-inducible *trc* promoter	Kirchner and Tauch, 2003

Read Processing, Mapping and Visualization

Paired-end reads were mapped to the *C. glutamicum* ATCC 13032 reference genome sequence accession number BX927147 (Kalinowski et al., 2003) with bowtie2 v2.2.7 (Langmead and Salzberg, 2012) using the default settings for paired-end read mapping.

False-positive primary transcriptome cDNA reads containing the barcode sequence TACCCTAG at their 5′-ends were discarded. The remaining R1 cDNA reads were mapped to the *C. glutamicum* ATCC 13032 reference genome sequence accession number BX927147 (Kalinowski et al., 2003) with bowtie2 v2.2.7 (Langmead and Salzberg, 2012) using the default settings for single-end read mapping. Read Explorer v.2.2 (Hilker et al., 2014) was used for the visualization of short read alignments, transcription start site (TSS) detection and differential gene expression analysis.

Identification of Transcription Start Sites (TSS)

Transcription start sites (TSS) were detected essentially as described by Wittchen et al. (2018). Primary 5′-end cDNA library data were analyzed with the software ReadXplorer v2.2 (Hilker et al., 2016) using the *Transcription analysis* function. The parameters for TSS detection were chosen by ReadXplorer using its automatic parameter estimation. TSS were detected with at least 10 read starts and a minimal coverage increase of 100%. The resulting list of predicted TSS was manually checked for false-positives.

Differential Gene Expression Analysis

Differential gene expression analysis of *C. glutamicum* grown with and without phenol (3.4 mM), including normalization, was performed using the whole transcriptome data and Bioconductor package DESeq2 (Love et al., 2014) included in the software ReadXplorer v2.2 (Hilker et al., 2016). The signal intensity value (*a*-value) was calculated by the log2 mean of normalized read counts, and the signal intensity ratio (*m*-value) by log2 fold-change. The evaluation of the differential RNA-seq data was performed using an adjusted *p*-value cut-off of $P \leq 0.01$ and a signal intensity ratio (*m*-value) cut-off of ≥ 1 or ≤ -1.

In vitro Transcription

The *in vitro* transcription assay was carried out essentially as described previously (Holátko et al., 2012). The holo-RNAP was reconstituted from the RNAP core enzyme isolated from *C. glutamicum* and individual *C. glutamicum* sigma factors isolated as His-tagged recombinant proteins from *E. coli*. The RNAP core (100 nM) was mixed with the respective σ factor (σ^C, σ^D, σ^E, σ^H, or σ^M) in a molar ratio of 1:30. The holo-RNAP was assembled for 10 min at 37°C. The transcription mixture was incubated for 15 min at 37°C. The transcripts labeled with [α-^{32}P]UTP were separated in 5.5% polyacrylamide gel. *In vitro* transcription assays were done 2 or 3 times for each promoter, with essentially the same results.

Promoter Activity Measurements Using the Two-Plasmid System

Sigma factors were assigned to individual promoters *in vivo* using the two-plasmid system for *C. glutamicum* described recently (Dostálová et al., 2017) and similar that developed for the identification of σ^E-dependent promoters in *E. coli* (Rezuchova and Kormanec, 2001). In principle, the sigma factors overproduced using the expression vector pEC-XT99A drove transcription from the individual promoters transcriptionally fused to the *gfpuv* reporter gene in the other plasmid present in the cell, the promoter-test vector pEPR1. Promoters were cloned to pEPR1 as approximately 75-nt fragments using the restriction sites *Pst*I and *Bam*HI. The same pEC-XT99A constructs as described previously (Dostálová et al., 2017) were used to overexpress the *sig* genes after the addition of isopropyl-β-thiogalactopyranoside (IPTG). Two-plasmid strains were cultivated in 2xYT medium (containing Km and Tc) for 24 h and the cell samples were collected. The cells were disrupted with a FastPrep homogenizer (MP Biomedicals). The fluorescence of the cell-free extracts was determined with a Saphire2 microplate spectrophotometer (Tecan; excitation wavelength 397 nm; emission wavelength 509 nm). Cells harboring the pEPR1 construct and the expression vector without a *sig* gene were used as a control. To determine the background fluorescence of *C. glutamicum* cells, the strain only carrying the promoter-less vector pEPR1 was used. Protein concentration in the extract was determined by Bradford assay, and promoter activity was expressed in arbitrary units/mg protein.

Homology Modeling and Molecular Dynamics (MD) Simulations

The homology models of the σ^D and σ^H domains which recognize the −10 and −35 sequences of the respective promoters were produced by using the Swiss-Model server (Waterhouse et al., 2018). The crystal structures of *E. coli* σ^E, PDBid: 4LUP (for −10 element GTC) (Campagne et al., 2014) and PDBid: 2H27 (for −35 element GGAAC) (Lane and Darst, 2006) were used as templates. The nucleotides within the *E. coli* σ^E consensus were replaced to match the consensus for *C. glutamicum* σ^H or σ^D, where necessary. Molecular dynamics simulations were done using the software package AMBER (Salomon-Ferrer et al., 2013)

TABLE 2 | Promoter sequences of σ^D-dependent genes in *C. glutamicum* ATCC 13032 determined by RNA sequencing specific for transcription start sites.

Gene	Promoter sequence[A]	Distance TSS-start codon
cmt1	AGGTAAAGCGCCTG**TTAACG**TAATAG-CTTGAAATATA**GAT**GTAAATTAA**A**	173 nt
cg0420	CATCTGAGCAGTTA**GAAACG**GTATGT-CGGTAGTAACC**GAT**ACGATTTATT**G**	33 nt
lpd	ATTTCGGCAGAGTG**CTAACG**GTTAGG–CACTATTTTCC **GTT** AGTTCTTTT**G**	360 nt
cg0607	TTGCGCGTTAATAA **GGAA** **CA**ATATCG–GTGTGATTCGC**GAT**ATATTAATC**A**	49 nt
rsdA	GGTCAGCGATGGAA**GTAACA**GAGTTA-GGGAACTTCTC**GAT**CTACTGAGT**G**	158 nt
cmt3	TTTGGGGGAGGTT**GTTACA**AAACCATA CGTCTGTGAA**GAT**ATGACG**A**GT**G**	44 nt
cg1056	TTTTGACGACGCA**GTAACG**CAATCGGGG ATTGTGGTC**GAT**TCTTTAAGC**A**	84 nt
cg2047	CATTTTTTAGTGAC**GTAACA**TCAAAG-AAGTATTCACT**GAT**GTAAGTAGT**G**	120 nt
lppS	AAGGCATTCTGGAC**GTAACG**CTCCGG-CATCTACAAGG**GAT**GATCAAAAT**A**	225 nt
fadD2	GTTAGTTTGCAAAA**GTAATA**AAATGT-TCATCTTTGTC**GAT**GGTCACA**A**T**A**	30 nt
cmt2	AGTGTCACAACTTG**GTAACG**TGTGGG-CGGAAAAACAA**GAT**AGGCATCGA**G**	59 nt
	GTAAC^A/$_G$ **GAT**	

[A]The predicted −35 motif GTAAC^A/$_G$ and −10 motif GAT are in bold, underlined. Elements identical to the consensus of σ^H-controlled promoters are highlighted in red. The gaps were introduced to align the key motifs.

and Linux computer nodes with powerful NVIDIA GPUs that enable the accumulation of 50-ns MD trajectories at 280 K.

RESULTS

Mapping of Transcription Start Sites of σ^D-Dependent Genes by RNA-seq

RNA-seq with a *C. glutamicum* WT strain, a strain overexpressing *sigD* and a *sigD* deletion (Δ*sigD*) strain was performed previously (Taniguchi et al., 2017). Using this approach, the 29 genes were identified, which showed the increased transcription in *C. glutamicum* overexpressing *sigD* and decreased transcription in the Δ*sigD* strain. The genes selected may be those which are directly under the control of σ^D, or the genes whose transcription is influenced by an indirect effect of *sigD* overexpression or deletion.

To further investigate these σ^D-dependent genes and to map their transcriptional start sites (TSS), RNA-seq of 5′-enriched primary transcripts of *C. glutamicum* overexpressing *sigD* was used. The sequencing of primary 5′-end specific cDNA library allows the exact mapping of TSS. To detect these TSS, the data obtained from the primary 5′-end cDNA sequencing were mapped to *C. glutamicum* ATCC 13032 reference genome sequence, accession number BX927147 (Kalinowski et al., 2003) and analyzed via ReadXplorer (Hilker et al., 2016). To distinguish between the background and actual TSS signal, we considered a position to be +1 (TSS) if the number of read starts here was 10 times higher than at position −1. In this way the 5′-ends of the transcripts of the above mentioned 29 putative σ^D-dependent genes were detected. Since several genes were cotranscribed in operons, the total number of TSS was 23 (**Supplementary Table S2**). The 50-nt sequences (−49 to +1) were aligned at the TSS, and the consensus motifs within the region of the supposed promoters were searched using the software Improbizer (Ao et al., 2004) as described previously (Albersmeier et al., 2017). The consensus sequence or closely similar motifs within the −35 and −10 regions were found in 11 sequences (**Table 2**). The products of the respective genes are involved in the synthesis of corynomycolic acid (*fadD2*, *cmt1*, *cmt2*, *cmt3*), peptidoglycan formation (*lppS*), inhibition of σ^D activity (*rsdA*) or have hypothetical functions (**Table 3**). The σ^D is thus involved in the control of cell wall integrity and cell envelope stress response, as described previously in the strains *C. glutamicum* ATCC 13032 (Taniguchi et al., 2017) and *C. glutamicum* R (Toyoda and Inui, 2018).

The sequences were used to generate a sequence logo with Weblogo3 (**Figure 1**). The consensus sequences GTAAC^A/$_G$ as the −35 motif and GAT as the −10 motif are apparent.

In vitro Transcription From the σ^D-Controlled Promoters

The activity of the 11 proposed σ^D-dependent promoters, which were deduced from the TSS determination by RNA-seq, was tested using the *in vitro* transcription system (Holátko et al., 2012). The promoter sequence elements of the proposed σ^D-dependent promoters were apparently different from the consensus sequence of σ^A/σ^B-driven promoters (Pátek and

TABLE 3 | Products of σ^D-dependent genes in *C. glutamicum* ATCC 13032.

Gene ID[A]	Gene name	Function
cg0413	*cmt1*	Trehalose corynomycolyl transferase
cg0420		Hypothetical glycosyltransferase
cg0441	*lpd*	Dihydrolipoamide dehydrogenase
cg0607		Hypothetical secreted protein
cg0697	*rsdA*	Anti-sigma D
cg1052	*cmt3*	Trehalose corynomycolyl transferase
cg1056		Hypothetical membrane protein
cg2047		Hypothetical secreted protein
cg2720	*lppS*	L,D-transpeptidase
cg3179	*fadD2*	Long-chain fatty-acid-CoA ligase
cg3186	*cmt2*	Trehalose corynomycolyl transferase

[A]Genes are listed according to CoryneRegNet (http://www.coryneregnet.de/).

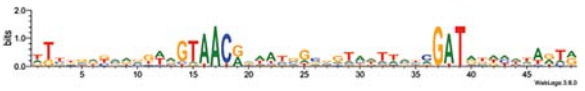

FIGURE 1 | Sequence logo of the 11 studied σ^D-dependent promoters. The logo was made using Weblogo3 (Crooks et al., 2004).

Nešvera, 2011; Albersmeier et al., 2017) and therefore ECF σ factors (σ^C, σ^D, σ^E, σ^H, and σ^M) were only used. This assay may directly prove whether a promoter is specifically recognized by RNAP associated with the chosen σ factor, and thus distinguish between direct and indirect control by the tested σ. As shown in **Figure 2**, all but one promoter were found to be exclusively σ^D-specific. The only exception was the promoter of *cg0607* (P*cg0607*), which was active with both σ^D and σ^H. The *in vitro* transcript level with σ^H was even higher than with σ^D (**Figure 2**). It is worth mentioning that P*cg0607* is the only one out of the 11 analyzed promoters that has the −35 sequence element GGAAC which is a consensus for σ^H-dependent promoters (Busche et al., 2012). The ECF σ factors σ^C, σ^E, and σ^M did not provide any signal in the assays (data not shown). The σ^H-specific *clpP1* promoter (Busche et al., 2012) was used as a control.

Determination of Activity of σ^D-Controlled Promoters *in vivo* Using Two-Plasmid System

To confirm the results of *in vitro* transcription, the activity of σ^D-dependent promoters was determined *in vivo* using the two-plasmid *C. glutamicum* cells carrying a *sig* gene in the expression vector pEC-XT99A and the analyzed promoter in the promoter-test vector pEPR1 (Dostálová et al., 2017). The promoter activity was measured as the fluorescence intensity of the Gfp reporter protein. The results of the assays with 7 most felicitous example promoters which confirmed the activity of σ^H in transcription are presented in **Figure 3**. As shown in the left part of **Figure 3**, all promoters exhibited high activity with the overexpressed *sigD*. Results with P*cg1056* were included to document that not all σ^D-controlled promoters are also recognized by σ^H, although there is no apparent reason found by inspection of the promoter sequence only. Activity of P*cg2047* with σ^H was approximately twice higher after induction at time point 3 (T3) and time point 6 (T6) although it was at the same level of the control. It is an unusual feature of this two-plasmid system in some cases, which we described in our previous paper (Dostálová et al., 2017). We concluded, therefore, that there was an activity of P*cg2047* initiated by σ^H.

The level of Gfp reporter fluorescence was lowest 3 h (T3) after the addition of the inducer (IPTG) in all cases and highest after 24 h (T24) in 10 of the 11 tested promoters. The promoters P*cmt2*, P*fadD2*, P*rsdA*, P*cg2047*, P*lppS*, P*lpd*, and P*cg0607* were also found to be active with σ^H, as shown in the right part of **Figure 3**. Although the maximal σ^H-induced activities were 1.5- to 64-fold lower than those with σ^D under the conditions used, the effect was apparent (**Figure 3**, right part). The promoter P*cg1056* is an example of a promoter which did not demonstrate any

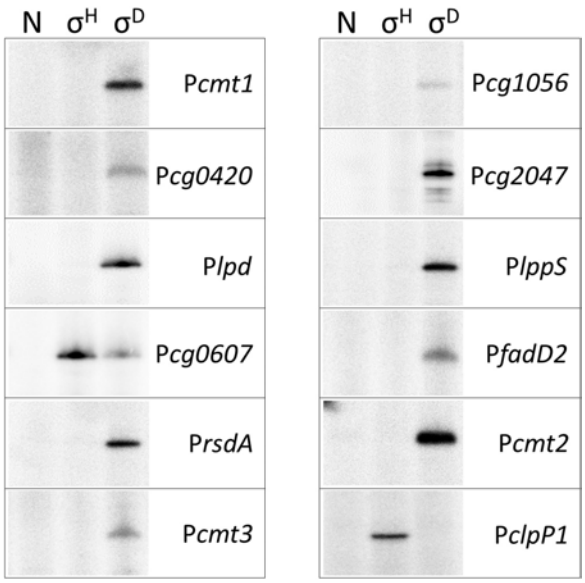

FIGURE 2 | *In vitro* transcription driven from σ^D-dependent promoters with reconstituted *C. glutamicum* holo-RNAPs (autoradiogram of the SDS-PAGE gel). The lanes with no sigma (N), σ^H and σ^D are shown. *In vitro* transcription was carried out as described previously (Holátko et al., 2012). The derivatives of the plasmid vector pRLG770 with inserted promoter fragments (approximately 75 nt) were used as DNA templates, recombinant RNAP core was isolated from *C. glutamicum*, and sigma factors were isolated as His-tagged proteins from *E. coli* using the pET-22b(+) constructs carrying the respective inserted *sig* genes (Holátko et al., 2012; Šilar et al., 2016). The σ^H-specific promoter P*clpP1* was used as a control. Representative results of 2–3 assays are shown.

increase in activity with *sigH* overexpression. Neither of the other overproduced σ factors supported a promoter activity increase with any of the promoters tested (data not shown). Interestingly, the trend of changes in the σ^H-directed promoter activity was mostly the opposite of that with σ^D: the activity with σ^H was highest 3 h after the addition of IPTG, then mostly decreased at T6, and the difference in Gfp level between the cells with IPTG-induced and non-induced σ^H-overproduction nearly vanished at T24 in most cases (**Figure 3**, right part). Due to this trend, σ^D- and σ^H-incited promoter activities were nearly comparable at T3. This effect was most apparent in P*cg0607*, which was also found to be active with σ^H by *in vitro* assay (**Figure 2**): this ratio between promoter activity with σ^D/σ^H was 1.5 at T3 but 20.5 at T24 (**Figure 3**). The overall conclusion is that most of the σ^D-controlled promoters are also to a lesser extent σ^H-activated.

Promoter Activity in the *sigD* Deletion Strain (Δ*sigD*)

To prove that σ^H is directly responsible for the minor activity of σ^D-controlled promoters *in vivo*, we tried to overexpress *sigH* in the Δ*sigD* strain also harboring pEPR1 with the target promoters. The Δ*sigD* strain grew slightly slower than the wild type strain (Taniguchi et al., 2017). However, the Δ*sigD* clones carrying two vector constructs grew extremely poorly. Therefore, we only succeeded in testing the clones with *Pcmt2*, *PlppS*, and *PrsdA*

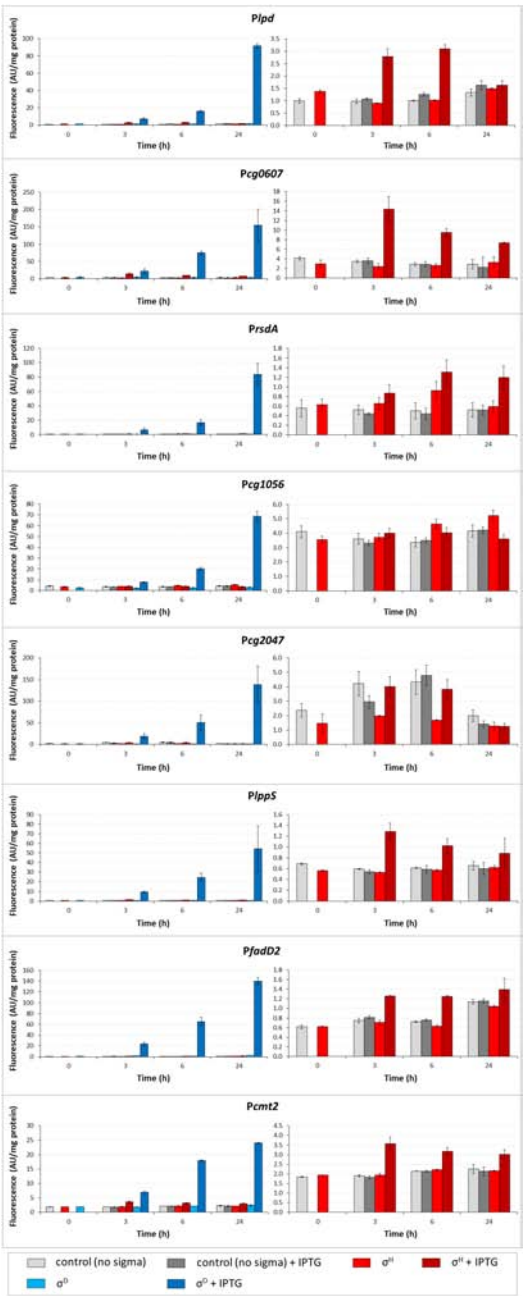

FIGURE 3 | Determination of promoter activity under *sigD* or *sigH* overexpression conditions using the two-plasmid assay. Promoter activity was measured as Gfpuv fluorescence intensity of cell extracts shown as bars in colors representing respective sigma factors. The *C. glutamicum* strains carried the pEC-XT99A constructs overexpressing *sigD* (blue bars) or *sigH* (red bars) after IPTG addition (added at time point 0, dark bars) and the promoter-test vector pEPR1 carrying the reporter *gfpuv* gene downstream of the target promoter (P*lpd*, P*cg0607* P*rsdA*, P*cg1056*, P*cg2047*, P*lppS*, P*fadD2,* or P*cmt2*). The strains harboring the pEPR1 with the target promoters and empty pEC-XT99A were used as the controls (gray bars). Only the σ^H-induced activity and controls are shown in the right panels to emphasize the minor recognition of σ^D-controlled promoters by σ^H. The background fluorescence intensity with control cells only carrying the empty vector pEPR1 was 0.25 ± 0.09 in all cases. AU, arbitrary units. The standard deviations of three biological replicates are depicted by error bars.

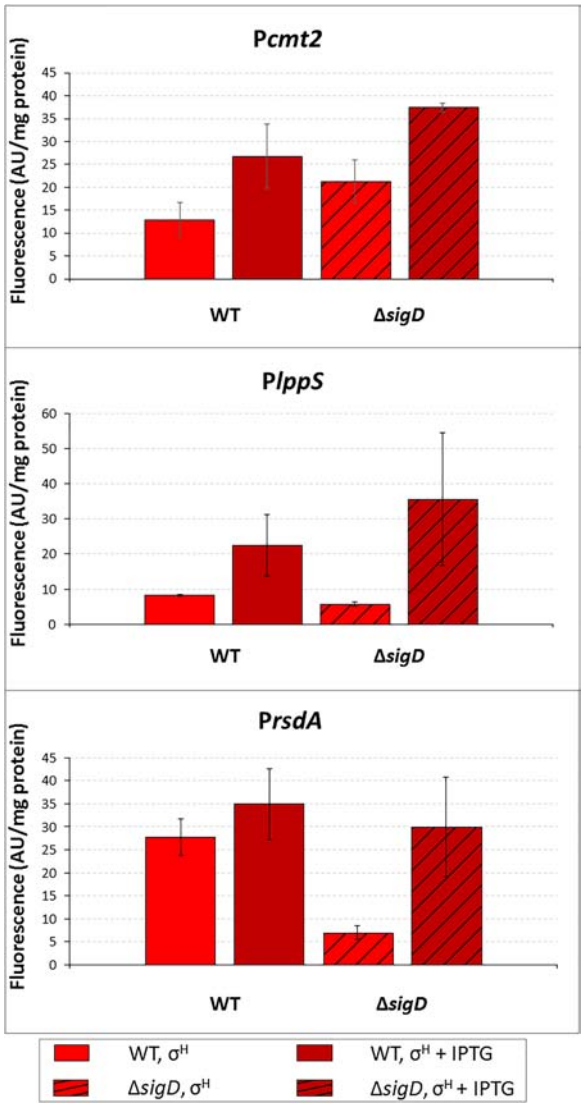

FIGURE 4 | Determination of promoter activity in *C. glutamicum* WT and Δ*sigD* strains under *sigH* overexpression conditions using the two-plasmid assay. The *C. glutamicum* strains carried the vector pEC-XT99A construct overexpressing *sigH* with IPTG and the promoter-test vector pEPR1 with a target promoter P*cmt2*, P*lppS* or P*rsdA*. The promoter activity was measured as the Gfpuv fluorescence intensity of the cell extracts after 6-h growth on complete agar plates with or without IPTG. Fluorescence of cultures without IPTG are shown as light bars; fluorescence of cultures with IPTG induction are shown as dark bars. Open bars depict fluorescence of the strains with WT background, hatched bars depict fluorescence of the strains with the Δ*sigD* background. AU, arbitrary units. The standard deviations of three biological replicates are depicted by error bars.

(cloned in pEPR1), moreover, only on a solid agar medium. The increase in promoter activity, (induction ratio of WT and Δ*sigD* strains with *sigH* overexpressed), was 2.1 and 1.8, respectively, for P*cmt2*, 2.2 and 3.5, respectively, for P*lppS* and 1.1 and 6.1, respectively, for P*rsdA* (**Figure 4**). Thus, RNAP+ σ^H was apparently directly active in transcription from all three tested σ^D-dependent promoters.

Analysis of *C. glutamicum* σ^D and σ^H Protein Sequence Similarity

To explain the observed function of σ^H in transcription from some σ^D-dependent promoters, the similarity of the amino acid sequences of *C. glutamicum* σ^D and σ^H proteins was analyzed. The level of overall similarity of the σ^D and σ^H sequences is very low (<25% identical AA), in contrast to *C. glutamicum* ECF sigma factors σ^H, σ^E, and σ^M, which exhibit a 25–38% mutual identity of AAs. However, when the regions which are thought to interact with the −35 and −10 promoter sequences (Lane and Darst, 2006; Campagne et al., 2014) were compared, some AAs were found to be identical or similar in σ^D and σ^H (shown in green and yellow, respectively, in **Figure 5**). As shown in **Figure 5**, majority of these AAs were also found to be conserved in the model ECF sigma factor, σ^E from *E. coli*, whose crystal structure was previously used for studies on sigma-promoter DNA interactions (Lane and Darst, 2006; Campagne et al., 2014).

Computer Modeling of σ^D and σ^H in Complexes With −10 and −35 Elements of σ^D- and σ^H-Controlled Promoters

We have shown that the consensus sequences of the *C. glutamicum* −10 and −35 elements recognized by σ^D (this study) and σ^H (Busche et al., 2012) differ (i.e., G**A**T vs. G**T**T at −10 and G**T**AA**C**$^{A}/_{G}$ vs. G**G**AA$^{T}/_{C}$ at −35). To identify the key AAs responsible for recognizing different nucleotides at the second position of these consensus sequences and to understand why σ^H is, to a certain extent, able to initiate transcription from the σ^D-dependent promoters, we used computer modeling tools. First, we created homology models of those σ^D and σ^H domains, which recognize the −10 and −35 sequences of the respective promoters. The structure of *E. coli* σ^E based on the crystal protein in complex with promoter DNA was used as a template (Lane and Darst, 2006; Campagne et al., 2014). It should be noted that the DNA promoter sequences recognized by *E. coli* σ^E are closer to the *C. glutamicum* consensus of the σ^H-specific −10 promoter element (GTC in *E. coli* σ^E, i.e., T at the second position in both cases) as well as the −35 element (GGAAC in *E. coli* σ^E, i.e., G in the second position in both cases). This also corresponds to the similarity of the AA sequences of *E. coli* σ^E and *C. glutamicum* σ^H which are supposed to interact with these nucleotides (Lane and Darst, 2006; Campagne et al., 2014) (shown in bold in **Figure 5**).

As for the −10 element, there is no X-ray or cryo-electron microscopy structure of the RNAP complex with any of the group IV (ECF) sigma factors described, and a model of the complete DNA transcription bubble is not yet available. The key nucleotide at the second position of the *C. glutamicum* −10 elements (i.e., A in σ^D and T in σ^H) is in close contact with the surface of the σ subunit in our homology models based on the *E. coli* σ^E crystal structure 4LUP (**Figure 6**). According to these models, the presence of Ala 60 in σ^D and Lys 53 in σ^H seems to be crucial for the recognition of the nucleotide at the second position of the −10 element. Ala 60 with the minimal side chain creates space for a larger adenine at the second position in the −10 element at σ^D (**Figure 6A**). In contrast, Lys 53 with a larger side chain fills the free space made by a smaller base, thymine, at the second position of the −10 consensus element at σ^H (**Figure 6B**).

As for the −35 element, template and non-template DNA strands clearly form a duplex. There is no potential conformational polymorphism that could appear with the −10 element, where the transcription bubble opens. Therefore, our homology models of σ^D and σ^H in complex with the respective −35 elements can be considered highly plausible. To verify the stability and reliability of these homology models, we introduced a water envelope into the models and carried out 50-ns MD simulations. It was found, that the hydrophobic interactions of the methyl group of T at the second position of the σ^D-consensus of the −35 element with the side chains of Val 169 and Ala 166 in σ^D are crucial for its recognition (**Figure 6D**). Conversely, a hydrogen bond with the side chain of Ser 171 is most important for the recognition of G at the second position of the σ^H-consensus of the −35 element (**Figure 6E**). The hydrogen bond between the hydroxyl group of Thr 168 and the phosphate group of the sugar-phosphate DNA backbone provides another stabilizing interaction.

We used the established models to investigate why σ^H is, to some degree, capable of recognizing σ^D-controlled promoters.

−10 Element

The larger side chain of Lys 53 in σ^H must interact with the larger adenine at the second position of the GAT consensus instead of the small side chain of Ala 60 in σ^D, if we consider the recognition of the −10 GAT motif of a σ^D-controlled promoter by σ^H. This is possible since the Lys 53 side chain is highly flexible and therefore probably does not represent a major barrier to the larger adenine (**Figure 6C**). To test whether Ala 60 in σ^D and Lys 53 in σ^H play key roles in recognizing the −10 element in σ^D-controlled promoters, we designed the mutant σ^HLys-53-Ala for *in vivo* analysis.

−35 Element

With the −35 element within the σ^D-dependent promoter, thymine at the second position of the σ^D-promoter consensus (GTAAC), whose methyl group interacts with the side chains of the hydrophobic AAs Val 169 and Ala 166 in σ^D (**Figure 6D**), interacts with Thr 168 and Ser 171 in σ^H (**Figure 6F**). To assess these interactions in complex (σ^H/−35 element of σ^D-dependent promoter) in detail, we again performed an extensive 50-ns MD simulation. It was found that the side chain of Thr 168 in σ^H can rotate, and its methyl group then interacts with the methyl group of the thymine within GTAAC, which undoubtedly leads to a hydrophobic stabilization. Moreover, the hydroxyl group from the Ser 171 side chain forms a hydrogen bond with the oxygen atom of the thymine. To test whether the replacement of the AA sequence 168-ThrValMetSerArg-172 with AlaValArgValAla from σ^D can improve the recognition of σ^D-controlled promoters by σ^H, we designed the mutant σ^H168-AlaValArgValAla-172 for the *in vivo* analysis.

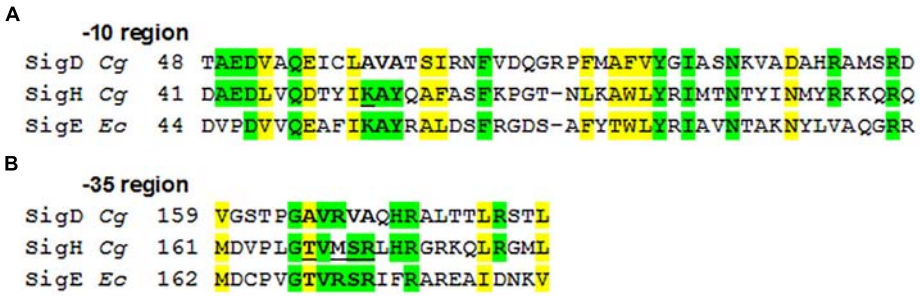

FIGURE 5 | Alignment of the σ AA sequences binding promoter –35 and –10 elements in *C. glutamicum*. *E. coli* σ^E, which was analyzed using its crystal structure (Lane and Darst, 2006; Campagne et al., 2014), is aligned for comparison. The AAs which are supposed to interact with the –10 **(A)** and –35 **(B)** elements (Lane and Darst, 2006; Campagne et al., 2014) are in bold. The σ^H AAs which we replaced with the corresponding AAs from σ^D by mutagenesis are underlined. Identical AAs are shown in green, similar in yellow; *Cg*, *C. glutamicum*; *Ec*, *E. coli*.

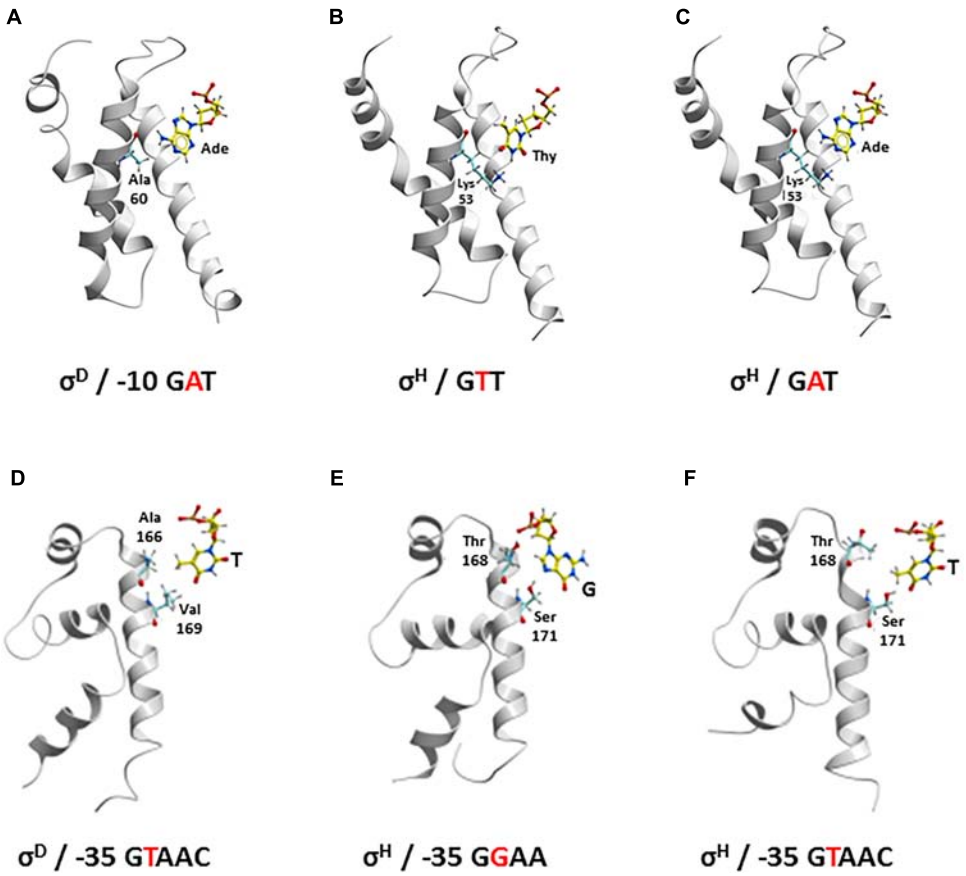

FIGURE 6 | Recognition of the nucleotide at second position of –10 element (yellow represents carbon; red, oxygen; blue, nitrogen; white, hydrogen, Ade, adenine; Thy, thymine) **(A–C)** by Ala 60 in σ^D and Lys 53 in σ^H (cyan, carbon) and at second position of –35 element (yellow, carbon) **(D–F)** by Ala 166 and Val 169 in σ^D and Thr 168 and Ser 171 in σ^H (cyan, carbon). –10: **(A)** σ^D and σ^D-dependent promoter; **(B)** σ^H and σ^H-dependent promoter; **(C)** σ^H and σ^D-dependent promoter –35: **(D)** σ^D and σ^D-dependent promoter; **(E)** σ^H and σ^H-dependent promoter; **(F)** σ^H and σ^D-dependent promoter.

Activity of σ^H-σ^D Mutants With the σ^D-Controlled Promoters

Most of the σ^D-controlled promoters were to a lesser extent also activated by σ^H, although the highly conserved sequences of the σ^H-specific promoters (−35 GGAA$^T/_C$, −10 GTT) differ from those of the identified σ^D-specific promoters (−35 GTAAC, −10 GAT). Computer modeling showed that σ^H can bind to the key regions of promoter DNA in a similar manner as σ^D to the analogous elements. Based on the results of the sequence similarity analysis and computer modeling, we designed

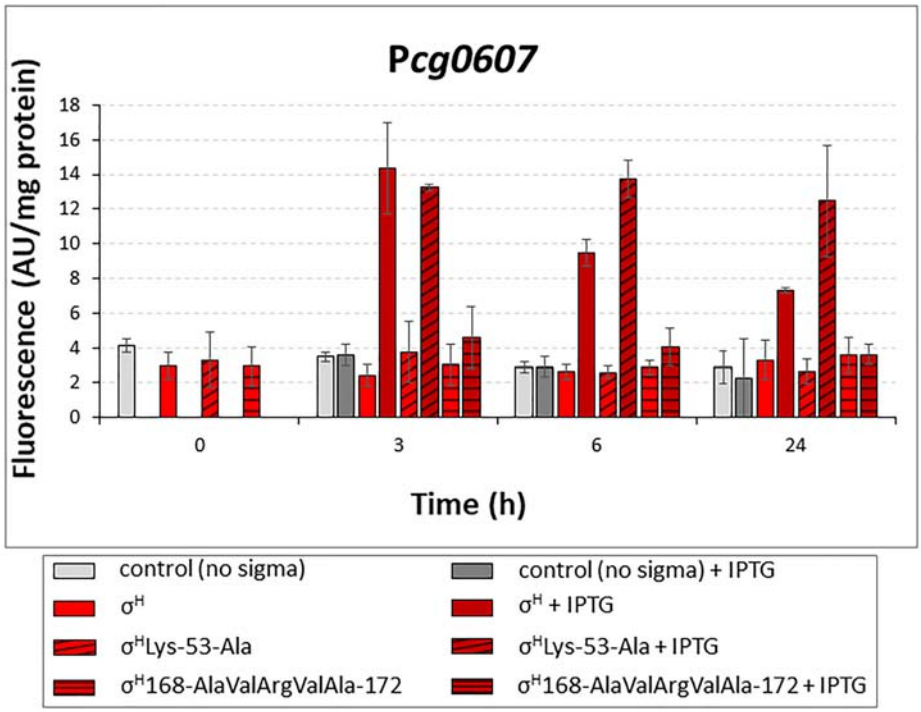

FIGURE 7 | Determination of promoter activity in *C. glutamicum* WT with overexpressed *sigH* or its mutants σ^HLys-53-Ala and σ^H168-AlaValArgValAla-172 by using two-plasmid assay. The *C. glutamicum* strains carried the vector pEC-XT99A overexpressing *sigH* (open bars), σ^HLys-53-Ala (cross-hatched bars) or σ^H168-AlaValArgValAla-172 (horizontally hatched bars) after IPTG addition and the promoter-test vector pEPR1 with the target promoter P*cg0607*. The strain with the empty expression vector pEC-XT99A was used as a control (gray bars). The promoter activity was measured as the Gfpuv fluorescence intensity of the cell extracts. Fluorescence of cultures without IPTG is shown as light bars; fluorescence of cultures with IPTG induction is shown as dark bars. AU, arbitrary units. The standard deviations of three biological replicates are depicted by error bars.

mutations to make σ^H more σ^D-like and possibly more efficient at transcription from σ^D-dependent promoters. We introduced the mutations into the *sigH* gene cloned in the expression vector pEC-XT99A, which resulted in the production of the mutant proteins σ^HLys-53-Ala or σ^H168-AlaValArgValAla-172. These mutant genes were used in the two-plasmid assays with the promoters which exhibited the highest activity with σ^H: P*cg0607*, P*lpps*, P*cmt2*, and P*rsdA*. We assumed that the overproduced σ^HLys-53-Ala and σ^H168-AlaValArgValAla-172 would trigger higher promoter activity in two-plasmid assays with the chosen σ^D-dependent promoters than σ^H. This assumption was only confirmed with σ^HLys-53-Ala and P*cg0607* (**Figure 7**). This effect was particularly apparent at T24, when promoter activity with σ^HLys-53-Ala was 1.7-fold higher than that with σ^H. This higher activity compared to other promoters could be explained by the unparalleled presence of the GGAA sequence in the −35 region of P*cg0607,* which is a consensus sequence of −35 elements in σ^H-dependent promoters. This result indicated that Lys 53 in σ^H and Ala 53 in σ^HLys-53-Ala (and Ala 60 in σ^D) most likely interact with the −10 promoter elements.

Contrary to the expectation, σ^H168-AlaValArgValAla-172 recognized Pcg0607 less efficiently. To assess how the mutant σ^H168-AlaValArgValAla-172 could interact with the σ^D-controlled promoters, we analyzed the homology model with this mutant σ factor in more detail. Using a 50-ns MD simulation, we found that the complex of σ^H168-AlaValArgValAla-172 with the −35 element of the σ^D-controlled promoter is probably not stable. This was something of a surprise given that the native σ^H was able to efficiently bind σ^D-controlled promoter DNA in previous MD simulations. A detailed analysis of the MD trajectories showed that this instability appeared to be due to the absence of Arg at the final position of the AA sequence AlaValArgValAla (ThrValMetSerArg in σ^H). The positively charged Arg 172 side chain of σ^H was found to create a significant stabilizing interaction (a salt bridge) with the negatively charged backbone of promoter DNA. This hypothesis, which might explain the low efficiency of the mutant σ^H168-AlaValArgValAla-172, may be tested in the future by creating additional mutations suggested by the *in silico* analysis.

Multiple Overlapping Promoters Upstream of the σ^D-Controlled Genes

In addition to the TSS ascribed to the σ^D-controlled promoters (**Table 2**), start sites of transcription driven from different overlapping or nearby promoters were detected by RNA-seq for 8 of the 11 analyzed genes. We suggest that most of these promoters are activated by σ^A and/or σ^B, and two are activated by σ^H, according to the upstream sequences (**Figure 8A**, in green and red, respectively). The putative housekeeping promoters

A

Promoter[a]	Sequence[b]	Distance TSS-start codon[c]	Assumed sigma factor
P1 *cmt1*	TTACCCACAACGGGCTGAAAACACACAGCTTTGGTTTATATTGTCGATTA	85 nt	σ^A/σ^B
P3 *cmt1*	TTTTGGCTCGTTATTCGAAAAGGTAAAGCGCCTGTTAACGTAATAGCTTG	193 nt	σ^A/σ^B
P2 *cg0420*	ATTCTTGGGCTCGAGTCTTCTTATAGTTTACAGATGTAAAATATTTTGCA	82 nt	σ^A/σ^B
P1 *lpd*	CGCACCCGGATGCACGACAATGACCCACTAAACACGTATCCTTGAATGCG	0 nt	σ^A/σ^B
P3 *lpd*	AAAAGTAGAAATTATCGACCTTTAACGCCATTGTGATTAGTATTTTGGCG	439 nt	σ^A/σ^B
P2 *cg0607*	ACCCCCGAATTCAAATCCGTGTTGCGCGTTAATAAGGAACAATATCGGTG	70 nt	σ^A/σ^B
P2 *cg2047*	TCTCTTGATATTCGCATCAAGCATTTTTTAGTGACGTAACATCAAAGAAG	141 nt	σ^A/σ^B
P1 *lppS*	ATTTGATTACTCAGGGAATGTTCGTTTAGTTTCCATCGTTTTCGCTAGTA	132 nt	σ^H
P3 *lppS*	AATGATAACGATTTGCTCACAAAACCATTGAAAAGGCCATTCTGGACGTA	258 nt	σ^A/σ^B
P2 *fadD2*	TTCGTCTTTTGTTGGAGGAACGGTCACTCGCTCAAGTAGTGTTAGTTTGC	69 nt	σ^H
P2 *cmt2*	TGGGCTGTGATAACTACCCAAGAGTGTCACAACTTGGTAACGTGTGGGCG	80 nt	σ^A/σ^B

B

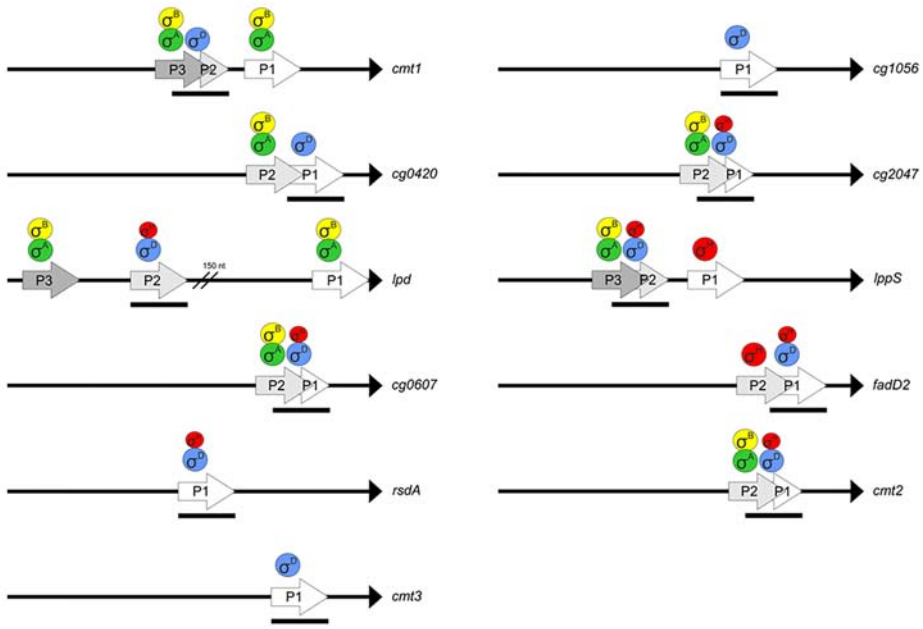

FIGURE 8 | Multiple promoters within upstream region of σ^D-dependent genes. **(A)** Sequences of putative σ^A/σ^B- or σ^H-dependent promoters within upstream region of σ^D-dependent genes. The promoters identified closest to the translation start codon were designated P1. The suggested –35 and –10 (or extended –10) promoter elements and the respective TSS are highlighted in green (σ^A/σ^B-dependent) or red (σ^H-dependent). TSS were detected by RNA-seq specific for transcription start sites. **(B)** Schematic representation of upstream regions of the genes with multiple promoters. To complete the studied promoter set, the fragments only carrying the σ^D-dependent promoters P*rsdA*, P*cmt3,* and P*cg1056* are also included. The proposed sigma factors regulating transcription from the individual promoters are shown above. Transcriptional starts are at the tips of the arrows. The length and positions of the bars below the arrows depict approximately the length and positions of the promoter-carrying DNA fragments (70 nt) used for both *in vitro* and *in vivo* assays. Translation initiation points are shown as black triangles.

are always located upstream of the σ^D-dependent promoters if there is a single additional σ^A- and/or σ^B-dependent promoter (upstream of the *cg0420*, *cg0607*, *cg2047*, and *cmt2* genes). Promoters which we consider to be σ^H-dependent according to the sequences of the putative −35 (GGAA) and −10 (GTT) elements were found upstream of *lppS* and *fadD2* genes. The detection of all TSS in the upstream regions of the σ^D-dependent genes was important to avoid effects of transcription started from the additional promoters. The position of the cloned promoter fragments for *in vivo* and *in vitro* assays could thus be chosen in such a way, that only the activity of the supposed σ^D-controlled promoters was determined. The organization of the multiple promoters within the upstream regions of the 8 genes is shown in **Figure 8B**. In the case of *fadD2*, the studied σ^D-dependent P1*fadD2* and the additional σ^H-dependent P2*fadD2* partially overlap and the activity of the

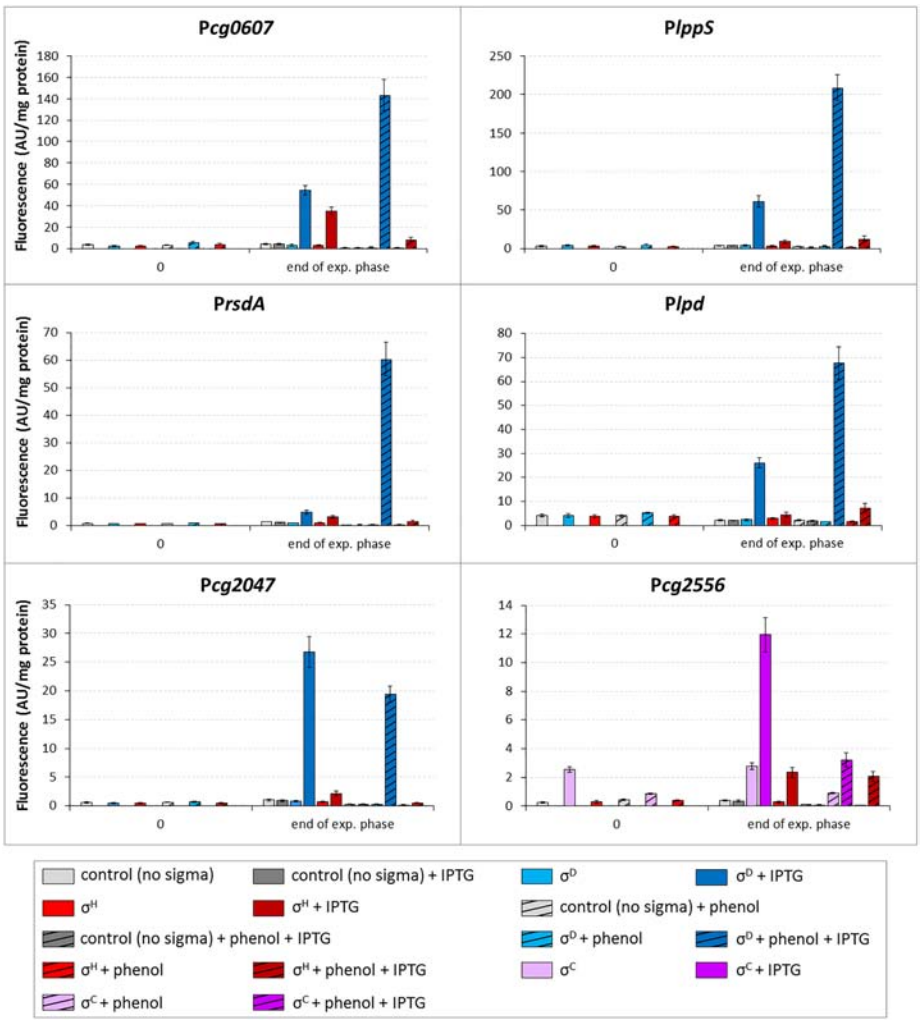

FIGURE 9 | Effect of phenol on activity of σ^D-dependent promoters. The *C. glutamicum* strains carried the vector pEC-XT99A overexpressing *sigH* (red bars), *sigD* (blue bars) or *sigC* (purple bars) after the addition of IPTG (added at OD_{600} = 1; dark bars) and the promoter-test vector pEPR1 constructs carrying the tested promoters (above the graphs). The strain overexpressing *sigC* and harboring pEPR1 with the σ^C-dependent promoter P*cg2556* (Dostálová et al., 2017), which is not activated by phenol, was used as a control (purple bars). Phenol (3.4 mM) was present in media from the beginning of cultivation (hatched bars). Plasmids carrying the pEPR1 construct and empty pEC-XT99A were used as controls (gray bars). The samples were taken at OD_{600} = 1 (0) and at the end of exponential growth phase. AU, arbitrary units. The standard deviations of three biological replicates are depicted by error bars.

additional σ^H-specific promoter might thus contribute to the overall σ^H-dependent activity of the fragment. However, such activity was not detected by *in vitro* transcription. *In vivo*, the σ^H-dependent activity was similarly low as in other cases. The σ^A- and/or σ^B-dependent promoters P3*cmt1*, P2*cg0420*, P2*cg0607*, P2*cg2047*, P3*lppS*, and P2*cmt2* (**Figures 8A,B**) were found to partially (mostly by the −10 region) reside on the 70-nt fragments with the analyzed σ^D-dependent promoters. However, their possible activity most probably did not interfere with the *in vivo* measurements of the effects of σ^D and σ^H overexpression.

Phenol as a Stressor

We have tested a number of stress conditions (heat shock, SDS, penicillin G, glycine, mitomycin C, phenol and limitation by glucose) to detect a slower growth of the *C. glutamicum* Δ*sigD* strain or to induce transcription from P*sigD* or from the promoters found to be σ^D-dependent (data not shown). Out of the conditions tested, only phenol exhibited a stronger inhibitory effect on the growth of the Δ*sigD* strain carrying the vector pEC-XT99A than on the growth of the analogous WT strain. We found that growth rate of *C. glutamicum* WT culture in 2xYT medium after the addition of 7.5 mM phenol decreased from 0.88 to 0.46 h^{-1} (1.9-fold), whereas the growth of the *C. glutamicum* Δ*sigD* decreased from 0.68 h^{-1} to 0.22 (3.1-fold). A difference in the effect of phenol was not significant in plasmidless strains.

To analyze the transcriptional response of *C. glutamicum* to phenol stress, we performed RNA-seq using the RNA isolated from the *C. glutamicum* WT cells grown in minimal medium with glucose (2%) or phenol (3.4 mM). Differential gene expression

analysis including normalization, was performed using the whole transcriptome data and Bioconductor package DESeq2 (Love et al., 2014) included in the software ReadXplorer v2.2 (Hilker et al., 2014). The evaluation of the differential RNA-seq data was performed using an adjusted *p*-value cut-off of $P \leq 0.01$ and a signal intensity ratio (*m*-value) cut-off of ≥ 1 or ≤ -1. According to the results (**Supplementary Tables S3**, **S4**), five genes previously found to be σ^D-dependent were more highly expressed on phenol than on glucose: *cg0607, lppS, rsdA, lpd,* and *cg2047* (**Supplementary Table S4**). The respective TSS identified by RNA-seq of 5′-enriched primary transcripts using the cultures grown on phenol were identical with those found using the *sigD* overexpressing strain.

The effect of phenol on the activity of the promoters P*cg0607,* P*lppS,* P*rsdA*, P*lpd,* and P*cg2047* was tested *in vivo* with the two-plasmid system. The strains carrying *sigD* or *sigH* inserted in pEC-XT99A and the promoters in pEPR1 were cultivated in minimal medium with glucose (2%) or phenol (3.4 mM). The promoter activity was measured in the extract of the cells before the addition of IPTG and at the end of exponential growth phase.

The activity of four promoters (P*cg0607*, P*lppS,* P*rsdA, and* P*lpd*) in the strains with overexpressed *sigD* was clearly higher after cultivation with phenol (**Figure 9**). The activity of the σ^C-dependent P*cg2556* used as a control was much lower in the medium with phenol under *sigC* overexpression conditions. The overexpression of *sigH* in the presence of phenol only resulted in a small increase in the P*lpd* activity. These results confirmed the data from RNA-seq (with the exception of P*cg2047* which was induced on phenol according to RNA-seq, but not in the two-plasmid assay). This is one of a few examples of the stress response to the action of phenolic compounds regulated by the ECF sigma factors in *C. glutamicum* (Chen et al., 2016, 2017). The phenol stress response mediated by ECF sigma factors will be further studied in *C. glutamicum* on the basis of the large amount of data produced by RNA-seq.

DISCUSSION

We recently began to study the function of *C. glutamicum* σ^D and its regulon for the first time (Taniguchi et al., 2017). The ECF sigma factor σ^D was found to be crucial for the envelope stress response, the synthesis of the mycomembrane and formation of the cell wall (Taniguchi et al., 2017; Toyoda and Inui, 2018). The genes of the σ^D regulon are involved in the synthesis of mycolic acids, the modification of peptidoglycan and other cell envelope-related functions. A subgroup of these genes which control mycolate metabolism are specific to the Mycolata group of bacteria, which include *Corynebacterium, Mycobacterium*, *Rhodococcus,* and *Nocardia* as the most important genera.

Sigma factors exhibiting a high level of similarity to *C. glutamicum* σ^D have been found in many bacteria. The highest level of AA identity with *C. glutamicum* σ^D was detected in σ^D proteins deduced from the respective genes in species closely related to *C. glutamicum* [*C. deserti* (94%), *C. callunae* (93%) and *C. efficiens* (90%)]. A lower level of identity (70–79%) was found with σ^D proteins from most of the phylogenetically more distant *Corynebacterium* species. The identity of *C. glutamicum* σ^D with σ^D proteins from other bacteria of the Mycolata group (e.g., genera *Mycobacterium*, *Rhodococcus,* and *Nocardia*) exhibited a range of 54–57%. All bacteria with a σ^D identity level higher than 45% (e.g., streptomycetes) belong to *Actinobacteria*. However, the functions of the genes of the σ^D regulons in these related bacteria are partially different. In addition to mycolate synthesis, the *M. tuberculosis*σ^D regulon is involved in virulence, lipid metabolism and gene expression under starvation conditions (Raman et al., 2004; Calamita et al., 2005).

A comparison of the promoter sequences of the putative σ^D-dependent genes among various bacteria was limited by the fact that either homologous genes were only found in a small number of *Corynebacterium* species (e.g., the genes *cg0420* and *cg2047* only occur in the genomes of three *C. glutamicum* strains) or no consensus sequences suggested for σ^D-dependent promoters were identified upstream of the homologous genes in the vast majority of other *Corynebacterium* species. Conservation of the putative σ^D-dependent promoter sequences among various bacteria was only found in the genes *cmt1* and *cmt2*, encoding trehalose corynomycolyl transferases.

Almost total conservation (37/38) of the −10 and −35 sequences (GTAAC − 15 nt – CTCGAT) in the P*rsdA* promoter was found in 38 *Corynebacterium* species encoding the anti-sigma factor RsdA. In other Actinobacteria (genera *Rhodococcus*, *Nocardia,* and *Mycobacterium*), a putative σ^D-dependent promoter is not present upstream of the *rsdA* gene but upstream of the *sigD* gene. Such an arrangement indicates that the *sigD-rsdA* operon is autoregulated by σ^D in these bacteria, in contrast to *C. glutamicum*, where σ^D seems to only control *rsdA* gene expression but not its own synthesis. Only two vegetative promoters were localized upstream of the *C. glutamicum* ATCC 13032 *sigD* gene (Pfeifer-Sancar et al., 2013).

We showed that σ^D played a dominant role in the transcription from all promoters tested in this study, however, low σ^H activity with most of these promoters was detected by the *in vivo* two-plasmid assay. This activity of the promoters was not observed when using *in vitro* transcription (with one exception). The promoter P*cg0607* was an exception and its efficiency documented by *in vitro* transcription was even higher with σ^H than with σ^D (**Figure 2**). The reason for this is probably that the −35 sequence GGAA within P*cg0607* is identical to the consensus of the −35 element of σ^H-controlled promoters. Similarly, the −10 element GTT, typical for σ^H-controlled promoters, was found in P*lpd*. Its activity with σ^H *in vivo* was also higher than that of other promoters (**Figure 3**). We can consider P*cg0607* and P*lpd* to be natural σ^D/σ^H-dependent hybrid promoters. However, it is apparent that the promoter efficiencies determined *in vivo* and *in vitro* do not correlate perfectly.

SigH plays a prominent role in the sigma regulatory network. Promoters controlled by σ^H were found to drive the transcription of *sigA* (Toyoda and Inui, 2015), *sigB* (Dostálová et al., 2017) and *sigM* (Nakunst et al., 2007). SigH, which also controls the expression of several genes encoding transcriptional regulators

(*clgR, sufR,* and *hspR*), is therefore considered to be a candidate for a global regulatory molecule (Schröder and Tauch, 2010). Overlap of the recognition specificities of σ^H and σ^E was described for some promoters (Šilar et al., 2016). In this study, an unexpected overlap of σ^H and σ^D in recognizing σ^D-dependent promoters has been proven.

To prove that the promoters are recognized directly with RNAP+σ^H, we measured the activities of P*cmt2*, P*lppS,* and P*rsdA* with σ^H in the Δ*sigD* strain. All three promoters were found to be active (**Figure 4**). The transcription driven by σ^H was apparently stronger in the absence of σ^D in the cell, probably because there was no competition with σ^D. Upstream regions of *cmt2* and *rsdA* carried no potential σ^H-specific promoter and the possible σ^H-specific promoter P1*lppS* was not included within the tested 70-nt P2*lppS* fragment (distance between TSS1 and TSS2 was 93 nt). Thus, it was apparently σ^H, which drove the detected activity of the σ^D-dependent promoter P2*lppS* in the Δ*sigD* mutant. Thus, σ^H was able to partially substitute for missing σ^D.

We have investigated the σ^D-dependent genes by different methods in *C. glutamicum* ATCC 13032 than those used in *C. glutamicum* R (Toyoda and Inui, 2018). In our study, differential gene expression analysis based on the obtained RNA-seq data of the whole transcriptome libraries (Illumina TruSeq stranded mRNA libraries) and RNA-seq of the 5′-enriched primary transcripts of *C. glutamicum* ATCC 13032 overexpressing *sigD* enabled us to not only discover the σ^D-regulated genes, but also precisely identify the TSS of the genes studied. Moreover, individual σ^D-dependent promoters were analyzed using *in vitro* transcription and *in vivo* two-plasmid assay. The *in vitro* assay revealed that P*cg0607* can directly drive transcription with RNAP+σ^H (**Figure 2**). Two σ^D-dependent genes of *C. glutamicum* ATCC 13032, *cg0420* and *cg2047* (encoding glycosyltransferase and a secreted protein, respectively), are not present on the *C. glutamicum* R chromosome. Another gene, *lpd* was not found to be σ^D-dependent in *C. glutamicum* R. The promoter P2*lpd* was localized 360 nt upstream of the translation initiation codon. There is a possibility that a potential small RNA, which was detected by RNA-seq, is transcribed from this promoter. P2*lpd* has a GTT sequence in the −10 region which is the consensus of σ^H-dependent promoters. The *lpd* gene (encoding dihydrolipoamide dehydrogenase) is known to play a role in the oxidative stress response in bacteria (Krisko et al., 2014). In *M. tuberculosis lpd* contributes to survival against host-generated reactive oxygen species (Daly et al., 2007). The activity of P2*lpd* was found to increase with *sigD* and, to a lesser extent, with *sigH* overexpression in the presence of phenol in *C. glutamicum* (**Figure 9**).

Based on the *in silico* analysis, the *sigH* mutants resulting in the production of the mutant proteins σ^HLys-53-Ala or σ^H168-AlaValArgValAla-172 were constructed. The mutation Lys-53-Ala within the −10 sequence-binding region of σ^H improved the σ^H-controlled activity of P*cg0607*, which is in agreement with the suggested crucial role of Ala in this position in recognizing the −10 element of σ^D-controlled promoters. The low promoter activity with σ^H mutant carrying 168-AlaValArgValAla-172 was probably due to the missing Arg 172, which may establish important stabilizing salt bridges with the sugar-phosphate backbone of DNA according to the *in silico* homology modeling.

Differential gene expression analysis of the transcriptome of *C. glutamicum* ATCC 13032 grown with or without phenol revealed that some σ^D-dependent genes (*cg0607*, *lppS, rsdA,* and *cg2047*) were higher transcribed under the phenol treatment. The promoters P*cg0607*, P*lppS,* P*rsd* and in addition P*lpd*, were also found to be induced by phenol in minimal medium by two-plasmid analysis (**Figure 9**). In *C. glutamicum* R, differential gene expression analyzed by microarrays showed that the σ^D-dependent genes play a role in the response to the lysozyme treatment (Toyoda and Inui, 2018). The changes in gene expression seem to be induced by the cell envelope stress exerted by the action of phenol or lysozyme.

Phenol in complete medium did not significantly slow the growth of the Δ*sigD* strain compared to the WT strain. However, when the replication of a single or even two plasmids placed a burden on the cell growth, these plasmid-harboring Δ*sigD* strains grew slower or did not grow at all. This extremely poor growth of Δ*sigD* strain with two plasmids was probably due to deficiencies in the cell envelope synthesis in combination with detrimental effects of supplemented antibiotics (Km and Tc) necessary for plasmid maintenance.

The function of σ^D-dependent genes and the organization of their transcription suggest that these genes play an important role not only in stress response, but also in cell homeostasis and in building a cell envelope during rapid growth under optimum conditions. Under optimal growth conditions, the transcription of the genes involved in corynomycolate synthesis is probably driven from additional σ^A- and/or σ^B-dependent promoters or σ^H-dependent promoters, which we detected upstream of many σ^D-dependent genes (**Figure 8A**). The transcription of σ^D-dependent genes from multiple promoters controlled by other sigma factors and the transcription from the σ^D-dependent promoters by σ^H may partially ensure the expression of these genes if the σ^D function is damaged or eliminated. However, these promoters are probably not strong enough to enable the cell to cope with the combined stress conditions if σ^D is missing. The low σ^H-triggered activity of the largely σ^D-controlled promoters, which is probably induced by modulation of the σ^H recognition specificity under particular physiological conditions, may contribute to fine-tuning transcription under various stresses, especially under the cell envelope stress.

Several genes of the *M. tuberculosis* σ^D regulon were found to be active in the stationary growth phase (Raman et al., 2004). Gfpuv fluorescence, which should reflect the activity of *C. glutamicum* σ^D-dependent promoters in our study, increased during cultivation and was found to be maximal at T24 (**Figure 3**). Interestingly, activity of the same promoters driven by σ^H exhibited the opposite trend. It therefore seems that σ^H may partially substitute for σ^D activity during the exponential phase.

The possible global regulator σ^H has been proven to play a crucial role in the hierarchy of σ factors, since it drives the transcription of at least three of them (σ^A, σ^B, and σ^M). Moreover, the regulatory overlaps of σ^H with transcriptional regulators

(Toyoda and Inui, 2015) and with several sigma factors including σ^D seem to control a number of physiological functions in *C. glutamicum* including heat, SOS, oxidative, chemical and cell surface stress responses. The accumulated evidence indicates that overlaps between the regulons of *C. glutamicum* ECF sigma factors are rather a common regulatory strategy how to cope with complex environmental stresses than an unusual exception.

AUTHOR CONTRIBUTIONS

MP and JK conceived the project and led the studies performed in Prague and Bielefeld, respectively. HD, TB, LR, and VŠ carried out the most experiments. TB and HD carried out RNA-seq and processed the data. JH did the *in vitro* transcription assays. JN performed the sequence analyses. IB carried out *in silico* analyses. All authors analyzed the results. MP and JN drafted the initial manuscript. All authors contributed to writing the final manuscript, reading, and approving the submitted version.

FUNDING

This work was supported by Grant 17-06991S from the Czech Science Foundation, Mobility Grant DAAD-18-11 from Czech Academy of Sciences (CAS) and Deutscher Akademischer Austauschdienst.

ACKNOWLEDGMENTS

Hironori Taniguchi (Wendisch Lab, Bielefeld University) is acknowledged for providing *sigD*-overexpressing *C. glutamicum* cultures for RNA isolation.

SUPPLEMENTARY MATERIAL

The Supplementary Material for this article can be found online at: https://www.frontiersin.org/articles/10.3389/fmicb.2018.03287/full#supplementary-material

TABLE S1 | Oligonucleotides used.

TABLE S2 | List of identified TSSs of SigD-upregulated genes and the respective sequences as detected by RNA-seq of transcriptome of *C. glutamicum* with overexpressed *sigD* cultivated on glucose.

TABLE S3 | List of identified TSSs of and the respective sequences as detected by RNA-seq of transcriptome of *C. glutamicum* WT cultivated on glucose.

TABLE S4 | List of identified SigD-dependent TSSs of SigD-upregulated genes and the respective sequences as detected by RNA-seq of transcriptome of *C. glutamicum* WT cultivated on phenol.

REFERENCES

Albersmeier, A., Pfeifer-Sancar, K., Rückert, C., and Kalinowski, J. (2017). Genome-wide determination of transcription start sites reveals new insights into promoter structures in the actinomycete *Corynebacterium glutamicum*. *J. Biotechnol.* 257, 99–109. doi: 10.1016/j.jbiotec.2017.04.008

Ao, W., Gaudet, J., Kent, W. J., Muttumu, S., and Mango, S. E. (2004). Environmentally induced foregut remodeling by PHA-4/FoxA and DAF-12/NHR. *Science* 305, 1743–1746. doi: 10.1126/science.1102216

Binder, S. C., Eckweiler, D., Schulz, S., Bielecka, A., Nicolai, T., Franke, R., et al. (2016). Functional modules of sigma factor regulons guarantee adaptability and evolvability. *Sci. Rep.* 6:22212. doi: 10.1038/srep22212

Busche, T., Šilar, R., Pičmanová, M., Pátek, M., and Kalinowski, J. (2012). Transcriptional regulation of the operon encoding stress-responsive ECF sigma factor SigH and its anti-sigma factor RshA, and control of its regulatory network in *Corynebacterium glutamicum*. *BMC Genomics* 13:445. doi: 10.1186/1471-2164-13-445

Calamita, H., Ko, C., Tyagi, S., Yoshimatsu, T., Morrison, N. E., and Bishai, W. R. (2005). The *Mycobacterium tuberculosis* SigD sigma factor controls the expression of ribosome-associated gene products in stationary phase and is required for full virulence. *Cell. Microbiol.* 7, 233–244. doi: 10.1111/j.1462-5822.2004.00454.x

Campagne, S., Marsh, M. E., Capitani, G., Vorholt, J. A., and Allain, F. H. (2014). Structural basis for -10 promoter element melting by environmentally induced sigma factors. *Nat. Struct. Mol. Biol.* 21, 269–276. doi: 10.1038/nsmb.2777

Chaturongakul, S., Raengpradub, S., Palmer, M. E., Bergholz, T. M., Orsi, R. H., Hu, Y., et al. (2011). Transcriptomic and phenotypic analyses identify coregulated, overlapping regulons among PrfA, CtsR, HrcA, and the alternative sigma factors σB, σC, σH, and σL in *Listeria monocytogenes*. *Appl. Environ. Microbiol.* 77, 187–200. doi: 10.1128/AEM.00952-10

Chen, C., Pan, J., Yang, X., Guo, C., Ding, W., Si, M., et al. (2016). Global transcriptomic analysis of the response of *Corynebacterium glutamicum* to vanillin. *PLoS One* 11:e0164955. doi: 10.1371/journal.pone.0164955

Chen, C., Pan, J., Yang, X., Xiao, H., Zhang, Y., Si, M., et al. (2017). Global transcriptomic analysis of the response of *Corynebacterium glutamicum* to ferulic acid. *Arch. Microbiol.* 199, 325–334. doi: 10.1007/s00203-016-1306-5

Chen, C., Zhang, Y., Xu, L., Zhu, K., Feng, Y., Pan, J., et al. (2018). Transcriptional control of the phenol hydroxylase gene phe of *Corynebacterium glutamicum* by the AraC-type regulator PheR. *Microbiol. Res.* 209, 14–20. doi: 10.1016/j.micres.2018.02.001

Cho, B. K., Kim, D., Knight, E. M., Zengler, K., and Palsson, B. O. (2014). Genome-scale reconstruction of the sigma factor network in *Escherichia coli*: topology and functional states. *BMC Biol.* 12:4. doi: 10.1186/1741-7007-12-4

Crooks, G. E., Hon, G., Chandonia, J. M., and Brenner, S. E. (2004). WebLogo: a sequence logo generator. *Genome Res.* 14, 1188–1190. doi: 10.1101/gr.849004

Dainese, E., Rodrigue, S., Delogu, G., Provvedi, R., Laflamme, L., Brzezinski, R., et al. (2006). Posttranslational regulation of *Mycobacterium tuberculosis* extracytoplasmic-function sigma factor sigma L and roles in virulence and in global regulation of gene expression. *Infect. Immun.* 74, 2457–2461. doi: 10.1128/IAI.74.4.2457-2461.2006

Daly, M. J., Gaidamakova, E. K., Matrosova, V. Y., Vasilenko, A., Zhai, M., Leapman, R. D., et al. (2007). Protein oxidation implicated as the primary determinant of bacterial radioresistance. *PLoS Biol.* 5:e92. doi: 10.1371/journal.pbio.0050092

Denyer, S. P. (1995). Mechanisms of action of antibacterial biocides. *Int. Biodeterior. Biodegr.* 36, 221–225. doi: 10.1016/0964-8305(96)00015-7

Dostálová, H., Holátko, J., Busche, T., Rucká, L., Rapoport, A., Halada, P., et al. (2017). Assignment of sigma factors of RNA polymerase to promoters in *Corynebacterium glutamicum*. *AMB Express* 7:133. doi: 10.1186/s13568-017-0436-8

Ehira, S., Teramoto, H., Inui, M., and Yukawa, H. (2009). Regulation of *Corynebacterium glutamicum* heat shock response by the extracytoplasmic-function sigma factor SigH and transcriptional regulators HspR and HrcA. *J. Bacteriol.* 191, 2964–2972. doi: 10.1128/JB.00112-09

Engels, S., Schweitzer, J. E., Ludwig, C., Bott, M., and Schaffer, S. (2004). *Clpc* and *clpP1P2* gene expression in *Corynebacterium glutamicum* is controlled by a regulatory network involving the transcriptional regulators ClgR and HspR as well as the ECF sigma factor σH. *Mol. Microbiol.* 52, 285–302. doi: 10.1111/j.1365-2958.2003.03979.x

Green, M. R., and Sambrook, J. (2012). *Molecular Cloning: A Laboratory Manual*, Fourth Edn. Cold Spring Harbor, NY: Cold Spring Harbor Laboratory Press.

Gruber, T. M., and Gross, C. A. (2003). Multiple sigma subunits and the partitioning of bacterial transcription space. *Annu. Rev. Microbiol.* 57, 441–466. doi: 10.1146/annurev.micro.57.030502.090913

Hanahan, D. (1985). "Techniques for transformation of *E. coli*," in *DNA Cloning. A Practical Approach*, Vol. 1, ed. D. M. Glover (Oxford: IRL), 109–135.

Hilker, R., Stadermann, K. B., Doppmeier, D., Kalinowski, J., Stoye, J., Straube, J., et al. (2014). ReadXplorer–visualization and analysis of mapped sequences. *Bioinformatics* 30, 2247–2254. doi: 10.1093/bioinformatics/btu205

Hilker, R., Stadermann, K. B., Schwengers, O., Anisiforov, E., Jaenicke, S., Weisshaar, B., et al. (2016). ReadXplorer 2-detailed read mapping analysis and visualization from one single source. *Bioinformatics* 32, 3702–3708. doi: 10.1093/bioinformatics/btw541

Holátko, J., Šilar, R., Rabatinová, A., Šanderová, H., Halada, P., Nešvera, J., et al. (2012). Construction of in vitro transcription system for *Corynebacterium glutamicum* and its use in the recognition of promoters of different classes. *Appl. Microbiol. Biotechnol.* 96, 521–529. doi: 10.1007/s00253-012-4336-1

Jordan, S., Hutchings, M. I., and Mascher, T. (2008). Cell envelope stress response in Gram-positive bacteria. *FEMS Microbiol. Rev.* 32, 107–146. doi: 10.1111/j.1574-6976.2007.00091.x

Kalinowski, J., Bathe, J., Bartels, D., Bischoff, N., Bott, M., Burkovski, A., et al. (2003). The complete *Corynebacterium glutamicum* ATCC 13032 genome sequence and its impact on the production of L-aspartate-derived amino acids and vitamins. *J. Biotechnol.* 104, 5–25. doi: 10.1016/S0168-1656(03)00154-8

Keilhauer, C., Eggeling, L., and Sahm, H. (1993). Isoleucine synthesis in *Corynebacterium glutamicum*: molecular analysis of the *ilvB-ilvN-ilvC* operon. *J. Bacteriol.* 175, 5595–5603. doi: 10.1128/jb.175.17.5595-5603.1993

Kirchner, O., and Tauch, A. (2003). Tools for genetic engineering in the amino acid-producing bacterium *Corynebacterium glutamicum*. *J. Biotechnol.* 104, 287–299. doi: 10.1016/S0168-1656(03)00148-2

Knoppová, M., Phensaijai, M., Veselý, M., Zemanová, M., Nešvera, J., and Pátek, M. (2007). Plasmid vectors for testing *in vivo* promoter activities in *Corynebacterium glutamicum* and *Rhodococcus erythropolis*. *Curr. Microbiol.* 55, 234–239. doi: 10.1007/s00284-007-0106-1

Kranz, A., Busche, T., Vogel, A., Usadel, B., Kalinowski, J., Bott, M., et al. (2018). RNAseq analysis of alpha-proteobacterium *Gluconobacter oxydans* 621H. *BMC Genomics* 19:24. doi: 10.1186/s12864-017-4415-x

Krisko, A., Copic, T., Gabaldon, T., Lehner, B., and Supek, F. (2014). Inferring gene function from evolutionary change in signatures of translation efficiency. *Genome Biol.* 15:R44. doi: 10.1186/gb-2014-15-3-r44

Lane, W. J., and Darst, S. A. (2006). The structural basis for promoter -35 element recognition by the group IV sigma factors. *PLoS Biol.* 4:e269. doi: 10.1371/journal.pbio.0040269

Langmead, B., and Salzberg, S. L. (2012). Fast gapped-read alignment with Bowtie 2. *Nat. Methods* 9, 357–359. doi: 10.1038/nmeth.1923

Love, M. I., Huber, W., and Anders, S. (2014). Moderated estimation of fold change and dispersion for RNA-seq data with DESeq2. *Genome Biol.* 15:550. doi: 10.1186/s13059-014-0550-8

Luo, Y., and Helmann, J. D. (2009). Extracytoplasmic function sigma factors with overlapping promoter specificity regulate sublancin production in *Bacillus subtilis*. *J. Bacteriol.* 191, 4951–4958. doi: 10.1128/JB.00549-09

Nakunst, D., Larisch, C., Hüser, A. T., Tauch, A., Pühler, A., and Kalinowski, J. (2007). The extracytoplasmic function-type sigma factor SigM of *Corynebacterium glutamicum* ATCC 13032 is involved in transcription of disulfide stress-related genes. *J. Bacteriol.* 189, 4696–4707. doi: 10.1128/JB.00382-07

Pátek, M., and Nešvera, J. (2011). Sigma factors and promoters in *Corynebacterium glutamicum*. *J. Biotechnol.* 154, 101–113. doi: 10.1016/j.jbiotec.2011.01.017

Pfeifer-Sancar, K., Mentz, A., Rückert, C., and Kalinowski, J. (2013). Comprehensive analysis of the *Corynebacterium glutamicum* transcriptome using an improved RNAseq technique. *BMC Genomics* 14:888. doi: 10.1186/1471-2164-14-888

Raman, S., Hazra, R., Dascher, C. C., and Husson, R. N. (2004). Transcription regulation by the *Mycobacterium tuberculosis* alternative sigma factor SigD and its role in virulence. *J. Bacteriol.* 186, 6605–6616. doi: 10.1128/JB.186.19.6605-6616.2004

Rezuchova, B., and Kormanec, J. (2001). A two-plasmid system for identification of promoters recognized by RNA polymerase containing extracytoplasmic stress response σE in *Escherichia coli*. *J. Microbiol. Methods* 45, 103–111. doi: 10.1016/S0167-7012(01)00237-8

Ross, W., Thompson, J. F., Newlands, J. T., and Gourse, R. L. (1990). E. coli Fis protein activates ribosomal RNA transcription in vitro and in vivo. *EMBO J.* 9, 3733–3742. doi: 10.1002/j.1460-2075.1990.tb07586.x

Salomon-Ferrer, R., Case, D. A., and Walker, R. C. (2013). An overview of the amber biomolecular simulation package. *WIREs Comput. Mol. Sci.* 3, 198–210. doi: 10.1002/wcms.1121

Schröder, J., and Tauch, A. (2010). Transcriptional regulation of gene expression in *Corynebacterium glutamicum*: the role of global, master and local regulators in the modular and hierarchical gene regulatory network. *FEMS Microbiol. Rev.* 34, 685–737. doi: 10.1111/j.1574-6976.2010.00228.x

Schulz, S., Eckweiler, D., Bielecka, A., Nicolai, T., Franke, R., Dotsch, A., et al. (2015). Elucidation of sigma factor-associated networks in *Pseudomonas aeruginosa* reveals a modular architecture with limited and function-specific crosstalk. *PLoS Pathog.* 11:e1004744. doi: 10.1371/journal.ppat.1004744

Seo, J. H., Hong, J. S., Kim, D., Cho, B. K., Huang, T. W., Tsai, S. F., et al. (2012). Multiple-omic data analysis of *Klebsiella pneumoniae* MGH 78578 reveals its transcriptional architecture and regulatory features. *BMC Genomics* 13:679. doi: 10.1186/1471-2164-13-679

Šilar, R., Holátko, J., Rucká, L., Rapoport, A., Dostálová, H., Kadeøabková, P., et al. (2016). Use of in vitro transcription system for analysis of *Corynebacterium glutamicum* promoters recognized by two sigma factors. *Curr. Microbiol.* 73, 401–408. doi: 10.1007/s00284-016-1077-x

Taniguchi, H., Busche, T., Patschkowski, T., Niehaus, K., Pátek, M., Kalinowski, J., et al. (2017). Physiological roles of sigma factor SigD in *Corynebacterium glutamicum*. *BMC Microbiol.* 17:158. doi: 10.1186/s12866-017-1067-6

Toyoda, K., and Inui, M. (2015). Regulons of global transcription factors in *Corynebacterium glutamicum*. *Appl. Microbiol. Biotechnol.* 100, 45–60. doi: 10.1007/s00253-015-7074-3

Toyoda, K., and Inui, M. (2016). The extracytoplasmic function sigma factor σC regulates expression of a branched quinol oxidation pathway in *Corynebacterium glutamicum*. *Mol. Microbiol.* 100, 486–509. doi: 10.1111/mmi.13330

Toyoda, K., and Inui, M. (2018). Extracytoplasmic function sigma factor σD confers resistance to environmental stress by enhancing mycolate synthesis and modifying peptidoglycan structures in *Corynebacterium glutamicum*. *Mol. Microbiol.* 107, 312–329. doi: 10.1111/mmi.13883

van der Rest, M. E., Lange, C., and Molenaar, D. (1999). A heat shock following electroporation induces highly efficient transformation of *Corynebacterium*

glutamicum with xenogeneic plasmid DNA. *Appl. Microbiol. Biotechnol.* 52, 541–545. doi: 10.1007/s002530051557

Waterhouse, A., Bertoni, M., Bienert, S., Studer, G., Tauriello, G., Gumienny, R., et al. (2018). SWISS-MODEL: homology modelling of protein structures and complexes. *Nucleic Acids Res.* 46, W296–W303. doi: 10.1093/nar/gky427

Wittchen, M., Busche, T., Gaspar, A. H., Lee, J. H., Ton-That, H., and Kalinowski, J. (2018). Transcriptome sequencing of the human pathogen *Corynebacterium diphtheriae* NCTC 13129 provides detailed insights into its transcriptional landscape and into DtxR mediated transcriptional regulation. *BMC Genomics* 19:82. doi: 10.1186/s12864-018-4481-8

Conflict of Interest Statement: The authors declare that the research was conducted in the absence of any commercial or financial relationships that could be construed as a potential conflict of interest.

frontiers in Microbiology

ORIGINAL RESEARCH
published: 14 January 2019
doi: 10.3389/fmicb.2018.03329

Structural and Physiological Exploration of *Salmonella* Typhi YfdX Uncovers Its Dual Function in Bacterial Antibiotic Stress and Virulence

Hye Seon Lee[1,2†], Soohyun Lee[3†], Jun-Seob Kim[3], Hae-Ran Lee[3], Ho-Chul Shin[1], Moo-Seung Lee[3], Kyeong Sik Jin[4], Cheol-Hee Kim[2], Bonsu Ku[1], Choong-Min Ryu[3,5]* and Seung Jun Kim[1,6]**

[1] Disease Target Structure Research Center, Korea Research Institute of Bioscience and Biotechnology, Daejeon, South Korea, [2] Department of Biology, Chungnam National University, Daejeon, South Korea, [3] Infectious Disease Research Center, Korea Research Institute of Bioscience and Biotechnology, Daejeon, South Korea, [4] Pohang Accelerator Laboratory, Pohang University of Science and Technology, Pohang, South Korea, [5] Department of Biotechnology, University of Science and Technology KRIBB School, Daejeon, South Korea, [6] Department of Bioscience, University of Science and Technology KRIBB School, Daejeon, South Korea

OPEN ACCESS

Edited by:
Daniela De Biase,
Sapienza University of Rome, Italy

Reviewed by:
Geqing Wang,
La Trobe University, Australia
Timothy James Wells,
The University of Queensland, Australia

***Correspondence:**
Bonsu Ku
bku@kribb.re.kr
Choong-Min Ryu
cmryu@kribb.re.kr
Seung Jun Kim
ksj@kribb.re.kr

† These authors have contributed equally to this work

Specialty section:
This article was submitted to Microbial Physiology and Metabolism, a section of the journal Frontiers in Microbiology

Received: 18 July 2018
Accepted: 21 December 2018
Published: 14 January 2019

Citation:
Lee HS, Lee S, Kim J-S, Lee H-R, Shin H-C, Lee M-S, Jin KS, Kim C-H, Ku B, Ryu C-M and Kim SJ (2019) Structural and Physiological Exploration of Salmonella Typhi YfdX Uncovers Its Dual Function in Bacterial Antibiotic Stress and Virulence. Front. Microbiol. 9:3329. doi: 10.3389/fmicb.2018.03329

YfdX is a prokaryotic protein encoded by several pathogenic bacteria including *Salmonella enterica* serovar Typhi, which causes one of the most fatal infectious diseases, typhoid fever. YfdX is a product of the *yfdXWUVE* operon and is known to be under the control of EvgA, a regulator protein controlling the expression of several proteins involved in response to environmental stress, in *Escherichia coli*. Nevertheless, unlike other proteins encoded by the same operon, the structural and physiological aspects of YfdX have been poorly characterized. Here, we identified a previously unknown pH-dependent stoichiometric conversion of *S*. Typhi YfdX between dimeric and tetrameric states; this conversion was further analyzed via determining its structure by X-ray crystallography at high resolution and by small-angle X-ray scattering in a solution state and via structure-based mutant studies. Biologically, YfdX was proven to be critically involved in *Salmonella* susceptibility to two β-lactam antibiotics, penicillin G and carbenicillin, as bacterial growth significantly impaired by its deficiency upon treatment with each of the two antibiotics was recovered by chromosomal complementation. Furthermore, by using *Galleria mellonella* larvae as an *in vivo* model of *Salmonella* infection, we demonstrated that *Salmonella* virulence was remarkably enhanced by YfdX deficiency, which was complemented by a transient expression of the wild-type or dimeric mutant but not by that of the monomeric mutant. The present study work provides direct evidence regarding the participation of YfdX in *Salmonella* antibiotic susceptibility and in the modulation of bacterial virulence, providing a new insight into this pathogen's strategies for survival and growth.

Keywords: STY3178, YfdX, *Salmonella* Typhi, antibiotics susceptibility, virulence

Abbreviations: CD, circular dichroism; DTT, dithiothreitol; MDR, multiple drug resistance; PDB, Protein Data Bank; SAXS, small-angle X-ray scattering; SEC-MALS, size exclusion chromatography-multiangle light scattering.

INTRODUCTION

Salmonella enterica serovar Typhi is a gram-negative bacterium that infects humans only (Hurley et al., 2014), causing systemic typhoid fever. Typhoid is one of the most widespread and hazardous infectious diseases in developing countries, with more than 16 million cases and 200,000 estimated deaths per year (Buckle et al., 2012; Dougan and Baker, 2014; Azmatullah et al., 2015). *S.* Typhi initially penetrates the small intestinal epithelial cells and then spreads through the bloodstream to other organs such as the spleen, liver, and bone marrow, where this bacterium multiplies and reenters the bloodstream causing symptoms including a high fever (Everest et al., 2001). A variety of antibiotics, such as ampicillin, chloramphenicol, trimethoprim-sulfamethoxazole, and ciprofloxacin, have already been used against *S.* Typhi (Kalra et al., 2003). Nevertheless, exposure to antibiotics over long periods has allowed *S.* Typhi to acquire resistance to various antibiotics through genetic changes: a phenomenon called "multiple drug resistance (MDR)" (Rowe et al., 1997; Kalra et al., 2003; Frye and Jackson, 2013). MDR strains exhibit strong resistance to antibiotics, and lead to treatment failure (Rowe et al., 1997; Parkhill et al., 2001; Kariuki et al., 2015; Karkey et al., 2018).

Bacterial resistance to antibiotics is acquired via a combination of a variety of strategies, which include alteration of a target protein, enzymatic deactivation, and restriction of antibiotic accessibility (Nikaido, 2009). How bacteria orchestrate these complicated events accompanying a change in the expression of several proteins has been under intensive investigation. It has been reported that EvgA, one of the response regulator proteins of *Escherichia coli*, constitutes a two-component system together with the sensor kinase EvgS and controls the expression of a wide range of genes involved in the response to stressors such as antibiotics and pH changes (Nishino and Yamaguchi, 2001, 2002; Masuda and Church, 2002; Nishino et al., 2003). The *yfdXWUVE* operon is one of the targets upregulated by EvgA (Masuda and Church, 2002; Nishino et al., 2003) and encodes formyl-CoA transferase YfdW (Gruez et al., 2003), oxalyl-CoA decarboxylase YfdU (Werther et al., 2010), acetyl-CoA:oxalate CoA-transferase YfdE (Mullins et al., 2013), putative transporter protein YfdV, and an uncharacterized protein YfdX, whose expression has been reported to be enhanced a 1000-fold by EvgA overproduction (Nishino and Yamaguchi, 2002; Nishino et al., 2003). Homologs of YfdX have been identified in various virulent bacterial species including *S.* Typhi (Parkhill et al., 2001), *S.* Typhimurium (McClelland et al., 2001), *Hafnia alvei* (Lazaro-Diez et al., 2016), *Shigella dysenteriae* (Kaur et al., 2014), and *Klebsiella pneumoniae* (Jiang et al., 2010). Furthermore, the crystal structure of *K. pneumoniae* YfdX in the tetramer-estimated form was determined and deposited at the PDB without accompanying publications (PDB code 3DZA). Recently, it has been reported that a bacterial protein STY3178, an ortholog of YfdX from the *S.* Typhi representative MDR strain CT18, interacts with three antibiotics ciprofloxacin, ampicillin, and rifampin (Saha et al., 2016b), has a chaperone-like activity (Saha et al., 2016a), and is modeled to interact with the outer-membrane protein STY3179 (Mondal et al., 2017), providing clues for understanding this protein. However, a number of unresolved issues about YfdX remain, with the absence of structural and physiological analyses, including its functional role during bacterial infection as well as its precise stoichiometry. *K. pneumoniae* YfdX appears to form a homotetramer in the crystal structure, whereas *S.* Typhi YfdX is proposed to form a trimer in solution according to dynamic light scattering, size exclusion chromatography, and nuclear magnetic resonance experiments (Saha et al., 2016b).

In this study, we attempted to answer such unresolved issues about the YfdX protein through structural, biochemical, and physiological analyses. An unexpected stoichiometric conversion of *S.* Typhi YfdX between the dimer and tetramer was identified, which was further analyzed via mutational assays based on crystal structure determination. Moreover, we found that *Salmonella* YfdX plays a significant role in bacterial susceptibility to penicillin G and carbenicillin and is involved in the negative regulation of bacterial virulence in an insect larvae model. These data collectively expand our understanding of this poorly studied protein.

MATERIALS AND METHODS

Crystallization and Structure Determination of *st*_YfdX

The DNA fragment coding for residues 10–186 of *st*_YfdX was cloned into the pET21a plasmid (Novagen). The protein was produced in the *E. coli* BL21(DE3) RIL strain (Novagen) at 18°C and purified on a Ni-NTA column (QIAGEN) first. The protein was further purified on a HiLoad 26/600 Superdex 75 prep grade gel filtration column (GE Healthcare), equilibrated with a buffer consisting of 20 mM Tris-HCl (pH 7.5), 200 mM NaCl, and 1 mM DTT. All crystals were obtained via the sitting-drop vapor diffusion method at 18°C by mixing and equilibrating 0.4 μL samples of the protein solution (20 mg/mL) with a precipitant solution as described in **Table 1**. Before data collection, crystals were immersed briefly in the reservoir solution containing a cryoprotectant reagent as shown in **Table 1**. Diffraction data were collected on the beamline 5C and 7A at the Pohang Accelerator Laboratory, South Korea, and processed using the *HKL* 2000 software (Otwinowski and Minor, 1997). The structure was determined by the molecular replacement method with the Phaser software (McCoy et al., 2007) using the structure of *kp*_YfdX (PDB code 3DZA) as a search model. Programs Coot (Emsley and Cowtan, 2004) and PHENIX (Adams et al., 2010) were used for the model building and refinement, respectively. Crystallographic data statistics are summarized in **Table 2**[1].

Preparation of Recombinant Proteins

Each of the DNA fragments encoding mutant *st*_YfdX proteins containing F42A·F45A·Y165A or Y100A·I137A

[1]The coordinates and the structure factors of the *st*_YfdX structures determined using crystals I, II, and III have been deposited in the PDB under the accession codes 6A02, 6A07, and 6A09, respectively.

TABLE 1 | Crystallization and cryoprotectant reagent conditions.

	Space group	Crystallization condition	Cryoprotectant reagent
Crystal I	*F222*	0.1 M sodium acetate (pH 4.6), 2.5 M sodium chloride, 12% PEG1500, 1.5% 2-methyl-2,4-pentanediol	15% glycerol
Crystal II	*F222*	0.1 M sodium acetate (pH 4.6), 2.5 M sodium chloride, 12% PEG1500, 1.5% 2-methyl-2,4-pentanediol	5% glycerol
Crystal III	*P222*	4% Tacsimate (pH 5.0), 12% PEG3350	20% glycerol

TABLE 2 | Data collection and structure refinement statistics.

PDB code	Crystal I (6A02)	Crystal II (6A07)	Crystal III (6A09)
Space group	*F222*	*F222*	*P222*
Unit cell dimensions			
a, b, c (Å)	88.8, 92.5, 95.5	88.8, 92,2, 95.4	72.4, 127.9, 170.4
α, β, γ (^{o})	90, 90, 90	90, 90, 90	90, 90, 90
Wavelength (Å)	0.9793	0.9793	0.9793
Resolution (Å)	50.0-1.4 (1.42-1.40)[b]	50.0-1.5 (1.53-1.50)[b]	50.0-2.3 (2.34-2.30)[b]
R_{sym}[a]	9.5 (27.1)	8.1 (28.0)	8.0 (27.7)
$I/\sigma(I)$	41.3 (4.7)	38.3 (5.6)	29.5 (4.9)
Completeness (%)	98.8 (96.5)	99.4 (99.5)	98.5 (91.2)
Redundancy	9.4	6.0	5.5
Refinement			
Resolution (Å)	50.0-1.4 (1.43-1.40)	50.0-1.5 (1.54-1.50)	50.0-2.3 (2.35-2.30)
Number of reflections	38,242	31,146	70,194
R_{work}[c]/R_{free}	18.9/21.3 (28.2/29.3)	18.2/21.5 (22.2/23.5)	18.0/23.3 (23.1/27.6)
Number of atoms			
Protein/water and ion	1326/198	1337/223	10668/587
RMSD			
Bond lengths (Å)/angles (^{o})	0.005/0.713	0.005/0.720	0.008/0.839
Ramachandran plot (%)			
Favored/allowed	98.2/1.8	98.8/1.2	98.2/1.8
Average B-values (Å^2)			
Protein/water and ion	17.1/27.2	19.1/30.0	37.4/38.7
Molprobity score	1.09 (99th percentile; N = 3363, 1.400 ± 0.25 Å)	1.05 (99th percentile; N = 4775, 1.501 ± 0.25 Å)	1.35 (100th percentile; N = 8821, 2.293 ± 0.25 Å)

[a] $R_{sym} = \Sigma\ |I_{obs} - I_{avg}|/I_{obs}$, *where* I_{obs} *is the observed intensity of individual reflection and* I_{avg} *is the average over symmetry equivalents.* [b] *The numbers in parentheses are statistics from the shell with the highest resolution.* [c] $R_{work} = \Sigma\ ||F_o| - |F_c||/\Sigma\ |F_o|$, *where* $|F_o|$ *and* $|F_c|$ *are the observed and calculated structure factor amplitudes, respectively.* R_{free} *was calculated with 10% of the data.*

substitutions and a DNA fragment encoding *kp*_YfdX was cloned into the pET21a plasmid. The recombinant proteins were produced and purified as was the wild-type *st*_YfdX.

Size Exclusion Chromatography-Multiangle Light Scattering Experiments

Size exclusion chromatography-multiangle light scattering (SEC-MALS) was performed using Superdex 75 Increase 10/300 GL (GE Healthcare). The differential refractive index spectra were recorded on Optilab T-rEX (Wyatt Technology Corporation), which was combined with high-performance liquid chromatography (Shimadzu) and DAWN HELEOS-II (Wyatt Technology Corporation). The weight-average molar mass was calculated using the ASTRA 6 software (Wyatt Technology Corporation).

Circular Dichroism Spectroscopy

Data were collected on a JASCO model J-815 spectropolarimeter with a 0.1-cm cuvette. The circular dichroism (CD) spectrum was recorded over the range of 200–260 nm in a nitrogen atmosphere with 0.1 mg/mL protein samples dissolved in 40 mM sodium phosphate buffer (pH 6.0 or 7.5). The spectrum comprised the accumulation of three scans at 0.2 nm intervals, which was corrected by subtracting signals from the buffer control. The raw CD signals were converted to mean residue ellipticity $[\theta_{MRE}]$ (in deg cm^2 dmol^{-1}) using the equation $[\theta_{MRE}] = \theta_{obs}/Cnl$, where θ_{obs} is the observed ellipticity (in millidegrees), C is the protein concentration (in molarity), n is the number of amino acid residues, and l is the pathlength (in millimeters).

Small-Angle X-Ray Scattering Experiments

Small-angle x-ray scattering (SAXS) measurements were carried out using the 4C SAXS II beamline at the Pohang Accelerator Laboratory, South Korea (Kim et al., 2017). Data were collected at 4°C with a sample-to-detector distance of 4,000 and 1,000 mm. Protein samples were prepared at pH 5.5 and 8.0, each of which was diluted to three different concentrations (1, 3, and 5 mg/mL). The SAXS data of each sample were collected in 10 successive frames of 5 s at 0.734 Å wavelength, which were measured in triplicates. Two-dimensional SAXS patterns were averaged and normalized for further analysis. Scattering intensities from the buffer solution were used as the experimental background. The scattering intensity data $I(q)$ as a function of q ($q = 4\pi\sin\theta/\lambda$, where θ is half of the scattering angle and λ is the wavelength; 0.01 Å^{-1} < q < 0.7 Å^{-1}) were obtained by radial averaging. CRYSOL (Svergun et al., 1995) and GNOM (Semenyuk and Svergun, 1991) were used to calculate the SAXS curves and distance distribution function $P(r)$, respectively. Molecular envelops were reconstructed using the *ab initio* shape determination program DAMMIF (Franke and Svergun, 2009). Fifteen independent models were generated, compared, and averaged to obtain the refined models using the programs DAMAVER and DAMSTART. Surface rendering was achieved using the program PyMOL. Structural diagrams were superimposed onto the reconstructed dummy atoms using SUPCOMB (Kozin and Svergun, 2001). Normalized spatial discrepancies were 3.13 for the tetramer and 3.32 for the MolA–Mol B dimer.

Knockout and Complementation of *yfdX*

Salmonella transformants carrying the pKD46 Red helper plasmid were cultured in the Luria-Bertani (LB) medium containing 100 μg/mL ampicillin and 10 mM L-arabinose at 30°C until turbidity at 600 nm reached 0.35–0.4. The cells were harvested and washed three times with ice-cold 10% glycerol and sterilized water to prepare electro-competent cells. A polymerase chain reaction (PCR) product containing the kanamycin resistance gene (amplified from pKD4) flanked upstream and downstream by sequences of the target gene (*yfdX*) was obtained using primers *yfdX*-p1 (5′-TGGCCGCAACAAACATGACTGATAACGTTACTCTGAATAATGACAAGATGTGTAGGCTGGAGCTGCTTC-3′) and *yfdX*-p2 (5′-GCGCGGCGTCGTGCTGCACGGAGTGCGTGGGTGATTCCTGAACTGACTGAATGGGAATTAGCCATGGTCC-3′). Next, 50 μL of electro-competent cells was mixed with 500 ng of the PCR product containing the 50 bp homologous sequence arms at each end of the kanamycin resistance cassette. Electroporation was performed in a 2-mm cuvette on Gene Pulser 3 (Bio-Rad) set at 2.5 kV, 25 μF, and 200 Ω. Transformants were screened on LB agar containing 50 μg/mL kanamycin. Knockouts were confirmed with primers *yfdX*-up97 (5′-GTGGGTTACCGGTTCTGAATAG-3′) and *yfdX*-dn43 (5′-CATAATGCTGCCTGCTGTAATG-3′). The kanamycin cassette was removed by pCP20 transformation (Datsenko and Wanner, 2000). For chromosomal complementation, the *yfdX*-kanamycin resistance cassette fusion PCR products were prepared using primers *yfdX*-ATG20 (5′-ATGGTTATCCTGTTTTCAGG-3′) and *yfdX*-dn_H_P2 (5′-TGTCAGACATAATGCTGCCTGCTGTAATGTATACAGCAGGCTGGGGGATAATGGGAATTAGCCATGGTCC-3′). Homologous recombination was performed as described above. For plasmid complementation, *yfdX* genes encoding wild-type or each mutant were cloned into the pNM12 vector harboring the *ara* promoter and ampicillin marker, which were then transformed into the *S.* Typhimurium UK-1 Δ*yfdX* strain.

Phenotype Microarrays

BiOLOG phenotypic microarray analyses were conducted following the manufacturer's instructions (BiOLOG, Inc.). In brief, bacteria were grown at 37°C for 16 h on LB agar media, and then scraped and resuspended in IF-0a. After that, 100 μL of a cell resuspension was inoculated into each well of phenotype microarray plates (#1–20). Respiration signals from 0 to 24 h shown in red were measured by BiOLOG OmniLog and then compared between the two strains. The microarray results were validated following the BiOLOG protocol with small modifications. To determine the minimum inhibitory concentration, serially diluted antibiotics were mixed with cell suspensions (5×10^5 cfu/mL), and then respiration signals were measured. All the experiments were conducted in triplicate.

Insect-Toxicity Assay

Injection assays with *Galleria mellonella* larvae were performed as described by Flury et al. (2016) with small variations. *G. mellonella* caterpillars purchased from S-WORM were grown at 30°C until they reached the fourth larval instar. Caterpillars were stored in the dark at 30°C for 3 days for stabilization. For injection, suspensions of overnight cultured bacterial cells were prepared in pH 7.4 PBS consisting of 137 mM NaCl, 2.7 mM KCl, 4.3 mM Na_2HPO_4, and 1.47 mM KH_2PO_4, and diluted to the desired concentration (10^5 cfu/μL). Bacterial cells resuspended in 2 μL of PBS were injected into larvae with a 5 μL microsyringe (MicroliterTM #701, Hamilton). The larvae were kept in Petri dishes at 30°C in the dark. For the evaluation of bacterial virulence, larvae were scored as live or dead for every 6 h up to 72 h. Each experiment consisted of three replicates per treatment with 10 larvae per replicate.

Bacterial RNA Isolation and Real-Time PCR

Salmonella Typhimurium UK1 strains were grown in the LB medium under aerobic conditions at 37°C for 4, 8, and 12 h before RNA isolation. The cells were stabilized using the RNA protect Bacteria Reagent (Qiagen), and total RNA was isolated using the RNeasy Kit (Qiagen). cDNA was synthesized with Superscript III Reverse transcriptase (Invitrogen). The mRNA levels of the coding regions of the *yfdX* gene were measured by quantification of cDNA using SYBR Green PCR Master Mix (Bio-Rad) with primers Q-ST-yfdX-F (5′-CTAGCAGGCGTCAGTGTTATT-3′) and Q-ST-yfdX-R (5′-ATGCCATCCTGAGCTGATTT-3′) monitored on a CFX connect real-time PCR detection system (Bio-Rad). The mRNA levels of the *yfdX* gene were normalized to the levels of 16S ribosomal RNA amplified with primers ST-16S-QF (5′-GTTAGCCGGTGCTTCTTCTG-3′) and ST-16S-QR (5′-TAGGCCTTCGGGTTGTAAAGT-3′).

RESULTS

Analysis of Stoichiometry of *S.* Typhi YfdX by SEC-MALS

The recombinant *S.* Typhi YfdX protein containing residues 10–186 from its total 199 amino acids, referred to as *st*_YfdX in this manuscript, was overexpressed in *E. coli* and purified on a Ni–NTA column and a size-exclusion chromatography column, equilibrated with a final buffer consisting of 20 mM Tris-HCl (pH 7.5), 200 mM NaCl, and 1 mM DTT (**Figure 1A**). To verify the stoichiometry of *st*_YfdX by means of the recombinant protein, we carried out SEC-MALS experiments, which is a useful tool for elucidating the molecular weight and stoichiometry of macromolecules in solution (Sahin and Roberts, 2012). Unexpectedly, the molecular weight of wild-type *st*_YfdX, which was concentrated to 10 mg/mL, was determined to be ∼42 kDa, suggesting that this protein exists as a dimer in solution, neither a trimer nor a tetramer, under this condition (**Figure 1B**). Increasing the concentration of the protein sample to 30 mg/mL did not alter its stoichiometry (**Figure 1B**). Based on the presence of the zinc ion coordination at the center of the *K. pneumoniae* YfdX (referred to as *kp*_YfdX) tetrameric structure (not shown), we suspected that a similar coordination might be necessary for

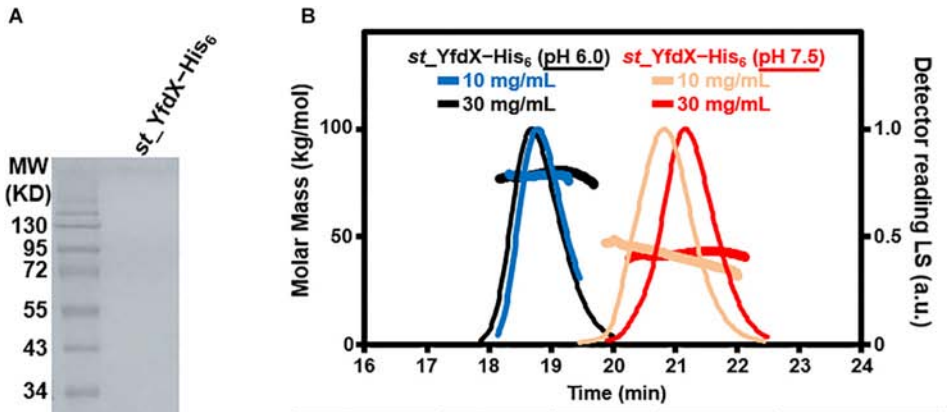

Protein	Conc.	Residues (a.a)	Mw (kg/mol)	Polydispersity (Mw/Mn)
*st*_YfdX–His_6 (pH 6.0)	10 mg/mL	190	78.4 (±0.166%)	1.000 (±0.235%)
	30 mg/mL		78.8 (±0.337%)	1.000 (±0.478%)
*st*_YfdX–His_6 (pH 7.5)	10 mg/mL		41.9 (±0.853%)	1.005 (±1.236%)
	30 mg/mL		42.1 (±0.311%)	1.000 (±0.439%)

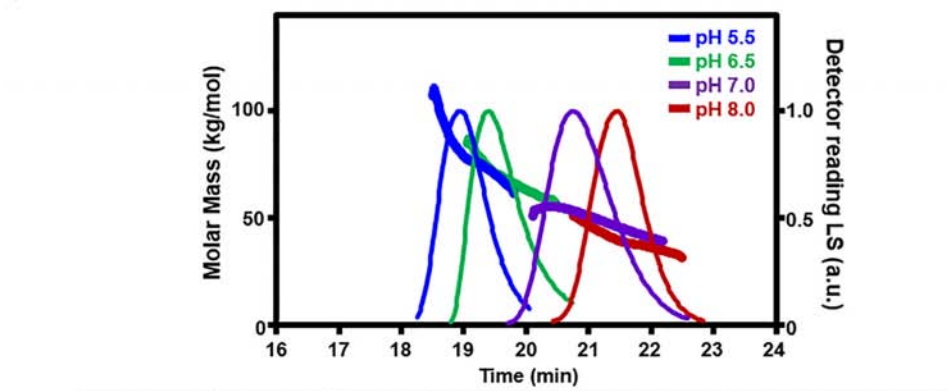

Protein	Buffer pH	Residues (a.a)	Mw (kg/mol)	Polydispersity (Mw/Mn)	Estimated ratio (%)	
					Tetramer	Dimer
*st*_YfdX–His_6 (10 mg/mL)	5.5	190	80.8 (±1.182%)	1.014 (±1.765%)	100	0
	6.0		78.4 (±0.166%)	1.000 (±0.235%)	94	6
	6.5		70.6 (±1.060%)	1.010 (±1.547%)	75	25
	7.0		50.9 (±1.114%)	1.008 (±1.619%)	26	74
	7.0*		52.6 (±0.544%)	1.012 (±0.784%)	30	70
	7.5		41.9 (±0.853%)	1.005 (±1.236%)	4	96
	8.0		40.4 (±1.318%)	1.009 (±1.965%)	0	100

FIGURE 1 | Preparation and SEC-MALS analysis of *st*_YfdX. **(A)** Purified *st*_YfdX–His_6 (20 μg) was loaded onto a sodium dodecyl sulfate polyacrylamide gel electrophoresis system and visualized by Coomassie blue staining together with the size markers. **(B)** SEC-MALS analysis of wild-type *st*_YfdX–His_6. (*Top*) Molar masses (in kg/mol) are plotted against the elution time (in min) from a size exclusion column. (*Bottom*) *st*_YfdX–His_6 is in the form of a dimer at pH 7.5 and a tetramer at pH 6.0. Mw, weight-average molar mass; Mn, number-average molar mass. **(C)** *st*_YfdX is in pH-dependent dimer–tetramer equilibrium. (*Top*) SEC-MALS analysis was carried out under various pH conditions. (*Bottom*) Molecular weight of *st*_YfdX–His_6 measured at the indicated condition are listed. The asterisk indicates the buffer condition (30 mM phosphate buffer pH 7.0 and 150 mM NaCl) used in the previous report (Saha et al., 2016b).

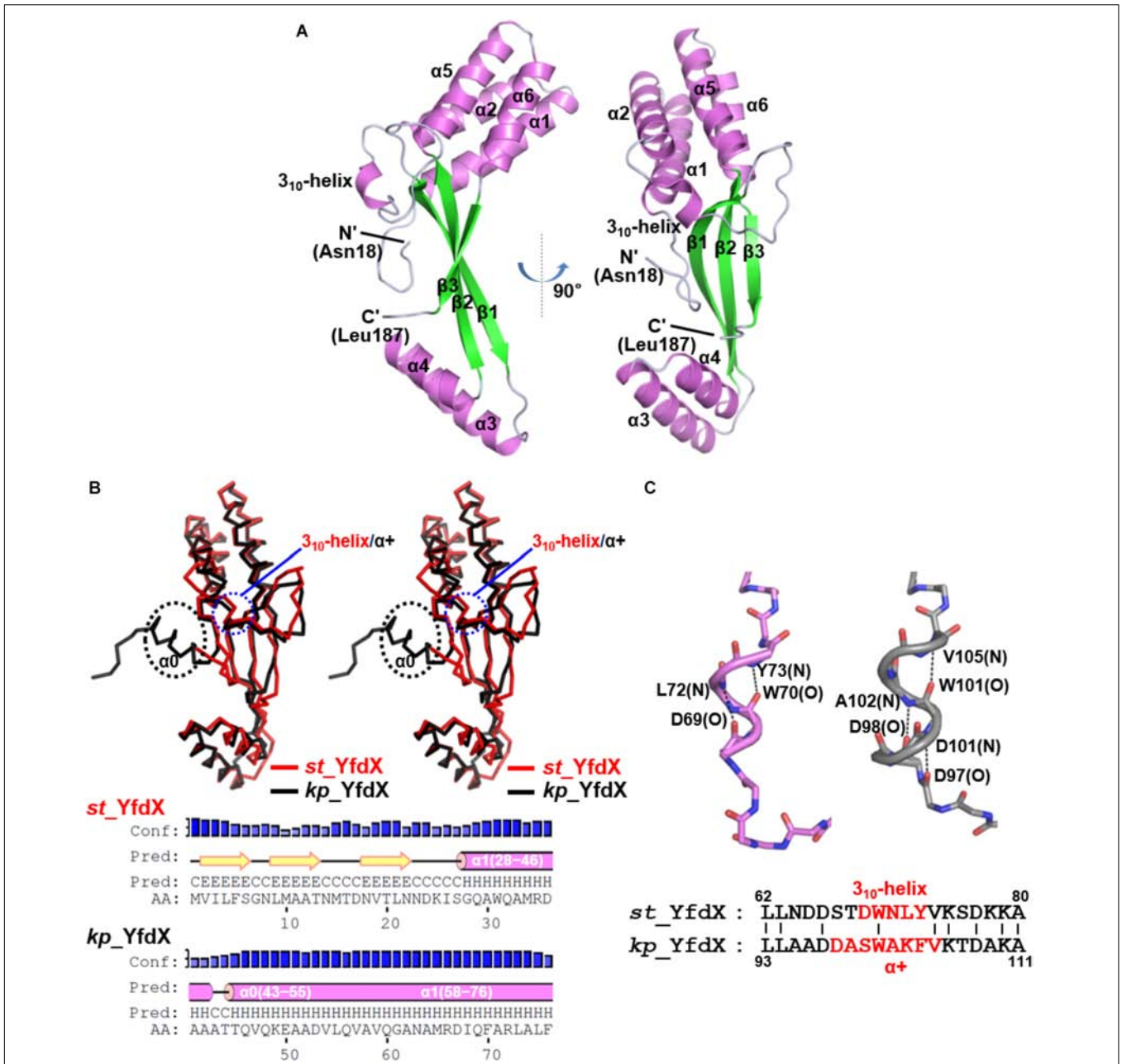

FIGURE 2 | Crystal structure of the *st*_YfdX monomer. **(A)** Two views of the *st*_YfdX monomeric structure are presented as ribbon drawings with the labeled secondary structures. **(B)** (*Top*) Stereo views of superimposed *st*_YfdX (red) and *kp*_YfdX (black) monomers shown as C_α traces. Remarkable differences at the secondary structural level between the two molecules are indicated. (*Bottom*) Secondary structure prediction of the amino- terminal region of the two proteins, which was obtained from the PSI-PRED server (http://bioinf.cs.ucl.ac.uk/psipred/). **(C)** (*Top*) Structural comparison of the 3_{10}-helix of *st*_YfdX (violet) and α+ of *kp*_YfdX (gray). Dashed lines highlight helical hydrogen bonding patterns with labels of the involved main chain amide or carbonyl groups. (*Bottom*) Sequence alignment. The residues constituting 3_{10}-helix or α+ helices are highlighted in red.

the formation of the high-order oligomeric structure of *st*_YfdX. Therefore, the recombinant *st*_YfdX protein was dialyzed against a buffer composed of 20 mM Bis-Tris-HCl (pH 6.0), 200 mM NaCl, and 1 mM DTT, with the intention of lowering pH to prevent zinc precipitation (Sayilgan et al., 2010; Park et al., 2015). Prior to zinc treatment, SEC-MALS experiments were conducted with the prepared protein sample, to use the data as a control. Surprisingly, we found that the molecular weights of the *st*_YfdX samples concentrated to 10 and 30 mg/mL, respectively, are ∼78–79 kDa (**Figure 1B**), and thus it was shown that *st*_YfdX forms a tetramer at pH 6.0, even without being treated with zinc chloride. The molecular weight of *st*_YfdX was then further analyzed by SEC-MALS at various pH conditions ranging from 5.5 to 8.0 at 0.5 intervals. As described in **Figure 1C**, the molar

mass of *st*_YfdX was shifted from 80.8 to 40.4 kDa, indicating that *st*_YfdX exists in a state of dynamic equilibrium between tetramer and dimer whose ratio is varied by pH. We also performed SEC-MALS on the recombinant *kp*_YfdX protein for comparison. As shown in **Supplementary Figure S1**, *kp*_YfdX exists as a tetramer at pH 6.0 and 7.5 but as a dimer at pH 10.0, showing that *kp*_YfdX also undergoes a pH-dependent transition between dimeric and tetrameric forms but the pH range is different from that of *st*_YfdX. Collectively, these data indicate that the recombinant *st*_YfdX protein can form a dimer or tetramer in solution, and this process is affected by pH of the solution.

Overall Structural Analysis of *st*_YfdX

Because structural information about *st*_YfdX was clearly indispensable for the corroboration of its stoichiometric properties, we attempted to elucidate its crystal structure. The purified recombinant protein was subjected to crystallization trials under 576 crystallization conditions. Rectangular crystals (space group *F*222) diffracted to the resolution of 1.4 Å were obtained in a crystallization condition with pH 4.6 (Crystal I; **Tables 1**, **2**), implying that this crystal might consist of the *st*_YfdX tetramer. Its asymmetric unit contains a single *st*_YfdX molecule that is composed of six α-helices, one 3_{10}-helix, and three β-strands (**Figure 2A**). These units are arranged to form three subdomains: a four-helical bundle (including α1, α2, α5, and α6), an antiparallel β-sheet (including β1–β3), and a two-helical bundle (including α3 and α4; **Figure 2A**). One 3_{10}-helix is located in the middle of the α2–β1 loop (**Figure 2A**). The *st*_YfdX monomer overlaps well with the *kp*_YfdX monomer when superimposed, with a root mean square deviation of 1.27 Å over 154 aligned residues out of a total of 170 residues (**Figure 2B**, top), which is consistent with high sequence homology between them (35% identity and 52% similarity; **Supplementary Figure S2**). One noticeable discrepancy is the presence of an additional α-helix (referred to as α0) ahead of α1 of *kp*_YfdX, which is not shown in *st*_YfdX (**Figure 2B**). The PSI-PRED server that accurately predicted the presence of helical portion at that position in *kp*_YfdX suggested that residues 1–17 of *st*_YfdX, including residues 1–9 (not contained in the construct used for crystallization) and residues 10–17 (not visible in the crystal structure) might not form the α-helical structure (**Figure 2B**), supporting that *st*_YfdX does not contain α0. Another difference at the secondary structural level is that although the short helix of *st*_YfdX next to α2 is a 3_{10}-helix containing i→i+3 hydrogen bonding, the corresponding helix of *kp*_YfdX is a canonical α-helix (referred to as α+) containing i→i+4 hydrogen bonding (**Figure 2C**). We noted that minor structural discrepancies between the two proteins are also evident in the 3_{10}-helix–β1 and β1–α3 loops (**Supplementary Figures 3A,B**).

Structural Analysis of the Oligomeric Form of *st*_YfdX

To verify the oligomeric state of *st*_YfdX, the intermolecular interactions and assembly were analyzed among *st*_YfdX molecules in crystals. Of note, we figured out that a tetramer-shaped oligomeric form of *st*_YfdX is shown in our crystal lattice (**Figure 3A**), which can be fairly well-matched to that of *kp*_YfdX (**Supplementary Figure S4**). In contrast, we could not find any crystallographic evidence for the formation of a *st*_YfdX trimer in our structure. We next structurally analyzed the intermolecular binding between *st*_YfdX monomers in the tetrameric form. The two *st*_YfdX molecules designated as Mol A and Mol B in **Figure 3** interact with each other mainly through very tight hydrophobic contacts. These contacts are mediated by bulky aromatic hydrophobic residues (Phe42, Phe45, and Tyr165) at the tip of a four-helical bundle (especially α1 and α6) of one monomer and a number of hydrophobic residues (Leu21′, Ile26′, Ile94′, Val96′, Ile110′, Ala113′, Met117′, Ile126′, Leu129′, Val134′, and Val136′) in the hydrophobic concave region consisting of a two-helical bundle (α3 and α4) and at the tip of a three-stranded β-sheet of the other monomer (**Figure 3B**, top). Atomic analysis further revealed 85 intermolecular carbon–carbon contacts (<4.5 Å) in the MolA–MolB binding interface, with more than half being provided by the three aromatic residues Phe42, Phe45, and Tyr165 (51 C–C contacts; 60%). This hydrophobic interaction is well-conserved in the structure of the *kp*_YfdX tetramer (**Supplementary Figure S3C**, top) as well, because the contact-involved residues are mostly conserved among YfdX proteins (**Supplementary Figure S2**; marked with asterisks). It should be noted that residues such as Trp31, Arg35, and Asn91 from the two *st*_YfdX monomers also reinforce the intermolecular interaction by providing hydrophobic interaction between two tryptophan residues and hydrocarbon portion of two arginine residues and hydrogen bonds between Arg35 and Asn91 (**Figure 3B**, bottom). Similar but slightly different hydrophobic interactions and hydrogen bonds contribute to the intermolecular interaction between *kp*_YfdX molecules (**Supplementary Figure S3C**, bottom).

In the case of two *st*_YfdX molecules designated as Mol A and Mol C in **Figure 3**, at a glance, β-strands from the two monomers appear to form a continuous six-stranded β-sheet. However, we found that no typical hydrogen bond at less than 3.5 Å is present between two facing β-strands (β3 and β3″) of the two *st*_YfdX monomers (**Figure 3C**, left), indicating that the six β-strands are discontinuous. Instead, the intermolecular association between the two three-stranded β-sheets is maintained by several side chains- and water molecules-mediated hydrogen bonds (**Figure 3C**, left). In the *kp*_YfdX crystal structure, the corresponding intermolecular interaction between two β-strands was reinforced by zinc ion coordination, in which two oxygen atoms from side chain carboxylates and four oxygen atoms from water molecules are involved (**Supplementary Figure S3D**, right). However, such a coordination is absent in the *st*_YfdX structure (**Supplementary Figure S3D**, left). Hydrophobic interactions provide additional force for the complex formation between Mol A and Mol C, which are mediated by Tyr100 and Ile137 from one molecule and Pro81″, Tyr87″, Leu158″, Leu170″, Val179″, and the hydrocarbon part of Thr154″, Lys163″, and Gln166″ from the

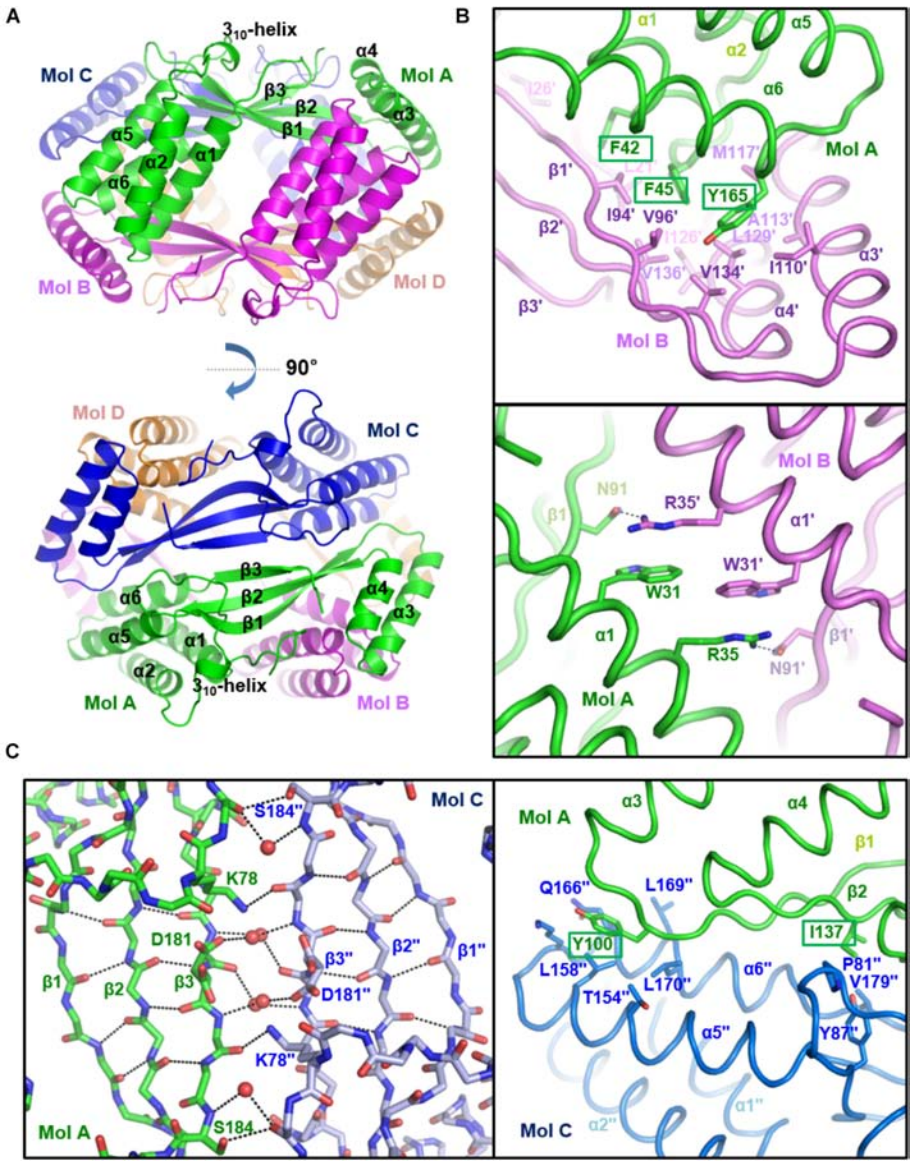

FIGURE 3 | Crystal structure of *st*_YfdX tetramer. **(A)** Two views of the *st*_YfdX tetrameric structure are presented as ribbon models. For clarity, only the secondary structures of Mol A are labeled. **(B)** Intermolecular interaction between Mol A (green) and Mol B (violet) of *st*_YfdX. Shown as stick representation and labeled are *st*_YfdX residues participating in the oligomeric assembly. Three bulky aromatic residues (Phe42, Phe45, and Tyr165) centered at the hydrophobic-interacting interface are marked with rectangles (*top*). Hydrogen bonds between Arg35 from one molecule and Asn91 form the opposite molecule are presented as dotted lines (*bottom*). **(C)** Intermolecular interaction between Mol A (green) and Mol C (blue) of *st*_YfdX. (*Left*) Shown as stick representation are the main chain atoms of three-stranded β-sheets from the two molecules and the side chain atoms of Lys78, Asp181, and Ser184. Water molecules mediating intermolecular hydrogen bonds are presented as red circles. Intra- and inter-molecular hydrogen bonds are indicated by dotted lines. (*Right*) Shown as a stick model and labeled are residues participating in intermolecular hydrophobic interactions. Two hydrophobic residues (Tyr100 and Ile137) that are presumed to play a key role in the Mol A–Mol C binding interaction are marked with rectangles.

opposite molecule (**Figure 3C**, right). Twenty-eight carbon–carbon contacts within 4.5 Å exist in the MolA–MolC binding interface, which is one third of those in the MolA–MolB binding interface. Similar hydrophobic interactions were also observed in the *kp*_YfdX structure (**Supplementary Figure S3E**), which are however a bit different from those in the *st*_YfdX structure along with the structural variation of β1–α3 loops (**Supplementary Figure S3B**). We found that Tyr100 and Ile137 of *st*_YfdX are conserved in *kp*_YfdX as Tyr131 and Ile168 (**Supplementary Figure S2**; marked with triangles), whereas their associating residues are relatively diverse in sequences between the two proteins. Overall, the interaction between Mol A and Mol B mainly depends on tight hydrophobic interaction and appears to be tight and dense (**Figure 3B**), whereas that between Mol A and Mol C is maintained by the combination of hydrogen bonds and loose hydrophobic

interaction but seems to be relatively weak and detachable (**Figure 3C**).

SEC-MALS and SAXS Exploration of *st*_YfdX

Whether the intermolecular interactions shown in the *st*_YfdX crystal structure indeed exist in solution was the next issue to be elucidated. Hence, we prepared two mutant *st*_YfdX proteins: *st*_YfdX(FFY), in which three core residues (Phe42, Phe45, and Tyr165; see **Figure 3B**, top) critical for the Mol A–Mol B interaction were substituted with alanine, and *st*_YfdX(YI), in which two hydrophobic residues (Tyr100 and Ile137; see **Figure 3C**, right) involved in the Mol A–Mol C interaction were mutated to alanine. These two proteins were expressed, purified, and finally equilibrated in two different solutions buffered with pH 6.0 Bis-Tris-HCl and pH 7.5 Tris-HCl, respectively, as was the wild-type protein. Introduction of such mutations did not affect *st*_YfdX protein folding, which was confirmed by CD spectroscopic analysis using wild-type and two mutant proteins (**Supplementary Figure S5**). SEC-MALS analysis was then performed on each protein sample, and the results were compared with one another and with those of wild-type. First, at both pH 6.0 and pH 7.5, the molecular weight of *st*_YfdX(YI) was ∼39 kDa (**Figures 4A,B**), indicating that structure-based alanine substitution of Tyr100 and Ile137 indeed abrogates the MolA–MolC interaction and therefore this mutant should exist as the MolA–MolB dimer (**Figure 4C**, right top). Next, the molecular weight of *st*_YfdX(FFY) was measured and found to be 20–21 kDa (**Figure 4A**) at both pH levels, showing that *st*_YfdX(FFY) exists in a monomeric form (**Figure 4C**, right bottom) but not as the MolA–MolC dimer (**Figure 4C**, left bottom). These data strongly indicate that when the very tight hydrophobic interaction-based MolA–MolB binding interface was impaired by the alanine substitution of Phe42, Phe45, and Tyr165, the relatively weak MolA–MolC interaction could not sustain the dimeric interface and thus it is in the monomeric form. As presented in **Figure 1B**, wild-type *st*_YfdX forms a tetramer at pH 5.5/6.0 but exists as a dimer at pH 7.5/8.0. We assume that the alteration of proton concentration might affect the formation of hydrogen bonds maintaining the MolA–MolC binding interface. The relatively weak MolA–MolC interaction is presumed not to be sustained at high pH conditions, and thus *st*_YfdX exists as the MolA–MolB dimer in that condition.

To further corroborate the pH-dependent conversion of *st*_YfdX between the two forms, SAXS data were collected using two protein samples equilibrated at pH 5.5 and 8.0, respectively (**Table 3**). We first confirmed that the calculated scattering intensity curves and distance distribution function $P(r)$ of the tetrameric and the MolA–MolB dimeric structures were nicely matched with the experimental observations (**Figures 5A,B**). Subsequently, the molecular envelope of the samples was derived from SAXS analysis. The envelope of *st*_YfdX at pH 5.5 was globular-shaped, in which the tetrameric crystal structure of *st*_YfdX could be successfully incorporated (**Figure 5C**, left). In contrast, that of *st*_YfdX at pH 8.0 was revealed to have a hemisphere-like shape that fitted well the MolA–MolB dimer (**Figure 5C**, right). Collectively, SEC-MALS and SAXS data demonstrate that *st*_YfdX switches between two different forms in a pH-dependent manner in the solution, whose conformation could be inferred from the crystal structure.

Crystallization and Structure Determination of $ZnCl_2$-Treated *st*_YfdX

As mentioned above, the pH-sensitive stoichiometric alteration of *st*_YfdX was detected during examination of the possibility of zinc coordination-mediated oligomerization. Even though such a zinc coordination was not shown in our crystal structure (**Supplementary Figure S3D**), we did not exclude such a possibility completely, and thus attempted crystallization of the *st*_YfdX protein sample equilibrated with the final buffer consisting of 20 mM Bis-Tris-HCl (pH 6.0), 200 mM NaCl, 1 mM DTT, and 1 mM $ZnCl_2$. Two forms of crystals were obtained that were diffracted to high resolution: rectangular crystals diffracted to 1.5 Å (space group *F*222; crystal II) under the same crystallization condition as that of crystal I, and board-shaped crystals diffracted to 2.3 Å (space group *P*222; crystal III) under the crystallization condition at pH 5.0 (see **Table 1**). The asymmetric units of crystals II and III contain one and eight *st*_YfdX molecules, respectively. We once again determined the structure of *st*_YfdX using these crystals (**Table 2**). The *st*_YfdX structures determined via crystals I–III were confirmed to be almost identical to each other; not only because the *st*_YfdX monomeric structures from crystals II and III were superimposed on each other and on that from crystal I with root mean square deviations in the range of 0.08–0.77 Å over ∼170 aligned residues, but also because tetramer-shaped oligomeric forms of *st*_YfdX were detected in the crystal lattices of both crystals II and III, as was the case for crystal I (**Supplementary Figure S4**). These data support that *st*_YfdX can form a tetramer. Nevertheless, oligomerization-contributing zinc coordination demonstrated in the *kp*_YfdX structure (**Supplementary Figure S3B**, right) was not found in all our crystal structures of *st*_YfdX (not shown), indicating that the zinc coordination is not necessary for formation of the tetramer of this protein.

Next, to understand the biological function of *st*_YfdX, a search for homologous structures on the Dali server (Holm and Sander, 1993) was carried out with the monomeric and tetrameric structures of *st*_YfdX. No homologous protein was identified in this search except for *kp*_YfdX (Z-score 20.1): a number of proteins containing a helical bundle were listed including *Nitrosomonas europaea* small metal-binding protein (Z-score 9.9) and *E. coli* cytochrome b_{562} (Z-score 8.5), but their structures overlapped with the *st*_YfdX structure only partially (**Supplementary Figure S6**), indicating that YfdX adopts a novel protein fold that has not been identified yet.

YfdX Modulates Antibiotic Susceptibility in *Salmonella*

Previous reports indicate that protein expression of *E. coli* YfdX is under control of EvgA, the response regulator factor that is intimately associated with the bacterial response to antibiotic stress (Nishino and Yamaguchi, 2001, 2002; Masuda and Church,

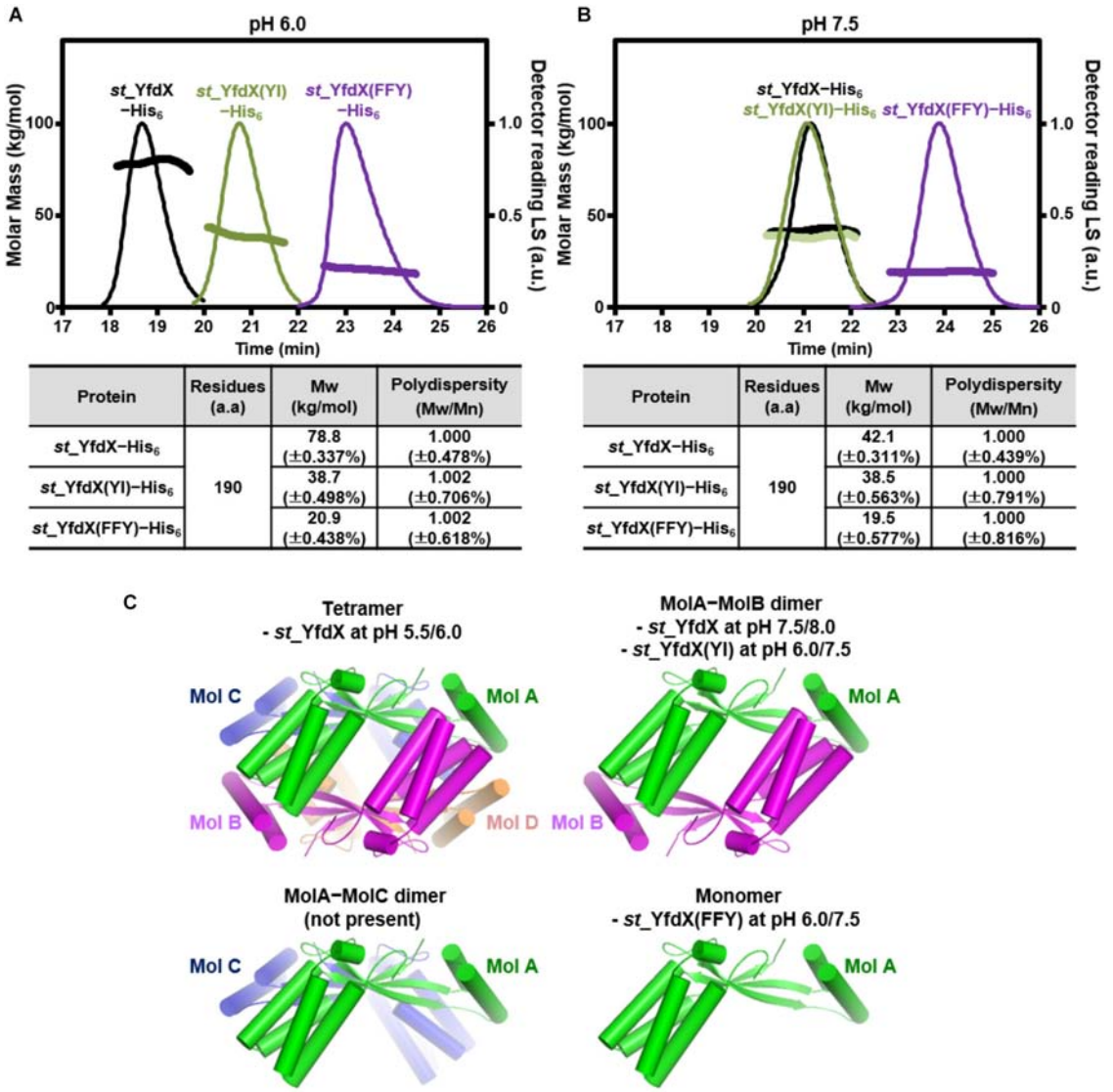

Protein	Residues (a.a)	Mw (kg/mol)	Polydispersity (Mw/Mn)
*st*_YfdX−His_6	190	78.8 (±0.337%)	1.000 (±0.478%)
*st*_YfdX(YI)−His_6		38.7 (±0.498%)	1.002 (±0.706%)
*st*_YfdX(FFY)−His_6		20.9 (±0.438%)	1.002 (±0.618%)

Protein	Residues (a.a)	Mw (kg/mol)	Polydispersity (Mw/Mn)
*st*_YfdX−His_6	190	42.1 (±0.311%)	1.000 (±0.439%)
*st*_YfdX(YI)−His_6		38.5 (±0.563%)	1.000 (±0.791%)
*st*_YfdX(FFY)−His_6		19.5 (±0.577%)	1.000 (±0.816%)

FIGURE 4 | SEC-MALS analysis of mutant *st*_YfdX. **(A,B)** Molecular weights of the *st*_YfdX(FFY) and *st*_YfdX(YI) mutants were analyzed and compared with each other and with those of the wild-type. All the experiments were conducted on protein samples prepared at 30 mg/mL. **(C)** Structural diagrams of *st*_YfdX proteins according to the crystal structure and SEC-MALS experiments.

TABLE 3 | Structural parameters obtained from the SAXS data of *st*_YfdX proteins in solution.

Model/sample	$R_{g,G}$[c] (Å)	$R_{g,p(r)}$[d] (Å)	D_{max}[e] (Å)	$MM_{calculated}$[f] (kDa)	MM_{SAX}[g] (kDa)	MM_{MALS}[h] (kDa)
Tetrameric model[a]	27.39 ± 0.04	26.91 ± 0.04	73.4	82.4	–	–
MolA-MolB model[a]	23.95 ± 0.01	23.86 ± 0.14	73.5	41.2	–	–
*st*_YfdX-His_6 at pH 5.5[b]	27.54 ± 0.21	26.90 ± 0.09	72.5	–	80.4	80.8
*st*_YfdX-His_6 at pH 8.0[b]	23.82 ± 0.21	23.84 ± 0.12	72.1	–	38.2	40.4

[a]*Models obtained from the st_YfdX structure determined using the crystal I.* [b]*Samples subjected to SAXS.* [c]$R_{g,G}$ *(radius of gyration) was obtained from the scattering data by the Guinier analysis.* [d]$R_{g,p(r)}$ *(radius of gyration) was obtained from the p(r) function by the program GNOM.* [e]D_{max} *(maximum dimension) was obtained from the p(r) function by the program GNOM.* [f]$MM_{calculated}$ *(molecular mass) was obtained from the amino acid sequence of protein.* [g]MM_{SAXS} *(molecular mass) was obtained from the SAXS experiments using BSA as a standard.* [h]MM_{MALS} *(molecular mass) was obtained from the MALS experiments using BSA as a standard (see* ***Figure 1C****).*

2002; Nishino et al., 2003). Even though the homolog of EvgA is absent in the genome of *S.* Typhi, we assumed that YfdX might also play a role in the response to antibiotics. Therefore, we analyzed the functional and physiological effects of *yfdX* gene expression in the *S.* Typhimurium UK-1 strain, whose YfdX (referred to as *stm*_YfdX in this manuscript) shares 98.0%

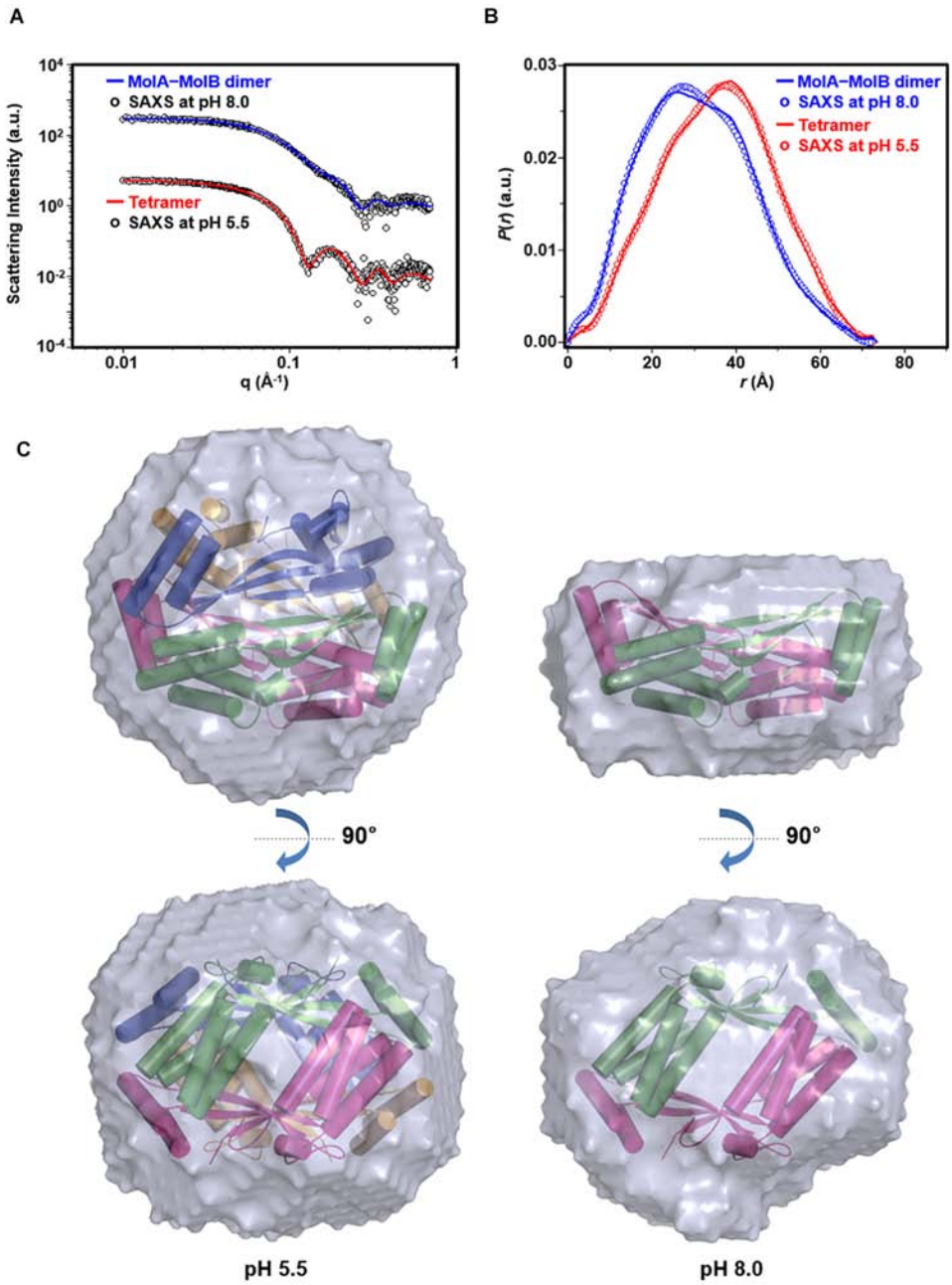

FIGURE 5 | SAXS analysis of *st*_YfdX. **(A)** X-ray scattering profiles in solution measured at 4°C. Circles indicate experimental data, whereas solid lines represent the theoretical SAXS curve calculated from the tetrameric (χ^2 = 0.583) and dimeric (χ^2 = 0.483) models shown in **Figure 4C** using the program CRYSOL. For clarity, each plot is shifted along the log *I*(*q*) axis. **(B)** Pair distance distribution *p*(*r*) functions in aqueous solution that were acquired by analyzing the experimental SAXS data using the program GNOM. Areas under curves were normalized to equal areas for ease of comparison. **(C)** The tetrameric (left) and dimeric (right) models of *st*_YfdX were docked into the reconstructed SAXS envelopes that were reconstructed as described in detail in Section "Materials and Methods."

identity (195 of 199 amino acids) with *st*_YfdX. First, the cellular expression level of *stm*_YfdX was examined in a time-dependent manner. As illustrated in **Supplementary Figure S7**, the transcription level of *stm*_YfdX was proportionally increased every 4 h and was higher at 12 h than at 4 or 8 h, indicating that cellular *stm*_YfdX was expressed in the exponential and, particularly, stationary phases. Next, phenotype microarrays were conducted by measuring the bacterial respiration rate to compare physiological changes upon antibiotic treatment between *S.* Typhimurium UK-1 wild-type and *yfdX*-deficient (Δ*yfdX*) strains. We found that the absence of YfdX makes the bacterium more susceptible to two antibiotics that are known to block cell wall synthesis, penicillin G and carbenicillin (**Figure 6A**). **Figure 6B** corroborates that the growth of the

Δ*yfdX* strain was remarkably restrained in the presence of each of the two antibiotics at the concentration where the wild-type strain grows well. Moreover, the growth of the Δ*yfdX* strain was completely (when treated with penicillin G) or considerably (when treated with carbenicillin) recovered by chromosomal complementation of the wild-type *S.* Typhi *yfdX* gene but not by that of the *yfdX* gene containing the FFY mutation (**Figure 6B**). These data collectively indicate that *Salmonella* YfdX performs significant functions in basal tolerance of this pathogenic bacterium against β-lactam antibiotics, and that its homooligomerization might be necessary for the functionality of this protein.

YfdX Deficiency in *Salmonella* Results in Promoted Bacterial Virulence

Given that various bacterial stress regulators are also known to be involved in bacterial virulence (Fang et al., 2016), we wondered whether *Salmonella* YfdX is able to modulate microbial virulence as well. A virulence screening system that is based on *G. mellonella* larvae as the *in vivo* model for *Salmonella* infection was employed to determine this issue. After injection of the *S.* Typhimurium UK-1 wild-type or Δ*yfdX* strain, the larval survival rate was recorded every 6 h for up to 48 h. Of note, the survival rate of larvae infected by the Δ*yfdX* strain (∼10% at 48 h) was significantly lower than that of larvae infected by the wild-type strain (∼60% at 48 h), indicating that *stm*_YfdX plays a role in attenuating bacterial virulence (**Figure 7A**). To confirm these results, we prepared *S.* Typhimurium UK-1 Δ*yfdX* strains in which YfdX-deficiency was complemented by arabinose-induced transient expression of wild-type *st*_YfdX or crystal structure-based mutant *st*_YfdX proteins including *st*_YfdX(FFY) and *st*_YfdX(YI) (see **Figures 3**, **4**). We first reconfirmed that the Δ*yfdX* strain-infected larvae show remarkably higher mortality than that of the wild-type strain-infected larvae at 21 h post-injection (**Figure 7B**, left). Subsequent analysis revealed that the *Salmonella* virulence was relieved by the transient expression of wild-type *st*_YfdX or *st*_YfdX(YI), but not by that of *st*_YfdX(FFY). Because *st*_YfdX(YI) and *st*_YfdX(FFY) exist in a dimeric and monomeric form, respectively (see **Figure 4**), these results imply that the oligomeric form but not the monomeric form of *st*_YfdX is functional and necessary to suppress *Salmonella* virulence. We also confirmed similar effects of *st*_YfdX on the larval survival rate by means of the *S.* Typhimurium 14028S strain (**Supplementary Figure S8**).

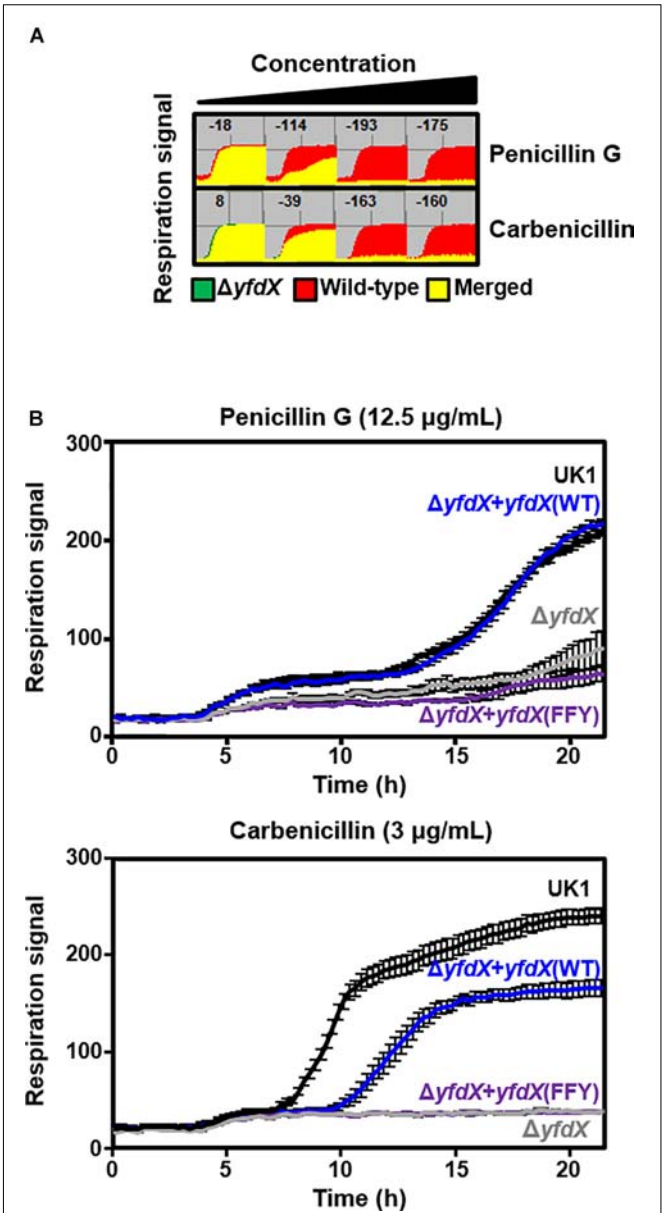

FIGURE 6 | Functionality of YfdX in antibiotic tolerance. **(A)** Phenotype arrays. Deficiency of YfdX enhanced susceptibility of *S.* Typhimurium to the indicated antibiotics. **(B)** Respiration of the *S.* Typhimurium UK-1 strains from 0 to 25 h was measured in the presence of each antibiotic at the indicated concentration.

DISCUSSION

Analysis of the Oligomeric Status of YfdX

In this study, we performed X-ray crystallographic and scattering, biochemical, and physiological analyses of *Salmonella*-derived YfdX, whose characteristics and biological function remain obscure despite recent research (Saha et al., 2016a,b; Mondal et al., 2017). One of the issues raised by a study on *st*_YfdX is about its stoichiometry (Saha et al., 2016b): *st*_YfdX indeed forms a trimer unlike *kp*_YfdX that appears to form a tetramer despite their high sequence homology. SEC-MALS analysis and structure determination by X-ray crystallographic and scattering analyses were carried out to resolve this issue, which led to the unexpected identification of a pH-related stoichiometric switch of *st*_YfdX (**Figures 1**–**5**). Although both the tetrameric (at pH 7.5/8.0) and dimeric form (at pH 5.5/6.0) were confirmed by SEC-MALS (**Figure 1**) and SAXS (**Figure 5**), *st*_YfdX was found to be in the tetrameric form in all the three crystal structures, presumably because of the increased opportunity of contacts in the crystal lattice (**Figure 3** and **Supplementary Figure S4**). Nevertheless, the dimeric structure of *st*_YfdX could

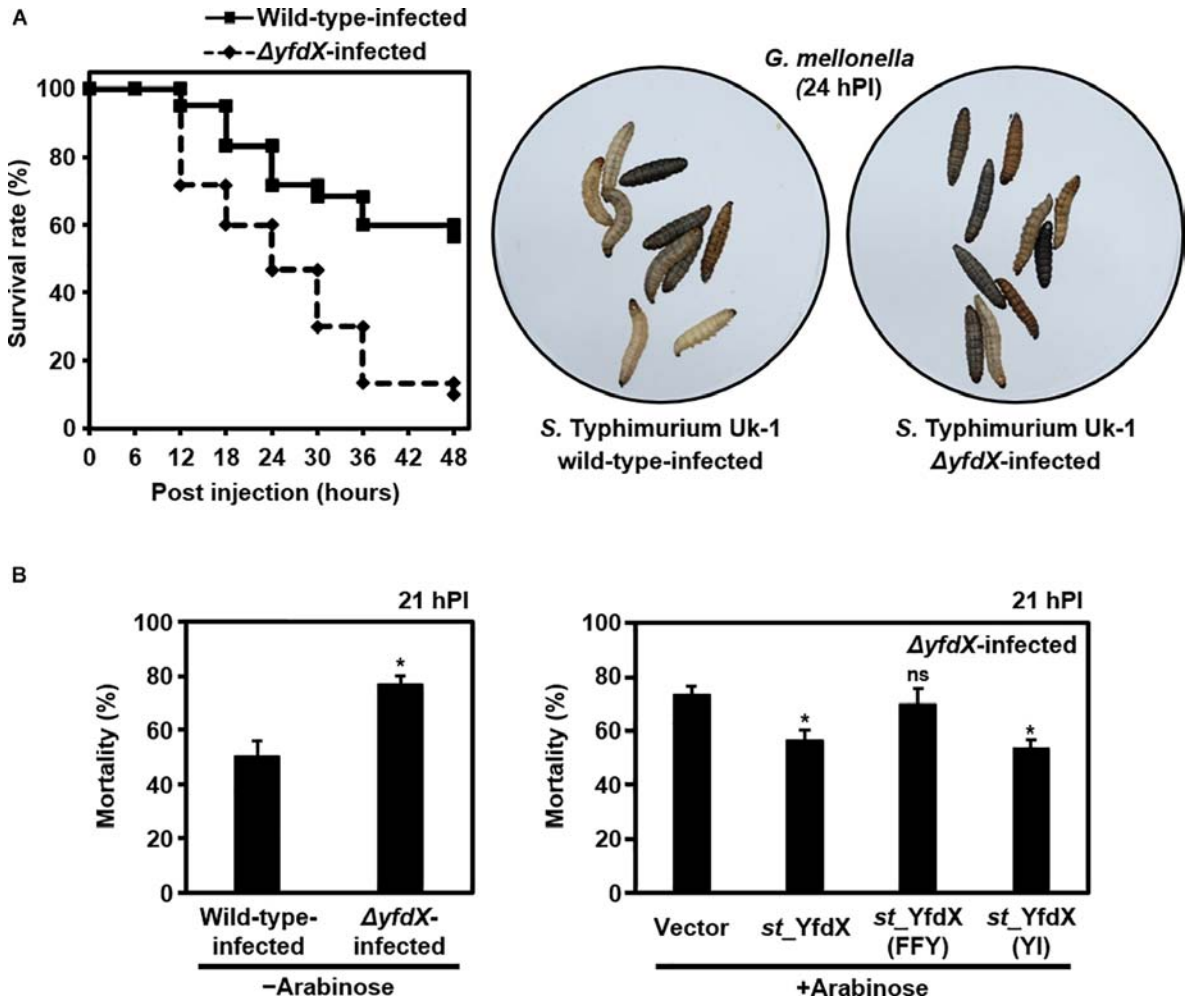

FIGURE 7 | YfdX reduces bacterial virulence. **(A)** *yfdX* deficiency enhanced *Salmonella* virulence to *Galleria mellonella* larvae. (*Left*) The survival rates of larvae infected by the *S*. Typhimurium UK-1 wild-type or Δ*yfdX* strain were measured every 6 h and compared. (*Right*) Pictures of *Salmonella*-infected larvae 24 h post-infection. White ones are alive, whereas black ones are dead. **(B)** Complementation assay. (*Left*) Mortality rates of wild-type or Δ*yfdX Salmonella* strain-infected larvae are compared. $^*P < 0.05$ (Student's *t*-test). (*Right*) Comparison of mortality rates of Δ*yfdX Salmonella*-infected larvae with the arabinose-induced transient expression of an empty vector (control), *st*_YfdX, *st*_YfdX(YI), or *st*_YfdX(FFY). ns, not significant; $^*P < 0.05$ versus transient expression of empty vector (Student's *t*-test).

be inferred from the combination of a structure-based mutational study accompanied by SEC-MALS analysis. Among the two hypothetical dimers illustrated in **Figure 4C**, the MolA–MolB form, but not the MolA–MolC form, is presumed to exist in solution, for the following reasons. First, the intermolecular interactions between MolA and MolB are clearly tighter and denser than those between MolA and MolC (**Figures 3B,C**). Second, the MolA–MolB interaction-null *st*_YfdX(FFY) mutant was revealed to be a monomer, not a dimer (**Figure 4B**), implying that the MolA–MolC interaction is not strong enough to sustain the complex formation. We speculate that the tetrameric form of *st*_YfdX observed at pH < 6.0 might involve assembly of two MolA–MolB dimers. SEC-MALS analysis also showed a pH-dependent gradual shift of the calculated molecular mass of *st*_YfdX from pH 5.5 to 8.0, indicating that *st*_YfdX is in a state of dynamic equilibrium between tetramer and dimer (**Figure 1C**). At pH 7.0, the molecular weight of *st*_YfdX was calculated to be ∼51–53 kDa, which presumably explains the reason that *st*_YfdX was estimated to form a trimer in the previous report (Saha et al., 2016b). Given the SEC-MALS analysis together with the crystallographic and SAXS structural analysis collectively (**Figures 1**–**5**), we consider that *st*_YfdX undergoes a continuous structural switch between dimer and tetramer rather than exists as a trimer.

Determination of the stoichiometry of *st*_YfdX was followed by corollary issues concerning the biological importance of such oligomerization. Chromosomal knockout and complementation assay using the *S.* Typhimurium UK-1 strain demonstrated that the monomer-forming mutant YfdX is non-functional (see **Figure 6**). The *G. mellonella* larvae-infection assay showed that the genetic knockout of YfdX could be complemented by the transient expression of the wild-type or the dimer-forming

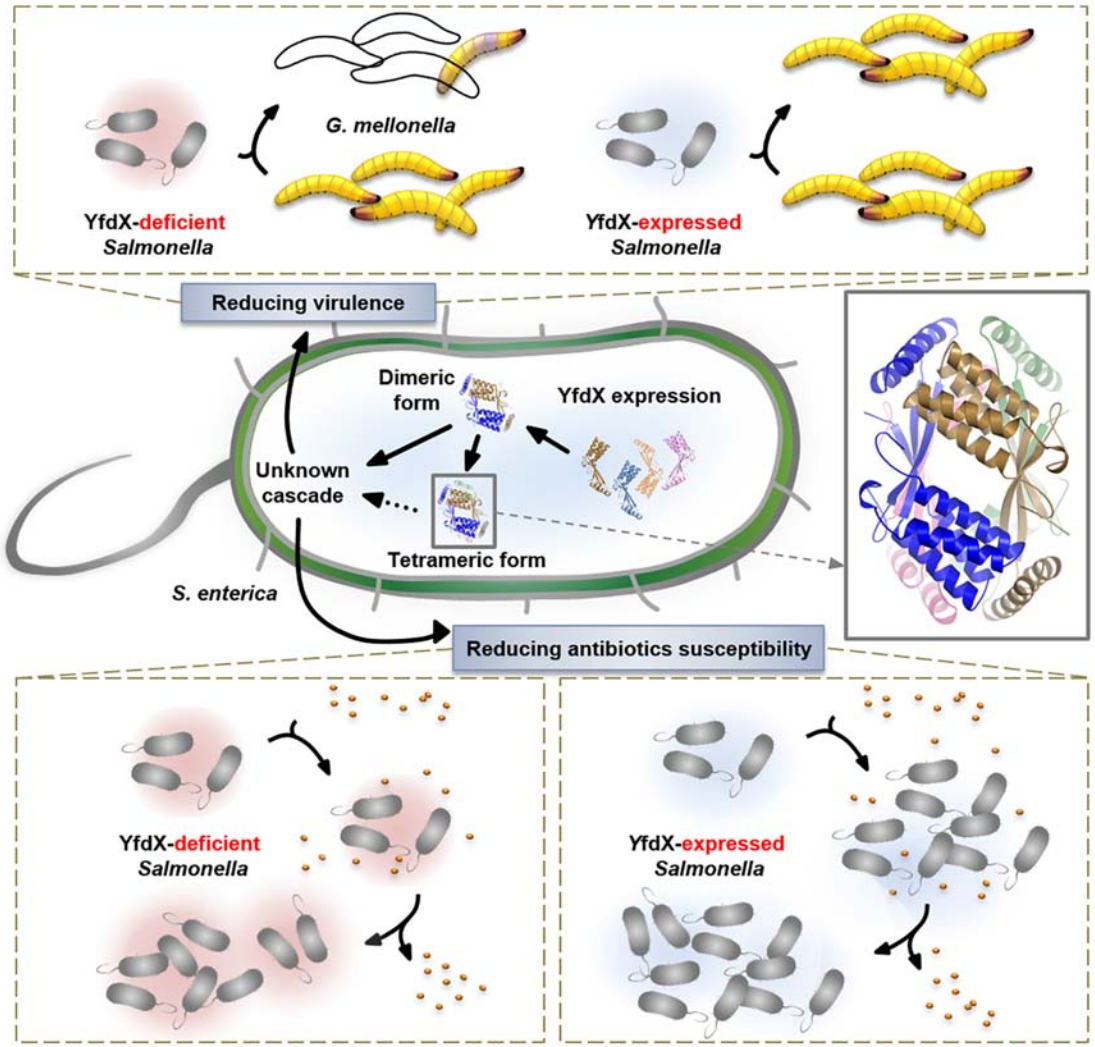

FIGURE 8 | Overall view of the physiological functionality of YfdX.

mutant, but not by that of the monomer-promoting mutant (see **Figure 7**). These data collectively suggest that the oligomerization of *st*_YfdX might be inevitable for its effectiveness. It is notable that we currently do not rule out the probability that the tetrameric and dimeric forms function differently in other cellular processes in which s*t*_YfdX is involved.

YfdX Acts a Critical Dual Function in Antibiotic Susceptibility and Virulence

Despite previous efforts examining the diverse biochemical properties of s*t*_YfdX (Saha et al., 2016a,b; Mondal et al., 2017), analysis of its functionality in live bacteria has been absent thus far, limiting our understanding of this protein. In this study, we demonstrated that YfdX is indeed involved in *Salmonella*'s tolerance to antibiotics, because its deficiency caused a remarkable increase in antibiotic susceptibility and impaired bacterial survival upon treatment with penicillin G and carbenicillin, which was compensated by chromosomal complementation with the wild-type *yfdX* but not with the monomer-promoting mutant *yfdX* (**Figure 6**). We also observed that the expression level of YfdX in *Salmonella* was higher in the stationary phase than that in the exponential phase (**Supplementary Figure S7**). Because tolerance to a variety of environmental stressors such as antibiotics and osmotic or acidic stress is vital for bacterial species, particularly in the stationary phase where bacterial growth is delayed or arrested, a number of bacterial proteins that are upregulated in this phase were found to be involved in a stress response and/or antibiotic tolerance (Hengge-Aronis, 1993; Battesti et al., 2011), which now should include YfdX. In addition, it was revealed for the first time that YfdX mitigates mortality of the *Salmonella* infection in our larval model (**Figure 7**), suggesting that YfdX is a negative regulator of bacterial virulence. Even though antibiotic resistance and bacterial virulence are different in their functionality and applicability, a number of biological processes have been reported

to be shared by the two mechanisms, including biofilm formation (Patel, 2005), upregulated expression of an efflux pump (Barbosa and Levy, 2000), regulation of cell permeability (Tsai et al., 2011), and cell wall alteration (Moya et al., 2008). Moreover, in a variety of gram-negative pathogenic bacteria such as *Staphylococcus aureus* and *Streptococcus pneumoniae*, bacteria strains resistant to antimicrobial molecules including β-lactams and glycopeptides show attenuated virulence when they infect mice (Rieux et al., 2001; Rudkin et al., 2012) or *G. mellonella* (Peleg et al., 2009), implying an association between the two mechanisms at the molecular level. Yet, the precise molecular mechanism of YfdX's action in the control of *Salmonella* antibiotic tolerance and bacterial virulence remains to be elucidated. One possibility is that YfdX may associate with membrane proteins and affect their function or localization, e.g., proteins involved in cell wall synthesis, as its deficiency led to the increased susceptibility to β-lactam antibiotics such as penicillin G and carbenicillin (**Figure 6**). Since a recent report shows simulated binding of *st*_YfdX to the outer-membrane protein STY3179, a *Salmonella* homolog of an adhesion and invasion locus protein from *Yersinia pestis* that interacts with the host extracellular matrix protein laminin (Yamashita et al., 2011), another possibility is that YfdX controls bacterial virulence by regulating host–pathogen interaction via binding to STY3179 or other unknown proteins. We suppose that future verification of the binding partner(s) of YfdX will be necessary to resolve this issue.

It has been reported that the EvgS-EvgA system controlling the expression of the *yfdXWUVE* operon in *E. coli* regulates the signaling pathways also associated with acid tolerance (Nishino and Yamaguchi, 2001, 2002; Masuda and Church, 2002; Nishino et al., 2003). We, therefore, raise a possibility that st_YfdX might participate not only in antibiotic susceptibility but also in acid tolerance of the bacterium or other processes such as pH homeostasis that is also implicated in *Salmonella* virulence (Rappl et al., 2003), in which its pH-dependent structural conversion could play some unknown role. However, at least under our assay conditions, the relation of st_YfdX with acid shock was shown to be unclear and inconsistent in the phenotype microarrays and in the minimum inhibitory concentration assays (unpublished data), and this issue remains to be resolved by future research as well.

CONCLUSION

We characterized various features of the *Salmonella*-derived YfdX protein, including the crystal structure that contains a novel fold, previously unknown stoichiometric features, proof of contribution to antibiotic response, and participation in the control of bacterial virulence (**Figure 8**). We believe that our biochemical and physiological findings will provide a rational basis for future research, augmented with the details of molecular mechanisms of the stress response in this pathogenic bacterium, in which much remains to be discovered.

AUTHOR CONTRIBUTIONS

BK, C-MR, and SJK conceived and designed the experiments. HSL, SL, J-SK, H-RL, and KSJ performed the experiments. HSL, SL, KSJ, BK, C-MR, and SJK analyzed the data. H-CS, M-SL, and C-HK contributed to reagents, materials, analysis tools. HSL, J-SK, BK, C-MR, and SJK wrote the manuscript.

FUNDING

This study was supported by the National Research Foundation of Korea (Grant No. NRF_2015M3A9B5030308) and by the BioNano Health-Guard Research Center as the Global Frontier Project (Grant No. H-GUARD_2013M3A6B2078954), which were funded by the Ministry of Science and ICT (MSIT) of South Korea. This study was also supported by the Korea Research Institute of Bioscience and Biotechnology Research Initiative Programs for Creative Research and for Disease Target Structural Research.

ACKNOWLEDGMENTS

This study involved the beamlines 4C, 5C, and 7A at the Pohang Accelerator Laboratory in South Korea. We are grateful to Dr. Eunha Hwang (Korea Basic Science Institute, South Korea) for helping with the SEC-MALS experiments and Dr. Myung Hee Kim and Dr. Jungwon Hwang (Korea Research Institute of Bioscience and Biotechnology, South Korea) for helping with the CD experiments.

SUPPLEMENTARY MATERIAL

The Supplementary Material for this article can be found online at: https://www.frontiersin.org/articles/10.3389/fmicb.2018.03329/full#supplementary-material

REFERENCES

Adams, P. D., Afonine, P. V., Bunkoczi, G., Chen, V. B., Davis, I. W., Echols, N., et al. (2010). PHENIX: a comprehensive python-based system for macromolecular structure solution. *Acta Crystallogr. D Biol. Crystallogr.* 66, 213–221. doi: 10.1107/S0907444909052925

Azmatullah, A., Qamar, F. N., Thaver, D., Zaidi, A. K., and Bhutta, Z. A. (2015). Systematic review of the global epidemiology, clinical and laboratory profile of enteric fever. *J. Glob. Health* 5:020407. doi: 10.7189/jogh.05.020407

Barbosa, T. M., and Levy, S. B. (2000). Differential expression of over 60 chromosomal genes in *Escherichia coli* by constitutive expression of MarA. *J. Bacteriol.* 182, 3467–3474. doi: 10.1128/JB.182.12.3467-3474.2000

Battesti, A., Majdalani, N., and Gottesman, S. (2011). The RpoS-mediated general stress response in *Escherichia coli*. *Annu. Rev. Microbiol.* 65, 189–213. doi: 10.1146/annurev-micro-090110-102946

Buckle, G. C., Walker, C. L., and Black, R. E. (2012). Typhoid fever and paratyphoid fever: systematic review to estimate global morbidity and mortality for 2010. *J. Glob. Health* 2:010401. doi: 10.7189/jogh.02.010401

Datsenko, K. A., and Wanner, B. L. (2000). One-step inactivation of chromosomal genes in *Escherichia coli* K-12 using PCR products. *Proc. Natl. Acad. Sci. U.S.A.* 97, 6640–6645. doi: 10.1073/pnas.120163297

Dougan, G., and Baker, S. (2014). *Salmonella enterica* serovar Typhi and the pathogenesis of typhoid fever. *Annu. Rev. Microbiol.* 68, 317–336. doi: 10.1146/annurev-micro-091313-103739

Emsley, P., and Cowtan, K. (2004). Coot: model-building tools for molecular graphics. *Acta Crystallogr. D Biol. Crystallogr.* 60, 2126–2132. doi: 10.1107/S0907444904019158

Everest, P., Wain, J., Roberts, M., Rook, G., and Dougan, G. (2001). The molecular mechanisms of severe typhoid fever. *Trends. Microbiol.* 9, 316–320. doi: 10.1016/S0966-842X(01)02067-4

Fang, F. C., Frawley, E. R., Tapscott, T., and Vazquez-Torres, A. (2016). Bacterial stress responses during host infection. *Cell Host Microbe* 20, 133–143. doi: 10.1016/j.chom.2016.07.009

Flury, P., Aellen, N., Ruffner, B., Pechy-Tarr, M., Fataar, S., Metla, Z., et al. (2016). Insect pathogenicity in plant-beneficial *Pseudomonads*: phylogenetic distribution and comparative genomics. *ISME J.* 10, 2527–2542. doi: 10.1038/ismej.2016.5

Franke, D., and Svergun, D. I. (2009). DAMMIF, a program for rapid ab-initio shape determination in small-angle scattering. *J. Appl. Crystallogr.* 42, 342–346. doi: 10.1107/S0021889809000338

Frye, J. G., and Jackson, C. R. (2013). Genetic mechanisms of antimicrobial resistance identified in *Salmonella enterica*, *Escherichia coli*, and *Enteroccocus* spp. isolated from U.S. food animals. *Front. Microbiol.* 4:135. doi: 10.3389/fmicb.2013.00135

Gruez, A., Roig-Zamboni, V., Valencia, C., Campanacci, V., and Cambillau, C. (2003). The crystal structure of the *Escherichia coli* YfdW gene product reveals a new fold of two interlaced rings identifying a wide family of CoA transferases. *J. Biol. Chem.* 278, 34582–34586. doi: 10.1074/jbc.C300282200

Hengge-Aronis, R. (1993). Survival of hunger and stress: the role of rpoS in early stationary phase gene regulation in *E. coli*. *Cell* 72, 165–168. doi: 10.1016/0092-8674(93)90655-A

Holm, L., and Sander, C. (1993). Protein structure comparison by alignment of distance matrices. *J. Mol. Biol.* 233, 123–138. doi: 10.1006/jmbi.1993.1489

Hurley, D., McCusker, M. P., Fanning, S., and Martins, M. (2014). *Salmonella*-host interactions – Modulation of the host innate immune system. *Front. Immunol.* 5:481. doi: 10.3389/fimmu.2014.00481

Jiang, Y., Yu, D., Wei, Z., Shen, P., Zhou, Z., and Yu, Y. (2010). Complete nucleotide sequence of *Klebsiella pneumoniae* multidrug resistance plasmid pKP048, carrying blaKPC-2, blaDHA-1, qnrB4, and armA. *Antimicrob. Agents Chemother.* 54, 3967–3969. doi: 10.1128/AAC.00137-10

Kalra, S. P., Naithani, N., Mehta, S. R., and Swamy, A. J. (2003). Current trends in the management of typhoid fever. *Med. J. Armed Forces India* 59, 130–135. doi: 10.1016/S0377-1237(03)80060-6

Kariuki, S., Gordon, M. A., Feasey, N., and Parry, C. M. (2015). Antimicrobial resistance and management of invasive *Salmonella* disease. *Vaccine* 33(Suppl. 3), C21–C29. doi: 10.1016/j.vaccine.2015.03.102

Karkey, A., Thwaites, G. E., and Baker, S. (2018). The evolution of antimicrobial resistance in *Salmonella* typhi. *Curr. Opin. Gastroenterol.* 34, 25–30. doi: 10.1097/MOG.0000000000000406

Kaur, G., Sathyabama, S., Arora, A., Verma, S., Mubin, N., Agrewala, J. N., et al. (2014). Genome sequencing, annotation and comparative genomic analysis of *Shigella dysenteriae* strain SD1D. *Gut Pathog.* 6:28. doi: 10.1186/1757-4749-6-28

Kim, K. W., Kim, J., Yun, Y. D., Ahn, H., Min, B., Kim, N. H., et al. (2017). Small-angle X-ray scattering beamline BL4C SAXS at pohang light source II. *Biodesign* 5, 24–29.

Kozin, M. B., and Svergun, D. I. (2001). Automated matching of high-and low-resolution structural models. *J. Appl. Cryst.* 34, 33–41.

Lazaro-Diez, M., Redondo-Salvo, S., Arboleya-Agudo, A., Ocejo-Vinyals, J. G., Chapartegui-Gonzalez, I., Ocampo-Sosa, A. A., et al. (2016). Whole-genome sequence of *Hafnia alvei* HUMV-5920, a human isolate. *Genome Announc.* 4:e00556. doi: 10.1128/genomeA.00556-16

Masuda, N., and Church, G. M. (2002). *Escherichia coli* gene expression responsive to levels of the response regulator EvgA. *J. Bacteriol.* 184, 6225–6234. doi: 10.1128/JB.184.22.6225-6234.2002

McClelland, M., Sanderson, K. E., Spieth, J., Clifton, S. W., Latreille, P., Courtney, L., et al. (2001). Complete genome sequence of *Salmonella enterica* serovar Typhimurium LT2. *Nature* 413, 852–856. doi: 10.1038/35101614

McCoy, A. J., Grosse-Kunstleve, R. W., Adams, P. D., Winn, M. D., Storoni, L. C., and Read, R. J. (2007). Phaser crystallographic software. *J. Appl Crystallogr.* 40, 658–674. doi: 10.1107/S0021889807021206

Mondal, M., Chakrabarti, J., and Ghosh, M. (2017). Molecular dynamics simulations on interaction between bacterial proteins: implication on pathogenic activities. *Proteins* 86, 370–378. doi: 10.1002/prot.25446

Moya, B., Juan, C., Alberti, S., Perez, J. L., and Oliver, A. (2008). Benefit of having multiple ampD genes for acquiring beta-lactam resistance without losing fitness and virulence in *Pseudomonas aeruginosa*. *Antimicrob. Agents Chemother.* 52, 3694–3700. doi: 10.1128/AAC.00172-08

Mullins, E. A., Sullivan, K. L., and Kappock, T. J. (2013). Function and X-ray crystal structure of *Escherichia coli* YfdE. *PLoS One* 8:e67901. doi: 10.1371/journal.pone.0067901

Nikaido, H. (2009). Multidrug resistance in bacteria. *Annu. Rev. Biochem.* 78, 119–146. doi: 10.1146/annurev.biochem.78.082907.145923

Nishino, K., Inazumi, Y., and Yamaguchi, A. (2003). Global analysis of genes regulated by EvgA of the two-component regulatory system in *Escherichia coli*. *J. Bacteriol.* 185, 2667–2672. doi: 10.1128/JB.185.8.2667-2672.2003

Nishino, K., and Yamaguchi, A. (2001). Overexpression of the response regulator evgA of the two-component signal transduction system modulates multidrug resistance conferred by multidrug resistance transporters. *J. Bacteriol.* 183, 1455–1458. doi: 10.1128/JB.183.4.1455-1458.2001

Nishino, K., and Yamaguchi, A. (2002). EvgA of the two-component signal transduction system modulates production of the yhiUV multidrug transporter in *Escherichia coli*. *J. Bacteriol.* 184, 2319–2323. doi: 10.1128/JB.184.8.2319-2323.2002

Otwinowski, Z., and Minor, W. (1997). Processing of X-ray diffraction data collected in oscillation mode. *Methods Enzymol.* 276, 307–326. doi: 10.1016/S0076-6879(97)76066-X

Park, S. M., Yoo, J. C., Ji, S. W., Yang, J. S., and Baek, K. (2015). Selective recovery of dissolved Fe, Al, Cu, and Zn in acid mine drainage based on modeling to predict precipitation pH. *Environ. Sci. Pollut. Res. Int.* 22, 3013–3022. doi: 10.1007/s11356-014-3536-x

Parkhill, J., Dougan, G., James, K. D., Thomson, N. R., Pickard, D., Wain, J., et al. (2001). Complete genome sequence of a multiple drug resistant *Salmonella enterica* serovar Typhi CT18. *Nature* 413, 848–852. doi: 10.1038/35101607

Patel, R. (2005). Biofilms and antimicrobial resistance. *Clin. Orthop. Relat. Res.* 437, 41–47. doi: 10.1097/01.blo.0000175714.68624.74

Peleg, A. Y., Monga, D., Pillai, S., Mylonakis, E., Moellering, R. C. Jr., et al. (2009). Reduced susceptibility to vancomycin influences pathogenicity in *Staphylococcus aureus* infection. *J. Infect. Dis.* 199, 532–536. doi: 10.1086/596511

Rappl, C., Deiwick, J., and Hensel, M. (2003). Acidic pH is required for the functional assembly of the type III secretion system encoded by *Salmonella* pathogenicity island 2. *FEMS Microbiol. Lett.* 226, 363–372. doi: 10.1016/S0378-1097(03)00638-4

Rieux, V., Carbon, C., and Azoulay-Dupuis, E. (2001). Complex relationship between acquisition of beta-lactam resistance and loss of virulence in *Streptococcus pneumoniae*. *J. Infect. Dis.* 184, 66–72. doi: 10.1086/320992

Rowe, B., Ward, L. R., and Threlfall, E. J. (1997). Multidrug-resistant *Salmonella* typhi: a worldwide epidemic. *Clin. Infect. Dis.* 24(Suppl. 1), S106–S109.

Rudkin, J. K., Edwards, A. M., Bowden, M. G., Brown, E. L., Pozzi, C., Waters, E. M., et al. (2012). Methicillin resistance reduces the virulence of healthcare-associated methicillin-resistant *Staphylococcus aureus* by interfering with the agr quorum sensing system. *J. Infect. Dis.* 205, 798–806. doi: 10.1093/infdis/jir845

Saha, P., Manna, C., Chakrabarti, J., and Ghosh, M. (2016a). Reversible thermal unfolding of a yfdX protein with chaperone-like activity. *Sci. Rep.* 6:29541. doi: 10.1038/srep29541

Saha, P., Manna, C., Das, S., and Ghosh, M. (2016b). Antibiotic binding of STY3178, a yfdX protein from *Salmonella* Typhi. *Sci. Rep.* 6:21305. doi: 10.1038/srep21305

Sahin, E., and Roberts, C. J. (2012). Size-exclusion chromatography with multi-angle light scattering for elucidating protein aggregation mechanisms. *Methods Mol. Biol.* 899, 403–423. doi: 10.1007/978-1-61779-921-1_25

Sayilgan, E., Kukrer, T., Yigit, N. O., Civelekoglu, G., and Kitis, M. (2010). Acidic leaching and precipitation of zinc and manganese from spent battery powders using various reductants. *J. Hazard Mater.* 173, 137–143. doi: 10.1016/j.jhazmat.2009.08.063

Semenyuk, A. V., and Svergun, D. I. (1991). GNOM – A program package for small-angle scattering data processing. *J. Appl. Cryst.* 24, 537–540.

Svergun, D., Barberato, C., and Koch, M. H. J. (1995). CRYSOL – A program to evaluate X-ray solution scattering of biological macromolecules from atomic coordinates. *J. Appl. Cryst.* 28, 768–773.

Tsai, Y. K., Fung, C. P., Lin, J. C., Chen, J. H., Chang, F. Y., Chen, T. L., et al. (2011). *Klebsiella pneumoniae* outer membrane porins OmpK35 and OmpK36 play roles in both antimicrobial resistance and virulence. *Antimicrob. Agents Chemother.* 55, 1485–1493. doi: 10.1128/AAC.01275-10

Werther, T., Zimmer, A., Wille, G., Golbik, R., Weiss, M. S., and Konig, S. (2010). New insights into structure-function relationships of oxalyl CoA decarboxylase from *Escherichia coli*. *FEBS J.* 277, 2628–2640. doi: 10.1111/j.1742-464X.2010.07673.x

Yamashita, S., Lukacik, P., Barnard, T. J., Noinaj, N., Felek, S., Tsang, T. M., et al. (2011). Structural insights into ail-mediated adhesion in *Yersinia pestis*. *Structure* 19, 1672–1682. doi: 10.1016/j.str.2011.08.010

Conflict of Interest Statement: The authors declare that the research was conducted in the absence of any commercial or financial relationships that could be construed as a potential conflict of interest.

frontiers in Microbiology

ORIGINAL RESEARCH
published: 27 February 2019
doi: 10.3389/fmicb.2019.00335

Single-Cell Approach to Monitor the Unfolded Protein Response During Biotechnological Processes With *Pichia pastoris*

Hana Raschmanová[1,2], Iwo Zamora[2], Martina Borčinová[2,3], Patrick Meier[2], Astrid Weninger[4], Dominik Mächler[2], Anton Glieder[4], Karel Melzoch[1], Zdeněk Knejzlík[5] and Karin Kovar[2]*

[1] Department of Biotechnology, University of Chemistry and Technology Prague, Prague, Czechia, [2] Institute of Chemistry and Biotechnology, School of Life Sciences and Facility Management, Zurich University of Applied Sciences ZHAW, Wädenswil, Switzerland, [3] Department of Genetics and Microbiology, Charles University, Prague, Czechia, [4] Institute of Molecular Biotechnology, Graz University of Technology, Graz, Austria, [5] Institute of Organic Chemistry and Biochemistry of the Czech Academy of Sciences, Prague, Czechia

OPEN ACCESS

Edited by:
John P. Morrissey, University College Cork, Ireland

Reviewed by:
Pau Ferrer, Luxembourg Institute of Science and Technology, Luxembourg
Dominik Mojzita, VTT Technical Research Centre of Finland Ltd, Finland

***Correspondence:**
Hana Raschmanová
raschmah@vscht.cz

Specialty section:
This article was submitted to Microbial Physiology and Metabolism, a section of the journal Frontiers in Microbiology

Received: *31 August 2018*
Accepted: *08 February 2019*
Published: *27 February 2019*

Citation:
Raschmanová H, Zamora I, Borčinová M, Meier P, Weninger A, Mächler D, Glieder A, Melzoch K, Knejzlík Z and Kovar K (2019) Single-Cell Approach to Monitor the Unfolded Protein Response During Biotechnological Processes With Pichia pastoris. Front. Microbiol. 10:335. doi: 10.3389/fmicb.2019.00335

Pichia pastoris (*Komagataella sp.*) is broadly used for the production of secreted recombinant proteins. Due to the high rate of protein production, incorrectly folded proteins may accumulate in the endoplasmic reticulum (ER). To restore their proper folding, the cell triggers the unfolded protein response (UPR); however, if the proteins cannot be repaired, they are degraded, which impairs process productivity. Moreover, a non-producing/non-secreting subpopulation of cells might occur, which also decreases overall productivity. Therefore, an in depth understanding of intracellular protein fluxes and population heterogeneity is needed to improve productivity. Under industrially relevant cultivation conditions in bioreactors, we cultured *P. pastoris* strains producing three different recombinant proteins: penicillin G acylase from *Escherichia coli* (*Ec*PGA), lipase B from *Candida antarctica* (*Ca*LB) and xylanase A from *Thermomyces lanuginosus* (*Tl*XynA). Extracellular and intracellular product concentrations were determined, along with flow cytometry-based single-cell measurements of cell viability and the up-regulation of UPR. The cell population was distributed into four clusters, two of which were viable cells with no UPR up-regulation, differing in cell size and complexity. The other two clusters were cells with impaired viability, and cells with up-regulated UPR. Over the time course of cultivation, the distribution of the population into these four clusters changed. After 30 h of production, 60% of the cells producing *Ec*PGA, which accumulated in the cells (50–70% of the product), had up-regulated UPR, but only 13% of the cells had impaired viability. A higher proportion of cells with decreased viability was observed in strains producing *Ca*LB (20%) and *Tl*XynA (27%). The proportion of cells with up-regulated UPR in *Ca*LB-producing (35%) and *Tl*XynA-producing (30%) strains was lower in comparison to the *Ec*PGA-producing strain, and a smaller proportion of *Ca*LB and *Tl*XynA (<10%) accumulated in the cells. These data provide an insight into the development of heterogeneity in a recombinant *P. pastoris* population during a biotechnological process.

A deeper understanding of the relationship between protein production/secretion and the regulation of the UPR might be utilized in bioprocess control and optimization with respect to secretion and population heterogeneity.

Keywords: unfolded protein response (UPR), stress response, *Pichia pastoris*, super folder green fluorescent protein (sfGFP), flow cytometry, single-cell, fed-batch culture, heterogeneity

INTRODUCTION

The yeast *Pichia pastoris* (*Komagataella phaffii*) is an established host for the biotechnological production of wide range of heterologous proteins, most of which are secreted (Cereghino and Cregg, 2000; Ahmad et al., 2014; Meehl and Stadheim, 2014; Juturu and Wu, 2018). The knowledge of this host and its use for the production of heterologous proteins is already advanced, but a more systematic and complex understanding of the *P. pastoris* cell factory is still needed, especially of intracellular metabolite fluxes, regulatory pathways and secretory machinery (Puxbaum et al., 2015; Zahrl et al., 2017). High-level expression of a heterologous gene may lead to an overload of the protein folding capacity of the endoplasmic reticulum (ER), and consequently to an accumulation of unfolded and/or misfolded proteins in the ER. As a response aiming to restore proper protein folding in the ER, and thus to eliminate the ER stress, the unfolded protein response (UPR) is triggered (Mattanovich et al., 2004; Guerfal et al., 2010). When the unfolded proteins cannot be repaired, they are eliminated within the ER-associated protein degradation (ERAD) pathway (Zahrl et al., 2018). The proportion of intracellularly degraded protein may be massive, up to 60% of the total (Pfeffer et al., 2011). Also, an interplay between protein synthesis and degradation to control protein homeostasis remains unclear, but was recently investigated in mammalian cells at single-cell level (Alber et al., 2018). The rate of protein degradation was shown to vary between cells (Alber et al., 2018). In a recombinant strain of *P. pastoris*, the co-existence of more sub-populations in terms of production and secretion of the recombinant protein was observed, where only part of the population actively secreted (Love et al., 2012). There was a sub-population with a stochastically changing rate of secretion (Love et al., 2010), a sub-population producing different amounts of the recombinant protein (Broger et al., 2011), and one not producing any at all (Broger et al., 2011). Intracellular protein accumulation and/or degradation, together with the existence of a non-secreting phenotype results in decreased productivity of a heterologous protein. Though an important aspect of productivity and approach to a strain's optimization, little attention is typically paid to intracellular product fluxes, stress responses (UPR, ERAD), strain heterogeneity in terms of growth and production/secretion, and cell physiology in microbial cultivation processes under industrially relevant cultivation conditions (Theron et al., 2018).

The UPR was investigated in *P. pastoris* at the point of clone selection (Aw et al., 2017), and in strains producing different recombinant proteins during fed-batch (Hohenblum et al., 2004; Resina et al., 2007; Sjöblom et al., 2012; Vogl et al., 2014; Zhong et al., 2014; Wang et al., 2017; Yu et al., 2017) or chemostat (Gasser et al., 2007; Hesketh et al., 2013; Rebnegger et al., 2014) bioreactor cultivations. Several recombinant proteins were shown to up-regulate UPR in *P. pastoris*, e.g., antibody fragments (Gasser et al., 2007; Khatri et al., 2011), human lysozyme (Hesketh et al., 2013), human trypsinogen (Hohenblum et al., 2004), lipase from *Rhizopus oryzae* (Resina et al., 2007), mucin-type protein fused with green fluorescent protein (GFP) (Sjöblom et al., 2012), membrane transporter proteins (Vogl et al., 2014), prolyl endopeptidase (Wang et al., 2017), phospholipase A_2 from *Streptomyces violaceoruber* (Yu et al., 2017) or human interleukin (Zhong et al., 2014). In contrast, the production of human serum albumin did not lead to induction of UPR (Hohenblum et al., 2004; Aw et al., 2017).

In *P. pastoris*, the UPR has so far been studied at the level of transcript of the genes involved in the UPR, using RNAseq (Yu et al., 2017), qPCR (Guerfal et al., 2010; Khatri et al., 2011; Sjöblom et al., 2012; Zhong et al., 2014; Wang et al., 2017), TRAC (Gasser et al., 2007), microarrays (Graf et al., 2008; Dragosits et al., 2010; Rebnegger et al., 2014; Vogl et al., 2014; Edwards-Jones et al., 2015; Aw et al., 2017) or sandwich hybridization assays (Resina et al., 2007). Alternatively, the UPR was detected at the level of protein with 2D electrophoresis (Dragosits et al., 2010; Vanz et al., 2014), Western blot (Zhong et al., 2014) or flow cytometry after immunofluorescent staining (Hohenblum et al., 2004). These methods can be laborious, time-consuming and expensive. Additionally, detection of the intracellular content of mRNA or protein requires previous cell disruption, which hinders the UPR monitoring during a running bioprocess. Recently, indirect detection of UPR levels based on metabolite biomarkers was suggested. This method can be applied in a high-throughput manner, and thus is more suitable for the screening scale (Tredwell et al., 2017). In yeast cell factories other than *P. pastoris*, easily detectable reporter proteins like β-galactosidase (Cox et al., 1993; Madzak and Beckerich, 2006) or super folder green fluorescent protein (sfGFP) (Lajoie et al., 2012) were previously used to monitor the UPR.

During fed-batch bioreactor cultivations of recombinant *P. pastoris* strains producing penicillin G acylase from *Escherichia coli* (*Ec*PGA), lipase B from *Candida antarctica* (*Ca*LB) or xylanase A from *Thermomyces lanuginosus* (*Tl*XynA), we systematically analyzed the production (secretion vs. intracellular accumulation) of the recombinant protein. Moreover, with flow cytometry, i.e., at the single-cell level, at-line and in a non-invasive manner, we also analyzed the up-regulation of UPR, cell physiology and heterogeneity of the *P. pastoris* strains. To monitor the up-regulation of UPR in the *P. pastoris* strains, a plasmid bearing a gene for sfGFP under the control of the *KAR2* promoter was integrated into the *P. pastoris* genome. The sfGFP

is a fast and robustly folding variant of GFP that is synthesized within a few minutes (Pédelacq et al., 2006; Khmelinskii et al., 2012), which makes it an appropriate biosensor for the immediate detection of folding events in the cell. *KAR2* is a gene involved in UPR, and its product, Kar2p protein, is an ER-resident chaperone that recognizes misfolded/unfolded proteins in the ER and assists proper protein folding (Dudek et al., 2009). Using flow cytometry for the detection of the sfGFP fluorescent signal, it was possible to monitor the activation of the *KAR2* promoter, i.e., up-regulation of the UPR at-line during the cultivation process.

MATERIALS AND METHODS

Culture Media

YPD medium contained 20 g glucose, 20 g peptone, 10 g yeast extract and 15 g agar per liter. YPD medium with 0.1 mg mL^{-1} Zeocin™ (Invitrogen, Carlsbad, USA) was used for the selection of the transformants containing the pPICZ-α-A plasmid with different recombinant genes. YPD medium with 0.1 mg mL^{-1} Nourseothricin (Jena Bioscience, Jena, Germany) was used for the selection of the strains containing the pREP-UPS_{KAR2}-sfGFP-NAT plasmid.

BMG (buffered minimal medium with glycerol) was used for screening the *P. pastoris* clones with integrated pREP-X-sfGFP-NAT or pREP-UPS_{KAR2}-sfGFP-NAT plasmid and for the flask cultivation of the *P. pastoris* strain producing *Ec*PGA (section 3.3). BMG medium contained 10 g glycerol, 13.4 g yeast nitrogen base with ammonium sulfate and without amino acids (YNB), and 0.4 mg biotin per liter and 100 mM potassium phosphate buffer (pH 6.0).

BMD1% (buffered minimal medium with 1% dextrose), BMM10 and BMM2 (buffered minimal media with 5 and 1% methanol, respectively) were used for the micro-scale cultivation screening in 96-deep well plates (Weis et al., 2004). The BMD1% medium contained 10 g glucose, 13.4 g YNB and 0.4 mg biotin per liter and 200 mM potassium phosphate buffer (pH 6.0). The BMM10 medium contained 50 mL methanol, 13.4 g YNB and 0.4 mg biotin per liter and 200 mM potassium phosphate buffer (pH 6.0). The BMM2 medium contained 10 mL methanol, 13.4 g YNB and 0.4 mg biotin per liter and 200 mM potassium phosphate buffer (pH 6.0).

BMGY (buffered complex medium with glycerol) was used for growth of the inoculum for the bioreactor cultivations. BMGY medium contained 10 g glycerol, 10 g yeast extract, 20 g peptone, 13.4 g YNB and 0.4 mg biotin per liter and 100 mM potassium phosphate buffer (pH 6.0).

Defined mineral medium used for batch bioreactor cultivations contained 30 g glycerol as a sole carbon source, 2.86 g K_2SO_4, 0.64 g KOH, 2.32 g $MgSO_4 \cdot 7H_2O$, 0.17 g $CaSO_4 \cdot 2H_2O$, 0.60 g EDTA disodium dehydrate, 7.23 g 85% H_3PO_4, 0.22 g NaCl, 0.1 mL polypropylene glycol (PPG), 4.35 mL filter sterilized PTM1 solution and 4.35 mL filter sterilized biotin solution per liter. The PTM1 stock solution contained 5.0 mL 96% H_2SO_4, 3.84 g $CuSO_4$, 0.08 g NaI, 3.0 g $MnSO_4 \cdot H_2O$, 0.2 g $Na_2MoO_4 \cdot 2H_2O$, 0.02 g H_3BO_3, 0.92 g $CoCl_2 \cdot 6H_2O$, 20.0 g $ZnCl_2$, and 65.0 g $FeSO_4 \cdot 7H_2O$ per liter. The biotin stock solution contained 0.20 g L^{-1} biotin. Before inoculation, the pH of the medium was adjusted to 5.5 using 8.5% NH_4OH.

Concentrated medium used in the first phase of fed-batch (growth phase) contained 588 g glycerol, 12 mL of filter sterilized PTM1 solution and 12 mL of filter sterilized biotin solution per 1,000 g feed solution. Concentrated medium used in the second phase of fed-batch (production phase) contained 1,000 g methanol, 12 mL of filter sterilized PTM1 solution and 12 mL of filter sterilized biotin solution per 1,000 g feed solution.

Plasmids

Construction of the UPR-Reporter Plasmid pREP-UPS_{KAR2}-sfGFP-NAT

The plasmid for monitoring the UPR in recombinant *P. pastoris* strains, named pREP-UPS_{KAR2}-sfGFP-NAT, carried a 324 base pair (bp) upstream region of the *KAR2* coding sequence containing one copy of the unfolded protein responsive element (UPRE) sequence, the *sfGFP* coding sequence (Khmelinskii et al., 2012), the nourseothricin acetyl transferase gene (*nat*) and the *HIS4* gene for integration of the plasmid into the *P. pastoris HIS4* locus. The construction of this plasmid is described in detail in **Supplementary Figure 1**. The plasmid map is provided in **Supplementary Files**.

Construction of Plasmids Bearing the Genes of the Model Recombinant Proteins

The expression cassettes for recombinant protein production contained the *AOX1* promoter, a secretion signal, the coding sequence of the heterologous gene (*Ec*PGA, *Ca*LB, *Tl*XynA), the *AOX1* terminator and the Zeocin resistance cassette. In the case of *Ec*PGA and *Ca*LB, the α-factor secretion signal from *S. cerevisiae* was used as the secretion signal, and in the case of *Tl*XynA, the natural secretion signal from *Thermomyces lanuginosus* was kept (Mellitzer et al., 2012b).

Construction of the expression plasmid carrying the *Ec*PGA gene (Sobotková et al., 1996) (pPICZαA_EcPGA) is described elsewhere (Borcinova et al., in preparation). Briefly, the coding sequence of the *Ec*PGA gene was codon optimized for *P. pastoris* and cloned into the pPICZα A plasmid (Invitrogen, Carlsbad, USA) via *XhoI* and *XbaI* restriction sites. The coding sequence of the *Ca*LB gene, codon optimized for *P. pastoris*, was PCR-amplified from the plasmid pBSY3S1Z_CaLB-WT (bisy e.U., Hofstätten an der Raab, Austria) using primers alphaMF-CALB_fw and CALB-AOX1TT_rev, and cloned into pBSYAOXsec_blunt containing the α-factor secretion signal from *S. cerevisiae* (bisy e.U., Hofstätten an der Raab, Austria) via *MlyI* restriction sites. The constructed plasmid was named pBSYAOXsec_CaLB. The natural secretion signal and the coding sequence of *Tl*XynA, codon optimized for *P. pastoris*, were PCR-amplified from the gBlock XylA_opt using primers PAOX1-XYL_fw and XYL-AOX1TT_rev, and cloned into pBSYAOX_blunt (bisy e.U., Hofstätten an der Raab, Austria) via *MlyI* restriction sites. The constructed plasmid was named pBSYAOX_TlXynA.

The nucleotide sequences of all the above-mentioned primers are provided in **Supplementary Table 1**. The plasmid maps are provided in **Supplementary Files**.

Strains

Electro-competent *P. pastoris* X33 (Invitrogen) cells were prepared and transformed [according to the protocol described by Lin-Cereghino et al. (2005)] with the plasmid DNA and the cells were regenerated in 1 mL of a 1:2 mixture of 1 M sorbitol and YPD medium for 2 h. For the transformation of *P. pastoris* cells with the UPR-reporter or -control plasmid, ∼500 ng of *SalI*-linearized plasmid pREP-UPS$_{KAR2}$-sfGFP-NAT or pREP-X-sfGFP-NAT was used. The transformants were plated out on selective YPD-agar plates with 0.1 mg mL^{-1} nourseothricin (Jena Bioscience, Jena, Germany) and incubated for 2–3 days at 28°C. Selected transformants were cultured overnight in 2 mL BMG at 250 rpm and 28°C, and the production of sfGFP was analyzed by flow cytometry (see chapter Flow Cytometry). An average-expressing clone from each construct was used for further studies. For the transformation of *P. pastoris* cells with the plasmid carrying the *Ec*PGA gene, pPICZαA_EcPGA, ∼5 μg of the linearized plasmid DNA were used and the transformants were selected on YPD-agar plates with Zeocin (Invitrogen, Carlsbad, USA) (Borcinova et al., in preparation). For the transformation of *P. pastoris* cells with the plasmids carrying the *Ca*LB or *Tl*XynA genes, ∼2 μg of *PmeI*-linearized plasmid pBSYAOXsec_CaLB or pBSYAOX_TlXynA, respectively were used for the transformation. The transformants were plated out on selective YPD-agar plates with 0.1 mg mL^{-1} Zeocin (Invitrogen, Carlsbad, USA) and incubated for 2–3 days at 28°C. Random transformants were screened in 96-deep well plates (see chapter Micro-Scale Cultivation Screening). All strains used in this study were stored in 24% glycerol at −80°C.

Micro-Scale Cultivation Screening

P. pastoris clones producing *Ca*LB or *Tl*XynA were cultured in 96-deep well plates in shakers (INFORS Multitron, Bottmingen, Switzerland) at 28°C, 320 rpm, and 80% relative humidity (Weis et al., 2004). After an initial batch phase for 60 h in 250 μL BMD1%, the cultures were induced with addition of 250 μL BMM2, i.e., 0.5% methanol. After 12, 24, and 48 h from the first induction, 50 μL of BMM10 was added to keep the methanol concentration at app. 0.5%. After 60 h from the first induction with methanol, the culture was centrifuged (4,000 rpm, 15 min, 4°C) and the enzymatic activity of *Ca*LB or *Tl*XynA was determined in the supernatant according to the protocols described in chapter Protein Analysis. From each construct, the clone with the highest enzymatic activity, irrespective of the number of integrated gene copies (not determined), was used for further studies.

Bioreactor Cultivations

Batch Cultivations for Determination of Growth Characteristics

A glycerol stock (1 mL) of the strain (all listed in **Table 1**) was thawed and used to inoculate 100 mL of BMGY medium. This first seed culture was grown for 48 h at 30°C and 150 rpm, and then 20 mL of the culture were used to inoculate 180 mL of sterile BMGY (i.e., 10% inoculation ratio). This second seed culture was grown for 12 h at 30°C and 150 rpm, and then aseptically transferred to a 3.6-liter bioreactor (Infors AG, Bottmingen, Switzerland) to achieve a 10% inoculation ratio. The batch volume was 2 L. After glycerol (30 g per liter) was consumed, i.e., after the end of glycerol batch, a batch phase with methanol was performed, which was initiated by pulsing 15 g of methanol per liter to the culture. The maximum specific growth rate of biomass and biomass/substrate yield with glycerol and methanol were calculated from the data obtained from the batch cultivation with glycerol and methanol, respectively (see chapter Data Analysis) for each strain, and were comparable for all strains (**Supplementary Table 2**).

Fed-Batch Cultivations

A glycerol stock (1 mL) of the strain (all listed in **Table 1**) was thawed and used to inoculate 100 mL of BMGY medium. This first seed culture was grown for 48 h at 30°C and 150 rpm, and then 60 mL of the culture were used to inoculate 540 mL of sterile BMGY (i.e., 10% inoculation ratio). This second seed culture was grown for 12 h at 30°C and 150 rpm, and then aseptically transferred to an 18-liter bioreactor (Bilfinger Industrietechnik, Salzburg, Austria) to achieve a 10% inoculation ratio. All cultivations were carried out as single experiments (i.e., without replication) at 30°C, pH 5.5, 0.5 bar overpressure, 3 VVM airflow (without oxygen enrichment) and agitation speed 1,100 rpm. Ammonium hydroxide (8.5%) and phosphoric acid (8.5%) were used for pH adjustment. The batch volume was 6 L and the end of batch was indicated by a rapid increase in dissolved oxygen concentration in the medium (after ∼12 h). To increase the biomass concentration, exponential feeding of a concentrated glycerol solution (58.8% w/w glycerol) was immediately initiated in order to keep specific growth rate μ at a constant value of 0.180 h^{-1} (app. 80% μ_{max} with glycerol) according to the feeding equation $F = 61.88 \cdot e^{0.18 \cdot t}$. After 2.5 h of glycerol feeding, exponential feeding of a concentrated methanol solution (100% w/w methanol) was initiated to keep the specific growth rate μ at a constant value of 0.008 h^{-1} (app. 15% μ_{max} with methanol), 0.016 h^{-1} (app. 30% μ_{max} with methanol) or 0.032 h^{-1} (app. 60% μ_{max} with methanol). The respective feeding equations were $F = 7.56 \cdot e^{0.008 \cdot t}$, $F = 12.52 \cdot e^{0.016 \cdot t}$ and $F = 22.44 \cdot e^{0.032 \cdot t}$. The feeding rates were calculated according to equation (3) in chapter Data Analysis. As parameters μ_{max} and $Y_{x/s,max}$ in equation (3), the average value of the maximum specific growth rates and maximum biomass/substrate yields of the strains Pp4 and Pp5 was used (since these strains were cultured as the first ones in the fed-batch cultivations). Samples were withdrawn regularly during fed-batch culture.

Substrate Analyses

The concentrations of glycerol and methanol in the centrifuged cultivation medium (14,000 rpm, 5 min) were determined by high-pressure liquid chromatography (HPLC) using an LC-20AB device equipped with autosampler SIL-20A, thermostated column oven CTO-20A and refractometer detector RID-10A (all produced by Shimadzu). The Aminex HPX-87H column, with an internal diameter (i.d.) of 7.8 mm (Bio-Rad, Munich, Germany), was run at 40°C at a flow rate of 0.6 mL min^{-1} under isocratic conditions, with 2.5 mM H_2SO_4 and an injection volume of 25 μL.

TABLE 1 | Overview of the fed-batch cultivations.

Recombinant protein	None		*Ec*PGA		*Ca*LB			*Tl*XynA
Strain	Pp1 (control)	Pp1 (control)	Pp4	Pp5 (control)	Pp10	Pp10	Pp10	Pp14
sfGFP expression	P_{KAR2}	P_{KAR2}	P_{KAR2}	No promoter (x)	P_{KAR2}	P_{KAR2}	P_{KAR2}	P_{KAR2}
$\mu_{methanol}$ (h^{-1}) set	0.016	0.032	0.016	0.016	0.016	0.032	0.008	0.016
$\mu_{methanol}$ (h^{-1}) reached	0.021 ± 0.001	0.039 ± 0.001	0.019 ± 0.002	0.021 ± 0.002	0.018 ± 0.001	0.036 ± 0.001	0.007 ± 0.001	0.019 ± 0.001

P. pastoris strains producing three different recombinant proteins and/or containing a reporter of UPR up-regulation were constructed. The recombinant proteins were EcPGA, CaLB, and TlXynA. The reporter of the up-regulation of UPR was a genome-integrated cassette consisting of the KAR2 promoter and sfGFP gene. Three strains contained the UPR reporter and produced a recombinant protein—EcPGA (Pp4), CaLB (Pp10), or TlXynA (Pp14). A control strain to verify the suitability of our UPR reporter produced EcPGA and contained a genome-integrated cassette carrying the sfGFP gene, but no promoter in front of this gene (Pp5). A control strain to examine the UPR up-regulation by cultivation conditions contained the UPR reporter, but produced none of the three recombinant proteins of interest (Pp1). In all processes, temperature was maintained at 30°C and pH at 5.5. All processes consisted of a batch phase with glycerol (30 g l^{-1}), a short (2.5 h) growth fed-batch with an exponential feeding of glycerol to maintain the specific growth rate at 0.2 h^{-1}, and a production fed-batch with an exponential feeding of methanol to maintain the specific growth rate at 0.008, 0.016, or 0.032 h^{-1}.

Biomass Concentration

The cells were harvested by centrifugation (14,000 rpm, 5 min), washed with distilled water and dried at 105°C until constant weight. The biomass concentration was then determined as cell dry weight (CDW).

Flow Cytometry

A BD Accuri™ C6 flow cytometer (BD Biosciences, Franklin Lakes, USA) equipped with a 20 mW 488 nm solid state blue laser was employed for measurements of the green fluorescence of sfGFP (FL1 530 ± 15 nm) during the flask experiments for the characterization of the *KAR2* upstream region (chapter Development of the UPR-Reporter Based on Characterization of the *KAR2* Upstream Region) and the for the characterization of the population producing recombinant *Ec*PGA (chapter Evaluation of the Flow Cytometry Data From Bioreactor Cultivations). Prior to analysis, cells were centrifuged (2,000 g, 5 min) and resuspended in phosphate-buffered saline (PBS) to an OD_{600} of 0.5. The data were analyzed using BD Accuri CFlow® Plus software (BD Biosciences, Franklin Lakes, USA).

Cells from the bioreactor experiments (chapters Evaluation of the Flow Cytometry Data From Bioreactor Cultivations and Physiology- and UPR-Related Effects of Production of Different Heterologous Proteins) were stained with propidium iodide (PI, Invitrogen, 1.0 mg/mL solution in water, P3566) and analyzed using a BD FACSCalibur 4CA flow cytometer (Becton Dickinson GmbH, Heidelberg, Germany) equipped with a 488-nm argon-ion laser, a 635-nm red diode laser, and the appropriate FACSFlow sheath fluid. Propidium iodide was used to assess cell viability as integrity of the cytoplasmic membrane, since PI effectively only enters cells with non-intact or damaged membranes and intercalates into double-stranded nucleic acids, resulting in a red fluorescence; such cells were considered as non-viable. The fluorescence emitted was collected in two optical channels, FL1 (515–545 nm) for the green fluorescence of sfGFP and FL3 (>650 nm) for the red fluorescence of propidium iodide. Samples were taken directly from the culture and were diluted with phosphate-buffered saline (PBS) to reach <100,000 events per 30 s analysis at a low flow speed (12 µL min^{-1}). The diluted *P. pastoris* cell suspension was incubated in the BD measuring tube with PI protected from light, and was thus measured directly. BD CellQuest Pro software was used in the cytometer, while the data were analyzed using FlowJo software (Tree Star Inc.).

The flow cytometry data from the bioreactor cultivations (chapters Evaluation of the Flow Cytometry Data From Bioreactor Cultivations, Physiology- and UPR-Related Effects of Production of Different Heterologous Proteins, and The Influence of Specific Growth Rate on *Ca*LB Production, Physiology and ER-Stress) were evaluated in RStudio, using principle component analysis (PCA) in order to reduce redundancy (e.g., cell size-based effects on sfGFP content). With PCA, the natural logarithm (ln) values of the measured flow cytometric data (FSC, SSC, FL1, FL2, FL3) were de-correlated and displayed in a two dimensional system of two principle components (PCs). The combination PC3-PC2, which described about 39.8% of the population variability, showed the lowest level of redundancy and was used for a clustering analysis. The clustering algorithm was developed for a sample of 10,000 measured cells from three different processes (cultivations of the strains producing *Ec*PGA and *Ca*LB, and the non-producing strain with $\mu_{methanol}$ 0.016 h^{-1}), using k-means. The number of clusters was allowed to vary from one to six in order to maximize the resulting Dunn index. The remaining measurements were then clustered according to the determined population centers, using a nearest neighbors approach.

Fluorescent Microscopy

For microscopic examination of cell size, morphology and fluorescence, phase contrast and epi-fluorescence microscopy were employed using an Olympus BX51 microscope (Olympus, Tokyo, Japan) equipped with a 120 W mercury vapor arc lamp and a U-MWB2 filter cube (excitation 450–480 nm, emission >515 nm). The microphotographs in **Supplementary Figure 6** were shot directly by camera (EOS 600D, Cannon, Tokyo, Japan).

Protein Analysis

Determination of Total Protein Concentration

Quick Start™ Bradford 1x Dye Reagent (Bio-Rad, Hercules, USA) was used for the determination of the total protein concentration (mg L^{-1}). The assay was performed according to the producer's instructions. Briefly, 250 μL of the reagent was mixed with 5 μL of the centrifuged supernatant (14,000 rpm, 5 min) in a 96-well plate, the plate was incubated for 5 min at room temperature and then the absorbance at 595 nm was measured. Bovine gamma-globulin (part of the kit) was used as a standard.

Penicillin G Acylase Activity Assay

The enzymatic activity of PGA was determined by measuring the amount of 6-APA generated by hydrolysis of penicillin G (Gao et al., 2006). 50–300 μL of the centrifuged supernatant (14,000 rpm, 5 min) were mixed with 100 mM sodium phosphate buffer (pH 8.0) to reach a total volume of 2 mL. Then, 1 mL of substrate solution (2% (w/v) penicillin G K^+ salt in 100 mM sodium phosphate buffer, pH 8.0) was added and the reaction mixture was incubated at 37°C for 8 min. In 2, 4 and 8 min after the addition of the substrate, 0.5 mL of the reaction mixture was withdrawn and the reaction was immediately stopped by the addition of 3 mL stop solution [mixture of 20% (v/v) acetic acid and 50 mM NaOH in ratio 2:1 (v/v)]. Then, 0.5 mL of p-dimethylamidobenzaldehyde solution in methanol (5 g L^{-1}) was added to the stopped reaction. After 15 min incubation of the mixture at room temperature, its absorbance at 415 nm was measured. One activity unit of PGA (U) is defined as the amount of PGA that is needed to produce 1 μmol 6-APA mL^{-1} min^{-1}.

For measurement of the intracellular *Ec*PGA, centrifuged cells from a 4 mL sample were washed with 0.1 M sodium phosphate buffer (pH 8.0) and stored at −80°C for a minimum of 1 h. The cell pellet was then resuspended to the original volume (4 mL) and diluted with 0.1 M sodium phosphate buffer (pH 8.0), to reach a maximum absorbance OD_{600} of 50–100. 1 mL of the diluted cell suspension was mixed with 1 mL of glass beads (0.25–0.50 mm) and vortexed for 20 min. The vortexed sample was centrifuged (8,000 rpm, 5 min, 4°C) and the supernatant was used for the PGA activity assay.

Lipase B Activity Assay

The enzymatic activity of *Candida antarctica* lipase B (*Ca*LB) was determined according to the colorimetric assay using p-nitrophenyl butyrate (pNPB) as a substrate (Krainer et al., 2012). 20 μL of the enzyme sample (culture supernatant) was transferred into a 96-well microtiter plate, and 180 μL of a freshly prepared pNPB working solution (100 μL pNPB stock solution in 10 mL of 300 mM Tris/HCl buffer, pH 8.0; pNPB stock solution was prepared by mixing 42 μL of pNPB (Sigma Aldrich) with 458 μL of DMSO and stored at −20°C) was added. The kinetics of the reaction were measured immediately at 405 nm for 6 min at 25°C. One activity unit (U) of *Ca*LB was defined as the amount of *Ca*LB that was needed to produce 1 μmol p-nitrophenolate mL^{-1} min^{-1}.

For the measurement of the intracellular *Ca*LB, centrifuged cells from a 0.5 mL sample were washed with PBS and stored at −20°C. The cell pellet was gently resuspended in Y-PER™ Yeast Protein Extraction Reagent (Thermo Scientific, Rockford, USA) in ratio 2.5 μL Y-PER per 1 mg WCW. The suspension was then incubated in the Eppendorf agitator at room temperature for 30 min and 600 rpm. Then, the sample was centrifuged (14,000 rpm, 10 min) and the supernatant was used for the *Ca*LB activity assay.

Xylanase a Activity Assay

The enzymatic activity of *Thermomyces lanuginosus* (*Tl*XynA) was determined according to the colorimetric *para*-hydroxybenzoic acid hydrazide (pHBAH) assay, which is used to detect reducing sugars released from polymers (Mellitzer et al., 2012a). For lignocellulosic substrate conversion, 20 μL of the enzyme sample (culture supernatant) or blank (50 mM sodium citrate buffer, pH 4.8) was mixed with 150 μL of the substrate solution (0.5% xylan in 50 mM sodium citrate buffer, pH 4.8). The mixture was incubated for 30 min at 50°C and 300 rpm. For the subsequent reducing-sugar assay, 50 μL of the substrate conversion reaction was mixed with 150 μL of pHBAH working solution (pHBAH stock solution was 5% w/v pHBAH in 0.5% v/v HCl; pHBAH working solution was prepared by mixing the stock solution with 0.5 M NaOH in 1:4 v/v ratio). The mixture was incubated at 99°C for 2 min, and then cooled to 4°C. Then, the absorption at 410 nm was measured. The activity (U L^{-1}) of *Tl*XynA was calculated from a standard curve, which was obtained after performing the assay with a series of standard solutions (0–200 U L^{-1}) of commercial xylanase from *Thermomyces lanuginosus* (X2753, Sigma Aldrich, St. Louis, USA).

For the measurement of intracellular *Tl*XynA, centrifuged cells from a 0.5 mL sample were washed with PBS and stored at −20°C. The cell pellet was gently resuspended in Y-PER™ Yeast Protein Extraction Reagent (Thermo Scientific, Rockford, USA) in ratio 2.5 μL Y-PER per 1 mg WCW. The suspension was then incubated in the Eppendorf agitator at room temperature for 30 min and 600 rpm. Then, the sample was centrifuged (14,000 rpm, 10 min) and the supernatant was used for the *Tl*XynA activity assay.

Fluorimetric Measurements

Spark 20M multimode microplate reader (Tecan, Männedorf, Switzerland) was used for measuring fluorescence of sfGFP. The mode Fluorescence Top Reading was used, with the excitation wavelength 485 ± 10 nm and emission wavelength 535 ± 10 nm.

qPCR

The sample taken during the bioreactor cultivation was centrifuged (14,000 rpm, 5 min) and the cell pellet was stored at −80°C. Total RNA was isolated from the cell pellets according to the protocol provided by Invitrogen (http://tools.thermofisher.com/content/sfs/manuals/easyselect_man.pdf). The cDNA was prepared using the iScript cDNA Synthesis Kit (Bio-Rad, Hercules, USA). qPCR was performed in QuantStudio™ 5 Real-Time PCR System (ThermoFisher Scientific, Waltham, USA), using the 5× HOT FIREPol® EvaGreen® qPCR Mix Plus (ROX) (Solis BioDyne, Tartu, Estonia). Relative expression of

KAR2 was monitored (primers q34 and q35), using *ACT1* as a reference (primers q24 and q25) and no-template as well as no-RT controls. The nucleotide sequences of the primers are provided in **Supplementary Table 1**. The fold-change of *KAR2* expression was evaluated using the $\Delta\Delta c_t$ method, relating all expression data to the expression of *KAR2* in the non-producing control strain in the sample taken 3 h after induction.

Statistical Analysis and Controls

Measurements of biomass concentration were carried out in duplicate. Flow cytometric measurements, measurements of enzyme activity and total protein concentration, and qPCR measurements were carried out in triplicate. The mean values was calculated and the errors were expressed as standard deviations.

Data Analysis

Maximum specific growth rate was calculated according to equation (1):

$$\mu_{\max} = \frac{\ln(x(t)) - \ln(x_0)}{t - t_0} \qquad (\mathrm{h}^{-1}) \tag{1}$$

where x is the biomass concentration (g L^{-1}) and t is the cultivation time (h).

Maximum biomass/substrate yield was calculated according to equation (2):

$$Y_{x/s,\max} = \frac{x_2 - x_1}{s_2 - s_1} \qquad (\mathrm{g\,g}^{-1}) \tag{2}$$

where s is the substrate concentration (g L^{-1}).

Exponential feeding rate was calculated according to equation (3):

$$F = F_0 \cdot e^{\mu \cdot t} = \frac{\mu \cdot V_0 \cdot x_0}{Y_{x/s,\max} \cdot s_0} \cdot e^{\mu \cdot t} \qquad (\mathrm{L\,h}^{-1}) \tag{3}$$

where F_0 is the initial feed rate (L h^{-1}), μ is the required specific growth rate (h^{-1}), V_0 is the initial working volume (L), x_0 is the initial biomass concentration (g L^{-1}) and s_0 is the concentration of carbon source in the feed solution (g L^{-1}).

Specific growth rate during fed-batch was calculated according to equation (4):

$$\mu(t) = \frac{\ln(x \cdot V) - \ln(x_0 \cdot V_0)}{t - t_0} \qquad (\mathrm{h}^{-1}) \tag{4}$$

where V is the working volume (L).

Approximate volume of supernatant was calculated according to equation (5):

$$V_s(t) = \frac{(V(t) \cdot \rho_{\mathrm{broth}}) - \frac{M_{x,\,WCW}}{1000}}{\rho_{\mathrm{supernatant}}} \qquad (\mathrm{L}) \tag{5}$$

where ρ_{broth} is the density of culture broth (kg L^{-1}), $M_{x,\mathrm{WCW}}$ is the mass of wet cells (g L^{-1}) and $\rho_{\mathrm{supernatant}}$ is the density of supernatant that is ∼1.03 kg L^{-1} (Potgieter et al., 2010)

The density of culture broth was calculated according to equation (6):

$$\rho_{\mathrm{broth}} \approx 0.000132 \cdot x_{\mathrm{WCW}} + 1.03 \qquad (\mathrm{kg\,L}^{-1}) \tag{6}$$

where x_{WCW} is the concentration of biomass wet cell weight (g L^{-1}).

The concentration of wet biomass (g L^{-1}) was calculated according to equation (7). This equation was determined and verified experimentally for the given strain and culture conditions.

$$\mathrm{WCW} \approx 4.2 \cdot \mathrm{CDW} \qquad (\mathrm{g\,L}^{-1}). \tag{7}$$

Product/biomass yield during fed-batch was calculated according to equation (8):

$$Y_{p/x} = \frac{\Delta(c_p \cdot V_S)}{\Delta(x \cdot V)} \qquad (\mathrm{U\,g}^{-1}) \tag{8}$$

where c_p is the product concentration (U L^{-1}).

RESULTS

We constructed a reporter for monitoring UPR up-regulation in living *P. pastoris* cells, which was based on the production of sfGFP upon the activation of the *P. pastoris KAR2* promoter. Using this reporter, UPR up-regulation was assessed in *P. pastoris* strains producing different recombinant proteins (*Ec*PGA, *Ca*LB, *Tl*XynA) during bioreactor fed-batch cultivations with methanol. Besides assessing the concentration of the secreted product in the cultivation medium, we also measured the residual/non-secreted product inside the cells. Flow cytometry was used as an at-line, single-cell and non-invasive method for the assessment of the UPR up-regulation (of the fluorescence of sfGFP), cell viability and population heterogeneity.

Development of the UPR-Reporter Based on Characterization of the *KAR2* Upstream Region

We aimed to use the *KAR2* upstream region for monitoring UPR in *P. pastoris* during bioreactor cultivations. The *KAR2* promoter within the *KAR2* upstream region has not yet been characterized in *P. pastoris*. So far, one copy of a potential UPRE (unfolded protein responsive element) sequence, which is a binding site of the transcription activator Hac1p of UPR-involved genes (Mori et al., 1996, 1998), was revealed in the *KAR2* upstream region of *P. pastoris* (Guerfal et al., 2010). The potential UPRE sequence is CAGCGTG, starting −84 bp upstream to the *KAR2* ATG (**Figure 1**). We prepared mutated variants (truncation and/or single nucleotide mutations) of the *P. pastoris KAR2* upstream region to check for the UPR-function of the potential UPRE (**Figure 1**). These variants were namely: (1) full length *KAR2* upstream region starting −324 bp upstream *KAR2* CDS (named FL); (2) truncated variant of the *KAR2* upstream region starting −190 bp upstream *KAR2* CDS, still containing the native UPRE sequence (named −190 bp); (3) truncated variant of the *KAR2*

FIGURE 1 | The upstream region of the *KAR2* CDS in *P. pastoris X33*. The nucleotide sequence located upstream of the *KAR2* CDS and downstream of the CDS of the previous gene (*BUD7*) in the genome of *P. pastoris* X33. One potential UPRE (CAGCGTG) was identified in the *KAR2* upstream region, starting −84 bp upstream of the *KAR2* CDS. The following variants of the *KAR2* upstream region were used to control the expression of *sfGFP*:

- full length *KAR2* upstream region (FL, −324 bp);
- truncated variant of *KAR2* upstream region, still containing native UPRE sequence (−191 bp);
- truncated variant of *KAR2* upstream region with two single mutations (84C→A, 78G→A) in the UPRE sequence (−191 bp mut.);

truncated variant of *KAR2* upstream region lacking the UPRE sequence (−77 bp).

upstream region starting −190 bp upstream *KAR2* CDS and with two single mutations (84C→A, 78G→A) disturbing the UPRE sequence (named −190 bp mut.); (4) truncated variant of the *KAR2* upstream region starting −77 bp upstream *KAR2* CDS, thus lacking the UPRE sequence (named −77 bp). These variants were inserted in front of the sfGFP gene in the pREP-P_{KAR2}-sfGFP plasmid, so the variant of the *KAR2* upstream region controlled the expression of sfGFP. Plasmid pREP-x-sfGFP, having no promoter in front of the sfGFP gene, was used as a negative control. The pREP-P_{KAR2}-sfGFP plasmids, as well as the pREP-x-sfGFP control plasmid were stably integrated into the *HIS4* locus of the *P. pastoris* X33 strain.

The strains were cultured in shake flasks with 100 mL YPD overnight to OD_{600} 2.0–3.0. The culture was then split into three parallels and incubated for 2 h. One of the parallels was cultured under normal (non-stress) conditions, while the other two parallels were cultured under experimentally-induced stress conditions, i.e., either in presence of 3 mM dithiothreitol (DTT) or under increased temperature (39°C). The activity of the different *KAR2* promoter variants was assessed according to the fluorescence of sfGFP with flow cytometry. Under non-stress conditions, the activities of the mutated *KAR2* upstream variants were lower than the activity of the full length (FL) variant (**Figure 2**), namely 1.2-fold in case of the −190 bp variant, 1.8-fold in case of −190 bp mut. variant and 6.7-fold in case of the −77 bp variant. Because the activity of the variant with the mutated potential UPRE sequence (−190 bp mut. variant) was lower than the activity of its non-mutated counterpart (−190 bp variant) and because the activity dramatically decreased when the potential UPRE sequence was missing in the −77 bp variant, we assume that the CAGCGTG might be the consensus UPRE motif in the *P. pastoris KAR2* upstream region, required for the functionality of the *KAR2* promoter. Against our expectations, up-regulation of the *KAR2* upstream region by DTT treatment was insignificant (**Figure 2**), even in the case of the FL and −190 bp variants. In contrast to DTT, increased temperature of 39°C led to a strong up-regulation of the promoter activity. Compared to the FL variant, which gave the strongest fluorescence signal at the increased temperature, fluorescence of the −190 bp, −190 bp mut., and −77 bp variants were lower (1.1-fold, 1.4-fold, and 10.2-fold, respectively). However, the increase of fluorescence of the heated (39°C) cells, when compared to the non-treated cells, was the most significant in the case of the −190 bp mut. variant (3.1-fold), while for the FL variant it was 2.3-fold, for the −190 bp variant 2.5-fold and for the −77 bp variant 1.5-fold. Because the activity of the variant with the mutated UPRE (−191 bp mut.) increased even more significantly after heat stress than the activity of the non-mutated variant (−191 bp), we assume that the potential UPRE does not function as a heat shock element. The fluorescence of the negative control strain producing no sfGFP (x), i.e., the background fluorescence signal, was considerably lower in comparison to strains with variants of the *KAR2* upstream region. Due to the highest sfGFP levels of the FL variant, we decided to use the plasmid bearing the $P_{KAR2(FL)}$-sfGFP to monitor the UPR in *P. pastoris*. The FSC-FL1 dot plots are provided in **Supplementary Figure 2**.

Validation of the P_{KAR2}-Based UPR Reporter in a Strain Over-producing Recombinant Protein in a Bioreactor Fed-Batch Cultivation

The plasmid $P_{KAR2(FL)}$-sfGFP was integrated into the *P. pastoris* strain producing *Ec*PGA to monitor the UPR during a bioreactor cultivation. Because the *Ec*PGA was previously observed to intracellularly accumulate in *P. pastoris* (Borcinova et al., in preparation; Marešová et al., 2017), we assumed that UPR would be up-regulated, and sfGFP would be strongly produced. The up-regulation of UPR upon production of *Ec*PGA was proved both by flow cytometric analysis of sfGFP fluorescence (**Supplementary Figures 4, 5**) and qPCR analysis of *KAR2* expression (**Figure 3**), when comparing the strain producing *Ec*PGA with a control strain producing no recombinant protein, both having the $P_{KAR2(FL)}$-sfGFP cassette integrated into their genome.

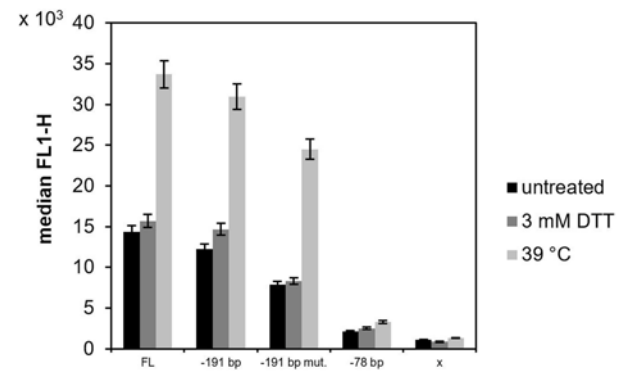

FIGURE 2 | The activity of different variants of the *KAR2* upstream region in *P. pastoris* X33. The promoter activity of the different variants of the *KAR2* upstream region was measured as a green fluorescence of sfGFP (channel FL1) with flow cytometry, as the gene of sfGFP was inserted downstream of the *KAR2* upstream region. A variant with no promoter in front of the sfGFP gene (x) was used as a negative control. *P. pastoris* strains with the different variants of the *KAR2* upstream region (FL, −190 bp, −190 bp mut., −77 bp) controlling *sfGFP* expression, and the negative control strain (*x-sfGFP*) were cultured overnight in shake flasks with YPD, then split into three parallels and further incubated for another 2 h. One parallel was cultured under normal conditions without experimental stress (black bars), the second parallel was cultured in the presence of 3 mM DTT (dark gray bars) and the third parallel was cultured at an increased temperature of 39°C (light gray bars). The displayed values are median FL1 values of all events belonging to a gate defined in a FSC-SSC dot plot (distinguishing *P. pastoris* cells from the background, data not shown). The error bar is showing a standard deviation of three measurements.

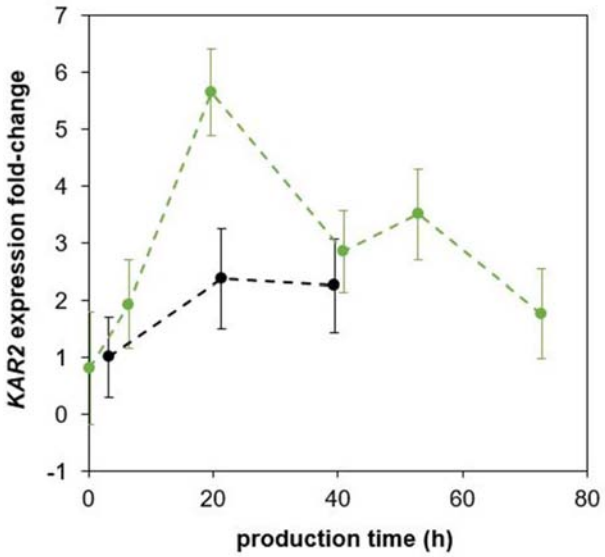

FIGURE 3 | Fold-change of *KAR2* expression in the *P. pastoris* strain producing *Ec*PGA and the non-producing control strain as obtained by qPCR analysis. The *P. pastoris* strains producing *Ec*PGA (green) and the control non-production strain (black) were cultured under the same cultivation conditions (30°C, pH 5.5), maintaining the specific growth rate of biomass with methanol at 0.016 h^{-1}. All relative expression data are related to the expression of *KAR2* in the non-producing control strain in the sample taken 3 h after induction.

Furthermore, we needed to exclude any potential negative effects of sfGFP production on the strain's growth, physiology and production properties, even though it was shown in *S. cerevisiae* that sfGFP fused to Kar2p did not significantly influence the growth of the strain, nor activated the UPR (Lajoie et al., 2012). Therefore, we prepared a control strain by integrating the negative control cassette x-sfGFP (lacking a promoter upstream the *sfGFP*, so producing no sfGFP, **Figure 2**), instead of the UPR reporter cassette ($P_{KAR2(FL)}$-sfGFP), to the *Ec*PGA-producing strain. The strains were cultured under the same cultivation conditions in bioreactors (**Table 1**). The specific growth rate with methanol during the production phase (**Table 1**), the production of *Ec*PGA (**Figure 4**) and viability (**Supplementary Figure 6**) were comparable in the two *Ec*PGA-producing strains, suggesting that the production of sfGFP did not impair the growth, production properties, nor viability of the *Ec*PGA-producing strain.

Since the production of sfGFP was shown not to influence the strain's physiology and turned out to be detectable with flow cytometry upon the up-regulation of the UPR, we decided to use the $P_{KAR2(FL)}$-sfGFP reporter system to monitor the UPR in two other recombinant strains, producing *Ca*LB and *Tl*XynA.

Evaluation of the Flow Cytometry Data From Bioreactor Cultivations

The *P. pastoris* strains producing and secreting *Ec*PGA, *Ca*LB and *Tl*XynA with the integrated $P_{KAR2(FL)}$-sfGFP cassette, the control strain with the integrated $P_{KAR2(FL)}$-sfGFP cassette producing none of the recombinant proteins, as well as the control strain without the integrated control x-sfGFP cassette producing *Ec*PGA were cultured under the same cultivation conditions (30°C, pH 5.5) during fed-batch cultivations with methanol, maintaining $\mu_{methanol}$ at 0.016 h^{-1} (ca 30% of $\mu_{max,methanol}$ of the strains). The achieved specific growth rate with methanol of all the strains was comparable (**Table 1**).

Flow cytometry was used to assess cell size and complexity (FSC and SSC, respectively), green fluorescence of sfGFP (FL1) referring to the activity of the *KAR2* promoter (UPR), and cell viability as red fluorescence of PI bound within cells with compromised cell membranes (FL3) during the cultivation. Two sub-populations with respect to the FSC signal were distinguished and observed in all strains over the production phase with methanol (examples of density plots are shown in **Supplementary Figure 3**). It is apparent from the FSC-FL1 dot plot overlay (**Supplementary Figure 4**) that the FL1 signal (fluorescence of sfGFP) correlated with FSC to some extent, and that the increase in FL1 over time was more significant in the case of cells with higher FSC. The time course of sfGFP fluorescence (median FL1) evaluated separately for the two sub-populations with different sizes (FSC) for all strains is provided in **Supplementary Figure 5**.

In order to reduce redundancy, such as for example the effect of cell size (FSC) on the sfGFP content (FL1) (see **Supplementary Figure 4**), the flow cytometric data were further evaluated using PCA (**Figure 5**). Based on the PCA, the following

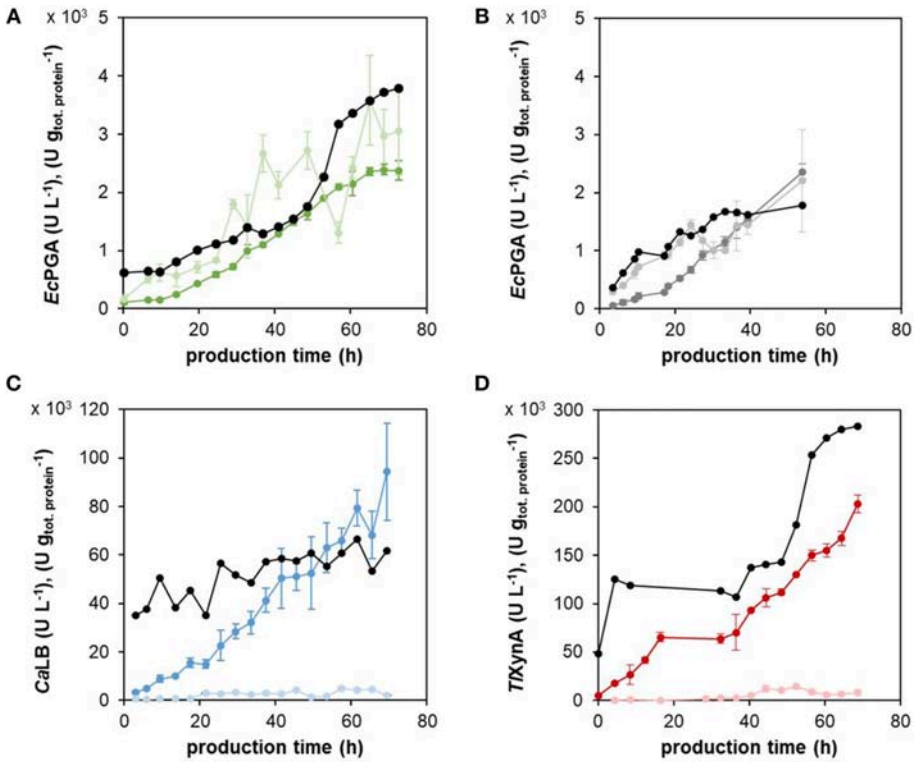

FIGURE 4 | The enzymatic activity of the different recombinant proteins in the centrifuged culture medium and cell extracts. The production of *Ec*PGA in the strain with the expression cassette $P_{KAR2(FL)}$-sfGFP **(A)** and in the control strain **(B)**, *Ca*LB **(C)**, and *Tl*XynA **(D)** was assessed as enzymatic activity (U L^{-1}) both in the culture medium, i.e., in the supernatant (dark green, dark gray, dark blue, dark red for *Ec*PGA, *Ec*PGA, *Ca*LB, *Tl*XynA, respectively), as well as in the cell extracts, i.e., inside the cells (light green, light gray, light blue, light red for *Ec*PGA, *Ec*PGA, *Ca*LB, *Tl*XynA, respectively). The concentrations were recalculated to the volume of the culture broth. The activities of the extracellular (secreted) enzyme were related to the mass of total extracellular protein (U $g^{-1}_{tot.protein}$, black in **A–D**). The strains with the integrated $P_{KAR2(FL)}$-sfGFP cassette for the monitoring of UPR and producing *Ec*PGA **(A)**, *Ca*LB **(C)**, or *Tl*XynA **(D)**, and the control strain with the integrated x-sfGFP cassette producing *Ec*PGA **(B)** were cultured under the same cultivation conditions (30°C, pH 5.5, $\mu_{methanol}$ 0.016 h^{-1}).

four sub-populations were distinguished: (I) smaller and less complex (lower FSC and SSC) viable cells with no UPR up-regulation; (II) larger and more complex (higher FSC and SSC, also including budding cells, i.e., two incompletely separated cells) viable cells with no UPR up-regulation; (III) viable cells with up-regulated UPR (increased FL1); and (IV) cells with impaired viability (increased FL3).

In order to additionally support the flow cytometry-based results indicating the heterogeneity of *P. pastoris* population with respect to cell size/complexity (FSC, SSC) and green fluorescence (FL1), we performed a shake flask cultivation of the strain producing *Ec*PGA (Pp4) for a microscopic evaluation of the population (**Supplementary Figure 7**). The strain was cultured in 25 mL BMG with subsequent methanol pulses, and analyzed by flow cytometry and fluorescent microscopy. According to the flow cytometric data (FSC-SSC, FSC-FL1), the division of the population into two sub-populations of different sizes and complexities was less pronounced in a shake flask (**Supplementary Figure 7**) than in a bioreactor (**Supplementary Figure 3**). Nevertheless, the population heterogeneity was observed microscopically in the shake flask culture; there were budding cells (two, rarely three connected cells), small oval cells (likely freshly separated cells after division) with weak fluorescence and big round cells with fluorescence of different intensities.

Physiology- and UPR-Related Effects of Production of Different Heterologous Proteins

The concentration (U L^{-1}) of the active enzyme (*Ec*PGA, *Ca*LB and *Tl*XynA) was assessed during fed-batch cultivation (cultivation conditions specified in 3.3) in the centrifuged cultivation medium as well as in the cells (**Figure 4**). A strong intracellular accumulation of *Ec*PGA was observed, as 50–70% of the total active *Ec*PGA remained in the cells over the whole production phase. In contrast, only a small proportion (2–10%) of the total active *Ca*LB or *Tl*XynA was detected in the cells after 20 h of production. Also, the total protein concentration (g L^{-1}) was assessed in the centrifuged cultivation medium and recalculated to the volume of the culture broth (**Supplementary Figure 8**). The activities of the extracellular (secreted) enzymes related to the mass of total extracellular protein are shown in **Figure 4**. In case of *Ca*LB (**Figure 4C**), the

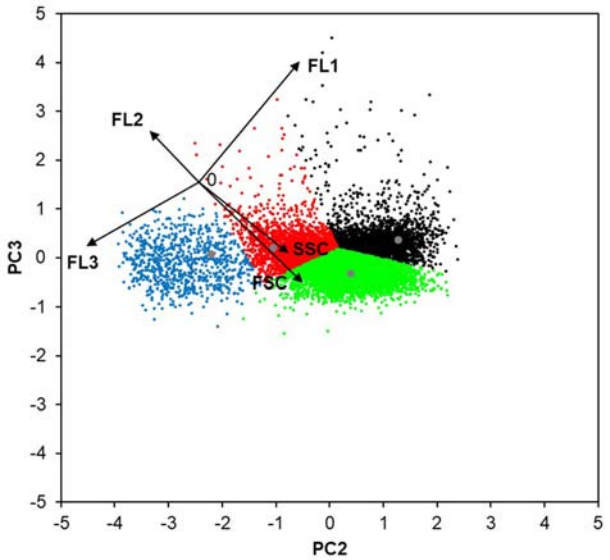

FIGURE 5 | The four sub-populations of *P. pastoris* cells defined with the use of PCA. The flow cytometric data (FSC, SSC, FL1, FL2, FL3) of 10,000 random cells from the bioreactor cultivations of the strains producing *Ec*PGA and *Ca*LB, and the non-producing strain (all at $\mu_{methanol}$ 0.016 h^{-1}) were analyzed with PCA. The lowest level of redundancy was observed when the data were displayed as the combination of PC2 and PC3 (describing ∼39.8% of the population variability), since the flow cytometric data (black vectors) were the most de-correlated. The length of each vector is 50 AU. The combination of PC3 and PC2 was used to establish the clustering method (population centers are displayed in gray). According to the FC signals (black arrows), the identified four clusters can be described as follows: smaller and less complex viable cells with no UPR up-regulation (red); larger and more complex viable cells with no UPR up-regulation (green); viable cells with up-regulated UPR (black); and cells with impaired viability (blue).

amount of active enzyme per mass of total protein (U $g^{-1}_{tot.protein}$) was more or less stable during the production phase, indicating that the portion of the active *Ca*LB in the secreted protein content was constant. In case of *Ec*PGA (**Figures 4A,B**) and *Tl*XynA (**Figure 4D**), the increase of active enzyme per mass of total protein after 40–50 h of production indicated an increased portion of the active enzyme in the extracellular protein content.

According to the flow cytometric data evaluated with PCA, the cell population was heterogeneous and the distribution of the cells into the four sub-populations (defined in chapter Evaluation of the Flow Cytometry Data From Bioreactor Cultivations) changed over the time course of the cultivation process (**Figure 6**). In the strains producing different recombinant proteins at the specific growth rate with methanol 0.016 h^{-1} (**Figures 6A–C**), the amount of the viable smaller and less complex cells increased after the shift to methanol, i.e., the start of the production phase, and was around 30% over the whole production phase. At the same time, the number of the viable bigger cells decreased. In the control non-producing strain (**Figure 6D**), the number of these smaller and less complex cells began to decrease again after some 20 h of growth on methanol, while the number of the viable larger cells increased proportionally. A decrease in viability was observed in all strains, including the control strain. Around 12% of the population of the control strain was stained with PI at the end of the cultivation, i.e., after 54 h of growth on methanol (**Figure 6D**), indicating that viability was impaired by long exposure of the cells to methanol. The production of *Ec*PGA did not have any negative effect on cell viability (**Figure 6A**), since the number of the PI-stained cells was comparable to the control non-producing strain. However, the production of *Ca*LB and *Tl*XynA impaired cell viability compared to the control strain; around 20% of the cells of the *Ca*LB- (**Figure 6B**) and the *Tl*XynA-producing strains (**Figure 6C**) had damaged membranes after 54 h of production. The number of damaged cells within the *Tl*XynA-producing strain further increased and was 27% by the end of the process, i.e., after 69 h of production (**Figure 6C**). The raw flow cytometry data showing the percentage of non-viable (PI-stained) cells are shown in **Supplementary Figure 6**. It can be seen that in case of *Tl*XynA, the percentage of the cells with impaired viability differed significantly in the two sub-populations of different FSC. While the viability of the "smaller" cells was comparable to the control strain (**Supplementary Figure 6A**), the viability of the "bigger" cells decreased dramatically (**Supplementary Figure 6B**).

There was only a slight up-regulation of UPR (around 4% of the population) observed in the non-producing control strain (**Figure 6D**). In contrast, a significant up-regulation of UPR was observed in all the production strains (**Figures 6A–C**). In the strain producing and also considerably intracellularly accumulating *Ec*PGA (**Figure 4A**), the number of cells with up-regulated UPR began to increase steeply right after induction of production (**Figure 6A**). After ∼30 h of production and until the end of the process, up to 60% of the cell population had an up-regulated UPR. Interestingly, in the strains producing *Ca*LB (**Figure 6B**) and *Tl*XynA (**Figure 6C**), the maximum portion of cells with up-regulated UPR (35% in case of *Ca*LB production and 26% in case of *Tl*XynA production) was also reached after 30 h of production, although further development was different. The portion of cells with up-regulated UPR was stable over the whole production phase in the *Ca*LB-producing strain, while it began to decrease in the *Tl*XynA-producing strain after 40 h of production and was 14% at the end of cultivation. The stagnation/decrease in the number of cells with an up-regulated UPR might have been caused by lysis of the damaged cells, which was enhanced in the case of production of *Ca*LB and *Tl*XynA, and a consequent release of the intracellular contents, including sfGFP, to the cultivation medium. Alternatively, also a potential loss of the expression cassette (Zhu et al., 2009) might have contributed to the stress relief, i.e., stagnation of the portion of cells with up-regulated UPR.

We further investigated the potential leakage of sfGFP from the cells by measuring the fluorescence of the cultivation medium (extracellular fluorescence) with a microplate fluorimeter. We compared the specific extracellular fluorescence (AU $gCDW^{-1}$) of the cultivation medium from the processes with the *Tl*XynA-producing strain, the non-producing control strain, and the control strain producing *Ec*PGA, but no sfGFP (**Figure 7**). For the *Tl*XynA-producing strain, we also measured the fluorescence

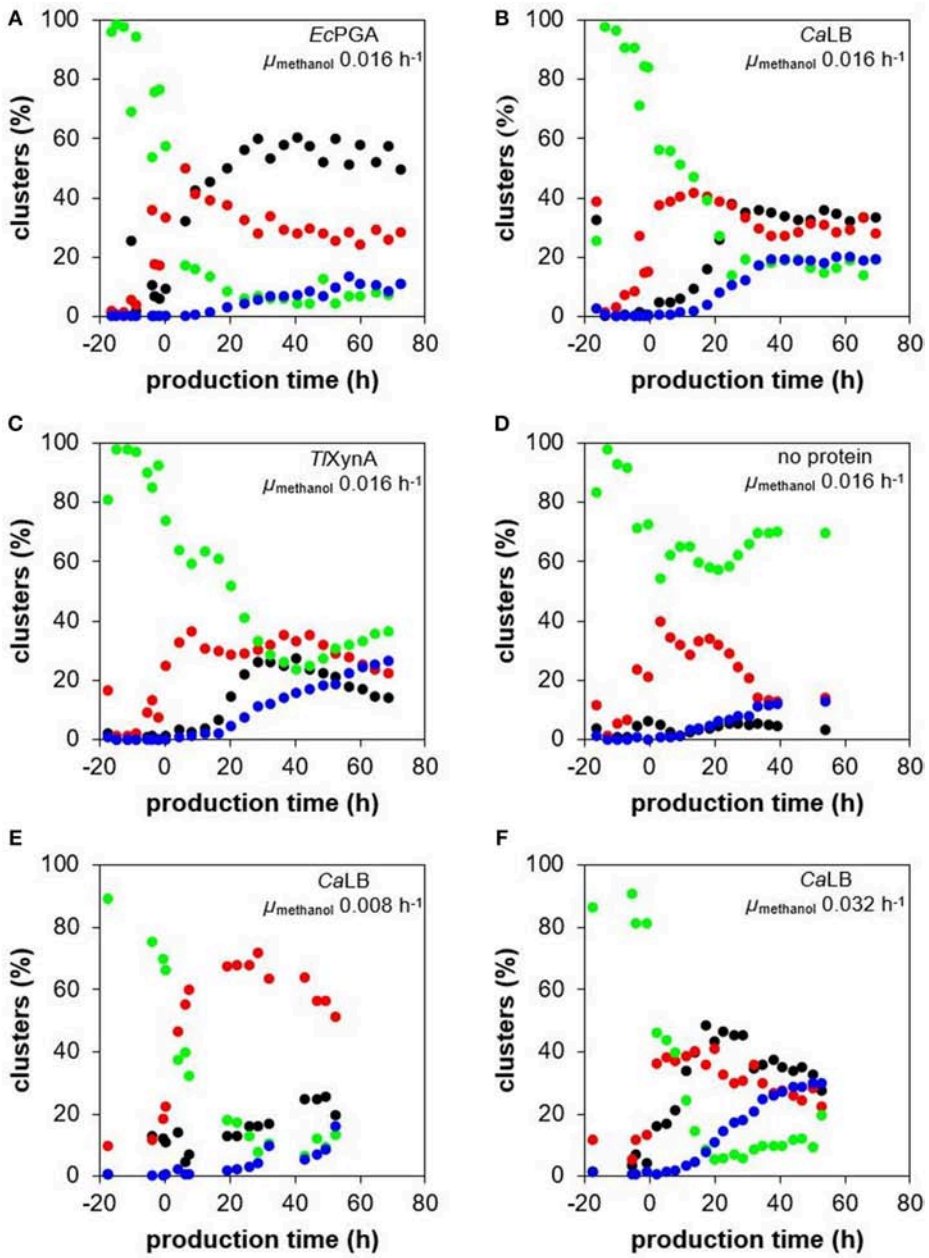

FIGURE 6 | Change of cell size and complexity, UPR up-regulation and viability during cultivations of *P. pastoris* strains producing different recombinant proteins. The *P. pastoris* strains producing *Ec*PGA **(A)**, *Ca*LB **(B)**, or *Tl*XynA **(C)**, as well as a control non-production strain **(D)** were cultured under the same cultivation conditions (30°C, pH 5.5), maintaining the specific growth rate of biomass with methanol at 0.016 h^{-1}. Additionally, the *P. pastoris* strain producing *Ca*LB was cultured at 30°C, pH 5.5 and at a specific growth rate of biomass with methanol of 0.008 h^{-1} **(E)** and 0.032 h^{-1} **(F)**. The four sub-populations identified with the PCA of the flow cytometric data were observed in all the cultivation processes: smaller and less complex viable cells with no UPR up-regulation (red ovals); larger and more complex viable cells with no UPR up-regulation (green ovals); viable cells with up-regulated UPR (black ovals); and cells with an impaired viability (blue ovals).

of the cell lysate (intracellular fluorescence). The specific extracellular fluorescence (AU $gCDW^{-1}$) in the case of the *Tl*XynA-producing strain began to increase after 15 h of the production phase, and continued increasing until the end of the cultivation. An increase in specific extracellular fluorescence was also observed for the control strains. Therefore, we assume that the increase in extracellular fluorescence was partly caused by the fluorescent background of the culture medium fed into the bioreactor. Nevertheless, after 30 h of production, the specific extracellular fluorescence in the cultivation with the *Tl*XynA-producing strain started to be higher than the specific extracellular fluorescence in cultivations with the control strains.

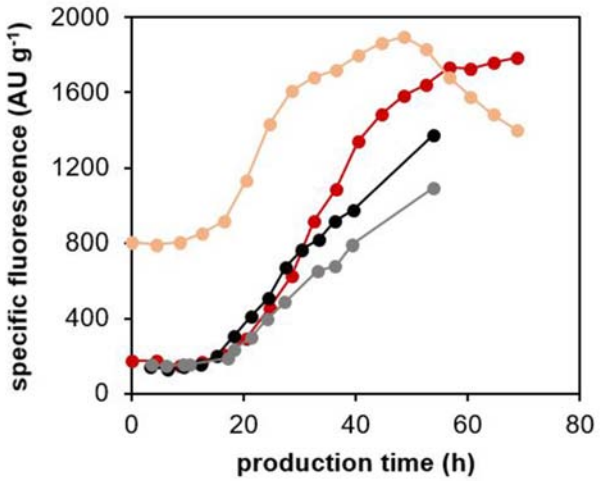

FIGURE 7 | Specific fluorescence of the culture medium and cell lysates of the *P. pastoris* strain producing *Tl*XynA, and the control strains. The *P. pastoris* strain producing *Tl*XynA was cultured at 30°C and pH 5.5, maintaining the specific growth rate of biomass with methanol during the production phase at 0.016 h^{-1}. Fluorescence of the centrifuged culture medium and of the cell lysates were measured with a fluorimeter. Specific extracellular fluorescence (dark red) and specific intracellular fluorescence (light red) were calculated from the measured fluorescence (AU) and CDW (g) values. As controls, the specific extracellular fluorescence of the *Ec*PGA-producing strain with no sfGFP production (gray), and the non-producing strain (black) are shown. The control strains were cultured under the same cultivation conditions as the *Tl*XynA-producing strain.

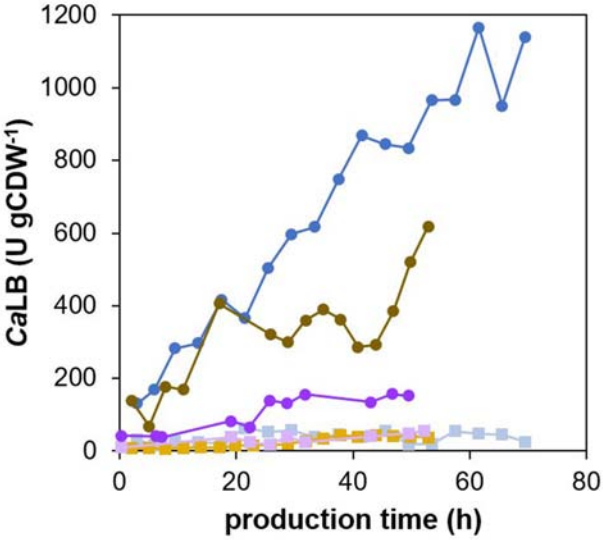

FIGURE 8 | *Ca*LB/biomass yield during cultivations of *P. pastoris* producing recombinant *Ca*LB under different specific growth rates with methanol. The *P. pastoris* strain producing *Ca*LB was cultured at 30°C and pH 5.5, maintaining the specific growth rate of biomass with methanol during the production phase at either 0.008 h^{-1} (purple), 0.016 h^{-1} (blue), or 0.032 h^{-1} (brown). The secreted (dark purple/blue/brown circles) as well as the intracellular (light purple/blue/brown squares) *Ca*LB/biomass yield were calculated.

Around the same time point, the number of cells with up-regulated UPR started to decrease, and the number of PI-stained cells in the population exceeded 12% (**Figure 6C**). The specific intracellular fluorescence measured with the fluorimeter also started to increase after the first 13 h of production, increased steeply until 30 h of production, and then less steeply until 50 h of production. After 50 h of production, it began to decrease. Based on these results, we assume that some of the *Tl*XynA-producing cells were really lysed and releasing sfGFP to the medium. The extracellular sfGFP is not measurable with flow cytometry, which can only detect fluorescence of the cells. Therefore, with our method, we were not able to detect cells with up-regulated UPR and damaged membranes, as a separate cluster.

The Influence of Specific Growth Rate on *Ca*LB Production, Physiology and ER-Stress

The *P. pastoris* strain producing and secreting *Ca*LB was cultured at 30°C and pH 5.5 during fed-batch cultivations with methanol, maintaining the specific growth rate of biomass with methanol at 0.008 h^{-1}, 0.016 h^{-1} or 0.032 h^{-1} (**Table 1**), which corresponded to 15, 30, and 60% of the maximum specific growth rate with methanol, respectively.

The concentration of the product was assessed in the culture broth as well as in the cell extracts, and the specific yield of *Ca*LB was calculated (**Figure 8**). During any of the cultivations with the three different specific growth rates with methanol, the product did not accumulate significantly inside the cells. During cultivation with a specific growth rate with methanol of 0.016 h^{-1}, the yield of secreted *Ca*LB increased steadily and was around 1,200 U $gCDW^{-1}$ at the end of the process, i.e., after 70 h of production. In the cultivation with a specific growth rate with methanol of 0.032 h^{-1}, the yield of the secreted *Ca*LB increased less steeply than in the cultivation with μ = 0.016 h^{-1} and was 600 U $gCDW^{-1}$ at the end of the process, i.e., after 53 h of production. The lowest yield of the secreted *Ca*LB, 150 U $gCDW^{-1}$ after 50 h of production, was reached in the cultivation with a specific growth rate with methanol of 0.008 h^{-1}.

The distribution of the cell population into four sub-populations, as determined by flow cytometry (PCA), differed for the three different specific growth rates with methanol over the time course of the process (**Figure 6**). The amount of viable smaller and less complex cells during the production phase was significantly higher (between 50 and 70%) at a growth rate of 0.008 h^{-1} (**Figure 6E**), than at growth rates of 0.016 h^{-1} (**Figure 6B**) or 0.032 h^{-1} (**Figure 6F**), where the portion of the viable smaller and less complex cells was 40% or lower during the production phase. The highest portion of cells with damaged membranes (30% after 53 h of production) was observed at μ 0.032 h^{-1} (**Figure 6F**); at μ 0.016 h^{-1}, it was around 20% after 53 h of production (**Figure 6B**), and at μ 0.008 h^{-1}, it was around 16% after 52 h of production (**Figure 6E**). The greatest impairment to the viability at μ 0.032 h^{-1} cannot be attributed to a high yield of secreted *Ca*LB (the highest was reached at μ 0.016 h^{-1}), nor to the faster feeding of methanol, since the portion

of PI-stained cells in a non-producing control strain cultured at μ 0.032 h^{-1} did not exceed 13% within a 55 h production phase (**Supplementary Figure 9**). The number of cells with up-regulated UPR slightly increased over the whole production phase at μ 0.008 h^{-1} and was 20–25% at the end of the process (**Figure 6E**). During the process with μ 0.032 h^{-1}, the maximum portion of cells with up-regulated UPR (48%) was reached after 17 h of production (**Figure 6F**), which was more and earlier, compared to cultivation at μ 0.016 h^{-1} (**Figure 6B**). After 17 h of production, the number of the cells belonging to the cluster with up-regulated UPR began to decrease and was 28% at the end of the process, i.e., after 53 h of production.

DISCUSSION

Novel Method of Monitoring Up-Regulation of UPR in *P. pastoris*

In *S. cerevisiae*, the UPRE from the *KAR2* promoter (Cox et al., 1993), or in *Yarrowia lipolytica*, the *KAR2* promoter (Madzak and Beckerich, 2006) were previously used to control the expression of the *lacZ* reporter gene. Induction of the UPR was then monitored as the production of β-galactosidase. We applied for the first time a similar approach to monitor the UPR in the yeast *P. pastoris*. But instead of *lacZ*, we fused the gene of the fast maturating sfGFP (Pédelacq et al., 2006; Khmelinskii et al., 2012) to the *KAR2* promoter (upstream region), to monitor its activity. We showed that the sfGFP signal increased after induction of recombinant protein production (**Figure 6**; **Supplementary Figure 6**), which was in accordance with the increase in *KAR2* expression, i.e., the UPR up-regulation (**Figure 3**). Importantly, the sfGFP fluorescence could have been quickly and easily detected with flow cytometry, which enabled a single-cell, at-line and non-invasive analysis of the UPR during fed-batch bioreactor cultivations. Moreover, cell viability, size and complexity were also analyzed simultaneously with flow cytometry.

P. pastoris Population Is Heterogeneous in Terms of Cell Size and Complexity, Up-Regulation of UPR and Cell Viability During Bioreactor Cultivations

Our work provides an interesting insight into the development of a heterogeneous cell population over the time course of a bioreactor cultivation (**Figure 6**). After the inoculation of the bioreactor, i.e., at the very beginning of the batch phase, the population was homogeneous, formed by larger and more complex cells (higher FSC). Already during the batch phase and further until the start of the production phase with methanol, the population became heterogeneous in terms of cell size and complexity, as the number of smaller and less complex cells (lower FSC) increased. After the start of the production phase, the increasing number of cells with up-regulated UPR was consistent with the decreasing number of viable large and complex cells, assuming that the UPR was being up-regulated mostly in these larger and complex cells. The number of cells with impaired viability increased with the decreasing number of smaller and less complex cells, as well as with the decreasing number of cells with up-regulated UPR. In other words, damaged cells likely arose from smaller and less complex cells, and partly from the large cells with up-regulated UPR. Also, the number of damaged cells increased at different rates and to different extents, depending on the product and specific growth rate with methanol. Cells with an up-regulated UPR and a damaged membrane were not detectable as a separate cluster with our method; as soon as the membrane was damaged, the sfGFP probably leaked out from the cells, so there was no measurable green fluorescence signal in these damaged cells.

The coexistence of *P. pastoris* cells of different sizes, especially during methanol feeding, was reported previously (Hohenblum et al., 2003). It was also shown that the non-producing cells were larger (as indicated by the mean FSC with flow cytometry) than the cells producing the recombinant antibody Fab fragment (Dragosits et al., 2010). According to another work (Aw et al., 2017), *P. pastoris* strains secreting a higher amount of a recombinant protein were shown to have larger cells (as determined by flow cytometry) than strains producing the same product, but lower titers. In our work, the median FSC during the production phase with methanol was comparable in case of the non-producing control strain (median FSC 14.0) and the strain producing *Ec*PGA (median FSC 15.3). The median FSC of the strains producing *Ca*LB and *Tl*XynA was lower (9.1 and 9.7, respectively). Moreover, in the case of the strain producing *Ca*LB, we observed a correlation between FSC and specific growth rate with methanol. The average FSC value (referring to cell size) over the production phase was 6.6 at the lowest growth rate of 0.008 h^{-1}. At growth rate 0.016 h^{-1}, the average FSC was 9.1 and at the highest growth rate 0.032 h^{-1}, the average FSC was 12.6. This trend was, however, not observed in the control strain producing no recombinant protein; the cell sizes were comparable at the specific growth rates with methanol of 0.016 h^{-1} (FSC 14.0) and 0.032 h^{-1} (FSC 12.1). In *S. cerevisiae*, several studies [summarized by Kacmar et al. (2006)] showed that cell size increased with an increasing specific growth rate. However, the increase in cell size was shown to be caused by the production of ethanol at higher growth rates, rather than by a higher specific growth rate (Kacmar et al., 2006).

The heterogeneity in terms of viability of the *P. pastoris* population producing a recombinant protein has been reported in many works (Hohenblum et al., 2003; Jahic et al., 2003; Hyka et al., 2010; Rebnegger et al., 2014, 2016; Zhong et al., 2014; Wang et al., 2016; Aw et al., 2017; Madjid Ansari et al., 2017; Reséndiz-Cardiel et al., 2017). To our best knowledge, the UPR has not been analyzed at the single-cell level in *P. pastoris* until now.

In our work, we did not measure the secretion and intracellular accumulation of the recombinant proteins (*Ec*PGA, *Ca*LB, *Tl*XynA) at a single-cell resolution, as previously shown using microengraving (Love et al., 2010, 2012) or tagging the protein of interest with eGFP (Broger et al., 2011). It was reported that the population of *P. pastoris* cells constitutively producing different recombinant proteins (eGFP, glycosylated/aglycosylated human Fc fragment) was heterogeneous in terms of protein secretion and growth rate. Independently from the type of recombinant protein, three sub-populations with regard to

protein secretion were identified: a large subpopulation (35%) that did not secrete the protein significantly but was viable, a subpopulation secreting the protein consistently, and a subpopulation with a changeable rate of protein secretion (Love et al., 2010, 2012). Heterogeneity in terms of protein production was also reported in the case of *P. pastoris* producing human membrane protein tagged with eGFP (Broger et al., 2011). The co-existence of the sub-populations with different fluorescence intensities indicated varying protein productivity, which was likely caused by varying copy numbers of the recombinant gene in the cells (Cregg et al., 2000). Also non-producing cells were identified within the population (Broger et al., 2011). Combining our method for the single-cell detection of cell size/complexity, UPR and viability with single-cell detection of the recombinant protein, or sorting the cells by FC according to their properties and subsequently measuring the product in the sorted subpopulations, it would be possible to relate the cell types characterized in this work (smaller vs. larger cells, cells with up-regulated UPR, cells with damaged membranes) to their secretion phenotype.

Production of Recombinant Proteins in *P. pastoris* Up-Regulates UPR and Impairs Viability

All three recombinant proteins used in this work, i.e., *Ec*PGA, *Ca*LB, and *Tl*XynA, up-regulated the UPR in *P. pastoris*, though to different extent, depending on the type of the recombinant protein (*Ec*PGA, *Ca*LB, *Tl*XynA, no protein), and, in the case of *Ca*LB, on the specific growth rate with methanol (0.008 h^{-1}, 0.016 h^{-1}, 0.032 h^{-1}). Interestingly, the maximum number of cells with an up-regulated UPR was always reached after 30 h of production, independent of the product, but probably depending on the specific growth rate with methanol.

The majority of studies report UPR up-regulation by (over)production of a recombinant protein (Hohenblum et al., 2004; Gasser et al., 2007; Resina et al., 2007; Khatri et al., 2011; Sjöblom et al., 2012; Hesketh et al., 2013; Vogl et al., 2014; Zhong et al., 2014; Wang et al., 2017; Yu et al., 2017). Only the induced production of secretory insulin precursor in *P. pastoris* was reported to be accompanied by a decrease in the amount of Kar2p in the cells upon methanol shift production (Vanz et al., 2014). This phenomenon was, however, recently explained not by a down-regulation of UPR, but by secretion of Kar2p along with the recombinant protein to the medium and/or by an enhanced autophagy of the ER, resulting in an extracellular release of Kar2p (Roth et al., 2018).

Generally, up-regulation of UPR may be more significant in a fed-batch mode than in chemostat cultures (Zahrl et al., 2017). Up-regulation of UPR was shown to correlate with the intracellular accumulation of human trypsinogen (Hohenblum et al., 2004) or interleukin (Zhong et al., 2014). In contrast, in the case of partial intracellular accumulation of the mucin-type protein fused with GFP, the ER folding stress was low; however there was a secretory bottle-neck in the Golgi system (Sjöblom et al., 2012). In another work, the UPR was reported to be up-regulated to a different extent in *P. pastoris* clones producing human serum albumin (HSA), which all contained only one copy of the gene coding for HSA (Aw et al., 2017); there was no clear correlation between up-regulation of the UPR, and product titers, but the ERAD was only up-regulated in clones with high secretion of HSA. The UPR was also shown to be down-regulated at lower specific growth rates (Rebnegger et al., 2014). In our work, the increasing specific growth rate with methanol resulted in a faster and stronger up-regulation of UPR.

In this work, the up-regulation was most significant in the case of *Ec*PGA (60% of the *Ec*PGA-producing cells exhibited up-regulated UPR), which strongly accumulated in the cells (up to 50–70% of the total active *Ec*PGA). As already discussed in the work of Marešová et al. (2017), the reason for poor secretion of *Ec*PGA might be its incorrect maturation in *P. pastoris* cells, which results in ER stress. A co-expression of *E. coli* chaperone genes might improve the secretion of proteins of bacterial origin (Summpunn et al., 2018). The recombinant *Ca*LB and *Tl*XynA in our work did not accumulate significantly inside the cells, yet we observed an up-regulation of the UPR. This was probably caused by the overexpression of the recombinant genes from the *AOX1* promoter, which resulted in a high load of protein in the ER. Since the post-translational modifications of *Tl*XynA involve formation of disulfide bonds (Gruber et al., 1998; Damaso et al., 2003), and in the case of *Ca*LB, also glycosylation (Uppenberg et al., 1994), we believe the capacity of the ER was exceeded. The up-regulation of UPR by the production of recombinant xylanase A in *P. pastoris* was reported previously (Lin et al., 2013); compared to a control non-producing strain, the fold change in *KAR2* expression analyzed by qPCR was ∼0.5 in a strain carrying one copy of the xylanase gene, and 1.9 in a strain carrying four copies of the xylanase gene. No ERAD up-regulation was observed, indicating that the xylanase was not degraded (Lin et al., 2013). Detectable amounts of Kar2p were also observed in the *P. pastoris* strain producing *Ca*LB (Samuel et al., 2013), but there was no comparison made to a non-producing strain. Overall, our results indicate that the up-regulation of UPR was not exclusively linked to poor secretion of the recombinant protein. Additionally, there was also no clear correlation between the intensity of UPR caused by the different proteins, and the mass of the secreted total protein (g) (**Supplementary Figure 8**). There is a general demand for more detailed characterization of the secretory machinery and the UPR in *P. pastoris*, information that is currently still derived from other yeasts (Puxbaum et al., 2015).

The viability of the cells was impaired by the production of *Ca*LB and *Tl*XynA, as the number of PI-stained cells in these strains was higher than in the non-producing control strain. In contrast to *Ca*LB and *Tl*XynA, the production of *Ec*PGA in our work did not enhance cellular damage, compared to the non-producing control strain. The impaired viability of *P. pastoris* resulting from production of recombinant protein is commonly observed, although to different extents, depending on the recombinant protein and cultivation conditions. For example, in the case of the production of recombinant human trypsinogen, 65% of cells were non-viable after ∼135 h of production with methanol (Hohenblum et al., 2003). The production of porcine trypsinogen at pH 4 and at a high cell density in fed-batch culture

resulted in more than 80% of damaged cells (Hyka et al., 2010). High viability was observed at very low, almost zero, specific growth rates (Rebnegger et al., 2016). In another study, however, there was no clear correlation between specific growth rates, viability and product yield; at the lowest specific growth rate (0.015 h^{-1}), the viability was 94%, while at the higher specific growth rates, the number of dead cells was even lower (Rebnegger et al., 2014). In our work, the increasing specific growth rate with methanol resulted in a larger fraction of damaged cells, but the highest specific yield of *Ca*LB was reached at the mid value within the range of the tested specific growth rates with methanol, i.e., at 0.016 h^{-1}.

CONCLUSIONS

Production and secretion of three different recombinant proteins (*Ec*PGA, *Ca*LB, *Tl*XynA) by *P. pastoris* was investigated along with up-regulation of the UPR and cell viability, which were assessed at the single-cell level in living cells and at-line with flow cytometry. In all three strains, as well as in a non-producing control strain, which were all cultured under the same cultivation conditions, a heterogeneous population consisting of four subpopulations developed after the induction of protein production. The distribution of the population into four fractions differed over the time course of the cultivation process and depended on the recombinant protein and the specific growth rate. Up-regulation of the UPR was especially strong when the recombinant protein was not properly secreted (*Ec*PGA), but was not linked exclusively to the intracellular accumulation. We observed no correlation between up-regulation of UPR and impaired viability, and also no clear correlation between viability and protein production (*Ca*LB). We believe these results emphasize the importance of a complex and systematic understanding of the biotechnological process, with a single-cell analysis of the production population, in order to enhance productivity of the bioprocess. We developed a reporter system for the UPR, which enables fast and easy monitoring of the UPR at the single-cell level and in a non-invasive manner. This method could be adapted to a broad range of biotechnologically important production hosts and also, with no necessary adaptation, could be used at the screening scale. By understanding the relationship between protein production/secretion and the tuning of the UPR, this monitoring system based on fluorescence measurement might be utilized in a feedback control of a bioprocess.

AUTHOR CONTRIBUTIONS

HR designed and conducted the experiments and wrote the manuscript. IZ created the program for the analysis of the flow cytometric data. MB and AW participated in the construction of the recombinant strains. PM participated in performing the bioreactor experiments and analyzing the data from the cultivation processes. DM presented this work at the conference Microbial Stress: from Systems to Molecules and Back in Kinsale, Ireland. ZK designed the expression cassette for monitoring the unfolded protein response and supervised the work. AG, KM, and KK supervised the work.

ACKNOWLEDGMENTS

The major part of this research was performed within the project Physiological response of *Pichia pastoris* to production of a heterologous protein (PHYRE) supported by the Swiss Government Excellence Scholarship. The work was also financially supported from specific university research (MSMT No 20-SVV/2017). Big thanks belongs to Marcel Straumann, Chiara Braun, Sonja Weichart, and Dr. Lukas Neutsch (all Zurich University of Applied Sciences ZHAW, Wädenswil, CH) for assisting with the bioreactor cultivations. The authors also thank Dr. Helena Marešová (Institute of Microbiology of the Czech Academy of Sciences, Czech Republic) for providing the plasmid carrying the *Ec*PGA, Prof. Dr. Michael Knop (Zentrum für Molekulare Biologie der Universität Heidelberg, Heidelberg, DE) for providing the plasmid pMaM60 and bisy e.U., Hofstätten for providing the plasmids pBSY3S1Z_CaLB-WT, pBSYAOXsec_blunt, and pBSYAOX_blunt. Further thanks goes to Prof. Dr. John Brooker for English proofreading.

SUPPLEMENTARY MATERIAL

The Supplementary Material for this article can be found online at: https://www.frontiersin.org/articles/10.3389/fmicb.2019.00335/full#supplementary-material

REFERENCES

Ahmad, M., Hirz, M., Pichler, H., and Schwab, H. (2014). Protein expression in *Pichia pastoris*: recent achievements and perspectives for heterologous protein production. *Appl. Microbiol. Biotechnol.* 98, 5301–5317. doi: 10.1007/s00253-014-5732-5

Alber, A. B., Paquet, E. R., Biserni, M., Naef, F., and Suter, D. M. (2018). Single live cell monitoring of protein turnover reveals intercellular variability and cell-cycle dependence of degradation rates. *Mol. Cell.* 71, 1079–1091. doi: 10.1016/j.molcel.2018.07.023

Aw, R., Barton, G. R., and Leak, D. J. (2017). Insights into the prevalence and underlying causes of clonal variation through transcriptomic analysis in *Pichia pastoris*. *Appl. Microbiol. Biotechnol.* 101, 5045–5058. doi: 10.1007/s00253-017-8317-2

Broger, T., Odermatt, R. P., Huber, P., and Sonnleitner, B. (2011). Real-time online flow cytometry for bioprocess monitoring. *J. Biotechnol.* 154, 240–247. doi: 10.1016/j.jbiotec.2011.05.003

Cereghino, J. L., and Cregg, J. M. (2000). Heterologous protein expression in the methylotrophic yeast *Pichia pastoris*. *FEMS Microbiol. Rev.* 24, 45–66. doi: 10.1111/j.1574-6976.2000.tb00532.x

Cox, J. S., Shamu, C. E., and Walter, P. (1993). Transcriptional induction of genes encoding endoplasmic reticulum resident proteins requires a transmembrane protein kinase. *Cell* 73, 1197–1206. doi: 10.1016/0092-8674(93)90648-A

Cregg, J. M., Cereghino, J. L., Shi, J., and Higgins, D. R. (2000). Recombinant protein expression in *Pichia pastoris*. *Mol. Biotechnol.* 16, 23–52. doi: 10.1385/MB:16:1:23

Damaso, M. C., Almeida, M. S., Kurtenbach, E., Martins, O. B., Pereira Jr., N., Andrade, C. M., et al. (2003). Optimized expression of a thermostable xylanase

from *Thermomyces lanuginosus* in *Pichia pastoris*. *Appl. Env. Microbiol.* 69, 6064–6072. doi: 10.1128/AEM.69.10.6064-6072.2003

Dragosits, M., Stadlmann, J., Graf, A., Gasser, B., Maurer, M., Sauer, M., et al. (2010). The response to unfolded protein is involved in osmotolerance of *Pichia pastoris*. *BMC Genomics* 11:207. doi: 10.1186/1471-2164-11-207

Dudek, J., Benedix, J., Cappel, S., Greiner, M., Jalal, C., Müller, L., et al. (2009). Functions and pathologies of BiP and its interaction partners. *Cell. Mol. Life Sci.* 66, 1556–1569. doi: 10.1007/s00018-009-8745-y

Edwards-Jones, B., Aw, R., Barton, G. R., Tredwell, G. D., Bundy, J. G., and Leak, D. J. (2015). Translational arrest due to cytoplasmic redox stress delays adaptation to growth on methanol and heterologous protein expression in a typical fed-batch culture of *Pichia pastoris*. *PLoS ONE* 10:e0119637. doi: 10.1371/journal.pone.0119637

Gao, B., Wang, X., and Shen, Y. (2006). Studies on characters of immobilizing penicillin G acylase on a novel composite support PEI/SiO_2. *Biochem. Eng. J.* 28, 140–147. doi: 10.1016/j.bej.2005.10.007

Gasser, B., Maurer, M., Rautio, J., Sauer, M., Bhattacharyya, A., Saloheimo, M., et al. (2007). Monitoring of transcriptional regulation in *Pichia pastoris* under protein production conditions. *BMC Genomics* 8:179. doi: 10.1186/1471-2164-8-179

Graf, A., Gasser, B., Dragosits, M., Sauer, M., Leparc, G. G., Tüchler, T., et al. (2008). Novel insights into the unfolded protein response using *Pichia pastoris* specific DNA microarrays. *BMC Genomics* 9:390. doi: 10.1186/1471-2164-9-390

Gruber, K., Klintschar, G., Hayn, M., Schlacher, A., Steiner, W., and Kratky, C. (1998). Thermophilic xylanase from thermomyces lanuginosus: high-resolution X- ray structure and modeling studies. *Biochemistry* 37, 13475–13485. doi: 10.1021/bi980864l

Guerfal, M., Ryckaert, S., Jacobs, P. P., Ameloot, P., Van Craenenbroeck, K., Derycke, R., et al. (2010). The HAC1 gene from *Pichia pastoris*: characterization and effect of its overexpression on the production of secreted, surface displayed and membrane proteins. *Microb. Cell Fact.* 9:49. doi: 10.1186/1475-2859-9-49

Hesketh, A. R., Castrillo, J. I., Sawyer, T., Archer, D. B., and Oliver, S. G. (2013). Investigating the physiological response of *Pichia* (Komagataella) *pastoris* GS115 to the heterologous expression of misfolded proteins using chemostat cultures. *Appl. Microbiol. Biotechnol.* 97, 9747–9762. doi: 10.1007/s00253-013-5186-1

Hohenblum, H., Borth, N., and Mattanovich, D. (2003). Assessing viability and cell-associated product of recombinant protein producing *Pichia pastoris* with flow cytometry. *J. Biotechnol.* 102, 281–290. doi: 10.1016/S0168-1656(03)00049-X

Hohenblum, H., Gasser, B., Maurer, M., Borth, N., and Mattanovich, D. (2004). Effects of gene dosage, promoters, and substrates on unfolded protein stress of recombinant *Pichia pastoris*. *Biotechnol. Bioeng.* 85, 367–375. doi: 10.1002/bit.10904

Hyka, P., Züllig, T., Ruth, C., Looser, V., Meier, C., Klein, J., et al. (2010). Combined use of fluorescent dyes and flow cytometry to quantify the physiological state of *Pichia pastoris* during the production of heterologous proteins in high-cell-density fed-batch cultures. *Appl. Env. Microbiol.* 76, 4486–4496. doi: 10.1128/AEM.02475-09

Jahic, M., Wallberg, F., Bollok, M., Garcia, P., and Enfors, S. O. (2003). Temperature limited fed-batch technique for control of proteolysis in *Pichia pastoris* bioreactor cultures. *Microb. Cell Fact.* 2:6. doi: 10.1186/1475-2859-2-6

Juturu, V., and Wu, J. C. (2018). Heterologous protein expression in *Pichia pastoris*: latest research progress and applications. *ChemBioChem* 19, 7–21. doi: 10.1002/cbic.201700460

Kacmar, J., Gilbert, A., Cockrell, J., and Srienc, F. (2006). The cytostat: a new way to study cell physiology in a precisely defined environment. *J. Biotechnol.* 126, 163–72. doi: 10.1016/j.jbiotec.2006.04.015

Khatri, N. K., Gocke, D., Trentmann, O., Neubauer, P., and Hoffmann, F. (2011). Single-chain antibody fragment production in *Pichia pastoris*: benefits of prolonged pre-induction glycerol feeding. *Biotechnol. J.* 6, 452–462. doi: 10.1002/biot.201000193

Khmelinskii, A., Keller, P. J., Bartosik, A., Meurer, M., Barry, J. D., Mardin, B. R., et al. (2012). Tandem fluorescent protein timers for *in vivo* analysis of protein dynamics. *Nat. Biotechnol.* 30, 708–714. doi: 10.1038/nbt.2281

Krainer, F. W., Dietzsch, C., Hajek, T., Herwig, C., Spadiut, O., and Glieder, A. (2012). Recombinant protein expression in *Pichia pastoris* strains with an engineered methanol utilization pathway. *Microb. Cell Fact.* 11:22. doi: 10.1186/1475-2859-11-22

Lajoie, P., Moir, R. D., Willis, I. M., and Snapp, E. L. (2012). Kar2p availability defines distinct forms of endoplasmic reticulum stress in living cells. *Mol. Biol. Cell* 23, 955–964. doi: 10.1091/mbc.e11-12-0995

Lin, X. Q., Liang, S. L., Han, S. Y., Zheng, S. P., Ye, Y. R., and Lin, Y. (2013). Quantitative iTRAQ LC-MS/MS proteomics reveals the cellular response to heterologous protein overexpression and the regulation of HAC1 in *Pichia pastoris*. *J. Proteomics* 91, 58–72. doi: 10.1016/j.jprot.2013.06.031

Lin-Cereghino, J., Wong, W. W., Xiong, S., Giang, W., Luong, L. T., Vu, J., et al. (2005). Condensed protocol for competent cell preparation and transformation of the methylotrophic yeast *Pichia pastoris*. *Biotechniques* 38, 44–48. doi: 10.2144/05381BM04

Love, K. R., Panagiotou, V., Jiang, B., Stadheim, T. A., and Love, J. C. (2010). Integrated single-cell analysis shows *Pichia pastoris* secretes protein stochastically. *Biotechnol. Bioeng.* 106, 319–325. doi: 10.1002/bit.22688

Love, K. R., Politano, T. J., Panagiotou, V., Jiang, B., Stadheim, T. A., and Love, J. C. (2012). Systematic single-cell analysis of *Pichia pastoris* reveals secretory capacity limits productivity. *PLoS ONE* 7:e37915. doi: 10.1371/journal.pone.0037915

Madjid Ansari, A., Majidzadeh,-A., K., Darvishi, B., Sanati, H., Farahmand, L., Norouzian, D., et al. (2017). Extremely low frequency magnetic field enhances glucose oxidase expression in *Pichia pastoris* GS115. *Enzyme Microb. Technol.* 98, 67–75. doi: 10.1016/j.enzmictec.2016.12.011

Madzak, C., and Beckerich, J.-M. (2006). A sensor of the unfolded protein response to study the stress induced in *Yarrowia* lipolytica strains by the production of heterologous proteins. *Microb. Cell Fact.* 5:P5. doi: 10.1186/1475-2859-5-S1-P5

Marešová, H., Palyzová, A., Plačková, M., Grulich, M., and Rajasekar, V. W., Štěpánek, V., et al. (2017). Potential of *Pichia pastoris* for the production of industrial penicillin G acylase. *Folia Microbiol. (Praha).* 62, 417–424. doi: 10.1007/s12223-017-0512-0

Mattanovich, D., Gasser, B., Hohenblum, H., and Sauer, M. (2004). Stress in recombinant protein producing yeasts. *J. Biotechnol.* 113, 121–135. doi: 10.1016/j.jbiotec.2004.04.035

Meehl, M. A., and Stadheim, T. A. (2014). Biopharmaceutical discovery and production in yeast. *Curr. Opin. Biotechnol.* 30, 120–127. doi: 10.1016/j.copbio.2014.06.007

Mellitzer, A., Glieder, A., Weis, R., Reisinger, C., and Flicker, K. (2012a). Sensitive high-throughput screening for the detection of reducing sugars. *Biotechnol. J.* 7, 155–162. doi: 10.1002/biot.201100001

Mellitzer, A., Weis, R., Glieder, A., and Flicker, K. (2012b). Expression of lignocellulolytic enzymes in *Pichia pastoris*. *Microb. Cell Fact.* 11:61. doi: 10.1186/1475-2859-11-61

Mori, K., Kawahara, T., Yoshida, H., Yanagi, H., and Yura, T. (1996). Signalling from endoplasmic reticulum to nucleus: transcription factor with a basic-leucine zipper motif is required for the unfolded protein-response pathway. *Genes Cells* 1, 803–817. doi: 10.1046/j.1365-2443.1996.d01-274.x

Mori, K., Ogawa, N., Kawahara, T., Yanagi, H., and Yura, T. (1998). Palindrome with spacer of one nucleotide is characteristic of the cis-acting unfolded protein response element in *Saccharomyces cerevisiae*. *J. Biol. Chem.* 273, 9912–9920. doi: 10.1074/jbc.273.16.9912

Pédelacq, J. D., Cabantous, S., Tran, T., Terwilliger, T. C., and Waldo, G. S. (2006). Engineering and characterization of a superfolder green fluorescent protein. *Nat. Biotechnol.* 24, 79–88. doi: 10.1038/nbt1172

Pfeffer, M., Maurer, M., Köllensperger, G., Hann, S., Graf, A. B., and Mattanovich, D. (2011). Modeling and measuring intracellular fluxes of secreted recombinant protein in *Pichia pastoris* with a novel 34S labeling procedure. *Microb. Cell Fact.* 10:47. doi: 10.1186/1475-2859-10-47

Potgieter, T. I., Kersey, S. D., Mallem, M. R., Nylen, A. C., and d'Anjou, M. (2010). Antibody expression kinetics in glycoengineered *Pichia pastoris*. *Biotechnol. Bioeng.* 106, 918–927. doi: 10.1002/bit.22756

Puxbaum, V., Mattanovich, D., and Gasser, B. (2015). Quo vadis? The challenges of recombinant protein folding and secretion in *Pichia pastoris*. *Appl. Microbiol. Biotechnol.* 99, 2925–2938. doi: 10.1007/s00253-015-6470-z

Rebnegger, C., Graf, A. B., Valli, M., Steiger, M. G., Gasser, B., Maurer, M., et al. (2014). In *Pichia pastoris*, growth rate regulates protein synthesis and secretion, mating and stress response. *Biotechnol. J.* 9, 511–525. doi: 10.1002/biot.201300334

Rebnegger, C., Vos, T., Graf, A. B., Valli, M., Pronk, J. T., Daran-Lapujade, P., et al. (2016). *Pichia pastoris* exhibits high viability and low maintenance-energy requirement at near-zero specific growth rates. *Appl. Environ. Microbiol.* 82, 4570–4583. doi: 10.1128/AEM.00638-16

Reséndiz-Cardiel, G., Arroyo, R., and Ortega-López, J. (2017). Expression of the enzymatically active legumain-like cysteine proteinase TvLEGU-1 of *Trichomonas vaginalis* in *Pichia pastoris*. *Protein Expr. Purif.* 134, 104–113. doi: 10.1016/j.pep.2017.04.007

Resina, D., Bollók, M., Khatri, N. K., Valero, F., Neubauer, P., and Ferrer, P. (2007). Transcriptional response of P-pastoris in fed-batch cultivations to *Rhizopus oryzae* lipase production reveals UPR induction. *Microb. Cell Fact.* 6:21. doi: 10.1186/1475-2859-6-21

Roth, G., Vanz, A. L., Lünsdorf, H., Nimtz, M., and Rinas, U. (2018). Fate of the UPR marker protein Kar2/Bip and autophagic processes in fed-batch cultures of secretory insulin precursor producing *Pichia pastoris*. *Microb. Cell Fact.* 17:123. doi: 10.1186/s12934-018-0970-3

Samuel, P., Prasanna Vadhana, A. K., Kamatchi, R., Antony, A., and Meenakshisundaram, S. (2013). Effect of molecular chaperones on the expression of *Candida antarctica* lipase B in *Pichia pastoris*. *Microbiol. Res.* 168, 615–620. doi: 10.1016/j.micres.2013.06.007

Sjöblom, M., Lindberg, L., Holgersson, J., and Rova, U. (2012). Secretion and expression dynamics of a GFP-tagged mucin-type fusion protein in high cell density *Pichia pastoris* bioreactor cultivations. *Adv. Biosci. Biotechnol.* 3, 238–248. doi: 10.4236/abb.2012.33033

Sobotková, L., Štěpánek, V., Plháčková, K., and Kyslík, P. (1996). Development of a high-expression system for penicillin G acylase based on the recombinant Escherichia coli strain RE3(pKA18). *Enzyme Microb. Technol.* 19, 389–397. doi: 10.1016/S0141-0229(96)00052-X

Summpunn, P., Jomrit, J., and Panbangred, W. (2018). Improvement of extracellular bacterial protein production in *Pichia pastoris* by co-expression of endoplasmic reticulum residing GroEL–GroES. *J. Biosci. Bioeng.* 125, 268–274. doi: 10.1016/j.jbiosc.2017.09.007

Theron, C. W., Berrios, J., Delvigne, F., and Fickers, P. (2018). Integrating metabolic modeling and population heterogeneity analysis into optimizing recombinant protein production by Komagataella *(Pichia) pastoris*. *Appl. Microbiol. Biotechnol.* 102, 63–80. doi: 10.1007/s00253-017-8612-y

Tredwell, G. D., Aw, R., Edwards-Jones, B., Leak, D. J., and Bundy, J. G. (2017). Rapid screening of cellular stress responses in recombinant *Pichia pastoris* strains using metabolite profiling. *J. Ind. Microbiol. Biotechnol.* 44, 413–417. doi: 10.1007/s10295-017-1904-5

Uppenberg, J., Hansen, M. T., Patkar, S., and Jones, T. A. (1994). The sequence, crystal structure determination and refinement of two crystal forms of lipase B from *Candida antarctica*. *Structure* 2, 293–308. doi: 10.1016/S0969-2126(00)00031-9

Vanz, A. L., Nimtz, M., and Rinas, U. (2014). Decrease of UPR- and ERAD-related proteins in *Pichia pastoris* during methanol-induced secretory insulin precursor production in controlled fed-batch cultures. *Microb. Cell Fact.* 13:10. doi: 10.1186/1475-2859-13-23

Vogl, T., Thallinger, G. G., Zellnig, G., Drew, D., Cregg, J. M., Glieder, A., et al. (2014). Towards improved membrane protein production in *Pichia pastoris*: general and specific transcriptional response to membrane protein overexpression. *N. Biotechnol.* 31, 538–552. doi: 10.1016/j.nbt.2014.02.009

Wang, J., Li, Y., and Liu, D. (2016). Improved production of *Aspergillus usamii* endo-β-1,4-Xylanase in *Pichia pastoris* via combined strategies. *Biomed Res. Int.* 2016: 3265895. doi: 10.1155/2016/3265895

Wang, X. D., Jiang, T., Yu, X. W., and Xu, Y. (2017). Effects of UPR and ERAD pathway on the prolyl endopeptidase production in *Pichia pastoris* by controlling of nitrogen source. *J. Ind. Microbiol. Biotechnol.* 44, 1053–1063. doi: 10.1007/s10295-017-1938-8

Weis, R., Luiten, R., Skranc, W., Schwab, H., Wubbolts, M., and Glieder, A. (2004). Reliable high-throughput screening with *Pichia pastoris* by limiting yeast cell death phenomena. *FEMS Yeast Res.* 5, 179–189. doi: 10.1016/j.femsyr.2004.06.016

Yu, X. W., Sun, W. H., Wang, Y. Z., and Xu, Y. (2017). Identification of novel factors enhancing recombinant protein production in multi-copy Komagataella phaffii based on transcriptomic analysis of overexpression effects. *Sci. Rep.* 7:16249. doi: 10.1038/s41598-017-16577-x

Zahrl, R. J., Mattanovich, D., and Gasser, B. (2018). The impact of ERAD on recombinant protein secretion in pichia pastoris (Syn komagataella spp.). *Microbiol.* 164, 453–463. doi: 10.1099/mic.0.000630

Zahrl, R. J., Peña, D. A., Mattanovich, D., and Gasser, B. (2017). Systems biotechnology for protein production in *Pichia pastoris*. *FEMS Yeast Res.* 17, 1–15. doi: 10.1093/femsyr/fox068

Zhong, Y., Yang, L., Guo, Y., Fang, F., Wang, D., Li, R., et al. (2014). High-temperature cultivation of recombinant *Pichia pastoris* increases endoplasmic reticulum stress and decreases production of human interleukin-10. *Microb. Cell Fact.* 13:163. doi: 10.1186/s12934-014-0163-7

Zhu, T., Guo, M., Sun, C., Qian, J., Zhuang, Y., Chu, J., et al. (2009). A systematical investigation on the genetic stability of multi-copy *Pichia pastoris* strains. *Biotechnol. Lett.* 31, 679–684. doi: 10.1007/s10529-009-9917-4

Conflict of Interest Statement: The authors declare that the research was conducted in the absence of any commercial or financial relationships that could be construed as a potential conflict of interest.

Advantages of publishing in Frontiers

OPEN ACCESS
Articles are free to read for greatest visibility and readership

FAST PUBLICATION
Around 90 days from submission to decision

HIGH QUALITY PEER-REVIEW
Rigorous, collaborative, and constructive peer-review

TRANSPARENT PEER-REVIEW
Editors and reviewers acknowledged by name on published articles

Frontiers
Avenue du Tribunal-Fédéral 34
1005 Lausanne | Switzerland

Visit us: www.frontiersin.org
Contact us: info@frontiersin.org | +41 21 510 17 00

REPRODUCIBILITY OF RESEARCH
Support open data and methods to enhance research reproducibility

DIGITAL PUBLISHING
Articles designed for optimal readership across devices

FOLLOW US
@frontiersin

IMPACT METRICS
Advanced article metrics track visibility across digital media

EXTENSIVE PROMOTION
Marketing and promotion of impactful research

LOOP RESEARCH NETWORK
Our network increases your article's readership